
Table of Contents

1	Introduction	1
1-1	Introduction to flight dynamics and control	2
1-1-1	Flight control surfaces	2
1-1-2	Flight control systems	4
1-2	Assumptions	13
1-3	Book outline	14
I	Equations of Motion	17
2	Reference Frames	19
2-1	Overview of reference frames	20
2-1-1	Inertial reference frame, F_I	20
2-1-2	Earth-centered, Earth-fixed reference frame (F_C)	22
2-1-3	Vehicle-carried normal Earth reference frame, F_E	22
2-1-4	Body-fixed reference frame, F_b	23
2-1-5	Vehicle reference frame, F_r	24
2-1-6	Aerodynamic (air-path) reference frame, F_a	26
2-2	Transformations between reference frames	28
2-2-1	Euler angles	28
2-2-2	Transformation matrices	33
2-2-3	Transformation from F_I to F_C	37
2-2-4	Transformation from F_C to F_E	38
2-2-5	Transformation from F_E to F_b	39
2-2-6	Transformation from F_E to F_a	40
2-2-7	Transformation from F_b to F_a	42
2-2-8	Coordinate transformations	44
2-3	Rotating reference frames	47
2-3-1	Vector time derivatives	47
2-3-2	Derivation of the angular velocity vector	52

3 Derivation of the Equations of Motion	57
3-1 Introduction	57
3-2 External forces and moments	58
3-2-1 External forces	58
3-2-2 External moments	60
3-3 The Equations of Translational Motion	61
3-3-1 Motion with respect to inertial space	61
3-3-2 Motion with respect to a rotating frame	63
3-3-3 Spherical position and Cartesian velocity	64
3-4 The Equations of Rotational Motion	69
3-4-1 General formulation	69
3-4-2 The Euler equations	70
3-4-3 The attitude equations	71
3-5 Simplifications of the equations of motion	75
3-5-1 Non-rotating Earth	77
3-5-2 Flat and Non-rotating Earth	77
3-5-3 Simplified equations in the body frame	78
4 Linearized Equations of Motion	83
4-1 Linearization about arbitrary flight condition in arbitrary body-fixed reference frame	85
4-1-1 Linearization of states	87
4-1-2 Linearization of forces and moments	87
4-1-3 Linearization of kinematic relations	92
4-2 Linearization about steady, straight, symmetric flight condition	94
4-2-1 Linearized set of equations	95
4-2-2 Moments and products of inertia	96
4-3 Equations of motion in non-dimensional form	98
4-3-1 Symmetric Motions	99
4-3-2 Asymmetric Motions	101
4-4 Symmetric equations of motion in state-space form	110
4-5 Asymmetric equations of motion in state-space form	112
II Dynamic Stability Analysis	115
5 Analysis of Symmetric Equations of Motion	117
5-1 Solution of the equations of motion	119
5-2 Stability criteria	130
5-3 The complete solution of the equations of motion	131
5-4 Approximate solutions	139

6 Analysis of Asymmetric Equations of Motion	143
6-1 Solution of the equations of motion	143
6-2 General character of the asymmetric motions	147
6-3 Routh-Hurwitz stability criteria for the asymmetric motions	150
6-4 Spiral and Dutch roll mode, the lateral stability diagram	156
6-5 Approximate solutions	157
7 Longitudinal Stability and Control Derivatives	161
7-1 Aerodynamic forces in the nominal flight condition	162
7-2 Derivatives with respect to airspeed	164
7-2-1 Stability derivative C_{X_u}	164
7-2-2 Stability derivative C_{Z_u}	165
7-2-3 Stability derivative C_{m_u}	165
7-3 Derivatives with respect to angle of attack	169
7-3-1 Stability derivative C_{X_α}	169
7-3-2 Stability derivative C_{Z_α}	170
7-3-3 Stability derivative C_{m_α}	173
7-4 Derivatives with respect to pitching velocity	174
7-5 Derivatives with respect to the acceleration along the top axis	182
7-6 Derivatives with respect to the elevator angle	185
7-6-1 Control derivative $C_{X_{\delta_e}}$	185
7-6-2 Control derivative $C_{Z_{\delta_e}}$	185
7-6-3 Control derivative $C_{m_{\delta_e}}$	186
7-7 Symmetric inertial parameters	186
8 Lateral Stability and Control Derivatives	189
8-1 Aerodynamic force and moments due to side slipping, rolling and yawing	189
8-2 Stability derivatives with respect to the sideslip angle	193
8-2-1 Stability derivative C_{Y_β}	193
8-2-2 Stability derivative C_{ℓ_β}	195
8-2-3 Stability derivative C_{n_β}	204
8-2-4 Stability derivative $C_{n_{\beta^2}}$	212
8-2-5 Stability derivative $C_{m_{\beta^2}}$	212
8-3 Stability derivatives with respect to roll rate	217
8-3-1 Stability derivative C_{Y_p}	217
8-3-2 Stability derivative C_{ℓ_p}	218
8-3-3 Stability derivative C_{n_p}	221
8-4 Stability derivatives with respect to yaw rate	225
8-4-1 Stability derivative C_{Y_r}	227
8-4-2 Stability derivative C_{ℓ_r}	229
8-4-3 Stability derivative C_{n_r}	231

8-5 The forces and moments due to aileron, rudder and spoiler deflections	232
8-6 Aileron control derivatives	234
8-6-1 Control derivative $C_{Y_{\delta_a}}$	234
8-6-2 Control derivative $C_{\ell_{\delta_a}}$	235
8-6-3 Control derivative $C_{n_{\delta_a}}$	235
8-7 Spoiler control derivatives	236
8-8 Rudder control derivatives	238
8-8-1 Control derivative $C_{Y_{\delta_r}}$	238
8-8-2 Control derivative $C_{\ell_{\delta_r}}$	240
8-8-3 Control derivative $C_{n_{\delta_r}}$	240
III Static Stability Analysis	243
9 Analysis of Steady Symmetric Flight	245
9-1 Aerodynamic center	246
9-1-1 Aerodynamic forces and moments acting on a wing	246
9-1-2 A compact description for the aerodynamic moment characteristics	254
9-1-3 The role of the aerodynamic center and $C_{m_{ac}}$ in static stability	259
9-1-4 The position of the aerodynamic center and $C_{m_{ac}}$ of a wing	268
9-1-5 Influence of wing shape on the aerodynamic center and $C_{m_{ac}}$	278
9-1-6 Characteristics of wing-fuselage-nacelle configurations	289
9-1-7 Aerodynamic effects of nacelles	300
9-2 Equilibrium in steady, straight, symmetric Flight	308
9-2-1 Conditions for equilibrium	308
9-2-2 Normal force on the horizontal tailplane	315
9-2-3 Hinge moment of the elevator	318
9-2-4 Flow direction and dynamic pressure at the horizontal tailplane	321
9-2-5 Effect of airspeed and center of gravity on tail load	335
9-2-6 Elevator deflection required for moment equilibrium	339
9-2-7 Stick forces in steady flight	341
10 Longitudinal Stability and Control in Steady Flight	345
10-1 Stick Fixed Static Longitudinal Stability	345
10-1-1 Stick fixed static longitudinal stability in gliding flight	346
10-1-2 Neutral point, stick fixed	351
10-1-3 Elevator trim curve and elevator trim stability	352
10-1-4 Influence of various parameters on elevator trim curve	362
10-1-5 Static longitudinal stability of tailless aircraft	364
10-1-6 Determination $C_{m_{\delta_e}}$ from measurements in flight	365
10-2 Stick Free Static Longitudinal Stability	370
10-2-1 Stick free static longitudinal stability in gliding flight	371

10-2-2 Neutral point, stick free	373
10-2-3 Elevator stick force curves and elevator stick force Stability	375
10-2-4 Effect of center of gravity and mass unbalance on stick force stability	385
10-2-5 Influence of design variables on control forces	390
10-2-6 Control forces a pilot can exert	391
10-2-7 Airworthiness requirements for steady straight symmetric flight	392
10-3 Longitudinal Control in Pull-Up Manoeuvres and Steady Turns	395
10-3-1 Characteristics of longitudinal control in turning flight	398
10-3-2 The stick displacement per g	401
10-3-3 The manoeuvre point, stick fixed	407
10-3-4 The stick force per g	410
10-3-5 The manoeuvre point, stick free	418
10-3-6 Non-aerodynamic means to influence the stick force Per g	422
11 Lateral Stability and Control in Steady Flight	425
11-1 Introduction	425
11-2 Equations of Equilibrium	425
11-3 Steady Horizontal Turns	427
11-3-1 Turns Using the Ailerons Only, $\delta_r = 0$	429
11-3-2 Turns Using the Rudder Only, $\delta_a = 0$	429
11-3-3 Coordinated Turns, $\beta = 0$	431
11-3-4 Flat Turns	432
11-4 Steady, Straight, Sideslipping Flight	432
11-5 Steady Straight Flight with One or More Engines Inoperative	436
11-6 Steady Rolling Flight	444
11-7 Control Forces and Hinge Moments for Lateral Control	449
11-7-1 Roll Control	449
11-7-2 Rudder Control	450
12 Space Applications	451
12-1 Introduction	451
12-2 Characteristic motion of a winged re-entry vehicle	451
12-2-1 Re-entry vehicle	451
12-2-2 Non-linear equations of motion	457
12-2-3 Linearization	460
12-2-4 State-space form	465
12-2-5 Nominal mission	474
12-2-6 Eigenvalues and eigenmotion	479
12-3 Eigenmotion of entry capsules	493
12-3-1 Nominal mission	494
12-3-2 State-Space Model	497
12-3-3 Eigenvalues and eigenmotion	500

A List of Symbols	507
B Nomenclature	519
B-1 Vectors	519
B-2 Reference frames	520
B-3 Superscripts and subscripts	521
B-4 Geometric of aircraft parameters	521
B-5 Aircraft Configurations	525
B-6 Flight Conditions	526
C General formulation of the equations of motion	527
C-1 Introduction	527
C-2 Time derivative of a vector in a rotating frame	528
C-3 Velocity and acceleration in a rotating frame	529
C-4 Translational motion	530
C-4-1 General formulation for an inertial frame	530
C-4-2 General formulation for a rotating frame	531
C-5 Rotational motion	533
C-5-1 General formulation	533
C-5-2 The angular momentum w.r.t. the centre of mass of a rigid body.	535
C-5-3 Derivation of the Euler equation of rotational motion	538
D Aircraft Parameters	541
D-1 Introduction	541
D-2 Linearized Equations of Motion	541
D-3 LTI-System Representation	542

Chapter 1

Introduction

This book discusses the theory of stability and control of aircraft at subsonic airspeeds. This book handles the theory of flight dynamics which describes the aircraft/spacecraft velocities (translational and rotational), position, and orientation in four dimensional space. Velocities, position, and orientation through time can be computed from the accelerations in time. The analysis of the flight dynamics is based on Newton's Second law: $F = ma$. If we know the forces acting on the aircraft/spacecraft and the mass distributions we can determine the accelerations. By integrating the accelerations with respect to time and by knowing the initial velocities, the velocities at each moment in time can be calculated. Likewise, by integrating the velocities with respect to time and knowing the initial position and orientation, the position and orientation at each time instant can be determined.

The dynamics, i.e. the 'behavior' through time, of the aircraft or spacecraft can be influenced by using controls, e.g. aerodynamic surfaces or thrusters. There are two types of flight dynamics analysis. The first concerns the stability. How does the aircraft react to movements of the controls or other types of disturbances? Does it have inherent stability? This type of analysis concerns the characteristics of the aircraft without the pilot aspect in it. The second type is about the aircraft/pilot connection. It is the analysis of the dynamics of the aircraft or spacecraft with respect to the ability of the pilot to control the craft. This is the field of 'handling qualities'. There are specific regulations that state the required 'handling qualities' for each type of aircraft. These regulations are usually defined in terms of responses of the aircraft to control inputs, like elevator, rudder or throttle inputs.

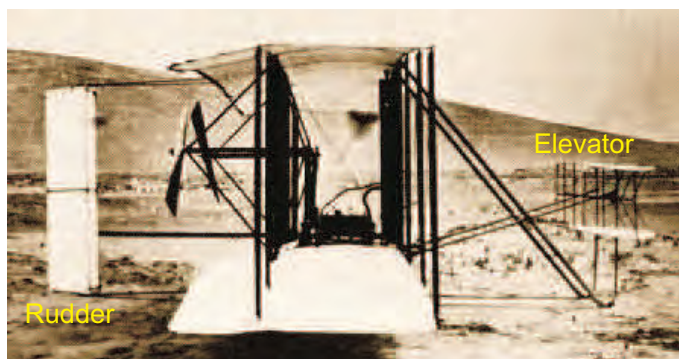
For aviation these regulations have matured through the years and are described in detail in regulation documents, such as the Joint Aviation Regulations (JAR) set up by the Joint Aviation Authorities (Europe) and the Federal Aviation Regulations set up by the Federal Aviation Administration (USA). The handling qualities of an aircraft are related to the control surfaces and control mechanism. There is a rich history on the development of control surfaces and control mechanism. The following section gives an overview. After that a list of terms and definitions used in flight dynamics is given. The setup of the book is to keep everything as general as possible and to simplify things through the use of assumptions where necessary. The assumptions which are used throughout the book are listed in section 1-2. Finally, the book outline will be given in section 1-3.

1-1 Introduction to flight dynamics and control

The Wright Flyer was the first powered piloted aircraft which had full attitude control (see figure 1-1). It had a double rudder to control *yaw*, a double elevator to control *pitch* and used warping of the wings to control *roll*. The control technique of using mechanical links connected to aerodynamic control surfaces was the founding of modern controlled flight. Modern aircraft still use the idea of pitch, roll, and yaw control through means of deflectable control surfaces. (Warping of wings requires flexible wings therefore limiting its field of application. Soon rigid wings with control surfaces where used.) However, over the years, many additional (control) surfaces have been developed. The location, shape, and purpose of each surface varies. Also the mechanisms to move the flight control surfaces, i.e. the flight control systems, have changed over the years. To fully comprehend the influences these development have on the field of flight dynamics and control, a short introduction is given in this section. First the control surfaces which have been developed throughout the years are addressed (section 1-1-1). Thereafter, in section 1-1-2, the mechanisms of translating pilot commands to the control surface deflections are discussed.



(a) First flight (Kittyhawk England, 10:35 AM, 17 Dec 1903)



(b) Profile view

Figure 1-1: The Wright Flyer I [146]

1-1-1 Flight control surfaces

Flight control surfaces have been developed throughout the years and many variants exist. A classification has been made for control surfaces. Two types are defined:

Primary flight control surfaces

Flight-critical control surfaces. If control of these surfaces is lost, control over the aircraft is (partially) lost and the aircraft is likely to crash.

Secondary flight control surfaces

Non-flight-critical control surfaces. If control of these surfaces is lost, complete control over aircraft is still possible.

The most obvious examples of *primary* flight control surfaces are the elevator, aileron, and rudder. These basic control surfaces are needed to control the aircraft about all three axis of the aircraft. Without any redundancy of these flight control surfaces, malfunction of one of these control surfaces would make the aircraft hard to control. Stable flight may still be possible if the pilot has thorough knowledge of the flight dynamics of the aircraft. Examples of *secondary* flight control surfaces are: speed brakes, lift dumpers, slats, flaps, and trim surfaces. Control over the orientation of the aircraft is still possible when these surfaces malfunction.

As said, many control surfaces have been developed. The difference between surfaces are, apart from their dimensions, the location on the aircraft and their purpose. In the following, a list is presented in which different types of control surfaces are explained briefly.

Ailerons

Purpose: provide roll control. *Location:* on the trailing edge of the main wing. *Extra information:* ailerons are placed either near the tip of the wing (Out-board ailerons) or near the root of the wing (In-board ailerons). Out-board ailerons are only active at low speeds. In-board ailerons are active at all speeds.

Elevators

Purpose: provide pitch control. *Location:* trailing edge of the horizontal stabilizer.

Rudders

Purpose: provide yaw control. *Location:* trailing edge of the vertical stabilizer.

Canards

Purpose: provide pitch control. *Location:* in front of the main wing. Canards can consist of a fixed surface with trailing edge control surface or the whole canard surface can be rotated and controlled.

Elevons

Purpose: provide pitch and roll control. *Location:* trailing edge of the main wing. *Extra information:* to provide pitch control, the elevons are extended symmetrically. For roll control the elevons are extended asymmetrically. Elevons are typically used on tailless delta-wing aircraft.

Flaperons

Purpose: provide roll control and additional lift. *Location:* trailing edge of main wing. *Extra information:* the flaperons is a combination of the ailerons and trailing edge flaps. The flap function is obtained by symmetrical extension of the flaperons. Roll control is obtained through asymmetric extension.

Flaps

Purpose: increase lift. *Location:* either on the leading-edge of the wing or the trailing edge of the wing. *Extra information:* the leading-edge and trailing-edge flaps are used to deform the shape of the wing cross-section (extending the camber line). The increase in wing surface causes an increase in lift. Therefore slower take-off and landing speeds are possible.

Slots

Purpose: increase lift (at higher angles of attack). *Location:* trailing edge of the wing. *Extra information:* a slot is an alternative to the trailing-edge flap. Slots outperform trailing-edge flaps by letting air flow through the wing such that, at high angles of attack, the collapse of airflow on the upper surface of an airfoil is reduced, thus maintaining maximum lift at high angles of attack.

Slats

Purpose: increase lift (at higher angles of attack). *Location:* leading edge of the wing. *Extra information:* the slat is actually a leading-edge slot. It delays wing stall at higher angles of attack.

Spoilers

Purpose: spoil lift, increase drag. *Location:* on main wing surface. *Extra information:* Spoiler have two main effects. By symmetric extension on both wings in flight, the spoilers act as speed brakes. During landing, symmetric extension will lead to a smaller roll-out distance. Asymmetric extension in flight will provide additional roll control without inducing wing twist to cause roll-reversal. There are two types of spoiler known: ground spoilers and flight spoilers. Ground spoilers are used during landing and extend further than flight spoilers (which are used in flight).

Speed brakes

Purpose: add drag to decelerate aircraft. *Location:* on wing surface. *Extra information:* speed brakes are aerodynamic surfaces which pop out of the wing at a near perpendicular angle to the airflow. This increases drag to the maximal possible extent.

Stabilators, Stabilons, and Tailerons (names are synonymous)

Purpose: provide pitch and roll control. *Location:* These surfaces are the two halves (left and right) of the horizontal stabilizer. *Extra information:* pitch control is achieved by rotating the horizontal stabilizer symmetrically. Roll control is achieved through asymmetric rotation. Stabilators are used to augment the surfaces which provide pitch (elevators, elevons, canards) and roll (ailerons, flaperons, spoilers) control.

Trim surfaces

Purpose: remove required control force exerted by the pilot. *Location:* trailing-edge of the vertical stabilizer (or part of the rudder) and/or trailing-edge of the horizontal stabilizer (or part of the elevator). *Extra information:* trim surfaces are used to balance the aerodynamic moment on control surfaces (during steady flight) such that the loads on the controls are eliminated. The pilot can then fly hands-free. Two main possibilities exist for the horizontal trim surface. Either the entire horizontal stabilizer acts as a trim surface (so-called variable-incidence horizontal stabilizer) or a smaller surface is used (trailing-edge surface of part of the elevator, creating the so-called variable camber horizontal stabilizer).

Each aircraft can have a different configuration regarding its control surfaces. In figures 1-2 to 1-6, several aircraft are depicted. Each figure shows the location of several specific control surfaces.

1-1-2 Flight control systems

How do you move the control surfaces of an aircraft and what does a pilot feel when moving a control stick or wheel? Why have the flight control systems changed so much through time? These are just a few questions which one can ask when looking at the history of flight control systems.

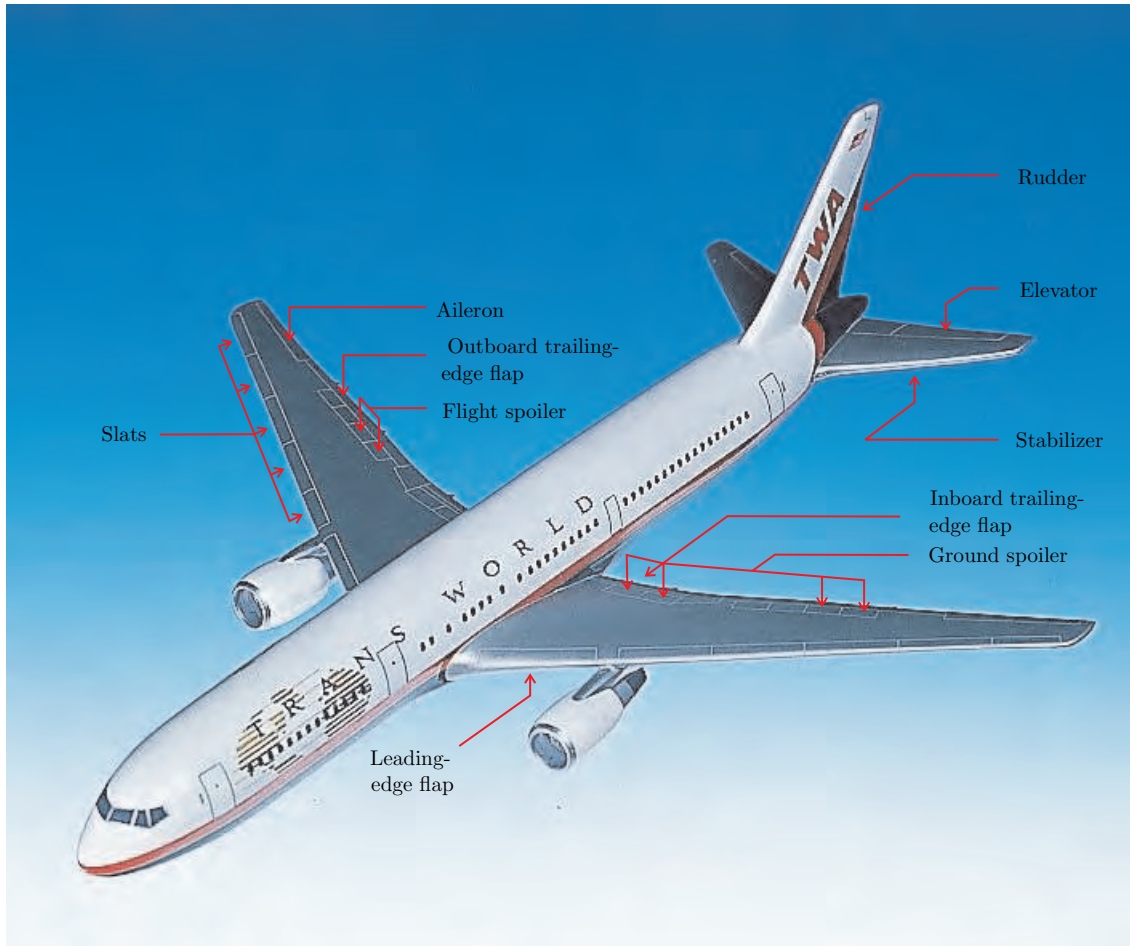


Figure 1-2: Boeing 767 3D-view [121]

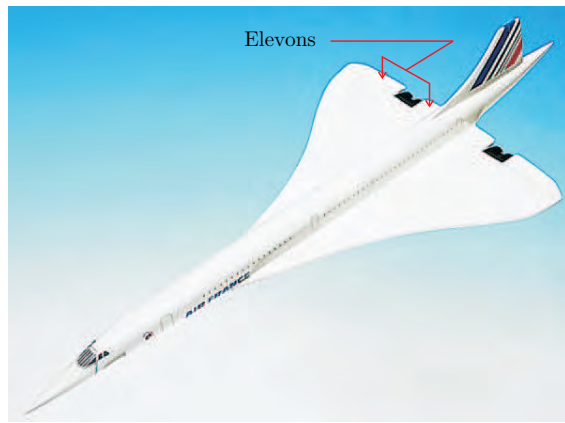


Figure 1-3: Concorde 3D-view [121]

In the development of control systems there have been two main drives. The first is the desire to build larger aircraft. Larger aircraft means larger aerodynamic surfaces which in turn means larger aerodynamic forces and thus larger control forces. The very first control systems were purely mechanical consisting of wires, springs, and wheels, which relied on the pilot strength



Figure 1-4: X-29 in flight [35]



Figure 1-5: 737-400 Flight and ground spoiler deployment on landing [32]

to move them. The control forces a pilot can generate (especially for larger periods of time) is limited, so when the aircraft size increased, something had to be done to the controls.

The second 'drive' in the development of control systems is the invention of the autopilot. With the development of new technical systems, like computers and electric actuators, it became possible to control the aircraft electrically.



Figure 1-6: Boeing 737 slats [32]

Looking at the past, several types of flight control systems can distinguished:

- Mechanical human powered system (reversible)
- Mechanical hydraulic powered system (irreversible/reversible)
- Fly-by-wire system (irreversible)

These different types will be briefly discussed in the next three sections.

Mechanical human powered flight control system

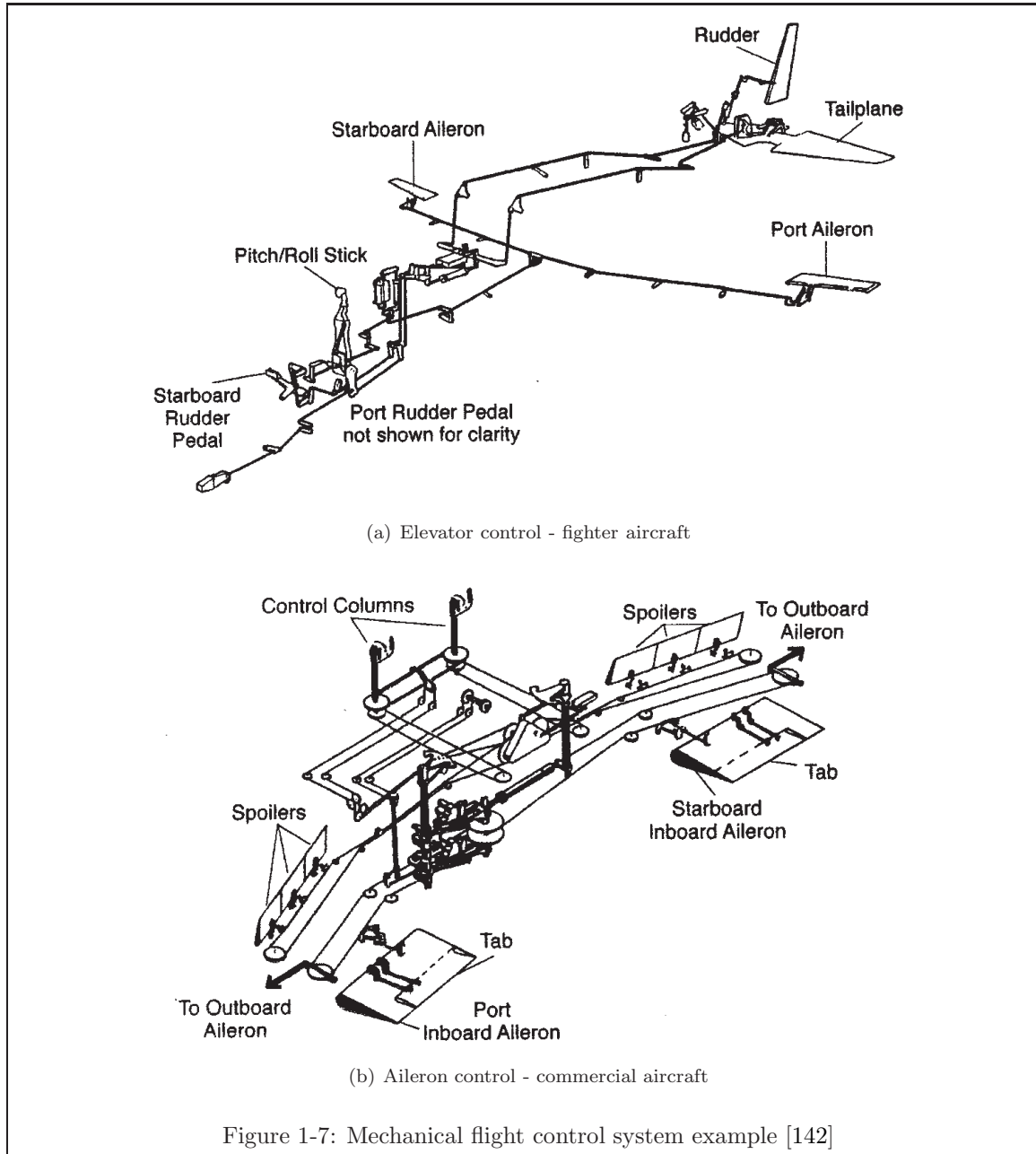
The first powered aircraft, the Wright Flyer, used a simple form of a mechanical human powered control systems. The pilot lay head-forward on the lower wing. With his left hand the pilot controlled the elevator pitch by moving a lever attached to the elevator. By using a cable system attached to a saddle, in which the pilot would lay, the pilot could control the warping of the wings by moving his hips sideways. This cable system was also connected to the rudder, thus creating two control surface movements with one movement of the pilot. This enabled the pilot to balance the aircraft and provided directional steering.

Although advanced in its time, the control system of the Wright Flyer was very simple indeed. An example of a more complicated system is the mechanical flight control system given in figure 1-7. One characteristic of a mechanical control system is that a direct linkage exists between the pilot and the control surfaces. Another characteristic is that it is reversible, i.e. the amount of control force needed to move an aerodynamic surface is directly felt by the pilot.

Mechanical flight control systems are found in small aircraft where control loads are not excessive. For flying larger aircraft, flight control systems had to be changed. Two mechanical solutions were developed. The first one is an attempt to extract the maximum mechanical advantage through levers and pulleys. The maximum reduction in forces in such a system is limited by the strength of the cables, levers, and pulleys. The second solution is the introduction of so-called control tabs (also known as servo tabs). These are small surfaces at the end of the control surface which reduce the required control force exerted by the pilot by using aerodynamic properties of the aircraft, see figure 1-8. In this case the pilot controls are directly linked to the control tabs.

The control tab generates an aerodynamic force which in turn moves the aerodynamic surface. The Boeing 707 used the concept of control tabs in its flight control system (see figure 1-9 and 1-10).

The ideas of extracting maximum mechanical advantage and using control tabs worked well for middle sized aircraft. However, when the aircraft became even larger, neither of the two solutions did suffice. This lead to the use of hydraulic power.



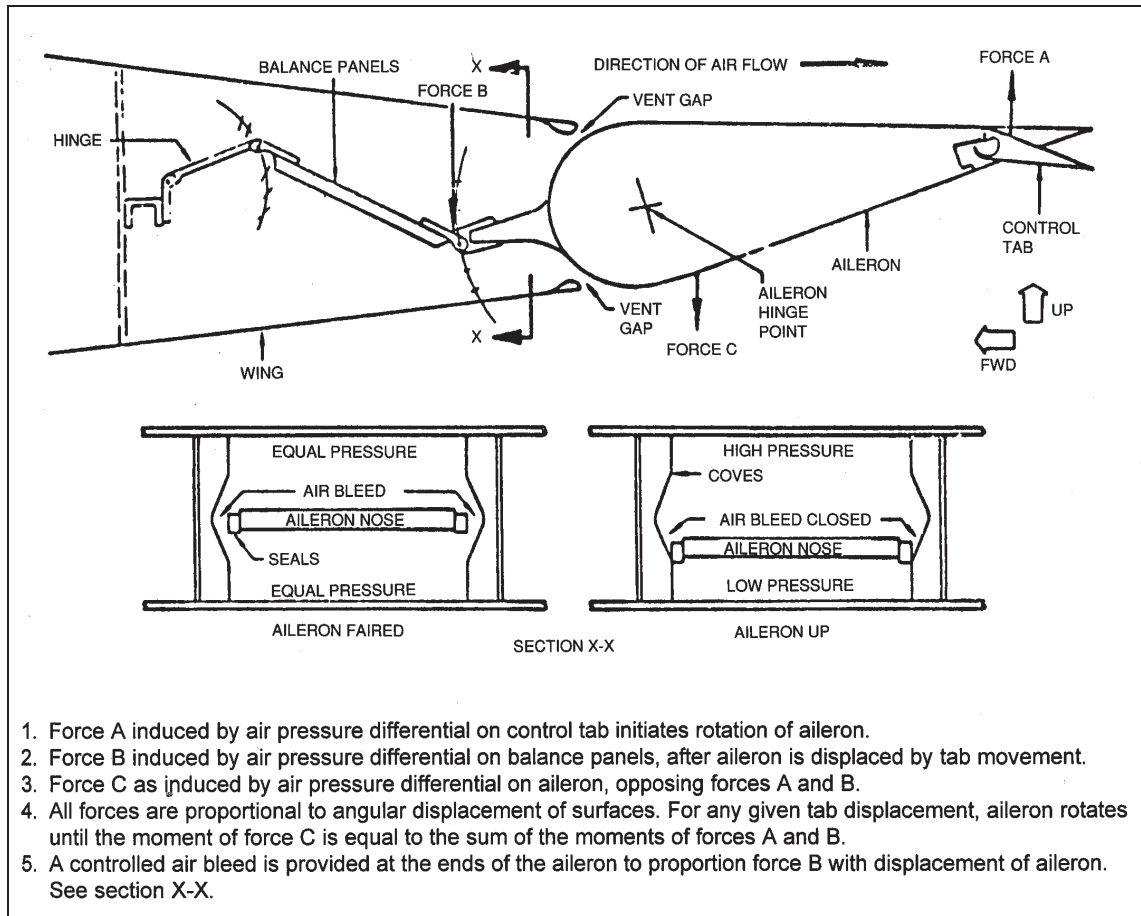


Figure 1-8: KC-135/707 Aileron Balance Panel Installation [142]

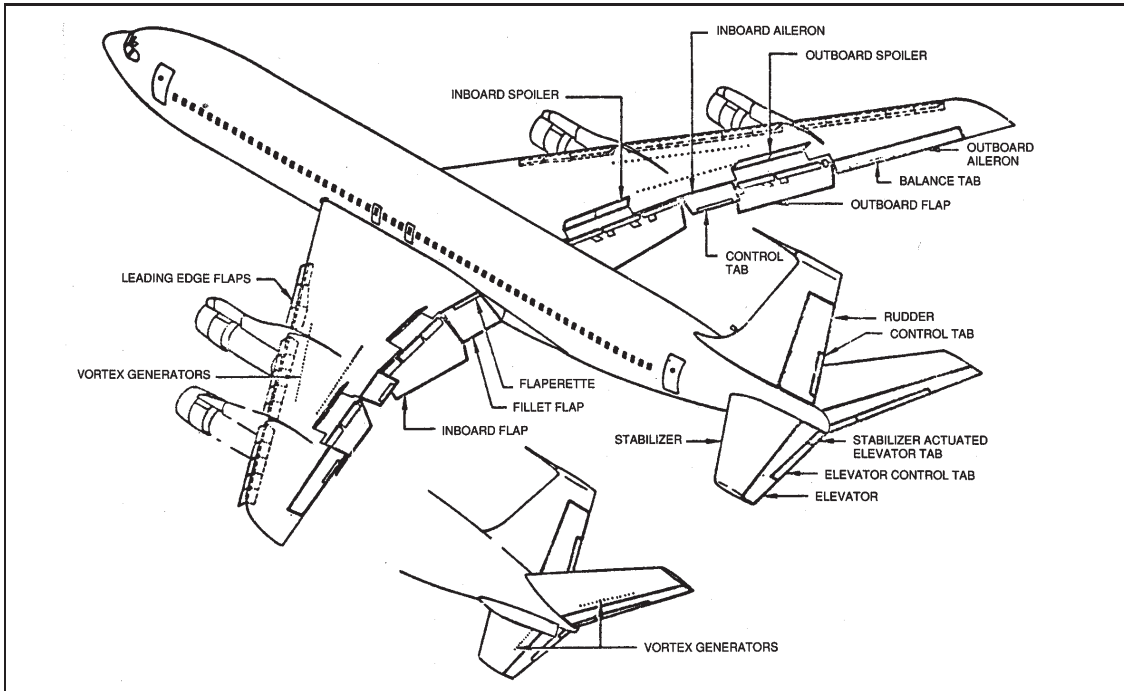


Figure 1-9: Boeing 707 Flight Control Surfaces [142]

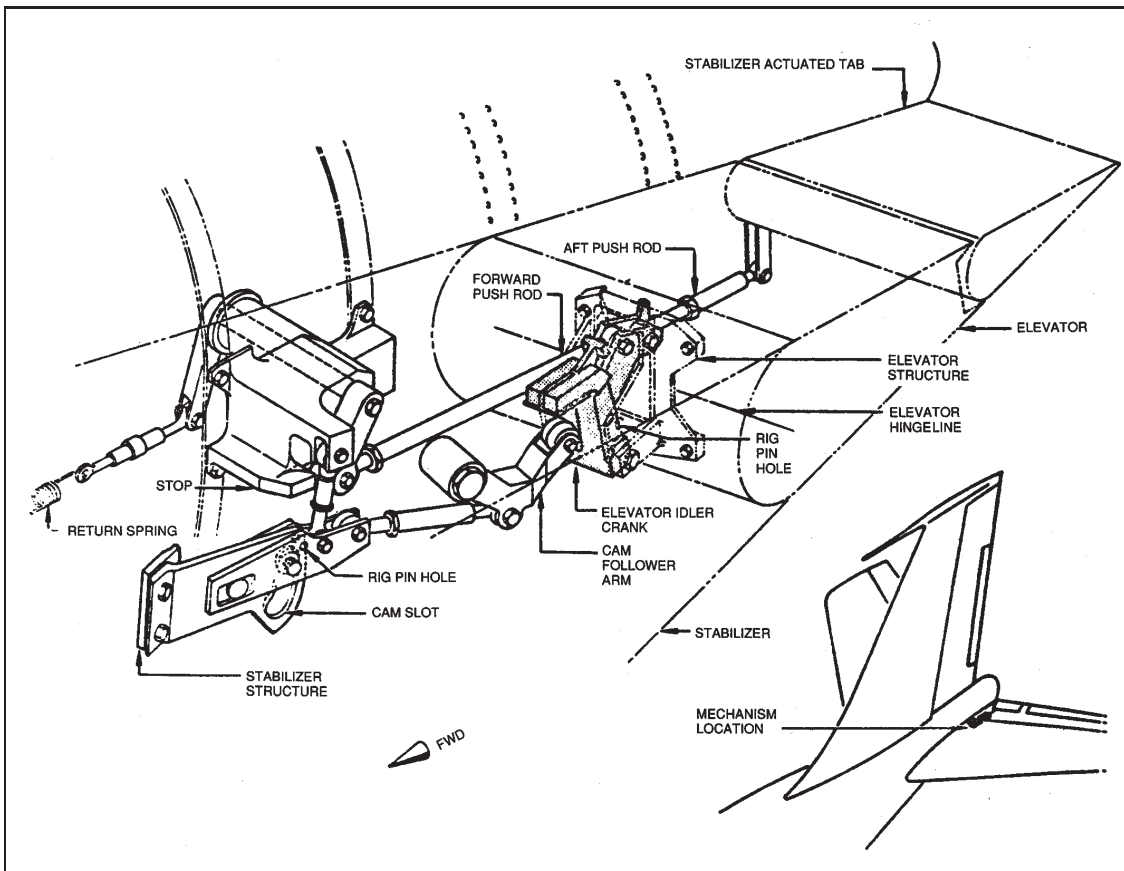


Figure 1-10: Boeing 707 Stabilizer-Actuated Tab Mechanism [142]

Mechanical hydraulic powered flight control systems

The development of large aircraft lead to the need for hydraulic powered flight control systems. The pilot could no longer generate the required control forces by using purely mechanical links. Hydraulic-power became the source of the control forces. The mechanical hydraulic powered flight control system consists of two parts:

1. A mechanical part (the same as for fully mechanical FCS)
2. A hydraulic part

The mechanical part transports the pilot commands to the hydraulic system. This is done by opening the appropriate set of servo valves of the hydraulic system. The hydraulic system then generates the forces for the actuators which move the aerodynamic surfaces. The Boeing 727 and 737 used such a flight control system (see figure 1-11). They both have a manual, mechanical linkage backup, in case of any failure of the primary flight control system. The backup system is called manual reversion since the control is done by the pilot and the force is directly felt by the pilot (thus noted as a *reversible* system). The mechanical hydraulic powered FCS is an *irreversible* system because the forces are not felt by the pilot. The feedback of forces tells the pilot a great deal about the current airspeed. In order to still keep the feeling of controlling the aircraft, artificial feel devices were installed that generate forces on the mechanical part of the FCS. The amount of force exerted on the mechanical system is made dependent on airspeed.

The Boeing 747 was the first aircraft in the Boeing series to have a fully powered actuation system. The manual reversion system was omitted from the FCS because the required control forces for any flight condition would have been too large to be generated by the pilot. The schematic layout of part of the flight control system of the Boeing 747 can be seen in figure 1-12.

The benefits of hydraulic-powered control surfaces with respect to human-powered control surfaces are two-fold. Firstly, the drag on the control surfaces is reduced by eliminating the need for control tabs. Also the control surface effectiveness is increased by eliminating control tabs. Secondly, the control surface flutter characteristics have improved since the hydraulic system introduces high mechanical stiffness. The main drawback of hydraulic-powered control surfaces is that it is an irreversible system.

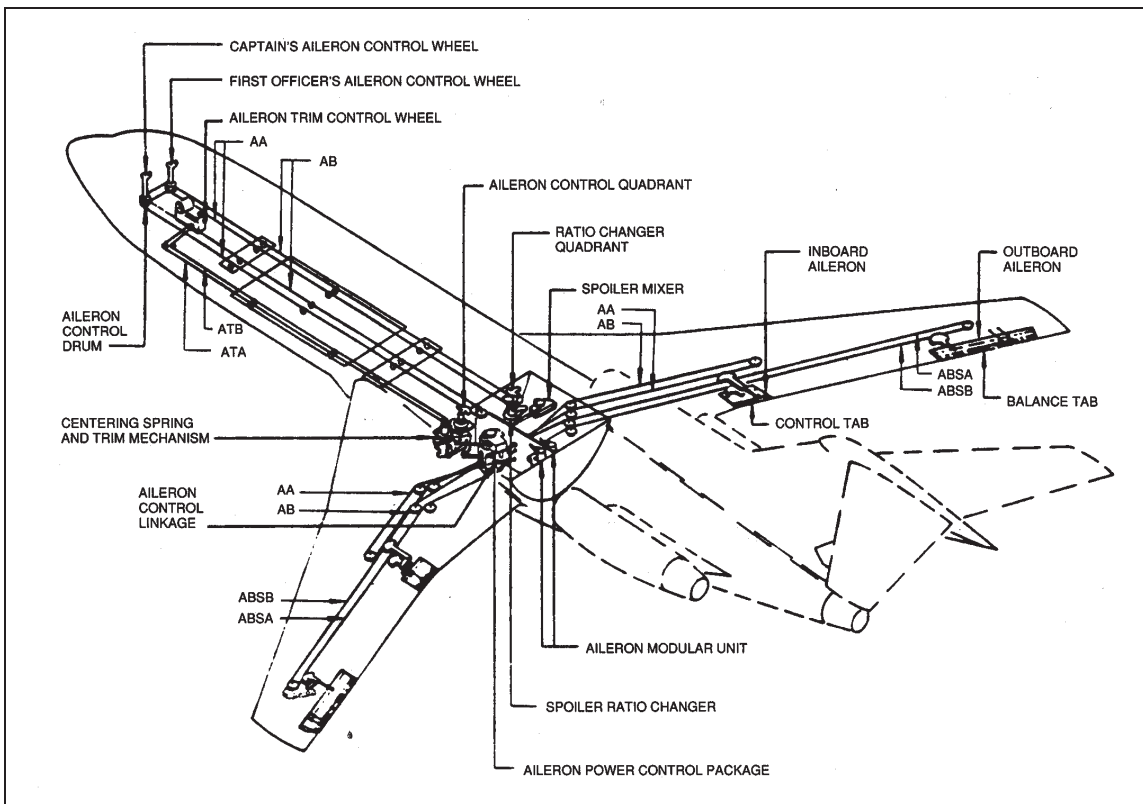


Figure 1-11: Boeing 727 Aileron Control and Trim Systems [142]

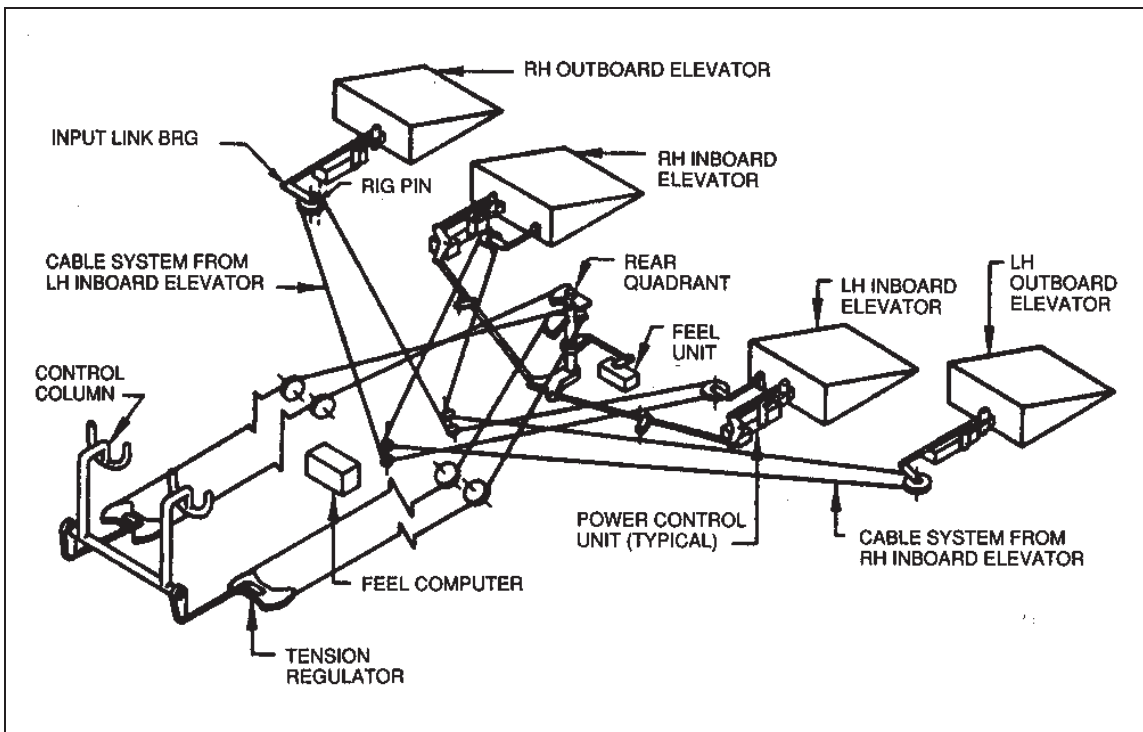


Figure 1-12: Boeing 747 Elevator Control System [142]

Fly-by-wire flight control system

With the invention of the (analog) computer it became possible to control an aircraft electronically. Initially the layout of the flight control system did not change very much. The mechanical part of the hydraulic powered control system was replaced by an electronic circuit and the cockpit controls now operate signal transducers which generate the appropriate commands. The only change to the hydraulic part of the system was the replacement of mechanical servo valves with electronic servo valves (the valves were operated by an electronic controller). This initial setup of the Fly-by-wire (FBW) FCS is known as the analog FBW FCS. The force feedback to the pilot is controlled by the electronic controller which drives an electric feel device.

The main advantage of the (initial) analog fly-by-wire FCS was that there was no longer a need for a complex, fragile, and heavy mechanical linkage between the pilot and the hydraulic system. The advantages of analog FBW FCS further increased when analog computers were developed. By replacing the electronic controller with analog computers the designer of the FCS has more flexibility with regard to setting the flight control characteristics. The pilot commands no longer needed to be interpreted as control surface deflection but more as 'intentions', like flying straight (column center) or commanding a constant pitch rate. The analog computer would then translate the pilot commands to actual control surface deflections. This concept opened the way for aircraft which were inherently unstable but could still be controlled as stable aircraft, the so-called *relaxed stability* concept.

The development of the digital computer expanded the application of the FBW FCS considerably. The analog computers had limited capabilities, but the possibilities with the digital computers were vast. Now, the flying and handling characteristics of an aircraft could be set precisely. More and more exotic (inherently unstable) aircraft could be flown with the help of a digital FBW FCS.

The next step in the development of flight control systems was to replace the heavy and high maintenance hydraulic mechanism. They were replaced with electrical power circuits. These circuits power electrical or self-contained electro-hydraulic actuators that are controlled by the digital flight control computers. This type of flight control system is also known as Power-by-wire FCS. Other developments are Fly-by-optics FCS which use light pulses instead of electric pulses to transport pilot commands. Even more futuristic developments are the designs of intelligent FCS which can reconfigure themselves when the aircraft sustains damage. The FCS can choose the best set of control surfaces to perform the desired/commanded motion.

1-2 Assumptions

In this book the derivation for the equations of motion will be kept as general as possible. The equations of motion are derived in chapter 3. Two assumptions are made during that derivation. These are:

Assumption 1: Spherical Earth

In reality the Earth is an ellipsoid. Assuming that the Earth is spherical will simplify the definition of latitude (see section 2-1-3). This in turn simplifies the transformation between reference frames which simplifies the equations of motion.

Assumption 2: Vehicle is a rigid body of constant mass

It is assumed that the vehicle under consideration does not deform under normal flight conditions. When this is true and the mass of the vehicle is constant then the matrix of inertia will be constant. This assumption implies no fuel consumption and no vehicle elastic modes.

After the general equations of motion are derived, other assumptions are used to simplify the equations. This reduced set of equations will be used to clarify certain aspects of flight dynamics in chapter 5 till 6. Whenever an assumption is used it will be clearly stated in the text. The following assumptions will be used in this book (after Chapter 3):

Assumption 3: Flat Earth

When the duration of the motion under consideration is short, the influence of the Earth's curvature is negligible. In such a case we can assume that the Earth is flat. This will make the vehicle carried normal Earth reference frame coincide with the normal Earth fixed reference frame.

Assumption 4: Non-rotating Earth

By neglecting the angular velocity of the Earth one neglects the influence of two types of acceleration, i.e. coriolis acceleration and centripetal acceleration. If real-life measured accelerations are used as input for simulations, one should remove the coriolis and centripetal components. Large errors are introduced if the time-span of the motion is large (in the order of hours).

Assumption 5: The vehicle has a plane of symmetry

If this is true then the orientation of the body-fixed reference frame can aligned with the principle axis of the vehicle in the symmetry plane. This will cause I_{xy} and I_{yz} to be zero.

Assumption 6: Aircraft has a conventional configuration

An aircraft with conventional configuration has one main wing, a horizontal and vertical stabilizor, ailerons, elevators, and one rudder. Such an aircraft is best suited for the explanation of flight dynamics principles. The reader can deduce the influence of other control systems (like the use of flaperons, elevons, etc.) by themselves. The basic principle of pitch, roll, and yaw control, remains. The only difference is that (stronger) coupling effects may be introduced.

Assumption 7: Zero wind velocity

No wind means that the undisturbed air is at rest relative to the Earth's surface. This means that the kinematic velocity is equal to the aerodynamic velocity.

Assumption 8: Resultant thrust lies in the symmetry plane

The means that the aerodynamic force caused by the engine(s), i.e. thrust, only influences the symmetric aerodynamic forces X , Z and the symmetric aerodynamic moment M .

1-3 Book outline

In part I, the derivation of the equations of motion for aircraft is given. Before the derivation is performed the reference frames which will be used are defined (see section 2-1). The building blocks of the equations of motion are the orientation and angular velocity of one reference frames to another. These block will be given in the remainder of chapter 2. The general equations of motion are derived in chapter 3. Simplification of the equations is performed thereafter to define the set of equations which will be used in the remainder of the book. Linearization of this set is performed in chapter 4.

In part II we will perform simulations with the symmetric (chapter 5) and asymmetric (chapter 6) linearized equations of motion. Stability and Control derivatives will be derived analytically. An analysis of the aircraft characteristics is performed for symmetric, steady flight, followed by an analysis on the characteristic modes for symmetric flight from the view of static stability. The same analysis and derivations as for symmetric flight will be done for asymmetric flight (chapter 8 and 11).

In part III, static stability and control is considered. First several aspects of aircraft aerodynamics, like the aerodynamic center and the process of deriving an state of equilibrium, are discussed (chapter 9). The aircraft characteristics for symmetric flight are explained and analyzed (chapter 7 and 10).

Finally, in chapter 12 we will look at the application of the flight dynamics theory to space applications.

Part I

Equations of Motion

Chapter 2

Reference Frames

This chapter defines the reference frames used in flight dynamics. A reference frame in this context is a coordinate system or set of axes within which to measure the position, orientation, and other properties of objects (e.g., aircraft and spacecraft) in it. First of all one needs at least *one* frame of reference to describe any motion or position. The need for *multiple* reference frames arises from two considerations. The first is that the definition of a vector makes more sense for one particular reference frame than for another. The aircraft's velocity vector expressed with respect to the Earth surface has a direct physical meaning while another decomposition will have no direct meaning (see Figure 2-1, where V_N is the velocity component due North, V_E is the velocity component due East, and V_D is the velocity component perpendicular to the Earth surface).

The other consideration is that the use of additional reference frames will make the derivation of the equations of motion easier. Certain motions are more easily described in a particular reference frame before a translation is made to the reference frame for which the equations of motion are derived.

Several reference frames will be used in subsequent chapters to derive the equations of motion. The orientation and state of the a vehicle (aircraft or spacecraft) can be defined in these reference frames. An important aspect when using multiple reference frames is the transformation

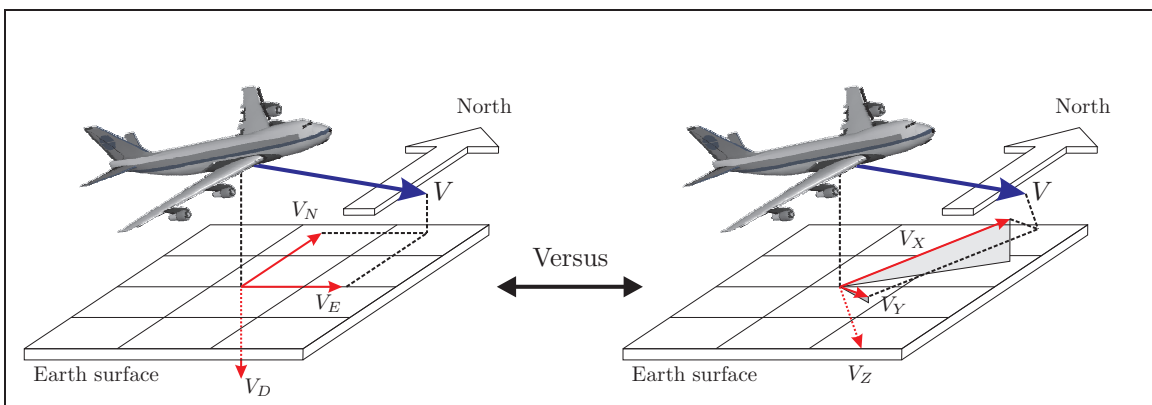


Figure 2-1: Aircraft velocity vector decomposition

of vector coordinates from one frame to another. A set of rotation angles is defined for each transformation. The rotation matrices given in this chapter are all defined using so-called Euler angles. The Euler angles are useful in many (normal-flight) cases. However, when certain situations occur such as in acrobatic flight or the (vertical) launch of a rocket, the Euler angle transformations will fail. A solution to this problem could be the use of Quaternions; this is, however, an advanced topic that is not discussed in the current lecture series.

The reference frames will be described in section 2-1. In Section 2-2, the transformations between the reference frames will be given using Euler angles. Transformation matrices will be established for every transformation between reference frames. The effect of changes in orientation between reference frames over time is an important aspect of deriving the equations of motion. This effect will be described in Appendix C, where the general derivation of the equations of motion can be found.

2-1 Overview of reference frames

In this section a total of six reference frames will be defined, divided into two categories: Earth-fixed and vehicle fixed. The reason for defining multiple reference frames is to make the derivation of the equations of motion easier and more meaningful. Due to the validity of Newton's Laws, in principle only one reference frame (an inertial reference frame) would suffice, but this would not make the understanding of flight dynamics easier.

2-1-1 Inertial reference frame, F_I

The first of the Earth-fixed frames is the inertial reference frame ($AX_IY_IZ_I$), also known as the Earth-Centered Inertial (ECI) reference frame, is a right-handed orthogonal axis-system. The origin is at the center of mass of the Earth. The Z_I -axis is directed to the north along the spin-axis of the Earth which goes through the poles of the Earth. The X_I -axis passes through the equator at the location where the ecliptic and the equator cross: the vernal equinox (see Figure 2-2, p. 21). ¹ The Y_I passes through the equatorial plane perpendicular to the X_I and Z_I to complete the coordinate axes system.

The spin-axis of the Earth does not remain in the same direction through time. Due to gravitational influences of the moon and other celestial bodies, the spin-axis 'wobbles' about a fictive mean spin-axis. This motion is known as polar motion . The definition of the inertial reference frame still holds although the choice of spin-axis orientation can differ per country. For purpose of clarity an International Celestial Reference System (or Conventional Celestial Reference System) has been defined. The coordinate system is defined by *the mean equator and equinox of J2000.0*. (The standard epoch J2000.0 is 12hr on January 1, 2000.) The mean equator and equinox are the fictitious equator and equinox, derived after removing the effects of nutation. For more information about polar motion the reader is directed to Ref. [100].

¹The ecliptic is defined as the great circle formed by the intersection of the plane of the Earth's orbit with the celestial sphere (it can be seen as the apparent annual path of the sun in the heavens).

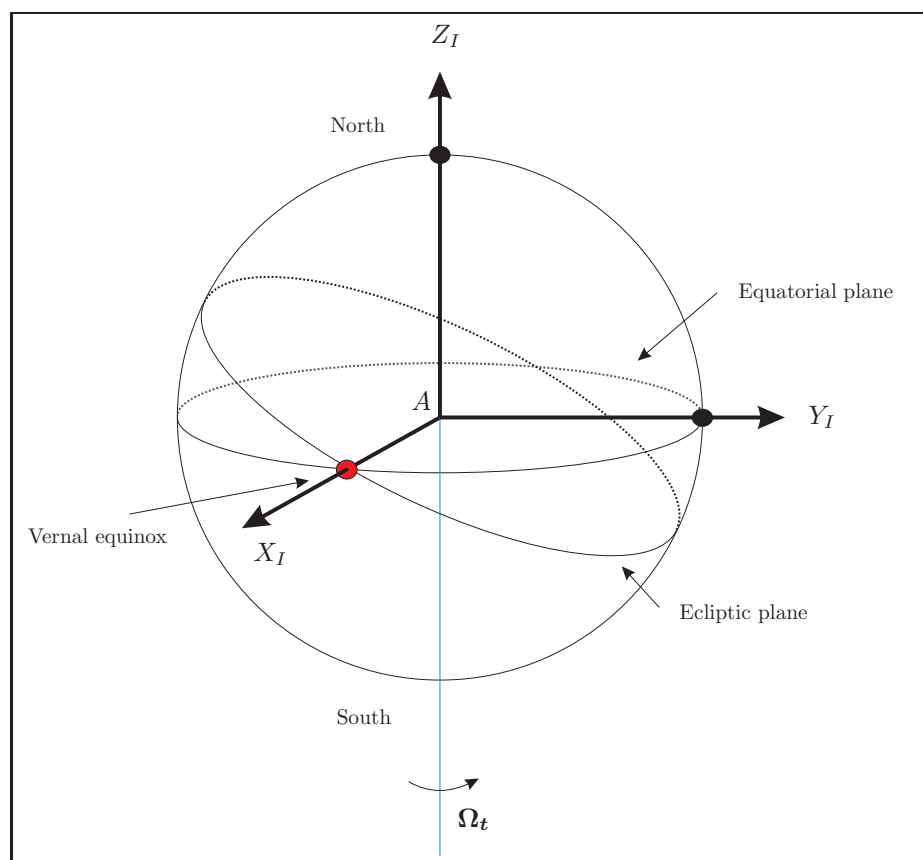


Figure 2-2: Definition of Earth-centered inertial reference frame

2-1-2 Earth-centered, Earth-fixed reference frame (F_C)

The second (and last) Earth-fixed frame is the Earth-centered, Earth-fixed reference frame (ECEF) ($AX_CY_CZ_C$), which is a right-handed coordinate axis-system very similar to the Earth-centered inertial reference frame. The difference between the two reference frames are the locations where the X -axis and Y -axis pass through the equatorial plane. The X_C -axis crosses the Greenwich meridian (see Figure 2-3, p. 22) while the X_I -axis passes through the vernal equinox (see Figure 2-2, p. 21). The Z_C -axis is directed along the spin-axis of the Earth, equal to the Z_I -axis. The Y_C passes through the equatorial plane perpendicular to the X_C end Z_C to complete the coordinate axes system. Since the X_C -axis is fixed to the Greenwich meridian, F_C is fixed to the Earth and will thus rotate about its Z_C -axis with the angular velocity of the Earth. This in contrast with the inertial reference frame which has no angular velocity.

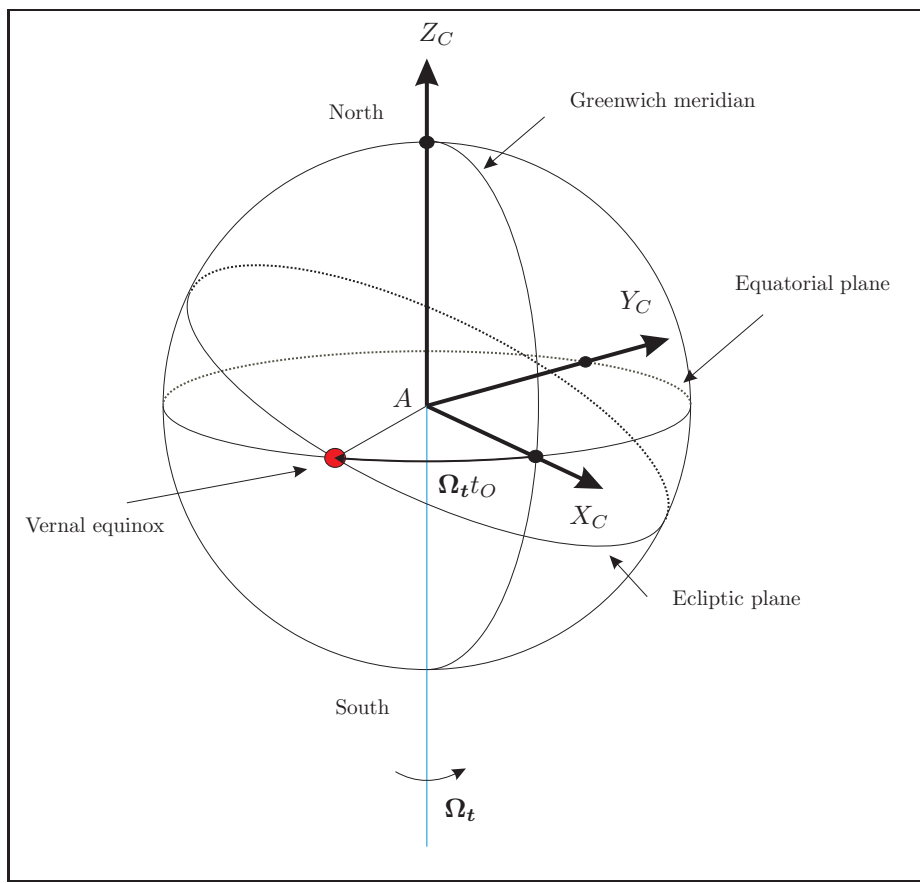


Figure 2-3: Definition of Earth-centered, Earth-fixed reference frame

2-1-3 Vehicle-carried normal Earth reference frame, F_E

The location of the origin O of this frame, sometimes also referred to as the *vertical* frame, is chosen as the aircraft's center of gravity. The X_EY_E plane is tangent to the Earth surface. The average Earth surface, the Earth geoid², is taken as a reference since the Earth surface changes constantly (see figure 2-4, p. 23). The X_E -axis is directed to the north and the Y_E -axis is directed

²Geoid: the particular equipotential surface that coincides with mean sea level and that may be imagined to extend through the continents. This surface is everywhere perpendicular to the force of gravity.

90 degrees to the right of the X_E axis. When the Earth is considered as a sphere, the Z_E -axis point to the center of the Earth (see Figure 2-5). The Earth is actually an ellipsoid such that the gravitational attraction vector g_r is no longer directed to the center of the Earth. Due to the rotational acceleration generated by the Earth's spin velocity Ω , the apparent gravitational pull is always tangent to the Earth geoid. A specific latitude can be defined for each vector in Figure 2-4 on page 23:

Φ_{gc} Geocentric latitude

Defined as angle between **AO** and the equatorial plane. It denotes the direction of the center of the Earth.

Φ_{gr} Gravitation latitude

Indicates the direction of the gravitational attraction g_r .

Φ_{gd} Geodesic latitude

Indicates the direction of apparent gravity (which is a combination of the gravitational attraction and the centripetal acceleration due to Earth rotational speed Ω). The direction of the apparent gravity is always perpendicular to the Earth geoid.

However, in the remainder of this book it is assumed that the Earth is a perfect sphere such that latitudes all become equal to each other and thus only one latitude angle exists.

Finally, It is stressed that the rotation of the X_EY_E -plane - also called the local horizontal plane - follows the variation of the Earth's curvature, and, therefore, does not follow the vehicle's rotational motion.

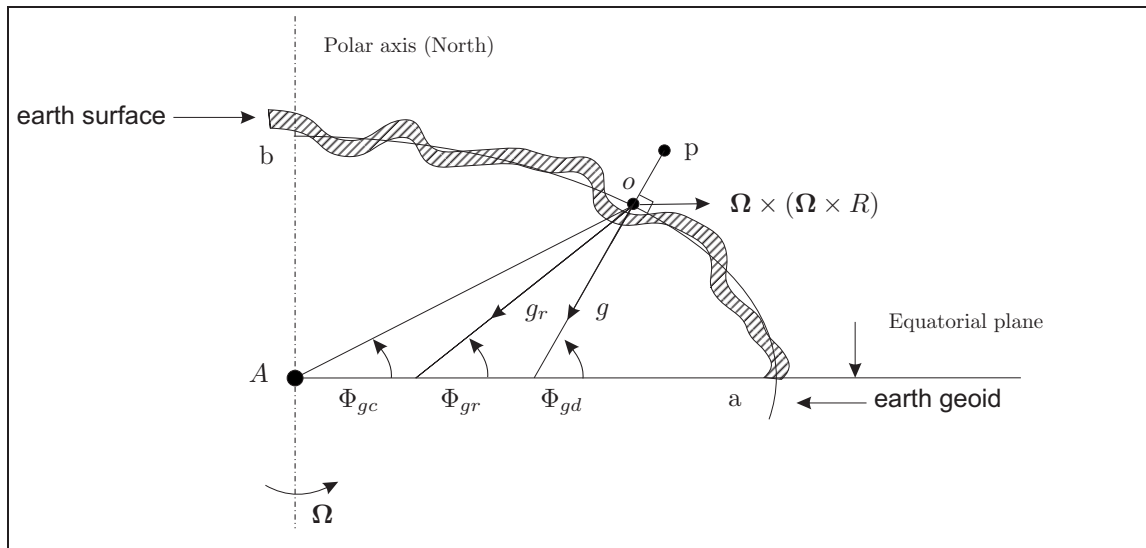


Figure 2-4: Earth geoid and latitude definitions

2-1-4 Body-fixed reference frame, F_b

The body-fixed reference frame ($GX_bY_bZ_b$) is a right-handed orthogonal axis-system with the origin at the aircraft's reference point. In general the center of mass of the aircraft is chosen as the aircraft's reference point. If the gravity field is constant than this point coincides with the center of gravity of the aircraft. The reference frame remains fixed to the aircraft even in

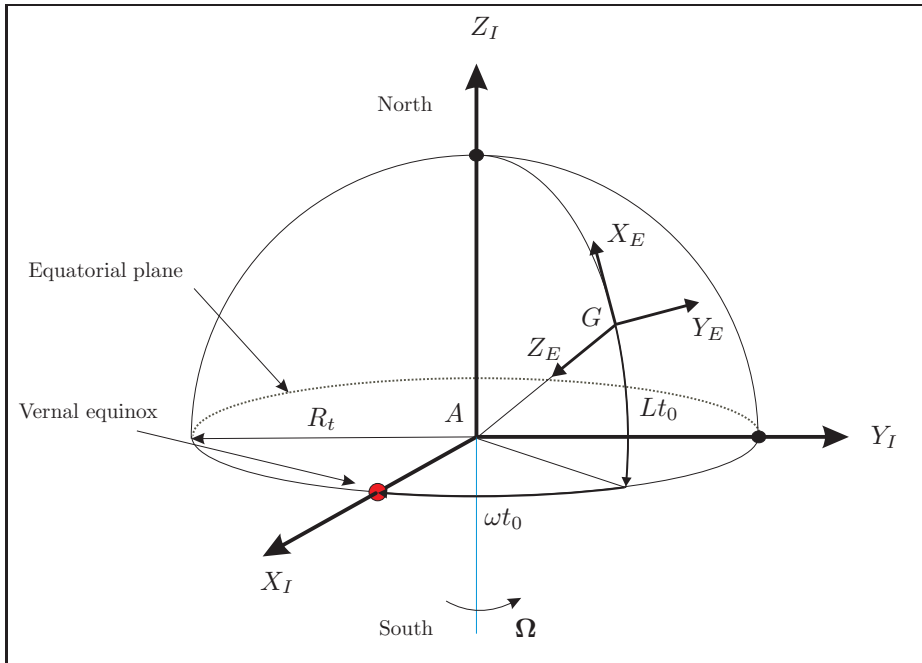


Figure 2-5: Vehicle carried normal Earth reference frame for spherical Earth

perturbed motion. The choice of the direction of the axes is rather arbitrary, the most commonly used orientation of the axes-system is depicted in Figure 2-6 (p. 25). The X_b -axis is in the symmetry plane of the aircraft³ and points forward.⁴ The actual direction is still arbitrary which influences the definition of the angle of attack (which will be explained in future sections). The Z_b -axis also lies in the symmetry plane and points downward. Finally the Y_b -axis is directed to the right, perpendicular to the symmetry plane.

Because the X -axis direction can be chosen arbitrarily, an infinite number of possible body-fixed reference frames exist. The most commonly used body-fixed reference-frame definition is the stability reference frame, F_S . For this reference frame to be defined, a reference flight condition must be chosen which is in most cases a condition of steady flight. For this condition the relative wind can be projected onto the plane of symmetry. The X_S -axis is chosen in this direction. The Z_S -axis is also in the plane of symmetry but perpendicular to the X_S -axis pointing downward. The Y_S -axis completes the reference frame. Once the orientation of the reference frame relative to the aircraft is chosen, it will remain fixed thereafter. A graphical description is given in Figure 2-7 (p. 25).

The stability reference frame will be used in subsequent sections of this book. The origin is chosen in the center of mass of the aircraft.

2-1-5 Vehicle reference frame, F_r

The vehicle frame of reference ($O_rX_rY_rZ_r$) is a *left-handed* orthogonal axis-system with the origin at an arbitrary, yet fixed and invariable, position. The reference frame is fixed to the vehicle.

³This is only possible under the assumption that such a plane exists.

⁴Forward, in this case, holds only for a more or less horizontal flight condition. For the vertical orientation of a launcher, the X_b -axis is positive pointing upwards. What is common, though, is that in both situations the axis points towards the nose of the vehicle.

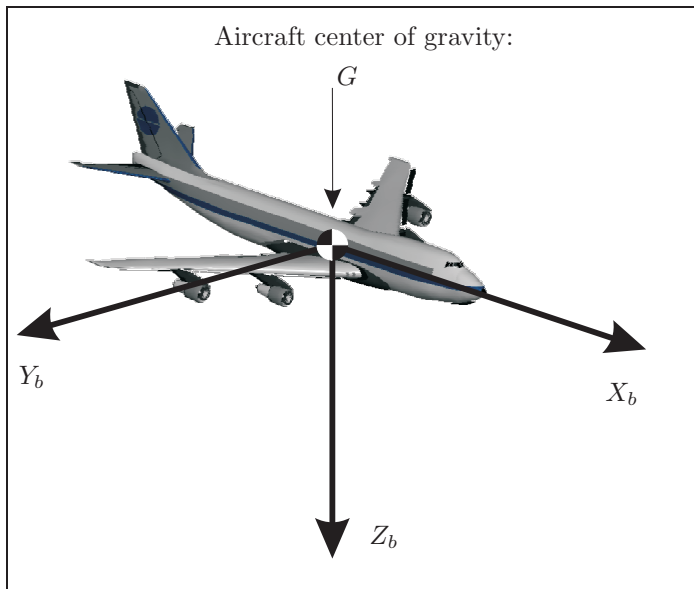


Figure 2-6: Body-fixed Reference Frame

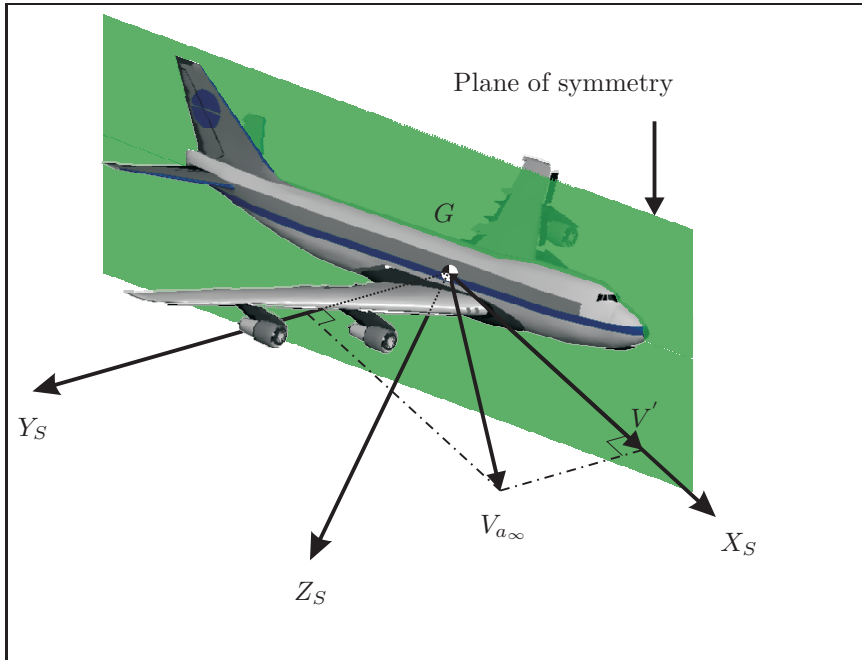


Figure 2-7: Stability Reference Frame

The usual definitions, in case of an aircraft, for the axes' directions are:

- X_r -axis
Parallel to the plane of symmetry, in a direction fixed and invariable relative to the aircraft.
The positive X_r -axis points to the rear of the aircraft.
- Y_r -axis
Perpendicular to the plane of symmetry. The positive Y_r -axis points to the left.

- Z_r -axis

Perpendicular to the $O_r X_r Y_r$ -plane. The positive Z_r -axis points upward in normal, upright, flight.

This frame of reference is used to prescribe locations of important parts of the aircraft, e.g. elevator hinge lines, location of aerodynamic centers, dimensions and positions of control surfaces, etcetera.

An example of the aircraft frame of reference is given in Figure 2-8 (p. 26).

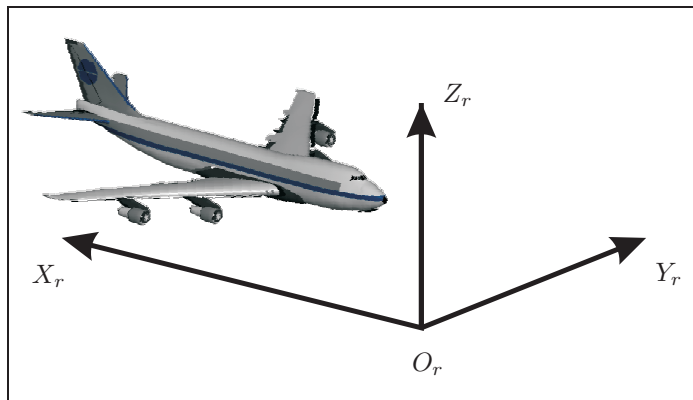


Figure 2-8: Left-handed (!) Aircraft Reference Frame F_r

2-1-6 Aerodynamic (air-path) reference frame, F_a

The aerodynamic (air-path) reference frame is coupled to the aerodynamic velocity \mathbf{V}_a (also known as air-path velocity or 'air velocity'). The aerodynamic velocity is defined as the velocity of the center of mass G relative to the undisturbed air. The origin of the reference frame is in general the same as that of the body-fixed reference frame F_b . The X_a -axis is in the direction of the aerodynamic velocity \mathbf{V}_a . The Z_a -axis is in the symmetry plane of the aircraft. The Y_a -axis is perpendicular to the $G X_b Z_b$ plane to complete the (right-orthogonal) axis system (see Figure 2-9, p. 27). The angles α_a and β_a are the aerodynamic angle of attack and the aerodynamic sideslip angle respectively. They denote the orientation of the aerodynamic reference frame with respect to the body-fixed reference frame.

The aerodynamic velocity expressed in the aerodynamic reference frame is denoted as:

$$\mathbf{V}_a^a = \begin{bmatrix} u_a^a \\ v_a^a \\ w_a^a \end{bmatrix} = \begin{bmatrix} V_a \\ 0 \\ 0 \end{bmatrix} \quad (2-1)$$

Common practice is to express the aerodynamic velocity vector in the body-fixed reference frame:

$$\mathbf{V}_a^b = \begin{bmatrix} u_a^b \\ v_a^b \\ w_a^b \end{bmatrix} = \begin{bmatrix} u \\ v \\ w \end{bmatrix} \quad (2-2)$$

The parameters (u, v, w) are commonly used to denote the components of any velocity vector along the axis of any reference frame. If the parameters are stated without any superscript then they are equal to the components of the aerodynamic velocity (in this book).

It is noted that when there is no wind, the aerodynamic reference frame is equal to the so-called kinematic (flight-path) reference frame. In that case the aerodynamic velocity is equal to the 'ground velocity', i.e., the velocity relative to the ground⁵.

⁵The ground velocity is always tangent to the ground track, i.e., the projection of the aircraft trajectory on the

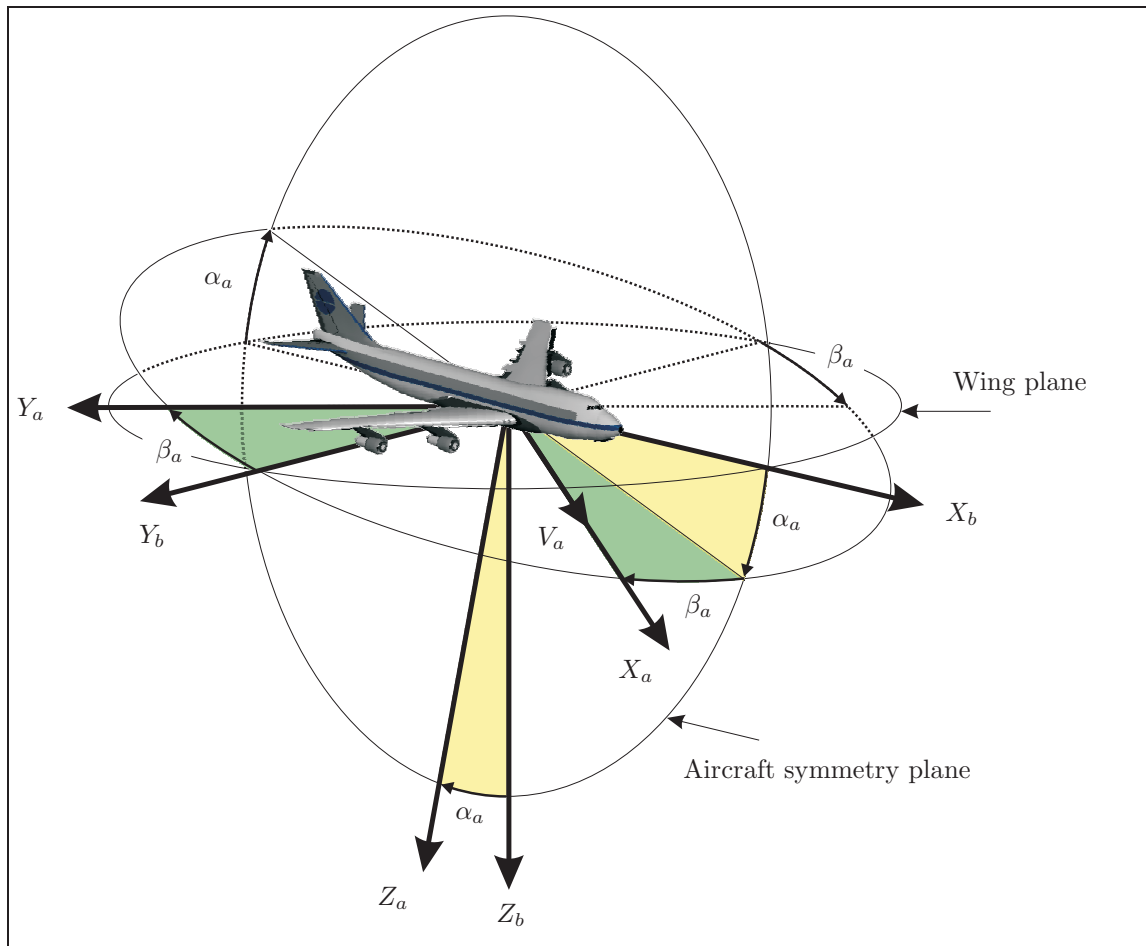


Figure 2-9: Aerodynamic Reference Frame in relation to Body-fixed Reference Frame

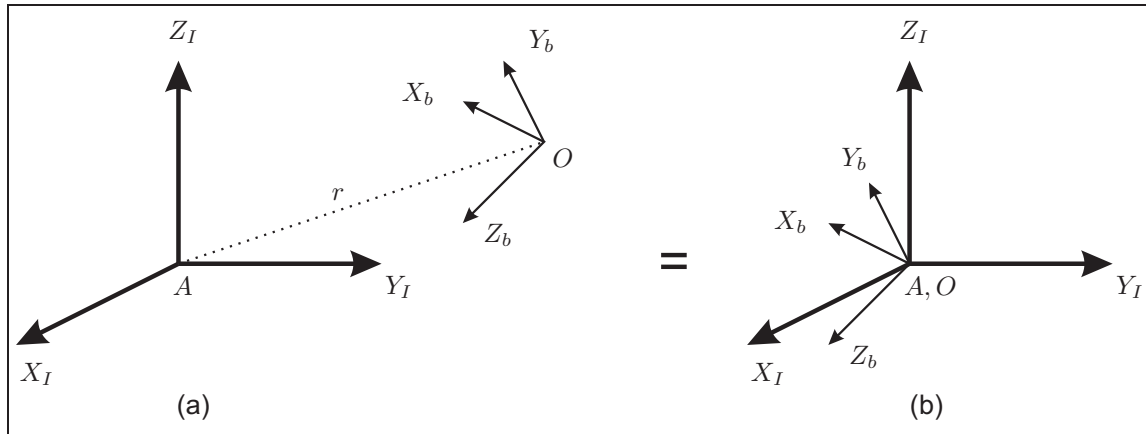


Figure 2-10: Euler angles define the attitude of F_b irrespectively of translation

2-2 Transformations between reference frames

The reference frames defined in the section 2-1 will be used to define position parameters (longitude, latitude, etc.) and vector parameters (airspeed, forces, moments, etc.). They are needed to express the motion of the aircraft (or spacecraft) by differential equations. To make equations of motion more readable, different motions will be expressed in different reference frames. To couple the motions in each reference frame to get the overall aircraft motion through time in one particular reference frame, a transformation between reference frames is necessary. In general terms, a transformation is composed of a translation of the origin of the starting frame towards the target frame, and a rotation that defines the difference in orientation of the two frames.

The rotation transformation between any two reference frames at any point in time can be described by (at most) three angles, known as Euler angles. Mathematically, the rotation using the three angles results in a particular transformation matrix. The Euler angles and the relevant transformation matrices will be explained in Section 2-2-1 and 2-2-2 (p. 33) respectively. Thereafter the most important transformations between reference frames and the angles (including the rotation sequence) which are needed to accomplish the transformation will be discussed (section 2-2-4 till 2-2-7, p. 38 till p. 47).

2-2-1 Euler angles

The *orientation* of a body in Euclidean space relative to an inertial reference frame can be described by three successive rotations through three *body-referenced* Euler angles⁶. Therefore a body-fixed reference frame is necessary⁷. Note that only the orientation of a reference frame is described by Euler angles, *not* the translation of one reference frame relative to another. This means that, in terms of Euler angles, position (a) in figure 2-10 (p. 28) is equivalent to position (b).

In principle the transition from the orientation of an inertial reference frame F_I to the orientation of a body-fixed reference frame F_b can be performed in 12 different ways. When starting from the orientation of the inertial reference frame, three consecutive rotations are performed. Each rotation is performed about one of the axes of the body-fixed reference frame. A maximum of three rotations are needed to arrive from the attitude of the inertial reference frame at the

⁶Named after Leonhard Euler (April 15, 1707 till September 18, 1783), a Swiss mathematician and physicist. He is considered to be one of the greatest mathematicians of all times.

⁷The rotation method given here is valid for any set of reference frames. To make the explanation easier to understand a body-fixed (non-inertial) and inertial reference frame are taken here.

orientation of the body-fixed reference frame. The only condition required to guarantee that transition to any attitude of the body-fixed reference frame is that no two consecutive rotations are about the same axis. Bearing this in mind one can set up six 'symmetric' sets of Euler angles:

$$\begin{aligned}\varphi_x \rightarrow \varphi_y \rightarrow \varphi_x, \quad \varphi_y \rightarrow \varphi_x \rightarrow \varphi_y, \quad \varphi_z \rightarrow \varphi_x \rightarrow \varphi_z \\ \varphi_x \rightarrow \varphi_z \rightarrow \varphi_x, \quad \varphi_y \rightarrow \varphi_z \rightarrow \varphi_y, \quad \varphi_z \rightarrow \varphi_y \rightarrow \varphi_z\end{aligned}$$

and six sets of 'asymmetric' Euler angles:

$$\begin{aligned}\varphi_x \rightarrow \varphi_y \rightarrow \varphi_z, \quad \varphi_y \rightarrow \varphi_x \rightarrow \varphi_z, \quad \varphi_z \rightarrow \varphi_x \rightarrow \varphi_y \\ \varphi_x \rightarrow \varphi_z \rightarrow \varphi_y, \quad \varphi_y \rightarrow \varphi_z \rightarrow \varphi_x, \quad \varphi_z \rightarrow \varphi_y \rightarrow \varphi_x\end{aligned}$$

where $\varphi_x, \varphi_y, \varphi_z$ denote rotations around the X -axis, Y -axis, and Z -axis. Any of these sets of Euler rotations allows transition to any attitude of F_b . One should bear in mind, however, that different sets of Euler angle rotation sequences will result in different magnitudes of the corresponding Euler angles. An example is given in the mini-tutorial on page 30.

Transformations using Euler angles are very often used because one can easily visualize the orientation changes per Euler angle. However, a major drawback exists, the so-called 'Euler angle singularity' or 'gimbal lock'. The exact meaning of this drawback will not be explained until Section 3-4-3, but it suffices to say that the singularity occurs at an pitch angle of 90° and -90° . During most (normal) aircraft manoeuvres these pitch angles will not be reached such that the singularity is of no concern.

Mini-tutorial: Rotation sequence using Euler angles

This tutorial shows why the specification of the rotation sequence is important. It will show that when a different rotation sequence is applied using a fixed set of angles will lead to a different orientation.

Suppose one wants to rotate a body about the origin of an inertial reference frame such that a transition is made from the initial orientation (Figure 2-11a, p. 31) to the final orientation (figure 2-11b). This transition will be done using Euler angles of 30° , -30° , and 60° for $\varphi_x, \varphi_y, \varphi_z$, respectively. The correct rotation sequence belonging to this set of Euler angles is the a-symmetric sequence: $\varphi_z \rightarrow \varphi_y \rightarrow \varphi_x$, the so-called 3-2-1 rotation. This sequence is the most common sequence in the aerospace industry. The initial rotation is taken about the axis of the starting reference axis system. After the first and the second rotation an intermediate reference frame is defined. The complete rotation sequence is stated as:

$$F_I \xrightarrow{\varphi_z} F_{I'} \xrightarrow{\varphi_y} F_{I''} \xrightarrow{\varphi_x} F_b$$

The rotations are visualized in Figure 2-12a till c (p. 32).

Now, what will happen if the Euler angles stay the same but the rotation sequence is altered? To show the consequences a second rotation sequence is applied:

$$F_I \xrightarrow{\varphi_x} F_{I'} \xrightarrow{\varphi_y} F_{I''} \xrightarrow{\varphi_z} F_b$$

The rotations are visualized in Figure 2-13a till c (p. 32).

As one can see, the end orientation of the body clearly differs from the previous case. The same end orientation can be reached using the second rotation scheme, but it would require a different set of Euler angles!

In subsequent sections the rotation sequences and the names of the Euler angles for each transition between specific reference frames are given. Only the transition between reference frames, mentioned in the previous section, will be discussed.

Using the Euler angles and the specific rotation sequences, one can set up so-called transformation matrices. These matrices can be used to transform vector coordinates in one reference frame to vector coordinates in another reference frame. The method of deriving such a transformation matrix will be discussed in the next section. In subsequent sections, the transformation matrices for each transition between reference frames will be specified.

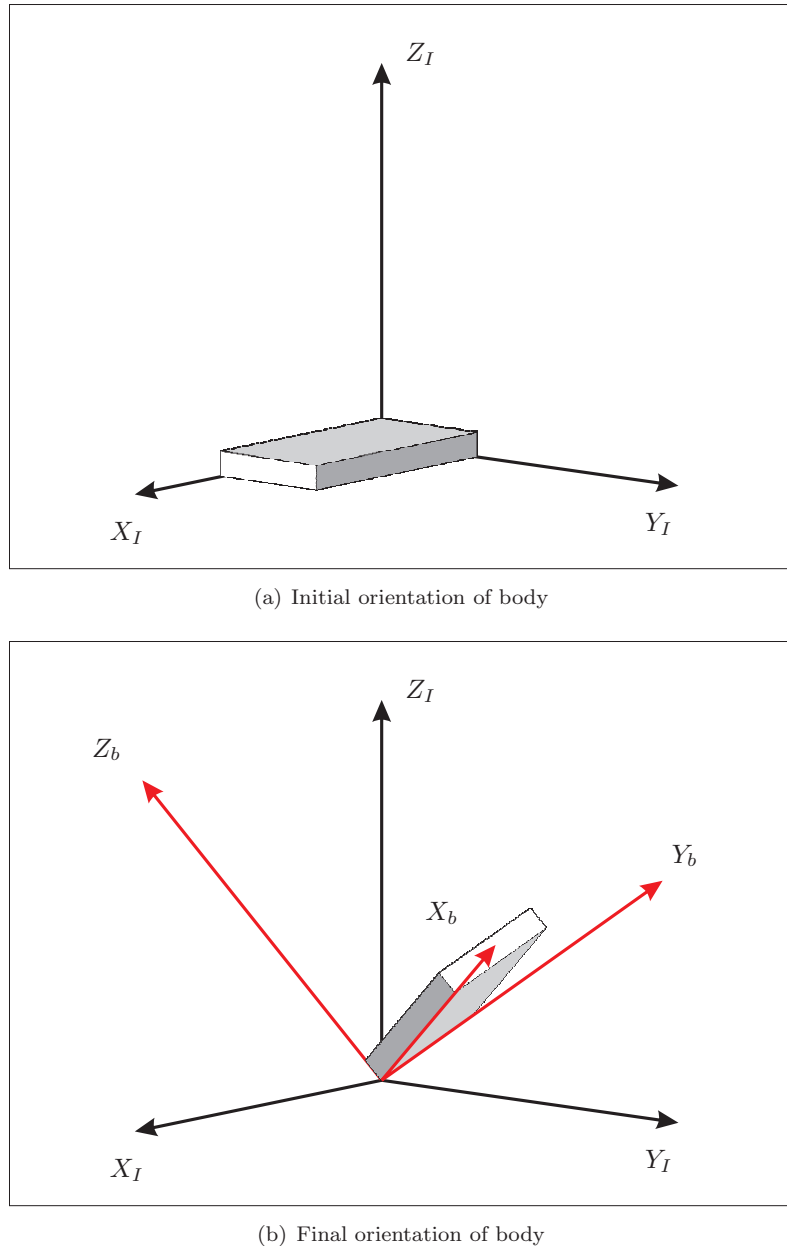


Figure 2-11: Euler angles tutorial: initial and end body orientation

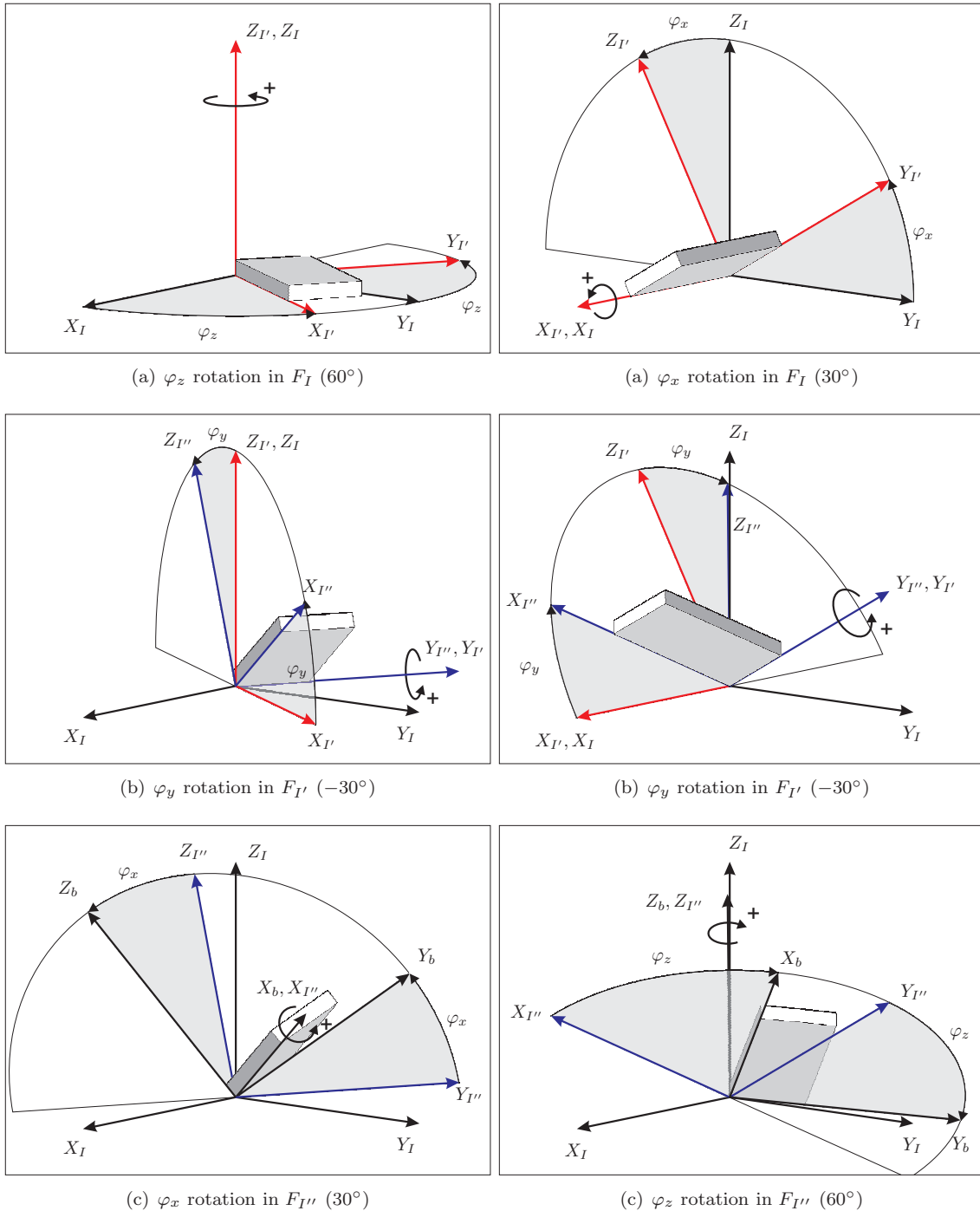


Figure 2-12: Euler angles tutorial: rotation sequence $\varphi_z \rightarrow \varphi_y \rightarrow \varphi_x$

Figure 2-13: Euler angles tutorial: rotation sequence $\varphi_x \rightarrow \varphi_y \rightarrow \varphi_z$

2-2-2 Transformation matrices

The transition between the *orientation* of one reference frame to another can be described in terms of Euler angles. These angles can be used to set up a so-called transformation matrix \mathbb{T} . Any *vector* which is expressed in one reference frame can be expressed in a second reference frame (see figure 2-14, p. 33).

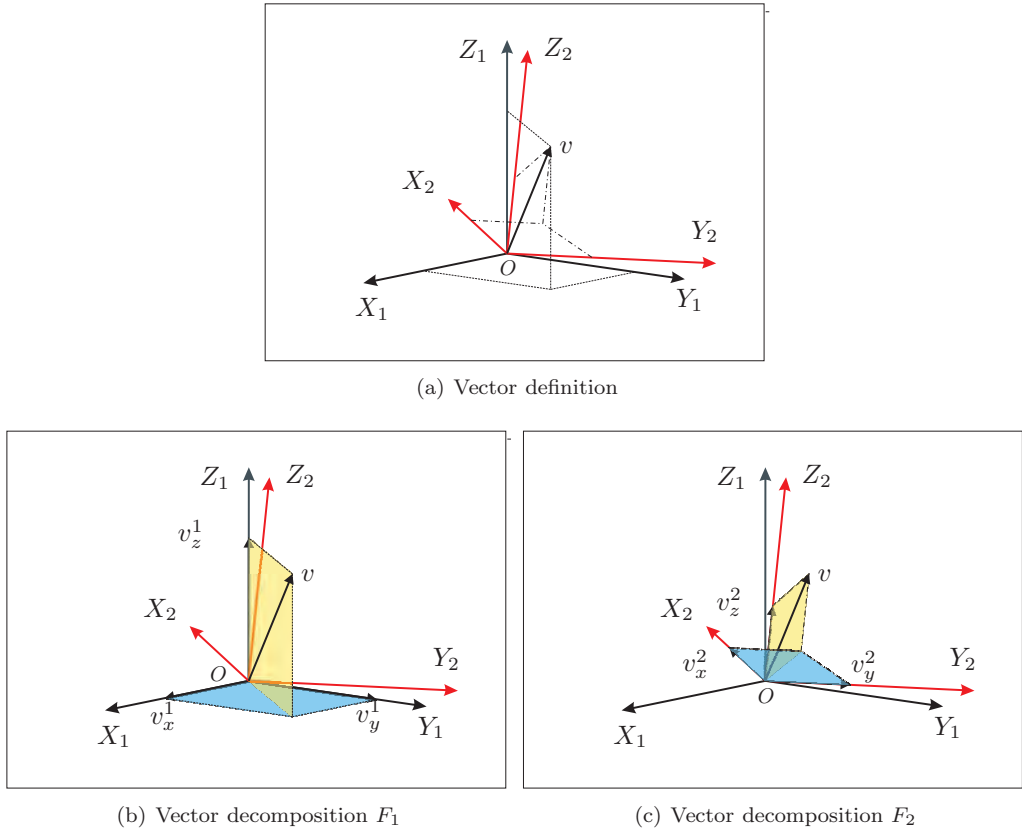


Figure 2-14: Simultaneous vector decomposition in two reference frames

The transition matrix contains the information necessary to calculate the coordinates of vector \mathbf{v} in the second reference frame F_2 when knowing the coordinates of vector v in the first reference frame F_1 :

$$\begin{bmatrix} v_x^2 \\ v_y^2 \\ v_z^2 \end{bmatrix} = \mathbb{T}_{21} \begin{bmatrix} v_x^1 \\ v_y^1 \\ v_z^1 \end{bmatrix} \quad (2-3)$$

The transformation matrix $\mathbb{T}_{2,1}$ must thus contain information regarding the *orientation* of reference frame F_1 with respect to reference frame F_2 . It does not contain any information about a possible translation between reference frame origins. When using Euler angles (see previous section) the transformation matrix can be defined as a multiplication of (at most) three (sub-)transformation matrices. Each (sub-)transformation matrix describes one rotation in the entire rotation sequence used in combination with the Euler angles. Thus the complete transformation

matrix can be defined as:

$$\begin{bmatrix} v_x^2 \\ v_y^2 \\ v_z^2 \end{bmatrix} = \mathbb{T}_{21''} \mathbb{T}_{1''1'} \mathbb{T}_{1',1} \begin{bmatrix} v_x^1 \\ v_y^1 \\ v_z^1 \end{bmatrix} \quad (2-4)$$

where $\mathbb{T}_{1',1}$ is the transformation matrix for the first rotation in the overall sequence expressing the vector \mathbf{v}^1 in terms of the axes of the intermediate reference frame $F_{1'}$, i.e. $\mathbf{v}^{1'}$. $\mathbb{T}_{1''1'}$ is the matrix for the second rotation expressing the vector $\mathbf{v}^{1'}$, which is expressed in $F_{1'}$, into to the second intermediate reference frame $F_{1''}$ ($\mathbf{v}^{1''}$). Finally the transition from $F_{1''}$ to F_2 is described by the transition matrix $\mathbb{T}_{21''}$ ($\mathbf{v}^{1''} \rightarrow \mathbf{v}^2$). Eq. (2-4) is obtained by substitution:

$$\left. \begin{array}{l} \mathbf{v}^{1'} = \mathbb{T}_{1',1} \mathbf{v}^1 \\ \mathbf{v}^{1''} = \mathbb{T}_{1''1'} \mathbf{v}^{1'} \\ \mathbf{v}^2 = \mathbb{T}_{21''} \mathbf{v}^{1''} \end{array} \right\} \mathbf{v}^2 = \mathbb{T}_{21''} \mathbb{T}_{1''1'} \mathbb{T}_{1',1} \mathbf{v}^1 \quad (2-5)$$

The information on a *single* rotation depends on the particular axis around which the rotation is performed. If the axis of rotation is the X -axis of the reference frame in which the vector is currently decomposed (F_1), then the coordinates of vector v in F_2 are given by (see figure 2-15, p. 35)):

$$\begin{aligned} v_x^2 &= 1.v_x^1 & +0.v_y^1 & +0.v_z^1 \\ v_y^2 &= 0.v_x^1 & +\cos \varphi_x \cdot v_y^1 & +\sin \varphi_x \cdot v_z^1 \\ v_z^2 &= 0.v_x^1 & -\sin \varphi_x \cdot v_y^1 & +\cos \varphi_x \cdot v_z^1 \end{aligned} \quad (2-6)$$

The transformation matrix is then defined as:

$$\mathbb{T}_{21} = \begin{bmatrix} 1 & 0 & 0 \\ 0 & \cos \varphi_x & \sin \varphi_x \\ 0 & -\sin \varphi_x & \cos \varphi_x \end{bmatrix} \quad (2-7)$$

The above transformation matrix is a so-called unit-axis transformation matrix, as it defines a rotation about a single axis. Since this axis is the X -axis, we define this unit-axis transformation by \mathbb{T}_x .

If the axis of rotation is the Y -axis of the reference frame in which the vector in currently decomposed (F_1), then the coordinates of vector \mathbf{v} in F_2 are given by (see figure 2-16, p. 35)):

$$\begin{aligned} v_x^2 &= \cos \varphi_y \cdot v_x^1 & +0.v_y^1 & -\sin \varphi_y \cdot v_z^1 \\ v_y^2 &= 0.v_x^1 & +1.v_y^1 & +0.v_z^1 \\ v_z^2 &= \sin \varphi_y \cdot v_x^1 & +0.v_y^1 & +\cos \varphi_y \cdot v_z^1 \end{aligned} \quad (2-8)$$

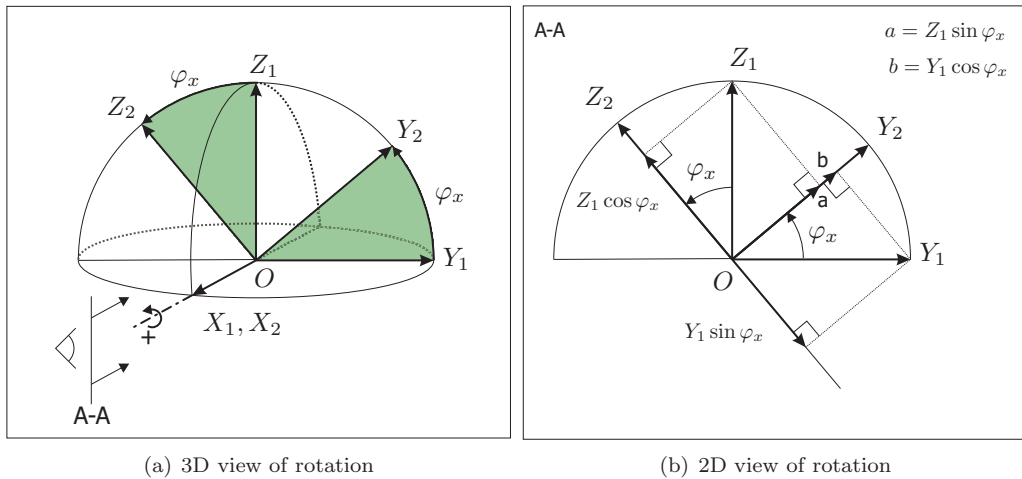
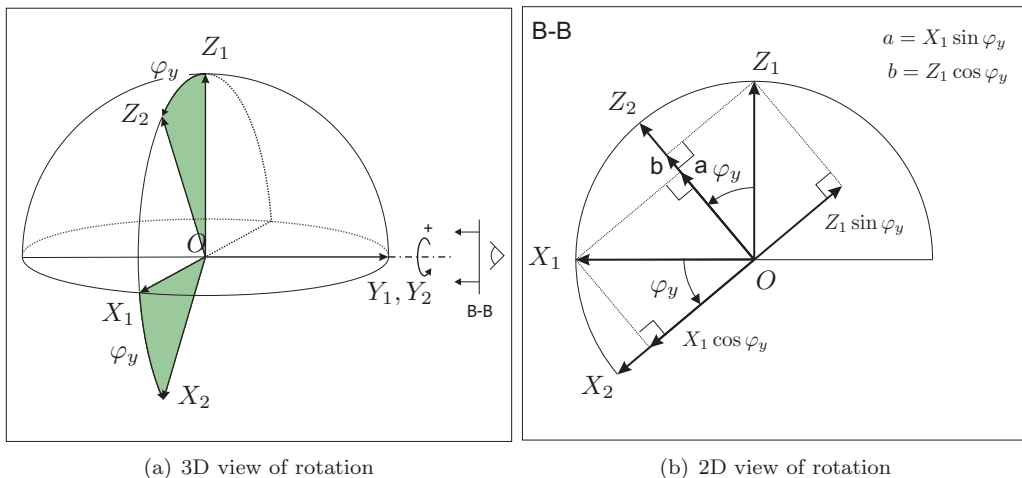
The transformation matrix is then defined as:

$$\mathbb{T}_{21} = \mathbb{T}_y = \begin{bmatrix} \cos \varphi_y & 0 & -\sin \varphi_y \\ 0 & 1 & 0 \\ \sin \varphi_y & 0 & \cos \varphi_y \end{bmatrix} \quad (2-9)$$

where \mathbb{T}_y is the second unit-axis transformation matrix.

If the axis of rotation is the Z -axis of the reference frame in which the vector in currently decomposed (F_1), then the coordinates of vector \mathbf{v} in F_2 are given by (see figure 2-17, p. 36)):

$$\begin{aligned} v_x^2 &= \cos \varphi_z \cdot v_x^1 & +\sin \varphi_z \cdot v_y^1 & +0.v_z^1 \\ v_y^2 &= -\sin \varphi_z \cdot v_x^1 & +\cos \varphi_z \cdot v_y^1 & +0.v_z^1 \\ v_z^2 &= 0.v_x^1 & +0.v_y^1 & +1.v_z^1 \end{aligned} \quad (2-10)$$

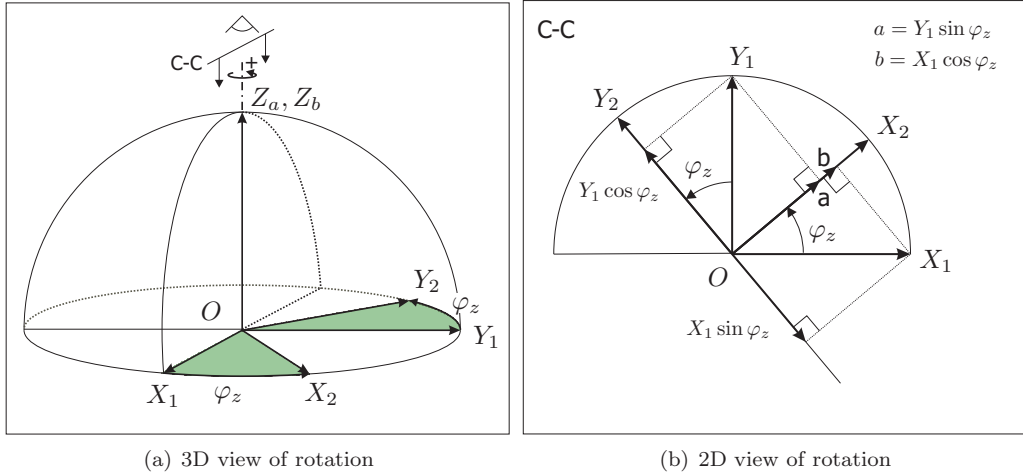
Figure 2-15: Vector decomposition for rotation about X -axisFigure 2-16: Vector decomposition for rotation about Y -axis

The transformation matrix is then defined as:

$$\mathbb{T}_{21} = \mathbb{T}_z = \begin{bmatrix} \cos \varphi_z & \sin \varphi_z & 0 \\ -\sin \varphi_z & \cos \varphi_z & 0 \\ 0 & 0 & 1 \end{bmatrix} \quad (2-11)$$

with \mathbb{T}_z being the third unit-axis transformation matrix.

If the rotation sequence is $\varphi_z \rightarrow \varphi_y \rightarrow \varphi_x$ the transformation for the entire rotation is described by:

Figure 2-17: Vector decomposition for rotation about Z -axis

$$\begin{aligned}
 \mathbf{v}_2 &= \mathbb{T}_{21} \mathbf{v}_1 \\
 &= \mathbb{T}_{21''} \mathbb{T}_{1''1'} \mathbb{T}_{1'1} \mathbf{v}_1 \\
 &= \begin{bmatrix} 1 & 0 & 0 \\ 0 & \cos \varphi_x & \sin \varphi_x \\ 0 & -\sin \varphi_x & \cos \varphi_x \end{bmatrix} \begin{bmatrix} \cos \varphi_y & 0 & -\sin \varphi_y \\ 0 & 1 & 0 \\ \sin \varphi_y & 0 & \cos \varphi_y \end{bmatrix} \begin{bmatrix} \cos \varphi_z & \sin \varphi_z & 0 \\ -\sin \varphi_z & \cos \varphi_z & 0 \\ 0 & 0 & 1 \end{bmatrix} \mathbf{v}_1 \\
 &= \begin{bmatrix} \cos \varphi_y \cos \varphi_z & \cos \varphi_y \sin \varphi_z & -\sin \varphi_y \\ \left(\begin{array}{c} \sin \varphi_x \sin \varphi_y \cos \varphi_z \\ -\cos \varphi_x \sin \varphi_z \end{array} \right) & \left(\begin{array}{c} \sin \varphi_x \sin \varphi_y \sin \varphi_z \\ +\cos \varphi_x \cos \varphi_z \end{array} \right) & \sin \varphi_x \cos \varphi_y \\ \left(\begin{array}{c} \cos \varphi_x \sin \varphi_y \cos \varphi_z \\ +\sin \varphi_x \sin \varphi_z \end{array} \right) & \left(\begin{array}{c} \cos \varphi_x \sin \varphi_y \sin \varphi_z \\ -\sin \varphi_x \cos \varphi_z \end{array} \right) & \cos \varphi_x \cos \varphi_y \end{bmatrix} \mathbf{v}_1
 \end{aligned} \tag{2-12}$$

Transformation matrix \mathbb{T}_{21} depend on the selected set of Euler rotations. This follows easily from the algebraic multiplication of the transformation matrices for a different sequence, for instance $\varphi_x \rightarrow \varphi_y \rightarrow \varphi_z$, resulting in a different matrix then given by Eq. (2-12).

Transformation matrices have special characteristics. These characteristics stem from two criteria. First of all, one wishes to apply a orthogonal transformation, i.e. a rotation from one orthogonal reference frame to another, thus the transformation matrix must also be orthogonal. Secondly, after the rotation of a reference frame, a vector must still have its original length. This implies that the determinant of the transformation matrix must be equal to 1. This leads to the following criteria for transformation matrices (see Ref. [179]):

1. The eigenvalues of the transformation matrix must satisfy one of the following (orthogonality property):
 - All eigenvalues are 1.
 - One eigenvalue is 1 and the other two are -1.
 - One eigenvalue is 1 and the other two are complex conjugates of the form $e^{i\theta}$ and $e^{-i\theta}$.

2. The determinant of the transformation matrix must be (normality property):

$$\det(\mathbb{T}) \equiv 1$$

When these criteria are met for a transformation matrix \mathbb{T} , i.e., the matrix is *orthonormal*, two important properties are guaranteed:

1. $\mathbb{T}_{ab}^{-1} = \mathbb{T}_{ab}^t = \mathbb{T}_{ba}$
2. $\mathbb{T}_{ab}^t \mathbb{T}_{ab} = \mathbb{T}_{ab}^{-1} \mathbb{T}_{ab} = \mathbb{I}$

Proof:

$$\begin{aligned} \mathbf{v}^2 &= \mathbb{T}_{21} \mathbf{v}^1 \xrightarrow{\text{(taking the inverse)}} \mathbf{v}^1 = \mathbb{T}_{21}^{-1} \mathbf{v}^2 \\ \mathbf{v}^1 &= \mathbb{T}_{12} \mathbf{v}^2 \xrightarrow{\text{(orthogonality)}} \mathbf{v}^1 = \mathbb{T}_{21}^t \mathbf{v}^2 \end{aligned} \quad \left. \begin{array}{l} \mathbb{T}_{21}^{-1} = \mathbb{T}_{21}^t \\ \mathbb{T}_{21}^t = \mathbb{T}_{21}^{-1} \end{array} \right\} \quad (2-13)$$

From property one follows property two.

These properties will be used during the derivation of the equations of motion and kinematic relations. In the following sections the transformation matrices will be derived which are frequently used in practice. As explained above, the particular form of each matrix strictly depends on the specific order of the rotation sequence. Each matrix belongs to one particular transformation between two reference frames and is thus only valid for the rotation sequence as stated per transformation.

2-2-3 Transformation from F_I to F_C

The transformation from the inertial reference frame F_I to the Earth-centered Earth-fixed reference frame F_C , is performed using a single rotation (see Figure 2-3 p. 22, and Figure 2-18 p. 39). The required rotation is one about the Z_I ($= Z_C$ axis) over an angle $\Omega_t t_O$, where Ω_t is the rotational speed of the Earth and t_O is known as the stellar time of point O .⁸

Effectively, this rotation maps the X_I - and Y_I -axis to their C -frame counterparts.

Angle sign and limits

$\Omega_t t_O$ is always positive and has a range of:

$$0 \leq \Omega_t t_O < 2\pi$$

and is fully repetitive.

Transformation matrix

$$\mathbf{X}^C = \mathbb{T}_{CI} \mathbf{X}^I \quad (2-14)$$

$$\mathbb{T}_{CI} = \begin{bmatrix} \cos \Omega_t t_O & \sin \Omega_t t_O & 0 \\ -\sin \Omega_t t_O & \cos \Omega_t t_O & 0 \\ 0 & 0 & 1 \end{bmatrix} \quad (2-15)$$

⁸The stellar time point is dependent on the definition of the I -frame, and the date and time of the considered epoch. For instance, for the definition of the inertial J2000 frame, it is exactly known what the orientation of the Earth, and thus the C -frame, was at January 1, 12h, 2000. Given the rotational rate of the Earth, one can easily calculate the angular position of the C -frame for any specified epoch since that date (or even before, if need be).

2-2-4 Transformation from F_C to F_E

The transformation from the Earth-centered Earth-fixed reference frame F_C to the vehicle-carried normal Earth reference frame is performed using two consecutive rotations (see Figure 2-18 p. 39). For the rotation sequence one intermediate reference frame will be defined, $F_{C'}$:

$$F_C \rightarrow F_{C'} \rightarrow F_E$$

The two rotations in sequence are:

1. Rotation τ about the Z_C -axis.
2. Rotation $-\delta - \frac{\pi}{2}$ about the Y_E -axis ($= Y'_C$ -axis).

where τ and δ are the geocentric longitude and latitude.

The first rotation over τ brings the Y_C -axis to the Y_E -axis. The second rotation consists of two parts. First the reference frame is rotated by $90^\circ = -\frac{\pi}{2}$ [rad] about the Y_E -axis to bring the X_E -axis in northern orientation, i.e. in Z_I -direction. Thereafter a rotation of $-\delta$ is performed to point the X_E -axis to the geographical north (seen from point O on the Earth surface).

It is stressed that in this case there is a translation transformation required to move the origin of the ECEF reference frame (i.e., the center of the Earth) to the center of gravity of the aircraft. This translation is covered by the radial distance, i.e., the sum of the (local) radius of the Earth and the vehicle altitude above the surface.

Angles sign and limits

τ is positive if the vehicle position is east of the Greenwich meridian (by definition of the C -frame, the X_C -axis passes through Greenwich, which is zero longitude), and negative when west. δ is positive if the vehicle location is on the northern hemisphere, and negative when south. The ranges of both angles are:

$$\begin{aligned} -\pi &\leq \tau < \pi \\ -\frac{\pi}{2} &\leq \delta \leq \frac{\pi}{2} \end{aligned}$$

Note that when the vehicle is exactly at one of the poles, the longitude is no longer defined.

Transformation matrix

$$\mathbf{X}^E = \mathbb{T}_{EC} \mathbf{X}^C \quad (2-16)$$

$$\begin{aligned} \mathbb{T}_{EC} &= \begin{bmatrix} -\sin \delta & 0 & \cos \delta \\ 0 & 1 & 0 \\ -\cos \delta & 0 & -\sin \delta \end{bmatrix} \begin{bmatrix} \cos \tau & \sin \tau & 0 \\ -\sin \tau & \cos \tau & 0 \\ 0 & 0 & 1 \end{bmatrix} \\ &= \begin{bmatrix} -\sin \delta \cos \tau & -\sin \delta \sin \tau & \cos \delta \\ -\sin \tau & \cos \tau & 0 \\ -\cos \delta \cos \tau & -\cos \delta \sin \tau & -\sin \delta \end{bmatrix} \end{aligned} \quad (2-17)$$

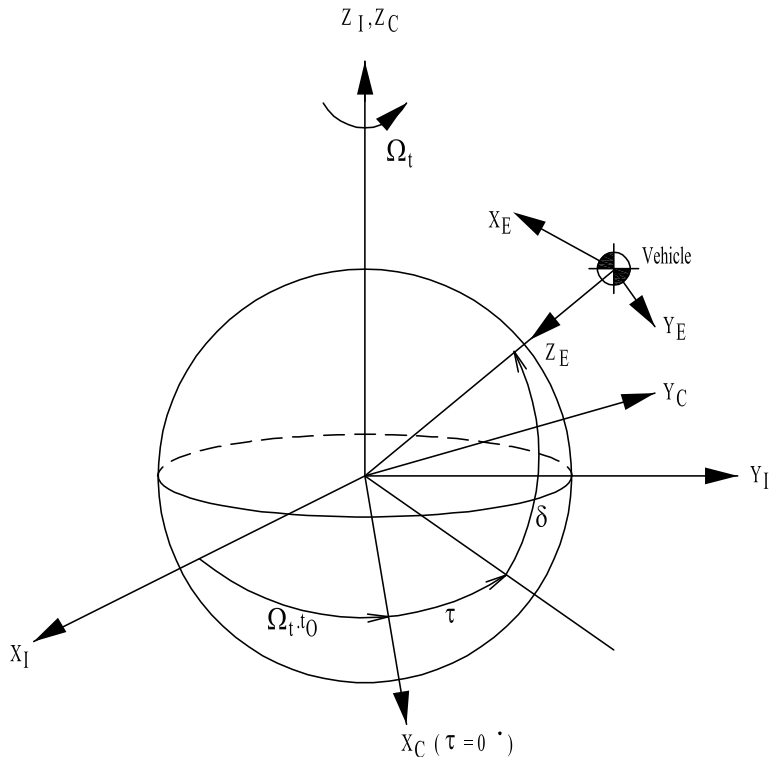


Figure 2-18: Relation between the inertial, the Earth-centered Earth-fixed and vehicle-carried normal Earth reference frames.

2-2-5 Transformation from F_E to F_b

The transformation from the vehicle carried normal Earth reference frame to the body-fixed reference frame is done in three consecutive rotations. For the rotation sequence two intermediate reference systems will be defined, i.e., $F_{E'}$ and $F_{E''}$:

$$F_E \rightarrow F_{E'} \rightarrow F_{E''} \rightarrow F_b$$

The three rotations in sequence are (see figure 2-19, p. 41):

- Rotation ψ yaw angle about the Z_E -axis
- Rotation θ pitch angle about the $Y_{E'}$ -axis
- Rotation φ roll angle about the X_b -axis (= $X_{E''}$ -axis)

In the aerospace industry the most commonly used rotation sequence is that of $\psi \rightarrow \theta \rightarrow \varphi$. Other sequences are also possible (see Section 2-2-1, p. 28). The yaw, pitch, and roll angle are the rotations about the Z , Y , and X -axis respectively. This set of angles is commonly confused with another set of angles, namely: the azimuth, climb, and bank angle. However the definitions of these angles are:

- azimuth angle: angle between X_b -axis and its projection on a predefined (local) vertical plane.
- climb angle: angle between X_b -axis and its projection on the (local) horizontal plane.

- bank angle: angle between Y_b -axis and its projection on the (local) horizontal plane.

Two definitions for the azimuth angle can be stated depending on the orientation of the X_E -axis:

- X_E is the direction of the geographic North: ψ_v true heading
- X_E is the direction of the magnetic North: ψ_m magnetic heading

The difference between the two headings is the magnetic declination dm , which is positive when the magnetic North is east of the geographic North.

Angles sign and limits

The positive rotation direction of the angles are in accordance with the definition of right-hand reference systems. In figure 2-19 (p. 41) a negative yaw angle ($-\psi$) is taken to enhance the graphical representation. The ranges of the angles according to convention are:

$$\begin{aligned} -\pi &\leq \psi < \pi \\ -\frac{\pi}{2} &< \theta < \frac{\pi}{2} \\ -\pi &\leq \varphi < \pi \end{aligned}$$

Transformation matrix

$$\mathbf{X}^b = \mathbb{T}_{bE} \mathbf{X}^E \quad (2-18)$$

$$\begin{aligned} \mathbb{T}_{bE} &= \mathbb{T}_{bE''} \mathbb{T}_{E''E'} \mathbb{T}_{E'E} \\ &= \begin{bmatrix} 1 & 0 & 0 \\ 0 & \cos \varphi & \sin \varphi \\ 0 & -\sin \varphi & \cos \varphi \end{bmatrix} \begin{bmatrix} \cos \theta & 0 & -\sin \theta \\ 0 & 1 & 0 \\ \sin \theta & 0 & \cos \theta \end{bmatrix} \begin{bmatrix} \cos \psi & \sin \psi & 0 \\ -\sin \psi & \cos \psi & 0 \\ 0 & 0 & 1 \end{bmatrix} \\ &= \begin{bmatrix} \cos \theta \cos \psi & \cos \theta \sin \psi & -\sin \theta \\ \left(\begin{array}{c} \sin \varphi \sin \theta \cos \psi \\ -\cos \varphi \sin \psi \end{array} \right) & \left(\begin{array}{c} \sin \varphi \sin \theta \sin \psi \\ +\cos \varphi \cos \psi \end{array} \right) & \sin \varphi \cos \theta \\ \left(\begin{array}{c} \cos \varphi \sin \theta \cos \psi \\ +\sin \varphi \sin \psi \end{array} \right) & \left(\begin{array}{c} \cos \varphi \sin \theta \sin \psi \\ -\sin \varphi \cos \psi \end{array} \right) & \cos \varphi \cos \theta \end{bmatrix} \quad (2-19) \end{aligned}$$

2-2-6 Transformation from F_E to F_a

The transformation from the vehicle carried normal Earth reference frame to the aerodynamic reference system is done in three consecutive rotations. For the rotation sequence two intermediate reference systems will be defined, $F_{E'}$ and $F_{E''}$:

$$F_E \rightarrow F_{E'} \rightarrow F_{E''} \rightarrow F_a$$

The three rotations in sequence are (see figure 2-19, p. 41):

- Rotation χ_a aerodynamic heading angle about the Z_E -axis
- Rotation γ_a aerodynamic flight-path angle about the $Y_{E'}$ -axis

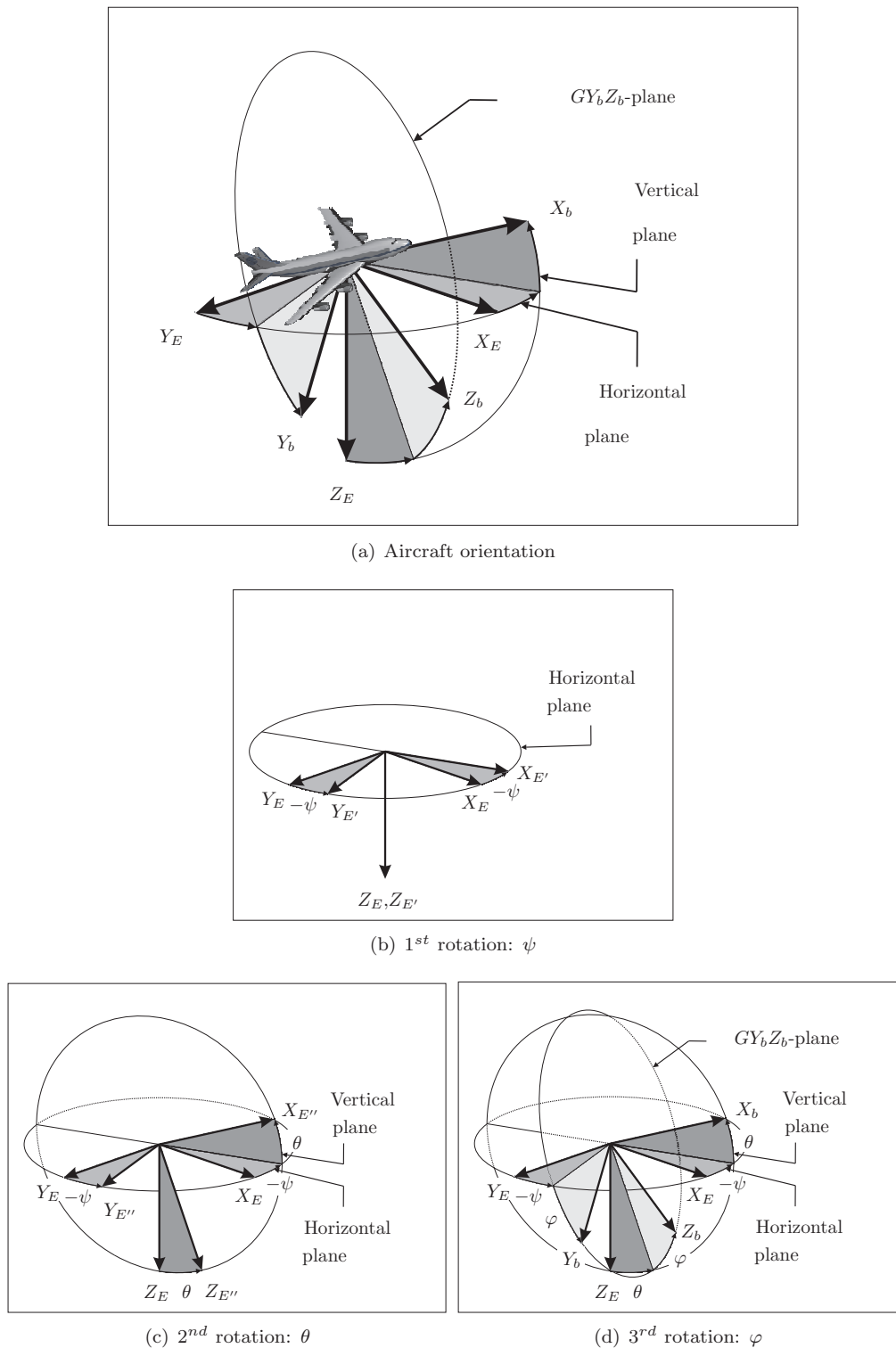


Figure 2-19: Transformation from vehicle carried normal Earth reference frame F_E to the body-fixed reference frame F_b

- Rotation μ_a aerodynamic bank angle about the X_a -axis ($=X_{E''}$ -axis)

The first two rotations, χ_a and γ_a , are used to 'bring' the X_a -axis parallel with the aerodynamic velocity vector. The third rotation, μ_a , is used to place the Z_a -axis into the symmetry plane of the aircraft.

Note that the definition of the bank angle is such that a positive angle represents a positive rotation around the velocity vector. For this reason, the bank angle is shown as $-\mu_a$ in Figure 2-20, p. 43. The rotation sequence is almost similar to that of the previous transformation $F_E \rightarrow F_b$ (Figure 2-19, p. 41) in the sense that we have a 3-2-1 rotation sequence. The difference is that for $F_E \rightarrow F_b$ we rotate over three positive angles, whereas for $F_E \rightarrow F_a$ the last angle ($=\mu_a$) is negative.

Angles sign and limits

For the definition of right-hand reference systems, one should define the positive rotation direction of the angles accordingly. For the γ_a and χ_a this is true, but the definition of μ_a violates this rule. As mentioned above, the reason for this is a physical one - it is related to the rotation about the velocity vector rather than a reference axis. However, in figure 2-20 (p. 43) besides a negative bank angle ($-\mu_a$) also a negative azimuth ($-\chi_a$) is indicated; the latter is only meant to enhance the graphical representation. The ranges of the angles according to convention are:

$$\begin{aligned} -\pi &\leq \chi_a < \pi \\ -\frac{\pi}{2} &\leq \gamma_a \leq \frac{\pi}{2} \\ -\pi &\leq \mu_a < \pi \end{aligned}$$

Transformation matrix

$$\mathbf{X}^a = \mathbb{T}_{aE} \mathbf{X}^E \quad (2-20)$$

$$\begin{aligned} \mathbb{T}_{aE} &= \mathbb{T}_{aE''} \mathbb{T}_{E''E'} \mathbb{T}_{E'E} \\ &= \begin{bmatrix} 1 & 0 & 0 \\ 0 & \cos \mu_a & -\sin \mu_a \\ 0 & \sin \mu_a & \cos \mu_a \end{bmatrix} \begin{bmatrix} \cos \gamma_a & 0 & -\sin \gamma_a \\ 0 & 1 & 0 \\ \sin \gamma_a & 0 & \cos \gamma_a \end{bmatrix} \begin{bmatrix} \cos \chi_a & \sin \chi_a & 0 \\ -\sin \chi_a & \cos \chi_a & 0 \\ 0 & 0 & 1 \end{bmatrix} \\ &= \begin{bmatrix} \cos \gamma_a \cos \chi_a & \cos \gamma_a \sin \chi_a & -\sin \gamma_a \\ \left(-\sin \mu_a \sin \gamma_a \cos \chi_a \right) & \left(-\sin \mu_a \sin \gamma_a \sin \chi_a \right) & -\sin \mu_a \cos \gamma_a \\ \left(-\cos \mu_a \sin \chi_a \right) & \left(+\cos \mu_a \cos \chi_a \right) & \cos \mu_a \cos \gamma_a \\ \left(\cos \mu_a \sin \gamma_a \cos \chi_a \right) & \left(\cos \mu_a \sin \gamma_a \sin \chi_a \right) & \cos \mu_a \cos \gamma_a \\ \left(-\sin \mu_a \sin \chi_a \right) & \left(+\sin \mu_a \cos \chi_a \right) & \end{bmatrix} \quad (2-21) \end{aligned}$$

Note that since we do not consider wind in these lecture notes, the subscript a may be dropped.

2-2-7 Transformation from F_b to F_a

The transformation from the body-fixed reference frame F_b to the aerodynamic reference frame F_a consists of two consecutive rotations. For the rotation sequence one intermediate reference frame will be defined, $F_{b'}$:

$$F_b \rightarrow F_{b'} \rightarrow F_a$$

The two rotations in sequence are (see figure 2-21, p. 45):

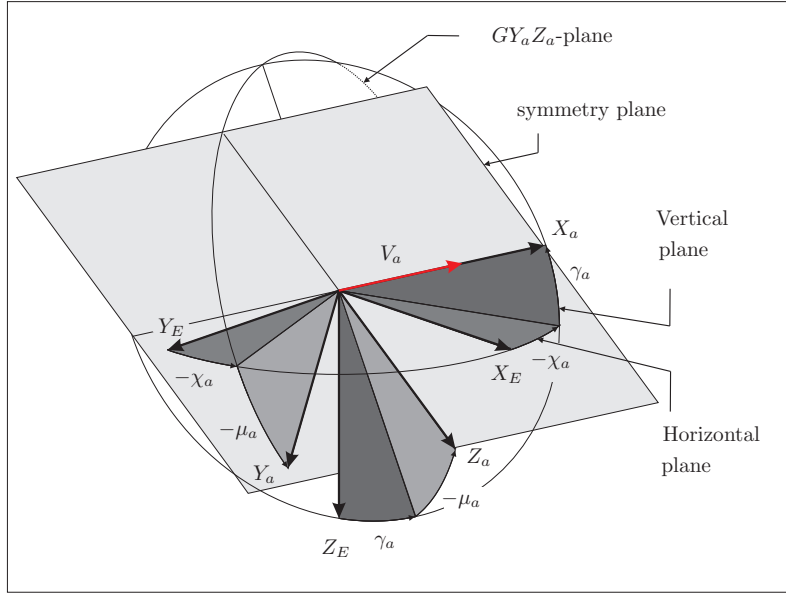


Figure 2-20: Transformation from vehicle carried normal Earth reference frame F_E to the aerodynamic reference frame F_a

- Rotation $-\alpha_a$ aerodynamic angle of attack about the Y_b -axis.
- Rotation β_a aerodynamic sideslip angle about the Z_a -axis ($= Z_{b'} - axis$).

The first rotation brings the X_b -axis to the $X_{b'}$ -axis and the Z_b -axis to the $Z_{b'}$ of the intermediate reference frame F'_b . Since the second and last rotation is about the $Z_{b'}$ -axis, the $Z_{b'}$ -axis is equal to the Z_a -axis. The second rotation bring the $X_{b'}$ -axis to the X_a -axis, thus into the direction of the aerodynamic velocity.

Angles sign and limits

The positive rotation direction of the angles are in accordance with the definition of right-hand reference systems. The angle of attack is positive if the body axis X_b lies above the X_a , thus if the nose of the aircraft is pointed above the aerodynamic velocity vector. The sideslip angle is positive when the body axis X_b lies left from the aerodynamic velocity vector (seen from the origin of the reference frame). The ranges of the angles according to convention are:

$$\begin{aligned} -\pi &\leq \alpha_a < \pi \\ -\frac{\pi}{2} &\leq \beta_a \leq \frac{\pi}{2} \end{aligned}$$

Transformation matrix

$$\mathbf{X}^a = \mathbb{T}_{ab} \mathbf{X}^b \quad (2-22)$$

$$\begin{aligned}
\mathbb{T}_{ab} &= \mathbb{T}_{ab'} \mathbb{T}_{b'b} \\
&= \begin{bmatrix} \cos \beta_a & \sin \beta_a & 0 \\ -\sin \beta_a & \cos \beta_a & 0 \\ 0 & 0 & 1 \end{bmatrix} \begin{bmatrix} \cos \alpha_a & 0 & \sin \alpha_a \\ 0 & 1 & 0 \\ -\sin \alpha_a & 0 & \cos \alpha_a \end{bmatrix} \\
&= \begin{bmatrix} \cos \beta_a \cos \alpha_a & \sin \beta_a & \cos \beta_a \sin \alpha_a \\ -\sin \beta_a \cos \alpha_a & \cos \beta_a & -\sin \beta_a \sin \alpha_a \\ -\sin \alpha_a & 0 & \cos \alpha_a \end{bmatrix}
\end{aligned} \tag{2-23}$$

Useful relations

The aerodynamic velocity vector can be related to the aerodynamic angle of attack and aerodynamic angle of sideslip. The aerodynamic velocity vector can be expressed in the body-fixed reference frame as stated in Eq. (2-2). Using this relation the magnitude of the aerodynamic velocity vector can be defined as:

$$V_a = \sqrt{u_a^b + v_a^b + w_a^b}$$

The aerodynamic angle of attack is defined as:

$$\alpha_a = \tan^{-1} \left(\frac{w_a^b}{u_a^b} \right)$$

Finally the aerodynamic angle of sideslip is defined as:

$$\beta_a = \sin^{-1} \left(\frac{v_a^b}{V_a} \right)$$

Again, in the absence of wind, the subscript a may be dropped. The above relations can only be used when the aerodynamic velocity is indeed known in body-frame components. If not - and the aerodynamic velocity has to be transformed using \mathbb{T}_{ba} , see Eq. (2-23), which depends on α_a and β_a - in Section 2-2-8 an alternative method is presented. Those transformations are given by Eqs. (2-36)-(2-38).

2-2-8 Coordinate transformations

In Sections 2-2-6 we saw that to calculate the transformation matrix \mathbb{T}_{aE} we need the angles γ_a (aerodynamic pitch angle, or flight-path angle), χ_a (aerodynamic yaw angle) and μ_a (aerodynamic roll angle). These angles are not readily available. In 3, where the equations of motion are derived, we will see that the state variables for velocity are V_N , V_E and V_D (see, for instance, Fig. 2-1), and that the attitude attitude of the vehicle is defined w.r.t. the E -frame, or, in other words, by the Euler angles φ , θ and ψ (see Section 2-2-5).

From the velocity components we can extract γ_a and χ_a , see also Fig. 2-22. The modulus of the velocity vector can directly be computed from the three Cartesian components,

$$V = \sqrt{V_N^2 + V_E^2 + V_D^2} \tag{2-24}$$

The projection of V in the local vertical plane gives

$$V \sin \gamma_a = -V_D \tag{2-25}$$

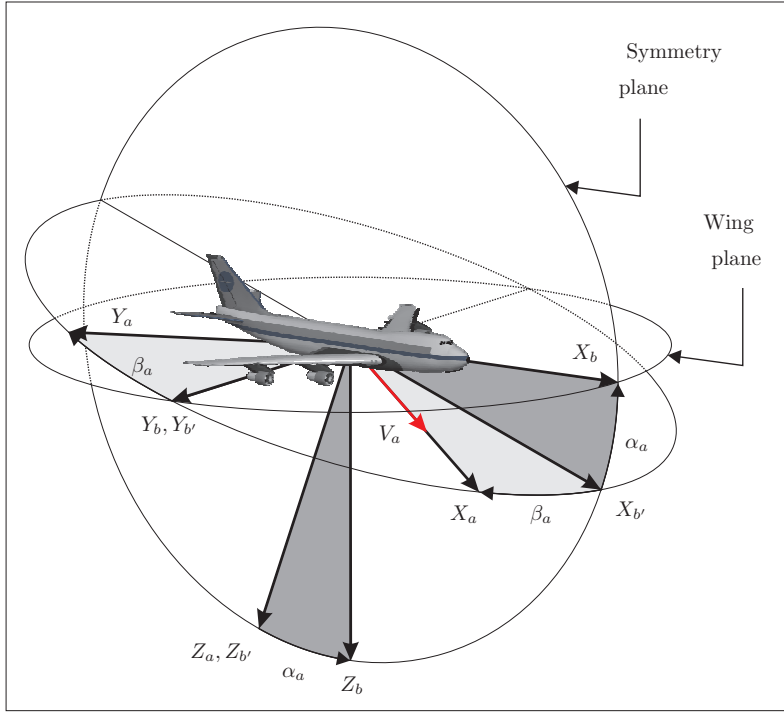


Figure 2-21: Transformation from the body-fixed reference frame F_b to the aerodynamic reference frame F_a

Because γ_a is restricted to values between -90° and 90° and since the arcsine function is defined for the same interval, we get from Eq. (2-25):

$$\gamma_a = \arcsin\left(\frac{-V_D}{V}\right) = -\arcsin\left(\frac{V_D}{V}\right) \quad (2-26)$$

As can be seen in the same figure, we find for the heading χ_a :

$$\tan \chi_a = \frac{V_E}{V_N} \Rightarrow \chi_a = \arctan\left(\frac{V_E}{V_N}\right) \quad (2-27)$$

In the previous section we showed that α_a and β_a can be derived from the velocity components in F_b . However, here we will show an alternative way that will also give us μ_a . To extract α_a , β_a and μ_a from the Euler angles, we rewrite \mathbb{T}_{Ea} :

$$\mathbb{T}_{Ea} = \mathbb{T}_{Eb} \mathbb{T}_{ba} \quad (2-28)$$

with \mathbb{T}_{Eb} given by the transpose of Eq. (2-19) and \mathbb{T}_{ba} by the transpose of Eq. (2-23):

$$\mathbb{T}_{Eb} = \begin{bmatrix} c\psi c\theta & c\psi s\theta s\varphi - s\psi c\varphi & s\psi s\varphi + c\psi s\theta c\varphi \\ s\psi c\theta & c\psi c\varphi + s\psi s\theta s\varphi & s\psi s\theta c\varphi - c\psi s\varphi \\ -s\theta & c\theta s\varphi & c\theta c\varphi \end{bmatrix} \quad (2-29)$$

$$\mathbb{T}_{ba} = \begin{bmatrix} c\alpha_a c\beta_a & -c\alpha_a s\beta_a & -s\alpha_a \\ s\beta_a & c\beta_a & 0 \\ s\alpha_a c\beta_a & -s\alpha_a s\beta_a & c\alpha_a \end{bmatrix} \quad (2-30)$$

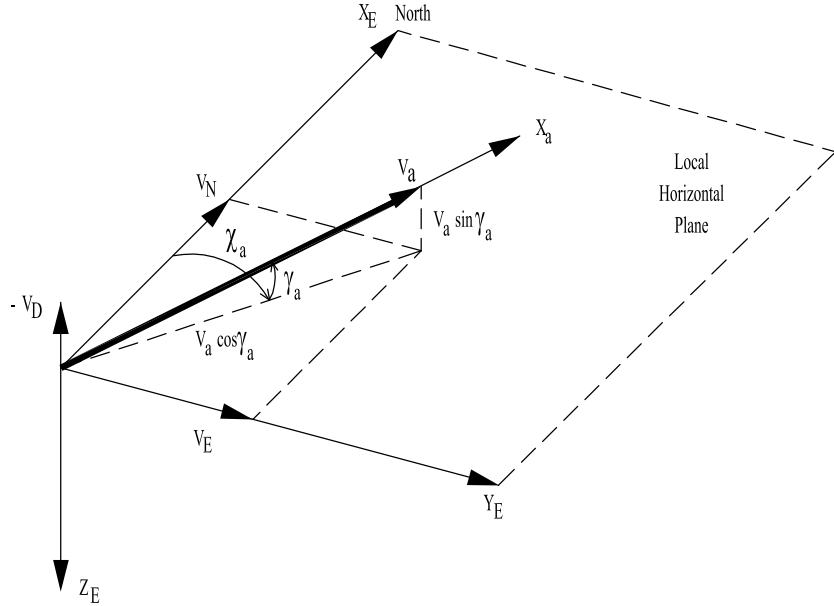


Figure 2-22: Relation between the spherical velocity components and Cartesian components in the V -frame.

In the above equations we have used the short-hand notation 's' for *sine* and 'c' for *cosine*. From Section 2-2-6, we know that \mathbb{T}_{Ea} can be written as:

$$\mathbb{T}_{Ea} = \mathbb{T}_z(-\chi_a) \mathbb{T}_y(-\gamma_a) \mathbb{T}_x(\mu_a) \quad (2-31)$$

Equating Eq. (2-28) with Eq. (2-31) gives us:

$$\mathbb{T}_{Eb} \mathbb{T}_{ba} = \mathbb{T}_z(-\chi_a) \mathbb{T}_y(-\gamma_a) \mathbb{T}_x(\mu_a) \quad (2-32)$$

Post-multiplying both sides with \mathbb{T}_{ab} yields

$$\mathbb{T}_{Eb} \mathbb{T}_{ba} \mathbb{T}_{ab} = \mathbb{T}_{Eb} = \mathbb{T}_z(-\chi_a) \mathbb{T}_y(-\gamma_a) \mathbb{T}_x(\mu_a) \mathbb{T}_{ab} \quad (2-33)$$

since $\mathbb{T}_{ba} \mathbb{T}_{ab} = \mathbb{I}$. Similarly, by first pre-multiplying both sides with $\mathbb{T}_z(\chi_a)$ (i.e., the inverse of $\mathbb{T}_z(-\chi_a)$) and then pre-multiplying both sides with $\mathbb{T}_y(\gamma_a)$ (the inverse of $\mathbb{T}_y(-\gamma_a)$), we finally get:

$$\mathbb{T}_{Xb} = \mathbb{T}_y(\gamma_a) \mathbb{T}_z(\chi_a) \mathbb{T}_{Eb} = \mathbb{T}_x(\mu_a) \mathbb{T}_{ab} \quad (2-34)$$

What we have now is a known transformation matrix on the left-hand side, \mathbb{T}_{Xb} , and a transformation matrix as a function of three unknown angles α_a , β_a and μ_a . The right-hand side can be written as:

$$\mathbb{T}_x(\mu_a) \mathbb{T}_{ab} = \begin{bmatrix} c\alpha_a c\beta_a & s\beta_a & s\alpha_a c\beta_a \\ -c\alpha_a s\beta_a c\mu_a - s\alpha_a s\mu_a & c\beta_a c\mu_a & c\alpha_a s\mu_a - s\alpha_a s\beta_a c\mu_a \\ c\alpha_a s\beta_a s\mu_a - s\alpha_a c\mu_a & -c\beta_a s\mu_a & c\alpha_a c\mu_a + s\alpha_a s\beta_a s\mu_a \end{bmatrix} \quad (2-35)$$

From Eq. (2-35), we find

$$\alpha_a = \arctan \left(\frac{\mathbb{T}_{Xb}(1, 3)}{\mathbb{T}_{Xb}(1, 1)} \right) \quad (2-36)$$

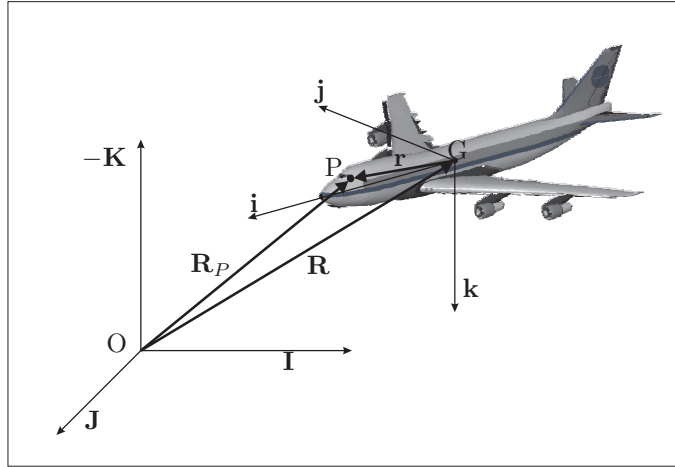


Figure 2-23: General situation for vector differentiation

$$\beta_a = \arcsin(\mathbb{T}_{Xb}(1, 2)) \quad (2-37)$$

$$\mu_a = -\arctan\left(\frac{\mathbb{T}_{Xb}(3, 2)}{\mathbb{T}_{Xb}(2, 2)}\right) \quad (2-38)$$

taking quadrant information into account. Note that $\beta_a = \pm 90^\circ$ is a singularity in the conversion. The notation $\mathbb{T}_{Xb}(i, j)$ means that we have to take the element at row i and column j of \mathbb{T}_{Xb} .

2-3 Rotating reference frames

2-3-1 Vector time derivatives

At any given moment in time we can express any vector in any reference frame. Vector expressions can be related through the relation

$$\mathbf{r}^2 = \mathbb{T}_{21}\mathbf{r}^1 \quad (2-39)$$

But what will happen if we look at this relation through time? What additional relations will we have? In this section we will incorporate the aspect of time by looking at the time derivatives of vectors. We will see that the properties of the reference frames, i.e. location, orientation, and velocities, with respect to each other must all be used to correctly specify vector derivative relations. In particular, these properties will be used in Appendix C, where the general formulation of the equations of motion is derived. This will be done both in the inertial reference frame and a rotating reference frame.

We will start this discussion by giving a general situation specified in Figure 2-23. Imagine that we have the inertial reference frame F_I ($O, \mathbf{I}, \mathbf{J}, \mathbf{K}$) and an body fixed reference frame F_b ($G, \mathbf{i}, \mathbf{j}, \mathbf{k}$) attached to an aircraft. As we can see, we have the following relation

$$\mathbf{R}_P = \mathbf{R} + \mathbf{r} \quad (2-40)$$

We can express this relation in either reference frame. Expressing it in the inertial reference frame we obtain

$$\begin{aligned} \mathbf{R}_P &= R_I \cdot \mathbf{I} + R_J \cdot \mathbf{J} + R_K \cdot \mathbf{K} + r_I \cdot \mathbf{I} + r_J \cdot \mathbf{J} + r_K \cdot \mathbf{K} \\ &= R_I \cdot \mathbf{I} + R_J \cdot \mathbf{J} + R_K \cdot \mathbf{K} + \mathbb{T}_{Ib}(r_i \cdot \mathbf{i} + r_j \cdot \mathbf{j} + r_k \cdot \mathbf{k}) \\ &= R_I \cdot \mathbf{I} + R_J \cdot \mathbf{J} + R_K \cdot \mathbf{K} + r_i \cdot \hat{\mathbf{i}} + r_j \cdot \hat{\mathbf{j}} + r_k \cdot \hat{\mathbf{k}} \end{aligned} \quad (2-41)$$

where $\hat{\mathbf{i}}, \hat{\mathbf{j}}, \hat{\mathbf{k}}$ are the unit vectors of reference frame F_b expressed in the inertial reference frame

$$\begin{aligned}\hat{\mathbf{i}} &= \mathbb{T}_{Ib}\mathbf{i} = \mathbb{T}_{Ib} \begin{bmatrix} 1 & 0 & 0 \end{bmatrix}^T \\ \hat{\mathbf{j}} &= \mathbb{T}_{Ib}\mathbf{j} = \mathbb{T}_{Ib} \begin{bmatrix} 0 & 1 & 0 \end{bmatrix}^T \\ \hat{\mathbf{k}} &= \mathbb{T}_{Ib}\mathbf{k} = \mathbb{T}_{Ib} \begin{bmatrix} 0 & 0 & 1 \end{bmatrix}^T\end{aligned}\quad (2-42)$$

The derivative of the vector \mathbf{R}_P , using the chain rule, is given by

$$\begin{aligned}\frac{d\mathbf{R}_P}{dt} &= \frac{d}{dt} \left(R_I \cdot \mathbf{I} + R_J \cdot \mathbf{J} + R_K \cdot \mathbf{K} + r_i \cdot \hat{\mathbf{i}} + r_j \cdot \hat{\mathbf{j}} + r_k \cdot \hat{\mathbf{k}} \right) \\ &= \dot{R}_I \cdot \mathbf{I} + \dot{R}_J \cdot \mathbf{J} + \dot{R}_K \cdot \mathbf{K} + \frac{d}{dt} \left(r_i \cdot \hat{\mathbf{i}} + r_j \cdot \hat{\mathbf{j}} + r_k \cdot \hat{\mathbf{k}} \right) \\ &= \left(\dot{R}_I \cdot \mathbf{I} + \dot{R}_J \cdot \mathbf{J} + \dot{R}_K \cdot \mathbf{K} \right) + \left(\dot{r}_i \cdot \hat{\mathbf{i}} + \dot{r}_j \cdot \hat{\mathbf{j}} + \dot{r}_k \cdot \hat{\mathbf{k}} \right) + \left(r_i \cdot \frac{d\hat{\mathbf{i}}}{dt} + r_j \cdot \frac{d\hat{\mathbf{j}}}{dt} + r_k \cdot \frac{d\hat{\mathbf{k}}}{dt} \right)\end{aligned}\quad (2-43)$$

since $\frac{d\mathbf{I}}{dt} = \frac{d\mathbf{J}}{dt} = \frac{d\mathbf{K}}{dt} = 0$. This derivative is the derivative with respect to the inertial reference frame since the vector \mathbf{R}_P is expressed in F_I during the derivation (and is expressed in F_I after the derivation). This fact is incorporated in the notation as follows

$$\frac{d\mathbf{R}_P}{dt} \Big|_I^I = \left(\dot{R}_I \cdot \mathbf{I} + \dot{R}_J \cdot \mathbf{J} + \dot{R}_K \cdot \mathbf{K} \right) + \left(\dot{r}_i \cdot \hat{\mathbf{i}} + \dot{r}_j \cdot \hat{\mathbf{j}} + \dot{r}_k \cdot \hat{\mathbf{k}} \right) + \left(r_i \cdot \frac{d\hat{\mathbf{i}}}{dt} \Big|_I^I + r_j \cdot \frac{d\hat{\mathbf{j}}}{dt} \Big|_I^I + r_k \cdot \frac{d\hat{\mathbf{k}}}{dt} \Big|_I^I \right)\quad (2-44)$$

The subscript next to the sign $|$ denotes the reference frame in which the derivative is taken. The previous relation is a very important one and we will analyze it piece by piece. The first three terms on the right hand side denote the translation of the origin of the body fixed reference frame. We can also write these terms as

$$\dot{R}_I \cdot \mathbf{I} + \dot{R}_J \cdot \mathbf{J} + \dot{R}_K \cdot \mathbf{K} = \frac{d\mathbf{R}}{dt} \Big|_I^I = \mathbf{V}_G^I\quad (2-45)$$

The second group of terms, denote the relative time derivative of \mathbf{r} with respect to F_b . It is the change in vector \mathbf{r} as we would see it if we stand at the origin of F_b . We will write these terms as

$$\left(\dot{r}_i \cdot \hat{\mathbf{i}} + \dot{r}_j \cdot \hat{\mathbf{j}} + \dot{r}_k \cdot \hat{\mathbf{k}} \right) = \frac{d\mathbf{r}}{dt} \Big|_b^I = \frac{\partial \mathbf{r}}{\partial t}\quad (2-46)$$

where $\frac{\partial}{\partial t}$ denotes the derivative with respect to the body fixed reference frame. It is called the *relative derivative*. The last group of terms contain information regarding the rotation of F_b as we will see later on.

Moving, non-rotating reference frame

As we can already guess, the relation for the time derivative when the body fixed reference frame is non-rotating is given by

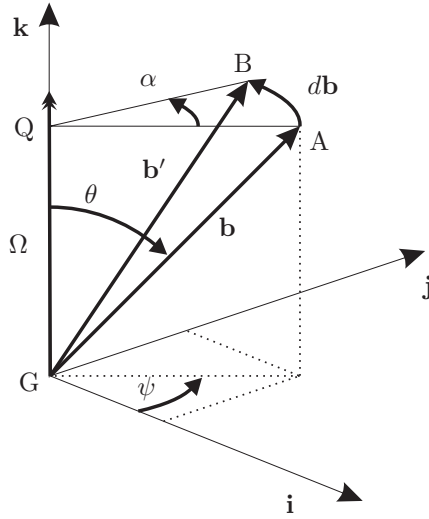
$$\begin{aligned}\frac{d\mathbf{R}_P}{dt} \Big|_I^I &= \left(\dot{R}_I \cdot \mathbf{I} + \dot{R}_J \cdot \mathbf{J} + \dot{R}_K \cdot \mathbf{K} \right) + \left(\dot{r}_i \cdot \hat{\mathbf{i}} + \dot{r}_j \cdot \hat{\mathbf{j}} + \dot{r}_k \cdot \hat{\mathbf{k}} \right) \\ &= \frac{d\mathbf{R}}{dt} \Big|_I^I + \frac{d\mathbf{r}}{dt} \Big|_b^I\end{aligned}\quad (2-47)$$

since the orientations (and the lengths) of the unit vectors $\mathbf{i}, \mathbf{j}, \mathbf{k}$ do not change.

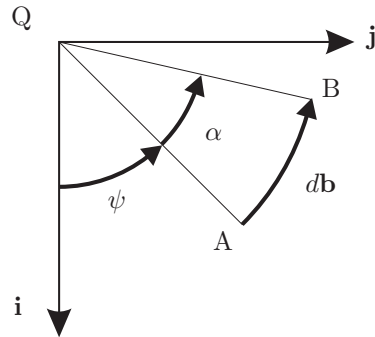
Non-moving, rotating reference frame

Now let us look at the situation where the body fixed reference frame is non-moving but rotating ($\frac{d\mathbf{R}}{dt} = 0$, angular velocity vector = $\boldsymbol{\Omega}$). In that case we have

$$\frac{d\mathbf{R}_P}{dt} \Big|_I^I = \left(\dot{r}_i \cdot \hat{\mathbf{i}} + \dot{r}_j \cdot \hat{\mathbf{j}} + \dot{r}_k \cdot \hat{\mathbf{k}} \right) + \left(r_i \cdot \frac{d\hat{\mathbf{i}}}{dt} \Big|_I^I + r_j \cdot \frac{d\hat{\mathbf{j}}}{dt} \Big|_I^I + r_k \cdot \frac{d\hat{\mathbf{k}}}{dt} \Big|_I^I \right)\quad (2-48)$$



(a) 3D view



(b) Top view

Figure 2-24: Change of a vector due to rotation vector Ω

We need the expressions of the unit vector time derivatives. To derive these expressions we will take a closer look at the change of a vector \mathbf{b} (of constant length) caused by a single rotation about the vector Ω (see figure 2-24). In the case that the rotation angle α goes to zero we have the following relation (α is replaced by the infinitely small angle $d\alpha$)

$$\lim_{\alpha \rightarrow 0} \{|d\mathbf{b}| = d\alpha |\mathbf{Q}\mathbf{A}| = d\alpha |\mathbf{b}| \sin \theta\} \quad (2-49)$$

We also have the following relation by definition

$$\frac{d\alpha}{dt} = |\Omega| \rightarrow d\alpha = |\Omega| dt \quad (2-50)$$

Combining relations we obtain

$$\lim_{\alpha \rightarrow 0} \{|d\mathbf{b}| = |\Omega| |\mathbf{b}| \sin \theta dt\} \rightarrow \left| \frac{d\mathbf{b}}{dt} \right| = |\Omega| |\mathbf{b}| \sin \theta \quad (2-51)$$

The latter equation is a scalar equation defining the relations between vector magnitudes and angles. The direction of $\left| \frac{d\mathbf{b}}{dt} \right|$ is perpendicular to the plane spanned by the vectors Ω and $\mathbf{Q}\mathbf{A}$,

thus we have

$$\frac{d\mathbf{b}}{dt} = \left| \frac{d\mathbf{b}}{dt} \right| \begin{bmatrix} -\sin \psi \\ \cos \psi \\ 0 \end{bmatrix} \quad (2-52)$$

Substituting the obtained relation for $\left| \frac{d\mathbf{b}}{dt} \right|$ gives

$$\frac{d\mathbf{b}}{dt} = |\boldsymbol{\Omega}| |\mathbf{b}| \sin \theta \begin{bmatrix} -\sin \psi \\ \cos \psi \\ 0 \end{bmatrix} = \begin{bmatrix} -|\boldsymbol{\Omega}| |\mathbf{b}| \sin \theta \sin \psi \\ |\boldsymbol{\Omega}| |\mathbf{b}| \sin \theta \cos \psi \\ 0 \end{bmatrix} \quad (2-53)$$

This relation is given exactly by the cross product of $\boldsymbol{\Omega}$ and \mathbf{b}

$$\boldsymbol{\Omega} \times \mathbf{b} = |\boldsymbol{\Omega}| \begin{bmatrix} 0 \\ 0 \\ 1 \end{bmatrix} \times |\mathbf{b}| \begin{bmatrix} \sin \theta \cos \psi \\ \sin \theta \sin \psi \\ 0 \end{bmatrix} = \begin{bmatrix} -|\boldsymbol{\Omega}| |\mathbf{b}| \sin \theta \sin \psi \\ |\boldsymbol{\Omega}| |\mathbf{b}| \sin \theta \cos \psi \\ 0 \end{bmatrix} \quad (2-54)$$

Thus we have the following important relation for the time derivative of a vector (of constant length) due to a rotation vector $\boldsymbol{\Omega}$

$$\frac{d\mathbf{b}}{dt} = \boldsymbol{\Omega} \times \mathbf{b} \quad (2-55)$$

Using this result in Eq. 2-48 yields

$$\begin{aligned} \frac{d\mathbf{R}_P}{dt} \Big|_I^I &= \left(\dot{r}_i \cdot \hat{\mathbf{i}} + \dot{r}_j \cdot \hat{\mathbf{j}} + \dot{r}_k \cdot \hat{\mathbf{k}} \right) + \left(r_i \cdot \frac{d\hat{\mathbf{i}}}{dt} \Big|_I^I + r_j \cdot \frac{d\hat{\mathbf{j}}}{dt} \Big|_I^I + r_k \cdot \frac{d\hat{\mathbf{k}}}{dt} \Big|_I^I \right) \\ &= \frac{dr}{dt} \Big|_b^I + r_i \cdot \boldsymbol{\Omega}_{bI}^I \times \hat{\mathbf{i}} + r_j \cdot \boldsymbol{\Omega}_{bI}^I \times \hat{\mathbf{j}} + r_k \cdot \boldsymbol{\Omega}_{bI}^I \times \hat{\mathbf{k}} \\ &= \frac{dr}{dt} \Big|_b^I + \boldsymbol{\Omega}_{bI}^I \times (r_i \cdot \hat{\mathbf{i}} + r_j \cdot \hat{\mathbf{j}} + r_k \cdot \hat{\mathbf{k}}) \\ &= \frac{dr}{dt} \Big|_b^I + \boldsymbol{\Omega}_{bI}^I \times \mathbf{r}^I \end{aligned} \quad (2-56)$$

The latter result is an important relation which is often used during the derivation of the equations of motion. Some remarks are in order:

- The time derivative $\frac{d\mathbf{r}}{dt} \Big|_b$ is the time derivative of the vector \mathbf{r} relative to the moving, rotating reference frame! It is the derivative of \mathbf{r} as seen by an observer standing in the origin of F_b .
- The rotation vector $\boldsymbol{\Omega}_{bI}$ denotes the relative angular velocity of reference frame F_b with respect to F_I . This angular velocity vector can be expressed in any reference frame as it is a vector. As usual, the superscript denotes in which reference frame it is expressed.
- The rotation vector has some useful properties:

- For any set of reference frames we have

$$\boldsymbol{\Omega}_{12}^2 = -\boldsymbol{\Omega}_{21}^2 \quad (2-57)$$

- and

$$\boldsymbol{\Omega}_{20}^2 = \boldsymbol{\Omega}_{21}^2 + \boldsymbol{\Omega}_{10}^2 \quad (2-58)$$

For mathematical proof of these two properties see [30], p. 228, as well as Section 2-3-2.

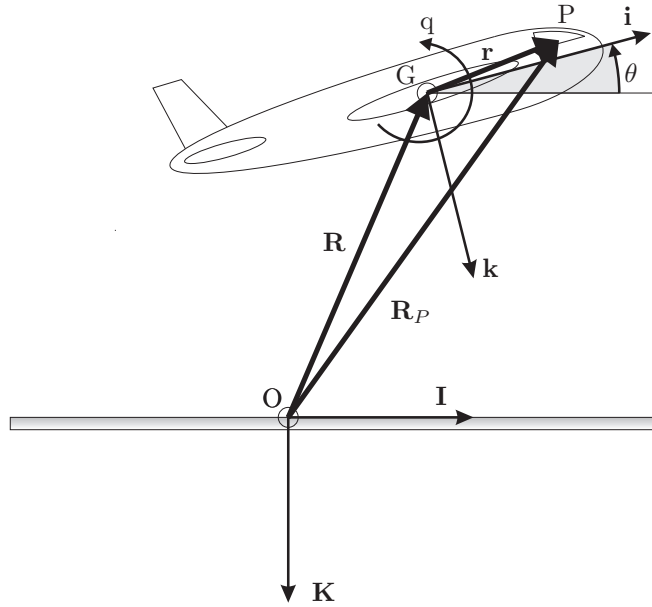


Figure 2-25: Example - derivation of pilot velocity with respect to F_E

Moving, rotating reference frame

If we combine the two relations obtained in the previous two sections, we get

$$\frac{d\mathbf{R}_P}{dt} \Big|_I = \frac{d\mathbf{R}}{dt} \Big|_I + \frac{d\mathbf{r}}{dt} \Big|_b + \boldsymbol{\Omega}_{bI} \times \mathbf{r} \quad (2-59)$$

This relation is valid for *any* two reference frames. Take one reference frame as the fixed (inertial) reference frame and let the other frame move with respect to the first. The most important aspect of this relation is that all terms should be expressed in the same reference frame otherwise the relation is not valid.

Example 2.1

Consider an aircraft with pitch angle θ (10 deg) and a pitch up rate q (5 deg/s) as depicted in Figure 2-25. The aircraft is flying with a speed of 200 m/s in the direction of \mathbf{I} at an altitude of 11 km at a distance of 5 km from point O , i.e. $\mathbf{R}^E = [5.10^3, 0, -11.10^3]^T$. The location of the pilot (point P) given with respect to the body fixed reference frame is $\mathbf{r}^b = [10, 0, -5]^T$. The vehicle carried normal Earth reference frame F_E is given by the quadruple $(O, \mathbf{I}, \mathbf{J}, \mathbf{K})$ and is fixed. The moving, rotating reference frame F_b is fixed to the aircraft in the center of gravity ($G, \mathbf{i}, \mathbf{j}, \mathbf{k}$). We will derive the velocity of the pilot with respect to F_E . The location of the pilot expressed in F_E is given by

$$\begin{aligned} \mathbf{R}_P^E &= \mathbf{R}^E + \mathbf{r}^E \\ &= R_I \cdot \mathbf{I} + R_J \cdot \mathbf{J} + R_K \cdot \mathbf{K} + r_I \cdot \mathbf{I} + r_J \cdot \mathbf{J} + r_K \cdot \mathbf{K} \\ &= R_I \cdot \mathbf{I} + R_J \cdot \mathbf{J} + R_K \cdot \mathbf{K} + \mathbb{T}_{lb}(r_i \cdot \hat{\mathbf{i}} + r_j \cdot \hat{\mathbf{j}} + r_k \cdot \hat{\mathbf{k}}) \\ &= R_I \cdot \mathbf{I} + R_J \cdot \mathbf{J} + R_K \cdot \mathbf{K} + r_i \cdot \hat{\mathbf{i}} + r_j \cdot \hat{\mathbf{j}} + r_k \cdot \hat{\mathbf{k}} \end{aligned} \quad (2-60)$$

This relation is given in inertial coordinates. The unit vectors of F_I are of course given by

$$\begin{aligned} \mathbf{I} &= [1 \ 0 \ 0]^T \\ \mathbf{J} &= [0 \ 1 \ 0]^T \\ \mathbf{K} &= [0 \ 0 \ 1]^T \end{aligned} \quad (2-61)$$

Since we have a single rotation, the transformation matrix is simply (see Section 2-2-5, $\psi = \phi = 0$)

$$\mathbb{T}_{Eb} = \mathbb{T}_{bE}^t = \begin{bmatrix} \cos \theta & 0 & \sin \theta \\ 0 & 1 & 0 \\ -\sin \theta & 0 & \cos \theta \end{bmatrix} \quad (2-62)$$

We can now express the unit vectors defining F_b in terms of F_o

$$\begin{aligned} \hat{\mathbf{i}} &= \mathbb{T}_{Eb}\mathbf{i} = \mathbb{T}_{Eb} \begin{bmatrix} 1 & 0 & 0 \end{bmatrix}^T = \begin{bmatrix} \cos \theta & 0 & -\sin \theta \end{bmatrix}^T \\ \hat{\mathbf{j}} &= \mathbb{T}_{Eb}\mathbf{j} = \mathbb{T}_{Eb} \begin{bmatrix} 0 & 1 & 0 \end{bmatrix}^T = \begin{bmatrix} 0 & 1 & 0 \end{bmatrix}^T \\ \hat{\mathbf{k}} &= \mathbb{T}_{Eb}\mathbf{k} = \mathbb{T}_{Eb} \begin{bmatrix} 0 & 0 & 1 \end{bmatrix}^T = \begin{bmatrix} \sin \theta & 0 & \cos \theta \end{bmatrix}^T \end{aligned} \quad (2-63)$$

Using previous results, the location of the pilot expressed in F_E is

$$\begin{aligned} \mathbf{R}_P^E &= \mathbf{R}^E + \mathbf{r}^E \\ &= \mathbf{R}^E + \mathbb{T}_{Ib}\mathbf{r}^b \\ &= \begin{bmatrix} 5.10^3 \\ 0 \\ -11.10^3 \end{bmatrix}^T + \begin{bmatrix} \cos 10^\circ & 0 & \sin 10^\circ \\ 0 & 1 & 0 \\ -\sin 10^\circ & 0 & \cos 10^\circ \end{bmatrix} \begin{bmatrix} 10 \\ 0 \\ -5 \end{bmatrix} \\ &= \begin{bmatrix} 5.10^3 + 10 \cos 10^\circ - 5 \sin 10^\circ \\ 0 \\ -11.10^3 - 10 \sin 10^\circ - 5 \cos 10^\circ \end{bmatrix} \\ &\approx \begin{bmatrix} 5008.98 \\ 0 \\ 11006.66 \end{bmatrix} \end{aligned} \quad (2-64)$$

The angular velocity of F_b with respect to F_E expressed in F_E is given by:

$$\boldsymbol{\Omega}_{bE}^E = \begin{bmatrix} 0 \\ q \\ 0 \end{bmatrix} \quad (2-65)$$

We now have all the information required to determine the velocity of point P with respect to F_E and expressed in F_E :

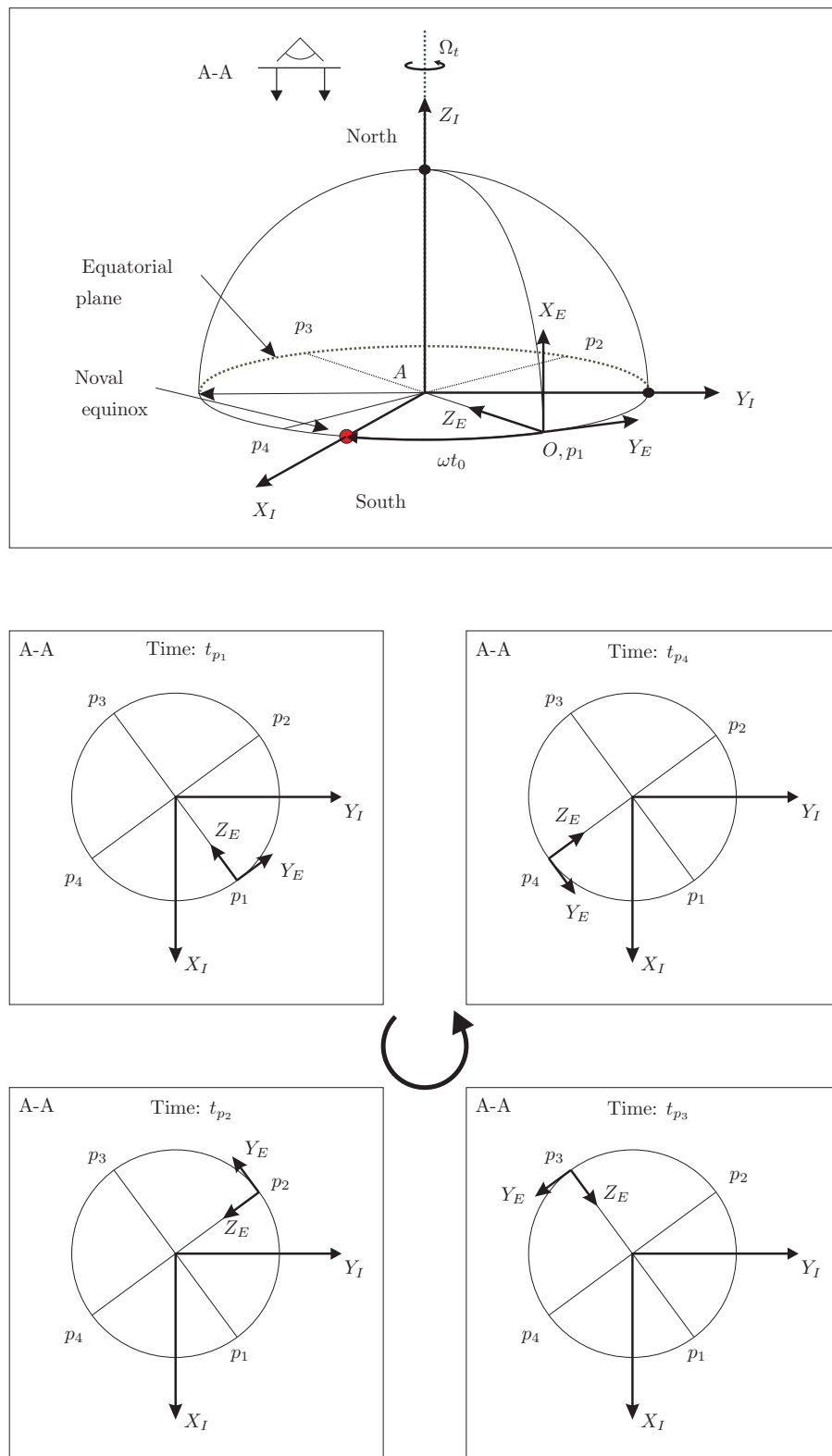
$$\begin{aligned} \mathbf{V}_P^E &= \frac{d\mathbf{R}_P}{dt} \Big|_E^E = \frac{d\mathbf{R}}{dt} \Big|_E^E + \frac{d\mathbf{r}}{dt} \Big|_b^E + \boldsymbol{\Omega}_{bE}^E \times \mathbf{r}^E \\ &= \begin{bmatrix} 200 \\ 0 \\ 0 \end{bmatrix} + \begin{bmatrix} 0 \\ 0 \\ 0 \end{bmatrix} + \begin{bmatrix} 0 \\ \frac{5\pi}{180} \\ 0 \end{bmatrix} \times \begin{bmatrix} 10 \cos 10^\circ - 5 \sin 10^\circ \\ 0 \\ -10 \sin 10^\circ - 5 \cos 10^\circ \end{bmatrix} \\ &= \begin{bmatrix} 200 + \frac{5\pi}{180} (-10 \sin 10^\circ - 5 \cos 10^\circ) \\ 0 \\ -\frac{5\pi}{180} (10 \cos 10^\circ - 5 \sin 10^\circ) \end{bmatrix} \end{aligned} \quad (2-66)$$

□

2-3-2 Derivation of the angular velocity vector

The rotational rate of one frame with respect to another can be derived on basis of the corresponding transformation matrix, or to be more precise, from the series of successive axis rotations. This will be illustrated with an example. Suppose we have a frame A , which will be rotated about the X -axis over an angle $d\alpha$, resulting in frame B (see Fig. 2-27a). The transformation matrix from frame A to frame B , \mathbb{T}_{BA} , can be obtained via a unit axis transformation

$$\mathbb{T}_{BA} = \mathbb{T}_x(d\alpha) \quad (2-67)$$

Figure 2-26: Angular velocity vector Ω_{EI}^E explanation

with \mathbb{T}_x given by (2-7).

If we have a look at the rotational rate of frame A with respect to frame B , we consider the rotation over $d\alpha$ to take place in a time interval dt . The rotational rate can therefore be expressed as $\dot{\alpha} = \frac{d\alpha}{dt}$. The orientation of this rotation vector must be collinear with the X_A -axis, of course, so

$$\boldsymbol{\Omega}_{BA} = \dot{\alpha} \mathbf{x}_A \quad (2-68)$$

with \mathbf{x}_A the unit vector in X -direction of the A -frame. Let us now introduce a second transformation, from frame B to frame C , and rotate about the Y -axis over an angle $d\beta$ (Fig. 2-27b).

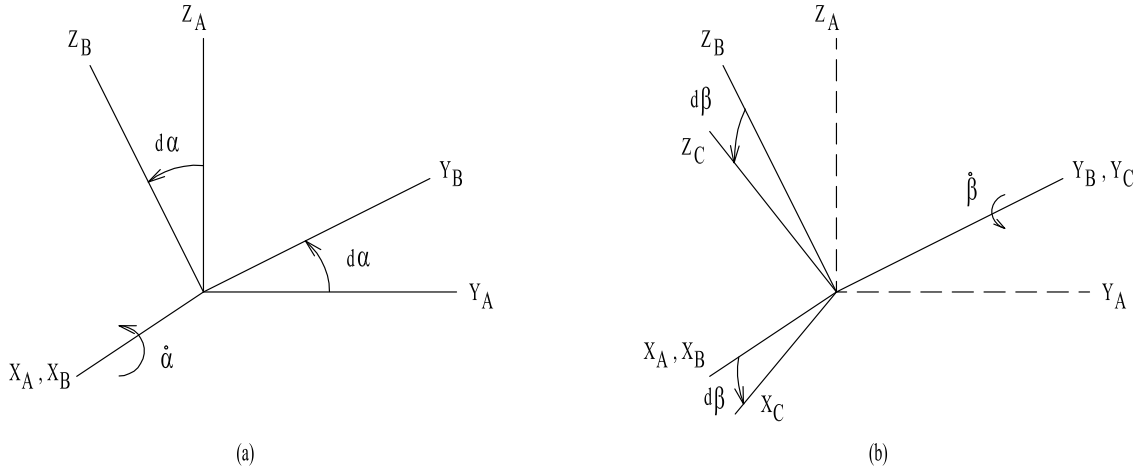


Figure 2-27: The transformation from frame A to frame B (a) and the one from frame B to frame C (b).

If we only had the rotation about the Y_B -axis, the rotational rate would have been, in accordance with the previous discussion:

$$\boldsymbol{\Omega}_{CB} = \dot{\beta} \mathbf{y}_B \quad (2-69)$$

The complete transformation matrix from frame A to frame C , \mathbb{T}_{CA} , is

$$\mathbb{T}_{CA} = \mathbb{T}_y(d\beta) \mathbb{T}_x(d\alpha) \quad (2-70)$$

Looking at the rotational rate of frame C with respect to frame A , we can decompose the rotation vector, just as we did with the transformation matrix:

$$\boldsymbol{\Omega}_{CA} = \boldsymbol{\Omega}_{CB} + \boldsymbol{\Omega}_{BA} \quad (2-71)$$

resulting in

$$\boldsymbol{\Omega}_{CA} = \dot{\beta} \mathbf{y}_B + \dot{\alpha} \mathbf{x}_A \quad (2-72)$$

Adding a third rotation, e.g., about the Z_C -axis over an angle $d\gamma$, resulting in frame D , gives for the transformation matrix

$$\begin{aligned} \mathbb{T}_{DA} &= \mathbb{T}_{DC} \mathbb{T}_{CB} \mathbb{T}_{BA} \\ &= |_D \mathbb{T}_z(d\gamma) |_C \mathbb{T}_y(d\beta) |_B \mathbb{T}_x(d\alpha) |_A \end{aligned} \quad (2-73)$$

and for the rotational rate

$$\begin{aligned}\boldsymbol{\Omega}_{DA} &= \boldsymbol{\Omega}_{DC} + \boldsymbol{\Omega}_{CB} + \boldsymbol{\Omega}_{BA} \\ &= \dot{\gamma}\mathbf{z}_C + \dot{\beta}\mathbf{y}_B + \dot{\alpha}\mathbf{x}_A\end{aligned}\tag{2-74}$$

The notation $\mathbb{T}_z(d\gamma)|_C$, as introduced above, makes it easy to derive the corresponding rotational rate: the index z means, that we are dealing with a rotation about the Z -axis, $|_C$ tells us that it is the Z_C -axis, and $d\gamma$ gives us the magnitude and direction of the rotational rate: $\dot{\gamma}$. Rotations about a negative angle will obviously get a minus sign in front of the rotational rate.

Note that if we derive the angular rate from the transformation matrix, the proof of Eq. (2-57) is easily given. For a given transformation matrix $\mathbb{T}_{AB} = \mathbb{T}_x(d\alpha)$ we know that the inverse transformation is given by its transpose. Effectively this means that $\mathbb{T}_{BA} = \mathbb{T}_x(-d\alpha)$, introducing a minus sign for the inverse rotation:

$$\boldsymbol{\Omega}_{BA} = -\boldsymbol{\Omega}_{AB}\tag{2-75}$$

Proof of Eq. (2-58) is more intuitive, and shown in Eqs. (2-73)-(2-74).

Chapter 3

Derivation of the Equations of Motion

3-1 Introduction

To describe the dynamics of a vehicle we need a model of that vehicle. The model we will use in subsequent chapters is governed by differential equations also known as the "Equations of Motion" (EOM). These EOM will be derived in this chapter. During the derivation the effects of rotating masses is not taken into account. It is assumed that the body is rigid.

The equations of motion are based on Newton's laws and are stated as follows (see [120] and [164]):

Newton's 1st law:

A body of constant mass is at rest or moves at a constant velocity, unless a force acts on the body.

Newton's 2nd law:

If a force acts on a body, the force is equal to the time derivative of the momentum, i.e. the product of mass and velocity of the body.

Newton's 3rd law:

If two bodies at rest, or moving at constant velocity, exert forces upon one another, the force on the first body is equal in magnitude but opposite in direction to the force of the second body.

Newton's laws are only valid when the motion of a body is expressed in an inertial reference frame, i.e., a frame with absolute translational velocity and absolute angular velocity equal to zero, or when it is expressed in a Galilean frame. A Galilean frame is one which is in rectilinear translation with respect to an inertial reference frame. This means that the angular velocity of such a frame is equal to zero and the translational velocity of the origin is constant. Normally, a reference frame based on stellar references is chosen as inertial reference frame. In these lecture notes, however, it is assumed that the absolute translational velocity of the Earth centered inertial reference frame F_I (see section 2-1-1) is negligible such that F_I can be seen as an inertial reference frame. The equations of motion will be derived with respect to the inertial reference frame F_I , but as explained in the previous chapter they can be expressed in any reference frame.

The general derivation can be found in C, as it is assumed to be common knowledge and should not hinder the flow of this chapter. Also, the common transition to rotating reference frames is discussed there. In this chapter, we will focus on the actual derivation of the equations of translational motion in the rotating E -frame, i.e., the vehicle-carried normal Earth reference frame. This can be found in Section 3-3. Then, in Section 3-4, the equations of rotational motion will be discussed. However, to have a better understanding of the external forces and moments driving the translational and rotational motion, we will begin this chapter with the external forces and moments are identified in 3-2.

Finally, at the end of section 3-5 the EOM for a flat, non-rotating Earth are derived. This section of EOM will be used in subsequent chapter to explain aircraft dynamics. A simple set of EOM is used to ensure a clear explanation.

3-2 External forces and moments

One could define three types of forces acting on an aircraft, originating from:

1. Gravity
2. Aerodynamics
3. Propulsion

The first two types of forces are by nature distributed forces. To make the equations of motion more easy to read, these distributed forces are 'replaced' by point forces acting at particular points on the body. Summation of all point forces will result in the total resultant force.

In general these forces will generate a moment about the point of reference, which on the aircraft is chosen at the center of gravity. This choice is made for two reasons. Firstly, the force due to gravity will not cause a moment since it acts at the center of gravity. Secondly, the center of gravity is also the origin of the body-fixed reference system such that no additional reference frames are needed.

External forces will be discussed first, next to be followed by the external moments.

3-2-1 External forces

We first consider the gravity vector.

Gravity

Using the assumption of a spherical Earth, the gravity vector is expressed in the vehicle carried normal Earth reference frame F_E as:

$$\mathbf{g}_G^E = \mathbf{g}_{r,G}^E = \begin{bmatrix} 0 \\ 0 \\ \frac{G m_t}{(R_t + h)^2} \end{bmatrix} \quad (3-1)$$

where:

G	: the constant of gravitation	$(6.664 \cdot 10^{-11} \text{ SI})$
m_t	: Earth total mass	$(5.983 \cdot 10^{24} \text{ kg})$
R_t	: mean Earth radius	$(6.368 \cdot 10^6 \text{ m})$

The gravity vector can be rewritten as a function of the gravity at zero altitude $\mathbf{g}_{r,0}$:

$$\mathbf{g}_{r,0} = \frac{g m_t}{R_t^2} \quad (3-2)$$

$$\mathbf{g}_r = \frac{\mathbf{g}_{r,0}}{\left(1 + \frac{h}{R_t}\right)^2} \quad (3-3)$$

When investigating Eq. (3-3) one can see that the gravity does not vary much with altitude. To have a difference of 1% in gravity one would have to travel 32 km in height:

$$\frac{\mathbf{g}_{r,2} - \mathbf{g}_{r,0}}{\mathbf{g}_{r,0}} = -0.01 = \frac{1}{\left(1 + \frac{h_2}{R_t}\right)^2} - 1 \quad (3-4)$$

$$\left(1 + \frac{h_2}{R_t}\right)^2 = \frac{1}{0.99} \quad (3-5)$$

$$h_2 = R_t \left(\sqrt{\frac{1}{0.99}} - 1 \right) \quad (3-6)$$

$$\approx 32 \text{ km} \quad (3-7)$$

This means that for normal aircraft the gravity vector magnitude can be assumed to be constant. For spaceflight, however, the distances traveled in height are much larger creating larger changes in gravity, and the variation of the magnitude of gravity can no longer be neglected. Another issue is the fact that the gravity experienced by a body traveling over the Earth surface changes with latitude. This effect is caused by the flattening of the Earth. A simple model for the gravity at zero altitude as a function of latitude was developed by Somigliana in 1929. The numerical version of that model is given by Eq. (3-8) (Ref. [30]).

$$g_{r,0} = 9.8703 (1.00335 + 0.00195 \sin^2 \delta) \quad (3-8)$$

where $g_{r,0}$ is the magnitude of the gravity.

To determine the gravity force one has to multiply the gravity acceleration with the total mass of the body. This force is also known as the weight of the body, i.e.

$$\mathbf{F}_G^E = \mathbf{W}_G^E = m \mathbf{g}_G^E \quad (3-9)$$

Aerodynamic forces

The flow of particles around a body creates pressure differences that cause the body to experience a force. For flight dynamics the considered particles are air particles, hence the forces are called aerodynamic forces. The overall resultant aerodynamic force which acts on the body can be composed by a summation of aerodynamic forces which act on each part of the aircraft. This includes the forces generated by the aerodynamic surfaces and by the engines, i.e. thrust. The thrust can be seen as an aerodynamic force since an engine creates disturbances in the airflow such that the aircraft is pulled forward.

The resultant aerodynamic force is usually decomposed into either the body-fixed reference frame or the aerodynamic reference frame. The decomposition into the body-fixed reference frame is denoted as:

$$\mathbf{F}_A^b = \begin{bmatrix} X^b \\ Y^b \\ Z^b \end{bmatrix} \quad (3-10)$$

The decomposition into the aerodynamic reference frame F_a is denoted as:

$$\mathbf{F}_A^a = \begin{bmatrix} X^a \\ Y^a \\ Z^a \end{bmatrix} \quad (3-11)$$

The two decompositions of the resultant aerodynamic force are related as follows:

$$\begin{aligned} \mathbf{F}_A^b &= \mathbb{T}_{ba} \mathbf{F}_A^a \\ \begin{bmatrix} X^b \\ Y^b \\ Z^b \end{bmatrix} &= \begin{bmatrix} \cos \beta_a \cos \alpha_a & -\sin \beta_a \cos \alpha_a & -\sin \alpha_a \\ \sin \beta_a & \cos \beta_a & 0 \\ \cos \beta_a \sin \alpha_a & -\sin \beta_a \sin \alpha_a & \cos \alpha_a \end{bmatrix} \begin{bmatrix} X^a \\ Y^a \\ Z^a \end{bmatrix} \end{aligned} \quad (3-12)$$

Propulsion forces

In aircraft dynamics studies it sometimes occurs that the propulsion force, or thrust, is included in the aerodynamic force. However, when extending the study of dynamics to spacecraft, for conventional launch vehicles (rockets) it is common to define the propulsion force separate from the aerodynamics. In case of air-breathing propulsion engines (RAM- and SCRAM-jets), applied in future launcher concepts (spaceplanes), the *calculation* of the propulsion forces is usually combined with the aerodynamics calculation, but the individual components are separated to get an aerodynamics force and a propulsion force. Therefore, while deriving the equations of motion we will consider an individual propulsion force. Similarly, if thrust-vector control is possible, a propulsion moment will be the result, that should be treated independently from the aerodynamic moment. Thrust vector control with launch vehicles is achieved by actively changing the orientation of the exhaust nozzle, thus creating a change in direction of the exhaust flow. This has a different direction of the propulsion force as result, and since the operating point of the propulsion force is not the center of gravity, it will create a propulsion moment. However, certain fighter jets also have active thrust-vector control. And, do no forget the case of a commercial airliner with two engines: if one of the engines fails, a very strong propulsion moment arises that has to be compensated for by the rudder (and vertical tail).

In these lecture notes, we assume that the propulsion force is defined in the body-fixed reference frame, F_b , and is defined as \mathbf{F}_P^b . The decomposition is denoted as:

$$\mathbf{F}_P^b = \begin{bmatrix} F_{P,x}^b \\ F_{P,y}^b \\ F_{P,z}^b \end{bmatrix} \quad (3-13)$$

3-2-2 External moments

The external moments are usually defined about the center of gravity G . Of course the point where the external forces act on the body can differ from the center of gravity, and they will then cause a moment about the center of gravity. In this section the external forces are reviewed to find out whether they produce additional moments about the center of gravity.

Gravity

Since the gravity force mg_G acts in the center of gravity, it will not cause a moment about the center of gravity.

Aerodynamic forces

The resultant aerodynamic force typically does not act in the center of gravity. It therefore causes a moment about the center of gravity. The resultant aerodynamic moment is defined in the body-fixed reference frame as:

$$\mathbf{M}_{A,G}^b = \begin{bmatrix} L^b \\ M^b \\ N^b \end{bmatrix}$$

The resultant aerodynamic moment is defined in the aerodynamic reference frame as:

$$\mathbf{M}_{A,G}^a = \begin{bmatrix} L^a \\ M^a \\ N^a \end{bmatrix} \quad (3-14)$$

Further details about the aerodynamic moment about the center of gravity will be given in chapter 4.

Propulsion forces

In case the propulsion force has a distinct operating point, and the direction of the thrust force can be changed such that the operating line does not pass through the center of gravity, a propulsion moment is the result. This moment is defined in the body reference frame, given by:

$$\mathbf{M}_{P,G}^b = \begin{bmatrix} M_{P,x}^b \\ M_{P,y}^b \\ M_{P,z}^b \end{bmatrix} \quad (3-15)$$

3-3 The Equations of Translational Motion

With the relatively low speeds encountered by present-day aircraft and spacecraft (that is, when compared to the speed of light), we can use classical or Newtonian mechanics to describe the motion of a vehicle flying in a planetary atmosphere. This kind of mechanics is based on the three Laws of Motion of Newton, Galileo's principle of relativity and the three classical conservation laws: conservation of mass, linear momentum and energy. This has been extensively treated in Appendix C, where the basic formulation of the equations of motion has been derived. In this chapter, we will start the discussion on the equations of translational motion by looking at the motion of a vehicle with respect to inertial space (Section 3-3-1). After presenting the general formulation, we will introduce and discuss the forces which arise from a variable mass of the vehicle. We conclude this section with addressing a Cartesian expression for the position and velocity. In Section 3-3-2, the motion of a vehicle when using a moving (or rotating) frame as a reference is described. After introducing the general formulation of the equations of motion, expressions when using Cartesian and spherical components for the position and velocity will pass review (Section 3-3-3).

3-3-1 Motion with respect to inertial space

Let us assume, that an arbitrary vehicle with variable mass m is subjected to an external force \mathbf{F}_{ext}^I . The vehicle (or, more precisely, the centre of mass, c.o.m.) is moving at a distance \mathbf{r}_{cm}^I from the origin of the inertial reference frame with an inertial velocity \mathbf{V}_I^I . Although we are discussing the translation of the c.o.m. of the vehicle, we will also assume that the vehicle (as a body, not as

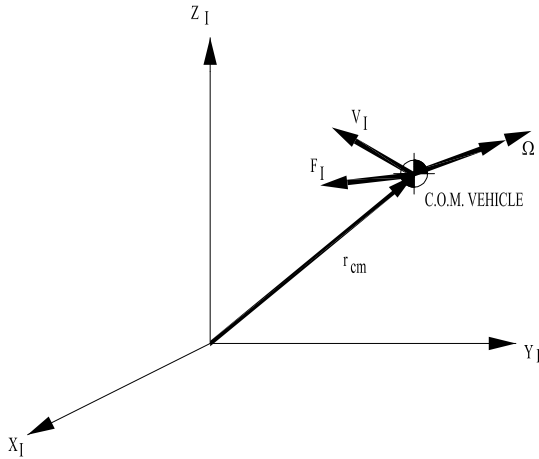


Figure 3-1: The motion of a body with respect to inertial space.

a mass point) is rotating w.r.t. the inertial frame, in order to derive an apparent force due to the rotation of the body with varying mass. The rotation¹ is given by Ω_{bI}^I . This situation is depicted in Fig. 3-1.

Starting with Newton's laws of motion, in Appendix C it was shown that the motion of this mass-varying body can be described as:

$$\mathbf{F}_{ext}^I = m \frac{d^2 \mathbf{r}_{cm}^I}{dt^2} + 2\Omega_{bI}^I \times \int_m \frac{\delta \tilde{\mathbf{r}}}{\delta t} dm + \int_m \frac{\delta^2 \tilde{\mathbf{r}}}{\delta t^2} dm \quad (3-16)$$

or

$$\mathbf{F}_{ext}^I + \mathbf{F}_C^I + \mathbf{F}_{rel}^I = m \frac{d^2 \mathbf{r}_{cm}^I}{dt^2} = m \frac{d\mathbf{V}_I^I}{dt} \quad (3-17)$$

In the above equations, the several terms have the following meaning:

\mathbf{F}_{ext}^I	= total of the external forces expressed in components of the inertial frame (N)
$\frac{d^2 \mathbf{r}_{cm}^I}{dt^2}$	= acceleration of the c.o.m. with respect to the inertial frame (m/s^2)
$\mathbf{F}_C^I = -2\Omega_{bI}^I \times \int_m \frac{\delta \tilde{\mathbf{r}}}{\delta t} dm$	= Coriolis force, due to time variations in mass distribution (N)
$\mathbf{F}_{rel}^I = - \int_m \frac{\delta^2 \tilde{\mathbf{r}}}{\delta t^2} dm$	= relative force, due to time variations in mass distribution (N)
$\Omega_{bI}^I = (p, q, r)^T$	= the rotation vector of the body frame with respect to the inertial frame, expressed in components along the inertial axes
$\tilde{\mathbf{r}}$	= the location of a mass element with respect to the c.o.m. of the vehicle (m)

Note that the notation $\frac{\delta \cdot}{\delta t}$ means that the derivative is taken of a vector expressed in the local (body) frame, as compared with $\frac{d \cdot}{dt}$, which is taken of a vector expressed in the inertial frame.

¹The rotational rate of, for instance, an aircraft, is commonly given by the components roll, pitch and yaw rate. This rotational rate is mathematically the rotational rate of the body frame with respect to the inertial frame, expressed in body-frame components, Ω_{bI}^b . In this section, the roll-rate components need to be expressed in the inertial frame to be consistent with other components.

For a rigid body (non-elastic body with constant mass), the Coriolis and relative force are zero, because the two (local) derivatives are zero, and the translational equation takes the familiar form:

$$\mathbf{F}_{ext}^I = m \frac{d^2 \mathbf{r}_{cm}^I}{dt^2} \quad (3-18)$$

Eq. (3-18) is a dynamic equation, meaning that it describes the motion of a body under the influence of external forces. The corresponding change in position can be described by the kinematic equation:

$$\frac{d\mathbf{r}_{cm}^I}{dt} = \mathbf{V}_I^I \quad (3-19)$$

Eq. (3-17), the equation of translational motion for a non-elastic mass-varying body has the same form as the one for a rigid body (and, as we will see in Section 3-4 the same is true for the equations of rotational motion). An important principle is involved here, the *Principle of Solidification*. This principle states [97] that *in general, equations of translational and rotational motion of an arbitrary variable mass system at time t can be written as the translational and rotational equations for a rigid body with mass M equal to the mass of the system at time t, while in addition to the true external forces and moments, two apparent forces and moments are applied: the Coriolis and relative forces and moments, respectively.*

3-3-2 Motion with respect to a rotating frame

Let us consider a vehicle with (variable) mass m , moving with a velocity \mathbf{V}_C with respect to the rotating Earth-Centered Earth-Fixed frame (index C) at a distance \mathbf{r}_{cm}^C from the centre of the central body (see Fig. 3-2). The vehicle is subjected to an external force \mathbf{F}_{ext}^C and has a rotation $\boldsymbol{\Omega}_{bI}^b$ w.r.t. the inertial planetocentric frame. The C -frame is fixed to the central body (with the origin in its c.o.m.) and rotates with an angular velocity $\boldsymbol{\Omega}_{CI}^C = (0, 0, \Omega_t)^T$.

For the equations of translational motion, the vehicle can be considered to be a mass point. Newton's Second Law, which describes the translational motion of a point mass with respect to an inertial frame, can be adjusted to be valid for a mass-varying system w.r.t. the rotating C -frame, as has been discussed at length in Appendix C:

$$\mathbf{F}_{ext}^C = m \frac{d^2 \mathbf{r}_{cm}^C}{dt^2} + 2m\boldsymbol{\Omega}_{CI}^C \times \frac{d\mathbf{r}_{cm}^C}{dt} + m\boldsymbol{\Omega}_{CI}^C \times (\boldsymbol{\Omega}_{CI}^C \times \mathbf{r}_{cm}^C) \quad (3-20)$$

or, remembering that $\frac{d\mathbf{r}_{cm}^C}{dt} = \mathbf{V}_C^C$,

$$m \frac{d\mathbf{V}_C^C}{dt} = \mathbf{F}_{ext}^C - 2m\boldsymbol{\Omega}_{CI}^C \times \mathbf{V}_C^C - m\boldsymbol{\Omega}_{CI}^C \times (\boldsymbol{\Omega}_{CI}^C \times \mathbf{r}_{cm}^C) \quad (3-21)$$

with

$\mathbf{V}_C^C = \frac{d\mathbf{r}_{cm}^C}{dt}$	=	relative velocity of the vehicle in the rotating frame C , expressed in components of C (m/s)
\mathbf{F}_{ext}^C	=	summation of all external forces acting on the vehicle, expressed in the C -frame (N)
$2\boldsymbol{\Omega}_{CI}^C \times \mathbf{V}_C^C$	=	apparent Coriolis acceleration due to the rotation of the frame (m/s^2)

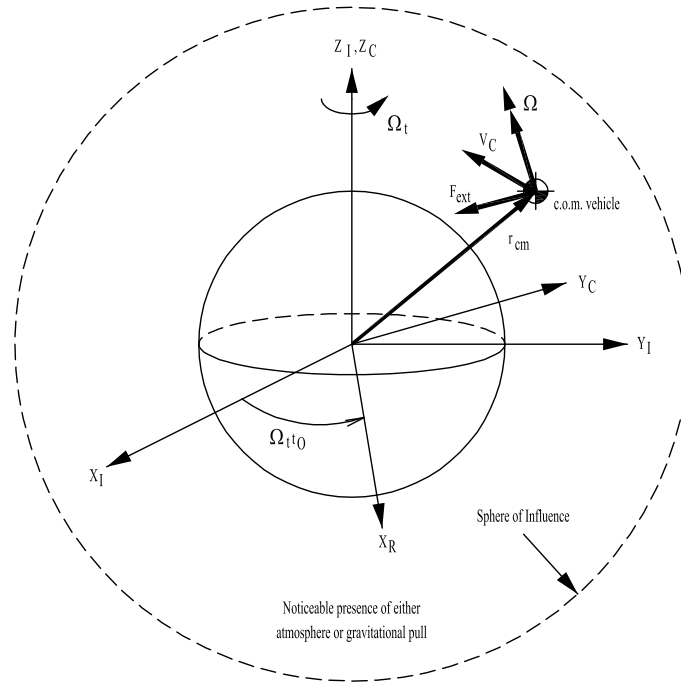


Figure 3-2: Definition of a vehicle moving in the sphere of influence of a celestial body. The inertial reference frame is indicated with index I . The Earth-centered Earth-fixed reference frame, with index C , is rigidly attached to the Earth and rotates with an angular velocity Ω_t , which is identical to the rotational rate of the Earth.

$$\begin{aligned}
 \boldsymbol{\Omega}_{CI}^C \times (\boldsymbol{\Omega}_{CI}^C \times \mathbf{r}_{cm}^C) &= \text{apparent transport acceleration of the vehicle due to angular rate of the rotating frame (m/s}^2\text{)} \\
 \frac{d^2 \mathbf{r}_{cm}^C}{dt^2} &= \text{acceleration of the vehicle in the rotating frame (m/s}^2\text{)} \\
 \boldsymbol{\Omega}_{CI}^C &= \text{the rotational rate of the } C\text{-frame, which is equal to the rotational rate of the central body (rad/s)}
 \end{aligned}$$

Note that in the above equation, we have assumed that the Coriolis force due to the variation in mass properties can be neglected. The relative force (or impulse thrust) is part of the external force vector.

Eq. (3-21) resolves the velocity vector in the rotating planetocentric frame. To obtain the position of the vehicle with respect to the same frame, we can simply write

$$\frac{d\mathbf{r}_{cm}^C}{dt} = \mathbf{V}_C^C \quad (3-22)$$

the so-called kinematic equation.

The position \mathbf{r}_{cm}^C and velocity \mathbf{V}_C^C can be expressed in either Cartesian or spherical coordinates, resulting in different equations of motion and a different strategy of solving these equations. In the following section, we will look at the combination of spherical components for the position and Cartesian components for the velocity.

3-3-3 Spherical position and Cartesian velocity

The definition of the spherical position is given by the familiar form of R , τ and δ (distance to center of the Earth, longitude and latitude), whereas the velocity is defined by the three Cartesian

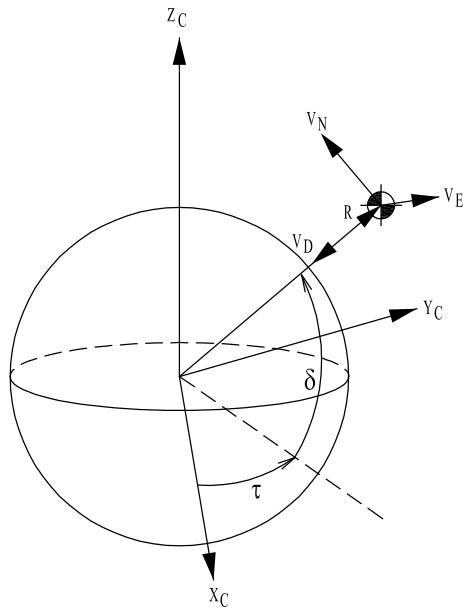


Figure 3-3: Definition of spherical position and Cartesian velocity.

components in the vehicle carried normal Earth reference frame (index E), V_N , V_E and V_D (see also Fig. 3-3). These components are in north, east and down direction.

Starting with the general formulation Eq. (3-21), it is easy to understand that not all of the available components are expressed in one and the same frame. To find scalar expressions for each of the three velocity derivatives, we will express each component, i.e., $\frac{d\mathbf{V}_C^E}{dt}$, $\frac{d\mathbf{r}_{cm}^C}{dt}$, \mathbf{F}_{ext}^C , $\boldsymbol{\Omega}_{CI}^C$, \mathbf{r}_{cm}^C and \mathbf{V}_C^E , in the E -frame.

Velocity vector \mathbf{V}_C^E

By definition the velocity vector expressed in one rotating frame will not change in magnitude when transforming it to another rotating reference frame. Therefore, the velocity w.r.t. the Earth-Centered Earth-Fixed reference frame will only change in the individual components when transforming to the E -frame. Therefore, with the definition given in Fig. 3-3, we can easily write the following relation:

$$\mathbf{V}_C^E = V_N \mathbf{x}_E + V_E \mathbf{y}_E + V_D \mathbf{z}_E \quad (3-23)$$

Position vector \mathbf{r}_{cm}^C

By definition of the E -frame - the negative Z_E -axis along \mathbf{r}_{cm} - the following equation holds:

$$\mathbf{r}_{cm}^E = -R \mathbf{z}_E \quad (3-24)$$

Rotation vector $\boldsymbol{\Omega}_{CI}^C$

The equation, which we have to solve is

$$\boldsymbol{\Omega}_{CI}^E = \mathbb{T}_{EC} \boldsymbol{\Omega}_{CI}^C \quad (3-25)$$

with Ω_{CI}^C given by $(0, 0, \Omega_t)^T$ and \mathbb{T}_{EC} given by Eq. (2-17), i.e.,

$$\mathbb{T}_{EC} = \begin{bmatrix} -c\tau s\delta & -s\tau s\delta & c\delta \\ -s\tau & c\tau & 0 \\ -c\tau c\delta & -s\tau c\delta & -s\delta \end{bmatrix} \quad (3-26)$$

where we have used the shorthand notation 'c' for *cosine* and 's' for *sine*. Eq. (3-25) results in

$$\Omega_{CI}^E = \Omega_t \cos \delta \mathbf{x}_E - \Omega_t \sin \delta \mathbf{z}_E \quad (3-27)$$

External forces \mathbf{F}_{ext}^C

The external forces have an aerodynamic, a thrust and a gravitational component, each of which are available in a different reference frame. Assuming there is no wind, the aerodynamic force is given w.r.t. the aerodynamic frame (index a), the thrust force is expressed in body-frame components and the gravitational force is either expressed in Cartesian C -frame components or spherical components in a frame similar to the E -frame. As discussed in Section 3-2, we will stick to the spherical definition. We will now look at the transformation of these forces to the E -frame.

For the aerodynamic force, we find

$$\mathbf{F}_A^E = \mathbb{T}_{Ea} \mathbf{F}_A^a \quad (3-28)$$

In Section 2-2-6, Eq. (2-21), \mathbb{T}_{aE} has been defined. We can calculate \mathbb{T}_{Ea} by transposing \mathbb{T}_{aE} (note again that the inverse transformation matrix is the transpose).

The propulsion force can be obtained with

$$\mathbf{F}_P^E = \mathbb{T}_{Eb} \mathbf{F}_P^b \quad (3-29)$$

where \mathbb{T}_{Eb} and \mathbf{F}_P^b are given by Eqs. (2-29) and (3-13), respectively.

The gravitational force, finally, is derived from Eq. (3-1) by multiplying this gravitational acceleration with the vehicle mass, m . As can be seen, \mathbf{g}_G^E is already defined in F_E , and thus also $\mathbf{F}_G^E = m \mathbf{g}_G^E$.

The total external force, \mathbf{F}_{ext}^E , is now written as

$$\mathbf{F}_{ext}^E = (F_x^E, F_y^E, F_z^E)^T = \mathbf{F}_A^E + \mathbf{F}_P^E + \mathbf{F}_G^E \quad (3-30)$$

Angular velocity of the E -frame

The last component that we need to evaluate the derivatives $\frac{d\mathbf{v}_C^C}{dt}$ and $\frac{d\mathbf{r}_{cm}^C}{dt}$ is the angular velocity of the E -frame. The orientation of the E -frame w.r.t. the C -frame, which depends on the position of the vehicle, or, to be more precise, on τ and δ . With the continuous motion of the vehicle, the E -frame has an angular velocity Ω_{EC} w.r.t. the C -frame. This rotation can be obtained from the corresponding transformation matrix (see Section 2-3-2).

While

$$\mathbb{T}_{EC} = |_E \mathbb{T}_y(-\frac{\pi}{2} - \delta) \mathbb{T}_z(\tau)|_C$$

we get

$$\boldsymbol{\Omega}_{EC} = -\dot{\delta}\mathbf{y}_E + \dot{\tau}\mathbf{z}_C \quad (3-31)$$

Note that the notation $|_E$ and $|_C$ indicates that at the corresponding place in the expression, a vector would be defined w.r.t. the E and C -frame, respectively. In the above case, it means that the transformation starts in the C -frame (right indication), after the rotation about the Z_C -axis an intermediate frame is reached (not indicated), and, finally, after a rotation about the Y -axis of the intermediate frame (which is equal to Y_E), we have reached the E -frame (left indication). See also Section 2-3-2.

To express \mathbf{z}_C in the direction of \mathbf{x}_E , \mathbf{y}_E and \mathbf{z}_E , we write:

$$[\mathbf{x}_C \mathbf{y}_C \mathbf{z}_C] = \mathbb{T}_{CE} [\mathbf{x}_E \mathbf{y}_E \mathbf{z}_E] \quad (3-32)$$

Transposing the matrix of Eq. (2-16), \mathbb{T}_{EC} , and carrying out the multiplication in Eq. (3-32) it follows for \mathbf{z}_C that

$$\mathbf{z}_C = \cos \delta \mathbf{x}_E - \sin \delta \mathbf{z}_E$$

and finally for $\boldsymbol{\Omega}_{EC}^E$:

$$\boldsymbol{\Omega}_{EC}^E = \dot{\tau} \cos \delta \mathbf{x}_E - \dot{\delta} \mathbf{y}_E - \dot{\tau} \sin \delta \mathbf{z}_E \quad (3-33)$$

Now, we have derived all the terms to evaluate the derivatives $\frac{d\mathbf{v}_C^C}{dt}$ and $\frac{d\mathbf{r}_{cm}^C}{dt}$.

The kinematic equations

As has been stated before, the kinematic equation is given by

$$\mathbf{V}_C^C = \frac{d\mathbf{r}_{cm}^C}{dt} \quad (3-34)$$

Substituting Eq. (3-24) gives

$$\frac{d\mathbf{r}_{cm}^E}{dt} = -\frac{dR}{dt} \mathbf{z}_E - R \frac{d\mathbf{z}_E}{dt} \quad (3-35)$$

For the time derivatives of each of the unit vectors \mathbf{x}_E , \mathbf{y}_E and \mathbf{z}_E we can write, as explained in Appendix C:

$$\begin{aligned} \frac{d\mathbf{x}_E}{dt} &= \boldsymbol{\Omega}_{EC}^E \times \mathbf{x}_E = -\dot{\tau} \sin \delta \mathbf{y}_E + \dot{\delta} \mathbf{z}_E \\ \frac{d\mathbf{y}_E}{dt} &= \boldsymbol{\Omega}_{EC}^E \times \mathbf{y}_E = \dot{\tau} \sin \delta \mathbf{x}_E + \dot{\tau} \cos \delta \mathbf{z}_E \\ \frac{d\mathbf{z}_E}{dt} &= \boldsymbol{\Omega}_{EC}^E \times \mathbf{z}_E = -\dot{\delta} \mathbf{x}_E - \dot{\tau} \cos \delta \mathbf{y}_E \end{aligned} \quad (3-36)$$

Here, we have used Eq. (3-33). Substituting Eq. (3-36c) in Eq. (3-35) yields

$$\frac{d\mathbf{r}_{cm}^E}{dt} = R \dot{\delta} \mathbf{x}_E + R \cos \delta \dot{\tau} \mathbf{y}_E - \dot{R} \mathbf{z}_E \quad (3-37)$$

Equating Eqs. (3-23) and (3-37), finally, results in the kinematic equations:

$$\dot{\delta} = \frac{V_N}{R} \quad (3-38)$$

$$\dot{\tau} = \frac{V_E}{R \cos \delta} \quad (3-39)$$

$$\dot{R} = -V_D \quad (3-40)$$

The dynamic equations

For the derivation of the dynamic equations, we have to evaluate three terms, i.e., the relative, Coriolis and transport acceleration, $\left[\frac{d\mathbf{V}_C^C}{dt} \right]_E$, $[2\boldsymbol{\Omega}_{CI}^C \times \mathbf{V}_C^C]_E$ and $[\boldsymbol{\Omega}_{CI}^C \times (\boldsymbol{\omega}_{CI}^C \times \mathbf{r}_{cm})]_E$. We will begin with the relative acceleration.

$$\begin{aligned} \left[\frac{d\mathbf{V}_C^C}{dt} \right]_E &= \frac{d}{dt} (V_N \mathbf{x}_E + V_E \mathbf{y}_E + V_D \mathbf{z}_E) \\ &= \dot{V}_N \mathbf{x}_E + V_N \frac{d\mathbf{x}_E}{dt} + \dot{V}_E \mathbf{y}_E + V_E \frac{d\mathbf{y}_E}{dt} + \dot{V}_D \mathbf{z}_E + V_D \frac{d\mathbf{z}_E}{dt} \end{aligned} \quad (3-41)$$

Substituting Eqs. (3-36) for the time derivatives of the unit vectors yields

$$\begin{aligned} \left[\frac{d\mathbf{V}_C^C}{dt} \right]_E &= (\dot{V}_N + \dot{\tau} V_E \sin \delta - \dot{\delta} V_D) \mathbf{x}_E + (\dot{V}_E - \dot{\tau} V_N \sin \delta - \dot{\tau} V_D \cos \delta) \mathbf{y}_E \\ &\quad + (\dot{V}_D + \dot{\delta} V_N + \dot{\tau} V_E \cos \delta) \mathbf{z}_E \end{aligned} \quad (3-42)$$

After expanding the vectorial multiplication for the Coriolis acceleration we obtain, using Eqs. (3-23) and (3-27):

$$[2\boldsymbol{\Omega}_{CI}^C \times \mathbf{V}_C^C]_E = 2\Omega_t [V_E \sin \delta \mathbf{x}_E - (V_D \cos \delta + V_N \sin \delta) \mathbf{y}_E + V_E \cos \delta \mathbf{z}_E] \quad (3-43)$$

and the double vector product to get the transport acceleration results in

$$[\boldsymbol{\Omega}_{CI}^C \times (\boldsymbol{\omega}_{CI}^C \times \mathbf{r}_{cm})]_E = \Omega_t^2 r \cos \delta (\sin \delta \mathbf{x}_E + \cos \delta \mathbf{z}_E) \quad (3-44)$$

Together with Eq. (3-30) for the external forces, we have expressed all components in the E -frame. If we substitute Eq. (3-30) and Eqs. (3-42) through (3-44) in Eq. (3-21), equate each of the three components along \mathbf{x}_E , \mathbf{y}_E and \mathbf{z}_E , this will give three scalar equations

$$\begin{aligned} \mathbf{x}_E : \dot{V}_N + \dot{\tau} V_E \sin \delta - \dot{\delta} V_D &= \frac{F_x^E}{m} - 2\Omega_t V_E \sin \delta - \Omega_t^2 R \sin \delta \cos \delta \\ \mathbf{y}_E : \dot{V}_E - \dot{\tau} V_N \sin \delta - \dot{\tau} V_D \cos \delta &= \frac{F_y^E}{m} + 2\Omega_t (V_D \cos \delta + V_N \sin \delta) \\ \mathbf{z}_E : \dot{V}_D + \dot{\delta} V_N + \dot{\tau} V_E \cos \delta &= \frac{F_z^E}{m} - 2\Omega_t V_E \cos \delta - \Omega_t^2 R \cos^2 \delta \end{aligned} \quad (3-45)$$

Finally, substituting Eqs. (3-38) and (3-39) for $\dot{\delta}$ and $\dot{\tau}$, and rearranging terms give the dynamic equations of motion:

$$\dot{V}_N = \frac{F_x^E}{m} - 2\Omega_t V_E \sin \delta - \Omega_t^2 R \sin \delta \cos \delta - \frac{V_E^2 \tan \delta - V_N V_D}{R} \quad (3-46)$$

$$\dot{V}_E = \frac{F_y^E}{m} + 2\Omega_t (V_D \cos \delta + V_N \sin \delta) + \frac{V_E}{R} (V_N \tan \delta + V_D) \quad (3-47)$$

$$\dot{V}_D = \frac{F_z^E}{m} - 2\Omega_t V_E \cos \delta - \Omega_t^2 R \cos^2 \delta - \frac{V_E^2 + V_N^2}{R} \quad (3-48)$$

3-4 The Equations of Rotational Motion

This section will describe the equations of rotational motion. Section 3-4-1 introduces the general formulation of the equations, and looks at the moments due to variable mass properties. In Section 3-4-2, the well-known (dynamical) Euler equations are presented. In Section 3-4-3, finally, we discuss the kinematic attitude equations in depth. These will be expressed with Euler angles.

3-4-1 General formulation

As a starting point, we consider a vehicle which is moving w.r.t. to an inertial frame, at a distance \mathbf{r}_{cm} from the origin. The vehicle is rotating with an angular velocity $\boldsymbol{\Omega}_{bI}^b$ w.r.t. this frame. The general form of the equation of rotational motion is given by

$$\begin{aligned} \mathbf{M}_{cm}^b &= \int_m \tilde{\mathbf{r}} \times \left(\frac{d\boldsymbol{\Omega}_{bI}^b}{dt} \times \tilde{\mathbf{r}} \right) dm + \int_m \tilde{\mathbf{r}} \times [\boldsymbol{\Omega}_{bI}^b \times (\boldsymbol{\Omega}_{bI}^b \times \tilde{\mathbf{r}})] dm + \\ &\quad + 2 \int_m \tilde{\mathbf{r}} \times \left(\boldsymbol{\Omega}_{bI}^b \times \frac{\delta \tilde{\mathbf{r}}}{\delta t} \right) dm + \int_m \tilde{\mathbf{r}} \times \frac{\delta^2 \tilde{\mathbf{r}}}{\delta t^2} dm \end{aligned} \quad (3-49)$$

or

$$\mathbf{M}_{cm}^b + \mathbf{M}_C^b + \mathbf{M}_{rel}^b = \int_m \tilde{\mathbf{r}} \times \left(\frac{d\boldsymbol{\Omega}_{bI}^b}{dt} \times \tilde{\mathbf{r}} \right) dm + \int_m \tilde{\mathbf{r}} \times [\boldsymbol{\Omega}_{bI}^b \times (\boldsymbol{\Omega}_{bI}^b \times \tilde{\mathbf{r}})] dm \quad (3-50)$$

For a derivation of Eq. (3-49), the reader is referred to Appendix C. In the above equations, the various terms have the following meaning:

\mathbf{M}_{cm}^b	=	total external moment about the vehicle's centre of mass, being of gravitational or aerodynamic origin (Nm)
$\mathbf{M}_C^b = -2 \int_m \tilde{\mathbf{r}} \times (\boldsymbol{\omega} \times \frac{\delta \tilde{\mathbf{r}}}{\delta t}) dm$	=	Coriolis moment due to time variations in mass distribution (Nm)
$\mathbf{M}_{rel}^b = - \int_m \tilde{\mathbf{r}} \times \frac{\delta^2 \tilde{\mathbf{r}}}{\delta t^2} dm$	=	relative moment due to time variations in mass distribution (Nm)
$\int_m \tilde{\mathbf{r}} \times \left(\frac{d\boldsymbol{\omega}}{dt} \times \tilde{\mathbf{r}} \right) dm$	=	apparent moment due to the angular acceleration of the vehicle with respect to the inertial frame (Nm)

$\int_m \tilde{\mathbf{r}} \times [\boldsymbol{\omega} \times (\boldsymbol{\omega} \times \tilde{\mathbf{r}})] dm$	=	apparent moment due to the angular velocity of the vehicle with respect to the inertial frame (Nm)
$\boldsymbol{\Omega}_{bI}^b = (p, q, r)^T$	=	the rotation vector of the body frame with respect to the inertial frame, expressed in components along the body axes
$\tilde{\mathbf{r}}$	=	the location of a mass element w.r.t. the c.o.m. of the vehicle (m)

Again, with the notation $\frac{\delta}{\delta t}$ means we refer to the derivative in the local (body) frame.

3-4-2 The Euler equations

Expanding the dynamic equations of rotational motion and expressing the components along the body axes, we get the so-called Euler equations, which give information about the angular accelerations. The full set of (non-linear) equations as obtained in Appendix C holds

$$\dot{\boldsymbol{\Omega}}_{bI}^b = \mathbf{I}^{-1} \left(\tilde{\mathbf{M}}_{cm}^b - \boldsymbol{\Omega}_{bI}^b \times \mathbf{I} \boldsymbol{\Omega}_{bI}^b \right) \quad (3-51)$$

with

$\tilde{\mathbf{M}}_{cm}^b = (M_x, M_y, M_z)^T$	=	sum of external, Coriolis and relative moments about the c.o.m., expressed in components along the body axes
$\mathbf{I} = \begin{bmatrix} I_{xx} & -I_{xy} & -I_{xz} \\ -I_{xy} & I_{yy} & -I_{yz} \\ -I_{xz} & -I_{yz} & I_{zz} \end{bmatrix}$	=	inertia tensor of the re-entry vehicle, referenced to the body frame
$\boldsymbol{\Omega}_{bI}^b = (p, q, r)^T$	=	the rotation vector of the body frame with respect to the inertial frame, expressed in components along the body axes

Solving the above equations asks for the inversion of the inertia tensor. However, in literature also analytical expressions can be found for \dot{p} , \dot{q} and \dot{r} [56].

In a number of cases, these equations can be simplified. In the case of a (mass-symmetrical) vehicle, two out of three products of inertia are equal to zero. When the plane of symmetry is the $X_B Z_B$ -plane, then $I_{xy} = I_{yz} = 0$. Eq. (3-51) then simplifies to

$$\begin{bmatrix} I_{xx} & 0 & -I_{xz} \\ 0 & I_{yy} & 0 \\ -I_{xz} & 0 & I_{zz} \end{bmatrix} \begin{bmatrix} \dot{p} \\ \dot{q} \\ \dot{r} \end{bmatrix} = \begin{bmatrix} M_x \\ M_y \\ M_z \end{bmatrix} - \begin{bmatrix} p \\ q \\ r \end{bmatrix} \times \begin{bmatrix} I_{xx} & 0 & -I_{xz} \\ 0 & I_{yy} & 0 \\ -I_{xz} & 0 & I_{zz} \end{bmatrix} \begin{bmatrix} p \\ q \\ r \end{bmatrix} \quad (3-52)$$

Solving this system of equations for \dot{p} , \dot{q} and \dot{r} leads to

$$\dot{p} = \frac{I_{zz}}{I^*} M_x + \frac{I_{xz}}{I^*} M_z + \frac{(I_{xx} - I_{yy} + I_{zz}) I_{xz}}{I^*} pq + \frac{(I_{yy} - I_{zz}) I_{zz} - I_{xz}^2}{I^*} qr \quad (3-53a)$$

$$\dot{q} = \frac{M_y}{I_{yy}} + \frac{I_{xz}}{I_{yy}} (r^2 - p^2) + \frac{I_{zz} - I_{xx}}{I_{yy}} pr \quad (3-53b)$$

$$\dot{r} = \frac{I_{xz}}{I^*} M_x + \frac{I_{xx}}{I^*} M_z + \frac{(I_{xx} - I_{yy}) I_{xx} + I_{xz}^2}{I^*} pq + \frac{(-I_{xx} + I_{yy} - I_{zz}) I_{xz}}{I^*} qr \quad (3-53c)$$

with $I^* = I_{xx} I_{zz} - I_{xz}^2$.

Even simpler expressions can be obtained, when we have two planes of symmetry. This is the case for rotational symmetric bodies. In that case, all three products of inertia are zero and Eqs. (3-53a)-(3-53c) simplify to

$$\dot{p} = \frac{M_x}{I_{xx}} + \frac{I_{yy} - I_{zz}}{I_{xx}} qr \quad (3-54a)$$

$$\dot{q} = \frac{M_y}{I_{yy}} + \frac{I_{zz} - I_{xx}}{I_{yy}} pr \quad (3-54b)$$

$$\dot{r} = \frac{M_z}{I_{zz}} + \frac{I_{xx} - I_{yy}}{I_{zz}} pq \quad (3-54c)$$

3-4-3 The attitude equations

In Section 3-4-1, the rotational rate of the body w.r.t. to the inertial planetocentric frame, expressed in components along the body axes is defined as

$$\boldsymbol{\Omega}_{bI}^b = p\mathbf{x}_b + q\mathbf{y}_b + r\mathbf{z}_b \quad (3-55)$$

In this section, we will use Euler angles to define the orientation of the body frame w.r.t. the E -frame (of which the XY -plane is the local horizontal plane). The three Euler angles are the yaw angle ψ , the pitch angle θ and the roll angle φ , and they arise from three successive rotations of the B -frame, starting from the E -frame (see also 2-19, p. 41).

1. A positive rotation about the Z_E -axis through the angle ψ resulting in frame $\mathbf{X}_{E'} = [\mathbf{x}_{E'} \ \mathbf{y}_{E'} \ \mathbf{z}_{E'}]$, with $\mathbf{z}_{E'} = \mathbf{z}_E$:

$$\mathbf{X}_{E'} = \mathbb{T}_z(\psi)\mathbf{X}_E \quad (3-56)$$

2. A positive rotation about the $Y_{E'}$ -axis through the angle θ resulting in frame $\mathbf{X}_{E''} = [\mathbf{x}_{E''} \ \mathbf{y}_{E''} \ \mathbf{z}_{E''}]$, with $\mathbf{y}_{E''} = \mathbf{y}'_E$:

$$\mathbf{X}_{E''} = \mathbb{T}_y(\theta)\mathbf{X}_{E'} \quad (3-57)$$

3. A positive rotation about the $X_{E''}$ -axis through the angle φ resulting in frame $\mathbf{X}_b = [\mathbf{x}_b \ \mathbf{y}_b \ \mathbf{z}_b]$, with $\mathbf{x}_b = \mathbf{x}_{E''}$:

$$\mathbf{X}_b = \mathbb{T}_x(\varphi)\mathbf{X}_{E''} \quad (3-58)$$

Using exactly the same rotations and order of rotations as above, we can write the following transformation:

$$\mathbf{X}_b = \mathbb{T}_{bE}\mathbf{X}_E \quad (3-59)$$

with, see also Eq. (2-19):

$$\mathbb{T}_{bE} = |_b\mathbb{T}_{bE''}|_{E''}\mathbb{T}_{E''E'}|_{E'}\mathbb{T}_{E'E}|_E = |_b\mathbb{T}_x(\varphi)|_{E''}\mathbb{T}_y(\theta)|_{E'}\mathbb{T}_z(\psi)|_E \quad (3-60)$$

The corresponding rotation can be derived from this transformation matrix and is given by

$$\boldsymbol{\Omega}_{bE} = \boldsymbol{\Omega}_{bE''} + \boldsymbol{\Omega}_{E''E'} + \boldsymbol{\Omega}_{E'E} = \dot{\varphi}\mathbf{x}_b + \dot{\theta}\mathbf{y}_{E''} + \dot{\psi}\mathbf{z}_E \quad (3-61)$$

Note again that $\mathbf{z}_{\mathbf{E}'} = \mathbf{z}_{\mathbf{E}}$, $\mathbf{y}_{\mathbf{E}''} = \mathbf{y}_{\mathbf{E}'}$ and $\mathbf{x}_{\mathbf{b}} = \mathbf{x}_{\mathbf{E}''}$.

On the other hand, we have the rotation of the vehicle w.r.t. the inertial frame, expressed in components along the body axes

$$\boldsymbol{\Omega}_{bI}^b = p\mathbf{x}_{\mathbf{b}} + q\mathbf{y}_{\mathbf{b}} + r\mathbf{z}_{\mathbf{b}}$$

which can be decomposed into

$$\boldsymbol{\Omega}_{bI}^b = \boldsymbol{\Omega}_{bE}^b + \boldsymbol{\Omega}_{EI}^b \quad (3-62)$$

The first term on the right-hand side of Eq. (3-62) describes the rotation of the vehicle w.r.t. the local horizontal plane, whereas the second term can be seen as the rotation of the local horizontal plane w.r.t. to the inertial frame, including a component due to the rotation of the central body. So if we subtract the second term from the vehicle's rotation vector, and equate the result with Eq. (3-61) we must be able to derive expressions for $\dot{\varphi}$, $\dot{\theta}$ and $\dot{\psi}$.

The rotation of the vehicle carried normal Earth reference frame w.r.t. the inertial frame can be derived from \mathbb{T}_{EI} , i.e.,

$$\mathbb{T}_{EI} = \mathbb{T}_y(-\frac{\pi}{2} - \delta)\mathbb{T}_z(\tau + \Omega_t t_O) \Rightarrow \boldsymbol{\Omega}_{EI} = -\dot{\delta}\mathbf{y}_{\mathbf{E}} + (\dot{\tau} + \Omega_t)\mathbf{z}_{\mathbf{I}} \quad (3-63)$$

Here we have used the fact that $\mathbf{z}_{\mathbf{C}} = \mathbf{z}_{\mathbf{I}}$, to combine τ and $\Omega_t t_O$ in a single rotation.

Summarizing, from Eqs. (3-61) and (3-63) we see that we have to transform $\mathbf{y}_{\mathbf{2}}$, $\mathbf{y}_{\mathbf{E}}$, $\mathbf{z}_{\mathbf{E}}$ and $\mathbf{z}_{\mathbf{I}}$ to $\mathbf{x}_{\mathbf{b}}$, $\mathbf{y}_{\mathbf{b}}$, $\mathbf{z}_{\mathbf{b}}$ in order to solve the following equation:

$$\boldsymbol{\Omega}_{bI}^b - \boldsymbol{\Omega}_{EI}^b = \boldsymbol{\Omega}_{bE}^b \quad (3-64)$$

Starting to work out $\mathbf{y}_{\mathbf{E}''}$, the relation between the intermediate E'' -frame and the B -frame is given by

$$[\mathbf{x}_{\mathbf{E}''} \quad \mathbf{y}_{\mathbf{E}''} \quad \mathbf{z}_{\mathbf{E}''}] = \mathbb{T}_{E''b} [\mathbf{x}_{\mathbf{b}} \quad \mathbf{y}_{\mathbf{b}} \quad \mathbf{z}_{\mathbf{b}}] \quad (3-65)$$

with

$$\mathbb{T}_{E''b} = \mathbb{T}_x(-\varphi) = \begin{bmatrix} 1 & 0 & 0 \\ 0 & c\varphi & -s\varphi \\ 0 & s\varphi & c\varphi \end{bmatrix} \quad (3-66)$$

so that

$$\mathbf{y}_{\mathbf{E}''} = \cos \varphi \mathbf{y}_{\mathbf{b}} - \sin \varphi \mathbf{z}_{\mathbf{b}} \quad (3-67)$$

In a similar manner we get for $\mathbf{y}_{\mathbf{E}}$ and $\mathbf{z}_{\mathbf{E}}$

$$[\mathbf{x}_{\mathbf{E}} \quad \mathbf{y}_{\mathbf{E}} \quad \mathbf{z}_{\mathbf{E}}] = \mathbb{T}_{Eb} [\mathbf{x}_{\mathbf{b}} \quad \mathbf{y}_{\mathbf{b}} \quad \mathbf{z}_{\mathbf{b}}] \quad (3-68)$$

where

$$\begin{aligned}\mathbb{T}_{Eb} &= \mathbb{T}_z(-\psi)\mathbb{T}_y(-\theta)\mathbb{T}_x(-\varphi) \\ &= \begin{bmatrix} c\psi c\theta & c\psi s\theta s\varphi - s\psi c\varphi & s\psi s\varphi + c\psi s\theta c\varphi \\ s\psi c\theta & c\psi c\varphi + s\psi s\theta s\varphi & s\psi s\theta c\varphi - c\psi s\varphi \\ -s\theta & c\theta s\varphi & c\theta c\varphi \end{bmatrix} \quad (3-69)\end{aligned}$$

so

$$\mathbf{y}_E = c\theta s\psi \mathbf{x}_b + (s\psi s\theta s\varphi + c\psi c\varphi) \mathbf{y}_b + (s\psi c\varphi s\theta - c\psi s\varphi) \mathbf{z}_b \quad (3-70)$$

$$\mathbf{z}_E = -s\theta \mathbf{x}_b + s\varphi c\theta \mathbf{y}_b + c\varphi c\theta \mathbf{z}_b \quad (3-71)$$

For \mathbf{z}_I , finally, we find:

$$\begin{bmatrix} \mathbf{x}_I & \mathbf{y}_I & \mathbf{z}_I \end{bmatrix} = \mathbb{T}_{Ib} \begin{bmatrix} \mathbf{x}_b & \mathbf{y}_b & \mathbf{z}_b \end{bmatrix} \quad (3-72)$$

with

$$\mathbb{T}_{Ib} = \mathbb{T}_{IE} \mathbb{T}_{Eb} \quad (3-73)$$

$$\mathbb{T}_{IE} = \mathbb{T}_{IC} \mathbb{T}_{CE} = \begin{bmatrix} -c(\tau + \Omega_t t_O) s\delta & -s(\tau + \Omega_t t_O) & -c(\tau + \Omega_t t_O) c\delta \\ -s(\tau + \Omega_t t_O) s\delta & c(\tau + \Omega_t t_O) & -s(\tau + \Omega_t t_O) c\delta \\ c\delta & 0 & -s\delta \end{bmatrix} \quad (3-74)$$

where \mathbb{T}_{IC} and \mathbb{T}_{CE} are given by the inverse transformation of Eq. (2-14) and Eq. (2-16), respectively, and \mathbb{T}_{Eb} is given by Eq. (3-69). Carrying out the matrix multiplication and solving for \mathbf{z}_I yields, after some manipulation,

$$\begin{aligned}\mathbf{z}_I &= [c\delta c\psi c\theta + s\delta s\theta] \mathbf{x}_b + \\ &\quad + [c\delta(c\psi s\theta s\varphi - s\psi c\varphi) - s\delta c\theta s\varphi] \mathbf{y}_b + \\ &\quad + [c\delta(s\psi s\varphi + c\psi s\theta c\varphi) - s\delta c\theta c\varphi] \mathbf{z}_b \quad (3-75)\end{aligned}$$

First, we will evaluate the left-hand side of Eq. (3-64). Substituting Eqs. (3-70) and (3-75) into Eq. (3-63), and subtracting the result from the vehicle's rotation vector Eq. (3-64), gives three components of a new rotation vector, $\boldsymbol{\Omega}_{bE}^b$, expressed in F_b , i.e., \tilde{p} , \tilde{q} and \tilde{r} :

$$\tilde{p} = p + c\theta s\psi \dot{\delta} - [c\delta c\psi c\theta + s\delta s\theta] (\dot{\tau} + \Omega_t) \quad (3-76)$$

$$\tilde{q} = q + (s\psi s\theta s\varphi + c\psi c\varphi) \dot{\delta} - [c\delta(c\psi s\theta s\varphi - s\psi c\varphi) - s\delta c\theta s\varphi] (\dot{\tau} + \Omega_t) \quad (3-77)$$

$$\tilde{r} = r + (s\psi c\varphi s\theta - c\psi s\varphi) \dot{\delta} - [c\delta(s\psi s\varphi + c\psi s\theta c\varphi) - s\delta c\theta c\varphi] (\dot{\tau} + \Omega_t) \quad (3-78)$$

In the above equations, $\dot{\tau}$ and $\dot{\delta}$ are given by the kinematic equations of translational motion Eqs. (3-38)-(3-39),

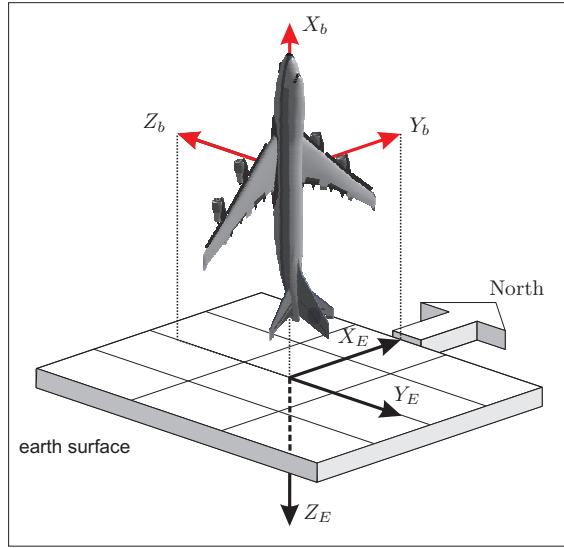


Figure 3-4: Euler angle singularity: Aircraft in vertical climb

$$\dot{\delta} = \frac{V_N}{R}$$

$$\dot{\tau} = \frac{V_E}{R \cos \delta}$$

Evaluating the right-hand side of Eq. (3-64), hereby substituting Eqs. (3-67) and (3-71) into Eq. (3-61), and equating the result with Eqs. (3-76)-(3-78), we get three expressions in $\dot{\varphi}$, $\dot{\theta}$ and $\dot{\psi}$. Written as a matrix equation, the result is

$$\begin{bmatrix} \tilde{p} \\ \tilde{q} \\ \tilde{r} \end{bmatrix} = \begin{bmatrix} 1 & 0 & -\sin \theta \\ 0 & \cos \varphi & \sin \varphi \cos \theta \\ 0 & -\sin \varphi & \cos \varphi \cos \theta \end{bmatrix} \begin{bmatrix} \dot{\varphi} \\ \dot{\theta} \\ \dot{\psi} \end{bmatrix} \quad (3-79)$$

Inverting the coefficient matrix, yields, finally, the kinematic attitude equations:

$$\dot{\varphi} = \tilde{p} + \sin \varphi \tan \theta \tilde{q} + \cos \varphi \tan \theta \tilde{r} \quad (3-80)$$

$$\dot{\theta} = \cos \varphi \tilde{q} - \sin \varphi \tilde{r} \quad (3-81)$$

$$\dot{\psi} = \frac{\sin \varphi}{\cos \theta} \tilde{q} + \frac{\cos \varphi}{\cos \theta} \tilde{r} \quad (3-82)$$

From Eqs. (3-80) and (3-82) it is clear that there is a singularity in the equations of motion for $\theta = \pm 90^\circ$. Let us focus on this singularity for a while. Imagine that the aircraft is in a vertical climb, see figure 3-4. If we try to determine the set of Euler angles for the particular case of vertical climb, it becomes clear that infinitely many sets satisfy this flight condition! One set is: $-90^\circ \rightarrow 90^\circ \rightarrow 0^\circ$. Another set is: $0^\circ \rightarrow 90^\circ \rightarrow 90^\circ$. The yaw and roll angle are now both defined about the same axis vertical axis. The singularity at $\theta = \pm 90^\circ$ can be avoided by choosing a different rotation sequence. However, another singularity will still exist for that new rotation sequence! For example, when the rotation sequence is $\varphi_y \rightarrow \varphi_x \rightarrow \varphi_z$ the singularity will lie at $\varphi_x = \pm 90^\circ$.

For a-symmetrical rotation sequences (see Section 2-2-1) the singularity is always at $\varphi_2 = \pm 90^\circ$, i.e. $\pm 90^\circ$ of the second rotation. Due to this rotation the axis for the third rotation will be aligned with the axis of the first rotation. It will therefore not matter how much the body is rotated in the first and third rotation, as long as the *subtraction* (for $\varphi_2 = +90^\circ$) or *summation* (for $\varphi_2 = -90^\circ$) of the two angles remains fixed! This can be shown mathematically by looking at the transformation matrix for the 3-2-1 rotation sequence (similar to \mathbb{T}_{bE} , section 2-2-5):

$$\begin{aligned} \mathbb{T}_{321} &= \mathbb{T}_{\varphi_x} \mathbb{T}_{\varphi_y} \mathbb{T}_{\varphi_z} \\ &= \begin{bmatrix} 1 & 0 & 0 \\ 0 & \cos \varphi_x & \sin \varphi_x \\ 0 & -\sin \varphi_x & \cos \varphi_x \end{bmatrix} \begin{bmatrix} \cos \varphi_y & 0 & -\sin \varphi_y \\ 0 & 1 & 0 \\ \sin \varphi_y & 0 & \cos \varphi_y \end{bmatrix} \begin{bmatrix} \cos \varphi_z & \sin \varphi_z & 0 \\ -\sin \varphi_z & \cos \varphi_z & 0 \\ 0 & 0 & 1 \end{bmatrix} \\ &= \begin{bmatrix} \cos \varphi_y \cos \varphi_z & \cos \varphi_y \sin \varphi_z & -\sin \varphi_y \\ \left(\begin{array}{c} \sin \varphi_x \sin \varphi_y \cos \varphi_z \\ -\cos \varphi_x \sin \varphi_z \end{array} \right) & \left(\begin{array}{c} \sin \varphi_x \sin \varphi_y \sin \varphi_z \\ +\cos \varphi_x \cos \varphi_z \end{array} \right) & \sin \varphi_x \cos \varphi_y \\ \left(\begin{array}{c} \cos \varphi_x \sin \varphi_y \cos \varphi_z \\ +\sin \varphi_x \sin \varphi_z \end{array} \right) & \left(\begin{array}{c} \cos \varphi_x \sin \varphi_y \sin \varphi_z \\ -\sin \varphi_x \cos \varphi_z \end{array} \right) & \cos \varphi_x \cos \varphi_y \end{bmatrix} \quad (3-83) \end{aligned}$$

Substituting $\varphi_y = 90^\circ$ will lead to:

$$\mathbb{T}_{321} = \begin{bmatrix} 0 & 0 & -1 \\ \left(\begin{array}{c} \sin \varphi_x \cos \varphi_z \\ -\cos \varphi_x \sin \varphi_z \end{array} \right) & \left(\begin{array}{c} \sin \varphi_x \sin \varphi_z \\ +\cos \varphi_x \cos \varphi_z \end{array} \right) & 0 \\ \left(\begin{array}{c} \cos \varphi_x \cos \varphi_z \\ +\sin \varphi_x \sin \varphi_z \end{array} \right) & \left(\begin{array}{c} \cos \varphi_x \sin \varphi_z \\ -\sin \varphi_x \cos \varphi_z \end{array} \right) & 0 \end{bmatrix}$$

Using the trigonometric rules of:

$$\begin{aligned} \sin(\varphi_x - \varphi_z) &= \sin \varphi_x \cos \varphi_z - \cos \varphi_x \sin \varphi_z \\ \sin(\varphi_z - \varphi_x) &= \cos \varphi_x \sin \varphi_z - \sin \varphi_x \cos \varphi_z \\ \cos(\varphi_x - \varphi_z) &= \sin \varphi_x \sin \varphi_z + \cos \varphi_x \cos \varphi_z \end{aligned}$$

one can rewrite the transformation matrix like:

$$\mathbb{T}_{321} = \begin{bmatrix} 0 & 0 & -1 \\ \sin(\varphi_x - \varphi_z) & \cos(\varphi_x - \varphi_z) & 0 \\ \cos(\varphi_x - \varphi_z) & -\sin(\varphi_x - \varphi_z) & 0 \end{bmatrix} = \begin{bmatrix} 0 & 0 & -1 \\ \sin A & \cos A & 0 \\ \cos A & -\sin A & 0 \end{bmatrix}$$

This means that the transformation matrix will be similar for a constant A , meaning that the entire collection of φ_x, φ_z satisfying $A = \varphi_x - \varphi_z$ can describe the same rotation. For $\varphi_y = -90^\circ$, the collection of φ_x, φ_z satisfying $A = \varphi_x + \varphi_z$ is obtained. The possibilities are infinite, therefore indicating the singularity. For symmetric rotation sequences the singularity is at 0° and 180° for the second rotation. In both cases the rotation axis for the third rotation is aligned with the first rotation, creating a singularity.

3-5 Simplifications of the equations of motion

The set of equations of motion derived in sections 3-3 and 3-4 are for a spherical, rotating Earth considering a rigid vehicle with constant mass moving in a changing gravity field. For the sake of convenience they are summarized below.

Translational motion:

$$\dot{V}_N = \frac{F_x^E}{m} - 2\Omega_t V_E \sin \delta - \Omega_t^2 R \sin \delta \cos \delta - \frac{V_E^2 \tan \delta - V_N V_D}{R} \quad (3-84)$$

$$\dot{V}_E = \frac{F_y^E}{m} + 2\Omega_t (V_D \cos \delta + V_N \sin \delta) + \frac{V_E}{R} (V_N \tan \delta + V_D) \quad (3-85)$$

$$\dot{V}_D = \frac{F_z^E}{m} - 2\Omega_t V_E \cos \delta - \Omega_t^2 R \cos^2 \delta - \frac{V_E^2 + V_N^2}{R} \quad (3-86)$$

$$\dot{\delta} = \frac{V_N}{R} \quad (3-87)$$

$$\dot{\tau} = \frac{V_E}{R \cos \delta} \quad (3-88)$$

$$\dot{R} = -V_D \quad (3-89)$$

Rotational motion:

$$\dot{\Omega}_{bI}^b = \mathbf{I}^{-1} \left(\tilde{\mathbf{M}}_{cm}^b - \boldsymbol{\Omega}_{bI}^b \times \mathbf{I} \boldsymbol{\Omega}_{bI}^b \right) \quad (3-90)$$

$$\dot{\varphi} = \tilde{p} + \sin \varphi \tan \theta \tilde{q} + \cos \varphi \tan \theta \tilde{r} \quad (3-91)$$

$$\dot{\theta} = \cos \varphi \tilde{q} - \sin \varphi \tilde{r} \quad (3-92)$$

$$\dot{\psi} = \frac{\sin \varphi}{\cos \theta} \tilde{q} + \frac{\cos \varphi}{\cos \theta} \tilde{r} \quad (3-93)$$

with

$$\tilde{p} = p + c\theta s\psi \dot{\delta} - [c\delta c\psi c\theta + s\delta s\theta] (\dot{\tau} + \Omega_t) \quad (3-94)$$

$$\tilde{q} = q + (s\psi s\theta s\varphi + c\psi c\varphi) \dot{\delta} - [c\delta (c\psi s\theta s\varphi - s\psi c\varphi) - s\delta c\theta s\varphi] (\dot{\tau} + \Omega_t) \quad (3-95)$$

$$\tilde{r} = r + (s\psi c\varphi s\theta - c\psi s\varphi) \dot{\delta} - [c\delta (s\psi s\varphi + c\psi s\theta c\varphi) - s\delta c\theta c\varphi] (\dot{\tau} + \Omega_t) \quad (3-96)$$

In this section, the influence of two commonly made assumptions on the equations of motion will be investigated. They are:

Non-rotating Earth

This assumption greatly reduces the complexity of the equations of motion. However, depending on the study case, it can introduce large errors during computations.

Flat Earth

If the distance traveled during the study case is small, then the curvature of the Earth will not play an important role in the changes of vehicle state. One could therefore assume that the Earth is flat, which simplifies the equations of motion. For larger distances, this assumption will cause significant errors.

3-5-1 Non-rotating Earth

If the Earth is assumed to be non-rotating then the angular velocity of the normal Earth fixed reference frame with respect to the inertial reference frame will be zero, i.e. $\Omega_t = 0$. This will simplify the equations of motions since in the force equations the term due to the rotation of the Earth will be zero. The dynamic equations of translational motion Eqs. (3-84)-(3-86) thus become:

$$\dot{V}_N = \frac{F_x^E}{m} - \frac{V_E^2 \tan \delta - V_N V_D}{R} \quad (3-97)$$

$$\dot{V}_E = \frac{F_y^E}{m} + \frac{V_E}{R} (V_N \tan \delta + V_D) \quad (3-98)$$

$$\dot{V}_D = \frac{F_z^E}{m} - \frac{V_E^2 + V_N^2}{R} \quad (3-99)$$

The kinematic relations do not contain terms with Ω_t , so Eqs. (3-87)-(3-89) are not affected. This also holds for the dynamic equations of rotational motion, since the motion is expressed w.r.t. inertial space. However, it is noted that the F_C -frame has become an inertial frame as well. The relative rotation Eqs. (3-94)-(3-96) in the kinematic attitude equations *do* change, but only the terms related to $\dot{\tau}$:

$$\tilde{p} = p + c\theta s\psi \dot{\delta} - [c\delta c\psi c\theta + s\delta s\theta] \dot{\tau} \quad (3-100)$$

$$\tilde{q} = q + (s\psi s\theta s\varphi + c\psi c\varphi) \dot{\delta} - [c\delta(c\psi s\theta s\varphi - s\psi c\varphi) - s\delta c\theta s\varphi] \dot{\tau} \quad (3-101)$$

$$\tilde{r} = r + (s\psi c\varphi s\theta - c\psi s\varphi) \dot{\delta} - [c\delta(s\psi s\varphi + c\psi s\theta c\varphi) - s\delta c\theta c\varphi] \dot{\tau} \quad (3-102)$$

3-5-2 Flat and Non-rotating Earth

Adding the assumptions of a flat Earth to a non-rotating Earth means that the Earth's radius becomes infinite. So, the terms with R in the denominator will become zero and disappear. This will result in the following equations, beginning with the equations from the previous section, Eqs. (3-97)-(3-102). It is noted that with this assumption the kinematic position equations *are* affected.

$$\dot{V}_N = \frac{F_x^E}{m} \quad (3-103)$$

$$\dot{V}_E = \frac{F_y^E}{m} \quad (3-104)$$

$$\dot{V}_D = \frac{F_z^E}{m} \quad (3-105)$$

$$\dot{\delta} = \dot{\tau} = 0 \quad (3-106)$$

$$\dot{R}\dot{h} = -V_D \quad (3-107)$$

$$\tilde{p} = p \quad (3-108)$$

$$\tilde{q} = q \quad (3-109)$$

$$\tilde{r} = r \quad (3-110)$$

The last three equations substituted in Eqs. (3-91)-(3-93) yields:

$$\dot{\varphi} = p + \sin \varphi \tan \theta q + \cos \varphi \tan \theta r \quad (3-111)$$

$$\dot{\theta} = \cos \varphi q - \sin \varphi r \quad (3-112)$$

$$\dot{\psi} = \frac{\sin \varphi}{\cos \theta} q + \frac{\cos \varphi}{\cos \theta} r \quad (3-113)$$

It is noted that Eqs. (3-111)-(3-113) are identical to Eqs. (3-91)-(3-93) but for the angular-rate components. An observation that can be made is the following. Suppose the Euler angles φ , θ and ψ would define the attitude of the vehicle w.r.t. the inertial frame (F_I), rather than the vehicle carried normal Earth reference frame (F_E). Then, without any assumptions made, we would end up with exactly the same equations as given by Eqs. (3-111)-(3-113). This is, of course, not completely out of the blue, since by putting a stop to the Earth's rotation we have effectively made the rotating Earth-centered Earth-fixed reference frame (F_C) an inertial reference frame.

The relations given in this section can directly be used to obtain the scalar form of the equations of motion for a flat, non-rotating Earth expressed in the body-fixed reference frame.

3-5-3 Simplified equations in the body frame

A simplified set of equations of motion is derived that will be used for the stability analyses in the remainder of these lecture notes.

The assumptions made here are:

- Vehicle is a rigid body.
- Vehicle mass is constant.
- Earth is flat.
- Earth is non-rotating.
- Body-fixed reference frame is chosen such that I_{xy} and I_{yz} are zero. Typically this means that the X_bZ_b -plane is a plane of mass symmetry.
- Effects of rotating masses are neglected.

Since the Earth is assumed to be flat the vehicle carried normal Earth reference frame and the Earth fixed reference frame have a constant orientation with respect to each other, in other words, they do not rotate. To simplify things we assume that the Earth-fixed frame - for the non-rotating Earth an inertial frame - has the same orientation as the E-frame at $t = 0$. The origin of this inertial frame is at the Earth's surface. Therefore, the two frames are only separated by a translation, and the rotation transformation matrix is the identity matrix.

The equations of motion will be expressed in the body-fixed reference frame (with the origin in the center of gravity G). The derivation starts with the force equations, Eqs. (3-103)-(3-105):

$$\frac{d\mathbf{V}_G}{dt} \Big|_E^E = \begin{bmatrix} \dot{V}_N \\ \dot{V}_E \\ \dot{V}_D \end{bmatrix} = \begin{bmatrix} \frac{F_x^E}{m} \\ \frac{F_y^E}{m} \\ \frac{F_z^E}{m} \end{bmatrix} = \frac{\mathbf{F}_{ext}^E}{m} \quad (3-114)$$

Our goal now is to obtain an expression in the form of

$$m \frac{d\mathbf{V}_G}{dt} \Big|_E^b = \mathbb{T}_{bE} \begin{bmatrix} F_x^E \\ F_y^E \\ F_z^E \end{bmatrix} = \begin{bmatrix} F_x^b \\ F_y^b \\ F_z^b \end{bmatrix} = \mathbf{F}_{ext}^b \quad (3-115)$$

Rather than transforming the external force components F_x^E , F_y^E and F_z^E to the b -frame we will look at the individual components and transform those, if required. As discussed before (Section 3-2-1) the gravitational force is expressed in the E -frame, and should therefore be transformed to the body frame. The aerodynamic force is either defined in the aerodynamic frame or with a simple transformation already available in the body frame. We assume the latter; since the propulsion force is also defined in the body frame, in this case we combine both forces into a single one, with components X^b , Y^b and Z^b .

$$\begin{aligned} \mathbf{F}_{ext}^b &= \mathbb{T}_{bE} \begin{bmatrix} 0 \\ 0 \\ mg_{r,0} \end{bmatrix} + \begin{bmatrix} X^b \\ Y^b \\ Z^b \end{bmatrix} \\ &= mg_{r,0} \begin{bmatrix} -\sin \theta \\ \sin \varphi \cos \theta \\ \cos \varphi \cos \theta \end{bmatrix} + \begin{bmatrix} X^b \\ Y^b \\ Z^b \end{bmatrix} \end{aligned} \quad (3-116)$$

with \mathbb{T}_{bE} given by Eq. (2-19). The acceleration in the E -frame is easily transformed to the body frame using the well-known relation for a time derivative in a rotating frame, Eq. (2-56). If we define $\mathbf{V}_G^E = (V_N, V_E, V_D)^T$, and we want to express the time-rate of change of this velocity in the body frame, then:

$$\begin{aligned} \frac{d\mathbf{V}_G}{dt} \Big|_E^b &= \frac{d\mathbf{V}_G}{dt} \Big|_b^b + \Omega_{bE}^b \times \mathbf{V}_G^b \\ &= \begin{bmatrix} \dot{u}_a^b \\ \dot{v}_a^b \\ \dot{w}_a^b \end{bmatrix} + \begin{bmatrix} p \\ q \\ r \end{bmatrix} \times \begin{bmatrix} u_a^b \\ v_a^b \\ w_a^b \end{bmatrix} \end{aligned} \quad (3-117)$$

Note that the rotational rate of the b -frame w.r.t. the E -frame is in this case identical to the rotational rate w.r.t. the I -frame, due to the assumption of a flat, non-rotating Earth. Further, since there is no wind, we can drop the sub-scripts and define the vector $[u, v, w]$ as the inertial velocity vector expressed in the body-fixed reference frame, i.e.:

$$\begin{bmatrix} u_a^b \\ v_a^b \\ w_a^b \end{bmatrix} = \begin{bmatrix} u \\ v \\ w \end{bmatrix} \quad (3-118)$$

Using this notation and expanding Eq. (3-117) yields

$$\frac{d\mathbf{V}_G}{dt} \Big|_E^b = \begin{bmatrix} \dot{u} + qw - rv \\ \dot{v} + ru - pw \\ \dot{w} + pv - qu \end{bmatrix} \quad (3-119)$$

Substituting Eq. (3-119) along with Eq. (3-116) into Eq. (3-115) will lead to the following set of force equations:

$$m \begin{bmatrix} \dot{u} + qw - rv \\ \dot{v} + ru - pw \\ \dot{w} + pv - qu \end{bmatrix} = mg_{r,0} \begin{bmatrix} -\sin \theta \\ \sin \varphi \cos \theta \\ \cos \varphi \cos \theta \end{bmatrix} + \begin{bmatrix} X \\ Y \\ Z \end{bmatrix} \quad (3-120)$$

For the relation between velocities, the following expression holds:

$$\begin{bmatrix} V_N \\ V_E \\ V_D \end{bmatrix} = \mathbb{T}_{Eb} \begin{bmatrix} u \\ v \\ w \end{bmatrix} \quad (3-121)$$

$$\begin{aligned} &= \begin{bmatrix} \cos \theta \cos \psi & \begin{pmatrix} \sin \varphi \sin \theta \cos \psi \\ -\cos \varphi \sin \psi \end{pmatrix} & \begin{pmatrix} \cos \varphi \sin \theta \cos \psi \\ +\sin \varphi \sin \psi \end{pmatrix} \\ \cos \theta \sin \psi & \begin{pmatrix} \sin \varphi \sin \theta \sin \psi \\ +\cos \varphi \cos \psi \end{pmatrix} & \begin{pmatrix} \cos \varphi \sin \theta \sin \psi \\ -\sin \varphi \cos \psi \end{pmatrix} \\ -\sin \theta & \begin{pmatrix} \sin \varphi \cos \theta \\ \cos \varphi \cos \theta \end{pmatrix} & \begin{pmatrix} \cos \varphi \cos \theta \\ \cos \varphi \cos \theta \end{pmatrix} \end{bmatrix} \begin{bmatrix} u \\ v \\ w \end{bmatrix} \\ &= \begin{bmatrix} \begin{pmatrix} [u \cos \theta + (v \sin \varphi + w \cos \varphi) \sin \theta] \cos \psi \\ -(v \cos \varphi - w \sin \varphi) \sin \psi \end{pmatrix} \\ \begin{pmatrix} [u \cos \theta + (v \sin \varphi + w \cos \varphi) \sin \theta] \sin \psi \\ +(v \cos \varphi - w \sin \varphi) \cos \psi \end{pmatrix} \\ u \sin \theta - (v \sin \varphi + w \cos \varphi) \cos \theta \end{bmatrix} \end{aligned} \quad (3-122)$$

The displacement of the aircraft's center of gravity relative to the Earth is obtained by integrating the three components of the ground speed with respect to time, hence,

$$x(t) = \int_0^t V_N dt \quad (3-123)$$

$$y(t) = \int_0^t V_E dt \quad (3-124)$$

$$h(t) = \int_0^t V_D dt \quad (3-125)$$

In terms of moment equations, the form does not change. The Euler equations relate the external moments to the (inertial) angular acceleration, see also Eq. (3-52) and the corresponding discussion :

$$\begin{bmatrix} I_{xx} & 0 & -I_{xz} \\ 0 & I_{yy} & 0 \\ -I_{xz} & 0 & I_{zz} \end{bmatrix} \begin{bmatrix} \dot{p} \\ \dot{q} \\ \dot{r} \end{bmatrix} = \begin{bmatrix} M_x \\ M_y \\ M_z \end{bmatrix} - \begin{bmatrix} p \\ q \\ r \end{bmatrix} \times \begin{bmatrix} I_{xx} & 0 & -I_{xz} \\ 0 & I_{yy} & 0 \\ -I_{xz} & 0 & I_{zz} \end{bmatrix} \begin{bmatrix} p \\ q \\ r \end{bmatrix} \quad (3-126)$$

The kinematic attitude equations are also still the same as before, see Eqs. (3-111)-(3-113):

$$\dot{\varphi} = p + \sin \varphi \tan \theta q + \cos \varphi \tan \theta r \quad (3-127)$$

$$\dot{\theta} = \cos \varphi q - \sin \varphi r \quad (3-128)$$

$$\dot{\psi} = \frac{\sin \varphi}{\cos \theta} q + \frac{\cos \varphi}{\cos \theta} r \quad (3-129)$$

Chapter 4

Linearized Equations of Motion

In the context of these lecture notes, the equations of motion of an aircraft may be used in several different ways. Most commonly, a disturbance function is given, such as a time-dependent control surface deflection or a gust velocity, and the response of the aircraft is then calculated. An inverse situation of this problem also exists, when a certain non-steady motion of the aircraft is given and the control surface deflection as a function of time causing this motion is to be found. In a third application of the equations of motions both the disturbing control surface deflection and the resulting aircraft motion have been measured in flight. The purpose is then to find expressions for the aerodynamic forces and moments in the equations of motion, as functions of the components of the motion and the disturbances, or stated differently, to define a mathematical model of the aircraft.

The problems described above can be solved by a variety of numerical algorithms. For example the numerical integration routines provided by MatLab[©] may readily be applied to solve the set of nonlinear ordinary differential equations derived in chapter 3, even in real time as needed for flight simulation. The present chapter focusses on the linearization of these nonlinear differential equations, resulting in a set of linear differential equations describing small deviations from a chosen reference condition. Performing simulations with a set of linearized equations will always lead to less accurate results. So why should we derive linearized versions of the equations of motion? The answer is that these linearized equations enable us to:

- study the so-called 'characteristic modes of aircraft',
- derive important handling quality and stability characteristic parameters
- design manual or automatic flight control systems using well established linear control theories.

The goal of these lecture notes is to provide insight into the characteristics of aircraft, presented in two ways: through determination of the characteristic modes on one hand and of stability and control derivatives on the other. Characteristic modes are described by the impulse response of the aircraft and are completely determined by the eigenvalues of the system. Stability and control derivatives describe the relation between the variation of the aircraft state due to variation of that state and due to variation of control input respectively.

The knowledge about the characteristics of the aircraft can be used to design control systems, such as autonomous control systems, like an autopilot, or performance increasing control systems

to be used during manual control.

The set of equations of motion used in this chapter is obtained by applying the following assumptions:

- Vehicle is a rigid body,
- Vehicle's mass is constant,
- Earth is non-rotating (see Section 3-5-1),
- Earth is flat (see Section 3-5-2),
- Gravity field is constant,
- Aircraft has a plane of symmetry and the body-fixed reference frame is chosen such that I_{xy} and I_{yz} are zero (see Section 3-4-2),
- Effects of rotating masses are neglected, and
- The resultant thrust vector lies in the symmetry plane and thus only affects the aerodynamic forces X , Z and the aerodynamic moment M .

Moreover we assume that the aircraft has a normal configuration with respect to control surfaces, i.e., it has ailerons (deflection δ_a), an elevator (deflection δ_e), a rudder (deflection δ_r), and engines (setting δ_t). The complete set of equations can be described by (see section 3-5-3):

$$\begin{aligned}
 F_x &= -W \sin \theta + X &= m(\dot{u} + qw - rv) \\
 F_y &= +W \cos \theta \sin \varphi + Y &= m(\dot{v} + ru - pw) \\
 F_z &= +W \cos \theta \cos \varphi + Z &= m(\dot{w} + pv - qu) \\
 \\
 \mathcal{M}_x &= L &= I_{xx} \dot{p} + (I_{zz} - I_{yy}) qr - I_{xz} (\dot{r} + pq) \\
 \mathcal{M}_y &= M &= I_{yy} \dot{q} + (I_{xx} - I_{zz}) rp + I_{xz} (p^2 - r^2) \\
 \mathcal{M}_z &= N &= I_{zz} \dot{r} + (I_{yy} - I_{xx}) pq - I_{xz} (\dot{p} - rq)
 \end{aligned} \tag{4-1}$$

where $W = mg_{r,0}$ has been used. The kinematic relations accompanying this set of equations are:

$$\begin{aligned}
 \dot{\varphi} &= p + q \sin \varphi \tan \theta + r \cos \varphi \tan \theta \\
 \dot{\theta} &= q \cos \varphi - r \sin \varphi \\
 \dot{\psi} &= q \frac{\sin \varphi}{\cos \theta} + r \frac{\cos \varphi}{\cos \theta}
 \end{aligned}$$

Linearization of the equations of motion can be performed about any given flight condition. The results generated with the linearized equations are valid for that flight condition and for the conditions close to that particular point (see figure 4-1). This means that there is a certain 'validity'-region about the initial state, i.e., the state about which the equations are linearized. It depends on the chosen flight condition and on the desired equation of motion output accuracy whether or not the aircraft moves quickly out of this region or not. If, for instance, a steady-state flight condition is chosen, the aircraft will remain close to this condition if no changes are made to the inputs. On the other hand, if we select an unstable or non-steady flight condition (with the same desired accuracy), the aircraft will deviate quickly from this point leaving us with a set of equations incapable of describing the motion accurately.

If we want to simulate the response of the aircraft along a particular trajectory which consists of multiple flight conditions, we could linearize the equations for multiple conditions and switch between sets as we move along the trajectory (see figure 4-1). Especially when we want to design a control system for the entire trajectory (for instance, to keep the aircraft on that trajectory) we

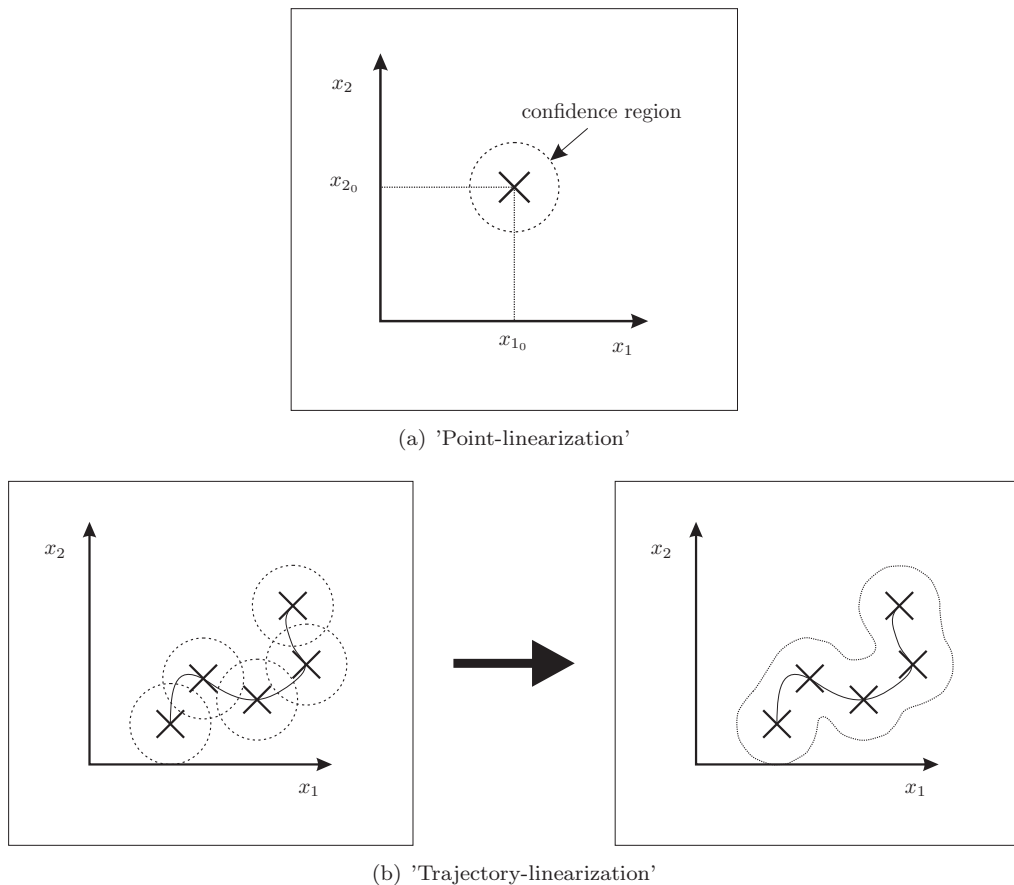


Figure 4-1: Linearization about a single point and a trajectory

can design a controller for each flight condition and switch between controllers. Also, linearizing the equations for multiple flight conditions gives us insight into the variation of the aircraft characteristics.

Linearization about one flight condition or about an entire flight trajectory boils down to the same thing. The technique of linearization about an arbitrary flight condition is described in section 4-1. No specific body-fixed reference frame is selected. In practice a steady state flight condition is usually chosen for the linearization. A steady state, straight, symmetric flight condition is chosen in section 4-2 for the linearization. At first no choices are made regarding the type of body-fixed reference frame. Thereafter we do make a choice and derive the linearized equation set for the same flight condition. The non-dimensional form of the latter set of equations is derived in section 4-3. The set is made non-dimensional to decouple the aerodynamic properties of the aircraft from its dimensions and mass, creating the opportunity to compare different aircraft types.

4-1 Linearization about arbitrary flight condition in arbitrary body-fixed reference frame

Linearization can be performed on any function which is differentiable. Consider a general function:

$$\mathbf{Y} = f(\mathbf{X})$$

which states that the output \mathbf{Y} is a function of the state \mathbf{X} which can have any dimension. This function can also be written in a Taylor expansion form. If we consider the state to be one dimensional and the function to be real then the Taylor expansion about state x_0 is given by:

$$\begin{aligned} y = & f(x_0) + f'(x_0)(x - x_0) + \frac{f'(x_0)}{2!}(x - x_0)^2 \\ & + \frac{f^{(3)}(x_0)}{3!}(x - x_0)^3 + \dots + \frac{f^{(n)}(x_0)}{n!}(x - x_0)^n + \dots \end{aligned} \quad (4-2)$$

where f' denotes the first derivative of function f with respect to x , and f'' denotes the second derivative etc. If the state \mathbf{X} is two dimensional, e.g. $\mathbf{X} = (x, u)$, the Taylor expansion about state (x_0, u_0) of a real function can be written as:

$$\begin{aligned} y = & f(x_0, u_0) + [f_x(x_0, u_0)\Delta x + f_u(x_0, u_0)\Delta u] \\ & + \frac{1}{2!}[f_{xx}(x_0, u_0)\Delta x^2 + 2f_{xu}(x_0, u_0)\Delta x\Delta u + f_{uu}(x_0, u_0)\Delta u^2] \\ & + \frac{1}{3!}[f_{xxx}(x_0, u_0)\Delta x^3 + 3f_{xxu}(x_0, u_0)\Delta x^2\Delta u \\ & + 3f_{xuu}(x_0, u_0)\Delta x\Delta u^2 + f_{uuu}(x_0, u_0)\Delta u^3] \\ & + \dots \end{aligned} \quad (4-3)$$

where f_x denotes the partial derivative of f with respect to x and f_u denotes the partial derivative of f with respect to u , etc. Of course the Taylor expansion can become rather large when the dimension of the state grows, however, the principle remains the same.

Linearization of a function about a point (known as the initial point of linearization or simply the initial point) is defined as expanding the function in a Taylor series and taking only the first term and the terms with a first (partial) derivative from that expansion. In other words disregarding terms which contain (partial) derivatives of order higher than 1. For a function with an n -dimensional state the linearized function about point \mathbf{X}_0 becomes:

$$\begin{aligned} \mathbf{Y} = & f(\mathbf{X}_0) + f_{x_1}(\mathbf{X}_0)\Delta x_1 + f_{x_2}(\mathbf{X}_0)\Delta x_2 + \dots + f_{x_n}(\mathbf{X}_0)\Delta x_n \\ = & f(\mathbf{X}_0) + \sum_{i=1}^n f_{x_i}(\mathbf{X}_0)\Delta x_i \end{aligned} \quad (4-4)$$

Example 4.1

Consider the following system of equations:

$$\begin{aligned} Y_1 &= x_1^2 + 3x_2^2 + 5 \\ Y_2 &= x_1^3 \end{aligned} \quad (4-5)$$

Applying Eq. (4-4), we get

$$\begin{aligned} Y_1 &= f(\mathbf{X}_0) + f_{x_1}(\mathbf{X}_0)\Delta x_1 + f_{x_2}(\mathbf{X}_0)\Delta x_2 \\ &= x_{10}^2 + 3x_{20}^2 + 5 + 2x_{10}\Delta x_1 + 6x_{20}\Delta x_2 \\ Y_2 &= f(\mathbf{X}_0) + f_{x_1}(\mathbf{X}_0)\Delta x_1 \\ &= x_{10}^3 + 3x_{10}^2\Delta x_1 \end{aligned} \quad (4-6)$$

□

The function can be replaced by the relations given by the equations of motion. In the next section the linearization of the states, i.e., the right hand side of the equations, is performed while in section 4-1-2 the forces and moments, i.e., the left hand side of the equations, are linearized. In section 4-1-3 the kinematic relations are linearized.

4-1-1 Linearization of states

The equations of motion can be written as:

$$\begin{aligned} F_x &= f(\dot{u}, v, w, q, r) \\ F_y &= f(\dot{v}, u, w, p, r) \\ F_z &= f(\dot{w}, u, v, p, q) \\ \mathcal{M}_x &= f(\dot{p}, \dot{r}, p, q, r) \\ \mathcal{M}_y &= f(\dot{q}, p, r) \\ \mathcal{M}_z &= f(\dot{p}, \dot{r}, p, q, r) \end{aligned} \quad (4-7)$$

Applying the Taylor expansion and neglecting the higher order terms will give:

$$\begin{aligned} F_x &= f(\mathbf{X}_0) + f_{\dot{u}}(\mathbf{X}_0) \Delta \dot{u} + f_v(\mathbf{X}_0) \Delta v + f_w(\mathbf{X}_0) \Delta w + f_q(\mathbf{X}_0) \Delta q + f_r(\mathbf{X}_0) \Delta r \\ F_y &= f(\mathbf{X}_0) + f_{\dot{v}}(\mathbf{X}_0) \Delta \dot{v} + f_u(\mathbf{X}_0) \Delta u + f_w(\mathbf{X}_0) \Delta w + f_p(\mathbf{X}_0) \Delta p + f_r(\mathbf{X}_0) \Delta r \\ F_z &= f(\mathbf{X}_0) + f_{\dot{w}}(\mathbf{X}_0) \Delta \dot{w} + f_u(\mathbf{X}_0) \Delta u + f_v(\mathbf{X}_0) \Delta v + f_p(\mathbf{X}_0) \Delta p + f_q(\mathbf{X}_0) \Delta q \\ \mathcal{M}_x &= f(\mathbf{X}_0) + f_{\dot{p}}(\mathbf{X}_0) \Delta \dot{p} + f_r(\mathbf{X}_0) \Delta \dot{r} + f_p(\mathbf{X}_0) \Delta p + f_q(\mathbf{X}_0) \Delta q + f_r(\mathbf{X}_0) \Delta r \\ \mathcal{M}_y &= f(\mathbf{X}_0) + f_{\dot{q}}(\mathbf{X}_0) \Delta \dot{q} + f_p(\mathbf{X}_0) \Delta p + f_r(\mathbf{X}_0) \Delta r \\ \mathcal{M}_z &= f(\mathbf{X}_0) + f_{\dot{p}}(\mathbf{X}_0) \Delta \dot{p} + f_r(\mathbf{X}_0) \Delta \dot{r} + f_p(\mathbf{X}_0) \Delta p + f_q(\mathbf{X}_0) \Delta q + f_r(\mathbf{X}_0) \Delta r \end{aligned} \quad (4-8)$$

where \mathbf{X}_0 denotes the state about which the linearization is performed. Taking the specific partial derivatives of the function using the equations in (4-1) and substituting the initial state for linearization results in:

$$\begin{aligned} F_x &= m(\dot{u}_0 + q_0 w_0 - r_0 v_0) + m(\Delta \dot{u} - r_0 \Delta v + q_0 \Delta w + w_0 \Delta q - v_0 \Delta r) \\ F_y &= m(\dot{v}_0 + r_0 u_0 - p_0 w_0) + m(\Delta \dot{v} + r_0 \Delta u - p_0 \Delta w - w_0 \Delta p + u_0 \Delta r) \\ F_z &= m(\dot{w}_0 + p_0 v_0 - q_0 u_0) + m(\Delta \dot{w} - q_0 \Delta u + p_0 \Delta v + v_0 \Delta p - u_0 \Delta q) \\ \mathcal{M}_x &= \left\{ \begin{array}{l} I_{xx}\dot{p}_0 + (I_{zz} - I_{yy}) q_0 r_0 - I_{xz}(\dot{r}_0 + p_0 q_0) + I_{xx}\Delta\dot{p} - I_{xz}\Delta\dot{r} \\ -I_{xz}q_0\Delta p + [(I_{zz} - I_{yy}) r_0 - I_{xz}p_0] \Delta q + (I_{zz} - I_{yy}) q_0 \Delta r \end{array} \right\} \\ \mathcal{M}_y &= \left\{ \begin{array}{l} I_{yy}\dot{q}_0 + (I_{xx} - I_{zz}) p_0 r_0 + I_{xz}(p_0^2 - r_0^2) \\ + I_{yy}\Delta\dot{q} + [(I_{xx} - I_{zz}) r_0 + I_{xz}p_0] \Delta p + [(I_{xx} - I_{zz}) p_0 + I_{xz}r_0] \Delta r \end{array} \right\} \\ \mathcal{M}_z &= \left\{ \begin{array}{l} I_{zz}\dot{r}_0 + (I_{yy} - I_{xx}) p_0 q_0 - I_{xz}(\dot{p}_0 - q_0 r_0) - I_{xz}\Delta\dot{p} + I_{zz}\Delta\dot{r} \\ + (I_{yy} - I_{xx}) q_0 \Delta p + [(I_{yy} - I_{xx}) p_0 + I_{xz}r_0] \Delta q + I_{xz}q_0 \Delta r \end{array} \right\} \end{aligned} \quad (4-9)$$

4-1-2 Linearization of forces and moments

The left hand side of the equations of motion can be written as, see Eq. (3-116):

$$\begin{aligned} F_x &= f(\theta, X) \\ F_y &= f(\theta, \varphi, Y) \\ F_z &= f(\theta, \varphi, Z) \\ \mathcal{M}_x &= f(L) \\ \mathcal{M}_y &= f(M) \\ \mathcal{M}_z &= f(N) \end{aligned} \quad (4-10)$$

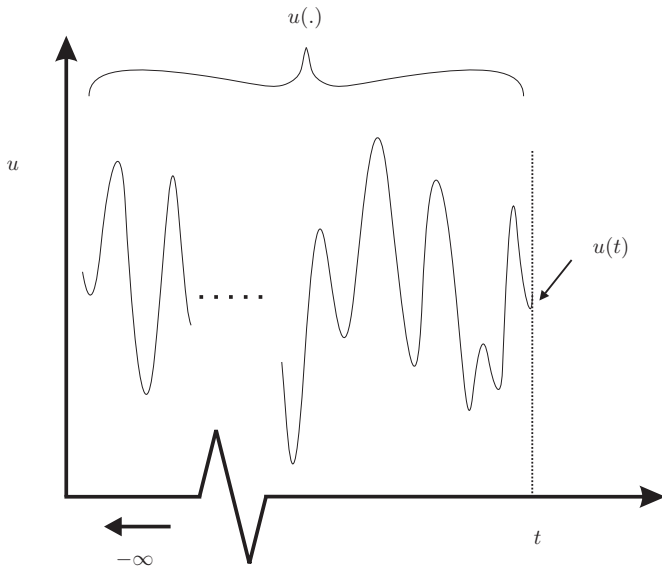


Figure 4-2: Example of a time-function: $u(.)$

where X, Y, Z are the aerodynamic forces and L, M, N are the aerodynamic moments, they are all dependent on the entire history of the aircraft state in time! The question is which states influence which forces and moments. The most general framework to be chosen is to assume that the aerodynamic forces and moments are functions of the components of the motion and control surface deflections, i.e.:

$$X, Y, Z, L, M, N \longrightarrow f(u(.), v(.), w(.), p(.), q(.), r(.), \delta_a(.), \delta_e(.), \delta_r(.), \delta_t(.)) \quad (4-11)$$

where the notation $(.)$ denote the dependence on the time-history of the parameters. The $(.)$ function contains information regarding the *entire* time history of a specific parameter. The aerodynamic forces and moments are thus a function of time-functions.

Let us take a look at the time-functions, taking for example $u(.)$, i.e., the time-function of the velocity along the X_b -axis (see figure 4-2). The information regarding the entire time history must now be molded into a form fit for the equations of motion. The method adopted here is to replace the time-function $u(.)$ by the following Taylor series:

$$\begin{aligned} u(.) &= u(t) + \dot{u}(t) \Delta t + \frac{1}{2!} \ddot{u}(t) \Delta t^2 + \frac{1}{3!} \dddot{u}(t) \Delta t^3 + \dots \\ &= u(t) + \sum_{i=1}^{\infty} \frac{1}{i!} \frac{d^i u}{dt^i} \Delta t^i \end{aligned} \quad (4-12)$$

It is assumed that if we take into account all possible derivatives of $u(t)$, that we have captured all information regarding the parameter history. In theory all the derivatives have an influence on the value of $u(.)$ on time t . However, it has been observed in practice that for most parameters the influences of the derivatives is limited and can be neglected in the relation (i.e., neglecting the summation term in equation (4-12)). A few exceptions are the derivatives $\frac{\partial Y}{\partial \dot{v}}$ and $\frac{\partial N}{\partial \dot{v}}$ with respect to the acceleration \dot{v} along the Y_B -axis and the derivatives $\frac{\partial Z}{\partial \dot{w}}$ and $\frac{\partial M}{\partial \dot{w}}$ with respect to the acceleration \dot{w} along the Z_B -axis. Of these four partial derivatives, the two relating the moments $\frac{\partial N}{\partial \dot{v}}$ and $\frac{\partial M}{\partial \dot{w}}$ (and of these two again $\frac{\partial M}{\partial \dot{w}}$) are by far the most important. In the following, all derivatives (with the exception of the previously mentioned four derivatives) will be neglected. By neglecting the influence of the derivatives we are in fact neglecting the influence of parameter variation through time. These influences arise from non-stationary wing-fuselage and tail interference. An example is given in the next mini-tutorial.

Mini-tutorial: Influence of non-stationary wing-fuselage and tail interference on aerodynamic forces and moments.

We look here at the wing-fuselage and tail interference in the case of cross-wind, i.e., $v \neq 0$. The discussion in this tutorial is hypothetical and is not proven here, it is only meant to present some insight into why the aerodynamic forces and moments are dependent on the history of all motion parameters.

Consider an aircraft flying at a velocity V which experiences at a certain moment a sudden cross-wind at time t (see figure 4-3(a)). Let us focus momentarily on the airflow over the wing and fuselage due to the cross-wind only (see figure 4-3(b)). At the root of the wing the airflow encounters the fuselage. Since the airflow cannot penetrate the fuselage it needs to follow a path around the fuselage. The airflow will be split in two, one part will travel over the fuselage and one will go underneath. The airflow underneath the fuselage will travel around the wing downwards, causing a decrease in the angle of attack for that section of the wing which leads to a decrease in lift. On the other side of the fuselage the opposite happens. So the lift on one side decreases and on the other side increases. This will cause a moment about the X_b -axis^a

Now consider the lift generating mechanism. The magnitude of lift is directly related with the strength of the vortices generated by the wings. If the lift decreases then the vortex strength will also decrease and vice versa. So, in our situation, we have a local decrease in vortex strength on one side and an increase on the other. This can be represented by placing an imaginary vortex with its centerline on the X_b -axis (see figure 4-3(c)). After time Δt the vortex hits the tail, therefore the tail will experienced a different airflow. The forces generated by this change in airflow will cause a rolling and yawing moment. This example shows that events on time t will still have effect at time $t + \Delta t$, showing the time-dependency of the aerodynamic force and moments on the motion parameters.

^aUnder the assumption that the X_b -axis is aligned with the fuselage.

By neglecting the time-dependency, the relations given by equation (4-11) can thus be redefined as:

$$X, Y, Z, L, M, N \longrightarrow f(u(t), v(t), \dot{v}(t), w(t), \dot{w}(t), p(t), q(t), r(t), \delta_a(t), \delta_e(t), \delta_r(t), \delta_t(t)) \quad (4-13)$$

When dropping the time notation (t), the relations given equation (4-10) can be rewritten as:

$$\begin{aligned} F_x &= f(\theta, u, v, w, p, q, r, \delta_a, \delta_e, \delta_r, \delta_t) \\ F_y &= f(\theta, \varphi, u, v, w, \dot{v}, p, q, r, \delta_a, \delta_e, \delta_r) \\ F_z &= f(\theta, \varphi, u, v, w, \dot{w}, p, q, r, \delta_a, \delta_e, \delta_r, \delta_t) \\ \mathcal{M}_x &= f(u, v, w, p, q, r, \delta_a, \delta_e, \delta_r) \\ \mathcal{M}_y &= f(u, v, w, \dot{w}, p, q, r, \delta_a, \delta_e, \delta_r, \delta_t) \\ \mathcal{M}_z &= f(u, v, w, \dot{v}, p, q, r, \delta_a, \delta_e, \delta_r) \end{aligned} \quad (4-14)$$

Linearizing these equations leads to:

$$\begin{aligned} F_x &= F_x(\mathbf{X}_0) + F_x(\Delta\mathbf{X}) \\ F_y &= F_y(\mathbf{X}_0) + F_y(\Delta\mathbf{X}) \\ F_z &= F_z(\mathbf{X}_0) + F_z(\Delta\mathbf{X}) \\ \mathcal{M}_x &= \mathcal{M}_x(\mathbf{X}_0) + \mathcal{M}_x(\Delta\mathbf{X}) \\ \mathcal{M}_y &= \mathcal{M}_y(\mathbf{X}_0) + \mathcal{M}_y(\Delta\mathbf{X}) \\ \mathcal{M}_z &= \mathcal{M}_z(\mathbf{X}_0) + \mathcal{M}_z(\Delta\mathbf{X}) \end{aligned} \quad (4-15)$$

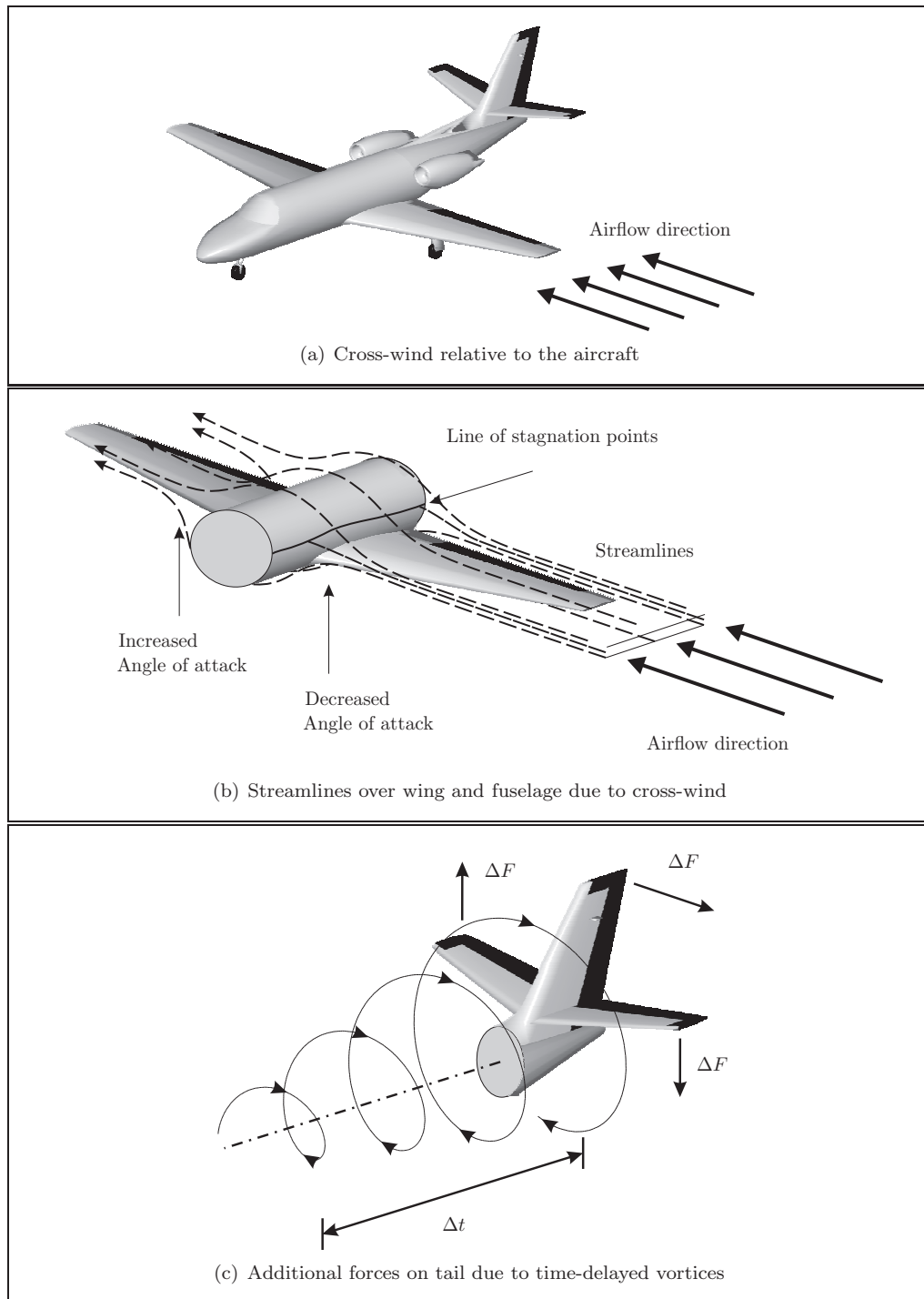


Figure 4-3: Airflow tutorial: example of time-dependent aerodynamic characteristics

with

$$\begin{aligned} F_x(\mathbf{X}_0) &= -W \sin \theta_0 + X_0 \\ F_y(\mathbf{X}_0) &= W \cos \theta_0 \sin \varphi_0 + Y_0 \\ F_z(\mathbf{X}_0) &= W \cos \theta_0 \cos \varphi_0 + Z_0 \\ M_x(\mathbf{X}_0) &= L_0 \\ M_y(\mathbf{X}_0) &= M_0 \\ M_z(\mathbf{X}_0) &= N_0 \end{aligned} \quad (4-16)$$

where X_0 , Y_0 , and Z_0 are the aerodynamic forces and L_0 , M_0 , and N_0 are the aerodynamic moments for the initial state of linearization, i.e., for $\mathbf{X}_0 = [u_0, v_0, w_0, p_0, q_0, r_0, \delta_{a0}, \delta_{e0}, \delta_{r0}]$. The second part of equation 4-15 can be written as:

$$\begin{aligned} F_x(\Delta\mathbf{X}) &= \left\{ \begin{array}{l} -W \cos \theta_0 \Delta\theta + X_u \Delta u + X_v \Delta v + X_w \Delta w + X_p \Delta p \\ + X_q \Delta q + X_r \Delta r + X_{\delta_a} \Delta \delta_a + X_{\delta_e} \Delta \delta_e + X_{\delta_r} \Delta \delta_r + X_{\delta_t} \Delta \delta_t \end{array} \right\} \\ F_y(\Delta\mathbf{X}) &= \left\{ \begin{array}{l} -W \sin \theta_0 \sin \varphi_0 \Delta\theta + W \cos \theta_0 \cos \varphi_0 \Delta\varphi \\ + Y_u \Delta u + Y_v \Delta v + Y_w \Delta w + Y_{\dot{v}} \Delta \dot{v} + Y_p \Delta p + Y_q \Delta q + Y_r \Delta r \\ + Y_{\delta_a} \Delta \delta_a + Y_{\delta_e} \Delta \delta_e + Y_{\delta_r} \Delta \delta_r \end{array} \right\} \\ F_z(\Delta\mathbf{X}) &= \left\{ \begin{array}{l} -W \sin \theta_0 \cos \varphi_0 \Delta\theta - W \cos \theta_0 \sin \varphi_0 \Delta\varphi \\ + Z_u \Delta u + Z_v \Delta v + Z_w \Delta w + Z_{\dot{w}} \Delta \dot{w} + Z_p \Delta p + Z_q \Delta q + Z_r \Delta r \\ + Z_{\delta_a} \Delta \delta_a + Z_{\delta_e} \Delta \delta_e + Z_{\delta_r} \Delta \delta_r + Z_{\delta_t} \Delta \delta_t \end{array} \right\} \\ M_x(\Delta\mathbf{X}) &= \left\{ \begin{array}{l} L_u \Delta u + L_v \Delta v + L_w \Delta w \\ + L_p \Delta p + L_q \Delta q + L_r \Delta r + L_{\delta_a} \Delta \delta_a + L_{\delta_e} \Delta \delta_e + L_{\delta_r} \Delta \delta_r \end{array} \right\} \\ M_y(\Delta\mathbf{X}) &= \left\{ \begin{array}{l} M_u \Delta u + M_v \Delta v + M_w \Delta w + M_{\dot{w}} \Delta \dot{w} + M_p \Delta p + M_q \Delta q \\ + M_r \Delta r + M_{\delta_a} \Delta \delta_a + M_{\delta_e} \Delta \delta_e + M_{\delta_r} \Delta \delta_r + M_{\delta_t} \Delta \delta_t \end{array} \right\} \\ M_z(\Delta\mathbf{X}) &= \left\{ \begin{array}{l} N_u \Delta u + N_v \Delta v + N_w \Delta w + N_{\dot{v}} \Delta \dot{v} \\ + N_p \Delta p + N_q \Delta q + N_r \Delta r + N_{\delta_a} \Delta \delta_a + N_{\delta_e} \Delta \delta_e + N_{\delta_r} \Delta \delta_r \end{array} \right\} \end{aligned} \quad (4-17)$$

As a consequence of the assumed symmetry of the aircraft and the linearization of the equations of motion a further simplification is possible. Suppose, a change in velocity $+ \Delta v$ along the Y_B -axis causes an extra force $\Delta X_{dv} = X_v \Delta v = dX$. Then, since the derivative is a constant, a change in velocity $- \Delta v$ will generate an extra force $\Delta X_{-dv} = X_v (-\Delta v) = -dX$. Mirroring the situation with $- \Delta v$ in the plane of symmetry must result in the situation with $+ \Delta v$, see figure 4-4. This means, however, that dX must be equal to zero and, as a consequence, X cannot vary linearly with Δv . Only a variation with Δv^2 , Δv^4 , Δv^6 etcetera is possible. Such terms of higher degree however, have already been neglected during the linearization. This leads to the conclusion that the asymmetric deviation Δv has no influence on the symmetric aerodynamic force X . A similar argument can be given for any of other combinations of symmetric and asymmetric variables.

Evidently, the following rules apply,

- Small asymmetric deviations and disturbances have no influence on the symmetric forces X and Z or on the symmetric moment M
- Small symmetric deviations and disturbances have no influence on the asymmetric force Y or on the asymmetric moments L and N

Expressed in a different way,

No aerodynamic coupling exists between the symmetric and the asymmetric degrees of freedom, as long as the deviations and disturbances remain small!

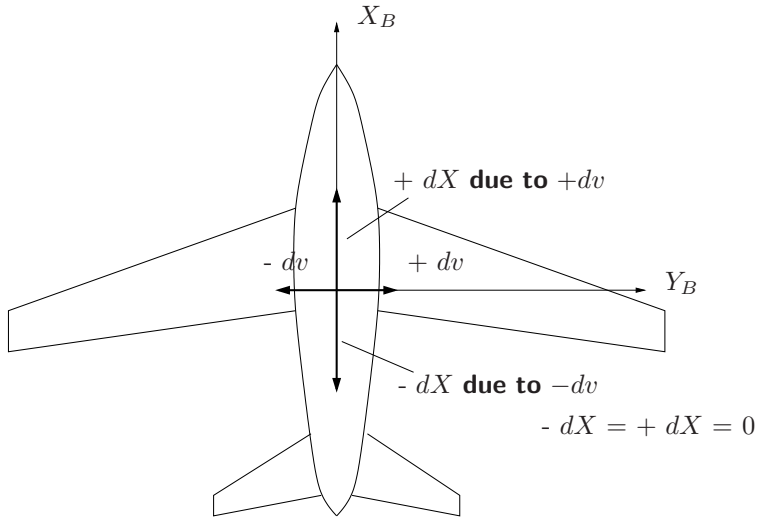


Figure 4-4: The impossibility of a force in the X_B -direction arising from a variation in velocity dv along the Y_B -axis

A single exception to this rule is the contribution $\frac{\partial^2 M}{\partial v^2} \cdot \Delta v^2$ to dM , which has in many practical situations a non-negligible magnitude at values of dv occurring in flight conditions where no other significant non-linearities are noticeable. In the following, however, this contribution of dv^2 to dM will not be further considered.

Under the previous assumptions, the linearized set of aerodynamic forces and moments and the weight can be written as follows:

$$\begin{aligned}
 F_x &= F_x(\mathbf{X}_0) - W \cos \theta_0 \Delta \theta + X_u \Delta u + X_w \Delta w + X_q \Delta q + X_{\delta_e} \Delta \delta_e + X_{\delta_t} \Delta \delta_t \\
 F_y &= F_y(\mathbf{X}_0) + \left\{ \begin{array}{l} W \cos \theta_0 \cos \varphi_0 \Delta \varphi \\ + Y_v \Delta v + Y_{\dot{v}} \Delta \dot{v} + Y_p \Delta p + Y_r \Delta r + Y_{\delta_a} \Delta \delta_a + Y_{\delta_r} \Delta \delta_r \end{array} \right\} \\
 F_z &= F_z(\mathbf{X}_0) + \left\{ \begin{array}{l} -W \sin \theta_0 \cos \varphi_0 \Delta \theta \\ + Z_u \Delta u + Z_w \Delta w + Z_{\dot{w}} \Delta \dot{w} + Z_q \Delta q + Z_{\delta_e} \Delta \delta_e + Z_{\delta_t} \Delta \delta_t \end{array} \right\} \\
 \mathcal{M}_x &= \mathcal{M}_x(\mathbf{X}_0) + L_v \Delta v + L_p \Delta p + L_r \Delta r + L_{\delta_a} \Delta \delta_a + L_{\delta_r} \Delta \delta_r \\
 \mathcal{M}_y &= \mathcal{M}_y(\mathbf{X}_0) + M_u \Delta u + M_w \Delta w + M_{\dot{w}} \Delta \dot{w} + M_q \Delta q + M_{\delta_e} \Delta \delta_e + M_{\delta_t} \Delta \delta_t \\
 \mathcal{M}_z &= \mathcal{M}_z(\mathbf{X}_0) + N_v \Delta v + N_{\dot{v}} \Delta \dot{v} + N_p \Delta p + N_r \Delta r + N_{\delta_a} \Delta \delta_a + N_{\delta_r} \Delta \delta_r
 \end{aligned} \tag{4-18}$$

where $F_x(\mathbf{X}_0), \dots, \mathcal{M}_x(\mathbf{X}_0), \dots$ remain the same (see equation 4-16).

4-1-3 Linearization of kinematic relations

The kinematic relations for a non-rotating flat Earth are functions of the Euler angles φ, θ and of the angular velocities p, q, r :

$$\begin{aligned}
 \dot{\varphi} &= f(\varphi, \theta, p, q, r) \\
 \dot{\theta} &= f(\varphi, q, r) \\
 \dot{\psi} &= f(\varphi, \theta, q, r)
 \end{aligned} \tag{4-19}$$

Linearization of these relations results in:

$$\begin{aligned}
 \dot{\varphi} &= \dot{\varphi}(\mathbf{X}_0) + \dot{\varphi}(\Delta \mathbf{X}) \\
 \dot{\theta} &= \dot{\theta}(\mathbf{X}_0) + \dot{\theta}(\Delta \mathbf{X}) \\
 \dot{\psi} &= \dot{\psi}(\mathbf{X}_0) + \dot{\psi}(\Delta \mathbf{X})
 \end{aligned} \tag{4-20}$$

with

$$\begin{aligned}\dot{\varphi}(\mathbf{X}_0) &= p_0 + q_0 \sin \varphi_0 \tan \theta_0 + r_0 \cos \varphi_0 \tan \theta_0 \\ \dot{\theta}(\mathbf{X}_0) &= q_0 \cos \varphi_0 - r_0 \sin \varphi_0 \\ \dot{\psi}(\mathbf{X}_0) &= q_0 \frac{\sin \varphi_0}{\cos \theta_0} + r_0 \frac{\cos \varphi_0}{\cos \theta_0}\end{aligned}\quad (4-21)$$

and

$$\begin{aligned}\dot{\varphi}(\Delta \mathbf{X}) &= \left\{ \begin{array}{l} \Delta p + \sin \varphi_0 \tan \theta_0 \Delta q + q_0 \cos \varphi_0 \tan \theta_0 \Delta \varphi \\ + q_0 \frac{\sin \varphi_0}{\cos^2 \theta_0} \Delta \theta + \cos \varphi_0 \tan \theta_0 \Delta r \\ - r_0 \sin \varphi_0 \tan \theta_0 \Delta \varphi + r_0 \frac{\cos \varphi_0}{\cos^2 \theta_0} \Delta \theta \end{array} \right\} \\ \dot{\theta}(\Delta \mathbf{X}) &= \cos \varphi_0 \Delta q - q_0 \sin \varphi_0 \Delta \varphi - \sin \varphi_0 \Delta r - r_0 \cos \varphi_0 \Delta \varphi \\ \dot{\psi}(\Delta \mathbf{X}) &= \left\{ \begin{array}{l} \frac{\sin \varphi_0}{\cos \theta_0} \Delta q + q_0 \frac{\cos \varphi_0}{\cos \theta_0} \Delta \varphi + q_0 \frac{\sin \varphi_0}{\cos \theta_0} \tan \theta_0 \Delta \theta + \\ \frac{\cos \varphi_0}{\cos \theta_0} \Delta r - r_0 \frac{\sin \varphi_0}{\cos \theta_0} \Delta \varphi + r_0 \frac{\cos \varphi_0}{\cos \theta_0} \tan \theta_0 \Delta \theta \end{array} \right\}\end{aligned}\quad (4-22)$$

Since the parameters of the linear velocity, i.e., V_N, V_E, V_D , are not included in the state vector, we do not have to linearize the equations relating these parameters with the state parameters $u, v, w, \varphi, \theta, \psi$. After we know the values for the state vector we can determine V_N, V_E, V_D using the relation given in Section 3-5-3:

$$\begin{aligned}\begin{bmatrix} V_N \\ V_E \\ V_D \end{bmatrix} &= \mathbb{T}_{bE}^t \begin{bmatrix} u \\ v \\ w \end{bmatrix} \\ &= \begin{bmatrix} \cos \theta \cos \psi & \begin{pmatrix} \sin \varphi \sin \theta \cos \psi \\ -\cos \varphi \sin \psi \end{pmatrix} & \begin{pmatrix} \cos \varphi \sin \theta \cos \psi \\ +\sin \varphi \sin \psi \end{pmatrix} \\ \cos \theta \sin \psi & \begin{pmatrix} \sin \varphi \sin \theta \sin \psi \\ +\cos \varphi \cos \psi \end{pmatrix} & \begin{pmatrix} \cos \varphi \sin \theta \sin \psi \\ -\sin \varphi \cos \psi \end{pmatrix} \\ -\sin \theta & \begin{pmatrix} \sin \varphi \cos \theta \\ \cos \varphi \cos \theta \end{pmatrix} & \end{bmatrix} \begin{bmatrix} u \\ v \\ w \end{bmatrix}\end{aligned}$$

At this point we have linearized the equations of motion and the kinematic relations. With this set of equations we are able to simulate any motion about the initial state of linearization \mathbf{X}_0 . During simulation one uses a state vector consisting of nine parameters:

$$\mathbf{x} = [u, v, w, p, q, r, \varphi, \theta, \psi]^T$$

and an input vector containing four input parameters:

$$\mathbf{u} = [\delta_a, \delta_e, \delta_r, \delta_t]^T$$

After rearranging the terms in the linearized equations of motion and kinematic relations one can write the relations in the state-space format:

$$\dot{\mathbf{x}}_0 + \Delta \dot{\mathbf{x}} = \mathbf{A}_0 \mathbf{x}_0 + \mathbf{A} \Delta \mathbf{x} + \mathbf{B}_0 \mathbf{u}_0 + \mathbf{B} \Delta \mathbf{u}$$

where $\mathbf{A}_0, \mathbf{A}, \mathbf{B}$ are constant matrices and the vector $\dot{\mathbf{x}}_0$ is also constant. The simulation is initialized at the initial state of linearization \mathbf{X}_0 . Bear in mind that this state includes information about the initial state vector *and* the initial input vector. If the initial state of linearization is a steady state, then the term $\dot{\mathbf{x}}_0$ will be zero meaning that the terms $\mathbf{A}_0 \mathbf{x}_0$ and $\mathbf{B}_0 \mathbf{u}_0$ cancel and the state-space format becomes:

$$\Delta \dot{\mathbf{x}} = \mathbf{A} \Delta \mathbf{x} + \mathbf{B} \Delta \mathbf{u}$$

The matrix \mathbf{A} contains the stability derivatives and inertial properties and the \mathbf{B} contains the control derivatives. The derivatives will be defined in section 4-3. The previous relation is used during simulations to determine the changes in state due to input changes.

The most common flying condition is a steady-state flight. In particular the steady, straight, symmetric flight conditions are often encountered. Therefore, most analyses of the characteristics of an aircraft are performed for such flight conditions. We will derive the linearized set of equations about a steady, straight, symmetric flight condition in the next section.

4-2 Linearization about steady, straight, symmetric flight condition

A steady, straight (wing level), symmetric flight condition has the following properties:

$$\begin{array}{llll} u \neq 0 & \dot{u} = 0 & p = 0 & \dot{p} = 0 \\ v = 0 & \dot{v} = 0 & q = 0 & \dot{q} = 0 \\ w \neq 0 & \dot{w} = 0 & r = 0 & \dot{r} = 0 \end{array}$$

$$\begin{array}{llll} \varphi = 0 & \dot{\varphi} = 0 & X \neq 0 & \dot{X} = 0 \\ \theta \neq 0 & \dot{\theta} = 0 & Y = 0 & \dot{Y} = 0 \\ \psi = 0 & \dot{\psi} = 0 & Z \neq 0 & \dot{Z} = 0 \end{array}$$

which in principle means that the state of the aircraft remains constant, i.e., all derivatives, the lateral velocity, and the angular velocities are zero. The conditions that u, w, X, Z are unequal to zero means that the aircraft has a velocity equal to $\sqrt{u^2 + w^2}$ and that the resultant aerodynamic force (including thrust component) $R = X + Z$ is equal in magnitude but opposite in sign with respect to the gravity vector W .

The set of linearized equations of motion is obtained by taking the flight condition described above as initial state for linearization. By substituting the properties in the general linearized equations of motion (equation (4-23)) we get:

$$\begin{aligned} F_x &= m(\Delta\dot{u} + w_0\Delta q) \\ F_y &= m(\Delta\dot{v} - w_0\Delta p + u_0\Delta r) \\ F_z &= m(\Delta\dot{w} - u_0\Delta q) \\ M_x &= I_{xx}\Delta\dot{p} - I_{xz}\Delta\dot{r} \\ M_y &= I_{yy}\Delta\dot{q} \\ M_z &= I_{zz}\Delta\dot{r} - I_{xz}\Delta\dot{p} \end{aligned} \tag{4-23}$$

The linearized forces and moments equation becomes:

$$\begin{aligned} F_x &= -W \cos \theta_0 \Delta \theta + X_u \Delta u + X_w \Delta w + X_q \Delta q + X_{\delta_e} \Delta \delta_e + X_{\delta_t} \Delta \delta_t \\ F_y &= +W \cos \theta_0 \Delta \varphi + Y_v \Delta v + Y_{\dot{v}} \Delta \dot{v} + Y_p \Delta p + Y_r \Delta r + Y_{\delta_a} \Delta \delta_a + Y_{\delta_r} \Delta \delta_r \\ F_z &= -W \sin \theta_0 \Delta \theta + Z_u \Delta u + Z_w \Delta w + Z_{\dot{w}} \Delta \dot{w} + Z_q \Delta q + Z_{\delta_e} \Delta \delta_e + Z_{\delta_t} \Delta \delta_t \\ M_x &= L_v \Delta v + L_p \Delta p + L_r \Delta r + L_{\delta_a} \Delta \delta_a + L_{\delta_r} \Delta \delta_r \\ M_y &= M_u \Delta u + M_w \Delta w + M_{\dot{w}} \Delta \dot{w} + M_q \Delta q + M_{\delta_e} \Delta \delta_e + M_{\delta_t} \Delta \delta_t \\ M_z &= N_v \Delta v + N_{\dot{v}} \Delta \dot{v} + N_p \Delta p + N_r \Delta r + N_{\delta_a} \Delta \delta_a + N_{\delta_r} \Delta \delta_r \end{aligned} \tag{4-24}$$

Here, we applied the knowledge that the aerodynamic forces are canceled by the weight terms for the initial state. Therefore they are removed from the equations. The linearized kinematic relations become (see equation 4-20 to 4-22):

$$\begin{aligned} \dot{\varphi} &= \Delta p + \tan \theta_0 \Delta r \\ \dot{\theta} &= \Delta q \\ \dot{\psi} &= \frac{1}{\cos \theta_0} \Delta r \end{aligned} \tag{4-25}$$

The aircraft body axes (F_b) used in the foregoing to describe the motions, have not yet been completely defined. The reference frame is fixed relative to the aircraft, but the direction of the X_b -axis in the plane of symmetry has not yet been defined. Often, the choice depends on the type of motion to be studied.

If the aircraft motion about a steady, straight, symmetric flight are to be determined, for instance to investigate the stability of the steady flight conditions, it is advantageous to use the so-called *stability reference frame*, see Section 2-1-4. This is a system of body axes, as previously defined, of which the X_S -axis is parallel to the direction of motion of the center of gravity in the steady initial flight condition. But during the disturbed motion of the aircraft the reference frame is fixed to the aircraft. This particular choice of the X_S -axis results in the equations of motion in,

$$\begin{aligned} u_0 &= V \\ w_0 &= 0 \end{aligned}$$

In addition, the angle of attack in the steady reference condition, measured relative to the X_S -axis, is zero,

$$\begin{aligned} \alpha_0 &= 0 \\ \theta_0 &= \gamma_0 \end{aligned} \tag{4-26}$$

A disadvantage of the stability axes becomes apparent, if the disturbed motions about several different equilibrium conditions have to be studied in succession. During each of these disturbed motions the X_S -axis and the Z_S -axis have a different direction relative to the aircraft. This implies, that the aerodynamic variables, the components of the motion and also the moments and products of inertia in each new case refer to a different attitude of the reference frame relative to the aircraft, although that attitude remains invariant during each of the disturbed motions.

In the following section the linearized set of equations for steady, straight, symmetric flight expressed in the stability reference frame is given. Thereafter the equations needed to determine the moment and products of inertia about the stability reference frame are given.

4-2-1 Linearized set of equations

In order to simplify the notation in the remainder of this chapter the changes in the variable angles relative to the reference condition are indicated without the letter Δ , e.g. θ rather than $\Delta\theta$, δ_e instead of $\Delta\delta_e$ ¹. The magnitude of the relevant variable in steady flight is indicated by the subscript 0 (0).

Since the aerodynamics are considered to be uncoupled, the set of equations can be split up into two parts. One describes the motion in the symmetry plane of the aircraft, i.e., the symmetric motion, and the other part describes the asymmetric motion. If the stability reference frame is used the equations of motion can now be written as follows,

¹During simulations one should bear in mind that u does not represent the true velocity along the X_b -axis. One should add the initial condition u_0 to obtain the true value for that velocity!

I Symmetric motion

$$\begin{aligned}
 -W \cos \theta_0 \theta & + X_u u + X_w w + X_q q + X_{\delta_e} \delta_e + X_{\delta_t} \delta_t = m \dot{u} \\
 -W \sin \theta_0 \theta & + Z_u u + Z_w w + Z_{\dot{w}} \dot{w} + Z_q q + Z_{\delta_e} \delta_e + Z_{\delta_t} \delta_t = m (\dot{w} - q V) \\
 M_u u + M_w w + M_{\dot{w}} \dot{w} + M_q q + M_{\delta_e} \delta_e + M_{\delta_t} \delta_t & = I_{yy} \dot{q} \\
 \dot{\theta} & = q
 \end{aligned} \tag{4-27}$$

II Asymmetric motion

$$\begin{aligned}
 W \cos \theta_0 \varphi & + Y_v v + Y_{\dot{v}} \dot{v} + Y_p p + Y_r r + Y_{\delta_a} \delta_a + Y_{\delta_r} \delta_r = m (\dot{v} + r V) \\
 L_v v + L_p p + L_r r + L_{\delta_a} \delta_a + L_{\delta_r} \delta_r & = I_{xx} \dot{p} - I_{xz} \dot{r} \\
 N_v v + N_{\dot{v}} \dot{v} + N_p p + N_r r + N_{\delta_a} \delta_a + N_{\delta_r} \delta_r & = I_{zz} \dot{r} - I_{xz} \dot{p} \\
 \dot{\psi} & = \frac{r}{\cos \theta_0} \\
 \dot{\varphi} & = p + r \tan \theta_0
 \end{aligned} \tag{4-28}$$

The kinematic relations remain the same, i.e.:

$$\begin{aligned}
 \dot{\varphi} & = p + \tan \theta_0 r \\
 \dot{\theta} & = q \\
 \dot{\psi} & = \frac{1}{\cos \theta_0} r
 \end{aligned} \tag{4-29}$$

4-2-2 Moments and products of inertia

The moments and products of inertia of the aircraft depend not only on the mass distribution of the aircraft, but also on the chosen directions of the axes of the reference frame relative to the aircraft (stability frame of reference F_S versus body-fixed frame of reference F_b). Due to the symmetry of the aircraft two of the three products of inertia are zero,

$$\begin{aligned}
 I_{yz} & = \int_m yz dm = 0 \\
 I_{xy} & = \int_m xy dm = 0
 \end{aligned}$$

This result does not depend on the directions of the two sets of body axes (stability and body-fixed frame of reference) in the plane of symmetry.

Suppose now, that for an arbitrary direction of the X_b -axis the magnitudes of the three moments of inertia and the remaining product of inertia are given. The direction of the X_b -axis is given by the angle $\varepsilon + \eta_1$ between the X_b -axis and the negative X_r -axis, see figure 4-5. This fixes also the direction of the Z_b -axis. If the X_b -axis has a different angle $\varepsilon + \eta_2$ with the negative X_r -axis, see figure 4-5, and the first and second reference frame are indicated by the subscripts 1 and 2 respectively, the following relations hold,

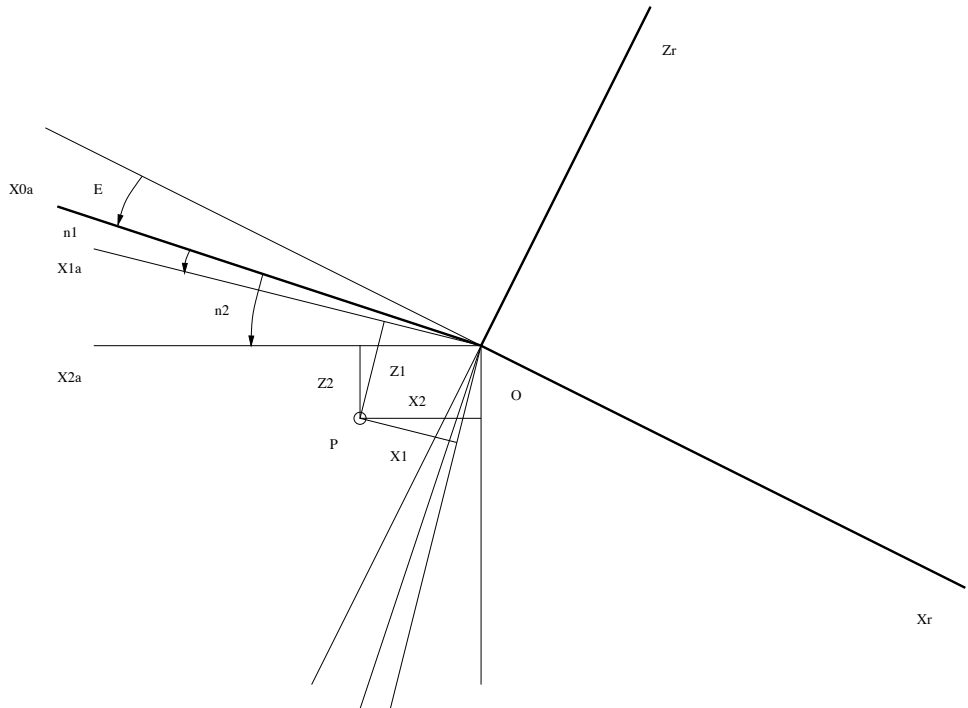


Figure 4-5: The angles between the principal inertial axes and the aircraft reference axes

$$\begin{aligned}x_2 &= x_1 \cos(\eta_2 - \eta_1) + z_1 \sin(\eta_2 - \eta_1) \\y_2 &= y_1 \\z_2 &= -x_1 \sin(\eta_2 - \eta_1) + z_1 \cos(\eta_2 - \eta_1)\end{aligned}$$

This leads to the following moments and products of inertia, relative to the new reference frame,

$$\begin{aligned}I_{xx_2} &= I_{xx_1} \cos^2(\eta_2 - \eta_1) + I_{z_1} \sin^2(\eta_2 - \eta_1) - I_{xz_1} \sin^2(\eta_2 - \eta_1) \\I_{yy_2} &= I_{yy_1} \\I_{zz_2} &= I_{xx_1} \sin^2(\eta_2 - \eta_1) + I_{z_1} \cos^2(\eta_2 - \eta_1) + I_{xz_1} \sin^2(\eta_2 - \eta_1) \\I_{xz_2} &= \frac{1}{2}(I_{xx_1} - I_{zz_1}) \sin(2(\eta_2 - \eta_1)) + I_{xz_1} \cos(2(\eta_2 - \eta_1))\end{aligned}\tag{4-30}$$

As could be expected, the moment of inertia about the Y_b -axis does not depend on the directions of the body axes in the plane of symmetry. For one particular direction of the X_b -axis, and correspondingly of the Z_b -axis, the product of inertia I_{xz} is zero. The axes having these directions are called the principal inertial axes in the plane of symmetry. They are indicated as X_0 - and Z_0 -axes and have an angle ε with the negative X_r - and Z_r -axis, see figure 4-5.

As the products of inertia I_{xy} and I_{yz} are always zero, the Y_b -axis is always a principal inertial axis. This follows also directly from the fact that the Y_b -axis is perpendicular to the plane of symmetry. If for an arbitrary direction $\varepsilon + \eta$ of the X_b -axis the inertial parameters are known the angle η of these axes with the principal inertial axes follow from equation (4-30) by equating I_{xz_2} and η_2 to zero,

$$\tan 2\eta = \frac{2 I_{xz}}{I_{xx} - I_{zz}}$$

Using the principal moments of inertia I_{x_0} and I_{z_0} , which can be calculated from equation (4-30) for a given value η by letting $\eta_2 = 0$, the inertial parameters for an arbitrary direction η of the body axes are,

$$I_{xx} = I_{xx_0} \cos^2 \eta + I_{zz_0} \sin^2 \eta$$

$$I_{yy} = I_{yy_0}$$

$$I_{zz} = I_{xx_0} \sin^2 \eta + I_{zz_0} \cos^2 \eta$$

$$I_{xz} = \frac{1}{2} (I_{xx_0} - I_{zz_0}) \sin 2\eta$$

4-3 Equations of motion in non-dimensional form

The differential equations derived in the foregoing can be applied directly to the calculation of the symmetric and asymmetric aircraft motions about a given condition of steady, straight, symmetric flight as a response to a given disturbance. Very often, however, the equations are used in a non-dimensional form. The reason for this practice is that the aerodynamic forces and moments in the equations are usually expressed in non-dimensional coefficients².

This leads to writing the entire equations in non-dimensional form. To this end, also the inertial characteristics and the time scale are made non-dimensional. One of the several ways in which this can be done, is discussed in the following.

As a starting point, three independent units are chosen, i.e., length having the dimension $[\ell]$, velocity with dimension $[\ell][t]^{-1}$ and mass with dimension $[m]$. The actual values of these units are,

	Symmetric motion:	Asymmetric motion:
length	\bar{c}	b
velocity	V	V
mass	$\rho S \bar{c}$	$\rho S b$

Evidently different units of length are used for the symmetric and the asymmetric motions, the mean aerodynamic chord \bar{c} and the wing span b respectively. These are also the customary lengths used to make the symmetric moment M and the asymmetric moments L and N , respectively, non-dimensional. The unit of mass chosen for both types of motion is the mass of a certain volume of air surrounding the aircraft equal to the wing area multiplied by the respective unit of length. With these units all variables in the equations of motion can be made non-dimensional, according to the schemes in tables 4-1 and 4-2.

Using these schemes, the way in which the equations of motion are made non-dimensional can now be discussed more in detail.

²With the non-dimensional form of the aerodynamic forces and moments, we can compare aircraft independent of aircraft dimensions and weight.

4-3-1 Symmetric Motions

For the symmetric motions the two force equations, in which each of the terms has the dimension of a force, i.e., X and Z , are made non-dimensional by a division by $\frac{1}{2}\rho V^2 S$. The moment equation, in which each of the terms has the dimension of a moment, i.e., M , is divided by $\frac{1}{2}\rho V^2 S \bar{c}$. Starting from equations (4-27) the result is,

$$-\frac{W \cos \theta_0}{\frac{1}{2}\rho V^2 S} \cdot \theta + \frac{X_u u + X_w w + X_q q + X_{\delta_e} \delta_e + X_{\delta_t} \delta_t}{\frac{1}{2}\rho V^2 S} = \frac{m \cdot \dot{u}}{\frac{1}{2}\rho V^2 S} \quad (4-31)$$

$$-\frac{W \sin \theta_0}{\frac{1}{2}\rho V^2 S} \cdot \theta + \frac{Z_u u + Z_w w + Z_q q + Z_{\delta_e} \delta_e + Z_{\delta_t} \delta_t}{\frac{1}{2}\rho V^2 S} = \frac{m (\dot{w} - q \cdot V)}{\frac{1}{2}\rho V^2 S} \quad (4-32)$$

$$\frac{M_u u + M_w w + M_q q + M_{\delta_e} \delta_e + M_{\delta_t} \delta_t}{\frac{1}{2}\rho V^2 S \bar{c}} = \frac{I_{yy} \dot{q}}{\frac{1}{2}\rho V^2 S \bar{c}} \quad (4-33)$$

$$\frac{\dot{\theta} \bar{c}}{V} = \frac{q \bar{c}}{V} \quad (4-34)$$

In elaborating the two force equations, use is made of the two equilibrium conditions,

$$\begin{aligned} W \sin \theta_0 &= X_0 \\ W \cos \theta_0 &= -Z_0 \end{aligned}$$

Using the previous scheme of table 4-1, these conditions are written as follows in equation (4-31),

$$\frac{-W \cos \theta_0}{\frac{1}{2}\rho V^2 S} = C_{Z_0} \quad (4-35)$$

and in equation (4-32),

$$\frac{-W \sin \theta_0}{\frac{1}{2}\rho V^2 S} = -C_{X_0} \quad (4-36)$$

Next, the partial derivatives of the aerodynamic forces and the moment are further elaborated. As an example the contribution $X_u \cdot u$ is considered. It is written as,

$$\frac{X_u \cdot u}{\frac{1}{2}\rho V^2 S} = \frac{X_u}{\frac{1}{2}\rho VS} \cdot \frac{u}{V} = \frac{X_u}{\frac{1}{2}\rho VS} \cdot \hat{u}$$

As both the left and right hand sides of this latter expression are non-dimensional, as \hat{u} is, the quotient $\frac{X_u}{\frac{1}{2}\rho VS}$ must also be non-dimensional. This quotient is called a stability derivative written as C_{X_u} ,

$$C_{X_u} = \frac{X_u}{\frac{1}{2}\rho VS}$$

and,

$$\frac{X_u \cdot u}{\frac{1}{2}\rho V^2 S} = C_{X_u} \cdot \hat{u}$$

It should be emphasized that for the stability derivative C_{X_u} in particular, but also for C_{Z_u} and C_{m_u} , the order of differentiation with respect to airspeed and non-dimensionalizing using the

factor $\frac{1}{2}\rho V^2 S$ in which the airspeed figures as well, is relevant for the resulting values of C_{X_u} , C_{Z_u} and C_{m_u} ,

$$C_{X_u} = \frac{1}{\frac{1}{2}\rho VS} \cdot \frac{\partial X}{\partial u} \neq \frac{\partial C_X}{\partial \dot{u}} \quad (4-37)$$

In a similar manner it follows,

$$\frac{X_w \cdot w}{\frac{1}{2}\rho V^2 S} = \frac{X_w}{\frac{1}{2}\rho VS} \cdot \frac{w}{V} = C_{X_\alpha} \alpha$$

where the stability derivative C_{X_α} is,

$$C_{X_\alpha} = \frac{X_w}{\frac{1}{2}\rho VS} = \frac{\partial C_X}{\partial \alpha}$$

Now the order of differentiation with respect to w and non-dimensionalizing using the factor $\frac{1}{2}\rho V^2 S$ may be changed, as $\frac{1}{2}\rho V^2 S$ does not contain the factor w .

The expressions for the different stability derivatives for symmetric motions are collected in table 4-3. The non-dimensional control derivatives are given in table 4-4. See also table 4-5 for the definition of the non-dimensional moments and products of inertia.

The non-dimensional equations for the symmetric motions now become,

$$\begin{aligned} C_{Z_0}\theta + C_{X_u}\hat{u} + C_{X_\alpha}\alpha + C_{X_q}D_c\theta + C_{X_{\delta_e}}\delta_e + C_{X_{\delta_t}}\delta_t &= 2\mu_c D_c\hat{u} \\ -C_{X_0}\theta + C_{Z_u}\hat{u} + C_{Z_\alpha}\alpha + C_{Z_{\dot{\alpha}}}D_c\alpha + C_{Z_q}D_c\theta + C_{Z_{\delta_e}}\delta_e + C_{Z_{\delta_t}}\delta_t &= 2\mu_c (D_c\alpha - D_c\theta) \\ C_{m_u}\hat{u} + C_{m_\alpha}\alpha + C_{m_{\dot{\alpha}}}D_c\alpha + C_{m_q}D_c\theta + C_{m_{\delta_e}}\delta_e + C_{m_{\delta_t}}\delta_t &= 2\mu_c K_Y^2 D_c \frac{q\bar{c}}{V} \\ \frac{\dot{\theta}\bar{c}}{V} &= \frac{q\bar{c}}{V} \end{aligned} \quad (4-38)$$

The four equations (4-38) are now rewritten in an ordered form. In this way, the following differential equations in the variables \hat{u} , α , θ and $\frac{q\bar{c}}{V}$ result in,

$$\begin{aligned} (C_{X_u} - 2\mu_c D_c)\hat{u} + C_{X_\alpha}\alpha + C_{Z_0}\theta + C_{X_q}\frac{q\bar{c}}{V} + C_{X_{\delta_e}}\delta_e + C_{X_{\delta_t}}\delta_t &= 0 \\ C_{Z_u}\hat{u} + [C_{Z_\alpha} + (C_{Z_{\dot{\alpha}}} + 2\mu_c)D_c]\alpha - C_{X_0}\theta + (C_{Z_q} + 2\mu_c)\frac{q\bar{c}}{V} + C_{Z_{\delta_e}}\delta_e + C_{Z_{\delta_t}}\delta_t &= 0 \\ -D_c\theta + \frac{q\bar{c}}{V} &= 0 \\ C_{m_u}\hat{u} + (C_{m_\alpha} + C_{m_{\dot{\alpha}}}D_c)\alpha + (C_{m_q} - 2\mu_c K_Y^2 D_c)\frac{q\bar{c}}{V} + C_{m_{\delta_e}}\delta_e + C_{m_{\delta_t}}\delta_t &= 0 \end{aligned} \quad (4-39)$$

or using matrix notation,

$$\begin{aligned} \begin{bmatrix} C_{X_u} - 2\mu_c D_c & C_{X_\alpha} & C_{Z_0} & C_{X_q} \\ C_{Z_u} & C_{Z_\alpha} + (C_{Z_{\dot{\alpha}}} - 2\mu_c)D_c & -C_{X_0} & C_{Z_q} + 2\mu_c \\ 0 & 0 & -D_c & 1 \\ C_{m_u} & C_{m_\alpha} + C_{m_{\dot{\alpha}}}D_c & 0 & C_{m_q} - 2\mu_c K_Y^2 D_c \end{bmatrix} \begin{bmatrix} \hat{u} \\ \alpha \\ \theta \\ \frac{q\bar{c}}{V} \end{bmatrix} \\ = \begin{bmatrix} -C_{X_{\delta_e}} & -C_{X_{\delta_t}} \\ -C_{Z_{\delta_e}} & -C_{Z_{\delta_t}} \\ 0 & 0 \\ -C_{m_{\delta_e}} & -C_{m_{\delta_t}} \end{bmatrix} \begin{bmatrix} \delta_e \\ \delta_t \end{bmatrix} \end{aligned} \quad (4-40)$$

and with,

$$\theta = \alpha + \gamma$$

the left hand side of equation (4-40) can also be expressed in the variables \hat{u} , γ , θ and $\frac{q\bar{c}}{V}$. If equation (4-40) is written as $P \mathbf{x} = Q \mathbf{u}$ with $\mathbf{x} = [\hat{u}, \gamma, \theta, \frac{q\bar{c}}{V}]^T$ and $\mathbf{u} = [\delta_e, \delta_t]^T$, matrix P is equal to,

$$\begin{bmatrix} C_{X_u} - 2\mu_c D_c & -C_{X_\alpha} & C_{X_\alpha} + C_{Z_0} & C_{X_q} \\ C_{Z_u} & -C_{Z_\alpha} - (C_{Z_\alpha} - 2\mu_c) D_c & C_{Z_\alpha} - C_{X_0} & C_{Z_\alpha} + C_{Z_q} \\ 0 & 0 & -D_c & 1 \\ C_{m_u} & -C_{m_\alpha} - C_{m_\alpha} D_c & C_{m_\alpha} & C_{m_\alpha} + C_{m_q} - 2\mu_c K_Y^2 D_c \end{bmatrix}$$

The right hand side of equation (4-40), i.e. $Q [\delta_e, \delta_t]^T$, remains unchanged with matrix Q equal to,

$$Q = \begin{bmatrix} -C_{X_{\delta_e}} & -C_{X_{\delta_t}} \\ -C_{Z_{\delta_e}} & -C_{Z_{\delta_t}} \\ 0 & 0 \\ -C_{m_{\delta_e}} & -C_{m_{\delta_t}} \end{bmatrix}$$

4-3-2 Asymmetric Motions

The equations for the asymmetric motions are made non-dimensional in close analogy with the foregoing. The force equation is again divided by $\frac{1}{2}\rho V^2 S$ and the two moment equations by $\frac{1}{2}\rho V^2 S b$. The result is,

$$\begin{aligned} \frac{W \cos \theta_0 \cdot \varphi}{\frac{1}{2}\rho V^2 S} + \frac{Y_v v + Y_i \dot{v} + Y_p p + Y_r r + Y_{\delta_a} \delta_a + Y_{\delta_r} \delta_r}{\frac{1}{2}\rho V^2 S} &= \frac{m(\dot{v} + r \cdot V)}{\frac{1}{2}\rho V^2 S} \\ \frac{L_v v + L_p p + L_r r + L_{\delta_a} \delta_a + L_{\delta_r} \delta_r}{\frac{1}{2}\rho V^2 S b} &= \frac{I_{xx} \dot{p} - I_{xz} \dot{r}}{\frac{1}{2}\rho V^2 S b} \\ \frac{N_v v + N_i \dot{v} + N_p p + N_r r + N_{\delta_a} \delta_a + N_{\delta_r} \delta_r}{\frac{1}{2}\rho V^2 S b} &= \frac{I_{zz} \dot{r} - I_{xz} \dot{p}}{\frac{1}{2}\rho V^2 S b} \\ \frac{\dot{\psi} b}{V} &= \frac{b}{V} \frac{r}{\cos \theta_0} \\ \frac{\dot{\varphi} b}{V} &= \frac{pb}{V} + \frac{rb}{V} \tan \theta_0 \end{aligned}$$

The component of the weight along the Z_S -axis is now written as,

$$\frac{W \cos \theta_0}{\frac{1}{2}\rho V^2 S} = \frac{W \cos \gamma_0}{\frac{1}{2}\rho V^2 S} = C_L$$

Next, the partial derivatives of the aerodynamic force and the two moments are expressed using the non-dimensional stability derivatives according to the scheme of table 4-6. See also table 4-7 and 4-8 for the definition of the non-dimensional control derivatives and the moments and products of inertia respectively. If in addition θ_0 in the kinematic relations is replaced by γ_0 , using equation (4-26), the non-dimensional equations for the asymmetric motions are,

$$\begin{aligned}
C_L \varphi + C_{Y_\beta} \beta + C_{Y_{\dot{\beta}}} D_b \beta + C_{Y_p} \frac{pb}{2V} + C_{Y_r} \frac{rb}{2V} + C_{Y_{\delta_a}} \delta_a + C_{Y_{\delta_r}} \delta_r &= 2\mu_b (D_b \beta + 2 \frac{rb}{2V}) \\
C_{\ell_\beta} \beta + C_{\ell_p} \frac{pb}{2V} + C_{\ell_r} \frac{rb}{2V} + C_{\ell_{\delta_a}} \delta_a + C_{\ell_{\delta_r}} \delta_r &= 4\mu_b (K_X^2 D_b \frac{pb}{2V} \\
&\quad - K_{XZ} D_b \frac{rb}{2V}) \\
C_{n_\beta} \beta + C_{n_{\dot{\beta}}} D_b \beta + C_{n_p} \frac{pb}{2V} + C_{n_r} \frac{rb}{2V} + C_{n_{\delta_a}} \delta_a + C_{n_{\delta_r}} \delta_r &= 4\mu_b (K_Z^2 D_b \frac{rb}{2V} \\
&\quad - K_{XZ} D_b \frac{pb}{2V}) \\
\frac{1}{2} D_b \psi &= \frac{1}{\cos \gamma_0} \frac{rb}{2V} \\
\frac{1}{2} D_b \varphi &= \frac{pb}{2V} + \frac{rb}{2V} \tan \gamma_0
\end{aligned} \tag{4-41}$$

In level flight ($\gamma_0 = 0$) the kinematic relations are reduced to,

$$\begin{aligned}
\frac{1}{2} D_b \psi &= \frac{rb}{2V} \\
\frac{1}{2} D_b \varphi &= \frac{pb}{2V}
\end{aligned}$$

By adding the latter of these two relations,

$$-\frac{1}{2} D_b \varphi + \frac{pb}{2V} = 0$$

the equations of motion (4-41) are changed into a set of four first order differential equations in β , φ , $\frac{pb}{2V}$ and $\frac{rb}{2V}$,

$$\begin{aligned}
[C_{Y_\beta} + (C_{Y_{\dot{\beta}}} - 2\mu_b) D_b] \beta + C_L \varphi + C_{Y_p} \frac{pb}{2V} + (C_{Y_r} - 4\mu_b) \frac{rb}{2V} + C_{Y_{\delta_a}} \delta_a + C_{Y_{\delta_r}} \delta_r &= 0 \\
-\frac{1}{2} D_b \varphi + \frac{pb}{2V} &= 0 \\
C_{\ell_\beta} \beta + (C_{\ell_p} - 4\mu_b K_X^2 D_b) \frac{pb}{2V} + (C_{\ell_r} + 4\mu_b K_{XZ} D_b) \frac{rb}{2V} + C_{\ell_{\delta_a}} \delta_a + C_{\ell_{\delta_r}} \delta_r &= 0 \\
(C_{n_\beta} + C_{n_{\dot{\beta}}} D_b) \beta + (C_{n_p} + 4\mu_b K_{XZ} D_b) \frac{pb}{2V} + (C_{n_r} - 4\mu_b K_Z^2 D_b) \frac{rb}{2V} + C_{n_{\delta_a}} \delta_a + C_{n_{\delta_r}} \delta_r &= 0
\end{aligned} \tag{4-42}$$

Using matrix notation, equations (4-42) are written as,

$$\begin{aligned}
&\begin{bmatrix} C_{Y_\beta} + (C_{Y_{\dot{\beta}}} - 2\mu_b) D_b & C_L & C_{Y_p} & C_{Y_r} - 4\mu_b \\ 0 & -\frac{1}{2} D_b & 1 & 0 \\ C_{\ell_\beta} & 0 & C_{\ell_p} - 4\mu_b K_X^2 D_b & C_{\ell_r} + 4\mu_b K_{XZ} D_b \\ C_{n_\beta} + C_{n_{\dot{\beta}}} D_b & 0 & C_{n_p} + 4\mu_b K_{XZ} D_b & C_{n_r} - 4\mu_b K_Z^2 D_b \end{bmatrix} \begin{bmatrix} \beta \\ \varphi \\ \frac{pb}{2V} \\ \frac{rb}{2V} \end{bmatrix} \\
&= \begin{bmatrix} -C_{Y_{\delta_a}} & -C_{Y_{\delta_r}} \\ 0 & 0 \\ -C_{\ell_{\delta_a}} & -C_{\ell_{\delta_r}} \\ -C_{n_{\delta_a}} & -C_{n_{\delta_r}} \end{bmatrix} \begin{bmatrix} \delta_a \\ \delta_r \end{bmatrix}
\end{aligned} \tag{4-43}$$

At the end of this section it should be noted that,

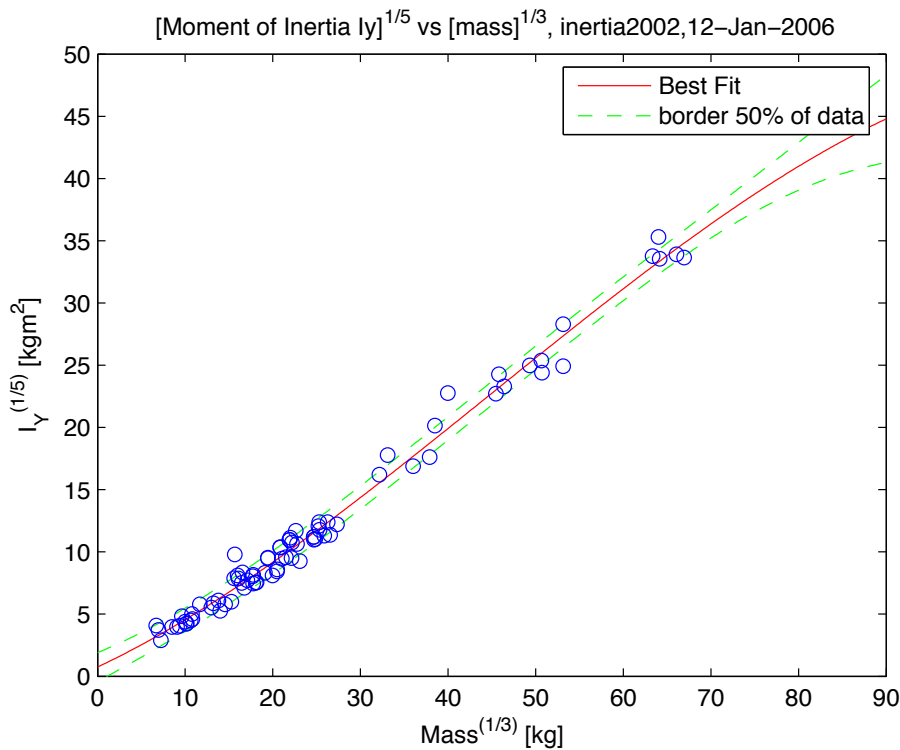


Figure 4-6: Relation between moment of inertia I_{yy} and the mass

- Often, especially in the British literature, the equations of motion are made non-dimensional using a unit of time not equal to $\frac{\bar{c}}{V}$, but $\tau_c \mu_c \frac{\bar{c}}{V}$ seconds for the symmetric motions and $\tau_b \mu_b \frac{b}{V}$ seconds rather than $\frac{b}{V}$ seconds for the asymmetric motions. The particular way of making the equations non-dimensional is determined in the first place by the habits of the user. None of the various methods offers clear advantages or disadvantages in comparison with other possible methods. This explains why only one method has been described in detail here.
- In chapters 7 and 8 attention is given to the methods used to obtain the various stability and control derivatives for the symmetric and asymmetric motions respectively.
- Reliable quantitative data on moments and products of inertia of aircraft are rare. Quantitative calculations can be time-consuming and may produce rather inaccurate results. The most reliable inertial parameters of aircraft are those obtained experimentally, usually by oscillating the suspended aircraft on the ground. Details on this experimental technique may be found in references [41, 102, 176, 181]. Figure 4-6 shows the relation between the moment of inertia I_{yy} and the mass for multiple types of aircraft. One can make educated guesses for the inertia properties of new types of aircraft using such figures.
- Appendix D lists symmetrical and asymmetrical inertial data, as well as stability and control derivatives for both the symmetric and asymmetric motions.

Dimensional parameter	Dimension	Divisor	Non-dimensional parameter
t	$[t]$	$\frac{\bar{c}}{V}$	$s_c = \frac{V}{\bar{c}} t$
$\frac{d}{dt}$	$[t]^{-1}$	$\frac{V}{\bar{c}}$	$D_c = \frac{\bar{c}}{V} \frac{d}{dt} = \frac{d}{ds_c}$
$\frac{d^2}{dt^2}$	$[t]^{-2}$	$\frac{V^2}{\bar{c}^2}$	$D_c^2 = \frac{\bar{c}^2}{V^2} \frac{d^2}{dt^2} = \frac{d^2}{ds_c^2}$
u	$[\ell][t]^{-1}$	V	$\hat{u} = \frac{u}{V}$
w	$[\ell][t]^{-1}$	V	$\alpha = \frac{w}{V}$
q	$[t]^{-1}$	$\frac{V}{\bar{c}}$	$\frac{q\bar{c}}{V}$
\dot{u}	$[\ell][t]^{-2}$	$\frac{V^2}{\bar{c}}$	$D_c \hat{u} = \frac{\dot{u}}{V} \frac{\bar{c}}{V} = \frac{\dot{u}\bar{c}}{V}$
\dot{w}	$[\ell][t]^{-2}$	$\frac{V^2}{\bar{c}}$	$D_c \alpha = \frac{\dot{w}}{V} \frac{\bar{c}}{V} = \frac{\dot{\alpha}\bar{c}}{V}$
\dot{q}	$[t]^{-2}$	$\frac{V^2}{\bar{c}^2}$	$D_c \frac{q\bar{c}}{V} = \dot{q} \frac{\bar{c}^2}{V^2}$
m	$[m]$	$\rho S \bar{c}$	$\mu_c = \frac{m}{\rho S \bar{c}}$
I_{yy}	$[m][\ell]^2$	$\rho S \bar{c} \cdot \bar{c}^2$	$\mu_c K_Y^2 = \frac{I_{yy}}{\rho S \bar{c}^3}$
k_y	$[\ell]$	\bar{c}	$K_Y = \frac{k_y}{\bar{c}}$
X	$[m][\ell][t]^{-2}$	$\frac{1}{2} \rho S \bar{c} \cdot \bar{c} \cdot \frac{V^2}{\bar{c}^2}$	$C_X = \frac{X}{\frac{1}{2} \rho V^2 S}$
Z	$[m][\ell][t]^{-2}$	$\frac{1}{2} \rho S \bar{c} \cdot \bar{c} \cdot \frac{V^2}{\bar{c}^2}$	$C_Z = \frac{Z}{\frac{1}{2} \rho V^2 S}$
M	$[m][\ell]^2[t]^{-2}$	$\frac{1}{2} \rho S \bar{c}^2 \cdot \bar{c} \cdot \frac{V^2}{\bar{c}^2}$	$C_m = \frac{M}{\frac{1}{2} \rho V^2 S \bar{c}}$

Table 4-1: Non-dimensional parameters in the equations of motion, symmetric motions

Dimensional parameter	Dimension	Divisor	Non-dimensional parameter
t	$[t]$	$\frac{b}{V}$	$s_b = \frac{V}{b} t$
$\frac{d}{dt}$	$[t]^{-1}$	$\frac{V}{b}$	$D_b = \frac{b}{V} \frac{d}{dt} = \frac{d}{ds_b}$
$\frac{d^2}{dt^2}$	$[t]^{-2}$	$\frac{V^2}{b^2}$	$D_b^2 = \frac{b^2}{V^2} \frac{d^2}{dt^2} = \frac{d^2}{ds_b^2}$
v	$[\ell][t]^{-1}$	V	$\beta = \frac{v}{V}$
p	$[\ell][t]^{-1}$	$\frac{2V}{b}$	$\frac{pb}{2V}$
r	$[t]^{-1}$	$\frac{2V}{b}$	$\frac{rb}{2V}$
\dot{v}	$[\ell][t]^{-2}$	$\frac{V^2}{b}$	$D_b \beta = \frac{\dot{v}}{V} \frac{b}{V} = \frac{\dot{\beta}b}{V}$
\dot{p}	$[t]^{-2}$	$\frac{2V^2}{b^2}$	$D_b \frac{pb}{2V} = \frac{\dot{p}b^2}{2V^2}$
\dot{r}	$[t]^{-2}$	$\frac{2V^2}{b^2}$	$D_b \frac{rb}{2V} = \frac{\dot{r}b^2}{2V^2}$
m	$[m]$	ρSb	$\mu_b = \frac{m}{\rho Sb}$
I_{xx}	$[m][\ell]^2$	$\rho Sb \cdot b^2$	$\mu_b K_X^2 = \frac{I_{xx}}{\rho Sb^3}$
I_{zz}	$[m][\ell]^2$	$\rho Sb \cdot b^2$	$\mu_b K_Z^2 = \frac{I_{zz}}{\rho Sb^3}$
J_{XZ}	$[m][\ell]^2$	$\rho Sb \cdot b^2$	$\mu_b K_{XZ} = \frac{J_{XZ}}{\rho Sb^3}$
k_x	$[\ell]$	b	$K_X = \frac{k_x}{b}$
k_z	$[\ell]$	b	$K_Z = \frac{k_z}{b}$

Table 4-2: Non-dimensional parameters in the equations of motion, asymmetric motions

Dimensional parameter	Dimension	Divisor	Non-dimensional parameter
Y	$[m][\ell][t]^{-2}$	$\frac{1}{2}\rho Sb \cdot b \cdot \frac{V^2}{b^2}$	$C_Y = \frac{Y}{\frac{1}{2}\rho V^2 Sb}$
L	$[m][\ell]^2[t]^{-2}$	$\frac{1}{2}\rho Sb^2 \cdot b \cdot \frac{V^2}{b^2}$	$C_\ell = \frac{L}{\frac{1}{2}\rho V^2 Sb}$
N	$[m][\ell]^2[t]^{-2}$	$\frac{1}{2}\rho Sb^2 \cdot b \cdot \frac{V^2}{b^2}$	$C_n = \frac{N}{\frac{1}{2}\rho V^2 Sb}$

Table 4-2: **(Continued)** Non-dimensional parameters in the equations of motion, asymmetric motions

Definition
$C_{X_u} = \frac{1}{\frac{1}{2}\rho VS} \cdot \frac{\partial X}{\partial u} \neq \frac{\partial C_X}{\partial \hat{u}}$
$C_{Z_u} = \frac{1}{\frac{1}{2}\rho VS} \cdot \frac{\partial Z}{\partial u} \neq \frac{\partial C_Z}{\partial \hat{u}}$
$C_{m_u} = \frac{1}{\frac{1}{2}\rho VS\bar{c}} \cdot \frac{\partial M}{\partial u} \neq \frac{\partial C_m}{\partial \hat{u}}$
$C_{X_\alpha} = \frac{1}{\frac{1}{2}\rho VS} \cdot \frac{\partial X}{\partial w} = \frac{\partial C_X}{\partial \alpha}$
$C_{Z_\alpha} = \frac{1}{\frac{1}{2}\rho VS} \cdot \frac{\partial Z}{\partial w} = \frac{\partial C_Z}{\partial \alpha}$
$C_{m_\alpha} = \frac{1}{\frac{1}{2}\rho VS\bar{c}} \cdot \frac{\partial M}{\partial w} = \frac{\partial C_m}{\partial \alpha}$
$C_{Z_{\dot{\alpha}}} = \frac{1}{\frac{1}{2}\rho S\bar{c}} \cdot \frac{\partial Z}{\partial \dot{w}} = \frac{\partial C_Z}{\partial \dot{\alpha}\bar{c}}$
$C_{m_{\dot{\alpha}}} = \frac{1}{\frac{1}{2}\rho S\bar{c}^2} \cdot \frac{\partial M}{\partial \dot{w}} = \frac{\partial C_m}{\partial \dot{\alpha}\bar{c}}$
$C_{X_q} = \frac{1}{\frac{1}{2}\rho VS\bar{c}} \cdot \frac{\partial X}{\partial q} = \frac{\partial C_X}{\partial \frac{qc}{V}}$
$C_{Z_q} = \frac{1}{\frac{1}{2}\rho VS\bar{c}} \cdot \frac{\partial Z}{\partial q} = \frac{\partial C_Z}{\partial \frac{qc}{V}}$
$C_{m_q} = \frac{1}{\frac{1}{2}\rho VS\bar{c}^2} \cdot \frac{\partial M}{\partial q} = \frac{\partial C_m}{\partial \frac{qc}{V}}$

Table 4-3: Stability derivatives, symmetric motions

Definition
$C_{X_{\delta_e}} = \frac{1}{\frac{1}{2}\rho V^2 S} \cdot \frac{\partial X}{\partial \delta_e} = \frac{\partial C_X}{\partial \delta_e}$
$C_{Z_{\delta_e}} = \frac{1}{\frac{1}{2}\rho V^2 S} \cdot \frac{\partial Z}{\partial \delta_e} = \frac{\partial C_Z}{\partial \delta_e}$
$C_{m_{\delta_e}} = \frac{1}{\frac{1}{2}\rho V^2 S \bar{c}} \cdot \frac{\partial M}{\partial \delta_e} = \frac{\partial C_m}{\partial \delta_e}$
$C_{X_{\delta_t}} = \frac{1}{\frac{1}{2}\rho V^2 S} \cdot \frac{\partial X}{\partial \delta_t} = \frac{\partial C_X}{\partial \delta_t}$
$C_{Z_{\delta_t}} = \frac{1}{\frac{1}{2}\rho V^2 S} \cdot \frac{\partial Z}{\partial \delta_t} = \frac{\partial C_Z}{\partial \delta_t}$
$C_{m_{\delta_t}} = \frac{1}{\frac{1}{2}\rho V^2 S \bar{c}} \cdot \frac{\partial M}{\partial \delta_t} = \frac{\partial C_m}{\partial \delta_t}$

Table 4-4: Control derivatives, symmetric motions

Definition
$\mu_c = \frac{m}{\rho S \bar{c}}$
$K_Y^2 = \frac{I_{yy}}{m \bar{c}^2}$

Table 4-5: Moments and products of inertia, symmetric motions

Definition
$C_{Y_\beta} = \frac{1}{\frac{1}{2}\rho VS} \cdot \frac{\partial Y}{\partial v} = \frac{\partial C_Y}{\partial \beta}$
$C_{\ell_\beta} = \frac{1}{\frac{1}{2}\rho VSb} \cdot \frac{\partial L}{\partial v} = \frac{\partial C_\ell}{\partial \beta}$
$C_{n_\beta} = \frac{1}{\frac{1}{2}\rho VSb} \cdot \frac{\partial N}{\partial v} = \frac{\partial C_n}{\partial \beta}$
$C_{Y_{\dot{\beta}}} = \frac{1}{\frac{1}{2}\rho VSb} \cdot \frac{\partial Y}{\partial \dot{v}} = \frac{\partial C_Y}{\partial \dot{\beta}}$
$C_{n_{\dot{\beta}}} = \frac{1}{\frac{1}{2}\rho Sb^2} \cdot \frac{\partial N}{\partial \dot{v}} = \frac{\partial C_n}{\partial \dot{\beta}}$
$C_{Y_p} = \frac{2}{\frac{1}{2}\rho VSb} \cdot \frac{\partial Y}{\partial p} = \frac{\partial C_Y}{\partial \frac{pb}{2V}}$
$C_{\ell_p} = \frac{2}{\frac{1}{2}\rho VSb^2} \cdot \frac{\partial L}{\partial p} = \frac{\partial C_\ell}{\partial \frac{pb}{2V}}$
$C_{n_p} = \frac{2}{\frac{1}{2}\rho VSb^2} \cdot \frac{\partial N}{\partial p} = \frac{\partial C_n}{\partial \frac{pb}{2V}}$
$C_{Y_r} = \frac{2}{\frac{1}{2}\rho VSb} \cdot \frac{\partial Y}{\partial r} = \frac{\partial C_Y}{\partial \frac{rb}{2V}}$
$C_{\ell_r} = \frac{2}{\frac{1}{2}\rho VSb^2} \cdot \frac{\partial L}{\partial r} = \frac{\partial C_\ell}{\partial \frac{rb}{2V}}$
$C_{n_r} = \frac{2}{\frac{1}{2}\rho VSb^2} \cdot \frac{\partial N}{\partial r} = \frac{\partial C_n}{\partial \frac{rb}{2V}}$

Table 4-6: Stability derivatives, asymmetric motions

Definition
$C_{Y_{\delta_a}} = \frac{1}{\frac{1}{2}\rho V^2 S} \cdot \frac{\partial Y}{\partial \delta_a} = \frac{\partial C_Y}{\partial \delta_a}$
$C_{\ell_{\delta_a}} = \frac{1}{\frac{1}{2}\rho V^2 S b} \cdot \frac{\partial L}{\partial \delta_a} = \frac{\partial C_\ell}{\partial \delta_a}$
$C_{n_{\delta_a}} = \frac{1}{\frac{1}{2}\rho V^2 S b} \cdot \frac{\partial N}{\partial \delta_a} = \frac{\partial C_n}{\partial \delta_a}$
$C_{Y_{\delta_r}} = \frac{1}{\frac{1}{2}\rho V^2 S} \cdot \frac{\partial Y}{\partial \delta_r} = \frac{\partial C_Y}{\partial \delta_r}$
$C_{\ell_{\delta_r}} = \frac{1}{\frac{1}{2}\rho V^2 S b} \cdot \frac{\partial L}{\partial \delta_r} = \frac{\partial C_\ell}{\partial \delta_r}$
$C_{n_{\delta_r}} = \frac{1}{\frac{1}{2}\rho V^2 S b} \cdot \frac{\partial N}{\partial \delta_r} = \frac{\partial C_n}{\partial \delta_r}$

Table 4-7: Control derivatives, asymmetric motions

Definition
$\mu_b = \frac{m}{\rho S b}$
$K_X^2 = \frac{I_{xx}}{mb^2}$
$K_Z^2 = \frac{I_{zz}}{mb^2}$
$J_{XZ} = \frac{I_{xz}}{mb^2}$

Table 4-8: Moments and products of inertia, asymmetric motions

4-4 Symmetric equations of motion in state-space form

The linearized ‘deviation equations’ for the symmetric motions, where $C_{X_q} = 0$, are, see equation (4-40),

$$\begin{bmatrix} C_{X_u} - 2\mu_c D_c & C_{X_\alpha} & C_{Z_0} & 0 \\ C_{Z_u} & C_{Z_\alpha} + (C_{Z_{\dot{\alpha}}} - 2\mu_c) D_c & -C_{X_0} & C_{Z_q} + 2\mu_c \\ 0 & 0 & -D_c & 1 \\ C_{m_u} & C_{m_\alpha} + C_{m_{\dot{\alpha}}} D_c & 0 & C_{m_q} - 2\mu_c K_Y^2 D_c \end{bmatrix} \begin{bmatrix} \hat{u} \\ \alpha \\ \theta \\ \frac{q\bar{c}}{V} \end{bmatrix} =$$

$$= \begin{bmatrix} -C_{X_{\delta_e}} & -C_{X_{\delta_t}} \\ -C_{Z_{\delta_e}} & -C_{Z_{\delta_t}} \\ 0 & 0 \\ -C_{m_{\delta_e}} & -C_{m_{\delta_t}} \end{bmatrix} \begin{bmatrix} \delta_e \\ \delta_t \end{bmatrix}$$

Linear Time Invariant (LTI) systems are given in the so called state-space form,

$$\dot{\mathbf{x}} = \mathbf{A} \mathbf{x} + \mathbf{B} \mathbf{u} \quad (4-44)$$

$$\mathbf{y} = \mathbf{C} \mathbf{x} + \mathbf{D} \mathbf{u} \quad (4-45)$$

with \mathbf{A} ($n \times n$) the state-matrix, \mathbf{B} ($n \times m$) the input-matrix, \mathbf{C} ($r \times n$) the output matrix and \mathbf{D} ($r \times m$) the direct matrix. Furthermore, \mathbf{x} ($n \times 1$) and \mathbf{y} ($r \times 1$) are the state and output vector respectively, while \mathbf{u} ($m \times 1$) is the input vector. Since the system is LTI, the matrices \mathbf{A} , \mathbf{B} , \mathbf{C} , and \mathbf{D} have constant elements.

This form can be obtained by rearranging equation (4-40). First, all terms without the differential operator D_c are placed on the right hand side of equation (4-40). Furthermore, the differential operator D_c is replaced by $\frac{\bar{c}}{V} \frac{d}{dt}$. The result is,

$$\begin{bmatrix} -2\mu_c \frac{\bar{c}}{V} \frac{d}{dt} & 0 & 0 & 0 \\ 0 & (C_{Z_{\dot{\alpha}}} - 2\mu_c) \frac{\bar{c}}{V} \frac{d}{dt} & 0 & 0 \\ 0 & 0 & -\frac{\bar{c}}{V} \frac{d}{dt} & 0 \\ 0 & C_{m_{\dot{\alpha}}} \frac{\bar{c}}{V} \frac{d}{dt} & 0 & -2\mu_c K_Y^2 \frac{\bar{c}}{V} \frac{d}{dt} \end{bmatrix} \begin{bmatrix} \hat{u} \\ \alpha \\ \theta \\ \frac{q\bar{c}}{V} \end{bmatrix} =$$

$$\begin{bmatrix} -C_{X_u} & -C_{X_\alpha} & -C_{Z_0} & 0 \\ -C_{Z_u} & -C_{Z_\alpha} & C_{X_0} & -(C_{Z_q} + 2\mu_c) \\ 0 & 0 & 0 & -1 \\ -C_{m_u} & -C_{m_\alpha} & 0 & -C_{m_q} \end{bmatrix} \begin{bmatrix} \hat{u} \\ \alpha \\ \theta \\ \frac{q\bar{c}}{V} \end{bmatrix} + \begin{bmatrix} -C_{X_{\delta_e}} & -C_{X_{\delta_t}} \\ -C_{Z_{\delta_e}} & -C_{Z_{\delta_t}} \\ 0 & 0 \\ -C_{m_{\delta_e}} & -C_{m_{\delta_t}} \end{bmatrix} \begin{bmatrix} \delta_e \\ \delta_t \end{bmatrix}$$

This equation can be written in the form,

$$\mathbf{P} \dot{\mathbf{x}} = \mathbf{P} \frac{d\mathbf{x}}{dt} = \mathbf{Q} \mathbf{x} + \mathbf{R} \mathbf{u} \quad (4-46)$$

with,

$$\mathbf{P} = \begin{bmatrix} -2\mu_c \frac{\bar{c}}{V} & 0 & 0 & 0 \\ 0 & (C_{Z_{\dot{\alpha}}} - 2\mu_c) \frac{\bar{c}}{V} & 0 & 0 \\ 0 & 0 & -\frac{\bar{c}}{V} & 0 \\ 0 & C_{m_{\dot{\alpha}}} \frac{\bar{c}}{V} & 0 & -2\mu_c K_Y^2 \frac{\bar{c}}{V} \end{bmatrix}$$

	x_{\dots}	z_{\dots}	m_{\dots}
u	$\frac{V}{\bar{c}} \frac{C_{X_u}}{2\mu_c}$	$\frac{V}{\bar{c}} \frac{C_{Z_u}}{2\mu_c - C_{Z_{\dot{\alpha}}}}$	$\frac{V}{\bar{c}} \frac{C_{m_u} + C_{Z_u} \frac{C_{m_{\dot{\alpha}}}}{2\mu_c - C_{Z_{\dot{\alpha}}}}}{2\mu_c K_Y^2}$
α	$\frac{V}{\bar{c}} \frac{C_{X_\alpha}}{2\mu_c}$	$\frac{V}{\bar{c}} \frac{C_{Z_\alpha}}{2\mu_c - C_{Z_{\dot{\alpha}}}}$	$\frac{V}{\bar{c}} \frac{C_{m_\alpha} + C_{Z_\alpha} \frac{C_{m_{\dot{\alpha}}}}{2\mu_c - C_{Z_{\dot{\alpha}}}}}{2\mu_c K_Y^2}$
θ	$\frac{V}{\bar{c}} \frac{C_{Z_0}}{2\mu_c}$	$-\frac{V}{\bar{c}} \frac{C_{X_0}}{2\mu_c - C_{Z_{\dot{\alpha}}}}$	$-\frac{V}{\bar{c}} \frac{C_{m_{\dot{\alpha}}} \frac{C_{m_{\dot{\alpha}}}}{2\mu_c - C_{Z_{\dot{\alpha}}}}}{2\mu_c K_Y^2}$
q	$\frac{V}{\bar{c}} \frac{C_{X_q}}{2\mu_c}$	$\frac{V}{\bar{c}} \frac{2\mu_c + C_{Z_q}}{2\mu_c - C_{Z_{\dot{\alpha}}}}$	$\frac{V}{\bar{c}} \frac{C_{m_q} + C_{m_\alpha} \frac{2\mu_c + C_{Z_q}}{2\mu_c - C_{Z_{\dot{\alpha}}}}}{2\mu_c K_Y^2}$
δ_e	$\frac{V}{\bar{c}} \frac{C_{X_{\delta_e}}}{2\mu_c}$	$\frac{V}{\bar{c}} \frac{C_{Z_{\delta_e}}}{2\mu_c - C_{Z_{\dot{\alpha}}}}$	$\frac{V}{\bar{c}} \frac{C_{m_{\delta_e}} + C_{Z_{\delta_e}} \frac{C_{m_{\dot{\alpha}}}}{2\mu_c - C_{Z_{\dot{\alpha}}}}}{2\mu_c K_Y^2}$
δ_t	$\frac{V}{\bar{c}} \frac{C_{X_{\delta_t}}}{2\mu_c}$	$\frac{V}{\bar{c}} \frac{C_{Z_{\delta_t}}}{2\mu_c - C_{Z_{\dot{\alpha}}}}$	$\frac{V}{\bar{c}} \frac{C_{m_{\delta_t}} + C_{Z_{\delta_t}} \frac{C_{m_{\dot{\alpha}}}}{2\mu_c - C_{Z_{\dot{\alpha}}}}}{2\mu_c K_Y^2}$

Table 4-9: Symbols appearing in the general state-space representation of equation (4-48)

$$\mathbf{Q} = \begin{bmatrix} -C_{X_u} & -C_{X_\alpha} & -C_{Z_0} & 0 \\ -C_{Z_u} & -C_{Z_\alpha} & C_{X_0} & -(C_{Z_q} + 2\mu_c) \\ 0 & 0 & 0 & -1 \\ -C_{m_u} & -C_{m_\alpha} & 0 & -C_{m_q} \end{bmatrix}$$

$$\mathbf{R} = \begin{bmatrix} -C_{X_{\delta_e}} & -C_{X_{\delta_t}} \\ -C_{Z_{\delta_e}} & -C_{Z_{\delta_t}} \\ 0 & 0 \\ -C_{m_{\delta_e}} & -C_{m_{\delta_t}} \end{bmatrix}$$

and $\mathbf{x} = [\hat{u} \ \alpha \ \theta \ \frac{q\bar{c}}{V}]^T$, while $\mathbf{u} = [\delta_e, \delta_t]^T$. The final state-space form is obtained by premultiplying equation (4-46) by the inverse of matrix \mathbf{P} ,

$$\dot{\mathbf{x}} = \mathbf{P}^{-1} \mathbf{Q} \mathbf{x} + \mathbf{P}^{-1} \mathbf{R} \mathbf{u} = \mathbf{A} \mathbf{x} + \mathbf{B} \mathbf{u} \quad (4-47)$$

In flight dynamics, equation (4-47) is usually written as,

$$\begin{bmatrix} \dot{\hat{u}} \\ \dot{\alpha} \\ \dot{\theta} \\ \dot{\frac{q\bar{c}}{V}} \end{bmatrix} = \begin{bmatrix} x_u & x_\alpha & x_\theta & 0 \\ z_u & z_\alpha & z_\theta & z_q \\ 0 & 0 & 0 & \frac{V}{\bar{c}} \\ m_u & m_\alpha & m_\theta & m_q \end{bmatrix} \begin{bmatrix} \hat{u} \\ \alpha \\ \theta \\ \frac{q\bar{c}}{V} \end{bmatrix} + \begin{bmatrix} x_{\delta_e} & x_{\delta_t} \\ z_{\delta_e} & z_{\delta_t} \\ 0 & 0 \\ m_{\delta_e} & m_{\delta_t} \end{bmatrix} \begin{bmatrix} \delta_e \\ \delta_t \end{bmatrix} \quad (4-48)$$

The definition of the newly introduced symbols are recapitulated in table 4-9. Dimensional eigenvalues λ are obtained using MATLAB's routine `eig.m` (for the state matrix A).

4-5 Asymmetric equations of motion in state-space form

Similar to Section 4-4 the linearized ‘deviation equations’ for the asymmetric motions, are, see equation (4-43),

$$\begin{bmatrix} C_{Y_\beta} + (C_{Y_\beta} - 2\mu_b)D_b & C_L & C_{Y_p} & C_{Y_r} - 4\mu_b \\ 0 & -\frac{1}{2}D_b & 1 & 0 \\ C_{\ell_\beta} & 0 & C_{\ell_p} - 4\mu_b K_X^2 D_b & C_{\ell_r} + 4\mu_b K_{XZ} D_b \\ C_{n_\beta} + C_{n_\beta} D_b & 0 & C_{n_p} + 4\mu_b K_{XZ} D_b & C_{n_r} - 4\mu_b K_Z^2 D_b \end{bmatrix} \begin{bmatrix} \beta \\ \varphi \\ \frac{pb}{2V} \\ \frac{rb}{2V} \end{bmatrix} = \begin{bmatrix} -C_{Y_{\delta_a}} & -C_{Y_{\delta_r}} \\ 0 & 0 \\ -C_{\ell_{\delta_a}} & -C_{\ell_{\delta_r}} \\ -C_{n_{\delta_a}} & -C_{n_{\delta_r}} \end{bmatrix} \begin{bmatrix} \delta_a \\ \delta_r \end{bmatrix}$$

These equations of motion are transformed to the state-space form as in,

$$\dot{\mathbf{x}} = \mathbf{A} \mathbf{x} + \mathbf{B} \mathbf{u} \quad (4-49)$$

This form can be obtained by rearranging equation (4-43). First, all terms without the differential operator D_b are placed on the right hand side of equation (4-43). Furthermore, the differential operator D_b is replaced by $\frac{b}{V} \frac{d}{dt}$. The result is,

$$\begin{bmatrix} (C_{Y_\beta} - 2\mu_b) \frac{b}{V} \frac{d}{dt} & 0 & 0 & 0 \\ 0 & -\frac{1}{2} \frac{b}{V} \frac{d}{dt} & 0 & 0 \\ 0 & 0 & -4\mu_b K_X^2 \frac{b}{V} \frac{d}{dt} & 4\mu_b K_{XZ} \frac{b}{V} \frac{d}{dt} \\ C_{n_\beta} \frac{b}{V} \frac{d}{dt} & 0 & 4\mu_b K_{XZ} \frac{b}{V} \frac{d}{dt} & -4\mu_b K_Z^2 \frac{b}{V} \frac{d}{dt} \end{bmatrix} \begin{bmatrix} \beta \\ \varphi \\ \frac{pb}{2V} \\ \frac{rb}{2V} \end{bmatrix} = \begin{bmatrix} -C_{Y_\beta} & -C_L & -C_{Y_p} & -(C_{Y_r} - 4\mu_b) \\ 0 & 0 & -1 & 0 \\ -C_{\ell_\beta} & 0 & -C_{\ell_p} & -C_{\ell_r} \\ -C_{n_\beta} & 0 & -C_{n_p} & -C_{n_r} \end{bmatrix} \begin{bmatrix} \delta_a \\ \delta_r \end{bmatrix} + \begin{bmatrix} -C_{Y_{\delta_a}} & -C_{Y_{\delta_r}} \\ 0 & 0 \\ -C_{\ell_{\delta_a}} & -C_{\ell_{\delta_r}} \\ -C_{n_{\delta_a}} & -C_{n_{\delta_r}} \end{bmatrix} \begin{bmatrix} \delta_a \\ \delta_r \end{bmatrix}$$

Again, this equation can be written in the form,

$$\mathbf{P} \dot{\mathbf{x}} = \mathbf{P} \frac{d\mathbf{x}}{dt} = \mathbf{Q} \mathbf{x} + \mathbf{R} \mathbf{u} \quad (4-50)$$

with in this case,

$$\mathbf{P} = \begin{bmatrix} (C_{Y_\beta} - 2\mu_b) \frac{b}{V} & 0 & 0 & 0 \\ 0 & -\frac{1}{2} \frac{b}{V} & 0 & 0 \\ 0 & 0 & -4\mu_b K_X^2 \frac{b}{V} & 4\mu_b K_{XZ} \frac{b}{V} \\ C_{n_\beta} \frac{b}{V} & 0 & 4\mu_b K_{XZ} \frac{b}{V} & -4\mu_b K_Z^2 \frac{b}{V} \end{bmatrix}$$

$$\mathbf{Q} = \begin{bmatrix} -C_{Y_\beta} & -C_L & -C_{Y_p} & -(C_{Y_r} - 4\mu_b) \\ 0 & 0 & -1 & 0 \\ -C_{\ell_\beta} & 0 & -C_{\ell_p} & -C_{\ell_r} \\ -C_{n_\beta} & 0 & -C_{n_p} & -C_{n_r} \end{bmatrix}$$

	y_{\dots}	l_{\dots}	n_{\dots}
β	$\frac{V}{b} \frac{C_{Y_\beta}}{2\mu_b}$	$\frac{V}{b} \frac{C_{\ell_\beta} K_Z^2 + C_{n_\beta} K_{XZ}}{4\mu_b (K_X^2 K_Z^2 - K_{XZ}^2)}$	$\frac{V}{b} \frac{C_{\ell_\beta} K_{XZ} + C_{n_\beta} K_X^2}{4\mu_b (K_X^2 K_Z^2 - K_{XZ}^2)}$
φ	$\frac{V}{b} \frac{C_L}{2\mu_b}$	0	0
p	$\frac{V}{b} \frac{C_{Y_p}}{2\mu_b}$	$\frac{V}{b} \frac{C_{\ell_p} K_Z^2 + C_{n_p} K_{XZ}}{4\mu_b (K_X^2 K_Z^2 - K_{XZ}^2)}$	$\frac{V}{b} \frac{C_{\ell_p} K_{XZ} + C_{n_p} K_X^2}{4\mu_b (K_X^2 K_Z^2 - K_{XZ}^2)}$
r	$\frac{V}{b} \frac{C_{Y_r} - 4\mu_b}{2\mu_b}$	$\frac{V}{b} \frac{C_{\ell_r} K_Z^2 + C_{n_r} K_{XZ}}{4\mu_b (K_X^2 K_Z^2 - K_{XZ}^2)}$	$\frac{V}{b} \frac{C_{\ell_r} K_{XZ} + C_{n_r} K_X^2}{4\mu_b (K_X^2 K_Z^2 - K_{XZ}^2)}$
δ_a	$\frac{V}{b} \frac{C_{Y_{\delta_a}}}{2\mu_b}$	$\frac{V}{b} \frac{C_{\ell_{\delta_a}} K_Z^2 + C_{n_{\delta_a}} K_{XZ}}{4\mu_b (K_X^2 K_Z^2 - K_{XZ}^2)}$	$\frac{V}{b} \frac{C_{\ell_{\delta_a}} K_{XZ} + C_{n_{\delta_a}} K_X^2}{4\mu_b (K_X^2 K_Z^2 - K_{XZ}^2)}$
δ_r	$\frac{V}{b} \frac{C_{Y_{\delta_r}}}{2\mu_b}$	$\frac{V}{b} \frac{C_{\ell_{\delta_r}} K_Z^2 + C_{n_{\delta_r}} K_{XZ}}{4\mu_b (K_X^2 K_Z^2 - K_{XZ}^2)}$	$\frac{V}{b} \frac{C_{\ell_{\delta_r}} K_{XZ} + C_{n_{\delta_r}} K_X^2}{4\mu_b (K_X^2 K_Z^2 - K_{XZ}^2)}$

Table 4-10: Symbols appearing in the general state-space representation of equation (4-52)

$$\mathbf{R} = \begin{bmatrix} -C_{Y_{\delta_a}} & -C_{Y_{\delta_r}} \\ 0 & 0 \\ -C_{\ell_{\delta_a}} & -C_{\ell_{\delta_r}} \\ -C_{n_{\delta_a}} & -C_{n_{\delta_r}} \end{bmatrix}$$

and $\mathbf{x} = [\beta \ \varphi \ \frac{pb}{2V} \ \frac{rb}{2V}]^T$, while $\mathbf{u} = [\delta_a \ \delta_r]^T$. The final state-space form is obtained by pre-multiplying equation (4-50) by the inverse of matrix \mathbf{P} ,

$$\dot{\mathbf{x}} = \mathbf{P}^{-1} \mathbf{Q} \mathbf{x} + \mathbf{P}^{-1} \mathbf{R} \mathbf{u} = \mathbf{A} \mathbf{x} + \mathbf{B} \mathbf{u} \quad (4-51)$$

In flight dynamics, equation (4-51) is usually written as,

$$\begin{bmatrix} \dot{\beta} \\ \dot{\varphi} \\ \dot{p} \\ \dot{r} \end{bmatrix} = \begin{bmatrix} y_\beta & y_\varphi & y_p & y_r \\ 0 & 0 & 2\frac{V}{b} & 0 \\ l_\beta & 0 & l_p & l_r \\ n_\beta & 0 & n_p & n_r \end{bmatrix} \begin{bmatrix} \beta \\ \varphi \\ \frac{pb}{2V} \\ \frac{rb}{2V} \end{bmatrix} + \begin{bmatrix} 0 & y_{\delta_r} \\ 0 & 0 \\ l_{\delta_a} & l_{\delta_r} \\ n_{\delta_a} & n_{\delta_r} \end{bmatrix} \begin{bmatrix} \delta_a \\ \delta_r \end{bmatrix} \quad (4-52)$$

The definition of the newly introduced symbols are recapitulated in table 4-10. Dimensional eigenvalues λ are obtained using MATLAB's routine `eig.m` (for the state-matrix \mathbf{A}).

Part II

Dynamic Stability Analysis

Chapter 5

Analysis of Symmetric Equations of Motion

Once the equations of motion of an aircraft have been derived and the required aerodynamic derivatives are known, it is possible to calculate the aircraft motions caused by an arbitrary control deflection or external disturbance. In the most general case, if the equations of motion to be used are non-linear, only a numerical integration of the equations is possible.

Many aircraft motions, however, may be considered as deviations from a condition of steady, straight, symmetric flight, small enough to permit linearization of the equations about that reference condition. In chapter 4 the linearization has been given. Thereafter it is possible to use analytical methods, such as the Laplace-transform, to solve the linearized equations. Even then, the computer remains a nearly indispensable tool to carry out the calculations.

If the motions of an aircraft about a given equilibrium condition are studied, it is, quite independent of the type of disturbance to be considered, of primary interest to know if the equilibrium is stable. The following discusses how this question is answered.

Stability is a characteristic of any equilibrium condition of any arbitrary system. The question of the stability of an equilibrium condition relates to the behaviour of the system after it has been subjected to a small deviation from the equilibrium due to some disturbance, once the disturbance has ceased to act. If, after some time, the system returns to the original equilibrium condition, that condition is stable. If the system does not return to the original condition but deviates increasingly with time, the equilibrium was unstable. Finally, the equilibrium condition is neutrally stable, if the deviation caused by the disturbance neither disappears nor keeps increasing with time.

If the motions of the system under study about the initial reference condition can be described by linear equations of motion, the stability of the equilibrium condition is independent of the type and magnitude of the disturbance and of the magnitude of the initial deviation from the equilibrium condition. The condition of linearity is, also in the case of aircraft, not always satisfied.

In the following, stability is a characteristic of an arbitrary steady flight condition. For the sake of simplicity the ‘stability of an aircraft’ is often referred to, whereas the stability of a certain

equilibrium condition of that aircraft is actually meant. This is not quite correct, since any particular aircraft may be in a stable and sometimes also in an unstable equilibrium condition. The behaviour of the aircraft once it has acquired a small deviation from an equilibrium condition is described by the linearized ‘deviation equations’, (4-39) and (4-42).

For simplicity’s sake, only the longitudinal stability is discussed in the following sections. The stability criteria to be derived and the methods used to solve the equations of motion are equally applicable to the asymmetric motions, see chapter 6.

To begin with, the linearized ‘deviation equations’ for the symmetric motions, where $C_{X_q} = 0$, are repeated here, see equation (4-40),

$$\begin{bmatrix} C_{X_u} - 2\mu_c D_c & C_{X_\alpha} & C_{Z_0} & 0 \\ C_{Z_u} & C_{Z_\alpha} + (C_{Z_\dot{\alpha}} - 2\mu_c) D_c & -C_{X_0} & C_{Z_q} + 2\mu_c \\ 0 & 0 & -D_c & 1 \\ C_{m_u} & C_{m_\alpha} + C_{m_\dot{\alpha}} D_c & 0 & C_{m_q} - 2\mu_c K_Y^2 D_c \end{bmatrix} \begin{bmatrix} \hat{u} \\ \alpha \\ \theta \\ \frac{q\bar{c}}{V} \end{bmatrix} = \begin{bmatrix} -C_{X_{\delta_e}} \\ -C_{Z_{\delta_e}} \\ 0 \\ -C_{m_{\delta_e}} \end{bmatrix} \delta_e$$

This is a group of four simultaneous, constant coefficient, linear differential equations of first order. The independent variable in the equations is, in the physical sense, the disturbance variable, i.e. the elevator deflection. The dependent variables are the four components of the motion.

According to the foregoing, the stability of the equilibrium condition is apparent from the aircraft’s motion, once it has acquired a deviation from the equilibrium situation due to a disturbance and the disturbance has ceased to act. In the equations of motion this means that the time history of the dependent variable is studied, assuming the independent variables to be all zero and assuming furthermore, that the dependent variables have been given non-zero initial conditions. As the equations are linear, the magnitude of the initial conditions, i.e. the magnitude of the assumed disturbances and the resulting deviations, have no influence on the stability of the equilibrium, as noted before. In the more general case, where the motions are described by non-linear equations, the magnitude of the disturbances may influence stability.

Since stability is then independent of the input, or the disturbance, the equations to be solved for the disturbed symmetric aircraft motions can now be written in the following homogeneous form,

$$\begin{bmatrix} C_{X_u} - 2\mu_c D_c & C_{X_\alpha} & C_{Z_0} & 0 \\ C_{Z_u} & C_{Z_\alpha} + (C_{Z_\dot{\alpha}} - 2\mu_c) D_c & -C_{X_0} & C_{Z_q} + 2\mu_c \\ 0 & 0 & -D_c & 1 \\ C_{m_u} & C_{m_\alpha} + C_{m_\dot{\alpha}} D_c & 0 & C_{m_q} - 2\mu_c K_Y^2 D_c \end{bmatrix} \begin{bmatrix} \hat{u} \\ \alpha \\ \theta \\ \frac{q\bar{c}}{V} \end{bmatrix} = \underline{0}$$

(5-1)

As the elevator angle has been assumed to remain constant, the stability to be determined from these equations is the so-called ‘stability, stick fixed’. The assumption is thus made that the pilot holds the control manipulator and thereby the elevator fixed, such that the elevator angle does indeed remain constant.

A highly realistic alternative is the situation where the pilot has trimmed the control force to zero and takes his hands off the control manipulator. In that case the control mechanism is free during the disturbed motion and the elevator may vary. The actual time history of the elevator angle during the disturbed motion then follows from one or more additional equations of motion describing the behaviour of the control mechanism in the ‘stick free’ condition.

The stability thus to be determined, is the so-called ‘stability, stick free’. The following general discussions of the stability of an equilibrium condition are valid both for the stability, stick fixed and the stability, stick free.

5-1 Solution of the equations of motion

The analytical solution of the linear differential equations considered here is based on the transformation of these equations into algebraic equations. This can be done in various ways.

The solution of the above homogeneous equations has the following general form, see for instance reference [112].

For the symmetric motions,

$$x = A_x e^{\lambda_c s_c} \quad (5-2)$$

where x represents any of the components of the motion, and the variables s_c is the time, made non-dimensional, see table 4-1, where,

$$s_c = \frac{V}{\bar{c}} t$$

The coefficient A_x in equation (5-2) is determined partly by the initial conditions given to the equations of motion. The variable λ_c in (5-2) to be discussed in detail later, can be either real or complex. From the solution (5-2) it can be seen at once if the equilibrium condition under study is stable.

For stability it is both necessary and sufficient that x goes to zero with increasing time. The requirement for stability then is,

$$\lim_{s_c \rightarrow \infty} x = 0$$

For finite values of the coefficient A_x it is the variable λ_c that determines entirely and only, if the stability requirement is met. It is, therefore, of primary interest to see how this λ_c is to be found. To this end it is only necessary to substitute the solution (5-2) of the equations of motion back

in these equations. The value or values of λ_c turning these equations into equalities are the ones looked for. Before performing the substitution, it may be realized that in equation (5-1),

$$D_c x = \frac{\bar{c}}{V} \frac{d}{dt} \left(A_x e^{\lambda_c \frac{V}{\bar{c}} t} \right) = \lambda_c x$$

(5-3)

$$D_c^2 x = \lambda_c^2 x$$

In the following, the equations for the symmetric motions are further analyzed.

Equations (5-2) and (5-3) are substituted in equation (5-1),

$$\begin{bmatrix} C_{X_u} - 2\mu_c \lambda_c & C_{X_\alpha} & C_{Z_0} & 0 \\ C_{Z_u} & C_{Z_\alpha} + (C_{Z_\alpha} - 2\mu_c) \lambda_c & -C_{X_0} & C_{Z_q} + 2\mu_c \\ 0 & 0 & -\lambda_c & 1 \\ C_{m_u} & C_{m_\alpha} + C_{m_\alpha} \lambda_c & 0 & C_{m_q} - 2\mu_c K_Y^2 \lambda_c \end{bmatrix} \begin{bmatrix} A_u \\ A_\alpha \\ A_\theta \\ A_q \end{bmatrix} e^{\lambda_c s_c} = \underline{0}$$

(5-4)

or, in a more compact notation,

$$[\Delta] \underline{A} e^{\lambda_c s_c} = \underline{0}$$

where $[\Delta]$ is the characteristic matrix and \underline{A} is the vector with elements A_u, A_α, A_θ and A_q .

By the substitution the equations of motion change from differential equations into simultaneous, linear, homogeneous algebraic equations. From these equations the non-zero common factor $e^{\lambda_c s_c}$ can be omitted without influencing the values of λ_c to be obtained,

$$[\Delta] \underline{A} = \underline{0} \quad (5-5)$$

These homogeneous equations are always satisfied by the so-called trivial solution,

$$\underline{A} = \underline{0}$$

which is a short notation for,

$$A_u = A_\alpha = A_\theta = A_q = 0$$

In equation (5-2) this means,

$$\hat{u} = \alpha = \theta = \frac{q\bar{c}}{V} = 0$$

This is the original equilibrium flight condition, which is evidently a particular case of the disturbed motion. This trivial solution is not further considered here. The homogeneous,

algebraic equations represented by equation (5-5) are in general inconsistent.

A simple example may serve to illustrate this fact. Suppose, the following two homogeneous, algebraic equations have been given,

$$a_{11} x_1 + a_{12} x_2 = 0$$

$$a_{21} x_1 + a_{22} x_2 = 0$$

Or,

$$\begin{bmatrix} a_{11} & a_{12} \\ a_{21} & a_{22} \end{bmatrix} \begin{bmatrix} x_1 \\ x_2 \end{bmatrix} = \underline{0}$$

From the first equation follows the solution,

$$x_2 = -\frac{a_{11}}{a_{12}} x_1$$

and from the second equation,

$$x_2 = -\frac{a_{21}}{a_{22}} x_1$$

These two solutions are consistent if,

$$-\frac{a_{11}}{a_{12}} = -\frac{a_{21}}{a_{22}}$$

or,

$$a_{11} a_{22} - a_{12} a_{21} = 0$$

Or, expressed in a different way,

$$\begin{vmatrix} a_{11} & a_{12} \\ a_{21} & a_{22} \end{vmatrix} = 0$$

If the coefficient determinant of the homogeneous, algebraic equations is zero, the equations are no longer inconsistent. But then they have become dependent.

In the case of aircraft motions considered here, the equations (5-5) and (5-4) have a solution only for a few particular values of λ_c . These are the values of λ_c resolving the inconsistency of the equations by making the equations dependent. These values of λ_c called the eigenvalues of the differential equations, are found according to the foregoing by equating the determinant of the square matrix $[\Delta]$ to zero. The determinant of $[\Delta]$ is called the characteristic determinant. The eigenvalues are then found from,

$$[\Delta] = 0$$

This ‘characteristic equation’ can be written more explicitly as,

$$\begin{vmatrix} C_{X_u} - 2\mu_c \lambda_c & C_{X_\alpha} & C_{Z_0} & 0 \\ C_{Z_u} & C_{Z_\alpha} + (C_{Z_\alpha} - 2\mu_c) \lambda_c & -C_{X_0} & C_{Z_q} + 2\mu_c \\ 0 & 0 & -\lambda_c & 1 \\ C_{m_u} & C_{m_\alpha} + C_{m_\alpha} \lambda_c & 0 & C_{m_q} - 2\mu_c K_Y^2 \lambda_c \end{vmatrix} = 0$$

For a further study of stability via the eigenvalues it is necessary to expand the above characteristic equation. The result may be expressed as,

$$A \lambda_c^4 + B \lambda_c^3 + C \lambda_c^2 + D \lambda_c + E = 0 \quad (5-6)$$

The four roots of this characteristic equation are the four eigenvalues λ_c to be found. According to equation (5-2) they determine if the original equilibrium condition is stable. The coefficients A to E in equation (5-6) are given with the more detailed discussion of dynamic longitudinal stability in section 5-3.

The resulting eigenvalues may finally be substituted in (5-5).

In general the roots of the characteristic equation are all different. After substitution in equation (5-2) they give the aircraft motion after a disturbance from the equilibrium situation. Assuming four different eigenvalues, the solution for the symmetric motions is,

$$\begin{bmatrix} \hat{u} \\ \alpha \\ \theta \\ \frac{q\bar{c}}{V} \end{bmatrix} = [A] \begin{bmatrix} e^{\lambda_{c_1} s_c} \\ e^{\lambda_{c_2} s_c} \\ e^{\lambda_{c_3} s_c} \\ e^{\lambda_{c_4} s_c} \end{bmatrix} \quad (5-7)$$

where the matrix $[A]$ can be written more explicitly as,

$$[A] = \begin{bmatrix} A_{u_1} & A_{u_2} & A_{u_3} & A_{u_4} \\ A_{\alpha_1} & A_{\alpha_2} & A_{\alpha_3} & A_{\alpha_4} \\ A_{\theta_1} & A_{\theta_2} & A_{\theta_3} & A_{\theta_4} \\ A_{q_1} & A_{q_2} & A_{q_3} & A_{q_4} \end{bmatrix} \quad (5-8)$$

Combination of equation (5-7) and (5-8) results in the solution of the homogeneous differential equations,

$$\begin{aligned} \hat{u} &= A_{u_1} e^{\lambda_{c_1} s_c} + A_{u_2} e^{\lambda_{c_2} s_c} + A_{u_3} e^{\lambda_{c_3} s_c} + A_{u_4} e^{\lambda_{c_4} s_c} \\ \alpha &= A_{\alpha_1} e^{\lambda_{c_1} s_c} + A_{\alpha_2} e^{\lambda_{c_2} s_c} + A_{\alpha_3} e^{\lambda_{c_3} s_c} + A_{\alpha_4} e^{\lambda_{c_4} s_c} \\ \theta &= A_{\theta_1} e^{\lambda_{c_1} s_c} + A_{\theta_2} e^{\lambda_{c_2} s_c} + A_{\theta_3} e^{\lambda_{c_3} s_c} + A_{\theta_4} e^{\lambda_{c_4} s_c} \\ \frac{q\bar{c}}{V} &= A_{q_1} e^{\lambda_{c_1} s_c} + A_{q_2} e^{\lambda_{c_2} s_c} + A_{q_3} e^{\lambda_{c_3} s_c} + A_{q_4} e^{\lambda_{c_4} s_c} \end{aligned}$$

Four out of the sixteen constants in $[A]$ are fixed by four initial conditions which must be given if the disturbed motion is to be determined completely. The remaining twelve constants then follow from twelve real or complex ratios of the components of the motion, mentioned earlier. From this brief discussion it may be seen, that the constants in $[A]$ have no influence whatsoever on the stability or instability of the equilibrium conditions.

The various possible types of eigenvalues λ_c and the corresponding motions, the so-called ‘eigen-motions’ are now studied, under the assumption that all eigenvalues are different.

Real eigenvalues

The part of the total aircraft response, i.e. the eigenmotion, corresponding to a real eigenvalue λ_c is described by an aperiodic exponential function, see figure 5-1. The equilibrium can only be stable, if all real eigenvalues are negative. Only then is,

$$\lim_{s_c \rightarrow \infty} A_x e^{\lambda_c s_c} = 0$$

If $\lambda_c = 0$, then,

$$A_x e^{\lambda_c s_c} = A_x$$

The eigenmotion corresponding to this particular value is a constant for any of the components of the motion. For $\lambda_c > 0$, all components of the motion tend to go to infinity with increasing time, because for any value of A_x ,

$$\lim_{s_c \rightarrow \infty} A_x e^{\lambda_c s_c} = \pm\infty$$

The speed at which for a given negative, real λ_c the corresponding eigenmotion converges to zero, is commonly expressed by two different characteristic times,

- The time to damp to half the amplitude, $T_{\frac{1}{2}}$. This is the time interval in which the exponential function decreases to half its original value. This means,

$$x(t + T_{\frac{1}{2}}) = \frac{1}{2} x(t)$$

or, using $s_c = \frac{V}{\bar{c}} t$:

$$e^{\lambda_c \frac{V}{\bar{c}} (t + T_{\frac{1}{2}})} = \frac{1}{2} e^{\lambda_c \frac{V}{\bar{c}} t}$$

From this follows,

$$T_{\frac{1}{2}} = \frac{\ln \frac{1}{2}}{\lambda_c} \frac{\bar{c}}{V} = -\frac{0.693}{\lambda_c} \frac{\bar{c}}{V}$$

- The time constant τ . This is the time interval in which the exponent decreases by 1 and the exponential function itself decreases by the factor $\frac{1}{e}$. Then,

$$x(t + \tau) = \frac{1}{e} x(t)$$

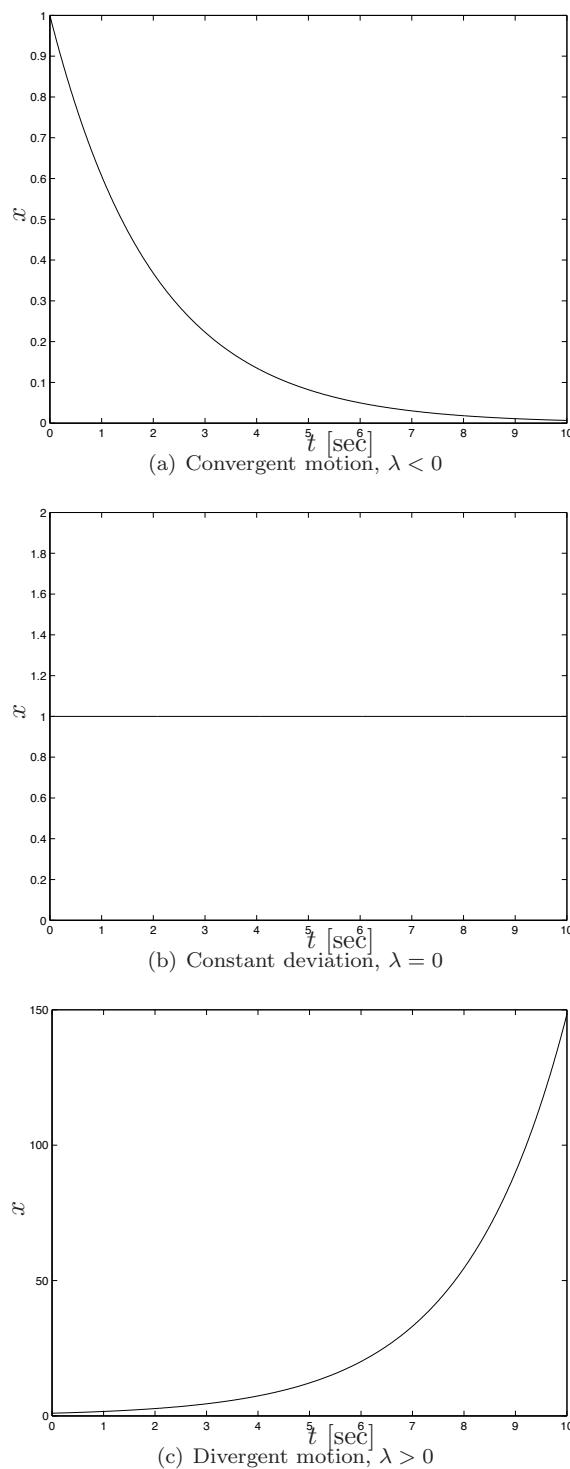


Figure 5-1: Aperiodic motions corresponding to a real eigenvalue λ

or,

$$e^{\lambda_c \frac{V}{\bar{c}}(t+\tau)} = \frac{1}{e} e^{\lambda_c \frac{V}{\bar{c}} t}$$

or

$$\lambda_c \frac{V}{\bar{c}} \tau = -1$$

$$\tau = -\frac{1}{\lambda_c} \frac{\bar{c}}{V}$$

The relations between $T_{\frac{1}{2}}$ and τ are,

$$\tau = 1.443 T_{\frac{1}{2}}$$

$$T_{\frac{1}{2}} = 0.693 \tau$$

Using the time constant, the eigenmotion corresponding to the real λ_c can be written as,

$$A_x e^{\lambda_c \frac{V}{\bar{c}} t} = A_x e^{-\frac{t}{\tau}}$$

If λ_c is positive and an aperiodic divergence results, $T_{\frac{1}{2}}$ and τ may still be used to indicate the level of divergence. In that case both $T_{\frac{1}{2}}$ and τ are negative. In those situations use is often made of the ‘time to double amplitude’ T_2 . It is the time interval in which the exponential function increases to twice its original value,

$$T_2 = -T_{\frac{1}{2}}$$

Complex Eigenvalues

In the case of a complex λ_c , the eigenvalue is written as,

$$\lambda_c = \xi_c + j \eta_c \quad j = \sqrt{-1}$$

Substituting of such an eigenvalue in equation (5-2) or (5-3) would lead to complex expressions for the components of the motion. But complex eigenvalues occur always in complex conjugate pairs, i.e.,

$$\lambda_{c1,2} = \xi_c \pm j \eta_c$$

The corresponding constants A_{x_1} and A_{x_2} in equation (5-2) are also complex conjugate, as the resultant motion can only be real. This means,

$$A_{x_{1,2}} = R_x \pm j Q_x$$

The eigenmotion belonging to the two complex conjugate roots of the characteristic equation, can now be written as,

$$\begin{aligned} A_{x_1} e^{\lambda_{c1}s_c} + A_{x_2} e^{\lambda_{c2}s_c} &= (R_x + j Q_x) e^{(\xi_c + j \eta_c)s_c} + (R_x - j Q_x) e^{(\xi_c - j \eta_c)s_c} = \\ &= [(R_x + j Q_x) e^{j\eta_c s_c} + (R_x - j Q_x) e^{-j\eta_c s_c}] e^{\xi_c s_c} \end{aligned}$$

Using the useful relationship $e^{j\phi} = \cos\phi + j \sin\phi$:

$$\begin{aligned} &= [(R_x + j Q_x) (\cos(\eta_c s_c) + j \sin(\eta_c s_c)) + (R_x - j Q_x) (\cos(\eta_c s_c) - j \sin(\eta_c s_c))] e^{\xi_c s_c} \\ &= [2R_x \cos(\eta_c s_c) - 2Q_x \sin(\eta_c s_c)] e^{\xi_c s_c} \end{aligned}$$

With a little help from the sine cosine identity $a \cos x + b \sin x = \sqrt{a^2 + b^2} \cos(x + \arctan \frac{b}{a})$ this results in

$$2\sqrt{R_x^2 + Q_x^2} e^{\xi_c s_c} \cos\left(\eta_c s_c + \arctan \frac{Q_x}{R_x}\right) \quad (5-9)$$

This part of the total response of the components of the motion is evidently a damped oscillation, i.e. ξ_c is negative.

The period P of the oscillation follows from the imaginary part η_c of the two eigenvalues. If the argument of the harmonic function has increased by 2π , a time P has elapsed,

$$\eta_c \frac{V}{\bar{c}} P = 2\pi$$

or,

$$P = \frac{2\pi}{\eta_c} \frac{\bar{c}}{V}$$

According to equation (5-9), the amplitude of the oscillation is,

$$2\sqrt{R_x^2 + Q_x^2} e^{\xi_c s_c}$$

Apparently, only the real part ξ_c of the eigenvalues determines if the amplitude converges to zero with increasing time, see figure 5-2. For stability it is necessary, that the real parts of all complex eigenvalues are negative. Only then is,

$$\lim_{s_c \rightarrow \infty} 2\sqrt{R_x^2 + Q_x^2} e^{\xi_c s_c} = 0$$

Various measures of the damping of an oscillation are in use.

- The time to damp to half amplitude, $T_{\frac{1}{2}}$. This characteristic has the same meaning as for the aperiodic motions. $T_{\frac{1}{2}}$ is now expressed by,

$$T_{\frac{1}{2}} = -\frac{0.693}{\xi_c} \frac{\bar{c}}{V}$$

If an oscillation has negative damping, i.e. it diverges, it means that $\xi_c > 0$ and $T_{\frac{1}{2}}$ is negative. Usually the time to double amplitude, T_2 of the oscillation is then given,

$$T_2 = -T_{\frac{1}{2}}$$

- The number of periods, $C_{\frac{1}{2}}$, in which the amplitude decreases to half its original value,

$$C_{\frac{1}{2}} = \frac{T_{\frac{1}{2}}}{P} = \frac{-0.693}{2\pi} \frac{\eta_c}{\xi_c} = -0.110 \frac{\eta_c}{\xi_c}$$

In analogy with T_2 is,

$$C_2 = -C_{\frac{1}{2}}$$

- The logarithmic decrement δ . This is the natural logarithm of the ratio of the oscillation's amplitude in two successive maxima,

$$\delta = \ln \frac{e^{\xi_c \frac{V}{\bar{c}}(t+P)}}{e^{\xi_c \frac{V}{\bar{c}}t}} = \xi_c \frac{V}{\bar{c}} P$$

or,

$$\delta = 2\pi \frac{\xi_c}{\eta_c} = -\frac{0.693}{C_{\frac{1}{2}}}$$

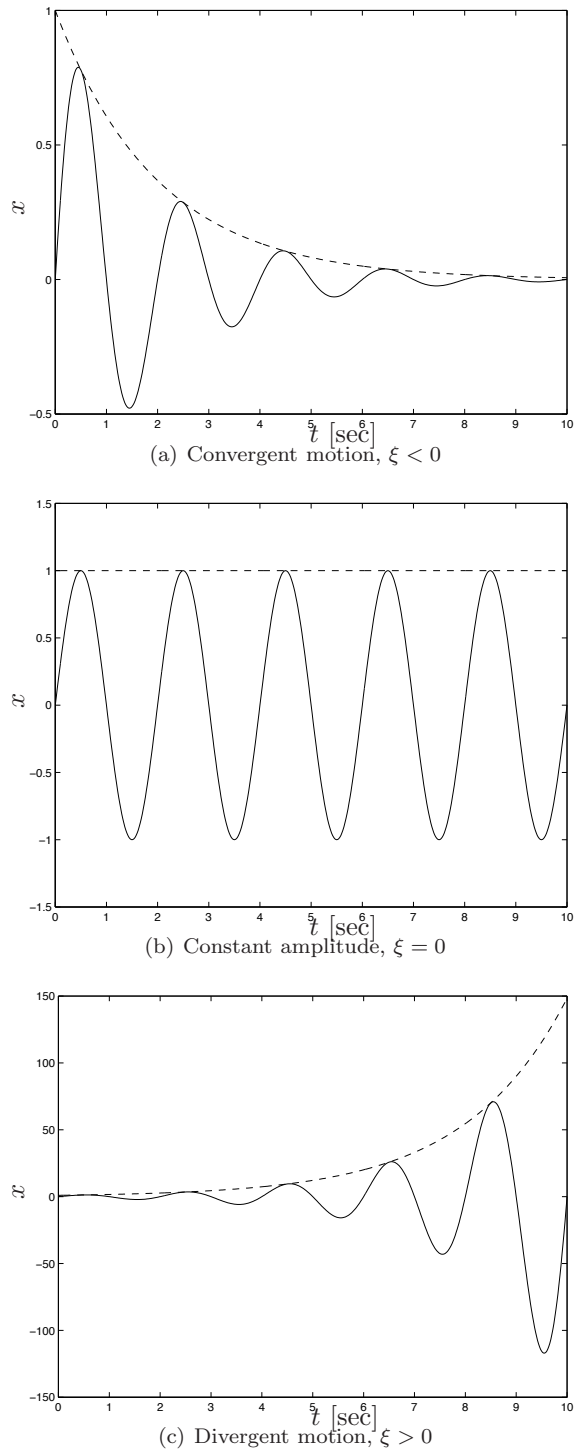


Figure 5-2: Periodic motion corresponding to a pair of complex, conjugate eigenvalues $\lambda_{1,2} = \xi \pm j\eta$

- The damping ratio ζ . The complex eigenvalues $\lambda_{c_{1,2}}$ are often written as follows,

$$\lambda_{c_{1,2}} = \left\{ -\zeta\omega_0 \pm j\omega_0\sqrt{1-\zeta^2} \right\} \frac{\bar{c}}{V} \quad (5-10)$$

Here ζ is the damping ratio and ω_0 is the undamped natural frequency (in rad/sec). If $\zeta = 0$, the eigenvalues are,

$$\lambda_{c_{1,2}} = \pm j\omega_0 \frac{\bar{c}}{V} = \pm\eta_c$$

The real part of $\lambda_{c_{1,2}}$ is then zero, the oscillation is accordingly undamped and the angular frequency of the oscillation is ω_0 . The relation between the period and the eigenfrequency ω_n of the damped oscillation is,

$$P = \frac{2\pi}{\omega_n}$$

With $P = \frac{2\pi}{\eta_c} \cdot \frac{\bar{c}}{V}$ it follows from equation (5-10) that,

$$\omega_n = \omega_0\sqrt{1-\zeta^2}$$

The relations between ω_0 , ζ , ξ_c and η_c can be derived to be,

$$\omega_0 = \sqrt{\xi_c^2 + \eta_c^2} \frac{V}{\bar{c}}$$

$$\zeta = \frac{-\xi_c}{\sqrt{\xi_c^2 + \eta_c^2}}$$

if $0 < \zeta < 1$ a damped oscillation occurs, because then λ_{c_1} and λ_{c_2} are complex and the real part $-\zeta\omega_0\frac{\bar{c}}{V}$ is negative. With increasing ζ the damping increases as well. The relations between $C_{\frac{1}{2}}$, δ and ζ are,

$$\delta = -2\pi \frac{\zeta}{\sqrt{1-\zeta^2}}$$

and,

$$C_{\frac{1}{2}} = 0.110 \frac{\sqrt{1-\zeta^2}}{\zeta}$$

If $\zeta = 1$, a transition occurs from a periodic to an aperiodic motion. The motion is then called critically damped. The characteristic equation in that particular case has two equal roots. If $\zeta > 1$, the motion is aperiodic, as both λ_{c_1} and λ_{c_2} are then real.

Finally, if $\zeta < 0$, the real part of the eigenvalues is positive, see equation (5-10). The considered equilibrium condition is then unstable. The motions diverge, in a periodic manner if $-1 < \zeta < 0$ and aperiodic if $\zeta < -1$.

At the end of this review of the stability of an equilibrium condition for the case where all eigenvalues are different, the findings can be summarized as follows.

The equilibrium is stable if all real eigenvalues and the real parts of the complex eigenvalues are negative. The disturbed motion then converges back to the original equilibrium condition. If at least one real or complex eigenvalue has a positive real part, then the equilibrium condition is unstable. In this case the disturbed motion diverges increasingly from the steady equilibrium flight condition. A transitional situation exists, where no eigenvalue has a positive real part, but a real eigenvalue or the real part of a pair of complex eigenvalues is just equal to zero. In such a situation, a deviation of constant magnitude or amplitude occurs. The equilibrium condition is then called neutrally stable.

Often, the eigenvalues, i. e. the roots of the characteristic equation, are depicted as points in the complex plane. Real eigenvalues are situated on the real axis at a distance of λ_c of the origin and complex eigenvalues have as coordinates $(\xi_c \pm j \eta_c)$.

The above stability criterion implies that all eigenvalues must be situated to the left of the imaginary axis. As soon as at least one eigenvalue is placed to the right of the imaginary axes, the equilibrium condition is unstable. If one or more eigenvalues are placed on the imaginary axis, whether or not in the origin of the system axis, and none lies in the right half of the plane, the equilibrium condition is neutrally stable.

The solution of the equations of motion for the case where two or more roots of the characteristic equation are equal, is not further discussed here. This topic is further discussed for instance in reference [112].

In order to determine the stability of the equilibrium condition according to the foregoing rules, it is always necessary to construct the characteristic determinant and to determine from it the values and types of eigenvalues.

In contrast with the foregoing, the following section discusses a method to determine the stability without an explicit calculation of the eigenvalues.

5-2 Stability criteria

Often a need exists to determine the stability of an equilibrium condition without resorting at once to the solution of the characteristic equation. Sometimes it is necessary to study the influence on the stability of systematic changes in the system under consideration. In such cases, fruitful use may be made of various so-called ‘stability criteria’. In this chapter only the Routh-Hurwitz criteria will be discussed. A more general stability criterion is that of Lyapunov of which the Routh-Hurwitz criteria are a particular case, see reference [112].

The Routh-Hurwitz Stability Criteria

In the foregoing it was shown, that the criterion for stability is that all real eigenvalues and all real parts of the complex eigenvalues are negative. Routh, see reference [147] and Hurwitz, see reference [81], derived criteria which the coefficients of an algebraic equation have to satisfy for all real roots and the real parts of the complex roots to be negative. It will be sufficient here to present only the stability criteria as they apply to the fourth order characteristic equation we derived in 5-1.

The characteristic equation is,

$$A \lambda_c^4 + B \lambda_c^3 + C \lambda_c^2 + D \lambda_c + E = 0 \quad (5-11)$$

The coefficients A, B, C, D and E are all real. Now Routh-Hurwitz states that when,

$$A > 0$$

The stability criteria are,

$$A > 0, B > 0, C > 0, D > 0, E > 0$$

and,

$$BCD - AD^2 - B^2E > 0$$

The latter expression,

$$R = BCD - AD^2 - B^2E$$

is often called Routh's discriminant.

If $A < 0$, the signs of B, C, D, E and R must also be negative to obtain negative real parts of the eigenvalues.

5-3 The complete solution of the equations of motion

As indicated already in section 5-1, an idea of the aircraft motions after a disturbance can be obtained by determining the roots of the characteristic equation (5-6). The general character of the symmetric motions is discussed in the following. To this end, a numerical example is discussed, along the lines presented in section 5-1.

According to equation (5-6) the characteristic equation for the symmetric motions is,

$$A \lambda_c^4 + B \lambda_c^3 + C \lambda_c^2 + D \lambda_c + E = 0$$

The coefficients A to E are obtained by expanding the characteristic determinant, see section 5-1. The coefficients A to E are,

$$A = 4\mu_c^2 K_Y^2 (C_{Z_{\dot{\alpha}}} - 2\mu_c)$$

$$B = C_{m_{\dot{\alpha}}} 2\mu_c (C_{Z_q} + 2\mu_c) - C_{m_q} 2\mu_c (C_{Z_{\dot{\alpha}}} - 2\mu_c) -$$

$$2\mu_c K_Y^2 \{C_{X_u} (C_{Z_{\dot{\alpha}}} - 2\mu_c) - 2\mu_c C_{Z_{\alpha}}\}$$

$$\begin{aligned}
C &= C_{m_\alpha} 2\mu_c (C_{Z_q} + 2\mu_c) - C_{m_\dot{\alpha}} \{2\mu_c C_{X_0} + C_{X_u} (C_{Z_q} + 2\mu_c)\} + \\
&C_{m_q} \{C_{X_u} (C_{Z_\dot{\alpha}} - 2\mu_c) - 2\mu_c C_{Z_\alpha}\} + 2\mu_c K_Y^2 (C_{X_\alpha} C_{Z_u} - C_{Z_\alpha} C_{X_u}) \quad (5-12)
\end{aligned}$$

$$\begin{aligned}
D &= C_{m_u} \{C_{X_\alpha} (C_{Z_q} + 2\mu_c) - C_{Z_0} (C_{Z_\dot{\alpha}} - 2\mu_c)\} - \\
&C_{m_\alpha} \{2\mu_c C_{X_0} + C_{X_u} (C_{Z_q} + 2\mu_c)\} + \\
&C_{m_\dot{\alpha}} (C_{X_0} C_{X_u} - C_{Z_0} C_{Z_u}) + C_{m_q} (C_{X_u} C_{Z_\alpha} - C_{Z_u} C_{X_\alpha}) \\
E &= -C_{m_u} (C_{X_0} C_{X_\alpha} + C_{Z_0} C_{Z_\alpha}) + C_{m_\alpha} (C_{X_0} C_{X_u} + C_{Z_0} C_{Z_u})
\end{aligned}$$

If the various aerodynamic and inertial parameters are known, the quantitative values of the coefficients A to E can be calculated. The eigenvalues λ_c are next obtained as the roots of the quartic characteristic equation (5-6).

In many practical situations a computer is available to obtain the eigenvalues λ_c . Very often the starting point for the calculations is then the characteristic determinant rather than the characteristic equation (5-6). When using a mathematical software package such as, e.g., MATLAB, it is merely necessary to provide the numerical values of the stability derivatives and the inertial parameters.

As an example the symmetric disturbed motions of a Cessna Ce500 ‘Citation’ are considered. The required data are given in table 5-1.

From these data follow the coefficients A to E , according to equation (5-12) and from these parameters the characteristic equation. From the coefficients A to E the stability can directly be assessed.

The eigenvalues are actually determined by MATLAB using the `roots.m` routine for root finding of polynomials. The resulting two pairs of complex conjugate eigenvalues are,

$$\lambda_{c_{1,2}} = -2.9107 \cdot 10^{-4} \pm j 6.6006 \cdot 10^{-3}$$

$$\lambda_{c_{3,4}} = -3.9161 \cdot 10^{-2} \pm j 3.7971 \cdot 10^{-2}$$

or with $\lambda = \lambda_c \frac{V}{\bar{c}}$,

$$\lambda_{1,2} = -8.6226 \cdot 10^{-3} \pm j 1.9544 \cdot 10^{-1}$$

$$\lambda_{3,4} = -1.1601 \cdot 10^0 \pm j 1.1240 \cdot 10^0$$

V	=	59.9 m/sec	m	=	4547.8 kg	\bar{c}	=	2.022 m
S	=	24.2 m ²	l_h	=	5.5 m	μ_c	=	102.7
K_Y^2	=	0.980	x_{cg}	=	0.30 \bar{c}			
C_{X_0}	=	0	C_{Z_0}	=	-1.1360			
C_{X_u}	=	-0.2199	C_{Z_u}	=	-2.2720	C_{m_u}	=	0
C_{X_α}	=	0.4653	C_{Z_α}	=	-5.1600	C_{m_α}	=	-0.4300
$C_{X_{\dot{\alpha}}}$	=	0	$C_{Z_{\dot{\alpha}}}$	=	-1.4300	$C_{m_{\dot{\alpha}}}$	=	-3.7000
C_{X_q}	=	0	C_{Z_q}	=	-3.8600	C_{m_q}	=	-7.0400
C_{X_δ}	=	0	C_{Z_δ}	=	-0.6238	C_{m_δ}	=	-1.5530

Table 5-1: Symmetric stability and control derivatives for the Cessna Ce500 ‘Citation’

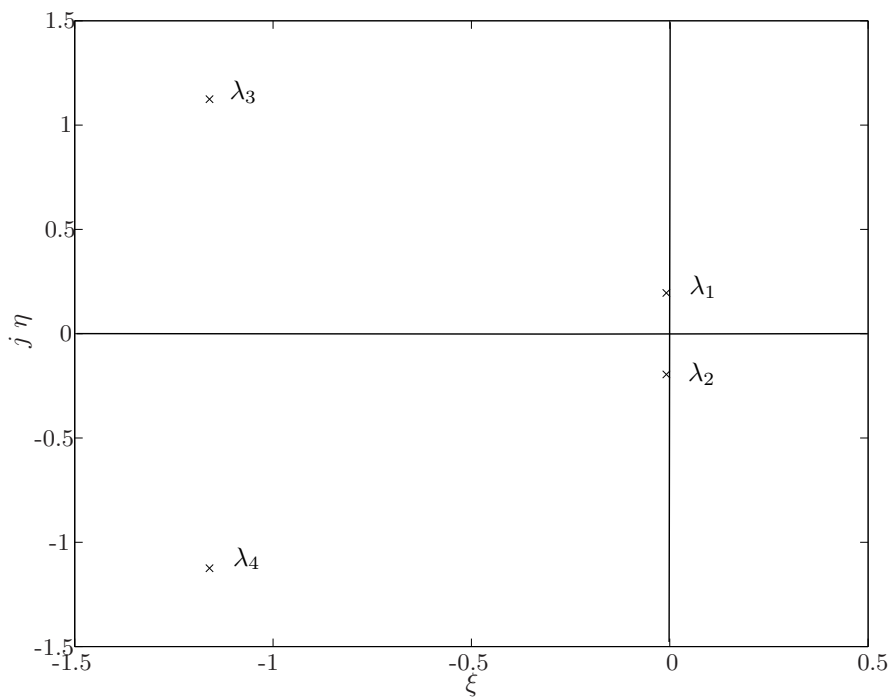


Figure 5-3: The location of the eigenvalues for the symmetric motions

Apparently, the disturbed motion is the sum of two periodic motions. The one corresponding to the eigenvalues $\lambda_{c_{1,2}}$ is a relatively slow, lightly damped oscillation, the other mode, corresponding to eigenvalues $\lambda_{c_{3,4}}$ has a much shorter period and is highly damped. Two such oscillations occur in nearly all situations with most categories of conventional aircraft. They are indicated as the long period oscillation, or ‘phugoid’, and the short period oscillation respectively.

The various characteristics of these motions derived in section 5-1 are next calculated from the eigenvalues λ_c . The results are,

- **Phugoid mode**

- $\lambda_{c_{1,2}} = -2.9107 \cdot 10^{-4} \pm j 6.6006 \cdot 10^{-3}$
- the period $P = 32.1391$ seconds
- the time to damp to half the amplitude $T_{\frac{1}{2}} \approx 81$ seconds
- the undamped natural frequency $\omega_0 = 0.1957$ rad/sec.
- the damping ratio $\zeta = 0.0441$

- **Short period mode**

- $\lambda_{c_{3,4}} = -3.9161 \cdot 10^{-2} \pm j 3.7971 \cdot 10^{-2}$
- the period $P = 5.5900$ seconds
- the time to damp to half the amplitude $T_{\frac{1}{2}} \approx 0.6$ seconds
- the undamped natural frequency $\omega_0 = 1.6153$ rad/sec.
- the damping ratio $\zeta = 0.7182$

Figure 5-3 shows the position of the eigenvalues in the complex plane. Here the dimensional eigenvalues are used,

$$\lambda = \lambda_c \frac{V}{\bar{c}}$$

$$\xi = \xi_c \frac{V}{\bar{c}}$$

$$\eta = \eta_c \frac{V}{\bar{c}}$$

Figures 5-4 and 5-5 show the time responses of the aircraft after some small disturbance. This calculation was made using the program package MATLAB. The actual disturbance used was a negative step elevator deflection ($\Delta\delta_e = -0.005$ Rad.). The parameters used in the simulation, as well as the flight condition, are given in table 5-1. In figure 5-4 the simulation of the phugoid mode is clearly seen, the period is approximately 32 seconds. The short period oscillation is best seen in figure 5-5, see the simulation of the pitch-rate q at the larger time scale. The high damping of this motion is also apparent.

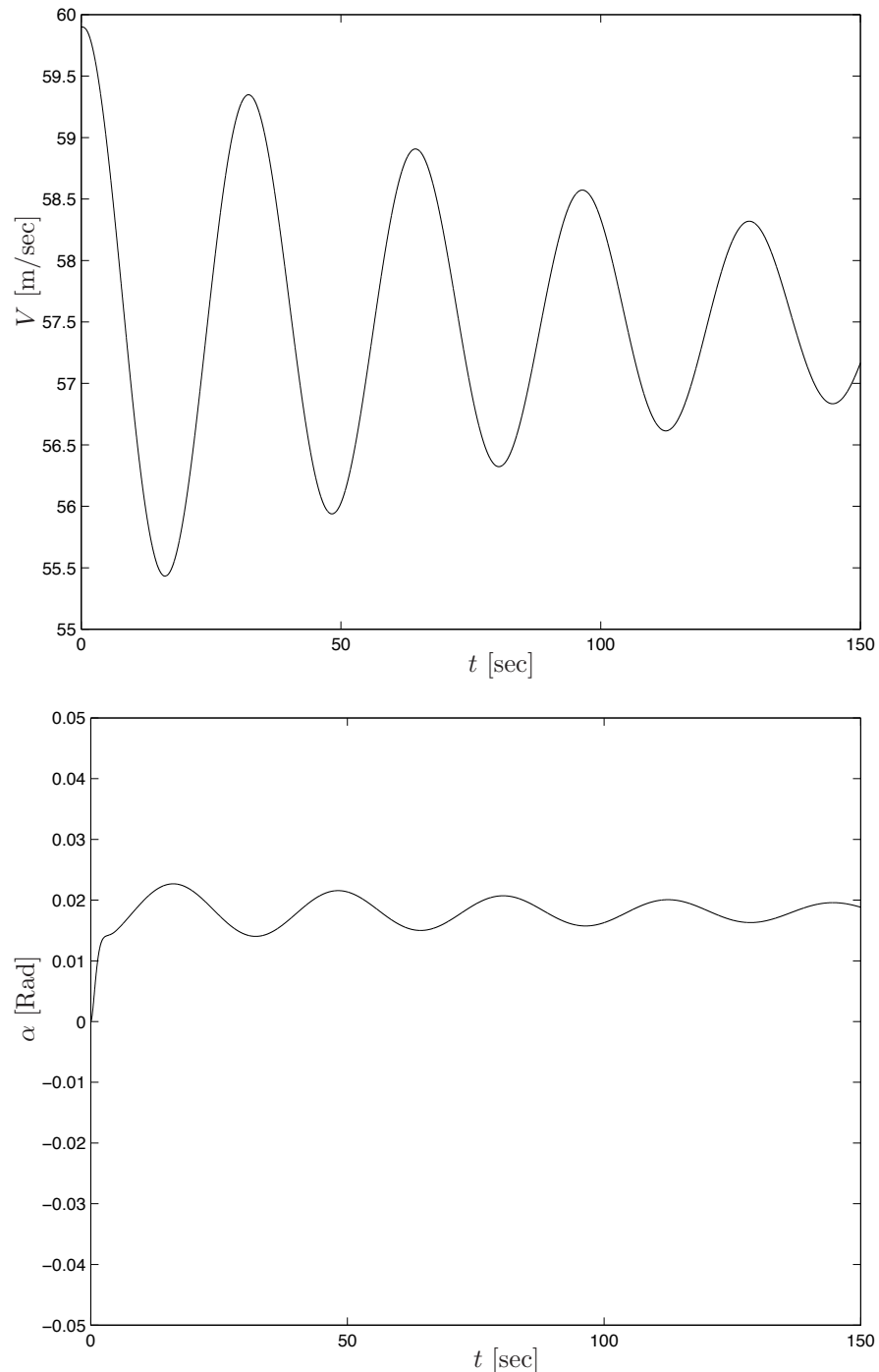


Figure 5-4: Response curves for a step elevator deflection ($\Delta\delta_e = -0.005$ [Rad]) for the Cessna Ce500 ‘Citation’, phugoid response

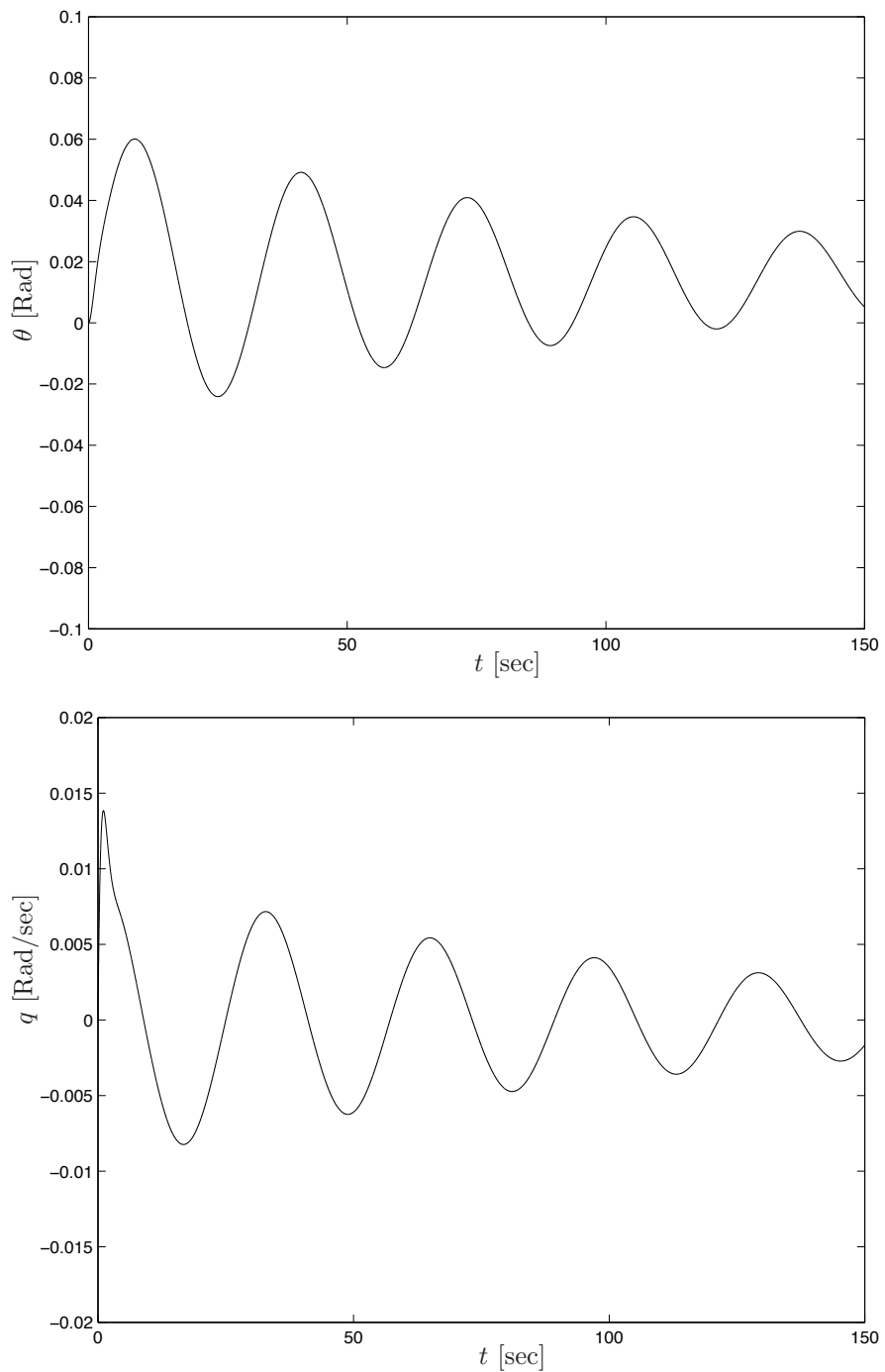


Figure 5-4: (**Continued**) Response curves for a step elevator deflection ($\Delta\delta_e = -0.005$ [Rad]) for the Cessna Ce500 ‘Citation’, phugoid response

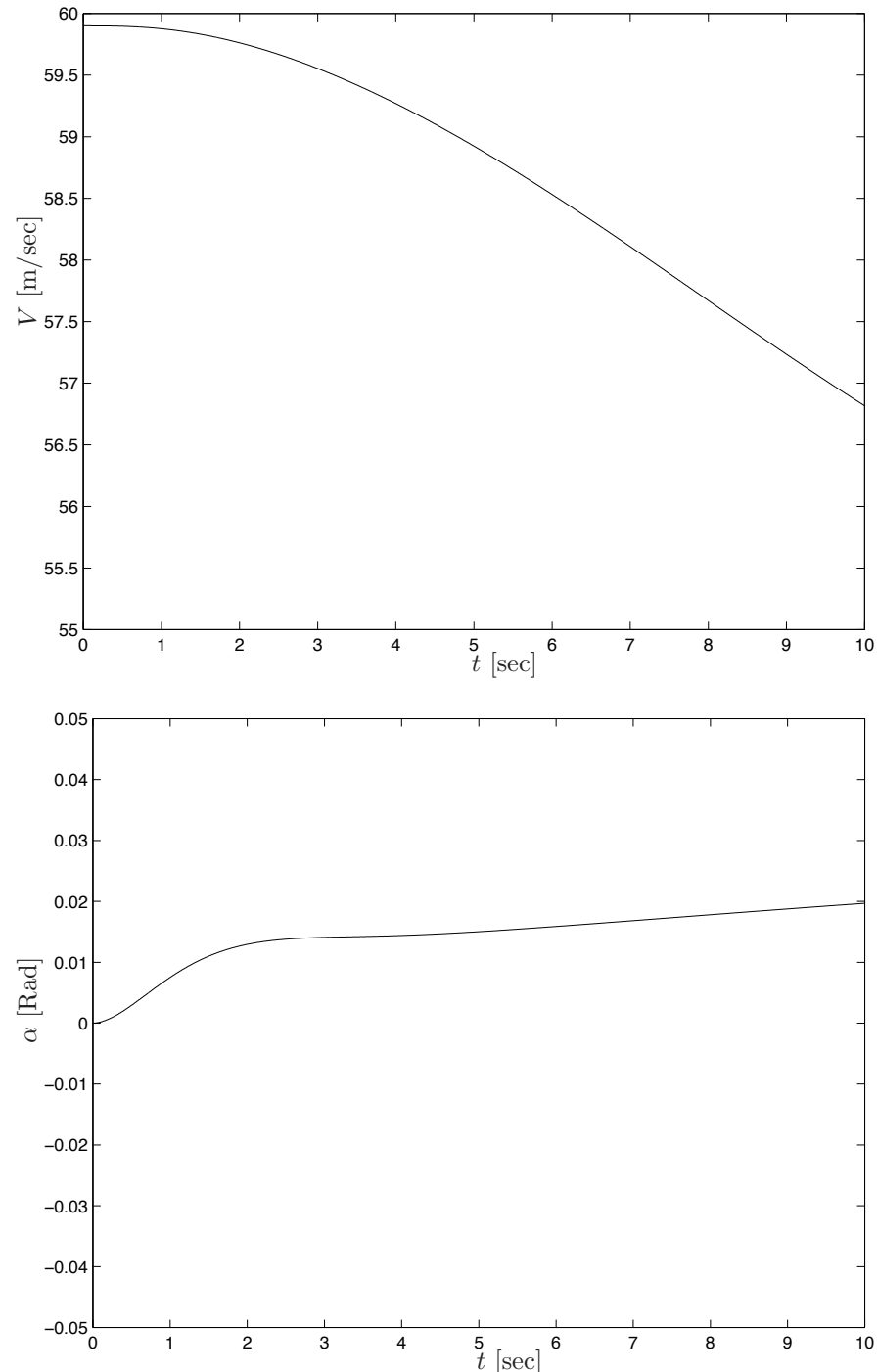


Figure 5-5: Response curves for a step elevator deflection ($\Delta\delta_e = -0.005$ [Rad]) for the Cessna Ce500 ‘Citation’, magnification of figure 5-4, short period response

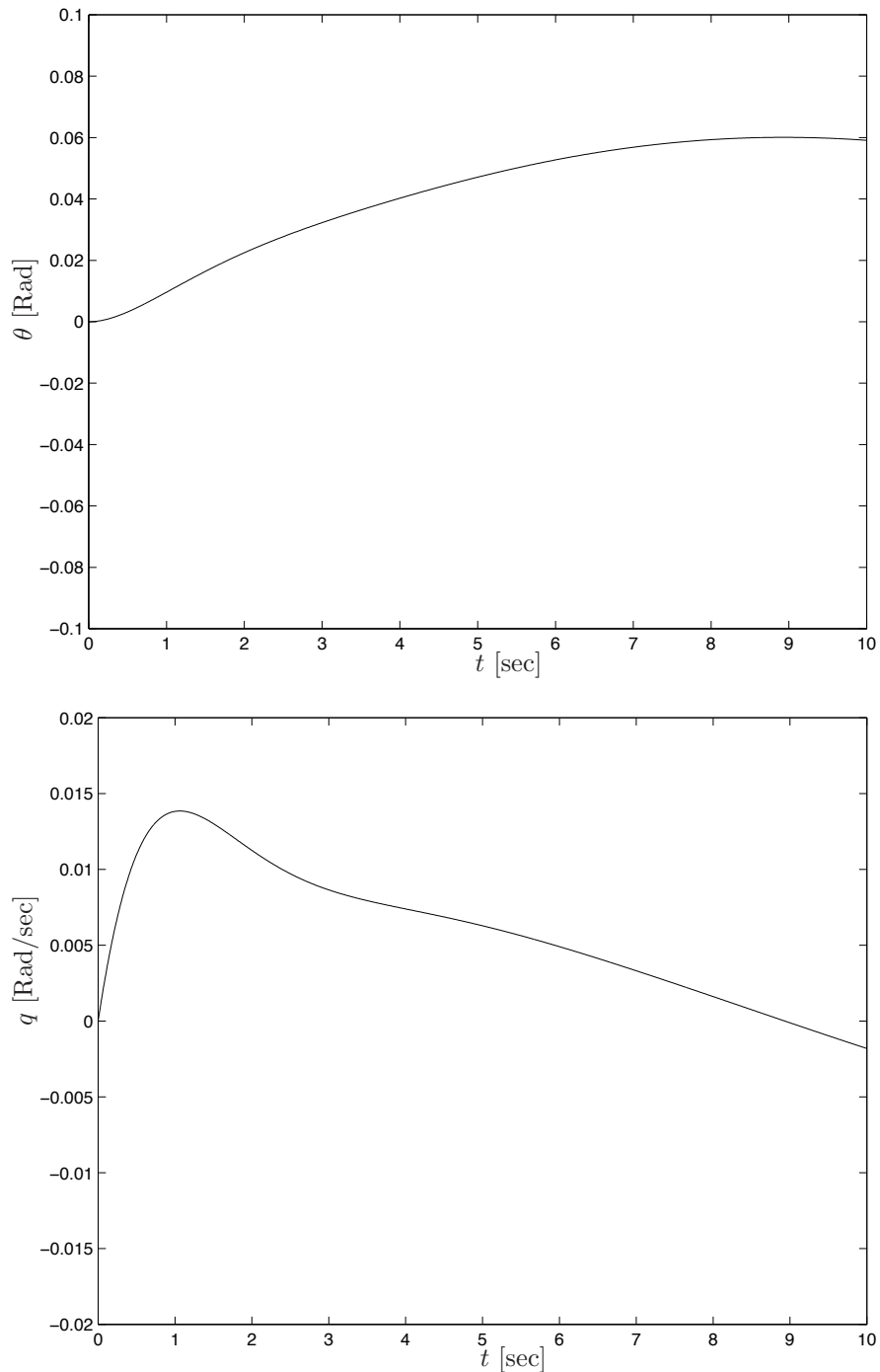


Figure 5-5: (**Continued**) Response curves for a step elevator deflection ($\Delta\delta_e = -0.005$ [Rad]) for the Cessna Ce500 ‘Citation’, magnification of figure 5-4, short period response

5-4 Approximate solutions

Figures 5-4 and 5-5 show some characteristic differences between the phugoid mode and the short period oscillation. The airspeed varies hardly during the short period oscillation. Due to the phugoid oscillation, airspeed and pitch angle vary in particular. The angular acceleration about the lateral axis, \dot{q} is almost zero during the long period oscillation. Also during this oscillation the variations of the angle of attack are relatively small if compared with the variations in angle of pitch. Since $\theta = \alpha + \gamma$, the changes in flight path angle γ will be nearly equal to those of θ .

Based on these characteristic differences, some approximating calculation methods for the short period and the long period oscillations can be given. The approximate solutions are useful to quickly and easily get some idea of the various characteristics of the two eigenmotions. Of course, the results are very handy for a quick check on the order of magnitude of results of complete computer calculations.

The accuracy of the approximating calculations depends of course on the unacceptability which depends on the type of aircraft. The following gives some calculation methods that generally produce satisfactory results for conventional aircraft. Even among the approximating calculations, some are more refined than others. Very often an apparently more refined calculation does not produce more accurate results, if compared with the complete calculation. A more detailed motivation for the various approximations can be found using the so-called eigenvectors of the eigenmotions. They are not discussed here.

1. Short period oscillation

(a) $V = \text{constant}$

The approximating calculation of the short period oscillation is based on the assumption that during this motion the airspeed remains constant. This implies that in the equations of motion $\dot{u} = 0$ and that the first column in equation (5-1) disappears. This also implies that the forces in the X_B -direction must remain in equilibrium during the entire motion. As a consequence, the X_B -equation can be entirely omitted. As an additional simplification, the initial steady flight condition is assumed to be level, so $\gamma_0 = 0$ and $C_{X_0} = 0$. This latter assumption causes the angle of pitch θ to disappear from the Z - and M equations, allowing the kinematic relation $-D_c\theta + \frac{q\bar{c}}{V} = 0$ to be omitted as well. In this way equations (5-1) are thus reduced to the following set of simpler equations,

$$\begin{bmatrix} C_{Z_\alpha} + (C_{Z_\alpha} - 2\mu_c) D_c & C_{Z_q} + 2\mu_c \\ C_{m_\alpha} + C_{m_\alpha} D_c & C_{m_q} - 2\mu_c K_Y^2 D_c \end{bmatrix} \begin{bmatrix} \alpha \\ \frac{q\bar{c}}{V} \end{bmatrix} = 0$$

The characteristic equation is obtained, just as in the discussion given in section 5-1, by equating the characteristic determinant to zero,

$$\begin{vmatrix} C_{Z_\alpha} + (C_{Z_\alpha} - 2\mu_c) \lambda_c & C_{Z_q} + 2\mu_c \\ C_{m_\alpha} + C_{m_\alpha} \lambda_c & C_{m_q} - 2\mu_c K_Y^2 \lambda_c \end{vmatrix} = 0$$

Expanding the determinant results in,

$$A\lambda_c^2 + B\lambda_c + C = 0$$

where,

$$A = 2\mu_c K_Y^2 (2\mu_c - C_{Z_\alpha})$$

$$B = -2\mu_c K_Y^2 C_{Z_\alpha} - (2\mu_c + C_{Z_q}) C_{m_\alpha} - (2\mu_c - C_{Z_\alpha}) C_{m_q}$$

$$C = C_{Z_\alpha} C_{m_q} - (2\mu_c + C_{Z_q}) C_{m_\alpha}$$

The roots of the characteristic equation are the two eigenvalues $\lambda_{c_{1,2}}$,

$$\lambda_{c_{1,2}} = \xi_c \pm j \eta_c = \frac{-B \pm j \sqrt{4AC - B^2}}{2A}$$

A further simplification is possible by omitting the derivatives C_{Z_α} and C_{Z_q} . They occur in the equations of motion in combination with the mass parameter $2\mu_c$ compared to which they are negligible. The coefficients A , B and C are then reduced to,

$$A = 4\mu_c^2 K_Y^2$$

$$B = -2\mu_c (K_Y^2 C_{Z_\alpha} + C_{m_\alpha} + C_{m_q})$$

$$C = C_{Z_\alpha} C_{m_q} - 2\mu_c C_{m_\alpha}$$

(b) $V = \text{constant}$, rotations in pitch only (γ is constant)

A further simplifying assumption is, that during the short period oscillation the trajectory of the aircraft c.g. is a straight line. If the initial steady flight condition is level flight the c.g. moves along a horizontal straight line. This means that the forces in the Z_B -direction remain in balance during the entire motion. As a consequence the Z -equation can be omitted. The only remaining motion is the rotation in pitch, i.e. only the M -equation remains. Because $\gamma = \theta - \alpha = 0$, α can be replaced by θ and $D_c \alpha$ by $D_c \theta$ in the M -equation.

With $D_c \frac{q\bar{c}}{V} = D_c^2 \theta$ the M -equation is then written as,

$$(C_{m_\alpha} + C_{m_\alpha} D_c + C_{m_q} D_c - 2\mu_c K_Y^2 D_c^2) \theta = 0$$

The characteristic equation has the coefficients,

$$A = -2\mu_c K_Y^2$$

$$B = C_{m_\alpha} + C_{m_q}$$

$$C = C_{m_\alpha}$$

2. Phugoid oscillation

(a) $\dot{q} = 0, \alpha = 0$

In this first, coarsest approximation of the long period oscillation the assumption is made that the angle of attack remains constant during this motion. As a consequence $\alpha = 0$ and also $\dot{\alpha} = 0$. This makes the α -column to disappear in equation (5-1) and one of the equations has become superfluous. Because $\dot{q} = 0$, the M -equation is omitted. The fact that $\alpha = 0$, may be seen as a consequence of a relatively high negative value of $C_{m\alpha}$. In such a case is also very nearly $C_m = 0$. If, finally, C_{Z_q} is neglected relative to $2\mu_c$ and again $C_{X_0} = 0$, the equations (5-1) now become,

$$\begin{bmatrix} C_{X_u} - 2\mu_c D_c & C_{Z_0} & 0 \\ C_{Z_u} & 0 & 2\mu_c \\ 0 & -D_c & 1 \end{bmatrix} \begin{bmatrix} \hat{u} \\ \theta \\ \frac{q\bar{c}}{V} \end{bmatrix} = 0$$

The characteristic equation is reduced to a quadratic, the coefficients are,

$$A = -4\mu_c^2$$

$$B = 2\mu_c C_{X_u}$$

$$C = -C_{Z_u} C_{Z_0}$$

The result permits a very simple approximation of the period. The undamped natural frequency ω_0 and the damping ratio ζ follow from the eigenvalues $\lambda_{c_{1,2}} = \xi_c \pm j \eta_c$ expressed in the coefficients A , B and C .

$$\omega_0 = \frac{V}{\bar{c}} \sqrt{\frac{C}{A}} = \frac{V}{\bar{c}} \sqrt{\frac{C_{Z_u} C_{Z_0}}{4\mu_c^2}} \quad (\text{sec}^{-1})$$

$$\zeta = -\frac{B}{2\sqrt{AC}} = \frac{-C_{X_u}}{2\sqrt{C_{Z_u} C_{Z_0}}}$$

For C_{X_u} , C_{Z_0} and C_{Z_u} the following approximations are introduced as discussed in sections 7-1, 7-2,

$$C_{X_u} = -2 C_D$$

$$C_{Z_0} = -C_L$$

$$C_{Z_u} = -2 C_L$$

For ω_0 and ζ then follows,

$$\omega_0 = \frac{V}{\bar{c}} \sqrt{\frac{2C_L^2}{4\mu_c^2}} = \frac{g\sqrt{2}}{V} \quad (\text{sec}^{-1})$$

$$\zeta = \frac{2C_D}{2\sqrt{2C_L^2}} = \frac{1}{2}\sqrt{2} \frac{C_D}{C_L}$$

According to this highly simplified calculation the damping of the long period oscillation is determined by the drag to lift ratio $\frac{C_D}{C_L}$. This ratio usually is in the order of 0.1. The

damping of the long period oscillation is, therefore, nearly always very low. In that case the period can be written as,

$$P = \frac{2\pi}{\omega_0 \sqrt{1 - \zeta^2}} \approx \frac{2\pi}{\omega_0} \quad (\text{sec})$$

With the above result for ω_0 , the period of the long period oscillation becomes,

$$P = \frac{2\pi}{g\sqrt{2}} V = 0.453 V \quad (\text{sec})$$

with V [m/sec].

According to this approximating calculation, the period in seconds of the long period oscillation is roughly 0.5 times the airspeed in [m/sec]. It should be remarked that for powered flight, the influence of C_{m_u} (neglected here) can be of considerable influence on the phugoid motion.

- (b) $\dot{q} = 0, \dot{\alpha} = 0$

A second, slightly more refined approximation of the long period oscillation goes less far than the previous one. Variations in α are now permitted, however, they are assumed to occur so slowly that $\dot{\alpha}$ remains negligible. In the equations (5-1) the contributions due to $D_c \frac{q\bar{c}}{V}$ and $D_c \alpha$ disappear, but none of the equations can be omitted. If C_{Z_q} and C_{X_0} are again neglected, the result is,

$$\begin{bmatrix} C_{X_u} - 2\mu_c D_c & C_{X_\alpha} & C_{Z_0} & 0 \\ C_{Z_u} & C_{Z_\alpha} & 0 & 2\mu_c \\ 0 & 0 & -D_c & 1 \\ C_{m_u} & C_{m_\alpha} & 0 & C_{m_q} \end{bmatrix} \begin{bmatrix} \hat{u} \\ \alpha \\ \theta \\ \frac{q\bar{c}}{V} \end{bmatrix} = 0$$

The coefficients of the characteristic equation, following from an expansion of the characteristic determinant, are,

$$A = 2\mu_c (C_{Z_\alpha} C_{m_q} - 2\mu_c C_{m_\alpha})$$

$$B = 2\mu_c (C_{X_u} C_{m_\alpha} - C_{m_u} C_{X_\alpha}) + C_{m_q} (C_{Z_u} C_{X_\alpha} - C_{X_u} C_{Z_\alpha})$$

$$C = C_{Z_0} (C_{m_u} C_{Z_\alpha} - C_{Z_u} C_{m_\alpha})$$

Chapter 6

Analysis of Asymmetric Equations of Motion

The asymmetric equations of motion will be treated along the same line as in chapter 5. Furthermore, the characteristic modes for the asymmetric aircraft motions will be discussed in this chapter, including several approximations for these modes. All simulations will be performed using a model of the Cessna Ce500 ‘Citation’.

6-1 Solution of the equations of motion

The equations for the disturbed asymmetric motions are obtained in the homogeneous form from equation (4-43), by omitting the terms due to the control surface deflections,

$$\begin{bmatrix} C_{Y\beta} + (C_{Y\dot{\beta}} - 2\mu_b)D_b & C_L & C_{Y_p} & C_{Y_r} - 4\mu_b \\ 0 & -\frac{1}{2}D_b & 1 & 0 \\ C_{\ell_\beta} & 0 & C_{\ell_p} - 4\mu_b K_X^2 D_b & C_{\ell_r} + 4\mu_b K_{XZ} D_b \\ C_{n_\beta} + C_{n_{\dot{\beta}}} D_b & 0 & C_{n_p} + 4\mu_b K_{XZ} D_b & C_{n_r} - 4\mu_b K_Z^2 D_b \end{bmatrix} \begin{bmatrix} \beta \\ \varphi \\ \frac{pb}{2V} \\ \frac{rb}{2V} \end{bmatrix} = 0 \quad (6-1)$$

The character of the asymmetric motions is discussed below, using a quantitative example.

Some characteristic parameters were derived for the symmetric eigenmotions in section 5-1. The same expressions also apply to the asymmetric motions, if the mean aerodynamic chord \bar{c} is replaced by the wing span b . The eigenvalues resulting from the characteristic equation are now indicated as λ_b .

The expressions for the time to damp to half an amplitude, and for the period, now read as follows,

- Aperiodic motion (λ_b real),

$$T_{\frac{1}{2}} = \frac{\ln \frac{1}{2}}{\lambda_b} \frac{b}{V} = -\frac{0.693}{\lambda_b} \frac{b}{V}$$

- Periodic motion corresponding to two complex, conjugate eigenvalues

$$\lambda_b = \xi_b \pm j \eta_b \quad j = \sqrt{-1}$$

$$P = \frac{2\pi}{\eta_b} \frac{b}{V}$$

$$T_{\frac{1}{2}} = -\frac{0.693}{\xi_b} \frac{b}{V}$$

$$C_{\frac{1}{2}} = \frac{T_{\frac{1}{2}}}{P} = \frac{-0.693}{2\pi} \frac{\eta_b}{\xi_b} = -0.110 \frac{\eta_b}{\xi_b}$$

$$\delta = \ln \frac{e^{\xi_b \frac{V}{b}(t+P)}}{e^{\xi_b \frac{V}{b}t}} = \xi_b \frac{V}{b} P = 2\pi \frac{\xi_b}{\eta_b} = \frac{0.693}{C_{\frac{1}{2}}}$$

In chapter 11 it was stated that C_{Y_β} and C_{n_β} are usually neglected, so it will be assumed here that,

$$C_{Y_\beta} = C_{n_\beta} = 0 \quad (6-2)$$

Expanding the characteristic determinant of equation (6-1),

$$\begin{vmatrix} C_{Y_\beta} + (C_{Y_\beta} - 2\mu_b) \lambda_b & C_L & C_{Y_p} & C_{Y_r} - 4\mu_b \\ 0 & -\frac{1}{2}\lambda_b & 1 & 0 \\ C_{\ell_\beta} & 0 & C_{\ell_p} - 4\mu_b K_X^2 \lambda_b & C_{\ell_r} + 4\mu_b K_{XZ} \lambda_b \\ C_{n_\beta} + C_{n_\beta} \lambda_b & 0 & C_{n_p} + 4\mu_b K_{XZ} \lambda_b & C_{n_r} - 4\mu_b K_Z^2 \lambda_b \end{vmatrix} = 0 \quad (6-3)$$

with the assumptions of equation (6-2), results in a quartic characteristic equation,

$$A \lambda_b^4 + B \lambda_b^3 + C \lambda_b^2 + D \lambda_b + E = 0$$

The coefficients A to E for the asymmetric motions are derived from the characteristic determinant, see (6-3),

$$A = 16\mu_b^3 (K_X^2 K_Z^2 - K_{XZ}^2)$$

$$B = -4\mu_b^2 \{ 2 C_{Y_\beta} (K_X^2 K_Z^2 - K_{XZ}^2) + C_{n_r} K_X^2 + C_{\ell_p} K_Z^2 + (C_{\ell_r} + C_{n_p}) K_{XZ} \}$$

$$C = 2\mu_b [(C_{Y_\beta} C_{n_r} - C_{Y_r} C_{n_\beta}) K_X^2 + (C_{Y_\beta} C_{\ell_p} - C_{\ell_\beta} C_{Y_p}) K_Z^2 +$$

$$\{(C_{Y_\beta} C_{n_p} - C_{n_\beta} C_{Y_p}) + (C_{Y_\beta} C_{\ell_r} - C_{\ell_\beta} C_{Y_r})\} K_{XZ} +$$

$$4\mu_b C_{n_\beta} K_X^2 + 4\mu_b C_{\ell_\beta} K_{XZ} + \frac{1}{2} (C_{\ell_p} C_{n_r} - C_{n_p} C_{\ell_r}) \Big]$$

$$D = -4\mu_b C_L (C_{\ell_\beta} K_Z^2 + C_{n_\beta} K_{XZ}) + 2\mu_b (C_{\ell_\beta} C_{n_p} - C_{n_\beta} C_{\ell_p}) +$$

$$\frac{1}{2} C_{Y_\beta} (C_{\ell_r} C_{n_p} - C_{n_r} C_{\ell_p}) + \frac{1}{2} C_{Y_p} (C_{\ell_\beta} C_{n_r} - C_{n_\beta} C_{\ell_r}) +$$

$$\frac{1}{2} C_{Y_r} (C_{\ell_p} C_{n_\beta} - C_{n_p} C_{\ell_\beta})$$

$$E = C_L (C_{\ell_\beta} C_{n_r} - C_{n_\beta} C_{\ell_r})$$

If the stability derivatives and inertial parameters are known for a certain aircraft configuration and flight condition, the coefficients A to E can be calculated. Using one of the common numerical methods, the eigenvalues may be obtained.

As an example the asymmetric disturbed motions of a Cessna Ce500 ‘Citation’ are studied. The required data are given in table 6-1.

From these data follow the coefficients A to E for the characteristic equation,

$$A \lambda_b^4 + B \lambda_b^3 + C \lambda_b^2 + D \lambda_b + E = 0$$

which can be obtained from equation(6-3). The roots of the characteristic polynomial are obtained by the program package MATLAB using the routine `roots.m`.

For a stable aircraft all eigenvalues λ_b must have negative real parts. When this is the case the disturbed motion will be positively damped. An explicit determination of the four eigenvalues, see also figure 6-1, for the Cessna Ce500 ‘Citation’ example become,

$$\lambda_{b_1} = -0.3291$$

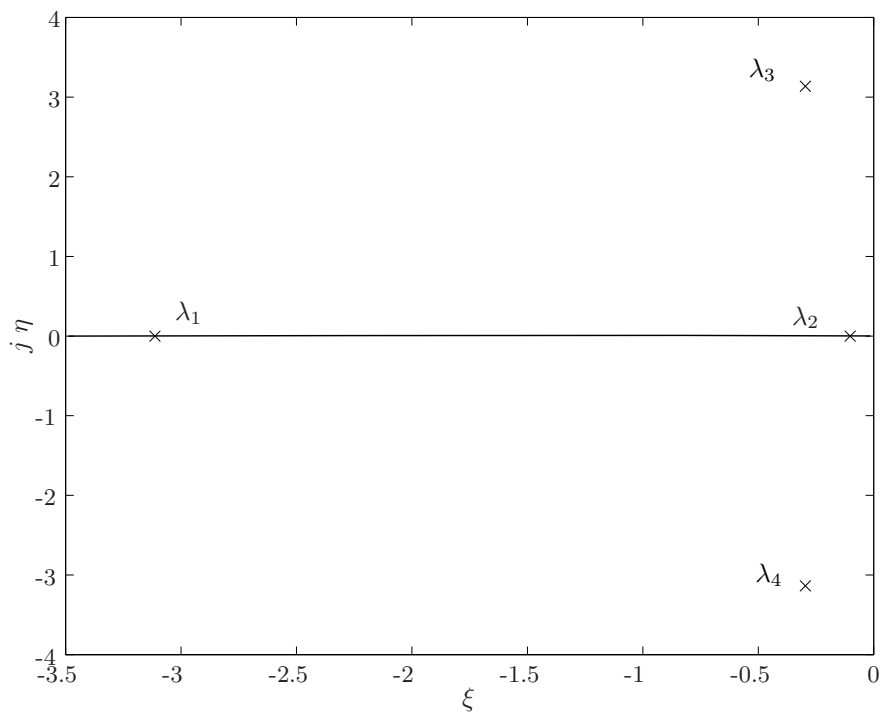
$$\lambda_{b_2} = -0.0108$$

$$\lambda_{b_{3,4}} = -0.0313 \pm j 0.3314$$

The disturbed asymmetric motions consist apparently of two aperiodic eigenmotions and one periodic motion. One of the two aperiodic motions appears to be well damped, the other one is only very lightly damped or may be even slightly undamped (which is the case for most aircraft. The characteristics of the eigenmotions are as follows,

V	=	59.9 m/sec	μ_b	=	15.5
S	=	24.2 m ²	K_X^2	=	0.012
b	=	13.36 m	K_Z^2	=	0.037
C_L	=	1.1360	K_{XZ}	=	0.002
C_{Y_β}	=	-0.9896	C_{ℓ_β}	=	-0.0772
C_{Y_p}	=	-0.0870	C_{ℓ_p}	=	-0.3444
C_{Y_r}	=	0.4300	C_{ℓ_r}	=	0.2800
$C_{Y_{\delta_a}}$	=	0	$C_{\ell_{\delta_a}}$	=	-0.2349
$C_{Y_{\delta_r}}$	=	0.3037	$C_{\ell_{\delta_r}}$	=	0.0286
					$C_{n_\beta} = 0.1638$
					$C_{n_p} = -0.0108$
					$C_{n_r} = -0.1930$
					$C_{n_{\delta_a}} = 0.0286$
					$C_{n_{\delta_r}} = -0.1261$

Table 6-1: Asymmetric stability and control derivatives for the Cessna Ce500 ‘Citation’

Figure 6-1: The location of the eigenvalues $\lambda = \lambda_b \frac{V}{b}$ for the asymmetric motions

- First aperiodic mode

- $\lambda_{b_1} = -0.3291$
- the time to damp to half the amplitude $T_{\frac{1}{2}} \approx 0.223$ seconds

- Second aperiodic mode

- $\lambda_{b_2} = -0.0108$
- the time to damp to half the amplitude $T_{\frac{1}{2}} \approx 6.782$ seconds

- Periodic mode

- $\lambda_{b_{3,4}} = -0.0313 \pm j 0.3314$
- the period $P = 2.004$ seconds
- the time to damp to half the amplitude $T_{\frac{1}{2}} \approx 2.340$ seconds
- the undamped natural frequency $\omega_0 = 3.1495$ rad/sec.
- the damping ratio $\zeta = 0.0940$

Figures 6-2 and 6-3 show the calculated responses for the aircraft, simulated by the program package MATLAB. In this particular case the disturbances are pulse-shaped rudder and aileron deflections.

6-2 General character of the asymmetric motions

From the time responses in figures 6-2 and 6-3 three eigenmotions may be distinguished, as was evident also from the eigenvalues.

- A highly damped aperiodic motion

The corresponding eigenvalue is $\lambda_{b_{11}}$, real and strongly negative. The motion is apparent mostly in the rate of roll. The damping of this motion is due primarily to the damping rolling moment generated by the wing when rotating about the longitudinal axis, i.e. the moment $C_{\ell_p} \cdot \frac{pb}{2V}$.

- Aperiodic mode in which the aircraft sideslips, yaws and rolls

The motion is characterized by the eigenvalue λ_{b_2} real, lightly positively or negatively damped. Depending on the sign of λ_{b_2} this eigenmotion converges or diverges. If the motion diverges ($\lambda_{b_2} > 0$), the aircraft after a disturbance enters into a sideslipping turn with ever increasing angle of roll and decreasing radius. During this motion the aircraft sideslips towards the inside of the turn, see figure 6-4. The aircraft is than called spirally unstable, as the aircraft describes a descending spiral. The eigenmotion is called the spiral motion. If it is damped, the aircraft has ‘spiral stability’.

- Periodic mode in which the aircraft sideslips, yaws and rolls

This eigenmotion is determined by the eigenvalues $\lambda_{b_{3,4}} = \xi_b \pm j \eta_b$. Figure 6-5 shows the general character of the motion. Rolling and yawing velocity are presented for the case where the motion is damped $\xi_b < 0$. This motion is generally called ‘Dutch roll’. The name seems to be inspired by the resemblance to the motion of a skater on the ice.

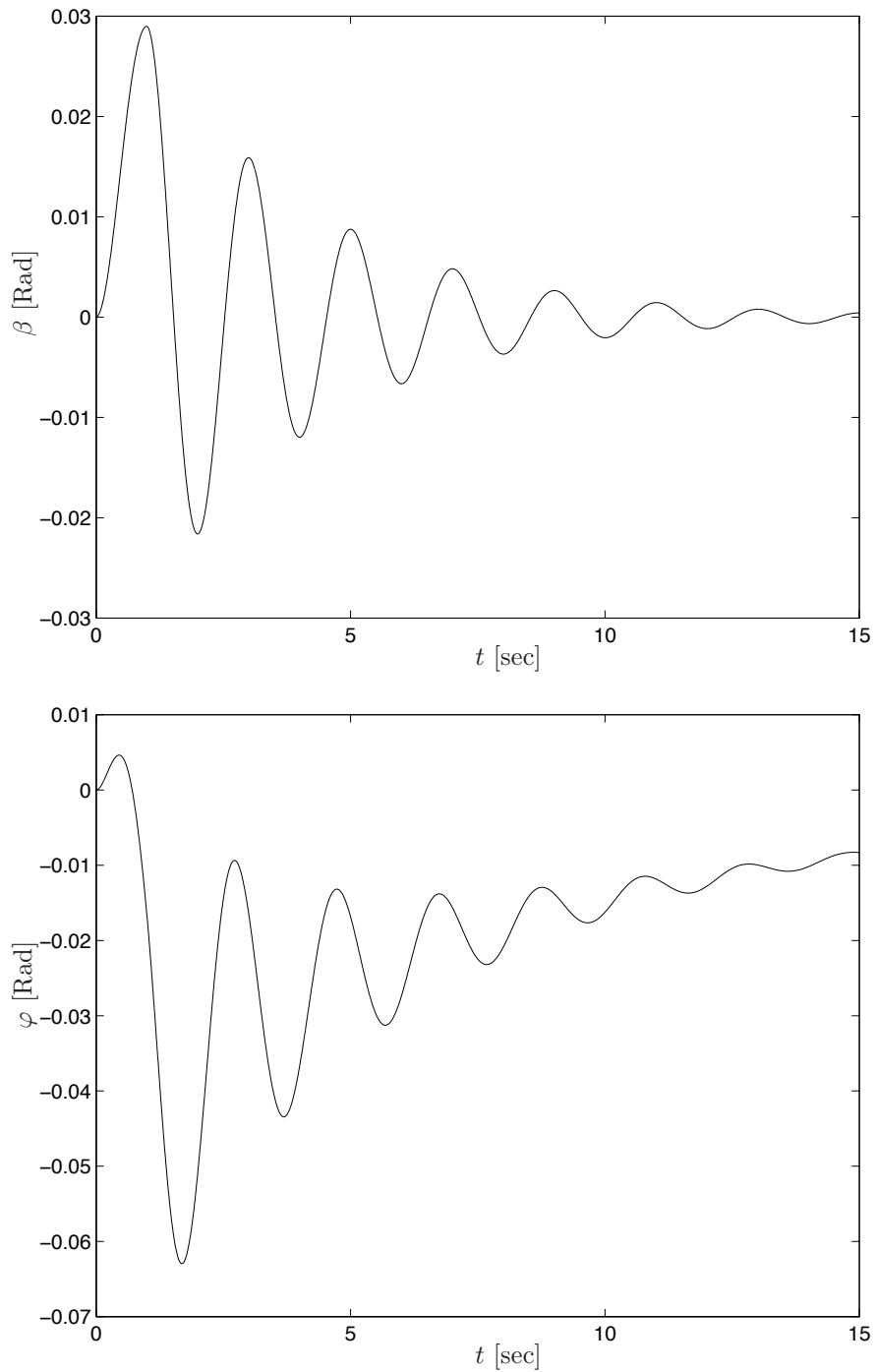


Figure 6-2: Response curves for a pulse-shaped rudder deflection ($\Delta\delta_r = +0.025$ [Rad] during 1 second) for the Cessna Ce500 ‘Citation’

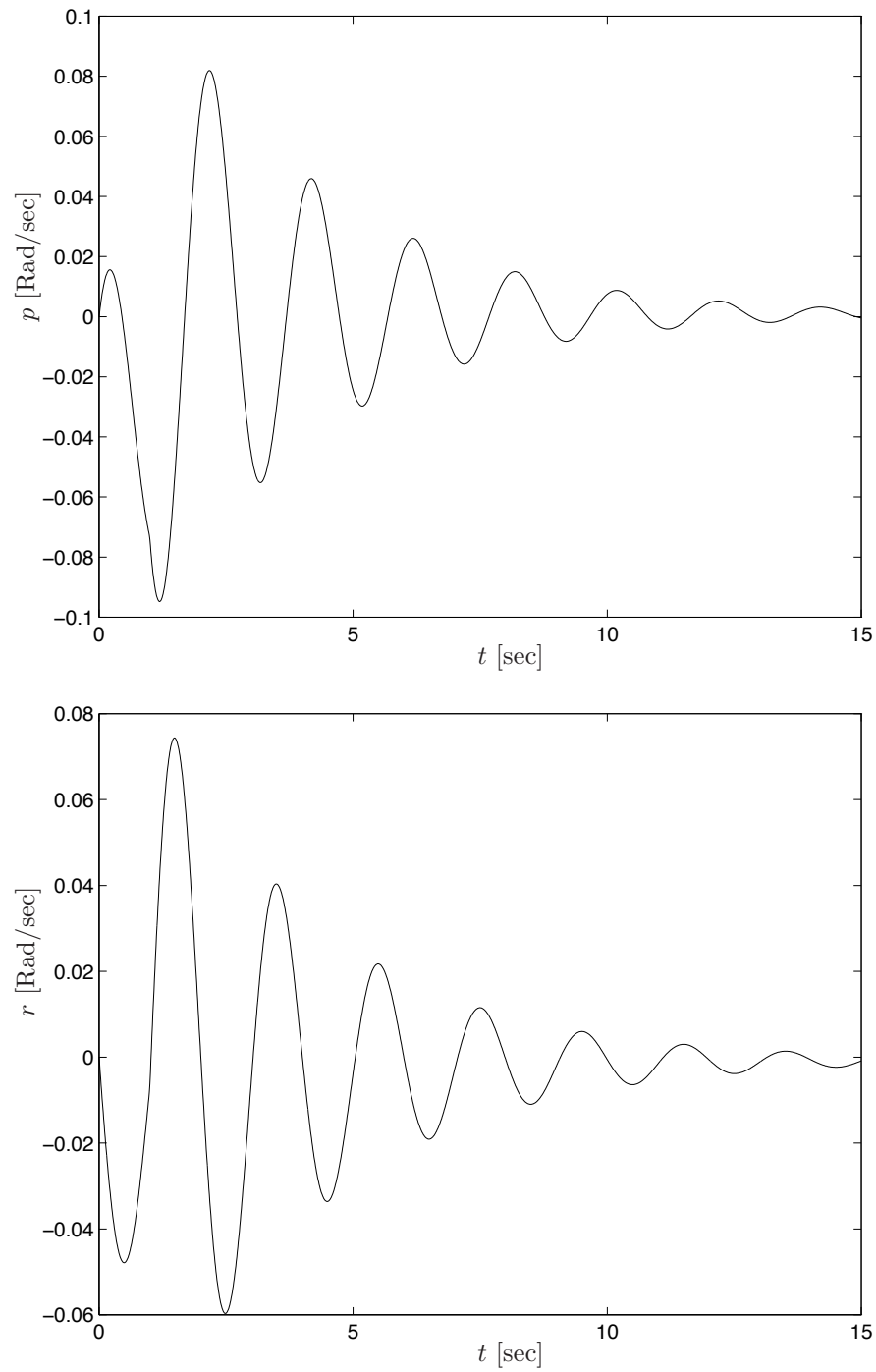


Figure 6-2: (**Continued**) Response curves for a pulse-shaped rudder deflection ($\Delta\delta_r = +0.025$ [Rad] during 1 second) for the Cessna Ce500 ‘Citation’

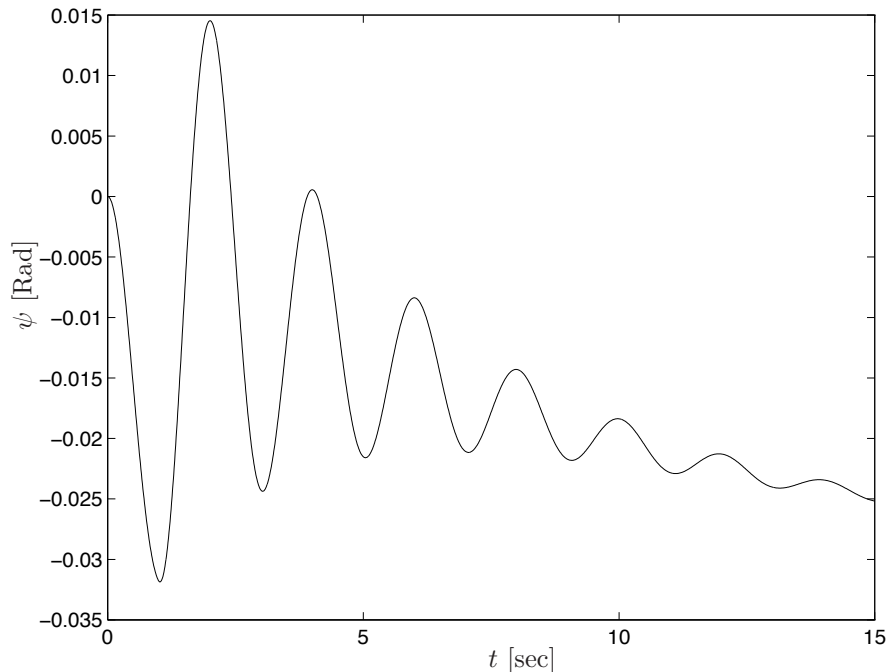


Figure 6-2: (**Continued**) Response curves for a pulse-shaped rudder deflection ($\Delta\delta_r = +0.025$ [Rad] during 1 second) for the Cessna Ce500 ‘Citation’

6-3 Routh-Hurwitz stability criteria for the asymmetric motions

The criteria for stability were discussed already in section 6-1. It can be proved, that in the transition from stability to instability the conditions $E > 0$ and $R > 0$ are the critical stability criteria. If only E becomes negative, one real eigenvalue changes sign. This means that one of the aperiodic motions changes from convergence to divergence. If R becomes more negative, the real part of the two complex, conjugate eigenvalues changes signs implying periodic divergence. According to the foregoing, the coefficient E determines the character of the aperiodic spiral motion and from the discriminant R follows the character of the (periodic) Dutch roll motion.

In the following the stability criteria are used for a further study of the spiral motion and the Dutch roll oscillation of the aircraft. To prepare for this discussion, the factors determining the signs of the coefficients A to E are investigated.

As a first approximation, the relatively small derivative C_{Y_p} is equated to zero and C_{Y_r} is neglected relative to $4\mu_b$. For aircraft having a straight wing without a large dihedral these assumptions are acceptable. Also, the coefficient K_{XZ} , the product of inertia, is omitted. K_{XZ} is relatively small, relative to K_X^2 and K_Y^2 . The remaining stability derivatives determining the magnitude and the signs of the coefficients A to E have, according to chapter 11, the following signs for conventional aircraft in normal flight,

$$C_{Y_\beta} < 0 \quad C_{\ell_p} < 0 \quad C_{n_p} < 0 \quad C_{\ell_r} > 0 \quad C_{n_r} < 0$$

The stability derivatives C_{ℓ_β} and C_{n_β} are practically the only ones the designer can manipulate to influence the lateral stability. As discussed in chapter 11, pleasant control characteristics require that,

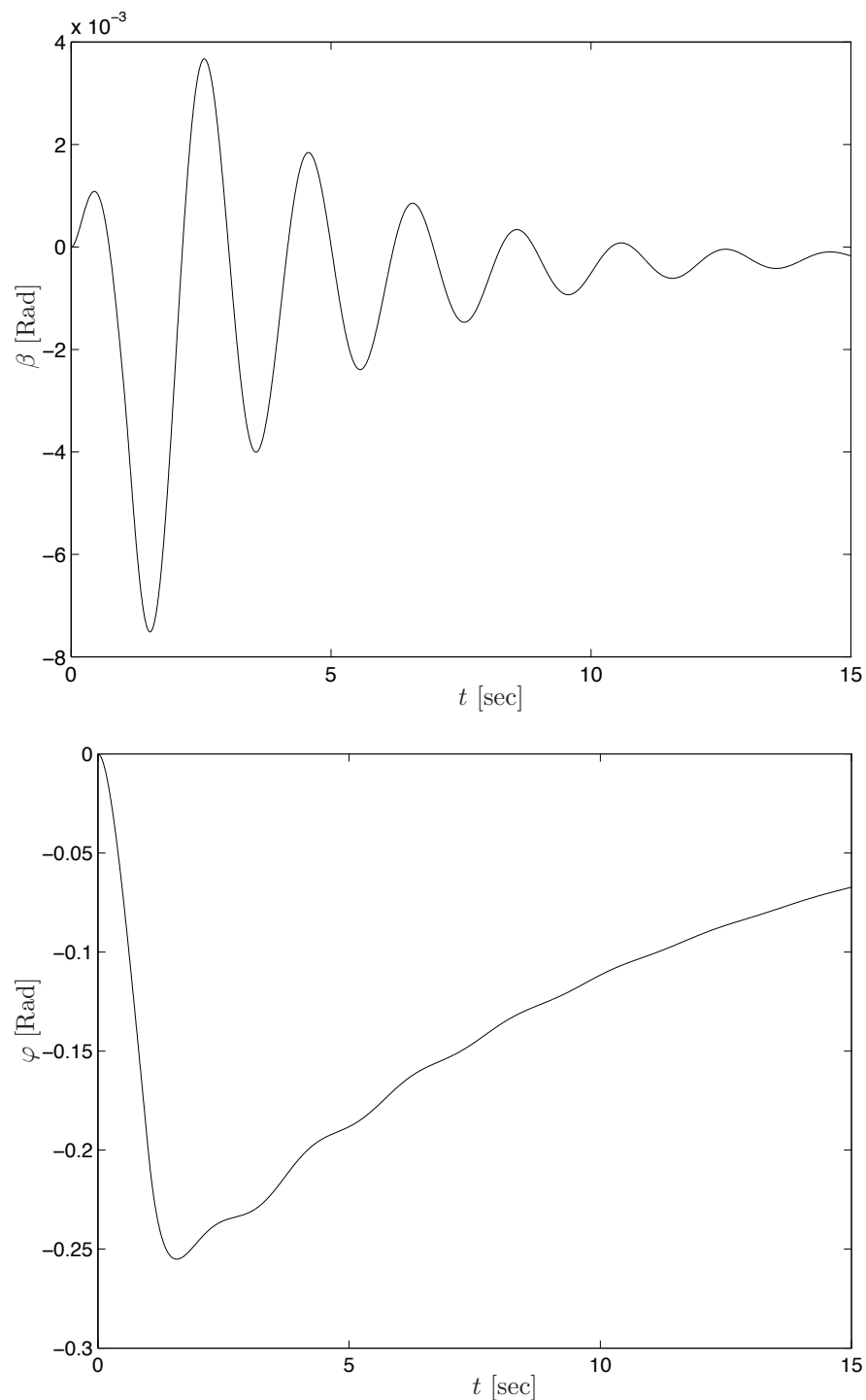


Figure 6-3: Response curves for a pulse-shaped aileron deflection ($\Delta\delta_a = +0.025$ [Rad] during 1 second) for the Cessna Ce500 ‘Citation’

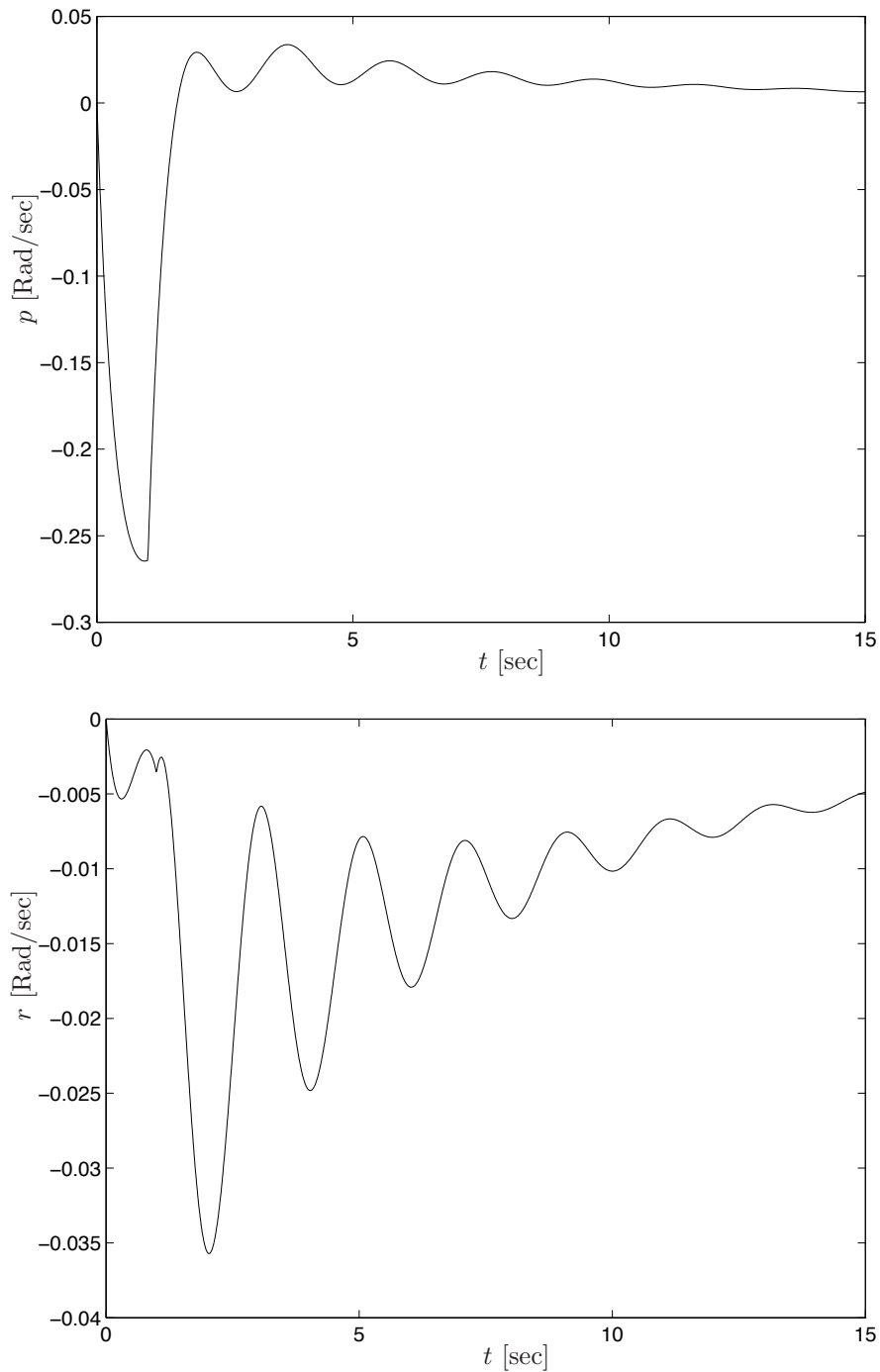


Figure 6-3: (**Continued**) Response curves for a pulse-shaped aileron deflection ($\Delta\delta_a = +0.025$ [Rad] during 1 second) for the Cessna Ce500 ‘Citation’

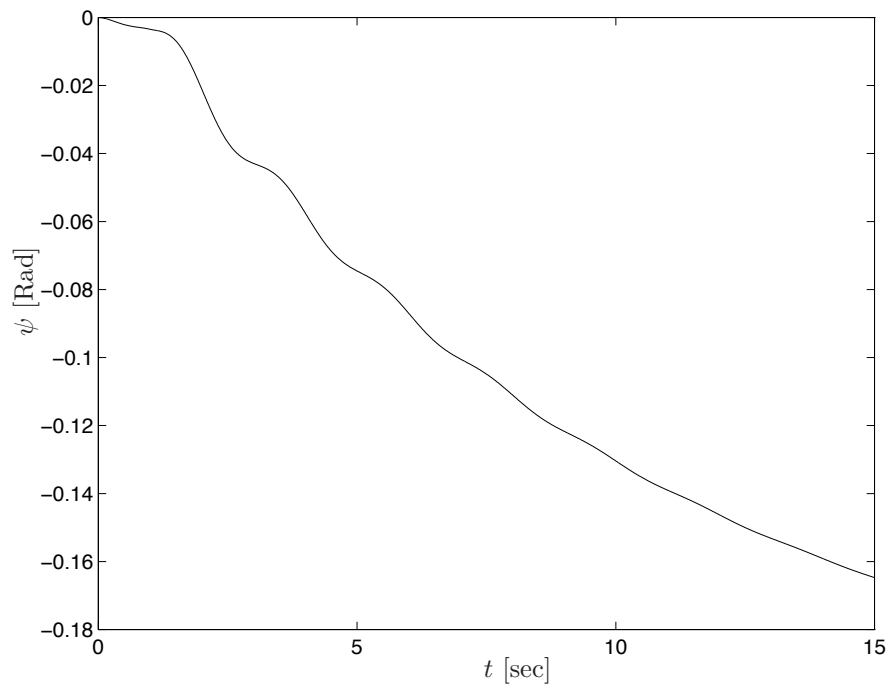


Figure 6-3: (Continued) Response curves for a pulse-shaped aileron deflection ($\Delta\delta_a = +0.025$ [Rad] during 1 second) for the Cessna Ce500 ‘Citation’

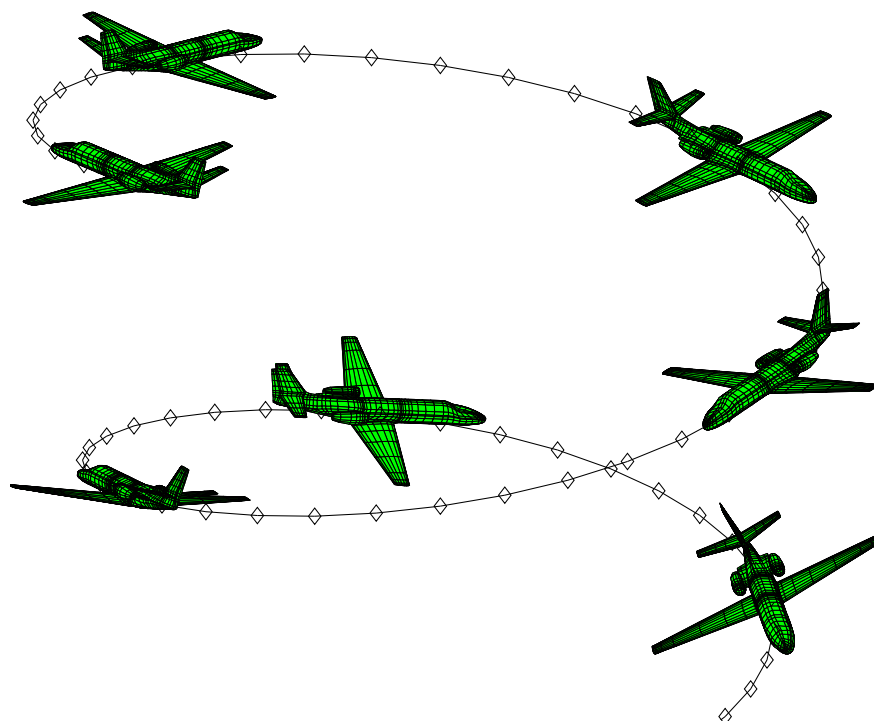


Figure 6-4: The spiral motion of an aircraft

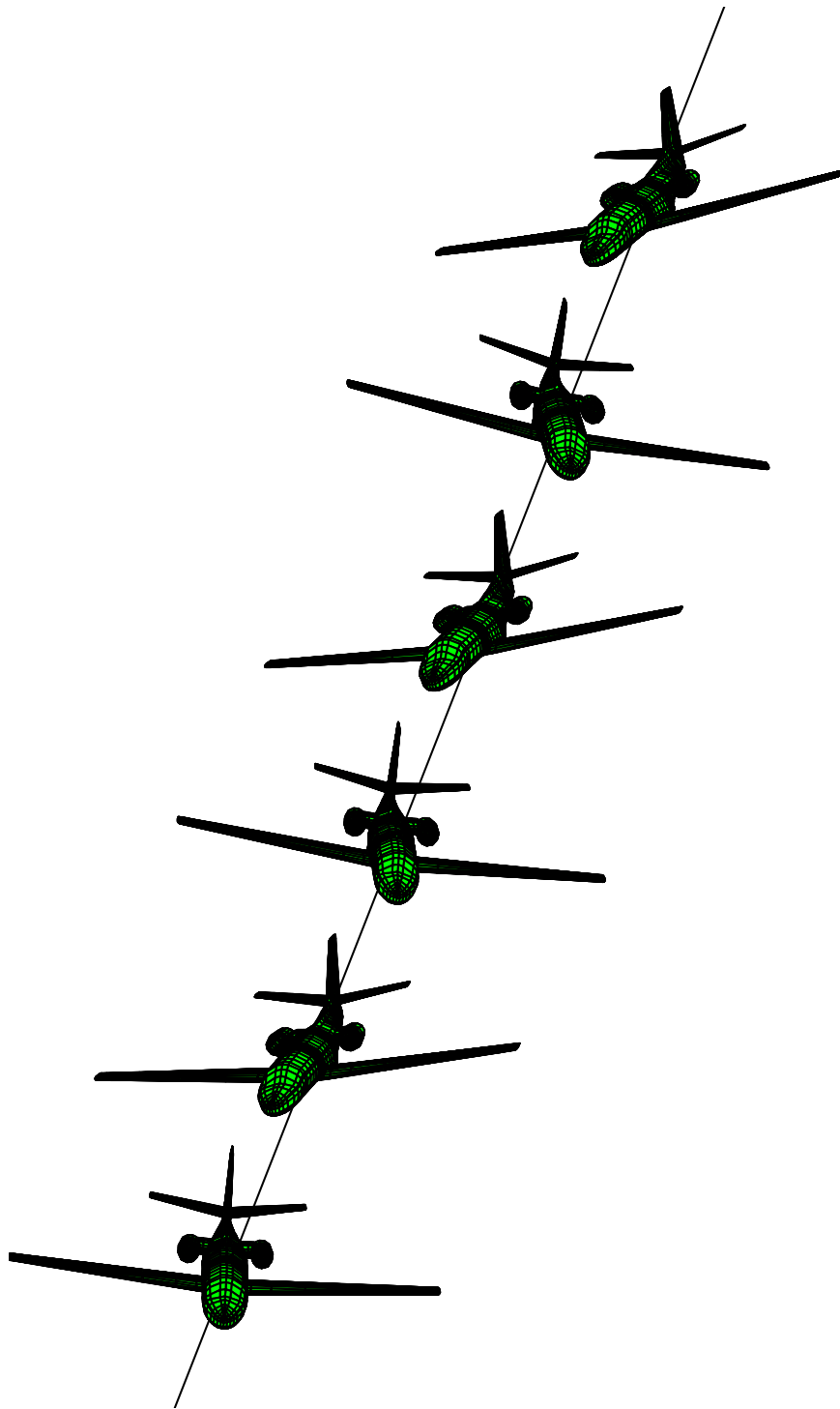


Figure 6-5: Characteristics of the Dutch Roll motion

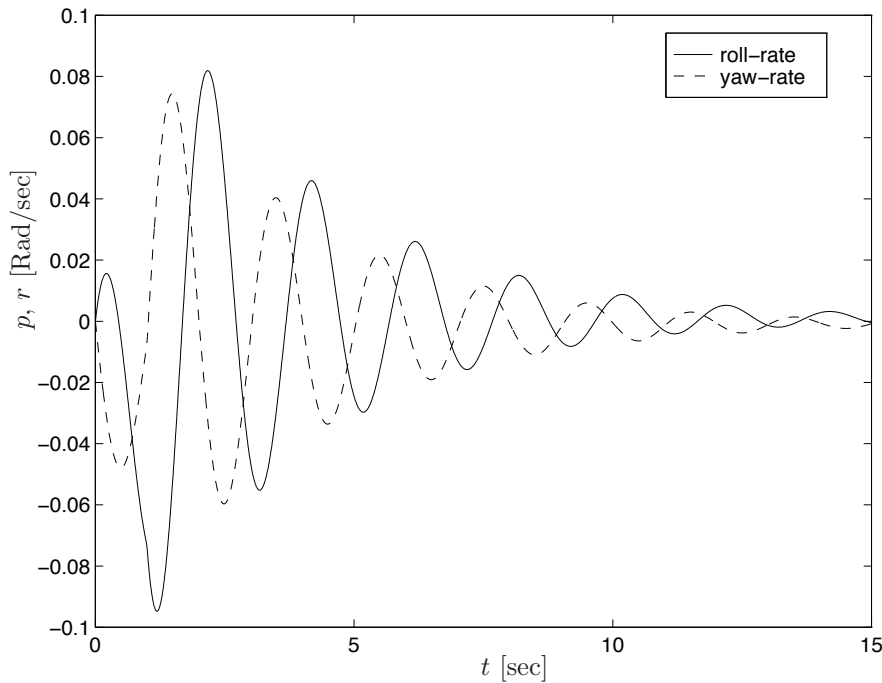


Figure 6-6: Roll- and yaw-rate characteristics of the Dutch Roll motion

$$C_{n_\beta} > 0 \quad C_{\ell_\beta} < 0$$

Neglecting C_{Y_p} , C_{Y_r} and K_{XZ} and using the known signs of the other derivatives and the inertial parameters the signs of the coefficients A to E can be established as follows,

$$A = 16\mu_b^3 K_X^2 K_Z^2 > 0$$

$$B = -4\mu_b^2 \{ 2 C_{Y_\beta} K_X^2 K_Z^2 + C_{n_r} K_X^2 + C_{\ell_p} K_Z^2 \} > 0$$

$$C = 2\mu_b \left[C_{Y_\beta} C_{n_r} K_X^2 + C_{Y_\beta} C_{\ell_p} K_Z^2 + 4\mu_b C_{n_\beta} K_X^2 + \frac{1}{2} (C_{\ell_p} C_{n_r} - C_{n_p} C_{\ell_r}) \right]$$

If $C_{n_\beta} > 0$ (the aircraft is then statically directionally stable), then $C > 0$.

$$D = -4\mu_b C_L C_{\ell_\beta} K_Z^2 + 2\mu_b (C_{\ell_\beta} C_{n_p} - C_{n_\beta} C_{\ell_p}) + \frac{1}{2} C_{Y_\beta} (C_{\ell_r} C_{n_p} - C_{n_r} C_{\ell_p})$$

If $C_L > 0$, $C_{\ell_\beta} < 0$ and $C_{n_\beta} > 0$, then also $D > 0$.

$$E = C_L (C_{\ell_\beta} C_{n_r} - C_{n_\beta} C_{\ell_r})$$

At positive values of C_L , the positive sign of E is determined by the condition,

$$C_{\ell_\beta} C_{n_r} - C_{n_\beta} C_{\ell_r} > 0$$

It appears that the above requirement for dynamic stability is identical to the one derived in chapter 11, see section 11-3. The latter was based on the criterion for good control characteristics in steady turns using the ailerons or the rudder only.

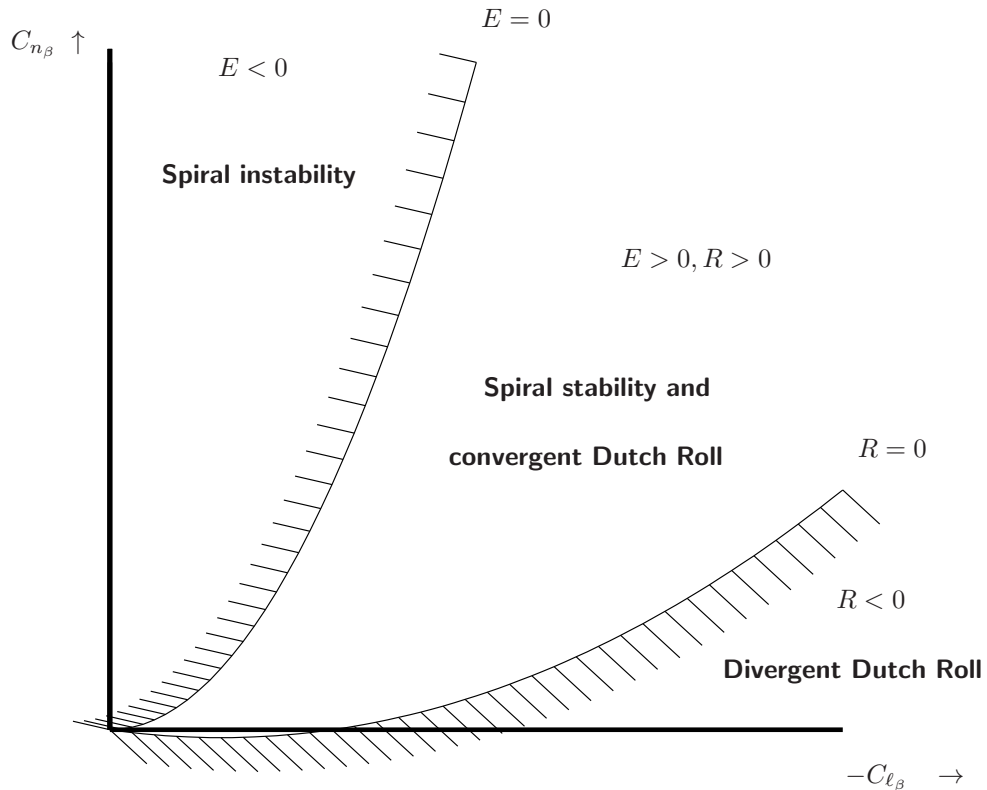


Figure 6-7: Lateral stability diagram

6-4 Spiral and Dutch roll mode, the lateral stability diagram

In the previous section it was stated that positive damping of the spiral motion required that $E > 0$ and for damping of the Dutch roll motion, $R > 0$. The magnitudes of E and R are influenced to a large extent by the effective dihedral C_{ℓ_β} and the static directional stability C_{n_β} . The derivative C_{ℓ_β} can be varied by changing the geometric dihedral of the wing; C_{n_β} is modified by varying the surface S_v of the vertical tailplane and the tail length l_v . But it should be remembered that changing S_v and/or l_v influences also some other stability derivatives, such as C_{n_r} and C_{Y_β} .

The effect of changes in C_{n_β} and C_{ℓ_β} on E and R is graphically depicted in the so-called lateral stability diagram, along the axes, C_{ℓ_β} and C_{n_β} are plotted, see figure 6-7.

For a particular aircraft, the boundaries $E = 0$ and $R = 0$ are plotted for a given aircraft configuration and flight condition in the lateral stability diagram. The remaining stability derivatives are assumed to remain constant, or to be adjusted to the external shape of the aircraft corresponding to each combination of C_{ℓ_β} and C_{n_β} .

The two curves $E = 0$ and $R = 0$ indicate the boundaries of areas in the diagram for spiral stability and a damped Dutch roll oscillation. The diagram indicates for any combination of C_{ℓ_β} and C_{n_β} the state of the dynamic lateral stability for the aircraft configuration and flight condition under study.

Only the most common case, where $C_{\ell_\beta} < 0$ and $C_{n_\beta} > 0$ is further discussed. Using the lateral stability diagram, the spiral motion is considered first. The criterion for spiral stability is,

$$C_{\ell_\beta} C_{n_r} - C_{n_\beta} C_{\ell_r} > 0$$

It follows, that spiral stability can be increased in two ways, e.g. by decreasing C_{n_β} or by increasing $-C_{\ell_\beta}$. Because other requirements on the control characteristic have to be met as well, a decrease in C_{n_β} may be hardly acceptable. A value of C_{ℓ_β} too large negative may not be acceptable either, as will be discussed below.

The effect of these conflicting requirements is, that it may be difficult to choose the external form of the aircraft such that it is spirally stable in all required aircraft configurations and flight conditions. The divergence from a spirally unstable equilibrium flight condition is often relatively slow. In order to avoid even less desirable characteristics, a certain slight degree of spiral instability may be unavoidable. The curve for $R = 0$, determining stability of the Dutch roll motion, appears to depend largely on the relative density $\mu_b = \frac{m}{\rho S b}$ of the aircraft. The curve for $R = 0$ moves upward in the lateral stability diagram with increasing μ_b . This means that for given aerodynamic characteristics (stability derivatives) the damping of the Dutch roll motion decreases with increasing μ_b .

In general, the Dutch roll motion of aircraft having a low wing loading, flying at relatively low altitudes are relatively well damped. A characteristic value of the damping for such aircraft is $\zeta \approx 0.15$ or $C_{\frac{1}{2}} \approx 0.7$.

For the Dutch roll motion it does not suffice to determine only the sign of R , because good flying qualities imply a certain minimal damping of the Dutch roll motion.

This minimal required damping has been made a function of the period of the motion, see reference [13]. This may be explained as follows. If the period is short, the reactions of the pilot will be too slow to stabilize the motion by suitable control deflections. In such a case a relatively high damping or a low value of $T_{\frac{1}{2}}$, or $C_{\frac{1}{2}}$, is required. If the period is longer, the damping of the motion may be lower, because in such a situation the pilot has less difficulty to improve the damping of the aircraft's motions via his control deflections.

However, the requirement relating the period and the minimal acceptable time to damp to half amplitude has turned out to provide insufficient guarantee for good flying qualities.

More recent requirements, see e.g. reference [13], stipulate that the damping of the Dutch roll has a certain minimal value depending on the roll to yaw ratio $\frac{|p|}{r}$ occurring during the Dutch roll motion. The interpretation of this ratio $\frac{|p|}{r}$ is shown in figure 6-6.

6-5 Approximate solutions

1. Heavily damped aperiodic rolling motion

The aperiodic rolling moment may be approximated by assuming that the aircraft can only roll about the longitudinal axis. This is permissible because this motion often disappears before the other eigenmotions of the aircraft have really started. If only the rolling motion is considered, in the equations (6-1) the angle of side slip β , and the non-dimensional yaw-rate $\frac{rb}{2V}$ disappear and the equations for the lateral force and the yawing moment can be omitted. In the remaining equation for the rolling moments the angle of roll φ does not occur, so the kinematic relation $-\frac{1}{2}D_b\varphi + \frac{pb}{2V} = 0$ is no longer needed. The rolling moment equation then reads,

$$(C_{\ell_p} - 4 \mu_b K_X^2 D_b) \frac{pb}{2V} = 0$$

It is easy to see, that this expression gives the real eigenvalue,

$$\lambda_{b_1} = \frac{C_{\ell_p}}{4 \mu_b K_X^2}$$

2. Dutch roll motion

(a) $\varphi = \frac{pb}{2V} = 0$

For a large category of conventional aircraft a certain approximation of the Dutch roll motion results if the rolling component is discarded in the Dutch roll motion. If φ and $\frac{pb}{2V}$ are set at zero, the φ - and $\frac{pb}{2V}$ -columns in the equations of motion disappear and the rolling moment equation can be omitted since the rolling moments have to remain in balance. Only the aerodynamic force Y - and the moment N -equations remain. As usual, C_{Y_β} and C_{n_β} are neglected, whereas C_{Y_r} is insignificant relative to $4 \mu_b$,

$$\begin{bmatrix} C_{Y_\beta} - 2\mu_b D_b & -4\mu_b \\ C_{n_\beta} & C_{n_r} - 4\mu_b K_Z^2 D_b \end{bmatrix} \begin{bmatrix} \beta \\ \frac{rb}{2V} \end{bmatrix} = 0$$

The coefficients of the quadratic characteristic equation become,

$$A = 8 \mu_b^2 K_Z^2$$

$$B = -2\mu_b (C_{n_r} + 2K_Z^2 C_{Y_\beta})$$

$$C = 4\mu_b C_{n_\beta} + C_{Y_\beta} C_{n_r}$$

From these coefficients ω_0 , ζ , P and $T_{\frac{1}{2}}$ can easily be obtained.

(b) $\varphi = \frac{pb}{2V} = 0$, yawing rotation only

A more restrictive assumption is that the trajectory of the aircraft's c.g. is a straight line during the oscillation. This implies that the course angle χ is constant, where $\chi = \beta + \psi = 0$, or $\beta = -\psi$. It implies as well that the Y -equation is superfluous. The remaining yawing moment equation is further simplified by the fact that $\frac{rb}{2V} = \frac{1}{2}D_b\psi$ and $\beta = -\psi$. The result is,

$$\left(-C_{n_\beta} + \frac{1}{2}C_{n_r} D_b - 2\mu_b K_Z^2 D_b^2 \right) \psi = 0$$

The coefficients A , B and C of the characteristic equation are,

$$A = -2\mu_b K_Z^2$$

$$B = \frac{1}{2}C_{n_r}$$

$$C = -C_{n_\beta}$$

The expressions for ω_0 and ζ are obtained very simply as,

$$\omega_0 = \frac{V}{b} \sqrt{\frac{C}{A}} = \frac{V}{b} \sqrt{\frac{C_{n_\beta}}{2\mu_b K_Z^2}}$$

$$\zeta = -\frac{B}{2\sqrt{AC}} = -\frac{C_{n_r}}{4\sqrt{2\mu_b K_Z^2 C_{n_\beta}}}$$

3. Aperiodic spiral motion

The aperiodic spiral motion is usually a very slow eigenmotion, in which the aircraft sideslips, yaws and rolls. It is, therefore, permissible to approximate the motion by assuming all linear and angular accelerations to be negligible. In the equations of motion this means,

$$D_b \beta = D_b \frac{pb}{2V} = D_b \frac{rb}{2V} = 0$$

In addition to C_{Y_r} , also C_{Y_p} is neglected.

$$\begin{bmatrix} C_{Y_\beta} & C_L & 0 & -4\mu_b \\ 0 & -\frac{1}{2}D_b & 1 & 0 \\ C_{\ell_\beta} & 0 & C_{\ell_p} & C_{\ell_r} \\ C_{n_\beta} & 0 & C_{n_p} & C_{n_r} \end{bmatrix} \begin{bmatrix} \beta \\ \varphi \\ \frac{pb}{2V} \\ \frac{rb}{2V} \end{bmatrix} = 0$$

Expanding the characteristic equation results in the eigenvalue,

$$\lambda_{b4} = \frac{2C_L(C_{\ell_\beta}C_{n_r} - C_{n_\beta}C_{\ell_r})}{C_{\ell_p}(C_{Y_\beta}C_{n_r} + 4\mu_b C_{n_\beta}) - C_{n_p}(C_{Y_\beta}C_{\ell_r} + 4\mu_b C_{\ell_\beta})}$$

It is easy to verify that the dominator is negative if all stability derivatives have their normal signs. For convergence of this motion it is necessary that $\lambda_{b4} < 0$, which means,

$$C_L(C_{\ell_\beta}C_{n_r} - C_{n_\beta}C_{\ell_r}) > 0$$

This corresponds to the requirement $E > 0$, derived in section 6-3.

4. Dutch roll motion and the aperiodic rolling motion

If the assumption is made that the c.g. moves along a straight line, but in addition the rolling motion is permitted, only the Y -equation disappears. The following equations in ψ and $\frac{pb}{2V}$ result,

$$\begin{bmatrix} -C_{\ell_\beta} + \frac{1}{2}C_{\ell_r}D_b + 2\mu_b K_{XZ}D_b^2 & C_{\ell_p} - 4\mu_b K_X^2 D_b \\ -C_{n_\beta} + \frac{1}{2}C_{n_r}D_b - 2\mu_b K_Z^2 D_b^2 & C_{n_p} + 4\mu_b K_{XZ}D_b \end{bmatrix} \begin{bmatrix} \psi \\ \frac{pb}{2V} \end{bmatrix} = 0$$

The characteristic equation is a cubic,

$$A \lambda_b^3 + B \lambda_b^2 + C \lambda_b + D = 0$$

The coefficients are then,

$$A = 4\mu_b^2 (K_X^2 K_Z^2 - K_{XZ}^2)$$

$$B = -\mu_b \{ (C_{\ell_r} + C_{n_p}) K_{XZ} + C_{n_r} K_X^2 + C_{\ell_p} K_Z^2 \}$$

$$C = 2\mu_b (C_{\ell_\beta} K_{XZ} + C_{n_\beta} K_X^2) + \frac{1}{4} (C_{\ell_p} C_{n_r} - C_{n_p} C_{\ell_r})$$

$$D = \frac{1}{2} (C_{\ell_\beta} C_{n_p} - C_{n_\beta} C_{\ell_p})$$

Evidently no explicit analytical solution to this cubic can be given. By using the approximation for the eigenvalue of the motion in roll, the characteristic equation may be reduced to a quadratic equation.

Chapter 7

Longitudinal Stability and Control Derivatives

In the following sections attention is given to the methods used to obtain the various stability and control derivatives for the symmetric motions. The corresponding methods used for the asymmetric motions will be discussed in chapter 8.

Evidently, the accuracy to which the derivatives can be determined has a direct influence on the accuracy of the calculated non-steady aircraft motions. The stability derivatives can be found not only by calculation from generalized data, but also from measurements. Flight tests with the actual aircraft can be made, or wind tunnel tests on a model. From comparisons of measured and calculated stability derivatives obtained in different ways, it appears that none of these various ways to obtain the various derivatives gives satisfactory results in all cases of practical interest. However, recent research suggests that Computational Fluid Dynamics' (CFD) techniques can also be used to estimate the stability and control derivatives with an accuracy comparable to results obtained by flight test techniques.

Calculated derivatives may be expected to show an acceptable correspondence with experimentally obtained values, only for conventional aircraft configurations. For less conventional configurations, calculated derivatives may be considered only as a very first approximation. In such situations measured stability derivatives are indispensable for calculations of stability and control characteristics on which some reliance has to be placed.

In the following the various stability derivatives are discussed in turn. When considering the forces and moments in the initial equilibrium condition, the contributions from the propulsive system are included; when discussing the stability derivatives these contributions are not considered.

Various calculation methods are mentioned, for more detailed discussions and quantitative data reference is made to the literature. All derivatives, with the exception of $C_{Z\alpha}$, $C_{m\alpha}$ and $C_{n\beta}$, are calculated under the assumption that the airflow is always stationary.

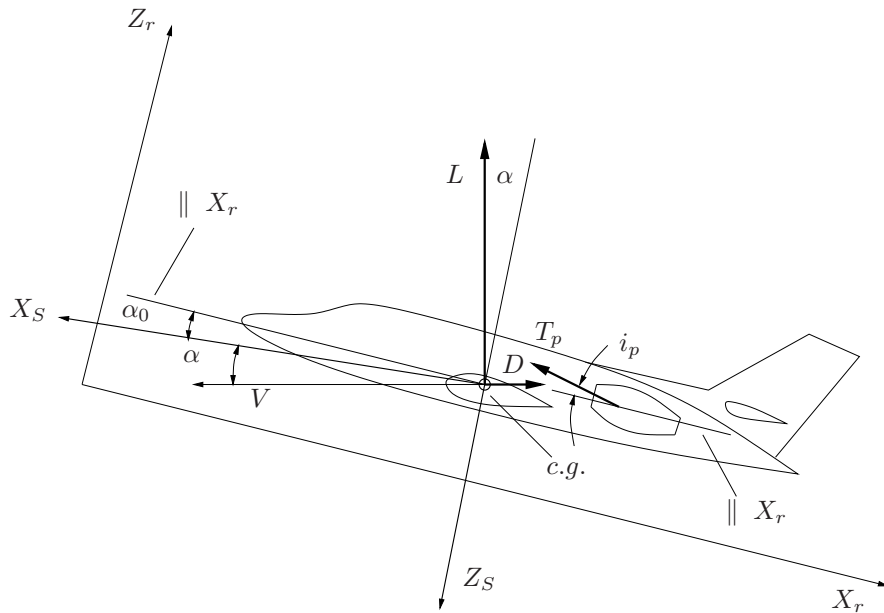


Figure 7-1: The attitude of the stability reference frame relative to the X_r - and Z_r -axis, after a disturbance from the equilibrium flight condition

7-1 Aerodynamic forces in the nominal flight condition

For the following discussions the direction of the X_s -axis of the system of stability axes is defined relative to the aircraft, using the fixed and invariable system of the aircraft reference axes, see figure 7-1 and chapter 2.

The angle between the negative X_r -axis and the positive X_s -axis is α_0 . Note: This is not the α_0 meant in equation (4-26). This angle remains constant during the disturbed motion and varies only if one other initial, steady flight condition is chosen.

The total aerodynamic force acting on the aircraft in symmetric flight is divided in,

1. The thrust of the propulsive system, T_p
2. The remaining aerodynamic force on the aircraft, consisting of the components,
 - (a) lift, L , perpendicular to the direction of the undisturbed flow
 - (b) drag, D , parallel to the direction of the undisturbed flow

These three forces are depicted in figure 7-1. The angle between T_p and the negative X_r -axis is i_p . In the following it is assumed that i_p is independent of the flight condition and does not change during the disturbed motion, as is the case with α_0 . Furthermore, α_0 and i_p are assumed to be small, so,

$$\cos(\alpha_0 + i_p) \approx 1$$

$$\sin(\alpha_0 + i_p) \approx \alpha_0 + i_p$$

The total aerodynamic moment acting on the aircraft in steady flight is not divided in contributions explicitly assigned to thrust, lift and drag.

The components X and Z of the total aerodynamic force along the X_S -axis and the Z_S -axis of the system of stability axes can now be calculated. From figure 7-1 it follows,

$$\begin{aligned} X &= L \sin \alpha - D \cos \alpha + T_p \\ Z &= -L \cos \alpha - D \sin \alpha - T_p (\alpha_0 + i_p) \end{aligned}$$

In non-dimensional form, after division by $\frac{1}{2}\rho V^2 S$, it follows,

$$\begin{aligned} C_X &= C_L \sin \alpha - C_D \cos \alpha + T'_c \\ C_Z &= -C_L \cos \alpha - C_D \sin \alpha - T'_c (\alpha_0 + i_p) \end{aligned} \tag{7-1}$$

where α is now the change in angle of attack relative to the value in the equilibrium situation. In equation (7-1) is,

$$T'_c = \frac{T_p}{\frac{1}{2}\rho V^2 S} = \frac{2D^2}{S} T_c$$

In the initial, steady flight condition (the equilibrium situation) $\alpha = 0$, therefore,

$$\begin{aligned} C_{X_0} &= -C_D + T'_c \\ C_{Z_0} &= -C_L - T'_c (\alpha_0 + i_p) \end{aligned}$$

In addition, the following relations hold because of equations (4-36) and (4-35) and $\alpha = 0$,

$$\begin{aligned} C_{X_0} &= \frac{W}{\frac{1}{2}\rho V^2 S} \sin \gamma_0 \\ C_{Z_0} &= -\frac{W}{\frac{1}{2}\rho V^2 S} \cos \gamma_0 \end{aligned} \tag{7-2}$$

or,

$$C_{X_0} = -C_{Z_0} \tan \gamma_0 \approx +C_L \tan \gamma_0$$

If the steady, initial condition is one of horizontal steady flight, then according to equation (7-2),

$$C_{X_0} = 0$$

and, by consequence,

$$C_D = T'_c$$

For the calculation of the moments reference is made to previous sections of this chapter. For the equations of motion it is important that in the initial steady flight condition the moments are balanced and therefore,

$$C_{m_0} = 0$$

7-2 Derivatives with respect to airspeed

Experimentally obtained values of the stability derivatives C_{X_u} , C_{Z_u} and C_{m_u} are rare. Nearly all measurements of stability derivatives in flight are restricted to the motions at constant airspeed. Measurements in wind tunnels are also invariably made at constant speed. Due to these circumstances it is usually not possible to compare calculated with measured values of C_{X_u} , C_{Z_u} and C_{m_u} . The expressions for the derivatives with respect to airspeed to be discussed in the following, should be used with care, since they have been calibrated against experimental data to an insufficient degree.

7-2-1 Stability derivative C_{X_u}

According to table 4-3, this derivative is equal to,

$$C_{X_u} = \frac{1}{\frac{1}{2}\rho VS} \frac{\partial X}{\partial V}$$

Also,

$$X = C_X \frac{1}{2}\rho V^2 S$$

From this follows,

$$\frac{\partial X}{\partial V} = C_X \rho VS + \frac{\partial C_X}{\partial V} \frac{1}{2}\rho V^2 S$$

and, by consequence,

$$C_{X_u} = 2 C_X + \frac{\partial C_X}{\partial V} V \quad (7-3)$$

where,

$$\frac{\partial C_X}{\partial V} V = \frac{\partial C_X}{\partial \hat{u}}$$

See also equation (4-37). The partial derivative with respect to airspeed is determined for deviations from the steady, initial flight condition in airspeed only, i.e. at $\alpha = 0$. This means that in equation (7-3),

$$C_X = C_{X_0}$$

and,

$$C_{X_u} = 2 C_{X_0} + \frac{\partial C_X}{\partial V} V \quad (7-4)$$

The starting point for the determination of the partial derivative $\frac{\partial C_X}{\partial V}$ is the expression for C_X at $\alpha = 0$,

$$C_X = -C_D + T'_c$$

Differentiating this expression with respect to V yields,

$$\frac{\partial C_X}{\partial V} = \frac{\partial T'_c}{\partial V} - \frac{\partial C_D}{\partial V} \quad (7-5)$$

7-2-2 Stability derivative C_{Z_u}

In analogy with equation (7-4) it follows for the derivative C_{Z_u} ,

$$C_{Z_u} = 2 C_{Z_0} + \frac{\partial C_Z}{\partial V} V \quad (7-6)$$

In the steady, initial flight condition is,

$$C_Z = -C_L - T'_c (\alpha_0 + i_p)$$

After differentiating it follows, in analogy with equation (7-5),

$$\frac{\partial C_Z}{\partial V} = -\frac{\partial C_L}{\partial V} - \frac{\partial T'_c}{\partial V} (\alpha_0 + i_p) \quad (7-7)$$

7-2-3 Stability derivative C_{m_u}

Following equations (7-4) and (7-6), C_{m_u} is written as,

$$C_{m_u} = 2 C_{m_0} + \frac{\partial C_m}{\partial V} V$$

Since $C_m = 0$ in the steady, initial condition, C_{m_u} is reduced to,

$$C_{m_u} = \frac{\partial C_m}{\partial V} V \quad (7-8)$$

The derivatives $\frac{\partial C_D}{\partial V}$, $\frac{\partial C_L}{\partial V}$ and $\frac{\partial C_m}{\partial V}$ may differ from zero due to various causes,

1. The variation of Mach number with airspeed. Due to the effects of compressibility, the aerodynamic coefficients vary with airspeed at Mach numbers higher than 0.6 to 0.7.
2. The variation of the aircraft's aeroelastic deformation with airspeed, or rather with dynamic pressure. This effect is not further considered here.
3. The variation of the Reynolds number with airspeed. This influence is entirely neglected for the small variations of airspeed considered here.
4. For a propeller-driven aircraft the contribution to the coefficients C_L , C_D and C_m made by those parts of the wing and the tailplane submerged in the slipstream, varies with airspeed via the thrust coefficient T'_c . For $\frac{\partial C_D}{\partial V}$ and $\frac{\partial C_L}{\partial V}$ the influences of compressibility and slipstream effects are taken separately. The same applies to $\frac{\partial C_m}{\partial V}$. The partial derivatives with respect to V then are,

$$\begin{aligned}\frac{\partial C_D}{\partial V} &= \frac{\partial C_D}{\partial M} \frac{\partial M}{\partial V} + \frac{\partial C_D}{\partial T'_c} \frac{\partial T'_c}{\partial V} \\ \frac{\partial C_L}{\partial V} &= \frac{\partial C_L}{\partial M} \frac{\partial M}{\partial V} + \frac{\partial C_L}{\partial T'_c} \frac{\partial T'_c}{\partial V} \\ \frac{\partial C_m}{\partial V} &= \frac{\partial C_m}{\partial M} \frac{\partial M}{\partial V} + \frac{\partial C_m}{\partial T'_c} \frac{\partial T'_c}{\partial V}\end{aligned}$$

Expressions (7-4), (7-6) and (7-8) can now be written as,

$$C_{X_u} = 2 C_{X_0} + \left(1 - \frac{\partial C_D}{\partial T'_c}\right) \frac{dT'_c}{dV} V - \frac{\partial C_D}{\partial M} M \quad (7-9)$$

$$C_{Z_u} = 2 C_{Z_0} - \left\{(\alpha_0 + i_p) + \frac{\partial C_L}{\partial T'_c}\right\} \frac{dT'_c}{dV} V - \frac{\partial C_L}{\partial M} M \quad (7-10)$$

$$C_{m_u} = \frac{\partial C_m}{\partial T'_c} \frac{dT'_c}{dV} V + \frac{\partial C_m}{\partial M} M \quad (7-11)$$

In equations (7-9), (7-10) and (7-11) the partial derivatives with respect to Mach number are not further considered here. The effects of compressibility, expressed here through the presence of the partial derivatives $\frac{\partial C_D}{\partial M}$, $\frac{\partial C_L}{\partial M}$ and $\frac{\partial C_m}{\partial M}$, are not the subject of this book. The slipstream effect, expressed through $\frac{\partial C_D}{\partial T'_c}$, $\frac{\partial C_L}{\partial T'_c}$ and the various contributions to $\frac{\partial C_m}{\partial T'_c}$, are not discussed in this book either.

The derivative $\frac{\partial T'_c}{\partial V}$ is now briefly discussed. The basic assumption is always that during the disturbed aircraft motions to be studied, the power setting of the engine(s), i.e. the throttle position and the setting of any other possible control lever, remains unchanged. Another assumption to be made when determining the variation of T'_c is that changes in airspeed always occur in a quasi-steady manner, i.e. so slowly that T'_c varies with airspeed just as in a series of steady flight conditions. If these assumptions are met, $\frac{\partial T'_c}{\partial V}$ can be calculated in a fairly simple manner. In the following $\frac{\partial T'_c}{\partial V}$ is derived for various types of propulsive systems.

1. Jet turbines and rocket motors

In studies on dynamic stability characteristics the usual assumption is that the thrust of these engines is independent of airspeed at constant throttle setting. This means,

$$T_p = T'_c \frac{1}{2} \rho V^2 S = \text{constant}$$

This results in,

$$\frac{dT'_c}{dV} = -\frac{2T'_c}{V}$$

At supersonic speeds in particular the thrust of a jet turbine does vary with airspeed. The correct value $\frac{dT'_c}{dV}$ then has to be obtained from more detailed calculations or from measurements.

2. Piston or turbine engines driving constant speed propellers

In this case, again at constant power setting, the power produced by the engine is approximately independent of airspeed. If the propeller efficiency is also assumed to be constant for relatively small variations in airspeed, then,

$$T_p V = \text{constant}$$

or,

$$T'_c V^3 = \text{constant}$$

This results in,

$$\frac{dT'_c}{dV} = -3 \frac{T'_c}{V}$$

3. Gliding flight

Finally, it should be noted that for any propulsive system in gliding flight ($T'_c = 0$) the following relation holds,

$$\frac{dT'_c}{dV} = 0$$

The foregoing expressions for $\frac{dT'_c}{dV}$ may be summarized as follows,

$$\frac{dT'_c}{dV} = -k \frac{T'_c}{V}$$

where k is,

1. in gliding flight, $k = 0$
2. jet turbines at subsonic speeds, rocket motors, $k = 2$
3. piston and turbine engines driving constant speed propellers, $k = 3$

As derived in the previous subsection,

$$C_{X_0} = -C_D + T'_c$$

$$C_{Z_0} = -C_L - T'_c (\alpha_0 + i_p)$$

Using these relations, equations (7-9), (7-10) and (7-11) can finally be written as,

$$C_{X_u} = -2 C_D + T'_c \left\{ 2 - k \cdot \left(1 - \frac{\partial C_D}{\partial T'_c} \right) \right\} - \frac{\partial C_D}{\partial M} M \quad (7-12)$$

$$C_{Z_u} = -2 C_L + T'_c \left\{ (-2 + k) (\alpha_0 + i_p) + k \cdot \frac{\partial C_L}{\partial T'_c} \right\} - \frac{\partial C_L}{\partial M} M \quad (7-13)$$

$$C_{m_u} = -k \cdot T'_c \cdot \frac{\partial C_m}{\partial T'_c} + \frac{\partial C_m}{\partial M} M \quad (7-14)$$

If $C_{X_0} \approx C_L \tan \gamma_0$ is used, equation (7-12) becomes,

$$C_{X_u} = 2 C_L \tan \gamma_0 - k \cdot T'_c \left(1 - \frac{\partial C_D}{\partial T'_c} \right) - \frac{\partial C_D}{\partial M} M \quad (7-15)$$

A few specific cases are,

1. Gliding flight at subsonic speed

Or, with $k = 0$, and,

$$\frac{\partial C_D}{\partial M} = \frac{\partial C_L}{\partial M} = \frac{\partial C_m}{\partial M} = 0$$

yields,

$$\begin{aligned} C_{X_u} &= 2 C_L \tan \gamma_0 = -2 C_D \\ C_{Z_u} &= -2 C_L \\ C_{m_u} &= 0 \end{aligned}$$

2. Level flight at subsonic speed for a jet- or rocket-propelled aircraft

Or, with $\gamma_0 = 0$, $k = 2$, $T'_c = C_D$ and,

$$\frac{\partial C_D}{\partial M} = \frac{\partial C_L}{\partial M} = \frac{\partial C_m}{\partial M} = 0$$

yields,

$$\begin{aligned} C_{X_u} &= -2 C_D \\ C_{Z_u} &= -2 C_L \\ C_{m_u} &= -2 C_D \frac{\partial C_m}{\partial T'_c} \end{aligned}$$

3. Level flight at subsonic speed for a propeller-driven aircraft having constant speed propellers

Or, with $\gamma_0 = 0$, $k = 3$, $T'_c = C_D$ and,

$$\frac{\partial C_D}{\partial M} = \frac{\partial C_L}{\partial M} = \frac{\partial C_m}{\partial M} = 0$$

yields,

$$\begin{aligned} C_{X_u} &= -3 C_D \left(1 - \frac{\partial C_D}{\partial T'_c} \right) \\ C_{Z_u} &= -2 C_L + C_D \left\{ -(\alpha_0 + i_p) + 3 \frac{\partial C_D}{\partial T'_c} \right\} \\ C_{m_u} &= -3 C_D \frac{\partial C_m}{\partial T'_c} \end{aligned}$$

7-3 Derivatives with respect to angle of attack

A change in angle of attack only is obtained by varying the speed w along the Z_S -axis. A pure α -motion is thus seen to be a steady motion where the aircraft performs a translation along the Z_S -axis (plunging motion). The stability derivatives C_{X_α} , C_{Z_α} and C_{m_α} pertaining to this type of motion may be obtained in a relatively simple way from wind tunnel measurements on a model of the aircraft. C_{X_α} and C_{Z_α} are derived from a measured or calculated polar curve corresponding to the specific aircraft configuration, whereas C_{m_α} follows from a measured or calculated moment curve $C_m - \alpha$. A discussion of each of the three derivatives is given below.

7-3-1 Stability derivative C_{X_α}

According to table 4-3, this derivative is equal to,

$$C_{X_\alpha} = \frac{1}{\frac{1}{2}\rho VS} \frac{\partial X}{\partial w} = \frac{\partial C_X}{\partial \alpha}$$

From equation (7-1) follows that,

$$C_X = C_L \sin \alpha - C_D \cos \alpha + T'_c$$

Taking the derivative with respect to α , leaving T'_c constant, results in,

$$C_{X_\alpha} = C_L \cos \alpha + C_{L_\alpha} \sin \alpha + C_D \sin \alpha - C_{D_\alpha} \cos \alpha$$

In the steady, initial condition $\alpha = 0$, leading to,

$$C_{X_\alpha} = C_L - C_{D_\alpha} \quad (7-16)$$

if C_X is expressed using C_N and C_T , C_{X_α} can be written as,

$$C_{X_\alpha} = -C_{T_\alpha} \cos \alpha_0 - C_{N_\alpha} \sin \alpha_0$$

If a parabolic polar curve is assumed, then,

$$C_D = C_{D_0} + \frac{C_L^2}{\pi Ae}$$

where C_{D_0} is the drag coefficient at $C_L = 0$. Then, C_{D_α} is,

$$C_{D_\alpha} = 2 \frac{C_{L_\alpha}}{\pi Ae} C_L$$

and C_{X_α} can be written as,

$$C_{X_\alpha} = C_L \left(1 - \frac{2C_{L_\alpha}}{\pi A e} \right)$$

Contrary to most stability derivatives, C_{X_α} is normally positive.

Using linearized potential flow theory (panel methods), absolute values of C_X as a function of α have been calculated for the Cessna Ce550 ‘Citation II’, see figure 7-3. The definition of the aircraft parts ‘wing’, ‘horizontal stabilizer’, ‘pylons’, ‘fuselage’, ‘vertical fin’ and ‘nacelles’ is given in figure 7-2. The main contribution to C_X is from the wing (induced drag).

7-3-2 Stability derivative C_{Z_α}

According to table 4-3, this derivative is equal to,

$$C_{Z_\alpha} = \frac{1}{\frac{1}{2}\rho VS} \frac{\partial Z}{\partial w} = \frac{\partial C_Z}{\partial \alpha}$$

C_Z has been written in equation (7-1) as,

$$C_Z = -C_L \cos \alpha - C_D \sin \alpha - T'_c (\alpha_0 + i_p)$$

This results in C_{Z_α} ,

$$C_{Z_\alpha} = C_L \sin \alpha - C_{L_\alpha} \cos \alpha - C_D \cos \alpha - C_{D_\alpha} \sin \alpha$$

which reduces for $\alpha = 0$ to,

$$C_{Z_\alpha} = -C_{L_\alpha} - C_D$$

As normally $C_D \ll C_{L_\alpha}$, a simplified expression for C_{Z_α} is,

$$C_{Z_\alpha} \approx -C_{L_\alpha}$$

The dominant contribution to C_{Z_α} is, of course, provided by the wing. But in some cases the contribution made by the horizontal tailplane is not negligible. Then it may be practical to express C_{Z_α} ,

$$C_{Z_\alpha} = -C_{N_{w_\alpha}} - C_{N_{h_\alpha}} \left(1 - \frac{d\varepsilon}{d\alpha} \right) \left(\frac{V_h}{V} \right)^2 \frac{S_h}{S} \quad (7-17)$$

Data for a quantitative determination of C_{Z_α} using equation (7-17) can be found in various places in the literature, see references [76] and [9].

Using linearized potential flow theory (panel methods), absolute values of C_Z as a function of α have been calculated for the Cessna Ce550 ‘Citation II’, see figure 7-4. The definition of the aircraft parts ‘wing’, ‘horizontal stabilizer’, ‘pylons’, ‘fuselage’, ‘vertical fin’ and ‘nacelles’ is given in figure 7-2. The main contribution to C_Z is from the wing.

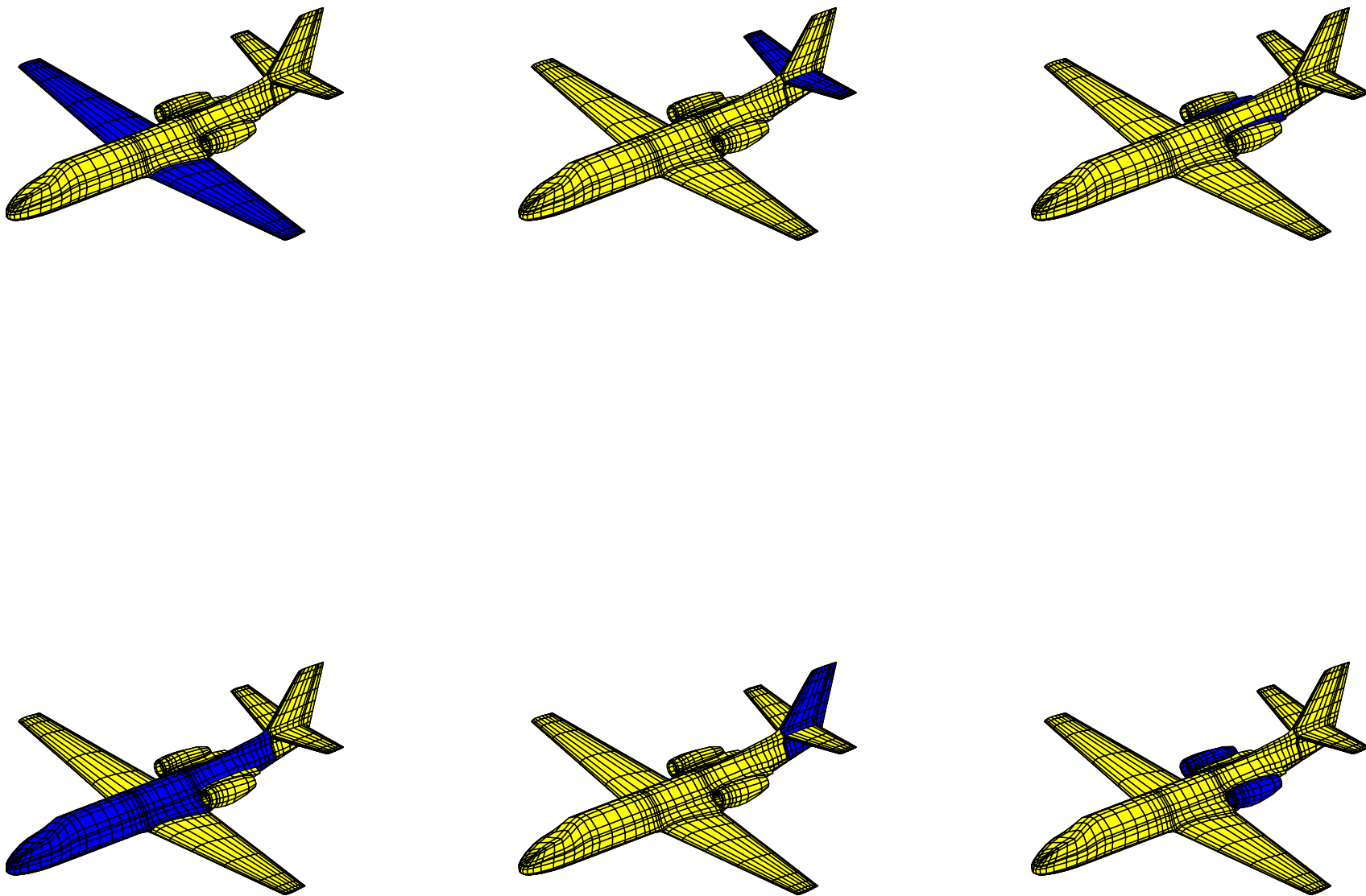


Figure 7-2: The definition of aircraft parts ‘wing’, ‘horizontal stabilizer’, ‘pylon’, ‘nacelles’, ‘vertical fin’ and ‘fuselage’ for the Cessna Ce550 ‘Citation II’ model (starting from the left top figure, in clockwise direction)

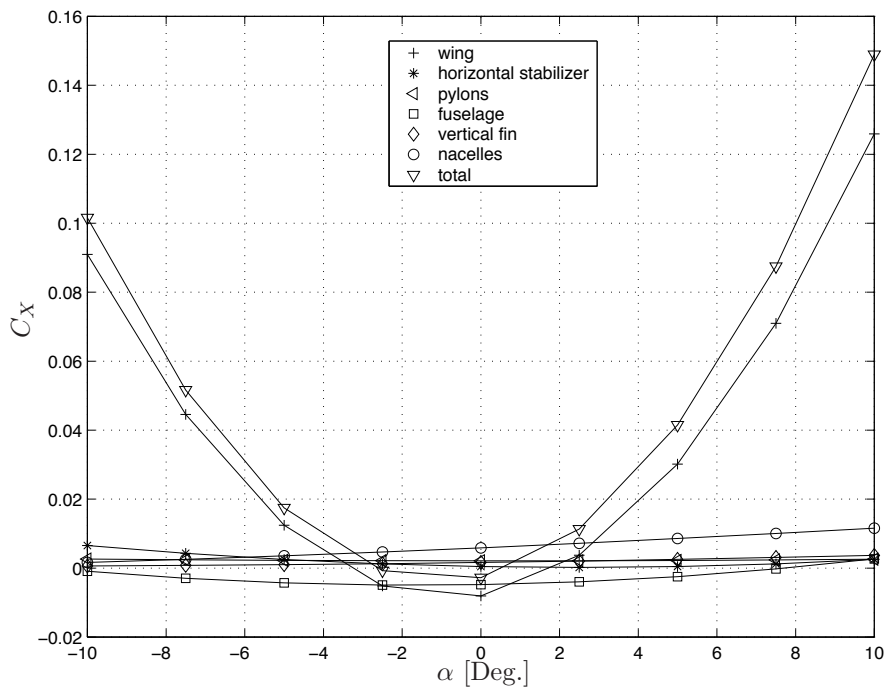


Figure 7-3: Calculated contributions of various aircraft parts to the force curve C_X versus α for the Cessna Ce550 'Citation II'

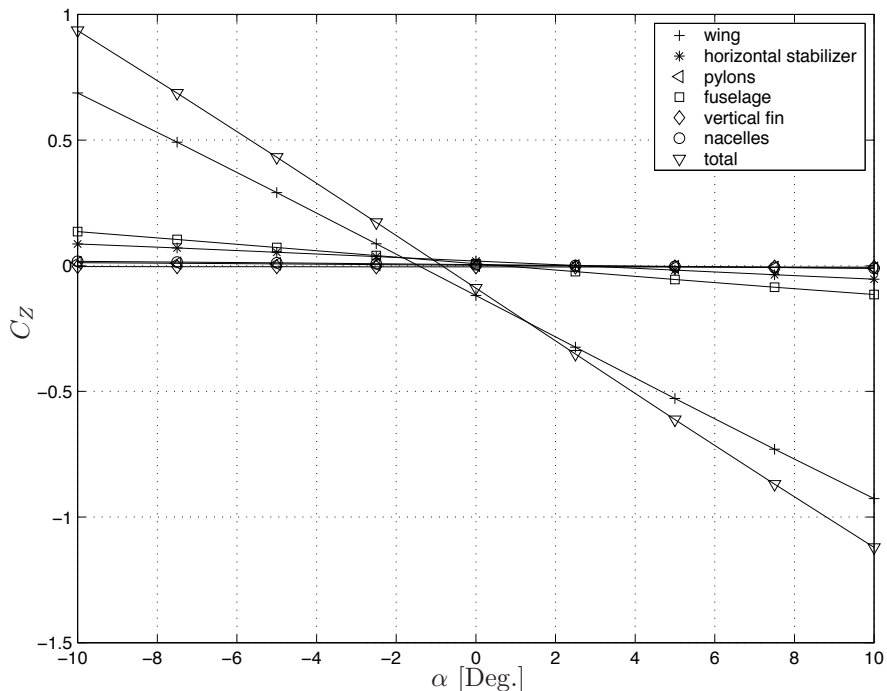


Figure 7-4: Calculated contributions of various aircraft parts to the force curve C_Z versus α for the Cessna Ce550 'Citation II'

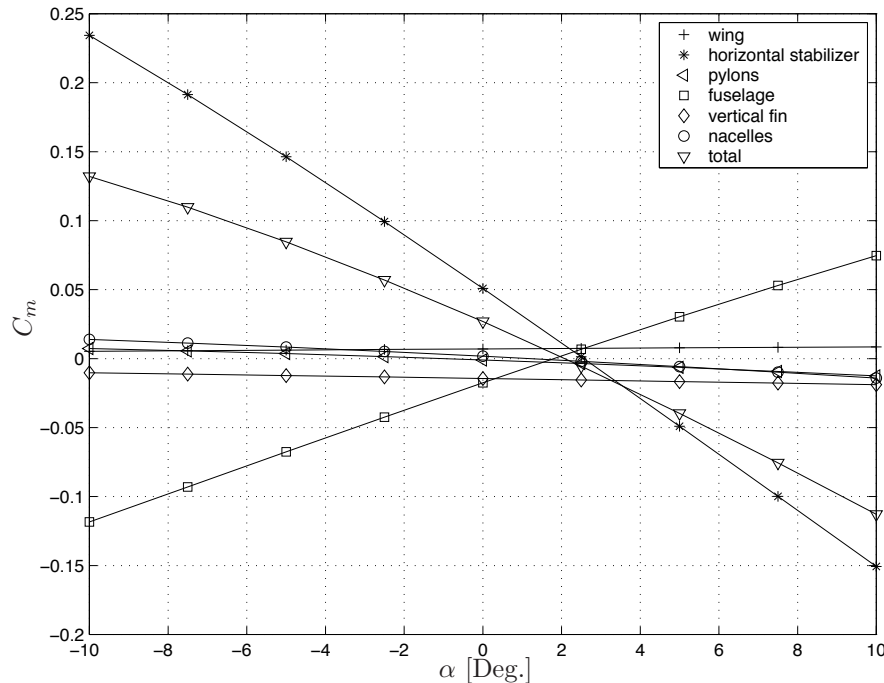


Figure 7-5: Calculated contributions of various aircraft parts to the moment curve C_m versus α for the Cessna Ce550 ‘Citation II’

7-3-3 Stability derivative C_{m_α}

According to table 4-3, this derivative is equal to,

$$C_{m_\alpha} = \frac{1}{\frac{1}{2}\rho V S \bar{c}} \frac{\partial M}{\partial w} = \frac{\partial C_m}{\partial \alpha}$$

In this chapter the simplified case is considered where the contributions of the tangential forces to C_m are neglected and the contributions of the thrust and slipstream effects are also not considered. It was found in chapter 9 for C_{m_α} ,

$$C_{m_\alpha} = C_{N_{w_\alpha}} \frac{x_{c.g.} - x_w}{\bar{c}} - C_{N_{h_\alpha}} \left(1 - \frac{d\varepsilon}{d\alpha}\right) \left(\frac{V_h}{V}\right)^2 \frac{S_h l_h}{S \bar{c}} \quad (7-18)$$

More general. C_{m_α} is the slope of the moment curve $C_m = C_m(\alpha)$ at the respective angle of attack at which according to section 7-1, $C_{m_0} = 0$. A calculation of C_{m_α} is possible using the references of chapter 9.

Using linearized potential flow theory (panel methods), absolute values of C_m as a function of α have been calculated for the Cessna Ce550 ‘Citation II’, see figure 7-5. The definition of the aircraft parts ‘wing’, ‘horizontal stabilizer’, ‘pylons’, ‘fuselage’, ‘vertical fin’ and ‘nacelles’ is given in figure 7-2. The main contributions to C_m are from the fuselage (destabilizing) and horizontal stabilizer (stabilizing).

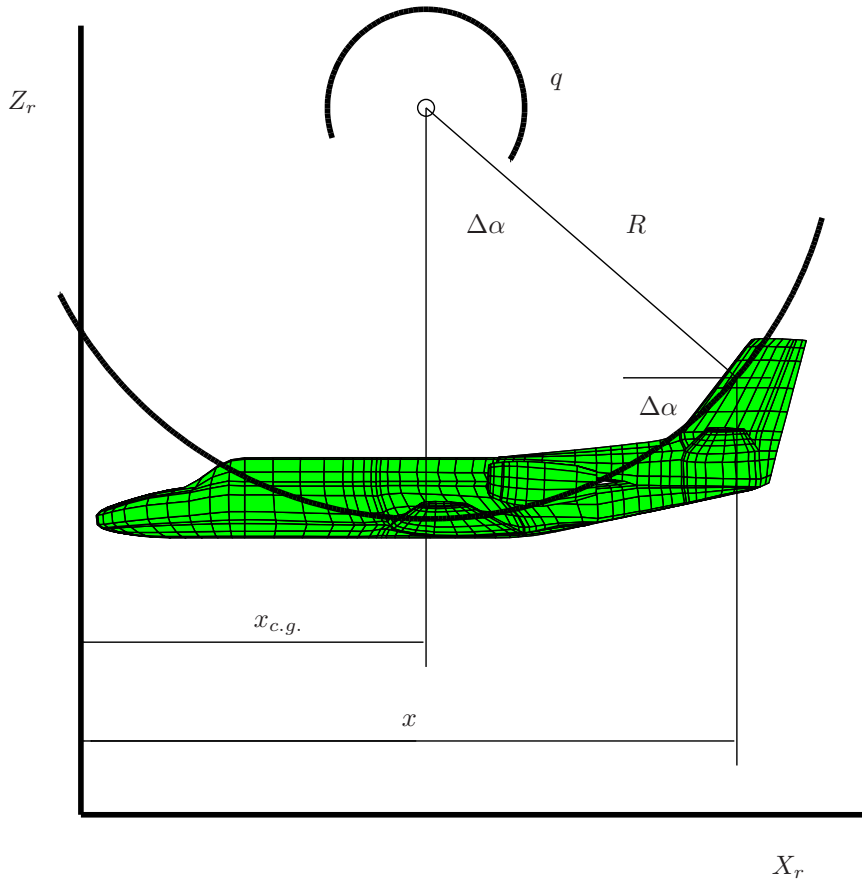


Figure 7-6: The pure q -motion, with $\Delta\alpha = \frac{x - x_{c.g.}}{R} = \frac{x - x_{c.g.}}{\bar{c}} \cdot \frac{q\bar{c}}{V}$

7-4 Derivatives with respect to pitching velocity

Before discussing the derivatives C_{X_q} , C_{Z_q} and C_{m_q} , the angular motion under consideration will be studied more closely. During the turning, symmetric motion, indicated here as q -motion, the center of rotation lies on the top axis through the aircraft's center of gravity, see figure 7-6. The distance R to the c.g. is,

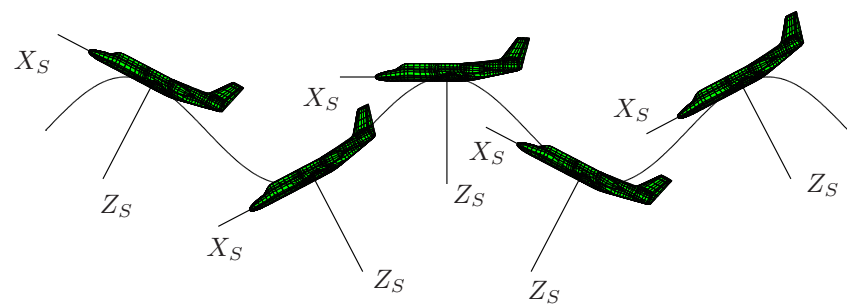
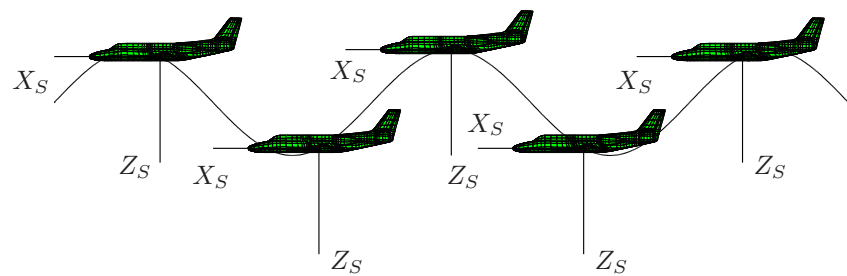
$$R = \frac{V}{q}$$

At a positive pitching velocity the center of rotation lies on the negative Z_S -axis, i.e. above the aircraft.

In all points of the aircraft, with the exception of the c.g. and all other points on the Z_S -axis, the geometric angle of attack is proportional to the angular velocity and to the distance in X_S -direction to the center of gravity,

$$\Delta\alpha = \frac{x - x_{c.g.}}{R} = \frac{x - x_{c.g.}}{\bar{c}} \cdot \frac{q\bar{c}}{V} \quad (7-19)$$

See also figure 7-6.

Figure 7-7: Harmonic q -motion, $\alpha = \text{constant}$, $\theta = \gamma$ Figure 7-8: Harmonic α -motion, $q = 0$

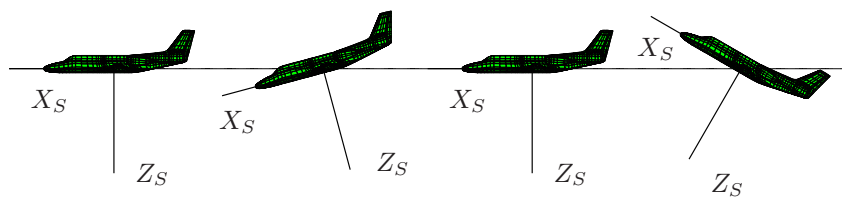


Figure 7-9: Combined harmonic q - and α -motion, $q = \dot{\alpha}$, $\gamma = \text{constant}$

The magnitude of the local airspeed varies (in principle) also with the angular velocity. This is because the local velocity in a given point varies proportional with the distance of that point to the center of rotation. Only in points at distance R of the center of rotation, i.e. also in the c.g., the magnitude of the local velocity does not vary with the rate of pitch. The aircraft's c.g. is the only point where during this q -motion neither the magnitude of the velocity, nor the direction, i.e. the geometric angle of attack, vary. Changes in the magnitude of the local airspeed and the geometric angle of attack at the aircraft's c.g. are described as the u -motion and the α - or plunging-motion respectively.

As far as the airflow at the center of gravity is concerned, the q -motion causes only a curvature of the streamlines. If the angular velocity during a q -motion is not constant, but varies harmonically with time, the aircraft describes due to this q -motion a sinusoidal trajectory, as indicated in figure 7-7. The most characteristic feature of this trajectory is, that the angle of attack at the aircraft's c.g. remains constant during this motion, i.e. $\dot{\alpha} = 0$. The center of gravity moves along an undulating trajectory, such that,

$$\dot{\theta} = q = \dot{\alpha} + \dot{\gamma} = \dot{\gamma}$$

Both the angle of pitch and the flight path angle will vary harmonically. In figure 7-8 the case for harmonic plunge is presented, i.e. α varies harmonically, however, now $q = 0$. An entirely different motion, to be distinguished very clearly from the q -motion, results if the center of rotation lies in the aircraft's c.g., see figure 7-9.

Then the angle of attack varies also in the center of gravity and,

$$\dot{\theta} = q = \dot{\alpha} \quad (7-20)$$

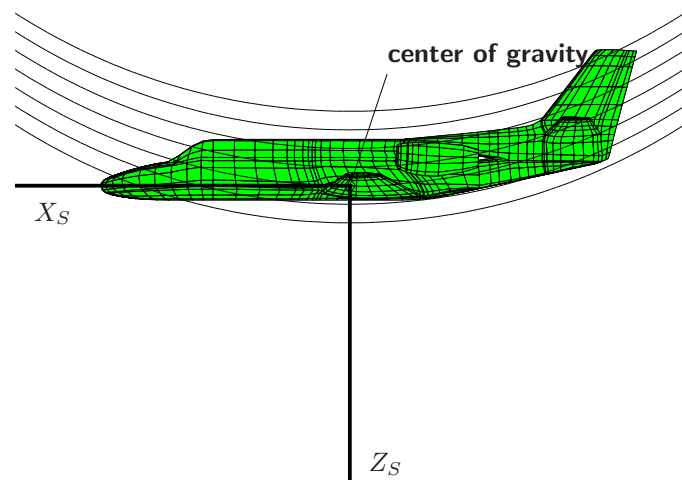
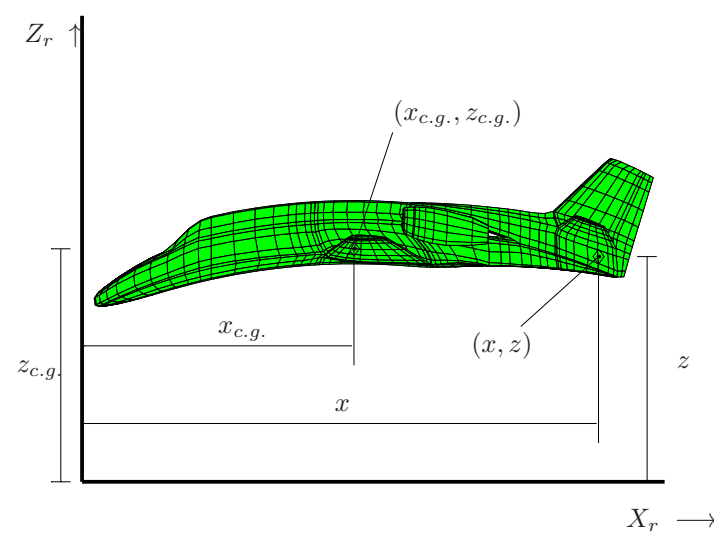


Figure 7-10: Aircraft in a curved flow field

Figure 7-11: Equivalent curved aircraft in a straight flow field with aircraft frame of reference, F_r

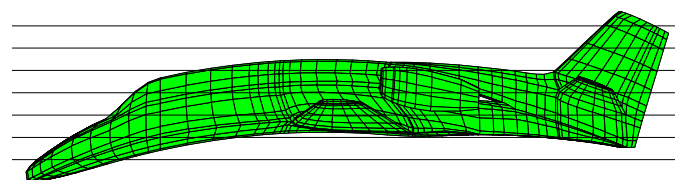


Figure 7-12: Equivalent curved aircraft in a straight flow field

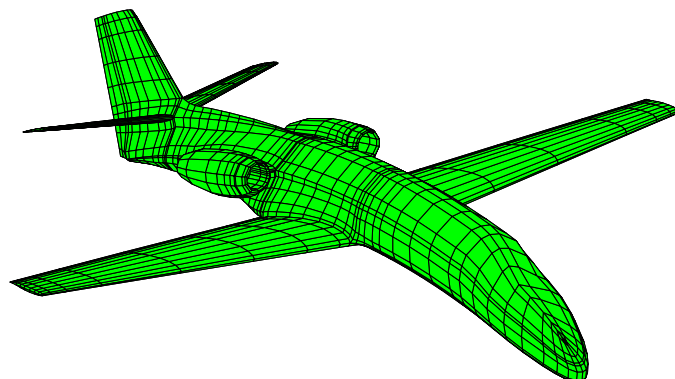


Figure 7-13: Equivalent curved aircraft in a straight flow field, 3-dimensional view

and, by consequence,

$$\dot{\gamma} = \dot{\theta} - \dot{\alpha} = 0 \quad (7-21)$$

According to equation (7-21) the center of gravity moves along a straight line, if the aircraft rotates while the c.g. is the center of rotation. This motion may be considered a superposition of a q -motion as defined above and a variable α -motion, such that the condition (7-20) is satisfied.

This q -motion is here the subject of discussion, the influence on the aerodynamic forces and moments due to an acceleration along the top axis during a non-steady α -motion is discussed in the next section.

The variation of the magnitude of the local airspeed with the distance to the center of rotation during the q -motion is usually neglected because of the small dimensions of the aircraft in the Z_S -direction if compared with common values of R . The only effect of the rotation is then a variation of the geometric angle of attack in the X_S -direction, expressed by equation (7-19), see figure 7-10.

A field of flow equivalent to that of the aircraft in curved flow can be obtained by placing a suitable curved aircraft in a field of parallel flow, see figures 7-11, 7-12 and 7-13.

The curvature of the aircraft or the wind tunnel model must be such that,

$$\Delta\alpha = -\frac{dz}{dx} = +\frac{x - x_{c.g.}}{\bar{c}} \frac{q\bar{c}}{V}$$

see equation (7-19), or,

$$\frac{z - z_{c.g.}}{\bar{c}} = -\frac{1}{2} \left(\frac{x - x_{c.g.}}{\bar{c}} \right)^2 \frac{q\bar{c}}{V}$$

The curvature is parabolic in the X_S -direction and proportional to $\frac{q\bar{c}}{V}$. For theoretical calculations it may be advantageous to use the curved aircraft in parallel flow. If, however, the stability derivatives would have to be measured using a curved model in parallel flow, it would be necessary to use a separate model for each value of $\frac{q\bar{c}}{V}$.

The changes in the forces X and Z and in the moment M caused by the q -motion are discussed in the following.

The change in X , expressed by the derivative C_{X_q} ,

$$C_{X_q} = \frac{1}{\frac{1}{2}\rho VS\bar{c}} \frac{\partial X}{\partial q} = \frac{\partial C_X}{\partial \frac{q\bar{c}}{V}}$$

is always neglected. The assumption thus is,

$$C_{X_q} = 0$$

Using linearized potential flow theory (panel methods), absolute values of C_X as a function of $\frac{q\bar{c}}{V}$ have been calculated for the Cessna Ce550 ‘Citation II’, see figure 7-14. The definition of the aircraft parts ‘wing’, ‘horizontal stabilizer’, ‘pylons’, ‘fuselage’, ‘vertical fin’ and ‘nacelles’ is given

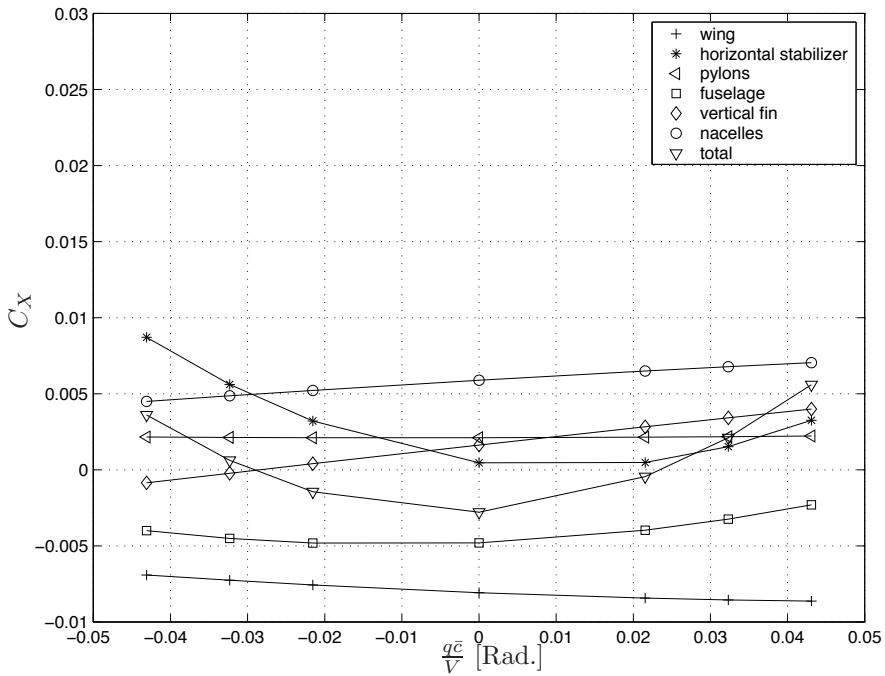


Figure 7-14: Calculated contributions of various aircraft parts to the force curve C_X versus $\frac{q\bar{c}}{V}$ for the Cessna Ce550 'Citation II'

in figure 7-2. All defined aircraft parts have a negligible contribution to C_X (as compared to the force curve C_X versus α , see figure 7-3).

The two remaining derivatives are C_{Z_q} and C_{m_q} ,

$$C_{Z_q} = \frac{1}{\frac{1}{2}\rho VS\bar{c}} \frac{\partial Z}{\partial q} = \frac{\partial C_Z}{\partial \frac{q\bar{c}}{V}}$$

$$C_{m_q} = \frac{1}{\frac{1}{2}\rho VS\bar{c}^2} \frac{\partial M}{\partial q} = \frac{\partial C_m}{\partial \frac{q\bar{c}}{V}}$$

Of these two derivatives C_{m_q} is the most important. For an aircraft having a horizontal tailplane, the largest contribution to C_{m_q} is provided by this tailplane. The change in wing lift caused by the angular velocity, i.e. by the curvature of the flow field, is small. Therefore, no change in downwash, as a reaction to a change in wing lift, is accounted for either. The contribution from the tailplane is calculated as follows.

According to equation (7-19) the change in angle of attack of the horizontal tailplane due to the rotation is,

$$\Delta\alpha_h = \frac{x_h - x_{c.g.}}{\bar{c}} \frac{q\bar{c}}{V} \approx \frac{l_h}{\bar{c}} \frac{q\bar{c}}{V}$$

This change in angle of attack causes a normal force at the tailplane,

$$\Delta C_{N_h} = C_{N_{h\alpha}} \left(\frac{V_h}{V} \right)^2 \frac{S_h}{S} \Delta\alpha_h$$

and this generates a moment about the aircraft's c.g.,

$$\Delta C_m = -C_{N_{h\alpha}} \Delta\alpha_h \left(\frac{V_h}{V}\right)^2 \frac{S_h l_h}{S\bar{c}} = -C_{N_{h\alpha}} \left(\frac{V_h}{V}\right)^2 \frac{S_h l_h^2}{S\bar{c}^2} \frac{q\bar{c}}{V}$$

As a consequence the contribution of the horizontal tailplane to C_{m_q} is,

$$(C_{m_q})_h = -C_{N_{h\alpha}} \left(\frac{V_h}{V}\right)^2 \frac{S_h l_h^2}{S\bar{c}^2}$$

and the contribution to C_{Z_q} is,

$$(C_{Z_q})_h = -C_{N_{h\alpha}} \left(\frac{V_h}{V}\right)^2 \frac{S_h l_h}{S\bar{c}}$$

A rough estimate of C_{Z_q} for the complete aircraft is sometimes taken as,

$$C_{Z_q} = 2 (C_{Z_q})_h = -2 C_{N_{h\alpha}} \left(\frac{V_h}{V}\right)^2 \frac{S_h l_h}{S\bar{c}}$$

For aircraft having a straight, slender wing C_{m_q} of the entire aircraft is usually approximated by multiplying the contribution of the tailplane with a factor 1.1 to 1.2, in order to account for the influence of the wing. For these conventional aircraft C_{m_q} can be expressed by,

$$C_{m_q} = -(1.1) C_{N_{h\alpha}} \left(\frac{V_h}{V}\right)^2 \frac{S_h l_h^2}{S\bar{c}^2}$$

Finally, a practical remark should be made. Often, quantitative data for the determination of C_{Z_q} and C_{m_q} are taken from publications of the American National Aeronautics and Space Administration (NASA). It is of interest to realize that NASA, and some other organizations as well, commonly relate the stability derivatives C_{Z_q} and C_{m_q} to $\frac{q\bar{c}}{V}$ rather than $\frac{q\bar{c}}{V}$.

In contrast to a u - or α -motion, the q -motion changes with a shift in the c.g. position. This can be seen as follows. In the new c.g. the change in angle of attack due to a rotation about the new center of rotation is, of course, again zero. This change in angle of attack at the new c.g. position $c.g.2$, $\Delta\alpha_{c.g.2}$ (where $\Delta\alpha_{c.g.1} = 0$), is the sum of a contribution from a rotation about the old c.g. ($c.g.1$) and a change in angle of attack due to an α -motion along the Z_S -axis. From this consideration C_{m_q} can be calculated in a straightforward manner.

In table 7-2 the expressions for the variations of C_{Z_q} and C_{m_q} with the c.g. position are given, based on the above discussion.

Using linearized potential flow theory (panel methods), absolute values of C_Z and C_m as a function of $\frac{q\bar{c}}{V}$ have been calculated for the Cessna Ce550 'Citation II', see figure 7-15 and figure 7-16. The definition of the aircraft parts 'wing', 'horizontal stabilizer', 'pylons', 'fuselage', 'vertical fin' and 'nacelles' is given in figure 7-2. The main contributions to C_Z are from the wing and the horizontal stabilizer. The main contribution to C_m is from the horizontal stabilizer. Note that both the slope of $C_Z - \frac{q\bar{c}}{V}$ and $C_m - \frac{q\bar{c}}{V}$ are representative for respectively the stability derivatives C_{Z_q} and C_{m_q} . E.g. from figure 7-15 it is obvious that C_{Z_q} indeed is approximately,

$$C_{Z_q} = 2 (C_{Z_q})_h$$

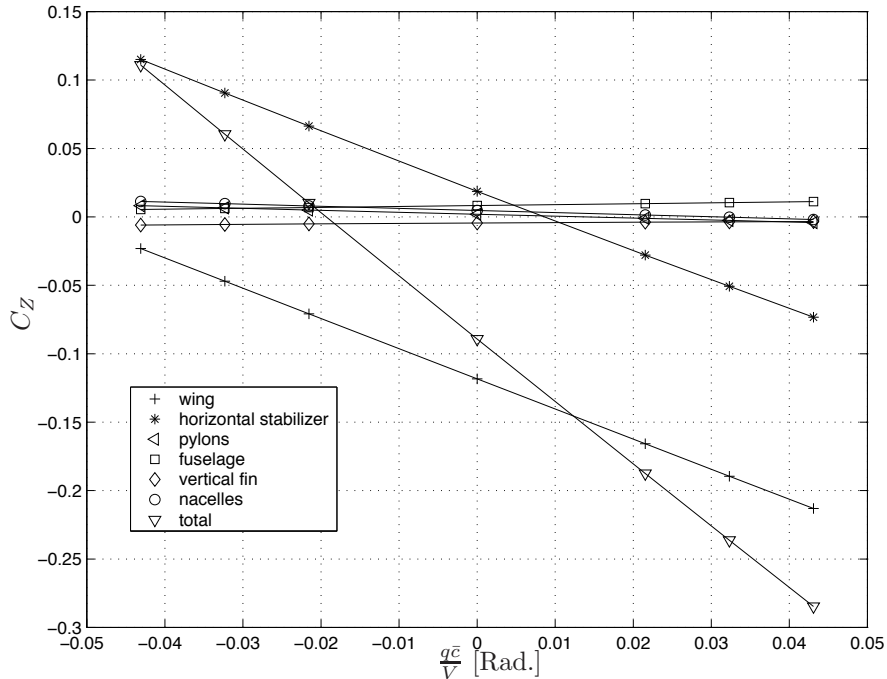


Figure 7-15: Calculated contributions of various aircraft parts to the force curve C_Z versus $\frac{q\bar{c}}{V}$ [Rad.] for the Cessna Ce550 ‘Citation II’

Furthermore, from figure 7-16 it also holds that C_{m_q} is indeed approximately,

$$C_{m_q} = 1.1 \left(C_{Z_q} \right)_h \frac{l_h}{\bar{c}}$$

7-5 Derivatives with respect to the acceleration along the top axis

If the components of airspeed u or w or the rate of pitch q of an aircraft experience a sudden change, a certain time interval passes before the pressure distribution over the entire aircraft has adjusted to the new flow condition. Usually, changes in the airspeed, i.e. in the component u , occur so slowly that this delayed adjustment is not noticeable.

Changes in u are, therefore, always assumed to occur in a quasi-steady fashion. On the other hand, changes in angle of attack, i.e. in the speed component w along the Z_S -axis, may occur much more quickly. Such changes are discussed in the following.

In reference [39] Cowley and Glauert were the first to point to the fact that an acceleration \dot{w} of the aircraft in the direction of the top axis has a non-negligible influence on the longitudinal moment C_m . This effect has an important influence on the damping of the symmetric motions. Following Cowley and Glauert, this effect is usually expressed through a stability derivative C_{m_α} . In order to account for the influence of the c.g. on this derivative C_{m_α} , it is necessary in principle to know as well the derivative C_{Z_α} which is in itself quite important.

As described earlier the relation between the aerodynamic coefficient C_m and the component of the motion α may be expressed in a Taylor series,

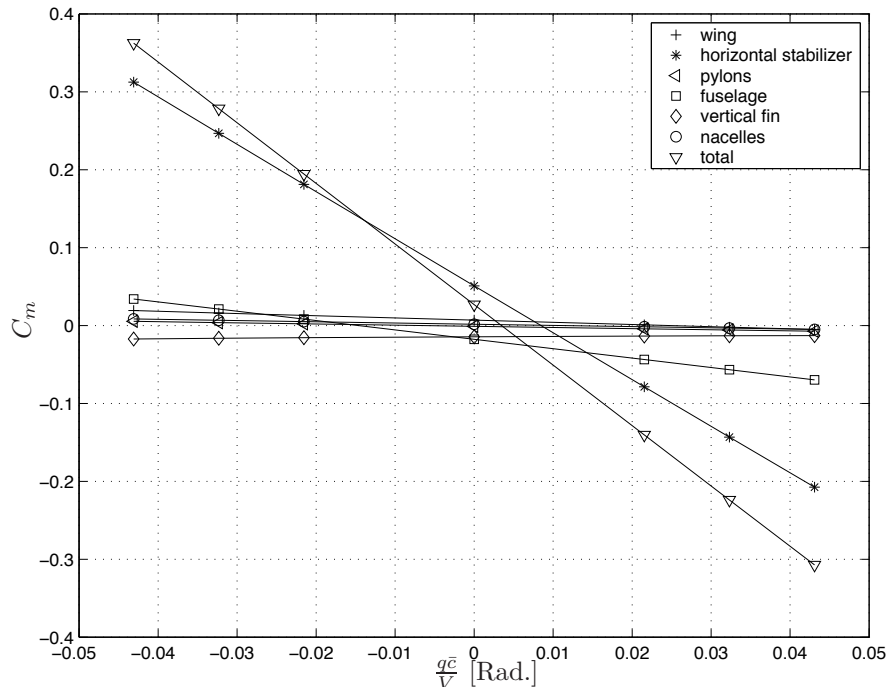


Figure 7-16: Calculated contributions of various aircraft parts to the moment curve C_m versus $\frac{\dot{q}\bar{c}}{V}$ for the Cessna Ce550 'Citation II'

$$\begin{aligned} \Delta C_m = & \frac{\partial C_m}{\partial \alpha} \Delta \alpha + \frac{\partial C_m}{\partial \frac{\dot{q}\bar{c}}{V}} \frac{\dot{q}\bar{c}}{V} + \frac{1}{2!} \left\{ \frac{\partial^2 C_m}{\partial \alpha^2} (\Delta \alpha)^2 + 2 \frac{\partial^2 C_m}{\partial \alpha \partial \frac{\dot{q}\bar{c}}{V}} \Delta \alpha \frac{\dot{q}\bar{c}}{V} + \right. \\ & \left. \frac{\partial^2 C_m}{\partial (\frac{\dot{q}\bar{c}}{V})^2} \left(\frac{\dot{q}\bar{c}}{V} \right)^2 \right\} + \frac{1}{3!} \{ \dots \} + \dots \dots \end{aligned} \quad (7-22)$$

In principle, the derivatives with respect to $\frac{\dot{q}\bar{c}^2}{V^2}$, $\frac{\dot{q}\bar{c}^3}{V^3}$, etcetera, could also be included in this series expansion. Experimental evidence shows, however, that the changes in angle of attack occur slowly enough to neglect any influences of the higher time derivatives than $\dot{\alpha}$. As usual, in the series (7-22) only the linear terms are maintained under the assumption that the values of $\Delta \alpha$ and $\frac{\dot{q}\bar{c}}{V}$ remain sufficiently small.

The change in the moment coefficient, ΔC_m , can then be written as,

$$\Delta C_m = \frac{\partial C_m}{\partial \alpha} \Delta \alpha + \frac{\partial C_m}{\partial \frac{\dot{q}\bar{c}}{V}} \frac{\dot{q}\bar{c}}{V}$$

or, in the common notation used in stability analyses,

$$\Delta C_m = C_{m_\alpha} \alpha + C_{m_{\dot{\alpha}}} \frac{\dot{\alpha}\bar{c}}{V} \quad (7-23)$$

The term $C_{m_{\dot{\alpha}}} \frac{\dot{\alpha}\bar{c}}{V}$ is then supposed to express the influence on C_m of the delayed adjustment of the airflow to changes in α .

For aircraft having a horizontal tailplane, this tailplane usually provides the most important contribution to C_{m_α} . A simplified explanation of this effect is the following.

In chapter 9 the angle of attack of the horizontal tailplane in steady, straight flight was expressed by equation (9-64),

$$\alpha_h = \alpha - \varepsilon + i_h$$

During the accelerated translation along the Z_S -axis here considered, i_h remains constant. In accordance with the conventions made in the present chapter, the explicit indication that a change in a variable is considered, is omitted. As a consequence $\alpha_h(t)$ can be written here as,

$$\alpha_h(t) = \alpha(t) - \varepsilon(t)$$

The horizontal tailplane is always situated in an air mass having passed the wing a brief time interval Δt ,

$$\Delta t \approx \frac{l_h}{V}$$

earlier. As a consequence, the downwash angle at the horizontal tailplane is at any time proportional to the wing angle of attack that brief time interval earlier,

$$\varepsilon(t) = \frac{d\varepsilon}{d\alpha} \alpha(t - \Delta t) \quad (7-24)$$

The angle of attack of the wing at the time $t - \Delta t$ can be written as,

$$\alpha(t - \Delta t) = \alpha(t) - \dot{\alpha} \Delta t + \frac{1}{2!} \ddot{\alpha} (\Delta t)^2 - \frac{1}{3!} \dots \dots$$

In this expression the time derivative of α higher than the first are omitted, as in equation (7-22). The result is,

$$\alpha(t - \Delta t) = \alpha(t) - \dot{\alpha} \Delta t$$

In equation (7-24) this leads to,

$$\varepsilon(t) = \frac{d\varepsilon}{d\alpha} \alpha(t) - \frac{d\varepsilon}{d\alpha} \dot{\alpha} \frac{l_h}{V}$$

and,

$$\alpha_h(t) = \alpha(t) \left(1 - \frac{d\varepsilon}{d\alpha} \right) + \frac{d\varepsilon}{d\alpha} \dot{\alpha} \frac{l_h}{V}$$

The term in the change in α_h proportional to $\dot{\alpha}$ is then,

$$\Delta\alpha_h(t) = + \frac{d\varepsilon}{d\alpha} \frac{l_h}{c} \frac{\dot{\alpha} \bar{c}}{V} \quad (7-25)$$

This $\Delta\alpha_h$ produces a force,

$$\Delta C_Z = -C_{N_{h\alpha}} \Delta \alpha_h \left(\frac{V_h}{V} \right)^2 \frac{S_h}{S}$$

and a longitudinal moment,

$$\Delta C_m = -C_{N_{h\alpha}} \Delta \alpha_h \left(\frac{V_h}{V} \right)^2 \frac{S_h l_h}{S \bar{c}}$$

Substituting equation (7-25) in the latter two expressions results in the desired, approximated, expressions for the stability derivatives,

$$C_{Z_{\dot{\alpha}}} = -C_{N_{h\alpha}} \left(\frac{V_h}{V} \right)^2 \frac{d\varepsilon}{d\alpha} \frac{S_h l_h}{S \bar{c}}$$

$$C_{m_{\dot{\alpha}}} = -C_{N_{h\alpha}} \left(\frac{V_h}{V} \right)^2 \frac{d\varepsilon}{d\alpha} \frac{S_h l_h^2}{S \bar{c}^2}$$

The variation of $C_{m_{\dot{\alpha}}}$ with the c.g. position is calculated by,

$$\Delta C_{m_{\dot{\alpha}}} = -C_{Z_{\dot{\alpha}}} \Delta \frac{x_{c.g.}}{\bar{c}}$$

In the calculation of $C_{Z_{\dot{\alpha}}}$ and $C_{m_{\dot{\alpha}}}$ attention should be given, as with C_{Z_q} and C_{m_q} , to the fact that in the literature these derivatives occur referenced to $\frac{\dot{\alpha}\bar{c}}{2V}$ rather than to $\frac{\dot{\alpha}\bar{c}}{V}$.

7-6 Derivatives with respect to the elevator angle

7-6-1 Control derivative $C_{X_{\delta_e}}$

According to table 4-3, this derivative is equal to,

$$C_{X_{\delta_e}} = \frac{1}{\frac{1}{2}\rho V^2 S} \frac{\partial X}{\partial \delta_e} = \frac{\partial C_X}{\partial \delta_e}$$

This derivative expresses the variation of aircraft drag with the elevator angle. Although the total drag caused by the elevator deflection may be non-negligible, especially at supersonic speed ('trim drag'), the variation in C_X with small variations of δ_e is commonly neglected. Or,

$$C_{X_{\delta_e}} = 0$$

7-6-2 Control derivative $C_{Z_{\delta_e}}$

According to table 4-3, this derivative is equal to,

$$C_{Z_{\delta_e}} = \frac{1}{\frac{1}{2}\rho V^2 S} \frac{\partial Z}{\partial \delta_e} = \frac{\partial C_Z}{\partial \delta_e}$$

If the aircraft has a horizontal tailplane, $C_{Z_{\delta_e}}$ can also be written more explicitly as,

$$C_{Z_{\delta_e}} = -C_{N_{h_{\delta_e}}} \left(\frac{V_h}{V} \right)^2 \frac{S_h}{S} \quad (7-26)$$

References [9, 110, 43, 46, 90, 106, 37] provide data to derive $C_{N_{h_{\delta_e}}}$ if the form and the dimensions of the stabilizer and the elevator are known. For tailless aircraft $C_{Z_{\delta_e}}$ should preferably be obtained from measurements on a wind tunnel model, see also references [43, 46, 106, 37].

7-6-3 Control derivative $C_{m_{\delta_e}}$

According to table 4-3, this derivative is equal to,

$$C_{m_{\delta_e}} = \frac{1}{\frac{1}{2}\rho V^2 S \bar{c}} \frac{\partial M}{\partial \delta_e} = \frac{\partial C_m}{\partial \delta_e}$$

If the aircraft has a horizontal tailplane, $C_{m_{\delta_e}}$ can be simply expressed using $C_{Z_{\delta_e}}$,

$$C_{m_{\delta_e}} = C_{Z_{\delta_e}} \frac{x_h - x_{c.g.}}{\bar{c}}$$

or,

$$C_{m_{\delta_e}} = -C_{N_{\delta_e}} \left(\frac{V_h}{V} \right)^2 \frac{S_h}{S} \frac{x_h - x_{c.g.}}{\bar{c}}$$

An approximation for $C_{m_{\delta_e}}$ is,

$$C_{m_{\delta_e}} = -C_{N_{\delta_e}} \left(\frac{V_h}{V} \right)^2 \frac{S_h l_h}{S \bar{c}}$$

This results in $C_{m_{\delta_e}}$, if $C_{Z_{\delta_e}}$ has been previously obtained using equation (7-26).

Of the three control derivatives $C_{m_{\delta_e}}$ has the largest effect on the aircraft motions. For aircraft having a horizontal tailplane, the influence of $C_{m_{\delta_e}}$ dominates to such an extent that very often $C_{Z_{\delta_e}}$ for these aircraft is neglected. This approximation is less applicable to tailless aircraft. The derivative $C_{m_{\delta_e}}$ for tailless aircraft is derived by the same calculation methods or wind tunnel measurements yielding also $C_{Z_{\delta_e}}$.

Table 7-1 summarizes the expressions for the stability and control derivatives discussed in the previous sections.

7-7 Symmetric inertial parameters

Reliable quantitative data on moments and products of inertia of aircraft are rare. Quantitative calculations are very time-consuming and may produce rather inaccurate results.

The most reliable inertial parameters of aircraft are those obtained experimentally, usually by oscillating the suspended aircraft on the ground. Details on this experimental technique can be found in references [180, 175, 42, 103].

$C_{X_0} = -C_D + T'_c \cos(\alpha_0 + i_p) = \frac{W}{\frac{1}{2}\rho V^2 S} \sin\gamma_0 \approx -C_D + T'_c$ $C_{Z_0} = -C_L - T'_c \sin(\alpha_0 + i_p) = -\frac{W}{\frac{1}{2}\rho V^2 S} \cos\gamma_0 \approx -C_L$ $C_{m_0} = 0$
$C_{X_u} = 2 C_L \tan \gamma_0$ $C_{Z_u} = -2 C_L$ $C_{m_u} = 0$
$C_{X_\alpha} = C_L - C_{D_\alpha} = -C_{T_\alpha} \cos\alpha_0 - C_{N_\alpha} \sin\alpha_0; \text{ if } C_D = C_{D_0} + \frac{C_L^2}{\pi Ae} \text{ then}$ $C_{X_\alpha} = C_L \left(1 - \frac{2C_{L_\alpha}}{\pi Ae}\right)$ $C_{Z_\alpha} = -C_{L_\alpha} - C_D \approx -C_{L_\alpha} \approx -C_{N_\alpha}$ $C_{m_\alpha} = C_{N_{w\alpha}} \frac{x_{c,g.}-x_w}{\bar{c}} - C_{N_{h\alpha}} \left(1 - \frac{d\varepsilon}{d\alpha}\right) \left(\frac{V_h}{V}\right)^2 \frac{S_h l_h}{S \bar{c}}$
$C_{X_q} = 0$ $C_{Z_q} = 2 (C_{Z_q})_h = -2 C_{N_{h\alpha}} \left(\frac{V_h}{V}\right)^2 \frac{S_h l_h}{S \bar{c}}$ $C_{m_q} = -(1.1 \text{ to } 1.2) (C_{m_q})_h = -(1.1 \text{ to } 1.2) \cdot C_{N_{h\alpha}} \cdot \left(\frac{V_h}{V}\right)^2 \frac{S_h l_h^2}{S \bar{c}^2}$
$C_{X_{\dot{\alpha}}} = 0$ $C_{Z_{\dot{\alpha}}} = -C_{N_{h\alpha}} \left(\frac{V_h}{V}\right)^2 \frac{d\varepsilon}{d\alpha} \frac{S_h l_h}{S \bar{c}}$ $C_{m_{\dot{\alpha}}} = -C_{N_{h\alpha}} \left(\frac{V_h}{V}\right)^2 \frac{d\varepsilon}{d\alpha} \frac{S_h l_h^2}{S \bar{c}^2}$

Table 7-1: Simplified formulae for the calculation of stability and control derivatives and coefficients in the initial, steady flight condition for the symmetric motions (without the effects of propellers and jets, aeroelasticity and compressibility of the air).

$C_{X_{\delta_e}} = 0$
$C_{Z_{\delta_e}} = -C_{N_{h_{\delta_e}}} \left(\frac{V_h}{V}\right)^2 \frac{S_h}{S}$
$C_{m_{\delta_e}} = -C_{N_{\delta_e}} \left(\frac{V_h}{V}\right)^2 \frac{S_h l_h}{S \bar{c}}$

Table 7-1: **(Continued)** Simplified formulae for the calculation of stability and control derivatives and coefficients in the initial, steady flight condition for the symmetric motions (without the effects of propellers and jets, aeroelasticity and compressibility of the air).

$C_{m_{\alpha_2}} = C_{m_{\alpha_1}} - C_{Z_\alpha} \frac{x_{c,g,2} - x_{c,g,1}}{\bar{c}}$
$C_{Z_{q_2}} = C_{Z_{q_1}} - C_{Z_\alpha} \frac{x_{c,g,2} - x_{c,g,1}}{\bar{c}}$
$C_{m_{q_2}} = C_{m_{q_1}} - C_{Z_{q_2}} \frac{x_{c,g,2} - x_{c,g,1}}{\bar{c}} - C_{m_{\alpha_1}} \frac{x_{c,g,2} - x_{c,g,1}}{\bar{c}} =$
$= C_{m_{q_1}} - (C_{Z_{q_1}} + C_{m_{\alpha_1}}) \frac{x_{c,g,2} - x_{c,g,1}}{\bar{c}} + C_{Z_\alpha} \left(\frac{x_{c,g,2} - x_{c,g,1}}{\bar{c}} \right)^2$
$C_{m_{\dot{\alpha}_2}} = C_{m_{\dot{\alpha}_1}} - C_{Z_{\dot{\alpha}}} \frac{x_{c,g,2} - x_{c,g,1}}{\bar{c}}$

Table 7-2: Influence of the center of gravity position on some stability derivatives

Chapter 8

Lateral Stability and Control Derivatives

In the previous chapter the equilibrium about the lateral axis and longitudinal control in steady, symmetric flight was studied. In addition, static longitudinal stability was considered since this is usually the most critical condition for dynamic longitudinal stability.

Studies in dynamic lateral stability relate to the asymmetric motions relative to a steady, symmetric flight condition. There is, however, not one specific ‘static lateral stability’ characteristic for the asymmetric disturbed motions. These disturbed asymmetric motions appear to be determined by more than just one stability derivative, while the inertial parameters also have an important influence.

In this chapter the lateral stability and control derivatives are discussed, whereas in chapter 11 the lateral equilibrium and lateral control in steady, asymmetric flight conditions will be studied, similar to chapter 10.

8-1 Aerodynamic force and moments due to side slipping, rolling and yawing

The asymmetric degrees of freedom of an aircraft are the following, see figure 8-1.

- The translation of the aircraft center of gravity along the Y_B -axis of the aircraft body axes, positive in the direction of this Y -axis. The component of airspeed along the Y_B -axis is indicated as v . If such a component is present the aircraft is said to be in sideslipping flight. The angle of sideslip β is the angle between the velocity vector \underline{V} of the center of gravity and the plane of symmetry, see figure 8-2,

$$\beta = \arcsin \left(\frac{v}{V} \right)$$

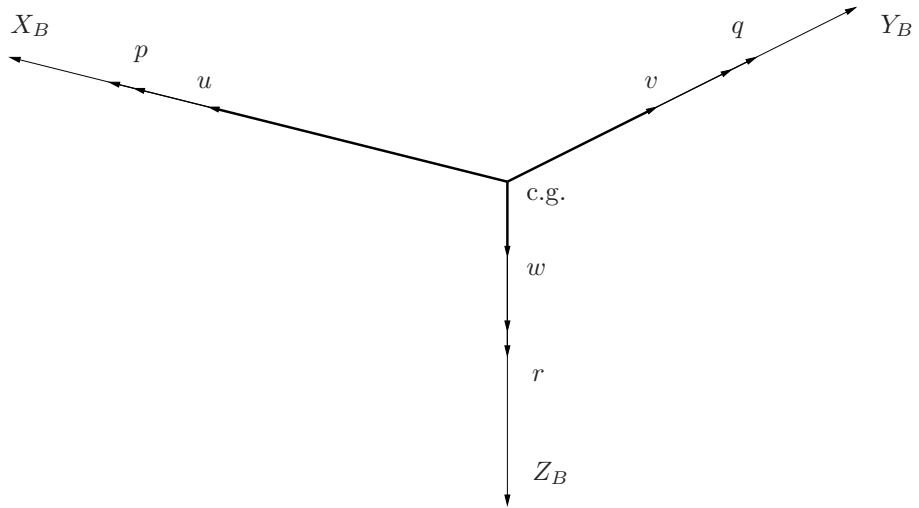
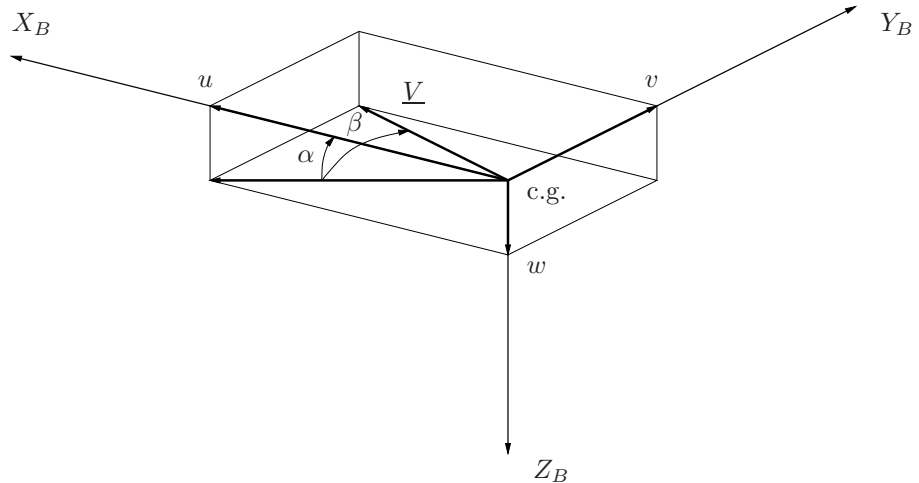


Figure 8-1: The six degrees of freedom of a rigid aircraft

Figure 8-2: Definition of the angle of attack α and sideslip angle β

or, at sufficiently small angles of sideslip,

$$\beta \approx \frac{v}{V} \quad (\text{Radians}) \quad (8-1)$$

The sideslip angle β is positive if the aircraft moves in the direction of the positive Y_B -axis, so to the right as seen by the pilot.

- The angular velocity about the X_B -axis, positive if the right wing moves down. The angular velocity about the X_B -axis, the rolling velocity, is indicated as p . Often the non-dimensional form $\frac{pb}{2V}$ is used.
- The angular velocity about the Z_B -axis, positive if the aircraft's nose moves to the right as seen by the pilot. The angular velocity about the Z_B -axis, the yawing velocity, is indicated as r . The non-dimensional yaw velocity about this top axis is $\frac{pb}{2V}$.

The asymmetric motions in general cause an aerodynamic force Y along the Y_B -axis, a moment L about the X_B -axis and a moment N about the Z_B -axis, see figure 8-3. As already noted in

section 4-1, asymmetric motions generally do not produce symmetric aerodynamic forces and moments. As a consequence the symmetric aerodynamic forces X and Z and the moment M , with a single exception, do not have to be considered.

The rolling moment L is commonly indicated as L' in situations where confusion with the lift L is possible.

The non-dimensional asymmetric forces and moments are defined as,

$$\begin{aligned} C_Y &= \frac{Y}{\frac{1}{2}\rho V^2 S} \\ C_\ell &= \frac{L}{\frac{1}{2}\rho V^2 S b} \\ C_n &= \frac{N}{\frac{1}{2}\rho V^2 S b} \end{aligned} \quad (8-2)$$

where C_ℓ and C_n are referenced to the wing span and not, like C_m , to the wing m.a.c., \bar{c} . The non-dimensional aerodynamic force and moments resulting from side slipping, rolling and yawing are determined by the partial derivatives with respect to the non-dimensional asymmetric components of the moment β , $\frac{pb}{2V}$ and $\frac{rb}{2V}$. These derivatives are,

- For sideslipping flight,

$$C_{Y_\beta} = \frac{\partial C_Y}{\partial \beta} \quad C_{\ell_\beta} = \frac{\partial C_\ell}{\partial \beta} \quad C_{n_\beta} = \frac{\partial C_n}{\partial \beta}$$

- For rolling flight,

$$C_{Y_p} = \frac{\partial C_Y}{\partial \frac{pb}{2V}} \quad C_{\ell_p} = \frac{\partial C_\ell}{\partial \frac{pb}{2V}} \quad C_{n_p} = \frac{\partial C_n}{\partial \frac{pb}{2V}}$$

- For yawing flight,

$$C_{Y_r} = \frac{\partial C_Y}{\partial \frac{rb}{2V}} \quad C_{\ell_r} = \frac{\partial C_\ell}{\partial \frac{rb}{2V}} \quad C_{n_r} = \frac{\partial C_n}{\partial \frac{rb}{2V}}$$

The derivatives with respect to $\frac{pb}{2V}$ and $\frac{rb}{2V}$ are indicated only with the subscript p and r respectively, to simplify the notation. The above mentioned partial derivatives are called the stability derivatives with respect to angle of sideslip, non-dimensional rolling velocity and non-dimensional yawing velocity, as these derivatives are used primarily in relation to the stability of aircraft flight. When using the stability derivatives it is assumed that the forces and moments vary linearly with β , $\frac{pb}{2V}$ and $\frac{rb}{2V}$. The additional assumption is made, that in symmetric flight C_Y , C_ℓ and C_n are zero. As a result, for instance in steady, straight sideslipping flight ($p = r = 0$), it can be written,

$$C_Y = C_{Y_\beta} \beta \quad C_\ell = C_{\ell_\beta} \beta \quad C_n = C_{n_\beta} \beta$$

For small deviations from the symmetric equilibrium condition to which the study of stability refers, this latter assumption is generally acceptable. Commonly, this assumption also

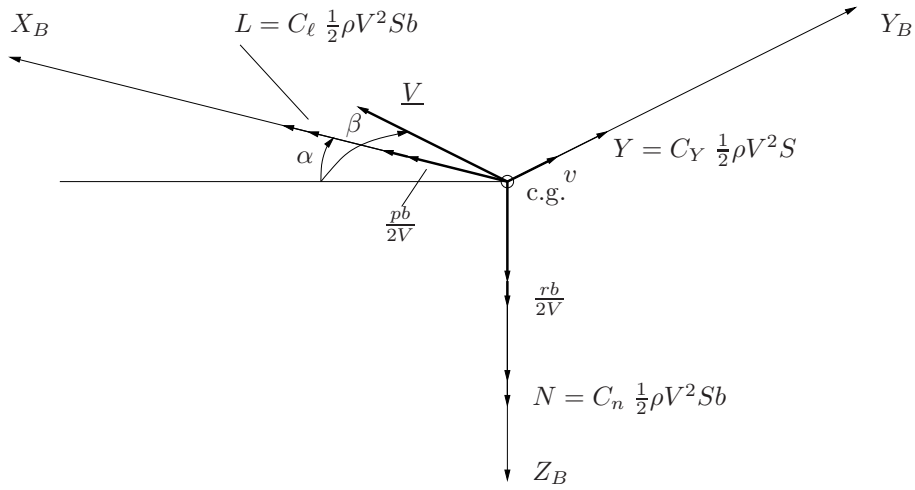


Figure 8-3: Asymmetric force and moments

holds when considering steady, asymmetric flight at values of β , $\frac{pb}{2V}$ and $\frac{rb}{2V}$ which are not too large.

During the non-steady motion of aircraft caused by a disturbance from the symmetric equilibrium condition the accelerations also generate aerodynamic forces and moments. These are usually small enough to be negligible. An exception is only made for the moment about the top axis caused by an acceleration along the Y_B -axis. The stability derivative describing this moment, indicated in accordance with the above as C_{n_β} , can be compared to the stability derivative C_{m_α} for the symmetric motions already discussed in section 7-5.

A deviation from the rule that asymmetric motions cause no symmetric forces and moments, is the change in pitching moment caused by a velocity about the lateral axis, v . In the study of stability, where small deviations from the symmetric equilibrium situation are considered, this change in C_m is commonly negligible. In steady asymmetric flight where large angles of sideslip occur, but also during take-off runs and during landing with cross wind, this pitching moment due to sideslip certainly has to be considered. The effect is expressed quantitatively by the derivative $C_{m_\beta^2}$.

Summarizing the above, the non-dimensional asymmetric aerodynamic forces and moments caused by the lateral motions are written as,

$$\begin{aligned} C_Y &= C_{Y_\beta} \beta + C_{Y_p} \frac{pb}{2V} + C_{Y_r} \frac{rb}{2V} \\ C_\ell &= C_{\ell_\beta} \beta + C_{\ell_p} \frac{pb}{2V} + C_{\ell_r} \frac{rb}{2V} \\ C_n &= C_{n_\beta} \beta + C_{n_\beta} \frac{\dot{\beta}b}{V} + C_{n_p} \frac{pb}{2V} + C_{n_r} \frac{rb}{2V} \end{aligned} \quad (8-3)$$

In the following the underlying mechanisms, magnitudes and signs of the stability derivatives are discussed. Figures 8-50 give a summary of the forces and moments acting on the aircraft due to β , $\frac{pb}{2V}$ and $\frac{rb}{2V}$. The usual signs of the corresponding stability derivatives are shown as well. Quantitative values of the stability derivatives have been compiled in appendix D for a number of aircraft in various flight conditions, see also reference [18].

When it comes to the actual calculation of stability derivatives, reference will be made to relevant references. An extensive list of references on the calculation of stability derivatives can be found in reference [165]. The calculation methods indicated in the references often rely on empirical data obtained from similar aircraft configurations. Calculation methods based entirely on theory result in most instances in insufficiently accurate results. Wind tunnel measurements remain necessary in later design stages to arrive at sufficiently accurate data. This applies in particular to the stability derivatives with respect to angle of sideslip, β , which have a predominant influence on lateral stability and lateral control characteristics of aircraft.

8-2 Stability derivatives with respect to the sideslip angle

8-2-1 Stability derivative C_{Y_β}

Sideslipping motion generates an aerodynamic lateral force, usually negative at positive angles of sideslip,

$$Y = C_{Y_\beta} \beta \frac{1}{2} \rho V^2 S \quad (8-4)$$

where C_{Y_β} is negative. The dominant contributions to C_{Y_β} are caused by the fuselage and the vertical tailplane, see figure 8-4. The contribution of the wing is generally negligible unless the wing has a large angle of sweep. The propulsion system may also give a contribution to C_{Y_β} that is not negligible.

The small contribution of the wing may, if necessary, be obtained for low airspeeds using references [10, 74, 34, 131, 167, 67].

The influence of the compressibility of the air can be accounted for using reference [60]. Calculation methods applicable to supersonic speeds are given in references [10, 74, 34, 3, 150, 2, 80]. The contribution of the fuselage arises in the same way as the normal force on a symmetric fuselage at a non-zero angle of attack. Calculation methods can be found in references [10, 74, 34, 3, 150, 2, 80].

The contribution of the vertical tailplane can, in analogy with the gradient of the normal force on the horizontal tailplane in the symmetric case, be written as,

$$(C_{Y_\beta})_v = C_{Y_{v\alpha}} \frac{d\alpha_v}{d\beta} \left(\frac{V_v}{V} \right)^2 \frac{S_v}{S} \quad (8-5)$$

Compare this equation to the corresponding expression for the horizontal tailplane,

$$(C_{N_\alpha})_h = C_{N_{h\alpha}} \frac{d\alpha_h}{d\alpha} \left(\frac{V_h}{V} \right)^2 \frac{S_h}{S}$$

In equation (8-5) $C_{Y_{v\alpha}} = \frac{C_{Y_v}}{\alpha_v}$ is the gradient of the normal force on the isolated vertical tailplane referenced to the area S_v of the vertical tailplane and the average local dynamic pressure $\frac{1}{2}\rho V_v^2$ at the vertical tailplane. The angle of attack α_v is the local angle of attack of the vertical tailplane measured in the $X_B O Y_B$ -plane and counted as positive if the airflow hits the tailplane from the left, see figure 8-5.

Even when disregarding the sign, α_v is generally not equal to β . Due to the presence of the fuselage and the wing-fuselage interaction a change in the component of the local velocity of the

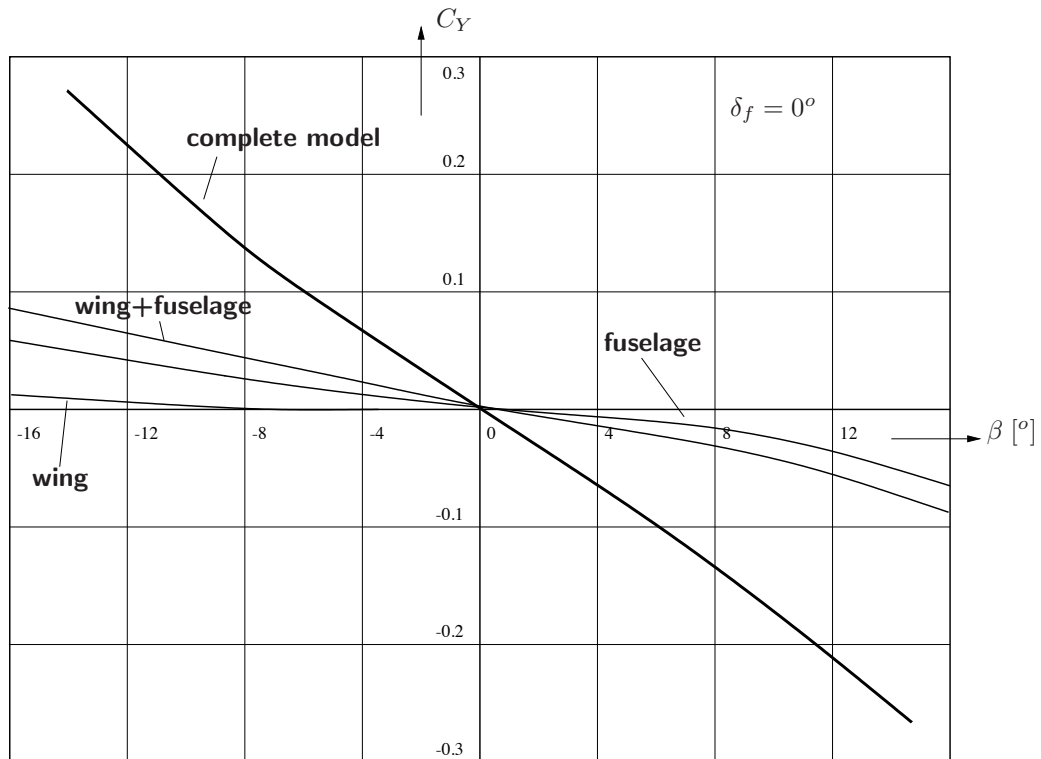


Figure 8-4: C_Y as a function of β measured on a model of the Fokker F-27 in gliding flight (from references [159, 161, 24])

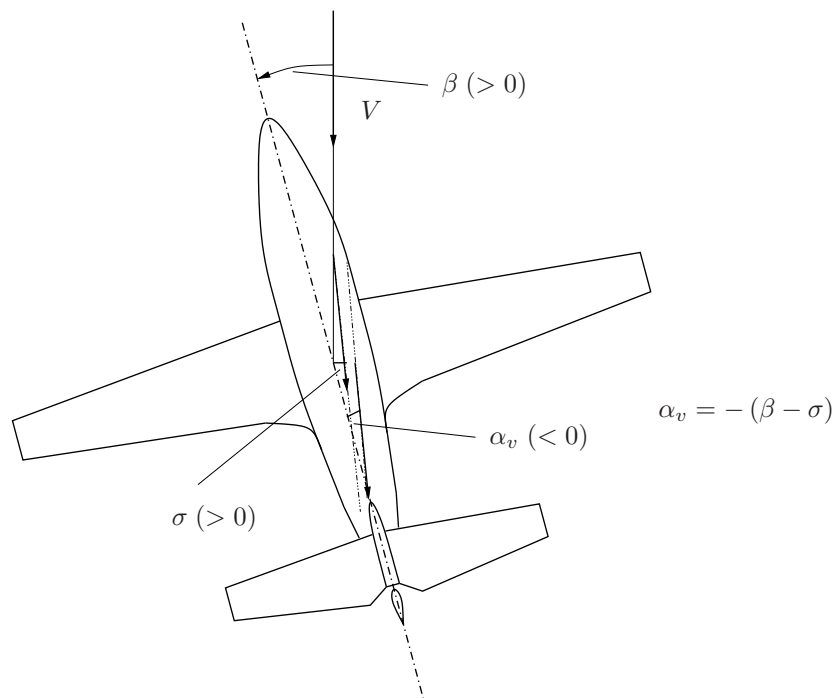


Figure 8-5: Relation between the sideslip angle β , the sidewash angle σ and the angle of attack α_v at the vertical tailplane

air parallel to the Y_B -axis occurs. The resulting change in the direction of the airflow is described using the sidewash angle σ , comparable to the downwash angle ε in symmetric flow. Consulting figure 8-5 it follows,

$$\alpha_v = -(\beta - \sigma) \quad (8-6)$$

The corresponding expression for the horizontal tailplane was, see equation (9-64),

$$\alpha_h = \alpha - \varepsilon + i_h$$

From equation (8-6) follows,

$$\frac{d\alpha_v}{d\beta} = -\left(1 - \frac{d\sigma}{d\beta}\right) \quad (8-7)$$

Substituting equation (8-7) in equation (8-5) results in,

$$(C_{Y_\beta})_v = -C_{Y_{v_\alpha}} \left(1 - \frac{d\sigma}{d\beta}\right) \left(\frac{V_v}{V}\right)^2 \frac{S_v}{S} \quad (8-8)$$

As a result of the sign convention for α_v , $C_{Y_{v_\alpha}}$ is positive like any normal force gradient. In the quantitative calculation of $C_{Y_{v_\alpha}}$ the presence of the horizontal tailplane, sometimes acting as an end plate to the vertical tail plane, has to be taken into account. Due to this effect the effective aspect ratio of the vertical tailplane may be considerably larger than its geometric aspect ratio. For subsonic airspeeds the calculation of $C_{Y_{v_\alpha}}$ can be made using references [10, 74, 111, 98, 125, 145, 141, 31]. For supersonic speeds references [117, 29, 114, 115] provide calculation methods.

If the angle of attack is not too large, $(\frac{V_v}{V})^2$ may usually be taken as 1 if the tailplane is not located in a slipstream. In the contrary case, $(\frac{V_v}{V})^2$ is determined in the same way as $(\frac{V_h}{V})^2$ for the horizontal tailplane. The magnitude of $\frac{d\sigma}{d\beta}$ will be discussed in more detail when dealing with C_{n_β} .

The propulsion system provides a negative contribution to C_{Y_β} caused by a lateral force in the propeller plane or in the plane of the engine inlet in the case of jet propulsion. This effect is a direct analogy with the normal force generated by a propeller or the engine air inlet if placed under a non-zero angle of attack. Calculation methods to determine this contribution are given in references [143, 144].

Using linearized potential flow theory (panel methods), C_Y as a function of β has been calculated for the Cessna Ce550 ‘Citation II’, see figure 8-6. The definition of the aircraft parts ‘wing’, ‘horizontal stabilizer’, ‘pylons’, ‘fuselage’, ‘vertical fin’ and ‘nacelles’ is given in figure 7-2. The main contributions to C_{Y_β} are from the vertical fin and the fuselage.

8-2-2 Stability derivative C_{ℓ_β}

The stability derivative C_{ℓ_β} is one of the primary lateral stability derivatives, usually indicated as the ‘effective dihedral’ of the aircraft. The explanation of this name lies in the fact that for conventional aircraft without wing sweep C_{ℓ_β} can usually be varied primarily changing the

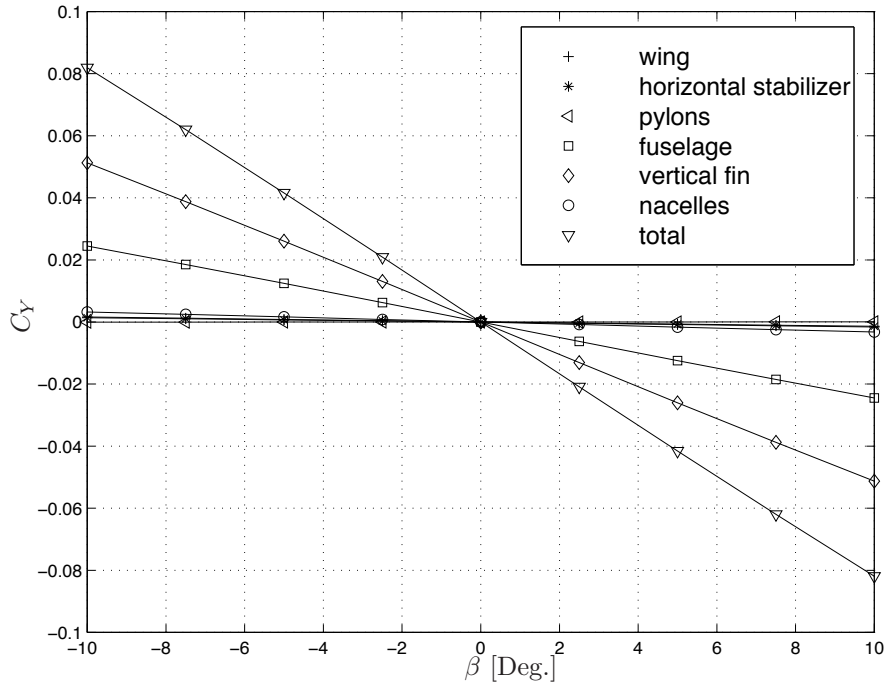


Figure 8-6: Aerodynamic force coefficient C_Y as a function of β for the Cessna Ce550 'Citation II', $\alpha = 0^\circ$

dihedral of the wing. To obtain desirable lateral control characteristics it is required that C_{ℓ_β} is negative. This can be illustrated as follows.

Suppose a disturbance causes an angle of roll to the right. Under the influence of the component of gravity along the Y_B -axis, the aircraft starts sideslipping to the right. A negative C_{ℓ_β} then causes a rolling moment trying to return the aircraft to an even keel, without interference by the pilot. In a qualitative sense this explains the desirability of a negative C_{ℓ_β} .

Apart from wing dihedral, wing sweep and the wing-fuselage interaction have a large influence on C_{ℓ_β} . The slipstream influence on C_{ℓ_β} of propeller driven aircraft can be considerable. The contributions of the fuselage and the tailplane are generally small.

The contribution of wing-dihedral to C_{ℓ_β} is caused by the difference in geometric angle of attack of the left and right hand halves of the wing in sideslipping flight. From subfigure b of figure 8-7 follows for the right wing without sweep and having not too large a dihedral,

$$V_{n_r} = w \cos \Gamma + v \sin \Gamma \approx w + v \Gamma$$

where for small values of α and β , see subfigure a of figure 8-7,

$$w \approx V \sin \alpha \approx V \alpha$$

and,

$$v \approx V \sin \beta \approx V \beta$$

resulting in,

$$V_{n_r} = V (\alpha + \beta \Gamma) \quad (8-9)$$

The geometric angle of attack of the right wing then is, see subfigure c of figure 8-7,

$$\alpha_{w_r} = \arctan \left(\frac{V_{n_r}}{u} \right) \approx \alpha + \beta \Gamma \quad (8-10)$$

In a similar manner it can be derived for the left wing,

$$V_{n_l} \approx V (\alpha - \beta \Gamma) \quad (8-11)$$

hence,

$$\alpha_{w_l} \approx \alpha - \beta \Gamma \quad (8-12)$$

The increase in lift on the right wing due to $\Delta\alpha_{w_r} = +\beta \cdot \Gamma$ and the decrease in lift on the left wing due to $\Delta\alpha_{w_l} = -\beta \cdot \Gamma$ are thus proportional to the geometric dihedral Γ . From the above it can be concluded that $(C_{\ell_\beta})_w$ will also be approximately proportional to Γ .

Swept wings experience an additional difference in lift between the two halves of the wing, independent of dihedral. This difference in lift is caused by the difference in the components of airspeed perpendicular to the wing leading edge on the $\frac{1}{4}$ -chord line. It can be seen from figure 8-8 that the difference in lift ΔL can be roughly approximated as,

$$\Delta L = C_L \frac{1}{2} \rho V^2 \frac{S}{2} \{ \cos^2(\Lambda - \beta) - \cos^2(\Lambda + \beta) \} \quad (8-13)$$

Further analysis results for small values of β in,

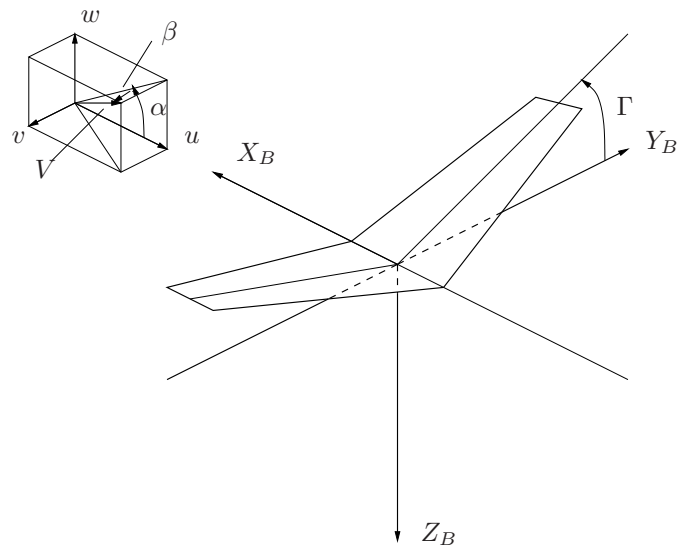
$$\Delta L = C_L \frac{1}{2} \rho V^2 S \sin 2\Lambda \cdot \beta \quad (8-14)$$

As the rolling moment of the wing $(C_{\ell_\beta})_w \cdot \beta$ will be proportional to ΔL , to a first approximation, this simple calculation shows that $(C_{\ell_\beta})_w$ will be approximately proportional to C_L and to $\sin 2\Lambda$, see figure 8-9.

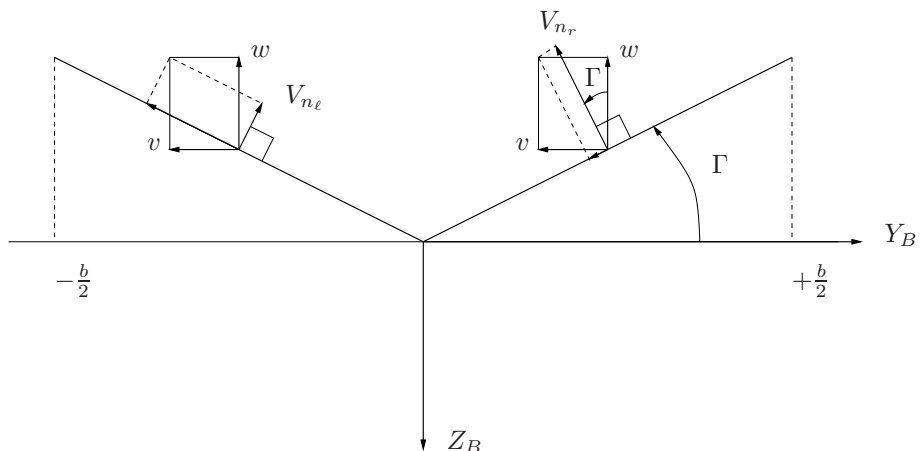
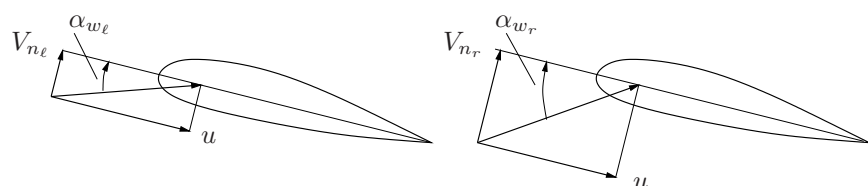
Flap deflection causes, at constant lift on the entire wing, a concentration of the lift at the center parts of the wing. Swept wings will have a less negative C_{ℓ_β} due to flap deflection. The same effect is obtained by applying negative wing-twist to swept wings.

The influence of dihedral and sweep on $(C_{\ell_\beta})_w$ are additive to a first order approximation. In summary it is seen from the foregoing that for a swept wing the contribution $(C_{\ell_\beta})_w$ is composed of one part proportional to the wing dihedral Γ (independent of C_L and wing sweep Λ) and of one part independent of Γ and proportional to C_L and $\sin 2\Lambda$. A consequence of the variation of C_{ℓ_β} with C_L is that swept wings often have a zero or even negative geometric dihedral, to avoid the unfavourable effects of too large and effective dihedral at large angles of attack. This will be further discussed when studying the dynamic lateral stability. Calculation methods to determine $(C_{\ell_\beta})_w$ are presented in references [10, 74, 131, 45, 140, 136].

The contribution of the fuselage itself to C_{ℓ_β} is very small. The wing fuselage interaction in sideslipping flight, however, can cause significant differences in the angles of attack of the two



(A) Wing with dihedral in sideslipping flight

(B) The normal velocities V_{n_ℓ} and V_{n_r} at two sides of the wing

(C) The angles of attack at the left and right wing

Figure 8-7: The origin of the difference in angles of attack at the left and right wing for a wing with dihedral in sideslipping flight

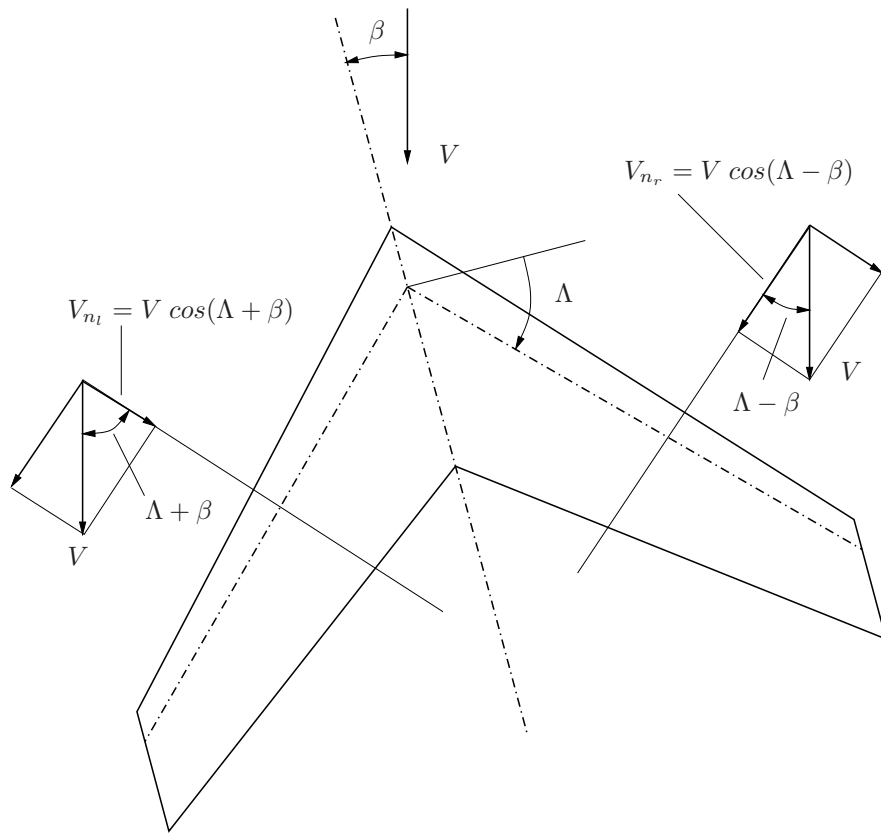


Figure 8-8: The origin of the difference in the velocities over the left and right wing for a swept wing in sideslipping flight

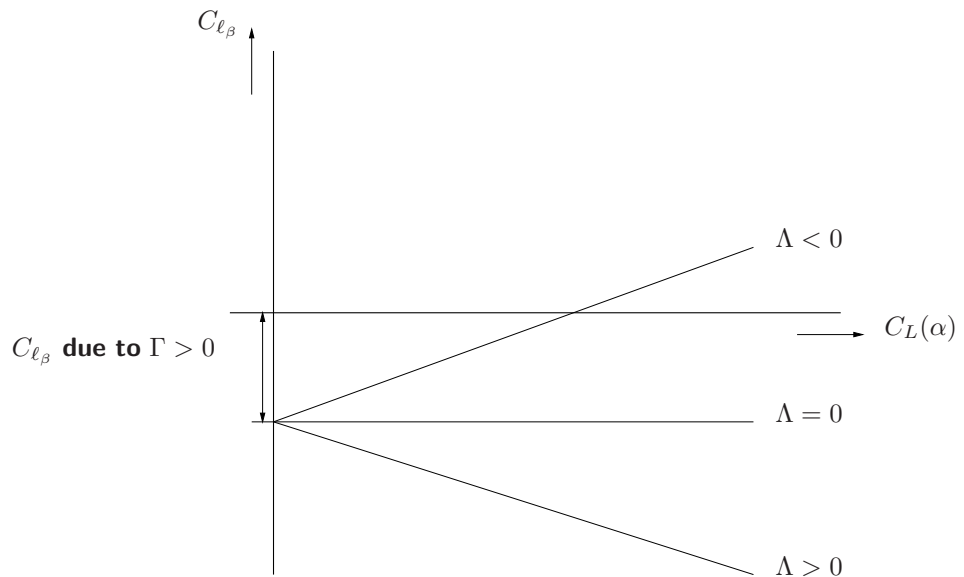


Figure 8-9: The variation of C_{ℓ_β} with C_L for swept wings

halves of the wing. This again has a strong influence on the rolling moment due to side-slip. Important for the way in which the rolling moment varies with angle of sideslip is the vertical position of the wing relative to the fuselage, see figure 8-13. The forward half wing of a low wing aircraft experiences a decrease in angle of attack due to sideslip. This produces a decrease in lift whereas the receding half wing experiences an increase in angle of attack and thus an increase in lift, due to the presence of the fuselage.

The situation is the reverse for a high wing aircraft. A positive angle of sideslip causes for a low wing aircraft an extra positive rolling moment, C_{ℓ_β} becomes less negative. On the other hand, $(C_{\ell_\beta})_v$ of a high wing aircraft becomes more negative. The magnitude of the contribution is strongly influenced by the shape of the fuselage and by its size compared to that of the wing. A detailed description of the influence of the wing-fuselage interaction on C_{ℓ_β} is given in reference [84]. A determination of C_{ℓ_β} of aircraft without tailplanes is possible using references [131, 167, 25, 45, 140, 136] for subsonic speeds and references [139, 89, 88, 116, 155] for supersonic speeds.

For example, see also the following illustrations; for the case of a high-wing-fuselage configuration in side-slipping flight, the configuration and velocity field are plotted in figure 8-10, while for the case of a low-wing-fuselage configuration in side-slipping flight, the configuration and velocity field are plotted in figure 8-11. Figure 8-12 presents the airflow around the Cessna Ce550 ‘Citation II’ in side-slipping flight. Particle traces depict the flow around the bottom side of the fuselage; as is obvious, the right wing induces a downwash in front of it, i.e. the particle traces follow a path below the wing and fuselage, while the left wing induces an upwash in front of it, i.e. the particle lines follow a path over the wing. In this figure a speedbar is given as well, depicting a measure for the local airspeed’s magnitude along particle traces. The results of these simulations were obtained using a panel method (linearized potential flow).

The contribution of the vertical tailplane to C_{ℓ_β} is usually not large for conventional aircraft, but may not be neglected for aircraft having a relatively large vertical tailplane. The magnitude of $(C_{\ell_\beta})_v$ follows from the magnitude and the position of the point of action of the lateral force $(C_{Y_\beta})_v \cdot \beta$. In the calculation of $(C_{\ell_\beta})_v$ the choice of the reference frame is important, as will be shown below.

In the study of stability, the so-called stability reference frame is commonly used. This is a system of aircraft body axes of which the X_S -axis in the plane of symmetry is chosen in the direction of the undisturbed flow. In this situation the rolling moment due to the side force on the vertical tailplane depends on the angle of attack of the aircraft.

From figure 8-15 follows for $(C_{\ell_\beta})_v$,

$$(C_{\ell_\beta})_v = (C_{Y_\beta})_v \left(\frac{z_v - z_{c.g.}}{b} \cos \alpha_0 - \frac{x_v - x_{c.g.}}{b} \sin \alpha_0 \right) \quad (8-15)$$

the ordinates x_v and z_v can be determined using the same references as indicated for the determination of $C_{Y_{v\alpha}}$.

The effective dihedral of a propeller driven aircraft having a propeller in front of the wing can experience an important change due to the interaction between the slipstream and the wing. Due to the increased dynamic pressure in the slipstream an extra rolling moment is generated in sideslipping flight, see figure 8-16. At a positive side-slip angle β this rolling moment acts in the right wing down sense, thus giving a positive contribution to C_{ℓ_β} . The contribution increases with

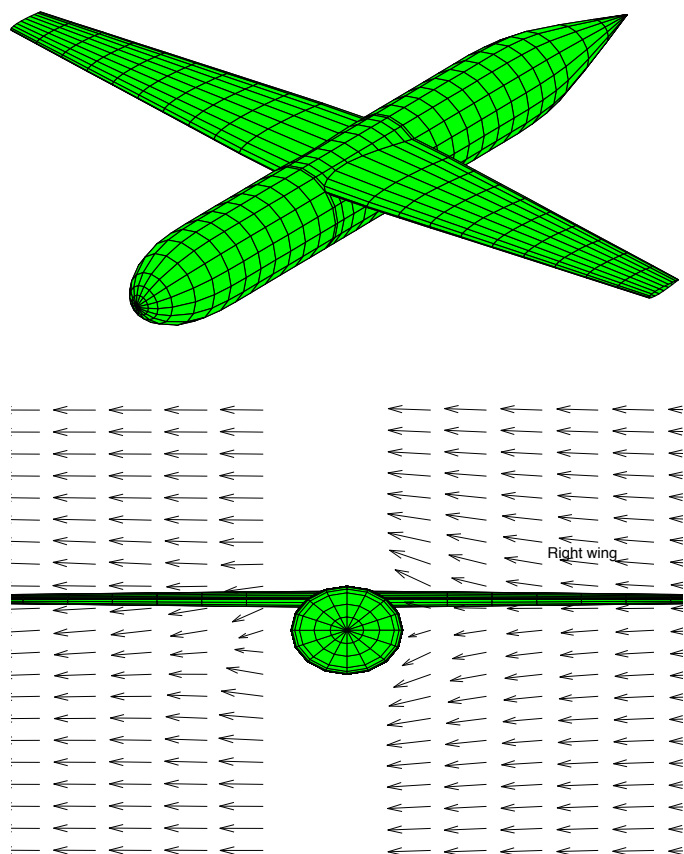


Figure 8-10: High-wing-fuselage configuration with the calculated velocity field in sideslipping flight ($\beta = 10^\circ$, $\alpha = 0^\circ$)

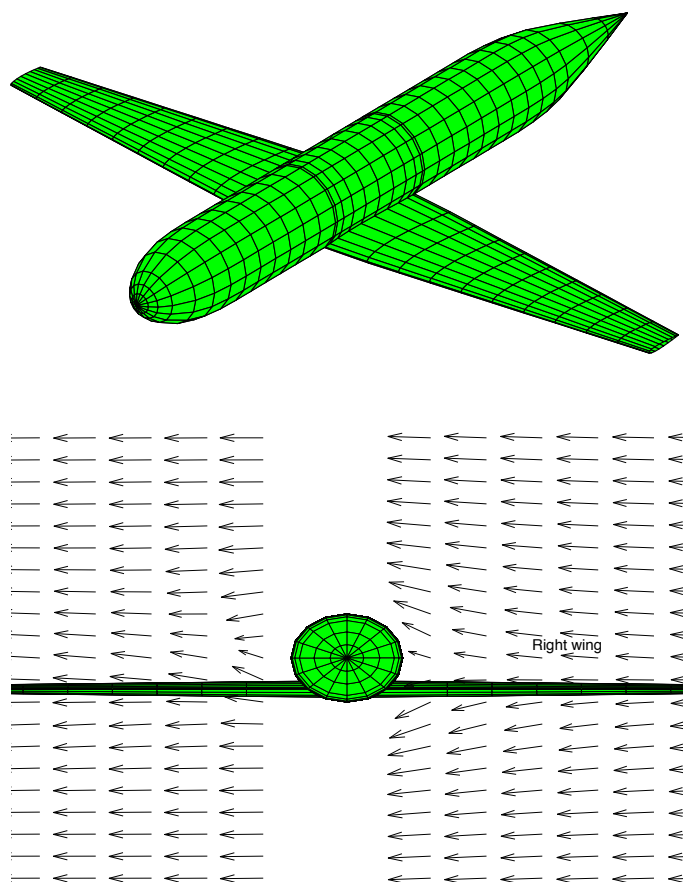


Figure 8-11: Low-wing-fuselage configuration with the calculated velocity field in sideslipping flight ($\beta = 10^\circ$, $\alpha = 0^\circ$)

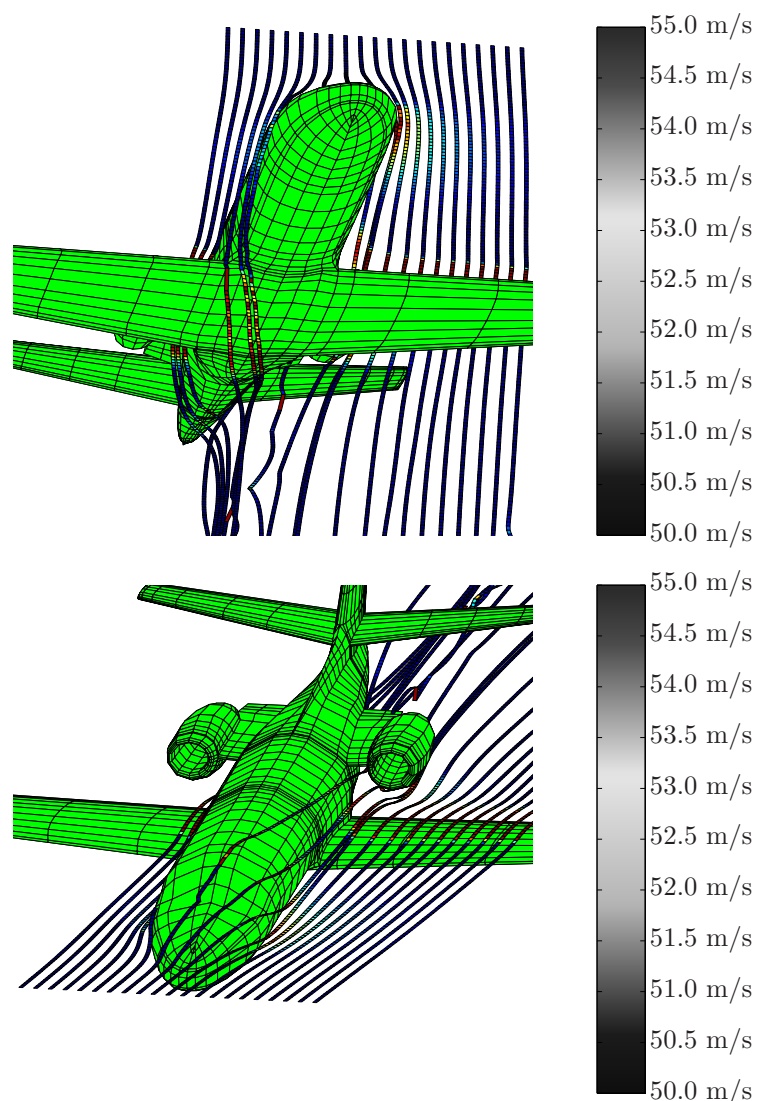


Figure 8-12: Calculated particle traces around the bottom half of the fuselage of the Cessna Ce550 'Citation II', sideslipping flight $\beta = 10^\circ$, $\alpha = 0^\circ$ (note: the speedbar is related to the magnitude of the airflow's velocity along the calculated particle traces)

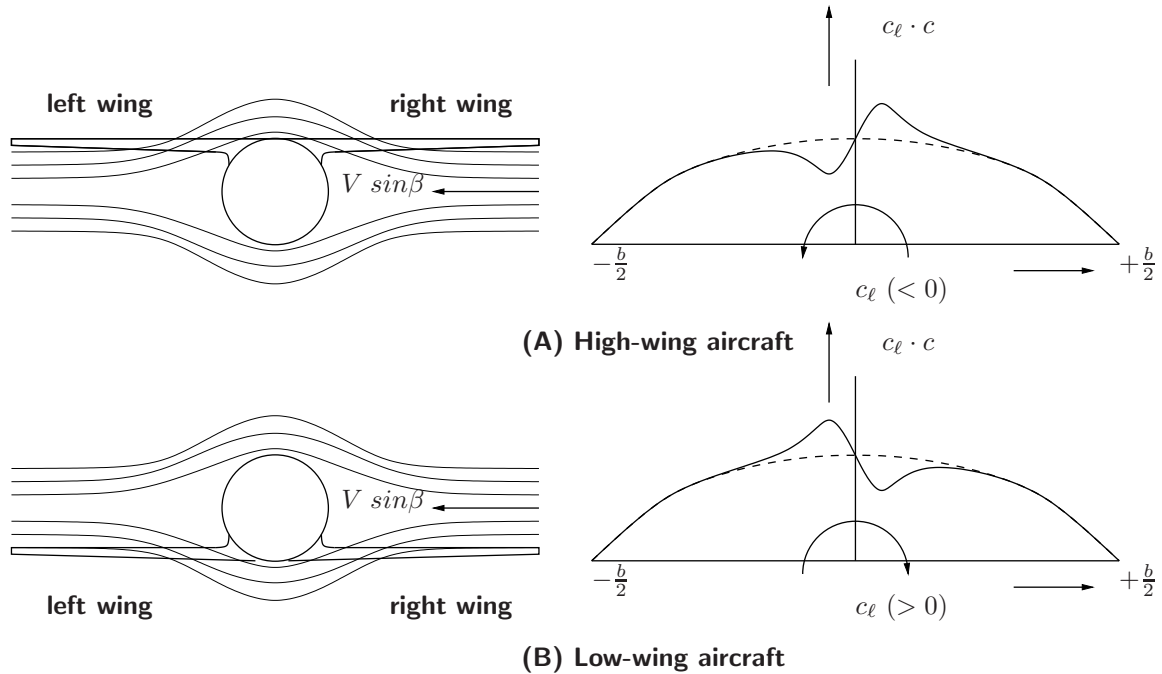


Figure 8-13: Origin of a rolling moment caused by wing-fuselage interactions in sideslipping flight

T_c and C_L . Deflection of the landing flaps will increase the effective angle of attack over the center part of the wing. It will further increase the effect of the slipstream on C_{ℓ_β} .

Using linearized potential flow theory (panel methods), C_ℓ as a function of β has been calculated for the Cessna Ce550 ‘Citation II’, see figure 8-14. The definition of the aircraft parts ‘wing’, ‘horizontal stabilizer’, ‘pylons’, ‘fuselage’, ‘vertical fin’ and ‘nacelles’ is given in figure 7-2. The main contributions to C_{ℓ_β} are from the vertical fin and the wing.

8-2-3 Stability derivative C_{n_β}

The stability derivative C_{n_β} is called the static directional, or weathercock, stability, as this derivative is geometrically directly comparable to the static longitudinal stability C_{m_α} .

For good control characteristics it is desirable that the angle of sideslip causes a moment about the top axis trying to reduce the sideslip. The desired sign of C_{n_β} is thus positive. The magnitude of C_{n_β} is determined by a small, positive contribution of the wing, an important destabilizing, negative contribution of the fuselage and a usually large stabilizing, positive contribution of the vertical tailplane, see figure 8-17. The contribution of the propulsion system may be either positive or negative.

The contribution to C_{n_β} of a wing without sweep is very small. The contribution of a swept back wing may be important especially at high C_L values due to the sideforce acting relatively far behind the center of gravity. This wing contribution may be calculated using the same references as for the determination of the contribution of the wing to C_{Y_β} .

The negative destabilizing contribution of the fuselage arises in a similar manner as the corresponding distribution of the fuselage to C_{m_α} in symmetric flight, see references [123, 2, 80, 3, 150, 22, 137].

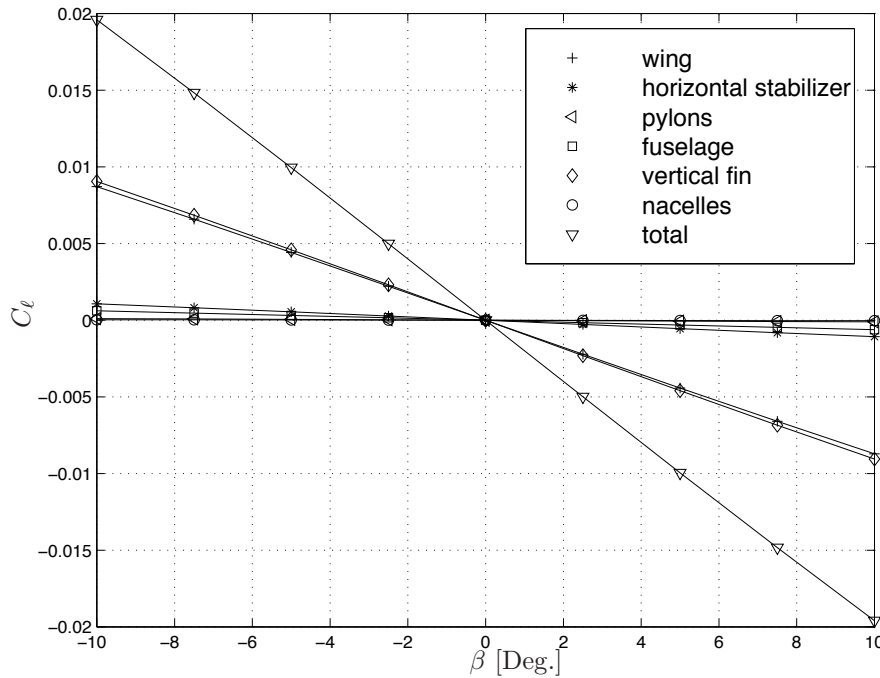


Figure 8-14: Aerodynamic moment coefficient C_ℓ as a function of β for the Cessna Ce550 'Citation II', $\alpha = 0^\circ$

The contribution of the vertical tailplane to C_{n_β} , expressed in the stability reference frame, follows from figure 8-15,

$$(C_{n_\beta})_v = - (C_{Y_\beta})_v \left(\frac{z_v - z_{c.g.}}{b} \sin \alpha_0 + \frac{x_v - x_{c.g.}}{b} \cos \alpha_0 \right) \quad (8-16)$$

In this expression $(C_{Y_\beta})_v$ is given by equation (8-8).

At small angles of attack with $x_v - x_{c.g.} = \ell_v$ follows from equations (8-8) and (8-16),

$$(C_{n_\beta})_v = C_{Y_{v_\alpha}} \left(1 - \frac{d\sigma}{d\beta} \right) \left(\frac{V_v}{V} \right)^2 \frac{S_v l_v}{Sb} \quad (8-17)$$

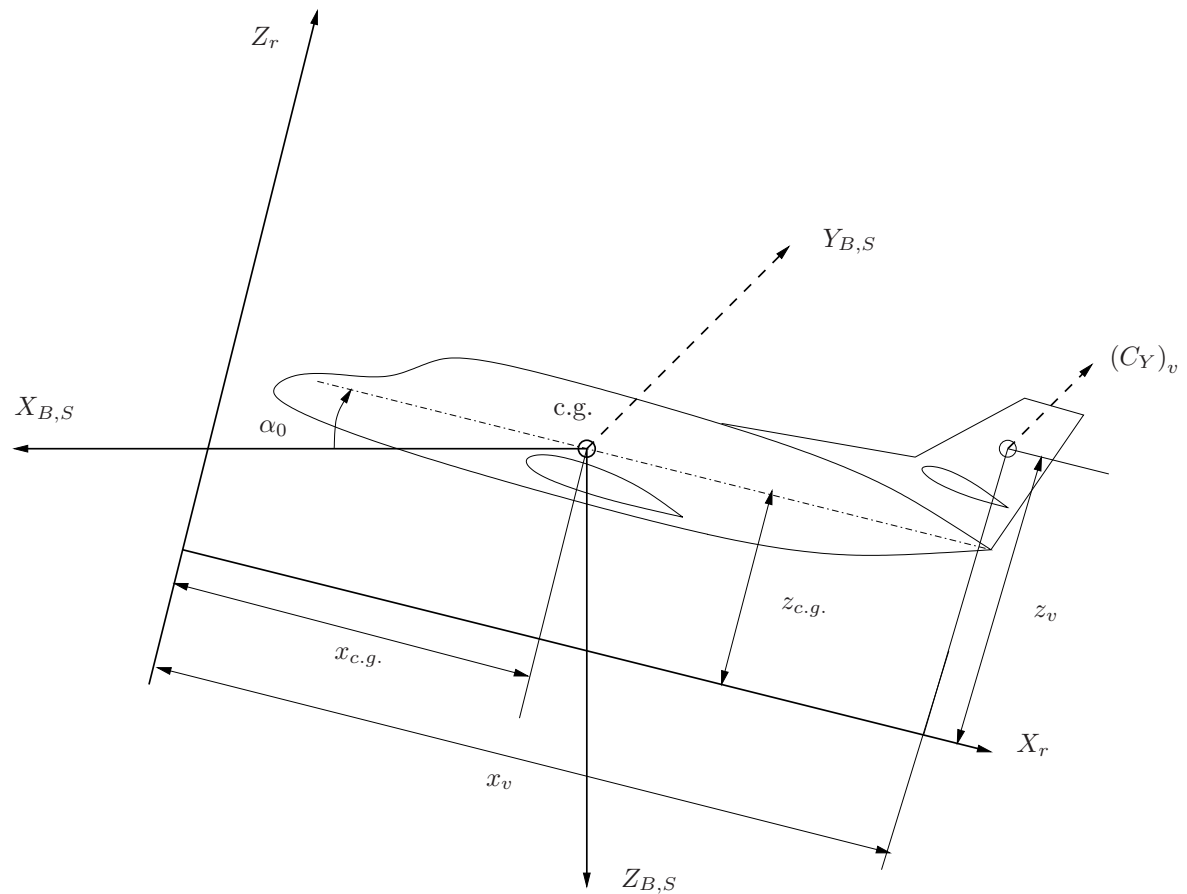
The corresponding expression for the horizontal tailplane is, see equation (10-7),

$$(C_{m_\alpha})_h = -C_{N_{h_\alpha}} \left(1 - \frac{d\varepsilon}{d\alpha} \right) \left(\frac{V_h}{V} \right)^2 \frac{S_h l_h}{S_c}$$

For the sake of simplicity l_v is often taken as the distance between the $\frac{1}{4}$ -chord points on the m.a.c.'s of the wing and the vertical tailplane.

Calculation methods to determine $C_{Y_{v_\alpha}}$ have been mentioned already in section 8-2.

The calculation of the sidewash gives rise to considerable difficulties in practice as the flow is strongly determined by the interaction between flow around the fuselage, the wing and the tailplane. The flow around an isolated fuselage can be presented schematically as in figure 8-18. A positive angle of sideslip causes a negative induced sidewash, or $\frac{d\sigma}{d\beta} < 0$.



$$(z_v - z_{c,g.}) \sin \alpha_0$$

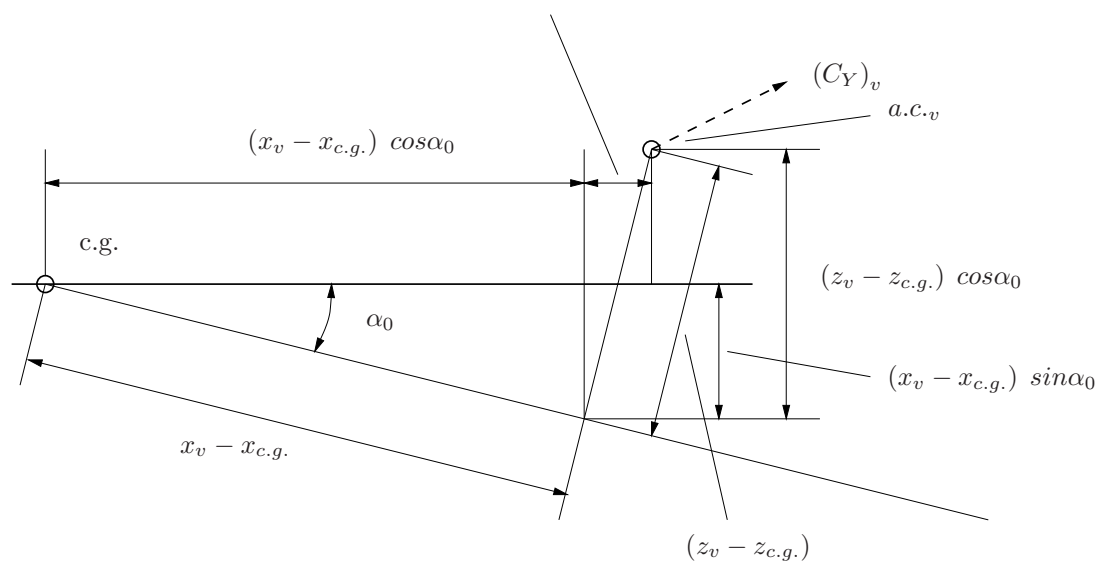
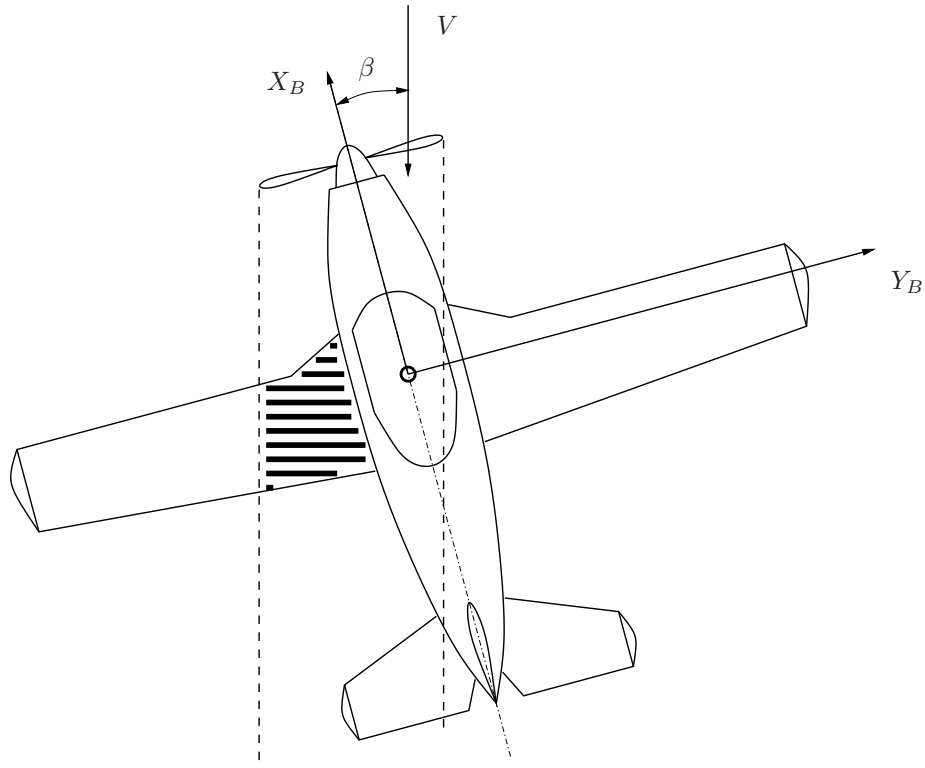
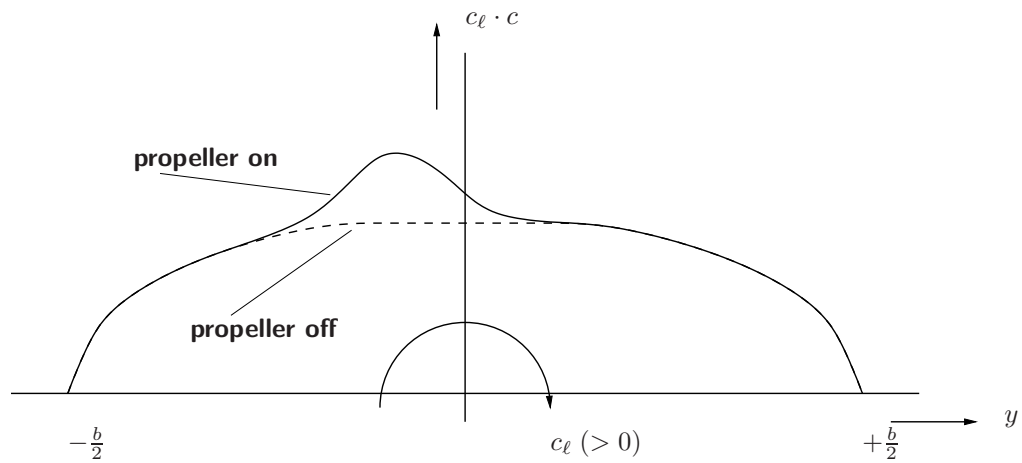


Figure 8-15: The position of the point of action of $(C_Y)_v$ relative to the X - and Z -axis in the stability reference frame



(A) The part of the wing submerged in the slipstream



(B) The change in lift distribution

Figure 8-16: The contribution of the slipstream to C_{ℓ_β}

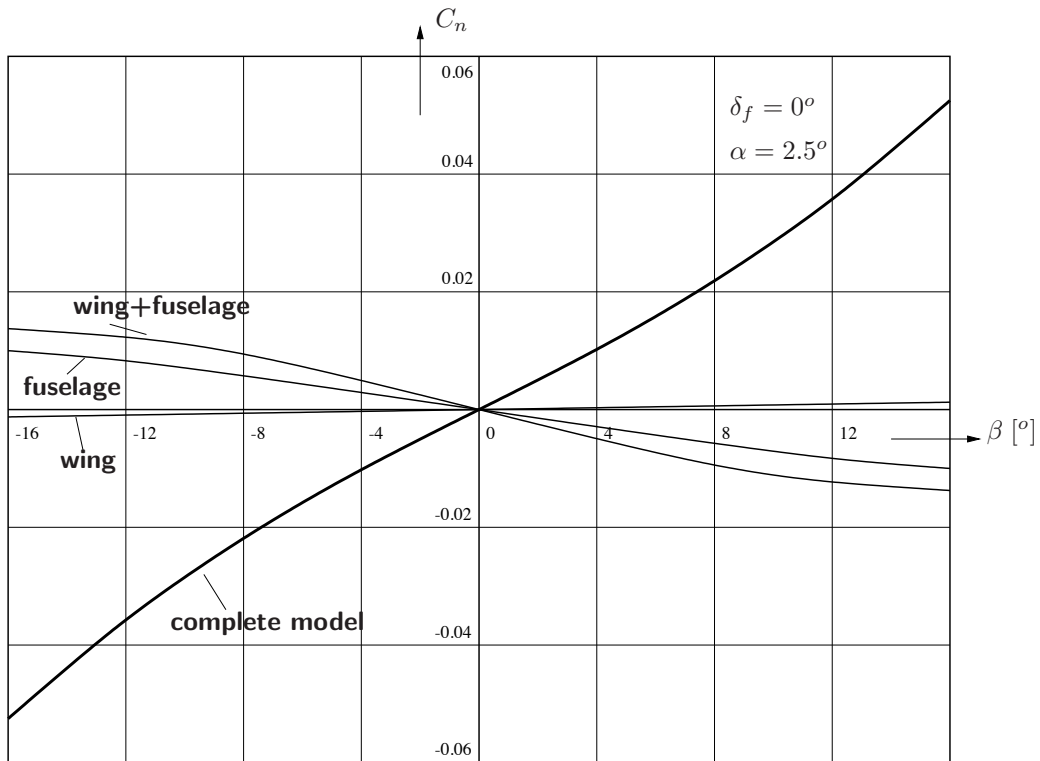


Figure 8-17: C_n as a function of β measured on a model of the Fokker F-27 in gliding flight (from references [159, 161, 24])

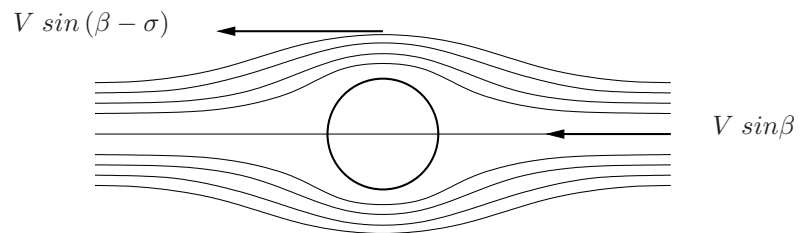
Another numerical example of the flow around a complete aircraft configuration in side-slip is given in figure 8-19. It is obvious from this figure that the determination of σ at the vertical tailplane will be difficult because of strong interactions between the fuselage, vertical tailplane and nacelles. Also in this figure speedbars have been added to give an impression of the magnitude of the local airspeed along the calculated particle traces. Note that the characteristic flow over the top of a fuselage in sideslip is given in figure 8-18, see also the examples given in figures 8-20 where particle traces have been given over the top of a fuselage of a large 4-engined transport aircraft in sideslip.

Earlier in section 8-2 the change in lift distribution in sideslip due to the presence of the fuselage was discussed. The extra lift distribution caused by the interaction also induces a side-wash at the location of the vertical tailplane. The difference in lift on the two halves of the wing causes a difference between the downwash at either side of the fuselage, see subfigures a and b of figure 8-21.

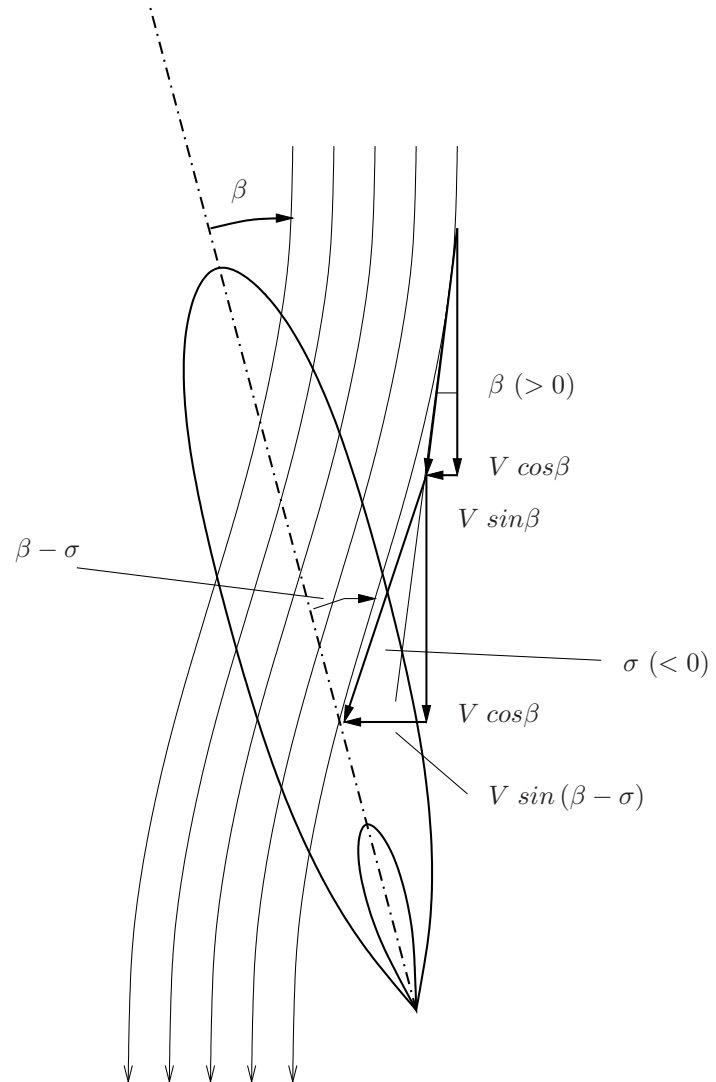
The downwash pattern is displaced laterally along with the main flow, over an angle β with the X -axis, see subfigure b of figure 8-21. The main effect, however, is a circulation about the fuselage. If a low wing aircraft sideslips to the right, the circulation is counter-clockwise, subfigure c of figure 8-21. This circulation generates at the vertical tailplane an extra negative sidewash. This induced cross-flow is stabilizing, as can also be seen from equation (8-17), $\Delta \frac{d\sigma}{d\beta} < 0$.

For a high wing aircraft in sideslip to the right, the sidewash is positive, the influence of the wing-fuselage interaction on $(C_{n_\beta})_v$ is thus seen to be destabilizing, $\Delta \frac{d\sigma}{d\beta} > 0$.

Figure 8-22 shows the results of measurements of the sidewash and the static directional stability illustrating the above. From this figure it can also be seen that the sidewash is greatly influenced by the presence of the horizontal tailplane. A low horizontal tailplane acts as an end plate to the vertical tailplane. This reduces the sidewash considerably. An accurate calculation of the



(A) Velocity components in a plane perpendicular to the fuselage axes



(B) The flow around the fuselage and the vertical tailplane

Figure 8-18: The sidewash induced by the fuselage at the vertical tailplane

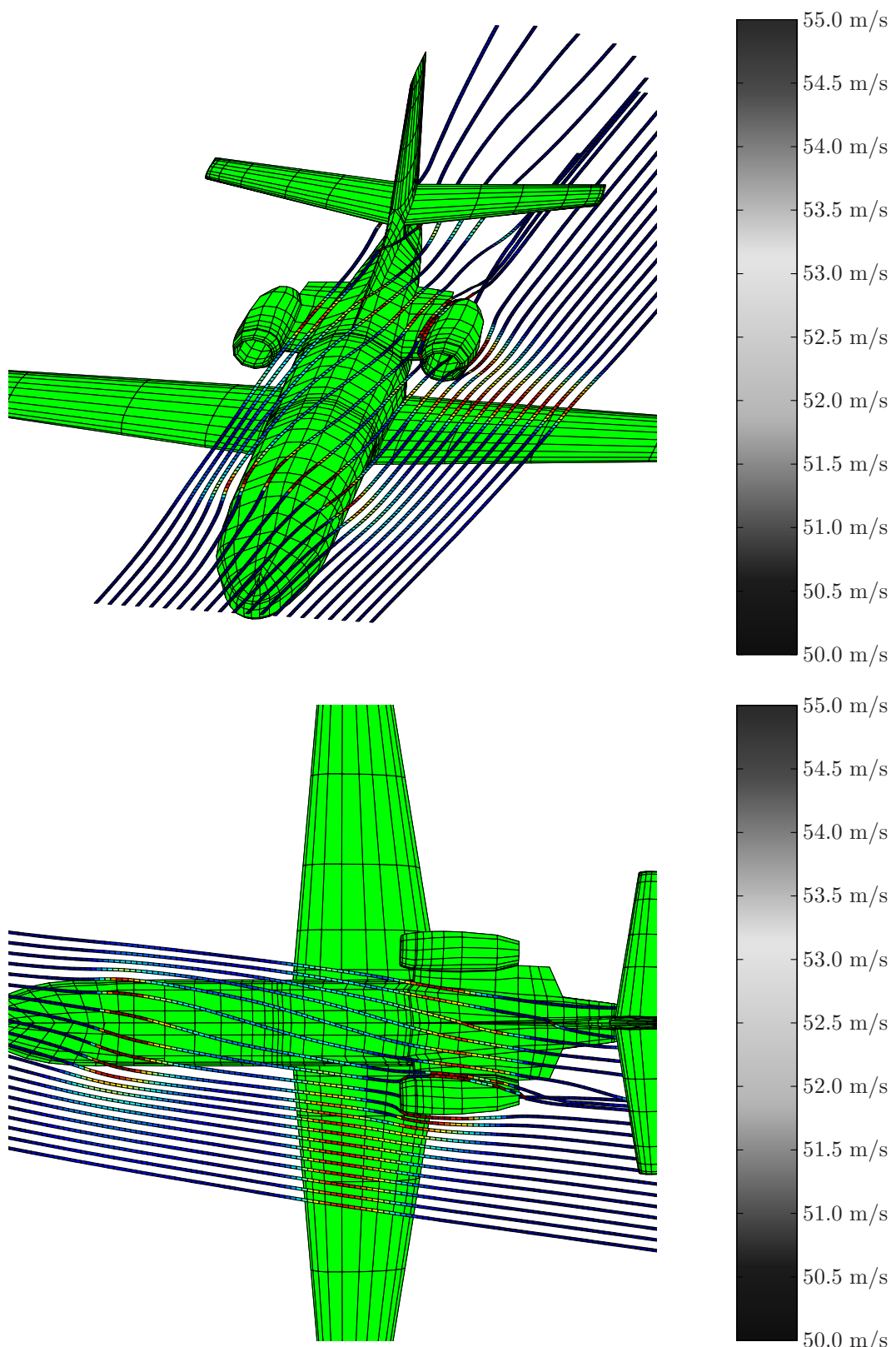


Figure 8-19: Calculated particle traces around the fuselage of the Cessna Ce550 'Citation II', sideslipping flight $\beta = 10^\circ$, $\alpha = 0^\circ$ (note: the speedbar is related to the magnitude of the airflow's velocity along the calculated particle traces)

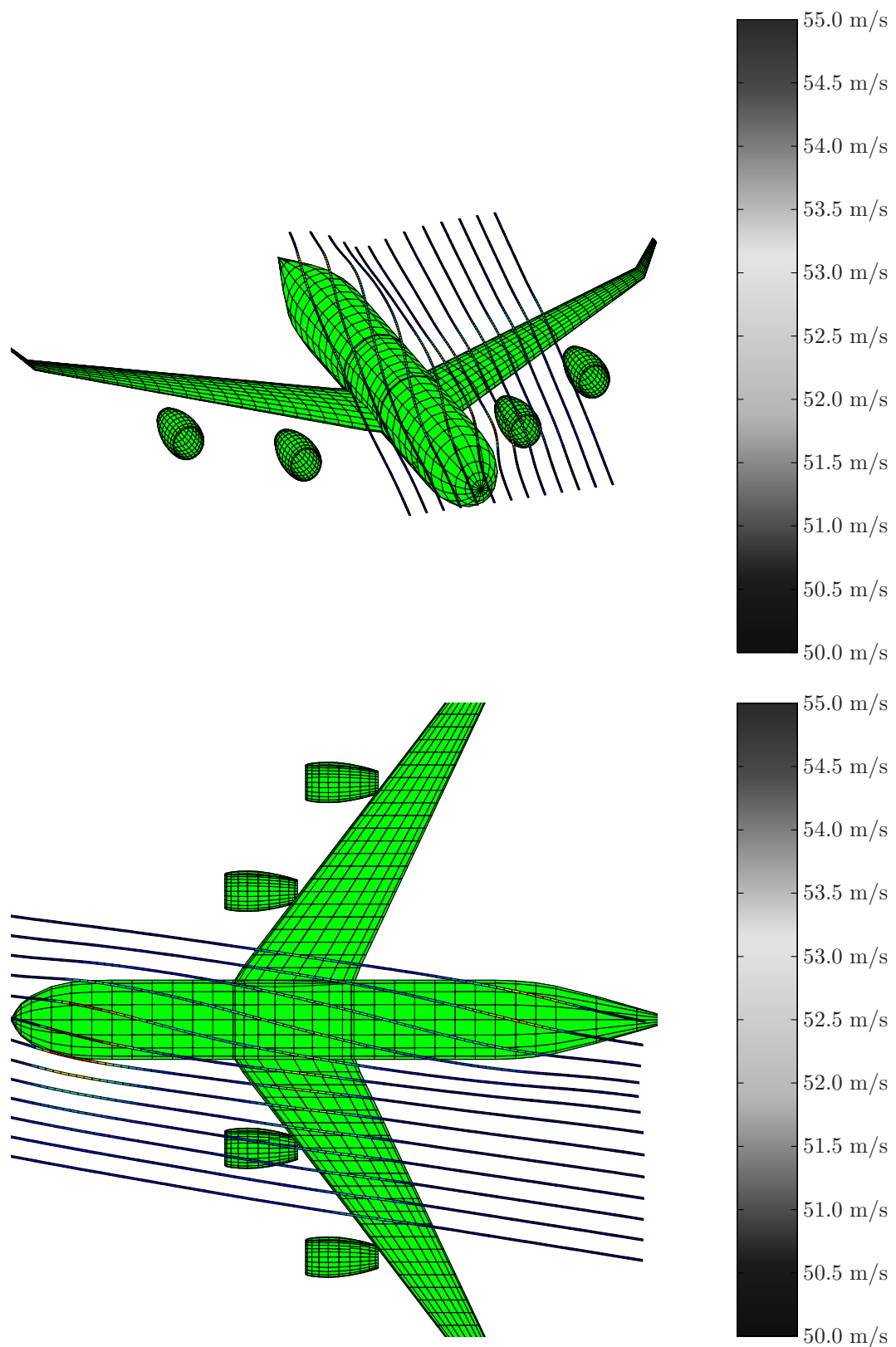


Figure 8-20: Calculated particle traces around the fuselage of a large 4-engined transport aircraft, sideslipping flight $\beta = 10^\circ$, $\alpha = 0^\circ$ (note: the speedbar is related to the magnitude of the airflow's velocity along the calculated particle traces)

average sidewash σ , or $\frac{d\sigma}{d\beta}$, at the vertical tailplane is not well possible, although references [83, 85, 86, 87, 96, 28] give calculation methods. In many cases results of systematic measurements on similar configurations are used to determine $\frac{d\sigma}{d\beta}$.

The contribution of the propulsion system to C_{n_β} is caused by the lateral force acting on the propeller or the engine inlet in cross-flow, see figure 8-23. If the propeller or the engine inlet is situated forward of the center of gravity this contribution is destabilizing. For propeller-driven aircraft the increased dynamic pressure in the slipstream causes a higher static directional stability, if the vertical tailplane is placed in the slipstream.

Using linearized potential flow theory (panel methods), C_n as a function of β has been calculated for the Cessna Ce550 ‘Citation II’, see figure 8-24. The definition of the aircraft parts ‘wing’, ‘horizontal stabilizer’, ‘pylons’, ‘fuselage’, ‘vertical fin’ and ‘nacelles’ is given in figure 7-2. The main contributions to C_{n_β} are from the fuselage (destabilizing contribution) and the vertical fin (stabilizing contribution).

8-2-4 Stability derivative C_{n_β}

The stability derivative C_{n_β} is a measure of the moment about the top axis caused during a change in the angle of sideslip when the aircraft executes an accelerated motion along the Y -axis. The derivative C_{n_β} corresponds entirely to the stability derivative C_{m_α} for the symmetric motions.

After a sudden change in the angle of sideslip a short interval passes before the changed sidewash, caused by the wing-fuselage interaction, has reached the vertical tailplane. As a consequence, the change of C_n with β does not occur as sudden as the change in β . This phenomenon is described using the stability derivative C_{n_β} .

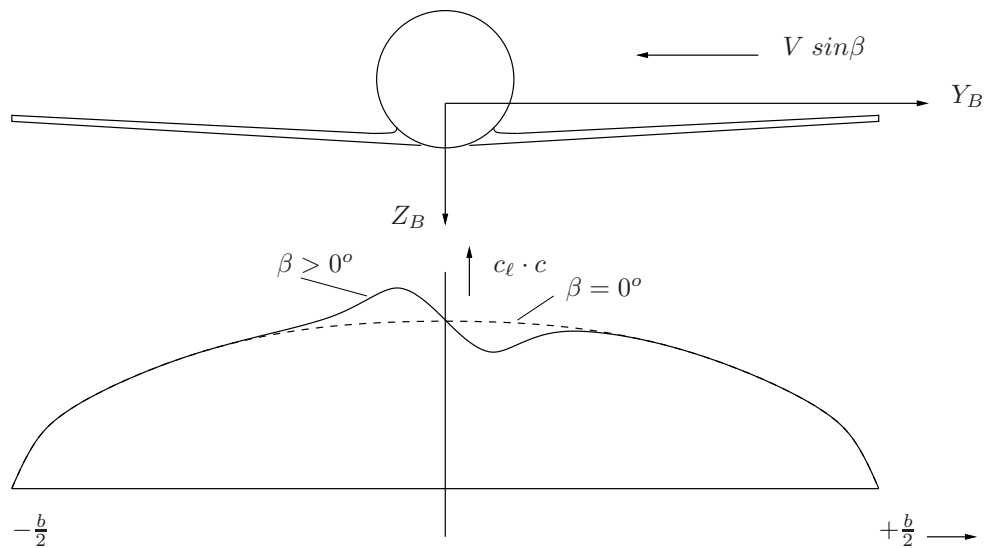
For aircraft with a straight wing of sufficiently large aspect ratio (e.g. $A > 4$ to 5), C_{n_β} is usually neglected. Also in the discussion of the dynamic lateral stability, C_{n_β} will not be considered. For aircraft having swept wings of low aspect ratio, C_{n_β} has to be determined using the results of systematic measurements on oscillating models, see for instance reference [59].

8-2-5 Stability derivative $C_{m_{\beta^2}}$

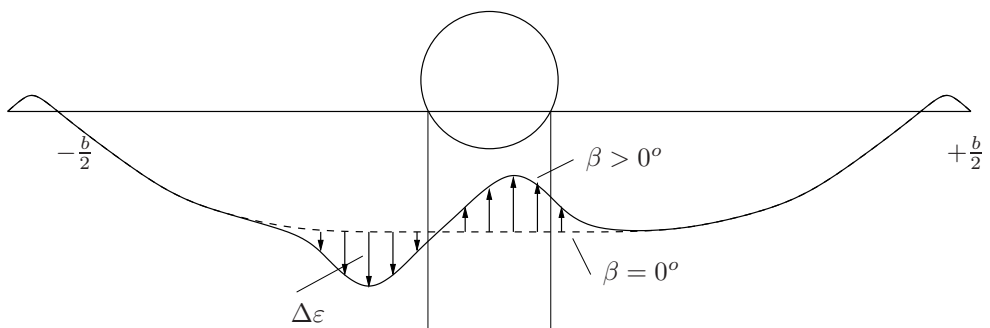
A sideslip can cause a pitching moment that may be considerable, especially at large angles of sideslip, see figure 8-25. It can be seen from this figure, as follows also from considerations of symmetry, that the change in pitching moment has the same sign for both positive and negative angles of sideslip. The stability derivative expressing the pitching moment due to sideslip is, therefore, written as $C_{m_{\beta^2}}$.

This moment is caused by the wing-fuselage interaction and the interaction between the fuselage and the tailplanes already discussed in relation to C_{n_β} . Reference [84] discusses the influence of wing-fuselage interactions on the pitching moment for combinations of a fuselage with a straight wing and a swept wing in a sideslip. Here also the vertical position of the wing relative to the fuselage is important.

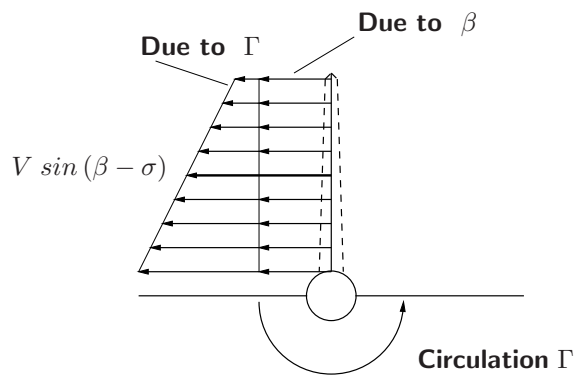
Especially at large angles of sideslip the change in pitching moment is determined to a large extent by the contribution of the horizontal tailplane, see references [135] and figure 8-25. The tailplane is located in the downwash field behind the wing, modified by the wing-fuselage interaction. If the tailplane is mounted low on the fuselage the field of flow is modified additionally by the fuselage



(A) The lift distribution of a low-wing aircraft sideslipping to the right



(B) The change in downwash behind the wing and fuselage



(C) The change in sidewash at the vertical tailplane

Figure 8-21: The effect of wing-fuselage interactions on the sidewash at the vertical tailplane of a low-wing aircraft in sideslipping flight

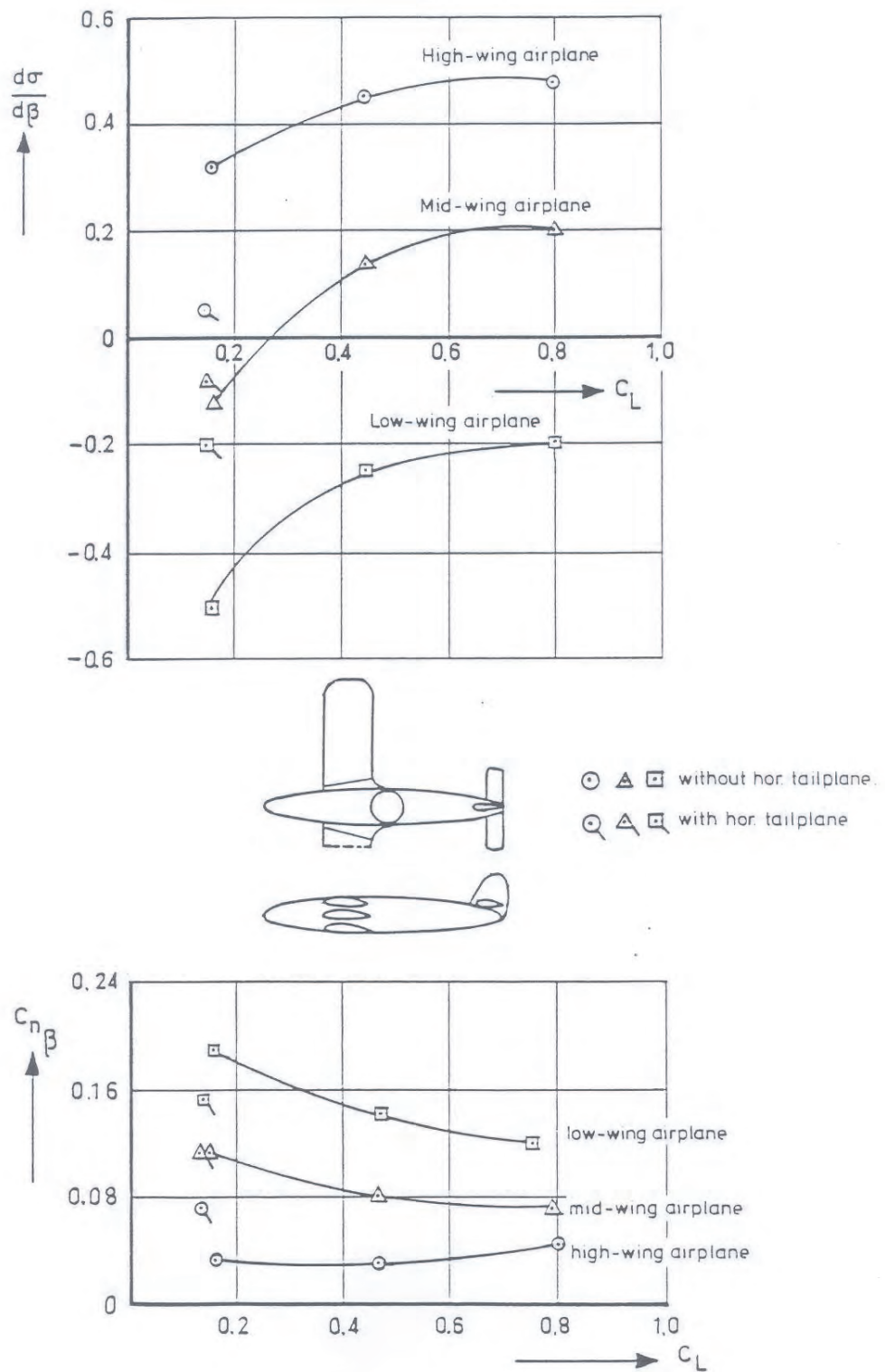


Figure 8-22: The effect of wing-fuselage interactions on the sidewash at the tailplanes and the derivative $C_{n\beta}$ (from reference [153])

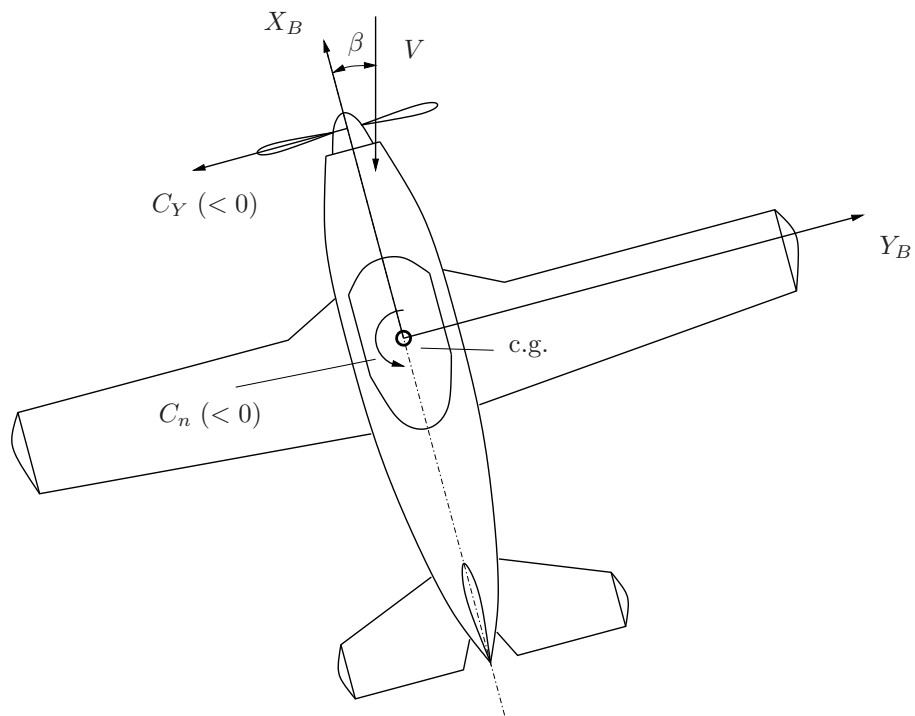


Figure 8-23: The contribution of the sideforce on the propeller to $C_{n\beta}$

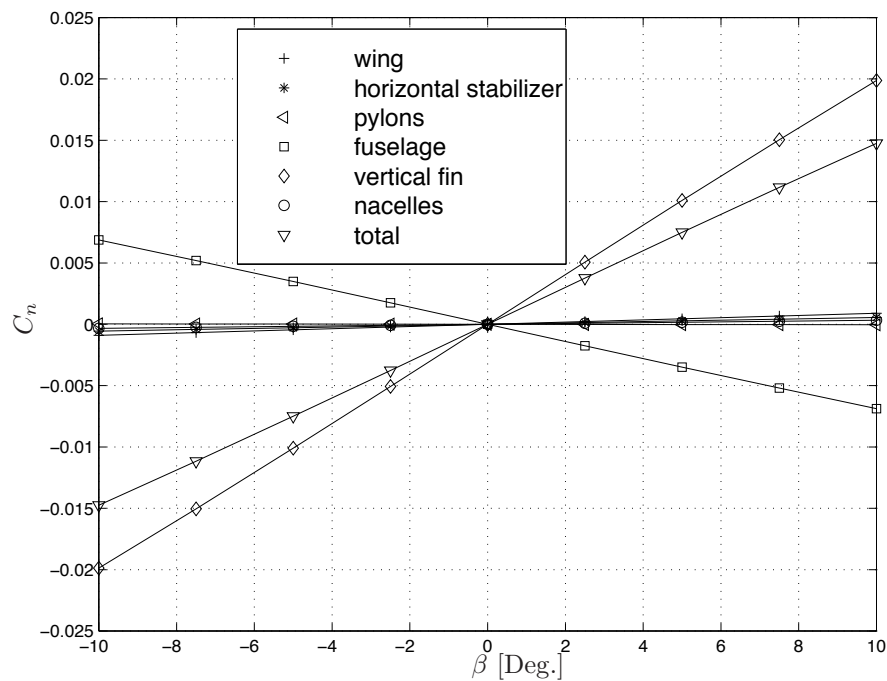


Figure 8-24: Aerodynamic moment coefficient C_n as a function of β for the Cessna Ce550 'Citation II', $\alpha = 0^\circ$

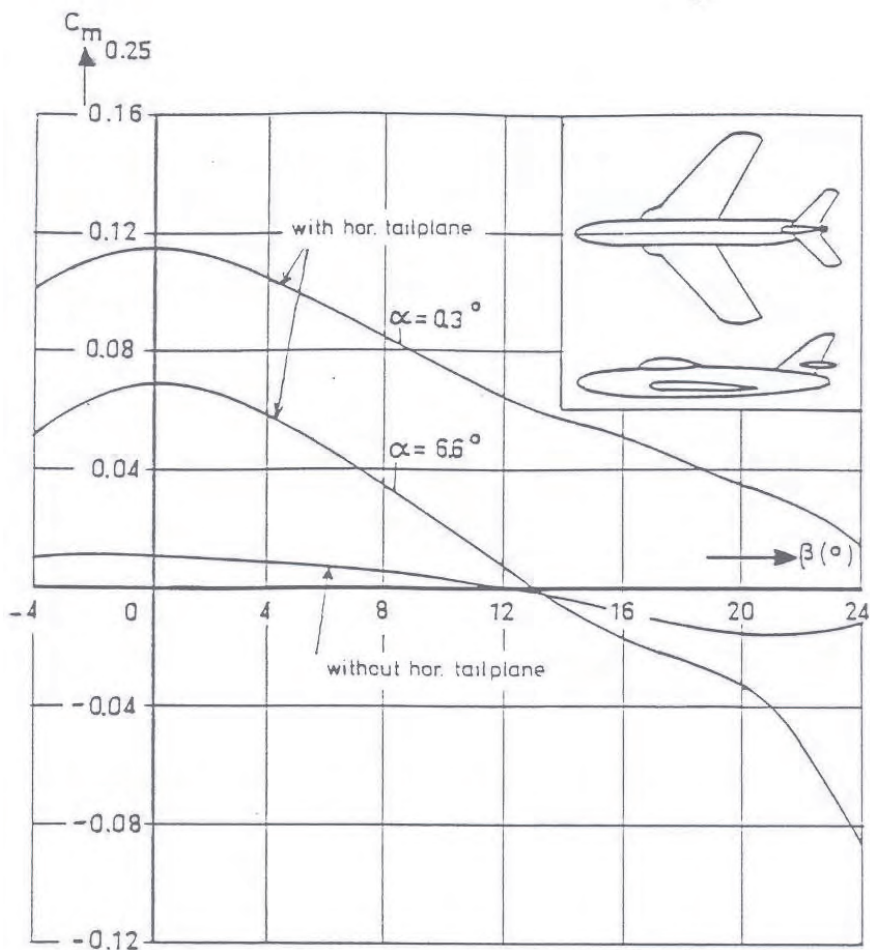


Figure 8-25: The pitching moment as a function of sideslip angle (from reference [135])

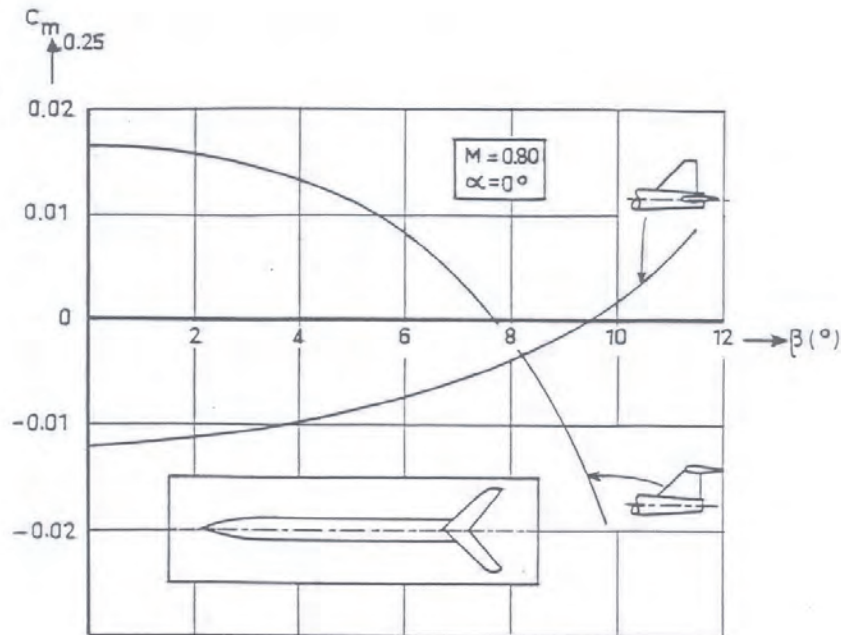


Figure 8-26: The influence of the vertical position of the horizontal tailplane on the variation of C_m in sideslipping flight for a fuselage with tailplanes (from reference [135])

and the vertical tailplane. The influence of the vertical position of the horizontal tailplane on C_m in sideslip is presented in figure 8-26. For a quantitative determination of $C_{m\beta^2}$ the designer has to rely on wind tunnel measurements and/or CFD simulations.

8-3 Stability derivatives with respect to roll rate

If the aircraft rolls about the X_B -axis, the geometric angle of attack of the various wing and tailplane chords varies proportional to the rolling-velocity p and to the distance of the chords to the X_B -axis, see figure 8-27. For a wing chord at a distance y from the plane of symmetry, the change in the geometric angle of attack is,

$$\Delta\alpha = \frac{p y}{V} = \frac{pb}{2V} \frac{y}{b/2} \quad (8-18)$$

Here y is measured in the system of aircraft body axes. For the sake of simplicity the aircraft c.g. is assumed to lie in the plane of symmetry. The non-dimensional rolling velocity $\frac{pb}{2V}$ is thus equal to the change in geometric angle of attack at the wing tip where $y = b/2$. This is also the helix angle of the helix described by the wing tip in rolling flight, which is why the rolling velocity is made non-dimensional by multiplying with $\frac{b}{2V}$.

8-3-1 Stability derivative C_{Y_p}

The derivative C_{Y_p} is always relatively small and is very often neglected. Only if the wing has a large sweep angle, or if a relatively large vertical tailplane is used, this derivative has to be taken into account. The origin of the contribution from a swept wing to C_{Y_p} will be explained when discussing $(C_{n_p})_w$. For swept back wings $(C_{n_p})_w$ is negative.

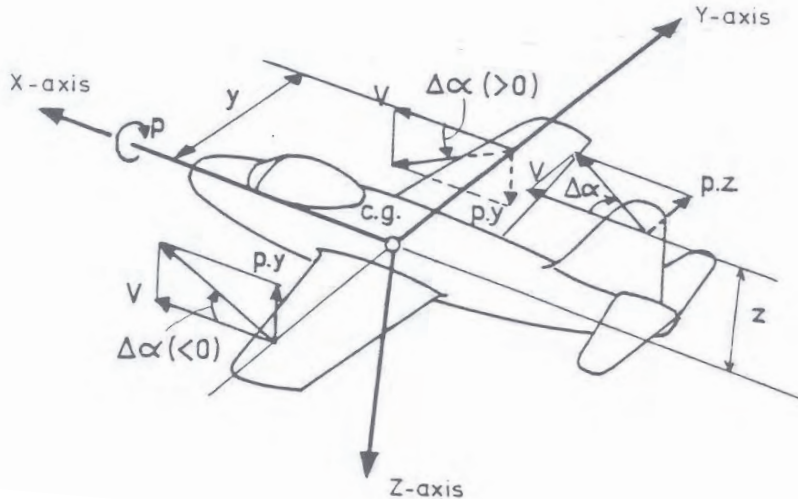


Figure 8-27: The variation of the local geometric angle of attack at the wing and the tailplane of a rolling aircraft

The contribution of the vertical tailplane to C_{Y_p} is caused by the change in angle of attack experienced by the vertical tailplane in rolling flight. A positive rolling velocity gives rise to a negative lateral force,

$$Y_v = (C_{Y_p})_v \frac{pb}{2V} \frac{1}{2} \rho V^2 S \quad (8-19)$$

Where $(C_{Y_p})_v$ is thus negative. In the determination of $(C_{Y_p})_v$ the sidewash at the vertical tailplane, induced by the rolling velocity has to be taken into account. This subject will be further discussed when dealing with C_{ℓ_p} . Calculation methods can be found in references [95, 31, 135, 114, 115].

Using linearized potential flow theory (panel methods), C_Y as a function of $\frac{pb}{2V}$ has been calculated for the Cessna Ce550 ‘Citation II’, see figure 8-28. The definition of the aircraft parts ‘wing’, ‘horizontal stabilizer’, ‘pylons’, ‘fuselage’, ‘vertical fin’ and ‘nacelles’ is given in figure 7-2. The main contributions to C_{Y_p} are from the wing, vertical fin and horizontal tailplane. The stability derivative C_{Y_p} is usually very small.

8-3-2 Stability derivative C_{ℓ_p}

The stability derivative C_{ℓ_p} is a measure of the moment about the X_B -axis due to rolling about this axis,

$$L = C_{\ell_p} \frac{pb}{2V} \frac{1}{2} \rho V^2 S b \quad (8-20)$$

In all normal flight conditions this moment opposes the rolling, trying to slow the motion down. C_{ℓ_p} is normally negative and a measure for the roll damping.

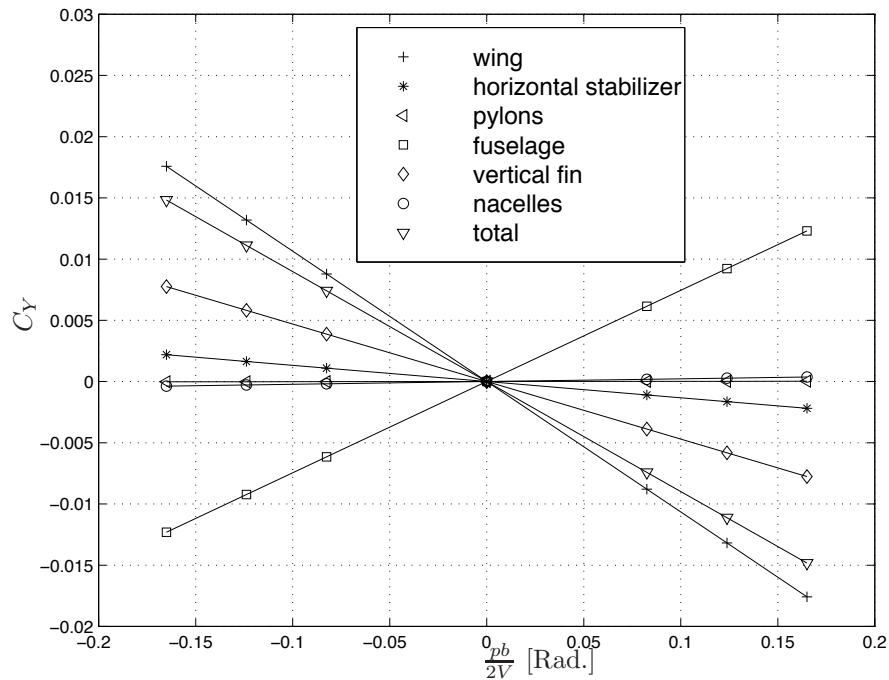
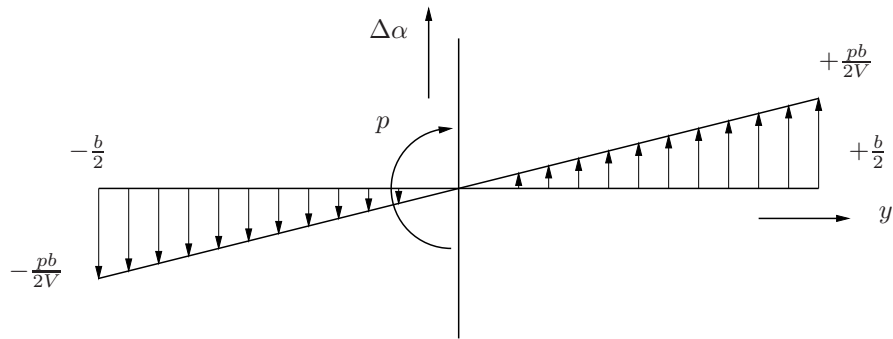
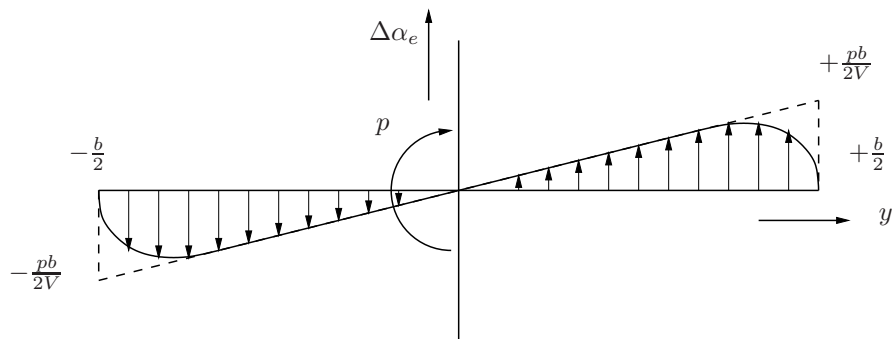


Figure 8-28: Aerodynamic force coefficient C_Y as a function of $\frac{pb}{2V}$ for the Cessna Ce550 'Citation II', $\alpha = 0^\circ$



(A) The variation in geometric angle of attack



(B) The variation in effective angle of attack

Figure 8-29: The variation of the local geometric and effective angle of attack along the span of a rolling wing

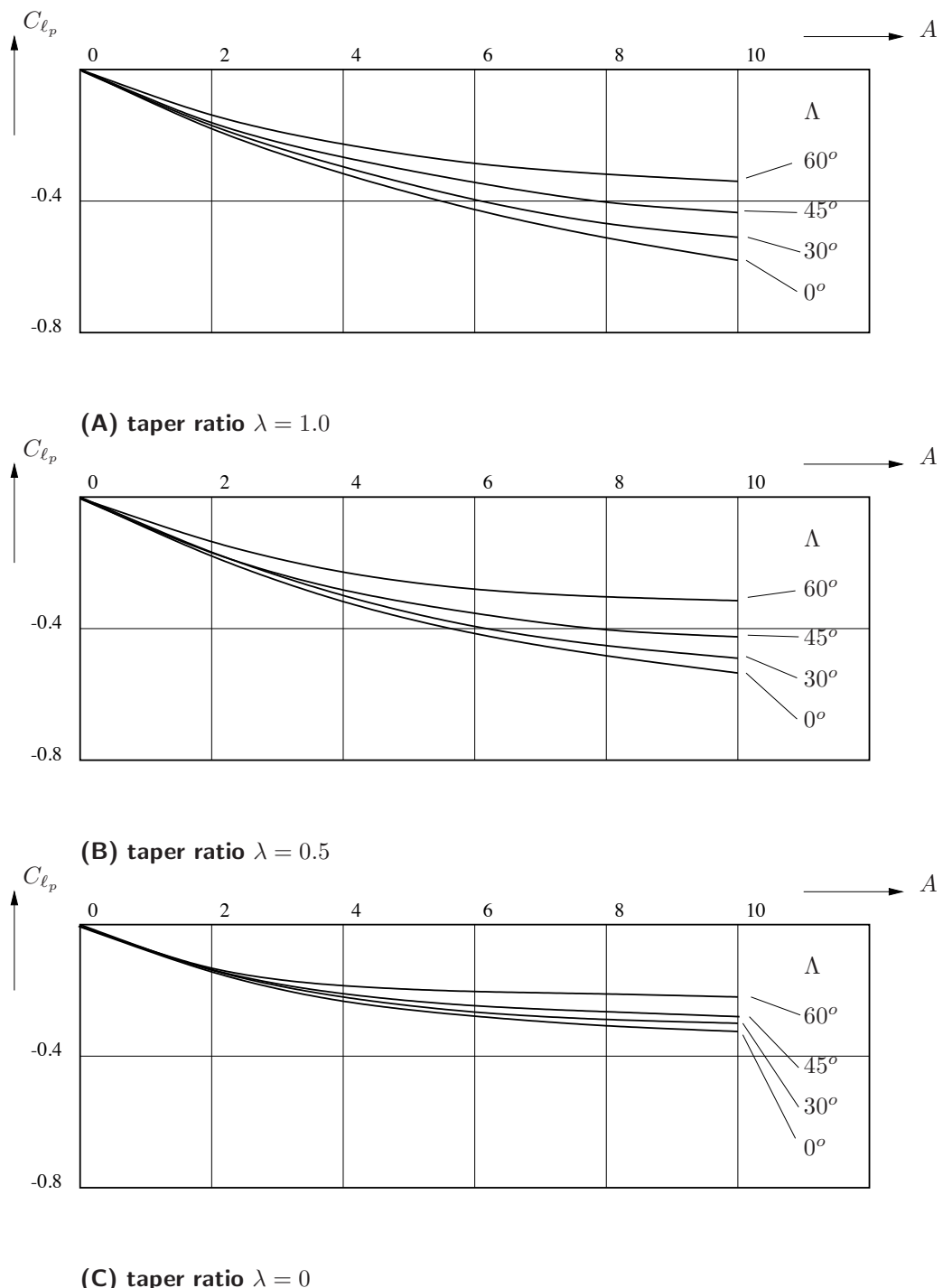


Figure 8-30: The roll-damping as a function of aspect ratio and sweep for various wing taper ratio's (from reference [34])

The dominant contribution to C_{ℓ_p} is generated by the wing. In some cases, the contribution from the tailplanes has to be taken into account as well. The contribution due to the fuselage, the wing-fuselage interaction and the propeller are usually negligible.

The contribution of the wing is caused by the change in geometric angle of attack and the resulting change in effective angle of attack along the wing span, see figure 8-29. An additional anti-symmetric lift distribution is generated causing a rolling moment opposite to the sense of the rotation. This has a damping effect on the rotation. Calculated values of C_{ℓ_p} for various wing planforms have been collected in figure 8-30. It can be seen that the roll damping of the wing increases in the absolute sense with the taper ratio, λ , and aspect ratio, A . The damping decreases with increasing wing sweep.

If the airflow over the wing remains attached, the wing contribution to C_{ℓ_p} is independent of C_L but proportional to the lift gradient $C_{L\alpha}$. If the lift gradient decreases at large angles of attack due to flow separation, C_{ℓ_p} decreases in the absolute sense as well. At very large angles of attack the down going wing may stall, causing a considerable reduction in wing damping. It is even possible that the influence of the loss in lift caused by the stall of the down going wing dominates the influence of the decrease in lift due to smaller angle of attack of the up going wing. In that case C_{ℓ_p} may become positive.

The lift distribution in rolling flight can be calculated using references [25, 45]. At subsonic speeds the wing contribution to C_{ℓ_p} can be determined with references [10, 74, 167, 133, 134, 66]. Reference [118] enables the wing contribution to be determined for angles of attack where the relation between c_ℓ and α of airfoils is non-linear. For supersonic speeds references [10, 74, 89, 88, 71] are available.

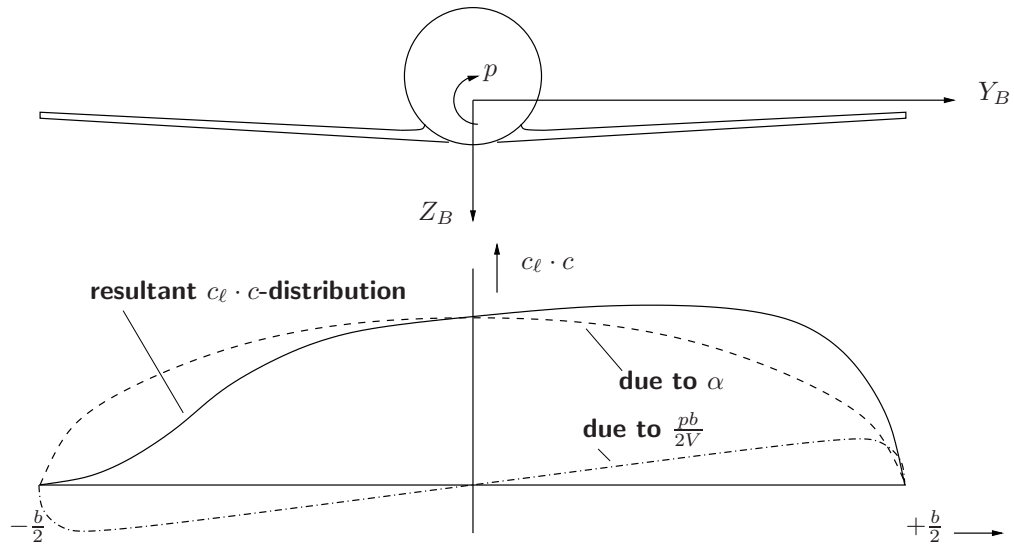
The contribution of the horizontal and the vertical tailplane to C_{ℓ_p} , caused by the same mechanism as the wing contribution, see figure 8-27, is generally much smaller than the wing contribution. Due to the smaller span of the tailplanes the maximum change in angle of attack is smaller than that of the wing.

A further decrease in the change of angle of attack at the horizontal and vertical tailplanes is caused by the change in downwash behind the rolling wing. Behind the downgoing wing the downwash increases, it decreases behind the upgoing wing, relative to non-rolling flight, see figure 8-31. This extra downwash distribution causes a circulation as depicted in subfigure c of figure 8-31. This downwash decreases the change in angle of attack along the span of the tailplanes. A further study of this phenomenon can be found in reference [95]. For conventional, subsonic aircraft the contributions of the tailplanes to C_{ℓ_p} can usually be neglected. Modern fighter aircraft and V/STOL-aircraft usually have relatively large tailplanes. Calculation of the tailplane contributions to C_{ℓ_p} for such aircraft is possible using references [141, 31, 29, 114, 115].

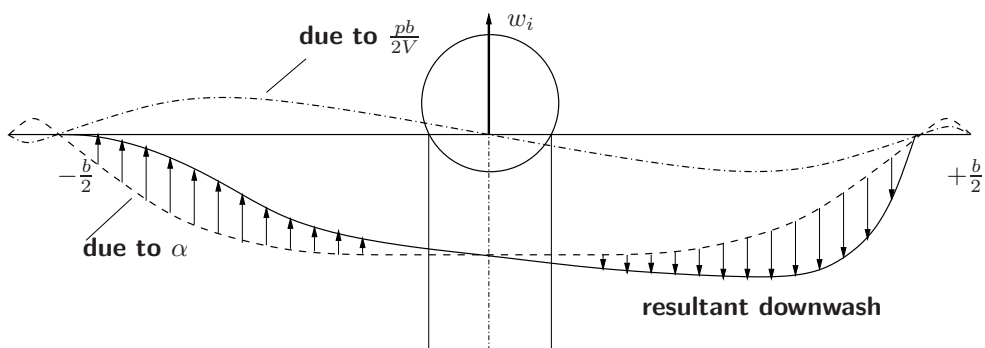
Using linearized potential flow theory (panel methods), C_ℓ as a function of $\frac{pb}{2V}$ has been calculated for the Cessna Ce550 ‘Citation II’, see figure 8-32. The definition of the aircraft parts ‘wing’, ‘horizontal stabilizer’, ‘pylons’, ‘fuselage’, ‘vertical fin’ and ‘nacelles’ is given in figure 7-2. The main contributions to C_{ℓ_p} is from the wing. The wing tries to damp the rolling motion.

8-3-3 Stability derivative C_{n_p}

This derivative is determined mainly by the contribution of the wing. Only a relatively large vertical tailplane produces a non-negligible contribution to C_{n_p} . Under normal conditions C_{n_p} is



(A) The change in lift distribution on a rolling wing



(B) The change in downwash behind a rolling wing

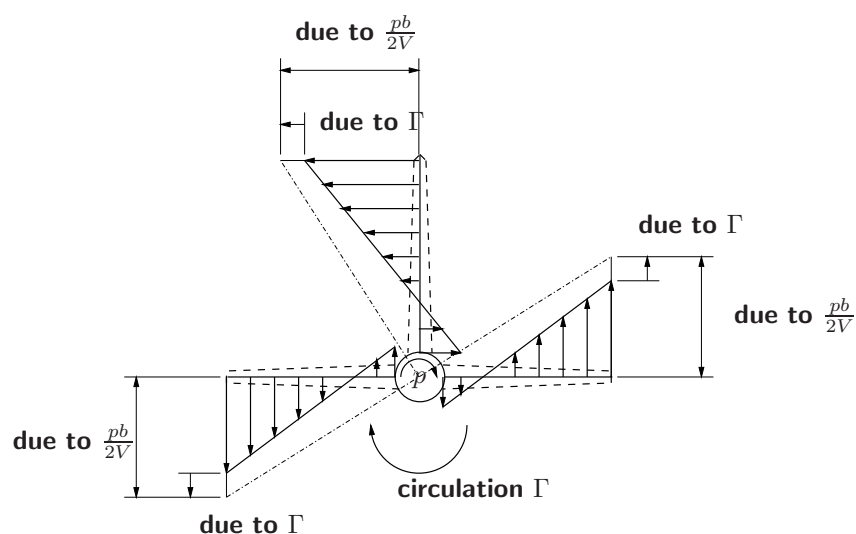
(C) The flow at the horizontal and vertical tailplanes due to p and Γ

Figure 8-31: The flow at the tailplanes of a rolling aircraft

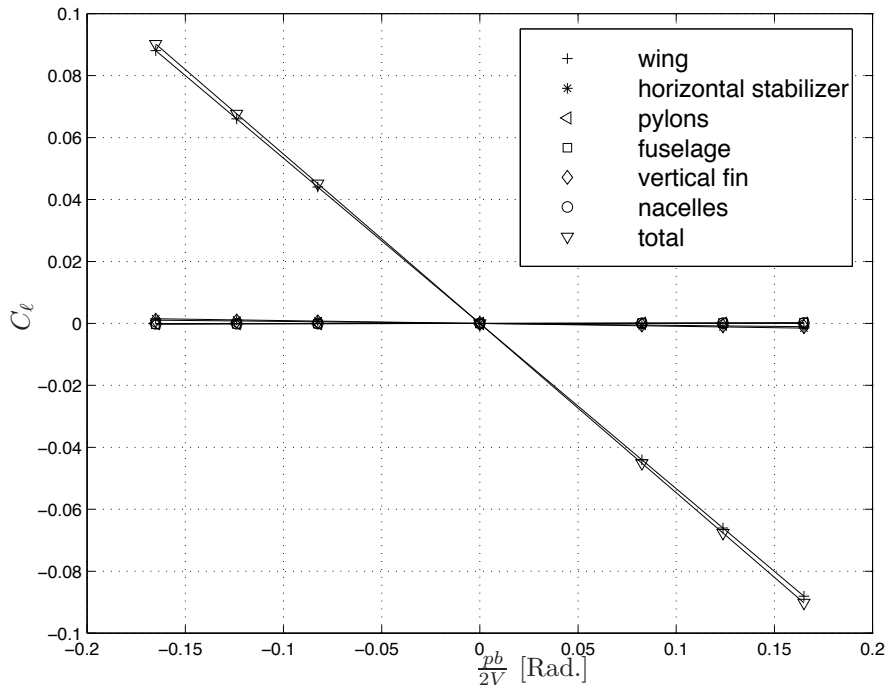


Figure 8-32: Aerodynamic moment coefficient C_ℓ as a function of $\frac{pb}{2V}$ for the Cessna Ce550 ‘Citation II’, $\alpha = 0^\circ$

negative.

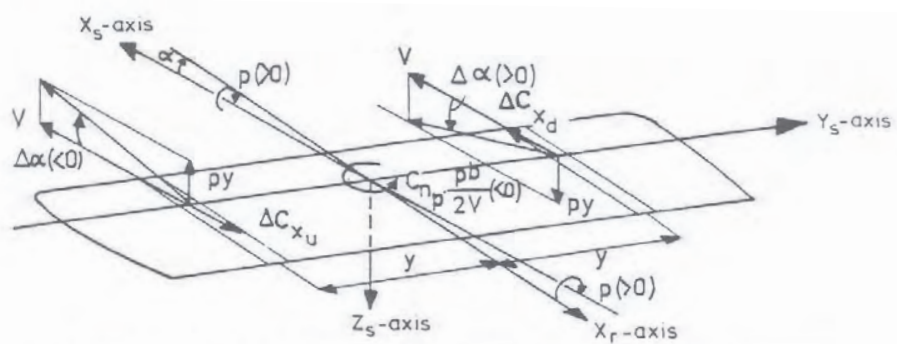
The generation of the wing’s contribution to C_{n_p} is illustrated in figure 8-33. In rolling flight an extra force in X_B -direction acts on each section of the wing. Since the local angle of attack varies along the wing span, it is essential to study the distribution of this extra force in the stability reference frame. The axes of the reference frame have a fixed direction relative to the aircraft. In this reference frame the down going wing experiences an extra forward force due to the increased angle of attack. The up going wing experiences an extra longitudinal force pointing backwards. As a result, a positive rolling velocity causes a negative yawing moment,

$$N = (C_{n_p})_w \frac{pb}{2V} \frac{1}{2} \rho V^2 S b \quad (8-21)$$

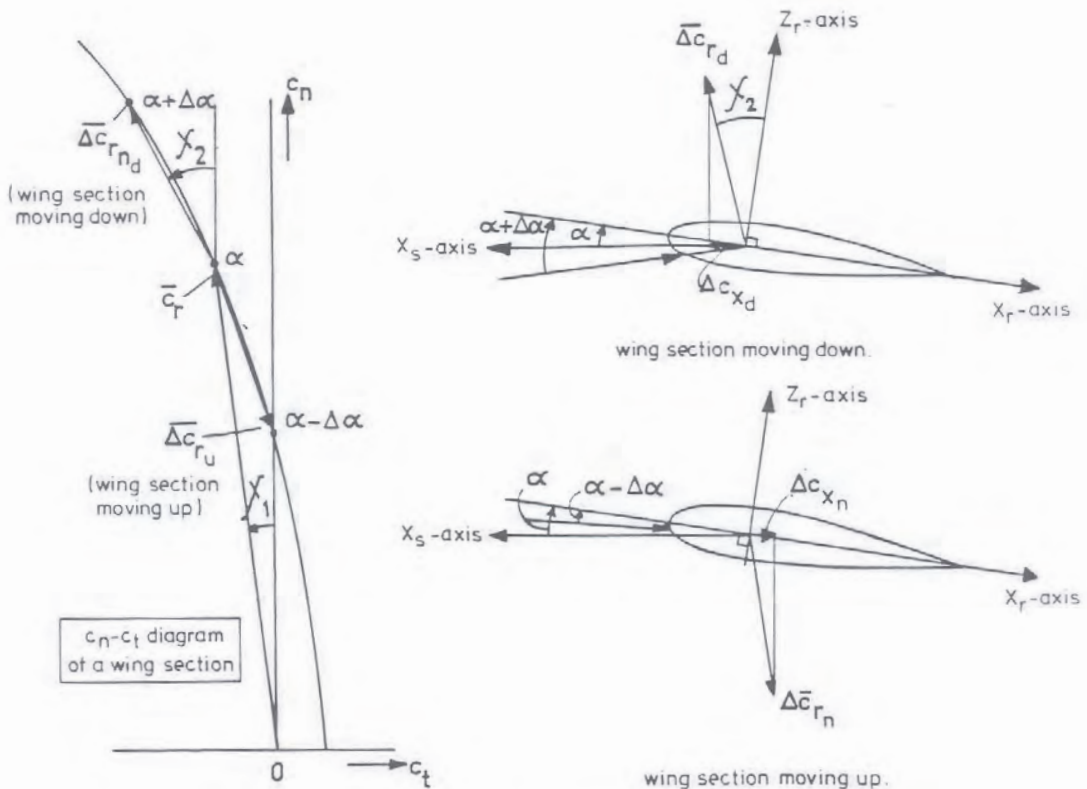
where $(C_{n_p})_w < 0$.

If flow separation occurs on the down going wing, the drag increases considerably causing the extra force in X_B - or X_S -direction to become negative. This renders $(C_{n_p})_w$ less negative or even positive. This applies also to wings with a sharp leading edge. Due to the absence of the suction peak on the airfoil’s nose, the resultant aerodynamic force and the change in the resultant aerodynamic force act here approximately perpendicular to the wing chord. From subfigure b of figure 8-33 it can be seen that for normal wings the extra force in X_S direction on the down going wing is positive (pointing forwards) and the extra force on the up going wing acts in the direction of the negative X_S direction. For normal wings $(C_{n_p})_w$ apparently is always negative.

For swept wings the change in resultant aerodynamic force acting on a section of the rolling wing has a component in the Y_B - or Y_S -direction, see figure 8-34. This lateral force has the same direction on both wing halves. This causes a resultant lateral force $(C_{Y_p})_w \cdot \frac{pb}{2V}$. This force generates a second, less important contribution to $(C_{n_p})_w$, depending on the c.g. position.



(a) The forces ΔC_X due to $\Delta\alpha$ of a rolling wing and the resultant yawing moment.



(b) Illustration of the change in the forces in X_s -and Z_s directions on the two sides of a rolling wing.

Figure 8-33: The origin of a negative yawing moment about the Z -axis of the stability reference frame for a wing having a positive rate of roll (attached flow)

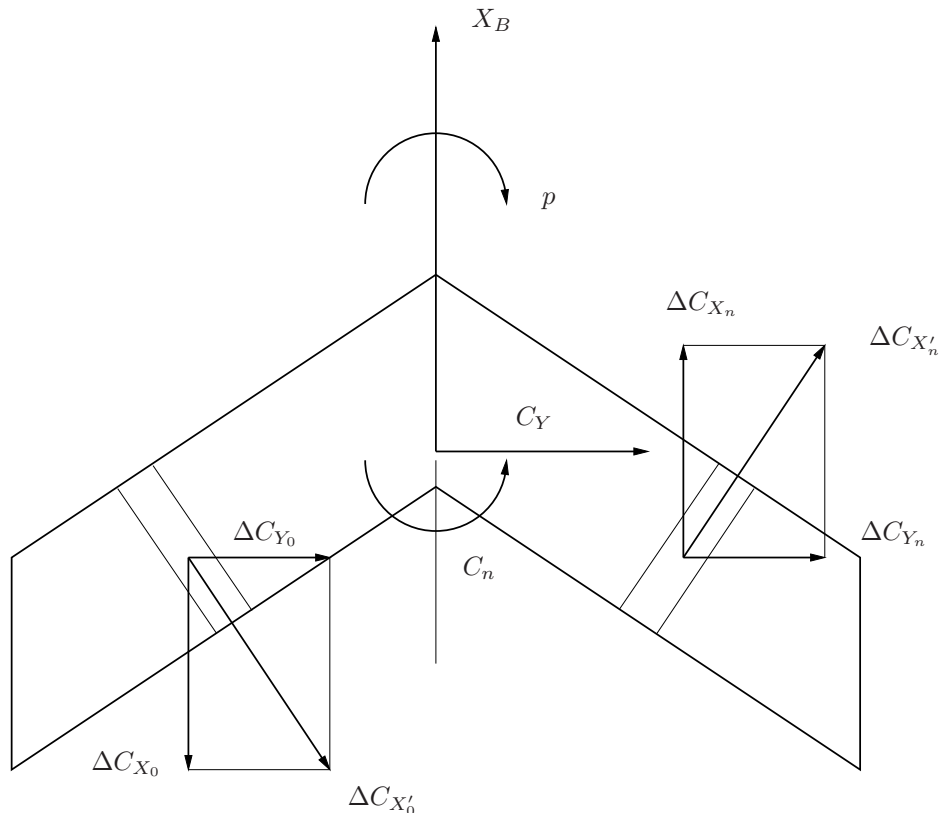


Figure 8-34: The side force and yawing moment on a rolling, swept back wing

Calculation methods to determine $(C_{Y_p})_w$ and $(C_{n_p})_w$ for subsonic speeds are given in references [10, 74, 131, 167, 68]. For supersonic speeds, see references [89, 88].

The contribution of the vertical tailplane to C_{n_p} follows directly from $(C_{Y_p})_v$ and the position of the point of action of $(C_{Y_p})_v$ using an expression in analogy with equation (8-16). The position of the point of action $(C_{Y_p})_v$ can be determined using the same references as given for the determination of the magnitude of $(C_{Y_p})_w$.

Using linearized potential flow theory (panel methods), C_n as a function of $\frac{pb}{2V}$ has been calculated for the Cessna Ce550 ‘Citation II’, see figure 8-35. The definition of the aircraft parts ‘wing’, ‘horizontal stabilizer’, ‘pylons’, ‘fuselage’, ‘vertical fin’ and ‘nacelles’ is given in figure 7-2. The main contributions to C_{n_p} are from the vertical fin, wing and horizontal stabilizer.

8-4 Stability derivatives with respect to yaw rate

Before going into a discussion of the derivatives with respect to yawing velocity, C_{Y_r} , C_{ℓ_r} and C_{n_r} separately, the motion to be considered needs further description. The notion of a so called ‘ r -motion’ is introduced here, in analogy with the ‘ q -motion’, see section 7-4. When performing such an r -motion, the aircraft moves along a curved trajectory in the XOY -plane, such that the velocity vector of the center of gravity remains in the plane of symmetry. By definition the angle of sideslip of the aircraft remains zero during an r -motion, see figure 8-36. Apparently, the r -motion causes merely a curvature of the streamlines in the XOY -plane. At the position of the c.g. the radius of curvature is R ,

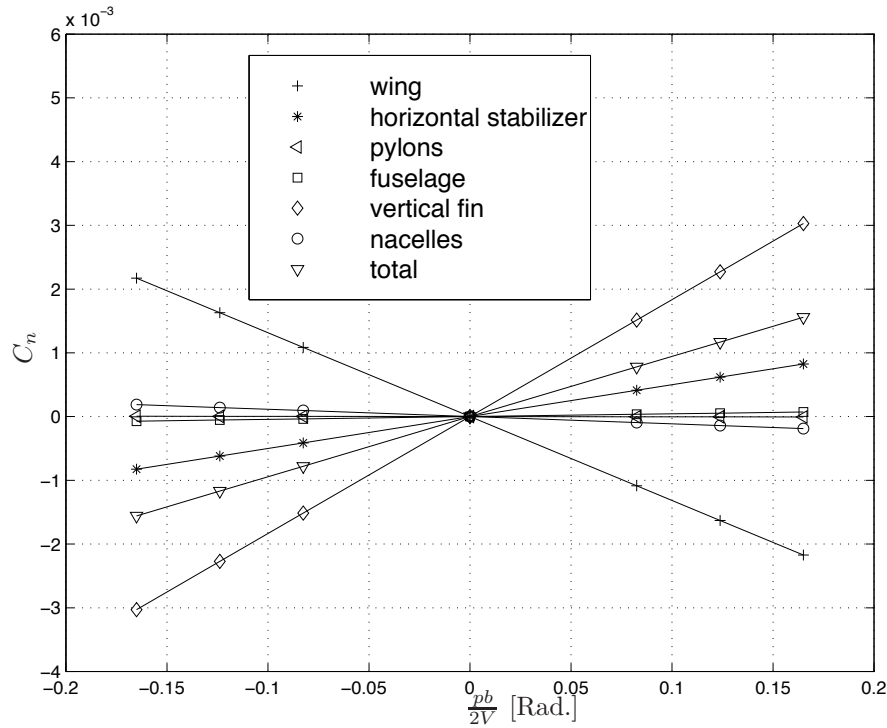


Figure 8-35: Aerodynamic moment coefficient C_n as a function of $\frac{pb}{2V}$ for the Cessna Ce550 ‘Citation II’, $\alpha = 0^\circ$

$$R = \frac{V}{r}$$

The center of rotation is situated at a distance R from the c.g. on the positive Y -axis if r is positive.

The effect of this r -motion is twofold. In the first place, and in analogy with the change in angle of attack caused by the q -motion, a change in the flow direction measured in planes parallel to the XOY -plane occurs at all points of the aircraft, see figure 8-37,

$$\Delta\alpha = \frac{rb}{2V} \frac{x - x_{c.g.}}{b/2} \quad (8-22)$$

As a consequence the airflow meets the vertical tailplane from the left if r is positive.

In the second place, the local speed of the airflow changes at all points of the aircraft by an amount, see figure 8-38,

$$\frac{\Delta V}{V} = -\frac{rb}{2V} \frac{y}{b/2} \quad (8-23)$$

As in equation (8-18), y is measured here in the stability reference frame. At positive r , the right wing has a lower airspeed and the left wing a larger airspeed than the aircraft center of gravity. Similar differences in airspeed occur in the plane of symmetry during the q -motion, but they are negligible due to the relatively small dimensions of the aircraft in Z -direction.

According to equation (8-23), $\frac{rb}{2V}$ is the non-dimensional change in airspeed occurring at the wing tip. The choice of the factor $\frac{b}{2V}$ to make the angular velocity non-dimensional thus has a geometric interpretation.

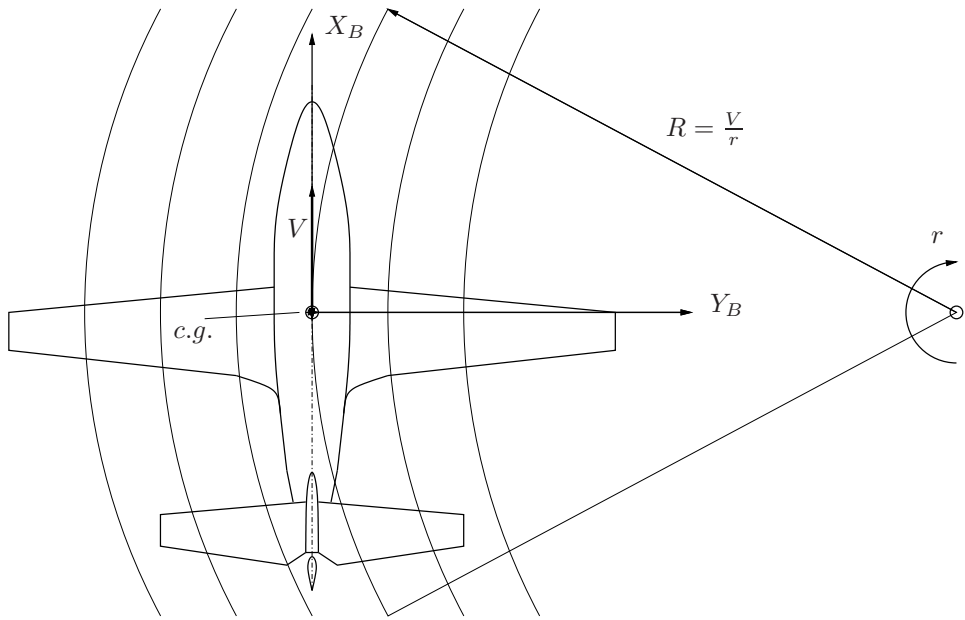


Figure 8-36: The pure 'r- motion'

8-4-1 Stability derivative C_{Y_r}

This derivative is usually of minor importance. The dominant contribution to C_{Y_r} is due to the vertical tailplane, C_{Y_r} is commonly positive.

The contribution of the wing is very small. Calculation methods are given in references [10, 74, 131, 167] for subsonic speeds and in references [89, 88] for supersonic speeds. The contributions of the fuselage and the wing-fuselage interaction are negligible, as is the contribution of the horizontal tailplane.

The lateral force on the vertical tailplane due to yawing can be written as,

$$Y_v = (C_{Y_r})_v \frac{rb}{2V} \frac{1}{2} \rho V^2 S \quad (8-24)$$

The lateral force is caused by the change in angle of attack $\Delta\alpha_v$ of the vertical tailplane, see figure 8-39. Accordingly,

$$Y_v = C_{Y_{v\alpha}} \Delta\alpha_v \frac{1}{2} \rho V_v^2 S_v \quad (8-25)$$

The change in angle of attack $\Delta\alpha_v$ follows from equation (8-22) with $x_v - x_{c.g.} = l_v$,

$$\Delta\alpha_v = \frac{rb}{2V} \frac{l_v}{b/2} \quad (8-26)$$

From equations (8-24), (8-25) and (8-26) it follows after some reduction,

$$(C_{Y_r})_v = 2 C_{Y_{v\alpha}} \left(\frac{V_v}{V} \right)^2 \frac{S_v l_v}{S b} \quad (8-27)$$

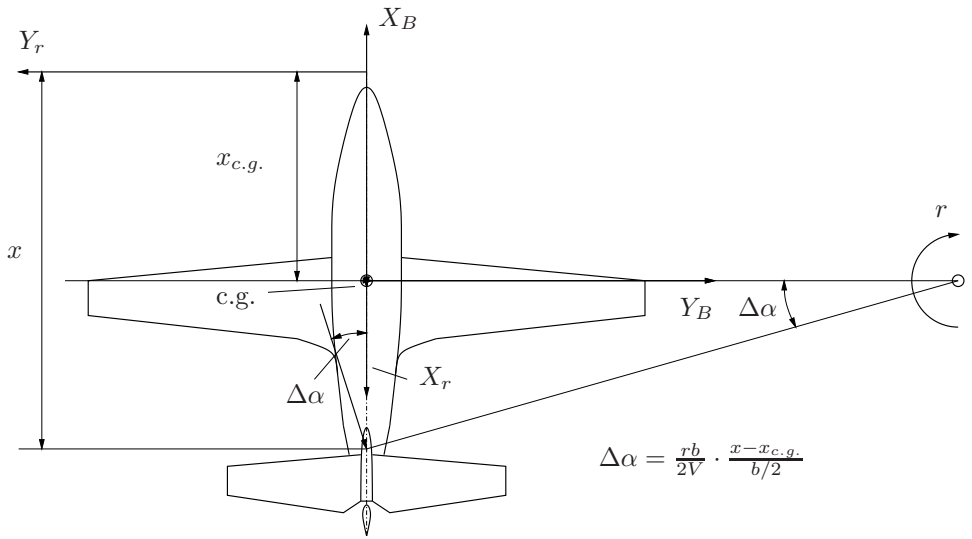


Figure 8-37: The change in geometric flow direction at an arbitrary point of the aircraft due to an 'r-motion'

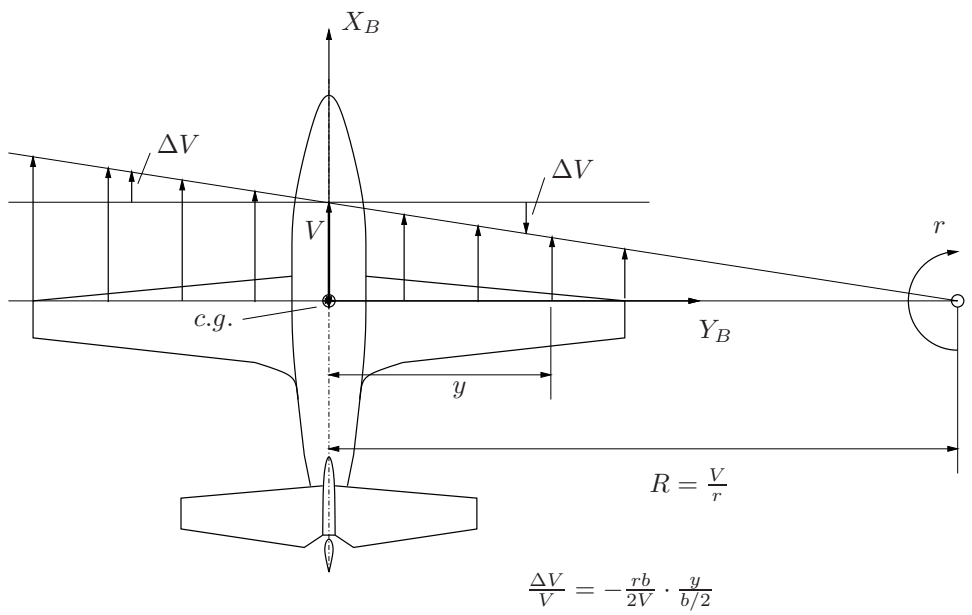


Figure 8-38: The variation in airspeed in spanwise direction due to an *r*-motion

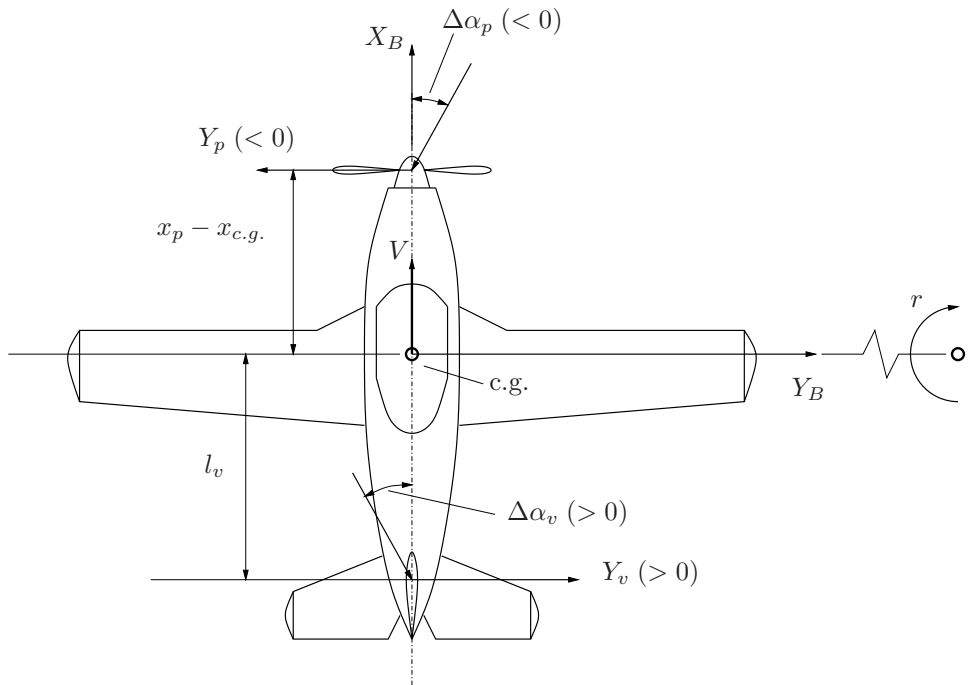


Figure 8-39: The side forces on the vertical tailplane and the propeller due to an r -motion.

From this expression it follows that $(C_{Y_r})_v$ is positive.

The values of $(C_{Y_r})_v$ calculated using equation (8-27) may not be very accurate due to the unknown influence of the wing-fuselage in the curved flow field on the flow direction at the vertical tailplane. For these reasons it is commonly necessary to use the results of wind tunnel measurements on similar configurations to determine $(C_{Y_r})_v$.

During the r -motion the propeller experiences an oblique inflow also causing a contribution to C_{Y_r} , see figure 8-39. In analogy with equation (8-27), $(C_{Y_r})_p$ can be written as,

$$(C_{Y_r})_p = 2 C_{Y_{p\alpha}} \left(\frac{V_p}{V} \right)^2 \frac{S_v}{S} \frac{x_p - x_{c.g.}}{b} \quad (8-28)$$

The derivative $(C_{Y_r})_p$ usually is negative. $C_{Y_{p\alpha}}$ and $\left(\frac{V_p}{V} \right)^2$ can be determined using references [143, 144].

Using linearized potential flow theory (panel methods), C_Y as a function of $\frac{rb}{2V}$ has been calculated for the Cessna Ce550 ‘Citation II’, see figure 8-40. The definition of the aircraft parts ‘wing’, ‘horizontal stabilizer’, ‘pylons’, ‘fuselage’, ‘vertical fin’ and ‘nacelles’ is given in figure 7-2. The main contributions to C_{Y_r} are from the vertical fin, the fuselage and the wing.

8-4-2 Stability derivative C_{ℓ_r}

The stability derivative C_{ℓ_r} is determined primarily by the contributions of the wing and the vertical tailplane. The contributions of the fuselage, the wing-fuselage interaction, the horizontal

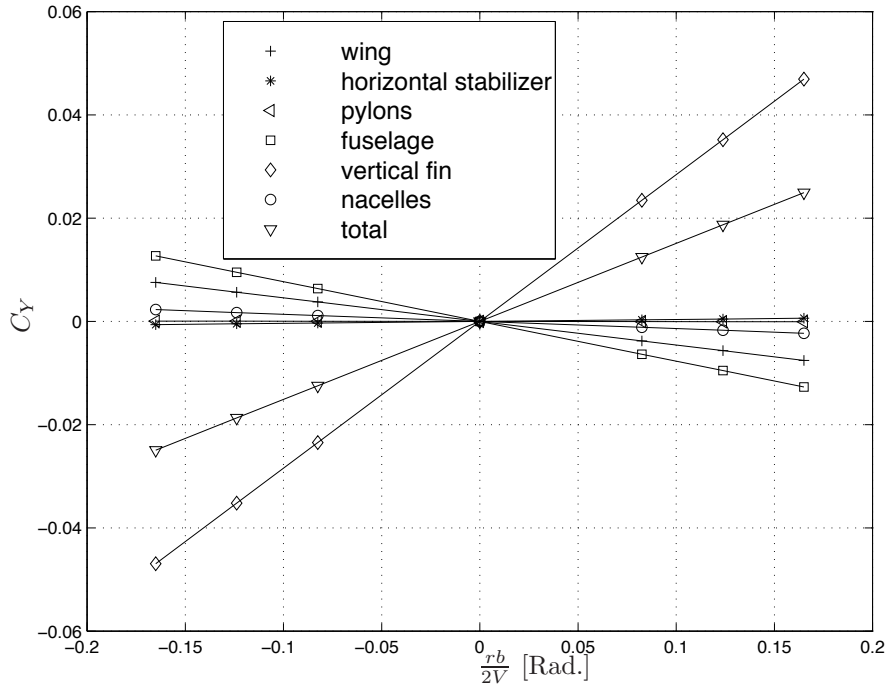


Figure 8-40: Aerodynamic force coefficient C_Y as a function of $\frac{rb}{2V}$ for the Cessna Ce550 'Citation II', $\alpha = 0^\circ$

tailplane and the propulsion system may usually be neglected. C_{ℓ_r} is always positive.

The contribution of the wing arises due to the differences in airspeed over the two wing halves during the r -motion, as described previously. At a positive yawing velocity, i.e. a rotation to the right, the left wing generates more lift than the right wing, causing a right wing down, positive, rolling moment,

$$L = (C_{\ell_r})_w \frac{rb}{2V} \frac{1}{2} \rho V^2 S b \quad (8-29)$$

This rolling moment, and thus $(C_{\ell_r})_w$, is proportional to the lift coefficient and at a given C_L dependent on the lift distribution over the wing span. Tapered wings show a higher lift concentration near the center of the wing, causing an increase in speed over the outer wing to have less effect. As a consequence, $(C_{\ell_r})_w$ decreases with λ at constant C_L . The same applies to wings having negative twist and to wings with deflected landing flaps. Swept back wings have a higher lift concentration on the outer wings. This causes $(C_{\ell_r})_w$ to increase somewhat with Λ . The derivative $(C_{\ell_r})_w$ can be calculated using references [10, 74, 131, 167, 33] for subsonic speeds and references [89, 88] for supersonic speeds.

The contribution of the vertical tailplane to C_{ℓ_r} is found from $(C_{Y_r})_v$ and the position of the point of action of $(C_{Y_r})_v$,

$$(C_{\ell_r})_v = (C_{Y_r})_v \left(\frac{z_v - z_{c.g.}}{b} \cos \alpha_0 - \frac{x_v - x_{c.g.}}{b} \sin \alpha_0 \right) \quad (8-30)$$

As $z_v - z_{c.g.}$ is usually positive, $(C_{\ell_r})_v$ is usually positive as well.

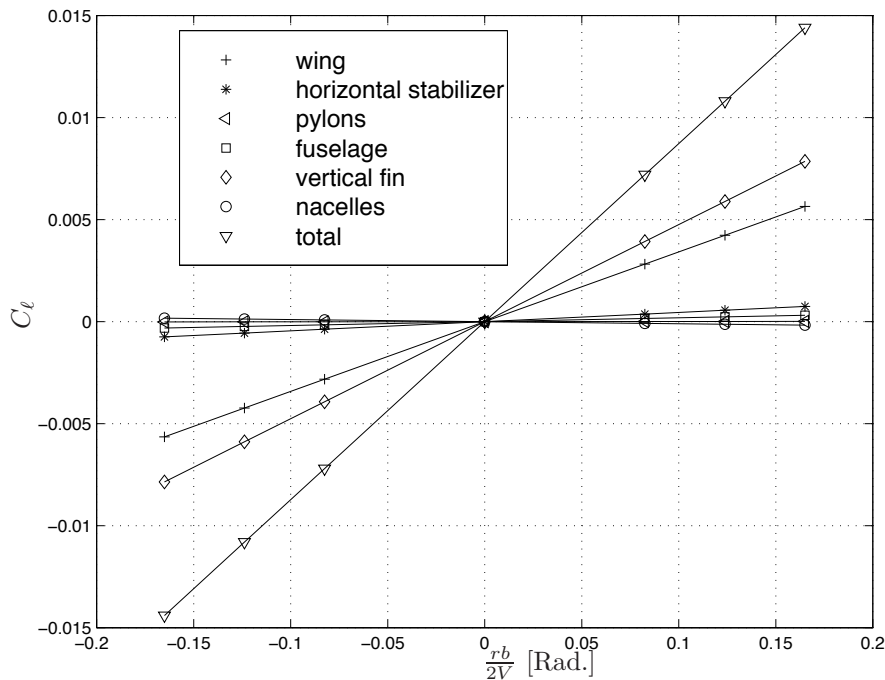


Figure 8-41: Aerodynamic moment coefficient C_{ℓ} as a function of $\frac{r_b}{2V}$ for the Cessna Ce550 ‘Citation II’, $\alpha = 0^\circ$

Using linearized potential flow theory (panel methods), C_{ℓ} as a function of $\frac{r_b}{2V}$ has been calculated for the Cessna Ce550 ‘Citation II’, see figure 8-41. The definition of the aircraft parts ‘wing’, ‘horizontal stabilizer’, ‘pylons’, ‘fuselage’, ‘vertical fin’ and ‘nacelles’ is given in figure 7-2. The main contributions to C_{ℓ_r} are from the vertical fin and the wing.

8-4-3 Stability derivative C_{n_r}

Similar to the derivatives C_{m_q} and C_{ℓ_p} , C_{n_r} is a measure of the aerodynamic moment about an axis caused by an angular velocity about the same axis. Under normal circumstances such a moment tries to slow down the motion, which implies that C_{n_r} is normally negative, again similar to C_{m_q} and C_{ℓ_p} . The dominant contribution to C_{n_r} is provided by the vertical tailplane. Additionally, only the wing, the fuselage and the propulsion system deliver non-negligible contributions.

The part provided by the wing is generated by the differences in drag between the two halves of the wing, caused by the differences in local airspeed. Calculation methods for subsonic speeds are found in references [10, 74, 131, 167] and in references [89, 88] for supersonic speeds.

The contribution due to the fuselage is small, but it may be non-negligible for modern configurations having a relatively large fuselage in comparison with the wing. A calculation is possible using references [150, 94].

The contribution of the vertical tailplane follows directly from, see equation (8-27) and the tail-length of the aircraft, see also figure 8-39,

$$(C_{n_r})_v = -(C_{Y_r})_v \frac{l_v}{b} \quad (8-31)$$

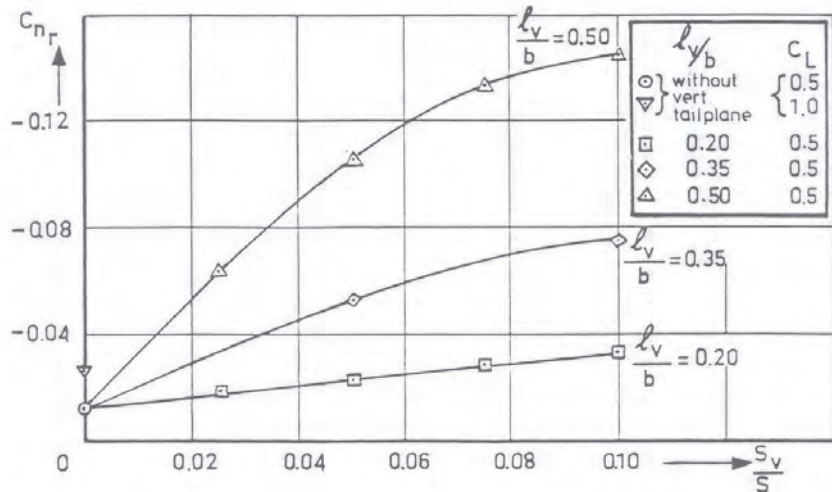


Figure 8-42: The effects of the size of the vertical tailplane and the taillength on C_{n_r} (from reference [94])

For the determination of $(C_{n_r})_v$ in the stability reference frame, at large angles of attack use has to be made of an expression in analogy with equation (8-16).

Figure 8-42 gives C_{n_r} of a model for different values of $\frac{l_v}{b}$ and $\frac{S_v}{b}$.

The contribution of the propeller to C_{n_r} follows in a similar manner from $(C_{Y_r})_p$. If the propeller is situated in front of the c.g., $(C_{Y_r})_p$ is negative. The damping moment is then increased by the propeller, see figure 8-39. Additionally, the increased dynamic pressure in the slipstream may cause an increase in the contribution of the vertical tailplane.

Using linearized potential flow theory (panel methods), C_n as a function of $\frac{r b}{2V}$ has been calculated for the Cessna Ce550 ‘Citation II’, see figure 8-43. The definition of the aircraft parts ‘wing’, ‘horizontal stabilizer’, ‘pylons’, ‘fuselage’, ‘vertical fin’ and ‘nacelles’ is given in figure 7-2. The main contributions to C_{n_r} are from the vertical fin and the fuselage.

8-5 The forces and moments due to aileron, rudder and spoiler deflections

For lateral control it is necessary to generate variable moments about the X_B -axis and the Z_B -axis. The moment about the X_B -axis is usually obtained by deflecting ailerons, at high airspeeds the use of spoilers is also quite common. The moment about the Z_B -axis is provided by the rudder.

The deflection of the ailerons or the spoilers generates in addition to the rolling moment L also a lateral force Y and a yawing moment N . Equally, rudder deflections cause not only a yawing moment, but also a lateral force and a rolling moment.

As is the case with the lateral motions of the entire aircraft, in principle no symmetric forces and moments are generated. Measures of the non-dimensional force C_Y and the non-dimensional moments C_ℓ and C_n due to control surface deflections are again the partial derivatives with respect to aileron deflection δ_a and the rudder deflection δ_r , these control derivatives are,

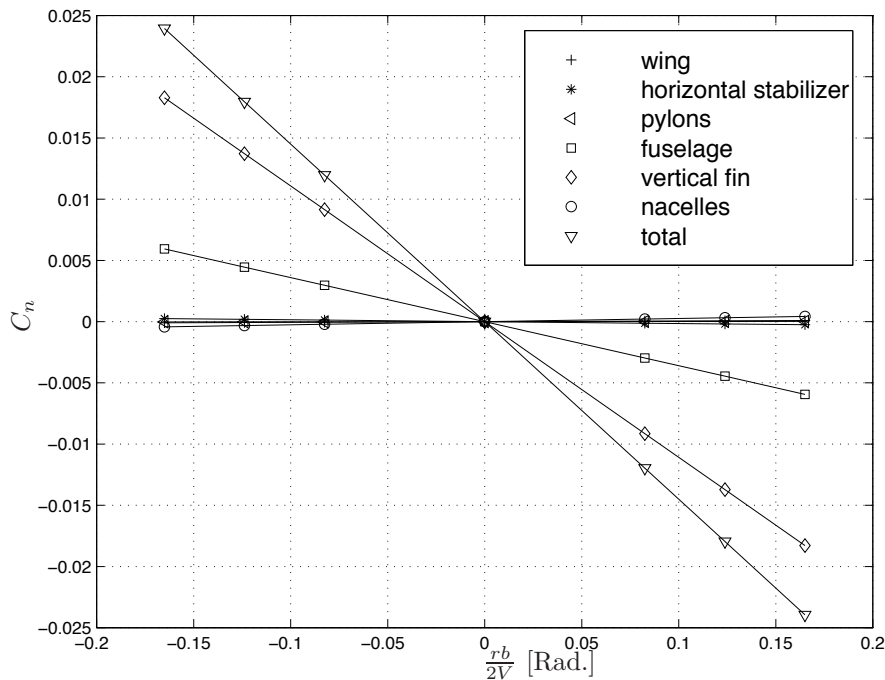


Figure 8-43: Aerodynamic moment coefficient C_n as a function of $\frac{rb}{2V}$ for the Cessna Ce550 'Citation II', $\alpha = 0^\circ$

1. aileron deflection,

$$C_{Y_{\delta_a}} = \frac{\partial C_Y}{\partial \delta_a} \quad C_{\ell_{\delta_a}} = \frac{\partial C_\ell}{\partial \delta_a} \quad C_{n_{\delta_a}} = \frac{\partial C_n}{\partial \delta_a}$$

2. rudder deflection,

$$C_{Y_{\delta_r}} = \frac{\partial C_Y}{\partial \delta_r} \quad C_{\ell_{\delta_r}} = \frac{\partial C_\ell}{\partial \delta_r} \quad C_{n_{\delta_r}} = \frac{\partial C_n}{\partial \delta_r}$$

When using the control deflections as measures for the forces and moments, in analogy with the stability derivatives, the assumption is made that the forces and moments vary linearly with δ_a and δ_r . For not too large control surface deflections, this assumption is usually quite acceptable. Appendix D provides, in addition to stability derivatives, also the control derivatives of some aircraft.

Figure 8-44 shows once more the positive direction of the control surface deflections. They are always measured in a plane perpendicular to the hinge axes of the surfaces. The deflection δ_a is defined as,

$$\delta_a = \delta_{a_{right}} - \delta_{a_{left}} \quad (8-32)$$

A positive deflection of the control stick, or a positive deflection of the control wheel (to the left), can be seen to produce a positive δ_a . Equally, a positive deflection of the rudder pedals (left pedal forward) causes a positive δ_r .

If spoilers are used, derivatives with respect to spoiler deflection δ_s are defined, in analogy with the above control deflections,

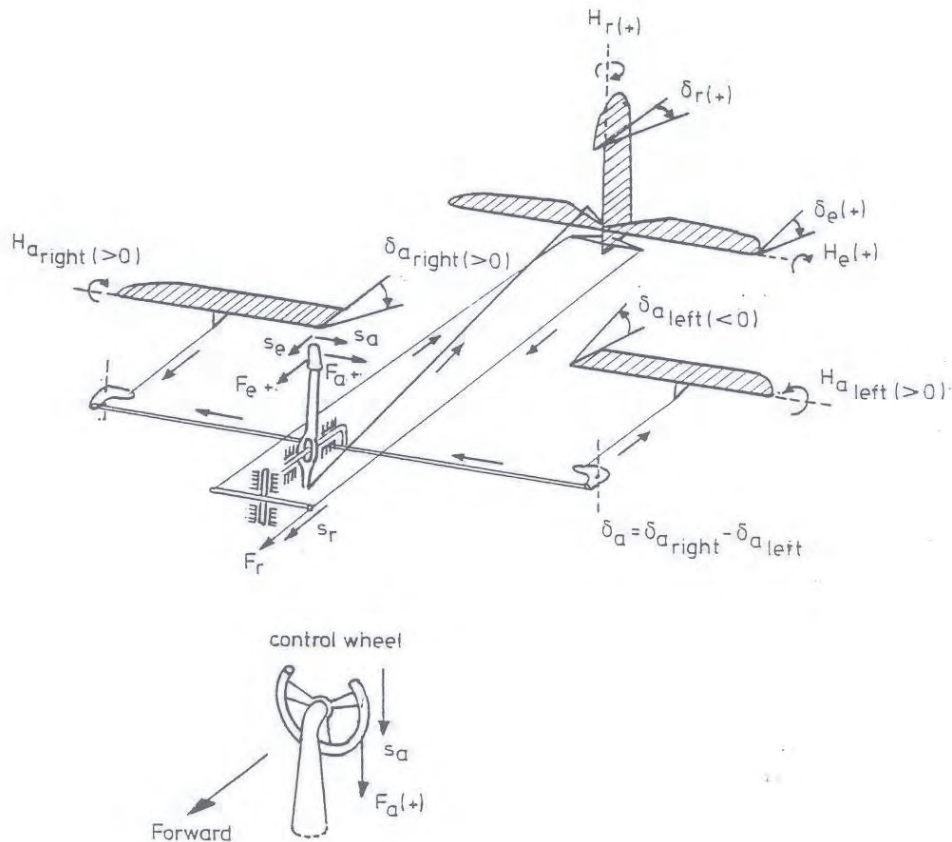


Figure 8-44: The positive direction of control deflections, control forces, control surface deflections and hinge moments

$$C_{Y_{\delta_s}} = \frac{\partial C_Y}{\partial \delta_s} \quad C_{\ell_{\delta_s}} = \frac{\partial C_\ell}{\partial \delta_s} \quad C_{n_{\delta_s}} = \frac{\partial C_n}{\partial \delta_s}$$

A spoiler deflection on the left wing is taken as positive. A positive δ_s corresponds with a positive deflection of the roll control manipulator. When using the derivatives with respect to δ_s great care is required, as for many spoiler configurations the forces and moments vary strongly non-linear with the spoiler deflection.

The control derivatives are discussed in the following. The use of spoilers for roll control is discussed in section 8-7.

8-6 Aileron control derivatives

8-6-1 Control derivative $C_{Y_{\delta_a}}$

The lateral force caused by an aileron deflection may be taken as zero for straight wings. On swept wings a lateral force does arise as is the case in rolling flight. The derivative $C_{Y_{\delta_a}}$ is very small in magnitude and is usually neglected.

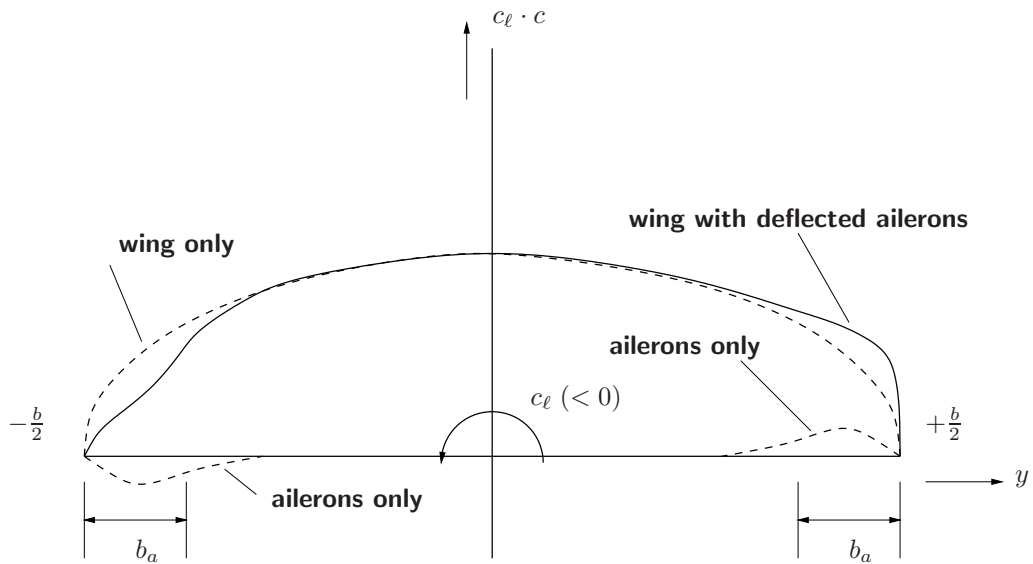


Figure 8-45: The effect of an aileron deflection on the lift distribution in spanwise direction

8-6-2 Control derivative $C_{\ell_{\delta_a}}$

This control derivative is, of course, the primary one for the ailerons. Due to a positive aileron deflection the lift on the right wing increases, on the left wing the lift decreases. The result is a rolling moment to the left, which is counted as negative, see figure 8-45,

$$L = C_{\ell_{\delta_a}} \delta_a \frac{1}{2} \rho V^2 S b \quad (8-33)$$

The derivative $C_{\ell_{\delta_a}}$ is negative and is also called the aileron effectivity. If the aeroelastic deformation of the wing is neglected, the influence of the Mach number is not considered and no flow separation on the wing in the area of the ailerons occurs, then $C_{\ell_{\delta_a}}$ may be considered as independent of C_L .

The magnitude of $C_{\ell_{\delta_a}}$ depends strongly on the dimensions and the location of the ailerons on the wing. Wing sweep and taper ratio also have an important influence on the aileron effectivity. For a given location and dimension of the ailerons, $C_{\ell_{\delta_a}}$ decreases in the absolute sense with increasing wing sweep and taper ratio (lower λ), especially when the wing aspect ratio is large.

The calculation of $C_{\ell_{\delta_a}}$ is possible, using references [10, 74, 166, 45, 107]. For supersonic speeds $C_{\ell_{\delta_a}}$ can be determined with reference [107]. In many instances measured values of $C_{\ell_{\delta_a}}$ obtained from flight tests turn out to be smaller in magnitude than was expected on the basis of calculations.

8-6-3 Control derivative $C_{n_{\delta_a}}$

The yawing due to aileron deflection arises because the drag of the wing having the downward deflected aileron increases, while that of the other side decreases, or perhaps increases less. As a consequence, a positive aileron deflection causes a positive yawing moment,

$$N = C_{n_{\delta_a}} \delta_a \frac{1}{2} \rho V^2 S b \quad (8-34)$$

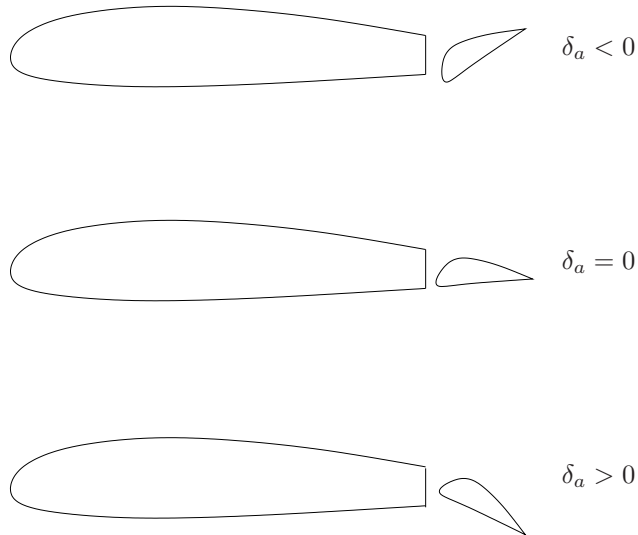


Figure 8-46: The Frise aileron

where $C_{n_{\delta_a}}$ is positive. To a first approximation $C_{n_{\delta_a}}$ is proportional to C_L . Too large values of $C_{n_{\delta_a}}$ are undesirable. If, for instance, the pilot wants to initiate a left turn, he deflects the roll control (stick or wheel) to the left to obtain the required negative roll-angle φ (left wing down). While the aircraft must obtain a negative yaw-rate (to the left), the positive aileron deflection generates a positive yawing moment, because $C_{n_{\delta_a}}$ is positive. This yawing moment causes the aircraft to yaw initially to the right. This effect is amplified by the usually positive yawing moment caused by the negative rolling velocity of the aircraft, C_{n_p} was seen to be negative. This initial yaw opposite to the desired direction is usually called the ‘adverse yaw’ of the aircraft.

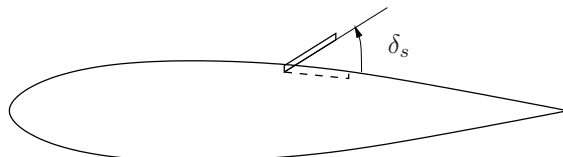
The derivative $C_{n_{\delta_a}}$ can be kept small in various ways. One of the means is the application of differential deflections of the ailerons when applying roll control. This implies that the downward deflection of the aileron is made smaller than the upward deflection of the other aileron. The difference in drag is reduced in this manner. An other method uses so called ‘Frise’ ailerons. The shape of the nose of these ailerons is such that the drag of the aileron strongly increases if it is deflected upward, see figure 8-46 and reference [166].

A calculation of $C_{n_{\delta_a}}$ having some accuracy is generally not possible. As a consequence it is always desirable to determine $C_{n_{\delta_a}}$ on the basis of experimentally obtained data, see reference [74].

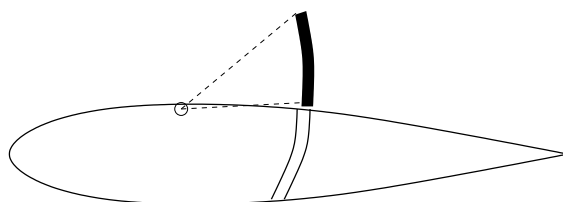
8-7 Spoiler control derivatives

At transonic and supersonic airspeeds roll control of the aircraft can often not be effected by ailerons alone. In such cases spoilers, or a combination of spoilers and ailerons are used. The latter solution is the more usual one.

A spoiler is nothing but a flap, deflected from the upper surface on one side of the wing to ‘spoil’ the airflow over that part of the wing, see subfigure a of figure 8-47. The local disturbance causes a decrease in lift and thereby generates a rolling moment. A deflection of the spoiler on the left wing is counted as positive. This causes, like an upward deflection of the left aileron, a negative rolling moment, hence $C_{n_{\delta_s}}$ is negative as $C_{n_{\delta_a}}$ is.



(A) Plate type spoiler



(B) Plugtype spoiler

Figure 8-47: Spoiler types

Spoilers are more effective if they are located closer to the wing leading edge. The response of the aircraft to spoiler deflection becomes slightly more sluggish in this way. Therefore, in practice spoilers are located mostly on the rear part of the wing chord.

Various causes make the use of spoilers on high speed aircraft more or less mandatory. In the first place, aileron effectivity decreases due to compressibility effects with increasing Mach number. On the other hand, the effectiveness of spoilers slightly increases with increasing Mach number. A second, even more important, phenomenon is the decrease in aileron effectivity due to wing deformation caused by aileron deflection.

Figure 8-48 shows how a downward deflection of the aileron causes the wing to twist such that the local angle of attack decreases. This counteracts the increase in lift due to the aileron deflection. Conversely, an upward deflection of the aileron causes an increase of the local angle of attack.

Such a decrease in aileron effectivity may be appreciable especially at high airspeeds, both due to the high dynamic pressure and to the rearward shift of the point of action of the local change in lift caused by the aileron deflection with increasing Mach number. In this way the resultant effect of an aileron deflection on highly swept wings with thin wing sections may even be opposite to the desired one. The effect is called ‘control reversal’ and the airspeed from which onward this occurs is the ‘reversal speed’. The point of action of the resultant change in lift for spoilers lies more forward on the chord than for ailerons. Hence, the wing twist is less and as a result the reversal speed is higher.

Finally and quite apart from the foregoing reasons, it is often not very well possible to use large ailerons on wings having a high sweep angle or a low aspect ratio. The trailing edges of such wings are taken up largely by landing flaps to obtain an acceptable low landing speed.

A spoiler deflection causes not only a reduction in lift, but also causes a strong increase in drag. A secondary advantage of the use of spoilers is, that due to this drag increase, $C_{n_{\delta_s}}$ is nearly always

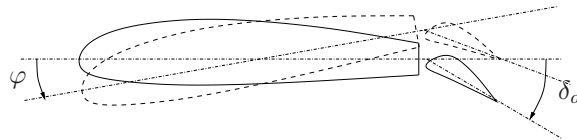


Figure 8-48: The local wing twist of a wing cross-section due to elastic deformation caused by an aileron deflection

negative, contrary to $C_{n\delta_a}$. The adverse yaw at the initiation of a turn is thereby decreased or even entirely avoided.

The increase in drag created by the deployment of spoilers may cause the designer to use the spoilers not only for roll control but as speed brakes as well. The spoilers are deflected symmetrically for this purpose. Symmetric deflection of spoilers situated in front of the landing flaps, when applied directly after touch down, provides the possibility to drastically decrease the wing lift during the roll out. A larger part of the weight acts on the undercarriage making the wheel brakes more effective, thus yielding an appreciable reduction in the stopping distance.

A disadvantage of spoilers is their low effectivity at small deflections, caused by re-attachment of the airflow behind the spoiler. So-called ‘plug type spoilers’, see subfigure b of figure 8-47 have better characteristics in this respect due to the open connection between lower and upper surface of the wing caused by the spoiler deflection. Re-attachment of the airflow is avoided in this manner. At large angles of attack the effectivity of the spoiler may also be low, especially if flow separation occurs at the trailing edge of the wing. A further disadvantage during the approach and landing phases is the decrease in total wing lift caused by the operation of the spoilers. This renders the precise control of the aircraft’s flight path slightly more difficult.

The hinge moment of a plain flap type spoiler, see subfigure a of figure 8-47, may be appreciable, and it usually changes non-linearly with the deflection angle. On the other hand, the hinge moment of a spoiler in the shape of a half circular plate, see subfigure b of figure 8-47, may be next to negligible. However, the total aerodynamic load on a spoiler of this type may be relatively high.

$C_{\ell\delta_s}$ and $C_{n\delta_s}$ can be determined using references [74]. Reference [61] gives theoretical calculation methods to determine $C_{\ell\delta_s}$ while reference [108] contains an extensive list of references on the use of spoilers.

8-8 Rudder control derivatives

8-8-1 Control derivative $C_{Y\delta_r}$

The rudder deflection causes a lateral force,

$$Y = C_{Y\delta_r} \delta_r \frac{1}{2} \rho V^2 S \quad (8-35)$$

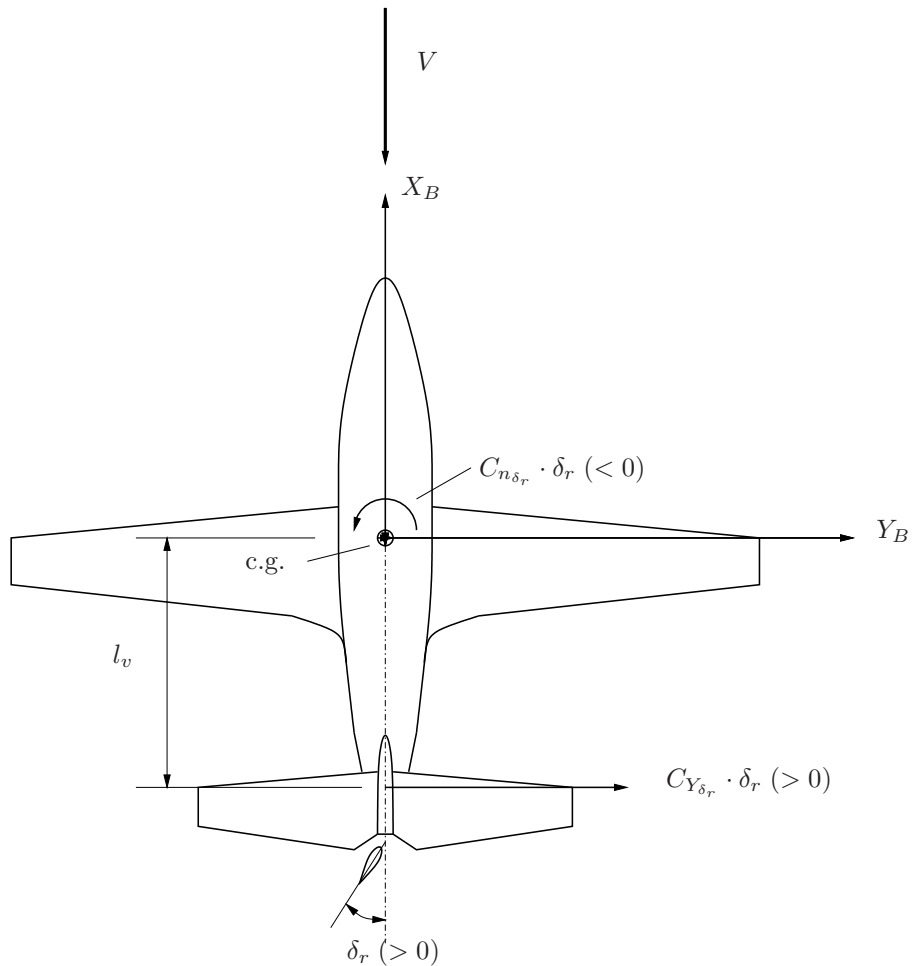


Figure 8-49: The side force and yawing moment due to a rudder deflection

A positive δ_r gives rise to a positive lateral force, see figure 8-49. The control derivative $C_{Y_{\delta_r}}$ is positive. The lateral force can be written as,

$$Y = C_{Y_{\delta_r}} \delta_r \frac{1}{2} \rho V_v^2 S_v \quad (8-36)$$

where $C_{Y_{\delta_r}}$ is the gradient of the normal, here lateral, force on the vertical tailplane. From equations (8-35) and (8-36) it follows,

$$C_{Y_{\delta_r}} = C_{Y_{\delta}} \left(\frac{V_v}{V} \right)^2 \frac{S_v}{S} \quad (8-37)$$

The derivative $C_{Y_{\delta_r}}$ is determined in a similar way as the derivative $C_{N_{h_{\delta}}}$ of the horizontal tailplane, see references [166, 44, 47, 135]. For supersonic speeds this derivative can be calculated with reference [107].

8-8-2 Control derivative $C_{\ell_{\delta_r}}$

A positive lateral force acting on the vertical tailplane, caused by a positive rudder deflection, causes a positive rolling moment,

$$L = C_{\ell_{\delta_r}} \delta_r \frac{1}{2} \rho V^2 S b \quad (8-38)$$

where $C_{\ell_{\delta_r}}$ is positive. In analogy with the contribution of the vertical tailplane $(C_{\ell_\beta})_v$, $(C_{\ell_p})_v$ and $(C_{\ell_r})_v$, the control derivative $C_{\ell_{\delta_r}}$ can be written as,

$$C_{\ell_{\delta_r}} = C_{Y_{\delta_r}} \left(\frac{z_v - z_{c.g.}}{b} \cos \alpha_0 - \frac{x_v - x_{c.g.}}{b} \sin \alpha_0 \right) \quad (8-39)$$

Large positive values of $C_{\ell_{\delta_r}}$ could be detrimental to good lateral control characteristics. In flight, when accurate lateral control is required, small deviations from the desired heading may be corrected by using rudder deflections, without recourse to the ailerons. This may give a result more quickly than changing the aircraft's heading via a change in angle of roll generated by the ailerons. If in such a situation a positive rudder deflection is used to yaw the aircraft to the left, a large positive $C_{\ell_{\delta_r}}$ causes an angle of roll to the right. Such a roll angle is associated with a turn to the right and opposes the desired yawing motion of the aircraft.

The effect just mentioned occurs mainly with aircraft having a highly mounted vertical tailplane, where $z_v - z_{c.g.}$ in equation (8-39) is large. In these aircraft the rudder and ailerons may be coupled mechanically such that a positive aileron deflection is generated by a positive rudder deflection. The moment $C_{\ell_{\delta_a}} \cdot \delta_a$ then opposes the moment $C_{\ell_{\delta_r}} \cdot \delta_r$.

8-8-3 Control derivative $C_{n_{\delta_r}}$

The primary effect of a rudder deflection is the yawing moment,

$$N = C_{n_{\delta_r}} \delta_r \frac{1}{2} \rho V^2 S b \quad (8-40)$$

The control derivative $C_{n_{\delta_r}}$ follows from figure 8-49 at small α_0 and taking $x_v - x_{c.g.} = l_v$,

$$C_{n_{\delta_r}} = -C_{Y_{\delta_r}} \frac{l_v}{b} \quad (8-41)$$

At large angles of attack, $C_{n_{\delta_r}}$ follows from an expression in analogy with equation (8-16) for $(C_{n_\beta})_v$. The control derivative $C_{n_{\delta_r}}$ is negative.

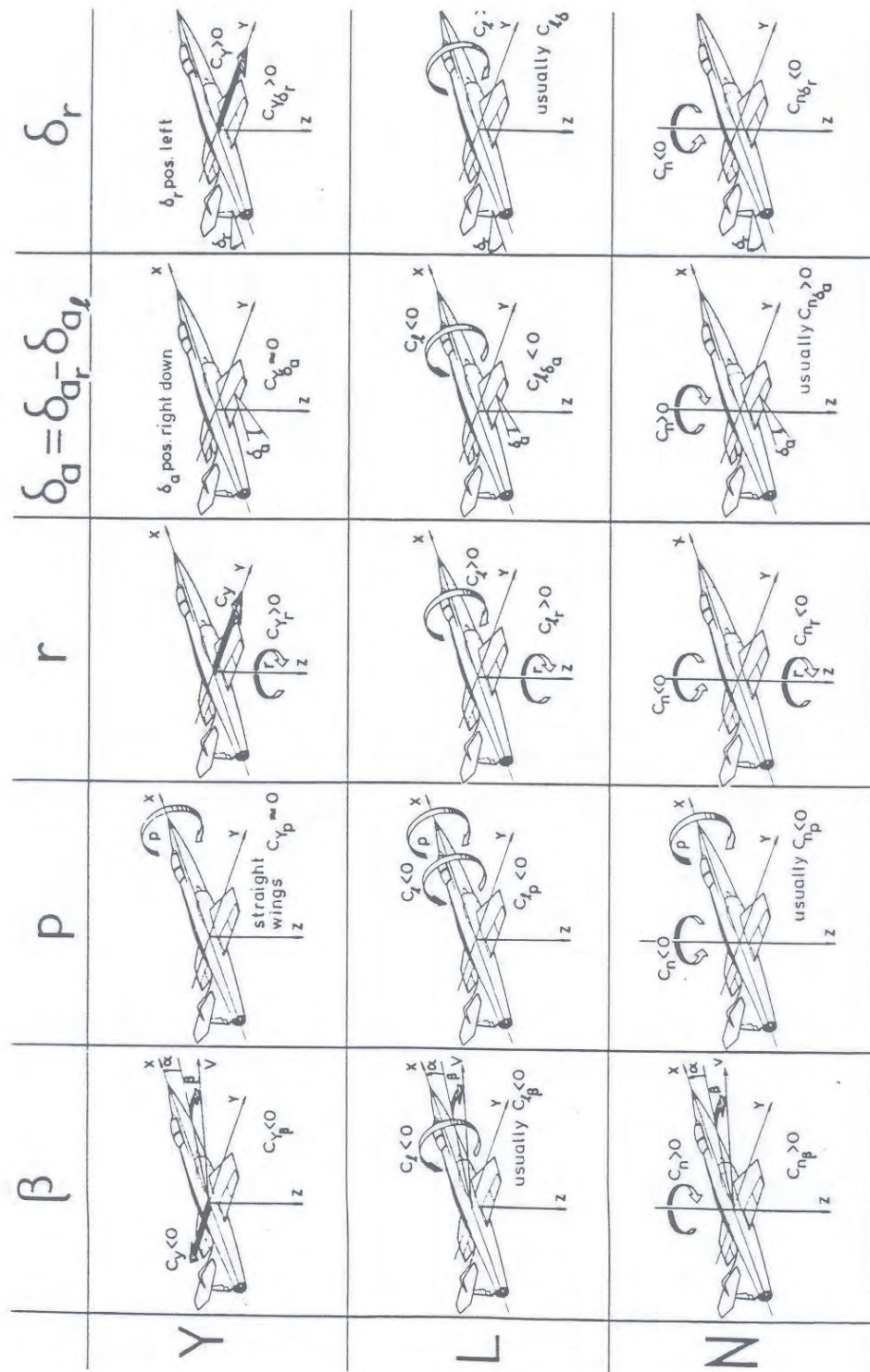


Figure 8-50: Asymmetric stability and control derivatives

Part III

Static Stability Analysis

Chapter 9

Analysis of Steady Symmetric Flight

The analysis of both static and dynamic stability and control characteristics of aircraft requires a mathematical model describing the effects of aerodynamic flow parameters as airspeed, angle of attack, angle of sideslip and body rotation rates on the aerodynamic forces and aerodynamic moments acting on the aircraft, see also chapters 3 and 4. Current practice is to extensively rely on tools from Computational Fluid Dynamics (CFD) to derive these characteristics from. It was and still is considered good practice, however, to augment and verify these results from CFD by using results from steady or rotary balance wind tunnel experiments with models of the complete aircraft or of isolated components. During the flight test campaign of the prototype aircraft these models can subsequently be improved by including flight test results using aerodynamic model identification techniques, see for example [101]. The disadvantage, however, of just using data from either CFD, wind tunnel experiments or flight tests on the complete model or actual aircraft is that it will not necessarily contribute much to the physical understanding of the resulting aerodynamic mechanisms leading to the observed aerodynamic force and moments characteristics. Also, there is still the problem of incorporating and interpreting the wind tunnel experimental results on isolated aircraft components.

This is the rationale behind the approach taken in the present chapter to first look at the characteristics of the isolated wing to which subsequently a fuselage and nacelles on the wing or fuselage are added. The final step is to add the effects of horizontal and vertical tail planes to this wing-body-nacelles composite.

The present chapter starts with an analysis of the aerodynamic forces and the aerodynamic moment acting on a symmetrical wing at some angle of attack. It is shown that the introduction of the concept of aerodynamic center leads to a surprisingly simple model for the force and moment characteristics. The concept of static stability is introduced and the necessary conditions to allow steady, stable flight. Next, it is shown how to derive a model of the force and moment characteristics of wings of arbitrary shape and twist from wing profile characteristics by applying classical 2-dimensional 'strip theory'. It is shown in particular how to compute the location of the wing aerodynamic center as well as the aerodynamic moment about it. Next, the isolated fuselage is discussed and the effect the fuselage has on the aerodynamic characteristics of the wing, and vice versa, the so called interference effects. In a similar way the effects of wing nacelles are discussed. The contribution of the horizontal tailplane to the aerodynamic forces and moment is discussed next. In classical aircraft configurations the horizontal tail plane is located somewhere behind the wing in the flow field induced by the wing-body-nacelles composite. This has a significant effect on the contribution of the tail plane to the aerodynamic forces in the plane of symmetry and on the

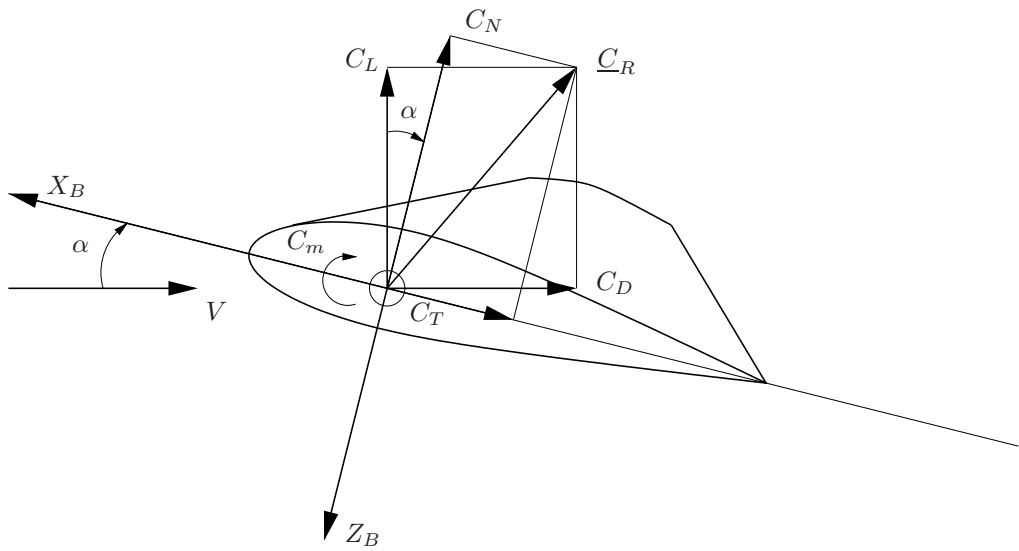


Figure 9-1: The aerodynamic forces and the moment acting on a wing in symmetric flight

pitching moment. The chapter proceeds with a general discussion on steady state flight conditions and is concluded with a discussion on the aerodynamic hinge moments of control surfaces.

9-1 Aerodynamic center

9-1-1 Aerodynamic forces and moments acting on a wing

A. Aerodynamic moment as a function of angle of attack

Figure 9-1 shows the components C_L and C_D , and C_N and C_T , of the dimensionless total aerodynamic force vector \underline{C}_R and the dimensionless aerodynamic moment C_m about a given arbitrary reference point, acting on a wing in symmetric flight, with

$$C_N = C_L \cos \alpha + C_D \sin \alpha$$

$$C_T = C_D \cos \alpha - C_L \sin \alpha$$

Figure 9-2 presents the familiar picture of C_L and C_D of a typical wing as a function of α , as measured in the wind tunnel. In addition the corresponding $C_N-\alpha$ and $C_T-\alpha$ curves are shown. From these figures it follows that the C_L and C_N curves are almost identical while the C_D and C_T are much more different. While C_L and C_N vary almost linearly with α over a large range of angles of attack, the relations between C_D and C_T and α is clearly non-linear. Figure 9-3 shows the relation between C_N and C_T of this wing. Note that C_T turns negative as α increases!

The aerodynamic moment coefficient C_m not only depends on α but also on the position of the selected reference point. This holds true also for the slope of the C_m versus α curve which, as we will show later is of crucial importance for longitudinal stability. It is easy to compute C_m for an arbitrary reference point from wind tunnel measurements about a fixed model suspension point.

Given the measured force and moment coefficients C_N and C_T and C_m about the suspension point (x_1, z_1) for some angle of attack, the moment about an arbitrary reference point (x_2, z_2) in the plane of symmetry can be computed as, see figure 9-4,

$$C_{m(x_2, z_2)} = C_{m(x_1, z_1)} + C_N \frac{x_2 - x_1}{\bar{c}} - C_T \frac{z_2 - z_1}{\bar{c}} \quad (9-1)$$

where x and z are coordinates in the aircraft reference frame F_r .

Figure 9-6 shows the resulting curves of C_m as a function of α for various positions of the reference point on the mac again for the case of a Fokker F-27 wing. From this figure it appears that,

1. The slope of the $C_m - \alpha$ curve strongly depends on the position of the reference point in the X_r -direction
2. In a large interval C_m varies almost linearly with α for reference points close to the mac

Figure 9-6 also shows the influence on the $C_m - \alpha$ curve of a change in position of the reference point parallel to the Z_r -axis. Now, the effect on the moment is much smaller. This is easily explained by equation (9-1), where C_T is small relative to C_N , see also figure 9-3. It appears that when the reference point is situated far below or above the mac, the moment is no longer a linear function of α which is due to the non-linear variation of C_T with α , see figure 9-2.

The dependence of the $C_m - \alpha$ curve on the selected reference point is a general phenomenon which does not apply to only wings but also to complete aircraft configurations. The relevant reference point in that case is the aircraft center of gravity, as we will see later.

It is possible to interpret the bundle of $C_m - \alpha$ curves in terms of some new concepts: the line of action of \underline{C}_R , the center of pressure, the aerodynamic center (ac) and the aerodynamic moment about the ac.

B. The line of action of \underline{C}_R and the center of pressure

The aerodynamic forces as well as the aerodynamic moment acting on the wing may also be obtained from the line of action along of the resulting aerodynamic force vector \underline{C}_R . The magnitude of the vector \underline{C}_R is,

$$C_R = \sqrt{C_L^2 + C_D^2} = \sqrt{C_N^2 + C_T^2}$$

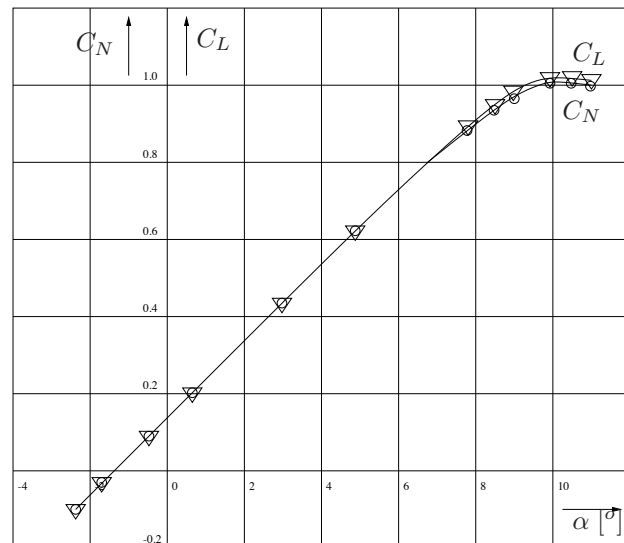
The direction of \underline{C}_R follows from the angle χ_1 , see figure 9-7, of the vector with the C_N -axis,

$$\chi_1 = \arctan \frac{C_T}{C_N}$$

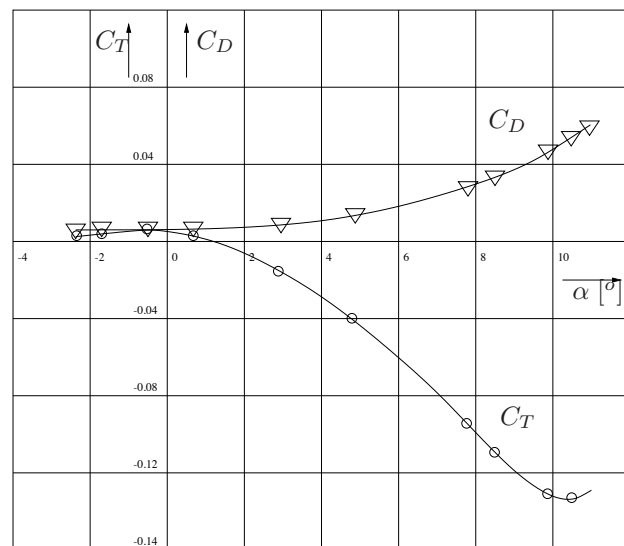
The position of the line of action of \underline{C}_R in the plane of symmetry, may be defined by its intersection with the (extended line through the) mac. This point is called the center of pressure.

The position of the center of pressure (x_d, z_0) for an arbitrary moment reference point (x_1, z_1) can be derived with equation (9-1) from $C_{m(x_1, z_1)}$,

$$C_{m(x_d, z_0)} = 0 = C_{m(x_1, z_1)} + C_N \frac{x_d - x_1}{\bar{c}} - C_T \frac{z_0 - z_1}{\bar{c}} \quad (9-2)$$

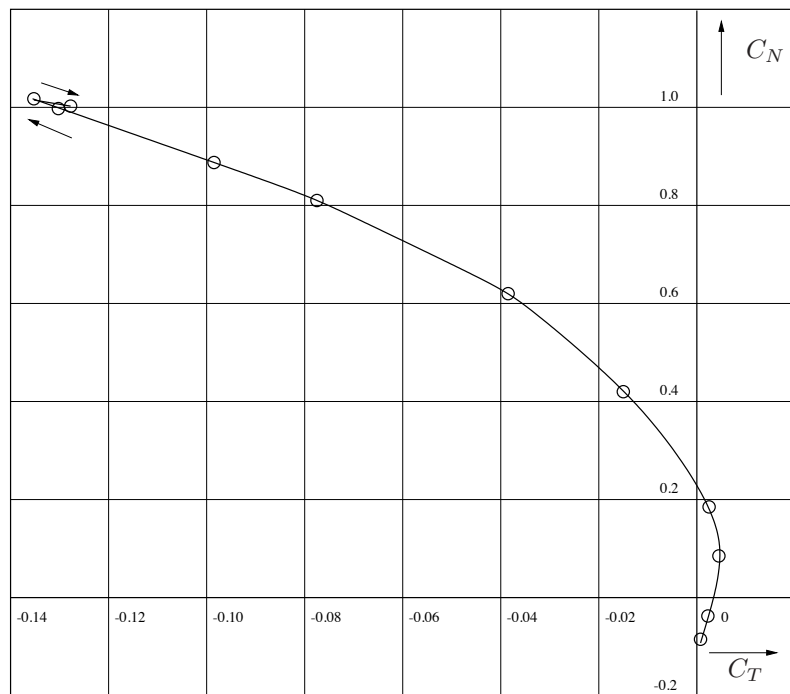
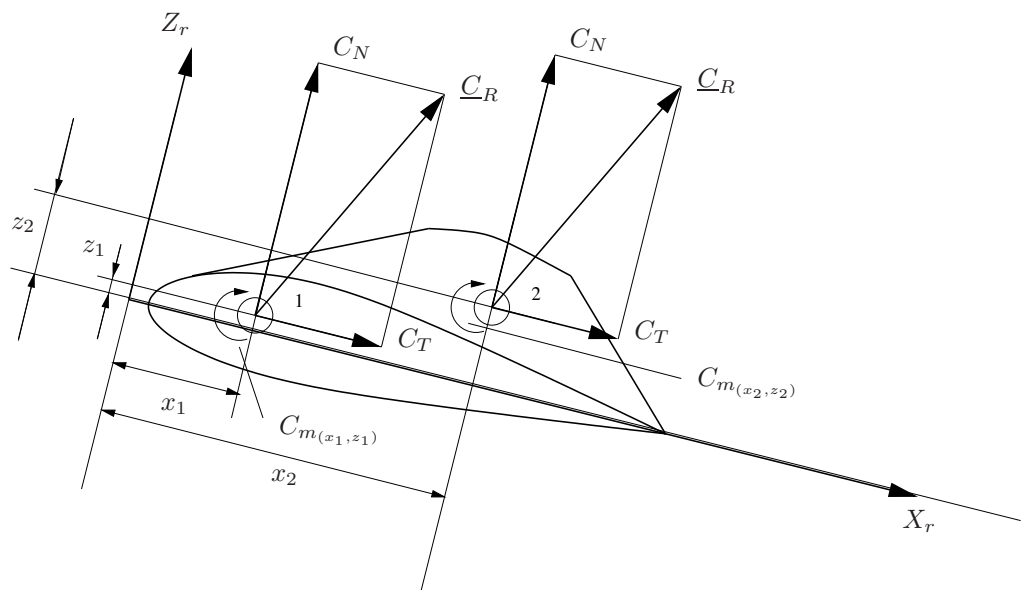


(A)



(B)

Figure 9-2: C_N , C_L and C_T , C_D as functions of α for the case of a Fokker F-27 wing (from reference [160])

Figure 9-3: C_N as a function of C_T for a Fokker F-27 wing (from reference [160])

$$C_{m(x_2, z_2)} = C_{m(x_1, z_1)} + C_N \frac{x_2 - x_1}{c} - C_T \frac{z_2 - z_1}{c}$$

Figure 9-4: The variation of the moment with changes in the reference point

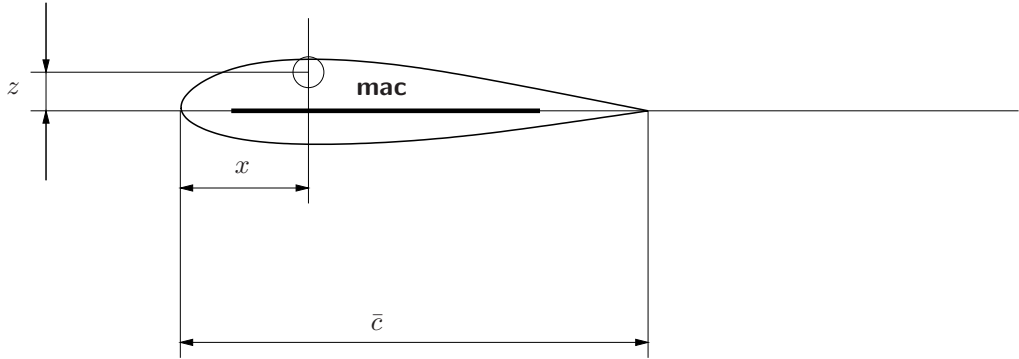


Figure 9-5: Location of point (x, z) with respect to the position of the mean aerodynamic chord

or simply

$$0 = C_{m(x_0, z_0)} + C_N \frac{x_d - x_0}{\bar{c}}$$

if the leading edge of the mac (x_0, z_0) is taken as the moment reference point. Now the center of pressure follows as,

$$\frac{x_d - x_0}{\bar{c}} = \frac{e}{\bar{c}} = -\frac{C_{m(x_0, z_0)}}{C_N} \quad (9-3)$$

It was shown above that for moment reference points on the mac, the wing aerodynamic moment C_m varies more or less linearly with the angle of attack, and thus also with C_N . The relation between $C_{m(x_0, z_0)}$ and C_N can then be written as,

$$C_{m(x_0, z_0)} = C_{m_0} + \frac{dC_{m(x_0, z_0)}}{dC_N} C_N \quad (9-4)$$

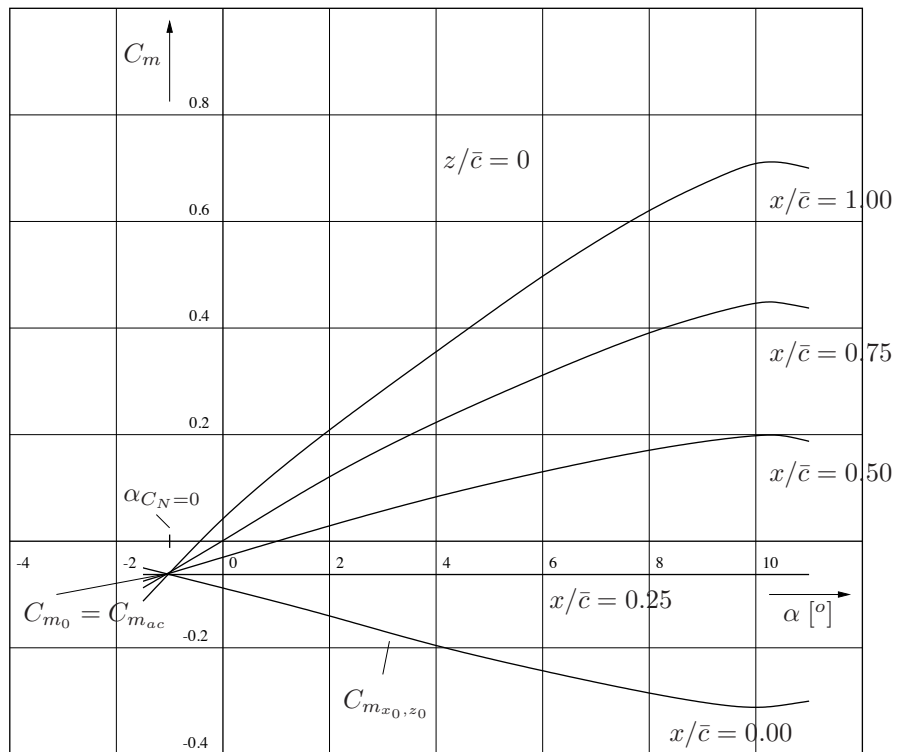
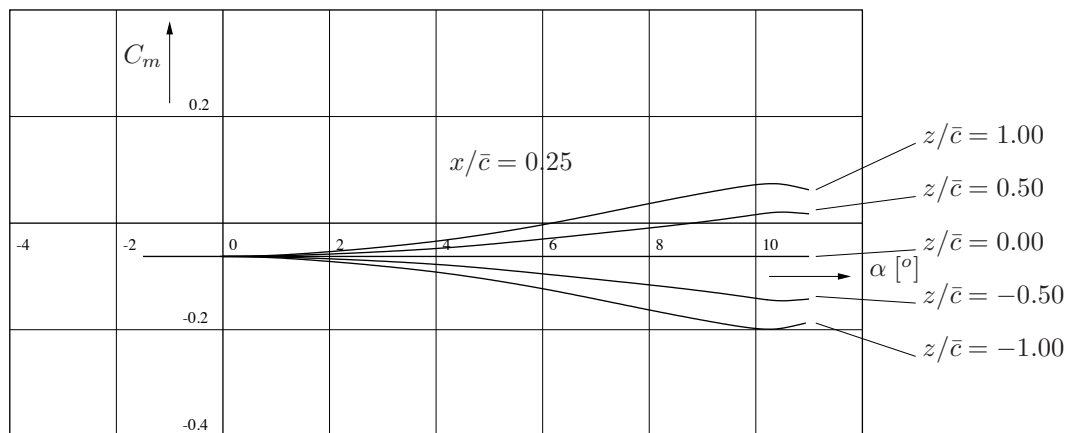
C_{m_0} denoting the value of C_m at $C_N = 0$. We note that all moment lines intercept at one single point at $\alpha_{C_N=0}$ with one value for C_{m_0} for all moment reference points. We note also that this and all other moment lines are close to straight up to an angle of attack of almost 10° . The center of pressure may now be written as,

$$\frac{e}{\bar{c}} = -\frac{C_{m_0}}{C_N} - \frac{dC_{m(x_0, z_0)}}{dC_N} \quad (9-5)$$

As $\frac{dC_{m(x_0, z_0)}}{dC_N}$ is negative, the center of pressure lies behind the leading edge of the mac for positive values of C_N .

Figure 9-9 shows the total aerodynamic force vector on the Fokker F-27 wing for a range of angles of attack. Figure 9-10 gives the corresponding position of the center of pressure.

The different ways to describe the aerodynamic moment characteristics of the wing, i.e. the $C_m - \alpha$ -curve and the line of action of \underline{C}_R with the center of pressure, both have their disadvantages. The $C_m - \alpha$ -curve for example is not unique but depends on the location of the reference point. In the other case of the line of action and the center of pressure both \underline{C}_R as well as the position of

(A) $\frac{x}{\bar{c}}$ variable(B) $\frac{z}{\bar{c}}$ variableFigure 9-6: Moment curves for various positions of the reference point for the Fokker F-27 wing
(from reference [160])

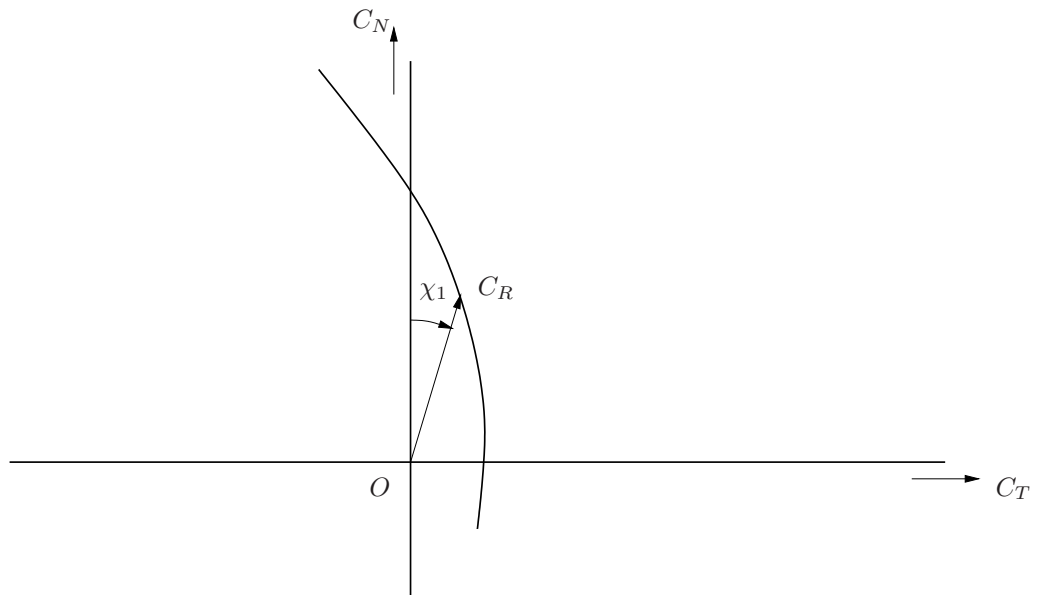


Figure 9-7: Definition of the angle χ_1

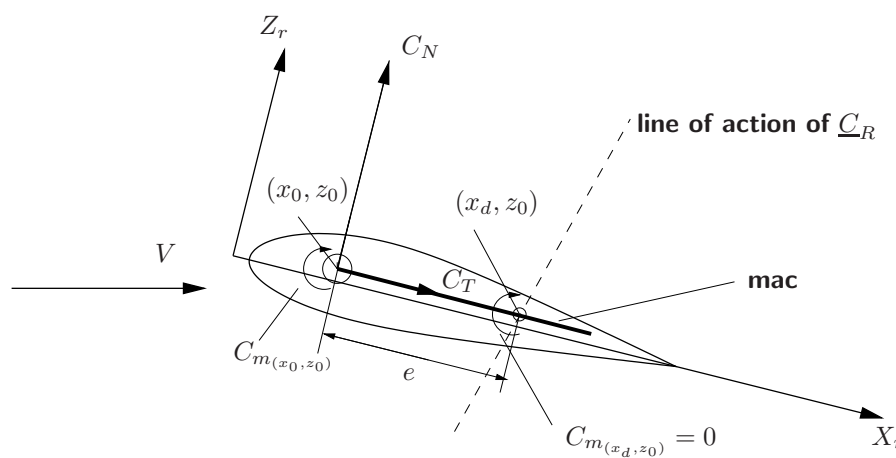


Figure 9-8: Definition of the center of pressure relative on the mean aerodynamic chord (mac)

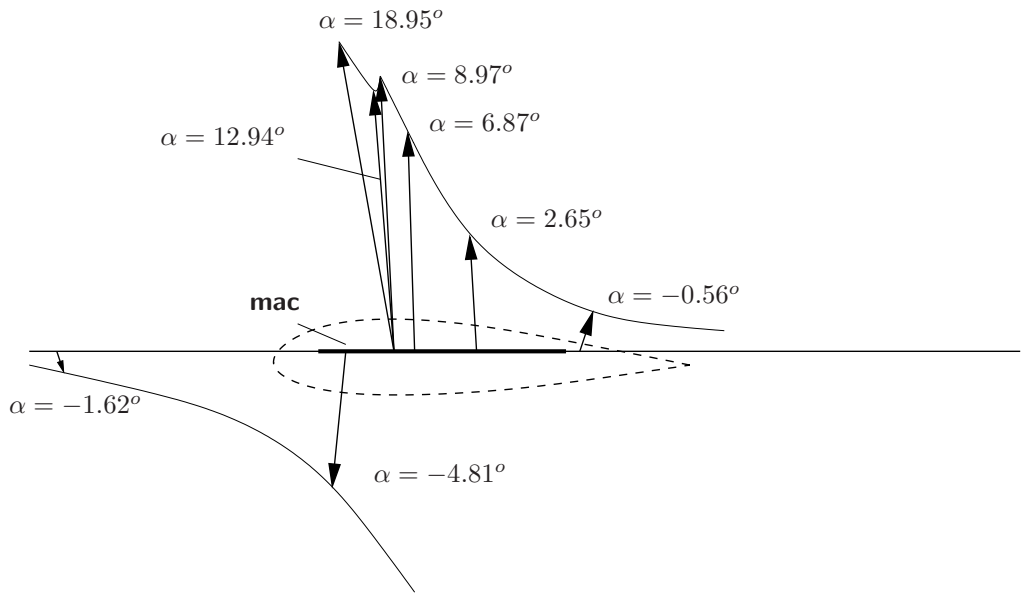


Figure 9-9: The magnitude of C_R and the position of the line of action of C_R as a function of the angle of attack for Fokker F-27 wing (from reference [160])

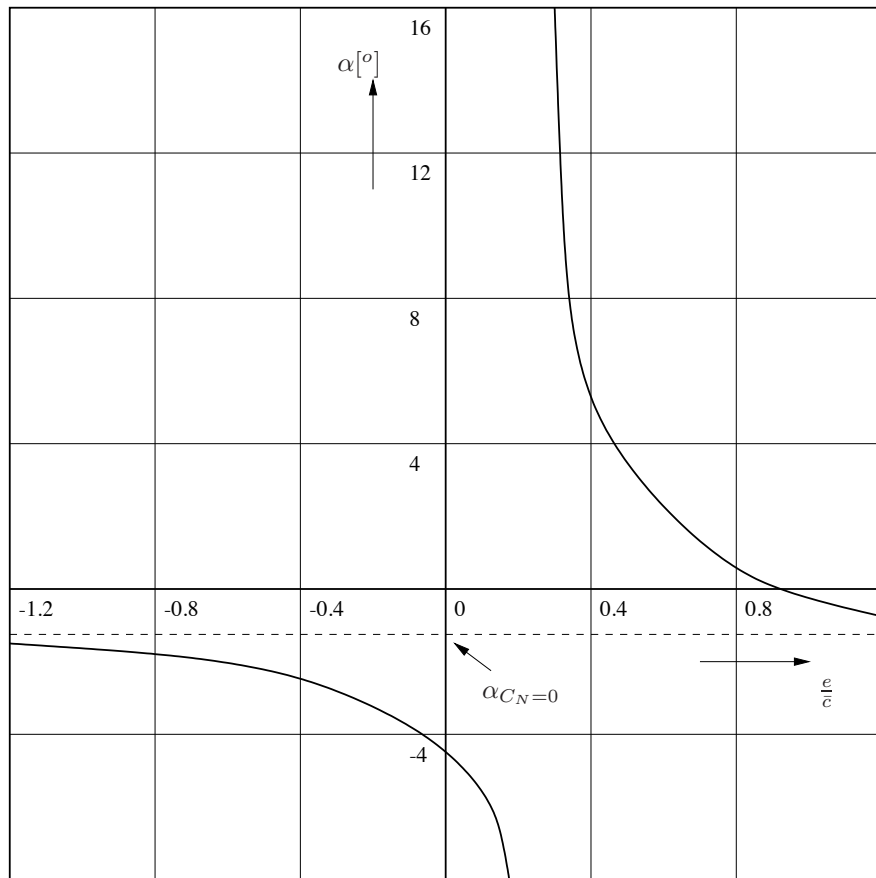


Figure 9-10: The position of the center of pressure as a function of the angle of attack for Fokker F-27 wing (from reference [160])

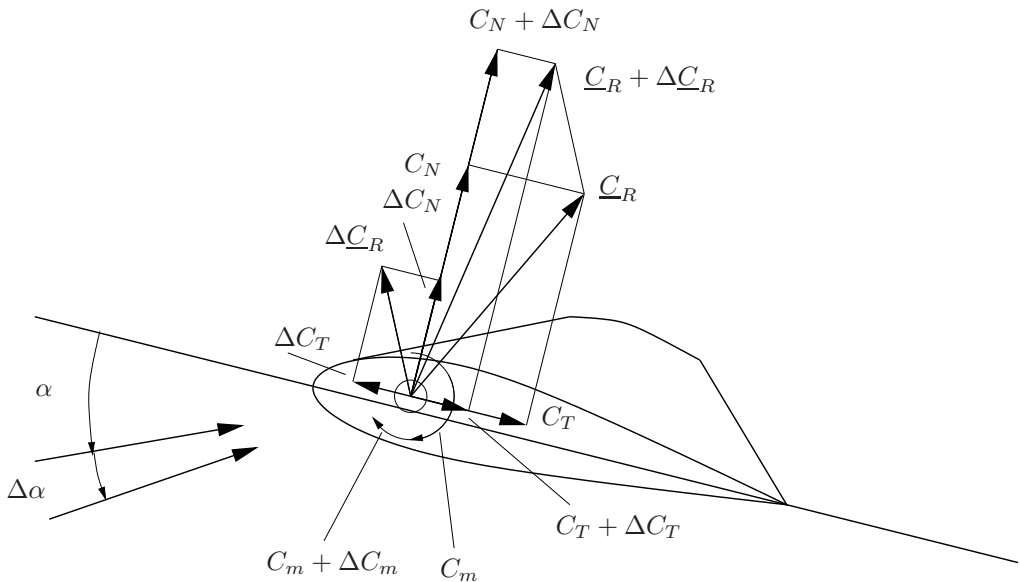


Figure 9-11: The aerodynamic forces and moment about an arbitrary point at two adjacent values of the angle of attack

the center of pressure depend on α . As a consequence the resulting 'picture' of the aerodynamic moment character is not simple to interpret, and easily leads to mistakes.

There, however, is an alternative and more attractive way to describe the aerodynamic moments which is based on the concept of the so called aerodynamic center. The aerodynamic center (ac) is a very special moment reference point with the important property that the aerodynamic moment about it is invariant, i.e. it does not change with the angle of attack! In many cases of practical interest also the position of the aerodynamic center (ac) is independent of the angle of attack. In the next section the aerodynamic center will be discussed in more detail.

9-1-2 A compact description for the aerodynamic moment characteristics

The following discussion it is shown that a moment reference point called the aerodynamic center (ac), about which aerodynamic moment ($C_{m_{ac}}$) is constant, does indeed exist. In this section the simplifying assumption is made that also the position of the ac does not vary with angle of attack.

A. The first metacenter, the neutral line and the neutral point

Figure 9-11 shows the forces and the moment about an arbitrary reference point at two adjacent angles of attack, α and $\alpha + \Delta\alpha$. Now the line of action of $\underline{\Delta C}_R$ in Figure 9-12, may readily be constructed as the vector difference of the aerodynamic forces corresponding to α and $\alpha + \Delta\alpha$.

About any point on the lines of action of \underline{C}_R and $\underline{C}_R + \underline{\Delta C}_R$ the aerodynamic moment at the respective angle of attack, i.e. α and $\alpha + \Delta\alpha$, is zero. Consequently, the moment about the point of intersection of the two lines, M_1 , equals zero both at α and $\alpha + \Delta\alpha$. In the limiting case, where $\Delta\alpha \rightarrow 0$, this point of intersection of the two adjacent lines of action is well known as the **first metacenter**, M_1 , in naval architecture.

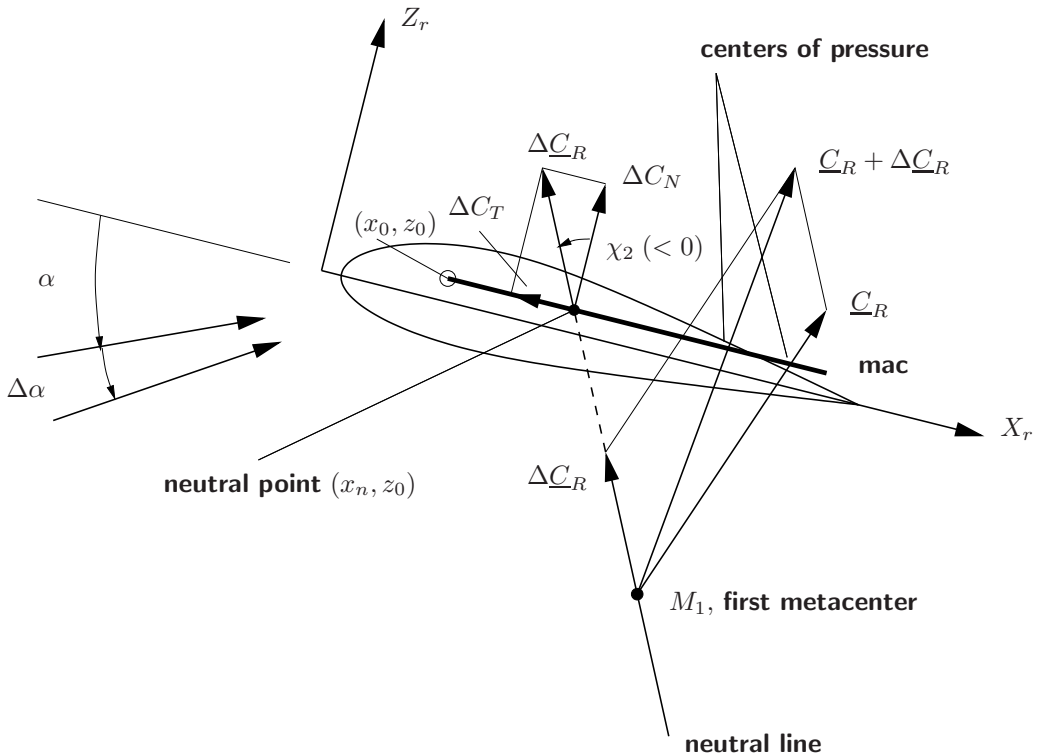


Figure 9-12: The line of action of the difference between aerodynamic force vectors at adjacent values of the angle of attack

We may conclude that in the first metacenter the following two conditions hold,

$$\begin{aligned} C_m &= 0 \\ \frac{dC_m}{d\alpha} &= 0 \end{aligned} \tag{9-6}$$

The physical meaning of the line of action of $\Delta\underline{C}_R$ is that for each reference point on the line the change of aerodynamic moment will be zero. Consequently, for infinitely small change of alpha the analytical expression for all points on the line of action of $d\underline{C}_R$ is,

$$\frac{dC_m}{d\alpha} = 0 \tag{9-7}$$

The line of action of $d\underline{C}_R$ is called the **neutral line**. The first metacenter turns out to be a special point on the neutral line where $C_m = 0$ as it is the intersection of the line of action of \underline{C}_R and the neutral line.

If the aerodynamic forces and the moment about the leading edge of the mac (x_0, z_0) are given the expression for the neutral line can be extracted from equations (9-1) and (9-7),

$$\frac{dC_{m(x_0, z_0)}}{d\alpha} + \frac{dC_N}{d\alpha} \frac{x - x_0}{\bar{c}} - \frac{dC_T}{d\alpha} \frac{z - z_0}{\bar{c}} = 0 \tag{9-8}$$

The intersection of the neutral line with the mac, where $z = z_0$, is called the **neutral point** of the wing. The distance of this neutral point (x_n, z_0) behind the leading edge of the mac follows

from equation (9-8),

$$\frac{x_n - x_0}{\bar{c}} = - \frac{dC_{m(x_0, z_0)}}{dC_N} \quad (9-9)$$

with,

$$z_n = z_0$$

The orientation of the neutral line follows from (see figure 9-12),

$$\chi_2 = \arctan \frac{dC_T}{dC_N} \quad (9-10)$$

B. The second metacenter and the aerodynamic center

Next, we consider two vectors $d\underline{C}_R$ at two values of the angle of attack, $\alpha_1 = \alpha$ and $\alpha_2 = \alpha + \Delta\alpha$. It follows that now, we have two neutral lines, one for α_1 and for α_2 . The point where these two neutral lines intersect satisfies the following conditions:

$$\begin{aligned} \left(\frac{dC_m}{d\alpha} \right)_{\alpha_1} &= 0 \\ \left(\frac{dC_m}{d\alpha} \right)_{\alpha_2} &= 0 \end{aligned}$$

see figure 9-13. In the limiting case where $\Delta\alpha \rightarrow 0$ the point of intersection follows from,

$$\frac{dC_m}{d\alpha} = 0 \quad (9-11)$$

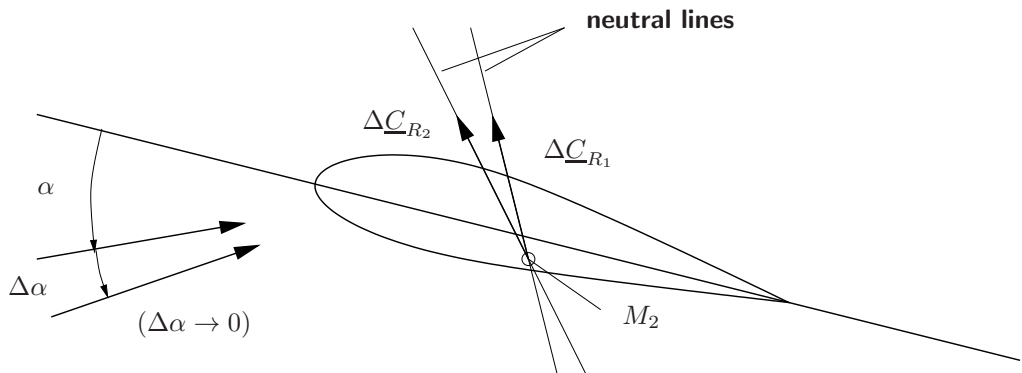
$$\frac{d^2C_m}{d\alpha^2} = 0 \quad (9-12)$$

The point of intersection of two neutral lines belonging to two adjacent angles of attack is called the **second metacenter**, M_2 in naval architecture. In aeronautical engineering this point is referred to as the aerodynamic center (ac).

In theoretical aerodynamics it is possible to prove that thin airfoils in a potential flow have an ac which is exactly invariant with the angle of attack. According to this thin airfoil theory, the ac of all thin airfoils is located at 25 % of the airfoil chord.

In experimental aerodynamics, measurements on two-dimensional wing airfoils show that in the range of angles of attack where no flow separation occurs there is indeed an ac position which is very nearly independent of the angle of attack. Also in the case of a complete wing in three-dimensional flow the ac turns out to have a constant position over a wide range of angles of attack in many cases for moderate to large aspect ratios and small to moderate sweep angles.

The . The location of the ac with coordinates x_{ac} and z_{ac} with respect to the leading edge of the mac follows from the conditions (9-11, 9-12),



second metacenter = aerodynamic center

Figure 9-13: The position of the aerodynamic center

$$\frac{dC_{m_{ac}}}{d\alpha} = 0$$

or,

$$\frac{dC_{m(x_0, z_0)}}{d\alpha} + \frac{dC_N}{d\alpha} \frac{x_{ac} - x_0}{\bar{c}} - \frac{dC_T}{d\alpha} \frac{z_{ac} - z_0}{\bar{c}} = 0 \quad (9-13)$$

and,

$$\frac{d^2C_{m_{ac}}}{d\alpha^2} = 0 \quad (9-14)$$

$$\frac{d^2C_{m(x_0, z_0)}}{d\alpha^2} + \frac{d^2C_N}{d\alpha^2} \frac{x_{ac} - x_0}{\bar{c}} - \frac{d^2C_T}{d\alpha^2} \frac{z_{ac} - z_0}{\bar{c}} = 0 \quad (9-15)$$

in which it was assumed that x_{ac} and z_{ac} are independent of α . After computing the two coordinates x_{ac} and z_{ac} of the ac by solving these equations, the aerodynamic moment about the ac, $C_{m_{ac}}$, follows by substitution into (9-1). This leads to the following expression for $C_{m_{ac}}$:

$$C_{m_{ac}} = C_{m(x_0, z_0)} + C_N \frac{x_{ac} - x_0}{\bar{c}} - C_T \frac{z_{ac} - z_0}{\bar{c}} \quad (9-16)$$

If C_N , C_T and $C_{m(x_0, z_0)}$ are known from measurements as functions of the angle of attack, it is possible in principle to obtain the coordinates x_{ac} and z_{ac} using the equations above (9-13). This would require, however, to differentiate the experimental data on C_N , C_T and C_m two times with respect to alpha, which maybe difficult to do.

An alternative way is to use the expressions for the neutral line (9-7),

$$\frac{dC_{m_{ac}}}{d\alpha} = 0$$

for two adjacent angles of attack. The coordinates x_{ac} and z_{ac} follow from their intersection .

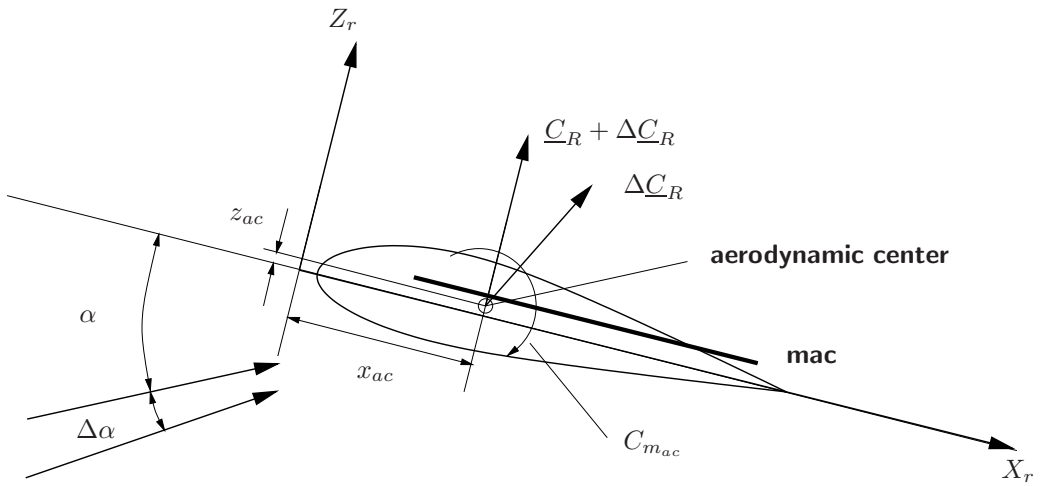


Figure 9-14: The aerodynamic forces and moment, using the ac as the moment reference point

With the concept of the aerodynamic center, the model of the aerodynamic forces and moment acting on a wing can be written in a very simple way. Each neutral line for any angle of attack α must pass through the ac. As by definition the moment $C_{m_{ac}}$ is constant, the model of the aerodynamic forces and moment acting on the wing thus consists of just a constant $C_{m_{ac}}$ about the ac of the wing and the total aerodynamic force \underline{C}_R through the ac for all angles of attack (see figure 9-14).

C. Replacing the ac by the neutral point

We have seen that the aerodynamic center is the moment reference point for which C_m is constant. It follows from practice that the position of the ac is indeed invariant for a range of angles of attack. Furthermore, it appears that the aerodynamic center is usually located very close to the wing's mac. This follows also from equation 9-15 if we take account of the virtually perfect linear relationships between $C_{m(x_0, z_0)}$ and alpha, and C_N and alpha. So, their second derivatives will vanish, resulting in $z_{ac} = z_0$, see again figure 9-6. By assuming that the ac is located exactly on the mac, the ac coincides with the neutral point. The following shows also that this simplification is usually quite acceptable.

As $C_{m_{ac}}$ is constant:

$$\frac{dC_{m_{ac}}}{d\alpha} = 0$$

it follows from equation (9-1) that,

$$\frac{dC_{m_{ac}}}{d\alpha} = \frac{dC_{m(x_0, z_0)}}{d\alpha} + \frac{dC_N}{d\alpha} \frac{x_{ac} - x_0}{\bar{c}} - \frac{dC_T}{d\alpha} \frac{z_{ac} - z_0}{\bar{c}} \quad (9-17)$$

In this expression $\frac{dC_T}{d\alpha}$ is relatively small compared to $\frac{dC_N}{d\alpha}$. Moreover, the distance from the ac to the mac is small (a few percent of \bar{c} at most). This means that the last term in equation eq: eq2p14 may be neglected and the x -coordinate of the ac $\frac{x_{ac}}{\bar{c}}$, follows from equation (9-17) as,

$$\frac{x_{ac} - x_0}{\bar{c}} = - \frac{dC_{m(x_0, z_0)}}{dC_N} \quad (9-18)$$

This result is identical to the expression for the location of the neutral point, equation (9-9), meaning that if the contribution of the tangential force is neglected in (9-17), the ac will indeed coincide with the neutral point.

With $z_{ac} = z_0$, $C_{m_{ac}}$ follows, with (9-1), from,

$$C_{m_{ac}} = C_{m(x_0, z_0)} + C_N \frac{x_{ac} - x_0}{\bar{c}} \quad (9-19)$$

and, clearly,

$$C_{m_{ac}} = C_{m(x_0, z_0)_{C_N=0}} = C_{m_0} \quad (9-20)$$

As has been shown, the ac and $C_{m_{ac}}$ can be obtained simply from experimental data on the aerodynamic moment about the leading edge of the mac. Next, using equation (9-18), x_{ac} is obtained from the slope of the $C_m - C_N$ -curve. According to equation (9-20), $C_{m_{ac}}$ is equal to C_{m_0} at $C_N = 0$. In many cases in the literature this simplified and approximated position of the ac is used. See for instance reference [50].

Finally if $\frac{x_{ac}}{\bar{c}}$ and $C_{m_{ac}}$ are known, the aerodynamic moment coefficient about an arbitrary reference point on the mac is given by the following very simple expression:

$$C_m(x) = C_{m_{ac}} + C_N \frac{x - x_{ac}}{\bar{c}}$$

The description of C_m using the ac and $C_{m_{ac}}$ derives its practical value from the fact that $C_{m_{ac}}$ is constant and the position of the ac is independent of the angle of attack. However, for wings with a low aspect ratios and/or a large sweep angle the variation of the ac with angle of attack may not always be negligible, not even at those angles of attack occurring in normal flight.

In order to enlarge the applicability of the ac and $C_{m_{ac}}$, a more general definition may be used in which $C_{m_{ac}}$ is kept constant but the ac is allowed to shift position depending on alpha.

9-1-3 The role of the aerodynamic center and $C_{m_{ac}}$ in static stability

If the $C_{m_{ac}}$ and the position of the ac (x_{ac}, z_{ac}) of a wing are known, the moment about an arbitrary point (x, z) is given by, see figure 9-15,

$$C_m(x, z) = C_{m_{ac}} + C_N \frac{x - x_{ac}}{\bar{c}} - C_T \frac{z - z_{ac}}{\bar{c}} \quad (9-21)$$

For qualitative discussions it usually is permissible to simplify equation (9-21), as was already indicated in section 9-1-2, by neglecting the contribution of the tangential force,

$$C_m = C_{m_{ac}} + C_N \frac{x - x_{ac}}{\bar{c}} \quad (9-22)$$

This simplified expression for C_m will often be used in the following discussions.

Suppose a model of a wing has been mounted in a wind tunnel so that the model is free to rotate about an axis through the moment reference point, serving now as the suspension point of the model. Furthermore, it is supposed that the center of gravity of the model has been made to

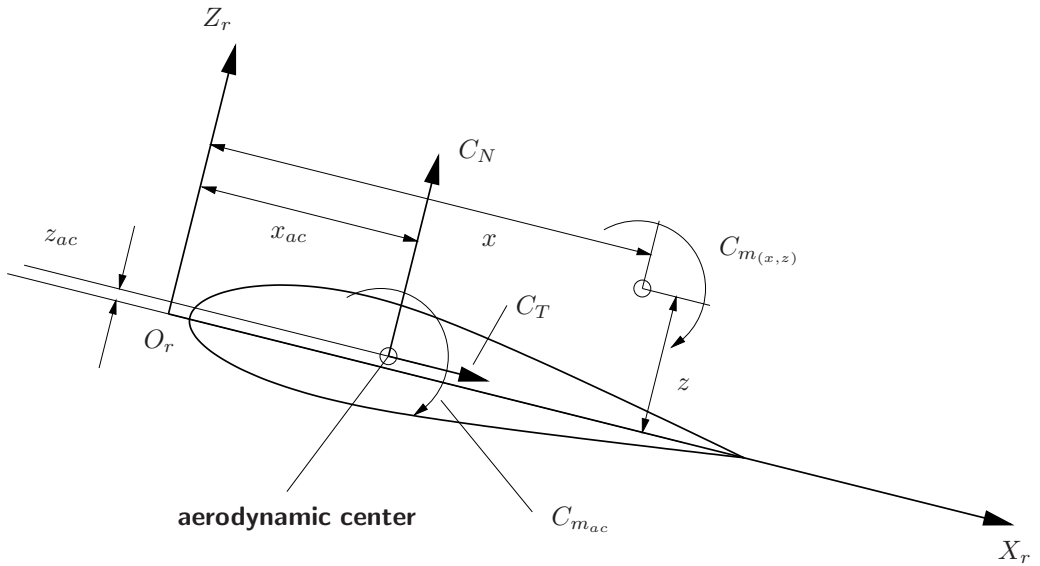


Figure 9-15: The moment about an arbitrary point (x, z) if the position of the ac and the $C_{m_{ac}}$ are known

coincide with this axis of rotation. Now a necessary condition for a steady equilibrium condition is $C_m = 0$.

Small disturbances will induce model attitude (i.e. angle of attack) deviations from the nominal equilibrium condition. If such a deviation causes an aerodynamic moment acting against the change in angle of attack the original equilibrium situation was a stable one. This means that an increase in angle of attack must give rise to a negative, nose-down, change in aerodynamic moment. The condition for stability may thus be written as:

$$\frac{dC_m}{d\alpha} < 0 \quad \text{at } C_m = 0 \quad (9-23)$$

It is easy to see that if $\frac{dC_m}{d\alpha} > 0$ at $C_m = 0$, the equilibrium is unstable. If a change in angle of attack causes no change in the aerodynamic moment, the equilibrium is said to be indifferent or neutrally stable. In that case $C_m = 0$ at all angles of attack and there will be equilibrium at any value of α .

The importance of the position of the suspension point relative to the ac of the wing is illustrated by considering the equilibrium of the moment and the stability of the equilibrium of the wing for different positions of the suspension point. From equation (9-22) follows for the equilibrium ($C_m = 0$),

$$C_m = C_{m_{ac}} + C_N \frac{x - x_{ac}}{\bar{c}} = 0 \quad (9-24)$$

and for the change of the moment with angle of attack,

$$\frac{dC_m}{d\alpha} = \frac{dC_N}{d\alpha} \frac{x - x_{ac}}{\bar{c}} \quad (9-25)$$

where $\frac{dC_N}{d\alpha}$ in the range of linear variation of C_N with α is always positive. Three cases are considered,

1. **suspension point ahead of the ac**, $\frac{x - x_{ac}}{\bar{c}} < 0$

According to equation (9-24), equilibrium is possible for either positive or negative values of C_N depending on the magnitude and the sign of $C_{m_{ac}}$, see figures 9-16 and 9-17. From equation (9-25) follows that $\frac{dC_m}{d\alpha} < 0$. This means that the equilibrium is stable, as can be seen from figures 9-16 and 9-17.

2. suspension point in the ac, $\frac{x-x_{ac}}{\bar{c}} = 0$

In this situation, equilibrium is possible only if $C_{m_{ac}} = 0$, see equation (9-24). If this is the case, equilibrium exists at any value of C_N , or α (see figure 9-18). The equilibrium is indifferent ($\frac{dC_m}{d\alpha} = 0$).

If $C_{m_{ac}} \neq 0$ no equilibrium situation is possible and as a consequence there can be no discussion of stability either (see figure 9-19).

3. suspension point behind the ac, $\frac{x-x_{ac}}{\bar{c}} > 0$

if $C_{m_{ac}} < 0$ equilibrium will exist at a certain positive C_N and for $C_{m_{ac}} > 0$ at a negative value of C_N (see figures 9-20 and 9-21). In both cases the equilibrium is unstable, $\frac{dC_m}{d\alpha} > 0$.

In summary it can be said that in the general case, i.e. where $C_{m_{ac}} \neq 0$, a condition of equilibrium ($C_m = 0$) is possible for any position of the suspension point ahead or behind the ac. The value of α or C_N for which $C_m = 0$ does depend on $C_{m_{ac}}$, see equation (9-24), but has by itself nothing to do with the stability of the equilibrium. At a given C_{N_α} the stability follows only from the position of the suspension point relative to the ac, see equation (9-25).

Summarizing,

- If the suspension point is situated ahead of the ac the model is always stable, $\frac{dC_m}{d\alpha} < 0$. If the suspension point moves back, the model becomes less stable as $\frac{dC_m}{d\alpha}$ becomes less negative.
- If the suspension point coincides with the ac, the slope of the moment curve is zero. In that case equilibrium is possible only if $C_{m_{ac}} = 0$. This equilibrium is said to be indifferent or neutrally stable.
- The equilibrium is always unstable if the suspension point lies behind the ac as then $\frac{dC_m}{d\alpha} > 0$.

In the foregoing the influence of a change in the x -coordinate of the moment reference point (the suspension point and rotation axis) was considered. In a similar way the influence of a change in the position of the ac at a constant position of the suspension point can be studied. Such a shift in ac location may be caused for instance by the influence of the fuselage on C_m as will be discussed later. From equation (9-25) it follows, that a forward shift of the ac (x_{ac} decreases) always has a destabilizing influence and a rearward shift of the ac a stabilizing effect.

In chapter 10 it is shown that the discussion given here for a wing, in a more extended form applies to the complete aircraft as well. The center of gravity of an aircraft has in this respect the same role as the axis of rotation of the wing. The slope of the moment curve ($C_m - \alpha$), with the center of gravity as the suspension point, is a measure of the static stability of the aircraft, i.e. its tendency to return the original angle of attack following a hypothetical disturbance.

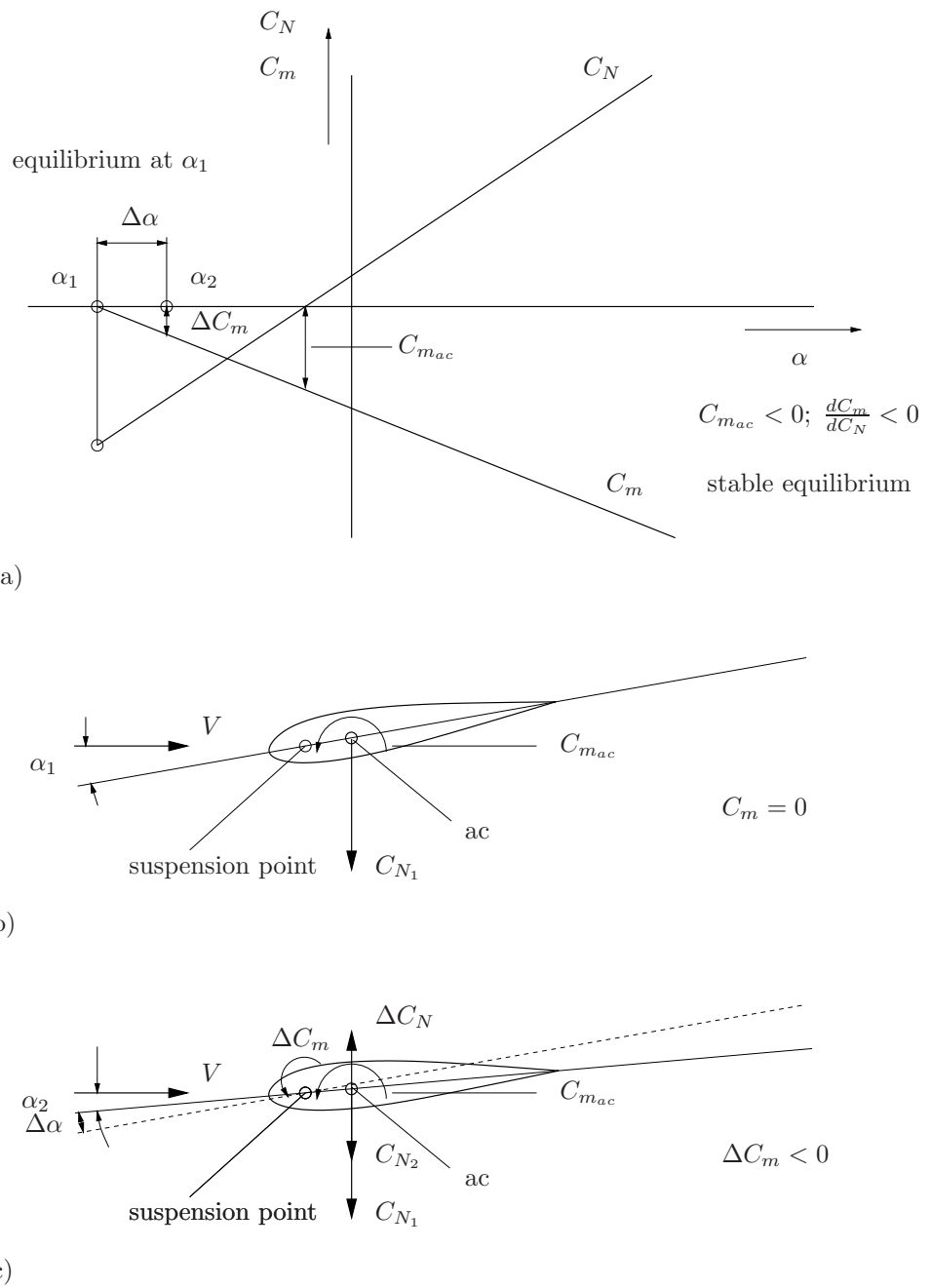
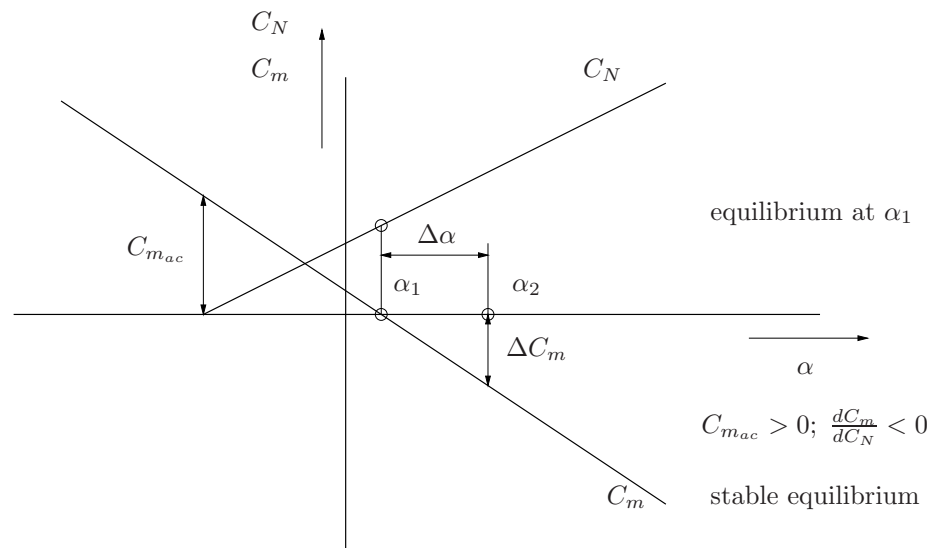
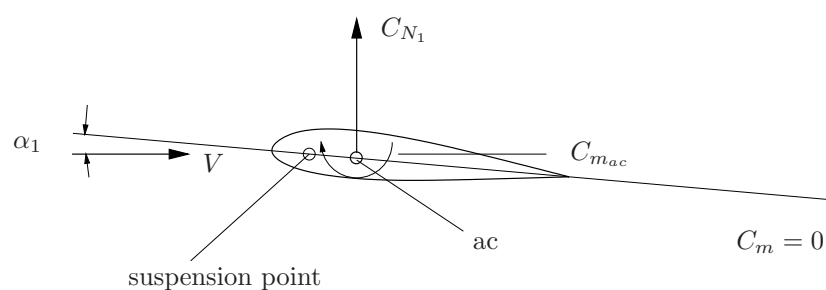


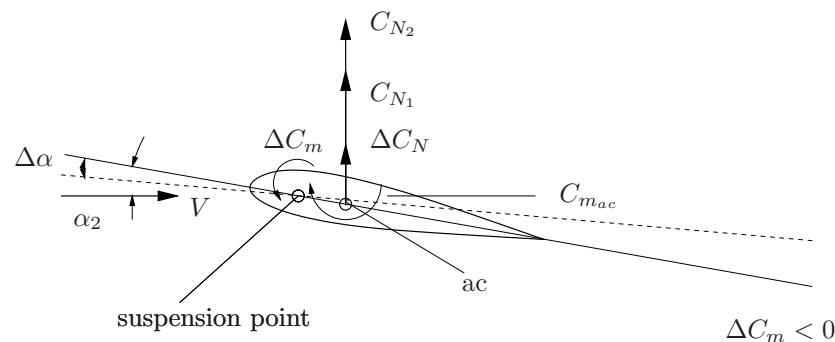
Figure 9-16: Equilibrium and stability of a wing, suspension point **ahead** of the ac, $C_{m_{ac}}$ **negative**



(a)



(b)



(c)

Figure 9-17: Equilibrium and stability of a wing, suspension point **ahead** of the ac, $C_{m_{ac}}$ **positive**

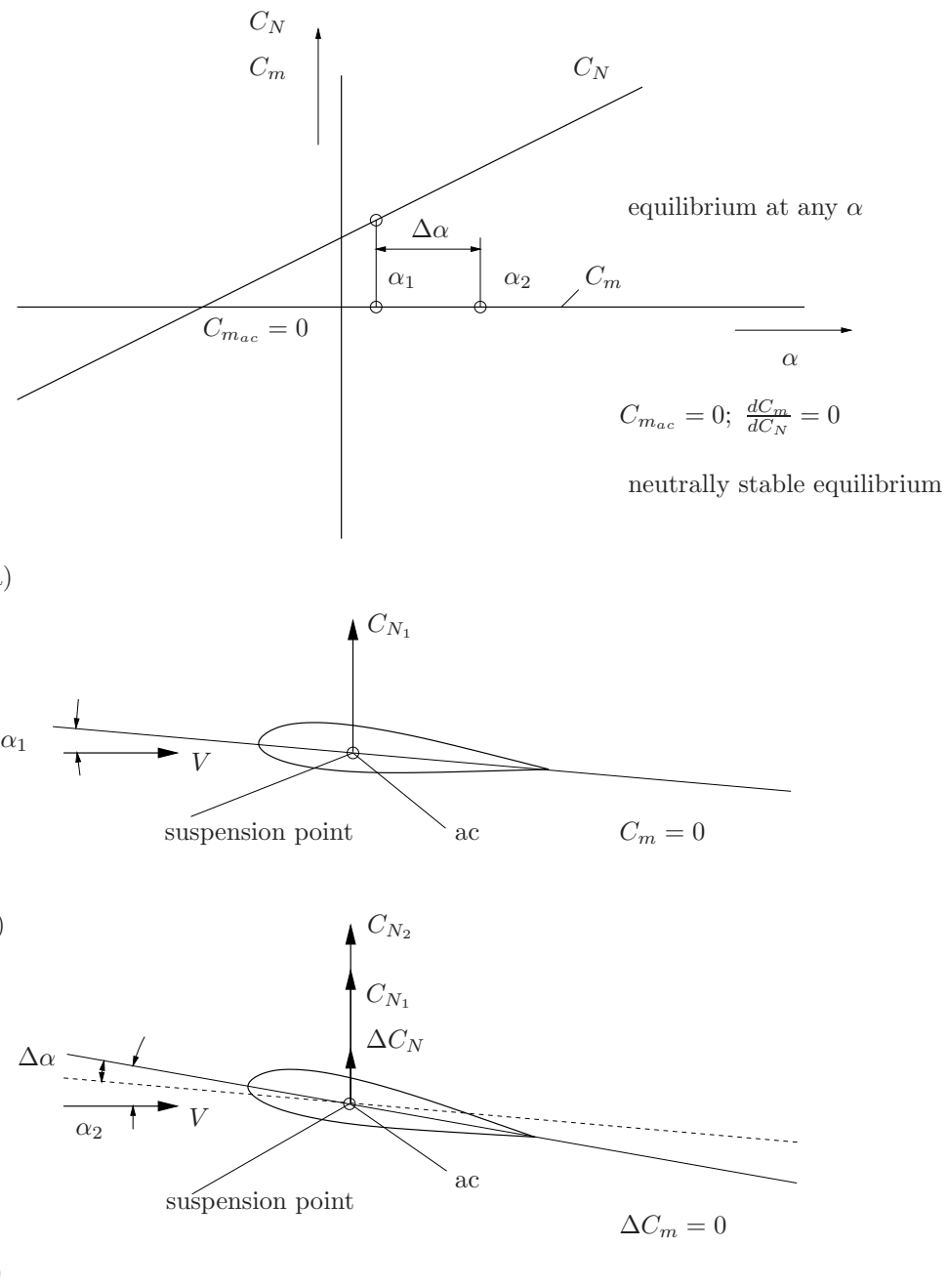


Figure 9-18: Equilibrium and stability of a wing, suspension point in the aerodynamic center, $C_{m_{ac}}$ equals 0

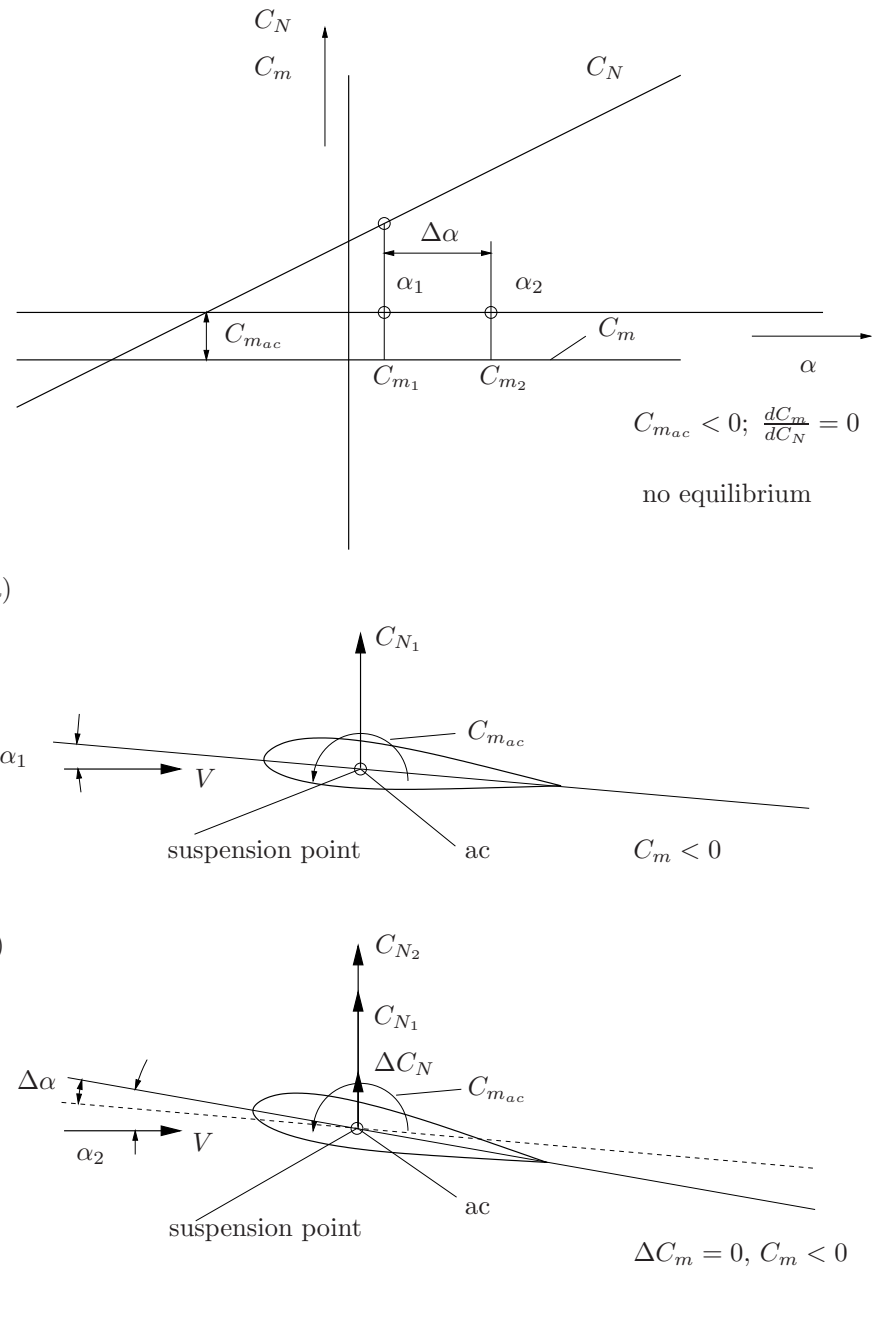
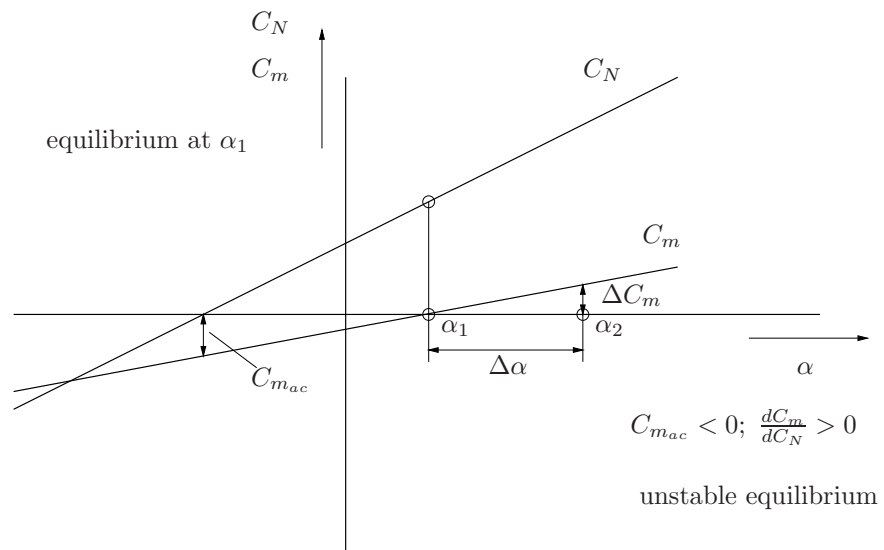
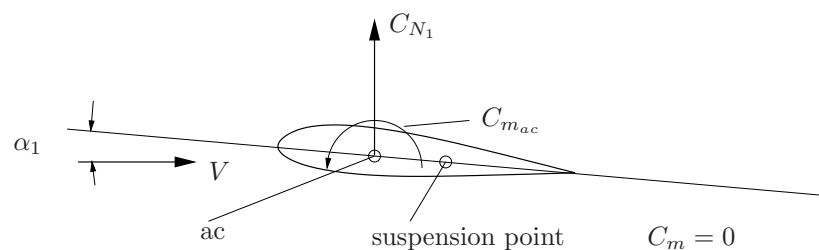


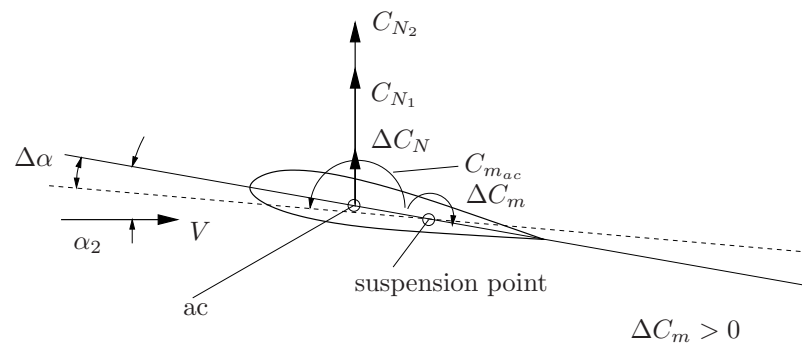
Figure 9-19: Equilibrium and stability of a wing, suspension point in the aerodynamic center, $C_{m_{ac}}$ negative



(a)



(b)



(c)

Figure 9-20: Equilibrium and stability of a wing, suspension point **behind** the ac, $C_{m_{ac}}$ **negative**

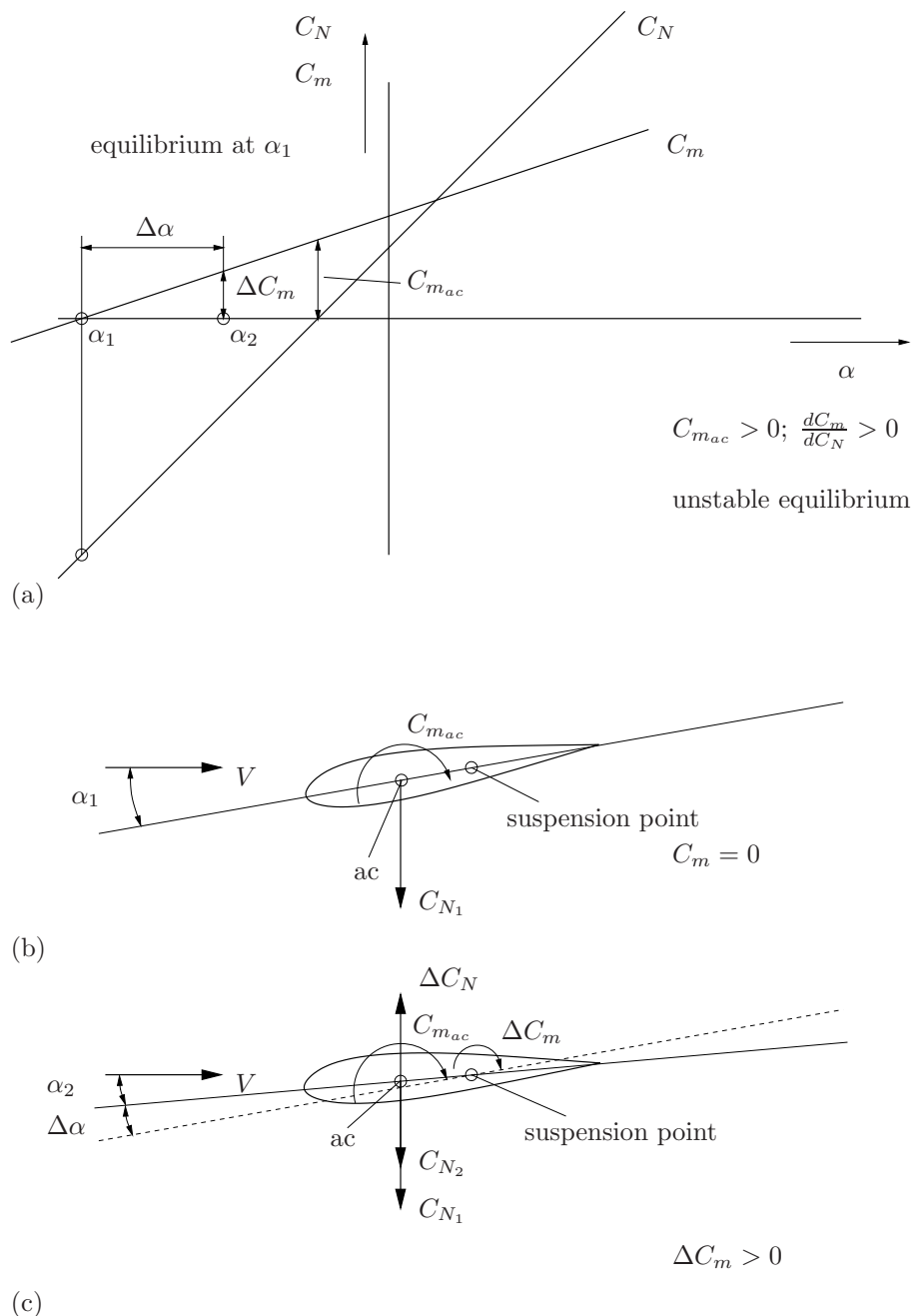


Figure 9-21: Equilibrium and stability of a wing, suspension point **behind** the ac, $C_{m_{ac}}$ **positive**

9-1-4 The position of the aerodynamic center and C_{mac} of a wing

In the foregoing sections an elegant and compact model was derived for the aerodynamic moment acting on a wing. Section 9-1-3 discussed how to use that model for analysis of static stability. The present section describes a method to derive such a model for a wing of arbitrary shape and twist from 'strip theory' rather than from wind tunnel measurements. The main motive to discuss this theory here is to allow the reader to understand the relationships between the parameters defining wing shape and the aerodynamic center ac and C_{mac} .

The basic idea behind strip theory is to derive the aerodynamic characteristics of wings of arbitrary geometry, dihedral and twist from the aerodynamic characteristics of two dimensional wing profiles.

A 'two-dimensional' dimensionless lift coefficient may be defined as $c_\ell = \frac{\ell}{\frac{1}{2}\rho V^2 c}$, in which ℓ denotes lift force per unit of length. In a similar way the two dimensional normal force coefficient c_n , drag coefficient c_d , tangential force coefficient c_t and moment coefficient c_m may be defined. Just for simplicity, below, the difference between the two dimensional lift and normal force is neglected, as well as the contributions of the drag or tangential force to the overall aerodynamic moment. The latter implies that effects of dihedral are neglected too. All formula's, however, may easily be extended to include these effects.

The simple model of the aerodynamic forces and moments developed in part c of section 9-1-2 is now used as the model for the aerodynamic forces and moment acting on a wing strip at a given span-wise location.

The lift distribution across the span of a wing can be divided into two parts. One part is the 'basic lift distribution' $c_{\ell_b}(y)$, which is the lift distribution at $\alpha_{C_L=0}$. This lift distribution depends on only on the geometry of the wing and the wing profiles applied. The other part is the 'additional lift' distribution $c_{\ell_a}(y)$ which depends on the wing geometry and wing profiles as well but in addition depends on the angle of attack, see figure 9-22.

Several examples of basic, additional and total lift distributions using a source/doublet singularity panel method (based on linearized potential flow) are given in figures 9-23 to 9-28. The figures clearly illustrate the effects of wing-twist, taper ratio and wing sweep angle.

We note that C_{mac} is the aerodynamic moment when $C_L = 0$. This must imply that C_{mac} is caused by the torque resulting from the basic lift distribution and the $c_{m_{ac}}$'s of the wing strip airfoils.

From the characteristics of the applied wing airfoils as well as the shape of the wing we now continue by computing the position of the ac, the magnitude of C_{mac} and lift gradient $C_{L\alpha}$.

The lift acting on a wing strip dy is,

$$dL = dL_a + dL_b = (c_{\ell_a} + c_{\ell_b}) \frac{1}{2}\rho V^2 c dy$$

This local lift force is assumed to act through the local ac, the constant moment $c_{m_{ac}}$ must be added, see figure 9-29. The moment due to the additional lift distribution about \bar{x}_0 , the leading edge of the mac, follows as,

$$M_a = -2 \int_0^{\frac{b}{2}} \left(c_{\ell_a} \frac{1}{2}\rho V^2 c \right) (x - \bar{x}_0) \cos \alpha dy$$

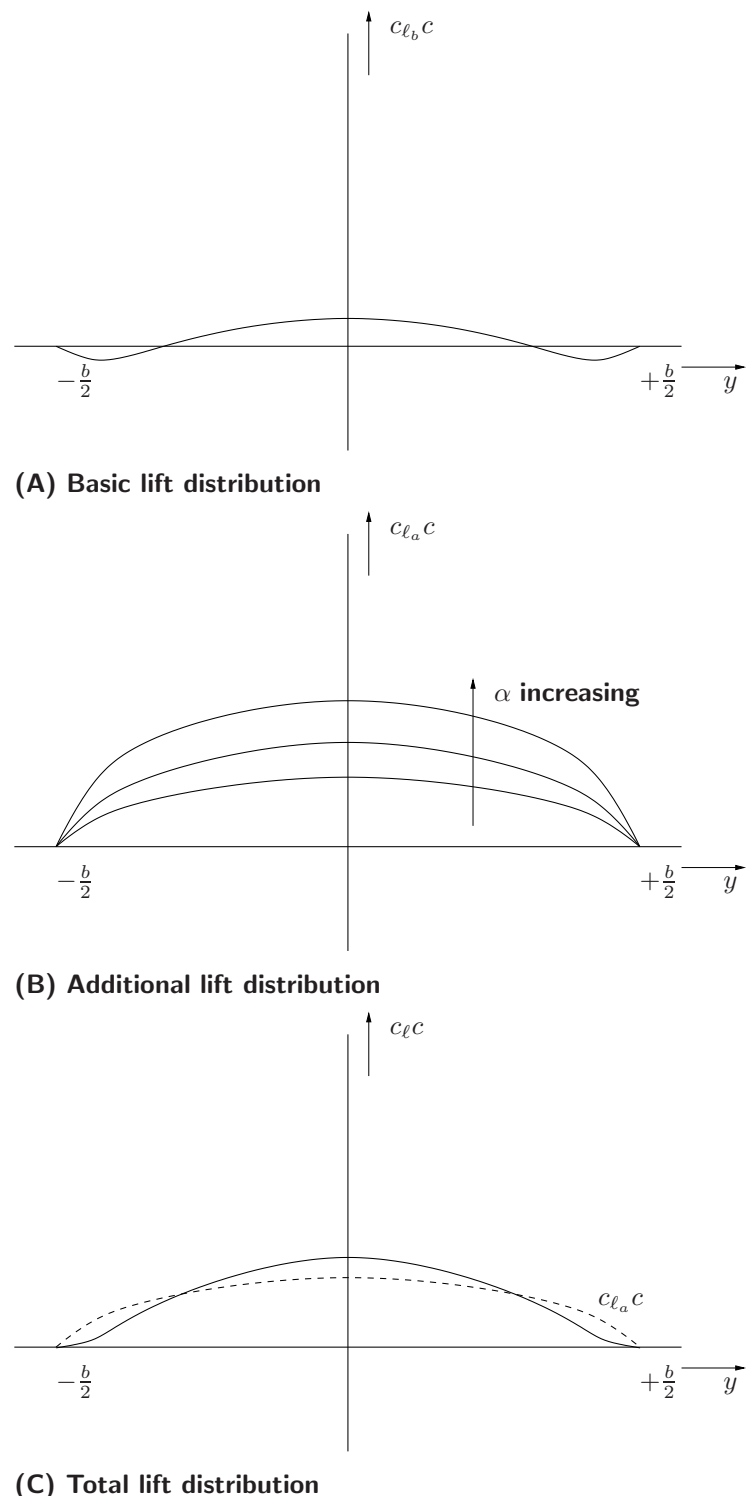


Figure 9-22: The basic, additional and total lift distribution of a wing with negative twist

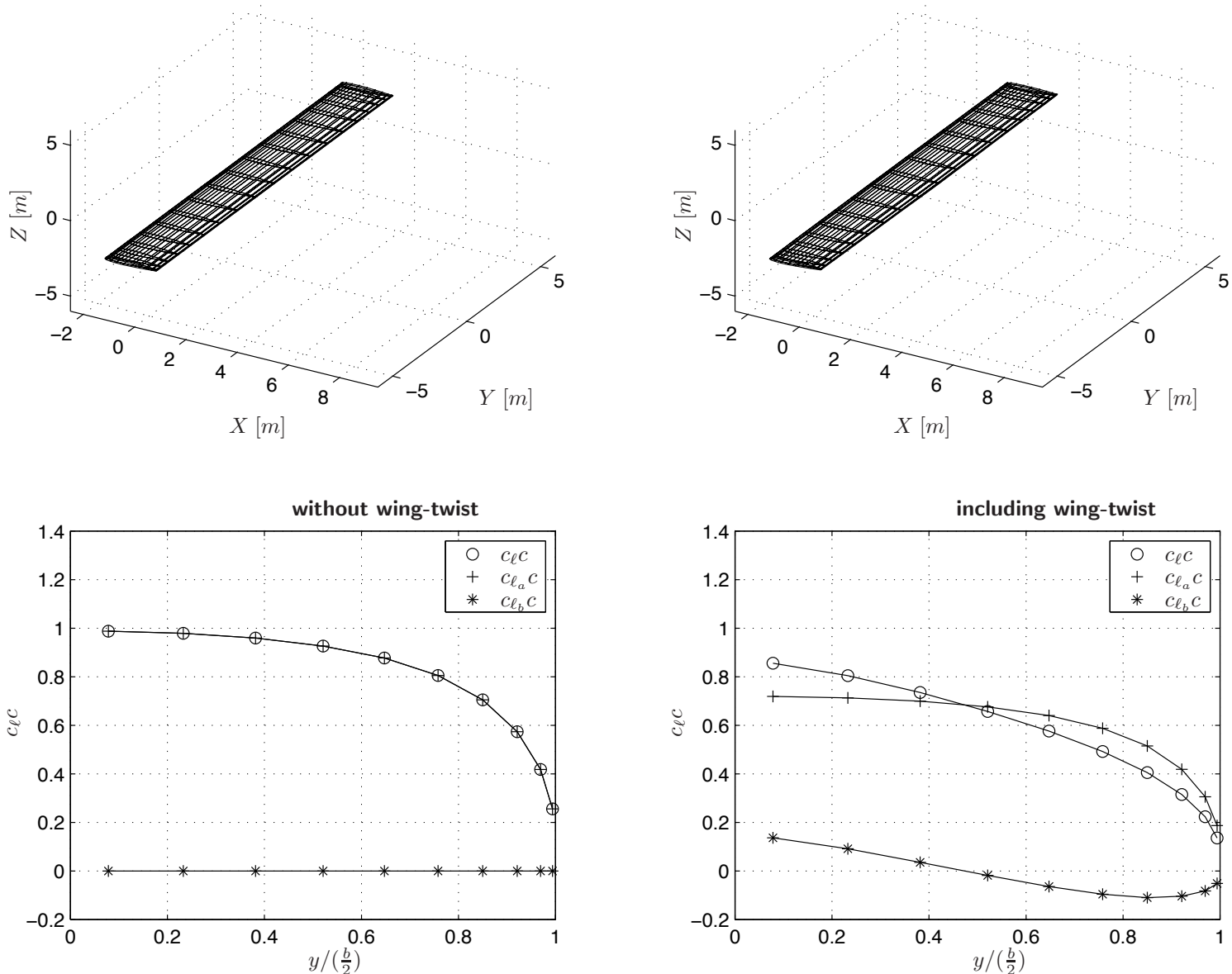


Figure 9-23: Numerical simulation of the basic lift distribution ($c_{\ell_b}c$ at $\alpha = \alpha_{C_L=0}$), additional lift distribution ($c_{\ell_a}c$) and total lift distribution ($c_{\ell}c$) for a wing without wing-twist (**left**, $\varepsilon = 0^\circ$) and a wing including wing-twist (**right**, $\varepsilon = -3^\circ$); NACA 0012 airfoil, $b = 16$ m, $S = 32$ m^2 , $\bar{c} = 2$ m, $\Gamma = 0^\circ$, $\Lambda = 0^\circ$, $\lambda = 1$, $\alpha_r = 0^\circ$, $\varepsilon = -3^\circ$, $\alpha = 5^\circ$. Results from a source/doublet singularity panel-method, linearized potential flow.

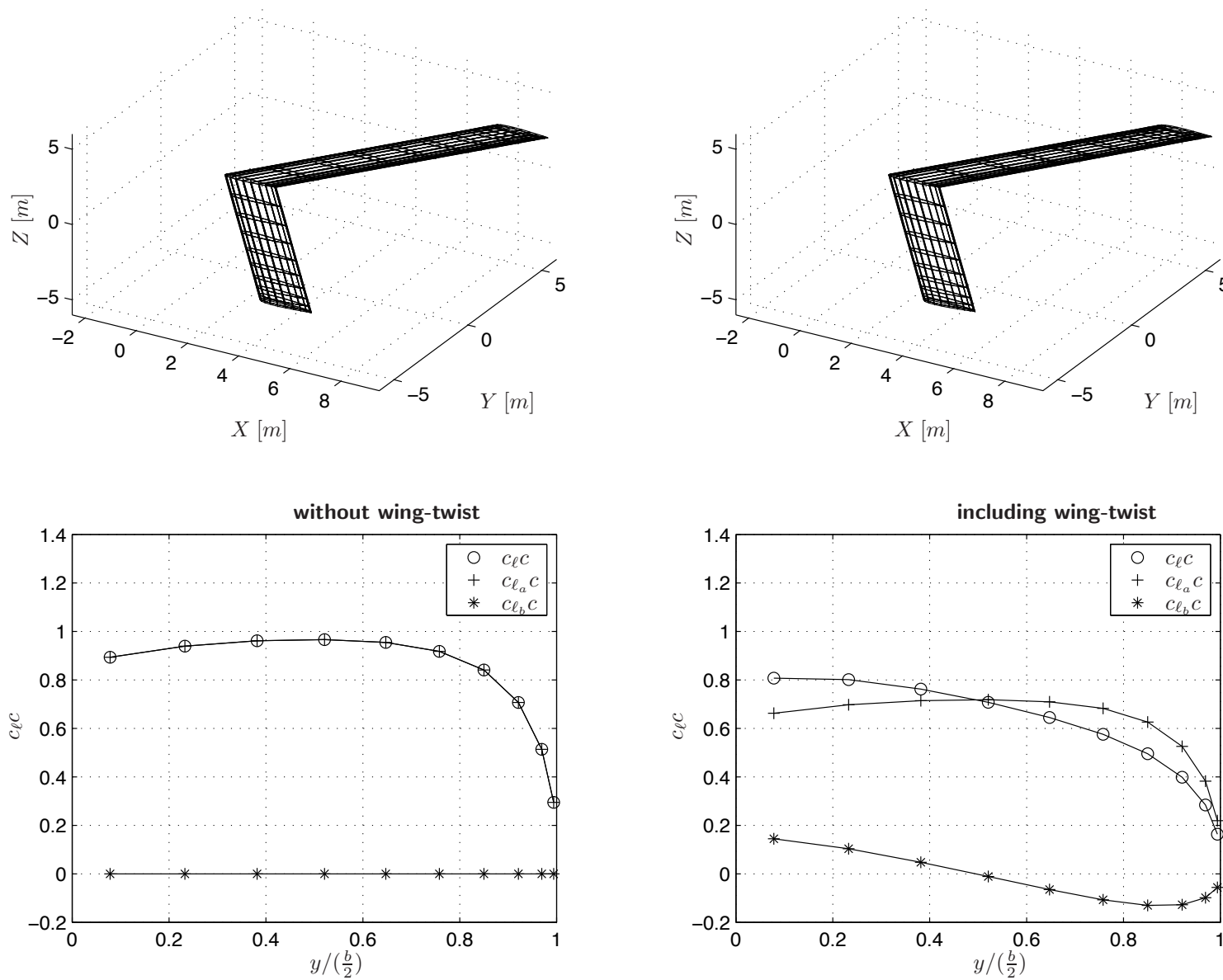


Figure 9-24: Numerical simulation of the basic lift distribution ($c_{\ell_b}c$ at $\alpha = \alpha_{CL=0}$), additional lift distribution ($c_{\ell_a}c$) and total lift distribution ($c_{\ell}c$) for a wing without wing-twist (**left**, $\varepsilon = 0^\circ$) and a wing including wing-twist (**right**, $\varepsilon = -3^\circ$); NACA 0012 airfoil, $b = 16\text{ m}$, $S = 32\text{ m}^2$, $\bar{c} = 2\text{ m}$, $\Gamma = 0^\circ$, $\Lambda = 37^\circ$, $\lambda = 1$, $\alpha_r = 0^\circ$, $\varepsilon = -3^\circ$, $\alpha = 5^\circ$. Results from a source/doublet singularity panel-method, linearized potential flow.

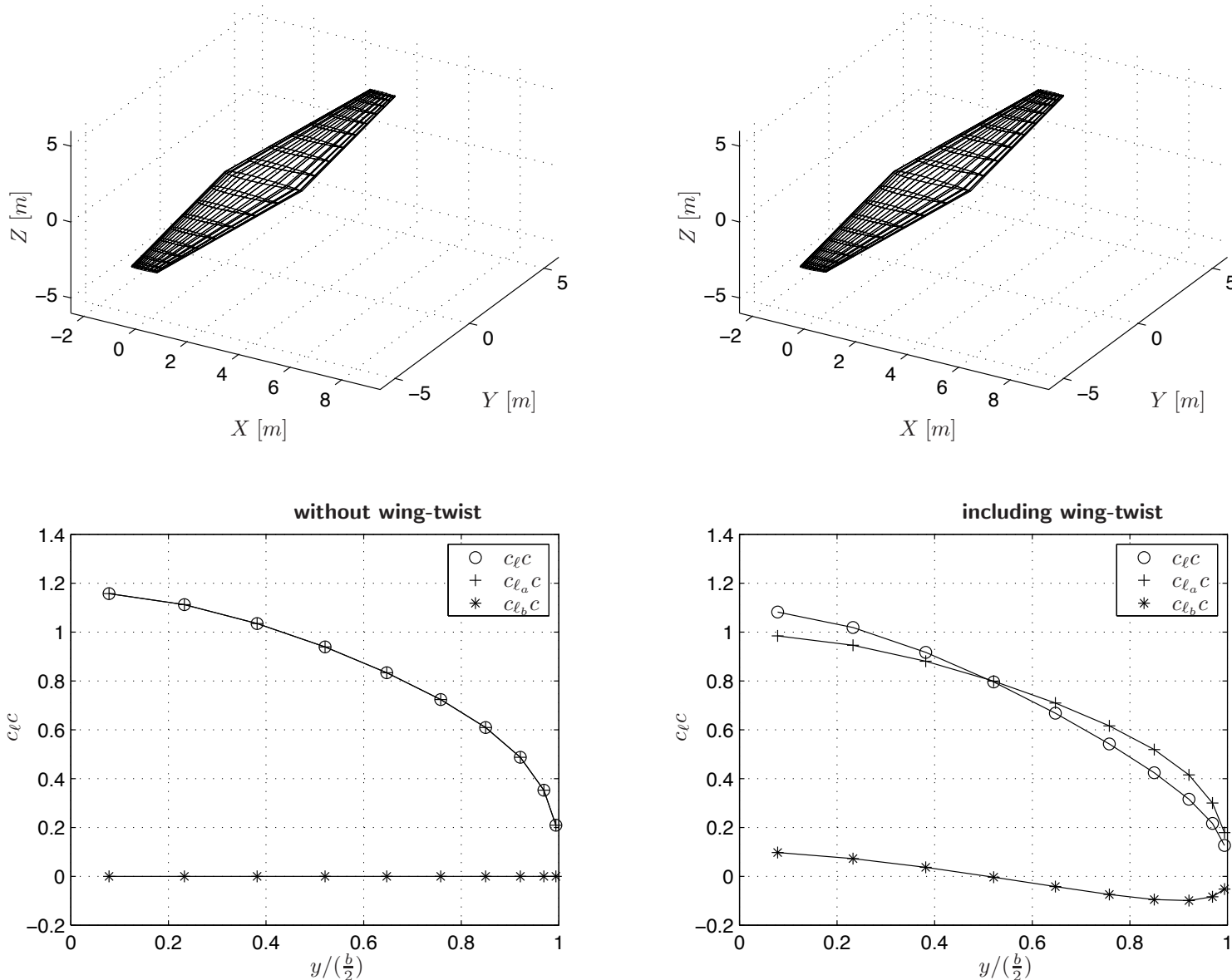


Figure 9-25: Numerical simulation of the basic lift distribution ($c_{\ell_b}c$ at $\alpha = \alpha_{C_L=0}$), additional lift distribution ($c_{\ell_a}c$) and total lift distribution ($c_{\ell}c$) for a wing without wing-twist (**left**, $\varepsilon = 0^\circ$) and a wing including wing-twist (**right**, $\varepsilon = -3^\circ$); NACA 0012 airfoil, $b = 16$ m, $S = 32$ m^2 , $\bar{c} = 2$ m, $\Gamma = 0^\circ$, $\Lambda = 0^\circ$, $\lambda = \frac{1}{3}$, $\alpha_r = 0^\circ$, $\varepsilon = -3^\circ$, $\alpha = 5^\circ$. Results from a source/doublet singularity panel-method, linearized potential flow.

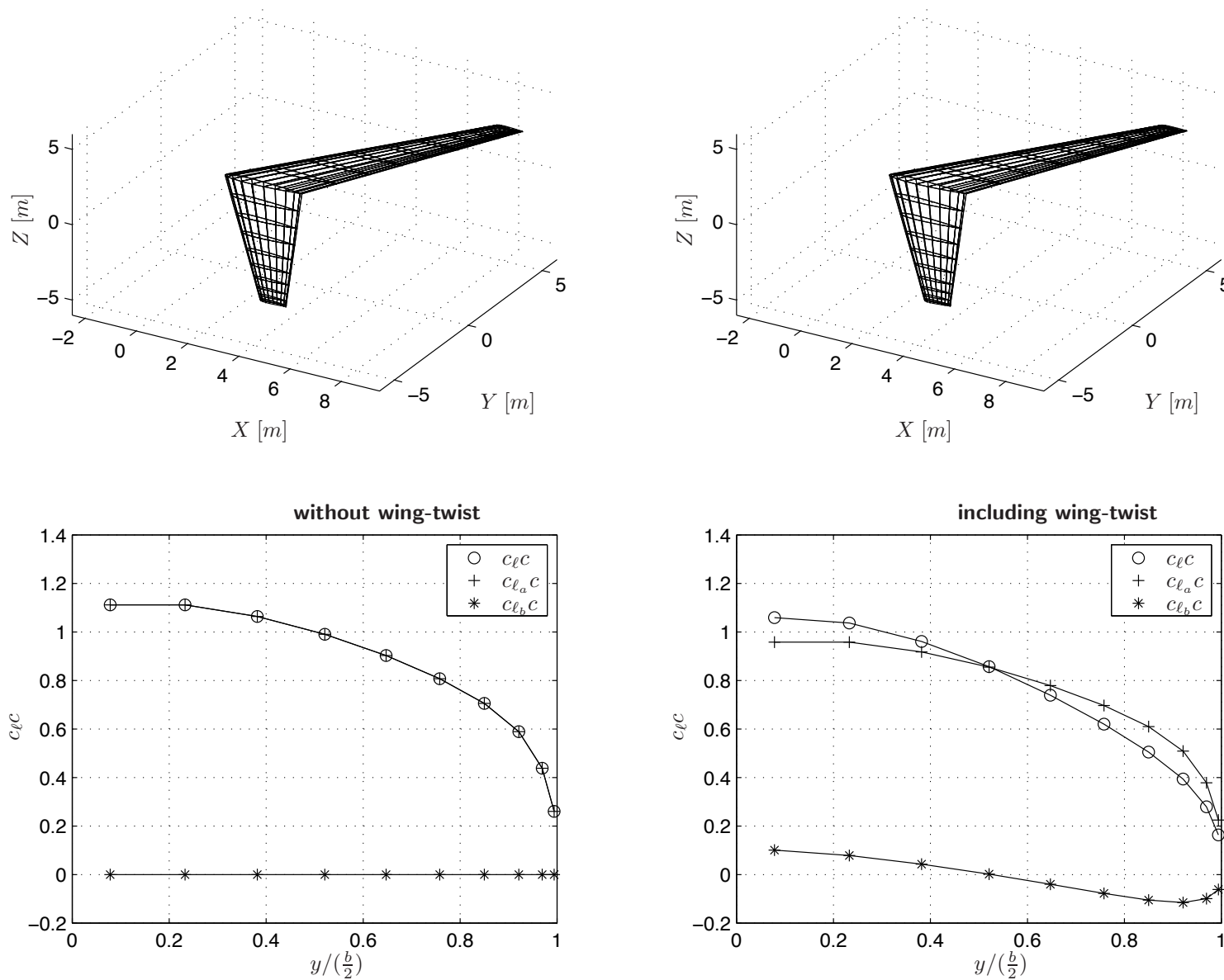


Figure 9-26: Numerical simulation of the basic lift distribution ($c_{\ell_b} c$ at $\alpha = \alpha_{C_L=0}$), additional lift distribution ($c_{\ell_a} c$) and total lift distribution ($c_{\ell c}$) for a wing without wing-twist (**left**, $\varepsilon = 0^\circ$) and a wing including wing-twist (**right**, $\varepsilon = -3^\circ$); NACA 0012 airfoil, $b = 16$ m, $S = 32$ m^2 , $\bar{c} = 2$ m, $\Gamma = 0^\circ$, $\Lambda = 37^\circ$, $\lambda = \frac{1}{3}$, $\alpha_r = 0^\circ$, $\varepsilon = -3^\circ$, $\alpha = 5^\circ$. Results from a source/doublet singularity panel-method, linearized potential flow.

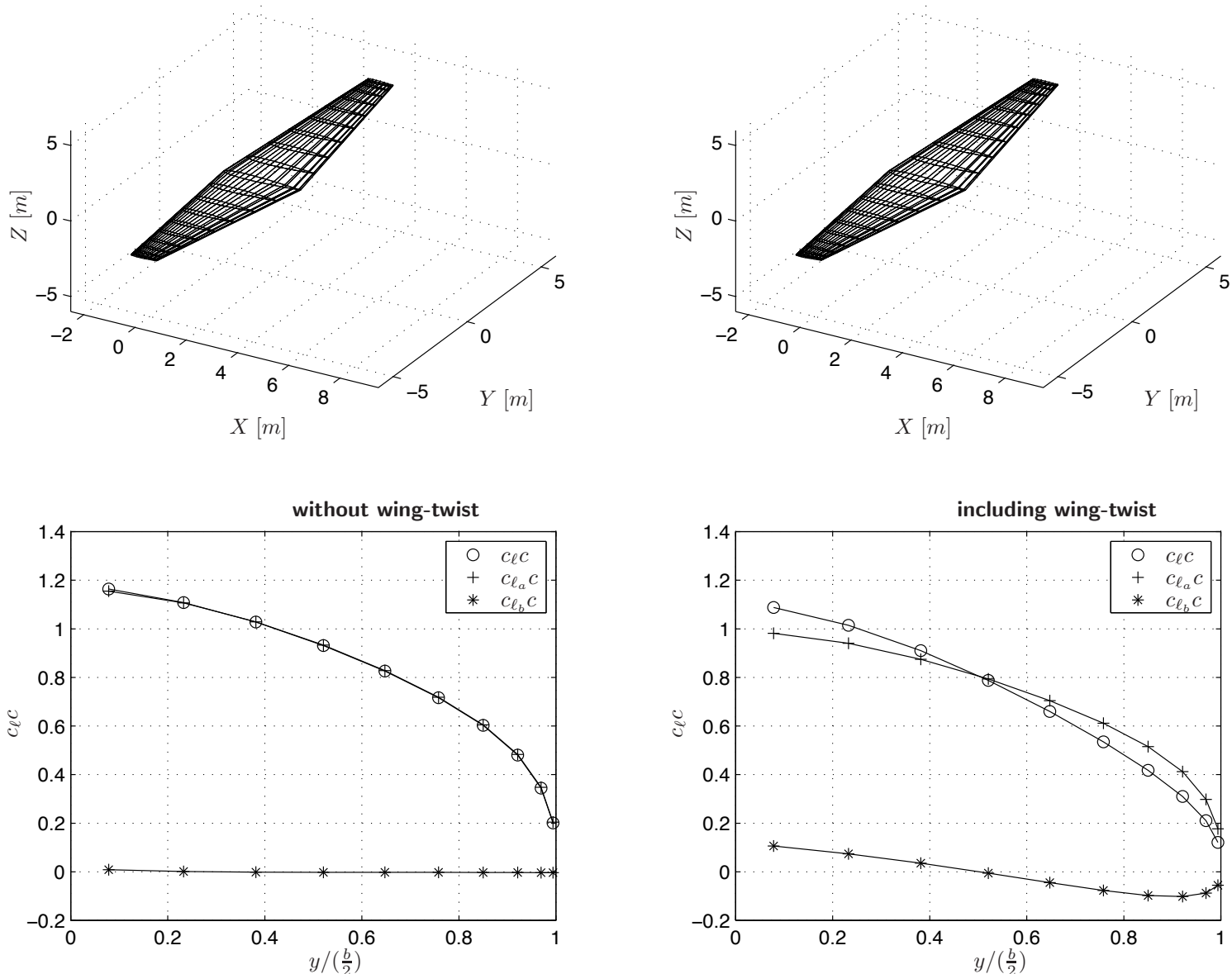


Figure 9-27: Numerical simulation of the basic lift distribution ($c_{\ell b}c$ at $\alpha = \alpha_{C_L=0}$), additional lift distribution ($c_{\ell_a}c$) and total lift distribution ($c_{\ell c}$) for a wing without wing-twist (**left**, $\varepsilon = 0^\circ$) and a wing including wing-twist (**right**, $\varepsilon = -3^\circ$); NACA 0012 airfoil, $b = 16$ m, $S = 32$ m^2 , $\bar{c} = 2$ m, $\Gamma = 5^\circ$, $\Lambda = 0^\circ$, $\lambda = \frac{1}{3}$, $\alpha_r = 0^\circ$, $\varepsilon = -3^\circ$, $\alpha = 5^\circ$. Results from a source/doublet singularity panel-method, linearized potential flow.

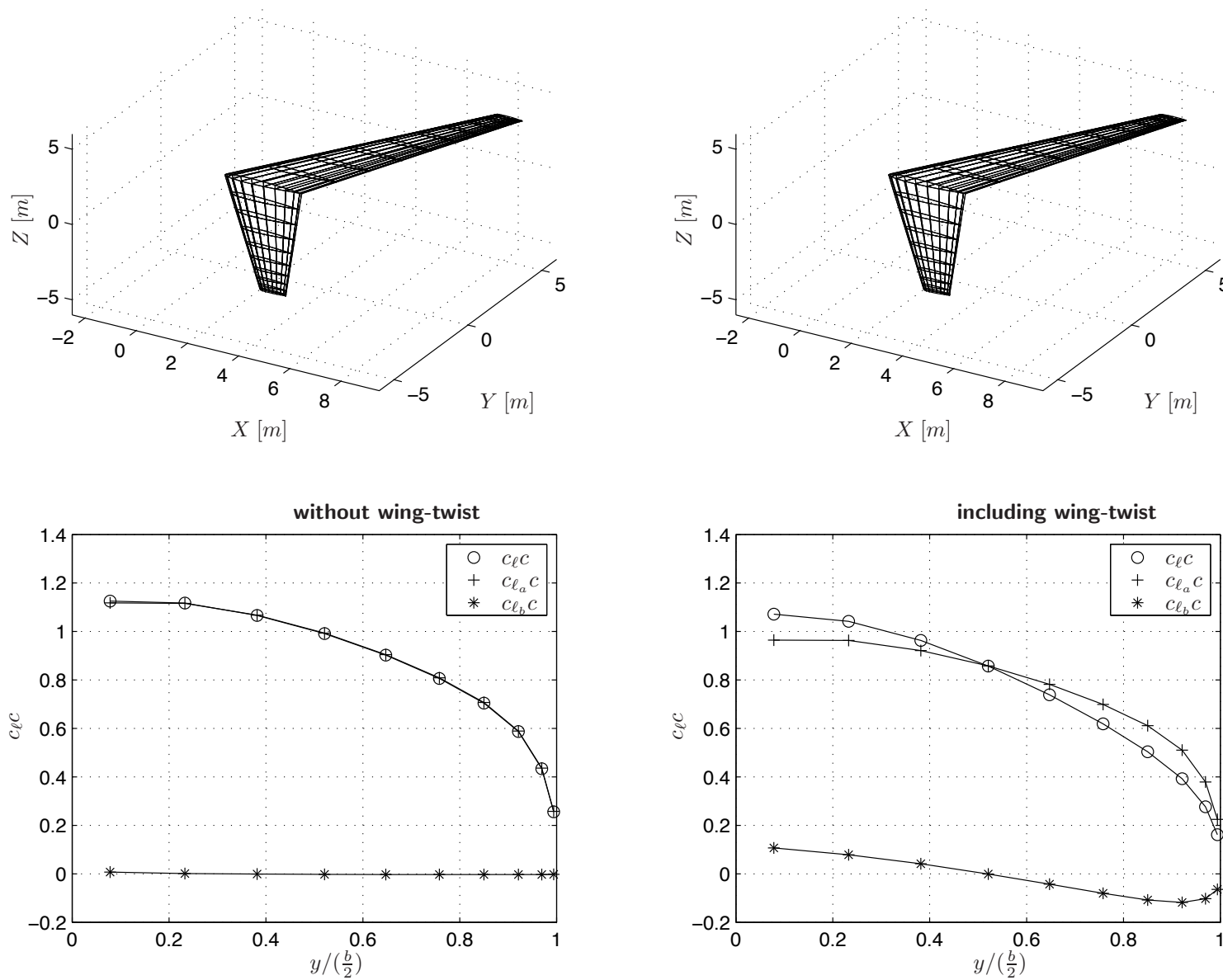


Figure 9-28: Numerical simulation of the basic lift distribution ($c_{\ell_b}c$ at $\alpha = \alpha_{C_L=0}$), additional lift distribution ($c_{\ell_a}c$) and total lift distribution ($c_{\ell}c$) for a wing without wing-twist (**left**, $\varepsilon = 0^\circ$) and a wing including wing-twist (**right**, $\varepsilon = -3^\circ$); NACA 0012 airfoil, $b = 16\text{ m}$, $S = 32\text{ m}^2$, $\bar{c} = 2\text{ m}$, $\Gamma = 5^\circ$, $\Lambda = 37^\circ$, $\lambda = \frac{1}{3}$, $\alpha_r = 0^\circ$, $\varepsilon = -3^\circ$, $\alpha = 5^\circ$. Results from a source/doublet singularity panel-method, linearized potential flow.

The resultant force of the additional lift distribution of the wing may be assumed to act through \bar{x}_{ac} the ac of the wing on the mac. So, the moment about the leading edge \bar{x}_0 of the mac due to the additional lift distribution may be written as,

$$M_a = -L_a (\bar{x}_{ac} - \bar{x}_0)$$

Combining the above two expressions results in,

$$L_a (\bar{x}_{ac} - \bar{x}_0) = 2 \int_0^{\frac{b}{2}} \left(c_{\ell_a} \frac{1}{2} \rho V^2 c \right) (x - \bar{x}_0) \cos \alpha dy$$

Using,

$$L = L_a = C_L \frac{1}{2} \rho V^2 S$$

and assuming $\cos \alpha \approx 1$, results in the required position of the ac of the wing,

$$\frac{\bar{x}_{ac} - \bar{x}_0}{c} = \frac{1}{C_L} \frac{2}{S\bar{c}} \int_0^{\frac{b}{2}} c_{\ell_a} c (x - \bar{x}_0) dy \quad (9-26)$$

The contribution of a wing strip dy to the total moment about \bar{x}_0 , the leading edge of the mac, follows from figure 9-29,

$$dM = \{c_{m_{ac}} c - c_{\ell} (x - \bar{x}_0) \cos \alpha\} \frac{1}{2} \rho V^2 c dy$$

The non-dimensional moment of the entire wing about \bar{x}_0 , if again $\cos \alpha \approx 1$, is obtained by integration along the wing span and division by $\frac{1}{2} \rho V^2 S \bar{c}$

$$C_m = \frac{2}{S\bar{c}} \left\{ \int_0^{\frac{b}{2}} c_{m_{ac}} c^2 dy - \int_0^{\frac{b}{2}} c_{\ell} c (x - \bar{x}_0) dy \right\} \quad (9-27)$$

or since,

$$c_{\ell} = c_{\ell_a} + c_{\ell_b}$$

equation (9-27) may be written as,

$$C_m = \frac{2}{S\bar{c}} \left\{ \int_0^{\frac{b}{2}} c_{m_{ac}} c^2 dy - \int_0^{\frac{b}{2}} c_{\ell_b} c (x - \bar{x}_0) dy - \int_0^{\frac{b}{2}} c_{\ell_a} c (x - \bar{x}_0) dy \right\} \quad (9-28)$$

According to equation (9-22), C_m about \bar{x}_0 , the leading edge of the mac, assuming again $C_N \approx C_L$, can be written as,

$$C_m = C_{m_{ac}} + C_L \frac{\bar{x}_0 - \bar{x}_{ac}}{\bar{c}} \quad (9-29)$$

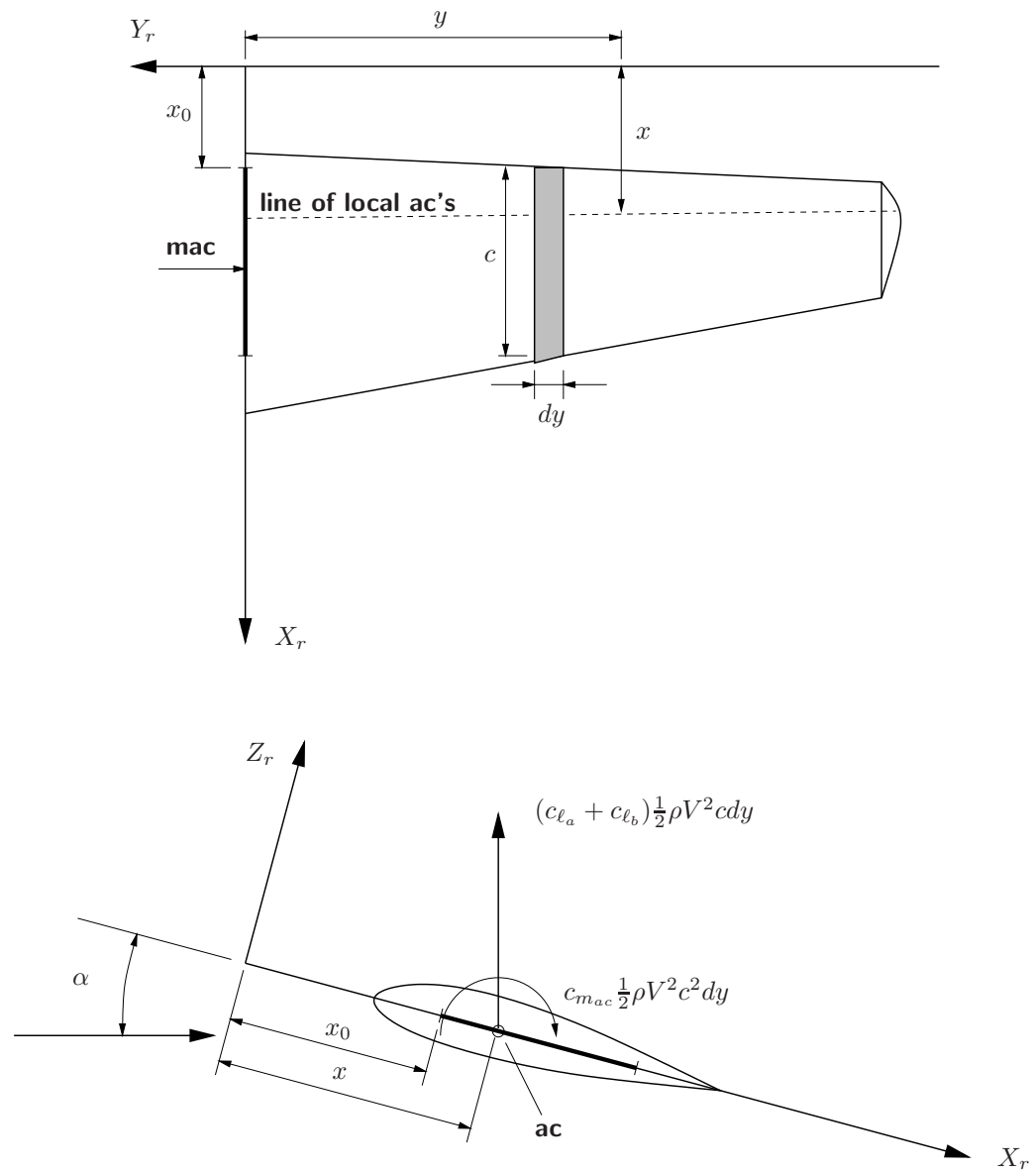


Figure 9-29: The calculation of the position of the ac and $C_{m_{ac}}$ for a wing with arbitrary geometry

Substituting equation (9-26) in equation (9-29) and equating equation (9-28) to equation (9-29) results in the expression for $C_{m_{ac}}$,

$$C_{m_{ac}} = \frac{2}{S\bar{c}} \left\{ \int_0^{\frac{b}{2}} c_{m_{ac}} c^2 dy - \int_0^{\frac{b}{2}} c_{\ell_b} c (x - \bar{x}_0) dy \right\} \quad (9-30)$$

We now have expressed the position of the ac of the wing as in equation (9-26) and the value of $C_{m_{ac}}$ in equation (9-30). These results are subject to the same simplifying assumptions as were made in part c of section 9-1-2,

1. The contribution of the tangential force to the moment is neglected and as a consequence the ac is located on the mac
2. The position of the ac is assumed to be independent of α

Reference [5] provides for a large number of wing shapes the values of \bar{x}_{ac} according to equation (9-26), in addition to the magnitudes of the first and second integral in equation (9-30). Data on the position of the ac and of $C_{m_{ac}}$ can be found in references [78, 163, 185].

9-1-5 Influence of wing shape on the aerodynamic center and $C_{m_{ac}}$

It is quite difficult to give general rules for the influence of the various wing geometry parameters describing the wing shape, such as aspect ratio and wing sweep on the aerodynamic moment curve of wings. The reason is, that the influence of one parameter strongly depends on the value of the others. Not too many experimental (wind tunnel) results are available in which those parameters were systematically varied. Most of these experimental results apply to wing-fuselage combinations, so variations of the influence of the fuselage with wing sweep, wing taper ratio, etcetera, are included in the experimental results. For these reasons it is not feasible to aim for completeness and a description of only a few of the more general effects of wing shape on the aerodynamic moment has to suffice.

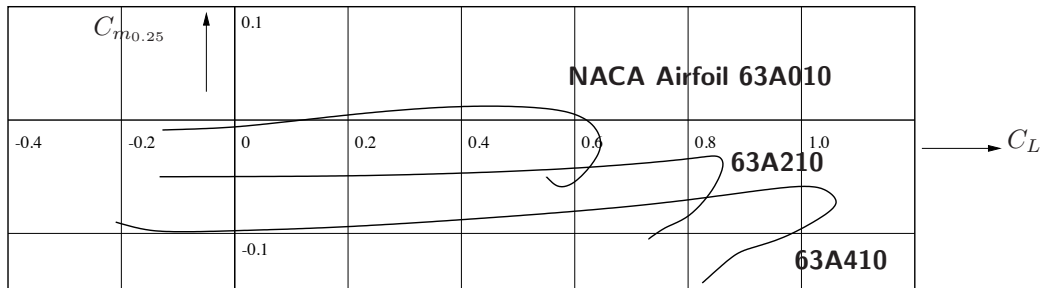
We have seen that the aerodynamic moment characteristics of a wing can be expressed in terms of a constant value of $C_{m_{ac}}$ and an approximated position of the ac on the wing mac. Relative to an arbitrary reference point (x_1, z_0) on the mac the aerodynamic moment may then be written as see equation (9-21),

$$C_{m_{(x_1, z_0)}} = C_{m_{ac}} + C_N \frac{x_1 - x_{ac}}{\bar{c}}$$

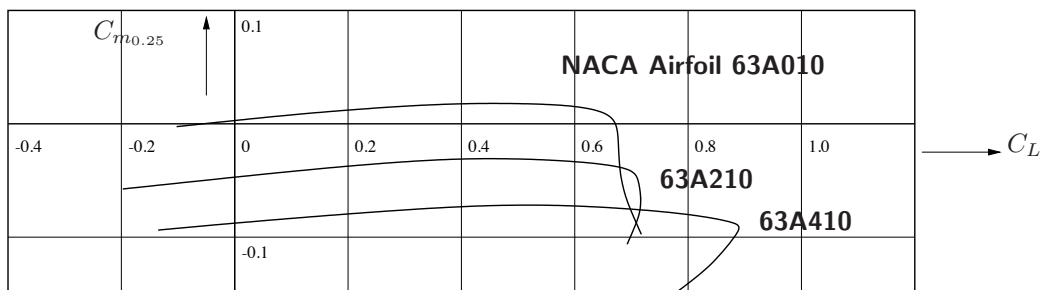
This equation is valid as far as linear wing strip theory is valid, so up to only 'moderate' values of the angle of attack, wing sweep angle and slender wings with moderate to large wing aspect ratios. For such wings, C_m and C_N vary more or less linearly with α if the same holds true for the individual wing strip profiles.

The $C_{m_{ac}}$ of a complete wing could be written as as, see equation (9-30),

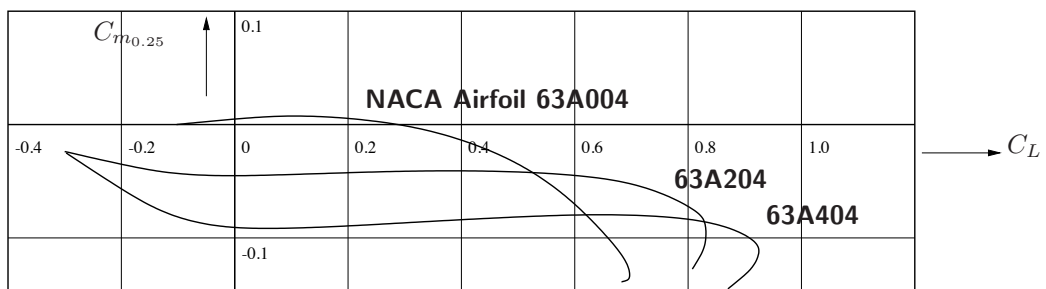
$$C_{m_{ac}} = \frac{2}{S\bar{c}} \left\{ \int_0^{\frac{b}{2}} c_{m_{ac}} c^2 dy - \int_0^{\frac{b}{2}} c_{\ell_b} c (x - \bar{x}_0) dy \right\}$$



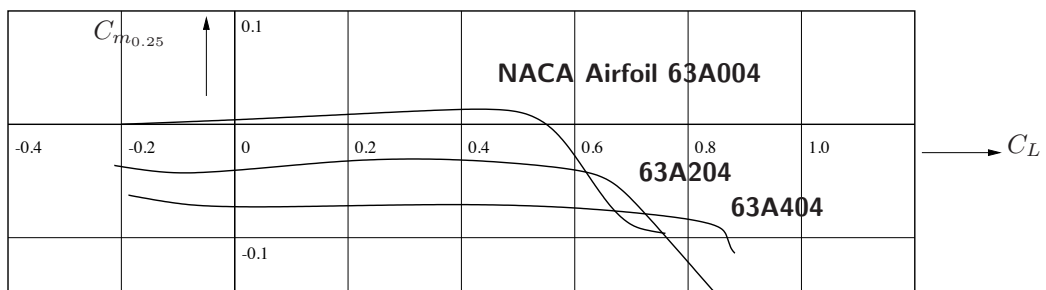
(A) $\lambda = 1, \Lambda = 0^\circ, A = 4, M = 0.6, \frac{t}{c} = 0.10$



(B) $\lambda = 1, \Lambda = 0^\circ, A = 2, M = 0.6, \frac{t}{c} = 0.10$

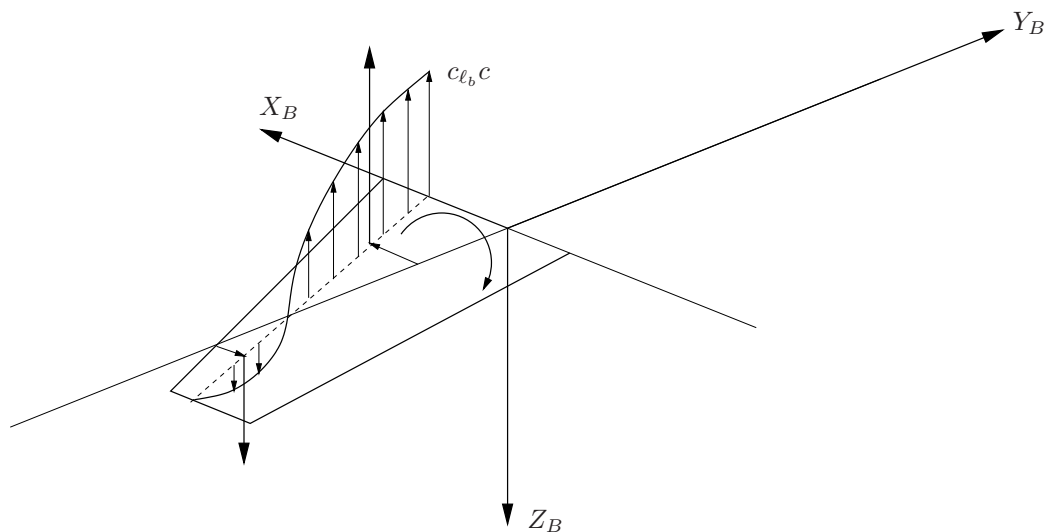


(C) $\lambda = 1, \Lambda = 0^\circ, A = 4, M = 0.6, \frac{t}{c} = 0.04$



(D) $\lambda = 1, \Lambda = 0^\circ, A = 2, M = 0.6, \frac{t}{c} = 0.04$

Figure 9-30: The influence of camber on the moment curves (from references [128, 127])



(A) The moment due to basic lift distribution (left wing)

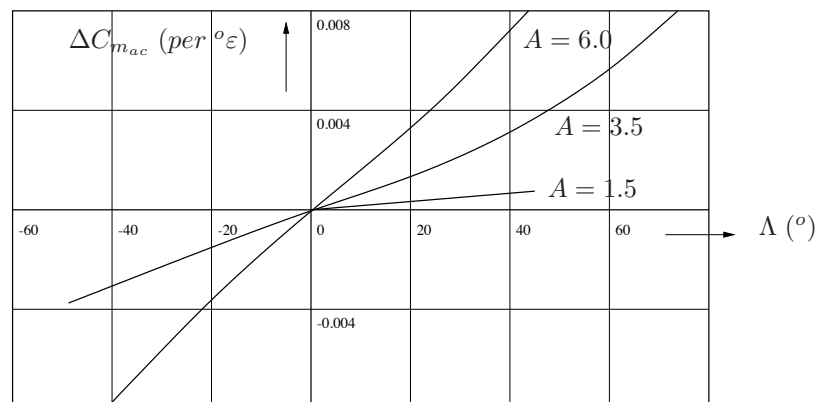
(B) $\Delta C_{m_{ac}}$ as a function of A and Λ , $\lambda = 0.5$

Figure 9-31: The variation of $C_{m_{ac}}$ with wing sweep Λ and angle of twist ε (from reference [50])

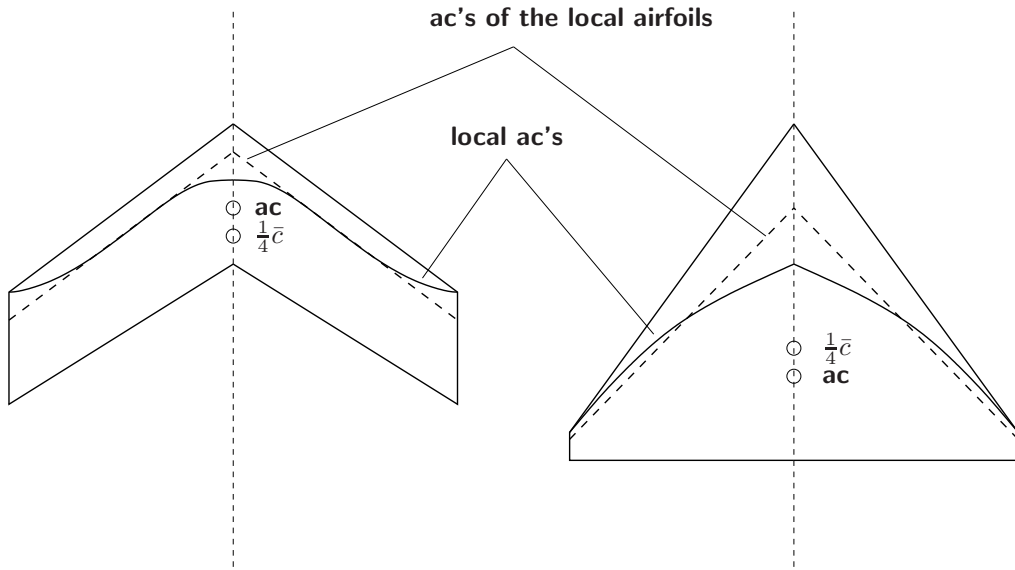


Figure 9-32: The positions of the local ac's of swept wings and delta wings

From this expression we see that C_{mac} is partly determined by the c_{mac} 's in the first integral, i.e. by the camber of the individual wing airfoils. However, from the second integral in equation (9-30) it appears that C_{mac} also depends on the wing twist in case the wings are swept, due to the contribution made of the basic lift distribution.

Straight wings have a constant factor $(x - \bar{x}_0)$ in the second integral in equation (9-30), reducing it to zero, and C_{mac} now only results from the contribution of the camber of the wing airfoils to the local c_{mac} . Increasing the camber leads to a more negative c_{mac} , see for example the wind tunnel results of figure 9-30. If a straight wing has a constant c_{mac} along the wing span, the result is $C_{mac} = c_{mac}$ thanks to the definition of the mac.

For sweptback wings having a negative wing twist the positive c_{ℓ_b} at the wing root and the negative c_{ℓ_b} at the tip will result in a positive ('tail-heavy') contribution to C_{mac} , see figure 9-31a. This contribution increases with wing sweep and aspect ratio, see figure 9-31b. Decreasing the taper ratio ($\lambda = \frac{c_t}{c_r}$) decreases again this effect.

The deflection of landing flaps may cause a significant increase of the camber of the wing cross-section over a part of the wing span. For straight wings the result is a more negative C_{mac} for the entire wing.

Flap deflection also causes a change of the basic lift distribution similar to the effect an increased negative twist at the wing tips. If the wing has positive (backward) sweep back, this change in the basic lift distribution induces itself a positive change in C_{mac} . As a consequence, the total change in C_{mac} due to flap deflection may even be positive. Calculations of this effect have been made for instance in references [130, 48].

The position of the ac is, (9-26),

$$\frac{x_{ac} - \bar{x}_0}{\bar{c}} = \frac{2}{C_L S \bar{c}} \int_0^{\frac{b}{2}} c_{\ell_a} c (x - \bar{x}_0) dy$$

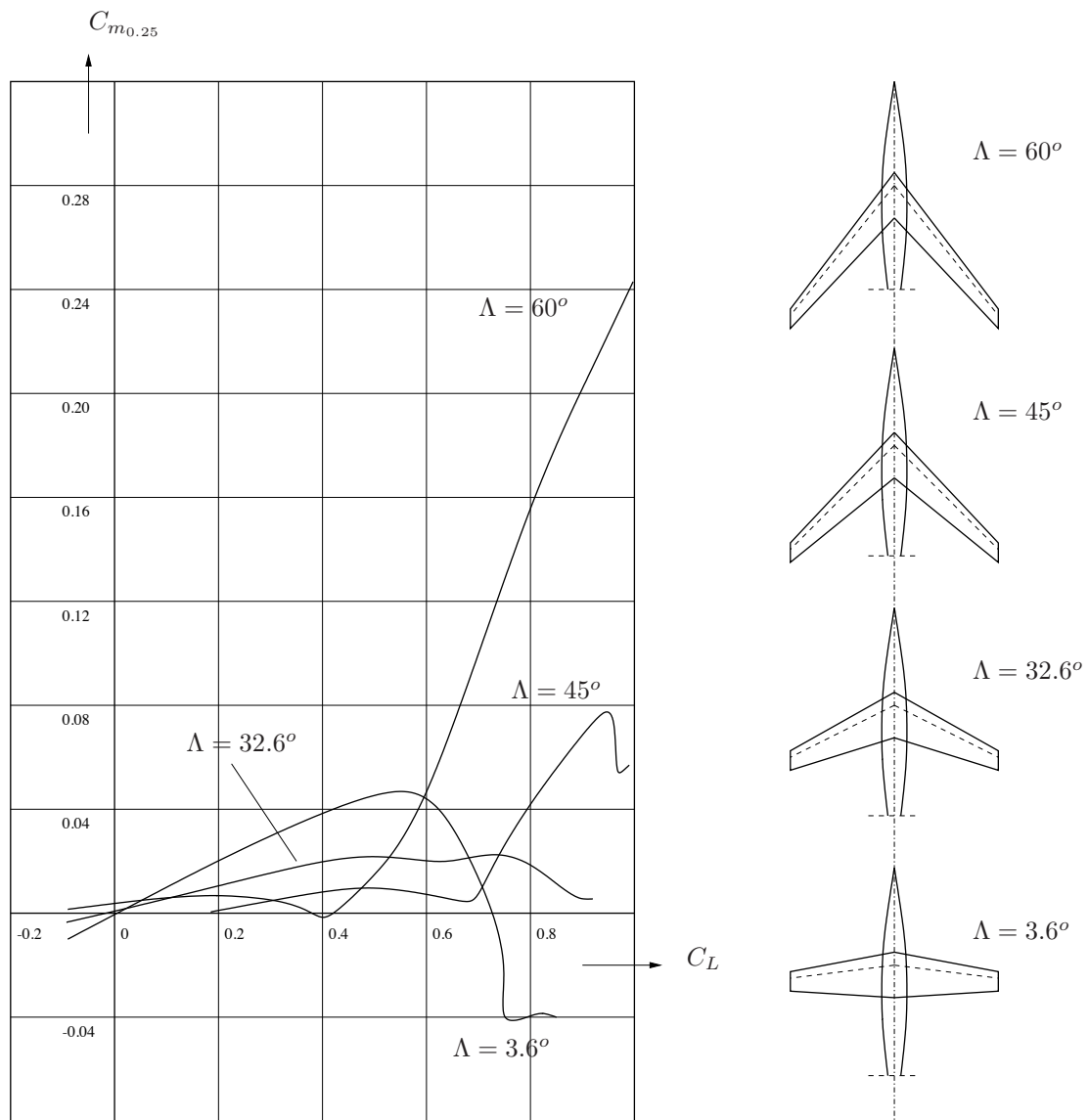


Figure 9-33: The influence of wing sweep on the moment curves of wings of aspect ratio $A = 4$, $\lambda = 0.6$, $\frac{t}{c} = 0.06$, $M = 0.40$ (from reference [182])

The position of local ac's of wing airfoils of straight wings with moderate to large aspect ratios correspond are close to the ac's in two-dimensional flow. As a consequence, the ac of such wings will lie around the 25 % position on the mac of the wing. Straight wings with low aspect ratio ($A < 3$), however, show an appreciable forward shift with decreasing aspect ratio. For these straight wings, flap deflection causes no significant shift of the ac.

The lift distribution in chordwise direction of swept wings and delta wings is strongly influenced by wing sweep. The result is that the local ac's of the wing no longer agree with the ac's of the local wing airfoils in two-dimensional flow, see figure 9-32.

The local ac's at the tips of swept back wings lie ahead of the ac's of the corresponding wing airfoils. Since for swept back wings the additional lift distribution is concentrated more near the wing tips, the ac of the complete wing will be situated ahead of the 25 % mac position. This forward shift increases with increasing sweepback angle and we know that this has a destabilizing influence, see also [5].

However, the combination of a swept back wing with a fuselage often shows a rearward shift of the ac with increasing sweepback angle, see the linear part of the moment curves up to $C_L \approx 0.4$ in figure 9-33. This is due to the influence of wing sweepback on the wing-fuselage interference, see also section 9-1-6.

If the taper ratio ($\lambda = \frac{c_t}{c_r}$) decreases, the contribution of the wing tips to the aerodynamic moment decreases. As the ac at the wing tip is shifted forward due to wing sweep, see 9-32, decreasing the taper-ratio of swept back wings moves the ac backwards, thus has a stabilizing effect, see the linear part of the moment curves up to $C_L \approx 0.4$ in figure 9-34.

Wing aspect ratio as such only has a relatively minor influence on the ac. Figure 9-35 for example shows the position of the ac as a function of aspect ratio for wings with 45° of sweep back angle .

Delta wings have local ac's situated behind the quarter-chord position over a large part of the wing span, see figure 9-32. In addition, the lift distribution of delta wings shows a concentration more towards the center parts of the wing. This causes the wing ac to be situated behind the 25 % mac position.

Wing aspect ratio and sweep back of delta wings cannot be varied independently. Increasing sweepback decreases aspect ratio, leading to a rearward shift of the ac, see figure 9-35. Similar to the case of swept wings, a fuselage added to a delta wing has a stabilizing effect (i.e. rearward shift of the ac), which increases with decreasing wing aspect ratio, and thus with increasing sweepback angle.

At sufficiently large angles of attack in particular the effects of flow separation result in non-linear moment curves for straight wings, wings with sweep back angle as well as for delta wings. Now, for these large angles of attack, the concepts of ac and C_{mac} start loosing their significance as in order to match the slope of the moment curve, not only the location of the ac, but also the value of the C_{mac} must be adapted. As also argued in reference [1] the characteristics of wings in such conditions may best be judged from aerodynamic moment curves for some suitable reference point as stability characteristics may still be deduced from the slope of the moment curves, as discussed earlier.

Straight wings usually exhibit large negative changes in $\frac{dC_m}{dC_L} \approx \frac{dC_m}{dC_N}$ at lift coefficients near $C_{L_{max}}$ due to flow separation. Figures 9-37 and 9-30 give examples of this phenomenon. As in flight such a negative (nose-down) change in C_m would help to decrease the angle of attack this is a favorable characteristic of straight wings.

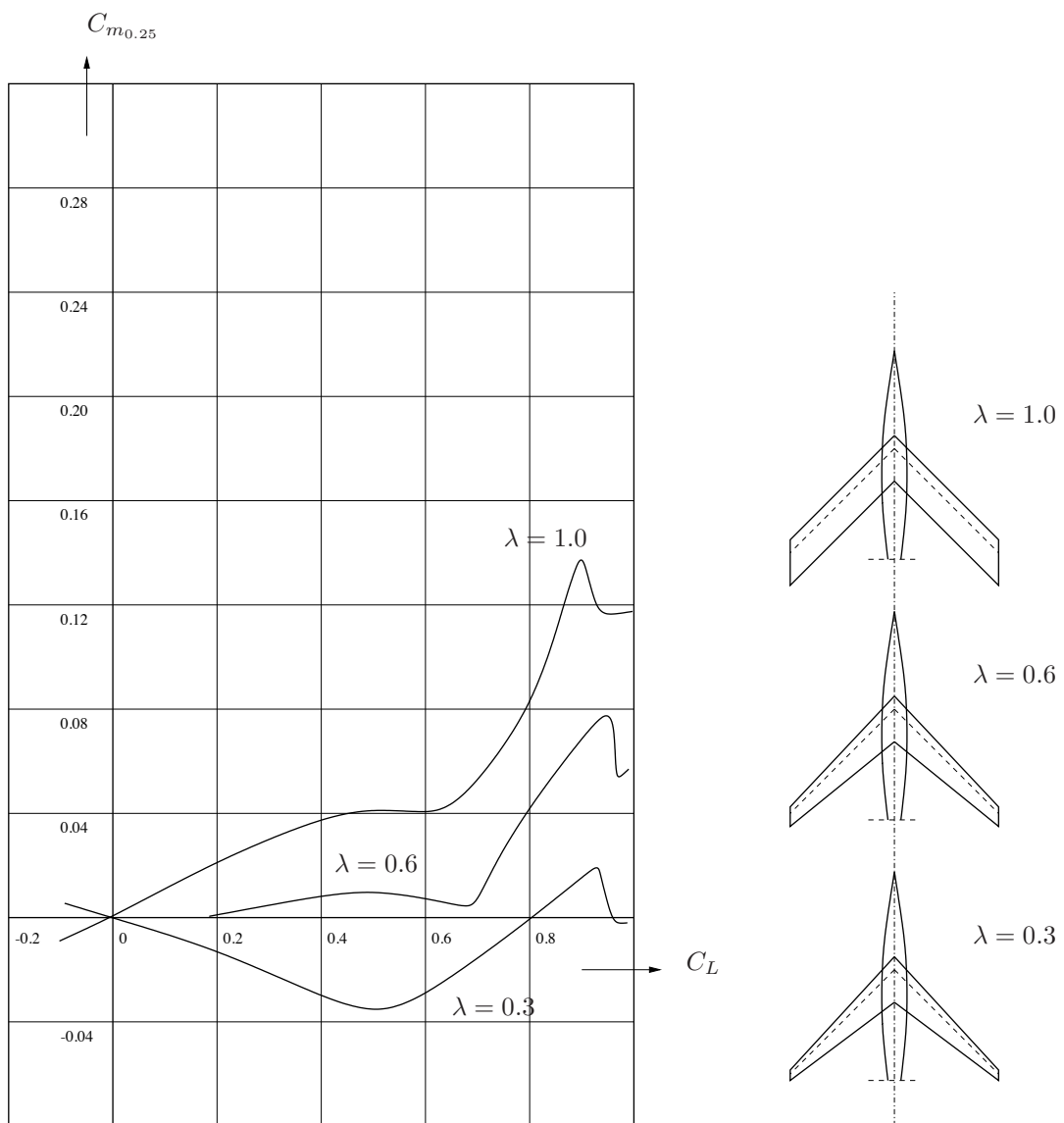


Figure 9-34: The influence of taper ratio on the moment curves of swept wings, $A = 4$, $\Lambda = 45^\circ$, $\frac{t}{c} = 0.06$, $M = 0.40$ (from reference [92])

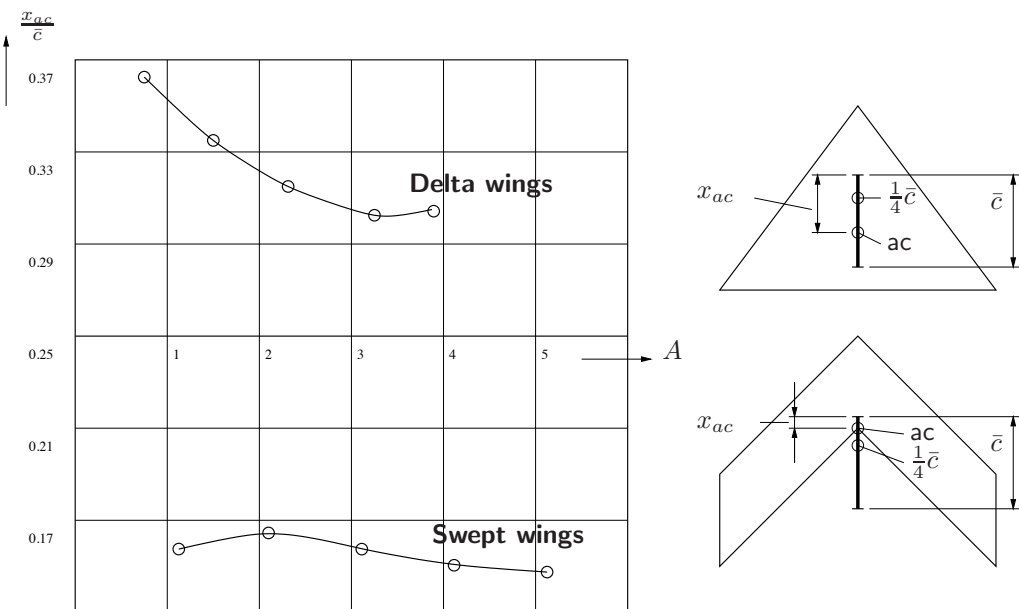


Figure 9-35: The position of the ac of delta wings and concept wings as a function of aspect ratio, $\Lambda = 45^\circ$ (from reference [170])

Swept wings, however, with moderate to large aspect ratios usually suffer from a large positive slope change increasing angle of attack. The change may start already at relatively small values of α . Figures 9-33, 9-34, 9-36 and 9-37 give examples.

These changes are caused by premature flow separation at the outer wings, predominantly caused by the high tip loading and the cross flow towards the wing tips. The result is an increasing thickness of the boundary layer and early flow separation. This effect occurs at lower C_L values, and the effect on C_m is stronger as sweep back angle and aspect ratio are larger. Figure 9-38 gives an indication of the combinations of aspect ratio and wing sweep angle for which destabilizing changes in the slope of the moment curves of the wing may be expected.

This 'sudden' change of slope of the moment curve is called '*pitch up*'. If it would occur in flight its overwhelming effect is to increase the angle of attack which evidently is highly undesirable and potentially very dangerous.

A horizontal tailplane has an important effect on the aerodynamic pitching moment and may be designed as to compensate for the adverse effect of '*pitch up*' as we will see later. However, even then '*pitch up*' remains a very undesirable wing characteristic which should best be avoided through design.

To avoid too much lift concentration near the wing tips (and the pitch up phenomenon) negative wing twist is often used. Camber and other shape parameters of the wing airfoils may be adjusted to obtain desired values of local $c_{\ell_{max}}$ without undue drag increases in cruising flight. To prevent cross-flow towards the wing tips (inducing early flow separation), several means may be applied such as boundary layer fences or a 'saw tooth' leading edge. Reference [72] provides an extensive compilation of the various methods and tools which may be employed for this purpose.

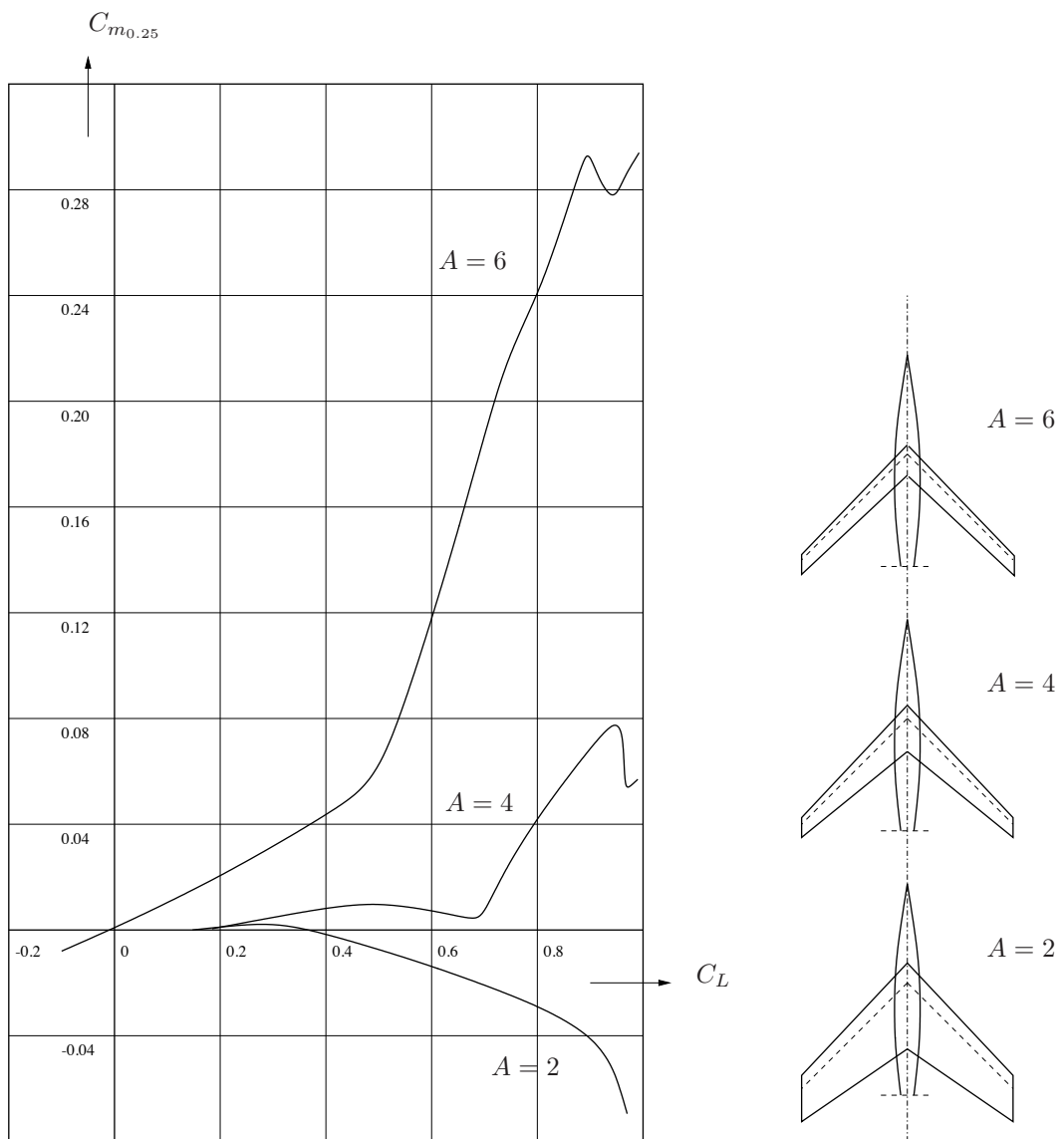


Figure 9-36: The influence of aspect ratio on the moment curve of swept wings, $\Lambda = 45^\circ$, $\lambda = 0.6$, $\frac{t}{c} = 0.06$, $M = 0.40$ (from reference [104])

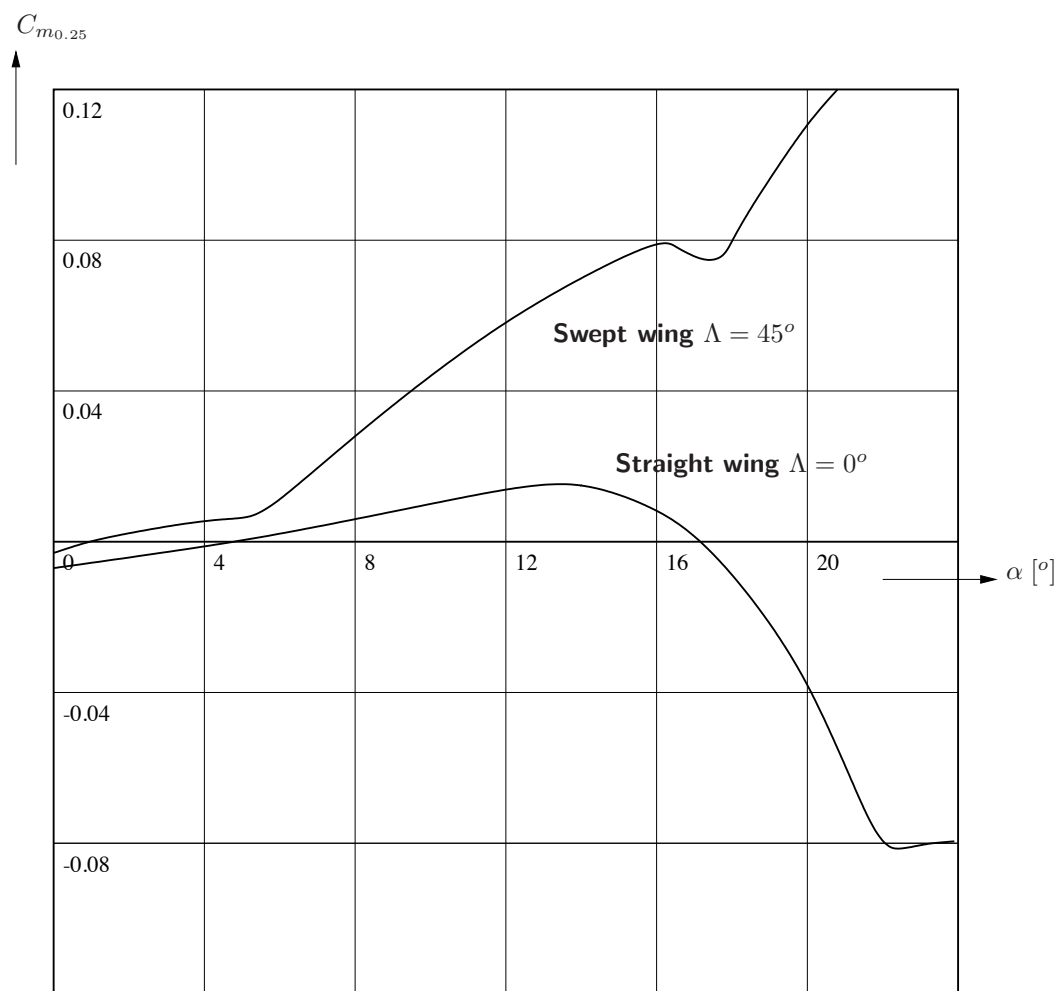


Figure 9-37: The moment curve of a straight wing and a swept wing, $A = 5$, $\lambda = 1$, $Re = 1 \cdot 10^6$ (DUT measurements)

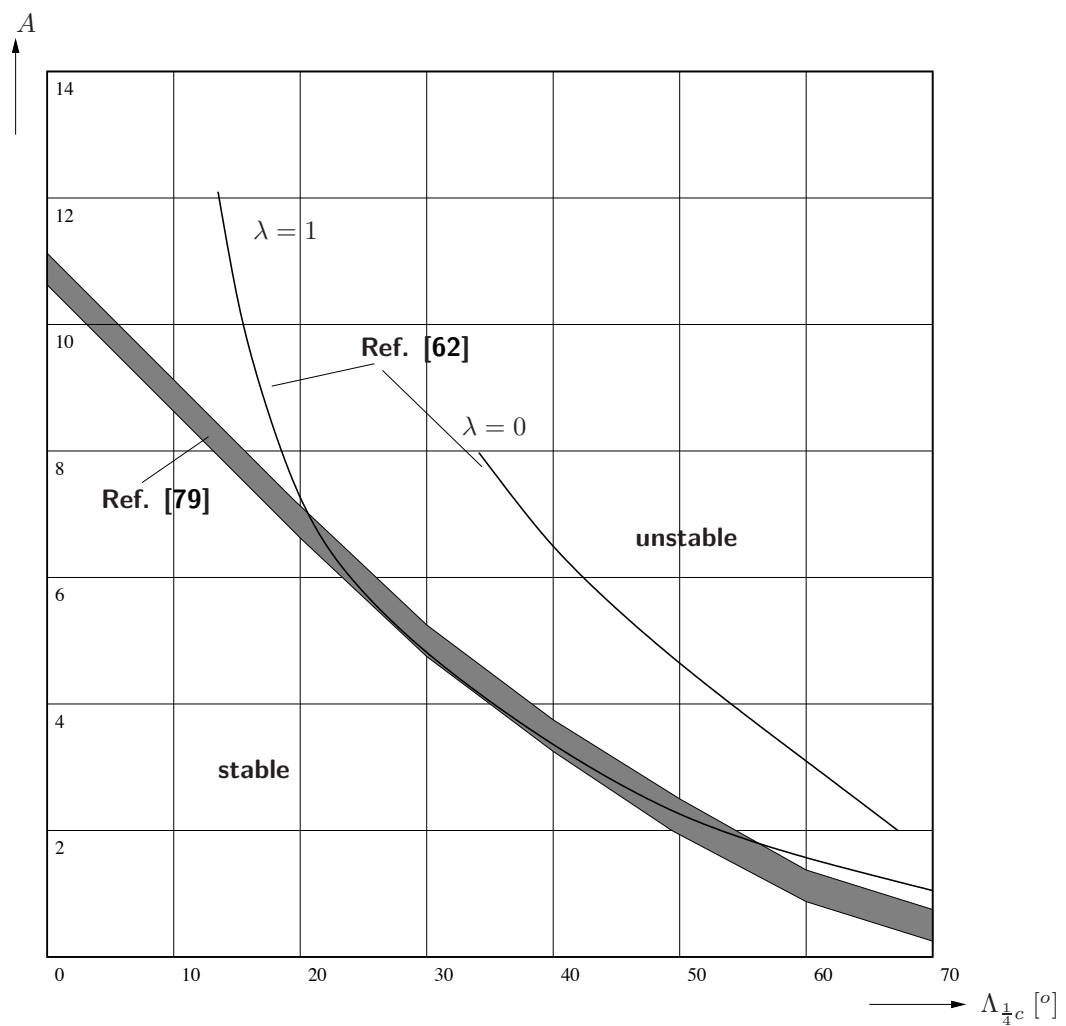


Figure 9-38: Boundaries for the combinations of aspect ratio and sweep angle for which destabilizing changes in the moment curves may be expected (from references [62, 79])

9-1-6 Characteristics of wing-fuselage-nacelle configurations

The model of the aerodynamic moment of the combination of a wing with fuselage and nacelles attached to the wing is in principle the same as for the isolated wing. At small angles of attack C_m varies linearly with C_N , as it does for the isolated wing. As a consequence, changes in the longitudinal moment caused by the fuselage and the nacelles are commonly expressed as a shift in the position of the ac and a change in $C_{m_{ac}}$. Neglecting again the contribution of the tangential force, the moment coefficient of the wing was written as, see equation (9-22),

$$C_{m_w} = C_{m_{ac_w}} + C_N \frac{x - x_{ac_w}}{\bar{c}}$$

In a similar way the moment of the combination of the wing with fuselage and nacelles can be expressed as,

$$C_{m_{w+f+n}} = C_{m_{ac_{w+f+n}}} + C_N \frac{x - x_{ac_{w+f+n}}}{\bar{c}}$$

At constant C_N the change in the moment is,

$$\Delta C_m = C_{m_{w+f+n}} - C_{m_w} = \Delta C_{m_{ac}} - C_N \frac{\Delta x_{ac}}{\bar{c}} \quad (9-31)$$

Similar to $C_{m_{ac_w}}$, also $C_{m_{ac_{w+f+n}}}$ is defined as constant and independent of the angle of attack. This means that $\Delta C_{m_{ac}}$ is independent of α as well. $\Delta C_{m_{ac}}$ is the change of C_m at $C_N = 0$ due to the addition of a fuselage (and nacelles).

The shift in the ac position then follows from equation (9-31),

$$\frac{\Delta x_{ac}}{\bar{c}} = -\frac{d(\Delta C_m)}{dC_N} = -\frac{1}{C_{N_\alpha}} \frac{d(\Delta C_m)}{d\alpha} \quad (9-32)$$

and the change in $C_{m_{ac}}$ is,

$$\Delta C_{m_{ac}} = (\Delta C_m)_{C_N=0} \quad (9-33)$$

The change in the longitudinal moment due to the presence of the fuselage and the wing's nacelles can be thought of as consisting of the contributions of the fuselage and the nacelles separately, the contribution of the wing-fuselage interference and the contribution of the wing-nacelle interference. Nacelles mounted at the rear fuselage are commonly regarded as part of the fuselage. Wing mounted nacelles exert an influence on the longitudinal moment similar to the fuselage. For these reasons only the effect of adding a fuselage to the wing is discussed in the following.

The change in the moment due to the presence of the fuselage, ΔC_m , can be written in the following expression,

$$C_{m_{w+f}} = C_{m_w} + \Delta C_m$$

where,

$$\Delta C_m = C_{m_f} + C_{m_i}$$

Here C_{m_f} denotes the longitudinal moment of the free fuselage in undisturbed flow while C_{m_i} denotes the wing-fuselage interference.

From wind tunnel tests the total ΔC_m can be simply obtained by comparing the moment curves of the isolated wing and the wing-fuselage combination at equal values of C_N . If, in addition, measurements have been made on the isolated fuselage, i.e. to determine C_{m_f} , C_{m_i} can be found as well.

For theoretical studies it appears to be useful to divide the total interference effect C_{m_i} into two parts,

1. $\Delta C_{m_{f.i.}}$; the change in the fuselage moment caused by situating the fuselage in the field of flow around the wing.
2. $\Delta C_{m_{w.i.}}$; the change in the wing moment caused by placing the wing in the field of flow around the fuselage.

So,

$$\Delta C_m = C_{m_f} + \Delta C_{m_{f.i.}} + \Delta C_{m_{w.i.}}$$

Usually, the total moment $C_{m_{f.i.}}$ contributed by the fuselage in the field of flow around the wing is calculated as one effect,

$$C_{m_{f.i.}} = C_{m_f} + \Delta C_{m_{f.i.}}$$

This results in,

$$\Delta C_m = C_{m_{f.i.}} + \Delta C_{m_{w.i.}}$$

In the following the latter two contributions to the change in C_m and the subsequent changes in the position of the ac and the $C_{m_{ac}}$ are discussed.

A. The moment on the fuselage positioned in the field of flow induced by the wing, the magnitude of $C_{m_{f.i.}}$

For a fuselage placed under a non-zero angle of attack in an inviscid and incompressible flow it is possible to prove that it will experience just an aerodynamic moment while the aerodynamic force will be zero. The mechanism behind this moment is illustrated in figure 9-39 (see also figure 9-40 for a numerical simulation of particle lines and pressure distribution over a slender fuselage, linearized potential flow). The magnitude of this moment acting on a slender fuselage of circular cross section in these conditions of incompressible, inviscid flow has been derived by Munk (reference [124]),

$$M_f = \rho V^2 \cdot \alpha_f \cdot (\text{Volume of Fuselage})$$

From this expression follows,

$$C_{m_f} = \frac{\pi \alpha_f}{2S\bar{c}} \int_0^{l_f} b_f^2(x) dx \quad (9-34)$$

Where,

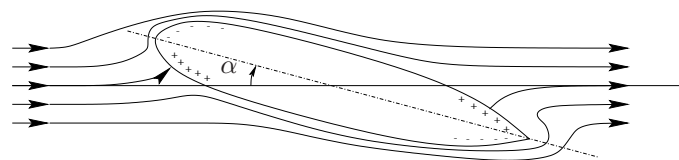


Figure 9-39: Pressure distribution over a fuselage in inviscid flow

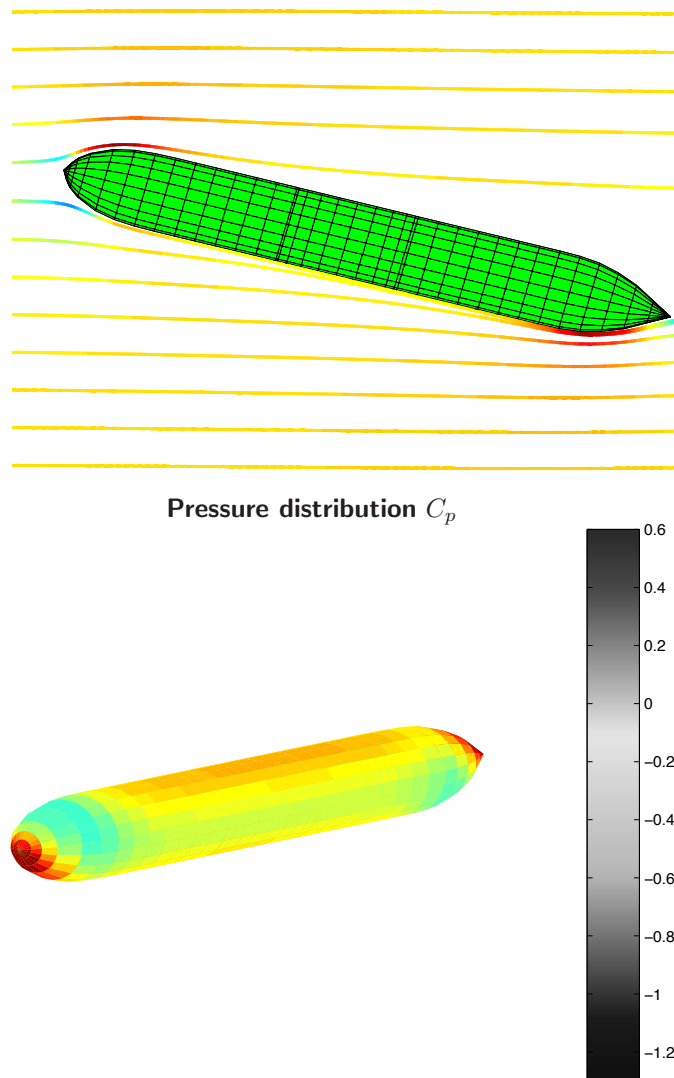


Figure 9-40: Numerical simulation of particle lines (top) and pressure distribution over a fuselage in inviscid flow, $\alpha = 10^\circ$, linearized potential flow

$b_f(x)$	local fuselage width
l_f	fuselage length
α_f	fuselage angle of attack, [Rad.]
S, \bar{c}	characteristic parameters of the wing to which C_{m_f} is referred

According to equation (9-34) the moment is positive (tail-heavy) at positive angles of attack and it increases with increasing angles of attack. The implication is that the idealized isolated fuselage is statically unstable at $\alpha_f = 0^\circ$ and cannot be in equilibrium at $\alpha_f \neq 0^\circ$.

If the wing and the fuselage are combined, the fuselage will experience the effect of air velocity variations as induced by the wing. This causes the angle of attack along the fuselage axis to be different from that of an isolated fuselage. As a consequence, also the pressure distribution over the fuselage is different from that of an isolated fuselage. The wing induced variation of the local angle of attack and the corresponding local normal force along the fuselage axis is shown schematically in figure 9-41. Ahead of the wing, for positive values of C_L , the upwash causes an increase of $\alpha_f(x)$ up to the wing leading edge. Across the wing chord the airflow is 'guided' parallel to the wing chord resulting in $\alpha_f(x)$ being zero. Behind the wing the local angle of attack along the fuselage is reduced due to the downwash induced by the wing. Results of some numerical simulations of the flowfield of the wing-fuselage combination of figure 9-42 are depicted in figures 9-43 and 9-44.

The result of the induced upwash in front of the wing is an increase in tail-down moment with increasing angle of attack, which as we know, is destabilizing. The wing induced downwash has the opposite effect, however, usually not enough to compensate fully the destabilizing effect of the wing induced flow field. Now it is not difficult to see that a long fuselage in front of the wing, as needed for transport aircraft with rear mounted engines, amplifies this effect.

As shown in the classical reference [123], the aerodynamic moment acting on a slender fuselage in an inviscid, incompressible flow field with induced velocities can be written as,

$$C_{m_{f.i.}} = \frac{\pi}{2S\bar{c}} \int_0^{l_f} b_f^2(x) \alpha_f(x) dx \quad (9-35)$$

Note that by substituting $\alpha_f(x)$ for the case of an isolated fuselage in (9-35) this equation should yield the same result as equation (9-34) !

$\alpha_f(x)$ can be expressed in terms of the wing angle of attack α as,

$$\alpha_f(x) = \alpha_{f_0} + \frac{d\alpha_f(x)}{d\alpha} (\alpha - \alpha_0) \quad (9-36)$$

where α_0 denotes $\alpha_{C_N=0}$ and α_{f_0} is the fuselage angle of attack at $\alpha = \alpha_0$. With equation (9-36) follows for $C_{m_{f.i.}}$,

$$C_{m_{f.i.}} = \frac{\pi\alpha_{f_0}}{2S\bar{c}} \int_0^{l_f} b_f^2(x) dx + \frac{\pi(\alpha - \alpha_0)}{2S\bar{c}} \int_0^{l_f} b_f^2(x) \frac{d\alpha_f(x)}{d\alpha} dx \quad (9-37)$$

in which the first term on the right hand side represents the fuselage moment at $C_N = 0$, and so $\Delta C_{m_{ac}}$ due to the fuselage is,

$$\Delta C_{m_{ac}} = (\Delta C_m)_{C_N=0} = \frac{\pi\alpha_{f_0}}{2S\bar{c}} \int_0^{l_f} b_f^2(x) dx \quad (9-38)$$

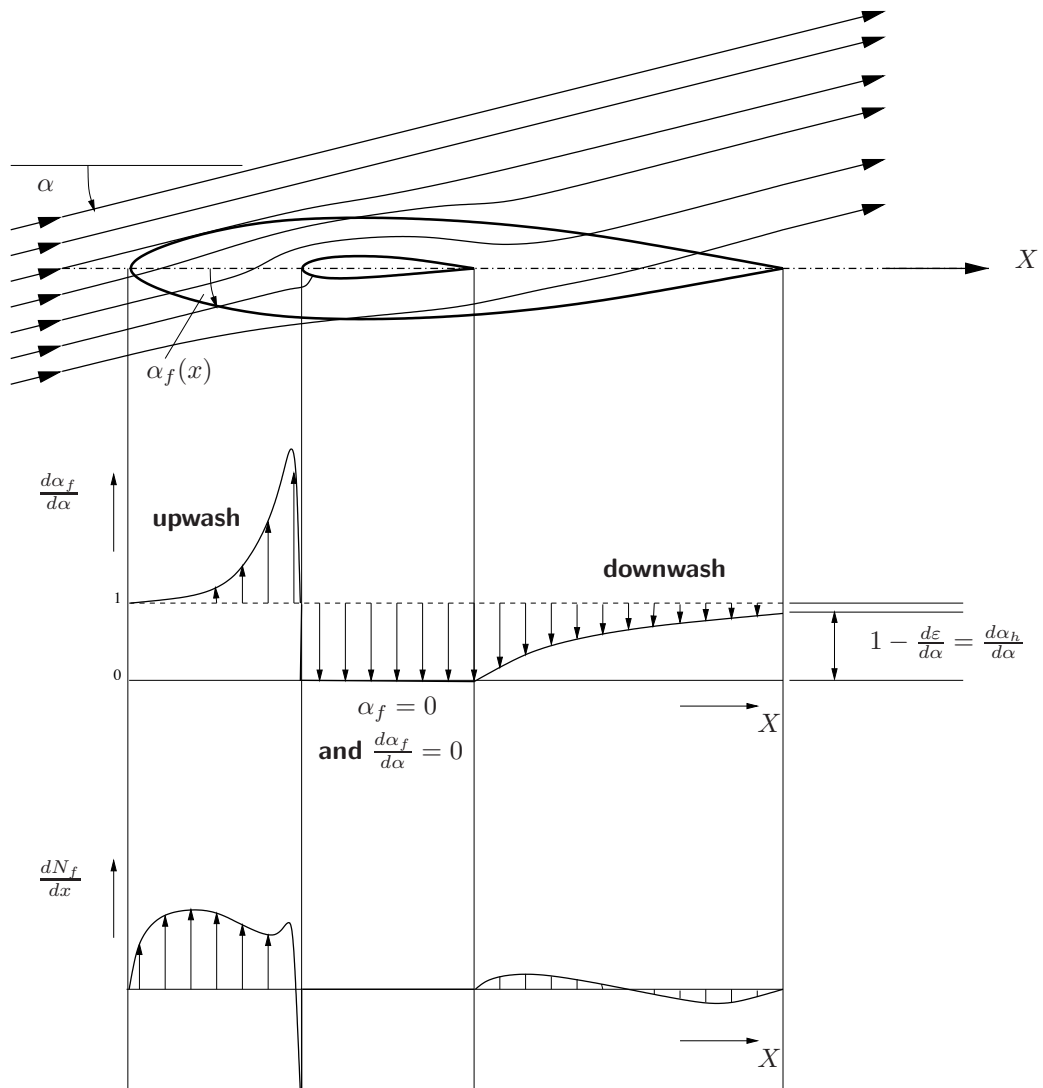


Figure 9-41: The variation of the angle of attack and the normal force along the fuselage axis in a wing induced flow field .

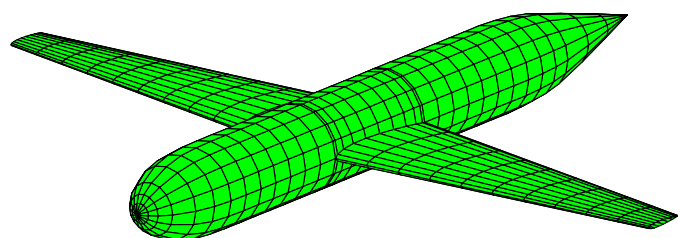


Figure 9-42: Wing-fuselage configuration as used in the flow field simulations depicted in figures 9-43 and 9-44 .

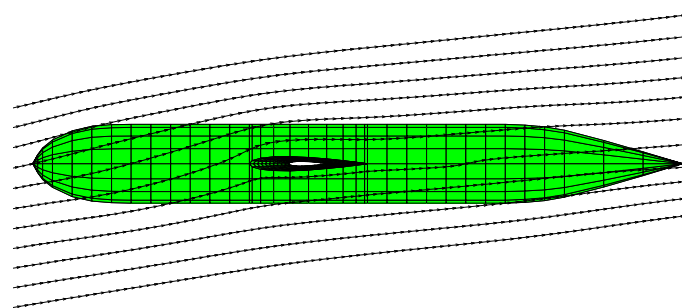


Figure 9-43: Numerical simulation of the velocity field of a wing-fuselage configuration, $\alpha = 10^\circ$.

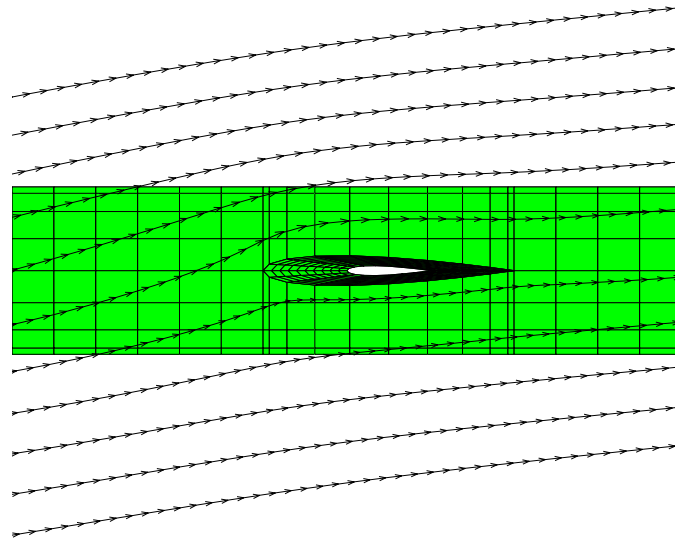


Figure 9-44: Numerical simulation of the velocity field of a wing-fuselage configuration, $\alpha = 10^\circ$, detail of figure 9-43 .

With equation (9-32) the shift in ac position due to the fuselage is,

$$\left(\frac{\Delta x_{ac}}{c} \right)_{f.i.} = -\frac{1}{C_{N_\alpha}} \frac{d C_{m_{f.i.}}}{d \alpha} = -\frac{1}{C_{N_\alpha}} \frac{\pi}{2S\bar{c}} \int_0^{l_f} b_f^2(x) \frac{d \alpha_f(x)}{d \alpha} dx \quad (9-39)$$

Reference [70] presents some classical semi-empirical correction formulas for $\Delta C_{m_{ac}}$ and $(\frac{\Delta x_{ac}}{c})_{f.i.}$ accounting for friction effects of fuselages of finite length.

Computing $C_{m_{f.i.}}$ with equation (9-37) is possible if the variation of $\frac{d \alpha_f}{d \alpha}$ along the fuselage axis is known. Some classical references are [123], [178] and [171]. Nowadays one would no doubt rather rely on some numerical method as used to compute the numerical simulations in the figures above.

Some nice qualitative results are shown in Figures 9-45 and 9-46. It turns out that both a reduction of aspect ratio and an increase of sweepback angles result in decreasing $\frac{d \alpha_f}{d \alpha}$ in front of the wing. This means that the contribution of the fuselage nose to $\frac{d C_{m_{f.i.}}}{d \alpha}$ becomes less stabilizing, see equation (9-39). The downwash angle behind the wing increases with decreasing wing aspect ratio and increasing sweepback angle, $\frac{d \varepsilon}{d \alpha}$ increases and $\frac{d \alpha_f}{d \alpha}$ is closer to zero. In this way the destabilizing contribution to $C_{m_{f.i.}}$ of the rear part of the fuselage behind the wing decreases as well. We conclude that both decreasing the wing aspect ratio and increasing the sweepback angle reduce the destabilizing effect of the fuselage to C_m .

B. The influence of the fuselage on the wing moment, the magnitude of $\Delta C_{m_{w.i.}}$

The influence of the fuselage on the characteristics of the wing itself consists of two parts,

1. The extra upwash induced by the presence of the fuselage over the wing root next to the fuselage, see figures 9-43, 9-44 and 9-47. Results of numerical simulations are shown in figure

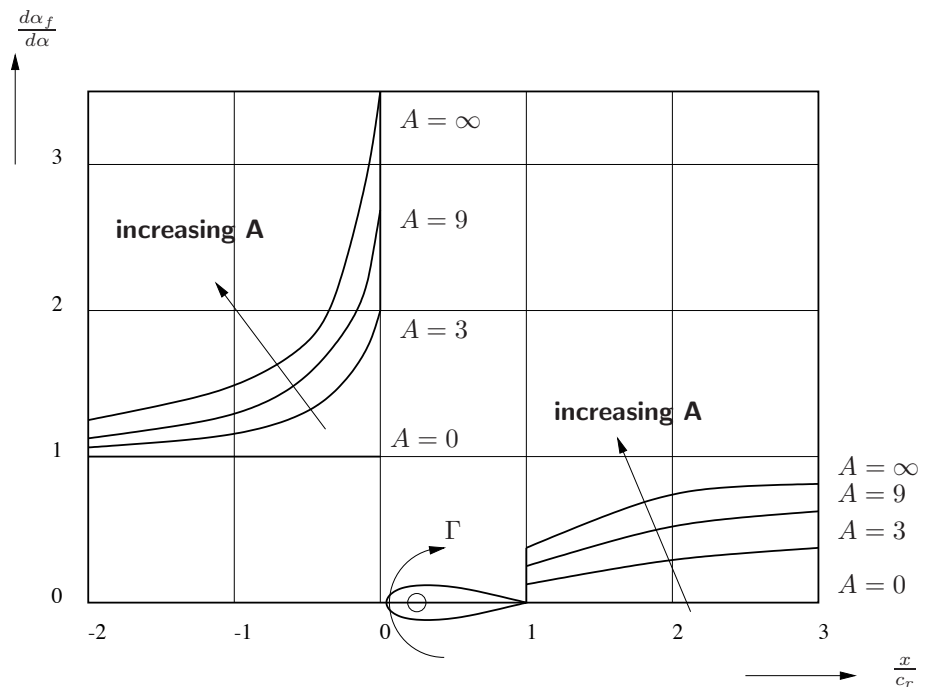


Figure 9-45: The influence of aspect ratio on the variation of $\frac{d\alpha_f}{d\alpha}$ along the fuselage axis ($\Lambda = 0$) (from reference [154])

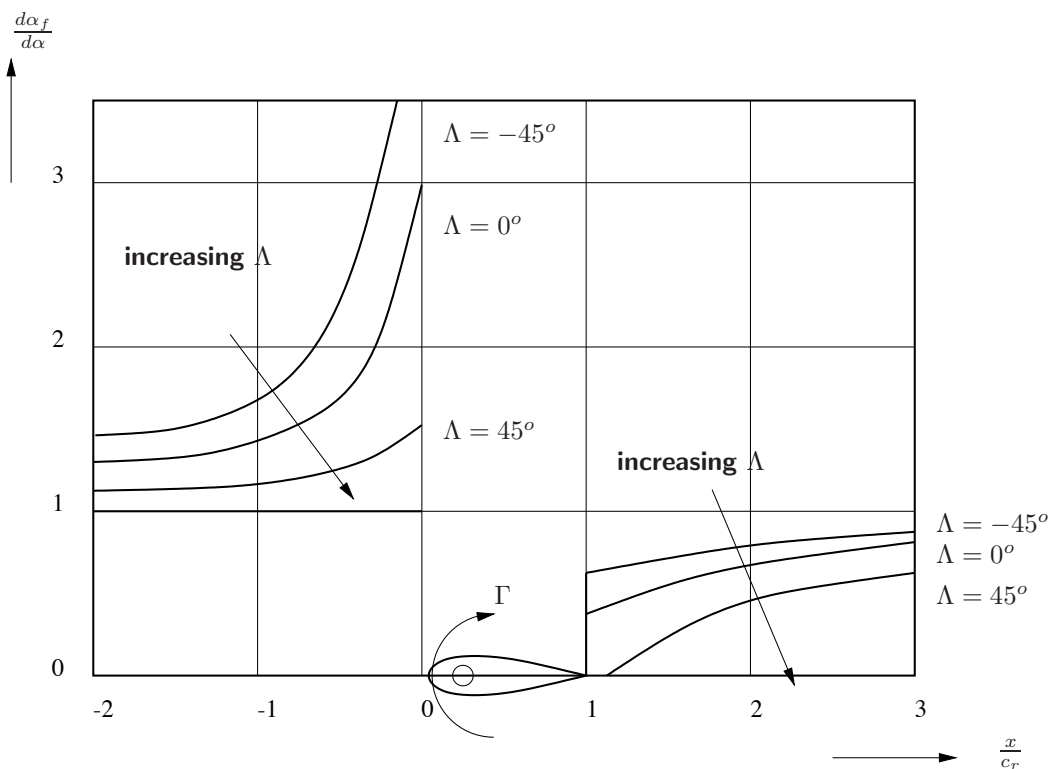


Figure 9-46: The influence of sweep angle of wings with $A = \infty$ on $\frac{d\alpha_f}{d\alpha}$ along the fuselage () (from reference [154])

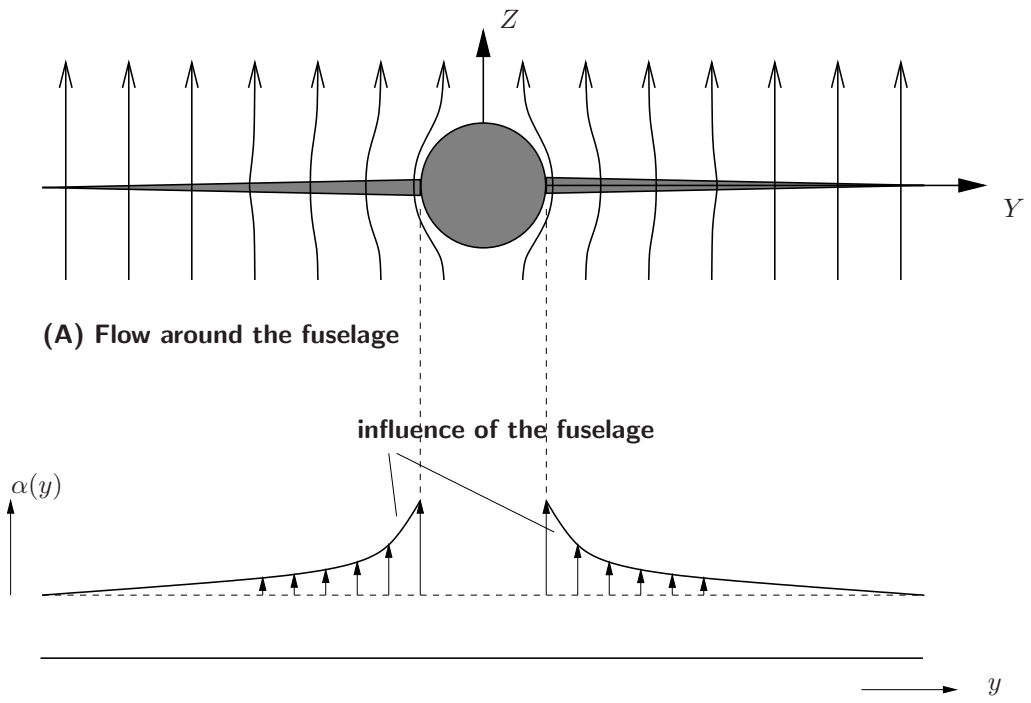


Figure 9-47: Fuselage induced variations of the local angle of attack along the wing span

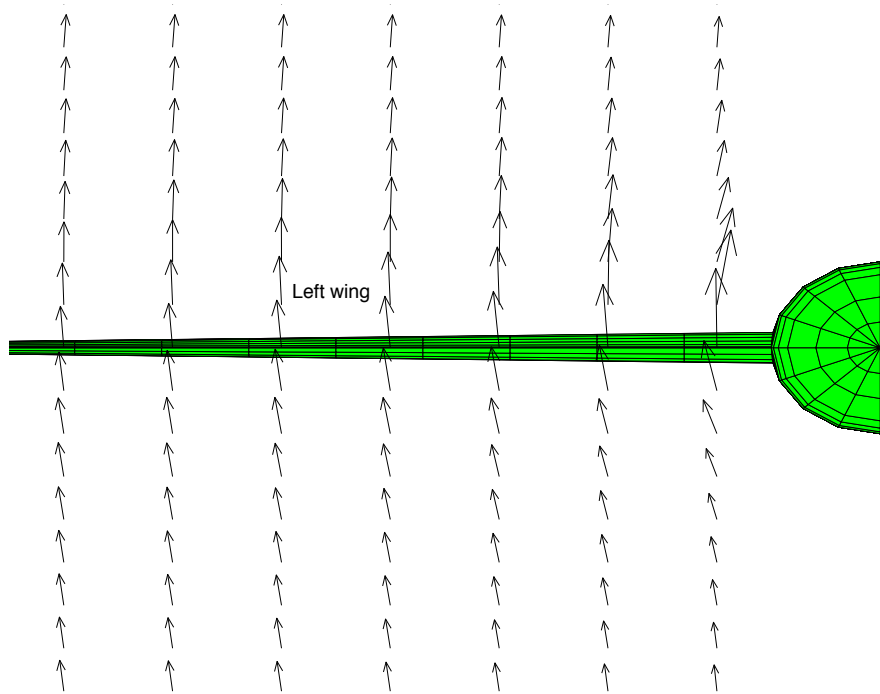


Figure 9-48: Numerical simulation of the fuselage induced upwash along the wing span, $\alpha = 5^\circ$

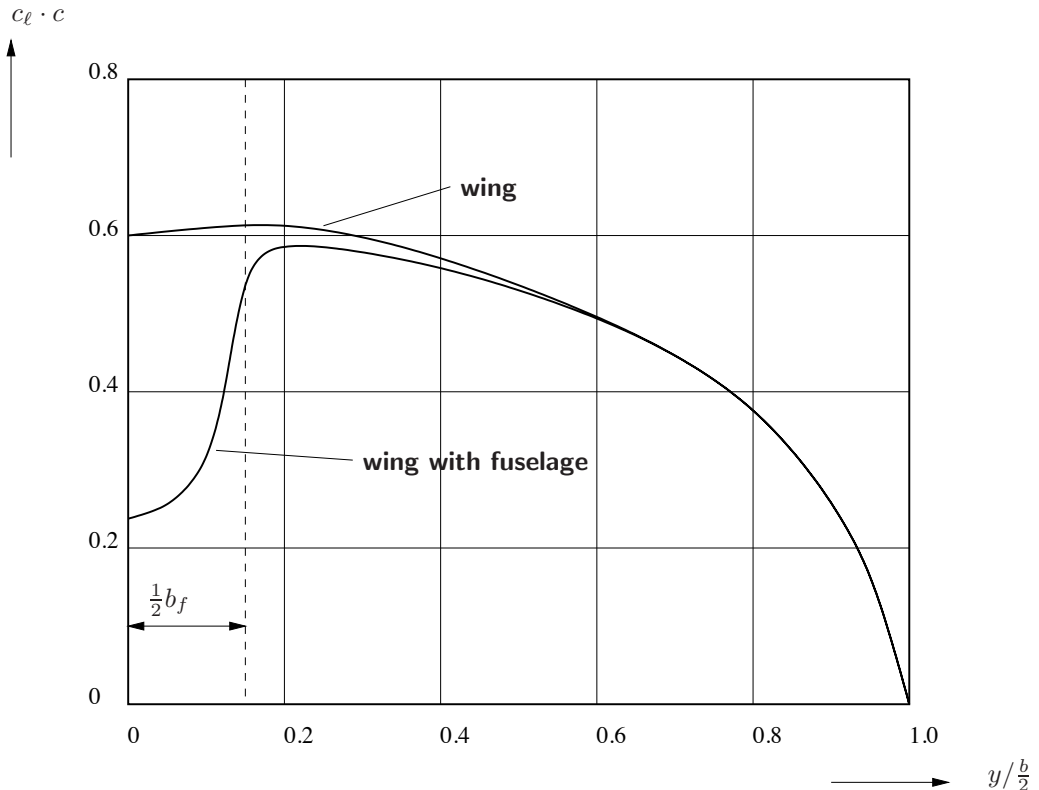


Figure 9-49: The $c_L \cdot c$ -distribution along the span of a wing with and without a fuselage (from reference [58])

9-48. These simulations were performed using the wing-fuselage configuration as of figure 9-42.

2. The change in lift distribution over that part of the wing covered by the fuselage, see figure 9-49.

A further look at the fuselage induced upwash learns that its effect on the wing moment is relatively small and can be usually be neglected, see reference [154]. The induced upwash of wing-mounted nacelles, however, may have a non-negligible effect, see reference [123].

Figure 9-49 shows measurements of the lift distribution across the span of a wing with and without fuselage. It appears that the fuselage affects lift only close to the fuselage. For straight wings this fuselage effect on the C_{mac} of the wing can safely be neglected.

For swept back wings, and also for delta wings, the ac of the entire wing lies behind the local ac's of the center wing profiles , see figure 9-50. This means that the lift reduction ΔC_{L_w} of the center part of the wing will induce in a nose-down change in moment, i.e. $\Delta C_{m_{w,i}}$ is negative. As ΔC_{L_w} is more or less proportional to C_L this effect is stabilizing , shifting ac of the wing rearward. For swept forward wings, however, the same effect causes a tail-down change in the wing moment and is destabilizing ,shifting the ac forward .

Reference [8] allows one to estimate $\Delta C_{m_{w,i}}$ with a simple method. The influence of the sweep

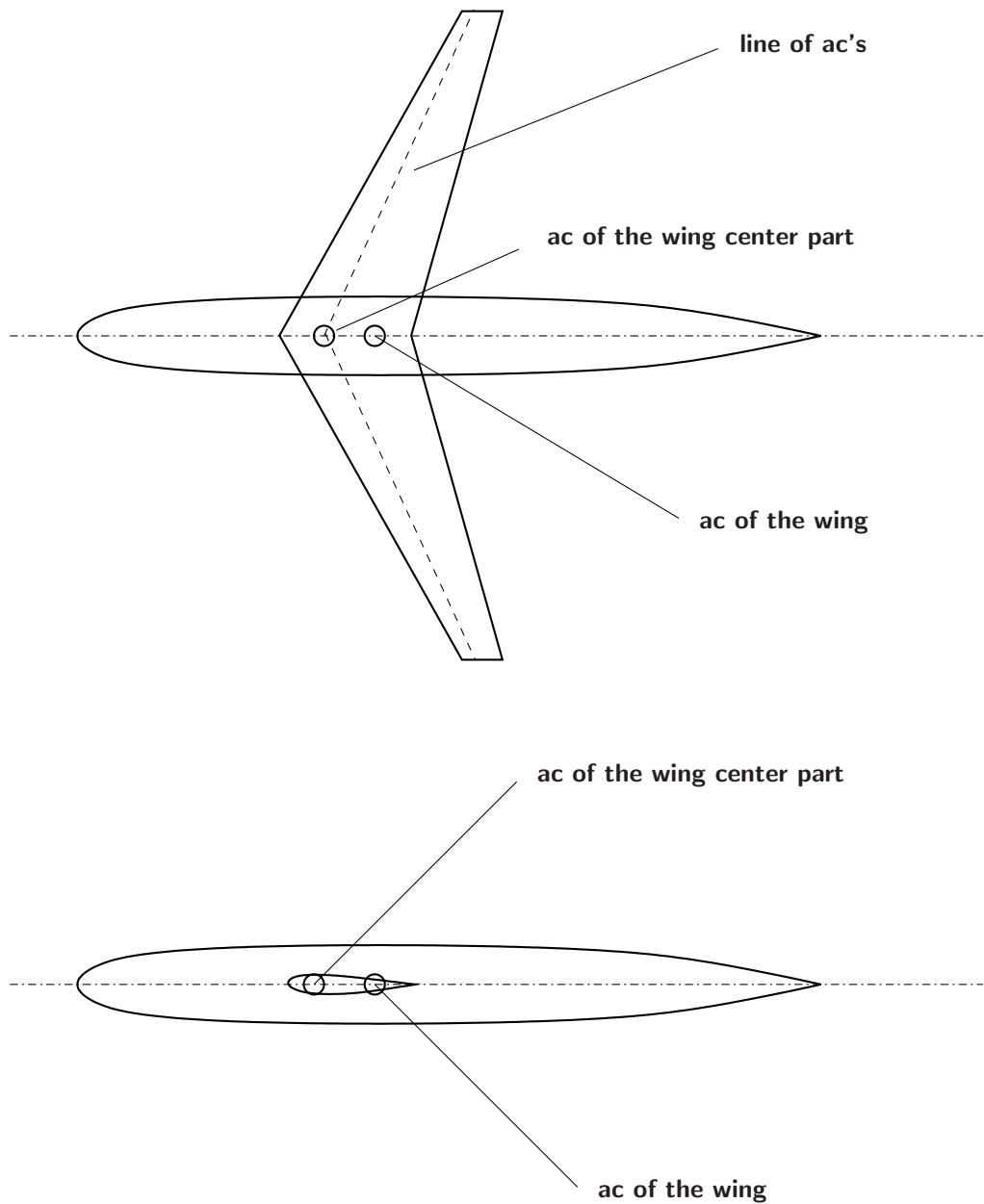


Figure 9-50: The change in wing moment due to loss in lift over the wing center part

angle on the ac as computed with,

$$\left(\frac{\Delta x_{ac}}{\bar{c}} \right)_{w.i.} = -\frac{1}{C_{N_\alpha}} \frac{d\Delta C_{m_{w.i.}}}{d\alpha} \quad (9-40)$$

is shown in figure 9-51 for a set of idealized wing-body configurations. The figure shows the contribution to Δx_{ac} caused by the fuselage in the wing induced field of flow $C_{m_{f.i.}}$ as derived from equation (9-37), the effect of the fuselage on aerodynamic moment of the wing $\Delta C_{m_{w.i.}}$ and the resulting shift of ac position caused by the fuselage, both calculated and measured.

From this figure it appears once again that the fuselage has a destabilizing influence, whereas a wing with positive sweepback angle has a stabilizing effect. As has already been noted in 9-1-5 this stabilizing influence of wing sweepback may compensate the destabilizing effect of the fuselage. The resulting shift of the ac may turn out to be stabilizing.

9-1-7 Aerodynamic effects of nacelles

Analysis of the aerodynamic effects of wing- or fuselage-mounted nacelles on the aerodynamic characteristics of a wing-fuselage configuration starts with the isolated nacelle .

In figure 9-52 a generic configuration of a engine nacelle including simulated particle lines is given for the case of an 'empty' nacelle (no engine thrust effects). Considering this nacelle at an angle-of-attack of $\alpha = 15^\circ$ it is obvious that the local airflow will conform to the exterior of the nacelle, the nacelle can be seen as a ring shaped wing .

Example: aircraft with wing-mounted nacelles

We first consider a transport aircraft model with swept back wings without its nacelles, see figure 9-53. The local airflow over the wing at the nacelle position is shown in figure 9-54. In figure 9-54 simulated particle lines are shown for an angle-of-attack $\alpha = 10^\circ$ as well as the non-dimensional pressure distribution coefficient C_p . The aerodynamic effect of the sweep angle on the non-dimensional pressure distribution C_p of the wing sections is evident from the increasing pressures moving to the wing tip.

Next we add nacelles to the wing . In figure 9-55 results are shown for the case of one nacelle per wing including simulated particle traces and non-dimensional sectional pressure distribution coefficients C_p . It is clear that the nacelle has a significant effect on the local pressure distribution resulting in a reduction of the local angle-of-attack as the airflow conforms to the external shape of the nacelle. This is confirmed by figure 9-56 showing the spanwise lift distribution expressed in terms of $c_l \cdot c$ for an angle-of-attack $\alpha = 10^\circ$ with and without nacelles.

Similar results are shown for the case of a four-engined model in figures 9-57 and 9-58.

The numerical examples shown above on the example case of a transport aircraft configuration show the potential benefits of numerical flow simulation tools as the source/doublet singularity panel-method, linearized potential flow applied in our case. We may use these methods in several ways to compute flow characteristics including pressure distributions and lift distributions, to analyze the effect of aircraft configuration changes including the effect of components as nacelles and, by computing results for a range of angle of attach values, computing the location of the aerodynamic center x_{ac} and the $C_{m_{ac}}$, and their variations for different configurations Δx_{ac} and $\Delta C_{m_{ac}}$. This includes the computation of the corresponding important effects on the downwash characteristics behind the wing, as we will see below.

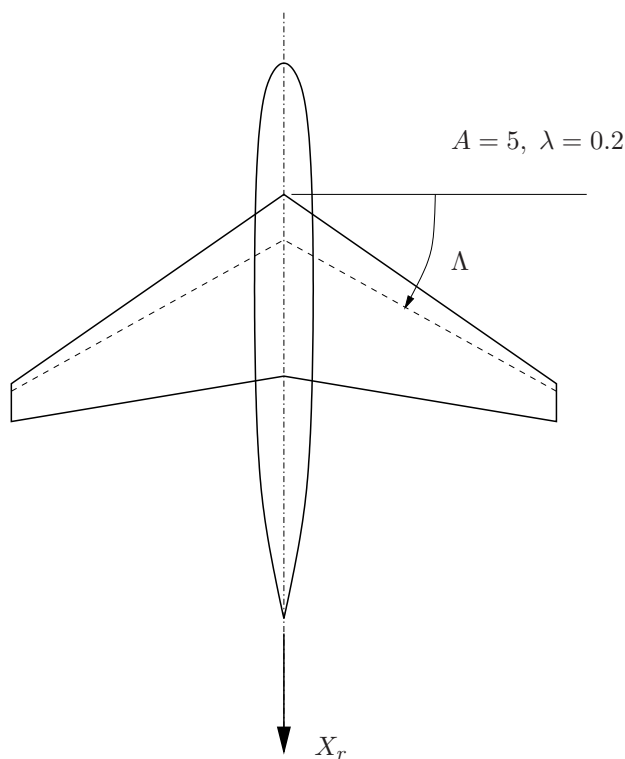
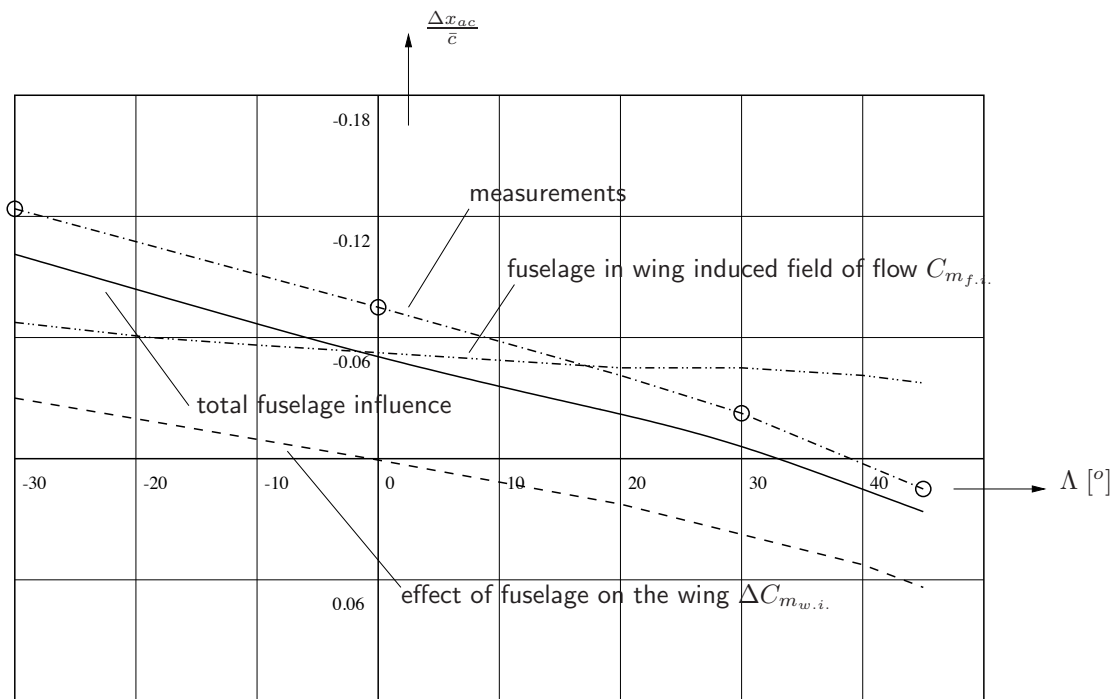


Figure 9-51: Shift of ac due to fuselage effects, as a function of wing sweep angle (from reference [152])

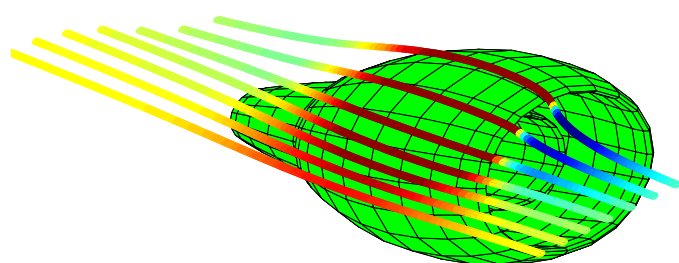


Figure 9-52: Flow simulations over a nacelle, $\alpha = 15^\circ$, computed with a source/doublet singularity panel-method, linearized potential flow

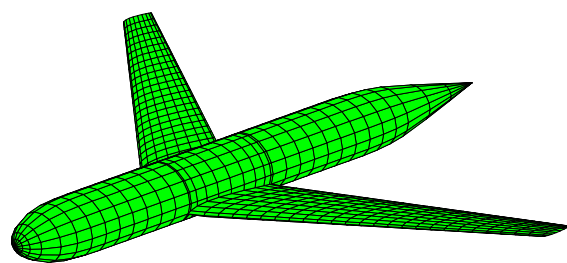


Figure 9-53: Generic Large Transport Aircraft (GLTA), no nacelles

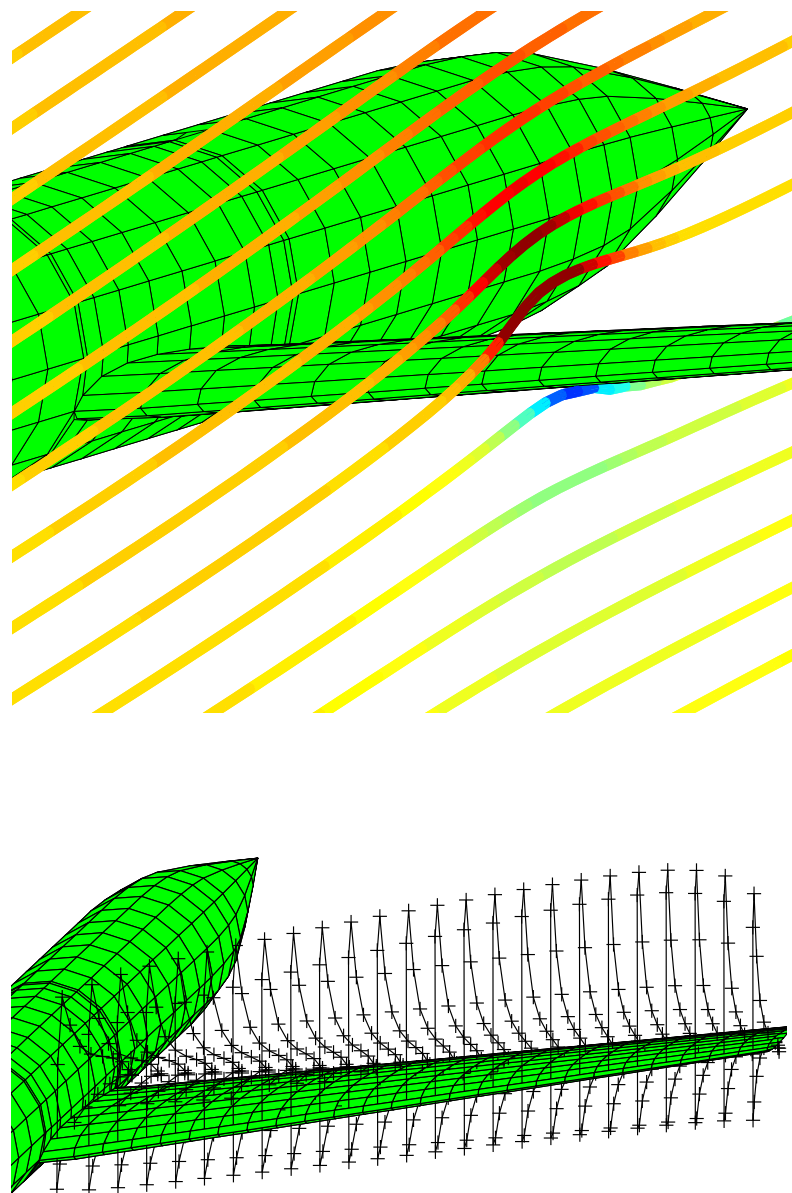


Figure 9-54: Particle lines in an $X_B O Z_B$ -plane (top) and non-dimensional sectional pressure distribution C_p (bottom) for the left wing of a generic transport aircraft model, no nacelles, $\alpha = 10^\circ$, computed with a source/doublet singularity panel-method, linearized potential flow

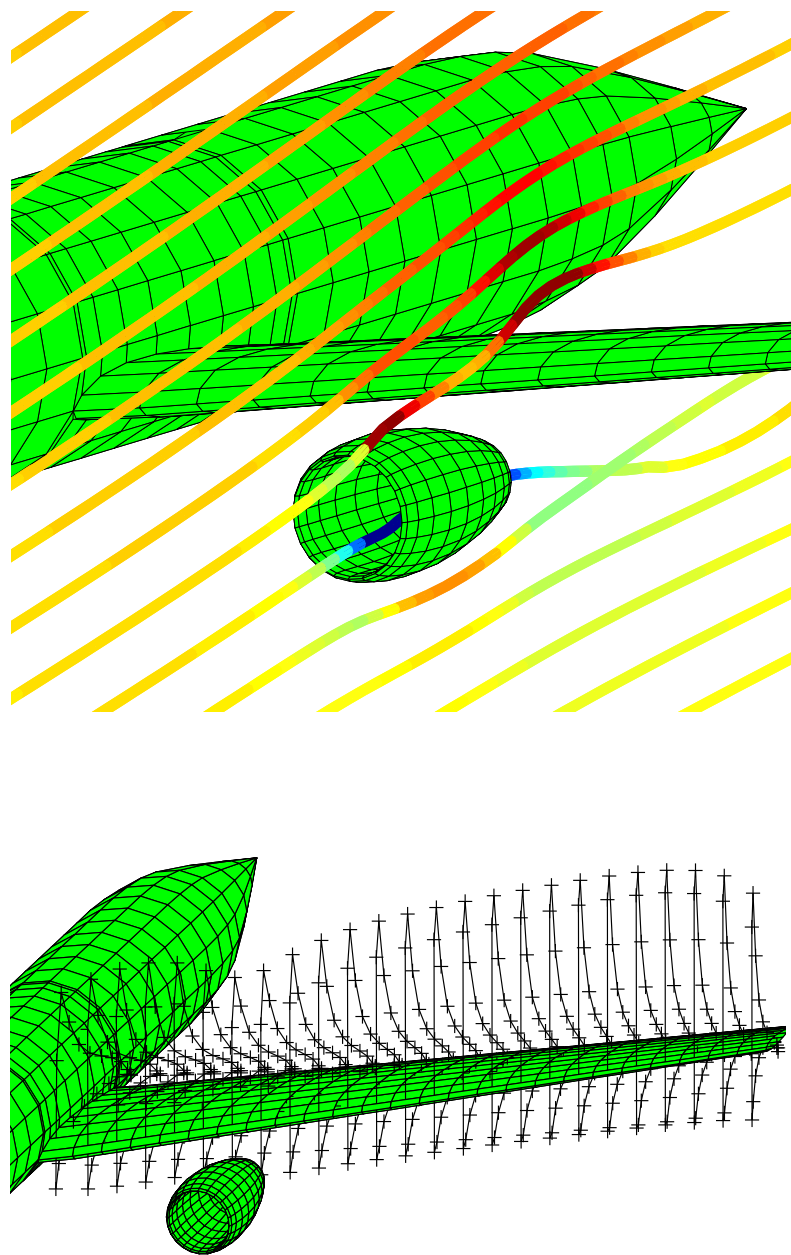


Figure 9-55: Particle lines in an $X_B O Z_B$ -plane (**top**) and non-dimensional sectional pressure distribution C_p (**bottom**) for the left wing of a twin-engined transport aircraft, $\alpha = 10^\circ$, computed with a source/doublet singularity panel-method, linearized potential flow

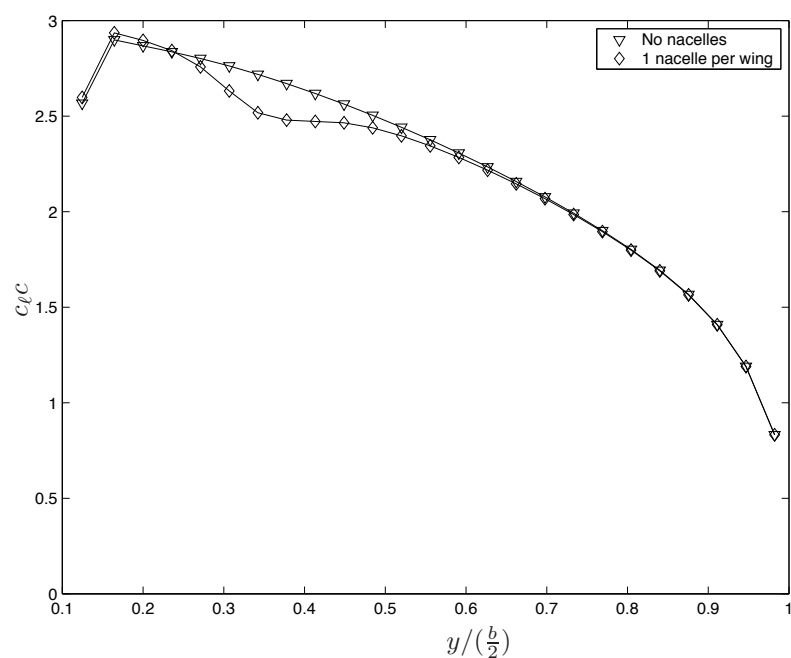
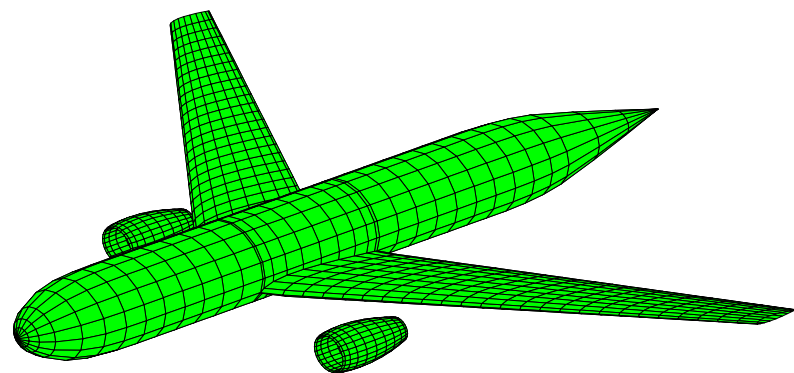


Figure 9-56: Spanwise lift distribution $c_{\ell}c$ at an angle-of-attack $\alpha = 10^\circ$ twin-engined transport aircraft configuration , source/doublet singularity panel-method, linearized potential flow

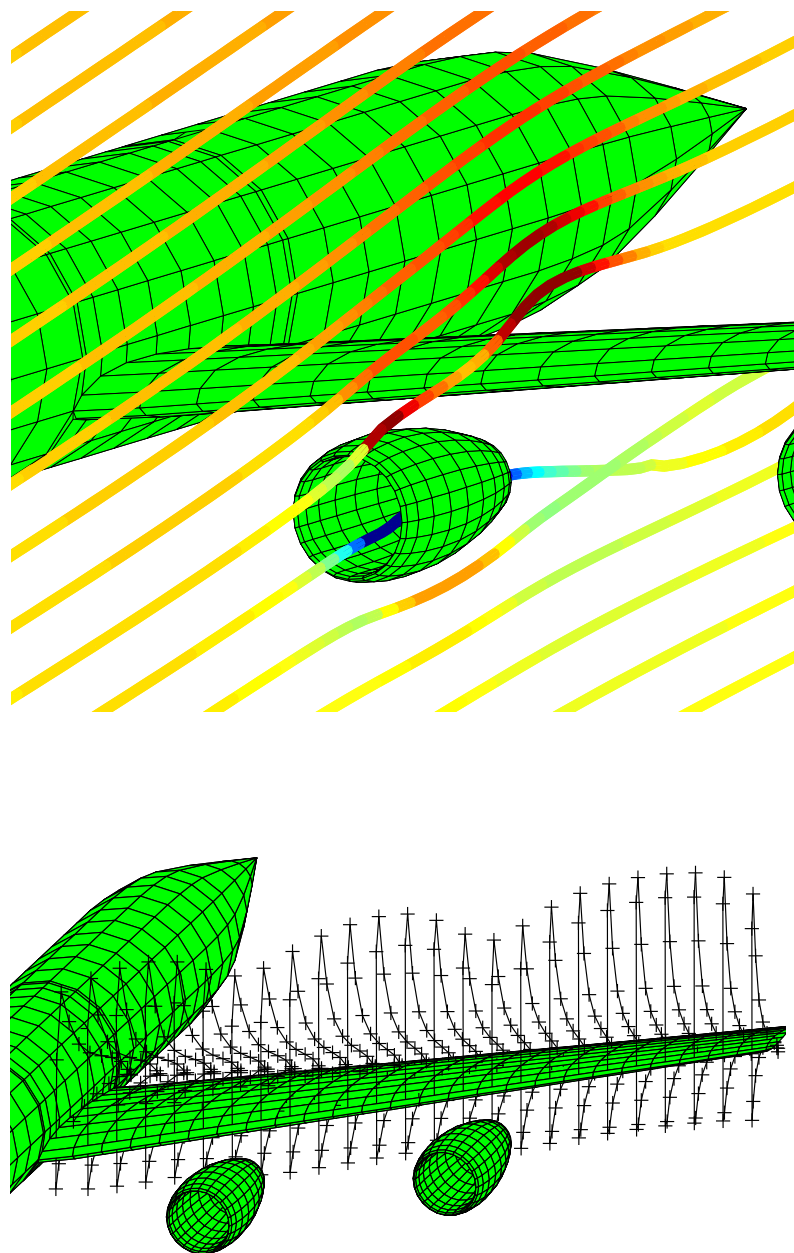


Figure 9-57: Particle lines in an $X_B O Z_B$ -plane and non-dimensional sectional pressure distribution coefficients C_p for the left wing of a four-engined transport aircraft , $\alpha = 10^\circ$, source/doublet singularity panel-method, linearized potential flow

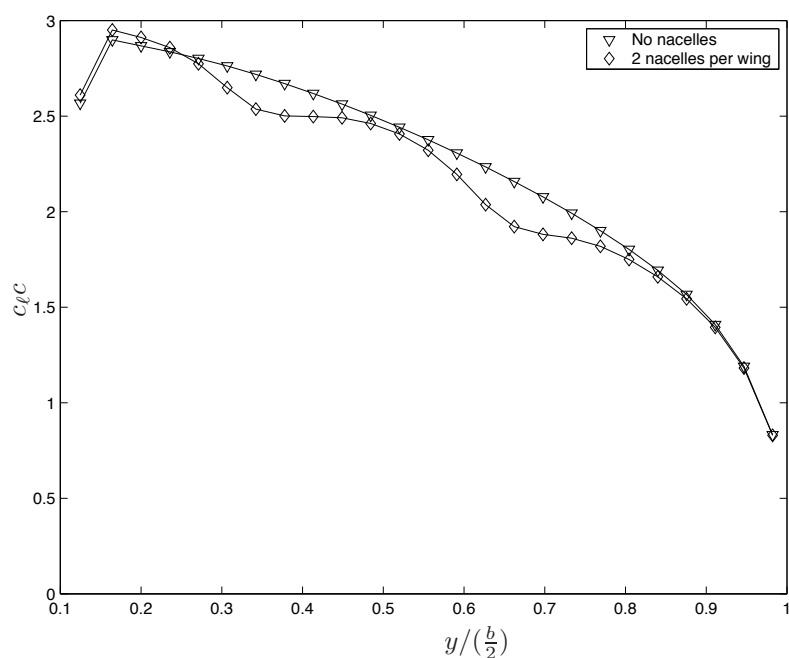
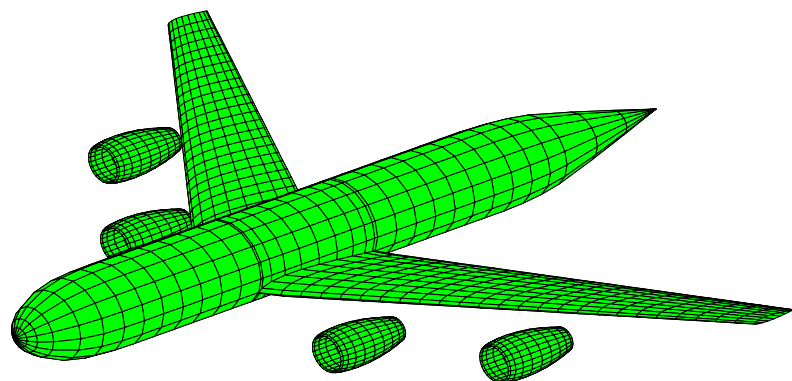


Figure 9-58: Four-engined transport aircraft with spanwise lift distribution $c_{\ell c}$ at an angle-of-attack $\alpha = 10^\circ$, source/doublet singularity panel-method, linearized potential flow

9-2 Equilibrium in steady, straight, symmetric Flight

The present section discusses steady, symmetric, straight flight conditions. The stability of these conditions is discussed in subsequent chapters.

For an aircraft it should be possible to obtain equilibrium of the (longitudinal) aerodynamic moment at any angle of attack and center of gravity position at which equilibrium of the forces is possible, i.e. at all feasible flight conditions, see reference [132]. To achieve this a horizontal tailplane with an elevator is used. The horizontal tailplane serves a dual purpose of generation a longitudinal moment about the center of gravity such that the resulting aerodynamic moment is zero and of changing the aerodynamic moment characteristics in a stable sense, as we will discuss in more detail later.

The following sections discuss the equilibrium of the forces and moments in steady, symmetric, straight flight conditions. In particular the contribution of the horizontal tailplane and the elevator to the longitudinal equilibrium of moments is considered. The stability of these conditions of equilibrium is the subject of next chapters.

9-2-1 Conditions for equilibrium

Since only steady flight is considered here, forces and moments due to mass and rotational inertia of the aircraft are omitted. The aircraft weight and the aerodynamic forces and moments are in equilibrium so,

$$\underline{W} + \underline{R} = 0$$

$$\underline{M} = 0$$

The forces and the moment are resolved in components along the aircraft body axes. In this way the conditions for equilibrium may be written as,

$$W_x + X = 0$$

$$W_y + Y = 0$$

$$W_z + Z = 0$$

$$L = 0$$

$$M = 0$$

$$N = 0$$

In the following, it is always assumed that the aircraft is symmetric and that in the considered flight conditions the flow around the aircraft has a plane of symmetry coinciding with that of the aircraft. In these symmetric flight conditions the resultant aerodynamic force \underline{R} and the weight vector \underline{W} lie in the plane of symmetry of the aircraft, so,

$$W_y = Y = 0$$

$$L = N = 0$$

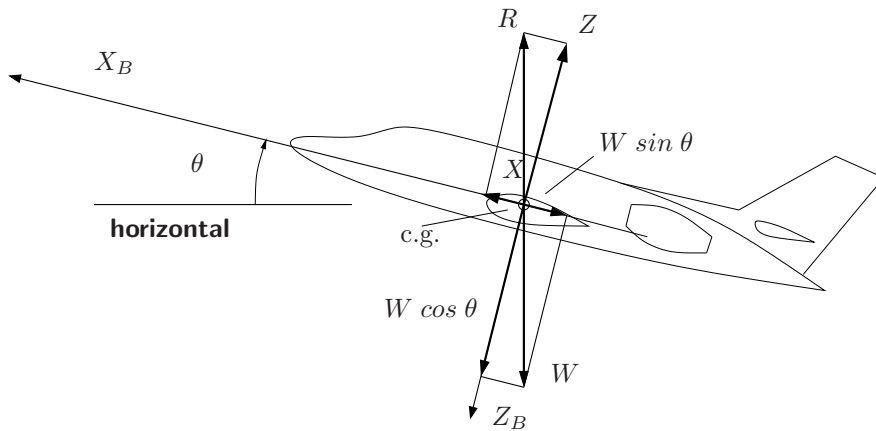


Figure 9-59: The equilibrium in steady, symmetric flight

The three conditions for equilibrium of these symmetric flight conditions are, see figure 9-59,

$$\begin{aligned} -W \sin \theta + X &= 0 \\ W \cos \theta - Z &= 0 \end{aligned}$$

$$M = 0$$

θ denoting the pitch angle.

These equations may also be written in terms of normal and tangential force N and T ,

$$T = W \sin \theta \quad (9-41)$$

$$N = W \cos \theta \quad (9-42)$$

$$M = 0 \quad (9-43)$$

with $T = X$ and $N = Z$. For simplicity , the aircraft body axes are chosen parallel to the aircraft reference axes, origin of the body axes remaining in the aircraft center of gravity. In the following, these conditions are further analyzed.

The resultant aerodynamic force R is built up from the contributions of the different parts of the aircraft. These parts also provide the elements of the resultant aerodynamic moment M . Three parts of the aircraft may be distinguished.

- Wing with fuselage and nacelles

The contributions of these parts of the aircraft usually are taken as one entity, the index w referring to the combination of the wing with fuselage and nacelles. The model of the forces acting on this part of the aircraft is given by the components N_w and T_w of the total aerodynamic force R_w , acting in the aerodynamic center (ac) of the wing with fuselage and nacelles (ac_w), and the aerodynamic moment M_{ac_w} acting about the ac_w .

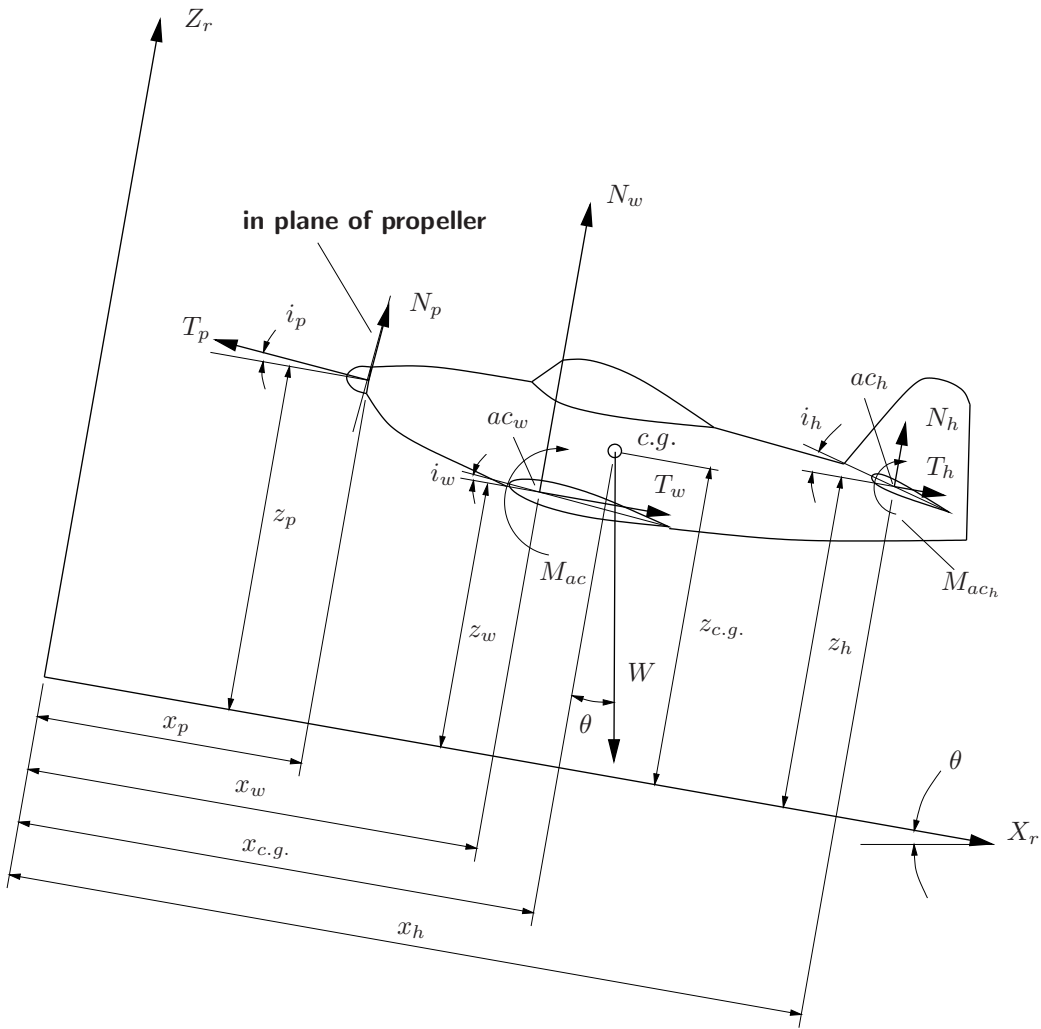


Figure 9-60: The forces and moments in steady, straight, symmetric flight

- **Horizontal tailplane**

Just as for the wing with fuselage and nacelles, the model of the forces acting on the horizontal tailplane is given by the components N_h and T_h , acting in the ac of the tailplane (ac_h), and the moment M_{ac_h} .

- **The propulsion unit**

The contribution of the propeller, or the jet engine, consists of the thrust T_p along the propeller or engine-axis and the normal force N_p acting in the plane of the propeller or in the plane of the engine inlet depending on the local angle of attack.

Figure 9-60 depicts the contributions of the various parts of the aircraft.

The symmetric conditions of equilibrium, equations (9-41), (9-42) and (9-43) can now be written as follows,

- Forces along the X_B -axis

$$T = +T_w + T_h - T_p \cos i_p + N_p \sin i_p = -W \sin \theta \quad (9-44)$$

- Forces along the Z_B -axis

$$N = +N_w + N_h + N_p \cos i_p + T_p \sin i_p = +W \cos \theta \quad (9-45)$$

- Moments about the Y_B -axis

$$\begin{aligned} M = & +M_{ac_w} + N_w (x_{c.g.} - x_w) - T_w (z_{c.g.} - z_w) + \\ & +M_{ac_h} + N_h (x_{c.g.} - x_h) - T_h (z_{c.g.} - z_h) + \\ & +(N_p \cos i_p + T_p \sin i_p) (x_{c.g.} - x_p) + \\ & +(T_p \cos i_p - N_p \sin i_p) (z_{c.g.} - z_p) = 0 \end{aligned} \quad (9-46)$$

Before bringing the expressions (9-44), (9-45) and (9-46) in a non-dimensional form, some new non-dimensional coefficients have to be defined. The non-dimensional coefficients of normal force and tangential force on the tailplane, and the moment about the ac of the tailplane are now defined by,

$$\begin{aligned} N_h &= C_{N_h} \frac{1}{2} \rho V_h^2 S_h \\ T_h &= C_{T_h} \frac{1}{2} \rho V_h^2 S_h \\ M_{ac_h} &= C_{m_{ac_h}} \frac{1}{2} \rho V_h^2 S_h \bar{c}_h \end{aligned} \quad (9-47)$$

The non-dimensional coefficients C_{N_h} , C_{T_h} and $C_{m_{ac_h}}$ are thus referred to the surface area S_h and the mac \bar{c}_h of the horizontal tailplane (see figure 9-61a) and the average local dynamic pressure $\frac{1}{2} \rho V_h^2$ at the horizontal tailplane. In general, this dynamic pressure is different from that of the undisturbed flow (at infinity). This is further discussed in section 9-2-4.

The thrust of the propeller and the normal force in the plane of the propeller may be written as,

$$T_p = T_c \rho V^2 D^2 \quad (9-48)$$

$$N_p = C_{N_p} \frac{1}{2} \rho V^2 S_p \quad (9-49)$$

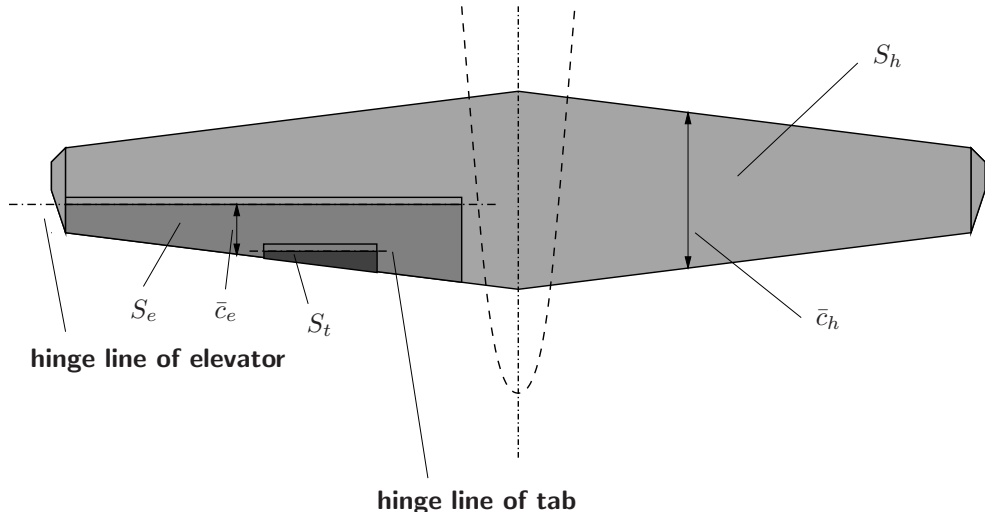
where D is the propeller diameter and $S_p = \frac{\pi}{4} D^2$ is the area of the propeller disc. The equations of equilibrium are made non-dimensional in the usual way by dividing equations (9-44) and (9-45) by $\frac{1}{2} \rho V^2 S$ and equation (9-46) by $\frac{1}{2} \rho V^2 S \bar{c}$. Using ,

$$-T_p \cos i_p + N_p \sin i_p \approx -T_p$$

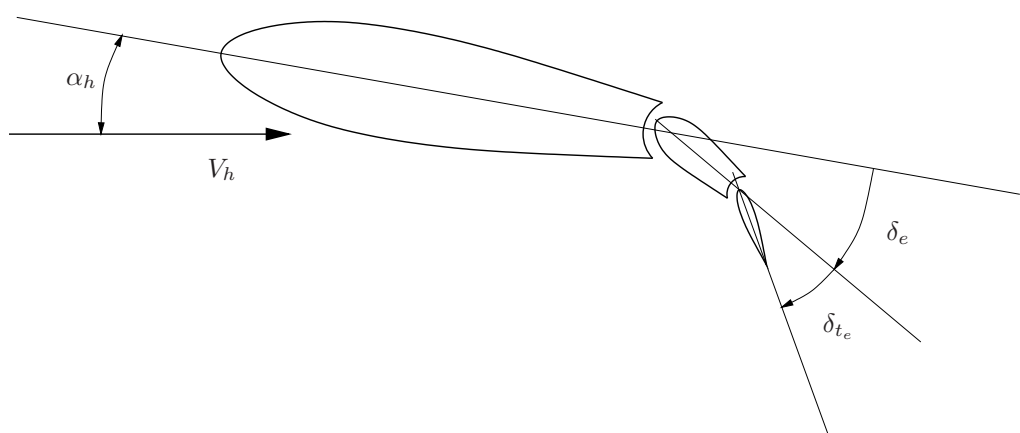
the result is,

$$C_T = +C_{T_w} + C_{T_h} \left(\frac{V_h}{V} \right)^2 \frac{S_h}{S} - T_c \frac{2D^2}{S} = -\frac{W}{\frac{1}{2} \rho V^2 S} \sin \theta \quad (9-50)$$

$$C_N = +C_{N_w} + C_{N_h} \left(\frac{V_h}{V} \right)^2 \frac{S_h}{S} + T_c \frac{2D^2}{S} \sin i_p + C_{N_p} \frac{S_p}{S} = \frac{W}{\frac{1}{2} \rho V^2 S} \cos \theta \quad (9-51)$$



(A) Geometry parameters of the horizontal tailplane, elevator and trim tab



(B) Positive deflections of α_h , δ_e and δ_{t_e}

Figure 9-61: Geometry parameters of the horizontal tailplane, elevator and trim tab, and their positive deflections

$$\begin{aligned}
C_m = & +C_{m_{acw}} + C_{N_w} \frac{x_{c.g.} - x_w}{\bar{c}} - C_{T_w} \frac{z_{c.g.} - z_w}{\bar{c}} + C_{m_{ach}} \left(\frac{V_h}{V} \right)^2 \frac{S_h}{S} \frac{\bar{c}_h}{\bar{c}} + \\
& + C_{N_h} \left(\frac{V_h}{V} \right)^2 \frac{S_h}{S} \frac{x_{c.g.} - x_h}{\bar{c}} - C_{T_h} \left(\frac{V_h}{V} \right)^2 \frac{S_h}{S} \frac{z_{c.g.} - z_h}{\bar{c}} + \\
& + \left(T_c \frac{2D^2}{S} \sin i_p + C_{N_p} \frac{S_p}{S} \right) \frac{x_{c.g.} - x_p}{\bar{c}} + T_c \frac{2D^2}{S} \frac{z_{c.g.} - z_p}{\bar{c}} = 0
\end{aligned} \quad (9-52)$$

These equilibrium equations may be used for different purposes such as to explore the set of feasible steady state flight conditions.

In the following, however, the purpose is an analysis of stability and flying qualities parameters. In that case it is permissible and even desirable to simplify the equations of equilibrium in such a way that only the most important contributions remain, resulting in the following simplifications ,

1. Propulsion effects, i.e. the terms with T_c and C_{N_p} are neglected.
2. The contribution of C_{T_h} to the force in X_B -direction in equation (9-50) and to the moment in equation (9-52) is neglected. This simplification is nearly always permissible.
3. The contribution of C_{T_w} to the moment in equation (9-52) is omitted. For large angles of attack, or in cases when the center of gravity is situated far above or below the ac_w , this simplification may not always be permissible.
4. The contribution of $C_{m_{ach}}$ is relatively small, even zero in case of symmetric airfoils, and so $C_{m_{ach}}$ in equation (9-52) is neglected too. The index w of $C_{m_{acw}}$ may therefore be omitted as well without raising confusion.

The resulting equations of equilibrium now read ,

$$C_T = C_{T_w} = -\frac{W}{\frac{1}{2}\rho V^2 S} \sin \theta \quad (9-53)$$

$$C_N = C_{N_w} + C_{N_h} \left(\frac{V_h}{V} \right)^2 \frac{S_h}{S} = \frac{W}{\frac{1}{2}\rho V^2 S} \cos \theta \quad (9-54)$$

$$C_m = C_{m_{ac}} + C_{N_w} \frac{x_{c.g.} - x_w}{\bar{c}} + C_{N_h} \left(\frac{V_h}{V} \right)^2 \frac{S_h}{S} \frac{x_{c.g.} - x_h}{\bar{c}} = 0 \quad (9-55)$$

The assumptions made in the model of the equilibrium lead to a very simple model, see figure 9-62.

The distance between the ac of the horizontal tailplane and the ac of the wing with fuselage and nacelles, $(x_h - x_w)$, is called the tail length l_h . For conventional aircraft,

$$l_h = x_h - x_w \approx x_h - x_{cg} \quad (9-56)$$

With (9-56) equation (9-55) may be written as,

$$C_m = C_{m_{ac}} + C_{N_w} \frac{x_{c.g.} - x_w}{\bar{c}} - C_{N_h} \left(\frac{V_h}{V} \right)^2 \frac{S_h l_h}{S \bar{c}} = 0 \quad (9-57)$$

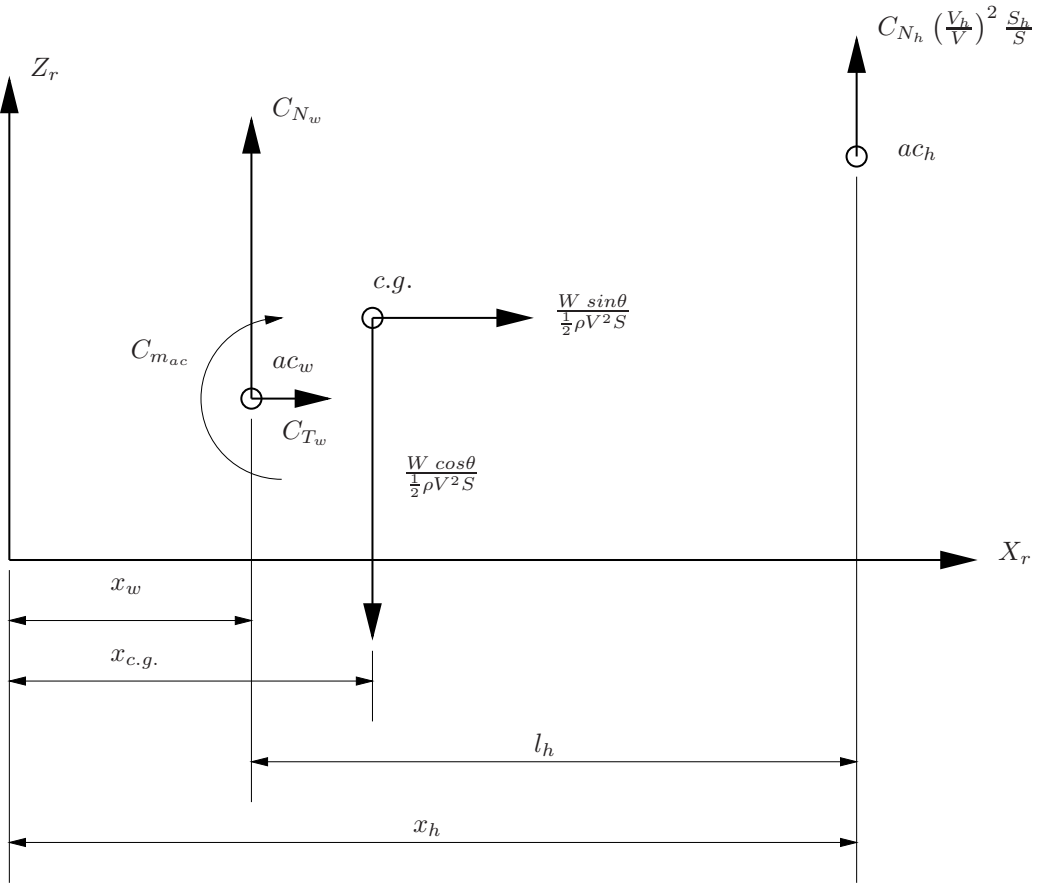


Figure 9-62: Simplified version of the equilibrium of forces and moments

or,

$$C_m = C_{m_w} + C_{m_h}$$

in which $\frac{S_h l_h}{S c}$ is called the 'tailplane volume'.

The tailplane serves to compensate for C_{m_w} through an appropriate deflection of the elevator or by adjusting the angle of incidence of the entire horizontal tailplane.

In this way the contribution C_{m_h} from the horizontal tailplane to the moment as generated by C_{N_h} , is equal and opposite to the contribution C_{m_w} of the wing with its fuselage and nacelles.

In the following sections the characteristics of the horizontal tailplane and the effects of the elevator are discussed in more detail. Also, expressions will be derived for the elevator angle and the pilot's control force necessary to maintain equilibrium for given flight conditions.

The equations of equilibrium (9-53), (9-54) and (9-55) apply to the conventional aircraft configurations where the horizontal tailplane is placed behind the wing. In the given form the expressions are valid also for aircraft where the horizontal 'tailplane' is located in front of the wing. In that case l_h in equation (9-57) is negative , see also equation (9-56).

For tailless aircraft the contribution of the horizontal tailplane obviously does not exist. In that case equation (9-57) reduces to,

$$C_m = C_{m_{ac}} + C_{N_w} \frac{x_{c.g.} - x_w}{\bar{c}} = 0 \quad (9-58)$$

see also figure 9-17.

The 'elevator' of tailless aircraft is situated at the trailing edge of the wing. Deflection of the elevator of such an aircraft causes a change of $C_{m_{ac}}$. The elevator deflection also has an influence on C_N which may be non-negligible in many cases. For tailless aircraft, equilibrium for some value of C_N is possible if $C_{m_{ac}}$ in equation (9-58) is made equal and opposite in sign to the moment of C_N about the center of gravity.

9-2-2 Normal force on the horizontal tailplane

The horizontal tailplane usually consists of a stabilizer and a control surface. In many cases a small auxiliary control surface is added to the control surface. This may be a trim tab, a balance tab or a servo tab. The non-dimensional pressure distribution over the horizontal tailplane is completely determined by three deflection angles,

1. The angle of attack of the horizontal tailplane, α_h
2. The control deflection angle, δ_e (index e stands for elevator)
3. The tab angle, δ_{t_e} (index t stands for tab)

Figure 9-61b shows the positive sense of the three angles α_h , δ_e and δ_{t_e} . Figure 9-63 shows the changes in the chordwise pressure distribution caused by changes in the local angle of attack, the control surface deflection and the tab angle deflection.

The non-dimensional normal force C_{N_h} as defined in equation (9-47) is determined by the local angle of attack and two deflection angles ,

$$C_{N_h} = C_{N_h} (\alpha_h, \delta_e, \delta_{t_e})$$

In figure 9-64 results are given of measurements of C_{N_h} as a function of α_h , δ_e and δ_{t_e} . It follows that in selected small intervals of α_h , δ_e and δ_{t_e} , C_{N_h} may be assumed to vary approximately linearly with these parameters. In the range of those small angle excursions a reasonable approximation of C_{N_h} is obtained by,

$$C_{N_h} = C_{N_{h_0}} + \frac{\partial C_{N_h}}{\partial \alpha_h} \alpha_h + \frac{\partial C_{N_h}}{\partial \delta_e} \delta_e + \frac{\partial C_{N_h}}{\partial \delta_{t_e}} \delta_{t_e} \quad (9-59)$$

A convenient shorthand notation is used for the aerodynamic partial derivatives introduced in equation (9-59), see table 9-1.

The expression (9-59) can be simplified a little. First we note that the influence of δ_{t_e} on C_{N_h} is usually small, see for example figure 9-64 and may be neglected.

Furthermore, many tailplanes have a symmetric or close to symmetric airfoils, so $C_{N_{h_0}} = 0$.

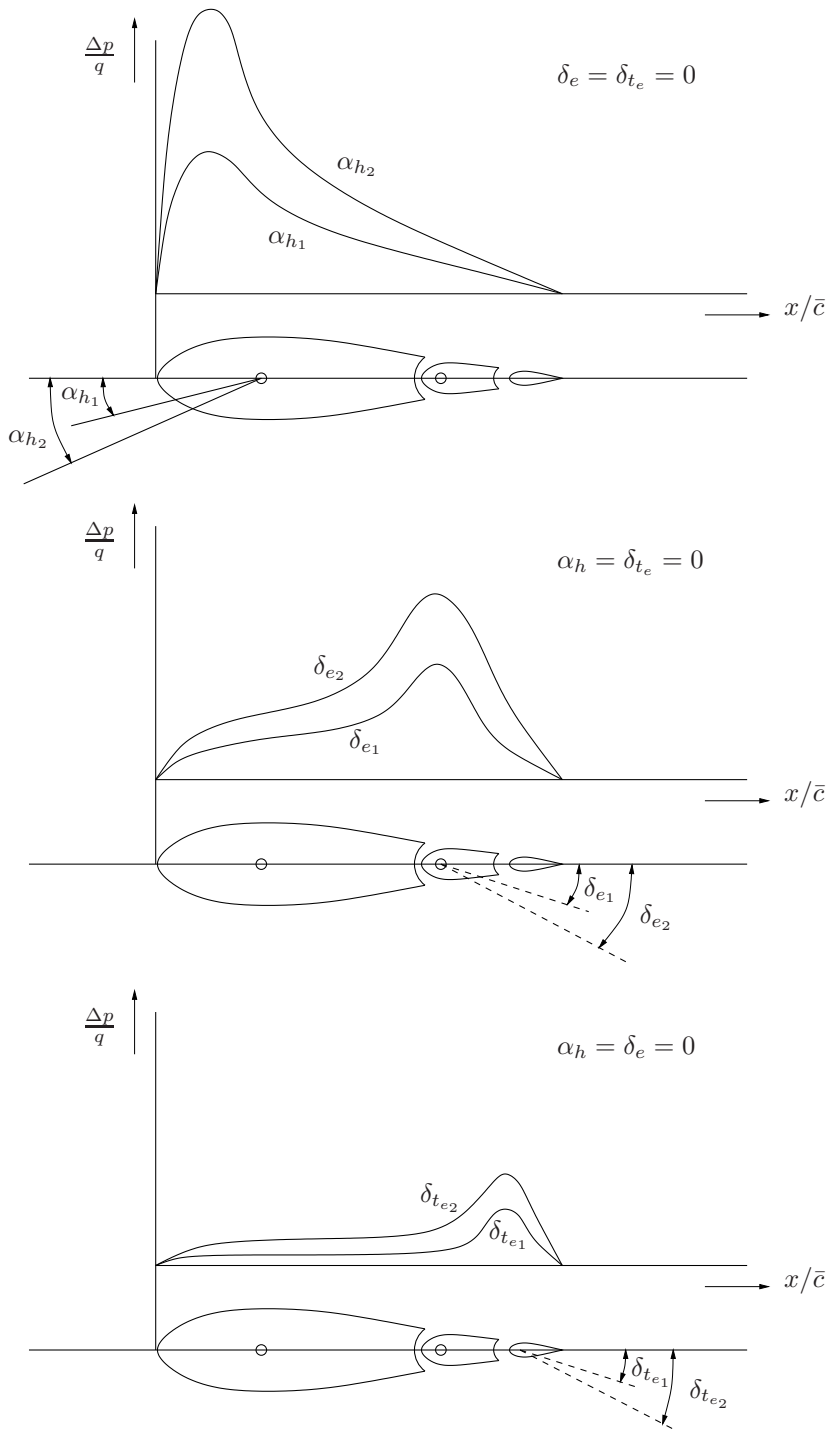
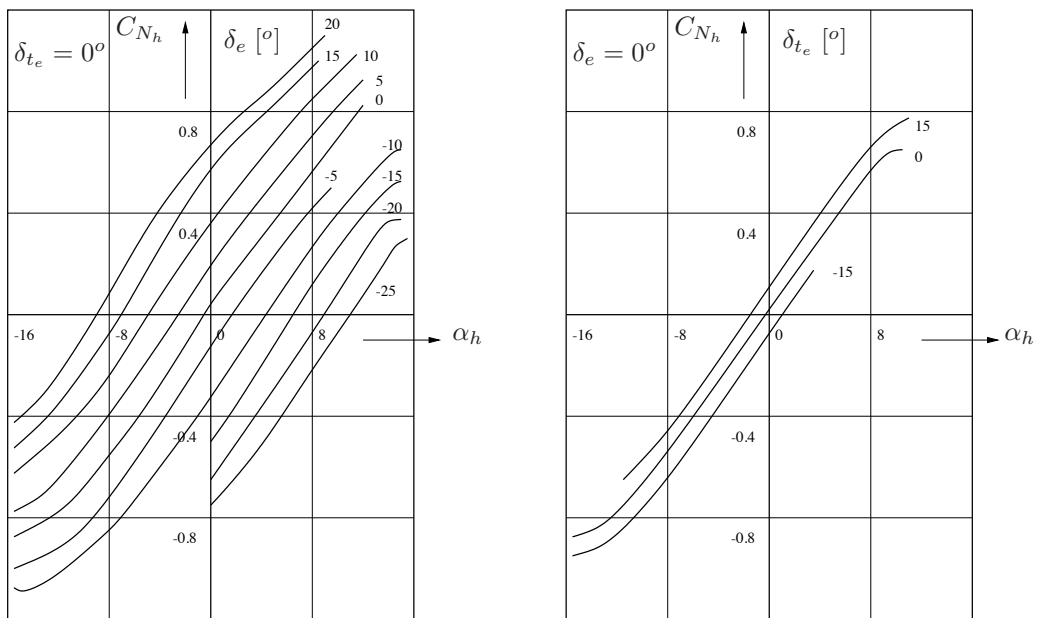


Figure 9-63: Pressure distributions over the tailplane chord due to α_h , δ_e and δ_{t_e}

		Normal force derivatives		
Derivative	$\frac{\partial C_{N_h}}{\partial \alpha_h}$		$\frac{\partial C_{N_h}}{\partial \delta_e}$	$\frac{\partial C_{N_h}}{\partial \delta_{t_e}}$
Shorthand notation	$C_{N_h\alpha}$		$C_{N_h\delta}$	$C_{N_h\delta_t}$

Table 9-1: Shorthand notation for the normal force derivatives on a tailplane

Figure 9-64: The normal force coefficient C_{N_h} as a function of α_h , δ_e and δ_{t_e} for the tailplane of the Fokker F-27 (Wind tunnel measurements from reference [17])

Using the shorthand notation (which corresponds to the American notation) this results in,

$$C_{N_h} = C_{N_{h_\alpha}} \alpha_h + C_{N_{h_\delta}} \delta_e \quad (9-60)$$

which serves as an approximation of the much more complex nonlinear relation,

$$C_{N_h} = C_{N_h} (\alpha_h, \delta_e, \delta_{t_e})$$

as may be obtained from wind tunnel measurements or flight test.

Both positive changes in the angle of attack α_h and the control deflection δ_e cause positive changes in C_{N_h} which means,

$$C_{N_{h_\alpha}} > 0 \quad \text{and} \quad C_{N_{h_\delta}} > 0$$

With references [75, 168, 4, 109, 65, 21], based on empirical data, it is possible to estimate $C_{N_{h_\alpha}}$ and $C_{N_{h_\delta}}$. The normal force gradient $C_{N_{h_\alpha}}$ can be obtained in principle using one of the available wing theories. The presence of the fuselage and the existence of an open gap between the stabilizer and the control surface must be taken into account, reducing the value of $C_{N_{h_\alpha}}$.

From measurements on two- and three-dimensional models it was shown that $C_{N_{h_\delta}}$ depends almost linearly on $C_{N_{h_\alpha}}$. This is reflected in figure 9-65 showing $\frac{C_{N_{h_\delta}}}{C_{N_{h_\alpha}}}$ to depend on the ratio of the control surface chord to the tailplane chord, $\frac{\bar{c}_e}{\bar{c}_h}$ and the trailing edge angle τ of the airfoil. This result holds for aerodynamically unbalanced control surfaces extending over the entire span of the horizontal tailplane with a closed gap between the horizontal tailplane ('stabilizer') and the control surface. However, $C_{N_{h_\delta}}$ is affected by several other factors such as cut-outs in the control surface at the fuselage and the vertical tailplane, a gap between the stabilizer and the aerodynamic shape of the nose of control surfaces (used to 'balance' or compensate hinge moments), see references [109, 65].

9-2-3 Hinge moment of the elevator

The aerodynamic hinge moment about the elevator hinge line, H_e , is determined by the pressure distribution over the elevator. This hinge moment is expressed by a non-dimensional coefficient, C_{h_e} ,

$$C_{h_e} = \frac{H_e}{\frac{1}{2} \rho V_h^2 S_e \bar{c}_e} \quad (9-61)$$

The hinge moment coefficient is thus referred to the average local dynamic pressure at the horizontal tailplane and to the surface S_e and the mac \bar{c}_e of the part of the control surface behind the hinge line, see figure 9-61a. The hinge moment is defined positive in the same direction as the control surface deflection.

Similar to C_{N_h} , also C_{h_e} depends on the three angles α_h , δ_e and δ_{t_e} , see the pressure distributions in figure 9-63,

$$C_{h_e} = C_{h_e} (\alpha_h, \delta_e, \delta_{t_e})$$

Measurements of C_{h_e} as a function of α_h , δ_e and δ_{t_e} are shown in figure 9-66. We now note that δ_{t_e} has an important effect on C_{h_e} .

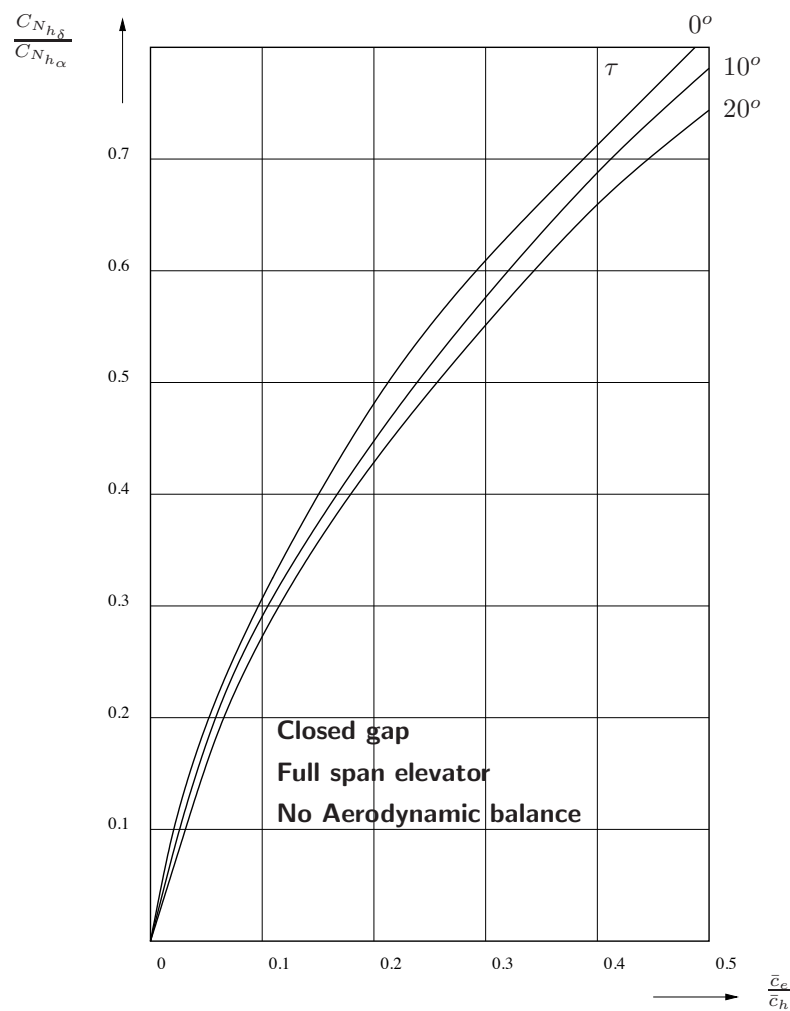


Figure 9-65: The quotient $\frac{C_{N_h\delta}}{C_{N_h\alpha}}$ as a function of $\frac{\bar{c}_e}{c_h}$ for various trailing edge angles τ (from reference [21])

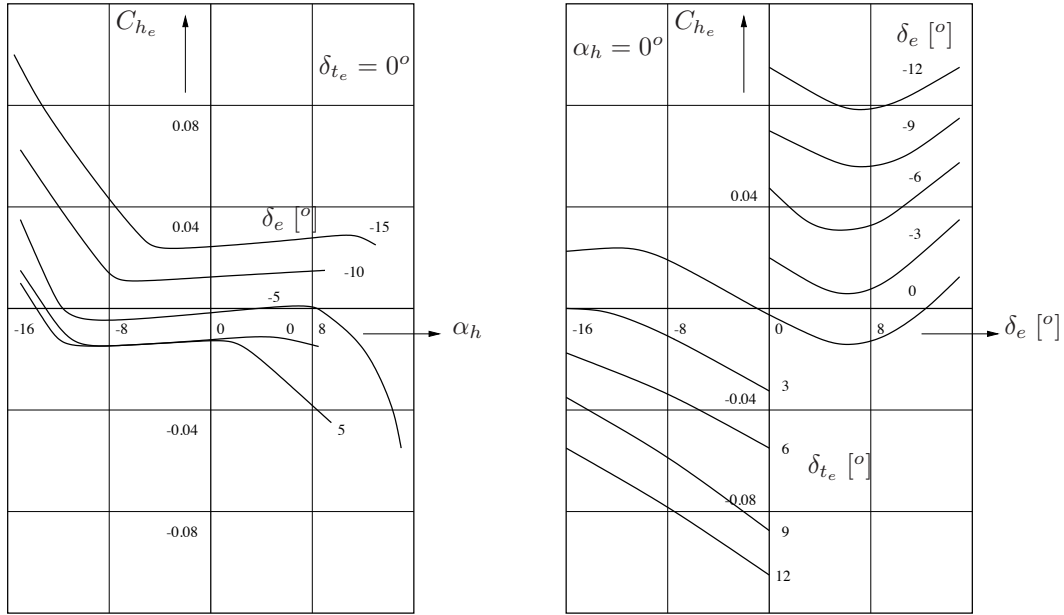


Figure 9-66: The hinge moment coefficient C_{he} as a function of α_h , δ_e and δ_{te} for a tailplane of the Fokker F-27 (wind tunnel measurements from reference [17])

		Hinge moment derivatives					
Derivative	$\frac{\partial C_{he}}{\partial \alpha_h}$	$\frac{\partial C_{he}}{\partial \delta_e}$	$\frac{\partial C_{he}}{\partial \delta_{te}}$	$\frac{\partial C_{ht_e}}{\partial \alpha_h}$	$\frac{\partial C_{ht_e}}{\partial \delta_e}$	$\frac{\partial C_{ht_e}}{\partial \delta_{te}}$	
American notation	C_{h_α}	C_{h_δ}	$C_{h_{\delta_t}}$	$C_{h_{t_\alpha}}$	$C_{h_{t_\delta}}$	$C_{h_{t_{\delta_t}}}$	

Table 9-2: Abbreviated notation for the hinge moment derivatives

Again for a limited interval of α_h , δ_e and δ_{te} variations a linear approximation for C_{he} may be written as,

$$C_{he} = C_{h_0} + \frac{\partial C_{he}}{\partial \alpha_h} \alpha_h + \frac{\partial C_{he}}{\partial \delta_e} \delta_e + \frac{\partial C_{he}}{\partial \delta_{te}} \delta_{te} \quad (9-62)$$

If a symmetric airfoil is used for the tailplane, $C_{h_0} = 0$. Using in addition the shorthand notation of table 9-2, C_{he} can be written as,

$$C_{he} = C_{h_\alpha} \alpha_h + C_{h_\delta} \delta_e + C_{h_{\delta_t}} \delta_{te} \quad (9-63)$$

Note that in equation (9-63), $C_{h_{\delta_t}}$ is the derivative of the moment about the elevator hinge axis with respect to the tab deflection. Table 9-2 also defines the derivatives $C_{h_{t_\alpha}}$, $C_{h_{t_\delta}}$ and $C_{h_{t_{\delta_t}}}$ which refer to the hinge moment about the tab hinge axis. These latter derivatives are made non-dimensional using S_t and c_t of the tab.

Computing the hinge moment derivatives of a control surface of given shape and dimensions is not always possible with sufficient accuracy. The shape of the tailplane, the airfoil and minute details

of the form of the gap between stabilizer and control surface have an effect on the derivatives. The main problem, however, is the relatively large influence of viscous effects which are difficult to account for quantitatively. Best is to obtain data on C_{h_e} from wind tunnel measurements, using as large a model of the tailplane as possible.

Depending on the location of the hinge line of the control surface the change in hinge moment, with increasing angle of attack and control surface deflection, will be negative in most cases, see also the pressure distributions given in figure 9-63. In that case both derivatives are negative,

$$C_{h_\alpha} < 0 \quad \text{and} \quad C_{h_\delta} < 0$$

If the hinge line would be moved backwards, however, in most cases it is the derivative C_{h_δ} which first changes sign to positive, see again 9-63, and would result in unacceptable flying qualities as discussed later. It follows from equation (9-61) that the hinge moment varies with the square of the airspeed and the cube of the dimensions of the aircraft. Fast and large aircraft would soon be confronted with very large hinge moments which would be difficult for pilots to handle by conventional mechanical control systems.

This led early mechanical flight control system designers to carefully aerodynamically balance control surfaces such that C_{h_α} and C_{h_δ} stay small, while keeping C_{h_δ} negative. As long as both C_{h_α} and C_{h_δ} are negative, the control surface is called aerodynamically under balanced. Shifting the hinge-line rearward will result in the control surface to become overbalanced with respect to the angle of attack, or with respect to the control deflection, or both. C_{h_α} and C_{h_δ} will then be positive see figure 9-67.

One of the means to change C_{h_α} and C_{h_δ} in the positive sense, is to employ a rearward shift of the hinge axis, or a forward extension of the nose of the control surface in front of the hinge line. As long as both C_{h_α} and C_{h_δ} are negative, the control surface is called aerodynamically underbalanced.

9-2-4 Flow direction and dynamic pressure at the horizontal tailplane

A horizontal tailplane located behind the wing experiences the field of flow disturbed by the wing, the fuselage, the nacelles and propellers. Mainly due to the downwash behind the wing, the average angle of attack α_h of the horizontal tailplane is decreased. If the horizontal tailplane lies in the wake produced by the wing, or in the boundary layer of the fuselage, the local average dynamic pressure at the horizontal tailplane is reduced. This is expressed in a value of $(\frac{V_h}{V})^2 < 1$ in equation (9-57).

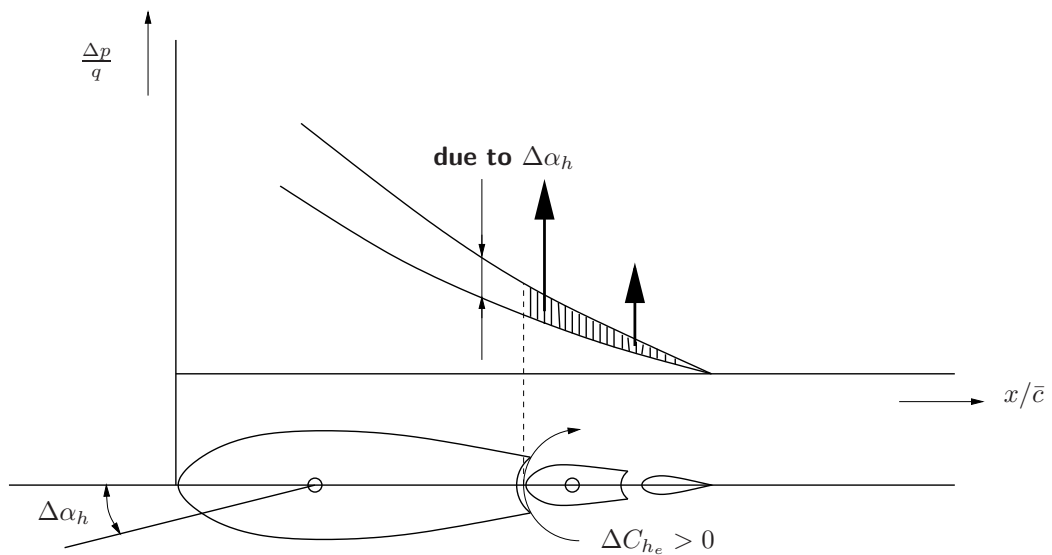
Both effects cause a change in the contribution of the horizontal tailplane to the moment about the aircraft's lateral axis. The slipstream of propeller driven aircraft and the exhaust stream of jet-propelled aircraft may also cause changes in α_h and $(\frac{V_h}{V})^2$.

If the average downwash angle at the location of the horizontal tailplane is designated ε , and the tailplane incidence setting relative to the X_r -axis is i_h , the average angle of attack of the horizontal tailplane follows from (see figure 9-68),

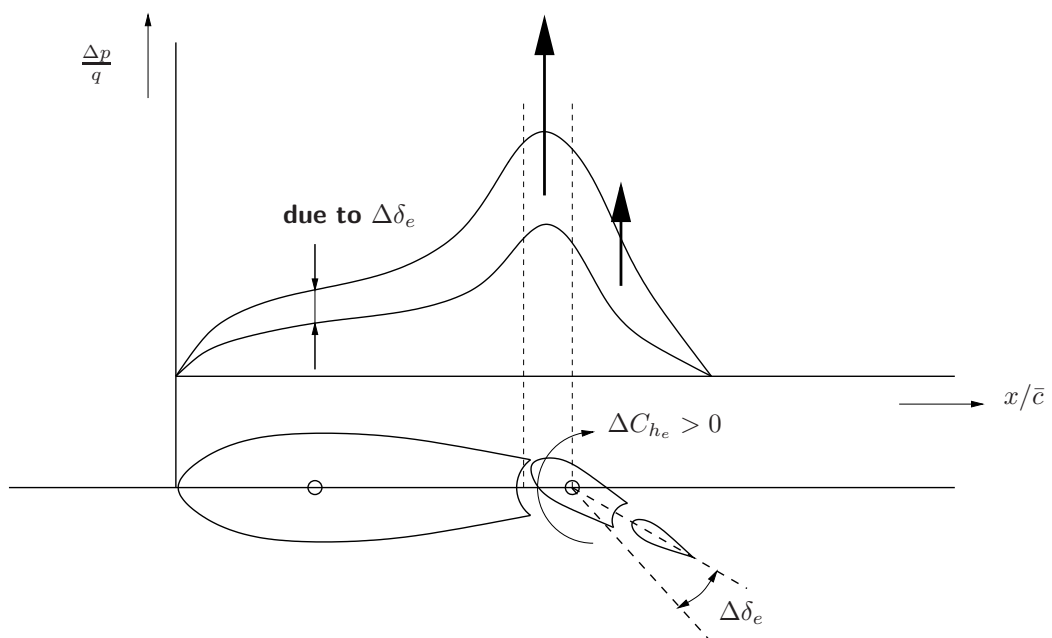
$$\alpha_h = \alpha - \varepsilon + i_h \tag{9-64}$$

The downwash angle is approximately proportional to C_L , in the range where C_L varies linearly with α ,

$$\varepsilon = (\alpha - \alpha_0) \frac{d\varepsilon}{d\alpha}$$

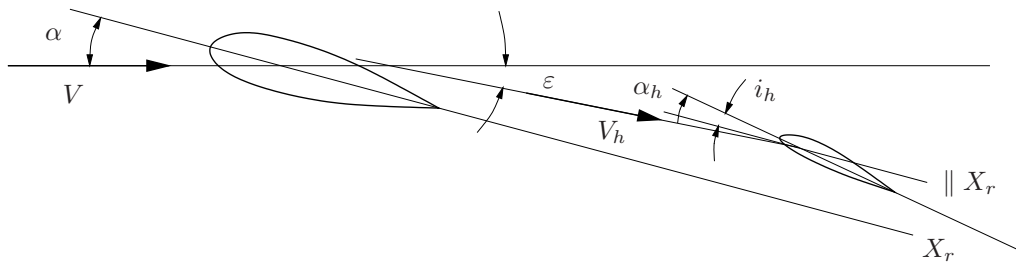


$$(A) \frac{\Delta C_{h_e}}{\Delta\alpha_h} > 0 \rightarrow C_{h_\alpha} > 0$$



$$(B) \frac{\Delta C_{h_e}}{\Delta\delta_e} > 0 \rightarrow C_{h_\delta} > 0$$

Figure 9-67: Overbalance with respect to angle of attack and elevator angle.



$$\alpha_h = \alpha - \varepsilon + i_h$$

Figure 9-68: The angle of attack α_h of the horizontal tailplane, $\alpha_h = \alpha - \varepsilon + i_h$

where $\alpha_0 = \alpha_{C_L=0}$ and $\frac{d\varepsilon}{d\alpha}$ is approximately constant. Thus α_h can be written as,

$$\alpha_h = (\alpha - \alpha_0) \left(1 - \frac{d\varepsilon}{d\alpha}\right) + (\alpha_0 + i_h) \quad (9-65)$$

From (9-65) the derivative of α_h with respect to α is,

$$\frac{d\alpha_h}{d\alpha} = \left(1 - \frac{d\varepsilon}{d\alpha}\right) \quad (9-66)$$

We will see below that this derivative is always smaller than one, resulting in a reduction of the positive contribution of the horizontal tailplane to the static stability of conventional aircraft with rear mounted tail planes.

The downwash angle ε and the factor $(\frac{V_h}{V})^2$ depend in the first place on the shape of the wing and on the location of the horizontal tailplane relative to the wing. The downwash behind the wing may be thought of as to be induced by a system of nested U shaped vortices. Part of each vortex is bound to the wing, inducing an upwash in front of the wing and a downwash behind the wing. The free, remaining parts of each vortex (the two antisymmetrical 'tails') leave the wing at the trailing edge of the wing in a vortex sheet of free vortices, reinforcing the downwash and reduce the upwash, see figure 9-69. The vertical velocities induced by these vortices result in the vortex sheet itself being pushed downwards, assuming the form as depicted in figure 9-70. While the inclination of the vortex sheet conforms to the upper and lower surfaces of the wing at the trailing edge (Joukowski condition), downstream the inclination decreases and the vortex sheet is 'bent' towards the direction of the undisturbed flow. Upwash, downwash and the vertical displacement of the vortex sheet are approximately proportional to C_L for a given wing geometry.

The boundary layers over the wing result in a 'wake' of reduced dynamic pressure which is assumed to coincide with the the vortex sheet.

The vertical displacement of the wing wake and vortex sheet increases with angle of attack but at a smaller rate than that of the horizontal tailplane , see figure 9-71. It is good practice to keep the horizontal tailplane out of the wing wake at all flight conditions. We conclude that this can indeed be assured by mounting it either high, keeping it above, or mounting it low, keeping it below the wake of the wing.

The tendency of a vortex plane is to roll-up, changing its shape until it is transformed into two tip vortices, see figure 9-72. This process depends on the lift distribution over the wing and it is intensified as the lift coefficients are larger and the wing aspect ratio smaller, see references [162, 184]. For wings with a large aspect ratio and a small sweep angle the roll-up of the vortex plane is of little importance in the range of practical angles of attack. For these wings we may compute the downwash at the horizontal tailplane by assuming a flat vortex plane, only slightly

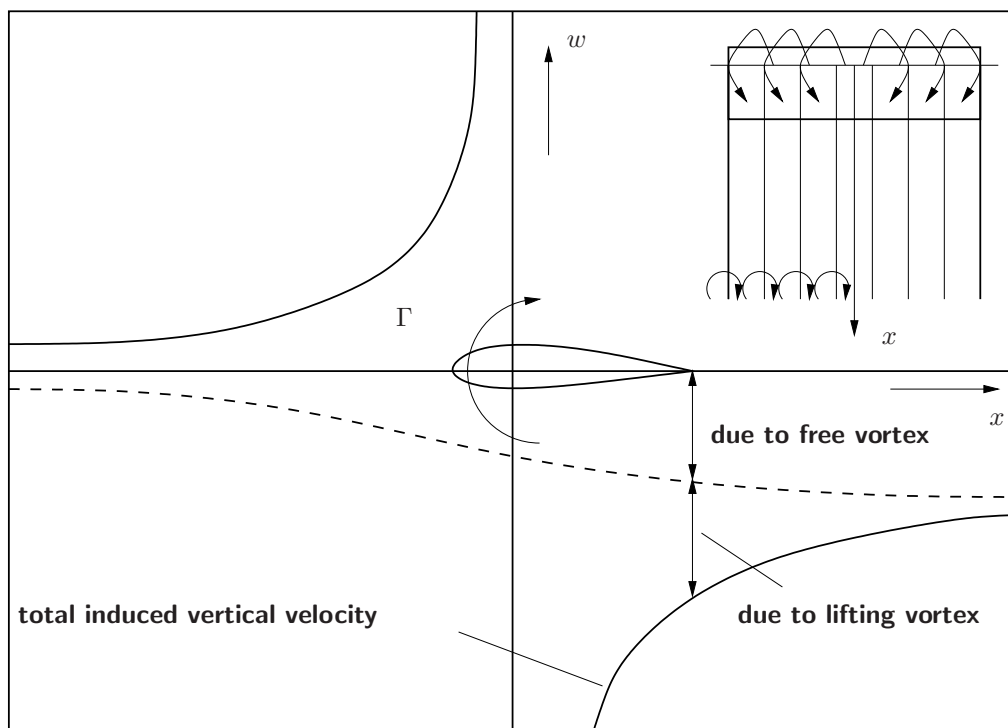


Figure 9-69: The contribution of the lifting and free vortices to the induced vertical velocities in front of and behind a wing

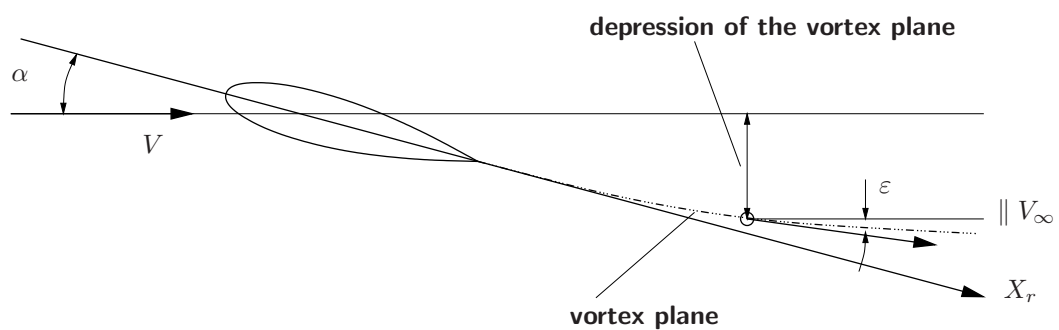


Figure 9-70: The position of the vortex plane behind the wing

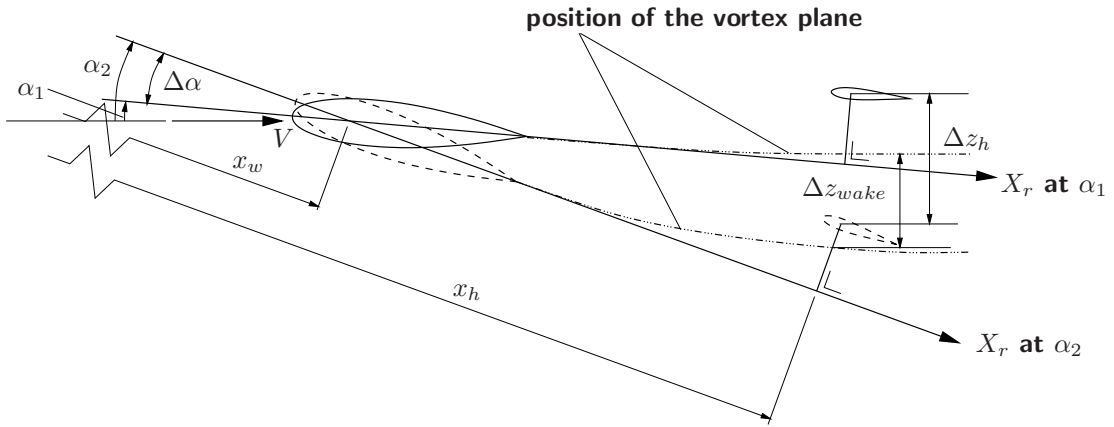


Figure 9-71: The vertical displacement of the wake and the tailplane relative to the flow field due to an increase in angle of attack $\Delta\alpha$; $\Delta z_h = \int_{x_w}^{x_h} \Delta \alpha \, dx = \Delta\alpha (x_h - x_w)$, $\Delta z_{wake} = \int_{x_w}^{x_h} \Delta \varepsilon(x) \, dx$, $\Delta z_{wake} < \Delta z_h$ as $\Delta\varepsilon(x)$ is smaller than $\Delta\alpha$. With increasing angle of attack the horizontal stabilizer moves downwards through the wake

curled at the edges. For small aspect ratio wings, or wings with a large sweep angle Λ , or both, however, this would be too rough an approximation. One would have to take account in these cases of the intricate deformed shape of the vortex sheet. The same holds true in cases where at some values of the angle of attack local flow separation occurs, often resulting in the 'functional' form of the wing to be different from what one would expect by considering just its geometry. The main effect of flow separation is to reduce downwash rather than to affect the shape (rolling-up) of the vortex sheet, as discussed below.

According to reference [126], the influence of the deformation and the rolling-up of the vortex sheet on the downwash close to the wing plane of symmetry may as well be neglected at low values of C_L .

Figure 9-73 gives the theoretical value for $\frac{d\varepsilon}{d\alpha}$ in the core of the vortex plane, as a function of aspect ratio and distance behind the wing, for wings having an elliptical lift distribution and attached (non separated) flow. The dominant influence of the wing aspect ratio is apparent.

A rough estimate of $\frac{d\varepsilon}{d\alpha}$ at sufficiently large distances behind the wing is possible for straight wings for not too small aspect ratios. The classical formula to be used is,

$$\frac{d\varepsilon}{d\alpha} = 2 \frac{C_{L_\alpha}}{\pi A} \approx \frac{2}{\pi A} 2\pi \frac{A}{A+2} = \frac{4}{A+2} \quad (9-67)$$

This expression results in values for $\frac{d\varepsilon}{d\alpha}$ for $A > 5$ which are in very good agreement with the more exact values given in figure 9-73 for an elliptical wing.

Figure 9-74 shows the variation in spanwise direction of the lift distribution $\frac{c_{Lc}}{2b}$ for wings of different taper ratios. Note that for wings with small values of $\lambda = \frac{c_t}{c_r}$ the average downwash angle near the plane of symmetry is larger than for wings with larger values of λ at the same values of C_L . This is caused by the higher lift loading near the wing center of former wings. As a consequence $\frac{d\varepsilon}{d\alpha}$ at the horizontal tailplane increases with decreasing λ . Sweepback of an untwisted wing causes a lower loading near the wing center. As a consequence, $\frac{d\varepsilon}{d\alpha}$ decreases with increasing sweep angle Λ , see also figure 9-75.

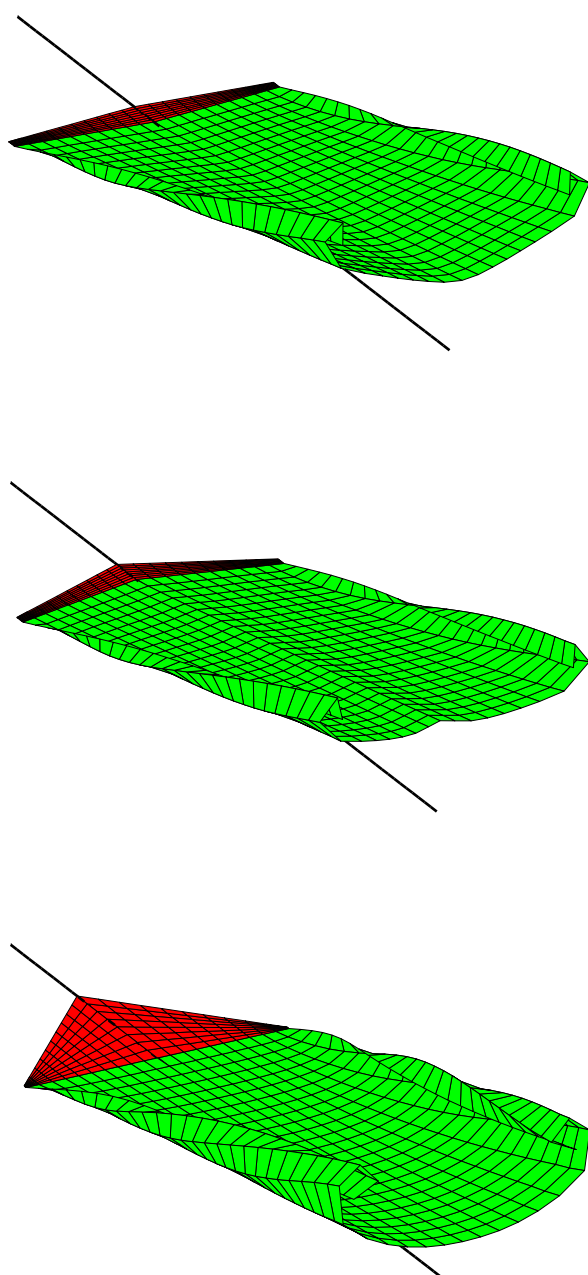


Figure 9-72: Numerical simulation of the deformation and wake roll-up of the vortex sheet behind a wing

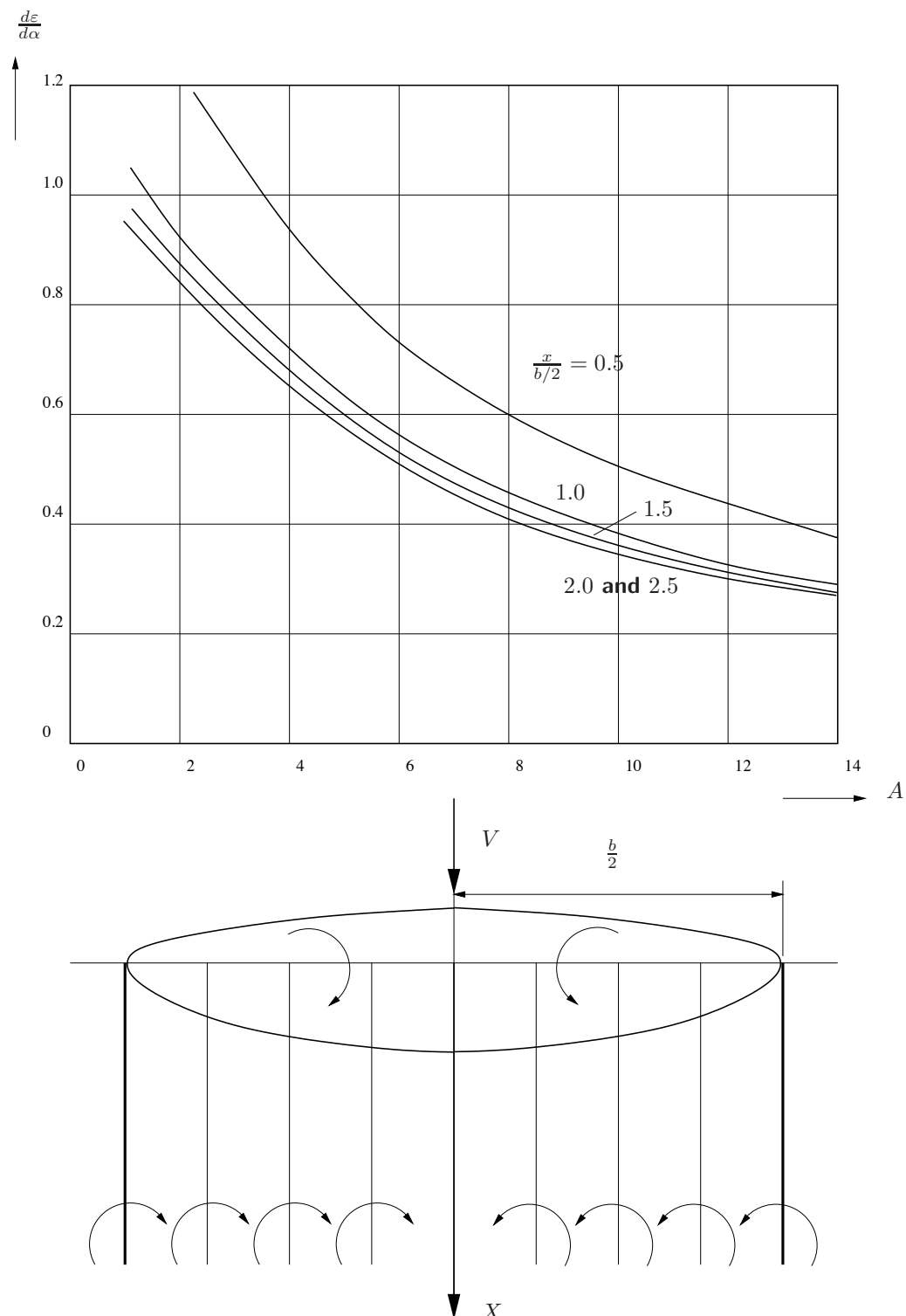


Figure 9-73: Computed values of $\frac{d\varepsilon}{d\alpha}$ behind a wing of elliptical lift distribution, as a function of aspect ratio and distance behind the wing

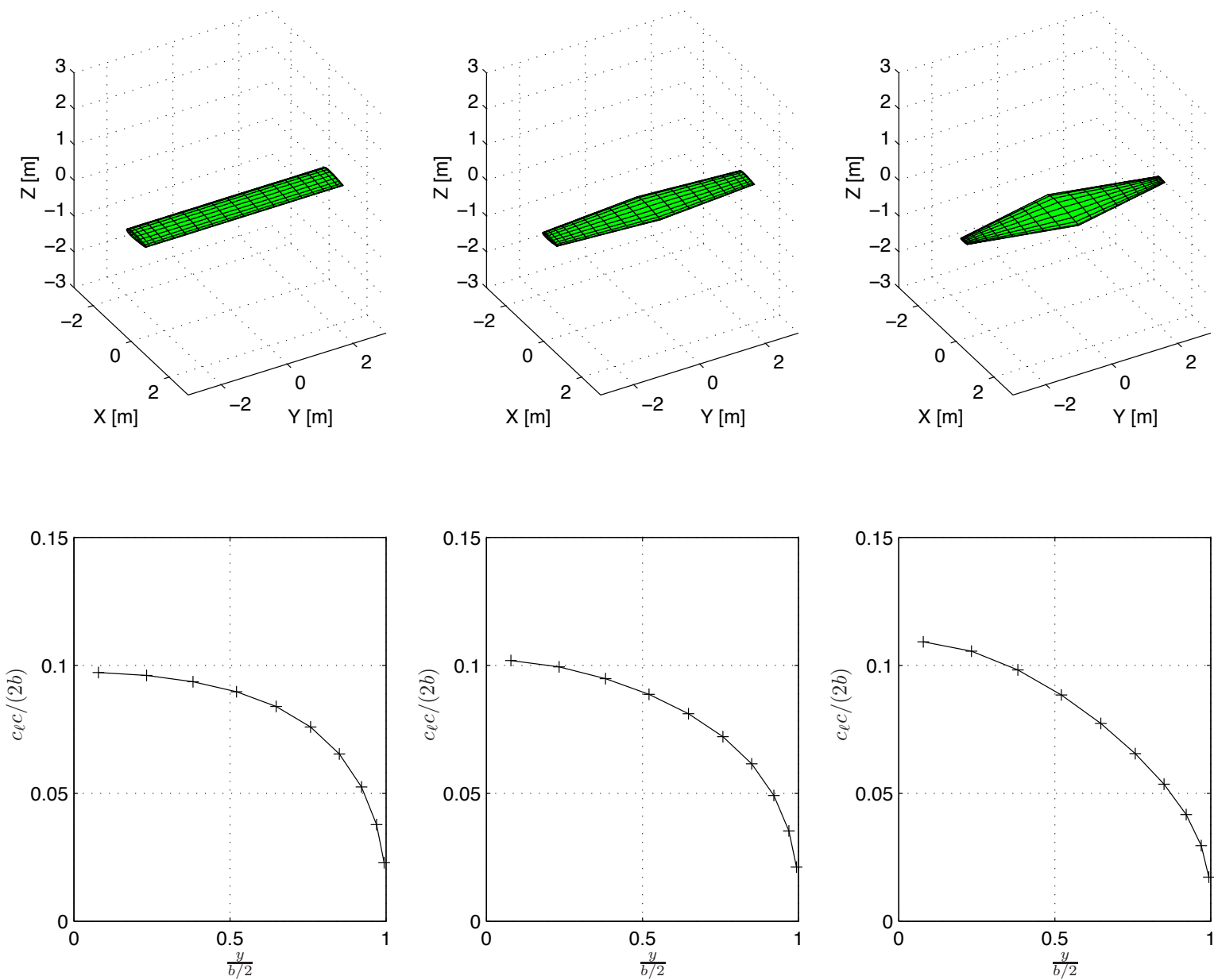


Figure 9-74: Numerical simulation of $\frac{c_L c}{2b}$ for wings with varying taper ratio λ ($C_L = 1.0$, $\Lambda = 0^\circ$, $A = 6$), computed with a source/doublet singularity method, also see reference [154]

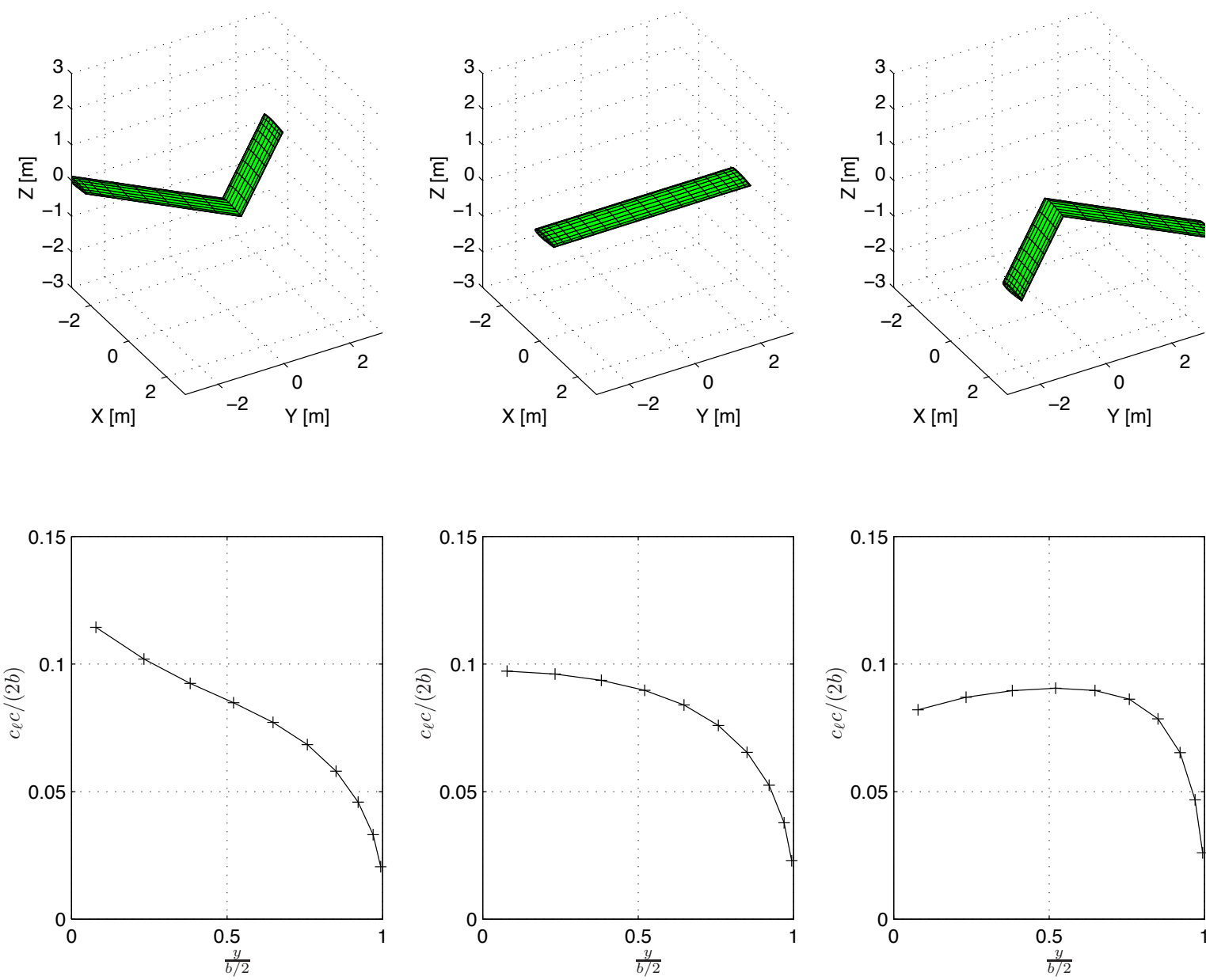


Figure 9-75: Numerical simulation of $\frac{C_L^c}{2b}$ for wings with varying sweep angle Λ ($C_L = 1.0$, $\lambda = 1$, $A = 6$), computed with a source/doublet singularity method, also see reference [154]

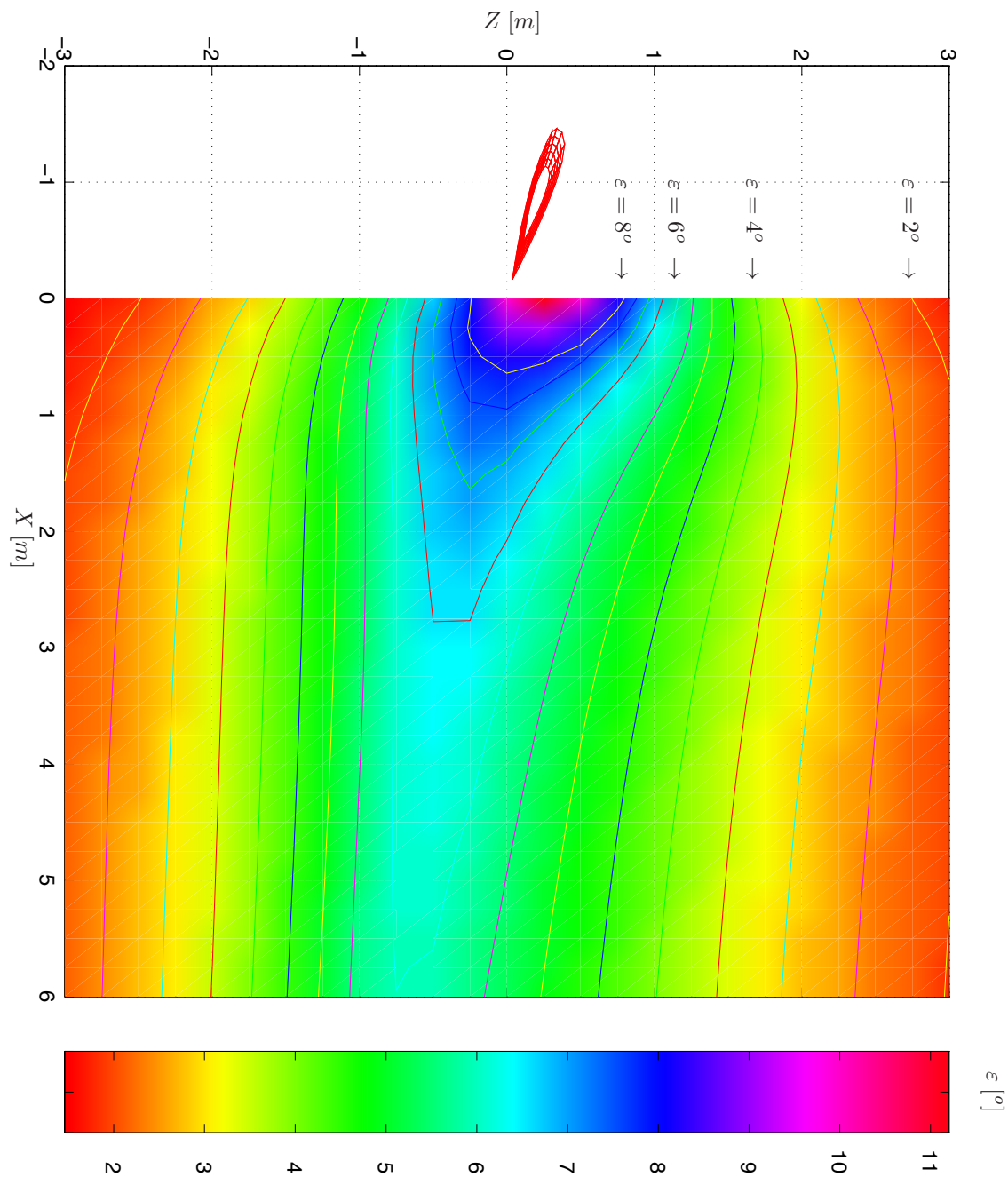


Figure 9-76: Numerical simulation of downwash angles in the plane of symmetry behind a wing ($\alpha = 13^\circ$, NACA 23014 airfoil, $A = 6$, $\lambda = 0.5$ and $C_L = 1.1615$, computed with a source/doublet singularity method, see also reference [157])

The downwash angle decreases with increasing distances above and below the vortex plane. Figure 9-76 shows the results of numerical simulations using a source and doublet singularity method (also known as ‘panel methods’). Measurements of the downwash angle in the plane of symmetry behind a tapered wing can be found in reference [157]. From figure 9-76 it is clear that the downwash in a certain distance above the wake is larger than in a point at the same distance below the wake. This is due to the fact that as a result of the depression of the wake and of the deformation of the vortex plane the free and the lifting vortices contribute more to the downwash above the wake than below the wake.

The field of flow behind wings with separated flow is significantly different from the case of attached flow. Flow separation will cause appreciable changes in $\frac{d\varepsilon}{d\alpha}$ with increasing angle of attack. A detailed discussion of these changes related to flow separation can be found in reference [126]. For straight wings with just little taper (so a large λ), flow separation starts near the wing root. The reduction in lift over the center wing results in a decrease of $\frac{d\varepsilon}{d\alpha}$. In addition a broad and deep wake is formed, causing a strong ‘inflow’ into the wake. Flow separation near the wing tips, occurring with highly tapered and swept back wings, causes an increase in downwash at the tailplane due to a concentration of lift force to the center of the wing caused by flow separation.

Swept wings and delta wings with thin airfoils often exhibit flow separation near the wing leading edge, already at small angles of attack. This leads to characteristic conical vortices above the wing. Such separation vortices may considerably increase the downwash.

The camber and nose shape of airfoils, wing twist, boundary layer fences, nose flaps and slats, all serve to influence the flow separation characteristics. It will be clear that these wing geometry parameters will also affect the downwash characteristics at the horizontal tailplane.

The fuselage causes a change in the flow behind the wing. This is due to the flow around the fuselage itself and due to the change in the wing lift distribution caused by the fuselage. The resultant influence on the average downwash at the horizontal tailplane is relatively small for slender wings. For wings of small aspect ratio the influence of the fuselage can be considerable and is strongly dependent of the position of the horizontal tailplane relative to the fuselage. If the tailplane is mounted on the fuselage a decrease in the average value of $(\frac{V_h}{V})^2$ occurs since part of the tailplane is in the boundary layer of the fuselage. In such cases a reduction in $(\frac{V_h}{V})^2$ of some 5 to 10% is often taken into account.

Example: aircraft with fuselage-mounted nacelles

The aerodynamic effects of fuselage-mounted nacelles are shown next on two aircraft models depicted in figures 9-77. These models represent a Cessna Ce550 Citation II with and without nacelles, respectively the top and bottom figure in figures 9-77.

In figures 9-78 the numerical simulation of $\frac{d\varepsilon}{d\alpha}$ (for $X = 5.0 \text{ m}$, $Z = 1.5 \text{ m}$) is given along the wing span (left wing) of the aircraft models presented in figures 9-77. Note that the top figure of figure 9-78 is a 2-dimensional representation (aft view) of the bottom figure. From figures 9-78 it follows that in the vicinity of the horizontal stabilizer the parameter $\frac{d\varepsilon}{d\alpha}$ is increased due to the presence of nacelles. This effect cannot be attributed to the induced velocities of free and bounded vortices but rather to the local airflow conforming to the external shape of the nacelles.

Flap deflection causes a concentration of lift at the center parts of the wing. This leads to an increased downwash ε and $\frac{d\varepsilon}{d\alpha}$.

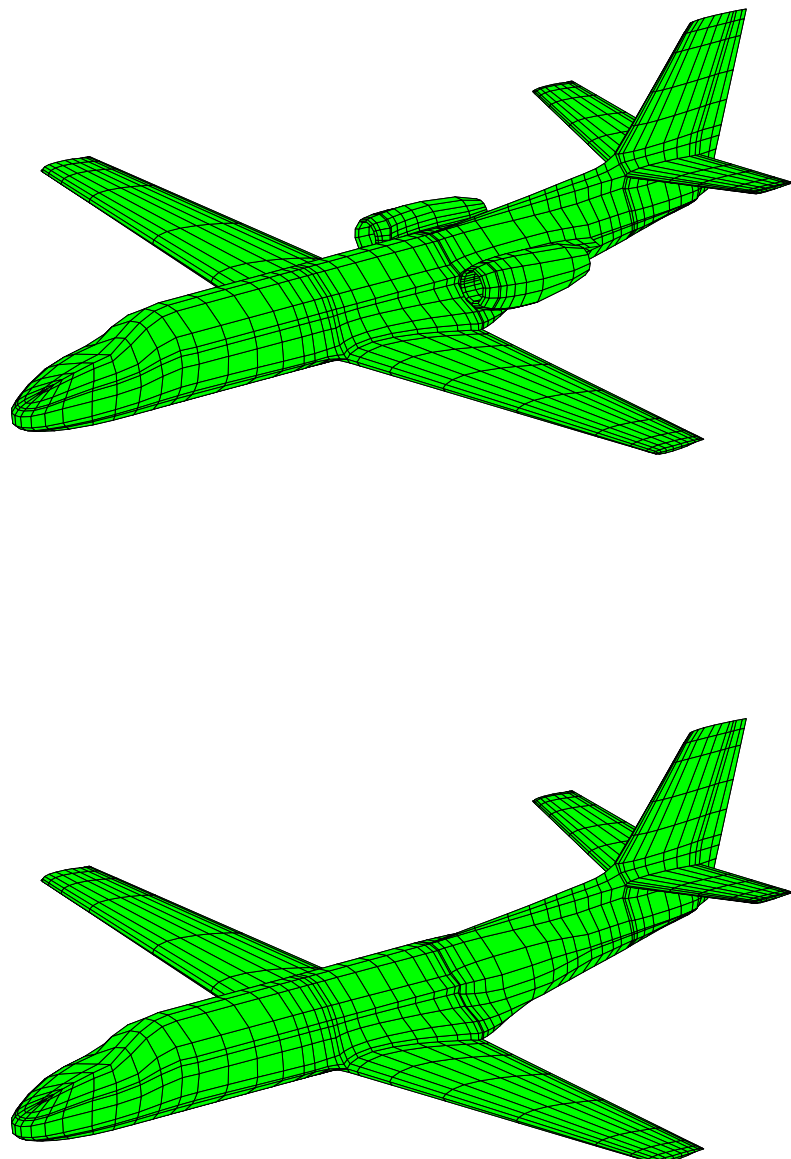


Figure 9-77: Cessna Ce550 Citation II configuration with and without nacelles

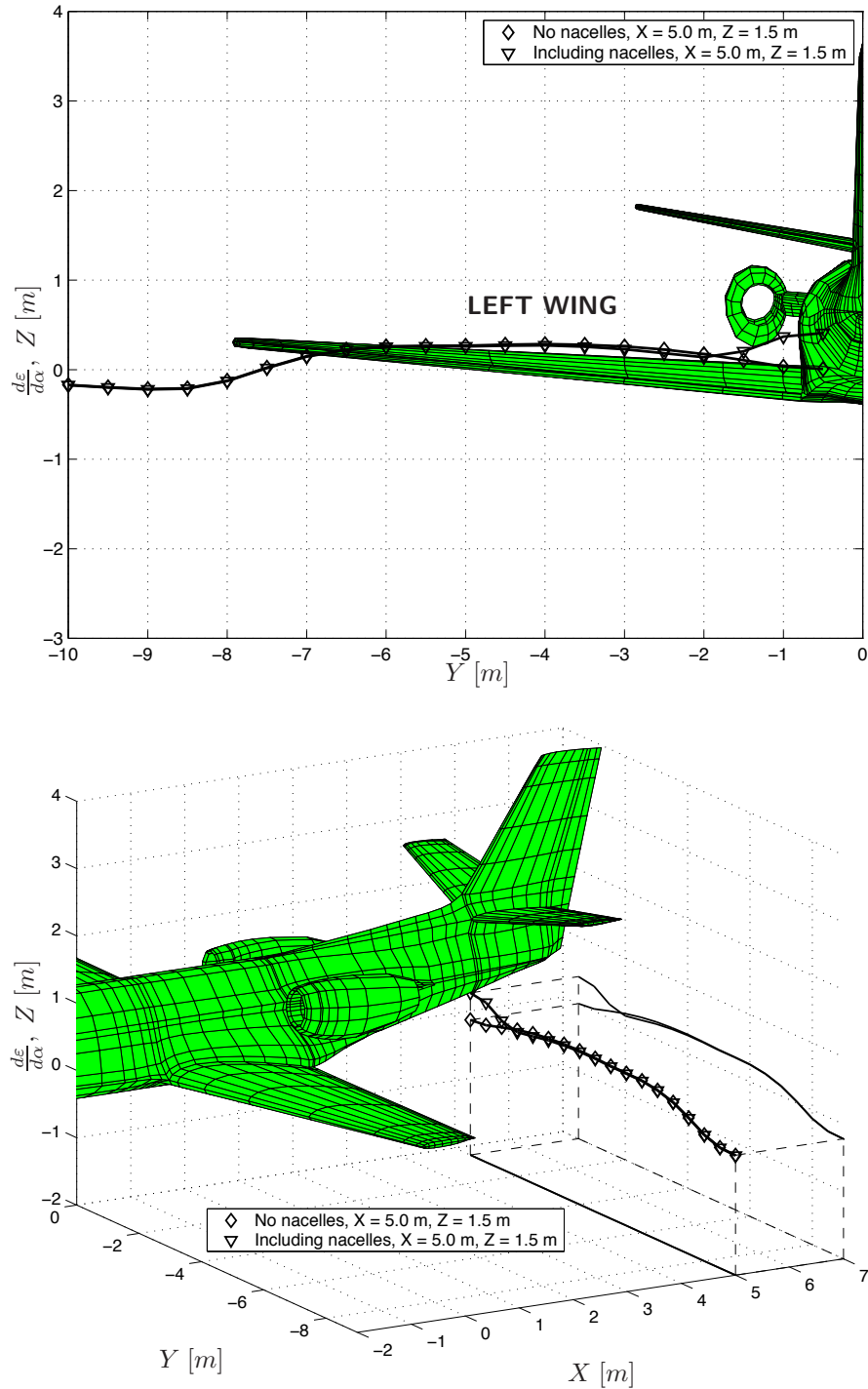


Figure 9-78: The effect of nacelles on $\frac{dC_l}{d\alpha}$ (at $X = 5.0 \text{ m}$, $Z = 1.5 \text{ m}$) aft of the wing of a Cessna Ce550 Citation II, computed with a source/doublet singularity panel-method, linearized potential flow

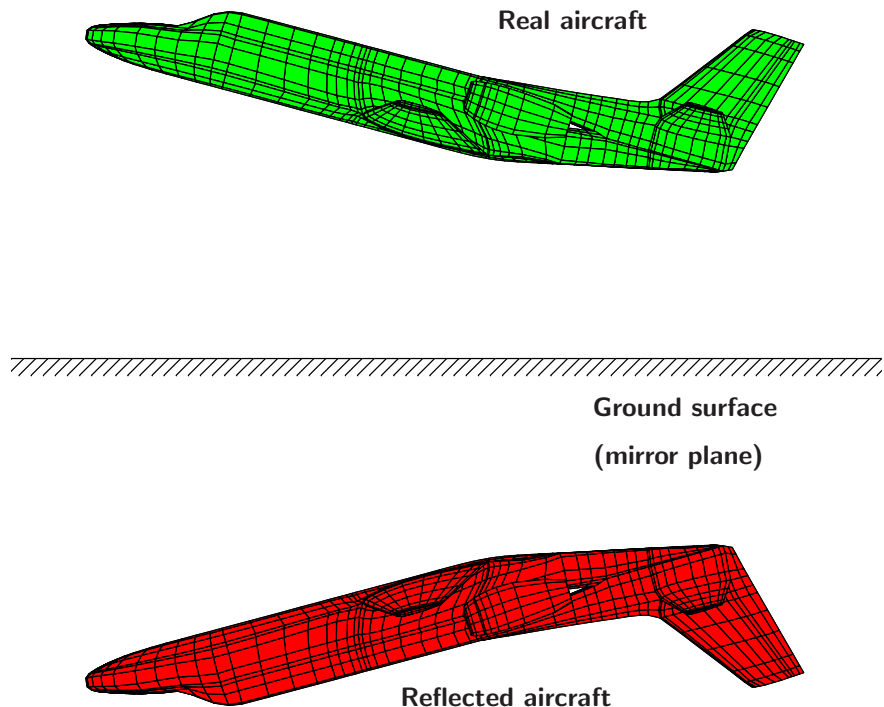


Figure 9-79: Calculation of ground effect

In take-off and landing the field of flow around and in particular behind the wing is strongly influenced by the proximity of the ground. Ground effect can be modeled by introducing additional 'mirror' lifting vortices and trailing vortices, see figure 9-79.

The mirror vortices cause a decrease in the induced angles of attack and a corresponding decrease in the effective angle of attack, proportional to the strength of the mirror vortices and thus to C_L . The result of ground effect is an increase in $C_{N_{w\alpha}}$ and $C_{N_{h\alpha}}$. As $C_{N_{h\delta}}$ is proportional to $C_{N_{h\alpha}}$, $C_{N_{h\delta}}$ increases as well.

The downwash angle behind the wing decreases due to the mirror vortices. This effect can also be understood directly, as the presence of the ground plane inhibits the downward flow behind the wing. Figure 9-80 gives an example of the change in ε at the horizontal tailplane caused by the ground effect. This figure also demonstrates that the reduction in $\frac{d\varepsilon}{d\alpha}$ due to ground effect can be quite important.

An additional consequence of the reduced downwash angles behind the wing is a smaller downward displacement of the wake, as compared with the situation without ground effect, see figure 9-80b . When choosing the vertical position of the horizontal tailplane in the course of the design process, this effect has to be taken into account.

For slender, straight wings without and with deflected flaps references [168, 156] shows how to compute the average downwash angle and the average dynamic pressure at the horizontal tailplane, see also reference [148]. The downwash behind swept wings can be determined with references

[77, 53, 49, 51, 169]. An extensive discussion of ground effect is given in reference [63]. The ground effect on the downwash and the wake can be calculated with reference [99].

For wings with a small aspect ratio or large sweep angle or both, the fuselage has a large influence on the flow at the horizontal tailplane and in case of flow separation, the flow field at the horizontal tailplane should be derived from measurements in the wind tunnel or by CFD simulations. An extensive summary and analysis of experimental data is given in reference [126], where also a method is described to estimate the characteristics of the horizontal tailplane.

9-2-5 Effect of airspeed and center of gravity on tail load

As discussed in section 9-2-1, a normal force acts on the horizontal tailplane to produce equilibrium of the longitudinal moment in an equilibrium situation. This normal force is called the tail load. The magnitude of the tail load N_h follows from equation (9-57) multiplied by $\frac{1}{2}\rho V^2 S \bar{c}$,

$$M = 0 = C_{m_{ac}} \frac{1}{2} \rho V^2 S \bar{c} + N_w (x_{c.g.} - x_w) - N_h l_h \quad (9-68)$$

or,

$$N_h = \frac{1}{l_h} \left\{ C_{m_{ac}} \frac{1}{2} \rho V^2 S \bar{c} + N_w (x_{c.g.} - x_w) \right\} \quad (9-69)$$

At small values of the angle of pitch θ , and if in addition $N_h \ll N_w$, it follows with equation (9-54),

$$N_w \approx W$$

The result becomes,

$$N_h \approx \frac{1}{l_h} \left\{ C_{m_{ac}} \frac{1}{2} \rho V^2 S \bar{c} + W (x_{c.g.} - x_w) \right\} \quad (9-70)$$

This also follows directly from figure 9-81, where the model of equilibrium of the forces and moment has been given in a strongly simplified form. It can be seen from equation (9-70) that the tail load N_h is needed,

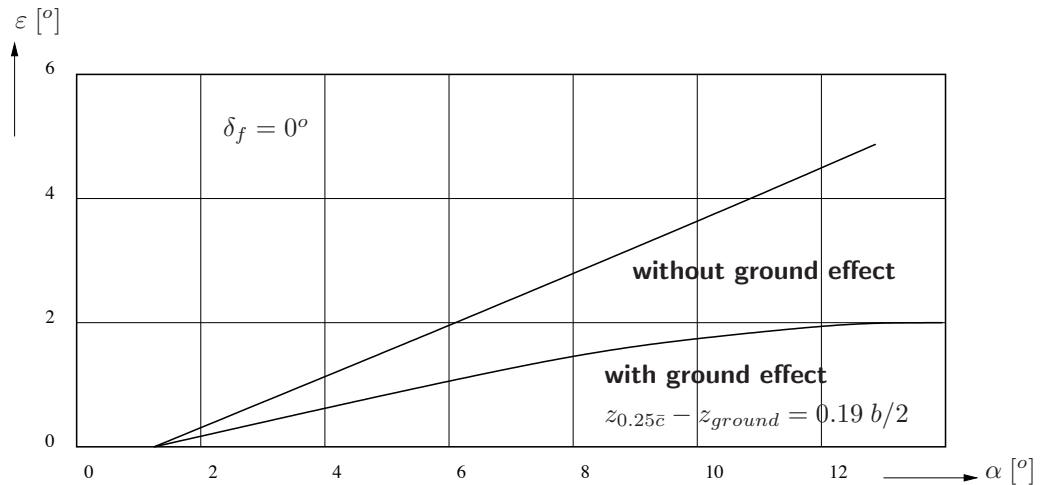
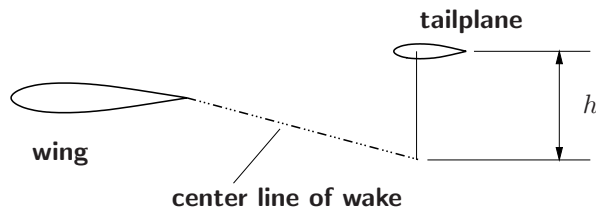
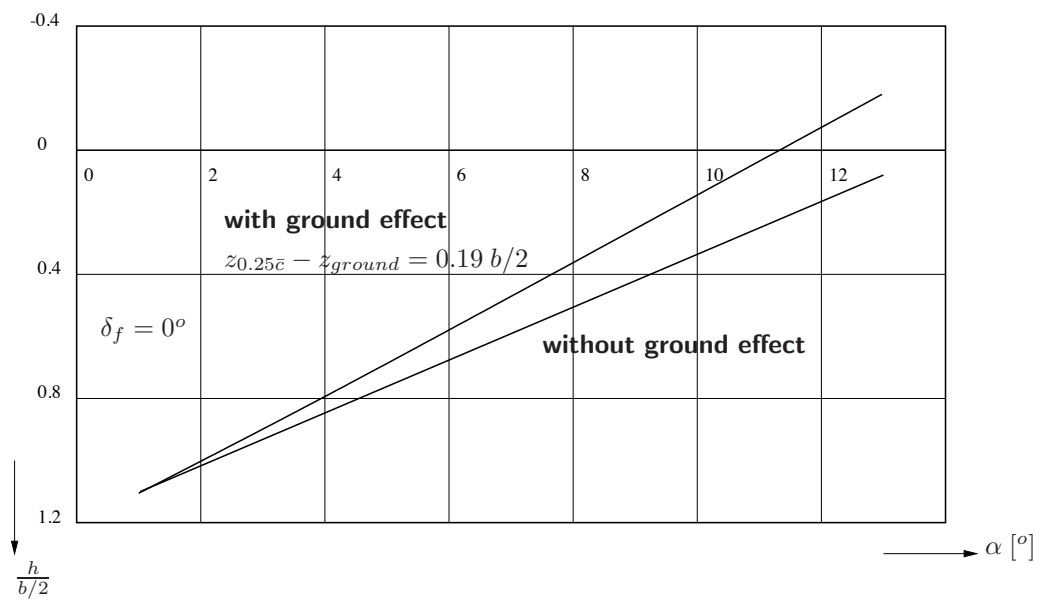
1. to compensate for the moment caused by the coefficient $C_{m_{ac}}$; this moment depends on the airspeed but not on center of gravity position; in addition it varies with flap deflection δ_f
2. to balance the moment of $N_w (\approx W)$ about the center of gravity; this moment is independent of airspeed, but varies with the center of gravity position

From equation (9-70) it can be seen that N_h varies quadratically with V and increases in the upward sense with a rearward shift of the center of gravity. Figure 9-82 gives a sketch of the variations of the tail load with airspeed for various c.g. positions and signs of $C_{m_{ac}}$.

The point of intersection of the parabola with the line $V = 0$, in actual flight the airspeed can, of course, not drop below V_{min} , follows from equation (9-70),

$$N_h = W \frac{x_{c.g.} - x_w}{l_h}$$

Figure 9-82 illustrates that due to the usually negative sign of $C_{m_{ac}}$ of the wing, fuselage and nacelles, the tail load reaches its largest positive value at the rearmost c.g. position and at

(A) The downwash angle ε as a function of α 

(B) The distance from the wake center line to the horizontal tailplane

Figure 9-80: The ground effect on the downwash angle ε and the location of the wake relative to the horizontal tailplane of a Siebel 204 D-1 aircraft

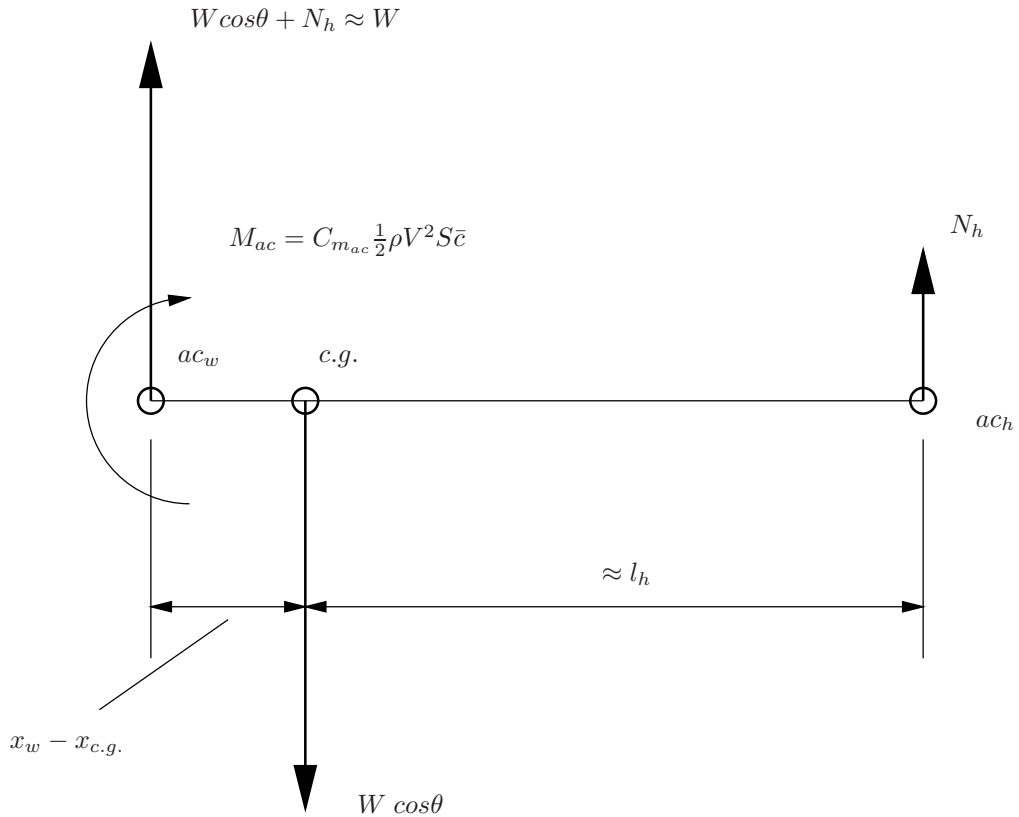
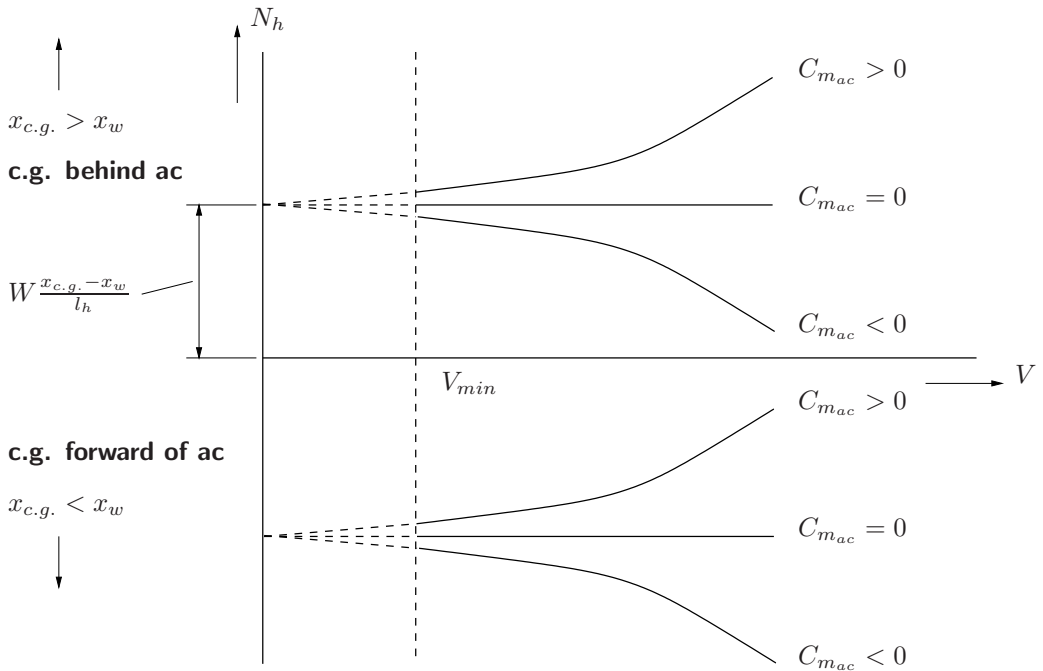


Figure 9-81: Simplified picture of the equilibrium of moments

Figure 9-82: The variation of the tail toad with airspeed at different c.g. positions and values of $C_{m_{ac}}$

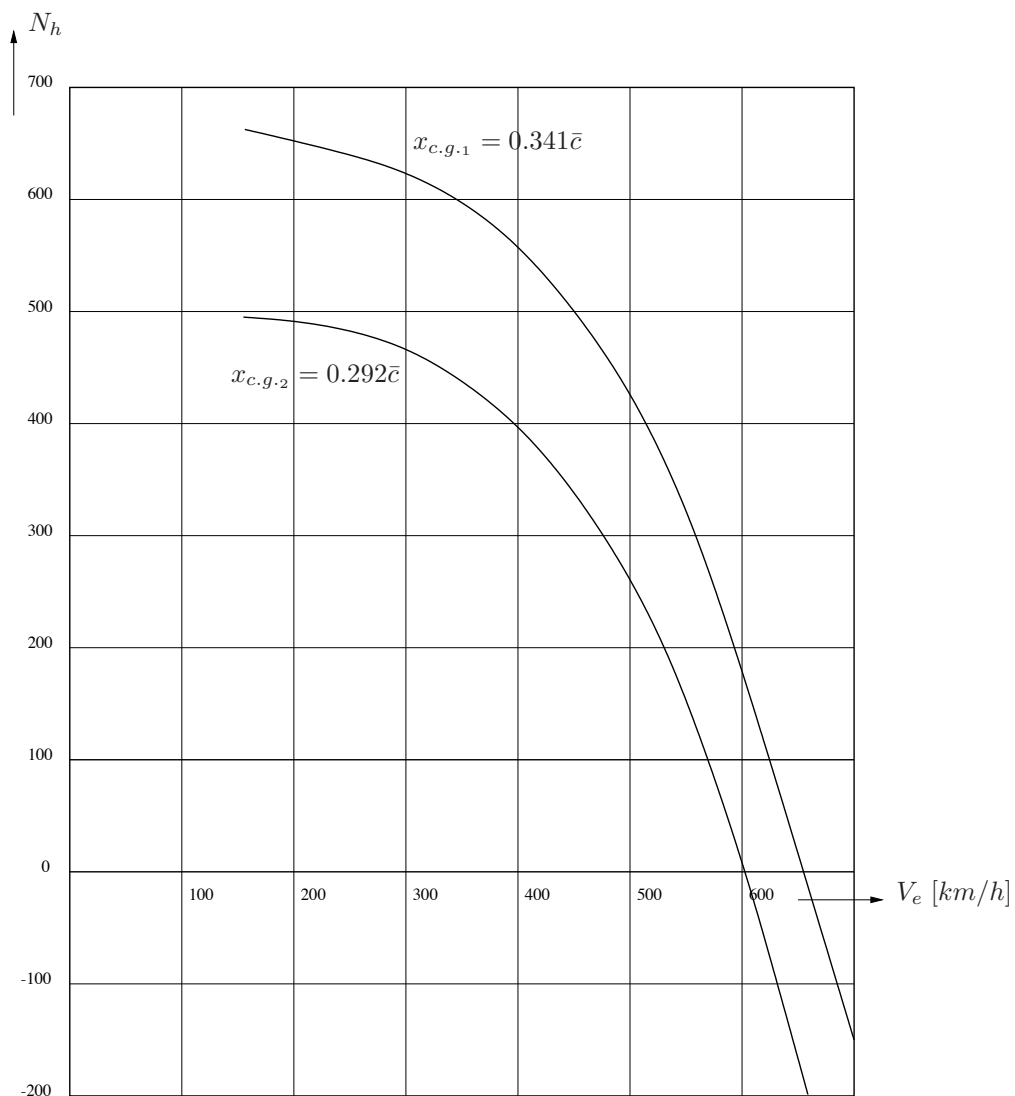


Figure 9-83: The tail load as a function of airspeed at two c.g. positions for De Havilland 'Mosquito II F' (from reference [26]), $W = 6800 \text{ kg}$, $S = 41.8 \text{ m}^2$, $l_h = 8.0 \text{ m}$ and $\bar{c} = 2.81 \text{ m}$

minimum airspeed. The largest negative, downward, tail load occurs for a given negative $C_{m_{ac}}$ at the most forward c.g. position and at a maximum airspeed.

Figure 9-83 presents tail loads measured in flight on a DeHavilland ‘Mosquito’. The influence of airspeed on N_h as well as of c.g. position agrees in principle with equation (9-70). From this figure it can be derived that for the range of airspeeds $350 < V_e < 500$ km/h : $x_w = 0.08 \bar{c}$ and $C_{m_{ac}} = -0.021$.

9-2-6 Elevator deflection required for moment equilibrium

The way in which the elevator is used to produce moment equilibrium follows from expression (9-57),

$$C_m = C_{m_{ac}} + C_{N_w} \frac{x_{c.g.} - x_w}{\bar{c}} - C_{N_h} \left(\frac{V_h}{V} \right)^2 \frac{S_h l_h}{S \bar{c}} = 0$$

C_{N_w} can be written in the linear range as,

$$C_{N_w} = C_{N_{w_\alpha}} (\alpha - \alpha_0) \quad (9-71)$$

In section 9-2-2, C_{N_h} has been expressed by, see equation (9-60),

$$C_{N_h} = C_{N_{h_\alpha}} \alpha_h + C_{N_{h_\delta}} \delta_e$$

while in section 9-2-4 the expression for the angle of attack of the horizontal tailplane α_h was found to be, see equation (9-65),

$$\alpha_h = (\alpha - \alpha_0) \left(1 - \frac{d\varepsilon}{d\alpha} \right) + (\alpha_0 + i_h)$$

Substituting equations (9-71), (9-60) and (9-65) in equation (9-57) results in the condition for moment equilibrium,

$$\begin{aligned} C_m &= C_{m_{ac}} + C_{N_{w_\alpha}} (\alpha - \alpha_0) \frac{x_{c.g.} - x_w}{\bar{c}} - \\ &\left[C_{N_{h_\alpha}} \left\{ (\alpha - \alpha_0) \left(1 - \frac{d\varepsilon}{d\alpha} \right) + (\alpha_0 + i_h) \right\} + C_{N_{h_\delta}} \delta_e \right] \left(\frac{V_h}{V} \right)^2 \frac{S_h l_h}{S \bar{c}} \\ &= 0 \end{aligned} \quad (9-72)$$

or, in an ordered form,

$$C_m = C_{m_0} + C_{m_\alpha} (\alpha - \alpha_0) + C_{m_{\delta_e}} \delta_e = 0 \quad (9-73)$$

with,

- a constant C_{m_0} ,

$$C_{m_0} = C_{m_{ac}} - C_{N_{h_\alpha}} (\alpha_0 + i_h) \left(\frac{V_h}{V} \right)^2 \frac{S_h l_h}{S \bar{c}} \quad (9-74)$$

- the static longitudinal stability, stick fixed C_{m_α} ,

$$C_{m_\alpha} = C_{N_{w_\alpha}} \frac{x_{c.g.} - x_w}{\bar{c}} - C_{N_{h_\alpha}} \left(1 - \frac{d\varepsilon}{d\alpha}\right) \left(\frac{V_h}{V}\right)^2 \frac{S_h l_h}{S \bar{c}} \quad (9-75)$$

- the elevator effectivity $C_{m_{\delta_e}}$,

$$C_{m_{\delta_e}} = -C_{N_{h_\delta}} \left(\frac{V_h}{V}\right)^2 \frac{S_h l_h}{S \bar{c}} \quad (9-76)$$

For a given aircraft the pilot can obtain equilibrium of the moment at a certain angle of attack, or $(\alpha - \alpha_0)$, and c.g. position, or C_{m_α} , see equation (9-75), by deflecting the elevator, i.e. by choosing δ_e such that the resultant C_m is equal to zero.

If the total moment C_m is written as the sum of the moment at $\delta_e = 0$ and the moment due to the elevator deflection,

$$C_m = (C_m)_{\delta_e=0} + C_{m_{\delta_e}} \delta_e \quad (9-77)$$

the condition for equilibrium of the total moment, $C_m = 0$, results in the required elevator deflection,

$$\delta_e = -\frac{1}{C_{m_{\delta_e}}} (C_m)_{\delta_e=0} \quad (9-78)$$

Since, according to equation (9-73),

$$(C_m)_{\delta_e=0} = C_{m_0} + C_{m_\alpha} (\alpha - \alpha_0) \quad (9-79)$$

the elevator angle δ_e becomes,

$$\delta_e = -\frac{1}{C_{m_{\delta_e}}} \{C_{m_0} + C_{m_\alpha} (\alpha - \alpha_0)\} \quad (9-80)$$

The above expressions are based on the simple model as derived in section 9-2-1. In addition, use has been made of several linear approximations. As a consequence, the above expressions are valid, strictly speaking, only for those angles of attack and elevator angles where C_{N_w} and C_{N_h} are proportional to α , or α_h and δ_e respectively. For more accurate calculations it will be better to rely on wind tunnel measurements of C_m for a range of values of interest of α , i_h and δ_e .

The above expressions apply to the case of an aircraft with a fixed stabilizer and a movable elevator. In many cases, however, the available power $|C_{m_{\delta_e}} \delta_e|_{max}$ is insufficient to obtain moment equilibrium at all desired c.g. positions over the entire range of airspeeds.

Often an adjustable stabilizer with a variable i_h is employed, and set such that $\delta_e = 0$. In that case C_{m_0} in equation (9-74) is of course no longer a constant. Some aircraft types have a movable horizontal tailplane with even no elevator at all, the so-called ‘flying-tail’. Expressions can be derived quite similarly for the value of i_h required for equilibrium in such cases.

We conclude this section on equilibrium and tail load with the following comments on equations (9-72) through (9-76),

- C_{m_α} , $C_{N_{w_\alpha}}$ and α_0 are fixed by the aerodynamic design of the wing, the fuselage and the nacelles.

- The required tail volume $\frac{S_h l_h}{S_c}$ follows primarily from the requirement that the aircraft shall be statically stable (i.e. $C_{m_\alpha} < 0$) at the rearmost permissible c.g. position, the derivative $C_{N_{h_\alpha}}$ following from the shape and size of the horizontal tailplane, see section 9-2-2.
- If the angle of incidence of the horizontal tailplane, i_h , is not adjustable, i_h is generally set such that the elevator angle is zero, minimizing the parasite tailplane drag .
- Both $\frac{d\varepsilon}{d\alpha}$ and $(\frac{V_h}{V})^2$ follow from the characteristics of the wing and the location of the horizontal tailplane relative to the wing and the fuselage, see section 9-2-4.
- For tail planes with fixed i_h , $(C_m)_{\delta_e=0}$ depends on angle of attack and c.g. position, and has to be compensated for by the moment generated by the elevator $C_{m_{\delta_e}} \delta_e$, see equation (9-77).
- For most aircraft the maximum, positive value of $C_{m_{\delta_e}} \cdot \delta_e$ (elevator up) required in any steady flight condition is larger than the minimum, negative (elevator down) value.
- The largest positive values of $C_{m_{\delta_e}} \cdot \delta_e$ will be needed to compensate for the largest value of $(C_m)_{\delta_e=0}$. The latter occurs at the most forward c.g. position and at the maximum angle of attack.

Ground effect usually produces a further negative contribution to $(C_m)_{\delta_e=0}$; as a consequence for many aircraft the required size of the elevator is determined by the requirement that the aircraft can take-off and land at the most forward c.g. position.

9-2-7 Stick forces in steady flight

To obtain equilibrium of the aerodynamic moment about the lateral axis through the center of gravity, the elevator must be deflected by applying a force on the control stick or wheel to compensate for the corresponding aerodynamic hinge moment. In many modern aircraft the connection between the pilot's control manipulator and the elevator is such that this effort provides only part of the total required hinge moment. Sometimes there is even no direct mechanical connection at all between the control stick or wheel and the control surface, such as in case of a Fly by Wire flight control system. These classes of control systems will not be discussed now, however, the concepts developed here and in subsequent chapters for mechanical flight control systems do in fact apply also to these types of flight control systems. In figure 9-84 a classical manual control system is depicted. The positive directions of the control deflections s , control forces F , surface angles δ and hinge moments H are as indicated. In the following the longitudinal control force required for equilibrium about the lateral axis, F_e , will be considered in more detail.

We now derive a simple model for the control force on the elevator control stick or wheel. Similar models can be derived for the aileron control force, F_a , and for the control force on the rudder pedals, F_r . If the control stick is displaced over a small distance ds_e , the work done by the control force F_e is $F_e \cdot ds_e$. Neglecting flexibility, the elevator deflects over an angle $d\delta_e$ and the work done by the hinge moment H_e is $H_e \cdot d\delta_e$. If the internal friction in the control system, as well as cable stretch, is neglected, the control system absorbs no work internally and the total amount of external work has to be zero if the stick and the elevator are again at rest after the displacement.

This implies that,

$$F_e \cdot ds_e + H_e \cdot d\delta_e = 0 \quad (9-81)$$

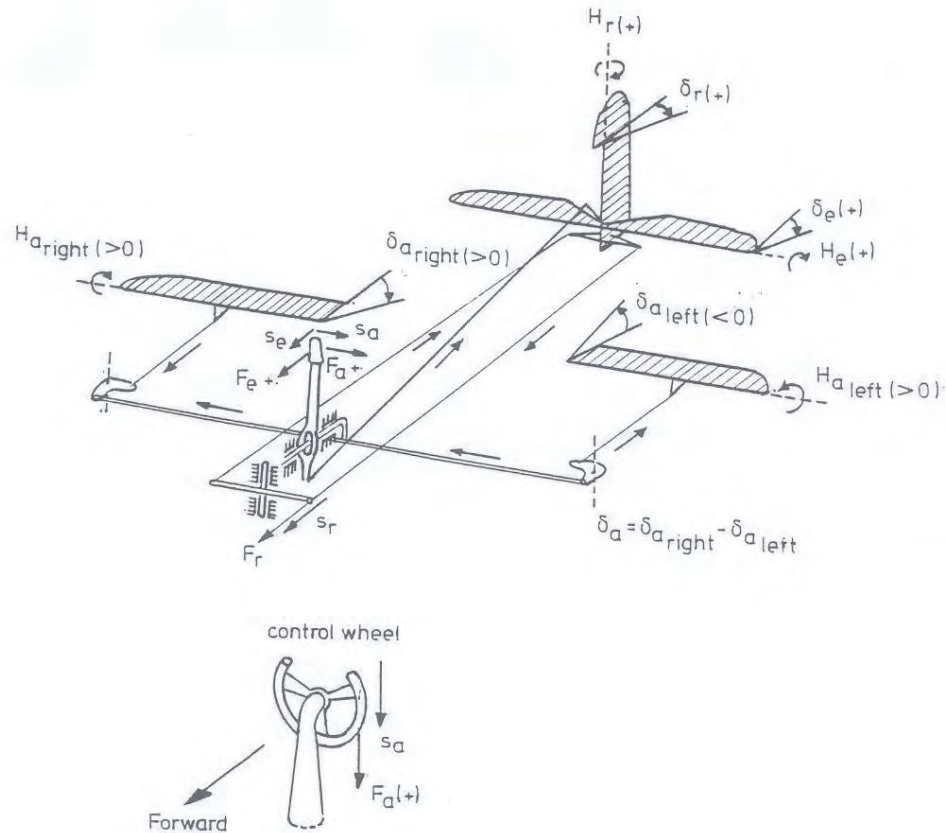


Figure 9-84: The positive direction of control deflections, control forces, control surface deflections and hinge moments

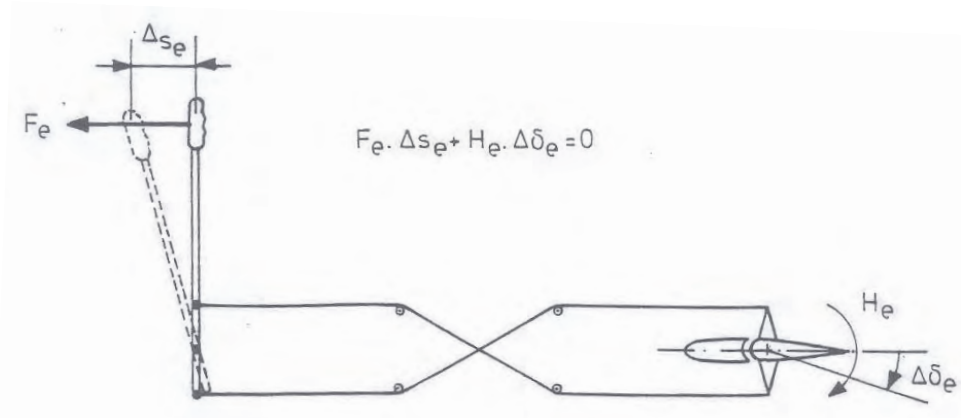


Figure 9-85: The relation between the control force and the hinge moment

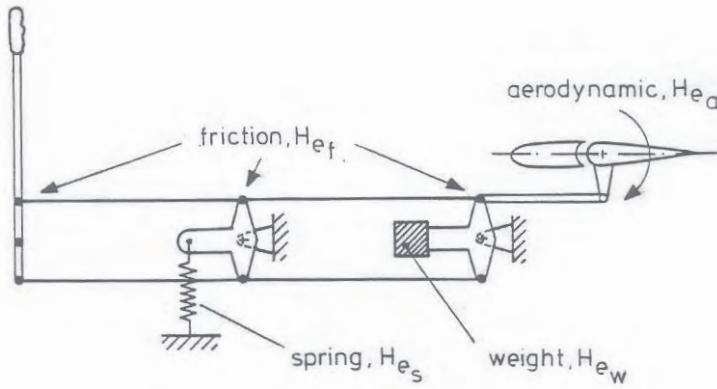


Figure 9-86: Contributions to the hinge moment

or, see also figure 9-85,

$$F_e = -\frac{d\delta_e}{ds_e} H_e \quad (9-82)$$

where the gear ratio $\frac{d\delta_e}{ds_e}$ is positive , see figure 9-84.

The total hinge moment to be balanced by the control force, see figure 9-86, consists of several components, i.e. the aerodynamic hinge moment (H_{e_a}), a hinge moment caused by friction in the control system (H_{e_f}) and, if the control surface is not statically balanced, a hinge moment (H_{e_w}) caused by the static unbalance. In many aircraft a spring is applied in the control system, giving rise to yet another component of the total hinge moment, H_{e_s} .

The total hinge moment then is,

$$H_e = H_{e_a} + H_{e_f} + H_{e_w} + H_{e_s}$$

For simplicity , the hinge moments due to friction, static unbalance and the spring will be omitted in the following. This results in,

$$H_e = H_{e_a}$$

Substituting equation (9-61) in (9-82) the longitudinal control force can then be written as,

$$F_e = -\frac{d\delta_e}{ds_e} \frac{1}{2} \rho V_h^2 S_e \bar{c}_e C_{h_e}$$

and, using the linearized expression as in equation (9-63) for C_{h_e} ,

$$F_e = -\frac{d\delta_e}{ds_e} \frac{1}{2} \rho V_h^2 S_e \bar{c}_e (C_{h_\alpha} \alpha_h + C_{h_\delta} \delta_e + C_{h_{\delta_t}} \delta_{t_e}) \quad (9-83)$$

Suppose now, that for a given c.g. position and angle of attack, or airspeed, the elevator angle, δ_e , required for equilibrium of the moment about the lateral axis has been determined according

to equation (9-80). Now the longitudinal control force required to maintain this elevator angle, for a given tab angle, δ_{t_e} , follows from equation (9-83). Chapter 7 deals in more detail with this control force as a function of airspeed, c.g. position and tab angle.

We conclude with some remarks on the required signs and magnitudes of the hinge moment derivatives $C_{h_{\delta_t}}$, C_{h_δ} and C_{h_α} .

- The required magnitude of $C_{h_{\delta_t}}$ (this is the case of a classical tail plane with fixed incidence of the horizontal tailplane, i_h) follows from the requirement that in steady flight conditions it must be possible to trim the control forces down to zero by adjusting the trim tab angle. A more detailed definition of aircraft configurations and flight conditions for which this requirement holds can be found in the airworthiness requirements, see references [11, 19, 6, 20, 12, 13, 7].
- The required magnitude of $C_{h_{\delta_t}}$ also depends of course on the allowable tab deflecting angles, δ_{t_e} , and on the values of C_{h_α} and C_{h_δ} .
- As has been mentioned before, in order to keep the required control forces within reasonable limits when changing either the aircraft configuration, indicated airspeed the steady flight condition or when executing turns or pull up maneuvers, C_{h_α} and C_{h_δ} should be small in an absolute sense.
- As shown in chapter 7 and mentioned above, C_{h_δ} must always be negative. Usually C_{h_α} is negative as well, but small positive values of C_{h_α} are permissible, even desirable and occur indeed in practice. When studying the control forces in more detail in chapter 7, this will be discussed in more detail.

Chapter 10

Longitudinal Stability and Control in Steady Flight

10-1 Stick Fixed Static Longitudinal Stability

In chapter 9 we discussed the equilibrium of the aerodynamic and gravitational forces in the plane of symmetry and the aerodynamic moment about the center of gravity. The also showed that the horizontal tailplane and its elevator play a crucial rôle in the equilibrium of the aerodynamic moment about the center of gravity. For the equilibrium, the following equations (9-53), (9-54) and (9-55), were derived,

$$\begin{aligned} C_T &= C_{T_w} = -\frac{W}{\frac{1}{2}\rho V^2 S} \sin \theta \\ C_N &= C_{N_w} + C_{N_h} \left(\frac{V_h}{V} \right)^2 \frac{S_h}{S} = \frac{W}{\frac{1}{2}\rho V^2 S} \cos \theta \\ C_m &= C_{m_{ac}} + C_{N_w} \frac{x_{cg} - x_w}{\bar{c}} + C_{N_h} \left(\frac{V_h}{V} \right)^2 \frac{S_h}{S} \frac{x_{cg} - x_h}{\bar{c}} = 0 \end{aligned}$$

For the equilibrium of the moments equation (9-57) was introduced,

$$C_m = C_{m_{ac}} + C_{N_w} \frac{x_{cg} - x_w}{\bar{c}} - C_{N_h} \left(\frac{V_h}{V} \right)^2 \frac{S_h l_h}{S \bar{c}} = 0$$

Equilibrium of forces and moments acting on an aircraft in flight is a necessary, but certainly not a sufficient condition for steady flight. A steady flight condition must also be stable as pointed out for example already in reference [132]. This means that after the occurrence of a small disturbance the aircraft should return to the original state of equilibrium. If this is the case, the equilibrium is called dynamically stable. Although, as remarked in reference [132], stability is strictly a characteristic of an equilibrium, it is common practice to call the aircraft itself dynamically stable if its equilibrium is stable.

The motions of aircraft after a disturbance, and along with it the dynamic stability, are determined by the equations of motion of the aircraft. A discussion of aircraft motions, using these equations of motion (see chapters 3 and 4), is postponed at this stage.

There is, as in reference [55], a simpler way to study stability. Experience has shown, that most critical requirements to be satisfied for dynamic stability can be expressed for most aircraft by the condition that the aircraft must be statically stable. The discussion of static stability is based on the equations for the equilibrium of the aircraft, see equations (9-53), (9-54) and (9-57). These equations are in fact special cases of the more general equations of motion.

When we discuss static longitudinal stability we refer to pitch attitude stability. So we just need to consider the expression for the longitudinal moment, equations (9-57) or (9-55) allowing us to study the change of aerodynamic moment caused by a change in angle of attack in a similar way as we did with the two dimensional wing profile, wings and wing-fuselage composites in section 9-1-3. Here we analize the static stability of complete aircraft including horizontal tail surfaces. New is also that we must consider static stability for the case of stick fixed (fixed elevator deflection) and the case of stick free (floating elevator). It will be shown that a close relationship exists between the way in which the stick position varies with airspeed, or angle of attack, in steady, straight flight on the one side and the static stability, stick fixed on the other. In a similar way it will be shown that static stability with stick free, is closely related to the way in which the stick force varies with airspeed in steady, straight flight. For simplicity , propulsion effects will be neglected and the dimensionless aerodynamic coefficients are assumed to be independent of airspeed. We could readily take these effects into account, at the cost, however, of much more cumbersome derivations.

It is interesting to note that steady flight conditions as discussed in the present chapter, are in fact just a special case of dynamic flight conditions described by equations of motion. This fact allows us to present an alternative way to derive static stability and control characteristics directly from the linearized equations of motion. The resulting expressions contain stability and control derivatives which do take account of things as propulsion effects, and so, are in a sense more general than those which were derived for the more simple case of the model above. We present these derivations from the linearized equations of motion in boxes under the heading of ‘Quick derivation of’ following the more elaborate analytical derivations based on the simplified model above.

10-1-1 Stick fixed static longitudinal stability in gliding flight

In section 9-1-3 the concept of static stability was presented for two dimensional wing profiles, wings and wing-fuselage composites. This discussion is now extended to a complete aircraft. Suppose the aircraft is in steady flight, so the moment about the center of gravity is zero, $C_m = 0$. If some external disturbance would cause an increase of the pitch angle and so of the angle of attack, we would like to see a negative, nose-down change in C_m , a nose down, restoring moment.

The condition for static longitudinal stability then is,

$$\frac{dC_m}{d\alpha} = C_{m_\alpha} < 0, \quad \text{at } C_m = 0 \quad (10-1)$$

If $C_{m_\alpha} = 0$ the static stability is called neutral. If $C_{m_\alpha} > 0$ the aircraft is statically unstable. To study the various contributions to the derivative C_{m_α} of the complete aircraft, the expression for the moment coefficient is reconsidered as in equation (9-72)

$$C_m = C_{m_{ac}} + C_{N_{w_\alpha}} (\alpha - \alpha_0) \frac{x_{cg} - x_w}{c} -$$

$$\left[C_{N_{h\alpha}} \left\{ (\alpha - \alpha_0) \left(1 - \frac{d\varepsilon}{d\alpha} \right) + (\alpha_0 + i_h) \right\} + C_{N_{h\delta_e}} \delta_e \right] \left(\frac{V_h}{V} \right)^2 \frac{S_h l_h}{S \bar{c}} \quad (10-2)$$

Equation (10-2) can be rearranged to combine the contributions of the wing with fuselage and nacelles (indicated by the index w) and the contribution of the horizontal tailplane (indicated by index h),

$$C_m = C_{m_w} + C_{m_h} \quad (10-3)$$

with,

$$C_{m_w} = C_{m_{ac}} + C_{N_{w\alpha}} (\alpha - \alpha_0) \frac{x_{cg} - x_w}{\bar{c}} \quad (10-4)$$

and,

$$C_{m_h} = - \underbrace{\left[C_{N_{h\alpha}} \underbrace{\left\{ (\alpha - \alpha_0) \left(1 - \frac{d\varepsilon}{d\alpha} \right) + (\alpha_0 + i_h) \right\}}_{\alpha_h} + C_{N_{h\delta_e}} \delta_e \right]}_{C_{N_h}} \left(\frac{V_h}{V} \right)^2 \frac{S_h l_h}{S \bar{c}} \quad (10-5)$$

Figures 10-1 schematically show the $C_m - \alpha$ -curves of the contributions according to equations (10-4) and (10-5) and of the complete aircraft configuration according to (10-2). Figure 10-2 presents the contributions of the various parts of the aircraft to the $C_m - \alpha$ -curve as measured in a wind tunnel on a model of the Fokker F-27. Figure 10-3 presents calculated moment curves for several parts of the Cessna Ce550 ‘Citation II’. This data was calculated using an inviscid panel method (linearized potential flow). The definition of the aircraft parts is presented in figure 7-2; these parts are: ‘wing’, ‘horizontal stabilizer’, ‘pylon’, ‘nacelles’, ‘vertical fin’ and ‘fuselage’ (in clockwise direction, starting from the left top figure). The results presented in figure 10-3 clearly show the destabilizing effect of the fuselage and the stabilizing effect of the horizontal tailplane, while the contribution of the wing and nacelles is almost indifferent.

The slopes of the moment curves follow from equations (10-4) and (10-5) by differentiating with respect to the angle α . Because the ‘stick fixed’ situation is considered, the elevator angle δ_e is taken constant,

$$C_{m_{\alpha_w}} = C_{N_{w\alpha}} \frac{x_{cg} - x_w}{\bar{c}} \quad (10-6)$$

$$C_{m_{\alpha_h}} = -C_{N_{h\alpha}} \left(1 - \frac{d\varepsilon}{d\alpha} \right) \left(\frac{V_h}{V} \right)^2 \frac{S_h l_h}{S \bar{c}} \quad (10-7)$$

Because the cg usually lies behind the ac of the combination of a wing with fuselage and nacelles, the derivative $C_{m_{\alpha_w}}$ is positive, see equation (10-6). This means, that even if the aircraft without the horizontal tailplane could be at equilibrium at all ($C_{m_w} = 0$), the equilibrium would be unstable, see also section 9-1-3. The contribution of the tailplane has a stabilizing effect, according to equation (10-7), $(C_{m_\alpha})_h < 0$. This contribution must be large enough, that C_{m_α} is, see equation (9-75),

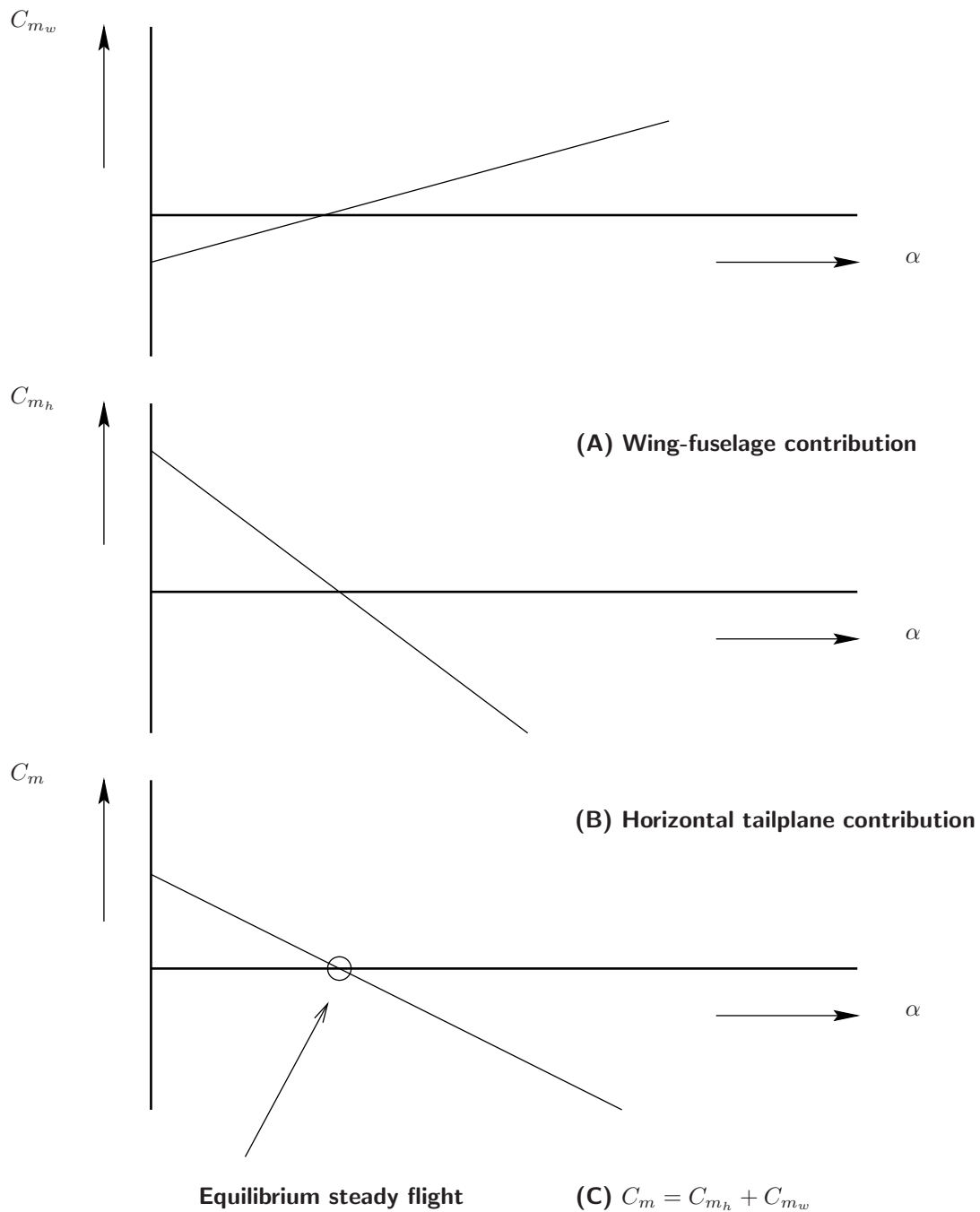


Figure 10-1: The contribution of various parts of the aircraft to the moment curve $C_m - \alpha$

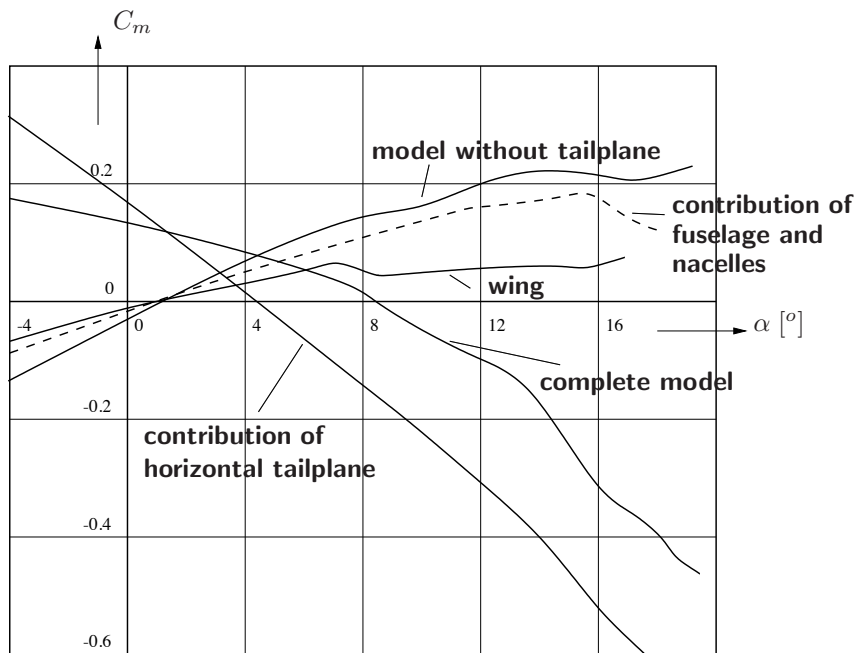


Figure 10-2: Measured contributions of various aircraft parts to the moment curve of the Fokker F- 27, reference point at $0.346 \bar{c}$ (from reference [158])

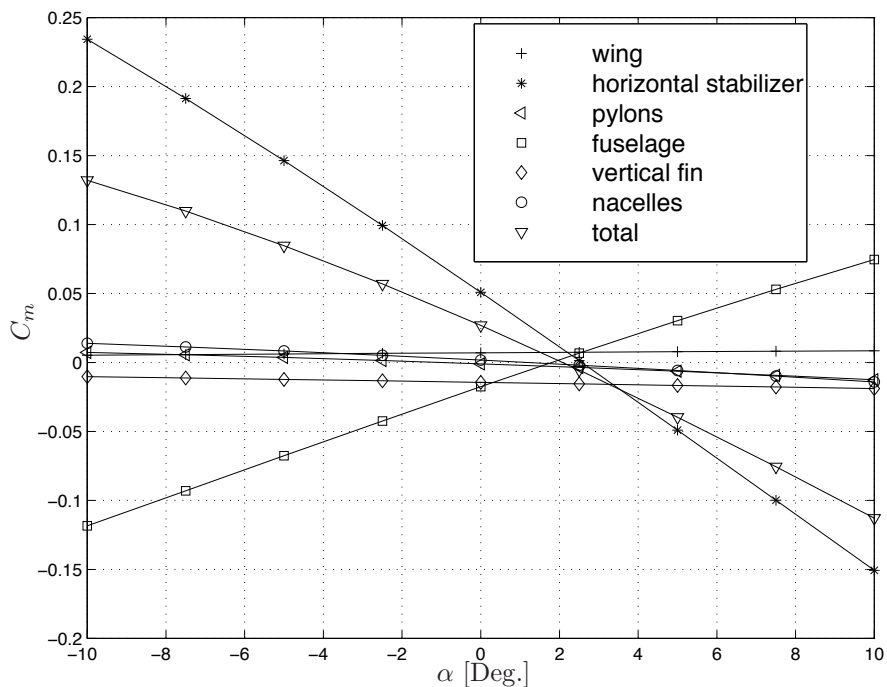


Figure 10-3: Calculated contributions of various aircraft parts to the moment curve of the Cessna Ce550 'Citation II'

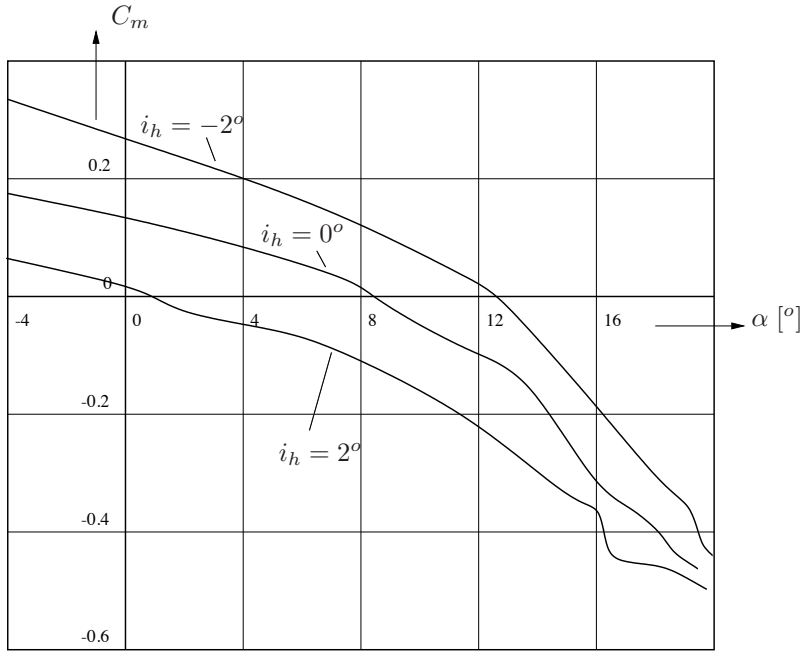


Figure 10-4: Influence of the tailplane incidence on the moment curve of the Fokker F-27, reference point at $0.346 \bar{c}$ (from reference [158])

$$C_{m_\alpha} = C_{N_{w_\alpha}} \frac{x_{cg} - x_w}{\bar{c}} - C_{N_{h_\alpha}} \left(1 - \frac{d\varepsilon}{d\alpha}\right) \left(\frac{V_h}{V}\right)^2 \frac{S_h l_h}{S \bar{c}}$$

is negative,

$$C_{m_\alpha} < 0$$

The important role of the horizontal tailplane for obtaining static stability is obvious, as already discussed in section 9-2-1. The horizontal tailplane is also essential to obtain equilibrium of the longitudinal moment.

As can be seen from a number of measured moment curves in figures 10-4 and 10-5, C_m varies almost linearly with α over a large range of angles of attack. But at large values of α , C_{m_α} is no longer constant. This is due to the contribution of C_T to the longitudinal moment and to the non-linearity caused by flow separation.

Strictly speaking, static stability is the slope of the moment curve C_{m_α} , only at $C_m = 0$. By varying i_h and δ_e the moment curve can be shifted up and down. If the angle of attack is not too large, the shifted moment curves are all parallel, see figure 10-4. A change in i_h influences C_m according to the expression in equation (9-73),

$$C_m = C_{m_0} + C_{m_\alpha} (\alpha - \alpha_0) + C_{m_{\delta_e}} \delta_e = 0$$

only by changes in C_{m_0} , which is independent of α , see equation (9-74)

$$C_{m_0} = C_{m_{ac}} - C_{N_{h_\alpha}} (\alpha_0 + i_h) \left(\frac{V_h}{V}\right)^2 \frac{S_h l_h}{S \bar{c}}$$

A change in δ_e influences C_m via the term $C_{m_{\delta_e}} \cdot \delta_e$, in principle again independent of α , see also equation (9-76),

$$C_{m_{\delta_e}} \delta_e = -C_{N_{h_{\delta_e}}} \left(\frac{V_h}{V} \right)^2 \frac{S_h l_h}{S \bar{c}} \delta_e$$

If C_m can be made zero at any angle of attack by a suitable choice of i_h or δ_e or both without influencing C_{m_α} , the slope of the moment curve at an angle of attack where $C_m \neq 0$ may be considered the static stability at that particular angle of attack α .

10-1-2 Neutral point, stick fixed

It follows from equation (9-75) and figure 10-5 that the cg position has a strong influence on the static stability. We will study this in more detail now. In order to obtain slightly more elegant expressions, we start with the expression for C_{m_α} obtained by differentiating equation (9-55) with respect to α ,

$$C_{m_\alpha} = C_{N_{w_\alpha}} \frac{x_{cg} - x_w}{\bar{c}} + C_{N_{h_\alpha}} \left(1 - \frac{d\varepsilon}{d\alpha} \right) \left(\frac{V_h}{V} \right)^2 \frac{S_h}{S} \frac{x_{cg} - x_h}{\bar{c}} \quad (10-8)$$

The only difference between equation (10-8) and the expression in equation (9-75), following from equation (9-57), is, that l_h has been replaced by $x_h - x_{cg}$. If the shift in cg positions are small relative to the tail length they are typically about 20 % of the mean aerodynamic chord \bar{c} and since l_h is typically 3 to 4 times \bar{c} , the contribution of the tailplane to C_{m_α} may be considered as constant to a first approximation.

The main effect of a change in cg position is a change in the contribution of the wing, fuselage and nacelles to C_{m_α} . Shifting the cg rearward (x_{cg} increases) will change the contribution of $C_{m_{w_\alpha}}$, usually already positive, to grow further in the positive sense. The result is, that C_{m_α} of the complete aircraft becomes less negative. A rearward shift of the center gravity thus has a destabilizing effect, see also figure 10-5. At a sufficiently far aft cg position the positive contribution of the wing-fuselage combination just compensates the negative contribution of the horizontal tailplane. Then,

$$C_{m_\alpha} = 0$$

This center of gravity position, at which the equilibrium of the moment is neutrally stable, stick fixed, is called the neutral point stick fixed (n.p.fix). This is the first interpretation of the neutral point, stick fixed. The abscissa of this point is $x_{n_{fix}}$. If the center of gravity coincides with this neutral point, it follows from equation (10-8) that,

$$C_{m_\alpha} = 0 = C_{N_{w_\alpha}} \frac{x_{n_{fix}} - x_w}{\bar{c}} + C_{N_{h_\alpha}} \left(1 - \frac{d\varepsilon}{d\alpha} \right) \left(\frac{V_h}{V} \right)^2 \frac{S_h}{S} \frac{x_{n_{fix}} - x_h}{\bar{c}} \quad (10-9)$$

From equation (10-9) the position of the neutral point is derived. To this end $C_{N_{w_\alpha}}$ is eliminated from equation (10-9) by multiplying the expression for the normal force gradient,

$$C_{N_\alpha} = C_{N_{w_\alpha}} + C_{N_{h_\alpha}} \left(1 - \frac{d\varepsilon}{d\alpha} \right) \left(\frac{V_h}{V} \right)^2 \frac{S_h}{S} \quad (10-10)$$

by,

$$\frac{x_{n_{fix}} - x_w}{\bar{c}}$$

The result is,

$$\frac{x_{n_{fix}} - x_w}{\bar{c}} = \frac{C_{N_{h\alpha}}}{C_{N_\alpha}} \left(1 - \frac{d\varepsilon}{d\alpha}\right) \left(\frac{V_h}{V}\right)^2 \frac{S_h l_h}{S \bar{c}} \quad (10-11)$$

where, as in an equation similar to equation (9-56),

$$l_h = x_h - x_w$$

in an aircraft fixed reference frame.

Next, equation (10-9) is subtracted from equation (10-8). Using equation (10-10), the resulting expression for C_m becomes,

$$C_{m_\alpha} = C_{N_\alpha} \frac{x_{cg} - x_{n_{fix}}}{\bar{c}} \quad (10-12)$$

Consider now by means of equation (10-12) a change in the moment dC_m due to a change in angle of attack $d\alpha$ such that $dC_m = C_{m_\alpha} d\alpha$. Since the accompanying change in the normal force is $dC_N = C_{N_\alpha} d\alpha$, equation (10-12) may be written as,

$$dC_m = dC_N \frac{x_{cg} - x_{n_{fix}}}{\bar{c}} \quad (10-13)$$

According to equation (10-13), the change in the moment dC_m may be interpreted as being caused by a change in the normal force dC_N , acting a distance $\frac{x_{cg} - x_{n_{fix}}}{\bar{c}}$ from the center of gravity, see figure 10-6. From this follows the second interpretation of the neutral point with stick fixed as the point of action on the m.ac of the normal force increment, caused by a step change of the angle of attack with fixed elevator angle deflection.

In concurrence with this second interpretation of the neutral point, the non-dimensional distance $\frac{x_{cg} - x_{n_{fix}}}{\bar{c}}$ is often called the '*stability margin*', stick fixed.

The present interpretation of the neutral point agrees entirely with its first introduction in section 9-1-2as the point of intersection of the line of action of an increment in the aerodynamic force, $d\underline{C}_R$ and the mean aerodynamic chord.

10-1-3 Elevator trim curve and elevator trim stability

A. Elevator trim curve

In section 9-2-6 the elevator angle required for equilibrium, i.e. for $C_m = 0$, was expressed in equation (9-80):

$$\delta_e = -\frac{1}{C_{m_{\delta_e}}} \{C_{m_0} + C_{m_\alpha} (\alpha - \alpha_0)\}$$

where C_m is the static stability according to equations (9-75) or (10-8). The constant C_{m_0} and the elevator efficiency $C_{m_{\delta_e}}$ were already expressed in equations (9-74) and (9-76) respectively,

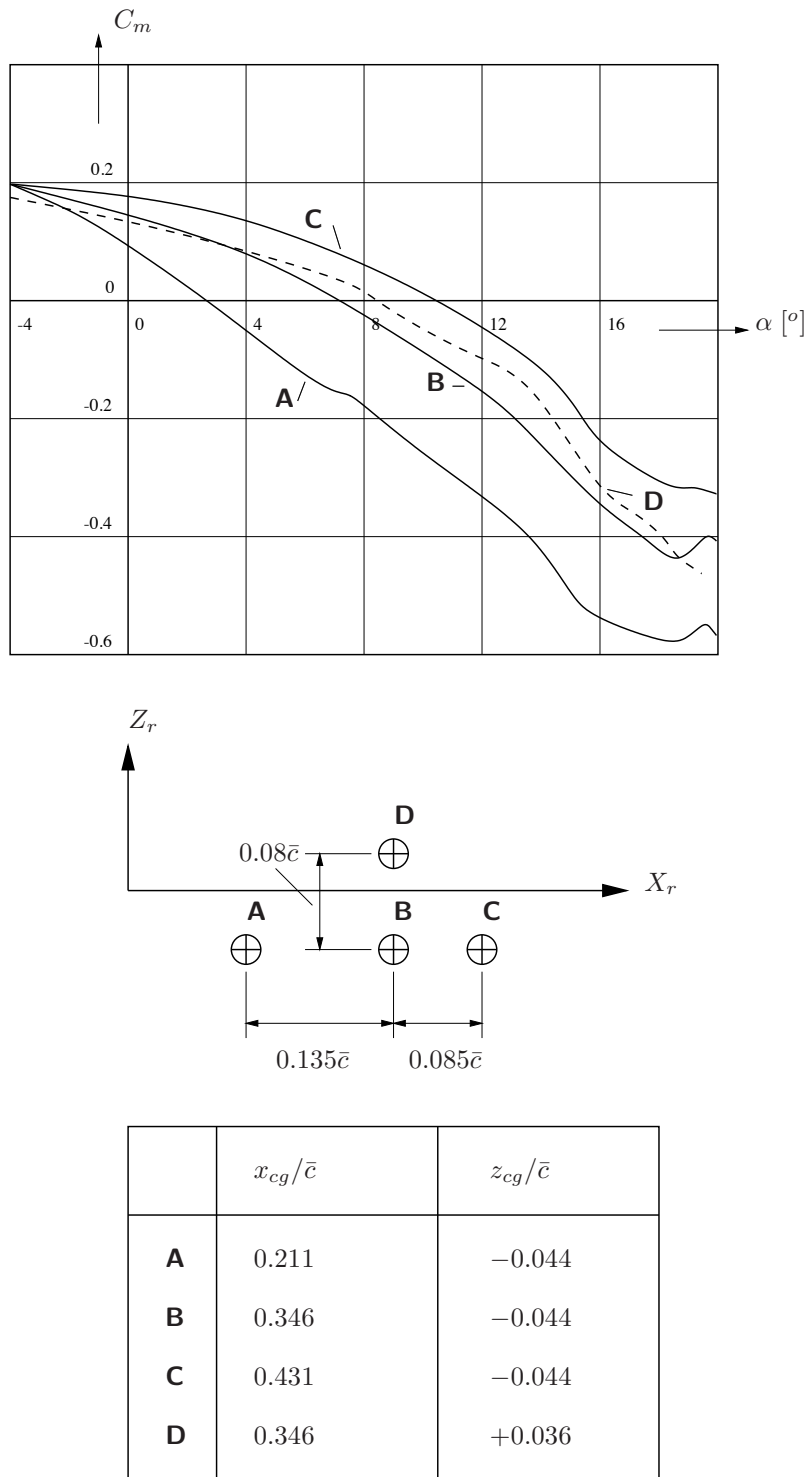


Figure 10-5: Influence of the position of the reference point (center of gravity) on the moment curves of the Fokker F-27, (from reference [158])

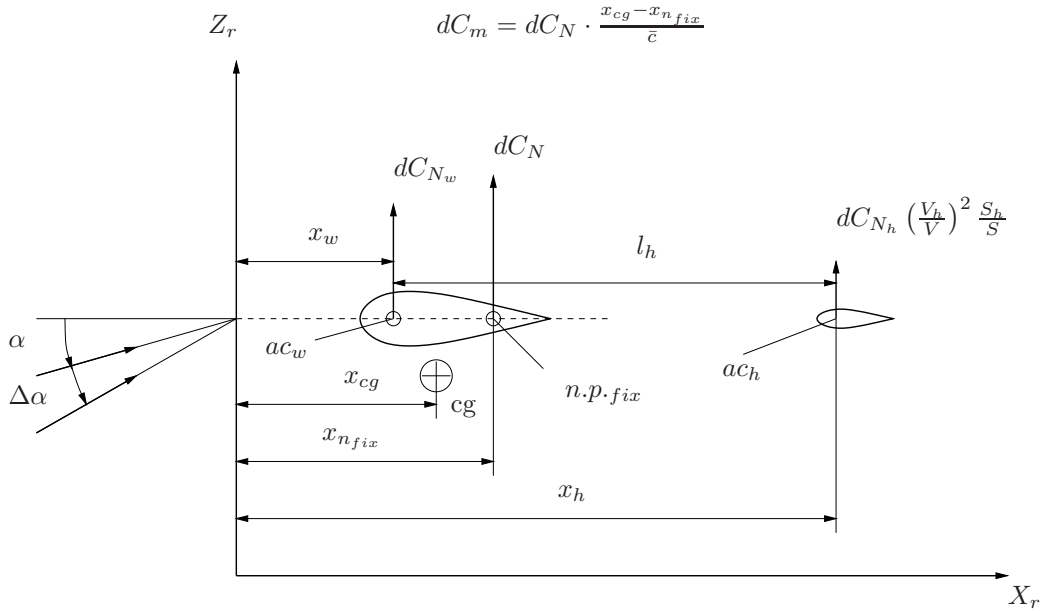


Figure 10-6: Change in the moment dC_m due to a change in the angle of attack $\Delta\alpha$

see section 10-1-1.

If $C_{m_{\delta_e}}$ and C_{m_α} are constant, the elevator angle required for equilibrium varies linearly with α , according to equation (9-80). The graphic representation of the elevator angle required for equilibrium as a function of α or airspeed V is known as the elevator trim curve.

The relation between the angle of attack α and the airspeed V is derived from the equilibrium in Z -direction, or in a slightly modified form,

$$C_N \approx C_{N_\alpha} (\alpha - \alpha_0) \approx \frac{W}{\frac{1}{2}\rho V^2 S} \quad (10-14)$$

From equation (9-80) follows with equation (10-14) the expression for the elevator trim curve δ_e as a function of V ,

$$\delta_e = -\frac{1}{C_{m_{\delta_e}}} \left(C_{m_0} + \frac{C_{m_\alpha}}{C_{N_\alpha}} \frac{W}{\frac{1}{2}\rho V^2 S} \right) \quad (10-15)$$

Figure 10-7 presents schematically some elevator trim curves and the corresponding moment curves for a statically stable ($C_{m_\alpha} < 0$), a neutrally stable ($C_{m_\alpha} = 0$) and a statically unstable ($C_{m_\alpha} > 0$) aircraft. It is common practice to plot an ‘elevator-up’ deflection in the upward direction, implying that the negative δ_e -axis points upwards. From these figures, and also from the expressions in equations (9-80) and (10-15), it can be seen that there is a close relation between the moment curve and the elevator trim curve. In particular the slope of the elevator-trim curve is directly related to the slope of the moment curve C_{m_α} , i.e. the static longitudinal stability, if $C_{m_{\delta_e}}$ is exactly constant.

B. Elevator stick position stability

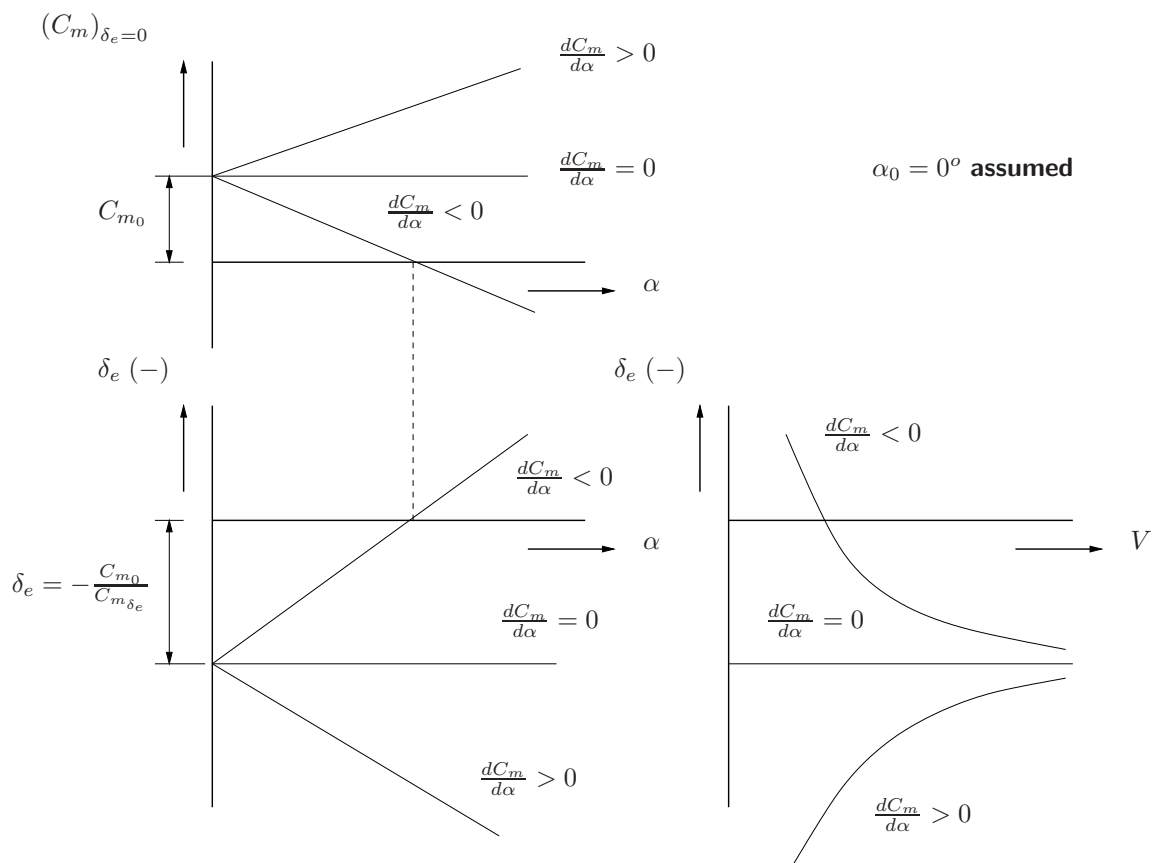


Figure 10-7: Moment curves and corresponding trim curves

The following discussion shows how the slope of the elevator trim curve is important for the pilot's opinion on the handling qualities of aircraft. The slope of the elevator trim curve $\delta_e - \alpha$ follows from equation (9-80) by differentiating with respect to α ,

$$\frac{d\delta_e}{d\alpha} = -\frac{C_{m_\alpha}}{C_{m_{\delta_e}}} \quad (10-16)$$

Considering that $C_{m_{\delta_e}}$ is always negative, it follows that for a statically stable aircraft ($C_{m_\alpha} < 0$) the slope of the trim curve $\delta_e - \alpha$ is always negative, i.e.,

$$\frac{d\delta_e}{d\alpha} < 0 \quad (10-17)$$

The slope $\frac{d\delta_e}{dV}$ of the elevator trim curve $\delta_e - V$ follows from equation (10-15) by differentiating with respect to V ,

$$\frac{d\delta_e}{dV} = \frac{4W}{\rho V^3 S} \frac{1}{C_{m_{\delta_e}}} \frac{C_{m_\alpha}}{C_{N_\alpha}} \quad (10-18)$$

For a statically stable aircraft ($C_{m_\alpha} < 0$) it follows from equation (10-18),

$$\frac{d\delta_e}{dV} > 0 \quad (10-19)$$

If the relation between the elevator angle and the airspeed in steady, straight flight is such that equation (10-19) is satisfied, the aircraft is said to have elevator trim stability, see also reference [173]. This concept of the elevator control position stability can be interpreted in two different ways, i.e.,

1. According to the first interpretation, trim stability (the slope $\frac{d\delta_e}{dV}$ of the elevator trim curve $\delta_e - V$) provides an indication of the static longitudinal stability of the aircraft. Elevator trim stability is a convenient characteristic to obtain the static stability both qualitatively and quantitatively from measurements in actual flight, see section 10-1-6 for a more detailed discussion.
2. The second interpretation of trim stability lies in the fact that an aircraft possessing such stability is pleasant for the pilot and safe to fly. This will be further illustrated in the following.

Suppose that from a given steady flight condition pilot elects to transition to another steady flight condition at a slightly lower airspeed and a corresponding larger angle of attack. He must therefore initiate a nose-up rotation of the aircraft over the small angle $\Delta\theta$, to obtain the required new angle of attack. This initial rotation is obtained through an initial moment ΔC_{m_i} about the lateral axis, generated by an initial elevator deflection $\Delta\delta_{e_i}$, see figure 10-8. If α and θ are intended to increase and as a consequence V is intended to decrease, the initial elevator displacement must be upward and the corresponding stick displacement directed aft. For any aircraft at any cg position the following holds,

$$\frac{\Delta\delta_{e_i}}{\Delta V} > 0$$

and,

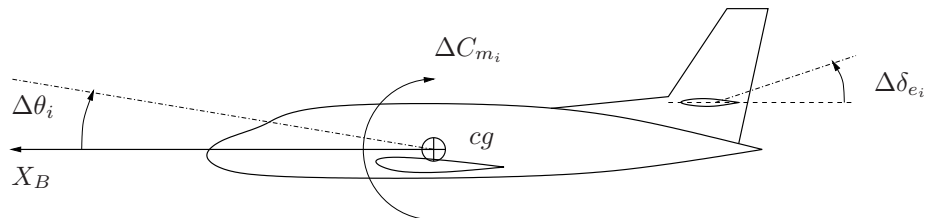


Figure 10-8: Initial control surface deflections

$$\frac{\Delta s_{e_i}}{\Delta V} > 0$$

Now it is known that it is pleasant for the pilot, because it eases the flying of the aircraft, if the initial control displacement Δs_{e_i} and the final control displacement Δs_{e_u} are in the same direction,

$$\frac{\Delta s_{e_u}}{\Delta s_{e_i}} > 0 \quad \Rightarrow \quad \frac{\Delta \delta_{e_u}}{\Delta \delta_{e_i}} > 0 \quad (10-20)$$

with the subscript u as in s_{e_u} and δ_{e_u} implying the final, or ultimate, control (surface) displacement.

There is no need for $\Delta \delta_{e_u}$ and $\Delta \delta_{e_i}$ to be of equal magnitude. In order to speed up the response of the aircraft, the pilot might well generate an initial control deflection larger than the final control displacement.

This has been indicated by the dashed line in figure 10-9a. Evidently, the following holds,

$$\frac{\Delta \delta_{e_u}}{\Delta \delta_{e_i}} = \frac{\frac{\Delta \delta_{e_u}}{\Delta V}}{\frac{\Delta \delta_{e_i}}{\Delta V}}$$

It was argued, that always $\frac{\Delta \delta_{e_i}}{\Delta V} > 0$. As a consequence equation (10-20) corresponds to the requirement $\frac{\Delta \delta_{e_u}}{\Delta V} > 0$ or, for infinitesimally small changes : $\frac{d \delta_e}{d V} > 0$.

It is thus seen, that equation (10-20) leads to the requirement in equation (10-19) for elevator control position stability. Figure 10-10 may serve as a further illustration of the importance of this desired control characteristic. The figure shows in a highly schematic way how the pilot handles the elevator control, if he or she wants to change the aircraft from one steady flight condition into another steady condition. The case of a trim curve showing control position stability is considered first.

Suppose again the pilot wants to reduce airspeed, starting from a steady flight condition (indicated '1' in the figure). Pulling the control wheel aft, will cause α and θ to increase, and soon after V to decrease. For an aircraft with positive elevator control position stability, the new elevator deflection δ_{e_2} corresponds to a new steady flight condition at a lower airspeed V_2 (see the flight condition indicated as '2' in figure 10-10). The response of the aircraft to the initial control displacement is in the direction of the desired new state equilibrium.

Figure 10-10 also shows the case of an aircraft with negative elevator control position stability. It can be seen, that the response of the aircraft to the initial control displacement is in the other direction as needed for the desired new steady flight condition. As a consequence a much more complicated time-history of the control displacement is needed to arrive at the steady flight

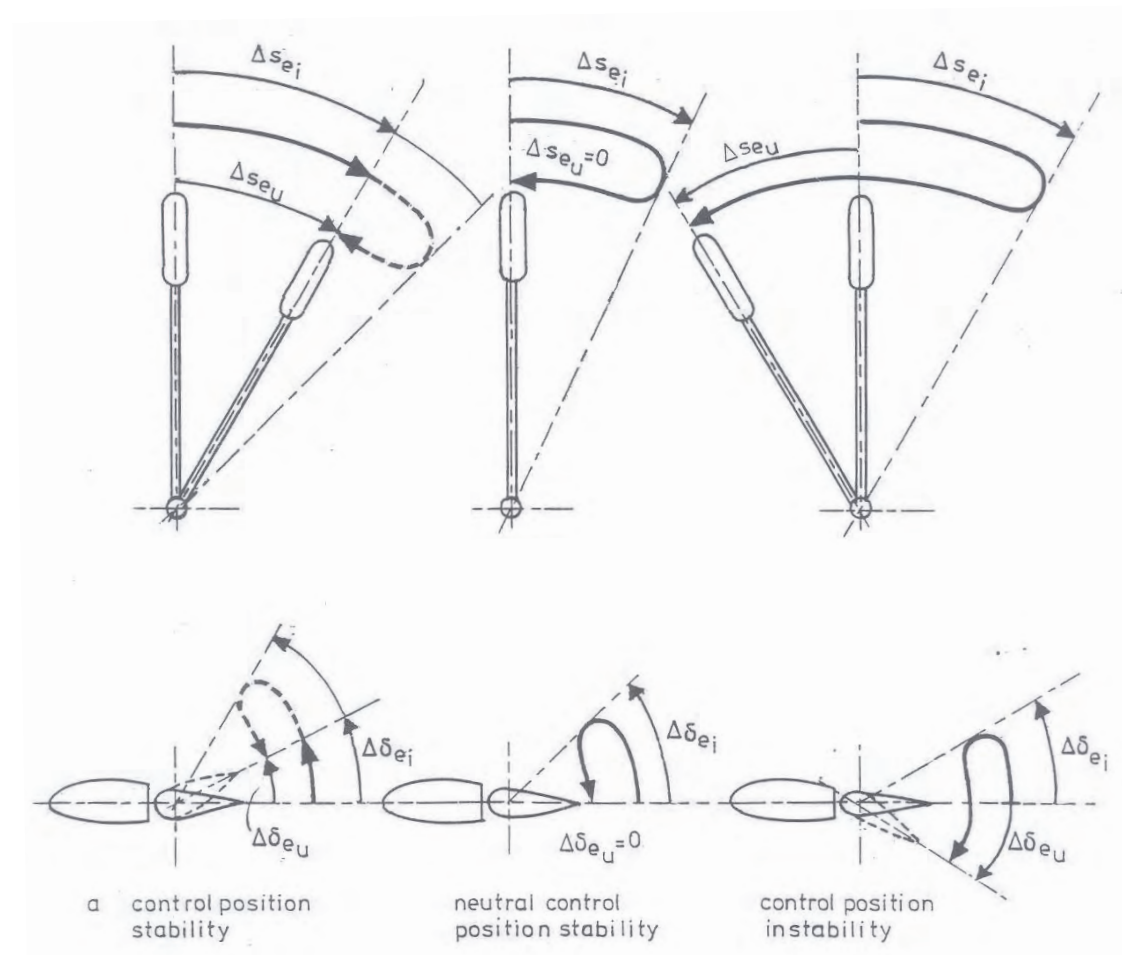


Figure 10-9: Initial and ultimate control displacement and control surface deflection for the transition to a lower airspeed

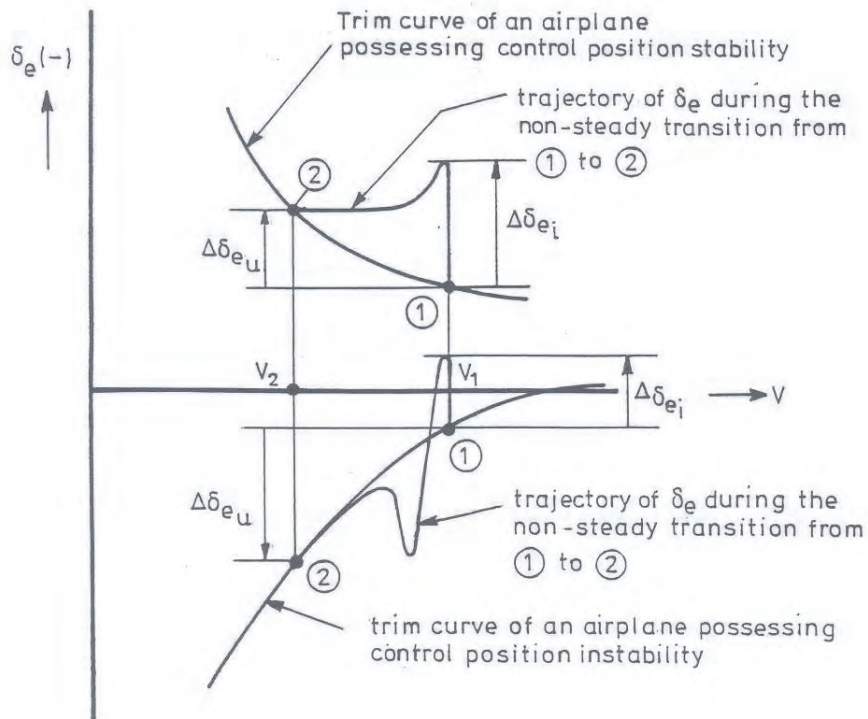


Figure 10-10: Aircraft responses to a control deflection

condition '2'. This characteristic where the initial control input and the final control input have different signs is considered to be an objectionable characteristic which pilots are supposed not to appreciate. Worse is, of course, that in this case this control characteristic reflects the fact that the aircraft is statically unstable, and would require a lot of attention and effort by the pilot to keep under control, and it might well be an impossible task for even the most gifted pilot.

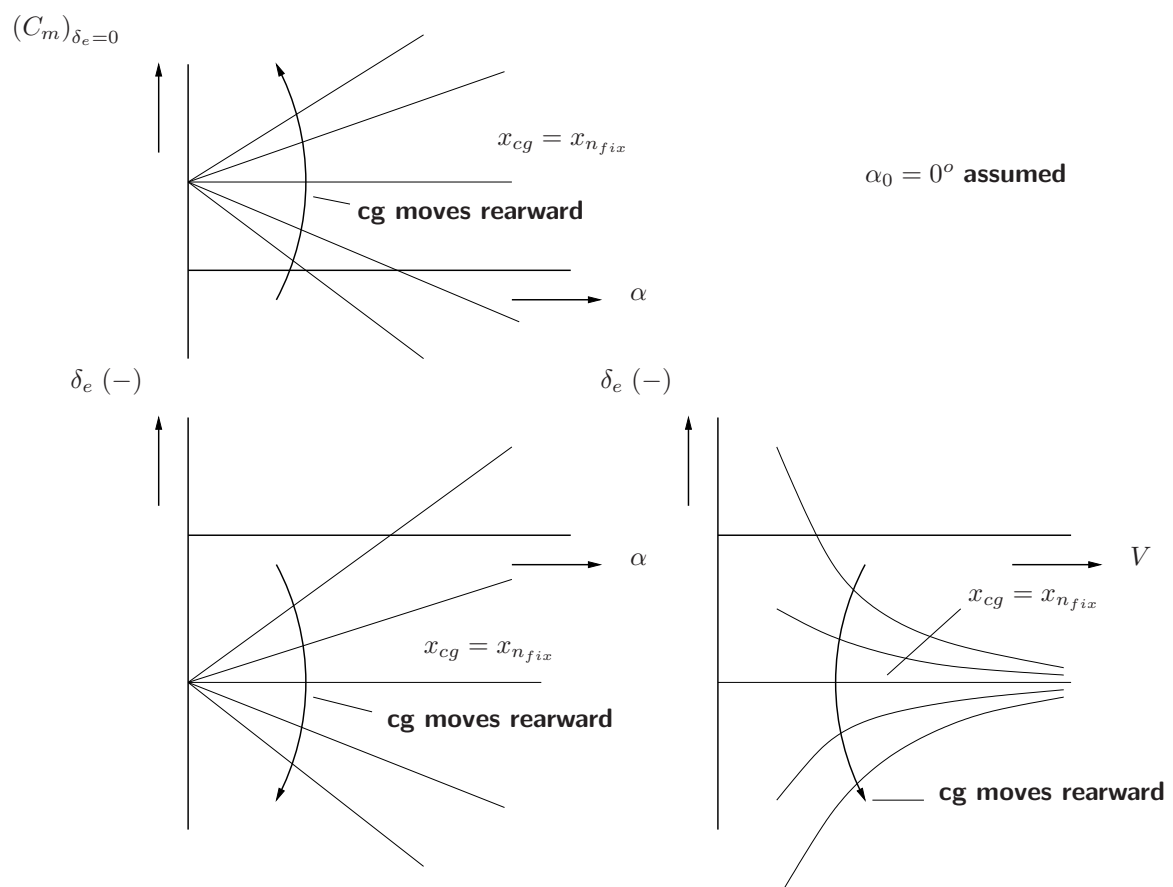


Figure 10-11: Influence of cg position on the trim curve

A quick derivation of stick position stability

We start with the symmetrical equations of motion, in which, for simplicity, the derivatives $C_{Z\dot{\alpha}}$ and C_{Z_q} were set to zero.

$$\begin{bmatrix} C_{X_u} - 2\mu_c D_c & C_{X_\alpha} & C_{Z_o} & 0 \\ C_{Z_u} & C_{Z_\alpha} - 2\mu_c D_c & 0 & 2\mu_c \\ 0 & 0 & -D_c & 1 \\ C_{m_u} & C_{m_\alpha} + C_{m\dot{\alpha}} D_c & 0 & C_{m_q} - 2\mu_c K_Y^2 D_c \end{bmatrix} \begin{bmatrix} \hat{u} \\ \alpha \\ \theta \\ \frac{q\bar{c}}{V} \end{bmatrix} + \begin{bmatrix} 0 \\ C_{Z_\delta} \\ 0 \\ C_{m_\delta} \end{bmatrix} \cdot \delta_e = 0$$

For stationary straight flight conditions, where $\frac{q\bar{c}}{V} = D_c\alpha = D_c\hat{u} = D_c\frac{q\bar{c}}{V} = 0$ these equations reduce to:

$$\begin{bmatrix} C_{X_u} & C_{X_\alpha} & C_{Z_o} \\ C_{Z_u} & C_{Z_\alpha} & 0 \\ C_{m_u} & C_{m_\alpha} & 0 \end{bmatrix} \cdot \begin{bmatrix} \hat{u} \\ \alpha \\ \theta \end{bmatrix} + \begin{bmatrix} 0 \\ C_{Z_\delta} \\ C_{m_\delta} \end{bmatrix} \cdot \delta_e = 0$$

Now, we introduce a small stick deflection $\Delta\delta_e$, in a trimmed flight condition with V_0, α_0, θ_0 . This results, after some time, in a new steady state flight condition with

$$V = V_0 + \Delta V (\Delta\hat{u} = \frac{\Delta V}{V_0}), \alpha = \alpha_0 + \Delta\alpha, \theta = \theta_0 + \Delta\theta$$

So,

$$\begin{bmatrix} C_{X_u} & C_{X_\alpha} & C_{Z_o} \\ C_{Z_u} & C_{Z_\alpha} & 0 \\ C_{m_u} & C_{m_\alpha} & 0 \end{bmatrix} \cdot \begin{bmatrix} \Delta\hat{u} \\ \Delta\alpha \\ \Delta\theta \end{bmatrix} + \begin{bmatrix} 0 \\ C_{Z_\delta} \\ C_{m_\delta} \end{bmatrix} \cdot \Delta\delta_e = 0$$

or

$$A_{ss} \cdot \Delta x - B \cdot \Delta\delta_e = 0$$

where

$$A_{ss} = \begin{bmatrix} C_{X_u} & C_{X_\alpha} & C_{Z_o} \\ C_{Z_u} & C_{Z_\alpha} & 0 \\ C_{m_u} & C_{m_\alpha} & 0 \end{bmatrix}, \Delta x = \begin{bmatrix} \Delta\hat{u} \\ \Delta\alpha \\ \Delta\theta \end{bmatrix} \text{ and } B = \begin{bmatrix} 0 \\ C_{Z_\delta} \\ C_{m_\delta} \end{bmatrix}$$

After dividing by $\Delta\delta_e$ we get:

$$\begin{bmatrix} C_{X_u} & C_{X_\alpha} & C_{Z_o} \\ C_{Z_u} & C_{Z_\alpha} & 0 \\ C_{m_u} & C_{m_\alpha} & 0 \end{bmatrix} \cdot \begin{bmatrix} \frac{\Delta\hat{u}}{\Delta\delta_e} \\ \frac{\Delta\alpha}{\Delta\delta_e} \\ \frac{\Delta\theta}{\Delta\delta_e} \end{bmatrix} + \begin{bmatrix} 0 \\ C_{Z_\delta} \\ C_{m_\delta} \end{bmatrix} = 0$$

$\frac{\Delta x}{\Delta\delta_e}$ now simply follows from

$$\frac{\Delta x}{\Delta\delta_e} = -A_{ss}^{-1} \cdot B$$

By applying Cramer's rule we find:

$$\frac{\Delta \hat{u}}{\Delta \delta_e} = \frac{\begin{vmatrix} 0 & C_{X_\alpha} & C_{Z_\alpha} \\ -C_{Z_\delta} & C_{Z_\alpha} & 0 \\ -C_{m_\delta} & C_{m_\alpha} & 0 \end{vmatrix}}{|A_{ss}|} = \frac{-C_{Z_\delta} C_{m_\alpha} + C_{m_\delta} C_{Z_\alpha}}{C_{Z_u} C_{m_\alpha} - C_{m_u} C_{Z_\alpha}}$$

If for simplicity the less usually important derivatives C_{Z_δ} and C_{m_u} are set to zero, we get:

$$\frac{\Delta \hat{u}}{\Delta \delta_e} = \frac{C_{m_\delta} C_{Z_\alpha}}{C_{Z_u} C_{m_\alpha}}$$

Substituting $C_{Z_\alpha} = -C_{N_\alpha}$, and $C_{Z_u} \approx -2C_L$ results in

$$\frac{\Delta \hat{u}}{\Delta \delta_e} = \frac{C_{m_\delta}}{2C_L} \cdot \frac{C_{N_\alpha}}{C_{m_\alpha}} \text{ or, } \frac{\Delta V}{\Delta \delta_e} = \frac{C_{m_\delta}}{2C_L} \cdot \frac{C_{N_\alpha}}{C_{m_\alpha}}.$$

After introducing:

$$C_L = \frac{W}{\frac{1}{2} \rho V_o^2 S}$$

we arrive at the well known expression for stick displacement stability:

$$\frac{d\delta_e}{dV} = \frac{4W}{\rho V_o^3 S} \cdot \frac{C_{m_\alpha}}{C_{N_\alpha}} \cdot \frac{1}{C_{m_\delta}}$$

For a statically stable aeroplane where $C_{m_\alpha} < 0$ and $\frac{d\delta_e}{dV} > 0$, which implies that for flight at a lower speed, an aft (negative) stick deflection is required.

10-1-4 Influence of various parameters on elevator trim curve

A. Influence of the center of gravity position

Using equation (10-12) the expression in equation (10-15) for the elevator trim curve can be rewritten as,

$$\delta_e = -\frac{1}{C_{m_{\delta_e}}} \left(C_{m_0} + \frac{W}{\frac{1}{2} \rho V^2 S} \frac{x_{cg} - x_{nfix}}{\bar{c}} \right) \quad (10-21)$$

The slope of the trim curve, the trim stability, follows from equations (10-18) and (10-12),

$$\frac{d\delta_e}{dV} = \frac{4W}{\rho V^3 S} \frac{1}{C_{m_{\delta_e}}} \frac{x_{cg} - x_{nfix}}{\bar{c}} \quad (10-22)$$

Equations (10-21) and (10-22) reveal the direct influence of the position of the center of gravity relative to the neutral point, stick-fixed, on the elevator angle required for equilibrium and on the elevator control position stability.

A rearward cg shift increases the elevator angle required for equilibrium, the elevator trim curve $\delta_e - V$ in figure 10-11 shifts downward. In addition when the cg shifts aft the stability margin decreases. The elevator control position stability, i.e. the slope of the trim curve, decreases, see also figure 10-11.

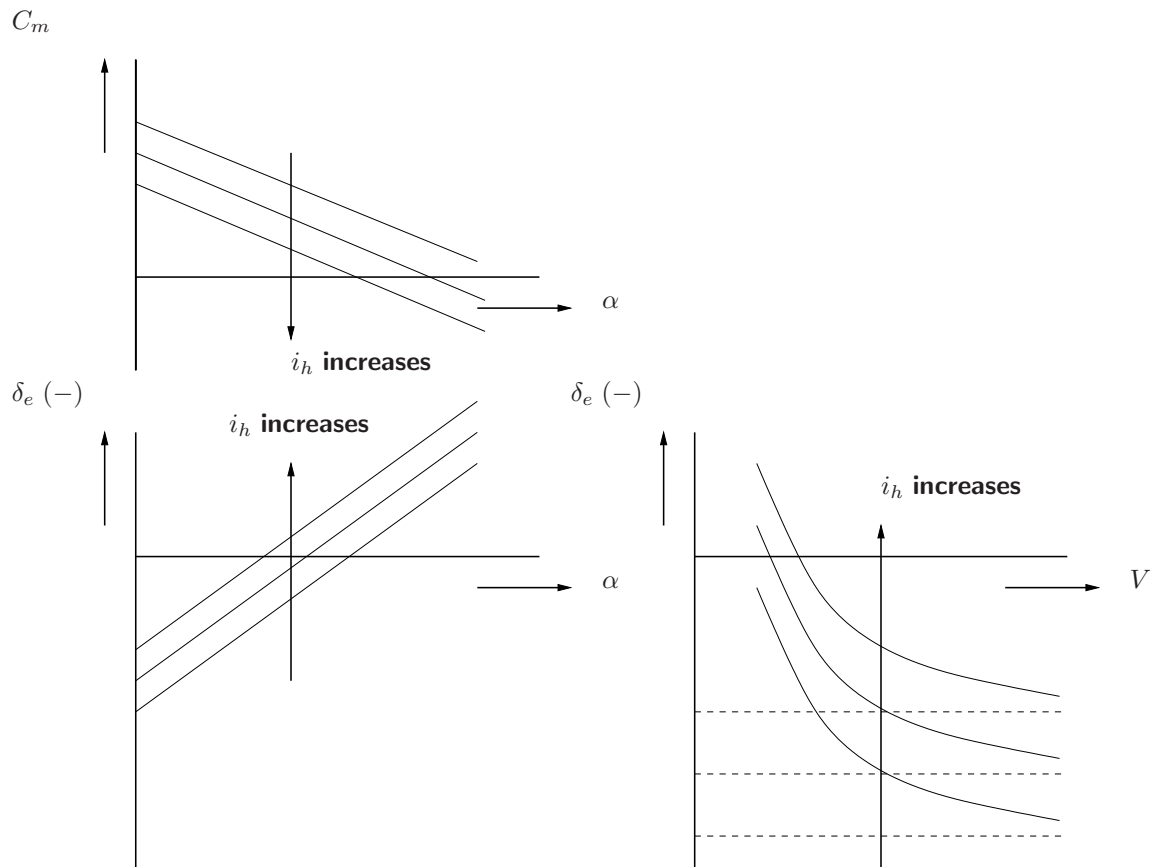


Figure 10-12: Influence of the tailplane angle of incidence on the trim curve (aircraft has control position stability)

B. Influence of the stabilizer setting

In the expression for the trim curve the part of the elevator angle independent of airspeed is obtained by letting in equation (10-21) $V = \infty$ (and by consequence $\alpha = \alpha_0$). Using equation (9-74), the resulting $\delta_{eV=\infty}$ is,

$$\delta_{eV=\infty} = -\frac{C_{m0}}{C_{m\delta_e}} = -\frac{1}{C_{m\delta_e}} \underbrace{\left\{ C_{m_{ac}} - C_{N_{h\alpha}} (\alpha_0 + i_h) \left(\frac{V_h}{V} \right)^2 \frac{S_h l_h}{S \bar{c}} \right\}}_{C_{m0}} \quad (10-23)$$

For many aircraft the stabilizer setting i_h can be varied in flight. From equation (10-23) it follows that such a change has an influence on $\delta_{eV=\infty}$. The stabilizer setting is adjusted in flight to reduce the elevator control force to zero in a given steady flight condition, see section 10-2. In such an aircraft the stabilizer thus has a function comparable to that of a trim tab. It follows from equation (10-23) that an increase of i_h (the stabilizer leading edge moves up) causes an increase in the negative sense of the part of δ_e independent of airspeed. The trailing edge of the elevator moves up as well. The simple explanation is that at constant airspeeds and cg positions the value of C_N required for equilibrium of the moment remains constant. This has been indicated schematically in figure 10-12.

C. Influence of the trim tab angle

Many aircraft, especially the smaller and slower ones, have a trim tab at the trailing edge of the elevator. If the tab angle δ_{te} is changed, the trim curve shifts parallel to itself. Qualitatively, this shift is entirely comparable to the shift caused by a change in the stabilizer angle of incidence i_h . Usually, the influence of a change in δ_{te} on the elevator trim curve is neglected, see also equation (9-60). Subfigure a of figure 10-21 shows a number of trim curves measured at constant cg positions and different trim tab angles.

D. Shape of the elevator trim curve

The shape of the trim curve not only depends on the variables discussed so far: the cg position, the stabilizer angle of incidence i_h and the trim tab angle δ_{te} . In addition, the influence of engine power setting can be appreciable, in particular for propeller-driven aircraft. Usually, an increase in engine power decreases the elevator control position stability. The Mach number effects and aeroelastic deformation can also have an important influence on the elevator trim curves, because they make the aerodynamic coefficient functions of airspeed. As noted in section 1-2 these phenomena will not be considered here.

10-1-5 Static longitudinal stability of tailless aircraft

The stability of tailless aircraft has already been discussed in section 9-1-3. It was shown, see figure 9-17, that equilibrium ($C_m = 0$) at positive values of C_N is possible only if $C_{m_{ac}} > 0$. The equilibrium is stable, i.e. $C_{m_{ac}} < 0$, if the center of gravity lies ahead of the ac,

$$x_{cg} < x_{ac} = x_w$$

By choosing a sufficiently forward cg position this condition can be satisfied. The requirement for a positive $C_{m_{ac}}$ needs a further discussion. In section 9-1-4 the following expression was derived for the $C_{m_{ac}}$ of a wing, see equation (9-30),

$$C_{m_{ac}} = \frac{2}{S\bar{c}} \left\{ \int_0^{\frac{b}{2}} c_{m_{ac}} c^2 dy - \int_0^{\frac{b}{2}} c_{\ell_b} c (x - x_0) dy \right\}$$

It is possible to obtain a positive $C_{m_{ac}}$ by choosing wing airfoil sections having a positive $c_{m_{ac}}$. Airfoils showing an S-shaped camber line possess at $c_{\ell} = 0$ a positive value for the moment coefficient. For wings having such airfoils the first integral in equation (9-30) is positive.

A second possibility to obtain a positive $C_{m_{ac}}$ is offered by the second integral in equation (9-30). As was discussed in section 9-1-4, this integral represents the moment due to the basic lift distribution. Figure 10-13 shows that this moment is positive at $C_L = 0$ for a wing having sweep back and negative wing twist.

Although it is thus shown that static longitudinal stability can be obtained without resorting to a horizontal tailplane, most aircraft nevertheless have a horizontal tailplane. The elevator of a tailless aircraft is placed at the trailing edge of the wing. The two parts of the elevator are commonly used as ailerons (or named as ‘elevons’) as well. Due to the relatively small distance to the aircraft center of gravity, elevons are less effective for pitch control than an elevator mounted on a tailplane. When the aircraft is in a trimmed condition, in general $\delta_e \neq 0$. The increased drag

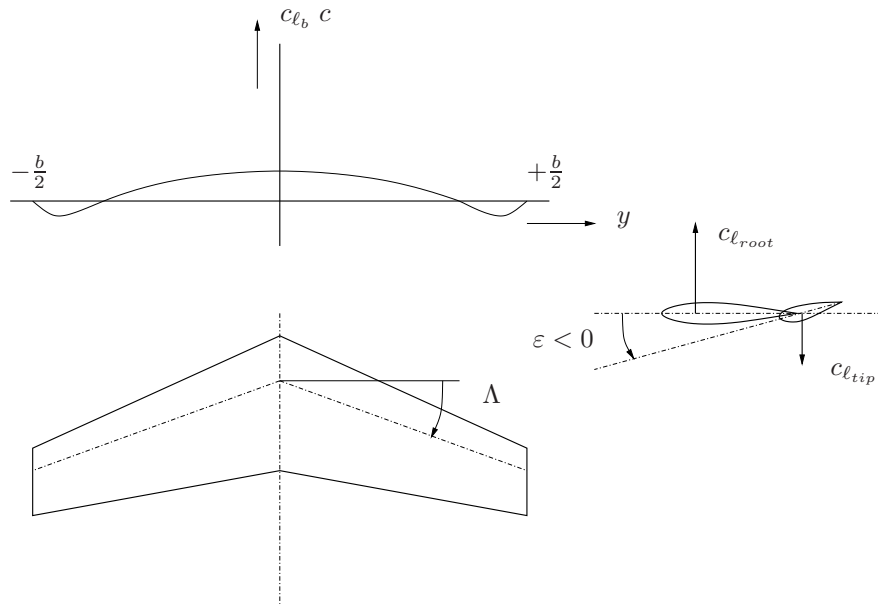


Figure 10-13: A positive $C_{m_{a.c.}}$ is obtained by combining sweepback and negative wing twist

due to the elevator deflection, called ‘trimdrag’, of the tailless aircraft may be one of the factors in favour of a design with a tailplane.

The horizontal tailplane also contributes to a considerable degree in the damping of the so-called short-period oscillation, occurring after a symmetric disturbance of the equilibrium, see chapter 5. This is an additional advantage of the horizontal tailplane.

Summarizing, it can be said that the horizontal tailplane contributes to,

- the equilibrium of the moment about the aircraft cg
- the static longitudinal stability
- the aerodynamic damping about the lateral axis

The price to be paid is, however,

- an increased aerodynamic drag
- an increased aircraft weight

10-1-6 Determination $C_{m_{\delta_e}}$ from measurements in flight

In section 9-2-6 the condition for equilibrium of the moment was written as, see equation (9-77),

$$C_m = (C_m)_{\delta_e=0} + C_{m_{\delta_e}} \delta_e$$

Suppose $C_{m_{\delta_e}}$ were known. From a trim curve, $\delta_e - V$, measured in flight the moment coefficient $(C_m)_{\delta_e=0}$ can be obtained as a function of V or α . In many cases $C_{m_{\delta_e}}$ varies markedly with flight condition, for instance under the influence of the wing wake or the slipstream. It follows that it is necessary to know $C_{m_{\delta_e}}$ in the flight conditions of interest, since a measured trim curve

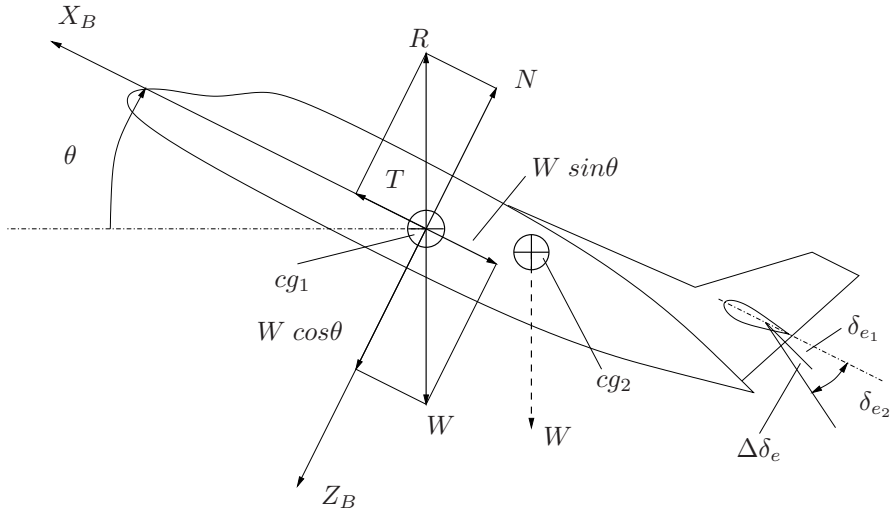


Figure 10-14: The determination of elevator efficiency from flight tests

is not a proper reflection of the moment curve $(C_m)_{\delta_e=0}$.

Methods to determine the elevator efficiency $C_{m_{\delta_e}}$ from measurements flight are all based on the principle of applying a known moment about the lateral axis in the flight conditions to be investigated. The extra elevator deflection needed to compensate for this moment is a measure of $C_{m_{\delta_e}}$ in that flight condition. The simplest manner to generate a known moment employs a shift of the center of gravity in the X -direction, for instance by shifting a known amount of ballast over a known distance.

In figure 10-14 cg positions (cg_1 and cg_2) have been indicated as well as the equilibrium at cg_1 . At constant elevator angle $\delta_e = \delta_{e1}$ no equilibrium exists about cg_2 . At constant α and δ_e , C_N does not change and it still passes through cg_1 . Equilibrium of the moment at cg_2 at constant α is obtained by changing the elevator angle. The change of the moment about cg_2 caused by $\delta_{e2} - \delta_{e1}$ is,

$$\Delta C_m = C_{m_{\delta_e}} (\delta_{e2} - \delta_{e1}) = C_{m_{\delta_e}} \Delta \delta_e$$

This moment is balanced by the moment of C_N about cg_2 , i.e.,

$$C_N \frac{x_{cg_2} - x_{cg_1}}{\bar{c}} + C_{m_{\delta_e}} (\delta_{e2} - \delta_{e1}) = 0 \quad (10-24)$$

The influence of the elevator deflection $\Delta \delta_e$ on C_N is neglected here, or,

$$\Delta C_N = C_{N_{h_\delta}} \Delta \delta_e \left(\frac{V_h}{V} \right)^2 \frac{S_h}{S} \ll C_N$$

From equation (10-24) it follows,

$$C_{m_{\delta_e}} = -\frac{1}{\Delta \delta_e} C_N \frac{\Delta x_{cg}}{\bar{c}} \quad (10-25)$$

The above means that if the trim curves have been measured at two cg positions differing in their x -coordinates, $C_{m_{\delta_e}}$ can be obtained with equation (10-25). In the foregoing the influence of the

cg position on $C_{m_{\delta_e}}$ has been neglected.

Because the tail volume $\frac{S_h l_h}{S \bar{c}}$ is obtained directly from the dimensions of the aircraft, use of equation (9-76) gives,

$$C_{N_{h_\delta}} \left(\frac{V_h}{V} \right)^2 = -C_{m_{\delta_e}} \frac{S \bar{c}}{S_h l_h} \quad (10-26)$$

The normal force gradient $C_{N_{h_\delta}}$ can only be obtained from flight tests if in addition $\left(\frac{V_h}{V} \right)^2$ has been measured along the span of the horizontal tailplane. Once the elevator efficiency $C_{m_{\delta_e}}$ has been measured as just described, the stability margin (stick fixed) can be derived from the slope of the trim curve, using equation (10-22).

If the aircraft is equipped with an adjustable stabilizer, the derivative $C_{m_{i_h}}$ can be obtained as well, once $C_{m_{\delta_e}}$ has been measured. To this end, the elevator angle required for equilibrium is measured in two flight conditions, differing only in the choice of the stabilizer angle of incidence but identical in all other respects. In section 9-2-4 the angle of attack α_h of the horizontal tailplane was derived as, see equation (9-64),

$$\alpha_h = \alpha - \varepsilon + i_h$$

From this expression it follows that if flight conditions do not change (both α and ε remain constant) a change in i_h influences only α_h , as expressed by,

$$\Delta \alpha_h = \Delta i_h$$

At constant α and ε , C_{N_h} has to remain constant as well to maintain the same steady flight conditions, where $C_m = 0$,

$$C_{N_h} = C_{N_{h_\alpha}} \alpha_h + C_{N_{h_\delta}} \delta_e = \text{constant}$$

or,

$$C_{N_{h_\alpha}} \Delta \alpha_h + C_{N_{h_\delta}} \Delta \delta_e = 0$$

The result is,

$$C_{N_{h_\alpha}} = -\frac{\Delta \delta_e}{\Delta i_h} C_{N_{h_\delta}}$$

As mentioned before, in general $C_{N_{h_\delta}} \cdot \left(\frac{V_h}{V} \right)^2$ will be determined, rather than C_{N_h} . If $\left(\frac{V_h}{V} \right)^2$ is not known, the procedure just described can only produce $C_{N_{h_\alpha}} \cdot \left(\frac{V_h}{V} \right)^2$,

$$C_{N_{h_\alpha}} \left(\frac{V_h}{V} \right)^2 = -\frac{\Delta \delta_e}{\Delta i_h} C_{N_{h_\delta}} \left(\frac{V_h}{V} \right)^2$$

By way of illustration, the following gives an example of the determination of stability characteristics from measured elevator trim curves. The aircraft in the example is a Fokker F-27, the measured trim curves were taken from reference [52]. Figure 10-15 shows two elevator trim curves $\delta_e - V_e$. They were measured at an engine power of 420 hp (approximately gliding flight) and a trim tab angle of $\delta_{t_e} = +4.5^\circ$. Apart from cg positions also the aircraft weight was different. For

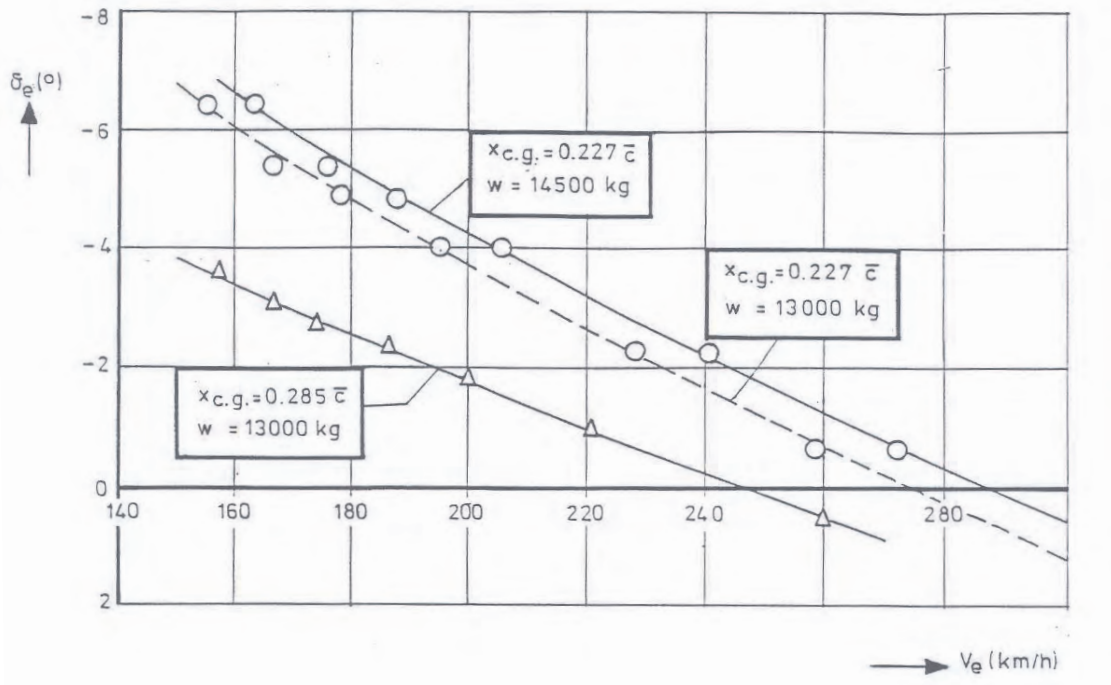


Figure 10-15: Trim curves for two cg positions of the Fokker F-27 (from reference [52])

this reason, the trim curve for $x_{cg} = 0.227 \bar{c}$, pertaining to an aircraft weight of 14,500 kg, was corrected to a weight of 13,000 kg. At a constant flight condition, i.e. at constant C_N and δ_e , the following holds,

$$V_{e2} = V_{e1} \sqrt{\frac{W_2}{W_1}}$$

The trim curve thus corrected is also shown in figure 10-15. In the first place $C_{m_{\delta_e}}$ is derived from the two trim curves belonging to the same aircraft weight of 13,000 kg. At $V_e = 240$ km/h, figure 10-15 shows that $\Delta\delta_e = 1.4^\circ$. The shift in cg position is $\frac{\Delta x_{cg}}{\bar{c}} = 0.058$.

At an aircraft weight of 13,000 kg the airspeed of $V_e = 240$ km/h corresponds to a normal force coefficient of $C_N = 0.681$. From equation (10-25) it then follows,

$$C_{m_{\delta_e}} = -\frac{1}{1.4} \cdot 0.681 \cdot 0.058 = -0.0282$$

with δ_e in degrees.

The tailplane volume of the present aircraft is $\frac{S_h l_h}{S \bar{c}}$. Using this value at $V_e = 240$ km/h it follows with equation (10-26),

$$C_{N_{h_\delta}} \left(\frac{V_h}{V} \right)^2 = +0.0303 \quad (\delta_e \text{ in degrees})$$

$$C_{N_{h_\delta}} \left(\frac{V_h}{V} \right)^2 = +1.7353 \quad (\delta_e \text{ in radians})$$

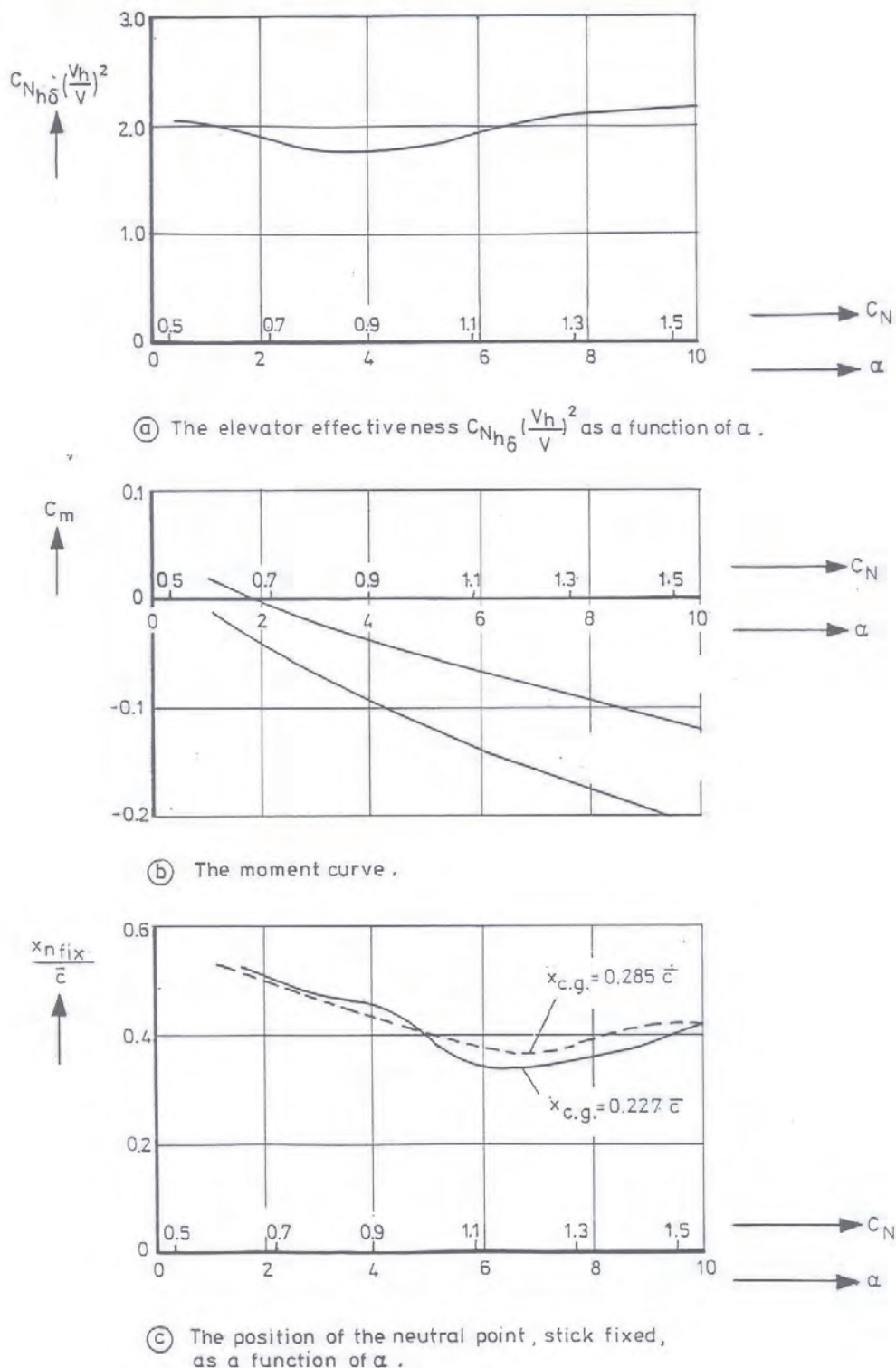


Figure 10-16: Some stability characteristics derived from the measured trim curves shown in figure 10-15 (Fokker F-27)

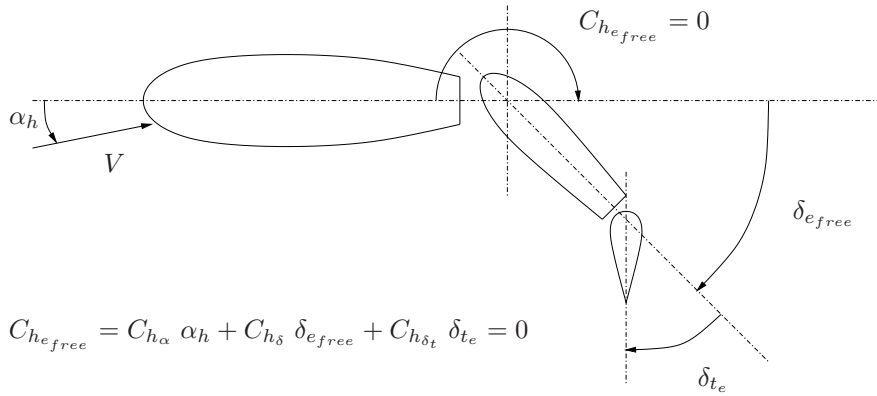


Figure 10-17: The equilibrium of the free elevator

Next, the position of the neutral point, stick fixed is derived by means of equation (10-22). Again at $V_e = 240$ km/h is $\frac{4W}{\rho_0 V_e^3 S} = 0.0204$ and at $x_{cg} = 0.277 \bar{c}$ the slope of the elevator trim curve is $\frac{d\delta_e}{dV_e} = +0.0502^\circ/\text{km/h}$ or $+0.187^\circ/\text{m/s}$. This results in,

$$\frac{x_{cg} - x_{n_fix}}{\bar{c}} = -0.187 \cdot 0.0282 \cdot 48.9 = -0.258$$

With $x_{cg} = 0.277 \bar{c}$ follows $x_{n_fix} = 0.485 \bar{c}$. If the same calculation is repeated for the trim curve measured at $x_{cg} = 0.285 \bar{c}$, the result is $x_{n_fix} = 0.490 \bar{c}$. Using the data obtained thus far the moment curves C_m versus V and C_m versus C_N can be derived. If in addition the relation C_N versus α of the aircraft is known, the moment curves C_m versus α can be calculated as well. Figure 10-16a shows the calculated values of $C_{N_{h_\alpha}} \cdot (\frac{V_h}{V})^2$ as a function of α . Figure 10-16b gives the C_m versus α curves and figure 10-16c shows the position of the neutral point, stick fixed, as a function of α and C_N .

10-2 Stick Free Static Longitudinal Stability

It was already noted in the previous section that it makes sense to study the static stability in the case of stick free. Two reasons can be given to study the static stability in this condition. The first is the requirement for the aircraft to remain stable if the pilot would release the stick. The second reason lies in the close relationship between the static stability, with stick free, and a certain characteristic of the way in which the elevator force required to maintain the elevator in the position for steady flight, varies with airspeed. This characteristic will be called the elevator stick (or control) force stability.

As in section 10-1, the concept of static stability is based entirely on the variation of the pitching moment with angle of attack. Leaving the elevator free only changes the contribution of the horizontal tailplane, and the elevator, to the pitching moment.

First we consider the behavior of the elevator in the control free situation. If the control stick or wheel is free, the control force F_e is zero. Neglecting the friction in the control mechanism this means that in the stick free situation the hinge moment is zero, $H_e = 0$, or,

$$C_{h_{e_free}} = 0$$

In this situation the elevator angle assumes a certain value, depending on the way the elevator is aerodynamically balanced and on the trim tab angle. This elevator angle, stick free, indicated as

$\delta_{e_{free}}$ see figure 10-17, varies with angle of attack. If the airfoil of the tailplane is symmetric, see equation (9-63), $C_{h_0} = 0$ and then,

$$C_{h_{e_{free}}} = C_{h_\alpha} \alpha_h + C_{h_\delta} \delta_{e_{free}} + C_{h_{\delta_t}} \delta_{t_e} = 0$$

This means that $\delta_{e_{free}}$ becomes,

$$\delta_{e_{free}} = -\frac{C_{h_\alpha}}{C_{h_\delta}} \alpha_h - \frac{C_{h_{\delta_t}}}{C_{h_\delta}} \delta_{t_e} \quad (10-27)$$

Differentiation with respect to α_h results in the variation of $\delta_{e_{free}}$, with α_h at constant trim tab angle,

$$\left(\frac{d\delta_e}{d\alpha_h} \right)_{free} = -\frac{C_{h_\alpha}}{C_{h_\delta}}$$

and the variation with α ,

$$\left(\frac{d\delta_e}{d\alpha} \right)_{free} = -\frac{C_{h_\alpha}}{C_{h_\delta}} \frac{d\alpha_h}{d\alpha} \quad (10-28)$$

Using equation (9-66),

$$\frac{d\alpha_h}{d\alpha} = 1 - \frac{d\varepsilon}{d\alpha}$$

results in,

$$\left(\frac{d\delta_e}{d\alpha} \right)_{free} = -\frac{C_{h_\alpha}}{C_{h_\delta}} \left(1 - \frac{d\varepsilon}{d\alpha} \right) \quad (10-29)$$

10-2-1 Stick free static longitudinal stability in gliding flight

The contribution of the horizontal tailplane to the pitching moment is, see equations (9-60) and (10-5),

$$C_{m_h} = - \left(C_{N_{h_\alpha}} \alpha_h + C_{N_{h_\delta}} \delta_e \right) \left(\frac{V_h}{V} \right)^2 \frac{S_h l_h}{S \bar{c}} \quad (10-30)$$

When studying the static longitudinal stability in section 10-1, the elevator control was assumed to be held fixed, the elevator angle δ_e was constant and did not change when α was slightly varied. If, however, in equation (10-30) the constant δ_e is replaced by the variable $\delta_{e_{free}}$, differentiation with respect to α results in the contribution of the horizontal tailplane with free elevator to the static longitudinal stability, stick free, $C_{m_{\alpha_{free}}}$,

$$\left(\frac{dC_{m_h}}{d\alpha} \right)_{free} = C_{m_{\alpha_{free}}} = - \left(C_{N_{h_\alpha}} \frac{d\alpha_h}{d\alpha} + C_{N_{h_\delta}} \left(\frac{d\delta_e}{d\alpha} \right)_{free} \right) \left(\frac{V_h}{V} \right)^2 \frac{S_h l_h}{S \bar{c}} \quad (10-31)$$

Substituting equation (9-66),

$$\frac{d\alpha_h}{d\alpha} = \left(1 - \frac{d\varepsilon}{d\alpha}\right)$$

and equation (10-29),

$$\left(\frac{d\delta_e}{d\alpha}\right)_{free} = -\frac{C_{h_\alpha}}{C_{h_\delta}} \left(1 - \frac{d\varepsilon}{d\alpha}\right)$$

results in,

$$C_{m_{\alpha_h free}} = -\left(C_{N_{h_\alpha}} - C_{N_{h_\delta}} \frac{C_{h_\alpha}}{C_{h_\delta}}\right) \left(1 - \frac{d\varepsilon}{d\alpha}\right) \left(\frac{V_h}{V}\right)^2 \frac{S_h l_h}{S \bar{c}} \quad (10-32)$$

If equation (10-32) is compared with the corresponding expression (10-7) for the contribution of the horizontal tailplane in the stick fixed situation, when $\delta_e = 0$ is constant,

$$C_{m_{\alpha_h fix}} = -C_{N_{h_\alpha}} \left(1 - \frac{d\varepsilon}{d\alpha}\right) \left(\frac{V_h}{V}\right)^2 \frac{S_h l_h}{S \bar{c}}$$

the concept of the normal force gradient of the tailplane in the stick free situation arises,

$$C_{N_{h_\alpha free}} = C_{N_{h_\alpha}} - C_{N_{h_\delta}} \frac{C_{h_\alpha}}{C_{h_\delta}} \quad (10-33)$$

Using this gradient in equation (10-32) results in close analogy with equation (10-7),

$$C_{m_{\alpha_h free}} = -C_{N_{h_\alpha free}} \left(1 - \frac{d\varepsilon}{d\alpha}\right) \left(\frac{V_h}{V}\right)^2 \frac{S_h l_h}{S \bar{c}} \quad (10-34)$$

The static stability, stick free, $C_{m_{\alpha_h free}}$, follows by adding to equation (10-34) the contribution of the wing, fuselage and nacelles,

$$C_{m_{\alpha free}} = C_{N_{w_\alpha}} \frac{x_{cg} - x_w}{\bar{c}} - C_{N_{h_\alpha free}} \left(1 - \frac{d\varepsilon}{d\alpha}\right) \left(\frac{V_h}{V}\right)^2 \frac{S_h l_h}{S \bar{c}} \quad (10-35)$$

Previously, the static stability, stick fixed, was derived as,

$$C_{m_\alpha} = C_{N_{w_\alpha}} \frac{x_{cg} - x_w}{\bar{c}} - C_{N_{h_\alpha}} \left(1 - \frac{d\varepsilon}{d\alpha}\right) \left(\frac{V_h}{V}\right)^2 \frac{S_h l_h}{S \bar{c}}$$

The expressions (9-75), (10-35) and (10-33) for $C_{N_{h_\alpha free}}$ indicate that the difference between the static stability stick fixed and stick free is entirely due to the term $C_{N_{h_\delta}} \frac{C_{h_\alpha}}{C_{h_\delta}}$. In this term $C_{N_{h_\delta}}$ is positive. The hinge moment derivatives C_{h_α} and C_{h_δ} were already discussed in chapter 9. They depend on the way the elevator is aerodynamically balanced. To keep the control forces at reasonably low levels, it is essential that both C_{h_α} and C_{h_δ} are made small in the absolute sense.

The required sign of C_{h_δ} follows from the behaviour of the free elevator in steady, trimmed flight, i.e. the situation where $F_e = 0$. In that situation $C_{h_e} = 0$. Suppose the elevator now obtains a small deviation $d\delta_e$ from the equilibrium position, due to some disturbance. The immediate effect is a hinge moment,

$$dC_{h_e} = C_{h_\delta} d\delta_e$$

if $C_{h_\delta} > 0$, the hinge moment will be positive if $d\delta_e$ is positive. Due to the hinge moment the change in elevator angle will further increase. The general conclusion is that an equilibrium position of a control surface in the controls free condition will be unstable if C_{h_δ} is positive; the control surface does not return to the equilibrium position after a disturbance has occurred. For this reason it is strictly necessary that C_{h_δ} is negative.

The above argument needs a slight extension. Suppose a control surface has a C_{h_δ} nearly equal to zero. In such a case actually two hinge moments are present, of nearly equal magnitude but of opposite sign, see the pressure distribution in figure 9-67. The resultant value of C_{h_δ} is due to the difference of these two hinge moments. A small variation in one of these moments, as may be caused by a small change in the shape of the control surface, due for instance to the tolerance in the manufacturing process, will have a large effect on C_{h_δ} if compared to the intended value. For this reason C_{h_δ} has to be not only negative, but should not be allowed to approach zero too closely. Common values are: $-0.2 \text{ to } -0.3 < C_{h_\delta} < -0.1$ (δ_e in Radians).

The sign of C_{h_δ} will be discussed in detail in section 10-2-3 in relation with the elevator control force stability. Here it can be said that C_{h_α} may be either negative or positive. Too large positive values of C_{h_α} , e.g. $C_{h_\alpha} >$ approximately 0.1 (with α_h in Radians), cannot be used because they may lead to dynamic instability, stick free. In the decision on the required values of C_{h_α} and C_{h_δ} the influence which ice accretion on the stabilizer and elevator has on the aerodynamic balance of the control surface, has to be taken into account as well. In the final choice of the elevator balance the non-linear relation between the hinge moment and α_h and δ_e at large angles is an additional important consideration.

From equations (10-33) and (10-35) it can be seen that depending on the sign of C_{h_α} the aircraft with free elevator control will be less statically stable ($C_{h_\alpha} < 0$), equally stable ($C_{h_\alpha} = 0$) or more stable ($C_{h_\alpha} > 0$) than it is in the control fixed situation.

10-2-2 Neutral point, stick free

As for the aircraft with fixed elevator control a certain center of gravity position exists also in the control free situation where C_{m_α} , here $C_{m_{\alpha_{free}}}$, is equal to zero. This center of gravity position is called the neutral point, stick free, indicated as $n.p._{free}$. The abscissa of this point is $x_{n_{free}}$. As in equation (10-11) the position of the neutral point, stick free, is obtained by letting $C_{m_{\alpha_{free}}} = 0$, see equation (10-35),

$$\frac{x_{n_{free}} - x_w}{\bar{c}} = \frac{C_{N_{\alpha_{free}}}}{C_{N_\alpha}} \left(1 - \frac{d\varepsilon}{d\alpha}\right) \left(\frac{V_h}{V}\right)^2 \frac{S_h l_h}{S \bar{c}} \quad (10-36)$$

Just like the neutral point, stick fixed, the neutral point, stick free, can be interpreted in a second way, in addition to the one just given. It is the point of action (on the m.ac) of the total change in normal force coefficient dC_N due to a change in angle of attack $d\alpha$ if the elevator control is left free.

In analogy with equation (10-12) it follows,

$$C_{m_{\alpha_{free}}} = C_{N_{\alpha_{free}}} \frac{x_{cg} - x_{n_{free}}}{\bar{c}}$$

with,

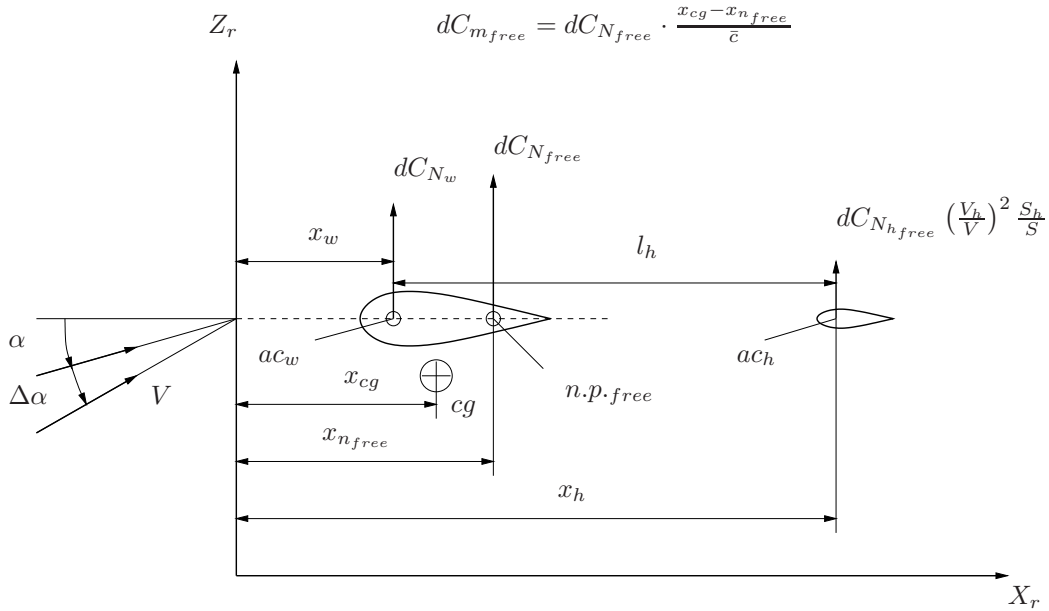


Figure 10-18: The change in the moment dC_{m_free} due to a change in angle of attack $\Delta\alpha$

$$C_{N_{\alpha_free}} \approx C_{N_{\alpha_fix}}$$

The latter expression is obtained by neglecting in equation (10-10) the difference in normal force gradient C_{N_α} due to the difference between $C_{N_{h_\alpha}}$ and $C_{N_{h_\alpha free}}$, as the contribution of the tailplane to C_{N_α} is relatively small when compared to the contribution of the wing.

The change in pitching moment dC_{m_free} due to a change in angle of attack $d\alpha$ with free elevator control then is,

$$dC_{m_free} = dC_{N_free} \frac{x_{cg} - x_{n_free}}{\bar{c}} \quad (10-37)$$

Figure 10-18 gives an illustration of this second interpretation of the neutral point, stick free.

The relative position of the two neutral points, stick fixed and stick free, follows from equations (10-11) and (10-36),

$$\frac{x_{n_free} - x_{n_fix}}{\bar{c}} = \frac{C_{N_{h_\alpha free}} - C_{N_{h_\alpha fix}}}{C_{N_\alpha}} \left(1 - \frac{d\varepsilon}{d\alpha}\right) \left(\frac{V_h}{V}\right)^2 \frac{S_h l_h}{S \bar{c}} \quad (10-38)$$

Using equation (10-33),

$$C_{N_{h_\alpha free}} = C_{N_{h_\alpha}} - C_{N_{h_\delta}} \frac{C_{h_\alpha}}{C_{h_\delta}}$$

the result is,

$$\frac{x_{n_free} - x_{n_fix}}{\bar{c}} = -\frac{C_{N_{h_\delta}}}{C_{N_\alpha}} \frac{C_{h_\alpha}}{C_{h_\delta}} \left(1 - \frac{d\varepsilon}{d\alpha}\right) \left(\frac{V_h}{V}\right)^2 \frac{S_h l_h}{S \bar{c}} = \frac{C_{m_\delta}}{C_{N_\alpha}} \frac{C_{h_\alpha}}{C_{h_\delta}} \left(1 - \frac{d\varepsilon}{d\alpha}\right) \quad (10-39)$$

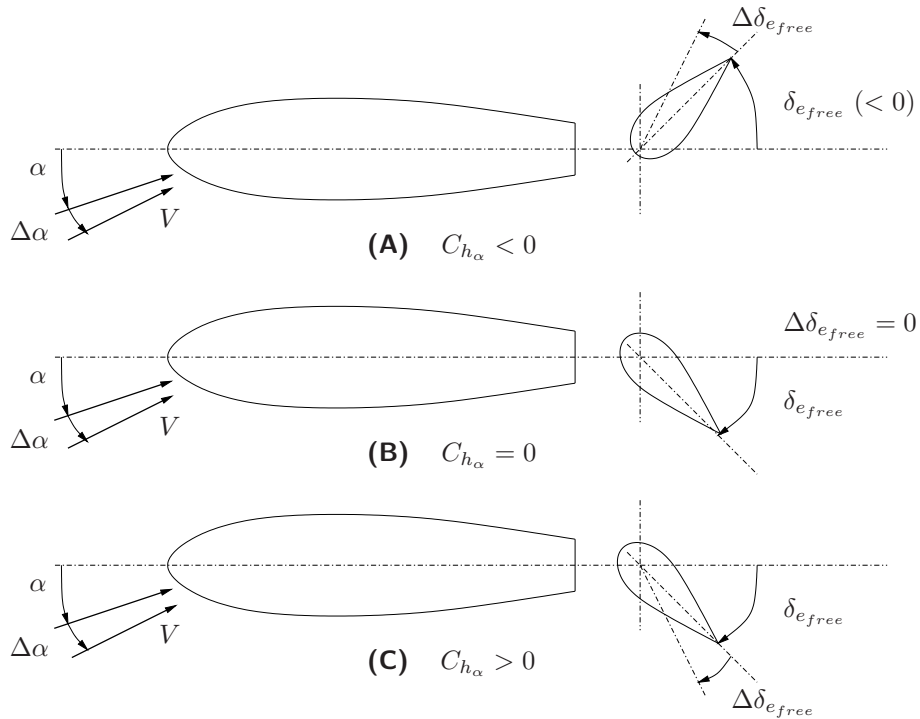


Figure 10-19: The behaviour of the free elevator after a change of the angle of attack

According to this latter expression the relative position of the two neutral points is determined primarily by the sign of C_{h_α} . A simple explanation of the influence of the sign of C_{h_α} on the static stability, stick free, is possible by looking at the behaviour of the free elevator, see figure 10-19. If $C_{h_\alpha} = 0$ the elevator angle $\delta_{e_{free}}$ does not vary with angle of attack according to equation (10-29). It is as if the controls were fixed, see subfigure b of figure 10-19. There is no difference between the static stability stick fixed and stick free, the two neutral points coincide.

If $C_{h_\alpha} < 0$ the elevator turns with the direction of the flow as the angle of attack varies, see subfigure a of figure 10-19. With an increase in angle of attack the trailing edge of the elevator moves up. The effect of freeing the elevator control is an extra downward force on the tailplane. This extra force promotes a further increase in angle of attack. As a consequence the static stability stick free is less than it is for stick fixed and $x_{n_{free}}$ is smaller than $x_{n_{fix}}$, if $C_{h_\alpha} < 0$. The influence of a positive C_{h_α} can be understood in the same way, see subfigure c of figure 10-19.

10-2-3 Elevator stick force curves and elevator stick force Stability

A. The control force curve

The elevator control force needed for equilibrium was derived in chapter 9 as,

$$F_e = -\frac{d\delta_e}{ds_e} \frac{1}{2} \rho V_h^2 S_e \bar{c}_e C_{h_e}$$

The following discussion is intended primarily for qualitative purposes. It is, therefore, permissible to express C_{h_e} here as a linear function of α_h , δ_e and δ_{t_e} , see equation (9-63). This leads to the following expression for F_e , see also equation (9-83),

$$F_e = -\frac{d\delta_e}{ds_e} \frac{1}{2} \rho V_h^2 S_e \bar{c}_e (C_{h_\alpha} \alpha_h + C_{h_\delta} \delta_e + C_{h_{\delta_t}} \delta_{t_e})$$

For a more accurate calculation of the control force in a given flight condition C_{h_e} has to be obtained from wind tunnel measurements for the correct values of α_h , δ_e and δ_{t_e} . In chapter 9 α_h was derived as, see equation (9-65),

$$\alpha_h = (\alpha - \alpha_0) \left(1 - \frac{d\varepsilon}{d\alpha} \right) + (\alpha_0 + i_h)$$

The elevator angle δ_e required for equilibrium about the lateral axis is, see equation (9-80),

$$\delta_e = -\frac{1}{C_{m_{\delta_e}}} \left\{ C_{m_0} + C_{m_{\alpha_{fix}}} (\alpha - \alpha_0) \right\}$$

Substitution of equations (9-65) and (9-80) in equation (9-83) results after some elaboration in,

$$F_e = -\frac{d\delta_e}{ds_e} \frac{1}{2} \rho V_h^2 S_e \bar{c}_e \left\{ C'_{h_0} + C'_{h_\alpha} (\alpha - \alpha_0) \right\} \quad (10-40)$$

where,

$$C'_{h_0} = -\frac{C_{h_\delta}}{C_{m_\delta}} C_{m_{ac}} - \frac{C_{h_\delta}}{C_{N_{h_\delta free}}} C_{N_{h_\delta free}} (\alpha_0 + i_h) + C_{h_{\delta_t}} \delta_{t_e} \quad (10-41)$$

$$\begin{aligned} C'_{h_\alpha} &= C_{h_\alpha} \left(1 - \frac{d\varepsilon}{d\alpha} \right) - \frac{C_{h_\delta}}{C_{m_\delta}} C_{m_{\alpha_{fix}}} = -\frac{C_{h_\delta}}{C_{m_\delta}} C_{m_{\alpha_{free}}} \\ &= -\frac{C_{h_\delta}}{C_{m_\delta}} C_{N_\alpha} \frac{x_{cg} - x_{n_{free}}}{\bar{c}} \end{aligned} \quad (10-42)$$

Furthermore,

$$(\alpha - \alpha_0) \approx \frac{W}{\frac{1}{2} \rho V^2 S} \frac{1}{C_{L_\alpha}} \approx \frac{W}{\frac{1}{2} \rho V^2 S} \frac{1}{C_{N_\alpha}} \quad (10-43)$$

Substituting equation (10-43) in equation (10-40) results in,

$$F_e = -\frac{d\delta_e}{ds_e} S_e \bar{c}_e \left(\frac{V_h}{V} \right)^2 \left(C'_{h_0} \frac{1}{2} \rho V^2 + C'_{h_\alpha} \frac{W}{S} \frac{1}{C_{N_\alpha}} \right) \quad (10-44)$$

According to equation (10-44) the elevator control force required to maintain steady flight consists of two parts. One is proportional to the dynamic pressure and thus varies with airspeed. The other part is independent of airspeed. The part depending on airspeed is considered first. It can be seen from equations (10-44) and (10-41) that this part varies by changing the trim tab angle or the stabilizer angle of incidence or both. Now suppose that i_h is constant. At a certain value of δ_{t_e} , C'_{h_0} will be equal to zero. This particular trim tab angle is called $\delta_{t_{e_0}}$. It is derived from equation (10-41) by letting,

$$C'_{h_0} = 0$$

The result is,

$$\delta_{t_{e_0}} = \frac{\frac{C_{h_\delta}}{C_{m_\delta}} C_{m_{ac}} + \frac{C_{h_\delta}}{C_{N_{h_\delta free}}} C_{N_{h_\delta free}} (\alpha_0 + i_h)}{C_{h_{\delta_t}}} \quad (10-45)$$

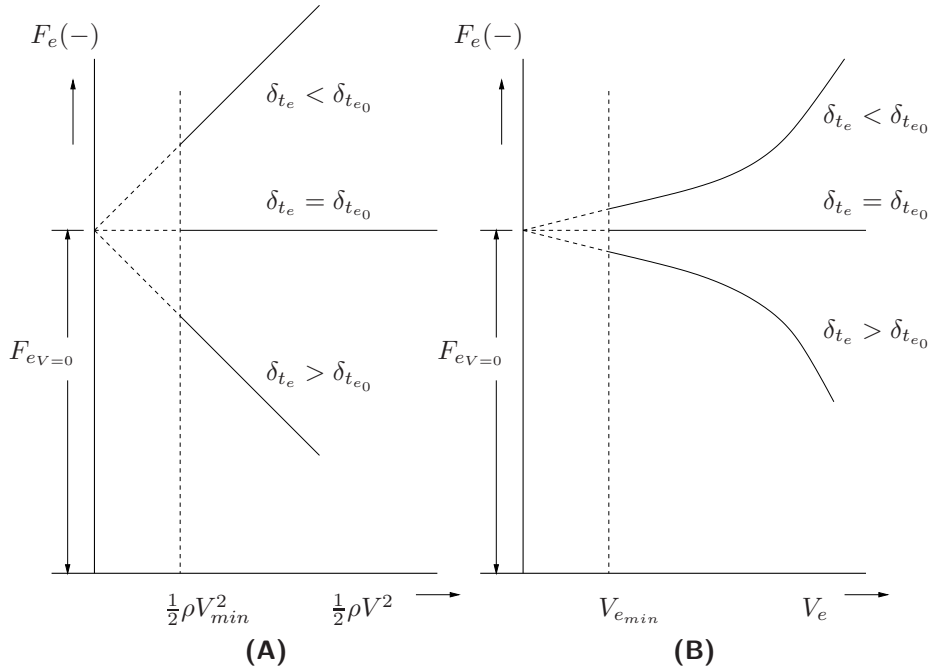


Figure 10-20: Schematic form of the elevator control force curve, F_e as a function of (a) dynamic pressure $\frac{1}{2}\rho V^2$ and (b) F_e as a function of equivalent airspeed V_e

Using equations (10-41) and (10-45), C'_{h_0} can now be written as,

$$C'_{h_0} = C_{h_{\delta_t}} (\delta_{te} - \delta_{te_0}) \quad (10-46)$$

After some elaboration the final expression for the elevator control force can now be obtained from equation (10-44), using equations (10-46) and (10-42). The result is,

$$F_e = \frac{d\delta_e}{ds_e} S_e \bar{c}_e \left(\frac{V_h}{V} \right)^2 \left\{ \frac{W}{S} \frac{C_{h_\delta}}{C_{m_{\delta_e}}} \frac{x_{cg} - x_{n_{free}}}{\bar{c}} - \frac{1}{2} \rho V^2 C_{h_{\delta_t}} (\delta_{te} - \delta_{te_0}) \right\} \quad (10-47)$$

The variation of the elevator control force with dynamic pressure or airspeed as expressed by equation (10-47) is shown schematically in figure 10-20. Negative elevator control forces, i.e. pull forces exerted by the pilot, are plotted upward in the figure, just like negative elevator angles. If the various aerodynamic characteristics in equation (10-47) may indeed be considered as constants, then F_e varies linearly with the dynamic pressure $\frac{1}{2}\rho V^2$, see subfigure a of figure 10-20, or quadratically with V , see subfigure b of figure 10-20. The measured trim curves and elevator control force curves shown in figure 10-21 show that in reality the various simplifying assumptions are not always satisfied.

The second part of the elevator control force is independent of airspeed, it is indicated as $F_{eV=0}$. According to equation (10-47) this part is determined by the position of the cg relative to the n.p._{free} or by the sign of the static stability, stick free. If the aircraft is statically stable, stick free ($x_{cg} < x_{n_{free}}$), $F_{eV=0}$ is negative.

The variation of the part of F_e depending on airspeed is determined by δ_{te} . If $\delta_{te} = \delta_{te_0}$, F_e does not vary with airspeed. If $\delta_{te} > \delta_{te_0}$ the control force increases in the positive sense with increasing airspeed, see figure 10-20, independent of the cg position. It was assumed that C_{h_δ} ,

$C_{m_{\delta_e}}$ and $C_{h_{\delta_t}}$ have the normal, negative sign.

The airspeed at which the control force is zero, is called the trim speed, indicated as V_{tr} . So,

$$V_{tr} = V_{F_e=0}$$

If the elevator control is let free at this airspeed, the control position does not change.

B. Elevator stick force stability

If the elevator control force curve at the trim speed satisfies the condition,

$$\left(\frac{dF_e}{dV} \right)_{F_e=0} > 0 \quad (10-48)$$

the aircraft is said to have elevator control force stability in that particular flight condition. Elevator control force stability is thus seen to depend only on the slope of the control force curve in the trimmed, i.e. $F_e = 0$, condition.

The expression will now be further analyzed. Differentiating equation (10-47) with respect to V yields the slope of the control force curve as,

$$\frac{dF_e}{dV} = -\frac{d\delta_e}{ds_e} S_e \bar{c}_e \left(\frac{V_h}{V} \right)^2 \rho V C_{h_{\delta_t}} (\delta_{t_e} - \delta_{t_{e0}}) \quad (10-49)$$

This expression holds for both trimmed and untrimmed conditions. The elevator control force stability follows by substituting in equation (10-49) the values of δ_{t_e} pertaining to V_{tr} . The trim speed V_{tr} is obtained from equation (10-47) by letting $F_e = 0$,

$$\frac{1}{2} \rho V_{tr}^2 C_{h_{\delta_t}} (\delta_{t_e} - \delta_{t_{e0}}) = \frac{W}{S} \frac{C_{h_{\delta_t}}}{C_{m_{\delta_e}}} \frac{x_{cg} - x_{n_{free}}}{\bar{c}} \quad (10-50)$$

Combining equations (10-49) and (10-50) results in the elevator control force stability,

$$\left(\frac{dF_e}{dV} \right)_{F_e=0} = -2 \frac{d\delta_e}{ds_e} S_e \bar{c}_e \left(\frac{V_h}{V} \right)^2 \frac{W}{S} \frac{C_{h_{\delta_t}}}{C_{m_{\delta_e}}} \frac{x_{cg} - x_{n_{free}}}{\bar{c}} \frac{1}{V_{tr}} \quad (10-51)$$

The direct relation between the control force stability as defined in equation (10-48) and the position of cg relative to the $n.p._{free}$ position can be seen from equation (10-51). If the aircraft is statically stable, stick free, it is control force stable according to equation (10-51) and vice versa.

Just like the control position stability, discussed in section 10-1, control force stability is important in two respects,

1. In the first place, the control force stability provides the possibility to ascertain from measurements in flight if the aircraft is statically stable, stick free, in a certain aircraft configuration and flight condition, see equation (10-51).
2. In the second place, and perhaps most important, an aircraft that is control force stable is more pleasant and safer to fly by the pilot. The latter subject will now be discussed.

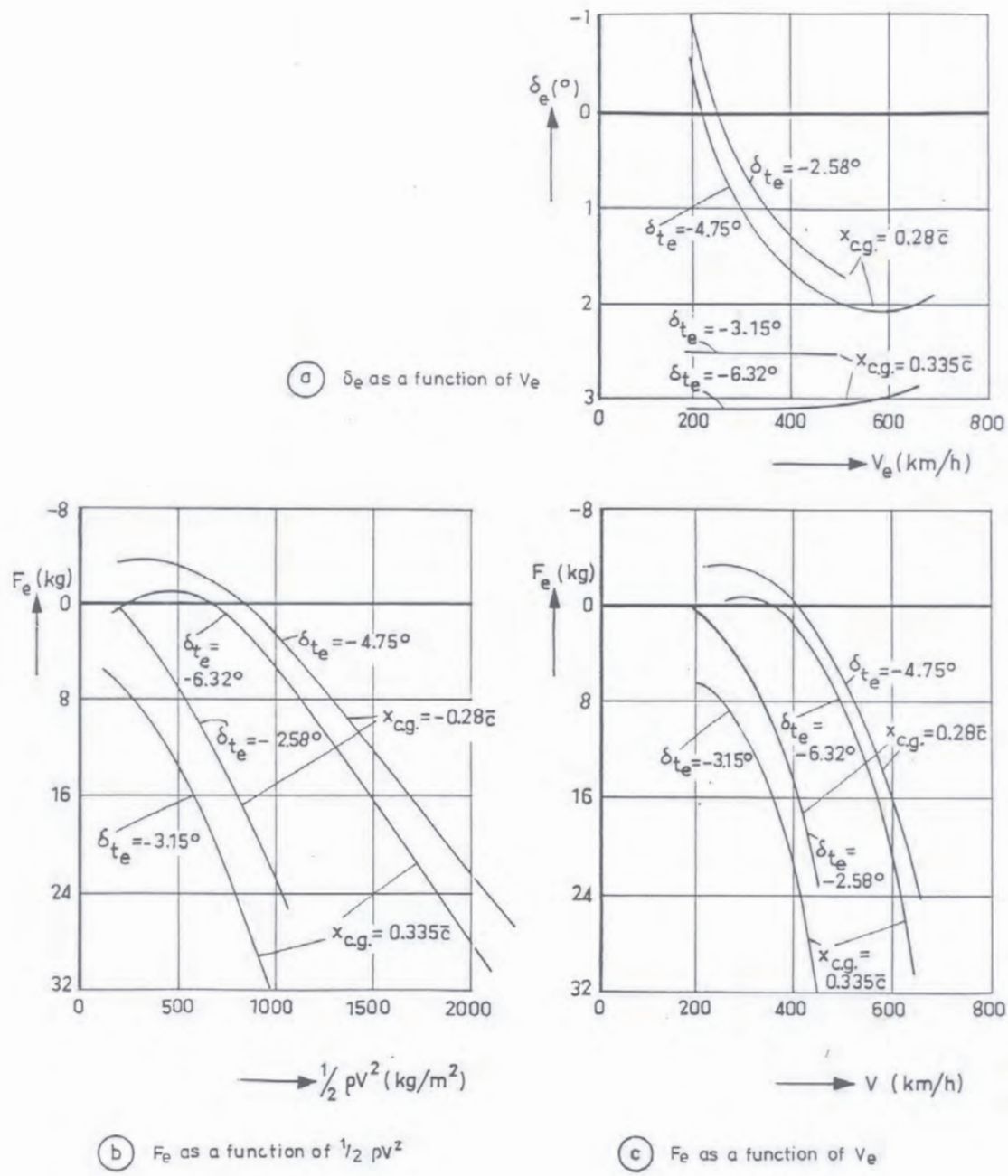


Figure 10-21: Measured trim curves and elevator control force curves for the De Havilland D.H.98 'Mosquito' M II F in gliding flight (from reference [27])

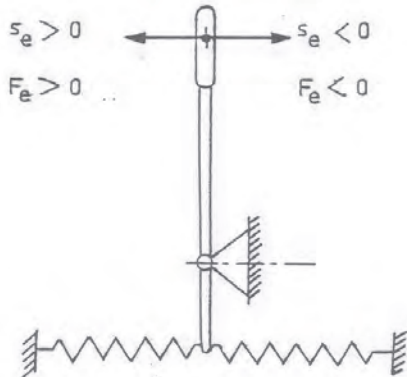


Figure 10-22: Schematic representation of the concept of 'positive feel', $\frac{dF_e}{ds_e}$

As a general rule it can be stated that it is highly desirable, if not imperative, that control displacements and the control forces required to generate and maintain these displacements both in manoeuvres and in steady flight conditions, have equal directions. This requirement can be expressed simply as,

$$\frac{dF_e}{ds_e} > 0 \quad (10-52)$$

The control manipulator, whether it is a stick or a wheel, then behaves as if it were pulled back to the neutral position by springs, see figure 10-22. The effect to the pilot is that he feels through the force he has to apply on the control manipulator in which direction and to what extent he has deflected the control. Generally it can be said that the pilot is far more sensitive to changes in the control forces he has to exert than to changes in the control column displacement.

Due to the adapted sign convention $\frac{d\delta_e}{ds_e} > 0$, the requirement as in equation (10-52) can then be written as,

$$\frac{dF_e}{d\delta_e} > 0$$

It was argued in subsection B of section 10-1-3 that the initial and the ultimate control displacement should be in the same direction. From the above it follows that this applies equally to the changes in the exerted control force.

Using the same sign convention for control displacements and control forces and considering the requirement for elevator control position stability, see equation (10-19),

$$\frac{d\delta_e}{dV} > 0$$

the corresponding requirement for elevator stick force stability is written as in equation (10-48),

$$\left(\frac{dF_e}{dV} \right)_{F_e=0} > 0$$

Inevitably, the control mechanism of the aircraft has a certain friction which was neglected so far. The magnitude of this friction, which is primarily static friction, has been expressed in section

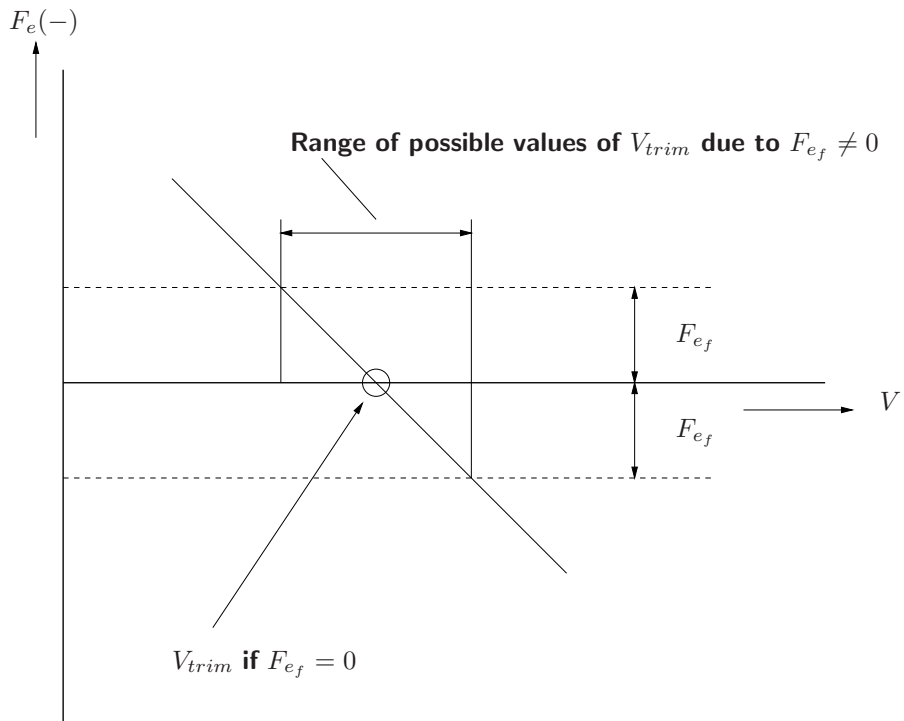


Figure 10-23: Uncertainty in trim speed due to friction in the control mechanism

9-2-7 in terms of an equivalent hinge moment H_{e_f} . A certain control force F_{e_f} is required to overcome this friction. If the airspeed in steady flight differs only slightly from V_{tr} the required control may be small as well. If $|F_e| < |F_{e_f}|$, no control force is required from the pilot. He can leave the control stick or wheel free, the required control position is maintained by the friction in the control mechanism, see figure 10-23.

The result is that in actual flight not one single trim speed exists, and any airspeed within the range where $F_e > F_{e_f}$ is then a trim speed.

In order to keep this uncertainty of the trim speed within acceptable limits the elevator control force stability must have a certain minimum positive value and, in addition, F_{e_f} has to be sufficiently small.

The U.S. military regulations, see reference [19], require,

$$\left(\frac{dF_e}{dV} \right)_{F_e=0} > 0.5 \text{ (lbs/3 kts)}$$

corresponding with,

$$\left(\frac{dF_e}{dV} \right)_{F_e=0} > 0.041 \text{ (kg/km/h)}$$

According to the same regulations the control force required to overcome the friction is limited to,

- **Light aircraft**

- control stick $F_{e_f} < 1.3 \text{ kg}$

- control wheel $F_{e_f} < 1.8 \text{ kg}$

• **Heavy aircraft**

- control stick $F_{e_f} < 2.3 \text{ kg}$
- control wheel $F_{e_f} < 3.2 \text{ kg}$

This control force is to be measured on the ground, the engines not running. In flight the control force needed to overcome the friction may be considerably less due to vibrations of the aircraft. The exact definitions of the terms ‘light’ and ‘heavy’ aircraft can be found in reference [19].

A quick derivation of stick force stability

We start with the symmetrical equations of motion, in which, for simplicity, the derivatives $C_{Z\dot{\alpha}}$ and C_{Z_q} were set to zero.

$$\begin{bmatrix} C_{X_u} - 2\mu_c D_c & C_{X_\alpha} & C_{Z_o} & 0 \\ C_{Z_u} & C_{Z_\alpha} - 2\mu_c D_c & 0 & 2\mu_c \\ 0 & 0 & -D_c & 1 \\ C_{m_u} & C_{m_\alpha} + C_{m\dot{\alpha}} D_c & 0 & C_{m_q} - 2\mu_c K_Y^2 D_c \end{bmatrix} \begin{bmatrix} \hat{u} \\ \alpha \\ \theta \\ \frac{q\bar{c}}{V} \end{bmatrix} + \begin{bmatrix} 0 \\ C_{Z_\delta} \\ 0 \\ C_{m_\delta} \end{bmatrix} \delta_e = 0$$

In stationary straight flight conditions $\frac{q\bar{c}}{V} = D_c \alpha = D_c \hat{u} = D_c \frac{q\bar{c}}{V} = 0$, so:

$$\begin{bmatrix} C_{X_u} & C_{X_\alpha} & C_{Z_o} \\ C_{Z_u} & C_{Z_\alpha} & 0 \\ C_{m_u} & C_{m_\alpha} & 0 \end{bmatrix} \cdot \begin{bmatrix} \hat{u} \\ \alpha \\ \theta \end{bmatrix} + \begin{bmatrix} 0 \\ C_{Z_\delta} \\ C_{m_\delta} \end{bmatrix} \cdot \delta_e = 0$$

The stick force can be written as:

$$F_e = -\frac{d\delta_e}{ds_e} 1/2\rho V_h^2 \cdot S_e \bar{c}_e \cdot (C_{h_\alpha} \cdot \alpha_h + C_{h_\delta} \cdot \delta_e + C_{h_{\delta_t}} \cdot \delta_{t_e})$$

writing it for simplicity as

$$F_e = K \cdot (C_{h_\alpha} \cdot \alpha_h + C_{h_\delta} \cdot \delta_e + C_{h_{\delta_t}} \cdot \delta_{t_e})$$

where

$$K = -\frac{d\delta_e}{ds_e} 1/2\rho V_h^2 \cdot S_e \bar{c}_e$$

We will concern ourselves with small variations ΔF_e of F_e and corresponding small deviations from a trimmed steady state condition at V_0, α_0, θ_0 . After some time, a new state of equilibrium will be reached:

$$V = V_o + \Delta V (\Delta \hat{u} = \frac{\Delta V}{V_o}), \alpha = \alpha_o + \Delta \alpha, \theta = \theta_o + \Delta \theta$$

As we are interested in stick force, we assume that the trim tab is not changed, so,

$$\Delta F_e = K \cdot (C_{h_\alpha} \cdot \Delta \alpha_h + C_{h_\delta} \cdot \Delta \delta_e)$$

where,

$$\Delta \alpha_h = (1 - \frac{d\varepsilon}{d\alpha}) \Delta \alpha$$

so

$$\Delta F_e = K \{ C_{h_\alpha} \Delta \alpha (1 - \frac{d\varepsilon}{d\alpha}) + C_{h_\delta} \Delta \delta_e \}$$

and

$$\Delta \delta_e = \frac{1}{K C_{h_\delta}} \Delta F_e - \frac{C_{h_\alpha}}{C_{h_\delta}} (1 - \frac{d\varepsilon}{d\alpha}) \Delta \alpha$$

If we now substitute $\Delta \delta_e$ into the equations of 'motion' for the case of steady state we get

$$\begin{bmatrix} C_{X_u} & C_{X_\alpha} & C_{Z_o} \\ C_{Z_u} & C_{Z_\alpha} & 0 \\ C_{m_u} & C_{m_\alpha} & 0 \end{bmatrix} \begin{bmatrix} \hat{u} \\ \alpha \\ \theta \end{bmatrix} + \begin{bmatrix} 0 \\ C_{Z_\delta} \\ C_{m_\delta} \end{bmatrix} \left\{ -\frac{C_{h_\alpha}}{C_{h_\delta}} (1 - \frac{d\varepsilon}{d\alpha}) \Delta \alpha + \frac{1}{K C_{h_\delta}} \Delta F_e \right\} = 0$$

or

$$\begin{bmatrix} C_{X_u} & C_{X_\alpha} & C_{Z_o} \\ C_{Z_u} & C_{Z_\alpha} - \frac{C_{h_\alpha}}{C_{h_\delta}} \cdot (1 - \frac{d\varepsilon}{d\alpha}) \cdot C_{Z_\delta} & 0 \\ C_{m_u} & C_{m_\alpha} - \frac{C_{h_\alpha}}{C_{h_\delta}} \cdot (1 - \frac{d\varepsilon}{d\alpha}) \cdot C_{m_\delta} & 0 \end{bmatrix} \begin{bmatrix} \Delta \hat{u} \\ \Delta \alpha \\ \Delta \theta \end{bmatrix} + \begin{bmatrix} 0 \\ C_{Z_\delta} \\ C_{m_\delta} \end{bmatrix} \frac{1}{K C_{h_\delta}} \Delta F_e = 0$$

Here we introduce two new stability derivatives for the case of stick free,

$$\begin{aligned} C_{Z_\alpha \text{ free}} &= C_{Z_\alpha} - \frac{C_{h_\alpha}}{C_{h_\delta}} (1 - \frac{d\varepsilon}{d\alpha}) \cdot C_{Z_\delta} \\ C_{m_\alpha \text{ free}} &= C_{m_\alpha} - \frac{C_{h_\alpha}}{C_{h_\delta}} \cdot (1 - \frac{d\varepsilon}{d\alpha}) \cdot C_{m_\delta} \end{aligned}$$

so,

$$A \Delta x_{ss} + B \frac{1}{K \cdot C_{h_\delta}} \Delta F_e = 0$$

with

$$A = \begin{bmatrix} C_{X_u} & C_{X_\alpha} & C_{Z_o} \\ C_{Z_u} & C_{Z_{\alpha free}} & 0 \\ C_{m_u} & C_{m_{\alpha free}} & 0 \end{bmatrix}, B = \begin{bmatrix} 0 \\ C_{Z_\delta} \\ C_{m_\delta} \end{bmatrix}, \Delta x_{ss} = \begin{bmatrix} \Delta \hat{u} \\ \Delta \alpha \\ \Delta \theta \end{bmatrix}$$

Multiplication by the inverse of A results in:

$$\Delta x_{ss} = -A^{-1} B \frac{1}{K \cdot C_{h_\delta}} \Delta F_e$$

or

$$x_{ss}' = \begin{bmatrix} \frac{\Delta \hat{u}}{\Delta F_e} K C_{h_\delta} \\ \frac{\Delta \alpha}{\Delta F_e} K C_{h_\delta} \\ \frac{\Delta \theta}{\Delta F_e} K C_{h_\delta} \end{bmatrix} = -A^{-1} B$$

and

$$\frac{\Delta F}{\Delta \hat{u}} = \frac{K C_{h_\delta}}{x_{ss}'(1)}$$

Finally, since $\Delta \hat{u} = \frac{\Delta V}{V}$, we get:

$$\frac{\Delta F}{\Delta V} = \frac{K C_{h_\delta}}{x_{ss}'(1) V} = -\frac{d\delta_e}{ds_e} C_{h_\delta} S_e \bar{c}_e^{1/2} \rho V_h^2 \frac{1}{x_{ss}'(1) V}$$

Applying Cramer's rule, we find:

$$\begin{aligned} x_{ss}'(1) &= -\frac{\begin{vmatrix} 0 & C_{X_\alpha} & C_{Z_o} \\ C_{Z_\delta} & C_{Z_{\alpha free}} & 0 \\ C_{m_\delta} & C_{m_{\alpha free}} & 0 \end{vmatrix}}{\begin{vmatrix} C_{X_u} & C_{X_\alpha} & C_{Z_o} \\ C_{Z_u} & C_{Z_{\alpha free}} & 0 \\ C_{m_u} & C_{m_{\alpha free}} & 0 \end{vmatrix}} = -\frac{\begin{vmatrix} C_{Z_o} & C_{Z_{\alpha free}} \\ C_{m_\delta} & C_{m_{\alpha free}} \end{vmatrix}}{\begin{vmatrix} C_{Z_o} & C_{Z_u} & C_{Z_{\alpha free}} \\ C_{Z_u} & C_{m_u} & C_{m_{\alpha free}} \end{vmatrix}} = \\ &= -\frac{C_{Z_\delta} C_{m_{\alpha free}} - C_{m_\delta} C_{Z_{\alpha free}}}{C_{Z_u} C_{m_{\alpha free}} - C_{m_u} C_{Z_{\alpha free}}} \end{aligned}$$

Now for simplicity we set

$$C_{Z_\delta} = 0, C_{m_u} = 0$$

resulting in:

$$x_{ss}'(1) = -\frac{-C_{m_\delta} C_{Z_{\alpha free}}}{C_{Z_u} C_{m_{\alpha free}}}$$

Since

$$C_{Z_\alpha} \approx -C_{N_\alpha}$$

and

$$C_{Z_u} \approx -2C_L = -2 \frac{W}{\frac{1}{2} \rho V^2 S}$$

we get:

$$x'_{ss}(1) = -\frac{C_{m_\delta} C_{Z_{\alpha_{free}}}}{C_{Z_u} C_{m_{\alpha_{free}}}}$$

With $C_{Z_{\alpha_{free}}} \approx C_{Z_{\alpha_{free}}}$ and $C_{Z_u} \approx -2 C_L = -2 \frac{W}{1/2\rho V^2 S}$,

$$x'_{ss}(1) = -\frac{C_{m_\delta} C_{Z_{\alpha_{free}}}}{2 \frac{W}{1/2\rho V^2 S} C_{m_{\alpha_{free}}}}.$$

We already derived:

$$\frac{\Delta F}{\Delta V} = \frac{K \cdot C_{h_\delta}}{x'_{ss}(1)} V = -\frac{d\delta_e}{ds_e} C_{h_\delta} \cdot S_e \bar{c}_e^{1/2} \rho V_h^2 \frac{1}{x'_{ss}(1)}, \frac{1}{V}$$

so:

$$\begin{aligned} \frac{\Delta F}{\Delta V} &= \frac{K \cdot C_{h_\delta}}{x'_{ss}(1)} V = -\frac{d\delta_e}{ds_e} C_{h_\delta} \cdot S_e \bar{c}_e^{1/2} \rho V_h^2 \frac{2}{C_{m_\delta}} \frac{W}{1/2\rho V^2 S} \cdot \frac{C_{m_{\alpha_{free}}}}{C_{N_{\alpha_{free}}}} \frac{1}{V} = \\ &= -\frac{d\delta_e}{ds_e} C_{h_\delta} \cdot S_e \bar{c}_e^{1/2} \rho V_h^2 \frac{2}{C_{m_\delta}} \frac{W}{1/2\rho V^2 S} \cdot \frac{x_{c.g.}}{\bar{c}} \end{aligned}$$

and since this formula applies to trim speed $V = V_{tr}$ we find:

$$\frac{dF}{dV} = -2 \frac{d\delta_e}{ds_e} C_{h_\delta} \cdot S_e \bar{c} \left(\frac{V_h}{V} \right)^2 \frac{W}{S} \frac{C_{h_\delta}}{C_{m_\delta}} \frac{x_{c.g.} - x_{n_{free}}}{\bar{c}} \frac{1}{V_{tr}}$$

10-2-4 Effect of center of gravity and mass unbalance on stick force stability

A. Influence of the center of gravity position

In the foregoing it was shown that the center of gravity has an influence only on the part $F_{e_{V=0}}$ of the control force which is independent of airspeed, see equation (10-47). If the cg is shifted in X -direction this constant term in equation (10-47) varies and, at a constant trim tab angle, the entire control force curve will shift up or down, parallel to itself.

If the cg is moved forward the control force curve will shift upwards (a larger pull force will be required) at constant δ_{t_e} and i_h . This agrees with the measured control force curves shown in figures 10-21 and 10-24.

The slope of the control force does not change at constant δ_{t_e} , but with the new cg position corresponds to another, higher trim speed. If the original trim speed is re-established by an additional downward deflection of the trim tab, it turns out, see for instance subfigure d of figure 10-24, that the elevator control force stability at constant trim speed has increased. So, strictly speaking, the elevator control force stability cannot be considered independent of the trim speed.

B. Trim tab angle and the stabilizer angle of incidence

From equation (10-47) it can be concluded that for a stick free, statically stable aircraft, any trim tab angle $\delta_{t_e} > \delta_{t_{e_0}}$ results in a certain airspeed where $F_e = 0$. The trim tab angle for a given V_{tr} is obtained from equation (10-50),

$$\delta_{t_e} = \delta_{t_{e_0}} + \frac{W}{1/2\rho V_{tr}^2 S} \frac{1}{C_{h_{\delta_t}}} \frac{C_{h_\delta}}{C_{m_{\delta_e}}} \frac{x_{cg} - x_{n_{free}}}{\bar{c}} \quad (10-53)$$

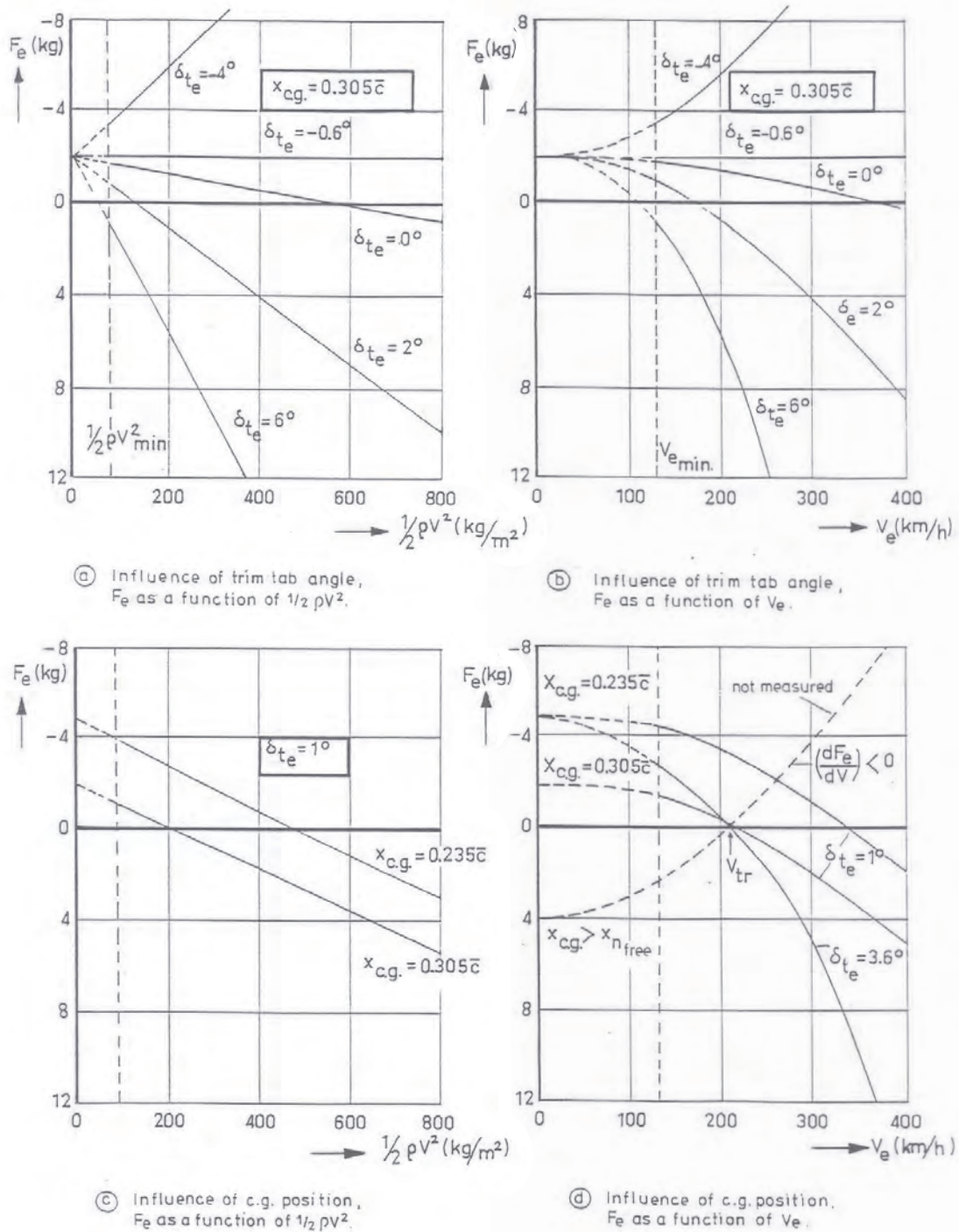


Figure 10-24: Measured elevator control force curves for the North American 'Harvard' II B in gliding flight (from reference [15])

It follows from equation (10-53) that for a given cg position the pilot can choose a certain trim speed where he can fly ‘hands-off’ by selecting the appropriate δ_{t_e} . If the stability margin stick free is positive, cg in front of the $n.p._{free}$, the trim speed is reduced by increasing δ_{t_e} , i.e. with increasing downward tab deflection. The trim wheel in the cockpit is turned backward to this end. Once a certain trim speed has been chosen the variation of the control force with airspeed in steady flight is fixed, according to equation (10-51), and so is the elevator control force stability.

It can be clearly seen in figure 10-24 from the measured elevator control forces that the slope of the control force curve indeed increases at a given airspeed by a downward deflection of the trim tab.

From the foregoing it becomes clear that for a given cg position a fixed relation exists between the trim tab angle and the corresponding trim speed.

The aircraft possesses elevator control force stability if according to equation (10-53),

$$\frac{d\delta_{t_e}}{dV_{tr}} < 0$$

The trim tab angle curve may be used to investigate the elevator control force stability. An example of a measured trim tab angle curve is shown in figure 10-25. As already mentioned in section 9-2-6, in some aircraft the elevator control forces are reduced to zero by adjusting the stabilizer angle of incidence. In such cases the elevator does not need to have a trim tab. It follows from equations (10-41) and (10-44) that both the horizontal stabilizer setting i_h and the trim tab angle δ_{t_e} figure in C'_{h_0} and $F_{eV=0}$.

It also follows from (10-41) and (10-44) that it is irrelevant whether the stabilizer or the trim tab is used to trim the control force to zero. If the stabilizer is used C'_{h_0} can be written in analogy with equation (10-46) as,

$$C'_{h_0} = C_{h_\delta} (i_h - i_{h_0}) \quad (10-54)$$

where i_{h_0} is the value of i_h for which $C'_{h_0} = 0$. The influence of i_h on the elevator control force stability is entirely comparable to that of δ_{t_e} .

C. Influence of a spring or an unbalanced mass in the control mechanism

Sometimes it is not possible to obtain satisfactory control forces and elevator control force stability in all required aircraft configurations and flight conditions by aerodynamic balancing of the elevator only. If at a given cg position and trim speed the elevator control force stability should become too low an unbalanced mass, a ‘bobweight’, see figure 10-26, or a spring, see figure 10-27, may be used in the control mechanism, see also figure 9-86. These devices increase $F_{eV=0}$ by a constant force $\Delta F_{eV=0}$, see figure 10-28. A spring to be used for this purpose is chosen in principle such that the applied force remains approximately constant over the entire range of control deflections. The entire control force curve will then be shifted upward, parallel to itself. A more detailed analysis shows, that now $C_{m_{free}}$ has become a function of airspeed. It also turns out that the $n.p._{free}$ position has moved backwards and consequently the stability margin, stick free, has been increased. The use of a spring or an unbalanced spring in the control mechanism is thus seen to have the same effect, as far as the control force curve is concerned, as a forward shift of the center of gravity.

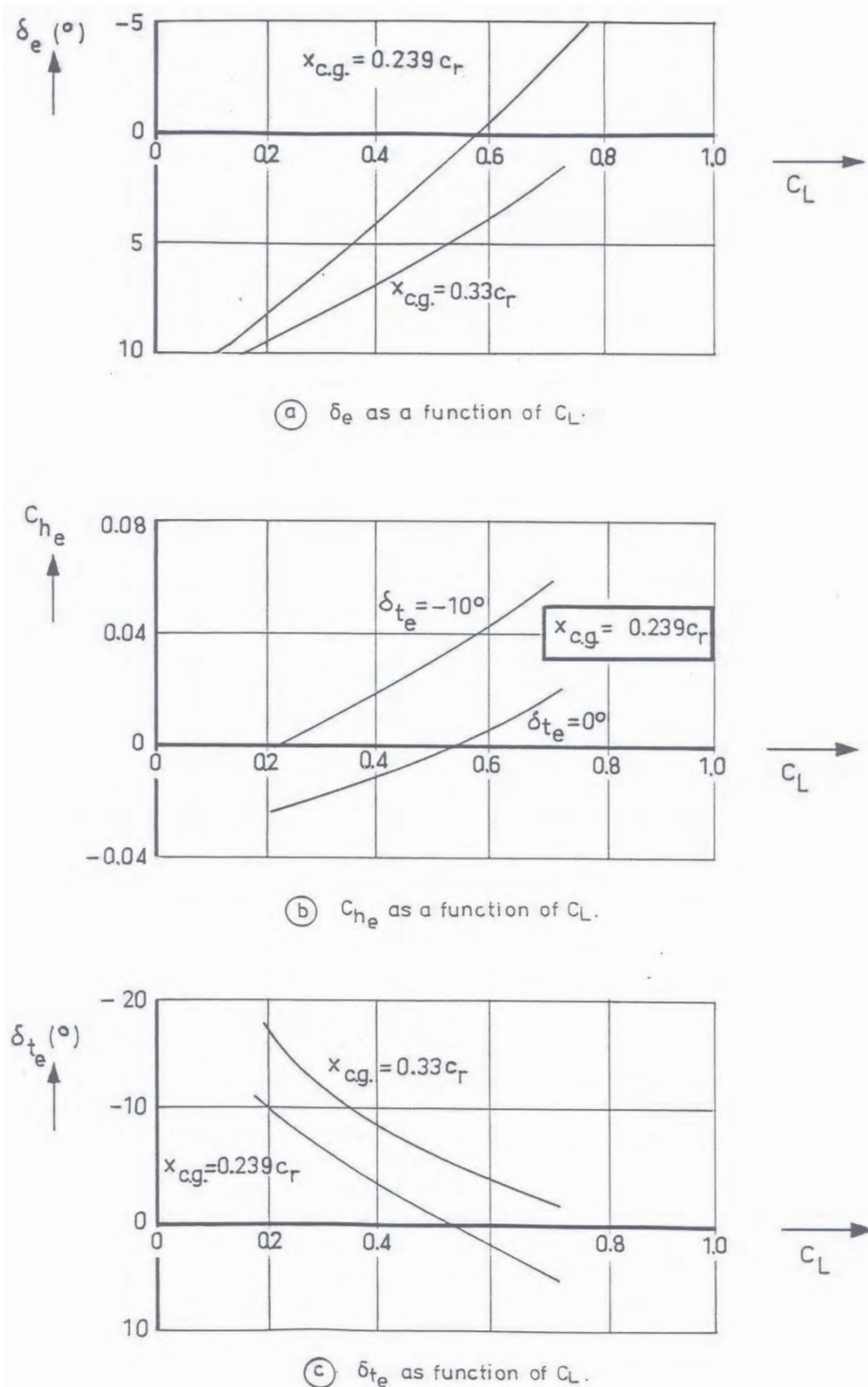


Figure 10-25: Trim curves, hinge moment coefficients and required trim tab angles as functions of C_L for the Siebel 204-D-1 aircraft (from reference [16])

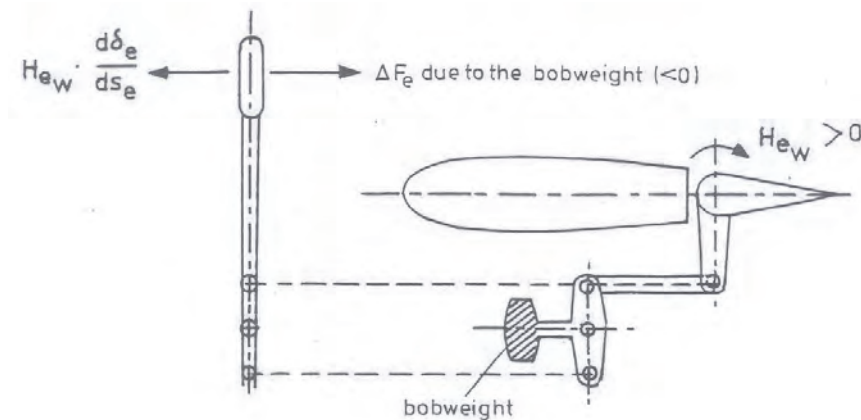


Figure 10-26: The influence of a bobweight in the control mechanism

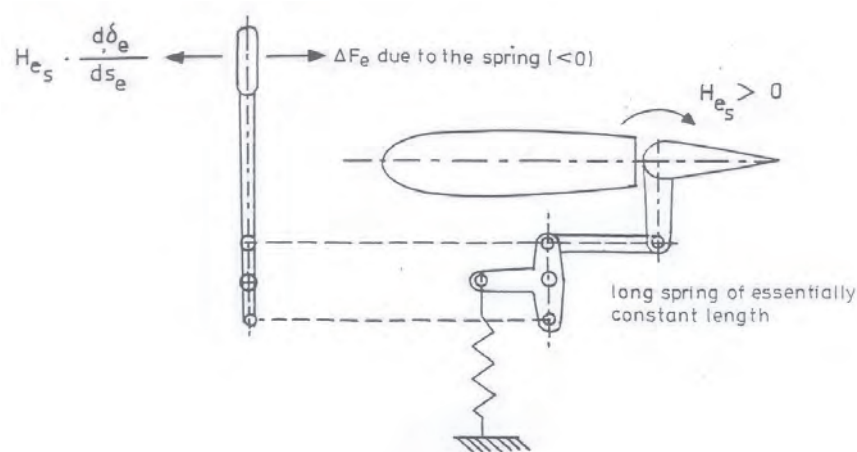


Figure 10-27: The influence of a spring in the control mechanism

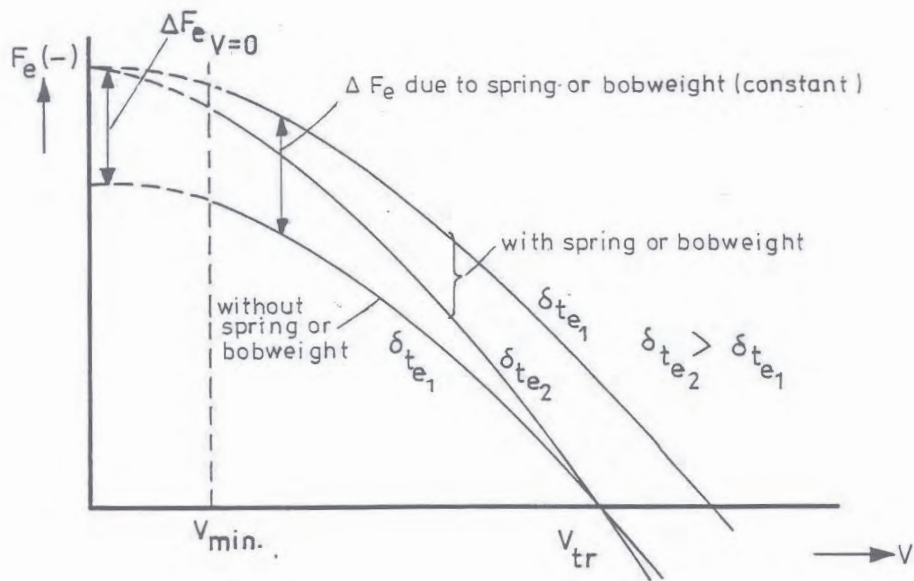


Figure 10-28: The influence of a spring or bobweight on the elevator control force curve

10-2-5 Influence of design variables on control forces

Another look at equation (10-47),

$$F_e = \frac{d\delta_e}{ds_e} S_e \bar{c}_e \left(\frac{V_h}{V} \right)^2 \left\{ \frac{W}{S} \frac{C_{h_\delta}}{C_{m_{\delta_e}}} \frac{x_{cg} - x_{n_{free}}}{\bar{c}} - \frac{1}{2} \rho V^2 C_{h_{\delta_t}} (\delta_{t_e} - \delta_{t_{e_0}}) \right\}$$

reveals that the variables of direct interest to the pilot are: $\frac{1}{2} \rho V^2$, x_{cg} , δ_{t_e} and i_h (they have already been discussed in previous sections). Other variables occurring in equation (10-47) are of interest in the design of the aircraft, such as $\frac{d\delta_e}{ds_e}$, S_e , \bar{c}_e , the tailvolume $\frac{S_h l_h}{S \bar{c}}$ and $C_{N_{h_\delta}}$ (or $C_{m_{\delta_e}}$), C_{h_δ} , $C_{h_{\delta_t}}$, $\frac{x_{n_{free}}}{\bar{c}}$. The following can be said on these variables. The control forces increase with the wing loading $\frac{W}{S}$. The control forces are in addition proportional to S_e and \bar{c}_e . Hence, for aircraft of identical shape the control forces vary with the third power of the dimensions.

The control gearing $\frac{d\delta_e}{ds_e}$ is determined by the fact that the extreme deflection of the control surface must correspond with the extreme displacement of the cockpit control column or stick. The range of elevator deflections $\Delta\delta_{e_{max}}$ is restricted aerodynamically, amounting to about 50° or 60° (25° to 30° to either side). The permissible range of control displacements $\Delta s_{e_{max}}$ is restricted by the dimensions of the human pilot and sometimes by the dimensions of the cockpit. The maximum value is about 40 cm.. The resulting value of $\frac{d\delta_e}{ds_e}$ turns out to be approximately 1.25 to $1.5^\circ/\text{cm}$. (2.2 to 2.6 Radians/m). Some aircraft have a variable gear ratio depending on the aircraft configuration.

The required value of $C_{m_{\delta_e}}$ is determined by the maximum required elevator power. Usually either the take-off or the landing at the most forward cg position is the most critical condition see section 9-2-6. The derivative $C_{h_{\delta_t}}$ determines the required size of the trim tab, taking into account the (limited) range of the trim tab angles. For a trim tab to be effective at any occurring value of α_h and δ_e the deflection should not be larger than $\pm 15^\circ$. The required size of the trim tab then

follows from the requirement that, according to the regulations, it must be possible to reduce the control force to zero in certain aircraft configurations, including the cg position, and over certain ranges of airspeed, see section 9-2-7.

The only remaining variables which the designer can use to influence the control forces are the stability margin, stick free and $C_{h\delta}$. Earlier was found, see equation (10-39),

$$\frac{x_{n_{free}} - x_{n_{fix}}}{\bar{c}} = - \frac{C_{N_{h\delta}}}{C_{N_\alpha}} \frac{C_{h\alpha}}{C_{h\delta}} \left(1 - \frac{d\varepsilon}{d\alpha}\right) \left(\frac{V_h}{V}\right)^2 \frac{S_h l_h}{S \bar{c}} = \frac{C_{m_{\delta_e}}}{C_{N_\alpha}} \frac{C_{h\alpha}}{C_{h\delta}} \left(1 - \frac{d\varepsilon}{d\alpha}\right)$$

This means that at a given position of the neutral point, stick fixed, $C_{h\alpha}$ and $C_{h\delta}$ are the only remaining variables with which the designer can manipulate the control forces. From the foregoing it will have become clear that the general requirement is for the center of gravity to be positioned forward of the neutral points, both stick fixed and stick free. The aircraft then possesses both elevator control position and force stability. If $C_{h\alpha}$ of the elevator as well as $C_{h\delta}$ are negative, the $n.p._{free}$ lies forward of the $n.p._{fix}$ position. The aft permissible cg position is limited by the $n.p._{free}$. It is possible to shift this n.p. aft by reducing $|C_{h\alpha}|$. The $n.p._{free}$ will even lie aft of the $n.p._{fix}$, if $C_{h\alpha} > 0$. This is one reason why a slight overbalance with respect to angle of attack is sometimes aimed for when balancing the elevator.

For many modern aircraft it turns out to be no longer possible to obtain acceptable control forces in all required aircraft configurations and flight conditions, merely by choosing $C_{h\alpha}$ and $C_{h\delta}$. In particular this is true for aircraft having a high wing loading $\frac{W}{S}$, a high maximum airspeed V_{max} and/or a large ratio of maximum to minimum airspeed $\frac{V_{max}}{V_{min}}$ (V/STOL-aircraft).

If purely aerodynamic means do not suffice additional use can be made in the first place of a spring or an unbalanced mass or both in the control mechanism. These devices also influence the dynamic stability, stick free, and sometimes in an unfavourable sense.

In more advanced cases, such as transonic, supersonic and some V/STOL-aircraft, springs and masses cannot offer a satisfactory solution. In those cases the aerodynamic hinge moments are balanced in total or in part by, usually hydraulic, control force amplifiers, i.e. control boosters, or by servo controls.

When hydraulic servo controls are used it would be sufficient for the pilot to apply only the very small forces needed to operate the servo valve. Experience has shown, however, that in the interest of safety of flight the pilot must have to exert forces in his control stick or wheel having the usual levels of magnitude and varying in the normal way with airspeed, control deflection and trim deflection. This requirement is met by the use of a separate installation in the flight control system, a so called ‘artificial feel unit’. This mechanism applies a force in the control manipulator which has to be balanced by the pilot’s control force. These artificially generated control forces are made to vary with $\frac{1}{2}\rho V^2$, δ_e and δ_{t_e} in such a way that the pilot’s control force shows indeed the variations found in an aircraft where the control manipulator has a direct mechanical linkage with the control surface.

10-2-6 Control forces a pilot can exert

The discussion in the previous sections centered around the control forces required to fly the aircraft. The following deals with forces a pilot can exert on his controls. Evidently the designer must ensure that the required control forces remain within the capabilities of even the least strongest amongst the pilot population.

Appropriate regulations aim to safeguard this requirement. The maximum control force a pilot can apply depends primarily on,

1. the individual person; strength and endurance differ appreciably from one person to another
2. the type of control manipulator (control wheel, center stick, side stick, rudder pedals)
3. the time during which the force must be exerted
4. the location of the control manipulator relative to the pilot

Regarding to these items, the following can be remarked.

Figure 10-29 clearly shows the large differences in the maximum possible control forces due to individual differences in strength and endurance of the test subjects. It appears that the largest force a pilot can exert is the rudder pedal force (curve a), the side force for aileron control is the smallest (curves d and e). It is also seen that the forces on a control wheel can be larger than those on a control stick. In the measurements of figure 10-29 the control manipulators were all handled by the right hand. This is in agreement with the situation in most single seat cockpits where the pilot uses his left hand to operate the engine throttle.

Figure 10-29 gives an indication of the maximum possible control forces as a function of the uninterrupted time period over which these forces have to be applied. The maximum possible control force decreases approximately logarithmically with increasing duration. The location of the control manipulator is not only important because it influences the maximum possible control forces. It also influences the pilot's comfort, see references [151, 69, 119, 36, 40]. For a large amount of information on the preferable locations of controls in the cockpit. Occasionally the aircraft flight condition can experience a rather sudden change. In view of such occurrences it is necessary to know how fast a pilot can change the control deflections under various levels of control force gradients. Information on this can be found in references [174, 129, 73]. It is evident that the required control forces may not surpass the possible control forces. The various Airworthiness Regulations contain requirements concerning the maximum permissible control forces under various circumstances. Table 10-1 gives the maximum forces as stipulated in the U.S. and the British Airworthiness Regulations, see references [6] and [7] respectively.

10-2-7 Airworthiness requirements for steady straight symmetric flight

The Airworthiness Regulations, see references [11, 19, 6, 20, 12, 13, 7], require that the aircraft is statically stable in the most important aircraft configurations and flight conditions. This means that the cg must be in front of the neutral point in those conditions. Sometimes the requirement is expressed in terms of an equivalent requirement regarding the control characteristics.

In view of the fact that the pilot is in general more sensitive to control forces and changes in control forces than to control positions and control displacements, the requirement usually stipulates that the aircraft possesses elevator control force stability in the relevant aircraft configurations and flight conditions at all permissible center of gravity positions. As discussed in section 10-2-2 this requirement can easily be reformulated into the condition that the center of gravity must be positioned in front of the neutral point stick free.

For the designer the emphasis may be slightly different. In section 10-2-4 it was seen that several possibilities exist to influence the control force through non-aerodynamic means. The arsenal of available tools is certainly not exhausted with the springs and unbalanced masses discussed in section 10-2-4. It is of great practical interest that several of these means may still be applied relatively easy in a late stage of the development of the aircraft, if the need arises, without great expense or drastic changes in the design. To change the elevator control position stability

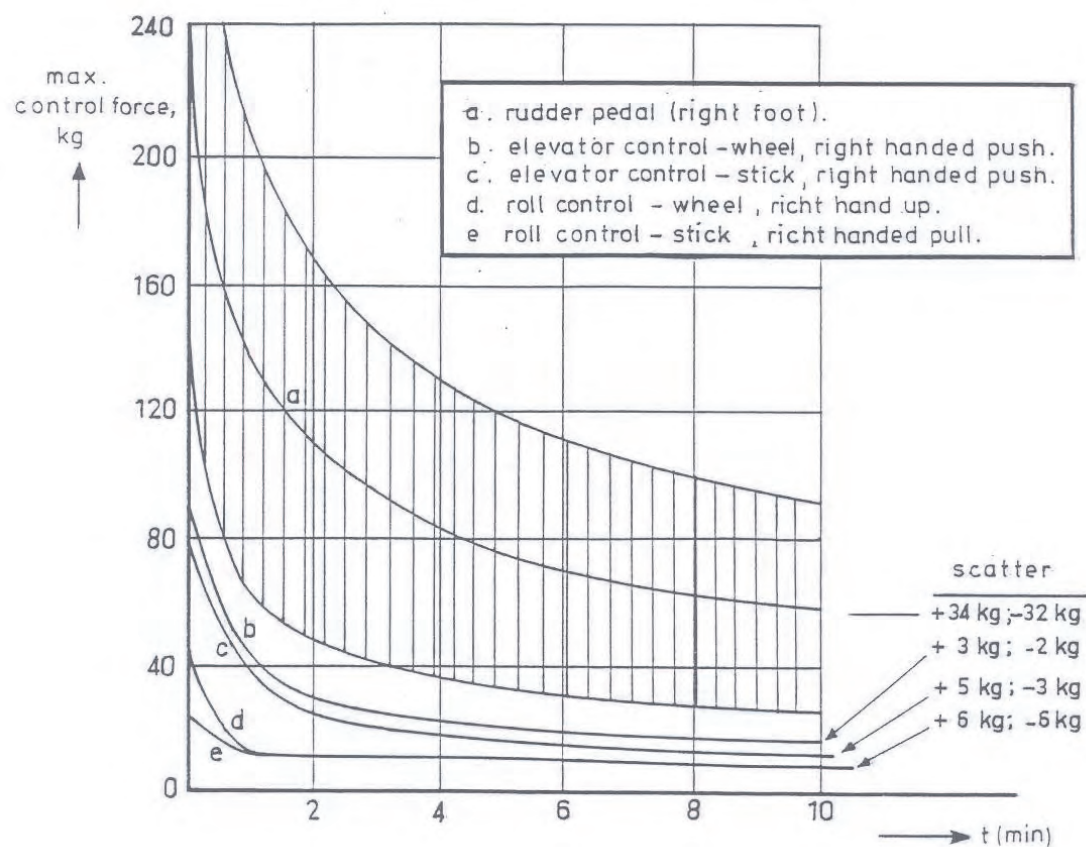


Figure 10-29: Maximum control forces as a function of the duration (from reference [151])

	Requirements according to	
	U.S. Civil (reference [7])	British Civil (reference [6])
Rudder pedals	82 kg (short intervals) 9 kg (long intervals)	82 kg (short intervals) 22.5 kg (long intervals)
Elevator control	35 kg (short intervals) 4.5 kg (long intervals)	22.5 kg (short intervals) 2.6 kg (long intervals)
Aileron control	27 kg (short intervals) 2.3 kg (long intervals)	
note that a ' <i>short interval</i> ' is regarded as a period of time lasting a few seconds while a ' <i>long interval</i> ' is regarded as a period of time lasting several minutes		

Table 10-1: Maximum permissible values of the required control forces, according to the U.S. and British Civil Airworthiness Regulations

or the static stability, stick fixed, usually turns out to be much more difficult since it requires considerably more drastic modifications in the design, see section 10-1-2.

This argument leads to an important design rule. Already in an early stage of the design of an aircraft it is essential to ensure that, in addition to other requirements to be met, the neutral point, stick fixed, in the prescribed aircraft configurations and flight conditions will lie behind the rearmost envisaged center of gravity position.

Experience has shown that during the development of an aircraft the center of gravity often shows the tendency to move a bit due to the successive design modifications. For this reason it may be wise to provide an additional margin when choosing the position of the neutral point, stick fixed, in the various aircraft configurations and flight conditions.

In the next section some control characteristics will be discussed concerning turning flight. Requirements to be met by the control characteristics in such flight conditions will prove to influence also the forward and rear limits of the permissible center of gravity positions.

10-3 Longitudinal Control in Pull-Up Manoeuvres and Steady Turns

The previous two sections dealt with the longitudinal control characteristics in steady straight flight. Control in turning and non steady flight, i.e. in manoeuvres, was not considered so far. It is by no means certain that an aircraft showing good control characteristics in steady, straight flight, also has similarly good control characteristics in manoeuvres. It is thus necessary to study these latter control characteristics and to this end express them quantitatively in appropriate terms. This way also allows to formulate quantitative requirements for desired control characteristics.

Of the many possible turning manoeuvres only two of the greatest general interest are considered here: the pull-up from a dive and the steady, coordinated, i.e. slip-free, horizontal turn.

During these two manoeuvres the aircraft has an angular, pitching, velocity about the lateral axis. In turns the pitching velocity q about the lateral axis is always accompanied by a yawing velocity r about the top axis, but because of the symmetry of the aircraft the influence of the asymmetric component r on the symmetric forces and moments can be neglected, see chapter 4.

An important purpose of the following discussion is to make longitudinal control in these manoeuvres accessible to quantitative study. Therefore, the control characteristics have to be expressed in characteristic variables, sufficiently simple to be manageable for the designer. To arrive at such characteristic variables some simplifying assumptions have to be made. Suppose the pilot of a normal stable aircraft wants to pull his aircraft up from a steady, straight, symmetric dive. In this context any descending flight will be called a dive. To achieve his purpose, he moves the elevator control back to a new position, which is assumed to be constant to simplify the discussion. The effect of this schematic control movement can be described as follows. Assuming a stable aircraft, first the pitching velocity q and the angle of attack α quickly increase to new approximately constant values depending on the ultimate control displacement. This motion occurs usually within a few seconds, often via a more or less well damped oscillation during which the airspeed remains very nearly constant. The aircraft motion, usually called the ‘short period oscillation’ will be discussed in more detail in chapter 5.

Figure 10-30 gives an example of such a symmetric motion caused by a step elevator deflection. Figure 10-31 presents the various measured components, the elevator deflection and the control force for a pull-up manoeuvre of an Auster J-5B ‘Autocar’.

Due to the increase in angle of attack the total lift on the aircraft becomes larger than the aircraft weight. This causes the trajectory of the cg to be curved, the aircraft is pulled up from the dive. If the pilot keeps the elevator angle constant, a second oscillation will occur. In contrast with the first oscillation, the second one is relatively slow and usually has a very low damping. After the second oscillation has also damped out, the pitching velocity q is zero and the airspeed as well as the angle of attack have assumed the new constant values corresponding to the new elevator angle in steady, straight flight. In actual flight, when pulling up from a dive the pilot will suppress the second, long-period, oscillation by means of suitable, small corrective elevator movements. This second oscillation, usually called ‘the slow oscillation’, or ‘phugoid’ will also be discussed in more detail in chapter 5.

In the following, only the first and relatively fast part of the motion is studied. The assumption is made that the airspeed remains constant at the level of the original steady flight condition. In addition to the assumption of a constant airspeed another simplification can be made. The normal load factor, n , is equal to 1 in the original straight flight.

Due to the control displacement initiating the pull-up from the dive, the value of n increases. If the short-period oscillation is sufficiently damped, the normal load factor remains very nearly constant during a brief time interval, see figures 10-30 and 10-31. This fact allows the normal

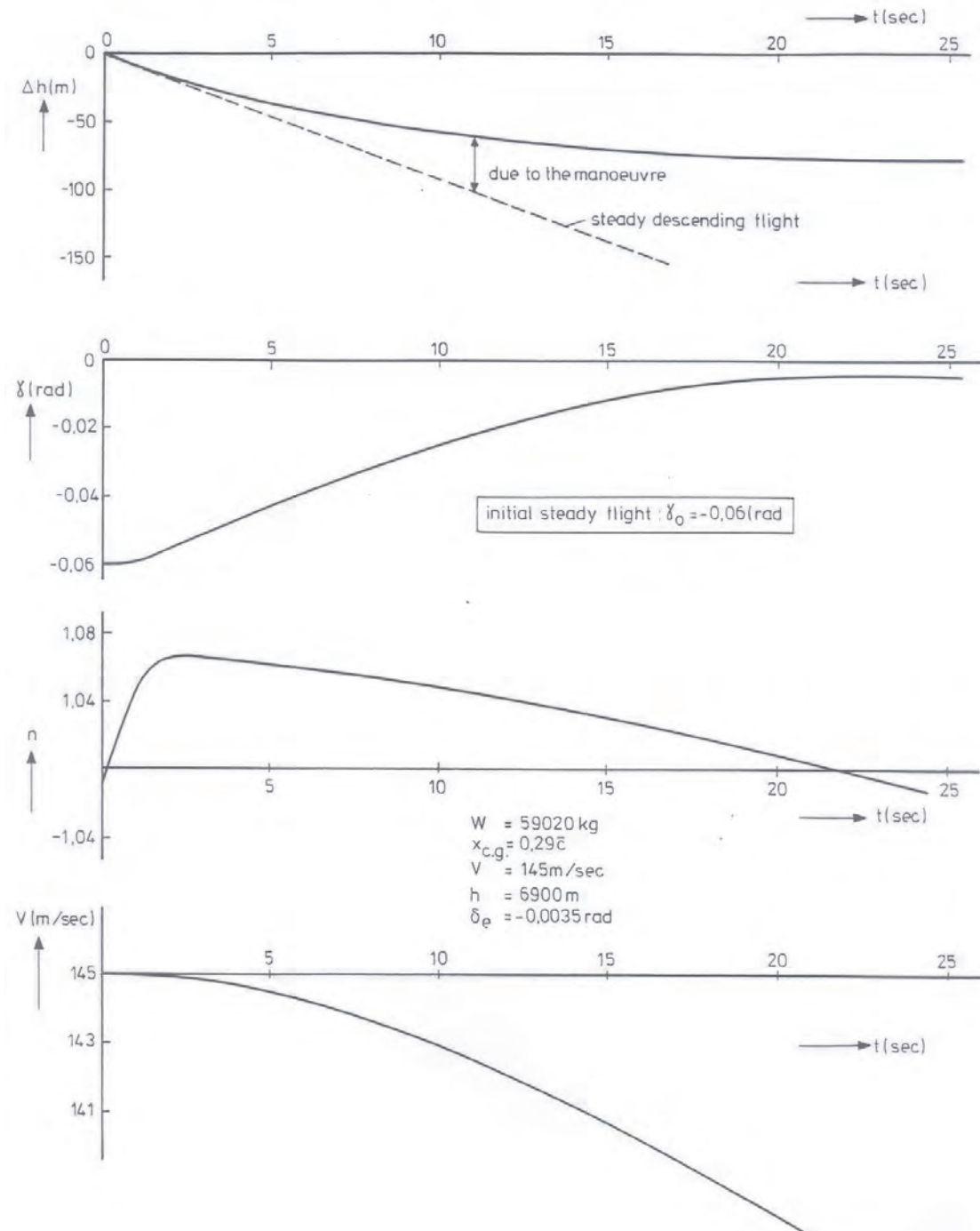


Figure 10-30: Response curves due to an elevator step deflection, Lockheed 1049 C 'Super Constellation'

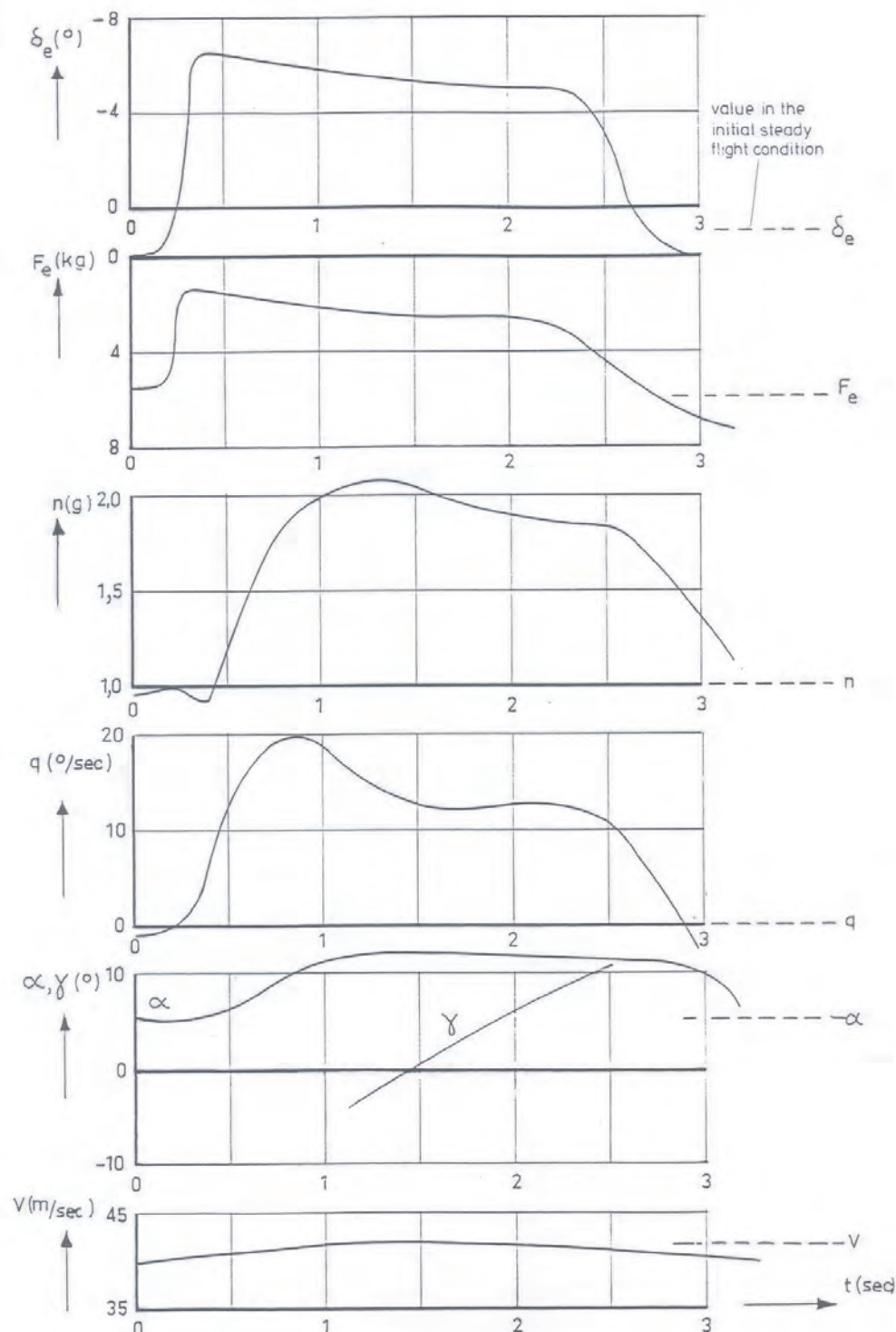


Figure 10-31: Response curves due to an elevator step deflection, Auster J-5B 'Autocar' (from reference [23])

load factor to be considered constant in the following, just like the airspeed.

Due to these two assumptions the pull-up trajectory is idealized to a steady flight condition. For steady turns the two simplifying and approximating assumptions concerning the aircraft motion need not to be made. The aircraft has by definition in a steady turn not only a constant airspeed but also a constant normal load factor.

In the following two notions will be derived characterizing longitudinal control in ‘steady’ pull-ups and in steady, horizontal, coordinated turns.

10-3-1 Characteristics of longitudinal control in turning flight

A notion characteristic for longitudinal control in turning flight should relate two aspects of the manoeuvre: on the one side the pilot’s action, the control displacement and the control force, and on the other hand a characteristic element of the resultant aircraft motion. For the latter the normal load factor n , mentioned before, is used,

$$n = \frac{N}{W} \quad (10-55)$$

In the initial steady flight condition $N = W$, or $n = 1$. Using this load factor, the ‘stick displacement per g’ and the ‘stick force per g’ are obtained, where g is the acceleration due to gravity. Just as with the elevator control position stability, the elevator angle is used rather than the stick displacement itself, so,

- stick displacement per g , $\frac{d\delta_e}{dn}$
- stick force per g , $\frac{dF_e}{dn}$

The load factor in these two expressions is not only characteristic for the change in the trajectory of the aircraft, it is also closely related to the loads imposed on the aircraft.

The two characteristics $\frac{d\delta_e}{dn}$ and $\frac{dF_e}{dn}$ express the extent to which the control position and control force have changed after the aircraft has changed at constant airspeed from a condition of steady, straight flight to another condition of steady, but turning flight or to steady turn at a load factor n . For the case of the pull-up manoeuvre it can be argued that $\frac{d\delta_e}{dn}$ and $\frac{dF_e}{dn}$ should have a negative sign. This argument is as follows.

In order to achieve a pull-up from a dive at a certain airspeed, an increase in angle of attack is needed. This requires an increase in the angle of pitch of the aircraft. This is the initial aircraft motion, the transition from the steady dive to the ‘steady’ pull-up manoeuvre. For this initial motion a tail-heavy moment ($\Delta C_m > 0$) is needed and because $C_{m_s} < 0$, an initial backward elevator control movement and an elevator deflection ‘trailing edge up’ ($\Delta\delta_{e_i} < 0$) are required.

It is argued in section 10-1-3 that a very general desirable control characteristic requires the final control displacement to have the same sign as the initial displacement. During the ‘steady’ pull-up manoeuvre at a constant, positive Δn this general characteristic requires that also the final $\Delta\delta_e$ is negative. This implies that the required sign is negative,

$$\frac{d\delta_e}{dn} < 0$$

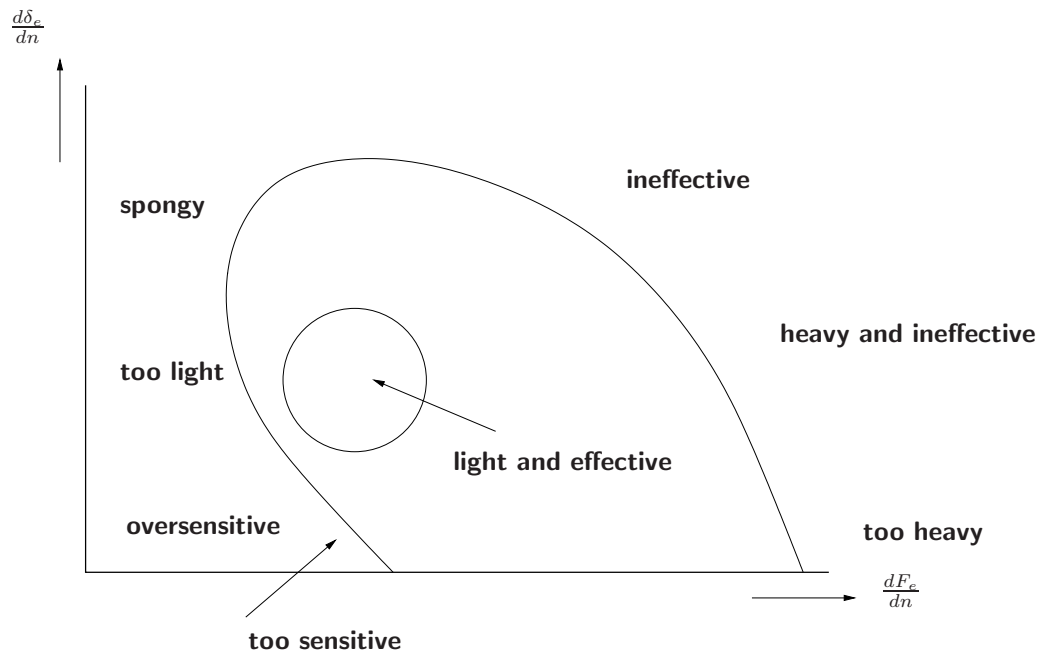


Figure 10-32: Description of the character of the control feel for various ratio's of the control force per g to the control displacement per g (from reference [183]).

Here it is argued that the change in control force required for a control displacement should have the same direction as the control displacement itself. As a consequence, since $\frac{d\delta_e}{ds} > 0$,

$$\frac{dF_e}{dn} < 0$$

It is of course desirable that also in a turn both the change in control position and control force are negative. In the pull-up manoeuvre as well as in a turn, a backward control movement and an extra pull force should be needed.

The stick force per g is generally assigned both a maximum and a minimum permissible value. If the stick force per g is too large in the absolute sense, the pilot will become tired too soon if he has to perform many manoeuvres. If, on the other hand, the stick force per g is too low, the aircraft is too sensitive to small unintentional variations in the control force. There is the additional risk that the aircraft may become overstrained due to a sudden control force.

The dynamic characteristics of the aircraft are also important here.

They have a direct bearing on the desired values of $\frac{d\delta_e}{dn}$ and $\frac{dF_e}{dn}$, see reference [91]. The following table 10-2 gives the maximum and minimum permissible values of the stick force per g , derived from the U.S. military requirements, see reference [19]. It will be seen that these values are related to the maximum permissible load factor n and thus to the strength of the aircraft.

A general rule is, that the absolute value of the stick force per g should not be lower than 1.4 kg . If the requirements of table 10-2 are applied to fighter aircraft having a $n_L = 6$, the result is that the stick force per g should be between -5.1 kg and -1.9 kg . For transport aircraft, usually having a $n_L = 2.5$, the boundaries are -32.2 kg and -13.6 kg . It is not sufficient to give a maximum and a minimum permissible value of the stick force per g . The relation between the stick displacement per g and the stick force per g is also important to achieve pleasant control characteristics. Figure 10-32 shows how various combinations of the stick

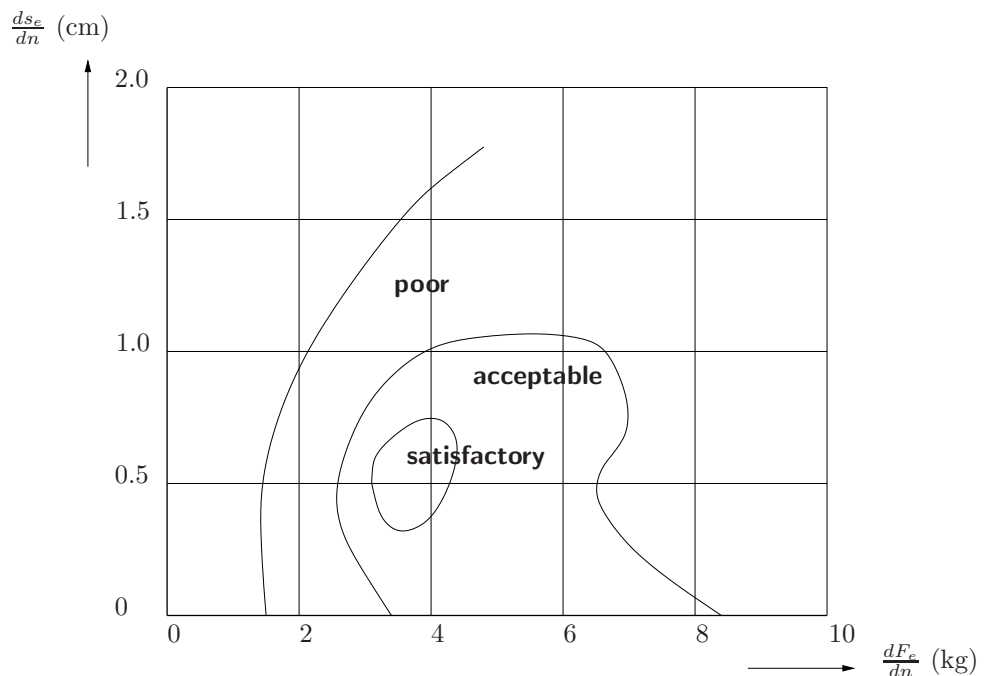


Figure 10-33: The influence of the stick displacement per g and the stick force per g on the pilot's opinion of the control characteristics at constant airspeed (from reference [91]).

	Maximum	Minimum
Trainer and fighter aircraft	$-\frac{25.4}{n_L - 1}$	$-\frac{9.5}{n_L - 1}$
Transport aircraft and bombers	$-\frac{54.4}{n_L - 1}$	$-\frac{20.4}{n_L - 1}$

Table 10-2: Permissible values of the stick force per g in kg

displacement per g and the stick force per g were judged. Figure 10-33 is another example of the influences of the two criteria on the pilot's opinion on the control characteristics of a fighter aircraft at constant airspeed. Quantitative requirements for the stick displacement per g do not exist.

In the following the stick displacement per g and the stick force per g are expressed as functions of the aerodynamic coefficients and the mass of the aircraft for the two cases,

1. The idealized **pull-up manoeuvre** previously discussed, where n and V are assumed to be constant.

The trajectory of the aircraft then is an arc of a circle in the vertical plane. The extent to which this idealized pull-up manoeuvre agrees with the actual motion of the aircraft may be judged from figures 10-30 and 10-31. It will be seen that n and V indeed remain very nearly constant over a brief time interval.

2. The **steady**, horizontal, coordinated **turn**.

10-3-2 The stick displacement per g

The calculation is based on the forces and moments acting on the aircraft both before and after the transition from the steady, straight flight to the idealized pull-up manoeuvre or the steady, horizontal turn. During both manoeuvres the airspeed is assumed to be constant. This implies, that the forces in X -direction are assumed to be in equilibrium and need not be further considered.

In the steady initial condition is,

$$N_0 = W$$

and,

$$M_0 = 0$$

or in non-dimensional form,

$$C_{N_0} = \frac{W}{\frac{1}{2}\rho V^2 S}$$

and,

$$C_{m_0} = 0$$

The index 0 here indicates the steady initial condition. After the transition is, using equation (10-55),

$$\Delta C_N = \frac{W}{\frac{1}{2}\rho V^2 S} \Delta n \quad (10-56)$$

and,

$$\Delta C_m = 0 \quad (10-57)$$

After the transition the angle of attack has increased an amount $\Delta\alpha$ and the aircraft has obtained an angular velocity q about the lateral axis. The elevator angle has changed by $\Delta\delta_e$. The variables describing the aircraft motion now are,

$$\alpha, \quad q \quad \text{or} \quad \frac{q\bar{c}}{V} \quad \text{and} \quad \delta_e \quad (V = \text{constant})$$

whereas in straight flight, considered so far, the variables are,

$$\alpha, \quad V \quad \text{and} \quad \delta_e \quad \left(\frac{q\bar{c}}{V} = 0 \right)$$

In chapter 3 the assumption was made that V would have no effect on the aerodynamic coefficients. Due to the change in angle of attack the aircraft experiences an extra normal force $C_{N_\alpha} \cdot \Delta\alpha$ and an extra moment $C_{m_\alpha} \cdot \Delta\alpha$. The moment due to the elevator deflection is $C_{m_{\delta_e}} \cdot \Delta\delta_e$. The pitching velocity q causes an aerodynamic force along the Z -axis. In section 7-4 a non-dimensional stability derivative C_{Z_q} was introduced,

$$C_{Z_q} = \frac{\partial C_Z}{\partial \frac{q\bar{c}}{V}} = -\frac{\partial C_N}{\partial \frac{q\bar{c}}{V}}$$

Using this stability derivative, the extra force along the Z -axis can be expressed as $C_{Z_q} \cdot \frac{q\bar{c}}{V}$. Here $\frac{q\bar{c}}{V}$ is the non-dimensional pitching velocity, see also section 7-4. A positive force $C_{Z_q} \cdot \frac{q\bar{c}}{V}$ is directed along the positive Z -axis (downward). Usually C_{Z_q} is negative.

The pitching velocity q gives also rise to an aerodynamic pitching moment about the lateral axis. This moment was expressed using another stability derivative, C_{m_q} , also discussed in 7-4,

$$C_{m_q} = \frac{\partial C_m}{\partial \frac{q\bar{c}}{V}}$$

The pitching moment due to q is $C_{m_q} \cdot \frac{q\bar{c}}{V}$. Usually C_{m_q} is negative.

From the foregoing follows for equations (10-56) and (10-57),

$$\Delta C_N = C_{N_\alpha} \Delta\alpha - C_{Z_q} \frac{q\bar{c}}{V} = \frac{W}{\frac{1}{2}\rho V^2 S} \Delta n \quad (10-58)$$

$$\Delta C_m = C_{m_\alpha} \Delta\alpha + C_{m_q} \frac{q\bar{c}}{V} + C_{m_{\delta_e}} \Delta\delta_e = 0 \quad (10-59)$$

Equation (10-59) results in,

$$\Delta\delta_e = -\frac{1}{C_{m_{\delta_e}}} \left(C_{m_\alpha} \Delta\alpha + C_{m_q} \frac{q\bar{c}}{V} \right)$$

The stick displacement per g results from differentiating this latter expression with respect to n ,

$$\frac{d\delta_e}{dn} = -\frac{1}{C_{m_{\delta_e}}} \left(C_{m_\alpha} \frac{d\alpha}{dn} + C_{m_q} \frac{d\frac{q\bar{c}}{V}}{dn} \right)$$

$\frac{d\alpha}{dn}$ follows from equation (10-58),

$$\frac{d\alpha}{dn} = \frac{1}{C_{N_\alpha}} \frac{W}{\frac{1}{2}\rho V^2 S} + \frac{C_{Z_q}}{C_{N_\alpha}} \frac{d\frac{q\bar{c}}{V}}{dn} \quad (10-60)$$

This results in,

$$\frac{d\delta_e}{dn} = -\frac{1}{C_{m_{\delta_e}}} \left\{ \frac{C_{m_\alpha}}{C_{N_\alpha}} \frac{W}{\frac{1}{2}\rho V^2 S} + \left(\frac{C_{m_\alpha} C_{Z_q}}{C_{N_\alpha}} + C_{m_q} \right) \frac{d\frac{q\bar{c}}{V}}{dn} \right\} \quad (10-61)$$

The relation between the non-dimensional pitching velocity $\frac{q\bar{c}}{V}$ and the normal load factor n is yet to be determined. A distinction has to be made here between the idealized pull-up manoeuvre and the steady, horizontal turn.

A. Derivation of $\frac{d\frac{q\bar{c}}{V}}{dn}$ for the pull-up manoeuvre

In the pull-up manoeuvre the bottom of the trajectory is considered, see figure 10-34. In this lowest point of the trajectory, the Z -axis is very nearly vertical and the total force along the Z -axis is $N - W$. The centripetal acceleration along the Z -axis is $V \cdot q$. As a consequence,

$$N - W = m V q$$

or, using equation (10-55),

$$\frac{q\bar{c}}{V} = \frac{g\bar{c}}{V^2} (n - 1)$$

This results in,

$$\frac{d\frac{q\bar{c}}{V}}{dn} = \frac{g\bar{c}}{V^2} \quad (10-62)$$

In chapter 4 a non-dimensional measure of the aircraft's mass μ_c was introduced. This so-called relative density is defined as,

$$\mu_c = \frac{m}{\rho S \bar{c}} = \frac{W}{g \rho S \bar{c}}$$

Using μ_c , equation (10-62) can be written as,

$$\frac{d\frac{q\bar{c}}{V}}{dn} = \frac{1}{2\mu_c} \frac{W}{\frac{1}{2}\rho V^2 S} \quad (10-63)$$

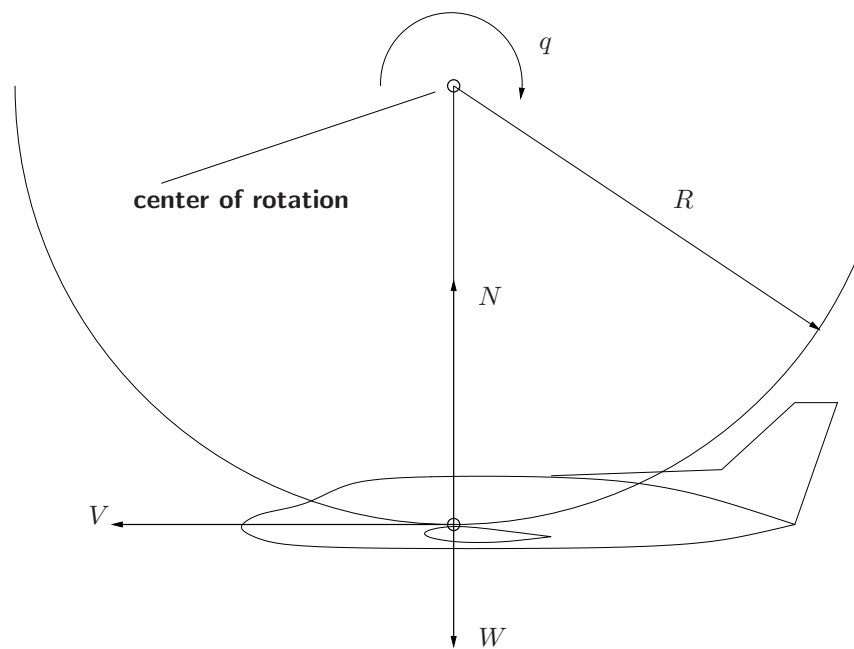


Figure 10-34: The forces and angular velocity q in the idealized pull-up manoeuvre

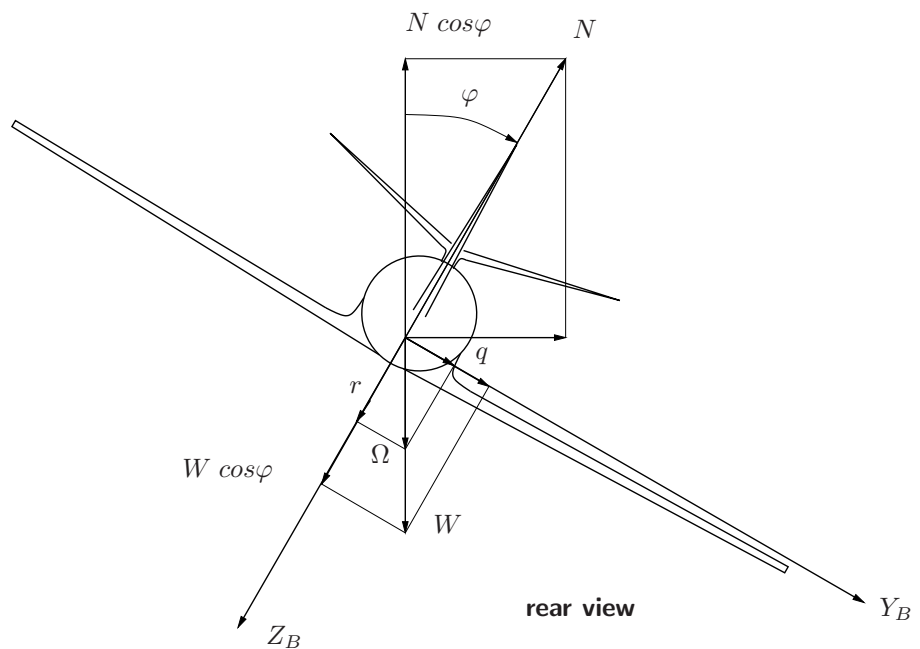


Figure 10-35: The forces and angular velocity in a steady horizontal turn

B. Derivation of $\frac{d\bar{q}}{dn}$ for the steady, horizontal turn

In this steady flight condition the resultant force along the Z -axis, see figure 10-35, is $N - W \cdot \cos \varphi$. The centripetal acceleration along the Z -axis is again $V \cdot q$, so,

$$N - W \cos \varphi = m V q$$

From figure 10-35 follows also,

$$N \cos \varphi = W$$

This relation and equation (10-55) result in,

$$\frac{q\bar{c}}{V} = \frac{g\bar{c}}{V^2} \left(n - \frac{1}{n} \right)$$

and after differentiation,

$$\frac{d\frac{q\bar{c}}{V}}{dn} = \frac{1}{2\mu_c} \frac{W}{\frac{1}{2}\rho V^2 S} \left(1 + \frac{1}{n^2} \right) \quad (10-64)$$

It follows from (10-64) that in steady, horizontal turns $\frac{q\bar{c}}{V}$ is a non-linear function of n . If equation (10-63) is substituted in equation (10-61), the resulting expression for the stick displacement per g in the pull-up manoeuvre can be written as,

$$\frac{d\delta_e}{dn} = -\frac{1}{C_{m_{\delta_e}}} \frac{W}{\frac{1}{2}\rho V^2 S} \left\{ \frac{C_{m_\alpha}}{C_{N_\alpha}} \left(1 + \frac{C_{Z_q}}{2\mu_c} \right) + \frac{C_{m_q}}{2\mu_c} \right\} \quad (10-65)$$

Using equations (10-64) and (10-61) the resulting expression for the steady turns reads,

$$\frac{d\delta_e}{dn} = -\frac{1}{C_{m_{\delta_e}}} \frac{W}{\frac{1}{2}\rho V^2 S} \left\{ \frac{C_{m_\alpha}}{C_{N_\alpha}} + \left(\frac{C_{m_\alpha}}{C_{N_\alpha}} \frac{C_{Z_q}}{2\mu_c} + \frac{C_{m_q}}{2\mu_c} \right) \left(1 + \frac{1}{n^2} \right) \right\} \quad (10-66)$$

A few simplifications can now be made. In equation (10-65) $2\mu_c$ is relatively large if compared to $|C_{Z_q}|$. Also, in equation (10-66) C_{m_q} is large in the absolute sense, if compared to $\frac{C_{m_\alpha}}{C_{N_\alpha}} C_{Z_q}$. This permits both equations (10-65) and (10-66) to be simplified to,

Pull-up manoeuvres

$$\frac{d\delta_e}{dn} = -\frac{1}{C_{m_{\delta_e}}} \frac{W}{\frac{1}{2}\rho V^2 S} \left(\frac{C_{m_\alpha}}{C_{N_\alpha}} + \frac{C_{m_q}}{2\mu_c} \right) \quad (10-67)$$

Steady turns

$$\frac{d\delta_e}{dn} = -\frac{1}{C_{m_{\delta_e}}} \frac{W}{\frac{1}{2}\rho V^2 S} \left\{ \frac{C_{m_\alpha}}{C_{N_\alpha}} + \frac{C_{m_q}}{2\mu_c} \left(1 + \frac{1}{n^2} \right) \right\} \quad (10-68)$$

It follows from equation (10-67) that in pull-up manoeuvres the control deflection and the elevator angle are linear functions of n . In steady, horizontal turns this is, according to equation (10-68),

not the case.

Then $\frac{d\delta_e}{dn}$ varies with n . The difference between $(\frac{d\delta_e}{dn})_{pull-up}$ and $(\frac{d\delta_e}{dn})_{turns}$ decreases with increasing n .

From equations (10-67) and (10-68) it follows also that both for the pull-up manoeuvres and the turns $\frac{d\delta_e}{dn}$ is proportional to the wingloading $\frac{W}{S}$ and to $\frac{1}{\frac{1}{2}\rho V^2}$. Figures 10-36 and 10-37 show measurements of the stick displacement per g in pull-up manoeuvres and steady turns of the Auster J-5B ‘Autocar’.

For both types of manoeuvres $\frac{d\delta_e}{dn}$ appears to have the desired negative sign. For this aircraft the relation between δ_e and n in pull-up manoeuvres is non-linear. From the measurements in figures 10-36 and 10-37 it is clear that the required control displacement for a steady turn is larger than for the pull-up manoeuvre at the same load factor n .

A quick derivation of the stick displacement per g

We start with the approximated equations of motion for constant speed, see chapter 10,

$$\begin{bmatrix} C_{Z_\alpha} & 2u_c + C_{Z_q} \\ C_{m_\alpha} & C_{m_q} \end{bmatrix} \cdot \begin{bmatrix} \alpha \\ \frac{q\bar{c}}{V} \end{bmatrix} + \begin{bmatrix} C_{Z_\delta} \\ C_{m_\delta} \end{bmatrix} \delta_e = 0$$

We consider a small deviation from steady straight flight with $\alpha = \Delta\alpha$, $q = \Delta q$ and $\Delta n = n - 1 = \frac{V}{g}\dot{\gamma} = \frac{V}{g}(\dot{\theta} - \dot{\alpha}) = \frac{V}{g}(q - \dot{\alpha})$. As we consider a steady state pull up manoeuvre we have $\dot{\alpha} = 0$, so

$$\Delta n = \frac{V}{g}q, \text{ so } \frac{q\bar{c}}{V} = \frac{g\bar{c}}{V^2}\Delta n$$

Substitution results in

$$\begin{bmatrix} C_{Z_\alpha} & 2u_c + C_{Z_q} \\ C_{m_\alpha} & C_{m_q} \end{bmatrix} \cdot \begin{bmatrix} \Delta\alpha \\ \frac{g\bar{c}}{V^2}\Delta n \end{bmatrix} + \begin{bmatrix} C_{Z_\delta} \\ C_{m_\delta} \end{bmatrix} \cdot \Delta\delta_e = 0$$

or with $Ax_{ss} + B\Delta\delta_e = 0$, in which

$$A = \begin{bmatrix} C_{Z_\alpha} & 2u_c + C_{Z_q} \\ C_{m_\alpha} & C_{m_q} \end{bmatrix}, \text{ and } B = \begin{bmatrix} C_{Z_\delta} \\ C_{m_\delta} \end{bmatrix}.$$

This can be solved as:

$$x_{ss} = \begin{bmatrix} \Delta\alpha \\ \frac{g\bar{c}}{V^2}\Delta n \end{bmatrix} = -A^{-1}B\Delta\delta_e, \text{ or } \begin{bmatrix} \frac{\Delta\alpha}{\Delta\delta_e} \\ \frac{\frac{g\bar{c}}{V^2}\Delta n}{\Delta\delta_e} \end{bmatrix} = -A^{-1}B$$

By applying Cramer's rule we get:

$$\frac{\Delta n}{\Delta\delta_e} = \frac{\begin{vmatrix} C_{Z_\alpha} & C_{Z_\delta} \\ C_{m_\alpha} & C_{m_\delta} \end{vmatrix}}{\begin{vmatrix} C_{Z_\alpha} & 2u_c + C_{Z_q} \\ C_{m_\alpha} & C_{m_q} \end{vmatrix}} = \frac{C_{Z_\alpha}C_{m_\delta} - C_{m_\alpha}C_{Z_\delta}}{C_{Z_\alpha}C_{m_q} - C_{m_\alpha}(2u_c + C_{Z_q})} \cdot \frac{V^2}{g\bar{c}}$$

or:

$$\frac{\Delta\delta_e}{\Delta n} = \frac{C_{Z_\alpha}C_{m_q} - C_{m_\alpha}(2u_c + C_{Z_q})}{C_{Z_\alpha}C_{m_\delta} - C_{m_\alpha}C_{Z_\delta}} \cdot \frac{g\bar{c}}{V^2}$$

When simplifying this expression by setting $C_{Z_\delta} \approx C_{Z_q} \approx 0$, and replacing C_{Z_α} by $-C_{N_\alpha}$ and u_c by $\frac{W}{g\rho S\bar{c}}$ we get:

$$\frac{d\delta_e}{dn} = \frac{\Delta\delta_e}{\Delta n} = -\frac{1}{C_{m_\delta}} \frac{W}{1/2\rho V^2 S} \cdot \left(\frac{C_{m_\alpha}}{C_{N_\alpha}} + \frac{C_{m_q}}{2\mu_c} \right)$$

10-3-3 The manoeuvre point, stick fixed

In equations (10-67) and (10-68) the first term between parantheses is $\frac{C_{m_\alpha}}{C_{N_\alpha}}$. From the discussion of the static longitudinal stability and the neutral point stick fixed, from section 10-1-2 follows,

$$\frac{C_{m_\alpha}}{C_{N_\alpha}} = \frac{x_{cg} - x_{n_{fix}}}{\bar{c}} \quad (10-69)$$

In equation (10-69) $x_{n_{fix}}$ is the x -coordinate of the neutral point, stick fixed, in gliding flight. The first contribution to $\frac{d\delta_e}{dn}$ then appears to be proportional to the distance of the center of gravity to the neutral point. As a consequence the stick displacement per g will decrease in the absolute

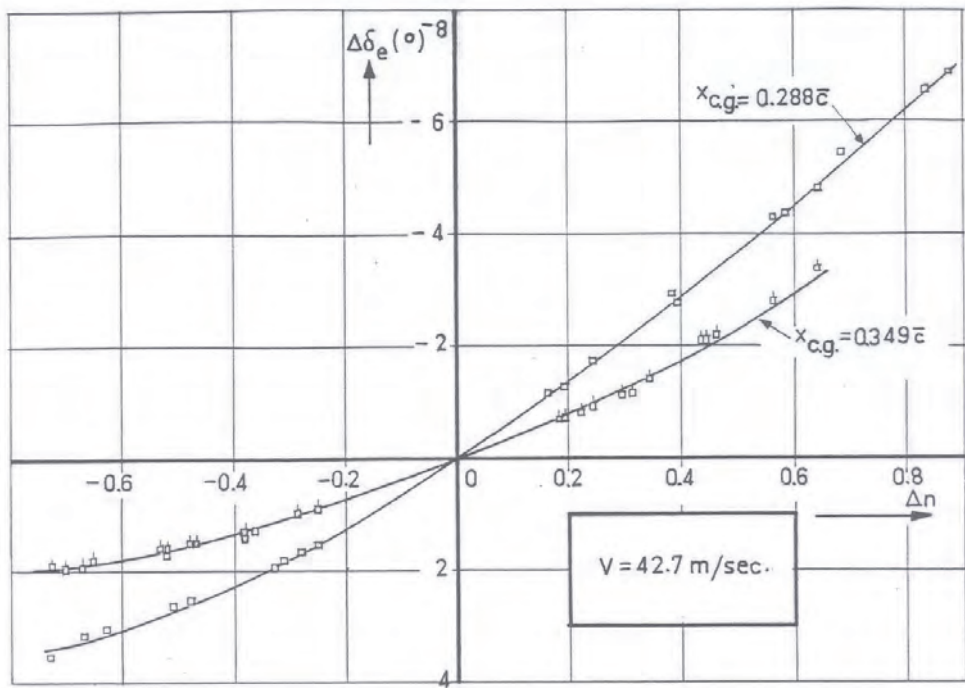


Figure 10-36: The incremental elevator deflection $\Delta\delta_e$ as a function of the incremental load factor Δn in pull-up manoeuvres, Auster J-5B 'Autocar' (from reference [23]).

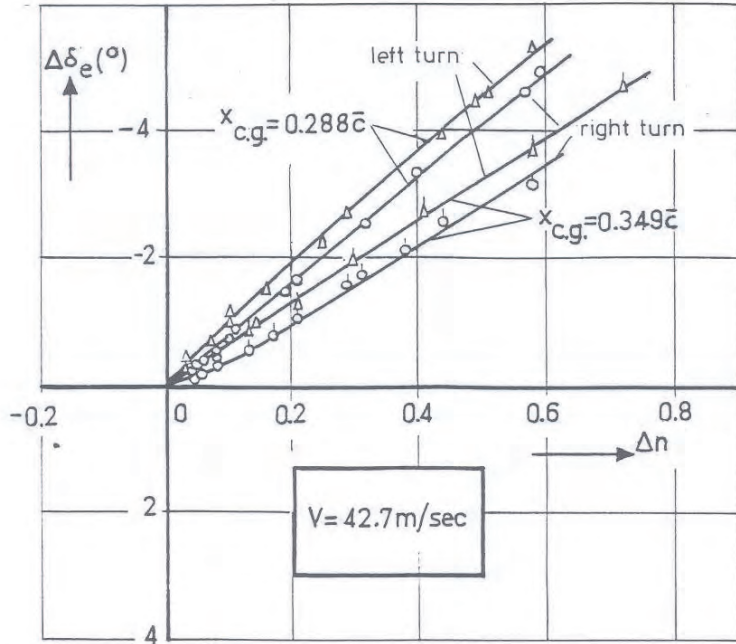


Figure 10-37: The incremental elevator angle $\Delta\delta_e$ as a function of the incremental load factor in turns, Auster J-5B 'Autocar' (from reference [23])

sense if the cg is shifted backward. This can clearly be seen in figures 10-36 and 10-37. It follows that there is a certain cg position where the stick displacement per g is zero. This is the case for the pull-up manoeuvres, if, see equation (10-67),

$$\frac{C_{m_\alpha}}{C_{N_\alpha}} + \frac{C_{m_q}}{2\mu_c} = \frac{x_{cg} - x_{n_{fix}}}{\bar{c}} + \frac{C_{m_q}}{2\mu_c} = 0 \quad (10-70)$$

The cg position at which the stick displacement per g is zero, is called the manoeuvre point, stick fixed, abbreviated as $m.p._{fix}$. The x -coordinate of this point is $x_{m_{fix}}$. From equation (10-70) follows, if $x_{cg} = x_{m_{fix}}$,

$$\frac{x_{m_{fix}} - x_{n_{fix}}}{\bar{c}} = -\frac{C_{m_q}}{2\mu_c} \quad (10-71)$$

Here C_{m_q} has been assumed independent of the cg position, see chapter 7. Combining equations (10-69) and (10-71) results in,

$$\frac{x_{cg} - x_{m_{fix}}}{\bar{c}} = \frac{C_{m_\alpha}}{C_{N_\alpha}} + \frac{C_{m_q}}{2\mu_c} \quad (10-72)$$

Next, equation (10-72) is substituted in equation (10-67). This results in an expression for the stick displacement per g as a function of cg position relative to the $m.p._{fix}$,

$$\frac{d\delta_e}{dn} = -\frac{1}{C_{m_{\delta_e}}} \frac{W}{\frac{1}{2}\rho V^2 S} \frac{x_{cg} - x_{m_{fix}}}{\bar{c}} \quad (10-73)$$

But the manoeuvre point, stick fixed, is not just the cg position at which the stick displacement per g vanishes. The manoeuvre point can be interpreted in yet another way, as explained in the following.

The normal force N can generally be written as, see equation (10-55),

$$N = n W$$

Then,

$$\frac{dC_N}{dn} = \frac{W}{\frac{1}{2}\rho V^2 S} \quad (10-74)$$

Substitution of equation (10-74) in equation (10-73) results in,

$$\frac{d\delta_e}{dn} = -\frac{1}{C_{m_{\delta_e}}} \frac{dC_N}{dn} \frac{x_{cg} - x_{m_{fix}}}{\bar{c}}$$

or,

$$C_{m_{\delta_e}} d\delta_e = -dC_N \frac{x_{cg} - x_{m_{fix}}}{\bar{c}} \quad (10-75)$$

Here $C_{m_{\delta_e}} \cdot d\delta_e$ is the change in the pitching moment due to the elevator deflection $d\delta_e$ and dC_N is the change in the normal force coefficient. According to equation (10-75) $C_{m_{\delta_e}} \cdot d\delta_e$ must be balanced by $dC_N \cdot \frac{x_{cg} - x_{m_{fix}}}{\bar{c}}$. This means that $\frac{x_{cg} - x_{m_{fix}}}{\bar{c}}$ is the arm of the force dC_N . Evidently,

the second interpretation of the manoeuvre point, stick fixed, is the point where the resultant change in normal force acts after the transition from a condition of steady, straight flight to a ‘steady’ pull-up manoeuvre, if the elevator angle were kept constant during this transition.

Since C_{m_q} is negative, it follows from equation (10-71) that the $m.p._{fix}$ always lies behind the $n.p._{fix}$. With increasing μ_c , i.e. with increasing flight altitude, the manoeuvre point moves forward. This can also be seen in figure 10-38 where the calculated position of the $m.p._{fix}$ of the Fokker F-27 ‘Friendship’ is shown.

Subfigure a of figure 10-38 clearly shows the forward shift of $m.p._{fix}$ and also the limiting position: $n.p._{fix}$. The latter position is attained when the term $\frac{C_{m_q}}{2\mu_c}$ becomes vanishingly small.

Thus far the manoeuvre point was discussed only in relation to the pull-up manoeuvres. Both interpretations of the manoeuvre point hold equally for the steady turns. The difference, however, is that then the position of the manoeuvre point is a function also of the load factor n . This can be seen as follows. From equations (10-68) and (10-69) follows for the steady turn,

$$\frac{x_{m_{fix}} - x_{n_{fix}}}{\bar{c}} = -\frac{C_{m_q}}{2\mu_c} \left(1 + \frac{1}{n^2}\right) \quad (10-76)$$

and by consequence,

$$\frac{x_{cg} - x_{m_{fix}}}{\bar{c}} = \frac{C_{m_\alpha}}{C_{N_\alpha}} + \frac{C_{m_q}}{2\mu_c} \left(1 + \frac{1}{n^2}\right) \quad (10-77)$$

The expression (10-73) is valid also for the stick displacement per g in steady turns, although the actual position of the manoeuvre point will be different from the position in the pull-up manoeuvre. From equation (10-76) it can be seen that $x_{m_{fix}}$ now depends not only on the flight altitude, but also on the load factor. If $n = 1$,

$$\frac{x_{m_{fix,turns}} - x_{n_{fix}}}{\bar{c}} = 2 \frac{x_{m_{fix,pull-up}} - x_{n_{fix}}}{\bar{c}} \quad (10-78)$$

With increasing n the manoeuvre point in turns shifts forward. At high values of n the manoeuvre points in the pull-up and in the turn very nearly coincide. This can be seen also in subfigure b of figure 10-38. It should be remembered that $n = 2$ in a steady, horizontal turn corresponds to an angle of roll $\varphi = 60^\circ$, ($n = \frac{1}{\cos \varphi}$). Apart from the stick displacement per g , the stick force per g is of particular interest. It is discussed in the following section.

10-3-4 The stick force per g

The elevator control force was written in section 9-2-7 as, see equation (9-83),

$$F_e = -\frac{d\delta_e}{ds_e} \frac{1}{2} \rho V_h^2 S_e \bar{c}_e (C_{h_\alpha} \alpha_h + C_{h_\delta} \delta_e + C_{h_{\delta_t}} \delta_{t_e})$$

The stick force per g is the derivative of the elevator control force with respect to the load factor in a pull-up manoeuvre or a steady turn. It is a measure of the change in elevator control force after the transition from a condition of steady, straight flight to a ‘steady’ pull-up manoeuvre or a steady turn. In equation (9-83) both α_h and δ_e are functions of the load factor n . It is assumed that the trim tab angle does not vary in the pull-up manoeuvre or the turn, δ_{t_e} is constant. The

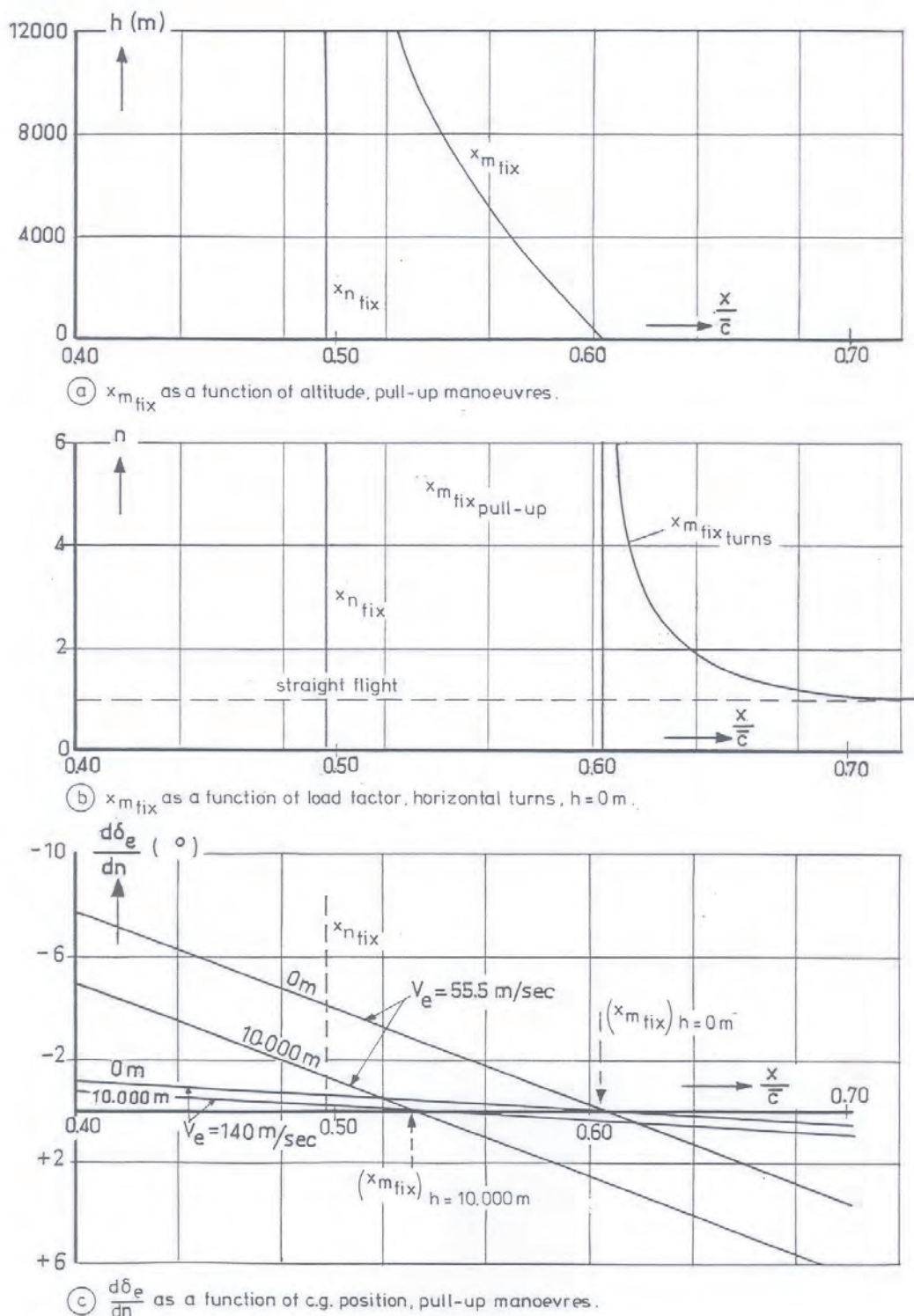


Figure 10-38: Calculated positions of the manoeuvre point, stick fixed, and the stick displacement per g of the Fokker F-27 'Friendship'

airspeed V and thus also V_h in equation (9-83) are assumed to be constant. The stick force per g is then obtained from equation (9-83),

$$\frac{dF_e}{dn} = -\frac{d\delta_e}{ds_e} \frac{1}{2} \rho V_h^2 S_e \bar{c}_e \left(C_{h_\alpha} \frac{d\alpha_h}{dn} + C_{h_\delta} \frac{d\delta_e}{dn} \right) \quad (10-79)$$

The stick displacement per g , the factor $\frac{d\delta_e}{dn}$ on the right hand side of equation (10-79), has already been determined in section 10-3-2. In order to find $\frac{dF_e}{dn}$ the derivative $\frac{d\alpha_h}{dn}$ needs to be determined.

The angle of attack α_h of the horizontal tailplane varies with n in the steady manoeuvres because both α and $q, \frac{q\bar{c}}{V}$, vary with n and,

$$\alpha_h = f \left(\alpha, \frac{q\bar{c}}{V} \right)$$

The partial variation of α_h with α alone was already discussed in section 9-2-4. For steady, straight flight it was found that, see equation (9-65),

$$\alpha_h = (\alpha - \alpha_0) \left(1 - \frac{d\varepsilon}{d\alpha} \right) + (\alpha_0 + i_h)$$

The partial variation of α_h with q alone will now be derived. In the idealized pull-up manoeuvre and in the steady turn the symmetric motion of the aircraft relative to the air can be considered as a pure rotation, with angular velocity q , about a center of rotation situated on the Z -axis above the center of gravity, see figure 10-39.

This position of the center of rotation is such that the local angle of attack at the center of gravity does not change due to the rotation.

When in chapter 4 the stability derivatives with respect to pitching velocity were discussed, it was shown that the principal effect of such a ‘ q -motion’ is a variation of the local, geometric angle of attack, proportional to the angular velocity q and the distance in x -direction to the center of gravity, see figure 10-39,

$$\Delta\alpha = \frac{x - x_{cg}}{R} = \frac{x - x_{cg}}{\bar{c}} \frac{q\bar{c}}{V} \quad (10-80)$$

At the horizontal tailplane the change in geometric angle of attack due to a q -motion is,

$$\Delta\alpha_h = \frac{x_h - x_{cg}}{\bar{c}} \frac{q\bar{c}}{V} \approx \frac{l_h}{\bar{c}} \frac{q\bar{c}}{V} \quad (10-81)$$

In steady, turning flight the total α_h is found by adding equation (9-65) and equation (10-81),

$$\alpha_h = (\alpha - \alpha_0) \left(1 - \frac{d\varepsilon}{d\alpha} \right) + (\alpha_0 + i_h) + \frac{l_h}{\bar{c}} \frac{q\bar{c}}{V} \quad (10-82)$$

From equation (10-82) follows the derivative with respect to n ,

$$\frac{d\alpha_h}{dn} = \left(1 - \frac{d\varepsilon}{d\alpha} \right) \frac{d\alpha}{dn} + \frac{l_h}{\bar{c}} \frac{d\frac{q\bar{c}}{V}}{dn} \quad (10-83)$$

The derivatives $\frac{d\alpha}{dn}$ and $\frac{d\frac{q\bar{c}}{V}}{dn}$ were already obtained previously, see equations (10-60), (10-63) and (10-64).

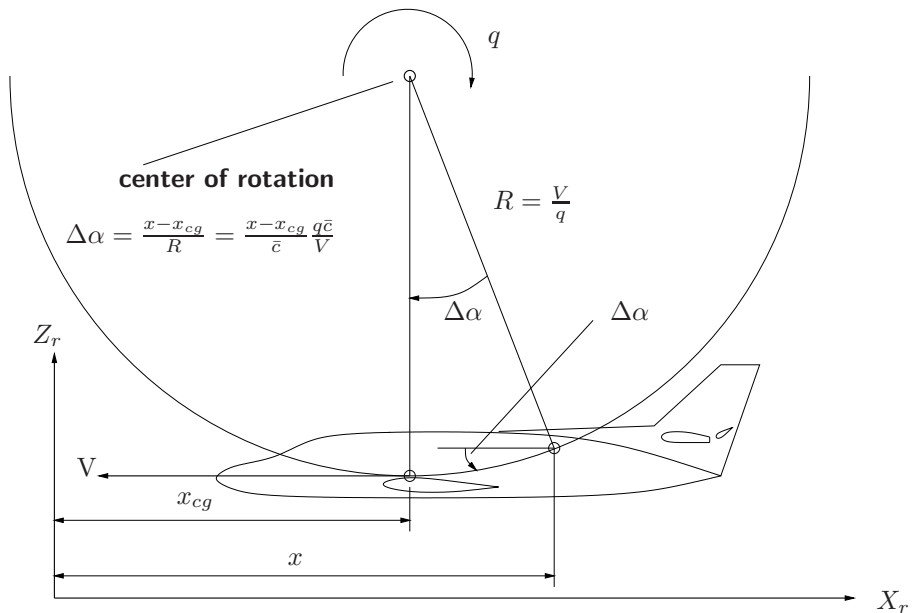


Figure 10-39: The variation of the angle of attack in an arbitrary point of the aircraft caused by a pure q -motion

All variables needed to determine $\frac{d\alpha_h}{dn}$ are now known. Substituting equations (10-60), (10-63) and (10-64) results in,

Pull-up manoeuvres

$$\frac{d\alpha_h}{dn} = \frac{W}{\frac{1}{2}\rho V^2 S} \left\{ \left(1 - \frac{d\varepsilon}{d\alpha} \right) \frac{1}{C_{N_\alpha}} + \frac{l_h}{\bar{c}} \frac{1}{2\mu_c} \right\} \quad (10-84)$$

Steady turns

$$\frac{d\alpha_h}{dn} = \frac{W}{\frac{1}{2}\rho V^2 S} \left\{ \left(1 - \frac{d\varepsilon}{d\alpha} \right) \frac{1}{C_{N_\alpha}} + \frac{l_h}{\bar{c}} \frac{1}{2\mu_c} \left(1 + \frac{1}{n^2} \right) \right\} \quad (10-85)$$

All factors in (10-79) are now known. Substituting and using the expressions already derived in sections 9-2-6 and 10-2-1, i.e. equation (9-76),

$$C_{m_{\delta_e}} = -C_{N_{h_\delta}} \left(\frac{V_h}{V} \right)^2 \frac{S_h l_h}{S \bar{c}}$$

equation (10-35),

$$C_{m_{\alpha_{free}}} = C_{N_{w_\alpha}} \frac{x_{cg} - x_w}{\bar{c}} - C_{N_{h_{\alpha_{free}}}} \left(1 - \frac{d\varepsilon}{d\alpha} \right) \left(\frac{V_h}{V} \right)^2 \frac{S_h l_h}{S \bar{c}}$$

and equation (10-33),

$$C_{N_{h_{\alpha_{free}}}} = C_{N_{h_\alpha}} - C_{N_{h_\delta}} \frac{C_{h_\alpha}}{C_{h_\delta}}$$

the stick force per g is obtained after some reformulation,

Pull-up manoeuvres

$$\frac{dF_e}{dn} = \frac{d\delta_e}{ds_e} \frac{W}{S} \left(\frac{V_h}{V} \right)^2 S_e \bar{c}_e \frac{C_{h_\delta}}{C_{m_{\delta_e}}} \left\{ \frac{C_{m_{\alpha_{free}}}}{C_{N_\alpha}} + \frac{1}{2\mu_c} \left(C_{m_q} - C_{m_{\delta_e}} \frac{C_{h_\alpha}}{C_{h_\delta}} \frac{l_h}{\bar{c}} \right) \right\} \quad (10-86)$$

Steady turns

$$\begin{aligned} \frac{dF_e}{dn} &= \frac{d\delta_e}{ds_e} \frac{W}{S} \left(\frac{V_h}{V} \right)^2 S_e \bar{c}_e \frac{C_{h_\delta}}{C_{m_{\delta_e}}} \left\{ \frac{C_{m_{\alpha_{free}}}}{C_{N_\alpha}} + \frac{1}{2\mu_c} \left(C_{m_q} - C_{m_{\delta_e}} \frac{C_{h_\alpha}}{C_{h_\delta}} \frac{l_h}{\bar{c}} \right) \right. \\ &\quad \left. \left(1 + \frac{1}{n^2} \right) \right\} \end{aligned} \quad (10-87)$$

The first term between the brackets of the expressions (10-86) and (10-87) is due to the static stability, stick free. The second term between the brackets in equation (10-86) can be simplified considerably. From equation (10-81) It can be seen that $\frac{l_h}{\bar{c}}$ is a measure of the change in angle of attack of the horizontal tailplane caused by the q -motion, i.e.,

$$\frac{d\alpha_h}{d\frac{q\bar{c}}{V}} = \frac{l_h}{\bar{c}} \quad (10-88)$$

The variation of the elevator angle with the angle of attack of the horizontal tailplane in the stick free situation was expressed in equation (10-27),

$$\left(\frac{d\delta_e}{d\alpha_h} \right)_{free} = -\frac{C_{h_\alpha}}{C_{h_\delta}}$$

Combining equations (10-88) and (10-27) results in,

$$\left(\frac{d\delta_e}{d\frac{q\bar{c}}{V}} \right)_{free} = \left(\frac{d\delta_e}{d\alpha_h} \right)_{free} \frac{d\alpha_h}{d\frac{q\bar{c}}{V}} = -\frac{C_{h_\alpha}}{C_{h_\delta}} \frac{l_h}{\bar{c}}$$

Evidently, the term $-C_{m_{\delta_e}} \cdot \frac{C_{h_\alpha}}{C_{h_\delta}} \cdot \frac{l_h}{\bar{c}}$ in equations (10-86) and (10-87) represents the moment due to the q -movement, caused by freeing the elevator for,

$$\Delta \left(\frac{dC_m}{d\frac{q\bar{c}}{V}} \right) = \Delta C_{m_q} = C_{m_{\delta_e}} \left(\frac{d\delta_e}{d\frac{q\bar{c}}{V}} \right)_{free} = -C_{m_{\delta_e}} \frac{C_{h_\alpha}}{C_{h_\delta}} \frac{l_h}{\bar{c}} \quad (10-89)$$

If a new derivative, C_{m_q} stick free, is introduced it can be written as,

$$C_{m_{q_{free}}} = C_{m_{q_{fix}}} + \Delta C_{m_q}$$

or, with equation (10-89),

$$C_{m_{q_{free}}} = C_{m_q} - C_{m_{\delta_e}} \frac{C_{h_\alpha}}{C_{h_\delta}} \frac{l_h}{\bar{c}} \quad (10-90)$$

With equations (10-90), (10-86) and (10-87) this can be written as,

Pull-up manoeuvres

$$\frac{dF_e}{dn} = \frac{d\delta_e}{ds_e} \frac{W}{S} \left(\frac{V_h}{V} \right)^2 S_e \bar{c}_e \frac{C_{h_\delta}}{C_{m_{\delta_e}}} \left\{ \frac{C_{m_{\alpha_{free}}}}{C_{N_\alpha}} + \frac{C_{m_{q_{free}}}}{2\mu_c} \right\} \quad (10-91)$$

Steady turns

$$\frac{dF_e}{dn} = \frac{d\delta_e}{ds_e} \frac{W}{S} \left(\frac{V_h}{V} \right)^2 S_e \bar{c}_e \frac{C_{h_\delta}}{C_{m_{\delta_e}}} \left\{ \frac{C_{m_{\alpha_{free}}}}{C_{N_\alpha}} + \frac{C_{m_{q_{free}}}}{2\mu_c} \left(1 + \frac{1}{n^2} \right) \right\} \quad (10-92)$$

From equations (10-91) and (10-92) the influence of the cg position on the stick force per g can be understood. If the cg moves aft, $C_{m_{\alpha_{free}}}$ decreases in the absolute sense and as a consequence the stick force per g decreases in the absolute sense.

From the above expressions it will be seen that contrary to the stick displacement per g the stick force per g is independent of airspeed if the aerodynamic derivatives in equations (10-91) and (10-92) are invariant with airspeed.

The variation of the stick force per g with the cg position is also evident from the measurements shown in figures 10-40 and 10-41. The stick force per g in steady turns is indeed, in the absolute sense, larger than in pull-up manoeuvres at the same load factor n . The relatively large scatter in the data points, visible mainly in figure 10-40, is thought to be caused by friction in the control system.

A quick derivation of stick force per g

Starting from the approximated equations of motion for constant speed, see chapter 10,

$$\begin{bmatrix} C_{Z_\alpha} & 2u_c + C_{Z_q} \\ C_{m_\alpha} & C_{m_q} \end{bmatrix} \cdot \begin{bmatrix} \alpha \\ \frac{q\bar{c}}{V} \end{bmatrix} + \begin{bmatrix} C_{Z_\delta} \\ C_{m_\delta} \end{bmatrix} \cdot \Delta\delta_e = 0$$

we substitute $\alpha = \Delta\alpha$, $q = \Delta q$ and $\Delta n = n - 1 = \frac{V}{g}\dot{\gamma} = \frac{V}{g}(\dot{\theta} - \dot{\alpha}) = \frac{V}{g}(q - \dot{\alpha})$, knowing that in a steady state pull up:

$$\Delta n = \frac{V}{g}q, \text{ so } \frac{q\bar{c}}{V} = \frac{g\bar{c}}{V^2}\Delta n$$

which results in:

$$\begin{bmatrix} C_{Z_\alpha} & 2u_c + C_{Z_q} \\ C_{m_\alpha} & C_{m_q} \end{bmatrix} \cdot \begin{bmatrix} \Delta\alpha \\ \Delta\frac{q\bar{c}}{V} \end{bmatrix} + \begin{bmatrix} C_{Z_\delta} \\ C_{m_\delta} \end{bmatrix} \cdot \Delta\delta_e = 0$$

The corresponding stick force is :

$$\Delta F_e = -\frac{d\delta_e}{ds_e} \cdot \frac{1}{2\rho V_h^2 S_e \bar{c}_e} \{ C_{h_\alpha} \cdot \Delta\alpha_h + C_{h_\delta} \cdot \Delta\delta_e \} = K \cdot \{ C_{h_\alpha} \cdot \Delta\alpha_h + C_{h_\delta} \cdot \Delta\delta_e \}$$

, with

$$K = -\frac{d\delta_e}{ds_e} \cdot \frac{1}{2\rho V_h^2 S_e \bar{c}_e}$$

and

$$\Delta\alpha_h = (1 - \frac{d\varepsilon}{d\alpha}) \cdot \Delta\alpha + \frac{\ell_h}{\bar{c}} \cdot \Delta\frac{q\bar{c}}{V}$$

So

$$\Delta\delta_e = \frac{\Delta F_e}{K} \frac{1}{C_{h_\delta}} - \frac{C_{h_\alpha}}{C_{h_\delta}} (1 - \frac{d\varepsilon}{d\alpha}) \cdot \Delta\alpha - \frac{C_{h_\alpha}}{C_{h_\delta}} \frac{\ell_h}{\bar{c}} \cdot \Delta\frac{q\bar{c}}{V}$$

Substituting this in the equations of motion results in:

$$\begin{aligned} & \begin{bmatrix} C_{Z_\alpha} & 2u_c + C_{Z_q} \\ C_{m_\alpha} & C_{m_q} \end{bmatrix} \cdot \begin{bmatrix} \Delta\alpha \\ \Delta\frac{q\bar{c}}{V} \end{bmatrix} + \\ & \quad \begin{bmatrix} C_{Z_\delta} \\ C_{m_\delta} \end{bmatrix} \cdot \left\{ \frac{\Delta F_e}{K} \frac{1}{C_{h_\delta}} - \frac{C_{h_\alpha}}{C_{h_\delta}} (1 - \frac{d\varepsilon}{d\alpha}) \cdot \Delta\alpha - \frac{C_{h_\alpha}}{C_{h_\delta}} \frac{\ell_h}{\bar{c}} \cdot \Delta\frac{q\bar{c}}{V} \right\} = \\ & \quad \begin{bmatrix} C_{Z_\alpha} - C_{Z_\delta} \frac{C_{h_\alpha}}{C_{h_\delta}} (1 - \frac{d\varepsilon}{d\alpha}) & 2u_c + C_{Z_q} - C_{Z_\delta} \frac{C_{h_\alpha}}{C_{h_\delta}} \frac{\ell_h}{\bar{c}} \\ C_{m_\alpha} - C_{m_\delta} \frac{C_{h_\alpha}}{C_{h_\delta}} (1 - \frac{d\varepsilon}{d\alpha}) & C_{m_q} - C_{m_\delta} \frac{C_{h_\alpha}}{C_{h_\delta}} \frac{\ell_h}{\bar{c}} \end{bmatrix} \cdot \begin{bmatrix} \Delta\alpha \\ \Delta\frac{q\bar{c}}{V} \end{bmatrix} + \\ & \quad \begin{bmatrix} C_{Z_\delta} \\ C_{m_\delta} \end{bmatrix} \cdot \frac{\Delta F_e}{K} \frac{1}{C_{h_\delta}} = 0 \end{aligned}$$

Now we introduce:

$$C_{Z_\alpha} - C_{Z_\delta} \frac{C_{h_\alpha}}{C_{h_\delta}} (1 - \frac{d\varepsilon}{d\alpha}) = C_{Z_\alpha \text{ free}}$$

$$C_{Z_q} - C_{Z_\delta} \frac{C_{h_\alpha}}{C_{h_\delta}} \frac{\ell_h}{\bar{c}} = C_{Z_q \text{ free}}$$

$$C_{m_\alpha} - C_{m_\delta} \frac{C_{h_\alpha}}{C_{h_\delta}} (1 - \frac{d\varepsilon}{d\alpha}) = C_{m_\alpha \text{ free}}$$

$$C_{m_q} - C_{m_\delta} \frac{C_{h_\alpha}}{C_{h_\delta}} \frac{\ell_h}{\bar{c}} = C_{m_q \text{ free}}$$

resulting in:

$$\begin{bmatrix} C_{Z_\alpha \text{ free}} & 2u_c + C_{Z_q \text{ free}} \\ C_{m_\alpha \text{ free}} & C_{m_q \text{ free}} \end{bmatrix} \cdot \begin{bmatrix} \Delta\alpha \\ \Delta\frac{q\bar{c}}{V} \end{bmatrix} + \begin{bmatrix} C_{Z_\delta} \\ C_{m_\delta} \end{bmatrix} \cdot \frac{\Delta F}{K} \frac{1}{C_{h_\delta}} = 0$$

or:

$$A \cdot \Delta x_{ss} + B \cdot \frac{\Delta F}{K} \frac{1}{C_{h_\delta}} = 0$$

Of which the solution is:

$$\Delta x_{ss} = -A^{-1} B \frac{\Delta F}{K} \frac{1}{C_{h_\delta}} \quad \text{with } \Delta x_{ss} = \begin{bmatrix} \Delta\alpha \\ \Delta\frac{q\bar{c}}{V} \end{bmatrix}$$

We may solve for $\Delta\frac{q\bar{c}}{V}$ as:

$$\begin{aligned} \Delta\frac{q\bar{c}}{V} &= \frac{\begin{vmatrix} C_{Z_\alpha \text{ free}} & C_{Z_\delta} \\ C_{m_\alpha \text{ free}} & C_{m_\delta} \end{vmatrix}}{\begin{vmatrix} C_{Z_\alpha \text{ free}} & 2u_c + C_{Z_q \text{ free}} \\ C_{m_\alpha \text{ free}} & C_{m_q \text{ free}} \end{vmatrix}} \cdot \frac{\Delta F}{K} \frac{1}{C_{h_\delta}} \\ &= \frac{C_{m_\delta} \cdot C_{Z_\alpha \text{ free}} - C_{Z_\delta} \cdot C_{m_\alpha \text{ free}}}{C_{Z_\alpha \text{ free}} C_{m_q \text{ free}} - C_{m_\alpha \text{ free}} (2u_c + C_{Z_q \text{ free}})} \cdot \frac{\Delta F}{K} \frac{1}{C_{h_\delta}} \end{aligned}$$

With good approximation we may set $C_{Z_q} = C_{Z_\delta} = 0$, so that $C_{Z_{\alpha \text{ free}}} = C_{Z_\alpha}$ and $C_{Z_{q \text{ free}}} = C_{Z_q} = 0$ so

$$\Delta\frac{q\bar{c}}{V} = \frac{C_{m_\delta} \cdot C_{Z_\alpha}}{C_{Z_\alpha} \cdot C_{m_q \text{ free}} - 2\mu_c C_{m_\alpha \text{ free}}} \cdot \frac{\Delta F}{K} \frac{1}{C_{h_\delta}}$$

and using $\Delta\frac{q\bar{c}}{V} = \frac{g\bar{c}}{V^2} \Delta n$ and $C_{Z_\alpha} = -C_{N_\alpha}$:

$$\begin{aligned} \frac{\Delta F}{\Delta n} &= K \cdot 2\mu_c \frac{g\bar{c}}{V^2} \frac{C_{h_\delta}}{C_{m_\delta}} \cdot \left\{ \frac{C_{m_\alpha \text{ free}}}{C_{N_\alpha}} + \frac{C_{m_q \text{ free}}}{2\mu_c} \right\} = \\ &- \frac{d\delta_e}{ds_e} \cdot \frac{1}{2\rho V_h^2 S_e \bar{c}_e} \frac{2.W}{g\rho S\bar{c}} \frac{g\bar{c}}{V^2} \frac{C_{h_\delta}}{C_{m_\delta}} \cdot \left\{ \frac{C_{m_\alpha \text{ free}}}{C_{N_\alpha}} + \frac{C_{m_q \text{ free}}}{2\mu_c} \right\} \end{aligned}$$

or:

$$\frac{dF_e}{dn} = - \frac{d\delta_e}{ds_e} \frac{W}{S} \cdot \left(\frac{V_h}{V} \right)^2 S_e \bar{c}_e \cdot \frac{C_{h_\delta}}{C_{m_\delta}} \left\{ \frac{C_{m_\alpha \text{ free}}}{C_{N_\alpha}} + \frac{C_{m_q \text{ free}}}{2\mu_c} \right\}$$

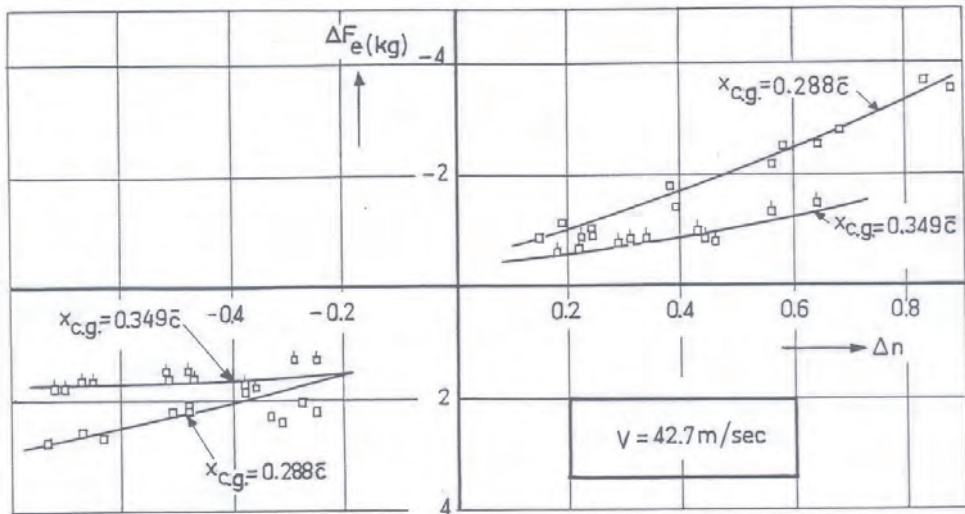


Figure 10-40: The incremental control force ΔF_e as a function of the incremental load factor Δn in pull-up manoeuvres, Auster J-5B ‘Autocar’ (from reference [23])

10-3-5 The manoeuvre point, stick free

In section 10-3-3 it was shown that at a certain cg position corresponding with the manoeuvre point, stick fixed, the stick displacement per g becomes zero. For the stick force per g also a certain cg position exists where $\frac{dF_e}{dn}$ is zero. This point is called the manoeuvre point, stick free. It is also indicated as $m.p._{free}$, the abscissa of this point is $x_{m_{free}}$. From the discussion in section 10-2-2 follows,

$$\frac{C_{m_{\alpha_{free}}}}{C_{N_\alpha}} = \frac{x_{cg} - x_{n_{free}}}{\bar{c}} \quad (10-93)$$

If $x_{cg} = x_{m_{free}}$ then $\frac{dF_e}{dn} = 0$, and,

$$\frac{C_{m_{\alpha_{free}}}}{C_{N_\alpha}} + \frac{C_{m_{q_{free}}}}{2\mu_c} = 0$$

For the pull-up manoeuvre the above can be written as, see equations (10-91) and (10-93),

$$\frac{x_{m_{free}} - x_{n_{free}}}{\bar{c}} = -\frac{C_{m_{q_{free}}}}{2\mu_c} \quad (10-94)$$

Since $C_{m_{q_{free}}}$ is again negative, the manoeuvre point, stick free, lies behind the neutral point, stick free in gliding flight. According to equations (10-93) and (10-94) is for the pull-up manoeuvres,

$$\frac{x_{cg} - x_{m_{free}}}{\bar{c}} = \frac{C_{m_{\alpha_{free}}}}{C_{N_\alpha}} + \frac{C_{m_{q_{free}}}}{2\mu_c} \quad (10-95)$$

For the stick force per g follows then with equations (10-91) and (10-95),

$$\frac{dF_e}{dn} = \frac{d\delta_e}{ds_e} \frac{W}{S} \left(\frac{V_h}{V} \right)^2 S_e \bar{c}_e \frac{C_{h_\delta}}{C_{m_{\delta_e}}} \frac{x_{cg} - x_{m_{free}}}{\bar{c}} \quad (10-96)$$

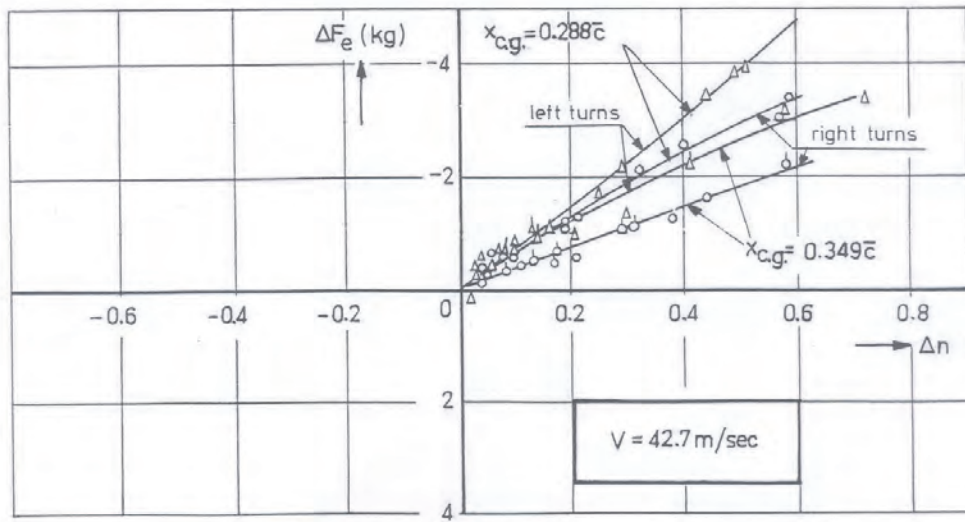


Figure 10-41: The incremental control force ΔF_e as a function of the incremental load factor Δn in turns, Auster J-5B 'Autocar' (from reference [23])

For the steady turns it can be derived in the same way,

$$\frac{x_{m_{free}} - x_{n_{free}}}{\bar{c}} = -\frac{C_{m_{q_{free}}}}{2\mu_c} \left(1 + \frac{1}{n^2}\right) \quad (10-97)$$

and consequently,

$$\frac{x_{cg} - x_{m_{free}}}{\bar{c}} = \frac{C_{m_{\alpha_{free}}}}{C_{N_\alpha}} + \frac{C_{m_{q_{free}}}}{2\mu_c} \left(1 + \frac{1}{n^2}\right) \quad (10-98)$$

This means that equation (10-96) is also true for the stick force per g in steady turns, although the position of the manoeuvre point, stick free, differs for the two types of manoeuvres, according to equations (10-94) and (10-97).

Just as in the case of the manoeuvre point, stick fixed, a second interpretation can be given of the manoeuvre point, stick free. To this end, the transition from a condition of steady, straight flight to a manoeuvre is separated in two phases. These will be considered separately one after another.

In the first phase, the aircraft is supposed to change with free elevator, from steady, straight flight to a turning manoeuvre. As far as the forces along the Z -axis are concerned this is a steady manoeuvre: equilibrium exists along the Z -axis. The change in normal force $dC_{N_{free}}$ due to this transition acts in a certain point, the abscissa of which is provisionally indicated as $x_{dC_{N_{free}}}$. The accompanying change in the pitching moment due to this transition then is,

$$dC_{m_{free}} = dC_N \frac{x_{cg} - x_{dC_{N_{free}}}}{\bar{c}}$$

The second and subsequent phase takes place at constant α , q and V . In this phase equilibrium of the pitching moment is obtained. The moment $dC_{m_{free}}$ is balanced by applying an appropriate

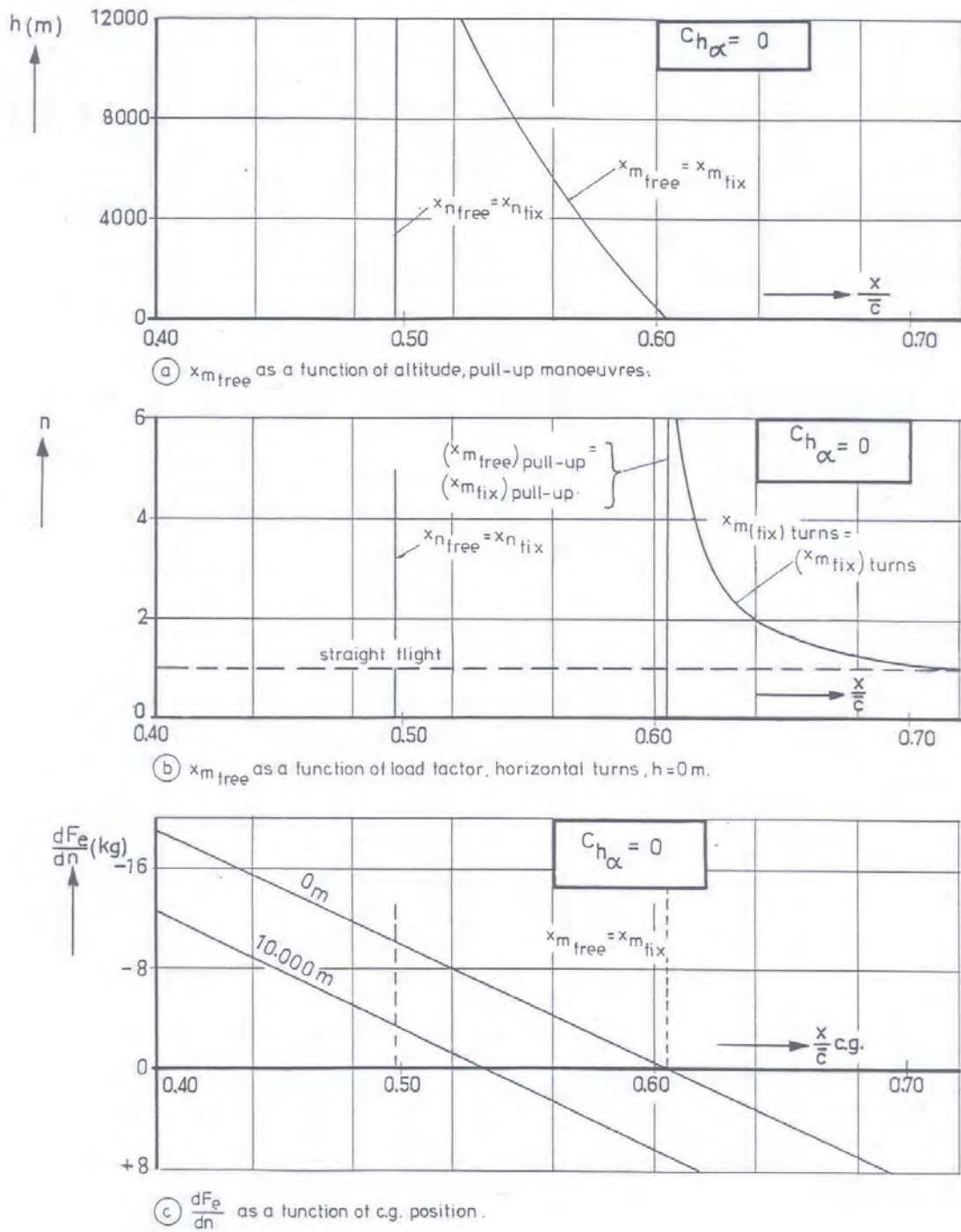


Figure 10-42: Calculated positions of the manoeuvre point, stick free, and the stick force per g of the Fokker F-27 'Friendship'

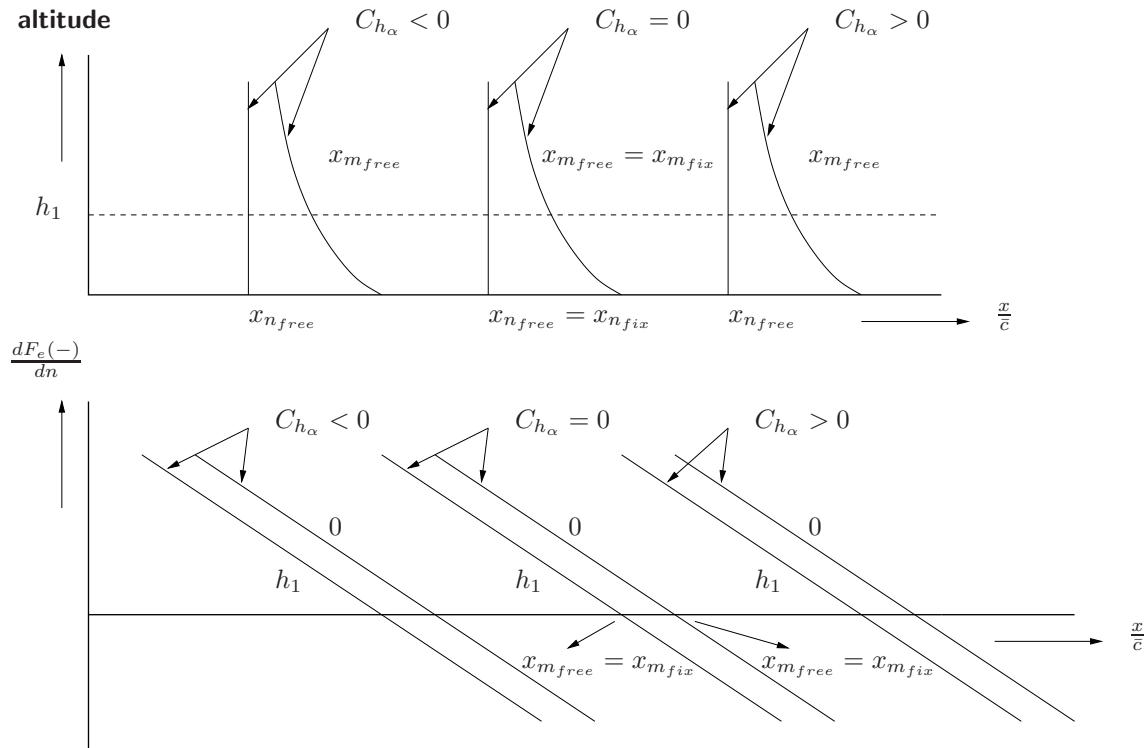


Figure 10-43: Influence of altitude and magnitude and sign of $C_{h\alpha}$ on the position of the manoeuvre point, stick free, and the stick force per g

elevator deflection $d\delta_e$ and the control force dF_e . The required elevator angle $d\delta_e$ is,

$$d\delta_e = -\frac{dC_{m_{free}}}{C_{m_{\delta_e}}} = -\frac{1}{C_{m_{\delta_e}}} dC_{N_{free}} \frac{x_{cg} - x_{dC_{N_{free}}}}{\bar{c}} \quad (10-99)$$

The required elevator control force dF_e follows from the change in the hinge moment occurring in the second phase. Note that in the first phase the elevator was free: $F_e = 0$. Thus,

$$dF_e = -\frac{d\delta_e}{ds_e} \frac{1}{2} \rho V_h^2 S_e \bar{c}_e dC_{h_e} \quad (10-100)$$

Since α_h is constant in the second phase (α and q remain constant), dC_{h_e} is,

$$dC_{h_e} = C_{h_\delta} d\delta_e \quad (10-101)$$

Substituting $d\delta_e$ according to equation (10-99) in equation (10-101) and subsequently in equation (10-100) results in,

$$dF_e = \frac{d\delta_e}{ds_e} \frac{1}{2} \rho V_h^2 S_e \bar{c}_e \frac{C_{h_\delta}}{C_{m_{\delta_e}}} dC_{N_{free}} \frac{x_{cg} - x_{dC_{N_{free}}}}{\bar{c}} \quad (10-102)$$

Next, the change in elevator control force dF_e is considered, following from the expression (10-96) for the stick force per g . With equation (10-74), where $dC_N = dC_{N_{free}}$, from equation (10-96) follows for both types of manoeuvres,

$$dF_e = \frac{d\delta_e}{ds_e} \frac{1}{2} \rho V_h^2 S_e \bar{c}_e \frac{C_{h_\delta}}{C_{m_{\delta_e}}} dC_{N_{free}} \frac{x_{cg} - x_{m_{free}}}{\bar{c}} \quad (10-103)$$

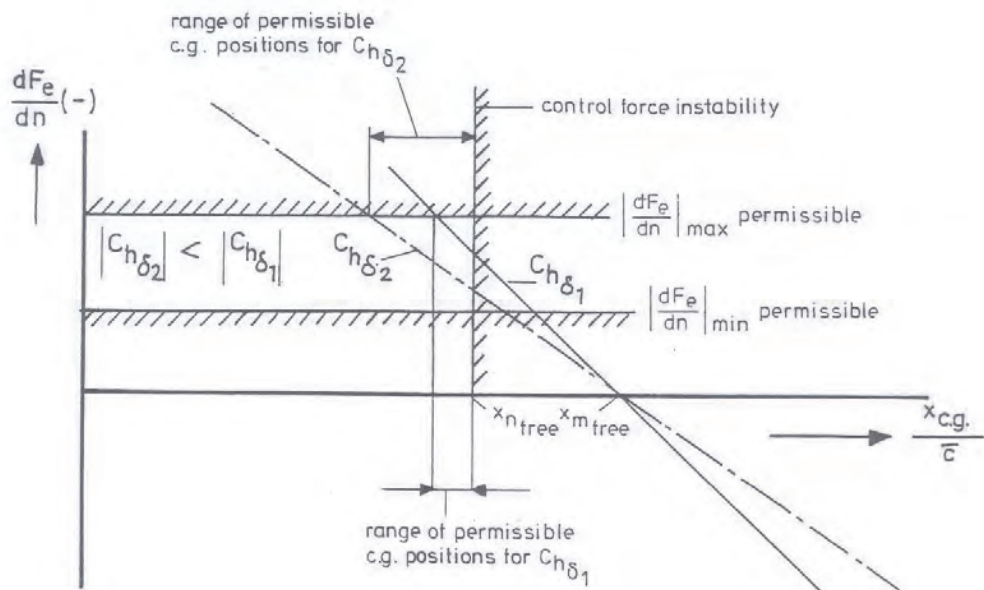


Figure 10-44: Increasing the range of permissible cg positions by decreasing $|C_{h\delta}|$

If the expressions (10-102) and (10-103) are now compared, it will be clear that the manoeuvre point, stick free, in equation (10-103) corresponds with the point of action of the change in normal force $dC_{N_{free}}$ in equation (10-102), caused by the transition with free elevator from steady, straight flight to a manoeuvre. This explains the second interpretation of the manoeuvre point, stick free.

Using equations (10-94) and (10-97) the position of the manoeuvre point was calculated for the Fokker F-27. The results are shown in figure 10-42. The $C_{h\alpha}$ of the elevator of this aircraft is approximately zero. As a result, there is no difference between the situations: control free and control fixed. It can be seen from the figure that the manoeuvre point moves forward with increasing flight altitude, approaching in the limit the neutral point. With increasing load factor n the manoeuvre point in steady turns approaches the manoeuvre point in pull-up manoeuvres.

Figure 10-43 indicates schematically how the position of the manoeuvre point, stick free, and $\frac{dF_e}{dn}$ change with flight altitude and with $C_{h\alpha}$.

Figure 10-44 shows the influence of $C_{h\delta}$ on the range of permissible center of gravity positions.

The discussion in section 10-3-1 referred to the fact that the stick force per g has an upper and a lower limit of permissible values. Other requirements remain also in force, such as those relating to the elevator control position and force stability. As a consequence it is sometimes not an easy matter to satisfy all requirements on the stability and control characteristics in all aircraft configurations and flight conditions stipulated in the regulations.

10-3-6 Non-aerodynamic means to influence the stick force Per g

Sometimes springs or unbalanced masses are installed in the control mechanism, to influence the elevator control force stability or the stick force per g or both.

In section 10-2-4 the influence was discussed of a spring or an unbalanced mass on the elevator control force stability and the position of the neutral point, stick free. The spring was assumed to

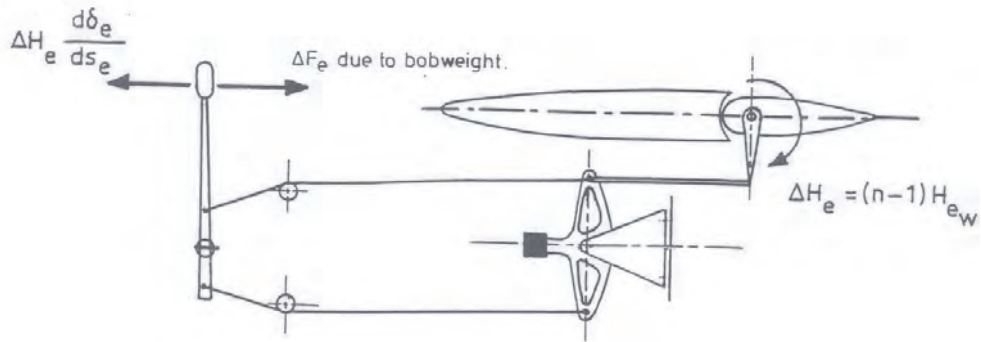


Figure 10-45: The incremental hinge moment due to a bobweight in the control mechanism in a pull-up manoeuvre at a load factor n

exert a constant hinge moment.

Such a spring has no influence on the stick force per g , but an unbalanced mass has.

Suppose, a mass has been installed in the control mechanism, see figure 10-45, such that in straight and level flight a static hinge moment H_{e_w} is generated.

In a manoeuvre at a load factor n an extra hinge moment $(n-1) \cdot H_{e_w}$ occurs. This hinge moment must be balanced by an extra control force ΔF_e ,

$$\Delta F_e = -\frac{d\delta_e}{ds_e} \Delta n H_{e_w}$$

The influence of the mass, sometimes called a ‘bobweight’, on the stick force per g is,

$$\Delta \frac{dF_e}{dn} = -\frac{d\delta_e}{ds_e} H_{e_w} \quad (10-104)$$

In this way it is seen that a modification of the stick force per g can be obtained which is independent of cg position and flight altitude. In some cases this may bring $\frac{dF_e}{dn}$ within the required limits.

By choosing the right combination of springs and bobweights it is possible in principle to vary both the elevator control force stability and the stick force per g independent of one another using non-aerodynamic means. If, however, the hinge moment generated by springs or bobweights or both becomes too large, the dynamic stability, stick free, may be influenced unfavorably. In addition, the possibility of the occurrence of flutter has to be investigated.

It was shown in this chapter that the stick displacement per g and the stick force per g must have a negative sign, whereas the magnitude of the stick force per g is additionally limited to lie within a certain range. These requirements may restrict both the forward and the rear limits of permissible cg positions. This remark is supplementary to what was noted in section 10-2-7.

There the rear limit of cg positions was said to be determined by the requirement that the aircraft must possess elevator control position and elevator control force stability. The forward limit of permissible cg positions was there shown to be dictated by the available elevator power in take-off or landing.

Chapter 11

Lateral Stability and Control in Steady Flight

11-1 Introduction

Using the equilibrium equations for asymmetric flight, the lateral control characteristics in some important steady, asymmetric flight conditions will be discussed in the following. To simplify the discussion only horizontal flight will be considered. In a condition of steady flight, in which the roll angle is constant by definition, the rolling velocity about the X_B -axis is zero. This is the case when the X_B -axis, along the velocity vector of the c.g., lies in the horizontal plane.

From the above follows that in steady, asymmetric horizontal flight the rolling velocity is always zero. The ‘steady’ rolling flight to be considered in section 11-6, is an approximated, quasi-steady flight condition giving in a simple manner insight in some important requirements on roll control for aircraft.

11-2 Equations of Equilibrium

In the most general case of a horizontal, steady, asymmetric condition of flight, the aircraft sideslips and yaws at constant β and $\frac{rb}{2V}$. The angle of roll φ of the aircraft differs from zero but the rolling velocity is zero. To maintain this flight condition, generally the ailerons as well as the rudder are deflected.

Not only the aerodynamic force Y along the Y_B -axis and the aerodynamic moments L and N about the X_B - and Z_B -axis respectively act on the aircraft, but also the component of the weight along the Y_B -axis. Since the pitch angle θ , measured in the stability reference frame, is zero in horizontal flight, the component of the weight along the Y_B -axis (or Y_S -axis) is,

$$W \sin \varphi$$

The combined forces along the Y_B -axis cause a centripetal acceleration in the Y_B -direction: $V \cdot r$, see figure 11-1. The resultant equation for the forces along the Y_B -axis, both in the aircraft and

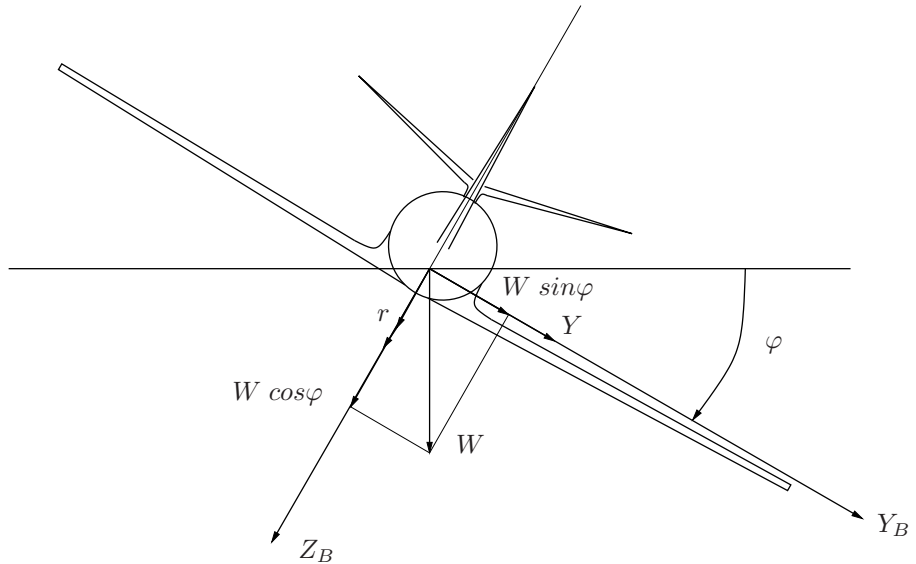


Figure 11-1: The forces along the Y_B -axis of an aircraft in steady, horizontal, asymmetric flight

the stability reference frame, then is,

$$W \sin \varphi + Y = m V r \quad (11-1)$$

whereas the equilibrium of the moments about the X_B - and Z_B -axes is expressed by,

$$L = 0 \quad (11-2)$$

$$N = 0 \quad (11-3)$$

The equations are made non-dimensional by dividing equation (11-1) by $\frac{1}{2}\rho V^2 S$, and both equations (11-2) and (11-3) by $\frac{1}{2}\rho V^2 S b$. This results for small values of φ in,

$$\begin{aligned} C_L \varphi - 4\mu_b \frac{r b}{2V} + C_Y &= 0 \\ C_\ell &= 0 \\ C_n &= 0 \end{aligned} \quad (11-4)$$

where,

$$C_L = \frac{W}{\frac{1}{2}\rho V^2 S}$$

and

$$\mu_b = \frac{m}{\rho S b}$$

is the non-dimensional mass parameter for the asymmetric motions, see chapter 4.

If the aerodynamic forces and moments in equation (11-4) are now expressed in the contributions arising from β , $\frac{rb}{2V}$, δ_a and δ_r , according to equations (8-2) and (8-3), the resulting asymmetric equilibrium equations for horizontal steady asymmetric flight become,

$$\begin{aligned} C_L \varphi + C_{Y_\beta} \beta + (C_{Y_r} - 4\mu_b) \frac{rb}{2V} + C_{Y_{\delta_a}} \delta_a + C_{Y_{\delta_r}} \delta_r &= 0 \\ C_{\ell_\beta} \beta + C_{\ell_r} \frac{rb}{2V} + C_{\ell_{\delta_a}} \delta_a + C_{\ell_{\delta_r}} \delta_r &= 0 \\ C_{n_\beta} \beta + C_{n_r} \frac{rb}{2V} + C_{n_{\delta_a}} \delta_a + C_{n_{\delta_r}} \delta_r &= 0 \end{aligned} \quad (11-5)$$

Based on the discussions in chapter 8, the control derivatives $C_{Y_{\delta_a}}$ and $C_{\ell_{\delta_r}}$ will be neglected in the following. In a first approximation used to study the various types of steady flight, C_{Y_r} , $C_{n_{\delta_a}}$ and $C_{Y_{\delta_r}}$ will also be dropped. In the thus simplified form the equilibrium equations read as,

$$C_L \varphi + C_{Y_\beta} \beta - 4\mu_b \frac{rb}{2V} = 0 \quad (11-6)$$

$$C_{\ell_\beta} \beta + C_{\ell_r} \frac{rb}{2V} + C_{\ell_{\delta_a}} \delta_a = 0 \quad (11-7)$$

$$C_{n_\beta} \beta + C_{n_r} \frac{rb}{2V} + C_{n_{\delta_r}} \delta_r = 0 \quad (11-8)$$

Or, using matrix notation,

$$\begin{bmatrix} C_L & C_{Y_\beta} & -4\mu_b & 0 & 0 \\ 0 & C_{\ell_\beta} & C_{\ell_r} & C_{\ell_{\delta_a}} & 0 \\ 0 & C_{n_\beta} & C_{n_r} & 0 & C_{n_{\delta_r}} \end{bmatrix} \begin{bmatrix} \varphi \\ \beta \\ \frac{rb}{2V} \\ \delta_a \\ \delta_r \end{bmatrix} = \underline{0}$$

In section 11-3 to 11-5 the lateral control characteristics of the aircraft in various steady, asymmetric flight conditions are studied, using the above equations. Because of the simplifications introduced, the considerations are primarily qualitative in nature, especially for larger deviations from symmetric flight.

11-3 Steady Horizontal Turns

In the three equations (11-6), (11-7) and (11-8) five variables occur. This implies, that steady turns at a given airspeed and yaw-rate $\frac{rb}{2V}$ can be flown in principle at infinitely many combinations of the remaining four variables δ_r , δ_a , β and φ . Only if one of these four variables has been fixed, the remaining three can be expressed as functions of $\frac{rb}{2V}$. In the following steady turns are studied in which each of the four variables mentioned are assumed separately to be equal to zero.

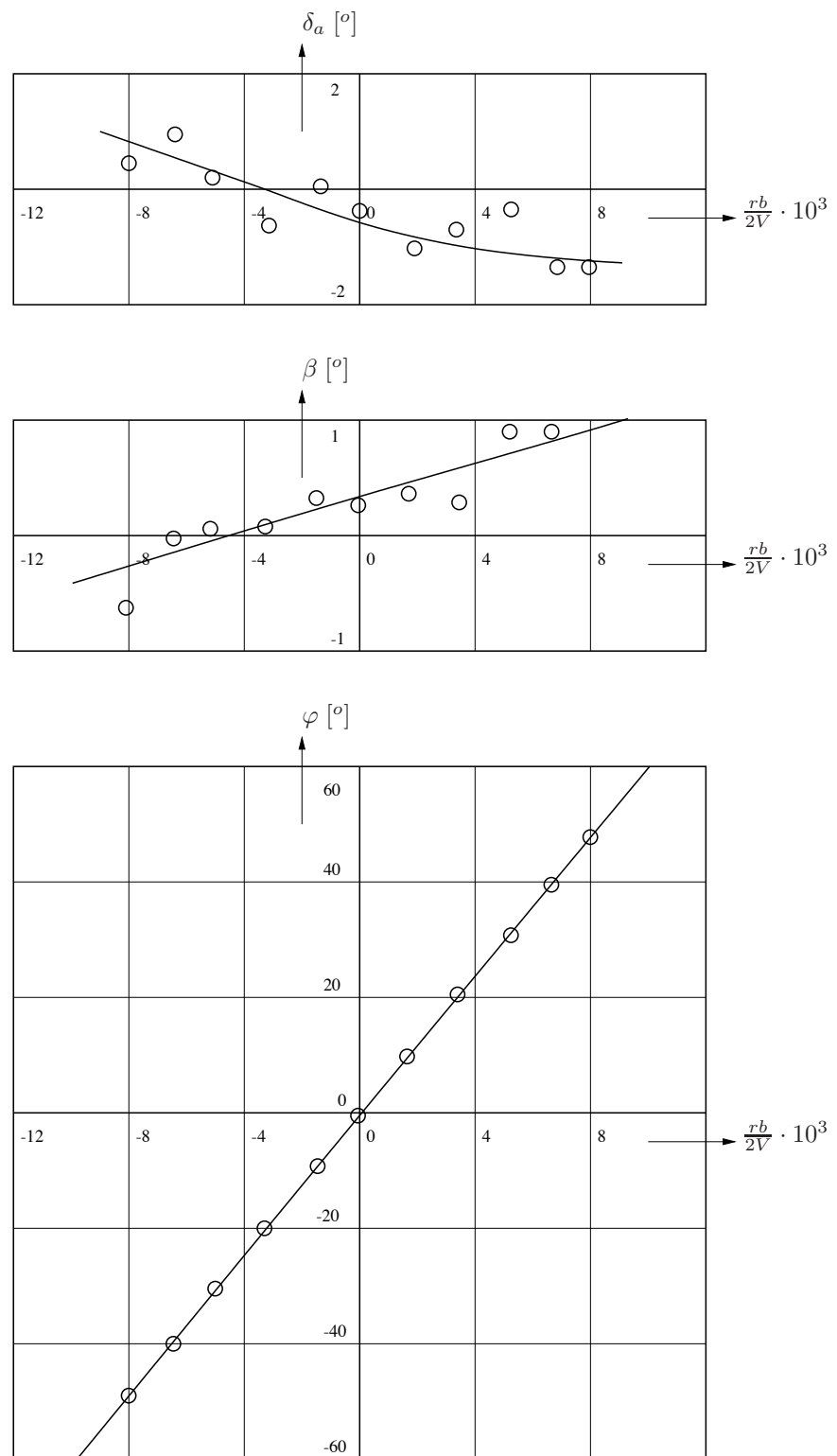


Figure 11-2: Steady turns using ailerons only, North American 'Harvard II B', gliding flight, $C_L = 0.31$, $x_{c.g.} = 0.304 \bar{c}$, $V = 78$ m/sec (from reference [14])

11-3-1 Turns Using the Ailerons Only, $\delta_r = 0$

Using equations (11-7) and (11-8) and the condition $\delta_r = 0$, it follows that the variation of the aileron angles with rate of yaw can be expressed as,

$$\frac{d\delta_a}{d\frac{rb}{2V}} = \frac{1}{C_{\ell_{\delta_a}}} \frac{C_{\ell_\beta} C_{n_r} - C_{\ell_r} C_{n_\beta}}{C_{n_\beta}} \quad (11-9)$$

Here $C_{\ell_{\delta_a}} < 0$ and $C_{n_\beta} > 0$.

To initiate a turn to the right using the ailerons only, a negative aileron deflection must be given to obtain a positive rolling velocity and a positive angle of roll. Using the same arguments as in chapter 10, it is desirable that in the ultimate steady flight condition the aileron control remains deflected in the direction of the initial control deflection, so $\frac{d\delta_a}{d\frac{rb}{2V}} < 0$. According to equation (11-9) the necessary condition for this is,

$$C_{\ell_\beta} C_{n_r} - C_{\ell_r} C_{n_\beta} > 0 \quad (11-10)$$

This latter condition corresponds to the condition for spiral stability which is discussed in chapter 6.

If $\delta_r = 0$ in the expressions (11-6) and (11-8), the variation of angle of roll with rate of yaw can be derived as,

$$\frac{d\varphi}{d\frac{rb}{2V}} = \frac{4\mu_b + C_{Y_\beta} \frac{C_{n_r}}{C_{n_\beta}}}{C_L} > 0 \quad (\text{for } C_L > 0) \quad (11-11)$$

and also,

$$\frac{d\beta}{d\frac{rb}{2V}} = -\frac{C_{n_r}}{C_{n_\beta}} > 0 \quad (C_{n_r} < 0, \quad C_{n_\beta} > 0) \quad (11-12)$$

In a turn to the right, with $\delta_r = 0$, the aircraft has a roll angle to the right ($\varphi > 0$) and the sideslip is towards the inside of the turn ($\beta > 0$). At practical values of φ and $\frac{rb}{2V}$ the angle of sideslip usually remains limited to a few degrees. Figure 11-2 shows the results of some measurements made in steady flight, using the ailerons only.

11-3-2 Turns Using the Rudder Only, $\delta_a = 0$

Using equations (11-7) and (11-8) and the condition $\delta_a = 0$, the variation of the rudder angle with rate of yaw is obtained as,

$$\frac{d\delta_r}{d\frac{rb}{2V}} = -\frac{1}{C_{n_{\delta_r}}} \frac{C_{\ell_\beta} C_{n_r} - C_{\ell_r} C_{n_\beta}}{C_{\ell_\beta}} \quad (11-13)$$

Here $C_{n_{\delta_r}} < 0$ and $C_{\ell_\beta} < 0$. It then follows that if the condition equation (11-10) for spiral stability is satisfied, in a turn to the right the rudder is also deflected to the right ($\delta_r < 0$). In

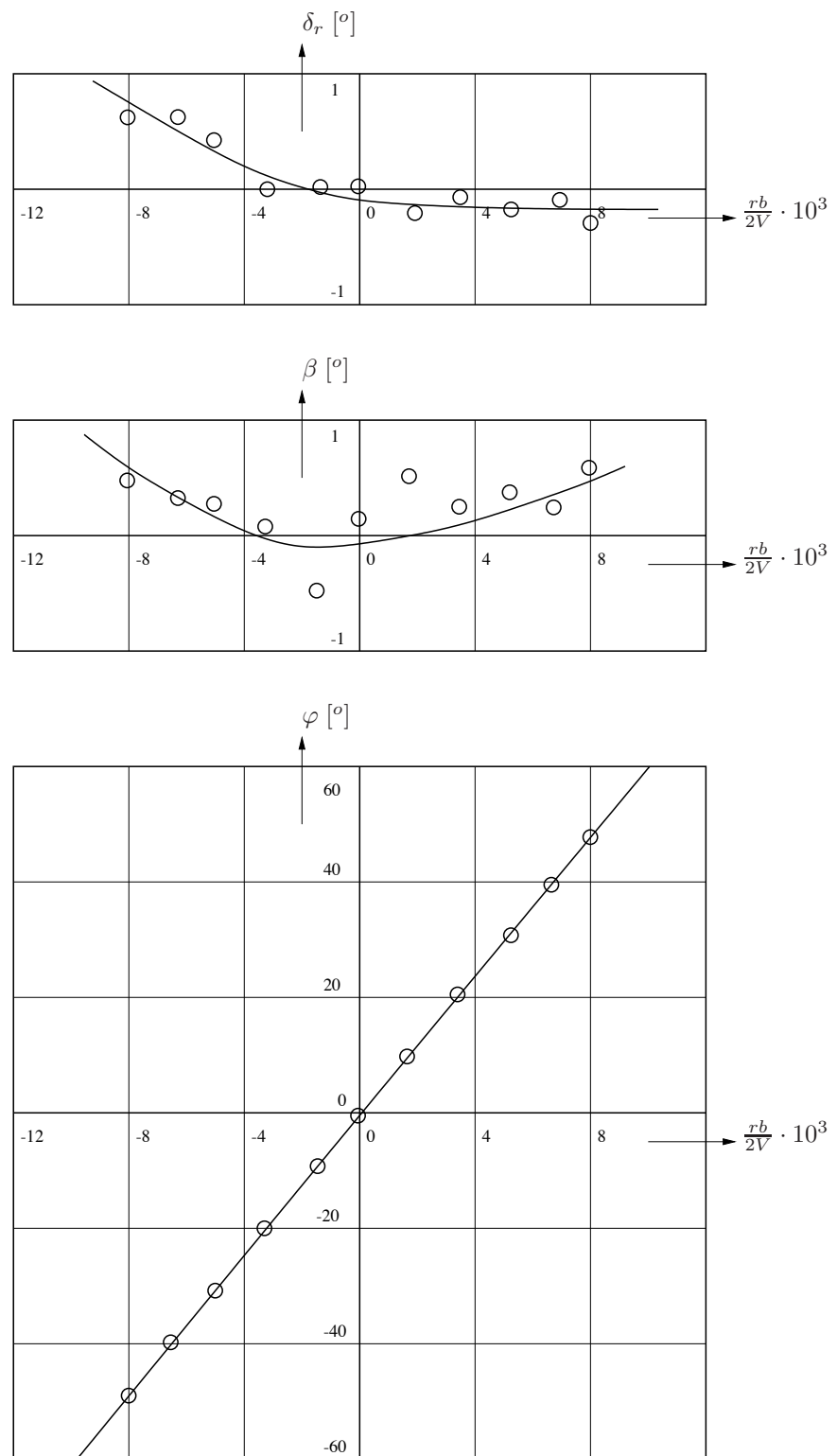


Figure 11-3: Steady turns using rudder only, North American 'Harvard II B', gliding flight, $C_L = 0.31$, $x_{c.g.} = 0.304 \bar{c}$, $V = 78$ m/sec (from reference [14])

analogy with equations (11-11) and (11-12) the following expressions for the variations of angle of roll and angle of sideslip hold,

$$\frac{d\varphi}{d\frac{rb}{2V}} = \frac{4\mu_b + C_{Y_\beta} \frac{C_{\ell_r}}{C_{\ell_\beta}}}{C_L} > 0 \quad (\text{for } C_L > 0) \quad (11-14)$$

and,

$$\frac{d\beta}{d\frac{rb}{2V}} = -\frac{C_{\ell_r}}{C_{\ell_\beta}} > 0 \quad (C_{\ell_r} > 0, \quad C_{\ell_\beta} < 0) \quad (11-15)$$

In a turn to the right, using the rudder only, the aircraft assumes again a positive angle of roll (to the right) and a positive, usually very small, angle of sideslip. Figure 11-3 shows the results of some measurements made in steady flight using the rudder only. As in figure 11-2, the control surface deflection and the angle of sideslip remain very small, even at angles of roll of $\pm 40^\circ$. As a consequence, the influence of the limited accuracy of the measurements and possible non-linearities is large enough to obscure a clear relation between the slopes of some measured curves and the expressions derived in this section, such as equation (11-15).

11-3-3 Coordinated Turns, $\beta = 0$

When flying a steady turn, the pilot's aim is in principle to keep the angle of sideslip zero. Then the drag is at a minimum. In addition, the coordinated turn is the most comfortable turn for passengers.

If $\beta = 0$, it follows from equation (11-6) that,

$$C_L \varphi = 4\mu_b \frac{rb}{2V} \quad (11-16)$$

This means that in the coordinated turn the component along the Y_B -axis of the centripetal acceleration is caused only by the lateral component of the aircraft weight. This is true, also for all objects in the aircraft. They do not experience a side force during the coordinated turn. As a consequence the pilot can also feel if he flies a well coordinated turn.

The variation of the roll angle with rate of yaw follows from equation (11-16),

$$\frac{d\varphi}{d\frac{rb}{2V}} = \frac{4\mu_b}{C_L} > 0 \quad (\text{for } C_L > 0) \quad (11-17)$$

The required control surface deflections follow from equations (11-7) and (11-8) with $\beta = 0$,

$$\frac{d\delta_a}{d\frac{rb}{2V}} = -\frac{C_{\ell_r}}{C_{\ell_{\delta_a}}} > 0 \quad (C_{\ell_r} > 0, \quad C_{\ell_{\delta_a}} < 0) \quad (11-18)$$

and,

$$\frac{d\delta_r}{d\frac{rb}{2V}} = -\frac{C_{n_r}}{C_{n_{\delta_r}}} < 0 \quad (C_{n_r} < 0, \quad C_{n_{\delta_r}} < 0) \quad (11-19)$$

In a coordinated turn to the right the aircraft has an angle of roll to the right. The rudder is deflected in the desirable negative direction (to the right). But the aileron is deflected to the left, in the direction opposite to that of the initial control deflection. As a matter of fact, this is less desirable, however it is inevitable in normal aircraft. Figure 11-4 shows the results of measurements made in steady, coordinated turns. The aileron angle turns out to be very nearly constant.

Quantitative calculations show very simply that the control surface deflections in each of the three types of steady turns just described remain usually small, see also figures 11-2, 11-3 and 11-4. It follows then that these flight conditions are not at all critical for the sizing of the control surfaces.

In cruising flight and usually also in the approach the differences between the coordinated turn ($\beta = 0$) and a turn using the ailerons only ($\delta_r = 0$) is so small as to make it attractive to the pilot to perform the lateral control using the roll control only. If the initiation of a turn is done not too quickly, the adverse yaw of a conventional aircraft will be small enough to render the use of the rudder unnecessary. Obviously, if the rudder need not be employed, the control of the aircraft is much easier, thereby improving the accuracy of the control of the aircraft.

11-3-4 Flat Turns

From equation (11-6) follows, if $\varphi = 0$,

$$\frac{d\beta}{d\frac{rb}{2V}} = \frac{1}{C_{Y_\beta}} 4\mu_b < 0 \quad (C_{Y_\beta} < 0) \quad (11-20)$$

Using equation (11-20) it is simple to derive that,

$$\frac{d\delta_a}{d\frac{rb}{2V}} > 0 \quad \frac{d\delta_r}{d\frac{rb}{2V}} < 0$$

In a flat turn to the right, the rudder angle is negative, just as in a turn to the right using the rudder only. In a flat turn the aircraft must perform a sideslip to the outside of the turn ($\beta < 0$ if $r > 0$) in order to obtain the lateral force required for the centripetal acceleration. Due to the combined sideslipping and yawing motions, a positive rolling moment (to the right) is generated. This requires a positive aileron deflection (to the left) for equilibrium about the X_B -axis. Figure 11-5 shows the results of some measurements made in steady, flat turns.

11-4 Steady, Straight, Sideslipping Flight

In general the pilot will try to avoid sideslipping in flight. The intentional use of steady, straight, sideslipping flight is limited to landings with cross wind and to the approach in flapless aircraft in order to control the flight path angle. A further discussion of steady, straight sideslipping flight is justified, however, because the aircraft may enter into a sideslip even without the pilot's intention.

Using the lateral control characteristics in steady, straight, sideslips, it is simple to verify if the effective dihedral, C_{ℓ_β} , and the static dimensional stability, C_{n_β} , have the correct sign.

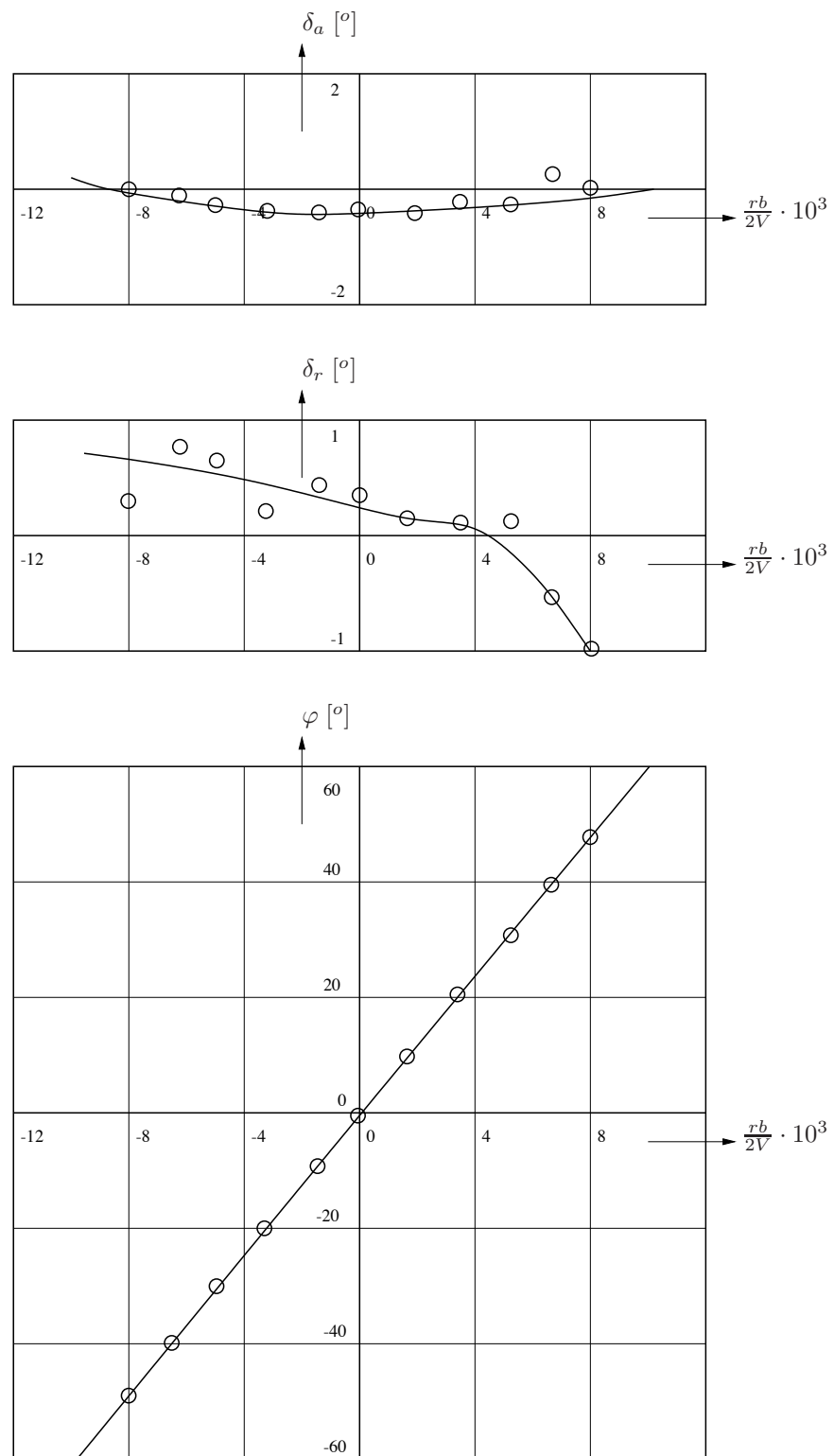


Figure 11-4: Steady coordinated turns, North American ‘Harvard II B’, gliding flight, $C_L = 0.31$, $x_{c.g.} = 0.304 \bar{c}$, $V = 78$ m/sec (from reference [14])

These two stability derivatives have a strong influence on the lateral control characteristics in general. They are also two important parameters in obtaining good lateral stability characteristics.

The equilibrium equations for steady, straight sideslip follow directly from the expressions (11-6), (11-7) and (11-8), by letting $\frac{rb}{2V} = 0$.

Neglecting small contributions, the equilibrium equations then become,

$$\begin{bmatrix} C_L & C_{Y_\beta} & 0 & 0 \\ 0 & C_{\ell_\beta} & C_{\ell_{\delta_a}} & 0 \\ 0 & C_{n_\beta} & 0 & C_{n_{\delta_r}} \end{bmatrix} \begin{bmatrix} \varphi \\ \beta \\ \delta_a \\ \delta_r \end{bmatrix} = 0 \quad (11-21)$$

The variation of the angle of roll with β follows from the first row of equation (11-21).

$$\frac{d\varphi}{d\beta} = -\frac{C_{Y_\beta}}{C_L} > 0 \quad (C_{Y_\beta} < 0, \quad C_L > 0) \quad (11-22)$$

Apparently, a positive angle of sideslip is associated with a positive angle of roll. A given angle of sideslip creates a large lateral force $C_{Y_\beta} \cdot \beta$ which has to be balanced in steady flight by a component of the weight along the Y_B -axis.

If the absolute value of C_{Y_β} is large, the equilibrium at a given angle of side-slip necessitates a large roll angle, as can be seen from equation (11-22).

A suddenly occurring angle of sideslip, caused for instance by a gust, gives also rise to a force along the Y_B -axis and hence to a sideward acceleration. The pilot senses this acceleration as a sideward force exerted upon him by his seat and seat belts. If, again C_{Y_β} is large in the absolute sense, this force will be relatively large, making it easier for the pilot to detect the presence of the sideslipping motion.

These arguments lead to the conclusion that a large negative value of C_{Y_β} may be considered as desirable.

To initiate a straight sideslip with a positive β (velocity vector pointing to the right of X_b -axis) the aircraft has to be given a positive rolling moment (to the right) and a negative yawing moment (to the left). This requires an initial aileron deflection to the right (negative) and an initial rudder deflection to the left (positive). It is then desirable that in the ultimate steady flight condition the aileron control is also deflected to the right and the rudder control to the left or,

$$\frac{d\delta_a}{d\beta} < 0 \quad \text{and} \quad \frac{d\delta_r}{d\beta} > 0$$

The required surface deflections follow from equation (11-21),

$$\frac{d\delta_a}{d\beta} = -\frac{C_{\ell_\beta}}{C_{\ell_{\delta_a}}} \quad (11-23)$$

$$\frac{d\delta_r}{d\beta} = -\frac{C_{n_\beta}}{C_{n_{\delta_r}}} \quad (11-24)$$

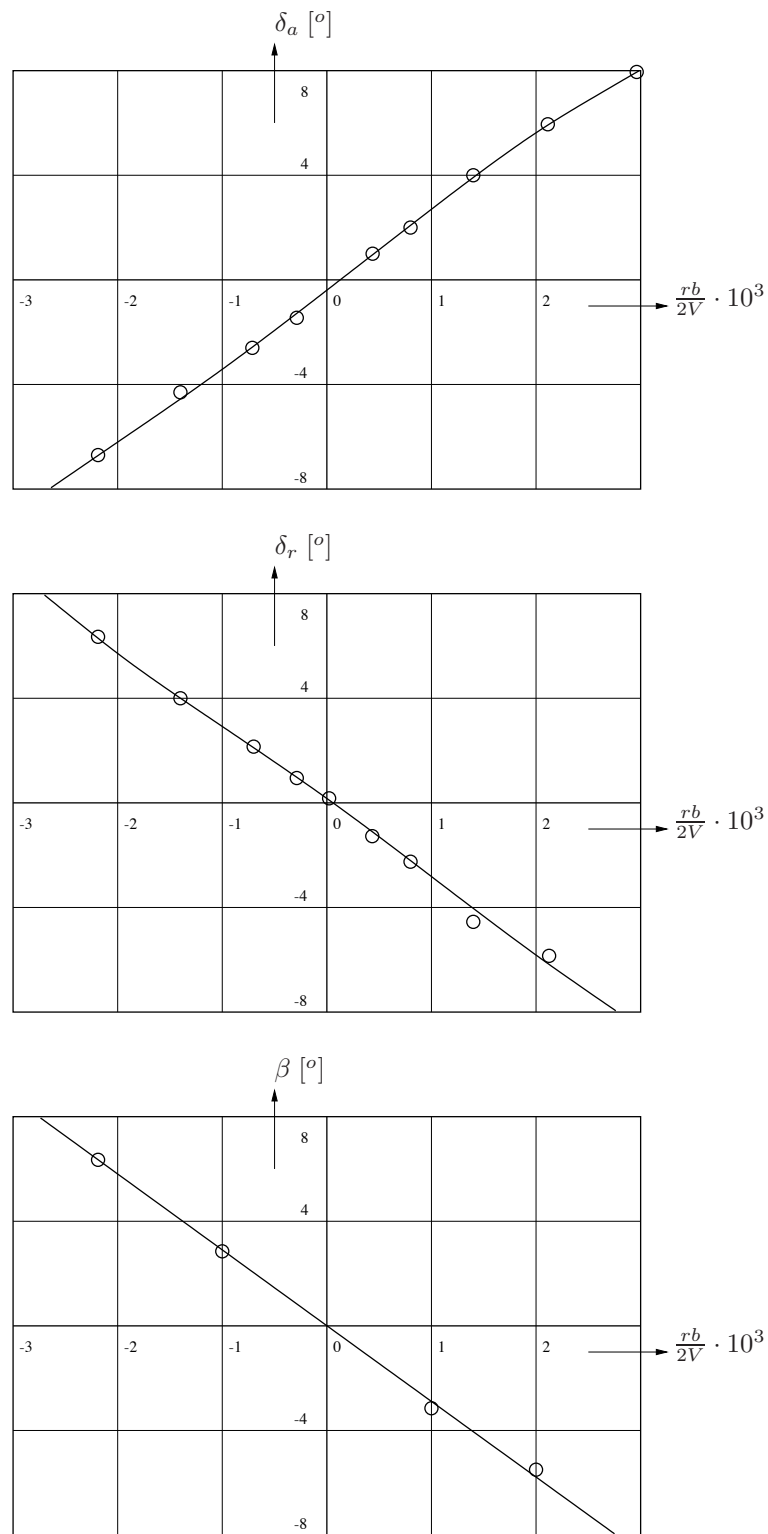


Figure 11-5: Steady flat turns, North American ‘Harvard II B’, gliding flight, $C_L = 0.31$, $x_{c.g.} = 0.304 \bar{c}$, $V = 78$ m/sec (from reference [14])

As both $C_{\ell_{\delta_a}}$ and $C_{n_{\delta_r}}$ are negative, the required directions of the control deflections in steady, straight sideslips are obtained, if,

$$C_{\ell_\beta} < 0 \quad \text{and} \quad C_{n_\beta} > 0$$

It will be shown in chapter 6 that the latter conditions have to be satisfied also to obtain lateral dynamic stability. Measurement of the control deflections in steady, straight sideslips offers a simple method to determine if these conditions are satisfied. Figure 11-6 shows some results of measurements, made in steady, straight sideslips.

As a final remark it can be said that the center of gravity position has an influence on the magnitude C_{n_β} , in analogy with the influence on C_{m_α} . As a consequence, the c.g. position also has some influence on the lateral stability and control. The importance of this influence is, however, generally much less than is the case for the longitudinal stability and control characteristics.

11-5 Steady Straight Flight with One or More Engines Inoperative

For multi-engined aircraft the requirement exists that the aircraft can continue flight if one engine becomes inoperative. This imposes requirements on the controllability and usually in particular on the available rudder power.

The most important consequences of the loss of the engine thrust from an engine not mounted in the plane of symmetry are a yawing moment due to the asymmetric thrust distribution and, in the case of a propeller-driven aircraft, a rolling moment caused by the resultant asymmetric lift distribution. The yawing moment can be written in non-dimensional form as,

$$C_{n_e} = k \frac{\Delta T_p y_e}{\frac{1}{2} \rho V^2 S b} \quad (11-25)$$

Here ΔT_p is the difference in thrust from the operative engine and the drag of the inoperative engine; y_e is the distance from the line of action of the thrust or drag to the plane of symmetry of the aircraft. ΔT_p may be considerably larger than the thrust of the operative engine if the inoperative engine is windmilling in the airstream. In the case of a propeller-driven aircraft, ΔT_p is minimal if the inoperative propeller is feathered, whereby the rotation is stopped.

The factor k in equation (11-25), which for propeller-driven aircraft may assume values of 1.5 to 2.0 in some instances, expresses the fact that the yawing moment actually occurring may be larger than would result from the changes in thrust only.

Figure 11-7 shows some results of measurements of C_{n_e} confirming this fact. The explanation of this effect lies in the increased lift of the part of the wing submerged in the slipstream. This increase in lift creates an extra downwash behind the wing which is now asymmetric. The downwash behind the operative propeller is larger than the downwash behind the inoperative propeller. In analogy with the airflow behind a high or low mounted wing in sideslipping flight, the differences in downwash create a circulation around the rear fuselage, thereby causing a cross-flow at the vertical tailplane. It is not difficult to verify that this cross-flow or sidewash causes an increase in the disturbing yawing moment.

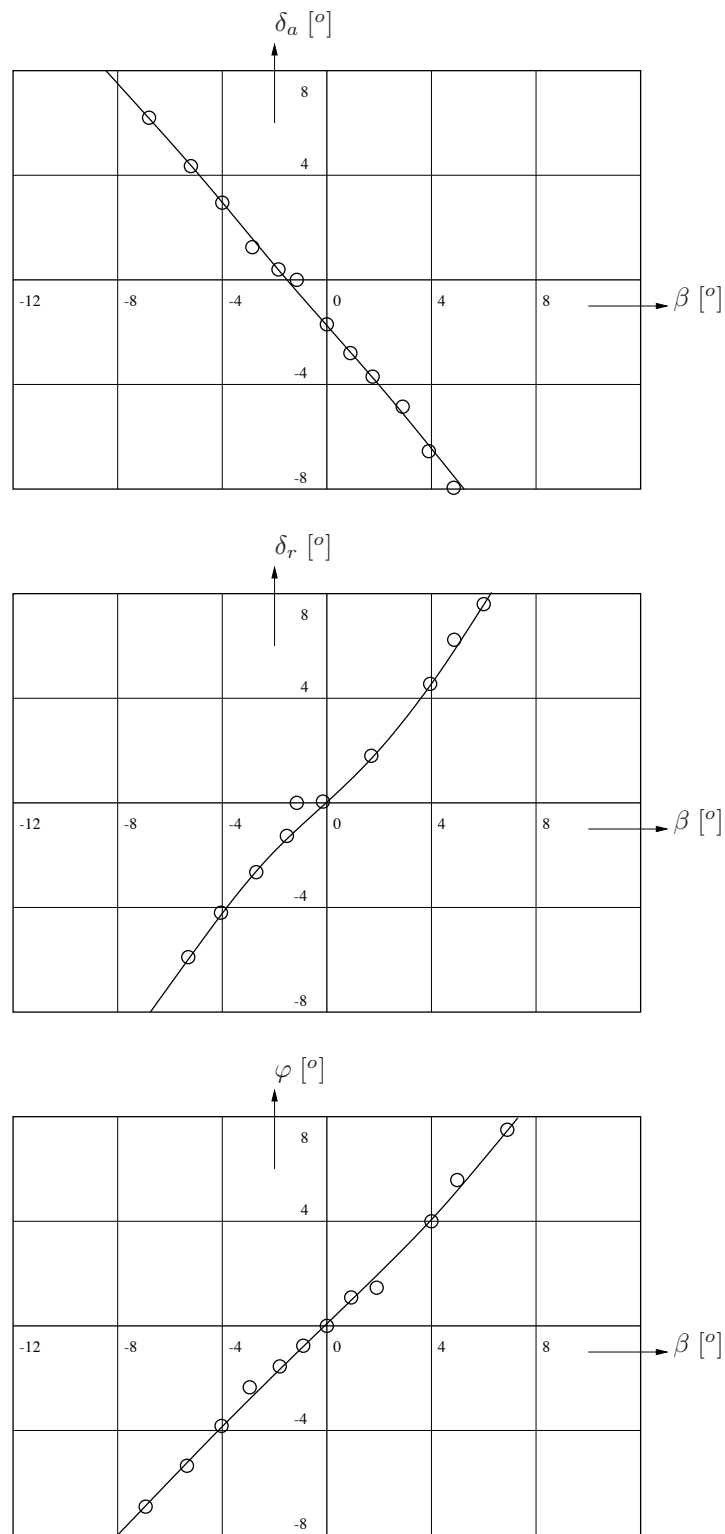


Figure 11-6: Steady, straight, sideslipping flight, North American ‘Harvard II B’, gliding flight, $C_L = 0.31$, $x_{c.g.} = 0.304 \bar{c}$, $V = 78$ m/sec (from reference [14])

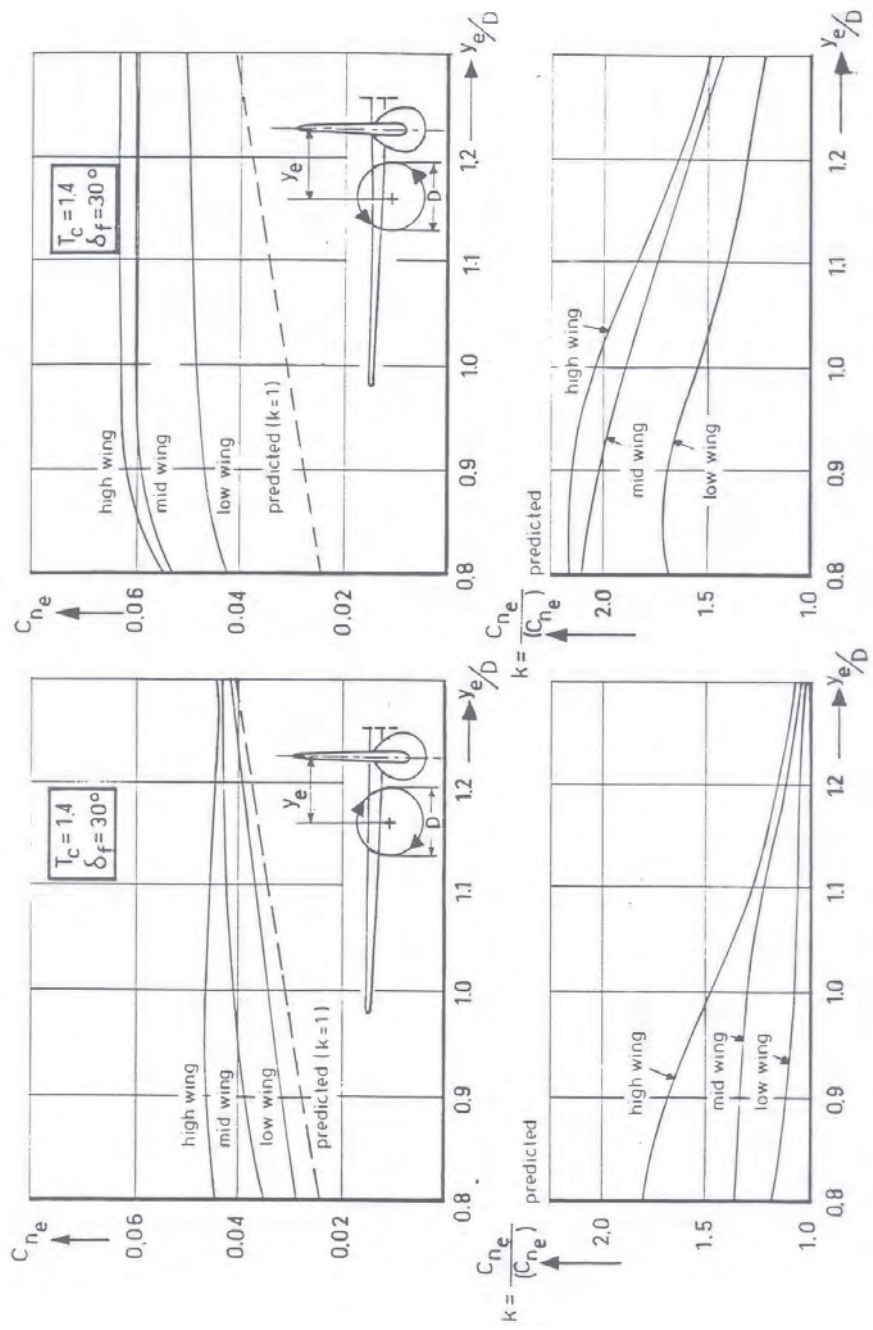


Figure 11-7: The magnitude of C_{n_e} due to an engine failure, as a function of the location and the sense of rotation of the propeller and the vertical position of the wing, measured on a model of a twin-engined propeller-driven aircraft (from reference [113]).

The experimental evidence in figure 11-7 shows that the direction of rotation of the propeller and the vertical position of the wing relative to the fuselage have an important influence on the magnitude of C_{n_e} . Reference [61] discusses this matter in detail. In general it can be concluded, that if the propellers turn clockwise, the loss of the left engine causes the largest disturbing yawing moment C_{n_e} . This engine is then called the critical engine. The rolling moment C_{ℓ_e} due to an inoperative engine is caused mainly by the difference in lift on both sides of the wing, behind the operative and the in-operative engine. Some results of measurements on C_{ℓ_e} are shown in figure 11-8.

If the right engine cuts out, both a positive C_{n_e} and a positive C_{ℓ_e} arise. Due to C_{n_e} the aircraft assumes a positive rate of yaw leading to a negative β . The rolling moment C_{ℓ_e} causes a positive rate of roll and thus a positive roll angle φ . The rolling motion is amplified by the contributions $C_{\ell_\beta} \cdot \beta (> 0)$ and $C_{\ell_r} \cdot \frac{rb}{2V} (> 0)$ due to the sideslipping and yawing motions. As a consequence, the roll angle may increase very rapidly.

The motion is counteracted by the yawing moments generated by p , r and β (C_{n_p} , C_{n_r} , C_{n_β} , and by the application of both a positive rudder deflection and a positive aileron deflection. A new condition of steady, straight flight may now be established, described by the following equilibrium equations in which a few minor contributions have been neglected,

$$\begin{bmatrix} C_L & C_{Y_\beta} & 0 & C_{Y_{\delta_r}} \\ 0 & C_{\ell_\beta} & C_{\ell_{\delta_a}} & 0 \\ 0 & C_{n_\beta} & 0 & C_{n_{\delta_r}} \end{bmatrix} \begin{bmatrix} \varphi \\ \beta \\ \delta_a \\ \delta_r \end{bmatrix} = - \begin{bmatrix} 0 \\ C_{\ell_e} \\ C_{n_e} \end{bmatrix} \quad (11-26)$$

In flight with asymmetrically distributed engine thrust very large rudder deflections may be required. As a consequence the lateral force caused by δ_r cannot be omitted in equation (11-26).

As the four variables φ , β , δ_a and δ_r occur in the equilibrium equations (11-26) there is not just one, single steady flight condition possible, but a whole range of conditions.

In practice two of the many possible conditions have special significance: steady flight at a roll angle equal to zero and the condition at which the angle of sideslip β is equal to zero. If $\beta = 0$ the aircraft drag is at a minimum, resulting in maximum flight performance.

If the right engine is inoperative, a positive rudder deflection (to the left) is required to balance C_{n_e} . In the flight condition at $\varphi = 0$, a positive angle of sideslip is necessary according to the top row of equation (11-26), to obtain an aerodynamic lateral force to balance the lateral force $C_{Y_{\delta_r}} \cdot \delta_r$, see figure 11-9. The aircraft performs a sideslipping motion in the direction of the inoperative engine.

In the flight condition with $\beta = 0$ the pilot must apply a negative roll angle, assuming again that the right engine is stopped, such that the component of the weight $C_L \cdot \varphi$ balances the lateral force $C_{Y_{\delta_r}} \cdot \delta_r$. The wing with the operative engine has to be kept low, see figure 11-10. In this situation the rudder deflection required for equilibrium is smaller than in the flight condition with $\varphi = 0$, where not only C_{n_e} but also the moment $C_{n_\beta} \cdot \beta$ acting in the same direction has to be balanced, see the bottom row in equation (11-26). The flight condition at $\varphi = 0$ is, therefore,

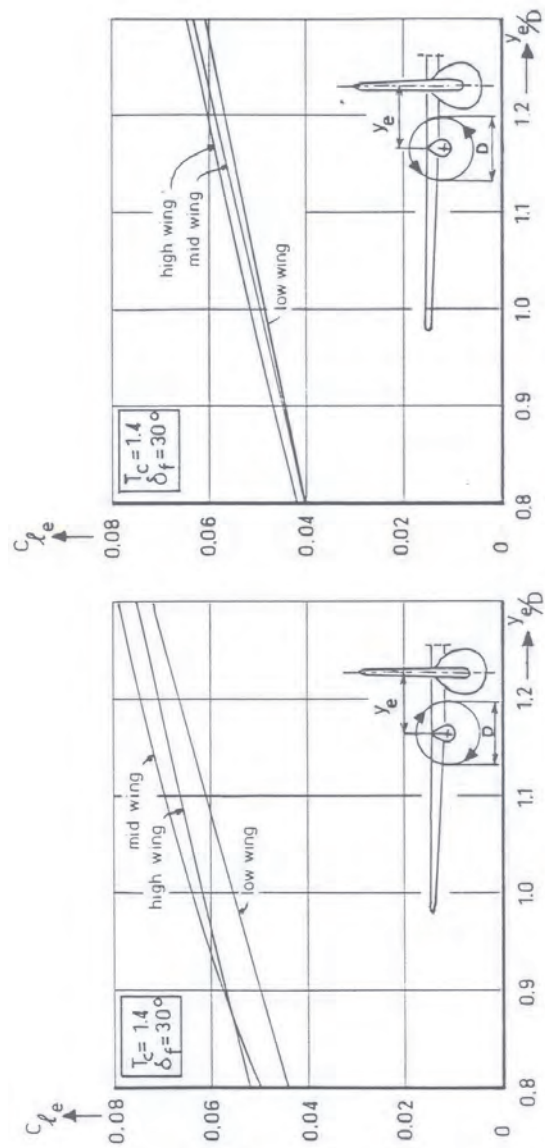


Figure 11-8: The magnitude of C_{ne} due to an engine failure, as a function of the location and the sense of rotation of the propeller and the vertical position of the wing, measured on a model of a twin-engined propeller-driven aircraft (from reference [113]).

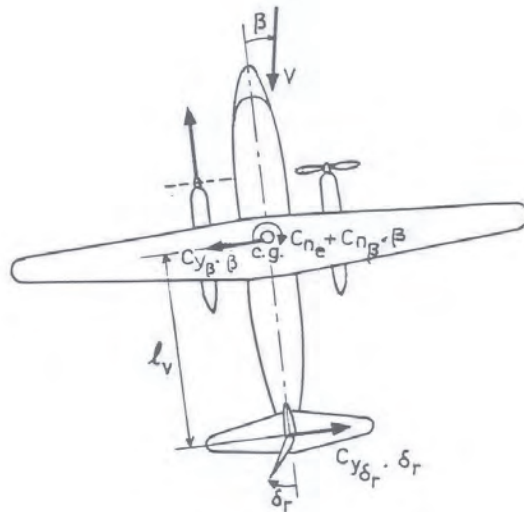


Figure 11-9: Steady, straight, single-engined flight at $\varphi = 0$

more critical for the determination of the required rudder power than the flight condition at $\beta = 0$.

Contrary to the moments $C_{n_{\delta_r}} \cdot \delta_r$ and $C_{n_\beta} \cdot \beta$, the disturbing yawing moment C_{n_e} depends strongly on airspeed. Taking the case of the propeller-driven aircraft, the engine power is constant at constant throttle setting.

To a first approximation this means,

$$T_p V = \text{constant}$$

From equation (11-25) then follows, that C_{n_e} in that case is inversely proportional to the cube of airspeed, V^3 . There will be an airspeed below which it is not possible to balance the yawing moment due to an engine failure, C_{n_e} , see figure 11-11. This airspeed is called the ‘minimum control speed’, $V_{m.c.}$. When determining $V_{m.c.}$ in flight, the regulations stipulate that $|\varphi|$ may not be larger than 5° .

High engine power and low airspeeds, and consequently large values of C_{n_e} at engine failure, occur during take-off and in climb immediately after take-off. In the take-off configuration at high C_L -values, the extra interference yawing moment, expressed by the factor k in equation (11-25), is also large. An additional factor is the fact that during take-off the aircraft is not allowed to lose height or to obtain large angles of roll.

The importance of the minimum control speed as an element in the choice of the take-off procedure to be followed, depends strongly on the type and location of the engine. Jet-propelled aircraft, having the engines mounted on the rear fuselage, often have a minimum control speed lower than the minimum airspeed for sustained flight.

For such aircraft the minimum control speed loses its significance. Handling the aircraft on the ground with failed engine may then be an important consideration. For twin-engined, propeller-driven aircraft, however, the minimum control speed in the take-off configuration is of extreme importance. Figure 11-12 shows some results of measurements on the Fokker F-27 with the right propeller feathered.

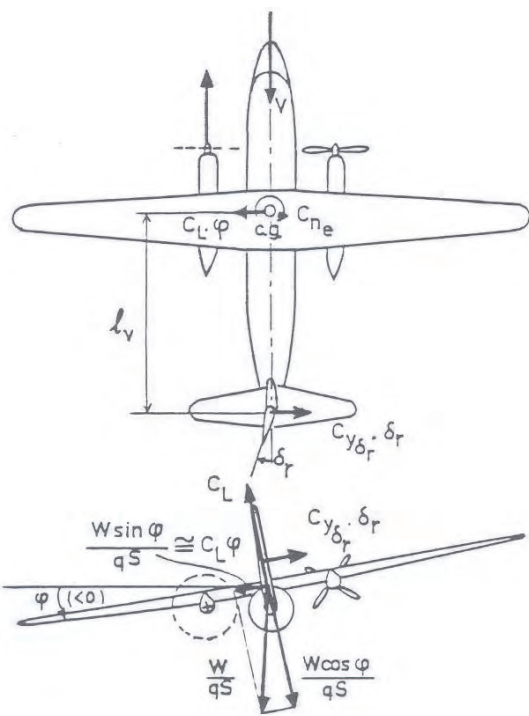
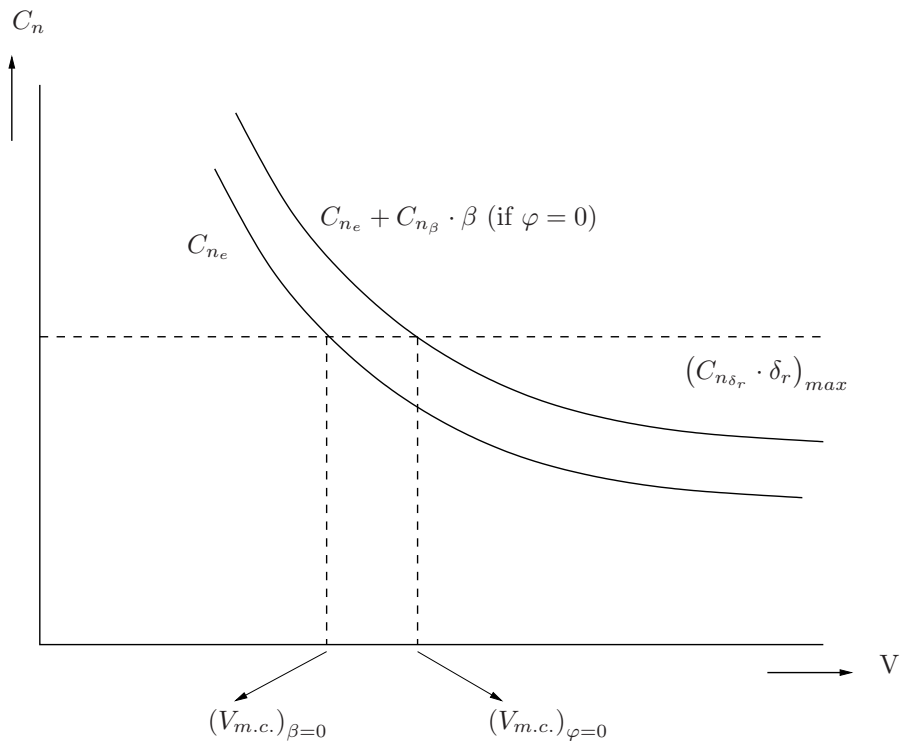
Figure 11-10: Steady, straight, single-engined flight at $\beta = 0$ 

Figure 11-11: Minimum control speed

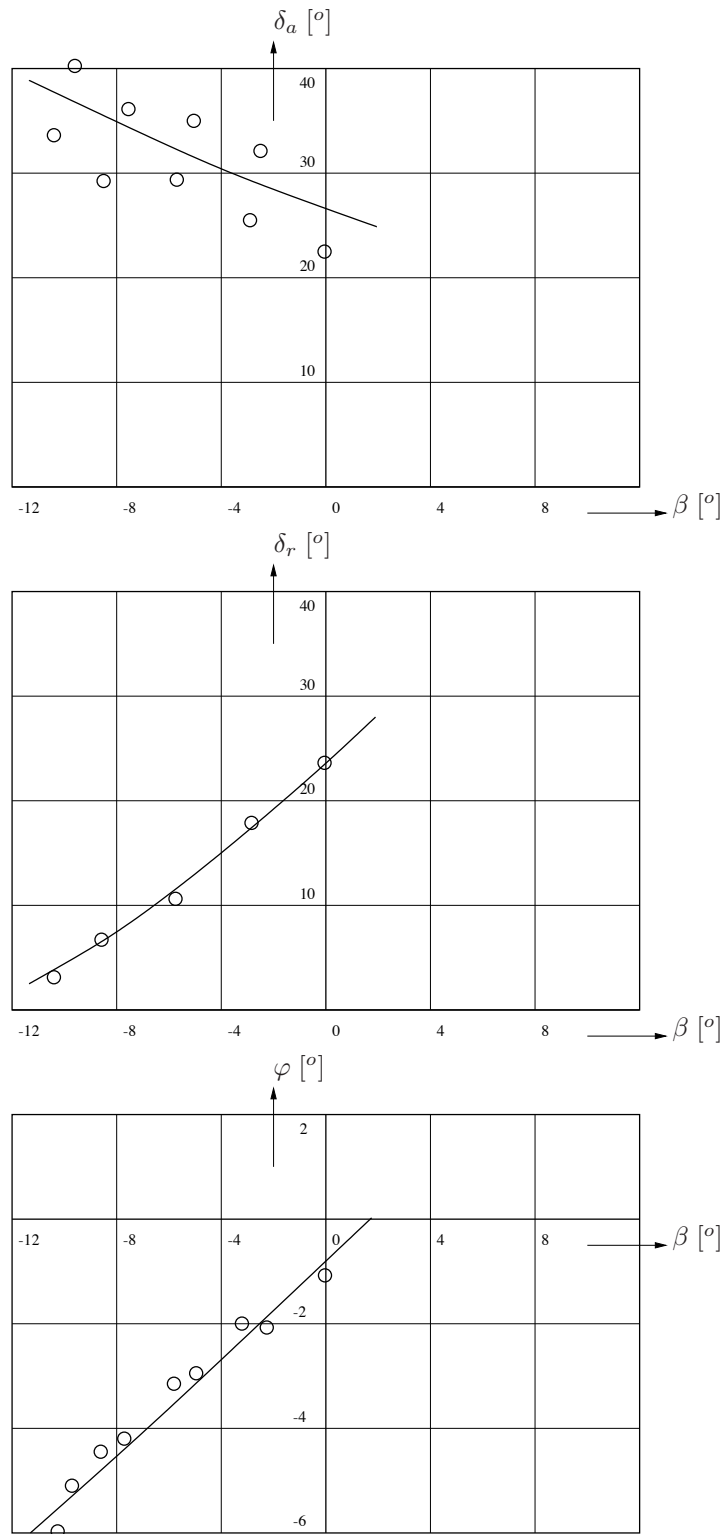


Figure 11-12: Steady, straight, sideslipping flight with the right propeller feathered, Fokker F-27, $h = 1850$ m, $C_L = 1.92$, $x_{c.g.} = 0.28 \bar{c}$, $V = 46.3$ m/sec (from reference [52])

11-6 Steady Rolling Flight

One of the measures for the manoeuvrability of an aircraft is the rate of roll obtained by giving a certain aileron deflection. The time required to establish a steady turn, is determined largely by this rate of roll. This is the reason why requirements exist for the attainable rates of roll. In many cases this fixes the required aileron power.

If the ailerons are deflected and then maintained in their deflected position, the aircraft will experience at first an angular acceleration about the X_B -axis. When the growing damping moment $C_{\ell_p} \cdot \frac{pb}{2V}$ has become equal to the rolling moment $C_{\ell_{\delta_a}} \cdot \delta_a$, the rate of roll will remain constant, if the simplifying assumption is made that during this rolling motion the aircraft will neither sideslip nor yaw. The resulting flight condition is that of steady rolling flight. It is possible to demonstrate, that this ‘steady’ condition is usually established relatively quickly. This makes it sensible to assess the manoeuvrability of an aircraft by means of the attainable rate of roll.

Under the influence of for instance the component of the weight $C_L \cdot \varphi$ and the yawing moments due to δ_a and p , the aircraft will not only roll but also sideslip and yaw. This means, that continuous rudder control would be required to make the aircraft perform a rolling flight at constant rate of roll without any sideslipping and yawing motions.

A real exactly steady rolling flight is thus not possible. The ‘steady’ rolling flight to be discussed below is, therefore, a quasi-steady flight condition in straight flight ($r = 0$) at constant rudder angle ($\delta_r = 0$), at small angles of roll φ and to the neglect of the angle of sideslip actually occurring ($\beta = 0$).

For this idealized flight condition the equation for the equilibrium of the aerodynamic moments about the X_B -axis is,

$$C_{\ell_p} \frac{pb}{2V} + C_{\ell_{\delta_a}} \delta_a = 0 \quad (11-27)$$

or,

$$\frac{pb}{2V} = -\frac{C_{\ell_{\delta_a}}}{C_{\ell_p}} \delta_a \quad (11-28)$$

where both $C_{\ell_{\delta_a}}$ and C_{ℓ_p} are negative. A positive aileron deflection is thus seen to cause a negative rate of roll.

In the discussion of $C_{\ell_{\delta_a}}$ and C_{ℓ_p} it was shown that these two derivatives are to a first approximation independent of C_L or the airspeed. According to equation (11-28) the rate of roll at a given aileron angle is thus proportional to airspeed, but the non-dimensional rate of roll is independent of V . From early investigations, see reference [64], it appeared that the pilot’s assessment of the manoeuvrability of the then considered aircraft, showed a better correlation with $\left(\frac{pb}{2V}\right)_{max}$ than with p_{max} . On this basis the requirements on manoeuvrability were expressed using the non-dimensional rate of roll.

As an example, older U.S. military regulations, see reference [19], required for a fighter aircraft,

$$\left(\frac{pb}{2V}\right)_{max} > 0.09$$

and for the other categories of aircraft,

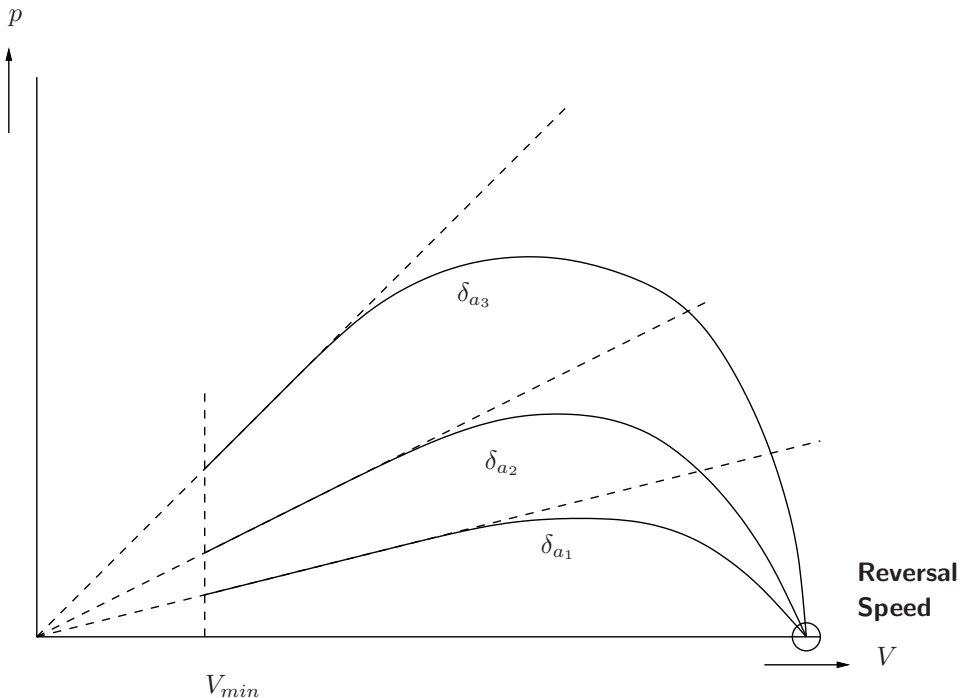


Figure 11-13: The limitation in the maximum attainable roll-rate due to elastic wing deformation

$$\left(\frac{pb}{2V} \right)_{max} > 0.07$$

Since the time when the requirements were formulated the range of possible airspeeds has increased so much, that the non-dimensional rate of roll, $\frac{pb}{2V}$, as the only criterion for the manoeuvrability of an aircraft about the X_B -axis, has lost some of its significance.

For V/STOL aircraft capable to operate at very low airspeeds, the rate of roll p resulting from the above requirements on $\frac{pb}{2V}$ would be too low at low values of V , to ensure good manoeuvrability. For such aircraft the additional requirement is sometimes used, that in the approach $\left(\frac{pb}{2V} \right)_{max}$, which can be seen as the maximum vertical speed of the wing tip due to rolling, must be at least be 10 ft/sec.

On the other hand, the rolling velocity at supersonic airspeed of a fighter aircraft having a small wing span according to the requirement on $\frac{pb}{2V}$, would be unreasonably large. At those high rates of roll, difficulties with the dynamic stability might occur, as at high rolling velocities the symmetric and the asymmetric aircraft motions at high rates of roll may become quite violently unstable. In later U.S. military Regulations, see reference [13], the requirement is given that fighter aircraft in the combat configuration must be capable to attain an angle of roll of $\varphi = 50^\circ$ within one second. For other aircraft configurations and flight conditions, as well as for other categories of aircraft, requirements on non-dimensional rate of roll are maintained.

It was discussed in section 8-7 that due the elastic deformation of the wing, $C_{\ell_{\delta_a}}$ will decrease in absolute value at high airspeed, or rather at high dynamic pressures. Due to this effect, the rate of roll no longer increases linearly with airspeed at a constant aileron deflection, see figure 11-13. At high airspeeds the rate of roll will even decrease. The reversal speed is reached when $C_{\ell_{\delta_a}} = 0$ and as a consequence also $p = 0$.

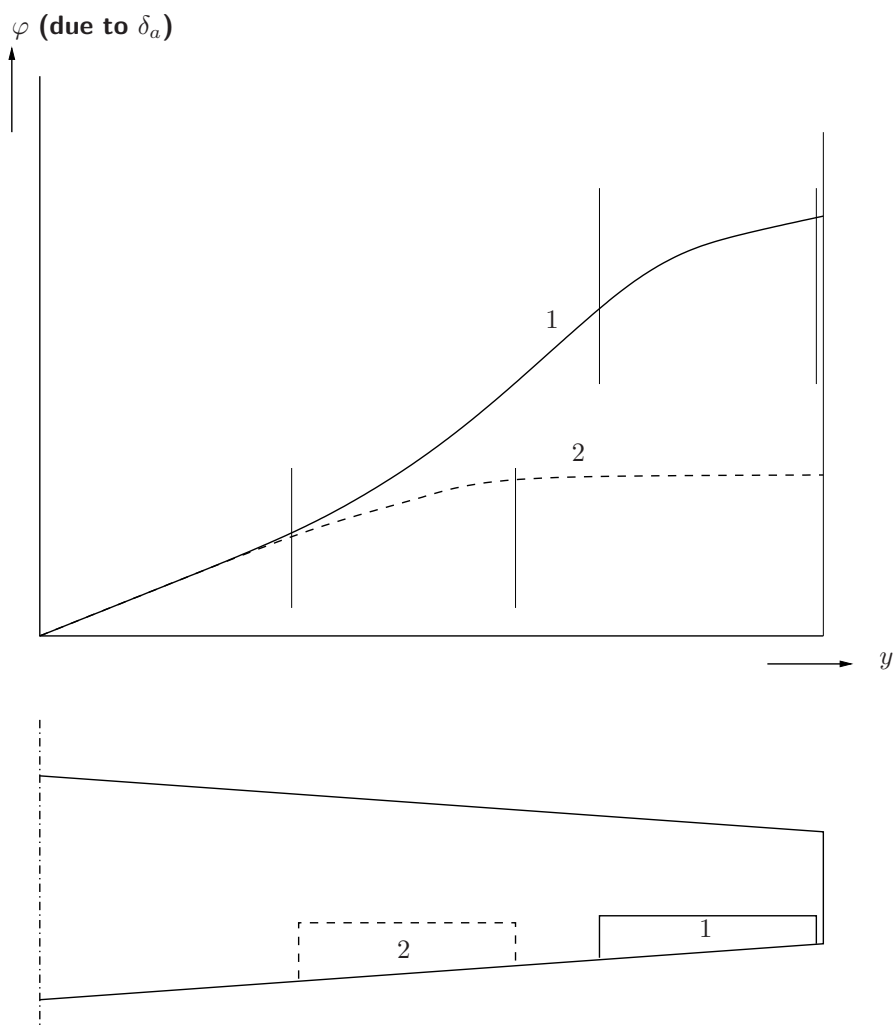


Figure 11-14: Variation of the wing twist angle φ along the wing span due to aileron deflection for two locations of the ailerons

The elastic wing twist may be reduced by locating the ailerons not at the wing tips, but more inboard. The sketch in figure 11-14 shows that this may considerably reduce the total twist at the wing tip, thereby reducing the loss in rolling moment generated by aileron deflection.

If the ailerons are located inboard, the outer part of the wing, generally possessing less torsional stiffness, will experience no further increase in wing twist. In cases where no satisfactory roll control can be obtained in this way, it may be necessary to use spoilers for roll control, as discussed in section 8-7.

The maximum achievable rate of roll p may be limited at high airspeeds by the maximum possible roll control force, rather than by the maximum aileron deflection. If no hydraulic servos are applied and if no differential aileron deflections are used, the roll control force can be written according to equation (11-40), if in addition $\delta_{t_a} = 0$, as,

$$F_a = -\frac{d\delta_a}{ds_a} \frac{1}{2} \rho V^2 S_a \bar{c}_a \left(C_{h_\alpha} \Delta\alpha_a + C_{h_\delta} \frac{1}{2} \delta_a \right) \quad (11-29)$$

It will be seen, that the required control force strongly increases with airspeed at a given aileron deflection.

In equation (11-29) $\Delta\alpha_a$ is the average effective change of angle of attack due to rolling over the span of the aileron. This average effective value can be equated to a geometric change in angle of attack at a distance y_m from the plane of symmetry, see figure 11-15. The expression is,

$$\Delta\alpha_a = \frac{pb}{2V} \frac{2y_m}{b} \quad (11-30)$$

For a given wing, y_m can be determined using reference [166]. The aileron deflection δ_a required for a steady, rolling flight at $\beta = 0$ follows from equation (11-28),

$$\delta_a = -\frac{pb}{2V} \frac{C_{\ell_p}}{C_{\ell_{\delta_a}}} \quad (11-31)$$

Substitution of equation (11-30) and (11-31) in (11-29) results in the following expression for the roll control force in a steady, rolling flight at $\beta = 0$, as a function of rate of roll p and airspeed V ,

$$F_a = -\frac{d\delta_a}{ds_a} \frac{1}{2} \rho V^2 S_a \bar{c}_a \left(C_{h_\alpha} \frac{2y_m}{b} - C_{h_\delta} \frac{1}{2} \frac{C_{\ell_p}}{C_{\ell_{\delta_a}}} \right) \frac{pb}{2V} \quad (11-32)$$

or,

$$F_a = -\frac{d\delta_a}{ds_a} \frac{1}{2} \rho V p \frac{b}{2} S_a \bar{c}_a \left(C_{h_\alpha} \frac{2y_m}{b} - \frac{C_{h_\delta} C_{\ell_p}}{2 C_{\ell_{\delta_a}}} \right) \quad (11-33)$$

If for a given aircraft the aerodynamic derivatives C_{h_α} , C_{h_δ} , C_{ℓ_p} and $C_{\ell_{\delta_a}}$ may be assumed to remain constant, at a given flight altitude (i.e. value of ρ) the roll control force is,

$$F_a = \text{constant} \cdot p \cdot V \quad (11-34)$$

In a diagram showing rate of roll as a function of V , curves for a constant control force will be hyperbola's, see figure 11-16. Due to wing twist, $C_{\ell_{\delta_a}}$ will decrease in absolute value with increasing airspeed, as discussed in section 8-7. For a real, elastic wing, the rate of roll achieved at a given control force will be smaller than for a rigid wing, just like the rate of roll resulting from a given aileron deflection, see figure 11-16.

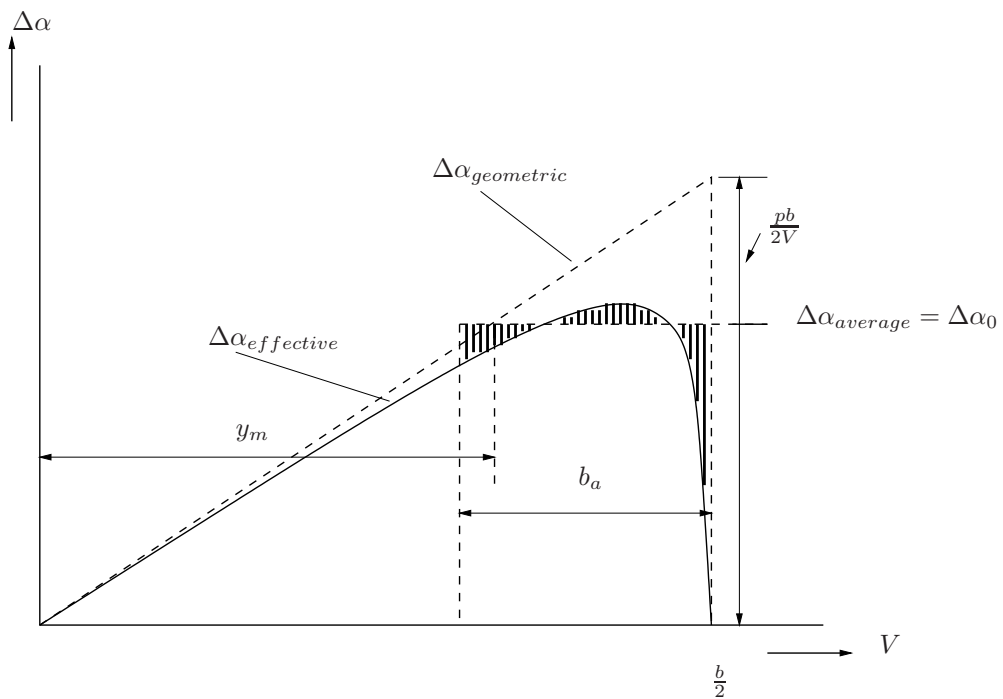


Figure 11-15: The average value of $\Delta\alpha$ along the aileron span in steady, rolling flight

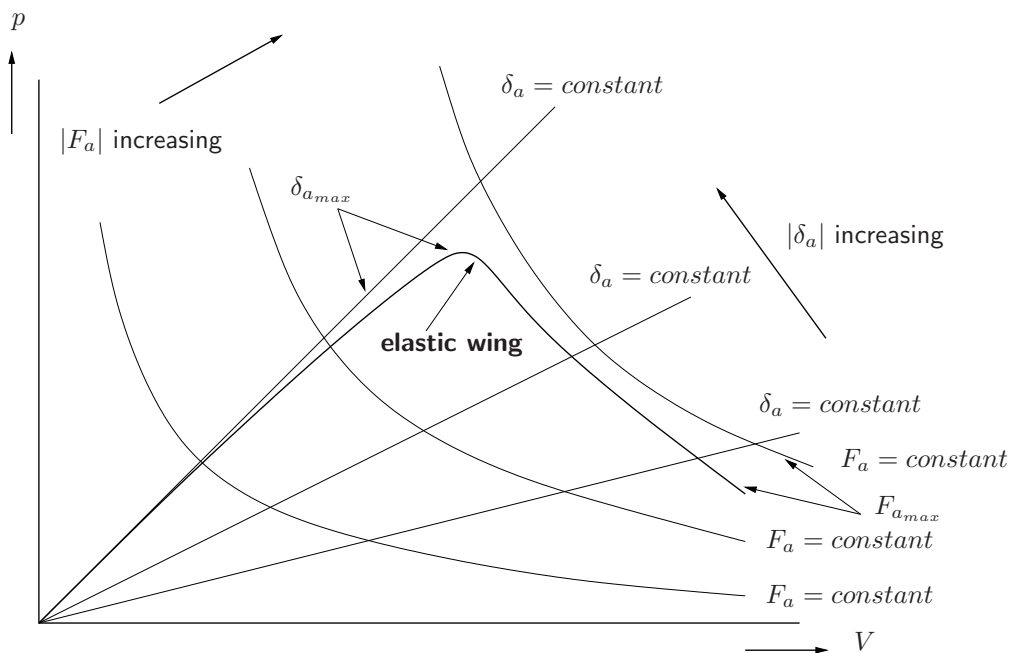


Figure 11-16: Roll-rate p as a function of airspeed V for various values of δ_a and F_a

11-7 Control Forces and Hinge Moments for Lateral Control

11-7-1 Roll Control

Using the same argument as in chapter 9 for the elevator control, the following expression applies to roll control in analogy with equation (9-77),

$$F_a \ ds_a + H_{a_r} \ d\delta_{a_r} + H_{a_l} \ d\delta_{a_l} = 0 \quad (11-35)$$

or,

$$F_a = - \left(\frac{d\delta_{a_r}}{ds_a} H_{a_r} + \frac{d\delta_{a_l}}{ds_a} H_{a_l} \right) \quad (11-36)$$

The hinge moments H_{a_r} and H_{a_l} can be written in the usual way as,

$$H_{a_r} = C_{h_{a_r}} \frac{1}{2} \rho V^2 S_{a_r} \bar{c}_{a_r}$$

$$H_{a_l} = C_{h_{a_l}} \frac{1}{2} \rho V^2 S_{a_l} \bar{c}_{a_l}$$

If $S_{a_r} = S_{a_l} = S_a$ (the area of one single aileron) and,

$$\bar{c}_{a_r} = \bar{c}_{a_l} = \bar{c}_a$$

the aileron control force in equation (11-36) becomes,

$$F_a = - \left(\frac{d\delta_{a_r}}{ds_a} C_{h_{a_r}} + \frac{d\delta_{a_l}}{ds_a} C_{h_{a_l}} \right) \frac{1}{2} \rho V^2 S_a \bar{c}_a \quad (11-37)$$

If no differential deflection of the ailerons is used, this expression can be further developed in a straightforward manner. Using equation (8-32),

$$\delta_{a_r} = -\delta_{a_l} = \frac{\delta_a}{2}$$

or,

$$\frac{d\delta_{a_r}}{ds_a} = -\frac{d\delta_{a_l}}{ds_a} = \frac{1}{2} \frac{d\delta_a}{ds_a}$$

Substitution in equation (11-37),

$$F_a = - \frac{1}{2} \frac{d\delta_a}{ds_a} \frac{1}{2} \rho V^2 S_a \bar{c}_a \left(C_{h_{a_r}} - C_{h_{a_l}} \right) \quad (11-38)$$

where,

$$C_{h_{a_r}} = C_{h_{0_r}} + C_{h_\alpha} \alpha_r + C_{h_\delta} \delta_{a_r} + C_{h_{\delta_t}} \delta_{t_{a_r}}$$

and,

$$C_{h_{a_l}} = C_{h_{0_l}} + C_{h_\alpha} \alpha_l + C_{h_\delta} \delta_{a_l} + C_{h_{\delta_t}} \delta_{t_{a_l}}$$

In asymmetric flight is $\alpha_r \neq \alpha_l$. Suppose now,

$$\alpha_r = \alpha + \Delta\alpha_a$$

then,

$$\alpha_l = \alpha - \Delta\alpha_a$$

The result is,

$$\alpha_r - \alpha_l = 2 \Delta\alpha_a$$

In addition, is,

$$\delta_{a_r} - \delta_{a_l} = \delta_a$$

$$\delta_{t_{a_r}} - \delta_{t_{a_l}} = \delta_{t_a}$$

$$C_{h_{0_r}} - C_{h_{0_l}} = 0$$

and thus,

$$C_{h_{a_r}} - C_{h_{a_l}} = C_{h_\alpha} 2 \Delta\alpha_a + C_{h_\delta} \delta_a + C_{h_{\delta_t}} \delta_{t_a} \quad (11-39)$$

Substitution of equation (11-39) in equation (11-38) finally results in,

$$F_a = -\frac{d\delta_a}{ds_a} \frac{1}{2} \rho V^2 S_a \bar{c}_a \left(C_{h_\alpha} \Delta\alpha_a + C_{h_\delta} \frac{\delta_a}{2} + C_{h_{\delta_t}} \frac{\delta_{t_a}}{2} \right) \quad (11-40)$$

The expression between parentheses is C_{h_α} of a single aileron.

11-7-2 Rudder Control

The applicable expression for the control force on the rudder pedals is entirely in analogy with equation (9-77) for the elevator control,

$$F_r = -\frac{d\delta_r}{ds_r} \frac{1}{2} \rho V_v^2 S_r \bar{c}_r (C_{h_\alpha} \alpha_v + C_{h_\delta} \delta_r + C_{h_{\delta_t}} \delta_{t_r}) \quad (11-41)$$

Calculation methods for the hinge moment derivatives in equation (11-40) and (11-41) have been mentioned in section 9-2-3.

Chapter 12

Space Applications

12-1 Introduction

This lecture series has focussed on the dynamic characteristics of subsonic aircraft. That allowed us to simplify the equations of motion such that we could use simplified expressions to derive the stability and control derivatives and to study, for instance, the characteristic motion. But what happens if the assumptions made to simplify the equations are no longer valid, for instance, because the velocity is so large that curvature effects of the Earth become important or even the fact that the Earth rotates. Also the fact that we have an atmosphere is not always the case, for instance when a Space Shuttle returns from the International Space Station it begins its mission outside the atmosphere and only gradually the atmospheric density and pressure start increasing. And satellites orbiting the Earth at sufficiently high orbits will never get in contact with the atmosphere, which means that the dynamic behaviour of these satellites is not governed by aerodynamic forces and moments at all.

In this chapter we will discuss several space applications such that the reader becomes aware of the different aspects that play a role in this kind of analyses. To this end, in Section 12-2 the characteristic motion of a winged re-entry vehicle will be discussed. Next, in Section 12-3 differences for entry capsules are highlighted.

12-2 Characteristic motion of a winged re-entry vehicle

12-2-1 Re-entry vehicle

To get a feeling for the influence of hypersonic velocities on the characteristic motion of aircraft-like vehicles we will use a reference vehicle that is similar to the Space Shuttle. The reason for doing so is that a complete mass and aerodynamic database is available for this vehicle, called HORUS-2B [38]. Initially, HORUS-2B was designed as a fully reusable second stage to the Ariane-5 launcher. Basically, the vehicle was unpowered although it had been equipped with a deorbitation engine and attitude-control thrusters. Later on, a rocket engine was added to the design and this adapted version became the manned, second stage of Sänger, the German Two-Stage-To-Orbit reference concept. Here, we use the original design being that of a winged, unpowered re-entry vehicle (see Figure 12-1). In Table 12-1, the main characteristics of HORUS are listed.

Total vehicle length	25.0 m
Maximum fuselage width	5.4 m
Maximum fuselage height	4.5 m
Wing span	13.0 m
Wing chord	23.0 m
Wing area	110.0 m ²
Maximum payload mass	7,000 kg
Re-entry mass	26,029 kg

Table 12-1: Main characteristics of HORUS-2B.

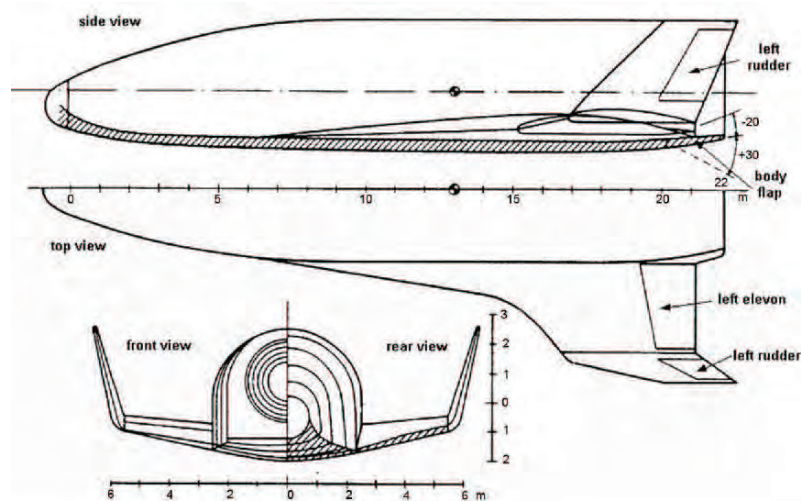


Figure 12-1: The HORUS-2B, based on [38].

The complete database of HORUS is described in ref. [38], where the aerodynamic coefficients are given in graphical form; the corresponding numerical values have been measured from these graphs. We will briefly summarise the key elements of the vehicle. The gross mass of the vehicle at re-entry is $m = 26,029$ kg. The c.o.m. is located in the vehicle's symmetry plane at 13 m from the nose (Figure 12-1). This configuration has the following principal moments of inertia:

$$\tilde{I}_{xx} = 119,000 \text{ kgm}^2 \quad \tilde{I}_{yy} = 769,000 \text{ kgm}^2 \quad \tilde{I}_{zz} = 806,000 \text{ kg m}^2$$

The inclination of the principal X -axis with respect to the X -axis of the body frame (negative for 'nose up') is -1.7° .

The HORUS-2B has a number of control surfaces, which have schematically been depicted in Figure 12-1: two rudders, two elevons and one body flap. The sign definitions for the deflection angles are as follows:

- Left and right rudder, deflection angles $\delta_{r,l}$ and $\delta_{r,r}$: positive outboard
- Left and right elevon, deflection angle $\delta_{e,l}$ and $\delta_{e,r}$: positive down
- Body flap, deflection angle δ_b : positive down

The rudders are outward movable only, which means that for yaw control only one rudder is active at a time. Deflecting both rudders at the same time would result in the so-called speed-brake function, but is not considered here¹. The elevons combine both the elevator and aileron function. The deflections commanded by the attitude controller should be combined to give the corresponding left and right elevon deflection.

In Figure 12-2, the entry control modes for HORUS have been depicted. The reaction control thrusters are operated in the early phase of re-entry, when dynamic pressure is too low to allow for aerodynamic control. The aileron and elevator start operating once the dynamic pressure has reached a minimum value of 100 N/m^2 . The rudder, which effectiveness is low, is being operated from a dynamic pressure of 150 N/m^2 and above. To support yaw control, the yaw thrusters continue to operate down to a Mach number of 1.

The control surfaces will only be effective above a certain dynamic pressure. For the upper layers of the atmosphere HORUS is equipped with reaction-control thrusters. These thrusters can also be used when large corrective manoeuvres are required and the control surfaces alone are not sufficient to deal with this. In Figure 12-2 the activation scheme of all control effectuators is shown. It is clear that the yaw thrusters are operational throughout the flight due to the low efficiency of the rudders.

The available thruster moments as well as the control-surface moments per degree deflection (linearised aerodynamics) have been plotted in Figure 12-3. It can easily be seen that for the elevons, there are three regions of a more or less linear increase with dynamic pressure. The rudder effectiveness seems to be completely linear with dynamic pressure. The dip in aileron effectiveness is because the elevator-trim deflection suddenly changes.

The aerodynamic database of HORUS-2B is based on some simplifying assumptions. The coefficients are steady coefficients for the untrimmed super/hypersonic flight regime, neglecting the following aerodynamic effects:

¹Speed brakes can be used in the approach and landing phase to increase the drag and therefore decrease the velocity. Since the entry guidance of HORUS is based on energy control by regulating the drag through the angle-of-attack dependency, it might be worthwhile to study the use the speedbrakes in this phase as well.

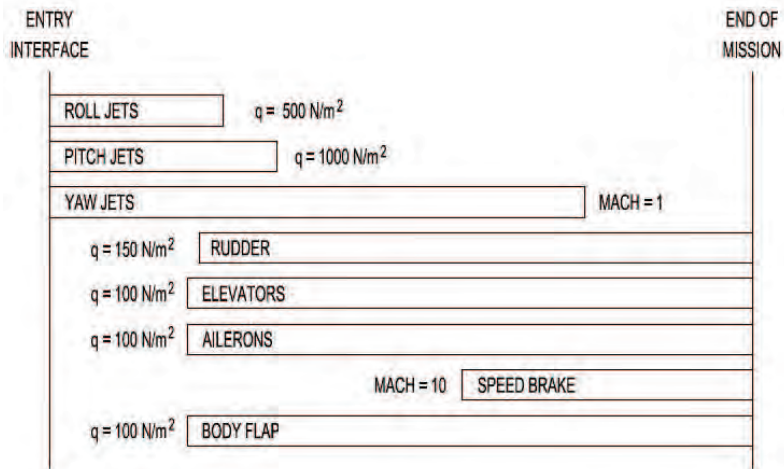


Figure 12-2: Entry control modes for HORUS.

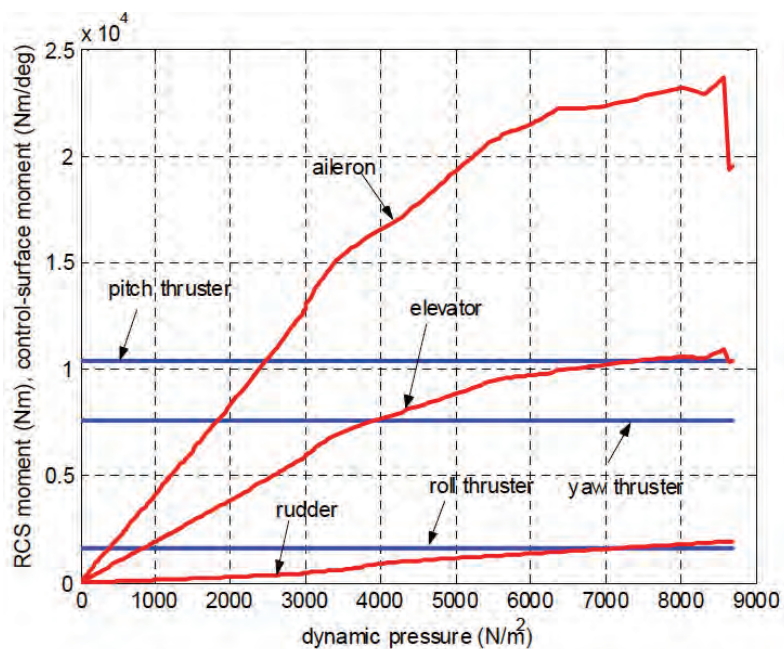


Figure 12-3: Maximum available moments (RCS thrusters) and moments per degree deflection (control surfaces).

- no aeroelastic effects (the vehicle is a non-elastic body);
- the influence of the Reynolds number on the skin-friction drag is not presented explicitly but included in the drag coefficient as averaged skin friction drag along a standard trajectory down to an altitude of 20 km. For trajectory calculations at lower altitudes, a drag altitude decrement is included in the data set. This decrement should be added to the total drag coefficient valid for 20 km;
- no special landing aerodynamics, like undercarriage drag, ground effects on pitch, lift and drag;
- no interference effects of the flaps;
- the influence of sideslip is simplified by linearisation over two degrees of angle of sideslip β . Note that β -derivatives or β -dependent coefficients can be extremely non-linear for $\beta > 2^\circ$.

The definition of the aerodynamic coefficients is the following:

$$C_D = C_{D_0} + \Delta C_{D_{r,l}} + \Delta C_{D_{e,l}} + \Delta C_{D_b} + \Delta C_{D_{e,r}} + \Delta C_{D_{r,r}} - \Delta C_{D_h} \quad (12-1)$$

with

$$\begin{aligned} C_{D_0} &= f(\alpha, M) \\ \Delta C_{D_{r,l}} &= f(\alpha, \delta_{r,l}, M) \\ \Delta C_{D_{e,l}} &= f(\alpha, \delta_{e,l}, M) \\ \Delta C_{D_b} &= f(\alpha, \delta_b, M) \\ \Delta C_{D_{e,r}} &= f(\alpha, \delta_{e,r}, M) \\ \Delta C_{D_{r,r}} &= f(\alpha, \delta_{r,r}, M) \\ C_{D_h} &= f(M, h) \end{aligned}$$

$$C_S = \Delta C_{S_{r,l}} + \Delta C_{S_{e,l}} + \Delta C_{S_{e,r}} + \Delta C_{S_{r,r}} + \left[\left(\frac{\partial C_S}{\partial \beta} \right)_0 + \Delta \left(\frac{\partial C_S}{\partial \beta} \right)_{e,l} + \Delta \left(\frac{\partial C_S}{\partial \beta} \right)_{e,r} \right] \beta \quad (12-2)$$

with

$$\begin{aligned} \Delta C_{S_{r,l}} &= f(\alpha, \delta_{r,l}, M) \\ \Delta C_{S_{e,l}} &= f(\alpha, \delta_{e,l}, M) \\ \Delta C_{S_{e,r}} &= f(\alpha, \delta_{e,r}, M) \\ \Delta C_{S_{r,r}} &= f(\alpha, \delta_{r,r}, M) \\ \left(\frac{\partial C_S}{\partial \beta} \right)_0 &= f(\alpha, M) \\ \Delta \left(\frac{\partial C_S}{\partial \beta} \right)_{e,l} &= f(\alpha, \delta_{e,l}, M) \\ \Delta \left(\frac{\partial C_S}{\partial \beta} \right)_{e,r} &= f(\alpha, \delta_{e,r}, M) \end{aligned}$$

$$C_L = C_{L_0} + \Delta C_{L_{e,l}} + \Delta C_{L_b} + \Delta C_{L_{e,r}} \quad (12-3)$$

with

$$\begin{aligned} C_{L_0} &= f(\alpha, M) \\ \Delta C_{L_{e,l}} &= f(\alpha, \delta_{e,l}, M) \\ \Delta C_{L_b} &= f(\alpha, \delta_b, M) \\ \Delta C_{L_{e,r}} &= f(\alpha, \delta_{e,r}, M) \end{aligned}$$

$$C_l = \Delta C_{l_{e,l}} + \Delta C_{l_{e,r}} + \left(\frac{\partial C_l}{\partial \beta} \right)_0 \cdot \beta \quad (12-4)$$

with

$$\begin{aligned} \Delta C_{l_{e,l}} &= f(\alpha, \delta_{e,l}, M) \\ \Delta C_{l_{e,r}} &= f(\alpha, \delta_{e,r}, M) \\ \left(\frac{\partial C_l}{\partial \beta} \right)_0 &= f(\alpha, M) \end{aligned}$$

$$C_m = C_{m_0} + \Delta C_{m_{e,l}} + \Delta C_{m_b} + \Delta C_{m_{e,r}} \quad (12-5)$$

with

$$\begin{aligned} C_{m_0} &= f(\alpha, M) \\ \Delta C_{m_{e,l}} &= f(\alpha, \delta_{e,l}, M) \\ \Delta C_{m_b} &= f(\alpha, \delta_b, M) \\ \Delta C_{m_{e,r}} &= f(\alpha, \delta_{e,r}, M) \end{aligned}$$

$$C_n = \Delta C_{n_{r,l}} + \Delta C_{n_{e,l}} + \Delta C_{n_{e,r}} + \Delta C_{n_{r,r}} + \left[\left(\frac{\partial C_n}{\partial \beta} \right)_0 + \Delta \left(\frac{\partial C_n}{\partial \beta} \right)_{r,l} + \Delta \left(\frac{\partial C_n}{\partial \beta} \right)_{e,l} + \Delta \left(\frac{\partial C_n}{\partial \beta} \right)_{e,r} + \Delta \left(\frac{\partial C_n}{\partial \beta} \right)_{r,r} \right] \beta \quad (12-6)$$

with

$$\begin{aligned} \Delta C_{n_{r,l}} &= f(\alpha, \delta_{r,l}, M) \\ \Delta C_{n_{e,l}} &= f(\alpha, \delta_{e,l}, M) \\ \Delta C_{n_{e,r}} &= f(\alpha, \delta_{e,r}, M) \\ \Delta C_{n_{r,r}} &= f(\alpha, \delta_{r,r}, M) \\ \left(\frac{\partial C_n}{\partial \beta} \right)_0 &= f(\alpha, M) \\ \Delta \left(\frac{\partial C_n}{\partial \beta} \right)_{r,l} &= f(\alpha, \delta_{r,l}, M) \\ \Delta \left(\frac{\partial C_n}{\partial \beta} \right)_{e,l} &= f(\alpha, \delta_{e,l}, M) \\ \Delta \left(\frac{\partial C_n}{\partial \beta} \right)_{e,r} &= f(\alpha, \delta_{e,r}, M) \\ \Delta \left(\frac{\partial C_n}{\partial \beta} \right)_{r,r} &= f(\alpha, \delta_{r,r}, M) \end{aligned}$$

Note that the current aerodynamic model of HORUS-2B does not comprise any damping coefficients, i.e.,

$$C_{l_p} = \frac{\partial C_l}{\partial \left(\frac{pb_{ref}}{V} \right)} = 0$$

$$C_{m_q} = \frac{\partial C_m}{\partial \left(\frac{qc_{ref}}{V} \right)} = 0$$

$$C_{n_r} = \frac{\partial C_n}{\partial \left(\frac{rb_{ref}}{V} \right)} = 0$$

The (supersonic) range of vehicle parameters and aerodynamic variables are given in Table 12-2. Furthermore, there is a drag dependency on the altitude. This dependency is given as a tabulated function of M (1.20 and 1.50) and h (0, 5, 10, 15 and 20 km).

α [°]	M [-]	δ_r [°]	δ_e [°]	δ_b [°]
0.0	1.2	0.0	-40.0	-20.0
5.0	1.5	10.0	-30.0	-10.0
10.0	2.0	20.0	-20.0	0.0
15.0	3.0	30.0	-10.0	10.0
20.0	5.0	40.0	0.0	20.0
25.0	10.0		10.0	30.0
30.0	20.0		20.0	
35.0			30.0	
40.0			40.0	
45.0				

Table 12-2: Parameter ranges for the super/hypersonic aerodynamic coefficients.

Summarized, the aerodynamic characteristics of HORUS are represented by tabulated functions of M , α and β , whereas the control-surface increments are also dependent on the related deflection angle. In total 34 tabulated coefficients are defined, i.e., 7 for C_D , 7 for C_S , 4 for C_L , 3 for C_l , 4 for C_m and 9 for C_n . These coefficients include the static derivatives with respect to the angle of sideslip. No dynamic derivatives have been specified.

12-2-2 Non-linear equations of motion

In Section 3-3 and Appendix C the non-linear equations of motion have been derived for both an inertial (Earth centered, index I) and rotating (Earth-Centred Earth-Fixed, index C) reference frame. Subsequently, in Section 3-3-3 the equations were set up for the vehicle carried Earth normal reference frame (index E). These equations formed the basis of the linearization process that would give us the non-dimensional equations in state-space form (Sections 4-3 through 4-5). Several steps were involved, notably simplifying the non-linear equations by assuming a non-rotating and flat Earth, and transforming the equations of translational motion to the body frame before linearization. For the study of the characteristic motion (or *eigenmotion*) of high-velocity entry vehicles, the assumptions of a non-rotating and flat Earth cannot be used, because of the large errors that will be otherwise introduced.

However, if these aspects are not ignored, setting up the equations of translational motion in the body frame is a complex process. For this reason, we will use a different set of equations as the starting point for the linearization. Traditionally, in re-entry studies either inertial Cartesian position and velocity elements are used, or a spherical position and velocity in a rotating frame, notably the C -frame. Because the latter definition makes it far easier to understand and interpret

the results, this will be our basis for linearization. On the downside, however, the full derivation is long and tedious, even though it follows the same steps as discussed in Section 3-3-2. Therefore, we will only present the final set of equations here. For more details on the derivation the interested reader is referred to the book of Vinh [177]. Our only assumptions that affect the equations are that the Earth is spherical (with a spherical gravity field) and rotates with a constant angular velocity Ω_t .

For the rotational motion we will use the Euler equations as derived in Section 3-4 and Appendix C. Here, we assume that the vehicle has a plane of mass symmetry (X_bY_b -plane), which means that $I_{xy} = I_{yz} = 0$. In terms of kinematic attitude equations we use a different set of Euler angles, notably the aerodynamic angles angle of attack, angle of sideslip and bank angle. These angles are in principle groundspeed based, but again, since there is no wind, they will be equal to their airspeed-based counterparts. Also in this case we will not derive the corresponding equations since also this derivation is long and tedious, although it follows the same steps in Section 3-4-3.

In Figure 12-4 the state variables for position and velocity are shown. The position is given by the distance R , longitude τ and latitude δ , whereas the velocity is expressed by its modulus, the groundspeed V , and two direction angles, i.e., flight-path angle γ and heading χ (note that since we do not consider wind, no subscript is added to differentiate between air- and groundspeed). The longitude is measured positively to the east ($-180^\circ \leq \tau < 180^\circ$). The latitude is measured along the appropriate meridian starting at the equator, positive in north direction ($0^\circ \leq \delta \leq 90^\circ$) and negative to the south. R , finally, is the distance from the c.o.m. of the central body to the c.o.m. of the vehicle. The relative velocity V (i.e., the modulus of the velocity vector \mathbf{V}) is expressed with respect to the C -frame. γ is the angle between \mathbf{V} and the local horizontal plane; it ranges from -90° to $+90^\circ$ and is negative when \mathbf{V} is oriented below the local horizon. χ defines the direction of the projection of \mathbf{V} in the local horizontal plane with respect to the local north and ranges from 0° to 360° . When $\chi = +90^\circ$, the vehicle is moving parallel to the equator to the east.

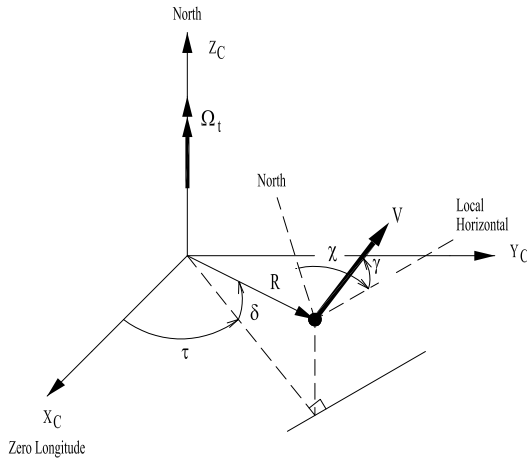


Figure 12-4: Definition of spherical position and velocity state variables.

The attitude of a vehicle, or, in mathematical terms, the orientation of the body-fixed reference frame with respect to the trajectory reference frame, is expressed by the so-called aerodynamic angles, i.e., the angle of attack α ($-180^\circ \leq \alpha < 180^\circ$, for a 'nose-up' attitude $\alpha > 0^\circ$), the angle of sideslip β ($-180^\circ \leq \beta < 180^\circ$, β is positive for a 'nose-left' attitude) and the bank angle μ ($-180^\circ \leq \mu < 180^\circ$, μ is positive when banking to the right), see also Figure 12-5. These angles form an asymmetric Euler set.

The angular rate of the body is here defined as the rotation of the body frame with respect to the inertial frame, expressed in components along the body axes. These components are called roll rate p , pitch rate q and yaw rate r (see again Figure 12-5).

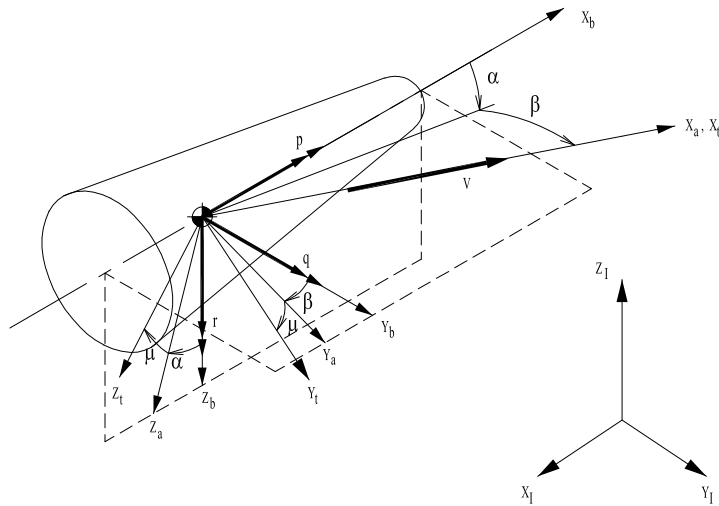


Figure 12-5: Definition of the aerodynamic attitude angles α , β and μ , and the angular rates p , q and r . Here, all states are positive.

Summarized, the dynamic equations of translational motion are given by

$$\dot{V} = -\frac{D}{m} - g \sin \gamma + \Omega_t^2 R \cos \delta (\sin \gamma \cos \delta - \cos \gamma \sin \delta \cos \chi) \quad (12-7)$$

$$\begin{aligned} V \dot{\gamma} = & \frac{L \cos \mu}{m} - g \cos \gamma + 2\Omega_t V \cos \delta \sin \chi + \frac{V^2}{r} \cos \gamma + \\ & + \Omega_t^2 R \cos \delta (\cos \delta \cos \gamma + \sin \gamma \sin \delta \cos \chi) \end{aligned} \quad (12-8)$$

$$\begin{aligned} V \cos \gamma \dot{\chi} = & \frac{L \sin \mu}{m} + 2\Omega_t V (\sin \delta \cos \gamma - \cos \delta \sin \gamma \cos \chi) + \frac{V^2}{r} \cos^2 \gamma \tan \delta \sin \chi + \\ & + \Omega_t^2 r \cos \delta \sin \delta \sin \chi \end{aligned} \quad (12-9)$$

whereas the kinematic position equations are given by

$$\dot{R} = \dot{h} = V \sin \gamma \quad (12-10)$$

$$\dot{\tau} = \frac{V \sin \chi \cos \gamma}{R \cos \delta} \quad (12-11)$$

$$\dot{\delta} = \frac{V \cos \chi \cos \gamma}{R} \quad (12-12)$$

The Euler equations of rotational motion are defined by (conform Eqs. (3-53a)-(3-53c)):

$$\dot{p} = \frac{I_{zz}}{I^*} M_x + \frac{I_{xz}}{I^*} M_z + \frac{(I_{xx} - I_{yy} + I_{zz}) I_{xz}}{I^*} pq + \frac{(I_{yy} - I_{zz}) I_{zz} - I_{xz}^2}{I^*} qr \quad (12-13)$$

$$\dot{q} = \frac{M_y}{I_{yy}} + \frac{I_{xz}}{I_{yy}} (r^2 - p^2) + \frac{I_{zz} - I_{xx}}{I_{yy}} pr \quad (12-14)$$

$$\dot{r} = \frac{I_{xz}}{I^*} M_x + \frac{I_{xx}}{I^*} M_z + \frac{(I_{xx} - I_{yy}) I_{xx} + I_{xz}^2}{I^*} pq + \frac{(-I_{xx} + I_{yy} - I_{zz}) I_{xz}}{I^*} qr \quad (12-15)$$

with $I^* = I_{xx}I_{zz} - I_{xz}^2$.

Finally, the kinematic attitude equations are given by:

$$\begin{aligned}\dot{\alpha} \cos \beta &= -p \cos \alpha \sin \beta + q \cos \beta - r \sin \alpha \sin \beta + \\ &+ \sin \mu \left[\dot{\chi} \cos \gamma - \dot{\delta} \sin \chi \sin \gamma + (\dot{\tau} + \omega_{cb}) (\cos \delta \cos \chi \sin \gamma - \sin \delta \cos \gamma) \right] + \\ &- \cos \mu \left[\dot{\gamma} - \dot{\delta} \cos \chi - (\dot{\tau} + \Omega_t) \cos \delta \sin \chi \right]\end{aligned}\quad (12-16)$$

$$\begin{aligned}\dot{\beta} &= p \sin \alpha - r \cos \alpha + \\ &+ \sin \mu \left[\dot{\gamma} - \dot{\delta} \cos \chi - (\dot{\tau} + \Omega_t) \cos \delta \sin \chi \right] + \\ &+ \cos \mu \left[\dot{\chi} \cos \gamma - \dot{\delta} \sin \chi \sin \gamma + (\dot{\tau} + \omega_{cb}) (\cos \delta \cos \chi \sin \gamma - \sin \delta \cos \gamma) \right]\end{aligned}\quad (12-17)$$

$$\begin{aligned}\dot{\mu} &= -p \cos \alpha \cos \beta - q \sin \beta - r \sin \alpha \cos \beta + \\ &+ \dot{\alpha} \sin \beta - \dot{\chi} \sin \gamma - \dot{\delta} \sin \chi \cos \gamma + (\dot{\tau} + \Omega_t) (\cos \delta \cos \chi \cos \gamma + \sin \delta \sin \gamma)\end{aligned}\quad (12-18)$$

In these equations, $\dot{\gamma}$, $\dot{\chi}$, $\dot{\delta}$ and $\dot{\tau}$ are given by Eqs. (12-8) through (12-12), and represent the effects of the rotation of the Earth and the rotation of the local horizontal plane, similar to the indicated effects in Eqs. (3-76)-(3-78). Note that the external moment components are expressed in the body-fixed reference frame.

12-2-3 Linearization

The characteristic motion, or the open-loop behaviour, of a vehicle, can be described by the eigenvalues and eigenvectors of the equations of motion. However, the eigenvalues and eigenvectors can only be obtained when the time derivatives of the states are given as a linear combination of the states. In other words: the equations of motion have to be linearised. As a result, the motion given by this linearised system should be regarded as an equilibrium trajectory, so that the characteristic motions are small deviations from this nominal path. To simplify the process of linearisation, we will make two assumptions, as we also did in Chapter 4. In this way we can already remove some terms from the equations, which would otherwise disappear during the linearization.

- We will consider a non-rotating Earth ($\Omega_t = 0$ rad/s), which is allowed since the rotation of the vehicle (and its local horizontal plane) is of a much higher frequency than the rotation of the Earth. As a result, the Coriolis and centripetal accelerations are zero as well,
- The vehicle is assumed to be rotationally symmetric (w.r.t. mass) around the X_b -axis of the body-fixed reference frame, which means that $I_{xz} = 0$.

With the above assumptions, we can neglect the smaller terms. The resulting equations of motion become:

$$\dot{V} = -\frac{D}{m} - g \sin \gamma \quad (12-19)$$

$$\dot{\gamma} = \left(\frac{V}{R} - \frac{g}{V} \right) \cos \gamma + \frac{(L \cos \mu - S \sin \mu)}{mV} \quad (12-20)$$

$$\dot{\chi} = \frac{V}{R} \cos \gamma \tan \delta \sin \chi - \frac{(L \sin \mu + S \cos \mu)}{mV \cos \gamma} \quad (12-21)$$

$$\dot{R} = V \sin \gamma \quad (12-22)$$

$$\dot{\tau} = \frac{V \cos \gamma \sin \chi}{R \cos \delta} \quad (12-23)$$

$$\dot{\delta} = \frac{V}{R} \cos \gamma \cos \chi \quad (12-24)$$

$$\dot{p} = \frac{M_x}{I_{xx}} + \frac{I_{yy} - I_{zz}}{I_{xx}} qr \quad (12-25)$$

$$\dot{q} = \frac{M_y}{I_{yy}} + \frac{I_{zz} - I_{xx}}{I_{yy}} pr \quad (12-26)$$

$$\dot{r} = \frac{M_z}{I_{zz}} + \frac{I_{xx} - I_{yy}}{I_{zz}} pq \quad (12-27)$$

Since the kinematic attitude equations are very complex, we will introduce another simplification. We assume that the vehicle's attitude is only marginally influenced by an asymmetric translational motion, or in other words: we assume that the vehicle's trajectory is parallel to the equator ($\delta = 0^\circ$ and $\chi = 90^\circ$), and remains that way ($\dot{\delta} = 0$ rad/s). In that case Eq. (12-16)-(12-18) reduce to:

$$\dot{\alpha} = q - (p \cos \alpha + r \sin \alpha) \tan \beta - \frac{L - mg \cos \gamma \cos \mu}{mV \cos \beta} \quad (12-28)$$

$$\dot{\beta} = p \sin \alpha - r \cos \alpha - \frac{S + mg \cos \gamma \sin \mu}{mV} \quad (12-29)$$

$$\dot{\mu} = -\frac{p \cos \alpha + r \sin \alpha}{\cos \beta} - \frac{L - mg \cos \gamma \cos \mu}{mV} \tan \beta + \frac{L \sin \mu + S \cos \mu}{mV} \tan \gamma \quad (12-30)$$

As we can see, the equations for χ , τ and δ are not coupled to the rest of the equations, so a 9-degrees-of-freedom linearised model for the state space formed by V , γ , R , p , q , r , α , β and μ can be derived.

The linearisation is performed as follows. As we saw in Chapter 4 the linearization was done by developing a Taylor series to first order of the equations of motion. The outcome of the linearization is a set of coupled linear differential equations, and can be written in matrix form:

$$\Delta \dot{\mathbf{x}} = \mathbf{A} \Delta \mathbf{x} + \mathbf{B} \Delta \mathbf{u} \quad (12-31)$$

where $\Delta \mathbf{x}$ is the $n \times 1$ error state vector, $\Delta \mathbf{u}$ is the $m \times 1$ noise input vector, and \mathbf{A} and \mathbf{B} are the $n \times n$ system or state matrix and $n \times m$ input matrix. The system matrix \mathbf{A} and input matrix \mathbf{B} can directly be derived from the non-linear equations of motion with:

$$\mathbf{A} = \begin{bmatrix} \frac{\partial f_1}{\partial x_1} & \dots & \frac{\partial f_1}{\partial x_n} \\ \vdots & \vdots & \vdots \\ \frac{\partial f_n}{\partial x_1} & \dots & \frac{\partial f_n}{\partial x_n} \end{bmatrix} \quad (12-32)$$

and

$$\mathbf{B} = \begin{bmatrix} \frac{\partial f_1}{\partial u_1} & \dots & \frac{\partial f_1}{\partial u_m} \\ \vdots & \vdots & \vdots \\ \frac{\partial f_n}{\partial u_1} & \dots & \frac{\partial f_n}{\partial u_m} \end{bmatrix} \quad (12-33)$$

evaluated at the nominal condition. In Eqs. (12-32) and (12-33), f_i are the equations of motion, \dot{V} , $\dot{\gamma}$, etc.

However, to provide more insight we will first explain the linearization process in a slightly more elaborate way. We assume an equilibrium value of each of the state variables (index 0), and we will look at small deviations from this equilibrium state. Note that the vehicle is not powered (no fuel consumption), which means that the mass properties are constant. So:

$$\begin{aligned} V &= V_0 + \Delta V \\ \gamma &= \gamma_0 + \Delta \gamma \\ R &= R_0 + \Delta R \\ p &= p_0 + \Delta p \\ q &= q_0 + \Delta q \\ r &= r_0 + \Delta r \\ \alpha &= \alpha_0 + \Delta \alpha \\ \beta &= \beta_0 + \Delta \beta = \Delta \beta \\ \mu &= \mu_0 + \Delta \mu \end{aligned} \quad (12-34)$$

Note that by definition of the nominal state, this also results in nominal aerodynamic forces D_0 , S_0 and L_0 , as well as nominal aerodynamic moments \mathcal{L}_0 , \mathcal{M}_0 and \mathcal{N}_0 . Similarly, the small state deviations give force and moment deviations ΔD , ΔS , ΔL , $\Delta \mathcal{L}$, $\Delta \mathcal{M}$ and $\Delta \mathcal{N}$.

The nominal position (R_0), velocity (V_0 and γ_0) and corresponding control history (α_0 , β_0 and μ_0) follow from the nominal trajectory (see Section 12-2-5), which leaves us with three unknowns p_0 , q_0 and r_0 . However, since we want no perturbation of the nominal control (α_0 and μ_0) when we are flying the vehicle, we can compute the equilibrium angular rates from the condition

$$\dot{\alpha} = \dot{\beta} = \dot{\mu} = 0 \quad (12-35)$$

or, using Eqs. (12-28)-(12-30),

$$q_0 = \frac{L_0}{mV_0} - \frac{g_0}{V_0} \cos \gamma_0 \cos \mu_0 \quad (12-36)$$

$$p_0 \sin \alpha_0 - r_0 \cos \alpha_0 = \frac{g_0}{V_0} \cos \gamma_0 \sin \mu_0 \quad (12-37)$$

$$p_0 \cos \alpha_0 + r_0 \sin \alpha_0 = \frac{L_0}{mV_0} \tan \gamma_0 \sin \mu_0 \quad (12-38)$$

Solving for p_0 , q_0 and r_0 gives us

$$p_0 = c_1 \sin \alpha_0 + c_2 \cos \alpha_0 \quad (12-39)$$

$$q_0 = \frac{L_0}{mV_0} - \frac{g_0}{V_0} \cos \gamma_0 \cos \mu_0 \quad (12-40)$$

$$r_0 = -c_1 \cos \alpha_0 + c_2 \sin \alpha_0 \quad (12-41)$$

with

$$c_1 = \frac{g_0}{V_0} \cos \gamma_0 \sin \mu_0$$

$$c_2 = \frac{L_0}{mV_0} \tan \gamma_0 \sin \mu_0$$

Note that since $\beta_0 = 0$, also $S_0 = 0$.

Substituting expressions Eq. (12-34) in Eqs. (12-19)-(12-30) gives us equations with nominal (e.g., V_0 , L_0 , etc.), first-order (e.g., ΔV_0 , ΔL_0 , etc.) and higher-order terms (e.g., $\Delta V \Delta \gamma$, $p_0 \Delta \alpha$, where the nominal rotational rates p_0 , q_0 and r_0 can be treated as perturbations, because they are small). So if we neglect now the higher-order terms and subtract the nominal state (i.e., $\dot{V}_0 = \dots$, etc.) we will get the linearized differential equations. As an example, Eq. (12-22) will be linearized:

$$\dot{R} = V \sin \gamma \quad (12-42)$$

Substituting $V = V_0 + \Delta V$, $\gamma = \gamma_0 + \Delta \gamma$ and $R = R_0 + \Delta R$ we obtain:

$$\dot{R}_0 + \Delta \dot{R} = (V_0 + \Delta V) \sin(\gamma_0 + \Delta \gamma) \quad (12-43)$$

Using the double-angle formula, $\sin(\gamma_0 + \Delta \gamma)$ expands to

$$\sin(\gamma_0 + \Delta \gamma) = \sin \gamma_0 \cos \Delta \gamma + \cos \gamma_0 \sin \Delta \gamma \quad (12-44)$$

Since $\Delta \gamma$ is small, $\sin \Delta \gamma \approx \Delta \gamma$ and $\cos \Delta \gamma \approx 1$, and the above equation reduces to:

$$\sin(\gamma_0 + \Delta \gamma) = \sin \gamma_0 + \cos \gamma_0 \Delta \gamma \quad (12-45)$$

With this result, Eq. (12-43) can be written as:

$$\dot{R}_0 + \Delta \dot{R} = V_0 \sin \gamma_0 + V_0 \cos \gamma_0 \Delta \gamma + \sin \gamma_0 \Delta V + \cos \gamma_0 \Delta V \Delta \gamma \quad (12-46)$$

The last term on the right-hand side, i.e., $\cos \gamma_0 \Delta V \Delta \gamma$, is a second-order term and can be neglected compared to the others, so we obtain:

$$\dot{R}_0 + \Delta \dot{R} = V_0 \sin \gamma_0 + V_0 \cos \gamma_0 \Delta \gamma + \sin \gamma_0 \Delta V \quad (12-47)$$

Finally, subtracting the nominal state, i.e., $\dot{R}_0 = V_0 \sin \gamma_0$, from both sides of Eq. (12-47) yields:

$$\Delta \dot{R} = V_0 \cos \gamma_0 \Delta \gamma + \sin \gamma_0 \Delta V \quad (12-48)$$

which is the result we have been looking for.

To conclude this example we go back to Eq. (12-31):

$$\Delta \dot{\mathbf{x}} = \mathbf{A} \Delta \mathbf{x} + \mathbf{B} \Delta \mathbf{u} \quad (12-49)$$

As said, the coefficients of \mathbf{A} are given by the partial derivatives evaluated at the nominal state. For our example with $f = V \sin \gamma$ conform Eq. (12-43), the corresponding derivatives are $\frac{\partial f}{\partial V}$ and $\frac{\partial f}{\partial \gamma}$. Evaluating these derivatives immediately gives

$$\left. \frac{\partial f}{\partial V} \right|_0 = \sin \gamma_0$$

and

$$\left. \frac{\partial f}{\partial \gamma} \right|_0 = V_0 \cos \gamma_0$$

Substituted into Eq. (12-49) gives, of course, the same result as Eq. (12-48), but obtained with a more straightforward approach.

The other equations follow in a similar manner. So, summarized, the following 9 first-order differential equations are obtained:

$$\Delta \dot{V} = -\frac{\Delta D}{m} + 2 \frac{g_0}{R_0} \sin \gamma_0 \Delta R - g_0 \cos \gamma_0 \Delta \gamma \quad (12-50)$$

$$\begin{aligned} \Delta \dot{\gamma} = & \left(-\dot{\gamma}_0 + \frac{2V_0}{R_0} \cos \gamma_0 \right) \frac{\Delta V}{V_0} + \left(\frac{2g_0}{R_0} - \frac{V_0^2}{R_0^2} \right) \frac{\cos \gamma_0}{V_0} \Delta R - \left(\frac{V_0^2}{R_0} - g_0 \right) \frac{\sin \gamma_0}{V_0} \Delta \gamma + \\ & - \frac{L_0}{mV_0} \sin \mu_0 \Delta \mu + \frac{\cos \mu_0}{mV_0} \Delta L - \frac{\sin \mu_0}{mV_0} \Delta S \end{aligned} \quad (12-51)$$

$$\Delta \dot{R} = \sin \gamma_0 \Delta V + V_0 \cos \gamma_0 \Delta \gamma \quad (12-52)$$

$$\Delta \dot{p} = \frac{\Delta M_x}{I_{xx}} \quad (12-53)$$

$$\Delta \dot{q} = \frac{\Delta M_y}{I_{yy}} \quad (12-54)$$

$$\Delta \dot{r} = \frac{\Delta M_z}{I_{zz}} \quad (12-55)$$

$$\begin{aligned} \Delta \dot{\alpha} = & \Delta q - \frac{1}{mV_0} \Delta L - \frac{g_0}{V_0} \cos \gamma_0 \sin \mu_0 \Delta \mu + \left(\frac{L_0}{mV_0^2} - \frac{g_0}{V_0^2} \cos \gamma_0 \cos \mu_0 \right) \Delta V + \\ & - \frac{g_0}{V_0} \sin \gamma_0 \cos \mu_0 \Delta \gamma - \frac{2g_0}{R_0 V_0} \cos \gamma_0 \cos \mu_0 \Delta R \end{aligned} \quad (12-56)$$

$$\begin{aligned} \Delta \dot{p} = & \sin \alpha_0 \Delta p - \cos \alpha_0 \Delta r - \frac{\Delta S}{mV_0} - \frac{g_0}{V_0} \cos \gamma_0 \cos \mu_0 \Delta \mu + \frac{g_0}{V_0^2} \cos \gamma_0 \sin \mu_0 \Delta V + \\ & + \frac{2g_0}{R_0 V_0} \cos \gamma_0 \sin \mu_0 \Delta R + \frac{g_0}{V_0} \sin \gamma_0 \sin \mu_0 \Delta \gamma \end{aligned} \quad (12-57)$$

$$\begin{aligned} \Delta \dot{\mu} = & -\cos \alpha_0 \Delta p - \sin \alpha_0 \Delta r - \left(\frac{L_0}{mV_0} - \frac{g_0}{V_0} \cos \gamma_0 \cos \mu_0 \right) \Delta \beta + \frac{L_0}{mV_0} \sin \mu_0 \Delta \gamma + \\ & + \frac{\tan \gamma_0}{mV_0} \left(\sin \mu_0 \Delta L + \cos \mu_0 L_0 \Delta \mu + \cos \mu_0 \Delta S - \frac{L_0}{V_0} \sin \mu_0 \Delta V \right) \end{aligned} \quad (12-58)$$

In deriving the above equations, we have used the central-field definition of the gravitational acceleration, i.e., $g = \frac{\mu}{R^2}$, which gives us

$$g_0 + \Delta g = \frac{\mu}{(R_0 + \Delta R)^2} = \frac{\mu}{R_0^2} \frac{1}{1 + 2 \frac{\Delta R}{R_0}} \approx \frac{\mu}{R_0^2} \left(1 - 2 \frac{\Delta R}{R_0} \right)$$

or

$$\Delta g = -2g_0 \frac{\Delta R}{R_0}$$

Now that we have linearised the equations of motion, we can write them in matrix form, also called the state-space form, see Eq. (12-31). This will be described in the following section.

12-2-4 State-space form

When equations of motion are written in state-space form, they have the following form in matrix notation, as discussed before:

$$\dot{\mathbf{x}} = \mathbf{Ax} + \mathbf{Bu} \quad (12-59)$$

with \mathbf{x} an $n \times 1$ state vector, \mathbf{u} an $m \times 1$ control vector, and \mathbf{A} and \mathbf{B} the $n \times n$ state (or system) and $n \times m$ control coefficient matrices, respectively. Eq. (12-59) is called the dynamics equation; to complete the description of the state of the vehicle we also need a so-called output equation:

$$\mathbf{y} = \mathbf{Cx} + \mathbf{Du} \quad (12-60)$$

In the above equation, \mathbf{y} is the $k \times 1$ output vector, and \mathbf{C} and \mathbf{D} are the $k \times n$ output and $k \times m$ direct transmission matrices, respectively. For the time being, we will restrict ourselves to the use of Eq. (12-59).

To write Eqs. (12-50)-(12-58) in state-space form, we must distinguish between state variables and control variables. The choice of state variables is obvious, if we look at the original equations of motion with their state variables. We write

$$\mathbf{x} = (\Delta V, \Delta \gamma, \Delta R, \Delta p, \Delta q, \Delta r, \Delta \alpha, \Delta \beta, \Delta \mu)^T$$

The selection of control variables is less clear. The principle of control is obvious: by changing the magnitude and direction of external forces (and therefore in principle also the external moments), the trajectory of the vehicle can be changed. The guidance system makes sure that the vehicle will follow its nominal trajectory by adjusting the angle of attack and bank angle, the control variables of the guidance system. These control variables determine the size and direction of the aerodynamic force vector, the only controllable external force acting on the unpowered vehicle. (The other external force is of gravitational origin; this force is depending on the position of the vehicle and cannot be controlled actively.)

The attitude controller has to guarantee that the commanded attitude is obtained (and maintained) with a certain accuracy in a finite time, which means that eventually there should be moment equilibrium. Note that the actual angle of attack and bank angle are given by the kinematic equations, which means that they have defined values depending on the rotation of the vehicle and thus the size and direction of the external moments. So whereas the forces acting on the centre of mass (c.o.m.) of the vehicle are the guidance control variables, the moments around the c.o.m. are the attitude control variables.

Inspecting the equations of motion, we find beside the three force components ΔD , ΔS and ΔL , three moment components, i.e., ΔM_x , ΔM_y and ΔM_z . Part of the moment components is determined by the vehicle, depending on its actual attitude. However, the remaining part is given (and can be changed) by, for instance, aerodynamic control surfaces, reaction control thrusters and momentum wheels, depending on the vehicle configuration and sub-systems. So for the selection of the attitude-control effectors, we must have a closer look at the vehicle, the HORUS-2B [38]. This vehicle is winged, without a major propulsion system, but with 5 aerodynamic control surfaces

(two rudders, two wing flaps² and a body flap) and a number of reaction control thrusters. The body flap is only used for trim, and does not have to be considered as a control. The two wing flaps, or elevons, can be deflected symmetrically (elevator function) and asymmetrically (aileron function). The rudders are outward movable only, and only one at a time.

It should be noted that by deflecting the control surfaces, an aerodynamic force is generated that gives a moment around the vehicle's c.o.m. depending on the moment arm, the distance to the c.o.m.. The deflection of a surface is in principle an analogous process, of course with a limited accuracy, which means that the generated moments are a continuous function of the deflection angle, as well as of flight and similarity parameters, such as the Mach number.

The reaction control system is only being used when the aerodynamic control surfaces are not sufficiently effective, e.g., in the upper layers of the atmosphere. The aerodynamic control surfaces are activated when their effectiveness is more than 10% of that of the corresponding thrusters and the thrusters are inhibited when their effectiveness is less than 10% of the corresponding aerodynamic surface³. Whereas the aerodynamic control moments are continuous functions, this is not the case with the reaction control moments. The principle of a thruster is that it is either ON or OFF. When it is on, it will generate a constant thrust force that will also result in a constant moment⁴. By switching the thrusters on and off repeatedly (so-called pulsing), the required moment can be approximated. Furthermore, in case there are more thrusters for generating moments about one particular axis, the magnitude of the moment can be varied by smartly combining the required thrusters. Here, however, we will assume continuous reaction control moments, for reasons of simplicity. Moreover, we will directly use the moments as control variables, instead of the thrust forces.

So, summarised we can write for the control vector \mathbf{u} :

$$\mathbf{u} = (\Delta\delta_e, \Delta\delta_a, \Delta\delta_r, \Delta M_{T,x}, \Delta M_{T,y}, \Delta M_{T,z})^T$$

with

- δ_e = elevator deflection angle (rad)
- δ_a = aileron deflection angle (rad)
- δ_r = rudder deflection angle (rad)
- $M_{T,x}$ = roll-thruster moment (Nm)
- $M_{T,y}$ = pitch-thruster moment (Nm)
- $M_{T,z}$ = yaw-thruster moment (Nm)

²To be more in line with other literature, we will not use the term *wing flaps*, but *elevons* since this control surface combines the elevator and aileron function.

³For the defined configuration of HORUS-2B, the maximal torque of the pitch thrusters is 10,400 Nm, the one of the roll thrusters is 1,600 Nm and the one of the yaw thrusters is 7,600 Nm. This results in activating the aerodynamic control surfaces at approximately 100 km and switching off the roll thrusters at about 75 km, while the yaw thrusters remain activated until the end of the descent.

⁴The thrust force is in principle depending on the atmospheric conditions, which change significantly during the flight. Since we do not have extended thruster models at our disposal, we will assume constant thrust forces. However, it is known from the experience with the Space Shuttle that the operation of the reaction control thrusters can be significantly influenced by atmospheric conditions.

These definitions of \mathbf{x} and \mathbf{u} result in the following state-space matrix equation:

$$\begin{aligned} \begin{pmatrix} \Delta\dot{V} \\ \Delta\dot{\gamma} \\ \Delta\dot{R} \\ \Delta\dot{p} \\ \Delta\dot{q} \\ \Delta\dot{r} \\ \Delta\dot{\alpha} \\ \Delta\dot{\beta} \\ \Delta\dot{\mu} \end{pmatrix} &= \begin{bmatrix} a_{VV} & a_{V\gamma} & a_{VR} & a_{Vp} & a_{Vq} & a_{Vr} & a_{V\alpha} & a_{V\beta} & a_{V\mu} \\ a_{\gamma V} & a_{\gamma\gamma} & a_{\gamma R} & a_{\gamma p} & a_{\gamma q} & a_{\gamma r} & a_{\gamma\alpha} & a_{\gamma\beta} & a_{\gamma\mu} \\ a_{RV} & a_{R\gamma} & a_{RR} & a_{Rp} & a_{Rq} & a_{Rr} & a_{R\alpha} & a_{R\beta} & a_{R\mu} \\ a_{pV} & a_{p\gamma} & a_{pR} & a_{pp} & a_{pq} & a_{pr} & a_{p\alpha} & a_{p\beta} & a_{p\mu} \\ a_{qV} & a_{q\gamma} & a_{qR} & a_{qp} & a_{qq} & a_{qr} & a_{q\alpha} & a_{q\beta} & a_{q\mu} \\ a_{rV} & a_{r\gamma} & a_{rR} & a_{rp} & a_{rq} & a_{rr} & a_{r\alpha} & a_{r\beta} & a_{r\mu} \\ a_{\alpha V} & a_{\alpha\gamma} & a_{\alpha R} & a_{\alpha p} & a_{\alpha q} & a_{\alpha r} & a_{\alpha\alpha} & a_{\alpha\beta} & a_{\alpha\mu} \\ a_{\beta V} & a_{\beta\gamma} & a_{\beta R} & a_{\beta p} & a_{\beta q} & a_{\beta r} & a_{\beta\alpha} & a_{\beta\beta} & a_{\beta\mu} \\ a_{\mu V} & a_{\mu\gamma} & a_{\mu R} & a_{\mu p} & a_{\mu q} & a_{\mu r} & a_{\mu\alpha} & a_{\mu\beta} & a_{\mu\mu} \end{bmatrix} \begin{pmatrix} \Delta V \\ \Delta \gamma \\ \Delta R \\ \Delta p \\ \Delta q \\ \Delta r \\ \Delta \alpha \\ \Delta \beta \\ \Delta \mu \end{pmatrix} + \\ + \begin{bmatrix} b_{Ve} & b_{Va} & b_{Vr} & b_{Vx} & b_{Vy} & b_{Vz} \\ b_{\gamma e} & b_{\gamma a} & b_{\gamma r} & b_{\gamma x} & b_{\gamma y} & b_{\gamma z} \\ b_{Re} & b_{Ra} & b_{Rr} & b_{Rx} & b_{Ry} & b_{Rz} \\ b_{pe} & b_{pa} & b_{pr} & b_{px} & b_{py} & b_{pz} \\ b_{qe} & b_{qa} & b_{qr} & b_{qx} & b_{qy} & b_{qz} \\ b_{re} & b_{ra} & b_{rr} & b_{rx} & b_{ry} & b_{rz} \\ b_{\alpha e} & b_{\alpha a} & b_{\alpha r} & b_{\alpha x} & b_{\alpha y} & b_{\alpha z} \\ b_{\beta e} & b_{\beta a} & b_{\beta r} & b_{\beta x} & b_{\beta y} & b_{\beta z} \\ b_{\mu e} & b_{\mu a} & b_{\mu r} & b_{\mu x} & b_{\mu y} & b_{\mu z} \end{bmatrix} \begin{pmatrix} \Delta \delta_e \\ \Delta \delta_a \\ \Delta \delta_r \\ \Delta M_{T,x} \\ \Delta M_{T,y} \\ \Delta M_{T,z} \end{pmatrix} \end{aligned} \quad (12-61)$$

Before we derive the 135 matrix elements a_{ij} and b_{ik} , one more task remains to be done as we already indicated above: the evaluation of the force and moment variations in Eqs. (12-39)-(12-55), i.e., ΔD , ΔS , ΔL , ΔM_x , ΔM_y , ΔM_z , as a function of state and control variables. Starting with ΔD , we must first study the aerodynamic database of the HORUS-2B to find the dependency of drag D on flight parameters and deflection angles [38]. We find:

$$D = f(M, \alpha, h, \delta_e, \delta_r, \delta_b)$$

with

- M = Mach number (-)
- α = angle of attack (rad)
- h = height (m)
- δ_e = elevon deflection angle (rad)
- δ_r = rudder deflection angle (rad)
- δ_b = body-flap deflection angle (rad)

ΔD can thus be written as

$$\Delta D = \frac{\partial D}{\partial M} \Delta M + \frac{\partial D}{\partial \alpha} \Delta \alpha + \frac{\partial D}{\partial h} \Delta h + \frac{\partial D}{\partial \delta_e} \Delta \delta_e + \frac{\partial D}{\partial \delta_a} \Delta \delta_a + \frac{\partial D}{\partial \delta_r} \Delta \delta_r + \frac{\partial D}{\partial \delta_b} \Delta \delta_b \quad (12-62)$$

To evaluate the partial derivatives, we write D as

$$D = C_D \bar{q} S_{ref} \quad (12-63)$$

with

- C_D = drag coefficient = $f(M, \alpha, h, \delta_r, \delta_e, \delta_b)$
- \bar{q} = $\frac{1}{2} \rho V^2$ = dynamic pressure (N/m^2) = $f(h, V)$
- S_{ref} = reference area (m^2)

The height dependency of the drag coefficient is only apparent for Mach numbers smaller than 1.5, and is small compared with the dependencies on Mach number and angle of attack. The body flap is only used for trim, so it has a nominal deflection angle only ($\Delta\delta_b = 0$). What remains are the contributions due to the elevators, ailerons and rudder. Since we are looking at corrective control only (the deflection angles are in principal in the order of a few degrees), and the contribution to the drag is small compared with the nominal drag, we will neglect these terms⁵. Eq. (12-62) simplifies to

$$\Delta D = \frac{\partial D}{\partial M} \Delta M + \frac{\partial D}{\partial \alpha} \Delta \alpha \quad (12-64)$$

Evaluating the first term on the right-hand side of Eq. (2.3.5) yields

$$\frac{\partial D}{\partial M} = \frac{\partial C_D}{\partial M} \bar{q} S_{ref} + \frac{\partial \bar{q}}{\partial M} C_D S_{ref} \quad (12-65)$$

Applying the definition of the Mach number,

$$M = \frac{V}{a} \quad (12-66)$$

with

a = speed of sound (m/s)

we obtain

$$\frac{\partial \bar{q}}{\partial M} = \frac{1}{2} \frac{\partial(\rho M^2 a^2)}{\partial M} = \rho_0 a_0^2 M_0 = \frac{\rho_0 V_0^2}{M_0} = \frac{2 \bar{q}_0}{M_0} \quad (12-67)$$

Furthermore,

$$\Delta M = \Delta \left(\frac{V}{a} \right) = \frac{1}{a_0} \Delta V = \frac{M_0}{V_0} \Delta V \quad (12-68)$$

In the above derivation, we have assumed that the variation of the speed of sound, which is a function of temperature (and thus altitude), is small and can be neglected with respect to other terms.

The second term on the right-hand side of Eq. (12-64) is easily derived as

$$\frac{\partial D}{\partial \alpha} = \bar{q}_0 S_{ref} \frac{\partial C_D}{\partial \alpha}$$

Summarising, we get for ΔD :

$$\Delta D = \left(\frac{M_0}{V_0} \frac{\partial C_D}{\partial M} + \frac{2 C_D}{V_0} \right) \bar{q}_0 S_{ref} \Delta V + \frac{\partial C_D}{\partial \alpha} \bar{q}_0 S_{ref} \Delta \alpha \quad (12-69)$$

The side force S is a function of M , α , β , δ_e , δ_a and δ_r . Again, we neglect the contribution due to the control surfaces, which results in

$$\Delta S = \frac{\partial S}{\partial M} \Delta M + \frac{\partial S}{\partial \alpha} \Delta \alpha + \frac{\partial S}{\partial \beta} \Delta \beta \quad (12-70)$$

⁵Due to a similar reasoning the contribution of the elevons to the lift force, as compared to the nominal lift force, can be neglected as well.

Evaluating all the terms in a similar way as above, we get for ΔS :

$$\Delta S = \frac{\partial C_S}{\partial \beta} \bar{q}_0 S_{ref} \Delta \beta \quad (12-71)$$

Note that $C_S = 0$ for $\beta = \beta_0 = 0^\circ$, which is also true for the derivatives w.r.t. M and α evaluated at β_0 .

For ΔL we find

$$\Delta L = \left(\frac{M_0}{V_0} \frac{\partial C_L}{\partial M} + \frac{2C_L}{V_0} \right) \bar{q}_0 S_{ref} \Delta V + \frac{\partial C_L}{\partial \alpha} \bar{q}_0 S_{ref} \Delta \alpha \quad (12-72)$$

The variation of the moments consist of an aerodynamic and a propulsive component, i.e.,

$$\Delta M_x = \Delta \mathcal{L} + \Delta M_{T,x} \quad (12-73a)$$

$$\Delta M_y = \Delta \mathcal{M} + \Delta M_{T,y} \quad (12-73b)$$

$$\Delta M_z = \Delta \mathcal{N} + \Delta M_{T,z} \quad (12-73c)$$

Only the aerodynamic contributions have to be expanded to a state-variable and control-variable contribution, because the thruster moments are already control variables (and are assumed to be state independent).

We will apply the same way of derivation as for the aerodynamic forces, with one difference. In this case, the contributions of the control surfaces cannot be neglected, because of their relative magnitude. Also, if we did, it would reduce the means of control to reaction control only. After inspecting the aerodynamic database, we find that the ailerons contribute to both the roll and yaw moment, the elevators to the pitch moment and the rudder to the yaw moment. Furthermore, there are no dynamic damping terms included in the definition of the moments as is usual the case, i.e.,

$$C_{l_p} = C_{m_q} = C_{n_r} = 0$$

but only because they have not been computed. This does not mean that they are zero, as we know from a similar vehicle, the Space Shuttle [172]. However, if we want to take the damping terms into account in the derivation, so that the model does not have to be expanded once these terms become available, or when we want to apply the model to another vehicle, we will see that in this case the related terms will vanish. In the previous section it was stated that the nominal rotational rates are small, and can be treated in a similar manner as the variations ΔV , $\Delta \beta$, etc. This means that when we derive the small variation around a nominal damping term like

$$C_{l_p} \frac{p_0 b_{ref}}{2V_0} \bar{q}_0 S_{ref} b_{ref}$$

the result is a second-order term and can thus be neglected. Therefore, the damping terms do not have to be included in our derivation. However, when the rotational rates p_0 , q_0 and r_0 are not small and can consequently not be neglected, the damping terms *will* appear in the model.

As a result, with the aerodynamic moments given by

$$\mathcal{L} = C_l \bar{q} S_{ref} b_{ref}$$

$$\mathcal{M} = C_m \bar{q} S_{ref} c_{ref}$$

$$\mathcal{N} = C_n \bar{q} S_{ref} b_{ref}$$

we get

$$\Delta \mathcal{L} = \frac{\partial C_l}{\partial \beta} \bar{q}_0 S_{ref} b_{ref} \Delta \beta + \frac{\partial C_l}{\partial \delta_a} \bar{q}_0 S_{ref} b_{ref} \Delta \delta_a \quad (12-74)$$

$$\Delta \mathcal{M} = \frac{M_0}{V_0} \frac{\partial C_m}{\partial M} \bar{q}_0 S_{ref} c_{ref} \Delta V + \frac{\partial C_m}{\partial \alpha} \bar{q}_0 S_{ref} c_{ref} \Delta \alpha + \frac{\partial C_m}{\partial \delta_e} \bar{q}_0 S_{ref} c_{ref} \Delta \delta_e \quad (12-75)$$

$$\Delta \mathcal{N} = \frac{\partial C_n}{\partial \beta} \bar{q}_0 S_{ref} b_{ref} \Delta \beta + \frac{\partial C_n}{\partial \delta_r} \bar{q}_0 S_{ref} b_{ref} \Delta \delta_r + \frac{\partial C_n}{\partial \delta_a} \bar{q}_0 S_{ref} b_{ref} \Delta \delta_a \quad (12-76)$$

Note that the nominal pitch coefficient $C_m = 0$ for trimmed flight. We will assume that trim is always guaranteed - see also Section 12-2-5 where the nominal trajectory will be discussed.

Finally, after substituting Eqs. (12-69), (12-71)-(12-72) and (12-74)-(12-76) in Eqs. (12-50)-(12-58) and rearranging terms, we find expressions for each of the coefficients a_{ij} and b_{ik} . The obtained stability model, which has the desired form of Eq. (12-59)

$$\dot{\mathbf{x}} = \mathbf{A}\mathbf{x} + \mathbf{B}\mathbf{u}$$

or, fully written out,

$$\begin{aligned} \begin{pmatrix} \Delta \dot{V} \\ \Delta \dot{\gamma} \\ \Delta \dot{R} \\ \Delta \dot{p} \\ \Delta \dot{q} \\ \Delta \dot{r} \\ \Delta \dot{\alpha} \\ \Delta \dot{\beta} \\ \Delta \dot{\mu} \end{pmatrix} &= \begin{bmatrix} a_{VV} & a_{V\gamma} & a_{VR} & 0 & 0 & 0 & a_{V\alpha} & 0 & 0 \\ a_{\gamma V} & a_{\gamma\gamma} & a_{\gamma R} & 0 & 0 & 0 & a_{\gamma\alpha} & a_{\gamma\beta} & a_{\gamma\mu} \\ a_{RV} & a_{R\gamma} & 0 & 0 & 0 & 0 & 0 & 0 & 0 \\ 0 & 0 & 0 & 0 & 0 & 0 & 0 & a_{p\beta} & 0 \\ a_{qV} & 0 & 0 & 0 & 0 & 0 & a_{q\alpha} & 0 & 0 \\ 0 & 0 & 0 & 0 & 0 & 0 & 0 & a_{r\beta} & 0 \\ a_{\alpha V} & a_{\alpha\gamma} & a_{\alpha R} & 0 & a_{\alpha q} & 0 & a_{\alpha\alpha} & 0 & a_{\alpha\mu} \\ a_{\beta V} & a_{\beta\gamma} & a_{\beta R} & a_{\beta p} & 0 & a_{\beta r} & 0 & a_{\beta\beta} & a_{\beta\mu} \\ a_{\mu V} & a_{\mu\gamma} & 0 & a_{\mu p} & 0 & a_{\mu r} & a_{\mu\alpha} & a_{\mu\beta} & a_{\mu\mu} \end{bmatrix} \begin{pmatrix} \Delta V \\ \Delta \gamma \\ \Delta R \\ \Delta p \\ \Delta q \\ \Delta r \\ \Delta \alpha \\ \Delta \beta \\ \Delta \mu \end{pmatrix} \\ &+ \begin{bmatrix} 0 & 0 & 0 & 0 & 0 & 0 \\ 0 & 0 & 0 & 0 & 0 & 0 \\ 0 & 0 & 0 & 0 & 0 & 0 \\ 0 & b_{pa} & 0 & b_{px} & 0 & 0 \\ b_{qe} & 0 & 0 & 0 & b_{qy} & 0 \\ 0 & b_{ra} & b_{rr} & 0 & 0 & b_{rz} \\ 0 & 0 & 0 & 0 & 0 & 0 \\ 0 & 0 & 0 & 0 & 0 & 0 \\ 0 & 0 & 0 & 0 & 0 & 0 \end{bmatrix} \begin{pmatrix} \Delta \delta_e \\ \Delta \delta_a \\ \Delta \delta_r \\ \Delta M_{T,x} \\ \Delta M_{T,y} \\ \Delta M_{T,z} \end{pmatrix} \end{aligned} \quad (12-77)$$

can now be used to study the open-loop behaviour of the vehicle. This will be described in the next section. In Eq. (12-77), the elements of matrix \mathbf{A} , i.e., a_{ij} , are given by:

$$a_{VV} = -\frac{1}{mV_0} \left(M_0 \frac{\partial C_D}{\partial M} \bar{q}_0 S_{ref} + 2D_0 \right) \quad (12-78)$$

$$a_{V\gamma} = -g_0 \cos \gamma_0 \quad (12-79)$$

$$a_{VR} = 2 \frac{g_0}{R_0} \sin \gamma_0 \quad (12-80)$$

$$a_{V\alpha} = -\frac{1}{m} \frac{\partial C_D}{\partial \alpha} \bar{q}_0 S_{ref} \quad (12-81)$$

$$a_{Vp} = a_{Vq} = a_{Nr} = a_{V\beta} = a_{V\sigma} = 0 \quad (12-82)$$

$$a_{\gamma V} = \frac{1}{V_0} \left(-\dot{\gamma}_0 + \frac{2V_0}{R_0} \cos \gamma_0 \right) + \frac{\cos \sigma_0}{mV_0^2} \left(M_0 \frac{\partial C_L}{\partial M} \bar{q}_0 S_{ref} + 2L_0 \right) \quad (12-83)$$

$$a_{\gamma\gamma} = - \left(\frac{V_0}{R_0} - \frac{g_0}{V_0} \right) \sin \gamma_0 \quad (12-84)$$

$$a_{\gamma R} = \left(\frac{2g_0}{V_0} - \frac{V_0}{R_0} \right) \frac{\cos \gamma_0}{R_0} \quad (12-85)$$

$$a_{\gamma\alpha} = \frac{\cos \sigma_0}{mV_0} \frac{\partial C_L}{\partial \alpha} \bar{q}_0 S_{ref} \quad (12-86)$$

$$a_{\gamma\beta} = - \frac{\sin \sigma_0}{mV_0} \frac{\partial C_S}{\partial \beta} \bar{q}_0 S_{ref} \quad (12-87)$$

$$a_{\gamma\sigma} = - \frac{L_0}{mV_0} \sin \sigma_0 \quad (12-88)$$

$$a_{\gamma p} = a_{\gamma q} = a_{\gamma r} = 0 \quad (12-89)$$

$$a_{RV} = \sin \gamma_0 \quad (12-90)$$

$$a_{R\gamma} = V_0 \cos \gamma_0 \quad (12-91)$$

$$a_{RR} = a_{Rp} = a_{Rq} = a_{Rr} = a_{R\alpha} = a_{R\beta} = a_{R\sigma} = 0 \quad (12-92)$$

$$a_{p\beta} = \frac{1}{I_{xx}} \frac{\partial C_l}{\partial \beta} \bar{q}_0 S_{ref} b_{ref} \quad (12-93)$$

$$a_{pV} = a_{p\gamma} = a_{pR} = a_{pp} = a_{pq} = a_{pr} = a_{p\alpha} = a_{p\sigma} = 0 \quad (12-94)$$

$$a_{qV} = \frac{M_0}{I_{yy} V_0} \frac{\partial C_m}{\partial M} \bar{q}_0 S_{ref} c_{ref} \quad (12-95)$$

$$a_{q\alpha} = \frac{1}{I_{yy}} \frac{\partial C_m}{\partial \alpha} \bar{q}_0 S_{ref} c_{ref} \quad (12-96)$$

$$a_{q\gamma} = a_{qR} = a_{qp} = a_{qq} = a_{qr} = a_{q\beta} = a_{q\sigma} = 0 \quad (12-97)$$

$$a_{r\beta} = \frac{1}{I_{zz}} \frac{\partial C_n}{\partial \beta} \bar{q}_0 S_{ref} b_{ref} \quad (12-98)$$

$$a_{rV} = a_{r\gamma} = a_{rR} = a_{rp} = a_{rq} = a_{rr} = a_{r\alpha} = a_{r\sigma} = 0 \quad (12-99)$$

$$a_{\alpha V} = -\frac{g_0}{V_0^2} \cos \gamma_0 \cos \sigma_0 - \frac{1}{mV_0^2} \left(M_0 \frac{\partial C_L}{\partial M} + C_L \right) \bar{q}_0 S_{ref} \quad (12-100)$$

$$a_{\alpha\gamma} = -\frac{g_0}{V_0} \sin \gamma_0 \cos \sigma_0 \quad (12-101)$$

$$a_{\alpha R} = -\frac{2g_0}{R_0 V_0} \cos \gamma_0 \cos \sigma_0 \quad (12-102)$$

$$a_{\alpha q} = 1 \quad (12-103)$$

$$a_{\alpha\alpha} = -\frac{1}{mV_0} \frac{\partial C_L}{\partial \alpha} \bar{q}_0 S_{ref} \quad (12-104)$$

$$a_{\alpha\sigma} = -\frac{g_0}{V_0} \cos \gamma_0 \sin \sigma_0 \quad (12-105)$$

$$a_{\alpha p} = a_{\alpha r} = a_{\alpha\beta} = 0 \quad (12-106)$$

$$a_{\beta V} = \frac{g_0}{V_0^2} \cos \gamma_0 \sin \sigma_0 \quad (12-107)$$

$$a_{\beta\gamma} = \frac{g_0}{V_0} \sin \gamma_0 \sin \sigma_0 \quad (12-108)$$

$$a_{\beta R} = \frac{2g_0}{R_0 V_0} \cos \gamma_0 \sin \sigma_0 \quad (12-109)$$

$$a_{\beta p} = \sin \alpha_0 \quad (12-110)$$

$$a_{\beta r} = -\cos \alpha_0 \quad (12-111)$$

$$a_{\beta\beta} = -\frac{1}{mV_0} \frac{\partial C_S}{\partial \beta} \bar{q}_0 S_{ref} \quad (12-112)$$

$$a_{\beta\sigma} = -\frac{g_0}{V_0} \cos \gamma_0 \cos \sigma_0 \quad (12-113)$$

$$a_{\beta q} = a_{\beta\alpha} = 0 \quad (12-114)$$

$$a_{\sigma V} = \frac{\tan \gamma_0 \sin \sigma_0}{mV_0^2} \left(M_0 \frac{\partial C_L}{\partial M} + C_L \right) \bar{q}_0 S_{ref} \quad (12-115)$$

$$a_{\sigma \gamma} = \frac{L_0}{mV_0} \sin \sigma_0 \quad (12-116)$$

$$a_{\sigma p} = -\cos \alpha_0 \quad (12-117)$$

$$a_{\sigma r} = -\sin \alpha_0 \quad (12-118)$$

$$a_{\sigma \alpha} = \frac{\tan \gamma_0 \sin \sigma_0}{mV_0} \frac{\partial C_L}{\partial \alpha} \bar{q}_0 S_{ref} \quad (12-119)$$

$$a_{\sigma \beta} = \frac{\tan \gamma_0 \cos \sigma_0}{mV_0} \frac{\partial C_S}{\partial \beta} \bar{q}_0 S_{ref} - \frac{L_0}{mV_0} + \frac{g_0}{V_0} \cos \gamma_0 \cos \sigma_0 \quad (12-120)$$

$$a_{\sigma \sigma} = \tan \gamma_0 \cos \sigma_0 \frac{L_0}{mV_0} \quad (12-121)$$

$$a_{\sigma R} = a_{\sigma q} = 0 \quad (12-122)$$

The elements of matrix \mathbf{B} , i.e., b_{ik} , are:

$$b_{Ve} = b_{Va} = b_{Vr} = b_{Vx} = b_{Vy} = b_{Vz} = 0 \quad (12-123)$$

$$b_{\gamma e} = b_{\gamma a} = b_{\gamma r} = b_{\gamma x} = b_{\gamma y} = b_{\gamma z} = 0 \quad (12-124)$$

$$b_{Re} = b_{Ra} = b_{Rr} = b_{Rx} = b_{Ry} = b_{Rz} = 0 \quad (12-125)$$

$$b_{pa} = \frac{1}{I_{xx}} \frac{\partial C_l}{\partial \delta_a} \bar{q}_0 S_{ref} b_{ref} \quad (12-126)$$

$$b_{px} = \frac{1}{I_{xx}} \quad (12-127)$$

$$b_{pe} = b_{pr} = b_{py} = b_{pz} = 0 \quad (12-128)$$

$$b_{qe} = \frac{1}{I_{yy}} \frac{\partial C_m}{\partial \delta_e} \bar{q}_0 S_{ref} c_{ref} \quad (12-129)$$

$$b_{qy} = \frac{1}{I_{yy}} \quad (12-130)$$

$$b_{qa} = b_{qr} = b_{qx} = b_{qz} = 0 \quad (12-131)$$

$$b_{ra} = \frac{1}{I_{zz}} \frac{\partial C_n}{\partial \delta_a} \bar{q}_0 S_{ref} b_{ref} \quad (12-132)$$

$$b_{rr} = \frac{1}{I_{zz}} \frac{\partial C_n}{\partial \delta_r} \bar{q}_0 S_{ref} b_{ref} \quad (12-133)$$

$$b_{rz} = \frac{1}{I_{zz}} \quad (12-134)$$

$$b_{re} = b_{rx} = b_{ry} = 0 \quad (12-135)$$

$$b_{\alpha e} = b_{\alpha a} = b_{\alpha r} = b_{\alpha x} = b_{\alpha y} = b_{\alpha z} = 0 \quad (12-136)$$

$$b_{\beta e} = b_{\beta a} = b_{\beta r} = b_{\beta x} = b_{\beta y} = b_{\beta z} = 0 \quad (12-137)$$

$$b_{\sigma e} = b_{\sigma a} = b_{\sigma r} = b_{\sigma x} = b_{\sigma y} = b_{\sigma z} = 0 \quad (12-138)$$

12-2-5 Nominal mission

The analysis of the characteristic motion is centred around a nominal reference trajectory. Such a reference trajectory is usually the result of an optimisation process, taking mission requirements, performance criteria and trajectory constraints into account. When neither a reference trajectory nor an optimisation program is at hand, one can generate one provided a control history is available. In ref. [38] a nominal control history of α and μ as a function of time is given. With this control history as guidance output and applying ideal control, we can generate the corresponding re-entry trajectory using the vehicle model described in this section and dynamics model to be discussed in the next section. The initial conditions for the simulation are:

$$\begin{aligned} V &= 7435.5 \text{ m/s} \\ \gamma &= -1.43^\circ \\ \chi &= 70.75^\circ \\ h &= 122 \text{ km} \\ \tau &= -106.58^\circ \\ \delta &= -22.3^\circ \end{aligned}$$

The vehicle is assumed to be heading towards a runway in Kourou (French Guyana). Some 80 km from the landing site guidance switches to the Terminal Area Energy Management (TAEM) logic. However, here the main focus is on the hypersonic entry and descent.

The simulation has been executed for a trimmed condition (pitch equilibrium only). Originally, for the Mach range between 1 and 20, trim was realised with the body flap as much as possible, and the rest with the elevons (elevator function). (For $0 < M \leq 1$, although this flight regime is not of interest here, the HORUS-2B is trimmed with the elevators, while having the body flap maximum up). However, the upper Mach boundary had to be changed to a dynamic pressure boundary $\bar{q} \geq 100 \text{ N/m}^2$, to prevent pitch instability and to be more in line with the body-flap activation of the Space Shuttle.

The nominal controls are shown in Figure 12-6. The nominal angle of attack is given as a function of flight time. HORUS enters the atmosphere with a high angle of attack of 40° . Because of this high angle, the maximum occurring heat flux can be kept sufficiently small. Further down the trajectory, the angle of attack is decreased in order to meet with the cross- and downrange requirements. The nominal bank-angle history [38] consists of absolute values only, guaranteeing a certain descent rate. The corresponding sign is determined by flying towards the targeting point near Kourou, while keeping the heading error within dead-band limits. Whenever the heading error exceeds the dead band, the sign of the bank angle is inverted. This manoeuvre, a so-called

bank reversal, usually takes between 10 and 20 s. Since ideal control is applied, i.e., the actual attitude is equated to the commanded attitude, the reversals show as vertical lines. We see four reversals at $t \approx 724$ s, $t \approx 1076$ s, $t \approx 1184$ s and $t \approx 1240$ s. The simulation is finished when the Terminal Area, 0.75° (≈ 83 km) from the runway, has been reached. This is about 1250 s after re-entry. In Figure 12-7, the altitude-velocity profile is plotted, whereas in Figure 12-8 the ground track is shown.

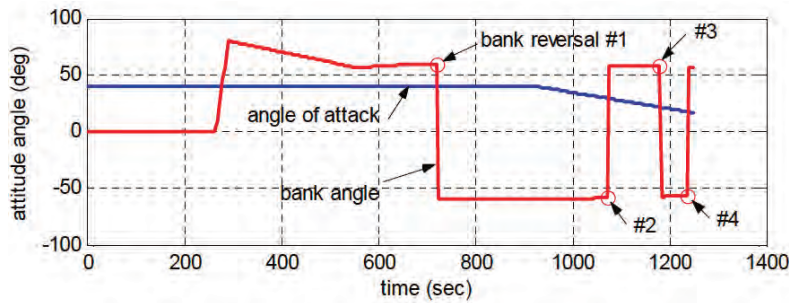


Figure 12-6: Nominal control history.

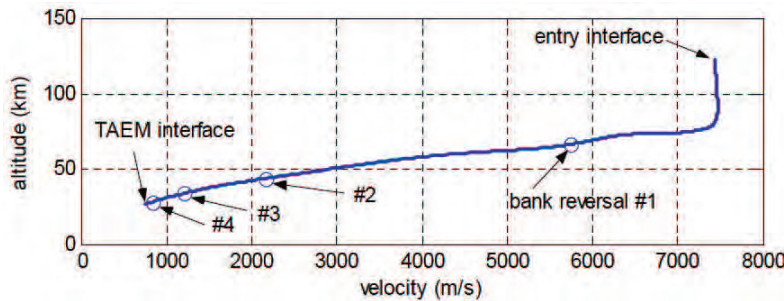


Figure 12-7: Altitude-velocity profile.

Studying the coefficients of \mathbf{A} and \mathbf{B} , we find that we need the following parameters of the nominal trajectory as a function of time:

$$\alpha_0, \mu_0, V_0, \gamma_0, R_0, \bar{q}_0, M_0, g_0, D_0, L_0$$

The control history provides α_0 and μ_0 ($\beta_0 = 0^\circ$), which we already discussed. The same holds for the altitude-velocity diagram shown in Figure 12-7, which provides V_0 and R_0 . The other relevant parameters are given in Figures 12-9 till 12-13. For a detailed discussion of the trajectory we refer to ref. [122]. It should be noted that in the curves for the drag and the lift, the trim drag and lift are included. These trim forces are too large to be ignored, as is usually done for conventional aircraft. In Figure 12-13, finally, the nominal body-flap and elevator deflection for trim stability are shown. We see that only at the end of the flight the body-flap deflection is saturated, and the elevons are required to provide the remaining trim moment. The deflections of the aerosurfaces take place with an infinite rate (zero time).

From coefficient $a_{\gamma V}$, we see that we need the value of $\dot{\gamma}_0$. This variable can be easily computed by substituting the related nominal values in Eq. (12-20),

$$\dot{\gamma}_0 = \left(\frac{V_0}{R_0} - \frac{g_0}{V_0} \right) \cos \gamma_0 + \frac{L_0 \cos \mu_0}{m V_0} \quad (12-139)$$

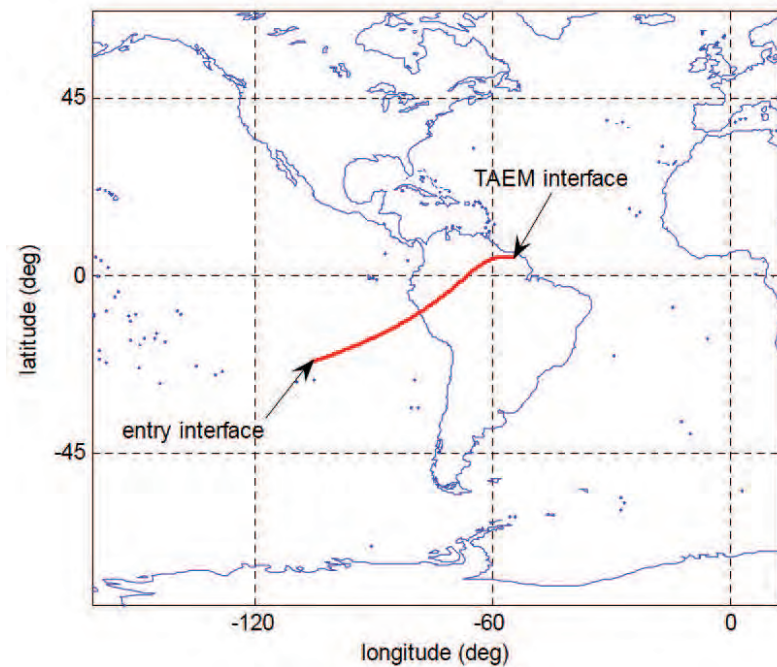


Figure 12-8: Ground track for nominal mission.

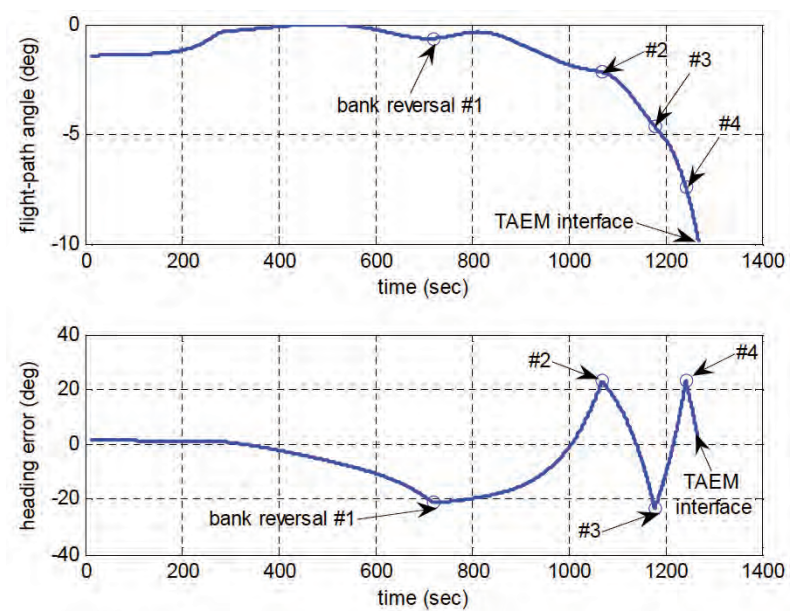


Figure 12-9: Nominal flight-path angle (top) and heading error (bottom) as a function of time.

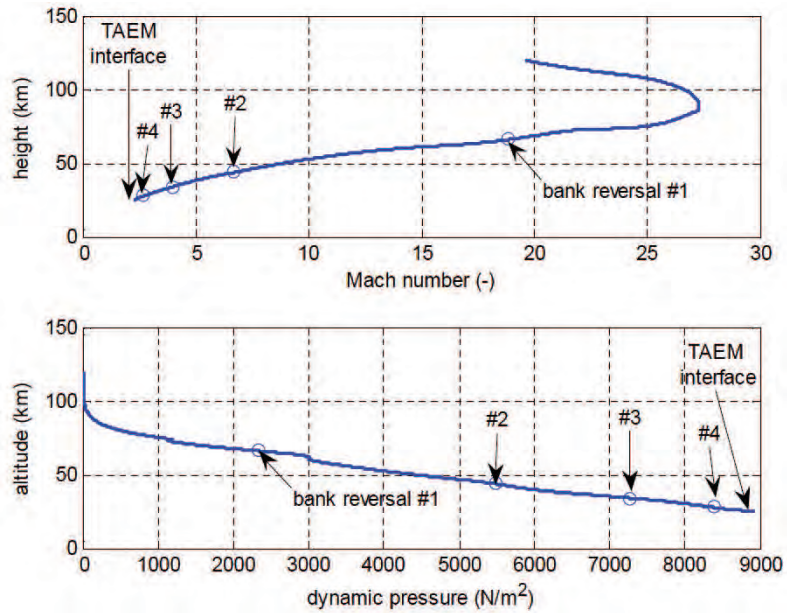


Figure 12-10: Nominal Mach number (top) and dynamic pressure (bottom) versus altitude.

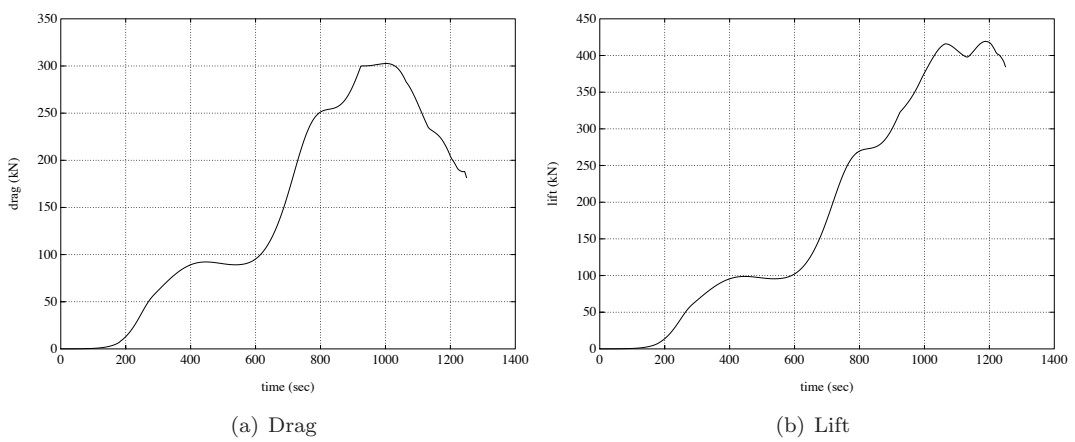


Figure 12-11: Nominal aerodynamic forces, including trim forces.

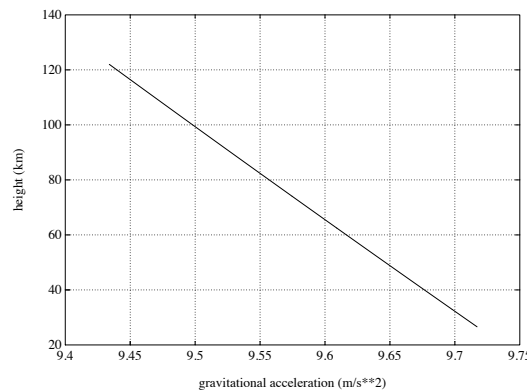


Figure 12-12: Nominal gravitational acceleration related to the height.

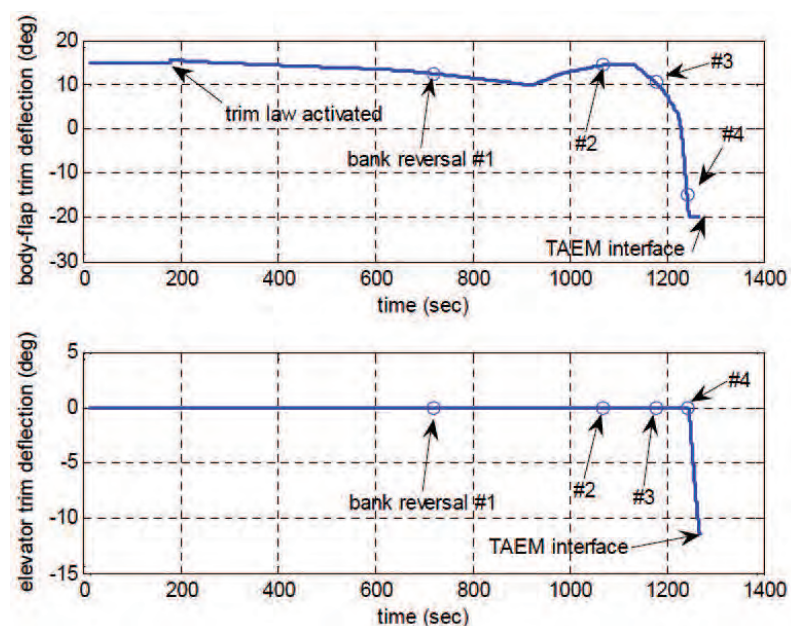


Figure 12-13: Trim deflection for body flap (top) and elevator (bottom) as a function of time.

Finally, we need the values of some aerodynamic coefficients and derivatives:

- $\frac{\partial C_D}{\partial M}$, $\frac{\partial C_D}{\partial \alpha}$, $\frac{\partial C_S}{\partial \beta}$, $\frac{\partial C_L}{\partial M}$, $\frac{\partial C_L}{\partial \alpha}$, $\frac{\partial C_l}{\partial \beta}$, $\frac{\partial C_n}{\partial \beta}$ with contributions of the base vehicle only,
- $\frac{\partial C_m}{\partial M}$, $\frac{\partial C_m}{\partial \alpha}$ with contributions of the base vehicle, the body flap and the elevons,
- $\frac{\partial C_l}{\partial \delta_a}$, $\frac{\partial C_m}{\partial \delta_e}$, $\frac{\partial C_n}{\partial \delta_a}$ with contributions of the elevons only, and
- $\frac{\partial C_n}{\partial \delta_r}$ with contributions of the rudder only.

With M_0 , α_0 and the trimmed deflection angles of body flap and elevator at hand, these derivatives can be computed off-line. After measuring from the graphs in ref. [38], the aerodynamic properties are given in tabular form, for which linear interpolation is used to extract the information for a particular flight situation. A derivative is computed by simply taking the derivative of the connecting line, when the flight situation is located in between two tabular values. At a boundary tabular value, either the left or right derivative is used; in case the flight condition is located at a tabular value somewhere in the table, the connecting line of the two neighbouring values is used.

12-2-6 Eigenvalues and eigenmotion

The system of equations, Eq. (12-7) through (12-18), is a time-varying system. Such a system cannot be easily studied in terms of natural motion, because this time-dependency will obscure the nature of the individual motion types. Also the non-linearities in the system make the behaviour of the system dependent on the magnitude of the input, so no crisp conclusions can be drawn from the results. Therefore, we will discretise the nominal trajectory into a number of time intervals. During each of the intervals, the state of the vehicle and other system parameters are assumed to be constant. For each of the time points, the system can be investigated. By linearising the equations of motion (see Section 12-2-3) and discretising the trajectory, the overall system has been divided into a sequence of Linear Time-Invariant systems (LTI systems) of the form presented in Section 12-2-4.

The part

$$\dot{\mathbf{x}} = \mathbf{A}\mathbf{x} \quad (12-140)$$

is known as the homogeneous part of the state equation, with which we can study the free response (also called open-loop behaviour, characteristic motion or eigenmotion) of the system. The eigenvalues λ of state matrix \mathbf{A} and the corresponding eigenvectors $\boldsymbol{\mu}$ can be computed from the following equation:

$$\mathbf{A}\boldsymbol{\mu} = \lambda\boldsymbol{\mu} \quad (12-141)$$

This equation can be solved by

$$\mathbf{A}\boldsymbol{\mu} - \lambda\boldsymbol{\mu} = (\mathbf{A} - \lambda\mathbf{I})\boldsymbol{\mu} = 0 \quad (12-142)$$

The condition for a non-trivial solution is

$$|\mathbf{A} - \lambda\mathbf{I}| = 0 \quad (12-143)$$

Standard algorithms are available to calculate the eigenvalues and corresponding eigenvectors of a given matrix A [138], which can also be found in software environments like Matlab[®]. The mathematical foundation of these algorithms is considered to be beyond the scope of these lecture notes.

With λ and μ , the eigenmotion $\mathbf{x}_{\lambda(t)}$ of the re-entry vehicle follows from ref. [105]:

$$\mathbf{x}_{\lambda}(t) = e^{\lambda t} \mu \quad (12-144)$$

Since we are dealing with a linear system of 9 coupled equations, Eq. (12-144) gives only one solution. The general form is, because of the linearity of the system, written as

$$\mathbf{x}_{\lambda}(t) = \sum_{i=1}^9 c_i e^{\lambda_i t} \mu_i \quad (12-145)$$

The constants c_i can be computed from specified initial conditions $\mathbf{x}(0)$, for instance an initial perturbation in the nominal angle of attack.

Before we start the discussion on the eigenvalues and eigenmotions of HORUS, we must note that it is not our intention to give a complete analysis of the open-loop behaviour of HORUS. We will restrict ourselves to a more general discussion, starting with a brief introduction on the relation between eigenvalues and eigenmotion. Then, we will introduce the characteristic motions which we find with subsonic, conventional aircraft and which have been discussed at length in Chapter 5 and 6. As we will see, the HORUS has similar motions in certain speed regimes. These characteristic motions will be discussed for a number of time points. To illustrate the eigenmotion, we will conclude this section by showing the results of a 6-dof open-loop re-entry simulation.

Having computed the eigenvalues and corresponding eigenvectors, how can we relate them to the actual motion of a vehicle? Based on the eigenvalues, we can see whether a component of the motion is (un)stable and (a)periodic, see also Figure 12-14. An eigenvalue can be real or complex. Complex eigenvalues appear in (conjugated) pairs and indicate a periodic eigenmotion, whereas real eigenvalues imply an aperiodic eigenmotion. The sign of the real part of the eigenvalue shows whether the eigenmotion will be converging (negative real part) or diverging (positive real part). When the real part is zero, the oscillations have a constant amplitude. A more detailed discussion can, amongst others, be found in refs. [54] and [105].

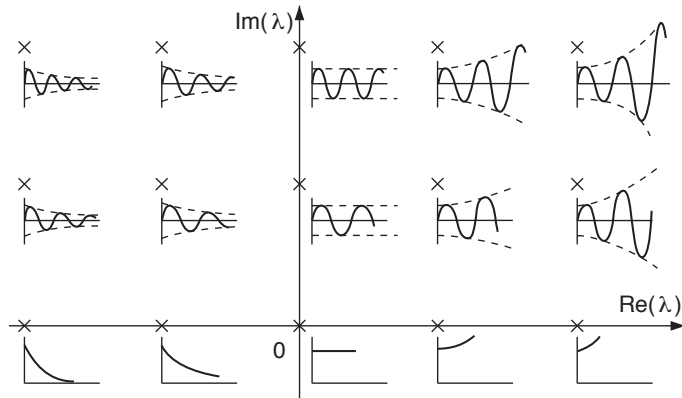


Figure 12-14: Impulse responses for various eigenvalue locations in the complex plane (based on ref. [54]), where the conjugate eigenvalues are omitted.

To characterise the eigenmotion we compute some specific coefficients, i.e., the *period* P , when a pair of complex conjugate eigenvalues represents a periodic motion, defined as

$$P = \frac{2\pi}{Im(\lambda)} \quad (12-146)$$

An aperiodic motion does not have a period, which also follows from the fact that the imaginary part of the eigenvalue is zero.

Next, we define the *halving time* $T_{\frac{1}{2}}$, indicating the time interval when the amplitude of the motion has become half its original value,

$$T_{\frac{1}{2}} = \frac{\ln \frac{1}{2}}{Re(\lambda)} \quad (12-147)$$

However, when the real part of the eigenvalue is positive, the halving time becomes negative. In that case it is better to speak of the *doubling time* of the (diverging) eigenmotion:

$$T_2 = \frac{\ln 2}{Re(\lambda)}$$

The *damping ratio* ζ for periodic eigenmotion (complex eigenvalues) can be computed with

$$\zeta = -\frac{Re(\lambda)}{\sqrt{Re(\lambda)^2 + Im(\lambda)^2}} \quad (12-148)$$

In the case of damped eigenmotion, ζ is positive (a negative damping ratio is in principle an amplification ratio). For aperiodic motion, ζ is not defined.

Finally, the *natural frequency* ω_n for periodic eigenmotion is defined to be

$$\omega_n = \sqrt{Re(\lambda)^2 + Im(\lambda)^2} \quad (12-149)$$

The natural frequency is the theoretical frequency of the eigenmotion when the energy of the system is constant during that motion, which means that the amplitude is constant. Again, for aperiodic motion ω_n is not defined. It should be noted that the natural frequency is more a mathematical notion rather than a physical one.

Using the above definitions, we can write a relation between the period on the one hand, and the damping ratio and the natural frequency on the other:

$$P = \frac{2\pi}{\omega_n \sqrt{1 - \zeta^2}} \quad (12-150)$$

Sofar, we have only discussed the stability characteristics of the eigenmotion, but we do not know yet in which of the state variables we can trace this motion. Studying the eigenvectors will help us to answer this question. Suppose we compute the modulus of each of the (complex) components of an eigenvector μ_i , then we can easily spot the components which are involved. Furthermore, computing the argument of the complex component, we get an impression of the phase difference between the related components.

In mathematical terms, see also Figure 12-15, the modulus z of a complex number λ is defined to be

$$z = \sqrt{Re(\lambda)^2 + Im(\lambda)^2} \quad (12-151)$$

and the argument θ is

$$\theta = \arctan\left(\frac{\operatorname{Im}(\lambda)}{\operatorname{Re}(\lambda)}\right) \quad (12-152)$$

Note that the argument of a real number is always 0 or π ($\lambda < 0$).

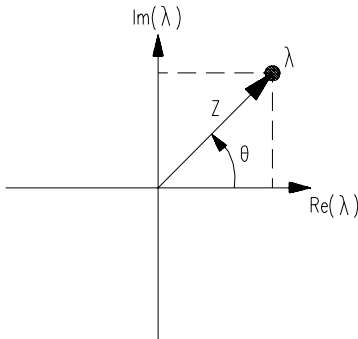


Figure 12-15: The modulus z and argument θ of a complex number.

Each component of the eigenvector can in principle be plotted as a time vector using z and θ , which will give us a visual aid to inspect the eigenmotion in the sense that the relative magnitude and phase difference of the related components can be distinguished, e.g., see [57]. Here, we will not do that but restrict to a numerical inspection of the more important components of the state vector.

Before we look at the eigenmotion of HORUS, we will briefly repeat the discussion on the eigenmotion of conventional subsonic aircraft in steady flight (see also Chapter 5 and 6), because we expect at least partly similar modes (a component of the eigenmotion) for HORUS. Five different modes can be distinguished, two longitudinal and three lateral modes. The longitudinal modes are called the short-period and the phugoid mode, whereas the lateral modes are called the lateral oscillation (or Dutch roll), the rolling convergence and the spiral mode. Furthermore, the longitudinal and lateral modes are decoupled, which means that a symmetric motion (e.g., a disturbance) will not affect the asymmetric motion and vice versa.

The *short-period oscillation* is a fast, periodic aircraft motion, which is usually well-damped. Because of the fast pitch rate, the aerodynamic forces acting on the vehicle are large. The flight path is nearly a straight line, and there is a negligible speed variation. The *phugoid* is a very slow oscillation which is poorly damped. The slowly oscillating speed results in small variations in the dynamic pressure and therefore the aerodynamic forces. Basically, the motion consists of translations in the aircraft plane of symmetry, while the rotation about the pitch axis is negligible. Since only the height and velocity are changing, the phugoid can be interpreted as a continuous exchange of potential and kinetic energy.

The *lateral oscillation* resembles the short-period oscillation, in that sense that it is usually a fast, well-damped aircraft motion (sometimes moderately damped). The large aerodynamic forces are in principal due to a rotation about the top axis (yaw). There is also a strong roll rate, but this does not influence the lateral oscillation that much. The flight path and the velocity almost have constant values. The *roll convergence* is a strongly damped, aperiodic eigenmotion, during which the aircraft rotates purely about the X -axis (roll). The roll convergence is aperiodic, because the roll angle does not have any influence on the external moments and thus the motion. The *spiral mode*, finally, is seen to consist mainly of yawing at nearly zero sideslip with some roll. The aerodynamic forces are very small, resulting in a large time constant. The spiral mode can be either a stable or unstable, aperiodic eigenmotion.

We will now have a look at the eigenmotion of HORUS. As we saw in Section 12-2-4, the system matrix \mathbf{A} is a 9x9 matrix, which means that there are 9 eigenvalues and corresponding eigenvectors. Inspecting \mathbf{A} will also tell us that there are some cross couplings between so-called symmetric (V, γ, R, q, α) and asymmetric variables (p, r, β, μ), indicating that the symmetric and asymmetric motion will not be completely decoupled. However, when these coupling terms are sufficiently small, decoupling will be possible. But this we will see later.

In Figures 12-16(a) through 12-16(d), the 9 eigenvalues of HORUS along the nominal trajectory are plotted. The first two figures show the eigenvalues in the complex plane, whereas the latter two give the imaginary and real parts of the eigenvalues as a function of flight time. Since it is not easy to see which modes the curves represent, we will only draw some general conclusions from these figures.

Figure 12-16(a) shows a mixture of complex and real eigenvalues, indicating that we can expect both periodic and aperiodic eigenmotions. The maximum imaginary parts of about 1.5 mean quite short periods. The real parts are between -1 and 1, which means that the modes can be either converging or diverging. Looking at Figure 12-16(c), we see in principle two major periodic eigenmotions emerge, which are, as we will find out later, the lateral oscillation (the two outer curves) and the short-period oscillation (the two inner curves). The discontinuous jumps in the inner curves are due to the linearisation of the aerodynamic coefficients and the linear table interpolation: when we go from one table range to another, the aerodynamic derivatives sometimes change discontinuously. Figure 12-16(d) indicates that most of the time the eigenmotions are very lightly damped or undamped. Only towards the end of the flight strong divergencies and convergencies appear.

To study the eigenmotion of HORUS in more detail, we have selected several time points for which we will compute the characteristic values (according to Eqs. (12-146) through (12-149)), and for which we will try to identify the modes by studying the eigenvectors. The selected time points are 1 ($t = 0$ s), 50 ($t = 196$ s), 100 ($t = 396$ s), 150 ($t = 596$ s), 200 ($t = 796$ s), 250 ($t = 996$ s), 300 ($t = 1196$ s) and 314 ($t = 1252$ s). The numerical results are presented in Table 12-3 through 12-10 at the end of this section.

In principle, we can trace the 5 motions which we discussed before for conventional aircraft. However, due to the larger speed regime and due to the distinct nature of the nominal trajectory (large bank angles as compared with the steady cruise flight of subsonic aircraft), we find some differences. Starting with time point 1, we find six eigenmodes. The first mode we have designated the short-period oscillation, because of the large-amplitude oscillations found in the angle of attack and pitch rate (note that the most important components of the eigenmotion have been printed bold).

Whereas in the aircraft case the height and velocity remained constant, it seems that here this is not the case, basically because of the much slower character of the re-entry short-period mode. However, it should be noted that despite the fact that the height component is the largest, only the relative difference is important. An amplitude of 0.0226 rad for the angle of attack means a 1-m amplitude for the height (or: $\Delta\alpha = 10^\circ$ gives $\Delta R \approx 6.7$ m). Moreover, we do not have such a rapid oscillation here: the period is about 850 s, whereas for conventional aircraft this is in the order of seconds. Also the motion is hardly damped, because of the absence of aerodynamic forces in the upper layers of the atmosphere. If it had not been for the angle of attack, we might also call this a phugoid-kind of motion. However, we have reserved that name for the second mode⁶.

The dominating components of the phugoid mode are the height and velocity, with the angle of attack more or less constant. Furthermore, looking at the period, we find that this eigenmotion is indeed much slower than the short-period oscillation ($P = 5,183$ s). A difference with the aircraft phugoid is that this mode is unstable, although the doubling time is more than 17,000 s. The next

⁶As we already find out, at this altitude it is not altogether useful to compare the characteristic modes of re-entry vehicles with those of aircraft, because of the completely different flight regime. However, we will stick to it because it is our only comparison method.

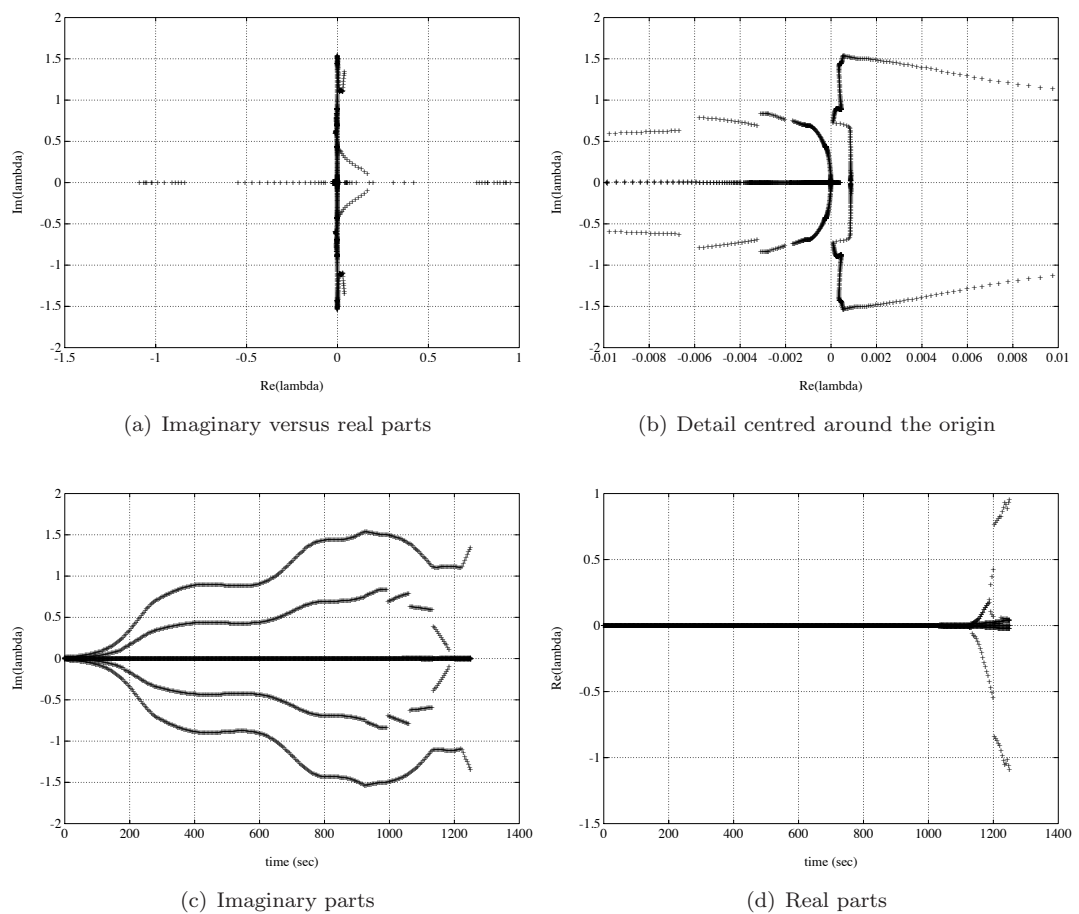


Figure 12-16: Variation of the eigenvalues along the nominal trajectory

mode, the lateral oscillation, compares well with its aircraft counterpart. Main components are the angle of sideslip and the bank angle, together with the corresponding angular rates. Initially, this mode is unstable, but as we will see later the oscillation changes into a damped one. The three remaining modes are all aperiodic. The first two have been given the common name *aperiodic roll mode* for obvious reasons: the bank angle is by far the largest component. Surprising is to see that in one mode the influence of the angle of sideslip is many orders larger⁷. This means that the first aperiodic roll mode can be compared with the roll convergence of conventional aircraft. Both modes are stable. The last aperiodic mode has been given the name *height mode*. This mode represents a lightly damped aperiodic motion, which has also been found by Sachs [149], while studying stability and control problems in hypersonic flight.

Now that we have established the basic modes of the eigenmotion, we can focus on the time history of these modes. The short period oscillation changes its nature and comes closer to the aircraft mode. Because at lower altitudes the aerodynamic forces are higher, the damping of this mode increases (although the damping remains low). The period decreases from $P \approx 850$ s at $t=0$ s, down to $P \approx 40$ s at $t = 96$ s down to $P \approx 9$ s at $t = 996$ s. Then, at time point 300 the periodic mode breaks into two aperiodic modes, of which one is strongly damped ($T_{\frac{1}{2}} = 1.4$ s) and the other one is strongly diverging ($T_2 = 1.9$ s). The half and doubling time decrease further for the last time point. Last but not least, the influence of the bank angle becomes stronger towards the end of the flight, a phenomenon which we will also see with the next mode, the phugoid (for the re-entry flight; not for conventional aircraft).

The phugoid damping ratio increases in time (apart from a small decrement at time point 150). It becomes a very well damped motion, with, for instance, a half time of 254 s at time point 200. The period of the phugoid decreases from over 5000 s ($t = 0$ s) to 430 s ($t = 1252$ s). One remark remains to be made and that is that at time point 100 the influence of the bank angle has changed a couple of orders of magnitude. This can be explained by the fact that initially the nominal trajectory is flown with zero bank angle, whereas later large bank angles are applied for lateral direction control. Because of this the influence of the bank angle in the phugoid becomes apparent, and a coupling (although small) exists between the symmetrical and asymmetrical motion).

As we mentioned before, the lateral oscillation is an unstable, periodic motion and this continues to be during the whole trajectory. But, some characteristics of the motion change. Towards time point 150, the negative damping coefficient gets smaller, which means that the motion becomes less unstable. From that point, the damping coefficient becomes more negative again. The period changes drastically during the first 100 s of flight (P changes from 373 s down to 19.3 s). It continues to decrease till time point 250 ($P = 4.2$ s), after which it varies only slightly. At $t = 396$ s, we see that the contribution of $\Delta\alpha$ has changed many orders of magnitude, indicating that due to a large bank angle a small coupling exists between the symmetrical and asymmetrical motion. Besides, the ratio between $\Delta\mu$ and $\Delta\beta$ changes from 1.39 to 1.36 indicating a slightly weaker coupling between the bank angle and the angle of sideslip at higher bank angles. Δh becomes the major component, although when we see this in proportion to the attitude angles it does not seem that major (for time point 100, an amplitude of 17.3° in the bank angle corresponds with an amplitude of 1 m in the height). The relative difference between the height and the attitude angles, however, becomes larger towards the end of the flight.

The aperiodic roll modes changes into a single unstable periodic roll mode with a small coupling to the angle of attack (an amplitude of $\Delta\mu = 10^\circ$ gives $\Delta\alpha = 0.33^\circ$) at time point 100. Moreover, the height becomes the major component. Again, this begins at the moment the vehicle starts banking. It should be noted that a small oscillation in the bank angle will result in a large amplitude in the height ($\Delta\mu = 0.1^\circ$ gives $\Delta h \approx 3,300$ m). However, at the next time point this mode changes again into two aperiodic modes, which are similar to the aperiodic height mode. For time points 200 and 250, a (very) stable periodic roll mode is back, while at time point 300 we have again two aperiodic modes. In this case, the stable mode is similar to the height mode,

⁷In principle, the eigenvalue of the second aperiodic roll mode is so small that for practical reasons it can be considered to be zero.

whereas the unstable one shows a coupling between the bank angle and the angle of attack, with the angle of attack the larger one.

The height mode already entered the discussion when we were focusing on the several roll modes. We will briefly finalise the discussion on characteristic modes. Initially, the height mode is stable. For time point 50, it has become unstable with an amplification ratio which is as large as the prior damping ratio. When the banking begins (time point 100), the eigenvalue related to the height mode is very small, and stays very small during the rest of the flight, being alternately positive and negative. For this reason, the height mode is not interesting to discuss any further, because for the short time of the flight this mode is practically indifferent. However, as we discussed before, for some time points the height mode consists of more than one aperiodic component. These additional modes have much larger eigenvalues and become the dominating modes for the height mode, although the damping and/or amplification remains very small.

In Figures 12-17 and 12-18 the eigenvalues have been separated for translational and rotational motion, and some of the discussed eigenmotions have been indicated.

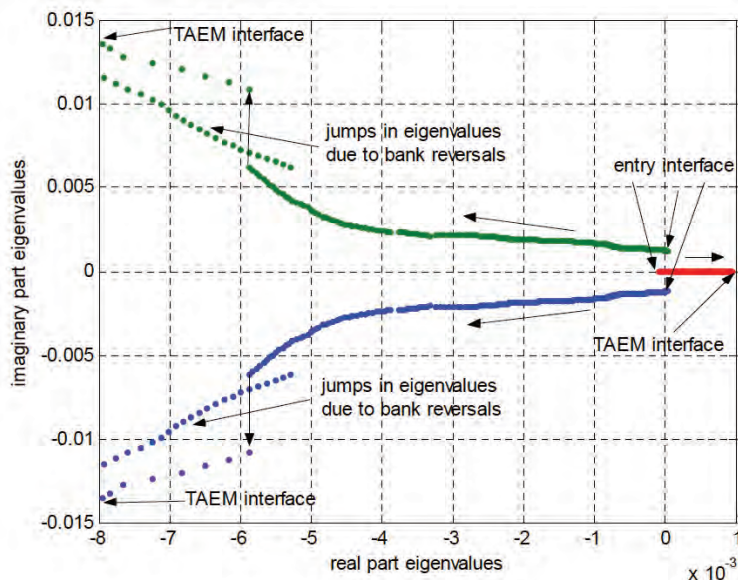


Figure 12-17: Eigenvalues for translational motion.

The free response according to Eq. (12-145) is in itself not that interesting. It will confirm what we have already seen in the tables with numerical results. Basically, the graphs will show us both periodic and aperiodic motions, either diverging or converging. Due to the sometimes long periods, the curves will not give us real insight in the eigenmotion at one particular moment in time. Only when the motion is, for instance, reasonably damped (or unstable, for that matter) and has a sufficiently short period, the resulting eigencurve can be quite informative. As an example, the curves for the angle of sideslip and the bank angle (the major variables for the lateral oscillation) have been plotted as a function of time for time point 300, see also Figure 12-19.

There is another more important reason for not looking into more detail at the curves representing the eigenmotion. The eigenvalues are computed for a certain point in time. When we compute the eigenmotion for a certain time interval (100 s in Figure 12-19), we assume that the dynamics of the vehicle are not changing (given by a constant system matrix and therefore constant eigenvalues). For a subsonic aircraft in steady (cruise) flight this can be a reasonable approximation, but for a re-entry vehicle this is most of the time not the case.

However, we thought it to be illustrative of the eigenmotion to simulate the descent of the HORUS-2B in the so-called open-loop 6-d.o.f. mode, i.e., a free-fall re-entry including attitude dynamics

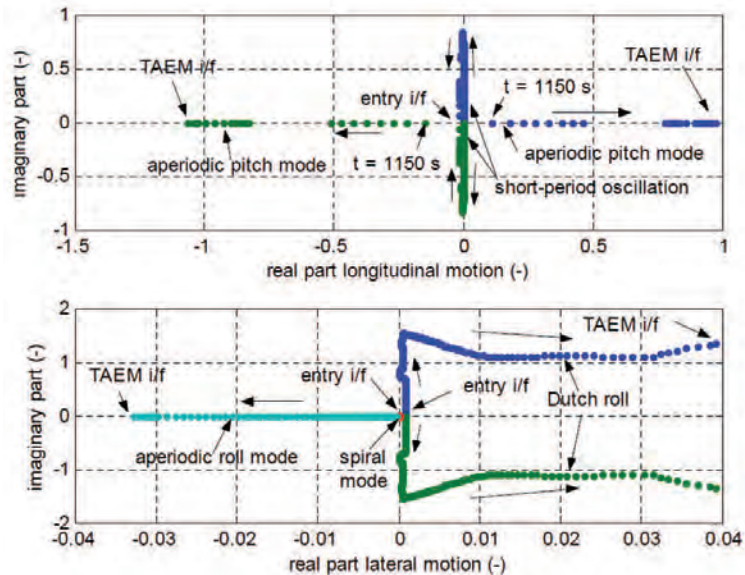
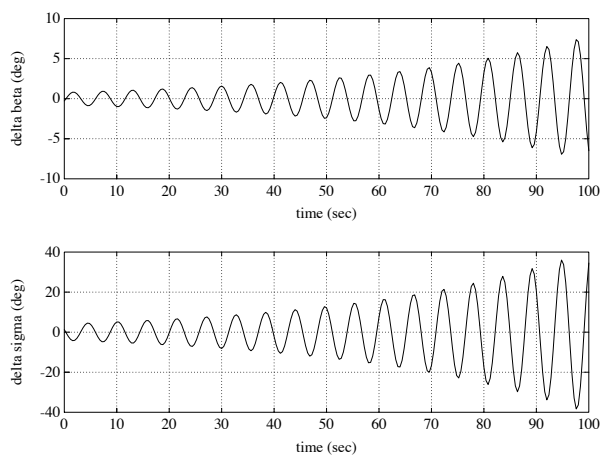


Figure 12-18: Eigenvalues for rotational motion.

Figure 12-19: The variation of the angle of sideslip and the bank angle with time (unstable lateral oscillation) for $t = 1196$ (time point 300). The period of this mode is 5.6 s, whereas the doubling time is 30.3 s.

but without attitude control. For the same initial conditions as given in Section 12-2-5⁸, the results (plots of the angle of attack, the angle of sideslip, the bank angle and the height as a function of flight time) are shown in Figures 12-20(a) through 12-20(d).

We see that right from the beginning the angle of attack is rapidly diverging, reaching a kind of stable oscillation after $t \approx 500$ s, however with an initial amplitude of $\pm 5^\circ$. After $t = 1,400$ s, the vehicle is in a state of severe unstable oscillations (with a pitch rate of a few hundred degrees per second). The angle of sideslip and the bank angle show only small oscillations, mainly induced by the angle-of-attack oscillations. Also these angles reach large values when $t > 1,400$ s. In Figure 12-20(d), we see that the vehicle is in fact doing a damped skipping flight, because of the strong variation in the aerodynamic forces. Finally, after more than 1,600 s the vehicle crashes on the Earth's surface.

A second simulation, now with zero initial attitude and angular rates, shows even worse results (Figures 12-21(a) through 12-21(c)). Beside large-amplitude oscillations in all three attitude angles, very unstable oscillations are reached after only 500 s (not plotted). It might not come as a surprise that also this time the vehicle crashes, even further off from the target. The conclusion from the above discussion is, that it is necessary to control the vehicle if we want it to have a stable flight and reach the landing area safely. However, that discussion is not part of the current lecture series.

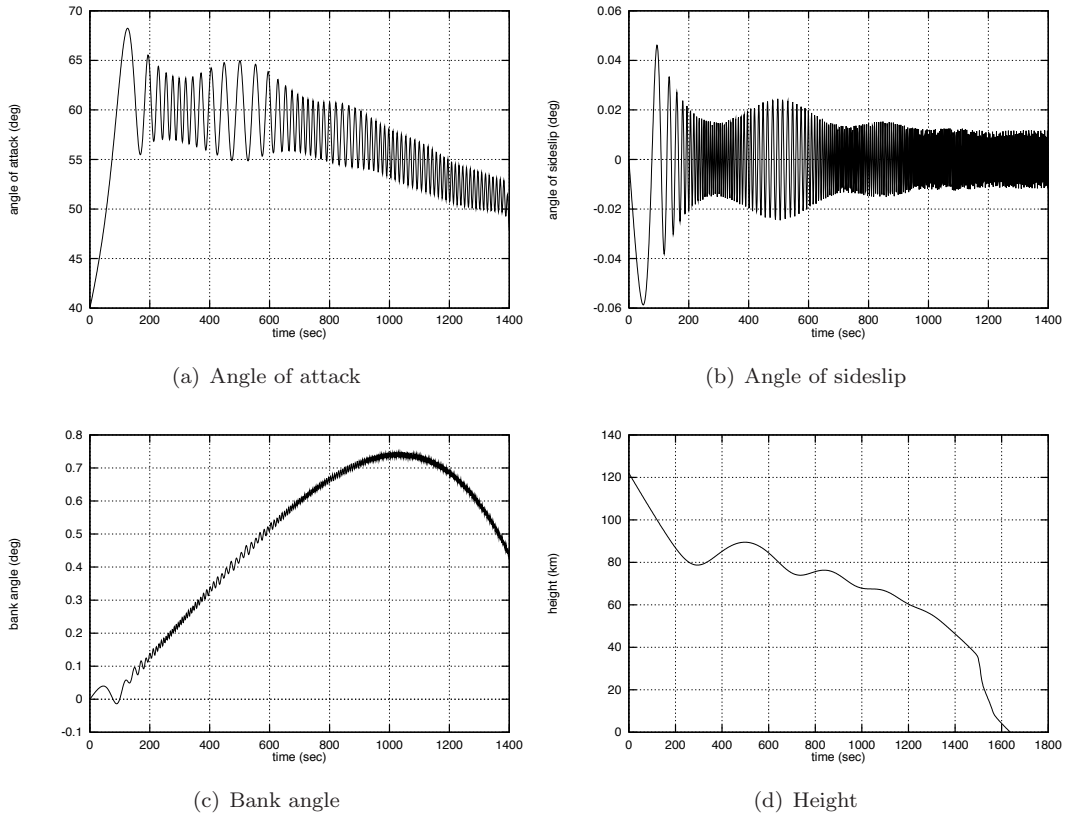


Figure 12-20: Open-loop simulation.

⁸Next to initial conditions for position and velocity, we need initial values for the attitude and angular rotation of the vehicle. The nominal attitude angles at $t = 0$ are $\alpha = 40^\circ$, $\beta = 0^\circ$ and $\mu = 0^\circ$, whereas the nominal pitch rate is $0.072663^\circ/\text{s}$ (the nominal roll and yaw rate are considered to be zero).

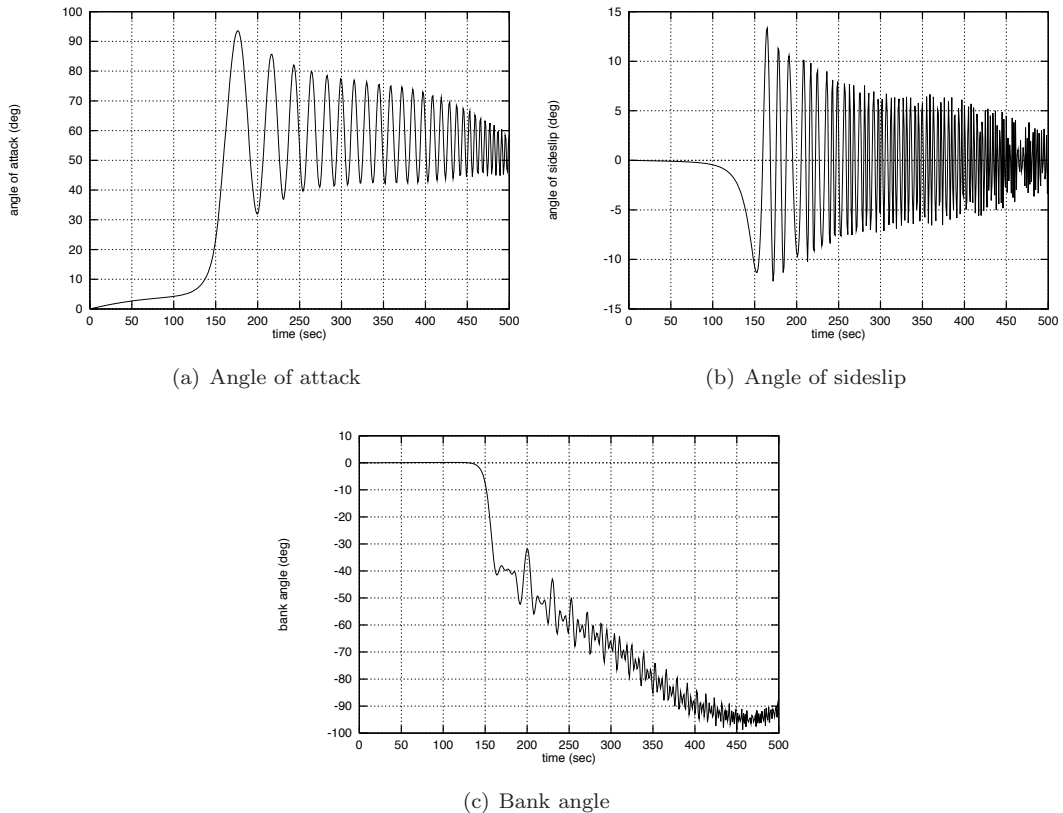


Figure 12-21: Open-loop simulation, zero initial attitude.

	short-period oscillation		phugoid		lateral oscillation		aperiodic roll mode		height mode
λ_i	Re	$-0.7302 \cdot 10^{-7}$		$0.4025 \cdot 10^{-4}$		$0.8677 \cdot 10^{-3}$	$-0.1735 \cdot 10^{-2}$	$-0.7925 \cdot 10^{-18}$	$-0.8402 \cdot 10^{-4}$
Im		$\pm 0.7415 \cdot 10^{-2}$		$\pm 0.1212 \cdot 10^{-2}$		± 0.0168	-	-	-
P (s)		847.3		5,183.0		373.8	∞	∞	∞
$T_{\frac{1}{2}}$ (s)		$0.949 \cdot 10^7$		-17,220.6		-798.9	399.4	$0.875 \cdot 10^{18}$	8,250.0
ζ (-)		$0.985 \cdot 10^{-5}$		-0.033		-0.052	-	-	-
ω_n (rad/s)		$0.742 \cdot 10^{-2}$		$0.121 \cdot 10^{-2}$		0.017	-	-	-
μ_i		z	θ (°)	z	θ (°)	z	θ (°)	z	z
ΔV		0.0129	10.7	$0.1271 \cdot 10^{-2}$	288.9	$0.1134 \cdot 10^{-15}$	6.2	$0.1678 \cdot 10^{-16}$	$0.2112 \cdot 10^{-15}$
$\Delta \gamma$		$0.9637 \cdot 10^{-6}$	331.7	$0.1632 \cdot 10^{-6}$	18.1	$0.4382 \cdot 10^{-20}$	325.8	$0.3441 \cdot 10^{-20}$	$0.6882 \cdot 10^{-21}$
ΔR		1.0000	63.3	1.0000	287.7	$0.2211 \cdot 10^{-14}$	51.1	$0.1475 \cdot 10^{-13}$	$0.3129 \cdot 10^{-12}$
Δp		$0.8551 \cdot 10^{-19}$	277.7	$0.2260 \cdot 10^{-23}$	291.9	0.0206	287.8	$0.2144 \cdot 10^{-2}$	$0.8153 \cdot 10^{-3}$
Δq		$0.1678 \cdot 10^{-3}$	6.1	$0.1804 \cdot 10^{-9}$	300.2	$0.3156 \cdot 10^{-17}$	318.3	$0.4950 \cdot 10^{-19}$	$0.4129 \cdot 10^{-19}$
Δr		$0.9334 \cdot 10^{-20}$	291.6	$0.7187 \cdot 10^{-24}$	0.4	$0.1542 \cdot 10^{-2}$	287.8	$0.1606 \cdot 10^{-3}$	$0.9716 \cdot 10^{-3}$
$\Delta \alpha$		0.0226	276.1	$0.3150 \cdot 10^{-7}$	281.9	$0.3891 \cdot 10^{-16}$	345.0	$0.3712 \cdot 10^{-16}$	$0.1735 \cdot 10^{-16}$
$\Delta \beta$		$0.1940 \cdot 10^{-17}$	21.6	$0.2444 \cdot 10^{-22}$	272.3	0.7277	20.8	$0.7814 \cdot 10^{-2}$	$0.1235 \cdot 10^{-15}$
$\Delta \sigma$		$0.2609 \cdot 10^{-17}$	11.3	$0.5346 \cdot 10^{-21}$	52.2	1.0000	11.7	1.0000	1.0000

Table 12-3: Eigenvalues and corresponding characteristic values for time point 1 ($t = 0$ s).

		short-period oscillation		phugoid		lateral oscillation		aperiodic roll mode		height mode
λ_i	Re	-0.2342·10 ⁻⁴		-0.1144·10 ⁻³		0.8723·10 ⁻³		-0.1769·10 ⁻²	0.1535·10 ⁻¹⁶	0.7921·10 ⁻⁴
Im		±0.1583		±0.1256·10 ⁻²		±0.3257		-	-	-
P (s)		39.7		5,002.9		19.3		∞	∞	∞
T _½ (s)		2,959.1		6,058.3		-794.6		392.0	-0.452·10 ¹⁷	-8,750.8
ζ (-)		0.148·10 ⁻³		0.091		-0.268·10 ⁻²		-	-	-
ω_n (rad/s)		0.158		0.126·10 ⁻²		0.326		-	-	-
μ_i		z	θ (°)	z	θ (°)	z	θ (°)	z	z	z
ΔV	0.3191	273.8	0.1277·10⁻²	76.0	0.3534·10⁻¹⁵	87.0	0.1622·10⁻¹⁵	0.2273·10⁻¹³	0.6449·10⁻³	
$\Delta \gamma$	0.2031·10 ⁻⁴	271.7	0.1690·10 ⁻⁶	345.2	0.1466·10 ⁻¹⁸	358.1	0.1344·10 ⁻¹⁸	0.8117·10 ⁻²⁰	0.8793·10 ⁻⁸	
ΔR	1.0000	1.8	1.0000	81.7	0.1821·10⁻¹¹	358.9	0.8659·10⁻¹²	0.3518·10⁻¹⁰	1.0000	
Δp	0.1769·10 ⁻¹⁶	271.7	0.8803·10 ⁻²¹	34.9	0.4007	1.3	0.2175·10 ⁻²	0.8197·10 ⁻³	0.4764·10 ⁻²¹	
Δq	0.5316·10⁻²	273.6	0.1936·10 ⁻⁹	285.7	0.6885·10 ⁻¹⁸	0.4	0.1162·10 ⁻¹⁹	0.1423·10 ⁻¹⁹	0.2771·10 ⁻⁹	
Δr	0.1096·10 ⁻¹⁷	272.4	0.1699·10 ⁻²¹	85.4	0.0291	1.3	0.1579·10 ⁻¹³	0.9790·10 ⁻³	0.8749·10 ⁻²¹	
$\Delta \alpha$	0.0336	3.6	0.4148·10 ⁻⁷	75.9	0.4179·10 ⁻¹⁷	81.3	0.2817·10 ⁻²⁰	0.7400·10 ⁻¹⁸	0.2094·10 ⁻⁷	
$\Delta \beta$	0.1322·10 ⁻¹⁶	2.3	0.1650·10 ⁻²²	350.2	0.7225	271.4	0.2129·10 ⁻⁴	0.5070·10 ⁻¹⁷	0.5994·10 ⁻²²	
$\Delta \sigma$	0.5658·10 ⁻¹⁶	1.1	0.1953·10 ⁻¹⁸	12.7	1.0000	271.0	1.0000	1.0000	1.0000	0.6410·10 ⁻¹⁸

Table 12-4: Eigenvalues and corresponding characteristic values for time point 50 ($t = 96$ s).

		short-period oscillation		phugoid		lateral oscillation		periodic roll mode		spiral mode
λ_i	Re	-0.2032·10 ⁻³		-0.9924·10 ⁻³		0.2225·10 ⁻³		0.1022·10 ⁻³		-0.1053·10 ⁻¹⁴
Im		±0.4292		±0.1359·10 ⁻²		±0.8844		±0.5608·10 ⁻³		-
P (s)		14.6		4,625.1		7.1		11,203.9		∞
T _½ (s)		3,410.4		698.4		-3,115.4		-6,784.2		0.658·10 ¹⁵
ζ (-)		0.474·10 ⁻³		0.590		-0.252·10 ⁻³		-0.179		-
ω_n (rad/s)		0.429		0.168·10 ⁻²		0.884		0.570·10 ⁻³		-
μ_i		z	θ (°)	z	θ (°)	z	θ (°)	z	θ (°)	z
ΔV	1.0000	270.6	0.1666·10⁻²	339.2	0.8536·10⁻²	270.1	0.5610·10⁻³	0.4	0.6115·10⁻⁵	
$\Delta \gamma$	0.2231·10 ⁻⁴	88.5	0.2385·10 ⁻⁶	76.0	0.1254·10 ⁻³	0.3	0.8066·10 ⁻⁷	335.9	0.2074·10 ⁻¹¹	
ΔR	0.3721	358.5	1.0000	22.3	1.0000	270.3	1.0000	55.6	1.0000	
Δp	0.4047·10 ⁻⁶	270.4	0.5151·10 ⁻⁹	56.3	0.3287	0.2	0.3382·10 ⁻⁹	29.0	0.1072·10 ⁻⁹	
Δq	0.0166	270.7	0.3228·10 ⁻⁹	321.3	0.1192·10 ⁻³	270.2	0.7965·10 ⁻⁹	280.7	0.7928·10 ⁻⁹	
Δr	0.2939·10 ⁻⁷	270.4	0.3740·10 ⁻¹⁰	56.3	0.0239	0.2	0.2456·10 ⁻¹⁰	29.0	0.1274·10 ⁻⁹	
$\Delta \alpha$	0.0387	0.6	0.5117·10 ⁻⁷	339.2	0.5723·10 ⁻³	0.1	0.1724·10 ⁻⁷	0.4	0.1878·10 ⁻⁹	
$\Delta \beta$	0.1304·10 ⁻⁶	0.4	0.6505·10 ⁻¹²	290.2	0.2182	270.2	0.1447·10 ⁻¹²	309.3	0.2645·10 ⁻²³	
$\Delta \sigma$	0.7566·10 ⁻⁶	348.9	0.1853·10⁻⁶	355.2	0.3020	270.2	0.5266·10⁻⁶	282.6	0.5107·10⁻⁶	

Table 12-5: Eigenvalues and corresponding characteristic values for time point 100 ($t = 396$ s).

		short-period oscillation		phugoid		lateral oscillation		spiral mode			
λ_i	Re	$-0.2537 \cdot 10^{-3}$		$-0.1090 \cdot 10^{-2}$		$0.4583 \cdot 10^{-3}$		$0.2865 \cdot 10^{-3}$	$-0.5696 \cdot 10^{-3}$	$0.3040 \cdot 10^{-14}$	
Im		± 0.4361		$\pm 0.1546 \cdot 10^{-2}$		± 0.9001		-	-	-	
P (s)		14.4		4,063.6		7.0		∞	∞	∞	
$T_{1/2}$ (s)		2,732.4		636.2		$-1,512.4$		-2,419.2	1,216.9	$-0.228 \cdot 10^{15}$	
ζ (-)		$0.582 \cdot 10^{-3}$		0.576		$-0.509 \cdot 10^{-3}$		-	-	-	
ω_n (rad/s)		0.436		$0.189 \cdot 10^{-2}$		0.900		-	-	-	
μ_i		z	θ (°)	z	θ (°)	z	θ (°)	z	z	z	
ΔV		1.0000	274.0	0.1815 $\cdot 10^{-2}$	82.2	0.9170 $\cdot 10^{-2}$	270.4	0.2713 $\cdot 10^{-3}$	0.1094 $\cdot 10^{-2}$	0.8003 $\cdot 10^{-5}$	
$\Delta \gamma$		0.4013 $\cdot 10^{-4}$	272.7	0.2974 $\cdot 10^{-6}$	1.2	0.1416 $\cdot 10^{-3}$	0.7	0.4491 $\cdot 10^{-7}$	0.8897 $\cdot 10^{-7}$	0.4561 $\cdot 10^{-11}$	
ΔR		0.5933	2.7	1.0000	306.6	1.0000	270.6	1.0000	1.0000	1.0000	
Δp		0.4450 $\cdot 10^{-6}$	273.7	0.5502 $\cdot 10^{-9}$	344.9	0.3603	0.6	0.9548 $\cdot 10^{-10}$	0.9607 $\cdot 10^{-9}$	0.6063 $\cdot 10^{-10}$	
Δq		0.0166	274.1	0.4104 $\cdot 10^{-9}$	54.0	0.1268 $\cdot 10^{-3}$	270.5	0.6327 $\cdot 10^{-9}$	0.2328 $\cdot 10^{-8}$	0.1015 $\cdot 10^{-8}$	
Δr		0.3231 $\cdot 10^{-7}$	273.7	0.3995 $\cdot 10^{-10}$	344.9	0.0262	0.6	0.6933 $\cdot 10^{-11}$	0.6976 $\cdot 10^{-10}$	0.7337 $\cdot 10^{-10}$	
$\Delta \alpha$		0.0380	4.0	0.5548 $\cdot 10^{-7}$	82.2	0.6003 $\cdot 10^{-3}$	0.5	0.8293 $\cdot 10^{-8}$	0.3343 $\cdot 10^{-7}$	0.2446 $\cdot 10^{-9}$	
$\Delta \beta$		0.1406 $\cdot 10^{-6}$	3.7	0.7542 $\cdot 10^{-12}$	39.8	0.2350	270.6	0.1982 $\cdot 10^{-13}$	0.3966 $\cdot 10^{-12}$	0.1012 $\cdot 10^{-22}$	
$\Delta \sigma$		0.8149 $\cdot 10^{-6}$	347.6	0.1603 $\cdot 10^{-6}$	281.8	0.3253	270.6	0.3505 $\cdot 10^{-6}$	0.1455 $\cdot 10^{-5}$	0.6027 $\cdot 10^{-6}$	

Table 12-6: Eigenvalues and corresponding characteristic values for time point 150 ($t = 596$ s).

		short-period oscillation		phugoid		lateral oscillation		roll divergence		spiral mode	
λ_i	Re	$-0.9485 \cdot 10^{-3}$		$-0.2730 \cdot 10^{-2}$		$0.3817 \cdot 10^{-3}$		$-0.6806 \cdot 10^{-4}$		$-0.8865 \cdot 10^{-15}$	
Im		± 0.6923		$\pm 0.2006 \cdot 10^{-2}$		± 1.432		$\pm 0.1084 \cdot 10^{-2}$		-	
P (s)		9.1		3,132.0		4.4		5,794.7		∞	
$T_{1/2}$ (s)		730.8		253.9		$-1,815.7$		10,183.9		$0.782 \cdot 10^{15}$	
ζ (-)		$0.137 \cdot 10^{-2}$		0.806		$-0.267 \cdot 10^{-3}$		0.063		-	
ω_n (rad/s)		0.692		$0.339 \cdot 10^{-2}$		1.432		$0.109 \cdot 10^{-2}$		-	
μ_i		z	θ (°)	z	θ (°)	z	θ (°)	z	θ (°)	z	
ΔV		1.0000	276.0	0.0025	319.8	0.1063 $\cdot 10^{-1}$	270.1	0.4720 $\cdot 10^{-3}$	72.2	0.4763 $\cdot 10^{-5}$	
$\Delta \gamma$		0.4694 $\cdot 10^{-4}$	275.1	0.6628 $\cdot 10^{-6}$	87.0	0.2809 $\cdot 10^{-3}$	0.5	0.2126 $\cdot 10^{-6}$	57.1	0.6368 $\cdot 10^{-11}$	
ΔR		0.3553	5.2	1.0000	50.9	1.0000	270.5	1.0000	330.7	1.0000	
Δp		0.7156 $\cdot 10^{-6}$	275.8	0.1981 $\cdot 10^{-8}$	288.2	0.5030	0.4	0.2391 $\cdot 10^{-9}$	323.5	0.1658 $\cdot 10^{-9}$	
Δq		0.0163	276.3	0.1057 $\cdot 10^{-8}$	304.4	0.1427 $\cdot 10^{-3}$	270.3	0.1008 $\cdot 10^{-8}$	4.8	0.7193 $\cdot 10^{-9}$	
Δr		0.5546E-07	275.8	0.1535 $\cdot 10^{-9}$	288.2	0.0390	0.4	0.1853 $\cdot 10^{-10}$	323.5	0.1947 $\cdot 10^{-9}$	
$\Delta \alpha$		0.0236	6.2	0.7242 $\cdot 10^{-7}$	319.8	0.4260 $\cdot 10^{-3}$	0.3	0.1356 $\cdot 10^{-7}$	72.2	0.1368 $\cdot 10^{-9}$	
$\Delta \beta$		0.1410 $\cdot 10^{-6}$	5.8	0.1911 $\cdot 10^{-11}$	324.5	0.2050	270.4	0.7395 $\cdot 10^{-13}$	49.9	0.2217 $\cdot 10^{-23}$	
$\Delta \sigma$		0.9087 $\cdot 10^{-6}$	328.9	0.1993 $\cdot 10^{-6}$	290.1	0.2867	270.4	0.3978 $\cdot 10^{-6}$	357.1	0.2623 $\cdot 10^{-6}$	

Table 12-7: Eigenvalues and corresponding characteristic values for time point 200 ($t = 796$ s).

		short-period oscillation	phugoid		lateral oscillation		roll divergence		spiral mode
λ_i	Re	-0.3245·10 ⁻²	-0.4386·10 ⁻²		0.1665·10 ⁻²		-0.1949·10 ⁻²		0.2946·10 ⁻¹⁴
Im		±0.6936	±0.2865·10 ⁻²		±1.496		±0.4996·10 ⁻⁴		-
P (s)		9.1	2192.8		4.2		12,577.2		∞
T _½ (s)		213.6	158.0		-416.2		355.7		-0.235·10 ¹⁵
ζ (-)		0.468·10 ⁻²	0.837		-0.111·10 ⁻²		1.000		-
ω_n (rad/s)		0.694	0.524·10 ⁻²		1.500		0.195·10 ⁻²		-
μ_i		z	θ (°)	z	θ (°)	z	θ (°)	z	θ (°)
ΔV		1.0000	283.5	0.2864·10 ⁻²	355.8	0.0138	271.5	0.8188·10 ⁻³	300.5
$\Delta \gamma$		0.1143·10 ⁻³	282.6	0.1725·10 ⁻⁵	325.9	0.5001·10 ⁻³	2.2	0.6430·10 ⁻⁶	300.1
ΔR		0.5387	13.0	1.0000	293.2	1.0000	272.2	1.0000	298.7
Δp		0.2483·10 ⁻⁵	283.1	0.8595·10 ⁻⁸	352.0	0.2990	2.2	0.2238·10 ⁻⁸	300.2
Δq		0.0127	284.2	0.5398·10 ⁻⁸	335.4	0.1345·10 ⁻³	271.7	0.3456·10 ⁻⁸	299.6
Δr		0.2959·10 ⁻⁶	283.1	0.1024·10 ⁻⁸	352.0	0.0356	2.2	0.2667·10 ⁻⁹	300.2
$\Delta \alpha$		0.0183	13.8	0.1486·10 ⁻⁶	355.8	0.4180·10 ⁻³	1.7	0.4247·10 ⁻⁷	300.5
$\Delta \beta$		0.3646·10 ⁻⁶	12.8	0.9533·10 ⁻¹¹	25.2	0.0947	272.2	0.9237·10 ⁻¹²	301.6
$\Delta \sigma$		0.6543·10 ⁻⁵	306.0	0.6393·10 ⁻⁶	28.3	0.1776	272.2	0.3700·10 ⁻⁶	298.5

Table 12-8: Eigenvalues and corresponding characteristic values for time point 250 ($t = 996$ s).

		former short-period oscillation	periodic pitch/roll mode		lateral oscillation		pitch/roll divergence		spiral mode
λ_i	Re	-0.5078	0.3695	-0.0157		0.0229	0.0814	-0.2892·10 ⁻³	0.9450·10 ⁻¹⁴
Im		-	-	±0.7035·10 ⁻²		±1.113	-	-	-
P (s)		∞	∞	893.1		5.6	∞	∞	∞
T _½ (s)		1.4	-1.9	44.3		-30.3	-8.5	2,396.8	-0.734·10 ¹⁴
ζ (-)		-	-	0.912		-0.021	-	-	-
ω_n (rad/s)		-	-	0.017		1.113	-	-	-
μ_i		z	z	z	θ (°)	z	θ (°)	z	z
ΔV		0.6721	0.5181	0.1758·10 ⁻²	9.3	0.0256	284.8	0.1215	0.3228·10 ⁻⁴
$\Delta \gamma$		0.4118·10 ⁻³	0.2972·10 ⁻³	0.1598·10 ⁻⁴	14.0	0.1027·10 ⁻²	17.9	0.6490·10 ⁻⁴	0.2695·10 ⁻⁶
ΔR		1.0000	1.0000	1.0000	349.9	1.0000	286.9	1.0000	1.0000
Δp		0.2036·10 ⁻⁴	0.1595·10 ⁻⁴	0.4226·10 ⁻⁶	48.5	0.0808	19.2	0.3478·10 ⁻⁵	0.3717·10 ⁻⁸
Δq		0.3447·10 ⁻²	0.1822·10 ⁻²	0.1025·10 ⁻⁶	278.8	0.7476·10 ⁻⁴	278.2	0.2963·10 ⁻⁴	0.6599·10 ⁻⁸
Δr		0.3419·10 ⁻⁵	0.2680·10 ⁻⁵	0.7098·10 ⁻⁷	48.5	0.0136	19.2	0.5842·10 ⁻⁶	0.6244·10 ⁻⁹
$\Delta \alpha$		0.7534·10 ⁻²	0.4372·10 ⁻²	0.3333·10 ⁻⁵	9.5	0.4170·10 ⁻³	16.0	0.2428·10 ⁻³	0.6126·10 ⁻⁷
$\Delta \beta$		0.1604·10 ⁻⁵	0.9150·10 ⁻⁶	0.1125·10 ⁻⁸	72.7	0.0140	290.4	0.4397·10 ⁻⁷	0.1669·10 ⁻¹²
$\Delta \sigma$		0.2726·10 ⁻⁴	0.7653·10 ⁻⁴	0.1671·10 ⁻⁴	48.9	0.0722	288.1	0.4241·10 ⁻⁴	0.3279·10 ⁻⁶

Table 12-9: Eigenvalues and corresponding characteristic values for time point 300 ($t = 1196$ s).

		former short-period oscillation	periodic pitch/roll mode	lateral oscillation	pitch/roll divergence	spiral mode	
λ_i	Re	-1.0884	0.9518	-0.0213	0.0392	0.0401	-0.1059·10 ⁻³ -0.9138·10 ⁻¹⁵
Im		-	-	±0.0146	±1.343	-	-
P (s)		∞	∞	430.4	4.7	∞	∞
T _{1/2} (s)		0.6	-0.7	32.6	-17.7	-17.3	6,544.1 0.759·10 ¹⁵
ζ (-)		-	-	0.825	-0.029	-	-
ω_n (rad/s)		-	-	0.026	1.343	-	-
μ_i		z	z	z	θ (°)	z	z
ΔV		0.9895	0.8871	0.6586·10⁻²	52.8	0.0268	339.8
$\Delta \gamma$		0.1275·10⁻²	0.1111·10⁻²	0.3613·10⁻⁴	68.9	0.1815·10⁻²	72.9
ΔR		1.0000	1.0000	35.0	1.0000	341.4	1.0000
Δp		0.3547·10⁻⁴	0.3566·10⁻⁴	0.1380·10⁻⁵	305.5	0.1259	74.5
Δq		0.0266	0.0220	0.5895·10⁻⁶	343.9	0.3583·10⁻³	336.1
Δr		0.1701·10⁻⁵	0.1710·10⁻⁵	0.6617·10⁻⁷	305.5	0.6041·10⁻²	74.5
$\Delta \alpha$		0.0267	0.0210	0.7066·10⁻⁵	52.8	0.4624·10⁻³	71.3
$\Delta \beta$		0.5123·10⁻⁵	0.4504·10⁻⁵	0.4726·10⁻⁸	339.9	0.0225	346.2
$\Delta \sigma$		0.2715·10⁻³	0.2695·10⁻³	0.4661·10⁻⁴	298.7	0.0911	342.9

Table 12-10: Eigenvalues and corresponding characteristic values for time point 314 ($t = 1252$ s).

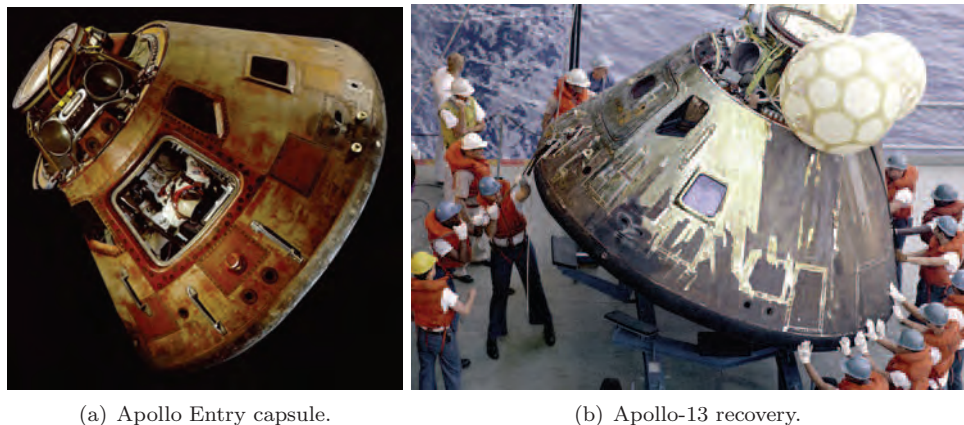
12-3 Eigenmotion of entry capsules

In the previous section we extensively described the eigenmotion of a winged entry vehicle and tried to relate it to the eigenmotion of conventional aircraft, flying at conventional speeds. It was concluded that:

- There are similar characteristic modes compared with conventional aircraft, yet with several differences,
- The absence of the atmosphere in the early re-entry phase makes everything slower,
- There is a coupling between symmetric and asymmetric motion,
- The open-loop, non-linear simulations show the necessity of control due to the severe oscillatory nature,
- Due to the time-variant and non-linear nature of re-entry missions, the eigenmodes are not distinguishable in an open-loop simulation.

The next step in the analysis of eigenmotion of space vehicles is to move away even further from conventional aircraft by looking at different vehicle shapes, albeit in similar velocity and altitude regimes as before. To identify the influence of the vehicle shape on the eigenmotion we have selected the Apollo capsule as the object of study, and consider the entry in the atmosphere after its return flight from the Moon.

The Apollo program was the spaceflight effort carried out by the United States' National Aeronautics and Space Administration (NASA) to land the first humans on Earth's Moon. Initiated in the early sixties of the previous century, Apollo followed the Mercury and Gemini programs and ran from 1961 to 1972. Its goal was accomplished with the Apollo-11 mission when astronauts Neil Armstrong and Buzz Aldrin landed their Lunar Module on the Moon on July 20, 1969, and walked on its surface. They safely landed on Earth on July 24 in the so-called Command Module (see Figure 12-22), a blunt entry capsule with an ablative heat shield. After this pioneering mission, another five Moon landings were carried out in a similar fashion.



(a) Apollo Entry capsule.

(b) Apollo-13 recovery.

Figure 12-22: Typical shape of a manned entry capsule. Images courtesy NASA.

To study the characteristic motion of the Apollo Command Module, the mission and vehicle will be introduced in the next sub-section (12-3-1). Since the state-space model for Apollo will be different from the model used for HORUS, in Sub-section 12-3-2 the differences will be highlighted. Then, in Sub-section 12-3-3 the time history of the eigenvalues is shown and the corresponding eigenmotion discussed.

12-3-1 Nominal mission

The model that is used in this study is that of an Apollo-like entry capsule (mass $m = 4976 \text{ kg}$), which is on a return leg from the Moon. It enters the atmosphere at 220 km altitude with a relative velocity of $V = 11 \text{ km/s}$, and a corresponding flight-path angle of $\gamma = -9.536^\circ$. To avoid excessive fuel consumption for attitude control, the z -location of the c.o.m. has been moved up from the symmetry axis to provide a natural hypersonic trim condition with an angle of attack of about $\alpha = -24.5^\circ$. Angle-of-attack control is therefore only used to stabilize the angle of attack around this trim condition; bank-angle-control is used to orient the lift in a lift-down condition to avoid skipping out of the atmosphere⁹, and is effectively the only guidance means. For attitude control the capsule is equipped with reaction-control thrusters only.

Apollo is a semi-ballistic capsule that flies with a low lift-to-drag ratio ($L/D \approx 0.3$), in a trajectory that is characterized by a high heat and mechanical load. The high heat load drove the design of the thermal protection system (TPS) towards the use of ablative materials, *i.e.*, materials that absorb the heat and consequentially slowly burn away, thus rejecting the heat from the vehicle.

Apollo enters the atmosphere with the heat shield facing the flow. Let us define a body frame with the origin in the theoretical apex of the vehicle, *i.e.*, if we would extend the smallest portion of the vehicle it would end in a point, which is called the *apex*. The x_B -axis is positive in the direction of the heat shield and intersects it in the centre of the circular cross section. The z_B -axis is positive pointing downwards for a nominal entry and the y_B -axis completes the right-handed system. In this frame of reference, the location of the centre of mass is given by $\mathbf{r}_{\text{cm}} = (2.57, 0.0, -0.137)^T$. Due to the (significant) shift of the centre of mass in z -direction, the capsule is not rotationally symmetric in mass, which means that one of the products of inertia is non-zero.

⁹When the entry velocity of a vehicle entering the atmosphere is significantly larger than the local circle velocity (about 7.8 km/s), the kinetic-energy of the vehicle is so large that the vehicle may bounce off the atmosphere, or *skip*. On one hand, one could use this skipping concept to reduce the energy level and enter the atmosphere after the second or third skip, but with the risk that the vehicle bounces off for good, when this is not carefully planned. On the other hand, when the vehicle should remain in the atmosphere during the initial entry, the lift should be oriented in a downward direction to "pull" the vehicle into the atmosphere. The latter guidance concept was chosen for Apollo, to avoid the chance of losing the vehicle and its crew.

The corresponding numerical values of moments and products of inertia are $I_{xx} = 5617.605456 \text{ kg/m}^2$, $I_{yy} = 4454.623056 \text{ kg/m}^2$, $I_{zz} = 4454.80176 \text{ kg/m}^2$, $I_{xy} = I_{yz} = 0.0 \text{ kg/m}^2$ and $I_{xz} = 1751.99984 \text{ kg/m}^2$.

The aerodynamic database used here is based on extensive wind-tunnel measurements done in the mid sixties as part of the Apollo-capsule design [82, 93]. What we need for our analysis are expressions for the aerodynamic forces and moments, as well as the first derivatives to be substituted in the linearized system discussed in Section 12-2-4. The drag, side and lift force appear to be functions of the states h and V , and the attitude angles α and β :

$$D(h, V, \alpha, \beta) = C_D(M(h, V), \alpha, \beta) \frac{1}{2} \rho(h) V^2 S_{ref} \quad (12-153)$$

$$S(h, V, \beta) = C_S(M(h, V), \beta) \frac{1}{2} \rho(h) V^2 S_{ref} \quad (12-154)$$

$$L(h, V, \alpha) = C_L(M(h, V), \alpha) \frac{1}{2} \rho(h) V^2 S_{ref} \quad (12-155)$$

where $\rho(h)$ is the altitude-dependent atmospheric density and $M(h, V)$ is the Mach number, through the speed-of-sound dependency with altitude a function of both h and V . S_{ref} is the aerodynamic reference area, with $S_{ref} = 12 \text{ m}^2$.

The aerodynamic roll, pitch and yaw moments, \mathcal{L} , \mathcal{M} and \mathcal{N} are functions of the states h, V, α, β, q and r [82, 93] and include the dynamic damping coefficients C_{m_q} and C_{n_r} . However, the quoted references do not give any data on the roll-moment coefficient. At most it will be a small value, so we can safely assume it to be zero:

$$\mathcal{L} = 0 \quad (12-156)$$

$$\mathcal{M}(h, V, \alpha, \beta) = \left(C_m(M(h, V), \alpha, \beta) + C_{m_q}(M(h, V), \alpha, \beta) \frac{qd_{ref}}{V} \right) \frac{1}{2} \rho(h) V^2 S_{ref} d_{ref} \quad (12-157)$$

$$\mathcal{N}(h, V, \alpha, \beta) = \left(C_n(M(h, V), \alpha, \beta) + C_{n_r}(M(h, V), \alpha, \beta) \frac{rd_{ref}}{V} \right) \frac{1}{2} \rho(h) V^2 S_{ref} d_{ref} \quad (12-158)$$

where d_{ref} is the aerodynamic reference length (*i.e.*, the vehicle diameter). The actual value is $d_{ref} = 3.9 \text{ m}$. Note that the force and moment coefficients are defined with respect to the apex - during the wind-tunnel campaign the mounting point of the wind-tunnel model - so the aerodynamic moments will also include a contribution of the forces to compensate for the distance between apex and centre of mass.

Knowing the state dependency of forces and moments will serve as input for obtaining the state-space formulation required to do the eigenmotion analysis. Before we move on to this we will briefly discuss the reference trajectory. Since we do not have the actual Apollo reference trajectory at our disposal, nor the models for the guidance, navigation and control system, we will generate the reference trajectory by simulating the mission in open loop. This means that given the initial conditions as stated before, we "drop" Apollo in the atmosphere and let it "fall" to the Earth's surface. The resulting motion thus includes the very eigenmotion that we want to study in the next sub-section. However, we saw in the previous section while discussing the open-loop motion of HORUS that the individual components of the eigenmotion cannot be discerned, so we will postpone that discussion until later.

In Figure 12-23 the altitude-velocity profile is shown. The entry begins at 220 km altitude and the first phase is characterized by an increase in velocity. This is always the case for entry vehicles, since the atmosphere is too thin to generate significant aerodynamic forces. Thus, the gravitational force dominates and pulls the vehicle down thereby increasing the vehicle's velocity. At a certain

combination of altitude and velocity the dynamic pressure starts building up and the retarding force is now larger than the gravitational pull, thus decreasing the vehicle's velocity.

The velocity rapidly decreases over just a small altitude range, resulting in a large mechanical load, or *g-load*. The *g-load* peaks at 18 g, which clearly shows the necessity to carefully control the flight path. Without a guidance system to properly plan the path and an attitude controller to maintain the commanded attitude the astronauts will not survive this particular entry. The final velocity shown in the plot ($V \approx 300$ m/s or $M = 1$) is attained after only 275 s of flight. One can easily understand that the thermal environment is challenging to say the least, if one knows that the only mechanism to reduce the kinetic energy is friction.

In Figure 12-24 the rotational states are shown. It is clear that the angle of attack stabilizes around a trim value, dictated by the location of the centre of mass (notably, the location in z -direction). Around $t \approx 230$ sec the vehicle behaviour becomes quite erratic, due to a combination of aerodynamic moments and non-linear couplings. Since the location of the centre of mass was determined to give a trim angle in the hypersonic regime, where the Mach effect is very small, a different trim equilibrium is found in the low hypersonic and supersonic regime. Here, the Mach effect is relatively strong.

However, the motion is not completely unstable as the angle of attack does not diverge more than a few degrees, with only a minor local (high-frequency) oscillation. The angle of sideslip is only marginally affected, although its behavior is also characterized by a high-frequency oscillation. The bank angle seems to be unstable as it keeps on decreasing. Main reason is that due to the roll-yaw coupling a bank-angle rotation is induced, and since there is no (roll) damping modelled, the rotation is undamped. The angular rates are oscillating rapidly, indicating that the aerodynamic moments keep on changing sign. This is consistent with the angle-of-attack oscillation around its trim value, representing a zero moment.

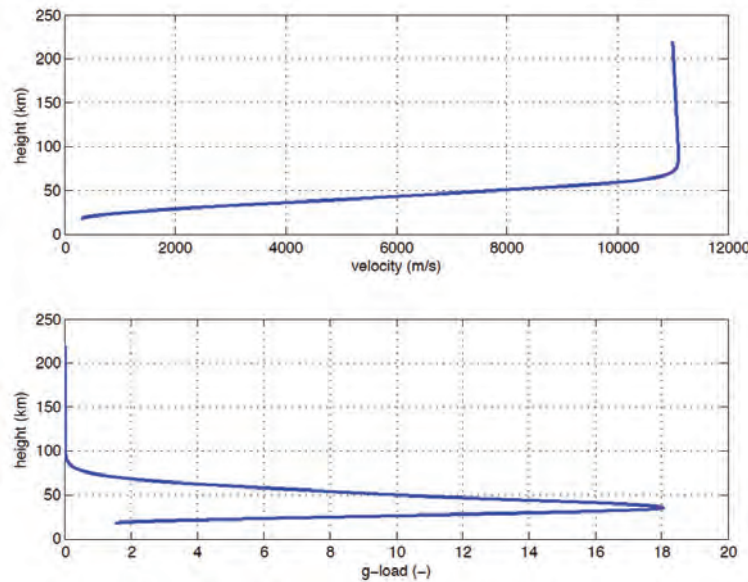


Figure 12-23: Altitude-velocity profile for a free-fall Apollo entry (top), and occurring *g-load* (bottom).

To do the eigenmotion analysis it would be better to have a smooth representation of the attitude angles, as the change of eigenvalues will then not suffer from the high-frequency oscillations. This seems justified as the induced eigenmotion should not have an influence on itself. Therefore, we will do a curve fit of the angle-of-attack and bank-angle profile and set the angle of sideslip to zero. This does not have an effect on the actual trajectory, because the trajectory dynamics are

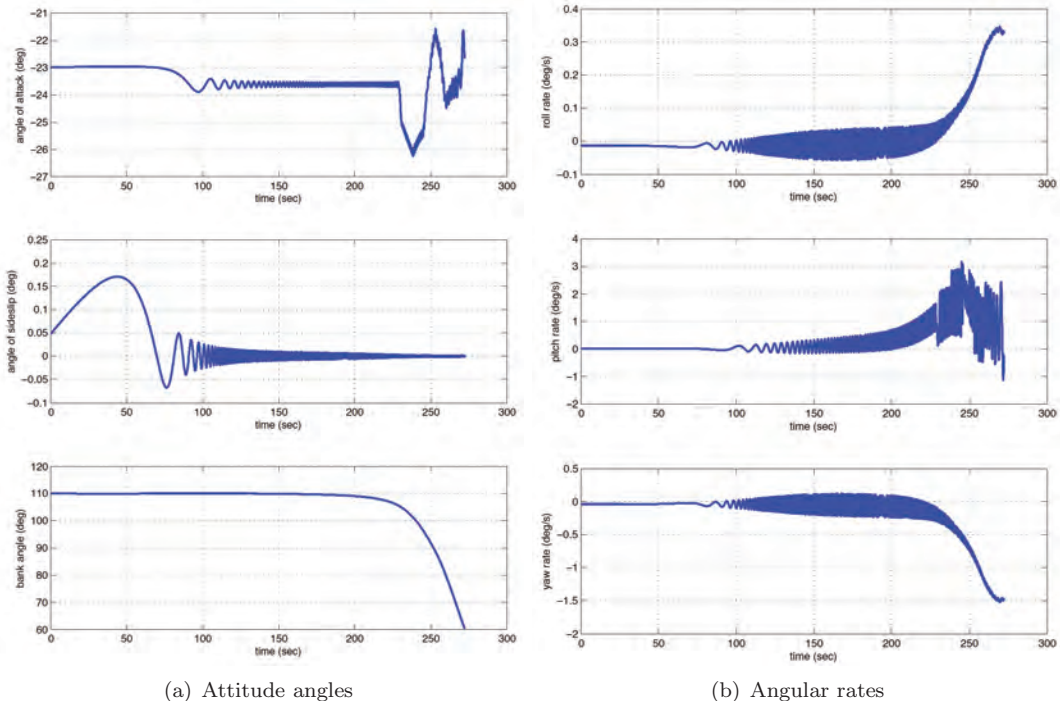


Figure 12-24: State variables for the rotational motion of a free-fall Apollo entry.

at least an order of magnitude slower, so the high-frequency attitude oscillations will average out. The resulting, smoothed angle of attack profile is shown in Figure 12-25(a). One might expect a larger influence towards the end of the flight, as the difference between actual and smoothed angle of attack is large. However, one should realize that the dynamic pressure has dropped significantly thus reducing the magnitude of the aerodynamic forces. At that moment, the forces have only a small influence on the shape of the trajectory. The induced oscillation in the bank angle is only small (Figure 12-25(b)), but is removed nonetheless to avoid any effect on the eigenmotion analysis.

12-3-2 State-Space Model

To calculate the eigenvalues and study the eigenmotion of the entry capsule we will, of course, follow the same approach as for the winged entry vehicle HORUS in the previous section. Starting from the non-linear equations of motion the equations are linearized with respect to state and control variables and put in state-space form:

$$\dot{\mathbf{x}} = \mathbf{Ax} + \mathbf{Bu} \quad (12-159)$$

with \mathbf{x} an $n \times 1$ state vector, \mathbf{u} an $m \times 1$ control vector, and \mathbf{A} and \mathbf{B} the $n \times n$ state (or system) and $n \times m$ control coefficient matrices, respectively.

In terms of state variables, there is no reason to change the ones we used before, so (see also Section 12-2-4):

$$\mathbf{x} = (\Delta V, \Delta \gamma, \Delta R, \Delta p, \Delta q, \Delta r, \Delta \alpha, \Delta \beta, \Delta \mu)^T$$

However, there are two fundamental differences with respect to HORUS that affect the definition of \mathbf{A} and \mathbf{B} . In the first place, the Apollo(-like) entry capsule does not have aerodynamic control

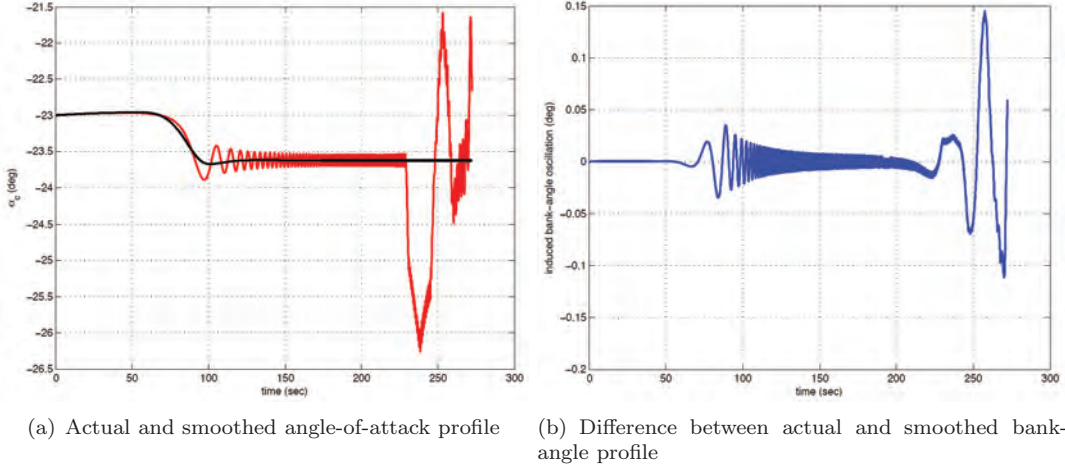


Figure 12-25: Smoothing applied to actual attitude profiles to obtain reference profile.

surfaces. The control system can only command the thrusters of the reaction control system to modify (or maintain) its attitude. This means that the control vector is now defined as

$$\mathbf{u} = (\Delta M_{T,x}, \Delta M_{T,y}, \Delta M_{T,z})^T$$

with

$$\begin{aligned} M_{T,x} &= \text{roll-thruster moment (Nm)} \\ M_{T,y} &= \text{pitch-thruster moment (Nm)} \\ M_{T,z} &= \text{yaw-thruster moment (Nm)} \end{aligned}$$

As a consequence, \mathbf{B} reduces to a 9x3 matrix (rather than 9x6). In the second place, we cannot assume that the vehicle is rotational symmetric in mass, as we did for HORUS. It may seem strange that we could assume this for an aircraft-like vehicle, but we did this after inspecting the values of moments and products of inertia; for HORUS I_{xz} is much smaller than the moments of inertia. In case of Apollo, I_{xz} is on average about 30% of the value of I_{xx} , I_{yy} and I_{zz} due to the shift in centre of mass. This value is far too large to be ignored, so it will introduce additional (coupling) terms in both \mathbf{A} and \mathbf{B} . Further, since the aerodynamic database of HORUS is more extensive, for Apollo some of the components disappear.

The linearization is done in exactly the same way as in the previous section and will not be repeated here. It is noted that the inclusion of the (aerodynamic) damping terms due to C_{m_q} and C_{n_r} do not give additional coefficients in \mathbf{A} , since these terms are of higher order. This has already been proven in Sub-section 12-2-4. The non-zero coefficients of \mathbf{A} and \mathbf{B} are shown in Eq. (12-77). Below, we will only list those coefficients that are different from the earlier definition.

The related elements of matrix \mathbf{A} , *i.e.*, a_{ij} , are given by

$$a_{pp} = I_{p1} q_0 \quad (12-160)$$

$$a_{pq} = I_{p1} p_0 + I_{p2} r_0 \quad (12-161)$$

$$a_{pr} = I_{p2} q_0 \quad (12-162)$$

$$a_{qp} = -2 \frac{I_{xz}}{I_{yy}} p_0 + \frac{I_{zz} - I_{xx}}{I_{yy}} r_0 \quad (12-163)$$

$$a_{qr} = \frac{I_{zz} - I_{xx}}{I_{yy}} p_0 + 2 \frac{I_{xz}}{I_{yy}} r_0 \quad (12-164)$$

$$a_{rp} = I_{r_1} q_0 \quad (12-165)$$

$$a_{rq} = I_{r_1} p_0 + I_{r_2} r_0 \quad (12-166)$$

$$a_{rr} = I_{r_2} q_0 \quad (12-167)$$

In the above coefficients, the following auxiliary variables have been used:

$$\begin{aligned} I_{p_1} &= \frac{I_{xx} - I_{yy} + I_{zz}}{I^*} \\ I_{p_2} &= \frac{(I_{yy} - I_{zz}) I_{zz} - I_{xz}^2}{I^*} \\ I_{r_1} &= \frac{(I_{xx} - I_{yy}) I_{xx} - I_{xz}^2}{I^*} \\ I_{r_2} &= \frac{(-I_{xx} + I_{yy} - I_{zz}) I_{xz}}{I^*} \\ I^* &= I_{xx} I_{zz} - I_{xz} I_{xz} \end{aligned}$$

As discussed earlier, the equilibrium angular rate components p_0 , q_0 and r_0 follow from the condition $\dot{\alpha} = \dot{\beta} = \dot{\mu} = 0$, and are given by Eqs. (12-39)-(12-41).

The non-zero elements of matrix **B**, i.e., b_{ik} , are:

$$b_{px} = \frac{I_{zz}}{I^*} \quad (12-168)$$

$$b_{pz} = \frac{I_{xz}}{I^*} \quad (12-169)$$

$$b_{qy} = \frac{1}{I_{yy}} \quad (12-170)$$

$$b_{rx} = \frac{I_{xz}}{I^*} \quad (12-171)$$

$$b_{rz} = \frac{I_{xx}}{I^*} \quad (12-172)$$

By inspecting the differences between the two system matrices **A** we can expect for Apollo an even stronger coupling between the three axes of motion than was the case for HORUS. This will show not only between longitudinal and lateral motion, but also as a stronger roll-yaw coupling in the lateral motion. Looking at **B** it is clear that also here the roll and yaw axes have a stronger coupling, which makes it harder to control the individual axes of the entry capsule. This means that a control moment exerted on the x -axis will induce a perturbing motion around the z -axis and vice versa. Control, however, is not part of the current discussion, so this remains an observation only.

12-3-3 Eigenvalues and eigenmotion

After linearizing the non-linear equations of motion and formulating the result in state-space form, we can evaluate \mathbf{A} at a number of discrete time points, as we already did in Sub-section 12-2-6. For each of the resulting LTI systems we can calculate the eigenvalues and eigenvectors, and derive a number of performance indicators: the *period* P , Eq. (12-146), the *halving time* $T_{\frac{1}{2}}$, Eq. (12-147), the *damping ratio* ζ , Eq. (12-148), and the *natural frequency* ω_n , Eq. (12-149). From the eigenvectors we calculate the modulus z , Eq. (12-151), and argument θ , Eq. (12-152). These parameters will help us to identify the type of eigenmode and the state variables involved in the eigenmotion.

Before we get to the detailed discussion of the eigenmotion, we will first have a look at the global picture, *i.e.*, the variation of all eigenvalues throughout the mission. In Figure 12-26 the eigenvalues for the coupled rotational and translational motion is shown (calculated from the 9×9 system matrix \mathbf{A}). The main observations are:

- there are two complex pairs, representing a longitudinal and lateral oscillation. The complex part is close to zero at entry but reaches large values (around 25) when the dynamic pressure (and thus the aerodynamic forces and moments) reach large values. This indicates a high-frequency oscillation when the vehicle is left to itself, and this is exactly what we saw earlier in Figure 12-24.
- The remaining 5 eigenvalues seem to be all real (*i.e.*, not complex), and what we will see later is that they are mainly related to altitude (and occasionally velocity). Therefore, we have indicated them by "height modes".
- Apart from one aperiodic eigenmode that is marginally unstable, all eigenmodes have negative real parts and are therefore stable.

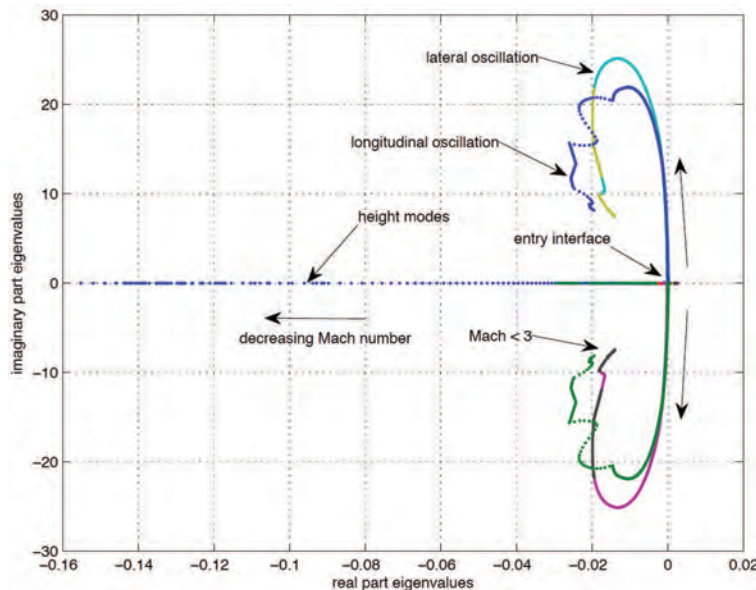


Figure 12-26: Eigenvalues for coupled rotational and translational motion. Evaluation done for discrete time points.

An aid in analyzing the time history of the eigenvalues is to assume that the translational and rotational motion are decoupled, an assumption that usually holds because the translational dynamics are at least an order of magnitude slower than the rotational dynamics. Also, similar to

what we do when analyzing aircraft motion, at first we can assume that the longitudinal and lateral motion are decoupled and verify this later. So, in Figures 12-27 and 12-28 the eigenvalues have been separated for translational and rotational motion. The shown eigenmodes confirm the ones indicated in Figure 12-26.

Additional information that is shown is that for the translational motion there is first an oscillatory height motion, which later separates into two aperiodic modes. Further, one of the aperiodic modes for translational motion is marginally unstable, whereas the height oscillation has a low frequency and is marginally stable. The other height modes are stable, and the damping increases with decreasing Mach number. For the lateral motion, there are also two aperiodic modes that are a combination of bank and height modes. These modes are either poorly damped or slightly unstable, an effect that becomes more apparent with decreasing Mach number. More details will follow from the inspection of the characteristic values.

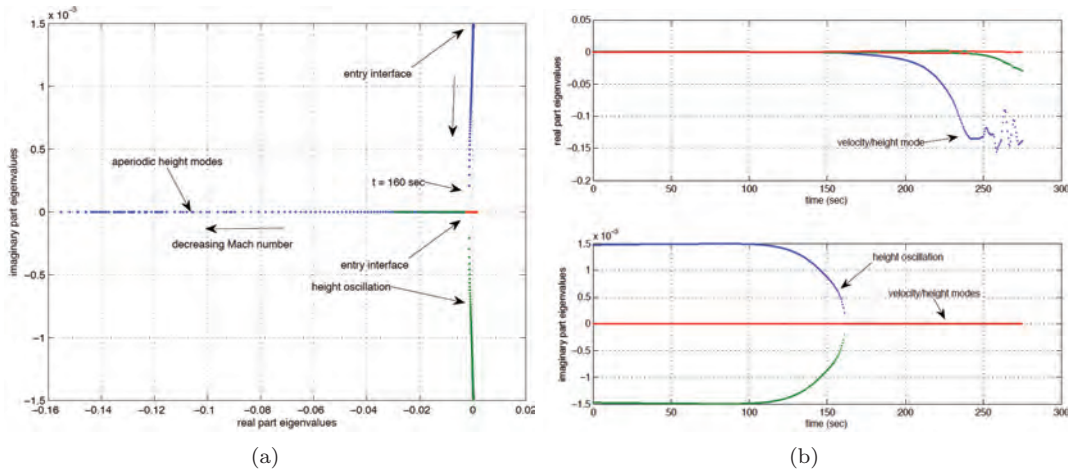


Figure 12-27: Eigenvalues for translational motion. Evaluation done for discrete time points.

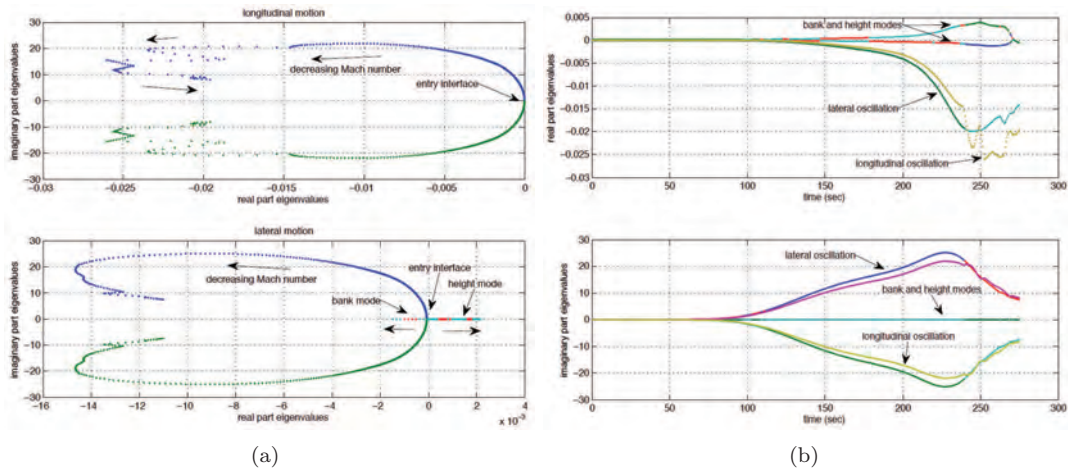


Figure 12-28: Eigenvalues for rotational motion. Evaluation done for discrete time points.

These characteristic values have been calculated for 7 time points ($t = 0, 50, 100, 150, 200, 250$ and 275 s) and are listed, together with eigenvalues and eigenvectors, in Tables 12-11 through 12-17. As we did for HORUS, we have labelled each of the eigenmotions with a name that closely resembles the nature of the eigenmotion. However, as we will see, there will be less relation with the corresponding modes for winged re-entry vehicles (and thus also for conventional aircraft).

We will begin the discussion by looking at the so-called *longitudinal* oscillation. In the tables we have put "longitudinal" between quotes, as it is clear that even though the angle of attack is the driving state in this motion, there is a very strong coupling with the bank angle, and to a lesser extent with the angle of sideslip. Note that this coupling mainly arises from the non-zero bank angle and the inertia coupling. In principle this motion is a combined symmetric and asymmetric motion. However, at the entry interface when the dynamic pressure (and thus the aerodynamic forces and moments) is practically zero, the motion is driven by inertia only so the coupling will not be so apparent. The eigenvalue shows small real and imaginary parts, yielding a period of $P = 885$ s and a very small damping ratio leading to an amplitude half time of about 75,000 (!) s. Effectively this means that the oscillation is indifferent, *i.e.*, undamped.

Gradually, however, with increasing dynamic pressure the aerodynamic moments increase, giving rise to faster oscillations - P decreases to 155 s at $t = 50$ s, 4.3 s at $t = 100$ s to the minimum value of $p = 0.4$ s between $t = 200$ and $t = 250$ s. So the motion becomes very high frequent, and if it were a true longitudinal mode it could possibly be compared with the short-period oscillation of conventional aircraft. However, in the short-period oscillation the velocity is not a "player", contrary to the current eigenmode. From a marginal contribution for $t < 50$ s, ΔV becomes a significant component at $t = 100$ s, and is the second largest component between $t = 200$ s and 250 s, indicating a significant coupling between translational and rotational motion. This coupling also manifests through the coupling with altitude for $t < 100$ s. The coupling with the lateral motion remains active up to $t = 100$ s, after which this coupling reduces to a minor one only. However, close to the end of flight ($t = 275$ s) the coupling is back, whereas the link with the translation motion has disappeared. Throughout the flight the oscillation is damped, although this effect is not so strong; towards the end of the flight the amplitude half time has become $T_{\frac{1}{2}} \approx 35$ s with a maximum damping ratio of $\zeta = 2.4 \cdot 10^{-3}$.

The second oscillatory eigenmode that we will discuss has been labelled *lateral oscillation*. Also here, in the table the "lateral" has been put in quotes, because it is not a "pure" lateral oscillation. In fact, up to $t = 100$ s, the altitude is the dominating state component, representing a strong coupling with a symmetric, translational motion. Also from the beginning, the angle of attack represents a significant component besides the angle of sideslip and bank angle that made us decide to call this mode lateral oscillation. So, also in this case the longitudinal and lateral motion are coupled. At $t = 100$ s, this coupling has disappeared and the yaw rate has popped up to be the main component (together with ΔR). The yaw rate becomes the only main component until the very end of the flight, and only then the angle of sideslip has become a significant contributor. So basically the lateral oscillation is better of being called yaw oscillation. With a little bit of imagination, one might compare this mode with the Dutch roll of conventional aircraft, as the main components are the roll and yaw rate, and the angle of sideslip and bank angle. In terms of period and damping, this mode is comparable to the longitudinal oscillation, slightly better damped (but still marginal) and with a shorter period. The fastest oscillation at $t = 200$ s has a period of $P = 0.3$ s. At $t > 200$ s the damping and period of the longitudinal and lateral oscillation are more or less the same, the former being only slightly better damped.

The third and last oscillation that we need to discuss is the so-called height oscillation, an eigenmode of translational motion that begins right at the entry interface. Initially unstable (again, with a very small negative damping ratio, so effectively indifferent) the real part of the eigenvalue slowly becomes negative (somewhere between $t = 100$ and 150 s) until it reaches its most negative value at $t \approx 160$ s (see also Figure 12-27). This eigenmode is a "pure" height mode, as the only state component involved is ΔR . It is a slow motion with a period P well in excess of 4,000 s. The smallest amplitude half time is at $t = 160$ s and is $T_{\frac{1}{2}} = 994$ s. At $t = 160$ s, the periodic eigenmode splits into two aperiodic height modes. Since there are more aperiodic height modes it becomes difficult to exactly pinpoint those two modes. It seems that the three modes, which have a period of $P_1 = 55.4$ s (stable mode), $P_2 = 509.3$ s (unstable mode) and $P_3 = 550.4$ s (stable mode) at $t = 200$ s are the modes related to translational motion, in particular if we study Figure 12-27. This figure shows the eigenvalues of a decoupled translational motion.

One interesting feature shows itself in these two aperiodic height modes. One of the two modes has both the velocity and the altitude as driving components, and could have been called a phugoid if it were not for the fact that this is an aperiodic mode rather than a periodic one. To distinguish from the height modes we have designated this one the *height/velocity* mode. It is the most stable of the discussed height modes with an amplitude half time reaching a value of as low as 5 s.

To conclude the discussion on height modes related to translational motion, we already mentioned that the third mode is an aperiodic height mode (the last column in each of the tables). This initially (marginally) stable mode becomes slightly unstable at $t = 150$ s, and after the separation of the periodic height mode shows an almost discrete jump in damping (the amplitude half time changes from 3,209 s to 509.3 s at $t = 200$ s). For the remaining part of the flight this mode is marginally unstable. All in all, the height modes are very slow eigenmotions not worth discussing any further.

The last eigenmodes that we discuss consist of a pair of (aperiodic) *bank modes*, one stable and one unstable. These modes begin at $t = 0$ s with only the bank angle as dominating state component. At $t = 50$ s, the height has become the dominating component (note: coupling between rotational and translational motion). Of course, at $t = 0$ the aerodynamic lift is practically zero, so banking would not affect the altitude. When the lift becomes larger, banking results in a smaller lift component in the vertical (symmetry) plane, which *has* an effect on the altitude. After $t = 100$ s the height has, in fact, become the only state component driving these eigenmotions (hence the name change to *height mode*). This is actually strange, since these modes originate from the lateral rotational motion and they have turned into modes linked with translational motion. The height modes also consist of one stable and one unstable mode, and represent (again) a very slow motion, and ultimately one with an amplitude half time almost equal to the flight duration ($T_{\frac{1}{2}} = 267.8$ s).

A final remark on the height modes is that in principle one cannot have a change in height unless there is also a change in velocity, *i.e.*, exchange of potential and kinetic energy. However, most of the time the height modes are so slow that also the velocity change is marginal, although this effect is still there. Only in case of the height/velocity mode with an amplitude half time below 100 s, the motion is fast enough to show. The coupling is a bit weaker towards the end of the flight, even though $T_{\frac{1}{2}} \approx 5$ s. The reason may be that, because the nominal velocity has reduced significantly, the aerodynamic drag (through the dynamic pressure) is also much smaller, and will have less influence on the velocity when the altitude (and thus the density) changes.

In summary, the eigenmotion of the entry capsule presents some fundamental differences with the winged re-entry vehicle discussed earlier. The longitudinal and lateral motion show a stronger coupling, and also include a coupling with the translational motion. These periodic modes are at least an order of magnitude faster compared to the corresponding modes of the winged re-entry vehicle discussed in the previous section, in fact, as fast as the short-period oscillation of conventional aircraft. However, other than the frequency of the oscillation there are no further similarities.

	"longitudinal" oscillation	"lateral" oscillation	bank mode	bank mode	height oscillation	height mode
λ_i Re	-9.2099·10 ⁻⁶	-1.1715·10 ⁻⁴	-4.3878·10 ⁻⁶	1.3114·10 ⁻⁴	3.1900·10 ⁻⁴	-4.9954·10 ⁻⁴
Im	$\pm 7.0963 \cdot 10^{-3}$	$\pm 8.1179 \cdot 10^{-3}$	-	-	$\pm 1.4721 \cdot 10^{-3}$	-
P (s)	885.4	774.0	∞	∞	4,268.1	∞
$T_{\frac{1}{2}}$ (s)	75,261	5,916.5	157,970	5,285.5	2,172.8	1,387.6
ζ (-)	1.2978·10 ⁻³	1.4430·10 ⁻²	-	-	-2.1178·10 ⁻¹	-
ω_n (rad/s)	7.0964·10 ⁻³	8.1188·10 ⁻³	-	-	1.5063·10 ⁻³	-
μ_i	$z \theta$ (°)	$z \theta$ (°)	z	z	$z \theta$ (°)	z
ΔV	0.0013 95.4	0.0009 176.8	0.0019	0.0015	0.0009 166.6	0.0001
$\Delta \gamma$	$< 10^{-4}$ 155.4	$< 10^{-4}$ 92.2	$< 10^{-4}$	$< 10^{-4}$	$< 10^{-4}$ 83.6	$< 10^{-4}$
ΔR	0.2888 70.5	0.8325 0.0	0.4694	0.7547	1.0000 0.0	1.0000
Δp	$< 10^{-4}$ -170.0	0.0002 -81.5	0.0007	$< 10^{-4}$	$< 10^{-4}$ 0.0	$< 10^{-4}$
Δq	0.0050 -89.9	0.0011 -3.3	$< 10^{-4}$	$< 10^{-4}$	$< 10^{-4}$ 0.0	$< 10^{-4}$
Δr	0.0014 -7.7	0.0042 -86.6	$< 10^{-4}$	0.0002	$< 10^{-4}$ 0.0	$< 10^{-4}$
$\Delta \alpha$	0.7006 180.0	0.1340 -94.1	0.0022	0.0022	$< 10^{-4}$ 0.0	$< 10^{-4}$
$\Delta \beta$	0.1598 82.1	0.4848 3.5	0.0012	0.0009	$< 10^{-4}$ 0.0	$< 10^{-4}$
$\Delta \sigma$	0.6327 -7.0	0.2320 145.7	0.8830	0.6561	$< 10^{-4}$ 0.0	$< 10^{-4}$

Table 12-11: Eigenvalues and corresponding characteristic values for time point $t = 0$ s.

	"longitudinal" oscillation	"lateral" oscillation	bank mode	bank mode	height oscillation	height mode
λ_i Re	-3.9798·10 ⁻⁰⁷	-1.2851·10 ⁻⁴	-4.5155·10 ⁻⁶	1.3373·10 ⁻⁴	2.4081·10 ⁻⁴	-3.8067·10 ⁻⁴
Im	$\pm 4.0473 \cdot 10^{-2}$	$\pm 4.5483 \cdot 10^{-2}$	-	-	$\pm 1.4881 \cdot 10^{-3}$	-
P (s)	155.3	138.2	∞	∞	4,222.3	∞
$T_{\frac{1}{2}}$ (s)	1,741,700	5,393.9	153,500	5,183.1	2,878.4	1,820.9
ζ (-)	9.8333·10 ⁻⁶	2.8254·10 ⁻³	-	-	-1.5975·10 ⁻¹	-
ω_n (rad/s)	4.0473·10 ⁻²	4.5483·10 ⁻²	-	-	1.5074·10 ⁻³	-
μ_i	$z \theta$ (°)	$z \theta$ (°)	z	z	$z \theta$ (°)	z
ΔV	0.0088 -89.6	0.0010 -0.6	0.0035	0.0019	0.0009 169.5	0.0001
$\Delta \gamma$	$< 10^{-4}$ -52.1	$< 10^{-4}$ -89.7	$< 10^{-4}$	$< 10^{-4}$	$< 10^{-4}$ 84.9	$< 10^{-4}$
ΔR	0.0731 -129.7	0.8395 180.0	0.9986	1.0000 0.0	1.0000 0.0	1.0000
Δp	$< 10^{-4}$ 29.3	0.0010 91.5	$< 10^{-4}$	$< 10^{-4}$	$< 10^{-4}$ 0.0	$< 10^{-4}$
Δq	0.0297 90.0	0.0012 179.0	$< 10^{-4}$	$< 10^{-4}$	$< 10^{-4}$ 0.0	$< 10^{-4}$
Δr	0.0017 178.4	0.0243 90.5	$< 10^{-4}$	$< 10^{-4}$	$< 10^{-4}$ 0.0	$< 10^{-4}$
$\Delta \alpha$	0.7332 0.0	0.0275 88.9	$< 10^{-4}$	$< 10^{-4}$	$< 10^{-4}$ 0.0	$< 10^{-4}$
$\Delta \beta$	0.0332 -91.6	0.4999 -179.5	$< 10^{-4}$	$< 10^{-4}$	$< 10^{-4}$ 0.0	$< 10^{-4}$
$\Delta \sigma$	0.6745 178.6	0.2097 -7.5	0.0522	0.0284	$< 10^{-4}$ 0.0	$< 10^{-4}$

Table 12-12: Eigenvalues and corresponding characteristic values for time point $t = 50$ s.

	"longitudinal" oscillation	lateral oscillation	height mode	height mode	height oscillation	height mode
λ_i Re	-1.4960·10 ⁻⁵	-1.5326·10 ⁻⁴	-4.8072·10 ⁻⁶	1.4592·10 ⁻⁴	1.4339·10 ⁻⁴	-2.3837·10 ⁻⁴
Im	± 1.4492	1.6539	-	-	$\pm 1.4875 \cdot 10^{-3}$	-
P (s)	4.3	3.8	∞	∞	4,224.0	∞
$T_{\frac{1}{2}}$ (s)	46,333.0	4,522.8	144,190	4,750.2	4,834.1	2,907.9
ζ (-)	1.0323·10 ⁻⁵	9.2665·10 ⁻⁵	-	-	-9.5951·10 ⁻²	-
ω_n (rad/s)	1.4492	1.6539	-	-	1.4944·10 ⁻³	-
μ_i	$z \theta$ (°)	$z \theta$ (°)	z	z	$z \theta$ (°)	z
ΔV	0.2252 -180.0	0.0008 -90.0	0.0030	0.0015	0.0009 173.7	$< 10^{-4}$
$\Delta \gamma$	$< 10^{-4}$ -178.9	0.0001 180.0	$< 10^{-4}$	$< 10^{-4}$	$< 10^{-4}$ 86.9	$< 10^{-4}$
ΔR	0.0404 91.3	0.6478 90.0	1.0000	1.0000	1.0000 0.0	1.0000
Δp	$< 10^{-4}$ -90.0	0.0264 0.0	$< 10^{-4}$	$< 10^{-4}$	$< 10^{-4}$ 0.0	$< 10^{-4}$
Δq	0.7116 0.0	0.0008 90.0	$< 10^{-4}$	$< 10^{-4}$	$< 10^{-4}$ 0.0	$< 10^{-4}$
Δr	0.0010 90.0	0.6488 0.0	$< 10^{-4}$	$< 10^{-4}$	$< 10^{-4}$ 0.0	$< 10^{-4}$
$\Delta \alpha$	0.4910 -90.0	0.0005 -0.0	$< 10^{-4}$	$< 10^{-4}$	$< 10^{-4}$ 0.0	$< 10^{-4}$
$\Delta \beta$	0.0005 180.0	0.3640 90.0	$< 10^{-4}$	$< 10^{-4}$	$< 10^{-4}$ 0.0	$< 10^{-4}$
$\Delta \sigma$	0.4473 90.0	0.1618 -90.2	$< 10^{-4}$	$< 10^{-4}$	$< 10^{-4}$ 0.0	$< 10^{-4}$

Table 12-13: Eigenvalues and corresponding characteristic values for time point $t = 100$ s.

	"longitudinal" oscillation		lateral oscillation	height mode	height mode	height oscillation	height mode
λ_i Re	-7.8191·10 ⁻⁴		-1.1030·10 ⁻³	-1.3343·10 ⁻⁵	2.2203·10 ⁻⁴	-6.9734·10 ⁻⁴	2.1600·10 ⁻⁴
Im	$\pm 1.0113 \cdot 10^1$		1.1589·10 ¹	-	-	$\pm 8.6942 \cdot 10^{-4}$	-
P (s)	0.6213		0.5422	∞	∞	7,226.8	∞
$T_{\frac{1}{2}}$ (s)	886.5		628.4	51,947.0	3,121.8	994.0	3,209.0
ζ (-)	7.7314·10 ⁻⁵		9.5176·10 ⁻⁵	-	-	6.2568·10 ⁻¹	-
ω_n (rad/s)	1.0113·10 ¹		1.1589·10 ¹	-	-	1.1145·10 ⁻³	-
μ_i	$z \theta$ (°)	$z \theta$ (°)	$z \theta$ (°)	z	z	$z \theta$ (°)	z
ΔV	0.3035 -180.0	0.0002	-90.0	0.0001	0.0002	0.0009 -114.1	0.0002
$\Delta \gamma$	$< 10^{-4}$ -179.8	0.0002	180.0	$< 10^{-4}$	$< 10^{-4}$	$< 10^{-4}$ 130.1	$< 10^{-4}$
ΔR	0.0091 90.2	0.1410 90.0		1.0000	1.0000	1.0000 0.0	bf 1.0000
Δp	$< 10^{-4}$ -90.1	0.0400 0.0	$< 10^{-4}$	$< 10^{-4}$	$< 10^{-4}$	$< 10^{-4}$ 0.0	$< 10^{-4}$
Δq	0.9444 0.0	0.0002	90.0	$< 10^{-4}$	$< 10^{-4}$	$< 10^{-4}$ 0.0	$< 10^{-4}$
Δr	0.0002 90.0	0.9854 0.0	$< 10^{-4}$	$< 10^{-4}$	$< 10^{-4}$	$< 10^{-4}$ 0.0	$< 10^{-4}$
$\Delta \alpha$	0.0934 -90.0	$< 10^{-4}$ -0.0	$< 10^{-4}$	$< 10^{-4}$	$< 10^{-4}$	$< 10^{-4}$ 0.0	$< 10^{-4}$
$\Delta \beta$	$< 10^{-4}$ 180.0	0.0787 90.0	$< 10^{-4}$	$< 10^{-4}$	$< 10^{-4}$	$< 10^{-4}$ 0.0	$< 10^{-4}$
$\Delta \sigma$	0.0848 90.0	0.0355	-90.0	$< 10^{-4}$	$< 10^{-4}$	$< 10^{-4}$ 0.0	$< 10^{-4}$

Table 12-14: Eigenvalues and corresponding characteristic values for time point $t = 150$ s.

	"longitudinal" oscillation		lateral oscillation	height mode	height mode	height/velocity mode	height mode	height mode
λ_i Re	-3.1788·10 ⁻³		-4.1027·10 ⁻³	-2.4495·10 ⁻⁶	4.8550·10 ⁻⁴	-1.2517·10 ⁻²	-1.2593·10 ⁻³	1.3609·10 ⁻³
Im	$\pm 1.7019 \cdot 10^1$		$\pm 1.9502 \cdot 10^1$	-	-	-	-	-
P (s)	0.4		0.3	∞	∞	∞	∞	509.3
$T_{\frac{1}{2}}$ (s)	218.1		169.0	282,970	1,427.7	55.4	550.4	
ζ (-)	1.8678·10 ⁻⁴		2.1037·10 ⁻⁴	-	-	-	-	-
ω_n (rad/s)	1.7019·10 ¹		1.9502·10 ¹	-	-	-	-	-
μ_i	$z \theta$ (°)	$z \theta$ (°)	$z \theta$ (°)	z	z	z	z	z
ΔV	0.3051 -180.0	0.0001	90.0	$< 10^{-4}$	0.0001	0.3605	0.0001	0.0001
$\Delta \gamma$	$< 10^{-4}$ -179.9	0.0002	0.0	$< 10^{-4}$	$< 10^{-4}$	$< 10^{-4}$	$< 10^{-4}$	$< 10^{-4}$
ΔR	0.0051 90.1	0.0826 -90.0		1.0000	1.0000	0.9328 1.0000		1.0000
Δp	$< 10^{-4}$ -90.1	0.0404	-180.0	$< 10^{-4}$	$< 10^{-4}$	$< 10^{-4}$	$< 10^{-4}$	$< 10^{-4}$
Δq	0.9493 0.0	0.0001	-90.0	$< 10^{-4}$	$< 10^{-4}$	$< 10^{-4}$	$< 10^{-4}$	$< 10^{-4}$
Δr	0.0001 90.0	0.9944 180.0		$< 10^{-4}$	$< 10^{-4}$	$< 10^{-4}$	$< 10^{-4}$	$< 10^{-4}$
$\Delta \alpha$	0.0558 -90.0	$< 10^{-4}$ 180.0	$< 10^{-4}$	$< 10^{-4}$	$< 10^{-4}$	$< 10^{-4}$	$< 10^{-4}$	$< 10^{-4}$
$\Delta \beta$	$< 10^{-4}$ 180.0	0.0472 -90.0	$< 10^{-4}$	$< 10^{-4}$	$< 10^{-4}$	$< 10^{-4}$	$< 10^{-4}$	$< 10^{-4}$
$\Delta \sigma$	0.0507 90.0	0.0213	89.9	$< 10^{-4}$	$< 10^{-4}$	$< 10^{-4}$	$< 10^{-4}$	$< 10^{-4}$

Table 12-15: Eigenvalues and corresponding characteristic values for time point $t = 200$ s.

	"longitudinal" oscillation		lateral oscillation	height mode	height mode	height/velocity mode	height mode	height mode
λ_i Re	-1.9744·10 ⁻²		-1.9696·10 ⁻²	2.6770·10 ⁻⁴	2.5881·10 ⁻³	-1.3210·10 ⁻¹	-4.6706·10 ⁻³	5.6919·10 ⁻⁴
Im	$\pm 1.5534 \cdot 10^1$		$\pm 1.5936 \cdot 10^1$	-	-	-	-	-
P (s)	0.4		0.4	∞	∞	∞	∞	
$T_{\frac{1}{2}}$ (s)	35.1		35.2	2,589.2	267.8	5.2	148.4	1,217.8
ζ (-)	1.2710·10 ⁻³		1.2359·10 ⁻³	-	-	-	-	-
ω_n (rad/s)	1.5534·10 ¹		1.5936·10 ¹	-	-	-	-	-
μ_i	$z \theta$ (°)	$z \theta$ (°)	$z \theta$ (°)	z	z	z	z	z
ΔV	0.1810 0.5	0.0008	90.4	$< 10^{-4}$	0.0002	0.3071	0.0004	0.0001
$\Delta \gamma$	0.0001 -0.2	0.0008	0.0	$< 10^{-4}$	$< 10^{-4}$	$< 10^{-4}$	$< 10^{-4}$	$< 10^{-4}$
ΔR	0.0002 -111.1	0.0460 -90.1		1.0000	1.0000	0.9517 1.0000		1.0000
Δp	0.0001 90.1	0.0411 -179.8		$< 10^{-4}$	$< 10^{-4}$	$< 10^{-4}$	$< 10^{-4}$	$< 10^{-4}$
Δq	0.9797 180.0	0.0021	-90.1	$< 10^{-4}$	$< 10^{-4}$	$< 10^{-4}$	$< 10^{-4}$	$< 10^{-4}$
Δr	0.0002 -91.8	0.9961 180.0		$< 10^{-4}$	$< 10^{-4}$	$< 10^{-4}$	$< 10^{-4}$	$< 10^{-4}$
$\Delta \alpha$	0.0631 90.1	0.0001	180.0	$< 10^{-4}$	$< 10^{-4}$	$< 10^{-4}$	$< 10^{-4}$	$< 10^{-4}$
$\Delta \beta$	$< 10^{-4}$ -8.0	0.0595 -90.0		$< 10^{-4}$	$< 10^{-4}$	$< 10^{-4}$	$< 10^{-4}$	$< 10^{-4}$
$\Delta \sigma$	0.0591 -90.1	0.0217	89.4	$< 10^{-4}$	$< 10^{-4}$	$< 10^{-4}$	$< 10^{-4}$	$< 10^{-4}$

Table 12-16: Eigenvalues and corresponding characteristic values for time point $t = 250$ s.

	"longitudinal" oscillation	lateral oscillation	height mode	height mode	height/velocity mode	height mode	height mode
λ_i	Re	$-1.9600 \cdot 10^{-2}$	$-1.4059 \cdot 10^{-2}$	$1.1446 \cdot 10^{-4}$	$-1.3974 \cdot 10^{-3}$	$-1.3847 \cdot 10^{-1}$	$-2.9344 \cdot 10^{-2}$
Im	± 8.1447	± 7.4652	-	-	-	-	-
P (s)	0.8	0.8	∞	∞	∞	∞	∞
$T_{\frac{1}{2}}$ (s)	35.4	49.3	6,055.6	496.0	5.0	23.6	11,939.0
ζ (-)	$2.4064 \cdot 10^{-3}$	$1.8833 \cdot 10^{-3}$	-	-	-	-	-
ω_n (rad/s)	8.1448	7.4652	-	-	-	-	-
μ_i	z	θ (°)	z	θ (°)	z	z	z
ΔV	0.0544	-178.8	0.0012	-89.0	$< 10^{-4}$	0.0003	0.1559
$\Delta \gamma$	0.0002	178.8	0.0010	-179.8	$< 10^{-4}$	$< 10^{-4}$	0.0001
ΔR	0.0002	-10.3	0.0267	89.8	1.0000	1.0000	1.0000
Δp	0.0002	-90.0	0.0439	-179.7	$< 10^{-4}$	$< 10^{-4}$	$< 10^{-4}$
Δq	0.9845	0.0	0.0043	89.3	$< 10^{-4}$	$< 10^{-4}$	$< 10^{-4}$
Δr	0.0024	89.4	0.9896	180.0	$< 10^{-4}$	$< 10^{-4}$	$< 10^{-4}$
$\Delta \alpha$	0.1209	-89.9	0.0006	-0.5	$< 10^{-4}$	$< 10^{-4}$	$< 10^{-4}$
$\Delta \beta$	0.0003	179.4	0.1278	-89.9	$< 10^{-4}$	$< 10^{-4}$	$< 10^{-4}$
$\Delta \sigma$	0.1149	89.5	0.0412	90.3	$< 10^{-4}$	$< 10^{-4}$	$< 10^{-4}$

Table 12-17: Eigenvalues and corresponding characteristic values for time point $t = 275$ s.

Appendix A

List of Symbols

Roman Symbols

a	Speed of sound
A	Center of the Earth, origin of F_I
A	Wing aspect ratio
b	Wing span
b_f	Local fuselage width
B	Moment of momentum, angular momentum
c	Local wing chord
c_f	Wing chord flap
$c_{a,e,r,t}$	Chord of aileron, elevator, rudder or tab, behind hinge line
c_r	Chord length in the plane of symmetry
c_t	Chord length at wing tip
c_m	Mean wing chord (Eng. notation: \bar{c})
\bar{c}	Mean aerodynamic chord (English notation: \bar{c})
$\bar{c}_{w,h,v}$	Mean aerodynamic chord of wing, horizontal tailplane, or vertical tailplane
$\bar{c}_{a,e,r,t}$	Mean aerodynamic chord of control surfaces and tabs, behind hinge line
c_d	Drag coefficient two-dimensional flow
CFD	Computational Fluid Dynamics
C_D	Drag coefficient three-dimensional flow
$c.g.$	Center of gravity

C_{h_e}	Hinge moment coefficient of the elevator. The indices a, r or t are used to indicate the hinge moment coefficients of the aileron, the rudder or a tab respectively	$\left[= \frac{H_e}{\frac{1}{2}\rho V_h^2 S_e \bar{c}_e} \right]$
C_{h_α}		$\left[= \frac{\partial C_h}{\partial \alpha_{a,h,v}} \right]$
C_{h_δ}		$\left[= \frac{\partial C_h}{\partial \delta_{a,e,r}} \right]$
$C_{h_{\delta_t}}$		$\left[= \frac{\partial C_h}{\partial \delta_{t_{a,e,r}}} \right]$
c_ℓ		$\left[= \frac{\ell}{\frac{1}{2}\rho V^2 \bar{c}} \right]$
C_ℓ		$\left[= \frac{L}{\frac{1}{2}\rho V^2 S_b} \right]$
C_L		$\left[= \frac{L}{\frac{1}{2}\rho V^2 S} \right]$
c_{ℓ_a}	Coefficient of the additional lift distribution	
c_{ℓ_b}	Coefficient of the basic lift distribution	
c_{ℓ_α}	Derivative of the lift-coefficient with respect to angle of attack, two-dimensional flow	$\left[= \frac{dc_\ell}{d\alpha} \right]$
C_{L_α}	Derivative of the lift-coefficient with respect to angle of attack, three-dimensional flow	$\left[= \frac{dC_L}{d\alpha} \right]$
C_{ℓ_e}	Coefficient of the rolling moment due to one inoperative engine	
C_{ℓ_p}		$\left[= \frac{\partial C_\ell}{\partial \frac{pb}{2V}} \right]$
C_{ℓ_r}		$\left[= \frac{\partial C_\ell}{\partial \frac{rb}{2V}} \right]$
C_{ℓ_β}		$\left[= \frac{\partial C_\ell}{\partial \beta} \right]$
$C_{\ell_{\delta_a}}$		$\left[= \frac{\partial C_\ell}{\partial \delta_a} \right]$
$C_{\ell_{\delta_r}}$		$\left[= \frac{\partial C_\ell}{\partial \delta_r} \right]$
c_m	Coefficient of the aerodynamic moment about the Y -axis, two-dimensional flow	$\left[= \frac{m}{\frac{1}{2}\rho V^2 c^2} \right]$
C_m	Coefficient of the aerodynamic moment about the Y -axis, three-dimensional flow	$\left[= \frac{M}{\frac{1}{2}\rho V^2 S \bar{c}} \right]$
$c_{m_{a.c.}}$	Coefficient of the moment about the aerodynamic center, two-dimensional flow	$= c_{m_0}$
$C_{m_{a.c.}}$	Coefficient of the moment about the aerodynamic center, three-dimensional flow	

C_{m_h}	Contribution of the horizontal tailplane to C_m	
C_{m_q}		$\left[= \frac{\partial C_m}{\partial \frac{qc}{V}} \right]$
C_{m_u}		$\left[= \frac{1}{\frac{1}{2}\rho V S \bar{c}} \frac{\partial M}{\partial u} \right]$
C_{m_w}	contribution of the wing with fuselage and nacelles to C_m	
C_{m_0}	C_m at $C_L = \delta_e = 0$	
$C_{m_{\alpha fix}}$	$\frac{\partial C_m}{\partial \alpha}$ at $\delta_e = \text{constant}$	
$C_{m_{\alpha free}}$	$\frac{\partial C_m}{\partial \alpha}$ at $F_e = 0$	
$C_{m_{\dot{\alpha}}}$		$\left[= \frac{\partial C_m}{\partial \frac{\dot{\alpha} \bar{c}}{V}} \right]$
$C_{m_{\beta^2}}$		$\left[= \frac{\partial C_m}{\partial \beta^2} \right]$
C_{m_δ}	Elevator efficiency	$\left[= \frac{\partial C_m}{\partial \delta_e} \right]$
c_n	Normal force coefficient, two-dimensional flow	$\left[= \frac{n}{\frac{1}{2}\rho V^2 c} \right]$
C_n	Yawing moment coefficient	$\left[= \frac{N}{\frac{1}{2}\rho V^2 S b} \right]$
C_N	Normal force coefficient, three-dimensional flow	$\left[= \frac{N}{\frac{1}{2}\rho V^2 S} \right]$
C_{n_e}	Yawing moment coefficient due to one inoperative engine	
C_{n_p}		$\left[= \frac{\partial C_n}{\partial \frac{pb}{2V}} \right]$
C_{n_r}		$\left[= \frac{\partial C_n}{\partial \frac{rb}{2V}} \right]$
C_{n_β}	Static directional stability	$\left[= \frac{\partial C_n}{\partial \beta} \right]$
$C_{n_{\delta_a}}$		$\left[= \frac{\partial C_n}{\partial \delta_a} \right]$
$C_{n_{\delta_r}}$		$\left[= \frac{\partial C_n}{\partial \delta_r} \right]$
C_{N_h}	Normal force coefficient of the horizontal tailplane	$\left[= \frac{N_h}{\frac{1}{2}\rho V_h^2 S_h} \right]$
$C_{N_{h_0}}$	C_{N_h} at $\alpha_h = \delta_e = \delta_{t_e} = 0$	
$C_{N_{h_\alpha}}$		$\left[= \frac{\partial C_{N_h}}{\partial \alpha_h} \right]$
$C_{N_{h_\delta}}$		$\left[= \frac{\partial C_{N_h}}{\partial \delta_e} \right]$
$C_{N_{h_{\delta_t}}}$		$\left[= \frac{\partial C_{N_h}}{\partial \delta_{t_e}} \right]$

C_{N_p}	Normal force coefficient on the propeller	$\left[= \frac{N_p}{\frac{1}{2}\rho V^2 S_p} \right]$
C_{N_w}	Coefficient of the normal force on the wing with fuselage and nacelles	$\left[= \frac{N_w}{\frac{1}{2}\rho V^2 S} \right]$
c_r	Coefficient of the resultant aerodynamic force, two-dimensional flow	$\left[= \frac{r}{\frac{1}{2}\rho V^2 \bar{c}} \right]$
C_R	Coefficient of the resultant aerodynamic force, three-dimensional flow	$\left[= \frac{R}{\frac{1}{2}\rho V^2 S} \right]$
c_t	Coefficient of the tangential force, two-dimensional flow	$\left[= \frac{t}{\frac{1}{2}\rho V^2 \bar{c}} \right]$
C_T	Coefficient of the tangential force, three-dimensional flow	$\left[= \frac{T}{\frac{1}{2}\rho V^2 S} \right]$
C_{T_h}	Coefficient of the tangential force of the horizontal tailplane	$\left[= \frac{T_h}{\frac{1}{2}\rho V_h^2 S_h} \right]$
C_{T_w}	Coefficient of the tangential force on the wing with fuselage and nacelles	$\left[= \frac{T_w}{\frac{1}{2}\rho V^2 S} \right]$
C_X		$\left[= \frac{X}{\frac{1}{2}\rho V^2 S} \right]$
C_{X_q}		$\left[= \frac{\partial C_X}{\partial \frac{q\bar{c}}{V}} \right]$
C_{X_u}		$\left[= \frac{1}{\frac{1}{2}\rho V S} \frac{\partial X}{\partial u} \right]$
C_{X_0}	C_X in steady flight	
C_{X_α}		$\left[= \frac{\partial C_X}{\partial \alpha} \right]$
$C_{X_{\delta_e}}$		$\left[= \frac{\partial C_X}{\partial \delta_e} \right]$
C_Y		$\left[= \frac{Y}{\frac{1}{2}\rho V^2 S} \right]$
C_{Y_p}		$\left[= \frac{\partial C_Y}{\partial \frac{pb}{2V}} \right]$
C_{Y_r}		$\left[= \frac{\partial C_Y}{\partial \frac{rb}{2V}} \right]$
C_{Y_β}		$\left[= \frac{\partial C_Y}{\partial \beta} \right]$
$C_{Y_{\delta_a}}$		$\left[= \frac{\partial C_Y}{\partial \delta_a} \right]$
$C_{Y_{\delta_r}}$		$\left[= \frac{\partial C_Y}{\partial \delta_r} \right]$

C_Z	$\left[= \frac{Z}{\frac{1}{2}\rho V^2 S} \right]$
C_{Z_q}	$\left[= \frac{\partial C_Z}{\partial \frac{q\bar{c}}{V}} \right]$
C_{Z_u}	$\left[= \frac{1}{\frac{1}{2}\rho VS} \frac{\partial Z}{\partial u} \right]$
C_{Z_0}	C_Z in steady flight
C_{Z_α}	$\left[= \frac{\partial C_Z}{\partial \alpha} \right]$
$C_{Z_{\dot{\alpha}}}$	$\left[= \frac{\partial C_Z}{\partial \frac{\dot{\alpha}\bar{c}}{V}} \right]$
$C_{Z_{\delta_e}}$	$\left[= \frac{\partial C_Z}{\partial \delta_e} \right]$
$C_{\frac{1}{2}}$	$\left[= \frac{T_{\frac{1}{2}}}{P} \right]$
d	Characteristic diameter of a jet engine
d	Drag, two-dimensional flow
D	Diameter of a propeller
D	Drag, three-dimensional flow
D	differential operator
D^2	
D_b	Non-dimensional differential operator, asymmetric motions
D_c	Non-dimensional differential operator, symmetric motions
e	Base of the natural logarithms
e	Distance of the center of pressure of a profile behind the leading edge
$F_{a,e,r}$	Aileron, elevator or rudder control force exerted by the pilot
G	Vehicle (aircraft) center of mass
h	Altitude
H_e	Hinge moment about the elevator hinge line, subscripts a, e, r indicate the aileron, elevator or rudder respectively
H_{a,e,r_a}	Aerodynamic hinge moment
H_{a,e,r_f}	Hinge moment due to friction in the control mechanism
H_{a,e,r_s}	Hinge moment due to a spring in the control mechanism
H_{a,e,r_w}	Hinge moment due to static unbalance of the control mechanism
	$\left[= C_{h_e} \frac{1}{2} \rho V_h^2 S_e \bar{c}_e \right]$

\underline{i}	Unit vector along the X -axis	
$i_{h,p}$	Angle of incidence of the horizontal tail or the propeller axis, relative to the X_m -axis	
I_x	Moment of inertia about the X-axis	$\left[= \int (y^2 + z^2) dm \right]$
I_{x_0}	Principle moment of inertia	
I_y	Moment of inertia about the Y-axis	$\left[= \int (x^2 + z^2) dm \right]$
I_{y_0}	Principle moment of inertia	
I_z	Moment of inertia about the Z-axis	$\left[= \int (x^2 + y^2) dm \right]$
I_{z_0}	Principle moment of inertia	
\underline{j}	Unit vector along the Y -axis	
J_{xy}	Product of inertia	$\left[= \int xy dm \right]$
J_{xz}	Product of inertia	$\left[= \int xz dm \right]$
J_{yz}	Product of inertia	$\left[= \int yz dm \right]$
k	Factor related to the variation of thrust with speed	
\underline{k}	Unit vector along the Z -axis	
k_x	Radius of gyration about the X-axis	$\left[= \sqrt{\frac{I_x}{m}} \right]$
k_y	Radius of gyration about the Y-axis	$\left[= \sqrt{\frac{I_y}{m}} \right]$
k_z	Radius of gyration about the Z-axis	$\left[= \sqrt{\frac{I_z}{m}} \right]$
k_{xz}		$\left[= \frac{J_{xz}}{m} \right]$
K_X	Non-dimensional radius of gyration about the X -axis	$\left[= \frac{k_x}{b} \right]$
K_Y	Non-dimensional radius of gyration about the Y -axis	$\left[= \frac{k_y}{b} \right]$
K_Z	Non-dimensional radius of gyration about the Z -axis	$\left[= \frac{k_z}{b} \right]$
K_{XZ}	Non-dimensional product of inertia	$\left[= \frac{k_{xz}}{b^2} \right]$
ℓ	Lift, two-dimensional flow	$\left[= c\ell \frac{1}{2} \rho V^2 c \right]$
l_f	Fuselage length	
l_h	Tail length, horizontal tail	$\left[= x_h - x_w \right]$
l_v	Tail length, vertical tail	
l_w	Length of the fuselage ahead of the wing	$\left[= x_v - x_w \right]$
LTI	Linear Time Invariant	

L	Rolling moment about the X -axis	$\left[= C_\ell \frac{1}{2} \rho V^2 S b \right]$
L	Lift, three-dimensional flow	$\left[= C_L \frac{1}{2} \rho V^2 S \right]$
L_g	Longitude	
L_t	Latitude	
m	Aerodynamic moment about the Y -axis, two-dimensional flow	$\left[= c_m \frac{1}{2} \rho V^2 c^2 \right]$
m	Mass	
mac	Mean aerodynamic chord	$[= \bar{c}]$
$m.p.$	Manoeuvre point	
M	Moment about the Y -axis, three-dimensional flow	$\left[= C_m \frac{1}{2} \rho V^2 S c \right]$
M	Mach number	$\left[= \frac{a}{V} \right]$
$\underline{M}, \mathcal{M}$	Total moment	
n	Normal force, two-dimensional flow	$\left[= c_n \frac{1}{2} \rho V^2 c \right]$
$n.p.$	Neutral point	
N	Normal force, three-dimensional flow	$\left[= C_N \frac{1}{2} \rho V^2 S \right]$
N	Yawing moment about the Z -axis	$\left[= C_n \frac{1}{2} \rho V^2 S b \right]$
N_h	Normal force on the horizontal tailplane	$\left[= C_{N_h} \frac{1}{2} \rho V_h^2 S_h \right]$
N_p	Normal force on the propeller	$\left[= C_{N_p} \frac{1}{2} \rho V^2 S_p \right]$
N_w	Normal force on the wing with fuselage and nacelles	$\left[= C_{N_w} \frac{1}{2} \rho V^2 S \right]$
O	Origin reference frames F_E and F_O	
p	Static pressure	
\dot{p}	Angular velocity about the X -axis	
P_0	Static pressure in undisturbed flow	
P	Period of an oscillation	
q	Dynamic pressure	$\left[= \frac{1}{2} \rho V^2 \right]$
\dot{q}	Angular velocity about the Y -axis	
r	Angular velocity about the Z -axis	
$\underline{r}, \mathbf{r}$	Vector indicating a position	
r	Resultant aerodynamic force, two-dimensional flow	$\left[= c_r \frac{1}{2} \rho V^2 c \right]$
R	Resultant aerodynamic force, three-dimensional flow	$\left[= C_R \frac{1}{2} \rho V^2 S \right]$
R	Routh's discriminant	
Re	Reynolds number	
$s_{a,e,r}$	Pilot's control deflection; aileron, elevator or rudder control respectively	

s_b	Non-dimensional parameter of time, asymmetric motions	$\left[= \frac{V}{b}t \right]$
s_c	Non-dimensional parameter of time, symmetric motions	$\left[= \frac{V}{\bar{c}}t \right]$
S	Wing area	
S_a	Area of one aileron, behind hinge line	
$S_{e,r,t}$	Area of elevator, rudder or tab respectively, behind hinge line	
$S_{h,v}$	Area of horizontal or vertical tailplane	
S_p	Area of the propeller disk	$\left[= \frac{\pi}{4}D^2 \right]$
t	Time	
t	Tangential force, two-dimensional flow	$\left[= c_t \frac{1}{2} \rho V^2 c \right]$
T	Tangential force, three-dimensional flow	$\left[= C_T \frac{1}{2} \rho V^2 S \right]$
T_c	Thrust coefficient of a propeller	$\left[= \frac{T_p}{\rho V^2 D^2} \right]$
T_c	Thrust coefficient of a jet engine	$\left[= \frac{T_p}{\frac{1}{2} \rho V^2 d^2} \right]$
T'_c	Thrust coefficient	$\left[= \frac{T_p}{\frac{1}{2} \rho V^2 S} \right]$
T_h	Tangential force on the horizontal tailplane	
T_w	Tangential force on the wing with fuselage and nacelles	
$T_{\frac{1}{2}}$	Time to damp to half amplitude	
T_2	Time to double amplitude	$\left[= -T_{\frac{1}{2}} \right]$
\hat{u}		$\left[= \frac{du}{V_0} \right]$
u	Component of \underline{V} along the X -axis	
$\Delta u, u$	Change in the component of V along the X -axis	
v	Component of \underline{V} along the Y -axis	
$\underline{V}, \mathbf{V}$	Velocity vector	
$\Delta v, v$	Change in the component of V along the Y -axis	
V	Magnitude of the airspeed vector \underline{V}	
\mathbf{V}_a	Aerodynamic velocity vector, velocity relative to a particle in the undisturbed air	
V_e	equivalent airspeed	
$V_{m.c.}$	Minimum control speed	
V_{trim}	Trimmed airspeed, V at which $F_e = 0$	
\mathbf{V}_k	Kinematic velocity vector, velocity relative to the normal Earth-fixed reference frame	
w	Component of \underline{V} along the Z -axis	
$\Delta w, w$	Change in the component of V along the Z -axis	
W	Aircraft weight	

x	x -coordinate, abscissa	
$x_{a.c.}$	Abscissa of the a.c. of the wing	
$x_{c.g.}$	Abscissa of the c.g.	
x_d	Abscissa of the center of pressure	
x_h	Abscissa of the a.c. of the horizontal tailplane	
$x_{m_{free}}$	Abscissa of the manoeuvre point, stick free	
$x_{m_{fixed}}$	Abscissa of the manoeuvre point, stick fixed	
$x_{n_{free}}$	Abscissa of the neutral point, stick free	
$x_{n_{fixed}}$	Abscissa of the neutral point, stick fixed	
x_p	Abscissa of the center of the propeller disk	
x_v	Abscissa of the a.c. of the vertical tailplane	
x_w	Abscissa of the a.c. of the wing with fuselage and nacelles	
x_0	Abscissa of the leading edge of the mac	
X	Component of the total aerodynamic force along the X -axis	$\left[= C_X \frac{1}{2} \rho V^2 S \right]$
y	y -coordinate, ordinate	
Y	Component of the total aerodynamic force along the Y -axis, lateral force	$\left[= C_Y \frac{1}{2} \rho V^2 S \right]$
z	z -coordinate	
z_h	z -coordinate of the a.c. of the horizontal tailplane	
z_p	z -coordinate of the center of the propeller disk	
z_v	z -coordinate of the a.c. of the vertical tailplane	
z_w	z -coordinate of the a.c. of the wing with fuselage and nacelles	
z_0	z -coordinate of the leading edge of the m.a.c.	
Z	component of the total aerodynamic force along the Z -axis	$\left[= C_Z \frac{1}{2} \rho V^2 S \right]$

Greek Symbols

α	angle of attack	
α_0	angle of attack of the X_a -axis at $C_L = 0$	
α_0	angle of attack in steady flight	
$\alpha_{h,v,w}$	angle of attack of the horizontal or vertical tailplane or the wing	
β	angle of sideslip	
γ	flight path angle, angle between \underline{V} , relative to the earth, and the horizontal plane	
γ_0	flight path angle in steady flight	
Γ	dihedral, angle between the Y_r -axis and the projection of the $\frac{1}{4}$ -chord line on the Y_rOZ_r -plane	
Γ_e	effective dihedral	
δ	logarithmic decrement	
δ_a	Total aileron deflection	
$\delta_{a_r}, \delta_{a_\ell}$	deflection of the right or left aileron	$[= \delta_{a_r} - \delta_{a_\ell}]$
δ_e	elevator deflection	
δ_f	flap deflection	
δ_r	rudder deflection	
δ_s	spoiler deflection	
δ_t	deflection of a trim tab	
ε	wing twist or washout angle	
ε	downwash angle, usually at the horizontal tailplane	
ε	angle between the X_r -axis and the principal inertial X -axis	
ζ	damping ratio of an oscillation	
η	propeller efficiency	
η	imaginary part of a complex eigenvalue	
η	angle between the principal inertial X -axis and the X_s -axis of the stability reference frame	
θ	angle of pitch, angle between the X_r -axis and the horizontal plane	
θ_0	angle of pitch in steady flight	
λ	Taper ratio	$\left[\lambda = \frac{c_t}{c_r} \right]$
λ	eigenvalue	
λ_b	non-dimensional eigenvalue, asymmetric motions	
λ_c	non-dimensional eigenvalue, symmetric motions	
Λ	angle of sweep, angle between the Y_r -axis and the projection of the $\frac{1}{4}$ -chord line on the X_rOY_r -plane	
μ_b	Relative density, asymmetric motions	$\left[= \frac{m}{\rho S b} \right]$
μ_c	Relative density, symmetric motions	$\left[= \frac{m}{\rho S c} \right]$

ν	Kinematic viscosity of the air
ξ	Real part of a complex eigenvalue
ρ	Air density
σ	Sidewash angle, usually at the vertical tailplane
τ	Time constant
τ	Trailing edge angle of a profile
φ	angle of roll, angle of the Y -axis and the intersection of the YOZ -plane and the horizontal plane
Φ	Bank angle, angle between the Y -axis and the horizontal plane
χ	Track angle
χ_1	Angle between the direction of \underline{C}_R and the Z -axis
χ_2	Angle between the neutral line and the Z -axis
ψ	Yaw angle
ω	Angular velocity
ω	Circular frequency
ω_0	Undamped natural frequency
$\underline{\Omega}$	Total angular velocity about the center of gravity
Ω	Angular velocity vector

Subscripts

<i>a</i>	Aerodynamic reference frame
<i>a</i>	Aerodynamic
<i>a</i>	Aerodynamic (velocity)
<i>a</i>	Aileron
<i>a.c.</i>	Aerodynamic center
<i>b</i>	Balance tab
<i>b</i>	Body-fixed reference frame
<i>c.g.</i>	Center of gravity
<i>e</i>	Elevator
<i>e</i>	Engine
<i>E</i>	Normal Earth-fixed reference frame
<i>f</i>	Flap
<i>f</i>	Fuselage
<i>f</i>	Friction
<i>fix</i>	$\delta_e = \text{constant}$
<i>free</i>	$F_e = 0, (C_{h_e} = 0)$
<i>h</i>	Horizontal tailplane
<i>i</i>	Initial
<i>i</i>	Interference
<i>I</i>	Inertial reference frame
<i>k</i>	Kinematic reference frame
<i>k</i>	Kinematic (velocity)
<i>n</i>	Nacelle
<i>O</i>	vehicle carried normal reference frame
<i>p</i>	Relating to the propulsive system
<i>r</i>	Vehicle reference frame
<i>r</i>	Rudder
<i>r</i>	Root of the wing
<i>s</i>	Spring in the control mechanism
<i>s</i>	Stability reference frame
<i>t</i>	tip
<i>t</i>	trim tab
<i>u</i>	ultimate, final
<i>v</i>	vertical tailplane
<i>w</i>	static unbalance
<i>w</i>	wing or wing with fuselage and nacelles
<i>x</i>	along the <i>X</i> -axis
<i>y</i>	along the <i>Y</i> -axis
<i>z</i>	along the <i>Z</i> -axis
0	initial, steady flight condition

Appendix B

Nomenclature

This appendix introduces several key notations and characters which will be used throughout the book. Knowing these notations and characters will facilitate the reading of the book and will improve the understanding of the text. We have tried to keep the reasoning behind the notations the same throughout the book. Only one exception exists and is with respect to the use of subscripts (see page 521).

B-1 Vectors

All vectors in this book are in three dimensional space, i.e. $\in \mathbb{R}^3$, unless defined otherwise. All vectors are in boldface. The superscript denotes the reference frame in which the vector is expressed while the subscript indicates the particular parameter in question. For example:

$$\mathbf{V}_k^b$$

is the kinematic (subscript k) velocity (vector \mathbf{V}) expressed in the body-fixed reference frame (superscript b). The legend for the subscripts en superscripts are given in the section on page 521.

Sometimes a second subscript is added. In that case the subscript denotes the point of origin of the vector or to which point or body the vector properties belong. For example:

$$\mathbf{V}_{k,G}^b$$

is the kinematic velocity of point G expressed in the body-fixed reference frame.

Four types of vectors have fixed component notations. Position vectors have components x, y, z while velocity vectors have components u, v, w . Acceleration components are denoted by a_x, a_y, a_z . Finally, the rotational velocity vector has components p, q, r . Other vectors do not have a fixed components notation. The same 'rules' regarding the superscript and the subscript notation apply for the components of the vectors.

A vector can be differentiated with respect to time which is always coupled to a reference frame (without a reference frame time differentiation only has a pure theoretical meaning). The time derivative of vector with respect to reference frame F_b is written as:

$$\frac{d\mathbf{X}}{dt}\Big|_b$$

Note that the derivative of a vector is again a vector. Thus the previous expression can be appended by a superscript denoting the reference frame in which the time derivative is expressed.

In cases where the meaning is obvious, the superscript and/or the subscripts are sometimes dropped, cleaning the text of any unnecessary notations which would only cloud the text. If any notation is simplified, it is explicitly mentioned so in the text.

B-2 Reference frames

A crucial element in this book is the definition of reference frames. All reference frames are right-handed orthogonal unless stated otherwise and are defined by their origin and orientation of the axes. A reference frame is denoted by F and its axes by X, Y, Z . The subscript appended to these letters indicates the reference frame we are talking about. For example:

$$F_b \longrightarrow (GX_bY_bZ_b)$$

is the body-fixed reference frame which has the origin in the vehicle center of mass G and has the axes X_b, Y_b, Z_b . A list of all reference frames used in this book is given next.

F_I	Inertial reference frame	(section 2-1-1)
F_C	Earth-centered, Earth-fixed reference frame	(section 2-1-2)
F_E	Vehicle carried normal Earth reference frame	(section 2-1-3)
F_b	Body-fixed reference frame	(section 2-1-4)
F_s	Stability reference frame	(section 2-1-4)
F_r	Vehicle reference frame	(section 2-1-5)
F_a	Aerodynamic reference frame	(section 2-1-6)

After chapter 2 the notations F_x, F_y, F_z are used to denote the total aerodynamic forces along the X, Y, Z -axis respectively. Although the context in which these parameters are used is different, care should be taken with the interpretation of the parameter F .

Transformation matrix

The *orientation* between reference frames is defined by a maximum of three Euler angles. The sequence of rotation combined with the set of angles enables us to transform any coordinate from one reference frame to another. A transformation matrix \mathbb{T} is used to quickly transform a complete vector. The subscripts indicate the reference frames involved in the transformation. For example:

$$\mathbf{X}^b = \mathbb{T}_{ba} \mathbf{X}^a$$

where \mathbf{X}^b is the vector \mathbf{X} expressed in reference frame F_b , \mathbb{T}_{ba} is the matrix for the transformation from frame F_a to F_b , and \mathbf{X}^a is the vector \mathbf{X} expressed in reference frame F_a .

Angular velocity vectors

When the orientation between reference frames is time-variant, one can define a rotation vector describing this change through time. The variable defining a rotation vector is $\boldsymbol{\Omega}$. The subscripts indicate which reference frames are involved while the superscript denotes the reference frame in which the vector is expressed. For example:

$$\boldsymbol{\Omega}_{ba}^b$$

is the rotation vector describing the angular velocity of reference frame F_b with respect to reference frame F_a (subscripts) expressed in frame F_b (superscript). One should be careful not to mix-up the interpretation of the subscripts for the angular velocity vectors and for the transformation matrices.

B-3 Superscripts and subscripts

At this point a distinction must be made between chapters 1 to 3 and the remainder of the book.

Chapters 1 to 3

For the first three chapters the main subject is the derivation of the equations of motion for the most general case of a spherical, rotating Earth. In those chapters the superscripts appended to a vector indicate the reference frame in which the vector is expressed. The possible superscripts are:

<i>I</i>	Inertial reference frame
<i>C</i>	Normal Earth-fixed reference frame
<i>E</i>	Vehicle carried normal Earth reference frame
<i>b</i>	Body-fixed reference frame
<i>s</i>	Stability reference frame
<i>p</i>	Principle axis reference frame
<i>z</i>	Zero-lift body axis reference frame
<i>a</i>	Aerodynamic reference frame
<i>k</i>	Kinematic reference frame

The subscripts in chapters 1 to 3 denote either reference frames (in case of transformation matrices and angular velocity vectors) or indicate a particular form of the vector. The subscript for the reference frames are the same as for the superscripts given above. The other subscripts are:

<i>a</i>	aerodynamic
<i>k</i>	kinematic

Remaining chapters

In the remainder of the book superscripts are not used often. One exception which occurs in chapter 4, is the superscript ' indicating the derivative with respect to parameter *i*, e.g. $f' = \frac{df}{di}$.

The function of the subscript changes considerably. A subscript in chapter 4 and subsequent chapters indicates the partial derivative of the function with respect to the parameter indicated by the subscript. For example:

$$X_u = \frac{\partial X}{\partial u}$$

B-4 Geometric of aircraft parameters

The geometric aircraft parameters are used to determine the aerodynamic force and moments and to make the equations of motion dimensionless. Figure B-2 illustrates the various parameters defining the geometry of the wing. The reference axes used in this figure are those of the Vehicle reference frame (see section 2-1-5).

- **Wing area, *S***

The area of the wing projection on the X_rOY_r -plane. Often the wing is partially covered by the fuselage and the engine nacelles. The wing area is then calculated using straight line extensions of the wing leading and trailing edges through the fuselage and the nacelles. The wing area can be expressed as,

$$S = \int_{-\frac{b}{2}}^{+\frac{b}{2}} c \, dy$$

where y is the coordinate in the Y_r -direction.

- **Wingspan, b**

The distance in Y_r -direction between the wing tips.

- **Mean aerodynamic chord, \bar{c}**

(mac) is defined as,

$$\bar{c} = \frac{1}{S} \int_{-\frac{b}{2}}^{+\frac{b}{2}} c^2 \, dy$$

One can define the location and orientation of the mean aerodynamic cord within the OX_rZ_r plane (see figure B-1). Four coordinates, $\bar{x}_o, \bar{x}_e, \bar{z}_o, \bar{z}_e$, determine the location and orientation of the mac. There definition is similar that of the mean aerodynamic chord:

$$\begin{aligned} \bar{x}_o &= \frac{1}{S} \int_{-\frac{b}{2}}^{+\frac{b}{2}} x_o(y) c(y) \, dy & \bar{x}_e &= \frac{1}{S} \int_{-\frac{b}{2}}^{+\frac{b}{2}} x_e(y) c(y) \, dy \\ \bar{z}_o &= \frac{1}{S} \int_{-\frac{b}{2}}^{+\frac{b}{2}} z_o(y) c(y) \, dy & \bar{z}_e &= \frac{1}{S} \int_{-\frac{b}{2}}^{+\frac{b}{2}} z_e(y) c(y) \, dy \\ \bar{\varepsilon} &= \frac{1}{S} \int_{-\frac{b}{2}}^{+\frac{b}{2}} \varepsilon(y) c(y) \, dy \end{aligned}$$

- **Mean or geometric chord, c_m**

Is very often used in the literature and is defined as:

$$c_m = \frac{S}{b}$$

- **Taper ratio, λ**

A measure of the variation in chord length along the span. It is expressed by,

$$\lambda = \frac{c_t}{c_r}$$

- **Aspect ratio, A**

Defined as,

$$A = \frac{b^2}{S}$$

- **Wing sweep, Λ**

The angle between the Y_r -axis and the projection of the 1/4-chord line on the X_rOY_r -plane (figure B-2). In some cases such as delta wings, only the angle between the Y_r -axis and the projection of the wing's leading edge on the X_rOY_r -plane is given.

- **Dihedral, Γ**

The dihedral of a wing is the angle between the Y_r -axis and the projection of the 1/4-chord line on the Y_rOZ_r -plane.

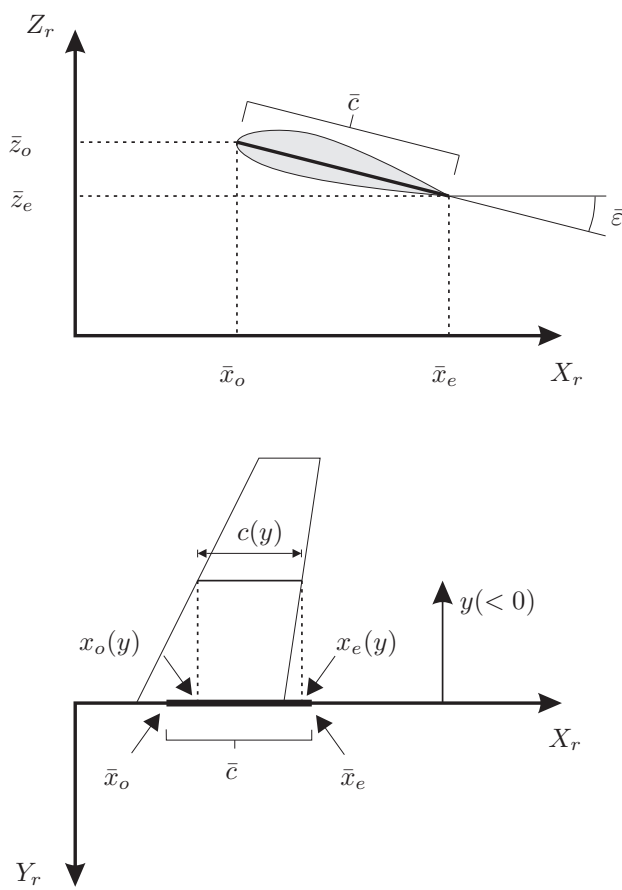


Figure B-1: Definition of the mean aerodynamic cord and related parameters

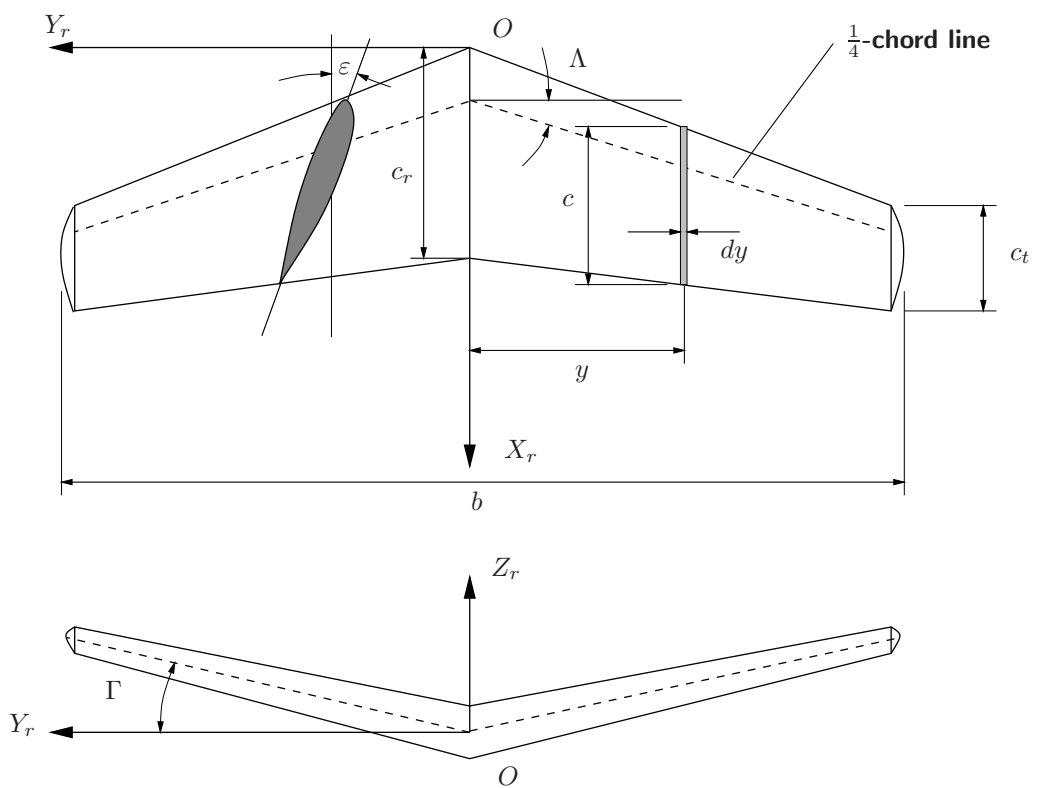


Figure B-2: Parameters defining the geometry of the wing

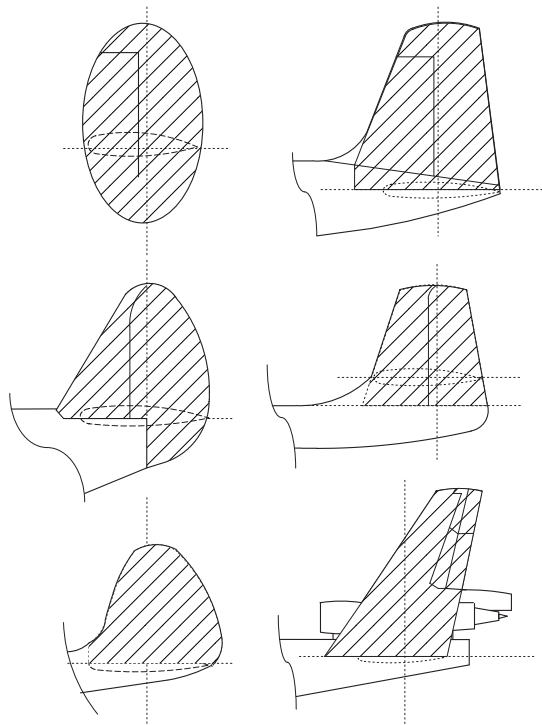


Figure B-3: Examples of definitions of the vertical tailplane area (see also NACA TN 775)

- **Washout or wing-twist, ε**

Expresses the variation in direction of the local wing chord relative to the direction of the chord line at the wing root. Neither the gradient of the washout ($\frac{d\varepsilon}{dy}$) nor the magnitude of wing sweep or dihedral need to be constant along the span. If necessary, these parameters are given as functions of the coordinate in span direction.

- **Wing airfoil**

The shape of the cross section of the wing parallel to the plane of symmetry.

The above geometric parameters apply not only to wings, but to tailplanes as well. Definitions of the geometric parameters for the elevator, or control surfaces in general, are given in chapter 7. It proves to be difficult to define the geometry of vertical tailplanes in a way applicable to all aircraft. In particular the distinction between fuselage and vertical tailplane is often hard to make. In many instances the division between vertical tailplane and dorsal fin is also more or less arbitrary. Usually the surface of the dorsal fin is not considered to be part of the vertical tailplane. Figure B-3 shows examples of definitions of vertical tailplanes, see reference [11]. Similar and other definitions are given in references [8] and [109].

B-5 Aircraft Configurations

The flight dynamic characteristics are dependent on the aircraft configuration. A full description of the aircraft configuration gives the aircraft's weight or mass, center of gravity position and internal as well as external loading, undercarriage position, control surface deflections, flap angle, airbrake and spoiler deflections. A description of the engine operating condition, such as throttle position, engine speed etcetera, is also required.

Some definitions as used in U.S. military requirements are briefly described below.

- **CR** (Cruising Flight)

Engine thrust or power for level flight at cruising speed, flaps in the position for cruising flight, undercarriage retracted.

- **L** (Landing)

Throttle closed, undercarriage down, flaps in the position for landing.

- **PA** (Powered Approach)

Undercarriage down, flaps and airbrakes in the normal position for the powered approach, engine thrust or power for level flight at $1.15 V_{S_L}$ or the normal airspeed in the powered approach, if the latter is lower.

NOTE: V_{S_L} is the stall speed (in the aircraft configuration for landing).

B-6 Flight Conditions

By specifying a specific flight condition, we specify (a part of) the state of the aircraft, i.e. we indicate which aircraft states are varying. This information can be used to deduce the equations of motion for that flight condition. The following definitions of flight conditions will be used throughout this book.

- **Steady flight**

An aircraft is in steady flight if the components of the aerodynamic velocity vector V_G (u, v, w) and the components of the body rotation vector (p, q, r) in the body-fixed reference frame F_b are constant. In this flight condition the aerodynamics force vector components in F_b and the aircraft's pitch and roll attitude (θ, φ) are constant too.

- **Straight flight**

An aircraft is in a straight flight condition, if the flightpath vector is straight.

- **Symmetric flight**

An aircraft is in symmetric flight, if the velocity vector of any point of the aircraft is parallel to the plane of symmetry (roll angle $\varphi = 0$).

- **Slipping flight**

An aircraft is in slipping flight, if the velocity vector of the aircraft's center of gravity is not parallel to the plane of symmetry of the aircraft.

Appendix C

General formulation of the equations of motion

C-1 Introduction

A vehicle, when moving in the sphere of influence of a celestial body, is subjected to a number of external forces, some of them may be atmospheric, gravitational, magnetic or perturbing forces caused by a third body, e.g. the Sun or another planet. This description generally holds for satellites orbiting the Earth or aircraft flying in the atmosphere of the Earth, where the application usually determines which forces to consider. The motion of the vehicle can be divided in the translation *of* the centre of mass (c.o.m.) and the rotation *about* its c.o.m.. The equations, which describe the corresponding motion are therefore called the equations of translational motion and the equations of rotational motion.

The basis for the equations motion is formed by Newton's Laws of Motion. For a point mass with constant mass, they read:

1. Every point mass continues in its state of uniform motion in a straight line (or rest), unless compelled to change that state by forces acting upon it.
2. The time rate of change of linear momentum of a point mass is proportional to the force acting upon that point mass and is collinear with and in the direction of that force.
3. The mutual forces of two point masses acting upon each other are equal in magnitude and opposite in direction (action = reaction).

The first and second law hold for a certain reference frame with respect to which a point mass, free of all external forces, moves in a straight line with a constant speed. Such a frame is called an inertial frame. However, Newton's laws can be modified to derive the equations of motion in a (rotating) non-inertial frame. In this chapter, we will derive the general formulation of the equations of motion for an elastic, mass-varying body w.r.t. a rotating (non-inertial) frame. In Section C-2 we will first discuss the basic mathematics of the time derivative of a vector in a rotating frame, and use this in the next Section C-3 to derive expressions for the velocity and acceleration in a rotating frame. Section C-4 will present the equations of translational motion, whereas Section C-5 will give the derivation of the equations of rotational motion. In that section, also the angular momentum with respect to the c.o.m. of a solid body is discussed, and used to formulate the so-called Euler equations.

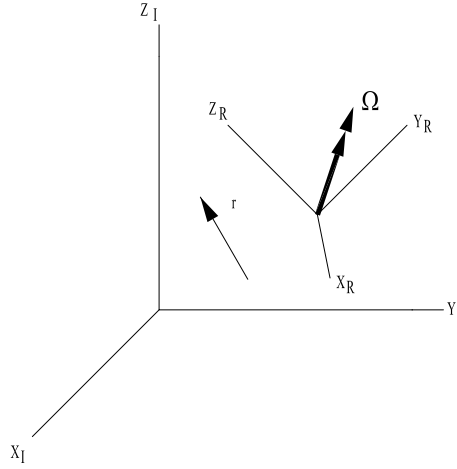


Figure C-1: Relative angular motion. The index I denotes the inertial frame, whereas the R -index stands for the rotating frame.

C-2 Time derivative of a vector in a rotating frame

Let us consider two frames: a fixed (inertial) frame with index I and a moving frame with index R which is rotating with an angular velocity $\boldsymbol{\Omega}$ with respect to the inertial frame¹. Suppose we want to take the time derivative of a vector \mathbf{r} expressed in the R -frame and we want to define the result in the I -frame. The begin situation is shown in Fig. C-1.

For the vector \mathbf{r} we can write:

$$\mathbf{r} = r_x \mathbf{x}_R + r_y \mathbf{y}_R + r_z \mathbf{z}_R \quad (\text{C-1})$$

in which \mathbf{x}_R , \mathbf{y}_R and \mathbf{z}_R are the unit axes in the R -frame. If we take the derivative of \mathbf{r} with respect to time, we get:

$$\begin{aligned} \frac{d\mathbf{r}}{dt} &= \frac{d}{dt} (r_x \mathbf{x}_R + r_y \mathbf{y}_R + r_z \mathbf{z}_R) \\ &= \frac{dr_x}{dt} \mathbf{x}_R + \frac{dr_y}{dt} \mathbf{y}_R + \frac{dr_z}{dt} \mathbf{z}_R + r_x \frac{d\mathbf{x}_R}{dt} + r_y \frac{d\mathbf{y}_R}{dt} + r_z \frac{d\mathbf{z}_R}{dt} \end{aligned} \quad (\text{C-2})$$

The end p of a vector \mathbf{r} , which is a function of time and which rotates with an angular velocity $\boldsymbol{\Omega}$ with respect to the inertial frame, will describe a curved path if the other end remains at a fixed point. The linear velocity of p with respect to inertial is given by (Cornelisse *et al.*, 1979):

$$\mathbf{V}_p = \boldsymbol{\Omega} \times \mathbf{r} \quad (\text{C-3})$$

For the last three terms of Eq. (C-2) we can write, using Eq. (C-3):

$$r_x \frac{d\mathbf{x}_R}{dt} + r_y \frac{d\mathbf{y}_R}{dt} + r_z \frac{d\mathbf{z}_R}{dt} = r_x \boldsymbol{\Omega} \times \mathbf{x}_R + r_y \boldsymbol{\Omega} \times \mathbf{y}_R + r_z \boldsymbol{\Omega} \times \mathbf{z}_R = \boldsymbol{\Omega} \times \mathbf{r} \quad (\text{C-4})$$

¹As a starting point we consider one of the two frames to be inertial. However, as this assumption is not actively used, it means that the derived equations will also be valid for two frames, which are rotating relatively to each other.

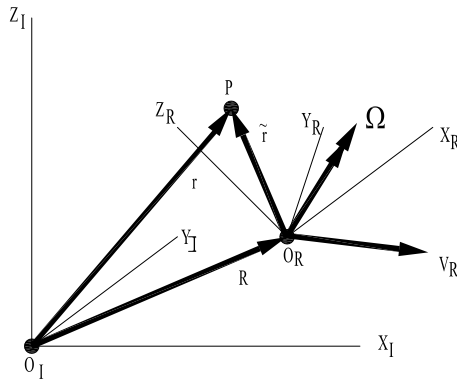


Figure C-2: Motion of a point p with respect to a fixed and a moving frame.

Finally, if we consider the first three terms of the right-hand side of Eq. (C-2) as the time derivative of \mathbf{r} expressed in the rotating frame, $\frac{\delta \mathbf{r}}{\delta t}$, we obtain:

$$\frac{d\mathbf{r}}{dt} = \frac{\delta \mathbf{r}}{\delta t} + \boldsymbol{\Omega} \times \mathbf{r} \quad (\text{C-5})$$

C-3 Velocity and acceleration in a rotating frame

We will now use Eq. (C-5) to derive expressions for the velocity and acceleration in a point p as given in Fig. C-2. If \mathbf{R} is the position of the rotating frame with respect to the inertial frame, \mathbf{r} and $\tilde{\mathbf{r}}$ the position vectors of p relative to the origins of the inertial and rotating frame, respectively, then:

$$\mathbf{r} = \mathbf{R} + \tilde{\mathbf{r}} \quad (\text{C-6})$$

The velocity of p with respect to the inertial frame is:

$$\mathbf{V}_I = \frac{d\mathbf{r}}{dt} = \frac{d\mathbf{R}}{dt} + \frac{d\tilde{\mathbf{r}}}{dt} \quad (\text{C-7})$$

Note that all derivatives are expressed in the inertial frame. Applying Eq. (C-5) yields:

$$\mathbf{V}_I = \frac{d\mathbf{R}}{dt} + \frac{\delta \tilde{\mathbf{r}}}{\delta t} + \boldsymbol{\Omega} \times \tilde{\mathbf{r}} \quad (\text{C-8})$$

The second term on the right-hand side is the relative velocity of p .

The acceleration of p with respect to the inertial frame is:

$$\mathbf{a}_I = \frac{d\mathbf{V}_I}{dt} = \frac{d^2\mathbf{R}}{dt^2} + \frac{d\boldsymbol{\Omega}}{dt} \times \tilde{\mathbf{r}} + \boldsymbol{\Omega} \times \frac{d\tilde{\mathbf{r}}}{dt} + \frac{d}{dt} \left(\frac{\delta \tilde{\mathbf{r}}}{\delta t} \right) \quad (\text{C-9})$$

Applying Eq. (C-5) again gives us

$$\mathbf{a}_I = \frac{d^2\mathbf{R}}{dt^2} + \frac{d\boldsymbol{\Omega}}{dt} \times \tilde{\mathbf{r}} + \boldsymbol{\Omega} \times (\boldsymbol{\Omega} \times \tilde{\mathbf{r}}) + 2\boldsymbol{\Omega} \times \frac{\delta \tilde{\mathbf{r}}}{\delta t} + \frac{\delta^2 \tilde{\mathbf{r}}}{\delta t^2} \quad (\text{C-10})$$

The different terms can be defined as:

$\frac{d^2\mathbf{R}}{dt^2}$	= absolute acceleration of the moving frame w.r.t. to the inertial frame
$\frac{\delta\Omega}{\delta t} \times \mathbf{r}$	= apparent (tangential) acceleration of p due to angular acceleration of moving frame
$\boldsymbol{\Omega} \times (\boldsymbol{\Omega} \times \mathbf{r})$	= apparent (centripetal) acceleration of p due to angular motion of moving frame. Together with the first two terms, the resulting acceleration is called the dragging acceleration.
$2\boldsymbol{\Omega} \times \frac{\delta\mathbf{r}}{\delta t}$	= Coriolis acceleration due to the motion of p in the moving frame
$\frac{\delta^2\mathbf{r}}{\delta t^2}$	= relative acceleration of p in the moving frame

Concluding, the absolute acceleration w.r.t. the inertial frame can be written as the summation of three terms, the dragging, Coriolis and relative acceleration.

C-4 Translational motion

C-4-1 General formulation for an inertial frame

We consider a mass system with N particles. Each particle has a constant mass m_i and a position vector \mathbf{r}_i w.r.t. the origin of the inertial frame. The number of particles is varying with time, so $N = N(t)$. The linear momentum of a particle w.r.t. the inertial frame is given by

$$\mathbf{J}_i = m_i \frac{d\mathbf{r}_i}{dt} \quad (\text{C-11})$$

According to Newton's second law the summation of the external and internal forces acting on the particle equals the change in linear momentum:

$$\mathbf{F}_i + \sum_{k=1}^N \mathbf{F}_{ik} = \frac{d\mathbf{J}_i}{dt} \quad (\text{C-12})$$

Summing over all particles yields

$$\sum_{i=1}^N \mathbf{F}_i + \sum_{i=1}^N \sum_{k=1}^N \mathbf{F}_{ik} = \sum_{i=1}^N \frac{d\mathbf{J}_i}{dt} \quad (\text{C-13})$$

The second term on the left-hand side is zero, since Newton's third law says $\mathbf{F}_{ik} = -\mathbf{F}_{ki}$ and a particle cannot exert a force on itself.

Defining $\mathbf{F}_I = \sum_{i=1}^N \mathbf{F}_i$ as the total external force acting on the system, and applying Eq. (C-11) we obtain

$$\mathbf{F}_I = \sum_{i=1}^N m_i \frac{d^2\mathbf{r}_i}{dt^2} \quad (\text{C-14})$$

When we consider a body, then the summation is replaced by an integration which gives us

$$\mathbf{F}_I = \int_m \frac{d^2\mathbf{r}}{dt^2} dm \quad (\text{C-15})$$

with \mathbf{r} as the location of a mass element w.r.t. the inertial frame. In Eq. (C-15), \int_m stands for integration of the full body (volume), i.e., it can be seen as a volume integral with three variables of integration. Defining the location of the c.o.m. of the body to be

$$\mathbf{r}_{\text{cm}} \int_m dm = \int_m \mathbf{r} dm \quad (\text{C-16})$$

and $\tilde{\mathbf{r}}$ as the position vector of the mass element w.r.t. the c.o.m., then

$$\mathbf{r} = \mathbf{r}_{\text{cm}} + \tilde{\mathbf{r}} \quad (\text{C-17})$$

Using the expression for the acceleration, which we found in the previous Section (Eq. C-10), realising that $\frac{d^2 \mathbf{R}}{dt^2} = \frac{d^2 \mathbf{r}_{\text{cm}}}{dt^2}$ and $\boldsymbol{\Omega}$ is the rotation of the body w.r.t. inertial space, and taking into account that $\int_m \tilde{\mathbf{r}} dm = 0$, which follows from substitution of Eq. (C-17) into Eq. (C-16), we can write for Eq. (C-15):

$$\mathbf{F}_I = m \frac{d^2 \mathbf{r}_{\text{cm}}}{dt^2} + 2\boldsymbol{\Omega} \times \int_m \frac{\delta \tilde{\mathbf{r}}}{\delta t} dm + \int_m \frac{\delta^2 \tilde{\mathbf{r}}}{\delta t^2} dm$$

(C-18)

with

\mathbf{F}_I	= total of the external forces expressed in components of the inertial frame (N)
$\frac{d^2 \mathbf{r}_{\text{cm}}}{dt^2}$	= acceleration of the c.o.m. with respect to the inertial frame (m/s^2)
$\mathbf{F}_C = -2\boldsymbol{\Omega} \times \int_m \frac{\delta \tilde{\mathbf{r}}}{\delta t} dm$	= Coriolis force, due to time variations in mass distribution (N)
$\mathbf{F}_{\text{rel}} = - \int_m \frac{\delta^2 \tilde{\mathbf{r}}}{\delta t^2} dm$	= relative force, due to time variations in mass distribution (N)
$\boldsymbol{\Omega} = (p, q, r)^T$	= the rotation vector of the body frame with respect to the inertial frame, expressed in components along the body axes
$\tilde{\mathbf{r}}$	= the location of a mass element with respect to the c.o.m. of the vehicle (m)

Eq. (C-18) describes the translational motion of an arbitrary body with variable mass distribution.

If we bring the two apparent forces due to the variation of the mass distribution to the left-hand side of Eq. (C-18), and designate the resulting force as $\tilde{\mathbf{F}}_I$, then the equation has the same form as the one for a rigid body (with a constant mass distribution), where both the Coriolis and the relative force are zero. This can be summarized by the *Principle of Solidification*, which states (Cornelisse *et al.*, 1979) that *in general, equations of translational and rotational motion of an arbitrary variable mass system at time t can be written as the translational and rotational equations for a rigid body with mass M equal to the mass of the system at time t, while in addition to the true external forces and moments, two apparent forces and moments are applied: the Coriolis and relative forces and moments, respectively.*

C-4-2 General formulation for a rotating frame

Let us now consider a vehicle moving in the sphere of influence of a celestial body. In Fig.C-3 we have established an inertial and a rotating planetocentric reference frame. The moving frame is rigidly attached to the central body, with its origin in its c.o.m., and hence rotates with the same rate as the central body, $\boldsymbol{\Omega}_R$. We assume that this rotational rate is constant. The vehicle has a

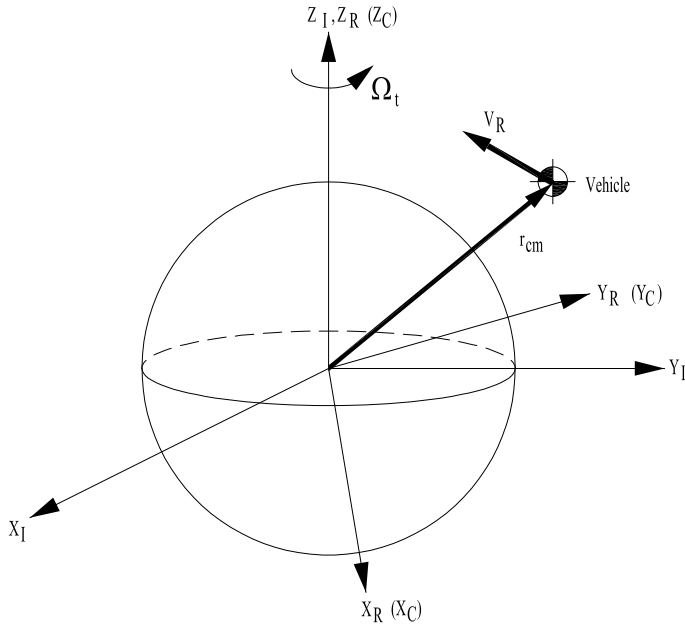


Figure C-3: The vehicle with respect to the two related reference frames. The index I indicates the inertial planetocentric reference frame, whereas R stands for the rotating planetocentric frame.

variable mass m and its c.o.m. is at a distance \mathbf{r}_{cm} from the c.o.m. mon origin of the two reference frames. It is moving with a velocity \mathbf{V}_R with respect to the moving frame.

In accordance with the vehicle location definition in the previous sub-section, we may write

$$\mathbf{r}_{\text{cm}_I} = \mathbf{R} + \mathbf{r}_{\text{cm}_R} = \mathbf{r}_{\text{cm}_R}$$

since the two frames are coinciding ($\mathbf{R} = \mathbf{0}$). Note that we have added the indices I and R to distinguish between the two position vectors.

Starting with Eq. (C-18), which describes the motion of the vehicle w.r.t. the inertial frame, we have

$$\mathbf{F}_I + \mathbf{F}_C + \mathbf{F}_{\text{rel}} = \tilde{\mathbf{F}}_I = m \frac{d^2 \mathbf{r}_{\text{cm}_I}}{dt^2} \quad (\text{C-19})$$

Expressing the acceleration of the c.o.m. w.r.t. the inertial frame in the rotating frame, we apply again Eq. (C-5) which gives us, equivalent to Eq. (C-10):

$$\begin{aligned} \mathbf{a}_R = \frac{d^2 \mathbf{r}_{\text{cm}_R}}{dt^2} &= \frac{d^2 \mathbf{R}}{dt^2} + \frac{d\Omega_R}{dt} \times \mathbf{r}_{\text{cm}_R} + \Omega_R \times (\Omega_R \times \mathbf{r}_{\text{cm}_R}) + \\ &+ 2\Omega_R \times \frac{\delta \mathbf{r}_{\text{cm}_R}}{\delta t} + \frac{\delta^2 \mathbf{r}_{\text{cm}_R}}{\delta t^2} \end{aligned} \quad (\text{C-20})$$

The first term on the right-hand side disappears, because $\mathbf{R} = \mathbf{0}$. Furthermore, we assumed that the central body is rotating with a constant angular rate, so also the second term is zero. Substitution of Eq. (C-20) into (C-19), and omitting the indices R for the sake of convenience,

we get the equation of translational motion of a mass-varying vehicle with respect to the rotating planetocentric frame:

$$\boxed{\mathbf{F}_R = m \frac{d^2 \mathbf{r}_{cm}}{dt^2} + 2m\boldsymbol{\Omega}_R \times \frac{d\mathbf{r}_{cm}}{dt} + m\boldsymbol{\Omega}_R \times (\boldsymbol{\Omega}_R \times \mathbf{r}_{cm})} \quad (C-21)$$

In the above equation, \mathbf{F}_R is the sum of the external forces *and the Coriolis and relative forces due to the variation of mass*, expressed in components of the R -frame. The other terms have the following meaning:

$$\begin{aligned} \frac{d^2 \mathbf{r}_{cm}}{dt^2} &= \text{apparent acceleration of the vehicle in the rotating frame} \\ 2\boldsymbol{\Omega}_R \times \frac{d\mathbf{r}_{cm}}{dt} &= \text{Coriolis acceleration due to the motion of the vehicle in the rotating frame} \\ \boldsymbol{\Omega}_R \times (\boldsymbol{\Omega}_R \times \mathbf{r}_{cm}) &= \text{apparent (or transport) acceleration of the vehicle due to angular rate of the rotating frame} \end{aligned}$$

Note that the derivatives $\frac{\delta}{\delta t}$ and $\frac{\delta^2}{\delta t^2}$ w.r.t. the rotating frame have been written with a conventional d , since there is no confusion about the frame.

C-5 Rotational motion

C-5-1 General formulation

We start the derivation, by looking at a single particle again. We multiply Eq. (C-12) vectorial with \mathbf{r}_i , yielding

$$\mathbf{r}_i \times \mathbf{F}_i + \sum_{k=1}^N \mathbf{r}_i \times \mathbf{F}_{ik} = \mathbf{r}_i \times \frac{d\mathbf{J}_i}{dt} \quad (C-22)$$

The moment of \mathbf{F}_i w.r.t. the origin of the inertial frame is defined as

$$\mathbf{M}_i = \mathbf{r}_i \times \mathbf{F}_i \quad (C-23)$$

and the angular momentum of the particle is

$$\mathbf{B}_i = \mathbf{r}_i \times \mathbf{J}_i = m_i \mathbf{r}_i \times \frac{d\mathbf{r}_i}{dt} \quad (C-24)$$

In the next sub-section we will discuss the angular momentum in more detail.

Substituting Eqs. (C-23-C-24) into Eq. (C-22) gives us

$$\mathbf{M}_i + \sum_{k=1}^N \mathbf{r}_i \times \mathbf{F}_{ik} = \mathbf{r}_i \times \frac{d\mathbf{J}_i}{dt} = \frac{d}{dt}(\mathbf{r}_i \times \mathbf{J}_i) = \frac{d\mathbf{B}_i}{dt} \quad (C-25)$$

Summing over all particles yields

$$\sum_{i=1}^N \mathbf{M}_i + \sum_{i=1}^N \sum_{k=1}^N \mathbf{r}_i \times \mathbf{F}_{ik} = \sum_{i=1}^N \frac{d\mathbf{B}_i}{dt} \quad (C-26)$$

The first term on the left-hand side is the total moment about the origin of the I -frame, \mathbf{M}_I . The second term is the total internal moment, which is equal to zero (which can be seen by taking the terms in pairs together). Eq. (C-26) can then be rewritten as

$$\mathbf{M}_I = \sum_{i=1}^N \frac{d\mathbf{B}_i}{dt} = \sum_{i=1}^N m_i \mathbf{r}_i \times \frac{d^2 \mathbf{r}_i}{dt^2} \quad (\text{C-27})$$

For a solid body, summation is replaced by integration:

$$\mathbf{M}_I = \frac{d\mathbf{B}}{dt} = \int_m \mathbf{r} \times \frac{d^2 \mathbf{r}}{dt^2} dm \quad (\text{C-28})$$

Suppose now we have a vehicle, which is rotating with an angular velocity $\boldsymbol{\Omega}$ w.r.t. the inertial frame, and we want to express the rotational motion of the vehicle using the external moment about the vehicle's c.o.m.. \mathbf{M}_I is the moment about the origin of the I -frame due to the external force \mathbf{F}_I . If the point, on which \mathbf{F}_I is acting is defined as \mathbf{r}_I , and $\tilde{\mathbf{r}}_I$ is the corresponding position w.r.t. the c.o.m. of the vehicle, then

$$\mathbf{M}_I = \mathbf{r}_I \times \mathbf{F}_I = (\mathbf{r}_{cm} + \tilde{\mathbf{r}}_I) \times \mathbf{F}_I \quad (\text{C-29})$$

so

$$\mathbf{M}_{cm} = \tilde{\mathbf{r}}_I \times \mathbf{F}_I = \mathbf{M}_I - \mathbf{r}_{cm} \times \mathbf{F}_I \quad (\text{C-30})$$

With \mathbf{M}_I and \mathbf{F}_I given by Eqs. (C-28) and (C-15), respectively, then we obtain with Eq. (C-17)

$$\mathbf{M}_{cm} = \int_m \tilde{\mathbf{r}} \times \frac{d^2 \mathbf{r}}{dt^2} dm \quad (\text{C-31})$$

Thus, with Eq. (C-10) we finally get for the equation of rotational motion for an arbitrary flexible body with variable mass:

$$\begin{aligned} \mathbf{M}_{cm} = & \int_m \tilde{\mathbf{r}} \times \left(\frac{d\boldsymbol{\Omega}}{dt} \times \tilde{\mathbf{r}} \right) dm + \int_m \tilde{\mathbf{r}} \times [\boldsymbol{\Omega} \times (\boldsymbol{\Omega} \times \tilde{\mathbf{r}})] dm + \\ & + 2 \int_m \tilde{\mathbf{r}} \times \left(\boldsymbol{\Omega} \times \frac{\delta \tilde{\mathbf{r}}}{\delta t} \right) dm + \int_m \tilde{\mathbf{r}} \times \frac{\delta^2 \tilde{\mathbf{r}}}{\delta t^2} dm \end{aligned} \quad (\text{C-32})$$

Here, the several terms on the right-hand side have the following meaning:

$2 \int_m \tilde{\mathbf{r}} \times (\boldsymbol{\Omega} \times \frac{\delta \tilde{\mathbf{r}}}{\delta t}) dm = -\mathbf{M}_C$	= Coriolis moment due to time variations in mass distribution (Nm)
$\int_m \tilde{\mathbf{r}} \times \frac{\delta^2 \tilde{\mathbf{r}}}{\delta t^2} dm = -\mathbf{M}_{rel}$	= relative moment due to time variations in mass distribution (Nm)
$\int_m \tilde{\mathbf{r}} \times \left(\frac{d\boldsymbol{\Omega}}{dt} \times \tilde{\mathbf{r}} \right) dm$	= apparent moment due to the angular acceleration of the vehicle with respect to the inertial frame (Nm)
$\int_m \tilde{\mathbf{r}} \times [\boldsymbol{\Omega} \times (\boldsymbol{\Omega} \times \tilde{\mathbf{r}})] dm$	= apparent moment due to the angular velocity of the vehicle with respect to the inertial frame (Nm)

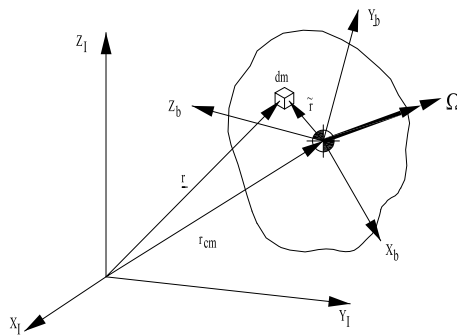


Figure C-4: The solid body with the two reference frames, the rotating body frame (index B) with the origin in the centre of mass and the inertial frame (index I).

C-5-2 The angular momentum w.r.t. the centre of mass of a rigid body.

The angular momentum of a particle was previously defined as

$$\mathbf{B}_i = \mathbf{r}_i \times \mathbf{J}_i = m_i \mathbf{r}_i \times \frac{d\mathbf{r}_i}{dt} \quad (C-33)$$

So the angular momentum \mathbf{B}_I of a solid body w.r.t. to the origin of an inertial frame can be expressed as

$$\mathbf{B}_I = \int_m \mathbf{r} \times \frac{d\mathbf{r}}{dt} dm \quad (C-34)$$

with \mathbf{r} given by Eq. (C-17). In Fig. C-4, the situation is schematically shown. We can distinguish two reference frames, an inertial one with index I and one, which is fixed to the body (index B), with the origin in the c.o.m., and therefore shares the rotational rates of the body (denoted as Ω). \mathbf{r} is the position of the mass element dm with respect to the inertial frame, $\tilde{\mathbf{r}}$ describes the same position but now measured from the c.o.m.. The location of the c.o.m. in the I -frame is indicated by \mathbf{r}_{cm} .

To compute the angular momentum with respect to the c.o.m. of a *rigid* body, we proceed as follows.

$$\frac{d\mathbf{r}}{dt} = \frac{d}{dt} (\mathbf{r}_{cm} + \tilde{\mathbf{r}}) = \frac{d\mathbf{r}_{cm}}{dt} + \frac{\delta \tilde{\mathbf{r}}}{\delta t} + \boldsymbol{\Omega} \times \tilde{\mathbf{r}} = \frac{d\mathbf{r}_{cm}}{dt} + \boldsymbol{\Omega} \times \tilde{\mathbf{r}} \quad (C-35)$$

Here, we have used Eqs. (C-17) and (C-5).

Substituting Eqs. (C-17) and (C-35) in Eq. (C-34) yields

$$\mathbf{B}_I = \int_m (\mathbf{r}_{cm} + \tilde{\mathbf{r}}) \times \left(\frac{d\mathbf{r}_{cm}}{dt} + \boldsymbol{\Omega} \times \tilde{\mathbf{r}} \right) dm \quad (C-36)$$

Writing out the terms in Eq. (C-36) results in:

$$\begin{aligned}\mathbf{B}_I &= \int_m \mathbf{r}_{cm} \times \frac{d\mathbf{r}_{cm}}{dt} dm + \int_m \mathbf{r}_{cm} \times (\boldsymbol{\Omega} \times \tilde{\mathbf{r}}) dm + \\ &+ \int_m \tilde{\mathbf{r}} \times \frac{d\mathbf{r}_{cm}}{dt} dm + \int_m \tilde{\mathbf{r}} \times (\boldsymbol{\Omega} \times \tilde{\mathbf{r}}) dm\end{aligned}\quad (C-37)$$

The first term on the right-hand side can be written as

$$\int_m \mathbf{r}_{cm} \times \frac{d\mathbf{r}_{cm}}{dt} dm = \mathbf{r}_{cm} \times \frac{d\mathbf{r}_{cm}}{dt} \int_m dm = m \mathbf{r}_{cm} \times \frac{d\mathbf{r}_{cm}}{dt} \quad (C-38)$$

with m as the total mass of the solid body. We were allowed to place the cross product outside the integral because \mathbf{r}_{cm} is independent of the variables of integration.

For the second term, we obtain, since $\boldsymbol{\Omega}$ is also independent of the variables of integration (each mass element in a rigid body has the same rotation vector):

$$\int_m \mathbf{r}_{cm} \times (\boldsymbol{\Omega} \times \tilde{\mathbf{r}}) dm = \mathbf{r}_{cm} \times \left(\boldsymbol{\Omega} \times \int_m \tilde{\mathbf{r}} dm \right) = 0 \quad (C-39)$$

since the definition of the c.o.m. prescribes that $\int_m \tilde{\mathbf{r}} dm$ equals zero.

The third term leads to:

$$\int_m \tilde{\mathbf{r}} \times \frac{d\mathbf{r}_{cm}}{dt} dm = -\frac{d\mathbf{r}_{cm}}{dt} \times \int_m \tilde{\mathbf{r}} dm = 0 \quad (C-40)$$

Eqs. (C-38-C-40) substituted in Eq. (C-37) gives

$$\mathbf{B}_I = m \mathbf{r}_{cm} \times \frac{d\mathbf{r}_{cm}}{dt} + \int_m \tilde{\mathbf{r}} \times (\boldsymbol{\Omega} \times \tilde{\mathbf{r}}) dm \quad (C-41)$$

We see that the angular momentum with respect to the origin of the inertial frame consists of two terms. The first one describes the angular momentum of the body if its mass is thought to be concentrated in the c.o.m. (point mass), expressed in c.o.m.ponents of the inertial frame. The second one is a correction term, which takes into account the finite dimensions of the body (instead of being a point mass). This correction term represents a contribution of all mass elements with respect to the c.o.m., i.e., the angular momentum of the body with respect to the c.o.m., and is denoted as \mathbf{B}_{cm} .

$$\mathbf{B}_{cm} = \int_m \tilde{\mathbf{r}} \times (\boldsymbol{\Omega} \times \tilde{\mathbf{r}}) dm \quad (C-42)$$

In the remainder of this sub-section we will derive expressions for each of the c.o.m.ponents of \mathbf{B}_{cm} . The following vector identity holds:

$$\mathbf{a} \times (\mathbf{b} \times \mathbf{c}) = \mathbf{b}(\mathbf{a} \cdot \mathbf{c}) - \mathbf{c}(\mathbf{b} \cdot \mathbf{a}) \quad (C-43)$$

If we write

$$\tilde{\mathbf{r}} = (x, y, z)^T$$

$$\boldsymbol{\Omega} = (p, q, r)^T$$

then

$$\tilde{\mathbf{r}} \cdot \tilde{\mathbf{r}} = x^2 + y^2 + z^2$$

$$\boldsymbol{\Omega} \cdot \tilde{\mathbf{r}} = px + qy + rz$$

Applying Eq. (C-43) to (C-42) results in

$$\int_m \tilde{\mathbf{r}} \times (\boldsymbol{\Omega} \times \tilde{\mathbf{r}}) dm = \int_m [\boldsymbol{\Omega}(\tilde{\mathbf{r}} \cdot \tilde{\mathbf{r}}) - \tilde{\mathbf{r}}(\boldsymbol{\Omega} \cdot \tilde{\mathbf{r}})] dm$$

and substituting the above results yields

$$\begin{aligned} \int_m & [p(x^2 + y^2 + z^2)\mathbf{x}_B + q(x^2 + y^2 + z^2)\mathbf{y}_B + r(x^2 + y^2 + z^2)\mathbf{z}_B + \\ & -x(px + qy + rz)\mathbf{x}_B - y(px + qy + rz)\mathbf{y}_B - z(px + qy + rz)\mathbf{z}_B] dm \end{aligned}$$

with \mathbf{x}_B , \mathbf{y}_B and \mathbf{z}_B being the unit vectors of the B -frame.

Writing out the three scalar equations gives the following expressions for the components of the angular momentum:

$$\begin{aligned} B_x &= \int_m [p(y^2 + z^2) - qxy - rxz] dm \\ B_y &= \int_m [-pyx + q(x^2 + z^2) - ryz] dm \\ B_z &= \int_m [-pzx - qzy + r(x^2 + y^2)] dm \end{aligned} \tag{C-44}$$

If we define

$$\begin{aligned} I_{xx} &= \int_m (y^2 + z^2) dm \\ I_{yy} &= \int_m (x^2 + z^2) dm \\ I_{zz} &= \int_m (x^2 + y^2) dm \end{aligned}$$

as the so-called moments of inertia, and

$$\begin{aligned} I_{xy} &= I_{yx} = \int_m xy dm \\ I_{xz} &= I_{zx} = \int_m xz dm \\ I_{yz} &= I_{zy} = \int_m yz dm \end{aligned}$$

as the products of inertia, Eqs. (C-44) can also be written as

$$\begin{aligned} B_x &= pI_{xx} - qI_{xy} - rI_{xz} \\ B_y &= -pI_{xy} + qI_{yy} - rI_{yz} \\ B_z &= -pI_{xz} - qI_{yz} + rI_{zz} \end{aligned} \quad (\text{C-45})$$

or, as a matrix equation:

$$\mathbf{B}_{\text{cm}} = \mathbf{I} \cdot \boldsymbol{\Omega} \quad (\text{C-46})$$

with

$$\mathbf{I} = \begin{bmatrix} I_{xx} & -I_{xy} & -I_{xz} \\ -I_{xy} & I_{yy} & -I_{yz} \\ -I_{xz} & -I_{yz} & I_{zz} \end{bmatrix}$$

called the inertia tensor.

C-5-3 Derivation of the Euler equation of rotational motion

Let us commence with the general formulation of the equation of rotational motion for a mass-varying body, Eq. (C-32)

$$\begin{aligned} \mathbf{M}_{\text{cm}} &= \int_m \tilde{\mathbf{r}} \times \left(\frac{d\boldsymbol{\Omega}}{dt} \times \tilde{\mathbf{r}} \right) dm + \int_m \tilde{\mathbf{r}} \times [\boldsymbol{\Omega} \times (\boldsymbol{\Omega} \times \tilde{\mathbf{r}})] dm + \\ &\quad + 2 \int_m \tilde{\mathbf{r}} \times \left(\boldsymbol{\Omega} \times \frac{\delta \tilde{\mathbf{r}}}{\delta t} \right) dm + \int_m \tilde{\mathbf{r}} \times \frac{\delta^2 \tilde{\mathbf{r}}}{\delta t^2} dm \end{aligned}$$

The last two terms on the right-hand side are the apparent moments due to elasticity and variation of mass. Bringing these terms to the other side, we get the same form of the equation as for a rigid body:

$$\begin{aligned} \mathbf{M}_{\text{cm}} + \mathbf{M}_C + \mathbf{M}_{\text{rel}} &= \tilde{\mathbf{M}}_{\text{cm}} = \int_m \tilde{\mathbf{r}} \times \left(\frac{d\boldsymbol{\Omega}}{dt} \times \tilde{\mathbf{r}} \right) dm + \\ &\quad + \int_m \tilde{\mathbf{r}} \times [\boldsymbol{\Omega} \times (\boldsymbol{\Omega} \times \tilde{\mathbf{r}})] dm \end{aligned} \quad (\text{C-47})$$

For a rigid body, we can derive the equation of rotational motion also in a different way. In the previous sub-section we found

$$\mathbf{B}_{\text{cm}} = \mathbf{I} \cdot \boldsymbol{\Omega} \quad (\text{C-48})$$

With Eqs. (C-5) and (C-28) we then find

$$\mathbf{M}_{\text{cm}} = \frac{d\mathbf{B}_{\text{cm}}}{dt} = \frac{\delta\mathbf{B}_{\text{cm}}}{\delta t} + \boldsymbol{\Omega} \times \mathbf{B}_{\text{cm}} \quad (\text{C-49})$$

The first term on the right-hand side of Eq. (C-49) can be written as

$$\frac{\delta\mathbf{B}_{\text{cm}}}{\delta t} = \frac{\delta\mathbf{I}}{\delta t} \cdot \boldsymbol{\Omega} + \mathbf{I} \cdot \frac{\delta\boldsymbol{\Omega}}{\delta t} = \mathbf{I} \cdot \frac{\delta\boldsymbol{\Omega}}{\delta t} \quad (\text{C-50})$$

since mass is invariant with time for a rigid body, and therefore also the inertia properties. Substituting Eq. (C-50) into Eq. (C-49), and applying Eq. (C-48) one more time we finally get

$$\mathbf{M}_{\text{cm}} = \mathbf{I} \cdot \dot{\boldsymbol{\Omega}} + \boldsymbol{\Omega} \times \mathbf{I} \cdot \boldsymbol{\Omega} \quad (\text{C-51})$$

According to the Principle of Solidification we can use the above equation for a mass-varying (non-rigid) body too, thereby taking the two apparent moments into account and at time t substituting the current mass properties, i.e., mass, and moments and products of inertia in the equations.

Appendix D

Aircraft Parameters

D-1 Introduction

In this appendix a list of stability and control derivatives are given for several aircraft. Also the inertial parameters, i.e. μ_b , μ_c , K_X^2 , K_Y^2 , K_Z^2 , K_{XZ} , etcetera, for these aircraft are provided.

D-2 Linearized Equations of Motion

In this section the linear equations of motion are given in which the inertia parameters and stability and control derivatives have to be substituted for simulation.

$$\begin{bmatrix} C_{X_u} - 2\mu_c D_c & C_{X_\alpha} & C_{Z_0} & C_{X_q} \\ C_{Z_u} & C_{Z_\alpha} + (C_{Z_{\dot{\alpha}}} - 2\mu_c) D_c & -C_{X_0} & C_{Z_q} + 2\mu_c \\ 0 & 0 & -D_c & 1 \\ C_{m_u} & C_{m_\alpha} + C_{m_{\dot{\alpha}}} D_c & 0 & C_{m_q} - 2\mu_c K_Y^2 D_c \end{bmatrix} \begin{bmatrix} \hat{u} \\ \alpha \\ \theta \\ \frac{q\bar{c}}{V} \end{bmatrix} = \\ = \begin{bmatrix} -C_{X_{\delta_e}} \\ -C_{Z_{\delta_e}} \\ 0 \\ -C_{m_{\delta_e}} \end{bmatrix} \delta_e$$

and as in equation (4-43),

$$\begin{bmatrix}
C_{Y_\beta} + (C_{Y_{\dot{\beta}}} - 2\mu_b)D_b & C_L & C_{Y_p} & C_{Y_r} - 4\mu_b \\
0 & -\frac{1}{2}D_b & 1 & 0 \\
C_{\ell_\beta} & 0 & C_{\ell_p} - 4\mu_b K_X^2 D_b & C_{\ell_r} + 4\mu_b K_{XZ} D_b \\
C_{n_\beta} + C_{n_{\dot{\beta}}} D_b & 0 & C_{n_p} + 4\mu_b K_{XZ} D_b & C_{n_r} - 4\mu_b K_Z^2 D_b
\end{bmatrix}
\begin{bmatrix}
\beta \\
\varphi \\
\frac{pb}{2V} \\
\frac{rb}{2V}
\end{bmatrix} =$$

$$= \begin{bmatrix}
-C_{Y_{\delta_a}} & -C_{Y_{\delta_r}} \\
0 & 0 \\
-C_{\ell_{\delta_a}} & -C_{\ell_{\delta_r}} \\
-C_{n_{\delta_a}} & -C_{n_{\delta_r}}
\end{bmatrix}
\begin{bmatrix}
\delta_a \\
\delta_r
\end{bmatrix}$$

D-3 LTI-System Representation

The LTI-system, or state-space, representation of the equations of motions are given below. The symmetric and asymmetric equations of motion in state-space form are, see equations (4-48) and (4-52),

Symmetric equations of motion

$$\begin{bmatrix}
\dot{u} \\
\dot{\alpha} \\
\dot{\theta} \\
\frac{\dot{q}\bar{c}}{V}
\end{bmatrix} = \begin{bmatrix}
x_u & x_\alpha & x_\theta & 0 \\
z_u & z_\alpha & z_\theta & z_q \\
0 & 0 & 0 & \frac{V}{\bar{c}} \\
m_u & m_\alpha & m_\theta & m_q
\end{bmatrix} \begin{bmatrix}
\hat{u} \\
\alpha \\
\theta \\
\frac{q\bar{c}}{V}
\end{bmatrix} + \begin{bmatrix}
x_{\delta_e} \\
z_{\delta_e} \\
0 \\
m_{\delta_e}
\end{bmatrix} \delta_e$$

Asymmetric equations of motion

$$\begin{bmatrix}
\dot{\beta} \\
\dot{\varphi} \\
\frac{\dot{p}b}{2V} \\
\frac{\dot{r}b}{2V}
\end{bmatrix} = \begin{bmatrix}
y_\beta & y_\varphi & y_p & y_r \\
0 & 0 & 2\frac{V}{b} & 0 \\
l_\beta & 0 & l_p & l_r \\
n_\beta & 0 & n_p & n_r
\end{bmatrix} \begin{bmatrix}
\beta \\
\varphi \\
\frac{pb}{2V} \\
\frac{rb}{2V}
\end{bmatrix} + \begin{bmatrix}
0 & y_{\delta_r} \\
0 & 0 \\
l_{\delta_a} & l_{\delta_r} \\
n_{\delta_a} & n_{\delta_r}
\end{bmatrix} \begin{bmatrix}
\delta_a \\
\delta_r
\end{bmatrix}$$

We refer to tables 4-9 and 4-10 for the definition of the parameters used in the above-mentioned state-space representations of the equations of motion.

In the following tables inertial parameters and stability and control derivatives for several aircraft are given.

V	=	59.9 m/sec	m	=	4547.8 kg	\bar{c}	=	2.022 m
S	=	24.2 m ²	l_h	=	5.5 m	μ_c	=	102.7
K_Y^2	=	0.980	x_{cg}	=	0.30 \bar{c}			
C_{X_0}	=	0	C_{Z_0}	=	-1.1360			
C_{X_u}	=	-0.2199	C_{Z_u}	=	-2.2720	C_{m_u}	=	0
C_{X_α}	=	0.4653	C_{Z_α}	=	-5.1600	C_{m_α}	=	-0.4300
$C_{X_{\dot{\alpha}}}$	=	0	$C_{Z_{\dot{\alpha}}}$	=	-1.4300	$C_{m_{\dot{\alpha}}}$	=	-3.7000
C_{X_q}	=	0	C_{Z_q}	=	-3.8600	C_{m_q}	=	-7.0400
$C_{X_{\delta_e}}$	=	0	$C_{Z_{\delta_e}}$	=	-0.6238	$C_{m_{\delta_e}}$	=	-1.5530
b	=	13.36 m	C_L	=	1.1360	μ_b	=	15.5
K_X^2	=	0.012	K_Z^2	=	0.037	K_{XZ}	=	0.002
C_{Y_β}	=	-0.9896	C_{ℓ_β}	=	-0.0772	C_{n_β}	=	0.1638
C_{Y_p}	=	-0.0870	C_{ℓ_p}	=	-0.3444	C_{n_p}	=	-0.0108
C_{Y_r}	=	0.4300	C_{ℓ_r}	=	0.2800	C_{n_r}	=	-0.1930
$C_{Y_{\delta_a}}$	=	0	$C_{\ell_{\delta_a}}$	=	-0.2349	$C_{n_{\delta_a}}$	=	0.0286
$C_{Y_{\delta_r}}$	=	0.3037	$C_{\ell_{\delta_r}}$	=	0.0286	$C_{n_{\delta_r}}$	=	-0.1261

Table D-1: Symmetric and asymmetric stability and control derivatives for the Cessna Ce500 ‘Citation’, Cruise

V	=	124.5 m/sec	m	=	16200 kg	\bar{c}	=	2.58 m
S	=	70.0 m ²				μ_c	=	137.5
K_Y^2	=	2.72	x_{cg}	=	0.32 \bar{c}			
C_{X_0}	=	0	C_{Z_0}	=	-0.45			
C_{X_u}	=	-0.09	C_{Z_u}	=	-0.90	C_{m_u}	=	0
C_{X_α}	=	0.15	C_{Z_α}	=	-5.90	C_{m_α}	=	-0.80
$C_{X_{\dot{\alpha}}}$	=	0	$C_{Z_{\dot{\alpha}}}$	=	-1.59	$C_{m_{\dot{\alpha}}}$	=	-6.50
C_{X_q}	=	0	C_{Z_q}	=	-7.36	C_{m_q}	=	-16.50
$C_{X_{\delta_e}}$	=	0	$C_{Z_{\delta_e}}$	=	-0.44	$C_{m_{\delta_e}}$	=	-1.80
b	=	29.00 m	C_L	=	0.45	μ_b	=	12.22
K_X^2	=	0.0127	K_Z^2	=	0.0342	K_{XZ}	=	0.0
C_{Y_β}	=	-0.90	C_{ℓ_β}	=	-0.09	C_{n_β}	=	0.11
C_{Y_p}	=	-0.23	C_{ℓ_p}	=	-0.60	C_{n_p}	=	0.02
C_{Y_r}	=	0.48	C_{ℓ_r}	=	0.23	C_{n_r}	=	-0.14
$C_{Y_{\delta_a}}$	=	0	$C_{\ell_{\delta_a}}$	=	-0.086	$C_{n_{\delta_a}}$	=	0.0
$C_{Y_{\delta_r}}$	=	0.29	$C_{\ell_{\delta_r}}$	=	0.029	$C_{n_{\delta_r}}$	=	-0.086

Table D-2: Symmetric and asymmetric stability and control derivatives for the Fokker F-27 ‘Friendship’, Cruise

V	=	66.75 m/sec	m	=	1199.8 kg	\bar{c}	=	1.494 m
S	=	16.17 m ²				μ_c	=	47.05
K_Y^2	=	0.6814						
C_{X_0}	=	0	C_{Z_0}	=	-0.310			
C_{X_u}	=	-0.093	C_{Z_u}	=	-0.620	C_{m_u}	=	0
C_{X_α}	=	0.18	C_{Z_α}	=	-4.631	C_{m_α}	=	-0.890
$C_{X_{\dot{\alpha}}}$	=	0	$C_{Z_{\dot{\alpha}}}$	=	-0.850	$C_{m_{\dot{\alpha}}}$	=	-2.600
C_{X_q}	=	0	C_{Z_q}	=	-1.95	C_{m_q}	=	-6.200
$C_{X_{\delta_e}}$	=	0	$C_{Z_{\delta_e}}$	=	-0.430	$C_{m_{\delta_e}}$	=	-1.28

Table D-3: Symmetric stability and control derivatives for the Cessna Ce-172 ‘Skyhawk’, Cruise

V	=	51.82 m/sec	m	=	5897 kg	\bar{c}	=	2.134 m
S	=	21.37 m ²				μ_c	=	105.56
K_Y^2	=	0.8979	x_{cg}	=	0.32 \bar{c}			
C_{X_0}	=	0	C_{Z_0}	=	-1.640			
C_{X_u}	=	0	C_{Z_u}	=	-3.72	C_{m_u}	=	-0.004
C_{X_α}	=	0.580	C_{Z_α}	=	-5.5296	C_{m_α}	=	-0.660
$C_{X_{\dot{\alpha}}}$	=	0	$C_{Z_{\dot{\alpha}}}$	=	-0.80	$C_{m_{\dot{\alpha}}}$	=	-2.50
C_{X_q}	=	0	C_{Z_q}	=	-2.050	C_{m_q}	=	-6.75
$C_{X_{\delta_e}}$	=	0	$C_{Z_{\delta_e}}$	=	-0.400	$C_{m_{\delta_e}}$	=	-0.980

Table D-4: Symmetric stability and control derivatives for the Learjet I, Approach

V	=	103.63 m/sec	m	=	3175 kg	\bar{c}	=	1.981 m
S	=	26.01 m ²				μ_c	=	58.35
K_Y^2	=	1.646						
C_{X_0}	=	0	C_{Z_0}	=	-0.191			
C_{X_u}	=	-0.06	C_{Z_u}	=	-0.402	C_{m_u}	=	0
C_{X_α}	=	0.06	C_{Z_α}	=	-5.510	C_{m_α}	=	-1.890
$C_{X_{\dot{\alpha}}}$	=	0	$C_{Z_{\dot{\alpha}}}$	=	-1.250	$C_{m_{\dot{\alpha}}}$	=	-4.550
C_{X_q}	=	0	C_{Z_q}	=	-4.05	C_{m_q}	=	-17.00
$C_{X_{\delta_e}}$	=	0	$C_{Z_{\delta_e}}$	=	-0.600	$C_{m_{\delta_e}}$	=	-2.00

Table D-5: Symmetric stability and control derivatives for the Beechcraft M99, Cruise

V	=	67.36 m/sec	m	=	255830 kg	\bar{c}	=	8.321 m
S	=	510.97 m ²	l_h	=	31.09 m	μ_c	=	49.12
K_Y^2	=	2.3345	x_{cg}	=	0.25 \bar{c}			
C_{X_0}	=	0	C_{Z_0}	=	-1.760			
C_{X_u}	=	0	C_{Z_u}	=	-3.3	C_{m_u}	=	0.071
C_{X_α}	=	0.630	C_{Z_α}	=	-5.933	C_{m_α}	=	-1.450
$C_{X_{\dot{\alpha}}}$	=	0	$C_{Z_{\dot{\alpha}}}$	=	-3.350	$C_{m_{\dot{\alpha}}}$	=	-1.650
C_{X_q}	=	0	C_{Z_q}	=	-2.825	C_{m_q}	=	-10.70
$C_{X_{\delta_e}}$	=	0	$C_{Z_{\delta_e}}$	=	-0.360	$C_{m_{\delta_e}}$	=	-1.400

Table D-6: Symmetric stability and control derivatives for the Boeing 747-100, Approach

V	=	129.1 m/sec	m	=	254240 kg	\bar{c}	=	8.321 m
S	=	510.97 m ²	l_h	=	31.09 m	μ_c	=	56.51
K_Y^2	=	2.488	x_{cg}	=	0.32 \bar{c}	ρ	=	1.058 kg m ⁻³
C_{X_0}	=	0	C_{Z_0}	=	-0.477			
C_{X_u}	=	-0.0478	C_{Z_u}	=	-0.954	C_{m_u}	=	-0.0252
C_{X_α}	=	0.687	C_{Z_α}	=	-4.487	C_{m_α}	=	-0.554
$C_{X_{\dot{\alpha}}}$	=	0	$C_{Z_{\dot{\alpha}}}$	=	6.62	$C_{m_{\dot{\alpha}}}$	=	-3.39
C_{X_q}	=	0	C_{Z_q}	=	-4.27	C_{m_q}	=	-19.45
$C_{X_{\delta_e}}$	=	0	$C_{Z_{\delta_e}}$	=	-0.353	$C_{m_{\delta_e}}$	=	-1.42

Table D-7: Symmetric stability and control derivatives for the Boeing 747-100, Holding, flaps up

V	=	73.0 m/sec	m	=	254240 kg	\bar{c}	=	8.321 m
S	=	510.97 m ²	l_h	=	31.09 m	μ_c	=	48.81
K_Y^2	=	2.488	x_{cg}	=	0.32 \bar{c}	ρ	=	1.125 kg m ⁻³
C_{X_0}	=	0	C_{Z_0}	=	-1.49			
C_{X_u}	=	-0.42	C_{Z_u}	=	-2.98	C_{m_u}	=	-0.185
C_{X_α}	=	1.59	C_{Z_α}	=	-5.293	C_{m_α}	=	-1.05
$C_{X_{\dot{\alpha}}}$	=	0	$C_{Z_{\dot{\alpha}}}$	=	6.70	$C_{m_{\dot{\alpha}}}$	=	-3.45
C_{X_q}	=	0	C_{Z_q}	=	-6.66	C_{m_q}	=	-21.98
$C_{X_{\delta_e}}$	=	0	$C_{Z_{\delta_e}}$	=	-0.353	$C_{m_{\delta_e}}$	=	-1.42

Table D-8: Symmetric stability and control derivatives for the Boeing 747-100, Approach, flaps 33°

V	=	66.142 m/sec	m	=	249650 kg	\bar{c}	=	8.321 m
S	=	510.97 m ²	l_h	=	31.09 m	μ_c	=	48.40
K_Y^2	=	3.77	x_{cg}	=	0.25 \bar{c}	ρ	=	1.125 kg m ⁻³
C_{X_0}	=	-0.0944	C_{Z_0}	=	-1.80			
C_{X_u}	=	-0.90	C_{Z_u}	=	-3.60	C_{m_u}	=	0
C_{X_α}	=	1.2542	C_{Z_α}	=	-5.344	C_{m_α}	=	-1.536
$C_{X_{\dot{\alpha}}}$	=	0	$C_{Z_{\dot{\alpha}}}$	=	-2.00	$C_{m_{\dot{\alpha}}}$	=	-1.70
C_{X_q}	=	0	C_{Z_q}	=	-2.84	C_{m_q}	=	-10.75
$C_{X_{\delta_e}}$	=	0	$C_{Z_{\delta_e}}$	=	-0.355	$C_{m_{\delta_e}}$	=	-1.409

Table D-9: Symmetric stability and control derivatives for the Boeing 747-100, Landing

V	=	145 m/sec	μ_b	=	17.219	h	=	6900 m
S	=	153.5 m ²	K_X^2	=	0.0283			
b	=	37.49 m	K_Z^2	=	0.0471			
m	=	59020 kg	K_{XZ}	=	0			
C_{Y_β}	=	-0.5960	C_{ℓ_β}	=	-0.1374	C_{n_β}	=	0.1173
C_{Y_p}	=	0	C_{ℓ_p}	=	-0.5200	C_{n_p}	=	-0.0210
C_{Y_r}	=	0.3690	C_{ℓ_r}	=	0.1440	C_{n_r}	=	-0.1800
$C_{Y_{\delta_a}}$	=	0	$C_{\ell_{\delta_a}}$	=	-0.0975	$C_{n_{\delta_a}}$	=	0.0052
$C_{Y_{\delta_r}}$	=	0.2150	$C_{\ell_{\delta_r}}$	=	0	$C_{n_{\delta_r}}$	=	-0.1030

Table D-10: Asymmetric stability and control derivatives for the Lockheed L1049C ‘Super Constellation’, Cruise

V	=	65.4 m/sec	μ_b	=	7.26	h	=	0 m
S	=	153.5 m ²	K_X^2	=	0.0326			
b	=	37.49 m	K_Z^2	=	0.0543			
m	=	51200 kg	K_{XZ}	=	0			
C_{Y_β}	=	-0.5610	C_{ℓ_β}	=	-0.1374	C_{n_β}	=	0.1173
C_{Y_p}	=	0	C_{ℓ_p}	=	-0.5200	C_{n_p}	=	-0.0626
C_{Y_r}	=	0.1945	C_{ℓ_r}	=	0.2750	C_{n_r}	=	-0.1800
$C_{Y_{\delta_a}}$	=	0	$C_{\ell_{\delta_a}}$	=	-0.0975	$C_{n_{\delta_a}}$	=	0.0052
$C_{Y_{\delta_r}}$	=	0.2150	$C_{\ell_{\delta_r}}$	=	0	$C_{n_{\delta_r}}$	=	-0.1030

Table D-11: Asymmetric stability and control derivatives for the Lockheed L1049C ‘Super Constellation’, Approach

V	=	77.1 m/sec	μ_b	=	7.185	h	=	0 m
S	=	470 m ²	K_X^2	=	0.052			
b	=	24.4 m	K_Z^2	=	0.249			
m	=	100000 kg	K_{XZ}	=	-0.066			
C_{Y_β}	=	-0.3640	C_{ℓ_β}	=	-0.1660	C_{n_β}	=	0.1360
C_{Y_p}	=	0	C_{ℓ_p}	=	-0.1410	C_{n_p}	=	-0.1430
C_{Y_r}	=	0	C_{ℓ_r}	=	0.2500	C_{n_r}	=	-0.2100
$C_{Y_{\delta_a}}$	=	0	$C_{\ell_{\delta_a}}$	=	-0.1010	$C_{n_{\delta_a}}$	=	0
$C_{Y_{\delta_r}}$	=	0.1290	$C_{\ell_{\delta_r}}$	=	0	$C_{n_{\delta_r}}$	=	-0.0790

Table D-12: Asymmetric stability and control derivatives for the BAC-Aerospatiale ‘Concorde’, Approach

V	=	660 m/sec	μ_b	=	1072	h	=	20000 m
S	=	18.6 m ²	K_X^2	=	0.0134			
b	=	6.7 m	K_Z^2	=	0.247			
m	=	11800 kg	K_{XZ}	=	0			
C_{Y_β}	=	-1.4200	C_{ℓ_β}	=	0.0100	C_{n_β}	=	0.4000
C_{Y_p}	=	0	C_{ℓ_p}	=	-0.3150	C_{n_p}	=	0
C_{Y_r}	=	0	C_{ℓ_r}	=	0	C_{n_r}	=	-1.4500
$C_{Y_{\delta_a}}$	=	-0.0735	$C_{\ell_{\delta_a}}$	=	-0.0500	$C_{n_{\delta_a}}$	=	0.0490
$C_{Y_{\delta_r}}$	=	0.3200	$C_{\ell_{\delta_r}}$	=	0.0100	$C_{n_{\delta_r}}$	=	-0.2000

Table D-13: Asymmetric stability and control derivatives for the North-American X-15 experimental aircraft, Cruise (unspecified)

V	=	40.2 m/sec	μ_b	=	5.56	h	=	0 m
S	=	23.23 m ²	K_X^2	=	0.0845			
b	=	14.63 m	K_Z^2	=	0.0192			
m	=	2315 kg	K_{XZ}	=	0			
C_{Y_β}	=	-0.6000	C_{ℓ_β}	=	-0.0560	C_{n_β}	=	0.0248
C_{Y_p}	=	0	C_{ℓ_p}	=	-0.5500	C_{n_p}	=	-0.0600
C_{Y_r}	=	0.1600	C_{ℓ_r}	=	0.1200	C_{n_r}	=	-0.0530
$C_{Y_{\delta_a}}$	=	0	$C_{\ell_{\delta_a}}$	=	-0.1120	$C_{n_{\delta_a}}$	=	0.0015
$C_{Y_{\delta_r}}$	=	0.2420	$C_{\ell_{\delta_r}}$	=	0	$C_{n_{\delta_r}}$	=	-0.0970

Table D-14: Asymmetric stability and control derivatives for the De Havilland Canada DHC-2 ‘Beaver’, Approach

Bibliography

- [1] J.H. Abbot and A.E. von Doenhoff. *Theory of wing sections*. Dover Publications, New York, 1960, (see also NACA Rep. 824).
- [2] H.J. Allan. Estimation of the forces and moments acting on inclined bodies of revolution at low mach numbers. Technical report, NACA R.M. A9 126, 1949.
- [3] H.J. Allen and E.W. Perkins. A study of effects of viscosity on flow over slender inclined bodies of revolution. Technical report, NACA Report 1048, 1951.
- [4] M.B. Ames and R.E. Sears. Determination of control surface characteristics from naca plain-flap and tab data. Technical report, NACA Rep. 721, 1941.
- [5] R.F. Anderson. Determination of the characteristics of tapered wings. Technical report, NACA Rep. 572, 1936.
- [6] Anonymous. British civil airworthiness requirements section d, aeroplanes. Technical report, Air Registration Board, London.
- [7] Anonymous. Civil air regulations (c.a.r.) 4b, airplane airworthiness-transport categories. Technical report, Civil Aeronautics Board, Washington D.C.
- [8] Anonymous. Data sheets, aerodynamics. Technical report, R. Ae. Soc. London.
- [9] Anonymous. Data sheets, aerodynamics, vols. i, ii and iii. Technical report, Royal Aeronautical Society.
- [10] Anonymous. Data sheets aerodynamics, vols, i, ii and iii. Technical report, Royal Aeron. Society, London.
- [11] Anonymous. Federal aviation regulations, subchapter c, aircraft, part 25. Technical report, F.A.A. Washington.
- [12] Anonymous. Icao, airworthiness of aircraft, annex 8, part iii. Technical report, Chapters 2 and 3.
- [13] Anonymous. Specification for flying qualities of piloted aeroplanes. Technical report, Bureau of Aeronautics, SR-119B, 1948.
- [14] Anonymous. Verslag der vliegproeven met het vliegtuig ft 404, type north-american “harvard ii b”, deel d: Statische stuurstanddwarsstabiliteit. Technical report, N.L.L. Rapport V. 1422 d, 1950 (in Dutch).

- [15] Anonymous. Samenvatting der resultaten van het experimentele onderzoek der vliegeigenschappen van het vliegtuig ft 404, type north american harvard ii b. Technical report, N.L.L. Rapport V 1599, 1951 (in Dutch).
- [16] Anonymous. Verslag van vliegproeven ter bepaling van langsstabiliteit en besturingseigenschappen in glijvlucht met beide schroeven in vaanstand van het vliegtuig ph-nll type siebel 204-d-1. Technical report, N.L.L. Rapport V 1698, 1953 (in Dutch).
- [17] Anonymous. F-27 staartvlakmodel 1:9. eigenschappen van het horizontale staartvlak. Technical report, N.L.L. Rapport A 1389, 1955 (in Dutch).
- [18] Anonymous. Verzameling van grootheden betreffende stabiliteit en besturing van moderne vliegtuigen. Technical report, N.L.L. T.M. V. 1864, 1960 (in Dutch).
- [19] Anonymous. Military specification, flying qualities of piloted airplanes. Technical report, MIL-F-8785B (A.S.G.), 1969.
- [20] Anonymouys. Ministry of aviation. design requirements for aircraft for the royal air force and royal navy. Technical report, Aviation publication 970, Part 6, 1948.
- [21] W.R. Bates. Collection and analysis of windtunnel data on the characteristics of isolated tail surfaces with and without end plates. Technical report, NACA T.N. 1291, 1947.
- [22] W.R. Bates. Static stability of fuselages having a relatively flat cross section. Technical report, NACA T.N. 3429, 1955.
- [23] H. Binkhorst. Metingen in de vlucht van de stuurverplaatsing per ‘g’ en de stuurkracht per ‘g’ in afvangmanoeuvres en in zuivere bochten van het vliegtuig austor j-5b “autocar”, ph-neh. Technical report, V.T.H.-Rapport 95, 1960 (in Dutch).
- [24] H. Binkhorst. Windtunnelmetingen aan een model van de fokker f-27 “friendship”. Technical report, VTH M47, 1961 (in Dutch).
- [25] J. Bird. Some theoretical low-speed span loading characteristics of swept wings in roll and sideslip. Technical report, NACA Report 969, 1950.
- [26] P.L. Bisgood and D.J. Lyons. Preliminary report of the flight measurement of aeroelastic distortions in relation to its effect on the control and longitudinal stability of a mosquito aircraft. Technical report, R. and M. 2371, 1949.
- [27] P.L. Bisgood and D.J. Lyons. Preliminary report on the flight-measurement of aeroelastic distortion in relation to its effects on the control and longitudinal stability of a mosquito aircraft. Technical report, R. and M. 2371, 1949.
- [28] P.J. Bobbitt. Tables for the rapid estimation of downwash and sidewash behind wings performing various motions at supersonic speeds. Technical report, NASA Memo 2-20-59 K, 1959.
- [29] P.J. Bobbitt and D.A. Malvestuto Jr. Estimation of forces and moments due to rolling for several slender-tail configurations at supersonic speeds. Technical report, NACA T.N. 2955, 1953.
- [30] J.L. Boiffier. *The Dynamics Of Flight, The Equations*. John Wiley & Sons, 1998.
- [31] K.W. Booth. Effect of horizontal-tail chord on the calculated subsonic span loads and stability derivatives of isolated unswept tail assemblies in sideslip and steady roll. Technical report, NASA Memo 4-1-59 L, 1959.
- [32] C. Brady. Boeing 737. <http://www.b737.org.uk/>, 1999.

- [33] J.P. Campbell and A. Goodman. A semi-empirical method for estimating the rolling moment due to yawing of airplanes. Technical report, NACA T.N. 1984, 1949.
- [34] J.P. Campbell and M.O. McKinney. Summary of methods for calculating dynamic lateral stability and response and for estimating lateral stability derivatives. Technical report, NACA Report 1098 and T.N. 2409, 1952, 1951.
- [35] NASA Dryden Flight Research Center. X-29 at high angle of attack with smoke generators. <http://www.dfrc.nasa.gov/gallery/photo/index.html>, 1991.
- [36] D.C. Cheatman. A study of the characteristics of human pilot control response to simulated lateral motions. Technical report, NACA Rep. 1197, 1954.
- [37] K.L. Coin. Equations and charts for the rapid estimation of hinge moment and effectiveness parameters for trailing edge controls having leading and trailing edges swept ahead of the mach lines. Technical report, NACA Rep. 1041, 1959.
- [38] MBB Space Communication and Propulsion Systems Division. Study on re-entry guidance and control. Technical report, ESA report reference: ESA CR (P) 2652, 1988.
- [39] W.L. Cowley and H. Glauert. The effect of the lag of the downwash on the longitudinal stability of an aeroplane on the rotary derivative. Technical report, R. and M. 718, 1921.
- [40] A. Damon, H.W. Stoudt, and R.A. McFarland. *The human body in equipment design*. Havard University Press., Cambridge (Mass.), 1967.
- [41] P. de Lange, J.H. Pelleboer, and J. Zaaijer. De coördinaten van het zwaartepunt en de grootte van het gewicht en massatraagheidsmoment van het vliegtuig dhc-2 “beaver”, ph-vth, ten behoeve van in oktober/november 1968 uitgevoerde metingen in niet-stationare symmetrische vlucht. Technical report, V.T.H. Memorandum M-165, 1970 (in Dutch).
- [42] P. de Lange, J.H. Pelleboer, and J. Zaaijer. De coördinaten van het zwaartepunt en de grootte van het gewicht en massatraagheidsmoment van het vliegtuig dhc-2 “beaver”, ph-vth, ten behoeve van in oktober/november 1968 uitgevoerde metingen in niet-stationare symmetrische vlucht. Technical report, V.T.H. Memorandum M-165, 1970 (in Dutch).
- [43] J. de Young. Spanwise loading for wings and control surfaces of low aspect ratio. Technical report, NACA T.N. 2011, 1950.
- [44] J. de Young. Spanwise loading for wings and control surfaces of low aspect ratio. Technical report, NACA T.N. 2011, 1950.
- [45] J. de Young. Theoretical antisymmetric span loading for wings of arbitrary plan at subsonic speeds. Technical report, NACA Report 1056, 1951.
- [46] J. de Young. Theoretical symmetric span loading due to flap deflection for wings of arbitrary plan form at subsonic speeds. Technical report, NACA Rep. 1071, 1952.
- [47] J. de Young. Theoretical symmetric span loading due to flap deflection for wings of arbitrary plan form at subsonic speeds. Technical report, NACA Report 1071, 1952.
- [48] J. de Young. Theoretical symmetric span loading due to flap deflection for wings of arbitrary plan forms at subsonic speeds. Technical report, NACA Rep. 1071, 1952.
- [49] J. de Young and W.H. Barling. Prediction of downwash behind swept-wing airplanes at subsonic speed. Technical report, NACA T.N. 3346, 1955.
- [50] J. de Young and C.W. Harper. Theoretical symmetric span loading at subsonic speeds for wings having arbitrary plan form. Technical report, NACA Rep. 921, 1948.

- [51] G.L. Decker. Prediction of downwash at various angles of attack for arbitrary tail locations. *Aero. eng. Rev.*, 15(7):22 to 27, 61, 1956.
 - [52] F.E. Douwes Dekker and W.J. Molier. Vliegeigenschappen van het fokker f-27 vliegtuig. Technical report, N.L.L. Rapport V. 1902, 1962 (in Dutch).
 - [53] F.D. Diederich. Charts and tables for use in calculations of downwash of wings of arbitrary plan form. Technical report, NACA T.N. 2353, 1951.
 - [54] A.F. D'Souza. *Design of control systems*. Prentice Hall, Inc., Englewood Cliffs, New Jersey, 1988.
 - [55] W.J. Duncan. *The principles of the control and stability of aircraft*. University Press, Cambridge, 1952.
 - [56] R.F. Antoniewicz E.L. Duke and K.D. Krambeer. Derivation and definition of a linear aircraft model. Technical report, NASA Reference Publication 1207, 1988.
 - [57] B. Etkin. *Dynamics of atmospheric flight*. John Wiley & Sons, Inc., New York, 1972.
 - [58] V.M. Falkner and D. Lehrians. Calculated loadings due to incidence of a number of straight and swept-back wings. Technical report, R. and M. 2596, 1948.
 - [59] L.R. Fischer and H.S. Fletcher. Effect of lag of sidewash on the vertical-tail contribution to oscillatory damping in yaw of airplane models. Technical report, NACA T.N. 3356, 1955.
 - [60] L.R. Fisher. Approximate corrections for the effects of compressibility on the subsonic stability derivatives of swept wings. Technical report, NACA T.N. 1854, 1949.
 - [61] R.W. Franks. The application of a simplified lifting-surface theory to the prediction of the rolling effectiveness of plain spoiler ailerons at subsonic speeds. Technical report, NACA R.M. A54 H 26a, 1954.
 - [62] G.C. Furlong and J.G. McHugh. A summary and analysis of the low-speed longitudinal characteristics of swept wings at high reynolds numbers. Technical report, NACA Rep. 1339, 1957.
 - [63] K. Gersten. Berechnung der aerodynamischen beiwerte von tragflügeln endlicher spannweite in bodennähe. *Abhandlungen der Braunschweig. Wissenschaft. Gesellschaft.*, XII:95 to 115, 1960 (in German).
 - [64] R.R. Gilruth and W.N. Turner. Lateral control required for satisfactory flying qualities based on flight tests of numerous airplanes. Technical report, NACA Report 715, 1941.
 - [65] H.J. Goett and J.P. Reeder. Effects of elevator nose shape, gap balance and tabs on the aerodynamic characteristics of a horizontal tail surface. Technical report, NACA Rep. 675, 1939.
 - [66] A. Goodman and G.H. Adair. Estimation of the damping in roll of wings through the normal flight range of lift coefficient. Technical report, NACA T.N. 1924, 1949.
 - [67] A. Goodman and J.D. Brewer. Investigation at low-speeds of the effect of aspect ratio and sweep on static and yawing stability derivatives of untapered wings. Technical report, NACA T.N. 1669, 1948.
 - [68] A. Goodman and L.E. Fisher. Investigations at low speeds of the effect of aspect ratio and sweep on rolling stability derivatives of untapered wings. Technical report, NACA Report 968, 1950.
-

- [69] M.N. Gough and A.P. Beard. Limitations of the pilot in applying forces to airplane controls. Technical report, NACA T.N. 550, 1936.
- [70] X. Hafer. Untersuchungen zur aerodynamik der fl ü gel-rumpf-anordnungen. Technical report, W.G.L. Jb., 1957, pages 181 to 208 (See also thesis of the same name, Fakult ä t f ü r Maschinenwesen, Braunschweig) (in German).
- [71] S.H. Harman and L. Jeffreys. Theoretical lift and damping-in-roll of thin wings with arbitrary sweep and taper at supersonic speeds. supersonic leading and trailing edges. Technical report, NACA T.N. 2114, 1950.
- [72] K.G. Hecks. The high speed shape. pitch-up and palliatives adopted on swept-wing aircraft. *Flight International*, 85:13 to 18, 1964.
- [73] H. Hertel. Ermittlung der gr ö ssten aufbringbaren steuer kr ä fte und erreichbaren geschwindigkeiten der steuerbet ä tigung. *Zeitschrift f ü r Flugtechnik und Motorluftschifffahrt*, 21 Jrg., page 36 to 45, 1930 (in German).
- [74] D.E. Hoak and J.W. Carlson. *USAF Stability and Control Handbook*. Douglas Aircraft Company Inc., 1961.
- [75] D.E. Hoak and J.W. Carlson. *USAF, Stability and Control Handbook*. Douglas Aircraft Co. Inc, 2 edition, 1968.
- [76] D.E. Hoak and J.W. Carlson. *USAF Stability and Control Handbook, 2nd ed.* Douglas Aircraft Co., Inc., 1968.
- [77] H.P. Hoggard and J.R. Hagerman. Downwash and wake behind untapered wings of various aspect ratios and angles of sweep. Technical report, NACA T.N. 1703, 1948.
- [78] V. Holmboe. Charts for the position of the aerodynamic centre at low speeds and small angles of attack for a large family of tapered wings. Technical report, Saab T.N. 27, 1954.
- [79] E.J. Hopkins. Lift, pitching moment and span load characteristics of wings at low speed as affected by variations of sweep and aspect ratio. Technical report, NACA T.N. 2284, 1951.
- [80] E.J. Hopkins. A semi-empirical method for calculating the pitching moment of bodies of revolution at low mach numbers. Technical report, NACA R.M. C14, 1951.
- [81] A. Hurwitz. Ueber die bedingungen, unter welchen eine gleichung nur wurzeln mit negativen re ä llen teilen besitzt. *Mathematische Werke*, Band II, Zahlentheorie und Geometrie:533 to 545, 1933.
- [82] North American Aviation Inc. Aerodynamic data manual for project apollo. Technical report, NASA-CR-82907, 1965.
- [83] W. Jacobs. The influence of the induced sidewind on the efficiency of the vertical tail. a simplified method for calculation. Technical report, F.A.A. Report 35, 1950.
- [84] W. Jacobs. Lift and moment changes due to the fuselage for a yawed aeroplane with unswept and swept wings. Technical report, F.A.A. Report 34, 1950.
- [85] W. Jacobs. The induced sidewind behind swept wings at subsonic velocities. Technical report, F.A.A. Report 41, 1951.
- [86] W. Jacobs. Theoretical and experimental investigations of interference effects of delta wing-vertical tail combinations with yaw. Technical report, F.A.A. Report 49, 1953.
- [87] W. Jacobs and E. Truckenbrodt. Der induzierte seitewind von flugzeugen. *Ing. Archiv*, 21:1 to 22, 1953 (in German).

- [88] A.L. Jones and A. Alksne. A summary of lateral stability derivatives calculated for wing plan forms in supersonic flow. Technical report, NACA Report 1052, 1951.
- [89] F.S. Malvestuto Jr. and K. Margolis. Theoretical stability derivatives of thin sweptback wings tapered to a point with swept back or sweptforward trailing edges for a limited range of supersonic speeds. Technical report, NACA Report 971, 1950.
- [90] J.B. Dods Jr. and B.E. Tinling. Summary of results of a windtunnel investigation of nine related horizontal tails. Technical report, NACA T.N. 3497, 1955.
- [91] R.P. Harper Jr. Flight evaluations of various longitudinal handling qualities in a variable stability jet fighter. Technical report, Cornell Aero. Lab. WADC T.R. 55-299, 1955.
- [92] T.J. King Jr. and T.B. Pasteur Jr. Wind-tunnel investigation of the aerodynamic characteristics in pitch of wing-fuselage combinations at high subsonic speeds. taper-ratio series. Technical report, NACA T.N. 3867, 1956.
- [93] W.C. Moseley Jr., R.H. Moore Jr., and J.E. Hughes. Stability characteristics of the apollo command module. Technical report, NASA TN D-3890, 1967.
- [94] W.E. Cotter Jr. Summary and analysis of data on damping in yaw and pitch for a number of airplane models. Technical report, NACA T.N. 1980, 1946.
- [95] W.H. Michael Jr. Analysis of the effects of wing interference on the tail contributions to the rolling derivatives. Technical report, NACA Report 1086, 1952.
- [96] W.H. Michael Jr. Investigation of mutual interference effects of several vertical tail-fuselage configurations in sideslip. Technical report, NACA T.N. 3135, 1954.
- [97] H.F.R. Schöyer J.W. Cornelisse and K.F. Wakker. *Rocket propulsion and spaceflight dynamics*. Pitman, London, 1979.
- [98] S. Katzoff and W. Mutterperl. The end-plate effect of a horizontal-tail surface on a vertical-tail surface. Technical report, NACA T.N. 797, 1941.
- [99] S. Katzoff and H.H. Sweburg. Ground effect on downwash angles and wake location. Technical report, NACA Rep. 738, 1943.
- [100] M. Kayton and W.R. Fried. *Avionics Navigation Systems*. John Wiley & Sons, Inc., 2 edition, 1997.
- [101] V. Klein. Estimation of aircraft aerodynamic parameters from flight data. *Aerospace Sci.*, 26:1 to 77, 1989.
- [102] C.C. Kranenburg, P. de Lange, and J.A. Mulder. Determination of the rigid body inertial characteristics of the de havilland dhc-2 “beaver” experimental aircraft from high accuracy measurements of free oscillations. Technical report, V.T.H. Report, LR-337, Delft University of Technology, Department of Aerospace, Delft, 1982.
- [103] C.C. Kranenburg, P. de Lange, and J.A. Mulder. Determination of the rigid body inertial characteristics of the de havilland dhc-2 “beaver” experimental aircraft from high accuracy measurements of free oscillations. Technical report, V.T.H. Report, LR-337, Delft University of Technology, Department of Aerospace Engineering, Delft, 1982.
- [104] R.E. Kuhn and J.W. Wiggins. Wind-tunnel investigations of the aerodynamic characteristics in pitch of wing-fuseage combinations at high subsonic speeds. aspect-ratio series. Technical report, NACA R.M. L52 A29, 1952.
- [105] B.C. Kuo. *Automatic control systems*. Prentice Hall, Inc., Englewood Cliffs, New Jersey, 1987.

- [106] R.A. Lagerstrom and M.E. Graham. Linearized theory of supersonic control surfaces. *Aero. Sci.*, 16:31 to 34, 1949.
- [107] R.A. Lagerstrom and M.E. Graham. Linearized theory of supersonic control surfaces. *Aero. Sci.*, 16:31 to 34, 1949.
- [108] J.G. Lowry. Data on spoiler-type ailerons. Technical report, NACA R.M. L53 124a, 1953.
- [109] D. Lyons and P.L. Bisgood. An analysis of the lift slope of aerofoils of small aspect ratio, including fins, with design charts for aerofoils and control surfaces. Technical report, R. and M. 2308, 1945.
- [110] D.J. Lyons and P.L. Bisgood. An analysis of the lift slope of aerofoils of small aspect ratio including fins with design charts for aerofoils and control surfaces. Technical report, R. and M. 2038,, 1945.
- [111] D.L. Lyons and P.L. Bisgood. An analysis of the lift slope of aerofoils of small aspect ratio including fins, with design charts for aerofoils and control surfaces. Technical report, R. and M. 2308, 1945.
- [112] J.G. Malkin. Theorie der stabilit ä t einer bewegung. Technical report, R. Oldenburg, M ü nchen, 1959 (in German).
- [113] J. Man é e. Windtunnel investigation of the influence of the aircraft configuration on the yawing and rolling moment of a twin-engined, propeller-driven aircraft with one engine inoperative. Technical report, N.L.L. Rapport A 1508 B (see also N.L.L. Rapport A 1508 A), 1963.
- [114] K. Margolis and P.J. Bobbitt. Theoretical calculations of the pressures, forces and moments at supersonic speeds due to various lateral motions acting on thin isolated vertical-tails. Technical report, NACA Report 1268, 1956.
- [115] K. Margolis and M.H. Elliot. Theoretical calculations of the pressures, forces and moments due to various lateral motions acting on tapered sweptback vertical tails with supersonic leading and trailing edges. Technical report, NASA T.N. D-383, 1960.
- [116] K. Margolis, W.L. Sherman, and M.E. Hannah. Theoretical calculation of the pressure distribution, span loading, and rolling moment due to sideslip at supersonic speeds for thin sweptback tapered wings with supersonic trailing edges and wing tips parallel to the axis of wing symmetry. Technical report, NACA T.N. 2898, 1953.
- [117] J.C. Martin and F.S. Mavestuto Jr. Theoretical forces and moments due to sideslip of a number of vertical tail configurations at supersonic speeds. Technical report, NACA T.N. 2412, 1951.
- [118] A.P. Martina. Method for calculating the rolling and yawing moments due to rolling for unswept wings with or without flaps or ailerons by use of non-linear section lift data. Technical report, NACA T.N. 2937, 1953.
- [119] W.H. McAvoy. Maximum forces applied by pilots to wheeltype controls. Technical report, NACA T.N. 628, 1937.
- [120] S.W. McCuskey. *An Introduction To Advanced Dynamics*. Addison-Wesley Publ. Co. Inc., 1958.
- [121] Silent Thunder Models. <http://www.silentthundermodels.com/>, October 2005.
- [122] E. Mooij. *Space Plane Flight Dynamics. Analysis of Guidance and Control Concepts*. PhD Thesis, Delft, The Netherlands, 1998.

- [123] H. Multhopp. Zur aerodynamik des flugzeugrumpfes. *Luftfahrtforschung*, 18:52 to 66 (in German), 1941.
- [124] M. Munk. The aerodynamic forces on airship hulls. Technical report, NACA Rep. 184, NACA Rep. 184,
- [125] H.E. Murray. Wind-tunnel investigation of end-plate effects of horizontal tails on a vertical tail compared with available theory. Technical report, NACA T.N. 1050, 1946.
- [126] R.H. Neely and R.F. Griner. Summary and analysis of horizontal-tail contribution to longitudinal stability of swept wing airplanes at low speeds. Technical report, NACA Rep. R-49, 1959.
- [127] W.H. Nelson and W.J. Krumm. The transonic characteristics of 38 cambered rectangular wings of varying aspect-ratio and thickness as determined by the transonic-bump technique. Technical report, NACA T.N. 3502, 1955.
- [128] W.H. Nelson and J.B. McDevitt. The transonic characteristics of 22 rectangular symmetrical wing models of varying aspect-ratio and thickness. Technical report, NACA T.N. 3501, 1955.
- [129] J.L. Overbeeke. Measurements of the control force-time relations for sudden movements of the controls. Technical report, N.L.L.-T.N. V 1816, 1958.
- [130] H.A. Pearson and R.F. Anderson. Calculation of the aerodynamic characteristics of tapered wings with partial-span flaps. Technical report, NACA Rep. 665, 1939.
- [131] H.A. Pearson and R.T. Jones. Theoretical stability and control characteristics of wings with various amounts of taper and twist. Technical report, NACA Report 635, 1938.
- [132] C.D. Perkins and R.E. Hage. *Airplane performance, stability and control*. John Wiley and Sons Inc., New York, Chapman and Hall Ltd. London, 1949.
- [133] W.J.G. Pinsker. A semi-empirical method for estimating the rotary rolling moment derivatives of swept and slender wings. Technical report, RAE T.N. Aero. 2641, 1959.
- [134] E.C. Polhamus. A simple method of estimating the subsonic lift and damping in roll of swept-back wings. Technical report, NACA T.N. 1862, 1949.
- [135] E.C. Polhamus. Some factors affecting the variation of pitching moment with sideslip of aircraft configurations. Technical report, NACA T.N. 4016, 1958.
- [136] E.C. Polhamus and W.C. Sleeman Jr. The rolling moment due to sideslip of swept wings at subsonic and transonic speeds. Technical report, NACA T.N. D-209, 1960.
- [137] E.C. Polhamus and K.P. Spreemann. Subsonic wind-tunnel investigation of the effects of fuselage afterbody on directional stability of wing-fuselage combinations at high angles of attack. Technical report, NACA T.N. 3896, 1956.
- [138] W.H. Press, B.P. Flannery, S.A. Teukolsky, and W.T. Vetterling. *Numerical recipes in C++*. Cambridge University Press, Cambridge, 1989.
- [139] P.E. Purser. An approximation to the effect of geometric dihedral on the rolling moment due to sideslip for wings at transonic and superonic speeds. Technical report, NACA R.M. L52 B01, 1952.
- [140] M.J. Queijo. Theoretical span load distributions and rolling moments for sideslipping wings of arbitrary plan form in incompressible flow. Technical report, NACA Report 1296, 1956.
- [141] M.J. Queijo and D.R. Riley. Calculated subsonic span loads and resulting derivatives of unswept and 45° sweptback tail surfaces in sideslip and in steady roll. Technical report, NACA T.N. 3245, 1945.

- [142] E.T. Raymond and C.C. Chenoweth. *Aircraft Flight Control Actuation System Design*. Society of Autonotive Engineers, Inc., 400 Commonwealth Drive, Warrendale, PA 15096-0001, USA, 1993.
- [143] H.S. Ribner. Formulas for propellers in yaw and charts of the side-force derivative. Technical report, NACA Report 819, 1945.
- [144] H.S. Ribner. Propellers in yaw. Technical report, NACA Report 820, 1945.
- [145] D.R. Riley. Effect of horizontal-tail span and vertical location on the aerodynamic characteristics of an unswept tail assembly in sideslip. Technical report, NACA Report 1171 and T.N. 2907, 1954, 1953.
- [146] Rosebut. Wright flyer 1. <http://www.earlyaviator.com/>, December 1903.
- [147] E.J. Routh. *Dynamics of a system of Rigid Bodies*. MacMillan and Co., London, 1905.
- [148] M.D. White R.R. Gilruth. Analysis and prediction of longitudinal stability of aircraft. Technical report, NACA Rep. 711, 1941.
- [149] G. Sachs. Stability and control problems in hypersonic flight - paper 35. Technical report, Space Course Munich, 1993.
- [150] A.H. Sacks. Aerodynamic forces, moments, and stability derivatives for slender bodies of general cross section. Technical report, NACA T.N. 3283, 1954.
- [151] J.C. Scheffer and A. Marx. Metingen ter bepaling van krachten die, afhankelijk van de tijdsduur, door een vlieger op de stuurorganen kunnen worden uitgeoefend. Technical report, N.L.L. Rapport V 1255, 1942 (in Dutch).
- [152] H. Schlichting. Calculation of the influence of a body on the position of the aerodynamic centre of aircraft with swept-back wings. Technical report, R. and M. 2582, 1952.
- [153] H. Schlichting and W. Frenz. Über den einfluss von fluegel und rumpf auf das seitenleitwerk. *Jahrbuch der Deutschen Luftfahrtforshung*, page 300 to 314, 1941 (in German).
- [154] H. Schlichting and E. Truckenbrodt. Aerodynamik des flugzeuges, bd 1 und 2. Technical report, Springer-Verlag, Berlin, 1959, (in German).
- [155] W.L. Sherman and K. Margolis. Theoretical calculations of the effects of finite sideslip at supersonic speeds on the span loading and rolling moment for families of thin sweptback tapered wings at an angle of attack. Technical report, NACA T.N. 3046, 1952.
- [156] A. Silverstein and S. Katzoff. Design charts for predicting downwash angles and wake characteristics behind plain and flapped wings. Technical report, NACA Rep. 648, 1939.
- [157] A. Silverstein, S. Katzoff, and W.K. Bullivant. Downwash and wake behind plain and flapped airfoils. Technical report, NACA Rep. 651, 1939.
- [158] C.L. Spigt and A. de Gelder. Windtunnelmetingen aan een model van de f-27 "friendship" uitgevoerd in de lage-snelheids tunnel van de onderafdeling der vliegtuigbouwkunde. Technical report, V.T.H. Memorandum M-42, 1959 (in Dutch).
- [159] C.L. Spigt and A. de Gelder. Windtunnelmetingen aan een model van de romp van de fokker f-27 "friendship". Technical report, VTH M41, 1959 (in Dutch).
- [160] C. Spoon. Windtunnel measurements on a model of the wing of the fokker f-27 "friendship". Technical report, V.T.H. M 46, 1958.
- [161] C. Spoon. Windtunnelmetingen aan een model van de vleugel van de fokker f-27 "friendship". Technical report, VTH M46, 1960 (in Dutch).

- [162] J.R. Spreiter and A.H. Sacks. The rolling-up of the trailing vortex sheet and its effect on the downwash behind wings. *Aero. Sci.*, 18(1):21 to 32, 72, 1951.
- [163] A. Stanbrook. The lift-curve and aerodynamic centre position of wings at supersonic and subsonic speeds. Technical report, R.A.E. T.N. Aero 2328, 1954.
- [164] J.L. Synge and B.A. Griffith. *Principles Of Mechanics*. McGraw-Hill Book Co., 1959.
- [165] H.H.B.M. Thomas. State of the art on estimation of derivatives. Technical report, AGARD Rep. 339 and M.o.A. Current Paper 664, 1960.
- [166] T.A. Toll. Summary of lateral control research. Technical report, NACA Rep. 868, 1947.
- [167] T.A. Toll and M.J. Queijo. Approximate relations and charts for low-speed stability derivatives of swept wings. Technical report, NACA T.N. 1581, 1948.
- [168] E. Torenbeek. *Synthesis of subsonic airplane design*. Delft University Press,, Delft, 1976.
- [169] H. Trienes and E. Truckenbrodt. Systematische abwindmessungen an pfeilförmigen Flügeln. *Ing. Archiv*, XX:26 to 36, 1652 (in German).
- [170] E. Truckenbrodt. Experimentelle und theoretische untersuchungen an symmetrisch angeströmten pfeil- und delta flügeln. Technical report, Z.f. Flw. Bd. 2, 1953, pages 185 to 201 (in German).
- [171] E. Truckenbrodt. Beitrage zur erweiterden traglinientheorie. Technical report, Z.f.Flw. Bd. 1, 1953, pages 31 to 37 (in German).
- [172] B.M. Trujillo. Determination of lift and drag characteristics of space shuttle orbiter using maximum likelihood estimation technique. Technical report, AIAA-86-2225, From: AIAA Atmospheric Flight Mechanics Conference (Williamsburg, Virginia, August 18-20, 1986, 1986.
- [173] H.J. van der Maas. Stuurstandslijnen van vliegtuigen; de bepaling ervan door middel van vliegproeven en hare betekenis voor de beoordeling der stabiliteit. Technical report, Verslagen en verhandelingen van de Rijks studiedienst voor Luchtvaart, Deel V, Amsterdam, 1929 (in Dutch).
- [174] T. van Oosterom. Measurements on the relation between magnitude and duration and on the rate of application of the control forces achieved by pilots in simulated manoeuvres. Technical report, AGARD Report 241, 1959.
- [175] C.H. v.d. Linden and A. Blauw. Experimental determination of the three moments of inertia and the product of inertia in the plane of symmetry of the n.l.r. laboratory aircraft siebel 204-d-1. Technical report, N.L.R. V. 1912, 1963 (in Dutch).
- [176] C.H. v.d. Linden and A. Blauw. Experimental determination of the three moments of inertia and the product of inertia in the plane of symmetry of the n.l.r. laboratory aircraft siebel 204-d-1. Technical report, N.L.R., V. 1912, 1963 (in Dutch).
- [177] N.X. Vinh. *Optimal trajectories in atmospheric flight*. Elsevier Scientific Publishing Company, Amsterdam, 1981.
- [178] J. Weissinger. The lift distribution of swept-back wings. Technical report, NACA T.M. 1120, 1947.
- [179] E.W. Weisstein. Rotation matrix. From MathWorld—A Wolfram Web Resource. <http://mathworld.wolfram.com/RotationMatrix.html>, 1999.

- [180] N.L. Wene. Measurement of aircraft moments of inertia. Technical report, AGARD Rep. 248, 1959.
- [181] N.L. Wener. Measurement of aircraft moments of inertia. Technical report, AGARD Rep. 248, 1959.
- [182] J.W. Wiggins and R.E. Kuhn. Wind-tunnel investigation of the aerodynamic characteristics in pitch of wing-fuselage combinations at high subsonic speeds. sweep series. Technical report, NACA R.M. L52 JWD 18, 1952.
- [183] J.C. Wimpenny. Stability and control in aircraft design. *J.R.A.S.*, 58:329 to 360, 1954.
- [184] R. Wurzbach. Das geschwindigkeitsfeld hinter einer auftrieb erzeugenden tragfl ä che von endlicher spannweite. *Z.f.Flw. Bd. 5,*, 12:360 to 365, 1957 (in German).
- [185] A.H. Yates. Notes on the mean aerodynamic chord and the mean aerodynamic centre of a wing. Technical report, J. R. Ae. S. Vol. 56, 1952, pages 461 to 474.